Volume 183 Number 1

THE BIOLOGICAL BULLETIN

AUGUST, 1992

Published by the Marine Biological Laboratory

THE
BIOLOGICAL BULLETIN

PUBLISHED BY
THE MARINE BIOLOGICAL LABORATORY

AUGUST, 1992

Printed and Issued by
LANCASTER PRESS, Inc.
PRINCE & LEMON STS.
LANCASTER, PA

THE BIOLOGICAL BULLETIN

THE BIOLOGICAL BULLETIN is published six times a year by the Marine Biological Laboratory, MBL Street, Woods Hole, Massachusetts 02543.

Subscriptions and similar matter should be addressed to Subscription Manager, THE BIOLOGICAL BULLETIN, Marine Biological Laboratory, Woods Hole, Massachusetts 02543. Single numbers, $30.00. Subscription per volume (three issues), $77.50 ($155.00 per year for six issues).

Communications relative to manuscripts should be sent to Michael J. Greenberg, Editor-in-Chief, or Carol L. Clapp, Managing Editor, at the Marine Biological Laboratory, Woods Hole, Massachusetts 02543. Telephone: (508) 548-3705, ext. 428. FAX: 508-540-6902. E-mail: pamel@hoh.mbl.edu.

POSTMASTER: Send address changes to THE BIOLOGICAL BULLETIN, Marine Biological Laboratory, Woods Hole, MA 02543.

Second-class postage paid at Woods Hole, MA, and additional mailing offices.
ISSN 0006-3185

INSTRUCTIONS TO AUTHORS

The Biological Bulletin aceepts outstanding original research reports of general interest to biologists throughout the world. Papers are usually of intermediate length (10–40 manuscript pages). A limited number of solicited review papers may be accepted after formal review. A paper will usually appear within four months after its aeceptance.

Very short, especially topical papers (less than 9 manuscript pages including tables, figures, and bibliography) will be published in a separate section entitled "Research Notes." A Research Note in *The Biological Bulletin* follows the format of similar notes in *Nature*. It should open with a summary paragraph of 150 to 200 words comprising the introduction and the eonelusions. The rest of the text should continue on without subheadings, and there should be no more than 30 references. References should be referred to in the text by number, and listed in the Literature Cited seetion in the order that they appear in the text. Unlike references in *Nature*, references in the Research Notes seetion should conform in punctuation and arrangement to the style of recent issues of *The Biological Bulletin*. Materials and Methods should be incorporated into appropriate figure legends. See the article by Lohmann *et al.* (October 1990, Vol. **179:** 214–218) for sample style. A Research Note will usually appear within two months after its acceptance.

The Editorial Board requests that regular manuscripts conform to the requirements set below; those manuscripts that do not conform will be returned to authors for correction before review.

1. ***Manuscripts.*** Manuscripts, including figures, should be submitted in triplicate. (Xerox copies of photographs are not aeceptable for review purposes.) The original manuscript must be typed in no smaller than 12 pitch, using double spacing (*including* figure legends, footnotes, bibliography, etc.) on one side of 16- or 20-lb. bond paper, 8½ by 11 inches. Please, no right justifieation. Manuscripts should be proofread earefully and errors correeted legibly in black ink. Pages should be numbered eonsecutively. Margins on all sides should be at least 1 ineh (2.5 em). Manuscripts should conform to the *Council of Biology Editors Style Manual*, 5th Edition (Council of Biology Editors, 1983) and to American spelling. Unusual abbreviations should be kept to a minimum and should be spelled out on first reference as well as defined in a footnote on the title page. Manuscripts should be divided into the following components: Title page, Abstract (of no more than 200 words), Introduction, Materials and Methods, Results, Discussion, Acknowledgments, Literature Cited, Tables, and Figure Legends. In addition, authors should supply a list of words and phrases under which the article should be indexed.

2. ***Title page.*** The title page consists of: a condensed title or running head of no more than 35 letters and spaces, the manuscript title, authors' names and appropriate addresses, and footnotes listing present addresses, acknowledgments or contribution numbers, and explanation of unusual abbreviations.

3. ***Figures.*** The dimensions of the printed page, 7 by 9 inches, should be kept in mind in preparing figures for publication. We recommend that figures be about 1½ times the linear dimensions of the final printing desired, and that the ratio of the largest to the smallest letter or number and of the thickest to the thinnest line not exceed 1:1.5. Explanatory matter generally should be included in legends, although axes should always be identified on the illustration itself. Figures should be prepared for reproduction as either line cuts or halftones. Figures to be reproduced as line euts should be unmounted glossy photographic reproductions or drawn in black ink on white paper, good-quality tracing cloth or plastic, or blue-lined coordinate paper. Those to be reproduced as halftones should be mounted on board, with both designating numbers or letters and scale bars affixed direetly to the figures. All figures should be numbered in consecutive order, with no distinetion between text and plate figures. The author's name and an arrow indicating orientation should appear on the reverse side of all figures.

4. ***Tables, footnotes, figure legends, etc.*** Authors should follow the style in a recent issue of *The Biological Bulletin* in preparing table headings, figure legends, and the like. Because of the high cost of setting tabular material in type, authors are asked to limit such material as much as possible. Tables, with their headings and footnotes, should be typed on separate sheets, numbered with consecutive Roman numerals, and placed after

the Literature Cited. Figure legends should contain enough information to make the figure intelligible separate from the text. Legends should be typed double spaced, with consecutive Arabic numbers, on a separate sheet at the end of the paper. Footnotes should be limited to authors' current addresses, acknowledgments or contribution numbers, and explanation of unusual abbreviations. All such footnotes should appear on the title page. Footnotes are not normally permitted in the body of the text.

5. ***Literature cited.*** In the text, literature should be cited by the Harvard system, with papers by more than two authors cited as Jones *et al.*, 1980. Personal communications and material in preparation or in press should be cited in the text only, with author's initials and institutions, unless the material has been formally accepted and a volume number can be supplied. The list of references following the text should be headed Literature Cited, and must be typed double spaced on separate pages, conforming in punctuation and arrangement to the style of recent issues of *The Biological Bulletin*. Citations should include complete titles and inclusive pagination. Journal abbreviations should normally follow those of the U. S. A. Standards Institute (USASI), as adopted by BIOLOGICAL ABSTRACTS and CHEMICAL ABSTRACTS, with the minor differences set out below. The most generally useful list of biological journal titles is that published each year by BIOLOGICAL ABSTRACTS (BIOSIS List of Serials; the most recent issue). Foreign authors, and others who are accustomed to using THE WORLD LIST OF SCIENTIFIC PERIODICALS, may find a booklet published by the Biological Council of the U.K. (obtainable from the Institute of Biology, 41 Queen's Gate, London, S.W.7, England, U.K.) useful, since it sets out the WORLD LIST abbreviations for most biological journals with notes of the USASI abbreviations where these differ. CHEMICAL ABSTRACTS publishes quarterly supplements of additional abbreviations. The following points of reference style for THE BIOLOGICAL BULLETIN differ from USASI (or modified WORLD LIST) usage:

A. Journal abbreviations, and book titles, all underlined (for *italics*)

B. All components of abbreviations with initial capitals (not as European usage in WORLD LIST *e.g., J. Cell. Comp. Physiol.* NOT *J. cell. comp. Physiol.*)

C. *All* abbreviated components must be followed by a period, whole word components *must not* (*i.e., J. Cancer Res.*)

D. Space between all components (*e.g., J. Cell. Comp. Physiol.*, not *J.Cell.Comp.Physiol.*)

E. Unusual words in journal titles should be spelled out in full, rather than employing new abbreviations invented by the author. For example, use *Rit Vísindafjélags Íslendinga* without abbreviation.

F. All single word journal titles in full (*e.g., Veliger, Ecology, Brain*).

G. The order of abbreviated components should be the same as the word order of the complete title (*i.e., Proc.* and *Trans.* placed where they appear, not transposed as in some BIOLOGICAL ABSTRACTS listings).

H. A few well-known international journals in their preferred forms rather than WORLD LIST or USASI usage (*e.g., Nature, Science, Evolution* NOT *Nature, Lond., Science, N.Y.; Evolution, Lancaster, Pa.*)

6. ***Reprints, page proofs, and charges.*** Authors receive their first 100 reprints (without covers) free of charge. Additional reprints may be ordered at time of publication and normally will be delivered about two to three months after the issue date. Authors (or delegates for foreign authors) will receive page proofs of articles shortly before publication. They will be charged the current cost of printers' time for corrections to these (other than corrections of printers' or editors' errors). Other than these charges for authors' alterations, *The Biological Bulletin* does not have page charges.

The Marine Biological Laboratory

Ninety-Fourth Report for the Year 1991 One-Hundred and Fourth Year

Officers of the Corporation

Denis M. Robinson, *Honorary Chairman of the Board of Trustees*
Sheldon J. Segal, *Chairman of the Board of Trustees*
Robert E. Mainer, *Vice Chairman of the Board of Trustees*
James D. Ebert, *President of the Corporation*
Harlyn O. Halvorson, *Director of the Corporation*
Robert D. Manz, *Treasurer*
Kathleen Dunlap, *Clerk of the Corporation*

Contents

Report of the Director

The Marine Resources Center

The most tangible and, in my mind, the most exciting development during 1991 was the construction of the long-awaited Marine Resources Center (MRC). As I write this report, the Center's grand opening is less than a month away, and after years of planning and dreaming, this state-of-the-art facility for the culture of marine animals is now a reality. We were fortunate to have received a total of $10.75 million from the Federal government for the construction of this building. I am pleased to report that the MRC will be completed on time and within budget.

Plans are moving forward to design and construct the Advanced Studies Laboratory which, together with the MRC, will constitute the Marine Biomedical Institute for Advanced Studies (MBIAS).

In last year's report, I expressed hope that by the next filing of the director's report, two other construction projects, namely the carpenter shop and the off-site parking lot, would be completed. I am pleased to say that the Devil's Lane parking area off Oyster Pond Road and the shuttle bus operation were fully functional by the beginning of summer 1991. The new carpenter shop next to the Broderick house was also in use by summer 1991.

Hurricane Bob

The most dramatic event of the season was Hurricane Bob, which hit Woods Hole on Monday, August 19, 1991. Fortunately, it occurred at low tide so the MBL sustained only minor water damage. However, like much of Cape Cod, the MBL was without electricity for five days, and emergency power was not sufficient to protect all research in the laboratories. The MBL received $39,793 from the Federal Emergency Management Agency for 75% of the damage to the sea wall and pilings, and $147,138 from its Business Interruption Insurance to cover the loss of five day's work, losses in the research labs, and physical damage to the campus and Waterfront Park. These experiences during Hurricane Bob have led us to update the MBL's emergency procedures.

Congressman Gerry Studds surveying the site of the new MRC.

The demolition of the Carpenters' Shop.

Salvage operations after Hurricane Bob.

Research

The Scientific Advisory Council was created in 1990 to provide advice to the Executive Committee on scientific programs, funding proposals, promotions for the scientists, and applications for year-round research.

In 1991, the Council's recommendations included the promotions of Brian Fry and Knute Nadelhoffer to associate scientist and the appointments of Andrew Miller and Rudolf Oldenbourg as assistant scientists and Norman Wainwright as senior scientist.

Further recommendations included developing program descriptions for the Neurobiology, Cell and Developmental Biology (henceforward to be known as Architectural Dynamics in Living Cells), and Molecular Evolution programs. The latter two have been completed, submitted to the Executive Committee, and endorsed. We are now ready to submit grant proposals to appropriate private sources. The Neurobiology program is still under review.

The Marine Resources Center.

Instruction

The 1991 education program was very successful. A team from the National Institutes of Health conducted a site visit of the Physiology course with a very positive outcome: five years of funding and many kudos for course director Thomas Pollard of The Johns Hopkins University and the course faculty. During the site visit several alums testified, including C. Ladd Prosser of the Physiology class of 1932.

Other highlights were the Cellular Neurobiology and Development of the Leech course under the leadership of David Weisblat of the University of California. David added a distinctly developmental flavor to the course and was also able to obtain funding from the National Science Foundation. A very lively two weeks were spent by students and faculty in the History of Biology course on Modern Evolutionary Biology led by Garland Allen of Washington University, St. Louis,

Trustees Bob Silver (l) and Jerry Melillo (r) shore up a tree felled by Hurricane Bob.

John Beatty of the University of Minnesota, and Jane Maienschein of Arizona State University.

Hurricane Bob played havoc with two of the August courses that use computers: Methods in Computational Neuroscience and Molecular Evolution. Heroic duty by the course personnel and local "techies" permitted students to capture and use the "dirty" electrical power supplied by the Loeb generator to model the nervous system and to do phylogenetic analyses, respectively.

The summer of 1991 marked the first year of a reinvigorated fellowship program under the leadership of MBL trustee, Ed Kravitz of Harvard University. Ed's *ad hoc* committee arranged fellows' weekly lunchtime presentations at Swope, and invitations to the Tokyo String Quartet benefit concert and dinner, to dinners prior to the Friday evening lectures, and to the Trustees' cocktail party. Eighteen fellowships, totalling about $120,000, were awarded to meritorious investigators in 1991. This is double the amount awarded in 1990. Several new fellowships were established at the MBL during 1991, most notably the Nikon International Fellowship and the Bernard Davis Fund. The Fellowships are listed in a separate section of this publication.

Library

The MBL/WHOI Library has been reorganized to reflect its newest mission to transform itself into a prototype information services center for scientific research and education. This signifies the development of computer networks and electronic databases that will be accessible to a growing number of scientists in Woods Hole and around the world. Under the leadership of director David Stonehill, the Library will continue to maintain traditional library serviees while simultaneously providing state-of-the-art information technologies.

Appointed Assistant Director for MBL Library Operations to maintain the traditional library operation is Judith Ashmore. Catherine Norton was named Director for Information Services to develop the computerized scientifie information systems.

Ecosystems Center

The Ecosystems Center continues to study the implications of accelerating changes in the earth's environments as a result of human interventions. Scientists from a variety of disciplines are carrying out long- and short-term experiments using advanced computer modelling and sophisticated spectrometers and gas and pressure similation chambers. Studies on acid rain, oxygen depletion, global warming, and sewage outfall are all underway.

The Lillie renovation

During the first quarter of 1991, the MBL won a matching grant amounting to $575,000 from the National Science Foundation to modernize the Lillie Research Building, the MBL's oldest and largest permanent laboratory. Our biggest challenge on this grant is to raise the matching funds by October 1992.

External Affairs

During 1991, the MBL consolidated the offices of Development, Public Information, Special Events, and the Associates' Liaison into the External Affairs Department. Hired to direct this department was Frank Carotenuto, who joined us from Clark University which not only completed but exceeded its fund drive.

Public programs

Again in 1991 the MBL offered a wide range of events for our neighbors in the Upper Cape community. The Tokyo String Quartet filled Lillie Auditorium in July for an outstanding concert, followed by a well-attended candlelight dinner on the Swope Terrace.

The Associates Lecture was presented by Dr. Gerald Fischbach who spoke on the Decade of the Brain.

The popular Falmouth Forum series began its third season in 1991. Sponsored by the MBL Associates, the early 1991 programs included a presentation by WHOI science writer, Victoria Kaharl, entitled "ALVIN in Wonderland"; a lecture on "The Legacy of Buckminster Fuller" by Gregory Watson, commissioner of the Massachusetts Department of Food and Agriculture; and readings by Annie Dillard, Pulitzer Prize winning author. Pediatrician T. Berry Brazelton kicked off the 1991–92 season with "Stresses and Supports for Parents in the 90s;" and Woods Hole sculptor, Elaine Pear Cohen, followed with a demonstration and lecture in December.

—Harlyn O. Halvorson

Report of the Treasurer

The year 1991 was one of constrained growth for the Laboratory. Our operations felt the pressure of a recessionary economy and tightened federal research budgets. Our capital base expanded dramatically, however, as federal government construction funds allowed us to near completion of our new Marine Resources Center, and as market appreciation and gifts increased our endowment by almost $2 million.

Total support and revenues increased from $17.0 to $20.8 million; this was due primarily to the continuation of construction of the Marine Resources Center, supported by a grant from the federal government; $4.2 million was received and expended on this project in 1991. Federal grant reimbursement of research increased from $4.9 million to $5.1 million; recovery of indirect costs grew proportionately. Total gifts received declined in 1991 although the use of gifts and gift balances to support the Laboratory's operations increased from $2.6 million to $2.9 million; this is due to the fact that the cash for a number of generous multi-year grants was received in the early years of the grants. We have invested the funds received, and are drawing them down over the years covered by the grants. Investment income declined, due to lowered interest rates and due to decreases in the invested balances from the multi-year grants just mentioned.

Total expenditures grew approximately $700,000. Of this more than $400,000 was for increases in research and $150,000 was increases in support of young scientists through fellowships, scholarships and stipends—this amount has doubled in the last two years. Expenses for administration rose approximately $180,000.

The Current Unrestricted Fund ended the year with an excess of support and revenues over expenses of $129,917 (Fig. 1). This combines the results of the Housing and Dining Auxiliary with all other Operations. The Housing and Dining Auxiliary had an excess of support and revenues over expenses of $134,862 of which $65,000 was used for scheduled repayment of debt owed on the Memorial Circle cottages and $69,862 (Fig. 2) was transferred to the Repairs and Replacements Reserve for housing. The operations of the Laboratory before the Housing and Dining operation experienced a deficiency of revenues to expenses of $4,945; this deficit was funded from our Unrestricted Quasi-Endowment. This near-balancing of the budget was achieved, however, only after incorporating the effect of a one-time change in the Laboratory's method of payment for Library periodicals, a change that improved the 1991 results by approximately $180,000.

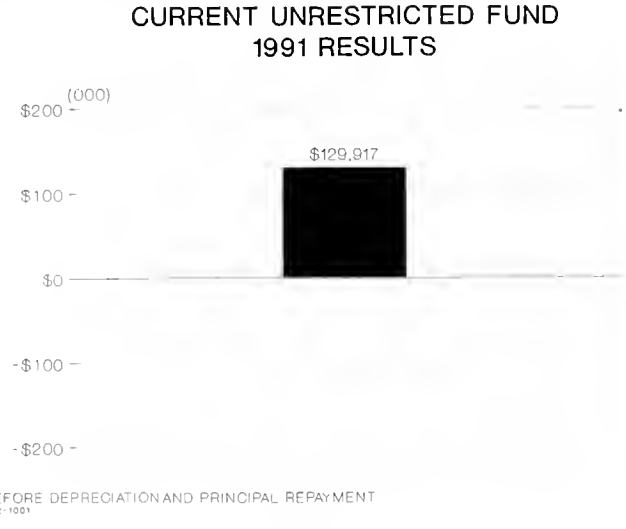

Figure 1

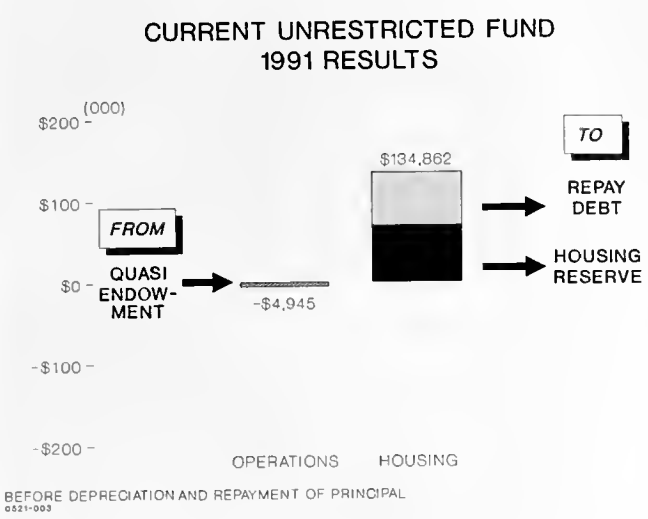

Figure 2

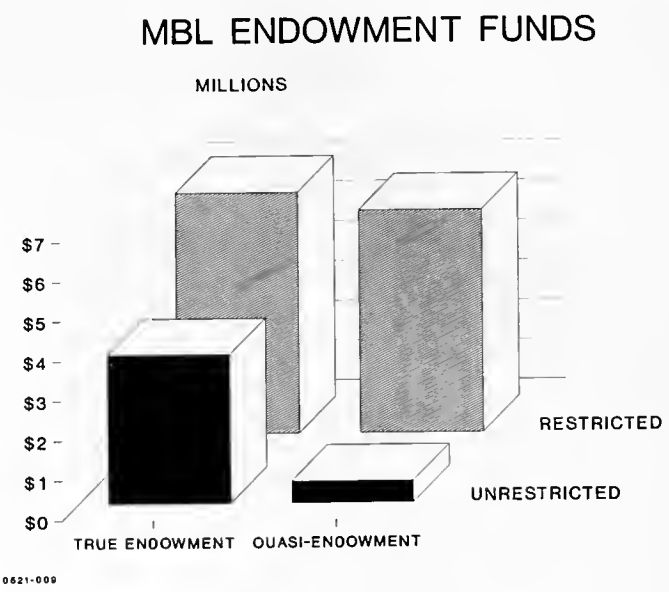

Figure 4

The balance sheet shows that we ended 1991 with continued excellent liquidity as cash and short term investments accounted for approximately two-thirds of current assets.

Land, buildings, and equipment, net of accumulated depreciation, grew by $4.3 million due primarily to the beginning of construction of the Marine Resources Center. When completed, this project is expected to total $9 million.

Investments for endowment and deferred support (gifts we have received for expenditure over multiple years) grew by approximately $1,900,000 due primarily to excellent capital appreciation of our portfolios. The steady growth of our Endowment Funds (Fig. 3) has improved the capitalization of the Laboratory, but the level is still modest for an institution of our size.

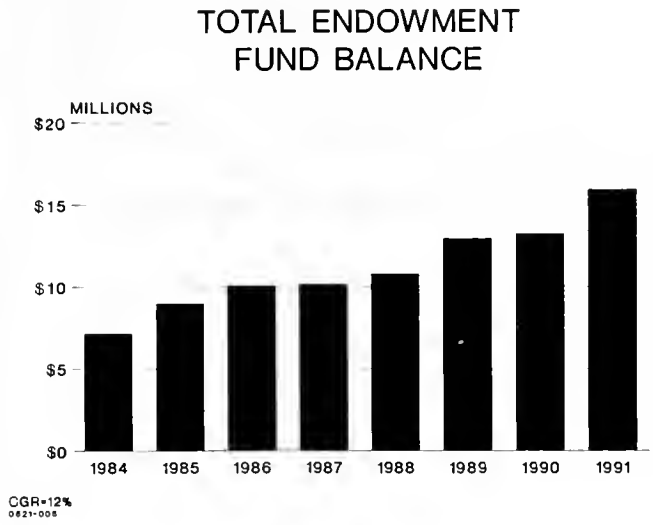

Figure 3

Our Endowment funds are defined in terms of the degree of discretion which the Laboratory may exercise with respect to them (Fig. 4). There are two principles of classification—whether principal may or may not be used ("Quasi" and "True" Endowment) and the degree of discretion the MBL may exercise in spending income (or for Quasi-Endowment, principal as well). Restricted Endowment constitute funds for which donors have specified activities or classes of activity. Unrestricted Endowment constitutes money for which the MBL may apply at its discretion. The lesson of Figure 4 is that the funds over which the MBL has the most discretion—Unrestricted Quasi-Endowment—are very slim. We intend to conserve those and to consider applying them only where there promises to be a significant return on our investment.

The Financial Statements have changed slightly this year. We have simplified the Statement of Support, Revenues, Expenses, and Changes in Fund Balances by condensing a number of categories. The most significant condensation is the line item "Services," which represents the various activities that the Laboratory engages in to support the scientists who come here—Marine Resources, Research Services, Library, *Biological Bulletin*, Dormitory and Dining Hall. Looking at this grouping does more than relieve the "eye strain"; it reveals a significant and sobering fact. The total expense of providing all such services is $3.8 million; the total "Fees for service" paid by users of those services is $3.2 million. Thus the Laboratory falls short of collecting the *direct cost* of the services it provides by $600,000. (The true cost would include an

allocation for administration, plant operations, and depreciation). How we will close or otherwise finance that gap is a significant, unmet challenge of the Laboratory.

Because we are not running a $600,000 deficit one might reasonably ask how it is being financed today. Some is funded by gifts, some by endowment income. The remainder is financed by not funding depreciation on much of our existing plant. The notable exception to this is the success we have had in funding depreciation of our housing. It remains my goal to reach the point where the MBL fully funds depreciation from its operations.

The operating budget for 1992 reflects a continued determination to maintain the current level of services at the Laboratory in the most cost-effective manner possible, while we redouble our efforts to generate more funds to support operations.

—Robert D. Manz

Coopers & Lybrand

certified public accountants

REPORT OF INDEPENDENT ACCOUNTANTS

To the Trustees of
Marine Biological Laboratory
Woods Hole, Massachusetts

We have audited the accompanying balance sheet of Marine Biological Laboratory as of December 31, 1991 and the related statement of support, revenues, expenses and changes in fund balances for the year then ended. We previously examined and reported upon the financial statements of the Laboratory for the year ended December 31, 1990, which condensed statements are presented for comparative purposes only. These financial statements are the responsibility of the Laboratory's management. Our responsibility is to express an opinion on these financial statements based on our audit.

We conducted our audit in accordance with generally accepted auditing standards. Those standards require that we plan and perform the audit to obtain reasonable assurance about whether the financial statements are free of material misstatement. An audit includes examining, on a test basis, evidence supporting the amounts and disclosures in the financial statements. An audit also includes assessing the accounting principles used and significant estimates made by management, as well as evaluating the overall financial statement presentation. We believe that our audit provides a reasonable basis for our opinion.

In our opinion, the financial statements referred to above present fairly, in all material respects, the financial position of Marine Biological Laboratory at December 31, 1991, and its support, revenues, expenses and changes in fund balances for the year then ended in conformity with generally accepted accounting principles.

Our audit was conducted for the purpose of forming an opinion on the basic financial statements taken as a whole. The supplemental schedules of support, revenues, expenses and changes in fund balances for current funds (Schedule I), endowment funds (Schedule II) and plant funds (Schedule III) as of December 31, 1991 are presented for purposes of additional analysis and are not a required part of the basic financial statements. Such information has been subjected to the auditing procedures applied in the audit of the basic financial statements and, in our opinion, is fairly stated, in all material respects, in relation to the basic financial statements taken as a whole.

Coopers & Lybrand

Boston, Massachusetts
April 17, 1992

MARINE BIOLOGICAL LABORATORY

BALANCE SHEETS

December 31, 1991
(with comparative totals for 1990)

ASSETS	*1991*	*1990*
Cash and cash equivalents	$ 373,365	$ 304,980
Restricted cash	6,994	—
Investments, at market (Notes B and H)	1,778,770	1,654,044
Accounts receivable, net of allowance for doubtful accounts of $6,000 and $5,000	458,275	540,983
Receivables due for costs incurred on grants and contracts	691,118	581,880
Other assets	239,970	35,679
Total current assets	3,548,492	3,117,566
Restricted cash (Note C)	587,579	545,796
Investments, at market (Notes B and H)	18,298,679	16,395,852
Deposits with trustee (Note G)	126,116	143,006
Fixed assets (Notes B and C):		
Land	689,660	689,660
Buildings	17,535,524	16,955,015
Equipment	2,933,618	2,819,202
Construction in progress	6,214,181	1,969,713
	27,372,983	22,433,590
Less accumulated depreciation	(10,050,276)	(9,459,548)
	17,322,707	12,974,042
Total assets	$39,883,573	$33,176,262

LIABILITIES AND FUND BALANCES	*1991*	*1990*
Current portion of long-term debt	$ 60,000	$ 65,000
Accounts payable and accrued expenses	822,084	774,139
Deferred income	308,019	679,849
Total current liabilities	1,190,103	1,518,988
Accounts payable (Note C)	587,579	—
Long-term debt (Note G)	1,140,000	1,200,000
Deferred support (Note J)	4,437,140	4,774,618
Annuities payable (Note B)	152,416	117,381
Total long-term liabilities	6,317,135	6,091,999
Commitments (Note C)	—	—
Total liabilities	7,507,238	7,610,987
Current unrestricted fund balances	21,398	19,518
Endowment fund balances:		
Quasi-endowment unrestricted	543,049	237,279
Endowment, income for unrestricted purposes	3,735,253	3,291,503
Endowment, income for restricted purposes	6,049,007	5,122,448
Quasi-endowment restricted	5,590,516	4,565,674
	15,374,776	12,979,625
Total endowment funds	15,917,825	13,216,904
Plant fund balances:		
Unrestricted	10,034,642	9,908,615
Repairs and replacement reserve	188,289	450,525
Restricted	6,214,181	1,969,713
Total plant funds	16,437,112	12,328,853
Total liabilities and fund balances	$39,883,573	$33,176,262

The accompanying notes are an integral part of the financial statements.

MARINE BIOLOGICAL LABORATORY

STATEMENT OF SUPPORT, REVENUES, EXPENSES AND CHANGES IN FUND BALANCES

for the year ended December 31, 1991
(with comparative totals for 1990)

	Current Funds				Endowment Funds		Plant Funds			
	Unrestricted									
	Operating Fund	Auxiliary Enterprises	Total	Restricted	Unrestricted	Restricted	Unrestricted	Restricted	1991 Total All Funds	1990 Total All Funds
SUPPORT AND REVENUES:										
Grant reimbursements of direct costs				$5,129,580					$ 5,129,580	$ 4,872,529
Grant for capital additions								$4,835,681	4,835,681	1,429,322
Recovery of indirect costs (Note J)	$3,319,506		$3,319,506						$3,319,506	3,136,240
Tuition				564,144					564,144	484,749
Fee for services	1,306,795	$1,731,624	3,038,419	173,858					3,212,277	3,031,862
Investment income	433,940		433,940	548,306					982,246	1,141,354
	5,060,241	1,731,624	6,791,865	6,415,888				4,835,681	18,043,434	14,096,056
Gifts (Note J)	318,685		318,685	1,652,189		$ 173,775			2,144,649	2,928,947
Change in deferred support (Note J)	362,288		362,288	(24,810)					337,478	(324,396)
	680,973		680,973	1,627,379		173,775			2,482,127	2,604,551
Miscellaneous revenue	28,651		28,651	240,352					269,003	339,256
Total support and revenues	5,769,865	1,731,624	7,501,489	8,283,619		173,775		4,835,681	20,794,564	17,039,863
EXPENSES:										
Research				5,685,198					5,685,198	5,228,030
Instruction				1,249,298					1,249,298	1,370,282
Scholarships, fellowships and stipends				529,044					529,044	356,253
Services	1,771,651	1,454,762	3,226,413	532,259					3,758,672	3,679,167
Administration	2,330,657	142,000	2,472,657						2,472,657	2,292,776
Plant operations	1,672,502		1,672,502	113,242			$ 47,991		1,833,655	1,757,391
Depreciation							608,327		608,327	601,501
Other				224,179			42,966		267,145	440,908
Total expenses	5,774,810	1,596,762	7,371,572	8,333,220		—	699,204	—	16,403,996	15,726,308
Excess (deficit) of support and revenues over expenses	(4,945)	134,862	129,917	(49,601)		173,775	(699,204)	4,835,681	4,390,568	1,313,555
Net realized gain on investments				121,308	$ 14,261	653,837			789,406	492,498
Net unrealized gain (loss) on investments				5,102	50,437	1,575,547			1,631,086	(420,657)
Total gain on investments	—			126,410	64,698	2,229,384	—	—	2,420,492	71,841
Transfers	6,825	(134,862)	(128,037)	(76,809)	241,072	(8,008)	562,995	(591,213)	—	—
Net change in fund balances	1,880	—	1,880	—	305,770	2,395,151	(136,209)	4,244,468	6,811,060	1,385,396
Fund balances, beginning of year	19,518	—	19,518	—	237,279	12,979,625	10,359,140	1,969,713	25,565,275	24,179,879
Fund balances, end of year	$ 21,398	—	$ 21,938	—	$ 543,049	$15,374,776	$10,222,931	$6,214,181	$32,376,335	$25,565,275

The accompanying notes are an integral part of the financial statements.

Marine Biological Laboratory

Notes to Financial Statements

A. *Purpose of the Laboratory:*

The purpose of Marine Biological Laboratory (the "Laboratory") is to establish and maintain a laboratory or station for scientific study and investigations, and a school for instruction in biology and natural history.

B. *Significant accounting policies:*

Basis of presentation—fund accounting

In order to ensure observance of limitations and restrictions placed on the use of resources available to the Laboratory, the accounts of the Laboratory are maintained in accordance with the principles of fund accounting. This is the procedure by which resources are classified into separate funds in accordance with specified activities or objectives. Separate accounts are maintained for each fund; however, in the accompanying financial statements, funds that have similar characteristics have been combined into fund groups. Accordingly, all financial transactions have been recorded and reported by fund group.

Externally restricted funds may only be utilized in accordance with the purposes established by the donor or grantor of such funds. However, the Laboratory retains full control over the utilization of unrestricted funds. Restricted gifts, grants, and other restricted support are accounted for in the appropriate restricted funds. Restricted current funds are reported as revenue as the related costs are incurred (see Note J).

Endowment funds are subject to restrictions which require that the principal be invested in perpetuity. Related investment income is available for use for restricted or unrestricted purposes by the Laboratory depending on donor restrictions. Quasi-endowment funds have been established by the Laboratory for the same purposes as endowment funds; however, the principal of these funds may be expended for various restricted and unrestricted purposes.

Accounting change

In 1991, certain revenues and expenses previously recorded on the cash basis have been accounted for on the accrual basis of accounting, resulting in decreases of $56,329 and $179,865 in current fund revenues and expenses, respectively. Prior year amounts were not restated. Certain other amounts in the prior year have been reclassified to conform to the current year's presentation.

Fixed assets

Land, buildings and equipment purchased by the Laboratory are recorded at cost. Donated fixed assets are recorded at fair market value at the date of the gift. Depreciation is computed using the straight-line method, full year convention over the asset's estimated useful life. Estimated useful lives are generally three to five years for equipment and twenty to forty years for buildings. When assets are sold or retired, the cost and accumulated depreciation are removed from the accounts and any resulting gain or loss is included in income for the period.

Contracts and grants

Revenues associated with contracts and grants are recognized in the statement of support, revenues, expenses and changes in fund balances as the related costs are incurred (see Note J). Reimbursement of indirect costs relating to government contracts and grants is based on negotiated indirect cost rates. Any over or underrecovery of indirect costs is recognized through future adjustments of indirect cost rates.

Investments

Investments purchased by the Laboratory are carried at market value. Money market securities are carried at cost plus accrued interest, which approximates market value. Donated investments are recorded at fair market value at the date of the gift. Land held for sale included in investments is carried at the initially recorded market value of $330,000. For determination of gain or loss upon disposal of investments, cost is determined based on the first-in, first-out method.

The Laboratory is the beneficiary of certain investments reported in the endowment funds which are held in trust by others. Every ten years the Laboratory's status as beneficiary of these funds is reviewed to determine that the Laboratory's use of these funds is in accordance with the intent of the donor. The market values of such investments are $4,717,316 and $4,125,093 at December 31, 1991 and 1990, respectively.

Investment income and distribution

The Laboratory follows the accrual basis of accounting except that investment income is recorded on a cash basis. The difference between such basis and the accrual basis does not have a material effect on the determination of investment income earned on a year-to-year basis.

Investment income includes income from a pooled investment account, which income is allocated to the participating funds on the market value unit basis (Note K).

Annuities payable

Amounts due to donors in connection with gift annuities are determined based on remainder value calculations which at December 31, 1991 assumed a rate of return of 10%, maximum payout terms of 18 years, and an interest payout rate of 8%.

C. *Land, buildings and equipment:*

As of December 31, 1991, the Laboratory has received funding of $6,805,394 for its current building program, principally the new Marine Resources Center. Included in assets at December 31, 1991 is restricted cash of $587,579 relating to this program. At December 31, 1991 the Laboratory was contractually obligated for approximately $3,425,000 of additional expenditures in connection with its building program for which it has in place an equal amount of funding commitments.

D. *Retirement plan:*

The Laboratory participates in the defined contribution pension program of the Teachers Insurance and Annuity Association College Equities Retirement Fund. Contributions amounted to $495,848 in 1991 and $451,665 in 1990.

E. *Pledges:*

As of December 31, 1992, the Laboratory has outstanding pledges of $543,951 (unaudited). Pledges are not included in the financial statements since it is not practicable to estimate the net realizable value of such pledges. These pledges are scheduled to be paid over the next four years in the amounts of $244,951, $165,000, $124,000 and $10,000, respectively.

F. *Interfund borrowings:*

Current fund interfund balances at December 31 are as follows:

	1991	*1990*
Due to restricted endowment fund	$ (4,150)	$(4,750)
Due to restricted quasi-endowment funds	(150,000)	(1,650)
	$(154,150)	$(6,400)

G. *Long-term debt:*

In 1989, the Laboratory issued $1,330,000 Massachusetts Industrial Finance Authority (MIFA) Series 1989 Bonds, which pay varying annual interest rates and mature on October 31, 2011. The Series 1989 Bonds are collateralized by a first mortgage on certain Laboratory property. The interest rate is adjustable and was 5.55% and 7.25% at December 31, 1991 and 1990, respectively. In compliance with the MIFA bond indenture, the Laboratory has on deposit with Shawmut Bank N.A., as trustee, investments of $126,116 in 1991 and $143,006 in 1990.

The aggregate amount of redemption due for each of the next five years is as follows:

1992	$ 60,000
1993	60,000
1994	60,000
1995	60,000
1996	60,000
Thereafter	900,000
	1,200,000
Less current portion	60,000
	$1,140,000

H. *Investments:*

The following is a summary of the cost and market value of investments at December 31, 1991 and 1990.

	Market		*Cost*	
	1991	*1990*	*1991*	*1990*
Certificates of deposit	$ 258,351	$ 502,360	$ 258,351	$ 502,360
Money market securities	1,767,300	2,090,735	1,767,300	2,090,735
U.S. Government securities	1,456,944	1,957,512	1,423,722	1,934,834
Corporate fixed income	8,387,547	6,809,264	7,718,034	6,663,376
Common stocks	7,864,060	6,346,778	4,589,543	4,284,591
Real estate	343,247	343,247	343,247	343,247
Total investments	$20,077,449	$18,049,896	$16,100,174	$15,819,143

Investments by fund group and related portfolios for the years ended December 31, 1991 and 1990, are as follows:

Current Funds				
Certificates of deposit	$ 258,351	$ 502,360	$ 258,351	$ 502,360
Money market securities	1,200,000	1,500,000	1,200,000	1,500,000
Library funds	320,419	—	317,557	—
Total	1,778,770	2,002,360	1,775,908	2,002,360

	Market		Cost	
Endowment and Quasi-Endowment				
General endowment trust fund	3,735,252	3,291,503	2,707,869	2,564,917
Library endowment trust fund	982,063	833,590	635,203	581,250
Ecosystems fund	4,488,315	3,755,777	3,411,559	3,153,183
Pooled funds	6,608,044	5,526,035	5,253,616	4,927,342
Instruction fund	2,141,758	2,297,384	1,972,772	2,246,844
Real estate	343,247	343,247	343,247	343,247
Total	18,298,679	16,047,536	14,324,266	13,816,783
Total investments	$20,077,449	$18,049,896	$16,100,174	$15,819,143

I *Tax-exempt status:*

The Laboratory is exempt from federal income tax under Section 501(c)3 of the Internal Revenue Code.

J. *Restricted current funds deferred support:*

The Laboratory defers recognition of revenue on current restricted funds until the related costs are incurred. Amounts received in excess of expenses are recorded as deferred support. The following summarizes the activity in the deferred support account:

	1991	*1990*
Balance at beginning of year	$4,774,618	$4,450,222
Additions:		
Gifts, endowment income and grants received	7,832,555	8,499,360
Net unrealized gains	121,308	19,868
Net realized gains	5,102	1,649
Transfers	36,777	—
Deductions:		
Funds expended under gifts and grants	8,333,220	7,977,187
Transfers	—	219,294
Balance at end of year	$4,437,140	$4,774,618

Deferred restricted gifts of $475,874 and $500,000 were expended in 1991 and 1990, respectively, for the support of indirect costs attributable to the Laboratory's instruction programs.

K. *Accounting for pooled investments*

Certain endowment fund assets are pooled for investment purposes. Investment income from the pooled investment account is allocated on the market value unit basis, and each endowment fund subscribes to or disposes of units on the basis of the market value per unit at the beginning of the calendar quarter within which the transaction takes place. The unit participation of the funds at December 31, 1991 and 1990 is as follows:

	1991	*1990*
Quasi-unrestricted	4,618	3,909
Quasi-restricted	7,415	7,436
Restricted endowment	40,687	39,401
	52,720	50,746

Pooled investment activity on a per-unit basis was as follows:

	1991	*1990*
Unit value at beginning of year	$108.90	$109.57
Unit value at end of year	128.42	108.90
Increase (decrease) in realized and unrealized appreciation	19.52	(.67)
Net income earned on pooled investments	5.15	5.99
Total return on pooled investments	$ 24.67	$ 5.32

L. *Financial Accounting Standard No. 106*

In December 1990, the Financial Accounting Standards Board (FASB) released Statement No. 106, "Employers' Accounting for Postretirement Benefits Other Than Pensions." This new standard requires employers to accrue, during the years that the employee renders the necessary service, the expected cost of benefits to be provided during retirement, and will apply to years beginning after December 15, 1994. The Laboratory is currently analyzing and interpreting the provisions of the Statement as it relates to its current and planned benefits program and its funding options. It is anticipated that adoption of this accounting standard will result in the Laboratory recording a significant liability.

MARINE BIOLOGICAL LABORATORY

STATEMENT OF SUPPORT, REVENUES, EXPENSES AND CHANGES IN FUND BALANCES

CURRENT FUNDS

for the year ended December 31, 1991

	Current Unrestricted Funds				
	Operating Fund	*Auxiliary Enterprises Fund*	*Total*	*Current Restricted Fund*	*Total*
SUPPORT AND REVENUES:					
Grant reimbursements of direct costs				$5,129,580	$5,129,580
Recovery of indirect costs	$3,319,506		$3,319,506		3,319,506
Tuition				564,144	564,144
Fees for services:					
Dormitories		$ 912,162	912,162		912,162
Dining hall		819,462	819,462		819,462
Library	426,630		426,630		426,630
Biological Bulletin	215,345		215,345		215,345
Research services	496,015		496,015	173,858	669,873
Marine resources	168,805		168,805		168,805
Investment income	433,940		433,940	548,306	982,246
	5,060,241	1,731,624	6,791,865	6,415,888	13,207,753
Gifts	318,685		318,685	1,652,189	1,970,874
Change in deferred support	362,288		362,288	(24,810)	337,478
	680,973		680,973	1,627,379	2,308,352
Miscellaneous revenue	28,651		28,651	240,352	269,003
Total support and revenues	5,769,865	1,731,624	7,501,489	8,283,619	15,785,108
EXPENSES:					
Research				5,685,198	5,685,198
Instruction				1,249,298	1,249,298
Scholarships, fellowships and stipends				529,044	529,044
Services:					
Dormitories		703,986	703,986		703,986
Dining hall		750,776	750,776		750,776
Library	493,431		493,431	347,873	841,304
Biological Bulletin	215,275		215,275		215,275
Research services	629,480		629,480	177,963	807,443
Marine resources	433,465		433,465	6,423	439,888
Administration:					
Administration	2,008,517	142,000	2,150,517		2,150,517
Sponsored projects administration	322,140		322,140		322,140
Plant operations	1,672,502		1,672,502	113,242	1,785,744
Other			—	224,179	224,179
Total expenses	5,774,810	1,596,762	7,371,572	8,333,220	15,704,792
Excess (deficit) of support and revenues over expenses	(4,945)	134,862	129,917	(49,601)	80,316
Net unrealized gain on investments				121,308	121,308
Net realized gain on investments			—	5,102	5,102
Total gain on investments			—	126,410	126,410
TRANSFERS AMONG FUNDS:					
Debt service		(65,000)	(65,000)		(65,000)
Acquisition of fixed assets	(69,446)		(69,446)	(58,545)	(127,991)
Repairs and replacement		(69,862)	(69,862)		(69,862)
Endowment transfer	50,000		50,000	200,000	250,000
Capitalize ecosystems income				(185,992)	(185,992)
Other	26,271		26,271	(32,272)	(6,001)
Total transfers among funds	6,825	(134,862)	(128,037)	(76,809)	(204,846)
Net change in fund balances	1,880	—	1,880	—	1,880
Fund balances, beginning of year	19,518	—	19,518	—	19,518
Fund balances, end of year	$ 21,398	—	$ 21,398	—	$ 21,398

SCHEDULE II

MARINE BIOLOGICAL LABORATORY

STATEMENT OF SUPPORT, REVENUES, EXPENSES AND CHANGES IN FUND BALANCES

ENDOWMENT FUNDS

for the year ended December 31, 1991

	Unrestricted	*Restricted*				
	Quasi-Endowment	*Endowment, Income for Unrestricted Purposes*	*Endowment, Income for Restricted Purposes*	*Quasi-Endowment*	*Total Restricted*	*Total*
SUPPORT AND REVENUES:						
Gifts			$ 21,450	$ 152,325	$ 173,775	$ 173,775
Total support and revenues			21,450	152,325	173,775	173,775
Net realized gain on investments	$ 14,261	$ 142,953	209,591	301,293	653,837	668,098
Net unrealized gain on investments	50,437	300,797	689,518	585,232	1,575,547	1,625,984
Total gain on investments	64,698	443,750	899,109	886,525	2,229,384	2,294,082
TRANSFERS AMONG FUNDS:						
Capitalize ecosystems income				185,992	185,992	185,992
Endowment transfers	(50,000)		6,000	(200,000)	(194,000)	(244,000)
Other transfers	291,072					291,072
Total transfers among funds	241,072		6,000	(14,008)	(8,008)	233,064
Net change in fund balances	305,770	443,750	926,559	1,024,842	2,395,151	2,700,921
Fund balances, beginning of year	237,279	3,291,503	5,122,448	4,565,674	12,979,625	13,216,904
Fund balances, end of year	$ 543,049	$ 3,735,253	$ 6,049,007	$ 5,590,516	$15,374,776	$15,917,825

MARINE BIOLOGICAL LABORATORY

STATEMENT OF SUPPORT, REVENUES, EXPENSES AND CHANGES IN FUND BALANCES

PLANT FUNDS

for the year ended December 31, 1991

	Unrestricted				
	Unrestricted	*Repairs and Replacement Reserve*	*Total Unrestricted*	*Restricted*	*Total*
SUPPORT AND REVENUES:					
Grant for capital additions				$4,835,681	$ 4,835,681
Total support and revenues				4,835,681	4,835,681
EXPENSES:					
Depreciation	$ 608,327		$ 608,327		608,327
Plant operations		$ 47,911	47,911		47,911
Other	42,966		42,966		42,966
Total expenses	651,293	47,911	699,204	—	669,204
Excess (deficit) of support and revenues over expenses	(651,293)	(47,911)	(699,204)	4,835,681	4,136,477
TRANSFERS AMONG FUNDS:					
Debt service	65,000		65,000		65,000
Acquisition of fixed assets	127,991		127,991		127,991
Capital additions	591,213		591,213	(591,213)	
Repairs and replacements	(6,884)	69,862	62,978		62,978
Other transfers		(284,187)	(284,187)		(284,187)
Total transfers among funds	777,320	(214,325)	562,995	(591,213)	(28,218)
Net change in fund balances	126,027	(262,236)	(136,209)	4,244,468	4,108,259
Fund balances, beginning of year	9,908,615	450,525	10,359,140	1,969,713	12,328,853
Fund balances, end of year	$10,034,642	$ 188,289	$10,222,931	$6,214,181	$16,437,112

Report of the Library Director

The MBL/WHOI Library was active and productive in 1991, with major activities in management, library operations, information systems, and grants.

Management

During 1991, the MBL Library Operations and the Information Systems divisions were separately established to dedicate management attention to the needs of each area. Judith Ashmore was appointed as Assistant Director for MBL Library Operations; Catherine Norton took up responsibility as Director of Information Systems. Subsequently, the Information Systems division became responsible for MBL administrative computing, instructional support, and MBL-wide data networking.

In January of 1992, the Library Director's position became a joint appointment with the Woods Hole Oceanographic Institution (WHOI). The WHOI Research Librarian and staff now report through the Library Director to serve WHOI and its scientists. This appointment allows MBL and WHOI to work more closely in developing the Library with common goals.

As I write this report in the spring of 1992, the Joint MBL/WHOI Library Advisory Committee, chaired by Dr. David Shepro, has met monthly since late 1991. This increased advisory effort has resulted in formal recommendations on Library access control and reductions in scientific journal subscriptions as well as substantial advice on other policy issues. The committee is now discussing the role of the book collection and will recommend acquisition and circulation policies for it. A second discussion is addressing inter-institutional alternatives for Library growth.

In 1991, accounting changes resulting from an initiative by the Library provided one-time savings of over $130,000 to MBL. In addition, these changes made it possible for the Information Systems division to provide 14 work stations for research services and administrative offices.

Library operations

The Library was recently accepted as a member of the Boston Library Consortium. This membership—the first new one in twenty years—provides MBL and WHOI scientists loan privileges and restricted access without cost to the collections of Boston College, the Massachusetts Institute of Technology, Tufts, Brandeis, Boston University, Northeastern, Wellesley, the University of Massachusetts and the Boston Public Library. It also provides experimental on-line access to the Colorado Association of Research Libraries (CARL) database of 70,000 current journal contents. And it makes MBL and WHOI part of research activities such as the ARIEL document delivery project.

Seven new journal subscriptions were requested, approved, and entered this year.

A detailed assessment of the book collection has been completed, measuring the collection against standards set by professional societies in major subject areas. The journal exchange program was reviewed, and distribution was discontinued for 125 copies of *The Biological Bulletin* for which no exchange subscription is received.

Policies have been established defining legitimate patrons of the MBL/WHOI Library, what services they

receive, and what charges are levied. This is the first time a uniform policy covering both MBL and WHOI has been established in these areas. Establishing them included working with high school and public libraries on the Cape and with institutions, such as the University of Rhode Island, that make frequent use of the collection.

Inter-library loan activity has expanded by 20% this year as electronic reference sources develop a broader array of citations, as Woods Hole scientists broaden their activity to new areas, and as reductions in the journal collection reduce the availability of material. Providing copies of articles swiftly and economically as an alternative to local journal subscriptions will be a high Library priority in the coming year.

The library services contract with the National Marine Fisheries Service (NMFS) was completed, negotiated, and expanded. The Library now serves the NMFS locations at Oxford, Maryland, and Sandy Hook, New Jersey, as well as the local NMFS installation.

A small but steady effort to improve our archives included repackaging the reprint collection in acid free boxes, reclassifying and repackaging the MBL photograph collection, and reclassifying and re-housing the MBL collection of teaching charts. A generous donation made it possible to build a cabinet that allowed the charts to be stored flat in the rare book room.

A program was instituted to preserve biographical material of people associated with the Marine Biological Laboratory. This archive provides continuity across the generations of scientists and administrators who have been a part of MBL. Contributions of copies or original material are solicited. The collection will be housed in the rare book room.

Information Systems

The Information Systems division worked rapidly on library systems, data networking, education, and administrative tasks.

The Library's scientific information services will make it possible for scientists to identify and obtain needed information rapidly wherever they are at the moment. The Information Systems division took the first step in that effort by deploying literature search services over the national data network. This service, the first distributed CD-ROM facility that works across a variety of desktop platforms, is now in use around the world.

Publishing Woods Hole scientific data was a major objective of the 1989 Library plan. The Information Systems division began this effort by electronically publishing Dr. LeBaron Colt's New England algae data.

All MBL buildings were interconnected with fiber optic data cables, all classrooms were equipped with data network outlets, and over 150 research and administrative data network connections were completed. A standard electronic mail and bulletin board service, connected to the national data networks, was established and maintained.

A pilot card access system for Library doors was developed and installed in three locations. This system gives senior scientific staff access after hours to the Copy Service Center and the Computer Reference area.

The Information Systems division worked hard to respond to the recommendations of the research services committee. Paperless financial transactions were established for the Chemistry Room and the Copy Service Center. Computers were obtained and installed in the Photo Lab and in Purchasing. A word processing facility for staff and students was established in the outer room to the Fellows Shop.

Standard word processing, spreadsheets, electronic mail, and document transfer facilities for administrative offices were established. Over a dozen installations of this system were made in six offices and the office staff were trained and supported in its use.

Grants and gifts

Library activities have successfully attracted major support over the past year.

I am pleased to report that in the spring of 1992, the National Library of Medicine awarded the Library a $455,000 grant to support instruction in medical informatics. This effort, extending over 3 years, will bring 30 students a year to MBL for instruction and will support a full-time teaching laboratory in medical informatics.

MBL is part of the ARIEL project in document transfer. A high resolution document scanning machine, linked to Boston academic libraries, will be granted to MBL as part of that project. The participating libraries are committed to 48-hour response to document requests; this begins the effort to develop document transfer as a direction in MBL library services.

The Library is developing scientific visualization capability both as a service to the MBL community and as a tool in library service. A joint proposal has been made to NSF by MBL and WHOI to establish a Woods Hole visualization center. The Library Director is co-principal investigator on the project which will, if

awarded, establish general visualization facilities at MBL and WHOI as well as facilities in individual research laboratories.

As part of the visualization effort, the Library has worked with the Digital Equipment Corporation to provide a DECstation 5000/240 with visualization software to the MBL community. This system is housed in the computer reference area and is used for a spectrum of biological and ecological applications.

Substantial private donations have generously supported the Library. Over $13,000 in individual donations were made to the Library during the year. The Henry Stommel Memorial Fund has endowed the atlas collection. Cambridge Scientific Abstracts has committed to support high resolution photographs of the teaching chart collection.

The Library is grateful for this support, and for the generous and continuing support of the entire MBL and WHOI community.

—David L. Stonehill

Educational Programs

Summer Courses

Biology of Parasitism (June 16 to August 16)

Director

John C. Boothroyd, Stanford University

Faculty

Jean-Francois Dubremetz, INSERM, France
Heidi Elmendorf-Singer, Stanford University School of Medicine
Alan Fairlamb, London School of Hygiene & Tropical Medicine, UK
Fred Finkelman, Uniformed Services University of the Health Sciences
Stephen Hajduk, University of Alabama, Birmingham
Kasturi Haldar, Stanford University
Fred Heinzel, University of California, San Francisco
Richard Komuniecki, University of Toledo
Richard Locksley, University of California, San Francisco
Patricia Maroney, Case Western Reserve University
Tim Nilsen, Case Western Reserve University
Vicki Pollard, University of Alabama, Birmingham
Steven M. Singer, Stanford University
Joseph Urban, U. S. Department of Agriculture
Donald Wigston, Emory University School of Medicine

Lecturers

Norma Andrews, Yale University School of Medicine
Robert Barker, Harvard School of Public Health
Steven Beverley, Harvard Medical School
Barry Bloom, Albert Einstein College of Medicine
Marty Chalfie, Columbia University
John David, Harvard School of Public Health
Dickson Despommier, Columbia University School of Public Health
Paul T. Englund, The Johns Hopkins School of Medicine
Jean Feagin, Seattle Biomedical Research Center
Ray Fetterer, Animal Parasitology Institute, BARC-East
Bruce M. Greene, University of Alabama
Marcelo Jacobs-Lorena, Case Western Reserve University
Anthony James, University of California School of Biological Sciences
Patricia Johnson, UCLA School of Medicine
Lloyd H. Kasper, Dartmouth Medical School
Phil Loverde, SUNY
John Mansfield, University of Wisconsin
Jim McKerrow, University of California, San Francisco
Ira Mellman, Yale University School of Medicine
Steve Meshnick, CUNY Medical School
Isaura Meza, CINVESTAV, Mexico
Rick Nelson, San Francisco General Hospital
Debra Peattie, Vertex Pharmaceuticals, Inc.
Jeff Ravetch, Sloan Kettering Memorial Cancer Center
David Russell, Washington University School of Medicine
Alan Sher, NIAID/NIH
Ethan Shevach, NIAID/NIH
Andy Spielman, Harvard School of Public Health
Tony Stretton, University of Wisconsin
Chris Tschudi, MacArthur Center for Molecular Parasitology, Yale University
Mervyn J. Turner, Merck Sharp & Dohme Research Laboratories
Elesabetta Ullu, MacArthur Center for Molecular Parasitology, Yale University
Lex H. T. van der Ploeg, Columbia University
Alice Wang, University of California
C. C. Wang, University of California
Paul Webster, Yale University School of Medicine
Tom Wellems, NIAID/NIH

Students

Dwight D. Bowman, Cornell University
Iris Bruchhaus, Berhard Nocht Institut fur Tropenmedizin, Germany
Laurence U. Buxbaum, The Johns Hopkins School of Medicine
Hilary F. Cadman, University of Zimbabwe, Zimbabwe
Pedro Clavijo, NYU School of Medicine
Laurie A. Ellis, Cornell University
Martha Espinosa-Cantellano, Center for Research & Advanced Studies, IPN, Mexico
Kristin M. Hager, University of Alabama, Birmingham
Sandra L. Halonen, Louisiana State University
Thomas S. Ilg, Max Planck-Institut fur Biologie, Tubingen, Germany

Morgana T. Lima, Federal University, Rio de Janeiro, Brazil
Patrick Lorenz, Swiss Tropical Institute, Switzerland
John F. McNally, Dublin City University, Ireland
Ricardo Mondragon, CINVESTAV, Mexico
Rupert J. Quinnell, London School of Hygiene, Brazil
Lidya B. Sanchez, NYU Medical Center
Andreas G. Seyfang, University of Tubingen, Germany
Keith E. Wilson, Oregon Health Sciences University
Nancy Wisnewski, Colorado State University
Yun Zhang, CUNY Medical School

Embryology: Cell Differentiation and Gene Expression in Early Development

(June 28 to August 2)

Directors

Eric H. Davidson, California Institute of Technology
J. R. Whittaker, MBL (Associate Director)

Faculty

Marianne Bronner-Fraser, University of California, Irvine
R. Andrew Cameron, California Institute of Technology
James A. Coffman, California Institute of Technology
Robert Crowther, MBL
Scott Fraser, California Institute of Technology
Janet Heasman, The Wellcome Trust, UK
Linda Huffer, MBL
Wendy Katz, California Institute of Technology
David Kosman, University of California, San Diego
Min Ku, Harvard University
Thomas E. Lallier, University of California, Irvine
Michael Levine, University of California, San Diego
David McClay, Jr., Duke University
Steven McKnight, Carnegie Institution of Washington
Jeffrey Miller, Duke University
Jane Rigg, California Institute of Technology
George Serbedzija, University of California
Sergei Sokol, Harvard University
Paul Sternberg, California Institute of Technology
Tanya Whitfield, The Wellcome Trust, CRC Institute, UK
Christopher C. Wylie, The Wellcome Trust, CRC Institute, UK

Students

Olga A. Alexandrova, Academy of Sciences of the USSR
Massimiliano Andreazzoli, University of Pisa, Italy
Paris Ataliotis, Ludwig Institute for Cancer Research, UK
Barry N. Bates, Purdue University
Claudio Bertuccioli, The Rockefeller University
Heidi L. Browning, University of Indiana
Susan M. Burden, Case Western Reserve University
Elizabeth A. Butler, University of Southampton, UK
Aaron W. Crawford, University of Utah
Mary E. Dickinson, Columbia University
Helen J. Doyle, University of California, San Francisco
Michael K. Dunn, Massachusetts General Hospital
Michael C. Figdor, Institute of Histology & Embryology, Austria
Ann Greig, University of North Carolina, Chapel Hill
Danielle R. Hamill, University of Kansas
Jing Huang, Fred Hutchinson Cancer Research Center
Barbara Hug, University of Utah
Seresh Jesuthasan, University of Oxford, UK
Rulang Jiang, Wesleyan University
Michael G. Laidlaw, Brown University
Elena Levine, University of California, San Francisco
Barbara E. Maclay, Duke University
Maria I. Morasso, NICHD/NIH
Ralf Sommer, University of Munich, Germany
Robert J. Wilson, National Institute for Medical Research, UK

Marine Ecology: Concepts, Techniques and Applications of Molecular Probes

(June 16 to July 27)

Director

Kenneth H. Nealson, Center for Great Lakes Studies, University of Wisconsin-Milwaukee

Faculty

Simona Bartl, Hopkins Marine Station, Stanford University
Thomas Chen, Center of Marine Biotechnology, University of Maryland
Stephanie Clendennen, Hopkins Marine Station, Stanford University
Douglas Crawford, University of Chicago
Denise Garvin, University of Wisconsin-Milwaukee
Chun-Mean Lin, Center of Marine Biotechnology, University of Maryland
Molly Nealson, Center for Great Lakes Studies, University of Wisconsin-Milwaukee
Dennis Powers, Hopkins Marine Station, Stanford University
Ragat Rohatgi, Harvard College
Daad Saffarini, University of Wisconsin-Milwaukee
Michael Shamblott, University of Maryland
Barbara Wimpee, Center for Great Lakes Studies, University of Wisconsin-Milwaukee
Charles Wimpee, University of Wisconsin-Milwaukee
Bih-Ying Yang, University of Maryland, Center of Marine Biotechnology

Lecturers

Edward DeLong, Woods Hole Oceanographic Institution
Sandra Nierzwicki-Bauer, Rensaleer Polytechnic Institute
Simon Silver, University of Illinois-Chicago
David Peterson, NASA-Ames
Thomas Schmidt, Miami University
Ivan Valiela, Woods Hole Ecosystem Group
Thomas Hollocher, Brandeis University
Joseph Montoya, Harvard University
Donal Manahan, University of Southern California
Dennis Powers, Hopkins Marine Station, Stanford University
Daniel Morse, University of California, Santa Barbara
Stephen Macko, University of Virginia
Ann Giblin, Ecosystems Center, MBL
Robert Haselkorn, University of Chicago
Mitchell Sogin, MBL

Students

Delynne Barnhisel, Michigan Technological University
Brenda W. Bennison, Florida State University
Joan Bernhard, Wadsworth Center for Laboratories and Research, New York State Dept. of Health
Richard Blakemore, University of New Hampshire

Lori Buchholz, Center for Great Lakes Studies, University of Wisconsin-Milwaukee
Francisco Calderon, University of Puerto Rico
Douglas Campbell, University of Western Ontario, Canada
Amy Collins, Finnegan, Henderson, Farabow, Garrett & Dunner, Esq., P.C.
Julie Dutcher, Center for Marine Science Research
Phyllis Henderson, University of Nevada/Truckee Meadows Community College
Brenden Holland, Texas A & M University
Marie A. Juinio, University of Rhode Island
Paul Kemp, Brookhaven National Laboratory
Robert Ladner, Rutgers University
Daniel Miller, Cornell University
Kathy Ann Miller, University of Puget Sound
Aileen Morse, Marine Science Institute, University of California, Santa Barbara
Paul Rawson, University of South Carolina
Joseph Sanger, University of Pennsylvania School of Medicine
Patricia Schulte, Hopkins Marine Station, Stanford University
James W. Swanson, Scripps Institute of Oceanography, University of California, San Diego
Tara Toolan, Harvard University
Ivan E. Tosques, University of Washington
Kathryn Van Alstyne, Kenyon College

Microbial Diversity
(June 16 to August 1)

Co-Directors
John Breznak, Michigan State University
Martin Dworkin, University of Minnesota

Faculty
Joseph Calabrese, West Virginia University
Pamela Contag, Stanford University Medical School
Christiane Dahl, University of Bonn, Germany
S. Courtney Frasch, University of Minnesota
Daniel R. Smith, University of Minnesota
Hans Trüper, University of Bonn, Germany

Students
Yvonne R. Boldt, University of Minnesota
Jurgen Breitung, Philipps-Universitat, Germany
Adriane I. Budavari, Swarthmore College
Ron Caspi, Scripps Institute of Oceanography, University of California, San Diego
Karl Fent, Woods Hole Oceanographic Institution
Weibong Hsing, University of Massachusetts
Heike Jager, Universitat Osnabruck, Germany
Mark D. Johnson, University of Alabama
Gudrun E. Karsten, Ruhr-University of Bochun, Germany
Monika Kern, University of Bonn, Germany
Mark A. Larsen, University of Puget Sound
Rixin Li, Texas A & M University
Chuzbao Lin, University of Illinois
R. Mohanraju, CAS-in Marine Biology, India
Sergei A. Ostroumov, SUNY, Stony Brook
Thomas P. Pitta, University of Connecticut
Sylvia S. Schnell, Universitat Tubingen, Germany
Steven C. Slater, Case Western Reserve University
Paul G. Tratnyek, Swiss Federal Institute, Switzerland
Gunter A. Wallner, Technische Universitat Munchen, Germany

Neural Systems & Behavior
(June 9 to August 1)

Co-Directors
Ronald Calabrese, Emory University
Martha Constantine-Paton, Yale University

Faculty
Thomas Abrams, University of Pennsylvania
Alexander Borst, Max-Planck Institut fur Biologische Kybernetik, Germany
Hollis Cline, University of Iowa
Yang Dan, Columbia University
Robert Douglas, University of British Columbia, Canada
Lise Eliot, Columbia University
Cole Gilbert, University of Arizona
Jurgen Haag, Max-Planck Institut fur Biologische Kybernetik, Germany
Jon Hayashi, University of Arizona
Sally Hoskins, City College of New York
Valerie L. Kilman, NPA Beckman Institute
John Koester, Columbia University/New York State Psychiatric Institute
Lynn T. Landmesser, University of Connecticut
Richard B. Levine, University of Arizona
Stephen G. Lisberger, University of California
Ann Lohoff, Columbia University
Poh Kheng Loi, University of Oregon
Eduardo Macagno, Columbia University
Rodney K. Murphey, University of Massachusetts-Amherst
Michael Nusbaum, University of Alabama School of Medicine
Mu-Ming Poo, Columbia University
Glen Prusky, Yale University
David J. Sandstrom, University of Oregon
Michael Stephen, Brown University
Leslie Stevens, Max-Planck Institut fur Entwickslungs Biologie, Germany
Nathan Tublitz, University of Oregon
Edgar Walters, University of Texas Medical School
Janis Weeks, University of Oregon
Angela Wenning, Universitat Konstanz, Germany
Laura R. Wolszon, Columbia University

Students
Miriam A. Ashley, University of California, Irvine
Dane M. Chetkovich, Baylor College of Medicine
Thomas A. Cleland, University of California, San Diego
Melissa J. Coleman, University of Alabama, Birmingham
Heather Cook, University of Toronto, Canada
Stafan B. Eichmuller, Free Institute of Berlin, Germany
Louise M. Freeman, University of California, Berkeley
James A. Glazier, AT & T Laboratories
Ashok Hegde, Columbia University
Carolyn T. Hue, University of Maryland
Lidija I. Ivic, University of Belgrade, Yugoslavia
Rebecca M. Johnston, University of Colorado, Boulder
William C. Lemon, Indiana University
Darren B. Orbach, The Rockefeller University
Barak A. Pearlmutter, Yale University

Stephen C. Pratt, Cornell University
Laura L. Stark, Yale University
Graciela A. Unguez-Munoz, University of California, Los Angeles
Michelle D. Withers, University of Arizona
Emma R. Wood, University of British Columbia, Canada

Neurobiology (June 16 to August 17)

Director
Irwin Levitan, Brandeis University

Faculty
Cecilia Armstrong, University of Pennsylvania
Hana Asmussen, University of Virginia Medical School
Gary Banker, University of Virginia
Andrew Czernik, The Rockefeller University
Jan De Weer, Duke University
Keith Elmslie, Case Western Reserve University
Stuart Firestein, Yale University School of Medicine
Robert French, University of Calgary, Canada
Sarah Garber, University of Alabama, Birmingham
Richard Horn, Roche Institute for Molecular Biology
Stephen Jones, Case Western Reserve University
Bechara Kachar, NIDCD/NIH
Leonard Kaczmarek, Yale University School of Medicine
Richard Kramer, Columbia University
John Marshall, Yale University School of Medicine
Randall McKinnon, Laboratory of Viral & Molecular Pathogenesis, NIH
Angus Nairn, The Rockefeller University
Randall Reed, The Johns Hopkins Medical School
Thomas Reese, NINDS/NIH
Talvinder Sihra, University of Dundee, Scotland
Carolyn Smith, NINDS/NIH
Donald Wigston, Emory University School of Medicine

Lecturers
Bill Agnew, Yale University
George Augustine, University of Southern California
Pancho Bezanilla, University of California, Los Angeles
David Brautigan, Brown University
Pietro DeCamilli, Yale University
Gerald Fischbach, Harvard University
Lloyd Greene, NYU
James Huettner, Harvard University
Richard Huganir, The Johns Hopkins School of Medicine
Shahid Khan, University of Cincinnati
Christopher Miller, Brandeis University
Daniel Oprian, Brandeis University
Mu Ming Poo, Columbia University
Gary Rudnick, Yale University
Stephen J. Smith, Stanford University
Ron Vale, University of California, San Francisco

Students
Frank G. Boess, Cambridge University, UK
Debra A. Fadool, University of Florida
Elizabeth P. Garcia, University of Maryland
Kobei Hatta, University of Oregon
David M. Holtzman, University of California, San Francisco
Stefanie Kaech, Friedrich Miescher-Institut, Switzerland
Meredith A. Levine-Lazaroff, Tufts University
Thomas S. Otis, Stanford University Medical Center
Renee S. Redman, Northwestern University
Laura B. Rosen, Harvard Medical School
Donna L. Senger, University of Alberta, Canada
Dake Zheng, Duke University Medical Center

Physiology: Cellular & Molecular Biology (June 16 to July 27)

Director
Thomas D. Pollard, The Johns Hopkins University

Faculty
William Busa, The Johns Hopkins University
Antony Galione, Oxford University, UK
Robert Jensen, The Johns Hopkins School of Medicine
John Jordan, University of Utah
Jonathan McMenamin-Balano, NYU School of Medicine
Andrew Murray, University of California, San Francisco
Roy Parker, University of Arizona
Stephen F. Parsons, University of North Carolina, Chapel Hill
Edward D. Salmon, University of North Carolina, Chapel Hill
Cynthia V. Stauffacher, Purdue University
Murray Stewart, MRC, UK
Katherine Swenson, Harvard Medical School
Edwin Taylor, University of Chicago
Katherine Wilson, The Johns Hopkins University School of Medicine
Katherine Pollard, Pomona College
Laura Machesky, The Johns Hopkins Medical School

Students
Catherine M. Asleson, University of Minnesota
Carrie L. Baker, The Johns Hopkins University
Mark F. Barreuther, Wesleyan University
Susanne M. Bockholt, University of North Carolina, Chapel Hill
Andreas Bremer, University of Basel, Mueller Institute, Switzerland
Rodney A. Brundage, University of Pennsylvania
Stuart K. Calderwood, Dana Farber Cancer Institute
Cianna L. Cooper, Boston University
John D. Cooper, State University of New York, Buffalo
Jeffrey A. Cruz, The Johns Hopkins University
Siew C. Ho, Harvard University
Andreas Hoenger, Mueller Institute, University of Basel, Switzerland
Miguel Holmgren, Chicago Medical School
Timothy M. Jinks, Princeton University
Henry J. Kaminski, Cleveland Veterans Affairs Medical Center
Eugene J. Kim, University of Pennsylvania
Richard J. Kowalski, Vanderbilt University
Anthony R. Maranto, Tufts Medical School & St. Elizabeth's Hospital
Alexander D. McDougall, University College of London, UK
Maura McGrail, University of Minnesota
Robert L. Morris, Harvard University
Martin P. Murphy, University of Cambridge, UK
Rudolf Oldenbourg, MBL
Puneet Opal, Northwestern University
Mark A. Pirner, University of Minnesota
Penny L. Post, Carnegie Mellon University
Homero L. Rey, University of California, Berkeley
Evelyn D. Rider, Harbor-UCLA Medical Center

Brian K. Romias, University of California, Los Angeles
Susan A. Safley, Emory University
Karen J. Schnetzer, Georgia Institute of Technology
David R. Sherwood, Duke University
Elizabeth F. Smith, Emory University
Richard S. Sucgang, Columbia University
Julia D. Wulfkuhle, Purdue University
Hana Yaari, Memorial Sloan Kettering Cancer Center

Short Courses

Analytical and Quantitative Light Microscopy in Biology, Medicine and Materials Science (May 16 to 24)

Co-Directors
Edward D. Salmon, University of North Carolina, Chapel Hill
Greenfield Sluder, Worcester Foundation for Experimental Biology
David E. Wolf, Worcester Foundation for Experimental Biology

Faculty and Course Assistants
Brad Amos, Medical Research Council, UK
Paul Blank, Gerontology Research Institute
Steven M. Block, Rowland Institute for Science
Orit Braha, Worcester Foundation for Experimental Biology
Richard Cardullo, Worcester Foundation for Experimental Biology
Gordon Ellis, University of Pennsylvania
Harvey Florman, Worcester Foundation for Experimental Biology
Jeff Gelles, Brandeis University
Linda Huffer, MBL
Shinya Inoué, MBL
Andrew Maniotis, Worcester Foundation for Experimental Biology
Christine McKinnon, Worcester Foundation for Experimental Biology
Frederick Miller, Worcester Foundation for Experimental Biology
Anthony Moss, Worcester Foundation for Experimental Biology
Stephen Parsons, University of North Carolina, Chapel Hill
Kenneth R. Spring, NHLBI/NHI
Robert V. Skibbens, University of North Carolina

Students
Joseph N. Benoit, Louisiana State University Medical Center
Pierre N. Bouchelouche, Herlev University Hospital, Denmark
Richard W. Cole, New York State Department of Health
Kathleen Collins, Whitehead Institute
Judy A. Drazba, NINDS/NIH
Kenneth W. Dunn, Columbia University Medical Center
John F. Dunne, Syntex Research
Stefan B. Eichmuller, Free Institute of Berlin, Germany
Douglas L. Eng, VA Medical Center
Robert M. Ezzell, Massachusetts General Hospital
Christian C. Felder, NIMH/NIH
Jeffrey T. Finer, Stanford University Medical Center
Harvey M. Fishman, University of Texas Medical School
Peter T. Harris, NIH
Liana Harvath, FDA-Bethesda
Sherwin S. Lehrer, Boston Biomedical Research Institute
Robert O. Messing, San Francisco General Hospital
Gradimir N. Misevic, University Hospital of Basel, Switzerland
Thomas D. Parsons, Emory University School of Medicine
Istvan Renyi, NIDDK/MDB/NIH
Rodney A. Rhodes, Indiana University School of Medicine
Sally Schroeter, Emory University School of Medicine
Russell J. Stewart, Harvard University
Arno Villringr, University of Munich, Germany
Mark E. Warchol, University of Virginia School of Medicine

Cellular Neurobiology and Development of the Leech (August 4 to 24)

Director
David A. Weisblat, University of California

Faculty and Course Assistants
Pierre Drapeau, Montreal General Hospital, Canada
Shirley Bissen, University of Missouri, St. Louis
Shawn Lockery, The Salk Institute
Kenneth J. Muller, University of Miami School of Medicine
John G. Nicholls, University of Basel, Switzerland
Michael Stephen, Brown University

Lecturers and Instructors
Ronald L. Calabrese, Emory University
Stefano Catarsi, Montreal General Hospital, Canada
Richard Kostriken, University of California
William Kristan, University of California, San Diego
Eduardo Macagno, Columbia University
David Merz, Montreal General Hospital, Canada
Robert Monette, Montreal General Hospital, Canada
Marty Shankland, Harvard Medical School
Cathy Wedeen, University of California

Students
Henrich M. Dircksen, University of Bonn, Germany
Siegward M. Elsas, University of California
Francisco Fernandez de Miguel, University of Basel, Switzerland
Roberto Gonzalez-Plaza, Universidad de Chile
Anne E. Luebke, University of Miami School of Medicine
Diana M. Neely, University of Basel, Switzerland
Collette N. O'Reilly, Simon Fraser University, Canada
Benet J. Pardini, Veterans Affairs Medical Center
Thomas J. Radosevich, Iowa State University
Felipe A. Ramirez, University of California
Blair E. Robertson, Oxford University, UK
Victoria Y. S. Wong, Columbia University

History of Biology: Modern Evolutionary Biology (August 4 to 17)

Directors
Garland Allen, Washington University
John M. Beatty, University of Minnesota
Jane Maienschein, Arizona State University

Faculty
Jonathan Hodge, University of Leeds, UK
David L. Hull, Northwestern University
Robert J. Richards, University of Chicago
V. Betty Smocovitis, Stanford University

Lecturers
Mark B. Adams, University of Pennsylvania
Ernst Mayr, Museum of Comparative Zoology, Harvard University
William B. Provine, Cornell University
Frank Sulloway, Massachusetts Institute of Technology

Students
Elizabeth M. Baker, Belmont Abbey College
Gillian A. Barker, University of California, San Diego
Mary M. Bartley, Cornell University
Robert W. Brackenbury, University of Cincinnati Medical Center
Joyce F. Cadwallader, St. Mary-of-the-Woods College
Eunice A. Cronin, Belmont Abbey College
Ernest F. DuBrul, University of Toledo
Elihu M. Gerson, Tremont Research Institute
Chirstiane Groeben, Naples Zoological Station, Italy
Kiyoon Kim, University of Oklahoma
Carol B. Knox, Northfield Mount Hermon School
Eric D. Kupferberg, Massachusetts Institute of Technology
Frank T. Kuserk, Moravian College
Olivier Lagueux, University of Toronto, Canada
Anne L. Larsen, Princeton University
Sherrie L. Lyons, University of Chicago
Arthur B. Millman, University of Massachusetts, Boston
Anne L. Mylott, Indiana University
Lennart Olsson, Uppsala University, Sweden
Ronald J. Overmann, National Science Foundation
Patricia A. Ross, University of Maryland
David W. Rudge, University of Pittsburgh
Clark T. Sawin, Tufts University School of Medicine
John R. Shaver, Michigan State University
Matti T. Sintonen, University of Helsinki, Finland
Jan B. Sloan, University Press of Kansas
Susan B. Spath, University of California, Berkeley
Tracy L. Teslow, University of Chicago
Sara F. Tjossem, Cornell University
David B. Walton, University of Chicago
Nadine M. Weidman, Cornell University
William C. Wimsatt, University of Chicago
James J. Youngblom, California State University

Methods in Computational Neuroscience
(August 4 to 31)

Directors
James M. Bower, California Institute of Technology
Christof Koch, California Institute of Technology
Kenneth D. Miller, California Institute of Technology
(Associate Director)

Lecturers and Instructors
Paul Adams, SUNY, Stony Brook
Edward Adelson, Massachusetts Institute of Technology
Richard Anderson, Massachusetts Institute of Technology
Joseph Atick, School of Natural Sciences
David Beeman, California Institute of Technology
David Berkowicz, Yale University Medical School
Bill Bialek, NEC Research Institute
Avis H. Cohen, University of Maryland
Erik de Schutter, California Institute of Technology
Rodney James Douglas, Medical Research Council, UK
Nancy Kopell, Boston University
Rudolfo Llinas, NYU Medical Center
David MacKay, California Institute of Technology
Eve Marder, Brandeis University
Michael V. Mascagni, Supercomputing Research Center
Bartlett Mel, California Institute of Technology
John Rinzel, NIH
Sylvie Ryckebusch, California Institute of Technology
Terrence Sejnowski, The Salk Institute
Michael Speight, California Institute of Technology
Roger Traub, IBM, T. J. Watson Research Center
John Uhley, California Institute of Technology
David van Essen, California Institute of Technology
Matthew Wilson, University of Arizona
Anthony Zador, Yale University
David Zipser, University of California, Santa Barbara

Students
Jeremy J. Ahouse, Brandeis University
Loren I. Alving, Mayo Clinic
Allison E. Balogh, The Johns Hopkins University
Lawrence J. Cauller, Brown University
Allan D. Coop, John Curtin School of Medical Research, Australia
Virginia E. De Sa, University of Rochester
Jennifer M. Groh, University of Pennsylvania
Yoram Gutfreund, Hebrew University, Israel
Aurora L. Isaac, Emory University
Daryl R. Kipke, Syracuse University
Gwendolen C. Littlewort, Oxford University, UK
John C. Middlebrooks, University of Florida
Pratik Mukherjee, The Rockefeller University
Venkatesh N. Murthy, University of Washington
Steven J. Nowlan, The Salk Institute
Klaus N. Obermayer, University of Illinois, Urbana-Champaign
Anke A. Post, University of Maryland, College Park
William C. Rose, The Johns Hopkins Medical School
Nava Rubin, Hebrew University, Israel
Subbakrishna Shankar, Case Western Reserve University
Diana K. Smetters, Massachusetts Institute of Technology
Jeffrey P. Utz, Hahnemann University
James L. Winslow, University of Toronto, Canada

Computational Neuroscience Workshop
(August 25 to 31)

Director
Terrence J. Sejnowski, The Salk Institute

Participants
Edward Adelson, Massachusetts Institute of Technology
John Allman, California Institute of Technology
Richard Andersen, Massachusetts Institute of Technology
Dana Ballard, University of Rochester
James Bower, California Institute of Technology
Charles Bruce, Yale University School of Medicine
James Buchannan, Marquette University
Joel Davis, Office of Naval Research
Robert Desimone, NIMH
Rodney Douglas, Medical Research Council, UK
Eric Knudsen, Stanford Medical School
Christof Koch, California Institute of Technology
Jan Koenderink, University of Uterecht, The Netherlands
Bartlett Mel, California Institute of Technology
Kenneth Miller, California Institute of Technology

Alexander Pentland, Massachusetts Institute of Technology
Michael Stryker, University of California School of Medicine
Lucia Vaina, Boston University
David Van Essen, California Institute of Technology
Jun Zhang, University of California, Berkeley
Steven Zucker, McGill University, Canada

Microinjection Techniques in Cell Biology (May 26 to June 1)

Director
Robert B. Silver, Cornell University

Faculty
Heather A. Bartlett, Cornell University
Karen Kindle, Cornell University
Douglas Kline, Kent State University
Katherine Luby-Phelps, University of Texas
D. William Provance, Jr., University of Texas

Students
Hilmar Bading, Harvard Medical School
Kathy J. Cooke, University of Chicago
Marwan E. El-Sabban, Cornell University
Nelson W. Ellmore, NCI/NIH
Jon P. Jacobson, University of Washington
Inge M. Janka, GSF-Forschungszentrum, Germany
Karl H. Kalland, Dana Farber Cancer Institute
Andrew P. Laudano, University of New Hampshire
Huguette Loevtrup, University of Umea, Sweden
Robert L. Myers, Manitoba Institute of Cell Biology, Canada
Asma Nusrat, Brigham & Women's Hospital
David C. Schwartz, NYU
Neil R. Smalheiser, University of Chicago
John D. Wilkinson, The Wellcome Research Labs, UK

Molecular Evolution (August 18 to 30)

Director
Mitchell L. Sogin, MBL

Faculty
Giorgio Bernardi, Institut Jacques Monod, France
Claude Bibeau, MBL
Michael Clegg, University of California
Dan Davison, University of Houston
Rob Dorit, Harvard University
Joseph Felsenstein, University of Washington
Laura Landweber, Harvard University
Diana Lipscombe, George Washington University
David R. Maddison, Harvard University
Roger Milkman, University of Iowa
Gary Olsen, University of Illinois
Norman Pace, Indiana University
Margaret Riley, University of Massachusetts, Amherst
Monica Riley, MBL
David Shub, SUNY, Albany
David Swofford, Illinois Natural History Survey
Bruce Walsh, University of Arizona
Mark Wheelis, University of California, Davis

Students
Barbara A. Best, University of California, Berkeley
Gregory C. Booton, Ohio State University
Ellen B. Braun-Howland, Rensselaer Polytechnic Institute
John H. Caldwell, University of Colorado Health Sciences
Jonathan B. Clark, University of Arizona
David A. Coleman, University of Houston
Vladimir Corredor, NYU Medical Center
Robert S. Coyne, Oberlin College
Keith A. Crandall, Washington University
Claire G. Cupples, Concordia University, Canada
Marta D. de Jesus, University of California, Los Angeles
Jamie Deneris, University of California
Claude W. dePamphilis, Vanderbilt University
Dominique A. Didier, University of Massachusetts, Amherst
Dali Ding, California Institute of Technology
Luis E. Eguiarte, University of California
Rebecca J. Gast, Ohio State University
Jonathan B. Geller, Stanford University
Patrick M. Gillevet, Harvard University
Solveig Gretarsdottir, University of Lund, Sweden
Margo G. Haygood, Scripps Institute of Oceanography, University of California, San Diego
John E. Hill, NYU Medical Center
Gregory J. Hinkle, University of Massachusetts, Amherst
Jim L. Holloway, Oregon State University
Anthony R. Kerlavage, NIH
Dawne V. Kipp, Ohio State University
Lisa M. Kordos, University of Houston
Subha Kovilur, University of Washington
Christina Ledje, University of Lund, Sweden
Youn-Ho Lee, Scripps Institute of Oceanography, University of California, San Diego
Barbara L. Lundrigan, University of Michigan
Jean Mariaux, Smithsonian Institution
Ann E. Montegut-Felkner, Rutgers University
Edward R. Moore, National Research Center for Biotechnology, Germany
Joanna L. Mountain, Stanford University Medical Center
Spencer V. Muse, North Carolina State University
William C. Navidi, University of Southern California
Trang D. Nguyen, University of California
Sandra A. Nierswicki-Bauer, Rensselaer Polytechnic Institute
Magnus Nordborg, Stanford University
Naomi E. Pierce, Princeton University
Yannick Pouliot, Montreal Neurological Institute, Canada
Steven C. Rassler, University of Iowa
Daniel P. Romero, University of California, San Francisco
Carl Saxinger, NIH
Christoph W. Sensen, Botanisches Institut, Germany
Timothy T. Stedman, Virginia Commonwealth University
Linda D. Strausbaugh, University of Connecticut
James W. Swanson, Scripps Institute of Oceanography, University of California, San Diego
Maximilian J. Telford, Oxford University, UK
Jeffrey L. Thorne, University of Washington
Richard E. Trimer, Rutgers University
Priscilla K. Tucker, University of Michigan
Diana Valencia, University of Utah
Marc A. Van Ranst, Albert Einstein College of Medicine
James Versalovic, Baylor College of Medicine
Francis X. Villablanca, University of California, Berkeley
Alfried P. Vogler, Yale University
James K. Wetterer, Princeton University
David A. Wheeler, Baylor College of Medicine
Brian M. Wiegmann, University of Maryland

Optical Microscopy & Imaging in the Biomedical Sciences (October 18 to 24)

Co-Directors

Nina S. Allen, Wake Forest University
Colin S. Izzard, SUNY, Albany

Faculty and Course Associates

Steve Brooks, Wake Forest University
Joseph A. DePasquale, SUNY, Albany
Kenneth Dunn, Columbia University College of Physicians & Surgeons
Robert Hard, SUNY, Buffalo
Kenneth A. Jacobson, University of North Carolina
Nancy L. Jones, Bowman Gray School of Medicine, Wake Forest University
Greta M. Lee, University of North Carolina
Frederick R. Maxfield, Columbia University College of Physicians & Surgeons
Loretta M. Memmo, SUNY, Albany
John M. Murray, University of Pennsylvania
Kenneth Orndorff, Dartmouth College
Timothy A. Ryan, Stanford University School of Medicine
John Sedat, University of California, San Francisco
Kenneth R. Spring, NHLBI/NIH

Students

Nathan M. Appel, NIH
Alex S. Bender, University of Miami School of Medicine
Reed C. Carroll, Harvard University
Carolyn M. Connelly, Boston University School of Medicine
Manoel L. Costa, Instituto Oswaldo Cruz, Brazil
Robert E. Donohue, National Heart, Lung and Blood Institute
Matjaz Flezar, Montreal Chest Hospital Centre, Canada
Ruy G. Jeager, NIH
Brian E. Kahn, Naval Research Laboratory
Federico Kalinec, NIH
Eric Karplus, Princeton University
Gene D. LeSage, Scott and White Clinic
Kiyoshi Okada, SUNY, Albany
Fredrick M. Pavalko, Indiana University School of Medicine
William A. Rowe, The Johns Hopkins University School of Medicine
Adrienne K. Salm, West Virginia University
Melvyn S. Tockman, The Johns Hopkins University
Beth M. Weiner, Harvard University
Xin Wen, Kodak Research Laboratory
Nancy K. Wills, University of Texas Medical Branch
Miriam E. Zolan, Indiana University

Pathogenesis of Neuroimmunologic Diseases (August 18 to 30)

Co-Directors

J. Murdoch Ritchie, Yale University School of Medicine
Byron H. Waksman, Foundation for Microbiology

Faculty

Vahi E. Amassian, SUNY Health Science Center, Brooklyn
Garry G. W. Arnason, University of Chicago
Etty N. Benveniste, University of Alabama, Birmingham
Joel A. Black, Yale University
Ivan Bodis-Wollner, Mt. Sinai School of Medicine
Richard D. Broadwell, University of Maryland School of Medicine
I. Nicholas Crispe, Yale School of Medicine
Judah A. Denburg, McMaster Medical Center, Canada
Daniel B. Drachman, The Johns Hopkins School of Medicine
Andrew G. Engel, Mayo Clinic
Diane E. Griffin, The Johns Hopkins School of Medicine
David A. Hafler, Brigham & Women's Hospital of Harvard Medical School
Stephen L. Hauser, Massachusetts General Hospital
William F. Hickey, Washington University School of Medicine
Jeffery Kocsis, Yale University
Norman Latov, College of Physicians & Surgeons of Columbia University
Michael Leahy, Falmouth Hospital, Falmouth, MA
Carl M. Leventhal, NINDS/NIH
W. Ian Lipkin, University of California
Cathy G. McAllister, Presbyterian University Hospital
Dale E. McFarlin, NINDS/NIH
Jerome B. Posner, Memorial Sloan-Kettering Cancer Center
Donald L. Price, The Johns Hopkins Hospital
Richard W. Price, University of Minnesota Health Center
James W. Prichard, Yale University Medical School
Anthony T. Reder, University of Chicago
Stephen C. Reingold, National Multiple Sclerosis Society
Jack Rosenbluth, NYU Medical Center
Benjamin F. Roy, Georgetown University School of Medicine
Clifford B. Saper, University of Chicago
Randolph B. Schiffer, Strong Memorial Hospital
Bhagwan T. Shahani, Massachusetts General Hospital
Moon L. Shin, University of Maryland, Baltimore
Michael E. Shy, Thomas Jefferson University Hospital
Raymond A. Sobel, Massachusetts General Hospital
Michele Solimena, Yale University Medical School
J. Wayne Streilein, University of Miami School of Medicine
Howard L. Weiner, Brigham & Women's Hospital of Harvard Medical School
Jerry Wolinsky, University of Texas Health Science Center at Houston
Scott Zamvil, Brigham & Women's Hospital of Harvard Medical School

Students

Sudhir S. Batchu, University of Missouri, Columbia
Neil W. Bindemann, University College, London, UK
Carlo Chizzolini, FIDIA Research Laboratories, Italy
Stephen D. Collins, VA Medical Center
Koen Gerritse, TNO Medical Biological Laboratory, The Netherlands
Laura S. Hair, Columbia Presbyterian Hospital
Christine J. Harling-Berg, Brown University
Carolyn G. Hatalski, University of California, Irvine
Ian C. D. Johnston, University Cambridge, UK
Daniel L. Kaufman, University of California, Los Angeles
Beum S. Kim, Yoido St. Mary's Hospital, Korea
Kyriacos A. Kyriallis, Cyprus Institute of Neurology & Genetics, Cyprus
Keiko Nakagaki, North Carolina State University
Suzanna L. Reid, University of Kentucky
David C. Silverberg, Moncton, New Brunswick, Canada
Andrew M. Snyder, University of Connecticut Health Center
Thomas R. Swift, Medical College of Georgia
Marie Tani, University Hospitals of Cleveland
Karl Vass, University of Vienna, Austria
Kathryn R. Wagner, The Johns Hopkins Medical Institute
Youbin Wang, Massachusetts General Hospital
Rupert Whittaker, University of Michigan

Summer Research Programs

Principal Investigators

Adams, James A., Northeast Fisheries Center University of Maryland, Eastern Shore
Akeson, R., University of Cincinnati
Alkon, Daniel L., NINDS/NIH
Armstrong, Clay, University of Pennsylvania
Armstrong, Peter B., University of California, Davis
Arnold, John M., University of Hawaii
Augustine, George J., University of Southern California and Duke University Medical Center

Baker, Robert, NYU Medical Center
Barlow, Jr., Robert B., Syracuse University
Barry, Daniel, University of Michigan Medical Center
Barry, Susan, University of Michigan
Bearer, Elaine, University of California, San Francisco
Beauge, Luis, Instituto M. y M. Ferreyra, Argentina
Bennett, M. V. L., Albert Einstein College of Medicine
Bezanilla, Francisco, University of California, Los Angeles
Bezprozvanny, Ilya, University of Connecticut Health Center
Bingham, Eula, University of Cincinnati
Bloom, George S., The University of Texas Southwestern Medical Center, Dallas
Bodznick, David, Wesleyan University
Borgese, Thomas A., Lehman College, CUNY
Boron, Walter, Yale University School of Medicine
Boyer, Barbara C., Union College
Brady, Scott T., The University of Texas Southwestern Medical Center, Dallas
Brown, Joel, Washington University School of Medicine
Browne, Robert, Wake Forest University
Bryant, Shirley H., University of Cincinnati
Burdick, Carolyn J., Brooklyn College, CUNY
Burger, Max M., Friedrich Miescher Institut, Switzerland

Cariello, Lucio, Stazione Zoologica
Chaet, A. B., University of West Florida
Chang, Donald C., Baylor College of Medicine
Chappell, Richard L., Hunter College, CUNY
Charlton, Milton, University of Toronto, Canada
Clay, John, NIH
Cohen, Lawrence B., Yale University School of Medicine
Cohen, William D., Hunter College, CUNY
Cooperstein, Sherwin J., The University of Connecticut Health Center
Cui, Jiamin, SUNY, Stony Brook
Cuppoletti, John, University of Cincinnati College of Medicine

D'Alessio, Giuseppe, University of Naples, Italy
D'Avanzo, Charlene, Hampshire College
DeWeer, Paul, University of Pennsylvania
Dowling, John E., Harvard University
Dunlap, Kathleen, Tufts Medical School

Eckberg, William R., Howard University
Ehrlich, Barbara E., University of Connecticut Health Center

Fishman, Harvey M., The University of Texas Medical Branch, Galveston

Gadsby, David, The Rockefeller University
Gainer, Harold, NINDS/NIH
Garber, Sarah S., University of Alabama, Birmingham
Garrick, Rita Anne, New Jersey Medical School and Fordham University
Gesteland, Robert C., University of Cincinnati College of Medicine
Giuditta, Antonio, University of Naples, Italy
Goldman, Robert D., Northwestern University Medical School
Gould, Robert M., Institute for Basic Research in Developmental Disabilities
Groome, James R., Utah State University

Haimo, Leah, University of California, Riverside
Hernandez-Cruz, Arturo, Roche Institute of Molecular Biology
Hershko, Avram, Technion, Israel
Highstein, Steven M., Washington University School of Medicine
Holz IV, George G., Howard Hughes Medical Institution, Massachusetts General Hospital
Hoskin, Francis C. G., Illinois Institute of Technology
Hunt, James M., Northwestern University

Ip, Wallace, University of Cincinnati College of Medicine

Johnston, Daniel, Baylor College of Medicine
Josephson, Robert K., University of California, Irvine

Kaminer, Benjamin, Boston University School of Medicine
Kaneshiro, Edna, University of Cincinnati
Kaplan, Ehud, The Rockefeller University
Kaplan, Ilene M., University College
Khan, Sohaib, University of Cincinnati College of Medicine
Koide, Samuel S., Population Council
Kremer, James R., University of Southern California
Kuznetsov, Sergei, Moscow State University, USSR

Landowne, David, University of Miami
Langford, George, University of North Carolina, Chapel Hill
Laufer, Hans, University of Connecticut
Lee, Robert K., University of Colorado
Levin, Jack, University of California School of Medicine, San Francisco
Levine, Robert Paul, Washington University School of Medicine
Lipicky, Raymond J., U.S. Food & Drug Administration
Lisman, John, Brandeis University
Llinas, Rodolfo R., New York University Medical Center

Malchow, Robert Paul, University of Illinois College of Medicine
Metuzals, Janis, University of Ottawa, Canada
Mindel, David P., University of Cincinnati
Moorman, Stephen J., University of Michigan
Mooseker, Mark S., Yale University

Nasi, Enrico, Boston University School of Medicine
Nelson, Leonard, Medical College of Ohio
Noe, Bryan D., Emory University School of Medicine
Norgren, Robert, University of Cincinnati

Obaid, Ana Lia, University of Pennsylvania School of Medicine

Pant, Harish, NINDS/NIH
Parsons, Thomas D., Emory University School of Medicine
Parysek, Linda, University of Cincinnati Medical School
Peckol, Paulette, Smith College

Quigley, James P., SUNY, Stony Brook

Rafferty, Nancy S., Northwestern University
Rakowski, Robert F., University of Health Sciences, Chicago Medical School
Reese, Thomas S., NINDS/NIH
Rieder, Conly, Wadsworth Center for Laboratories and Research
Ripps, Harris, University of Illinois College of Medicine
Rivera, Domingo, Clark University and University of California, Berkeley
Rohr, Stephen, University of Pennsylvania School of Medicine
Rome, Lawrence, University of Pennsylvania
Ross, William, New York Medical College
Ruderman, Joan V., Harvard Medical School
Russell, John M., University of Texas Medical Branch

Saavedra, Raul A., Children's Hospital and Harvard Medical School
Salzberg, Brian M., University of Pennsylvania School of Medicine
Sanger, Jean M., University of Pennsylvania School of Medicine
Sanger, Joseph W., University of Pennsylvania School of Medicine
Schroeter, Sally, Emory University
Segal, Sheldon, The Rockefeller Foundation
Sheetz, Michael P., Duke University Medical Center
Shilling, Fraser M., University of Southern California
Shipley, Michael T., University of Cincinnati College of Medicine
Silver, Robert B., Cornell University, N.Y. State College of Veterinary Medicine
Siwicki, Kathleen King, Swarthmore College
Sloboda, Roger D., Darmouth College
Smith, David V., University of Cincinnati College of Medicine
Smith, Stephen J., Stanford University School of Medicine
Sperelakis, Nicholas, University of Cincinnati College of Medicine
Spruston, Nelson, Baylor College of Medicine
Steffen, Walter, University of Minnesota
Steinacker, A., Washington University School of Medicine
Stemmer, Andreas C., MRC Laboratory of Molecular Biology, UK
Suprenant, Kathy A., University of Kansas
Sweeney, H. Lee, University of Pennsylvania School of Medicine

Telzer, Bruce, Pomona College
Treistman, Steven N., Worcester Foundation for Experimental Biology
Trinkaus, John P., Yale University
Troll, Walter, NYU Medical Center
Tytell, Michael, Bowman Gray School of Medicine, Wake Forest University

Ueno, Hiroshi, The Rockefeller University

Vale, Ronald, University of California, San Francisco
Vallee, Richard, Worcester Foundation for Experimental Biology
Van Egeraat, Jan M., Living State Physics Group, Vanderbilt University

Wadsworth, Patricia, University of Massachusetts
Wang, Rui, University of Alberta, Canada
Weiss, Dieter, Technical University, Munich, Germany
Wessel, Gary M., Brown University
Wonderlin, William F., West Virginia University
Worden, Mary Kate, Harvard Medical School

Yoshioka, Tohru, Waseda University, Japan

Zhou, Z. Jimmy, University of California
Zigman, Seymour, University of Rochester School of Medicine & Dentistry
Zottoli, Steven J., Williams College
Zukin, R. Suzanne, Albert Einstein College of Medicine

Other Research Personnel

Alberghina, Mario, University of Catania, Italy
Altamirano, Anibal A., University of Texas Medical Branch
Araneda, Ricardo, Albert Einstein College of Medicine
Auerbach, Peter S., Swarthmore College

Bartlett, Heather, Cornell University
Bartley, Annette D., Hunter College
Bersoff, Rochelle, Washington University School of Medicine
Bittner, George, University of Texas, Austin
Blanchard, Charles, Bio-Rad
Bowden, John, Emory University
Brehm, Paul, SUNY, Stony Brook
Breitwieser, Gerda E., The Johns Hopkins University School of Medicine
Brouer, Jan, University of Cincinnati
Buchanan, JoAnn, Stanford University School of Medicine
Buchanan, Roger, NIH
Buelow, Neal, Syracuse University

Bullock, Theodore H., University of California, San Diego
Burkey, Adam, Williams College

Caldwell, Jeremy, Albert Einstein College of Medicine
Caputo, Carlos, IVIC, Venezuela
Cohen, Avrum, Yale University School of Medicine
Cohen, Darien, University of North Carolina, Chapel Hill
Cohen, Darien L., University of North Carolina, Chapel Hill
Cohen, Ted, Yale University
Collin, Carlos, NINDS/NIH
Connor, John, Swarthmore College
Correa, Ana M., University of California, Los Angeles
Couch, Ernest, Texas Christian University
Crispino, Marianna, University of Naples, Italy

Danace, Hadi, University of Connecticut
DeFazio, Richard A., University of Southern California
Deffenbaugh, Max, Princeton University
Dehnbostel, Denise, University of Michigan
Dessev, George, Northwestern University Medical School
DiPolo, Reinaldo, IVIC, Venezuela
Dodds, Alister W., University of Oxford
Door, Reinhard, Universitat of Ulm, Germany
Doroshenko, Peter, AA Bogomoletz Institute of Physiology, USSR

Falk, Chun, Yale University School of Medicine
Fay, Richard, Parmly Hearing Institute, Loyola University of Chicago
Friedman, Richard N., Living State Physics Group, Vanderbilt University
Fujiki, Hirota, National Cancer Center Research Institute, Japan

Gallant, Paul E., NINDS/NIH
Gibson III, Daniel G., Worcester Polytechnic Institute
Gilbert, Susan P., Pennsylvania State University
Gill-Kumar, Pritam, U.S. Food and Drug Administration
Giordano, Daniela, University of Rome, Italy
Goldman, Anne E., Northwestern University Medical School
Gomez, Maria, Boston University School of Medicine
Gomez-Laganas, Froylan, University of Pennsylvania
Grant, Philip, NINDS/NIH
Grassi, Daniel, U.S. Food and Drug Administration
Gruner, John A., NYU Medical Center

Hainfeld, Colleen, Brown University
Haneji, Tatsuji, Chiba University, Japan
Hayden, James, Bio-Rad
Heintzelman, Matthew B., Yale University
Hernandez, Michael R., University of Texas Medical Branch
Herzog, Erik, Syracuse University
Hilfiker, Sabine, Biozentrum Basel
Hill, Susan D., Michigan State University
Hogan, Emilia, Yale University School of Medicine
Holmgren, Miguel, University of Health Sciences, Chicago Medical School

Inoue, Hiroko, University of Tokyo, Japan
Ito, Etsuro, Waseda University, Japan

Jacobson, Jonathan M., Emory University
Jaffe, David, Baylor College of Medicine
Johnson, Michelle R., Howard University
Johnston, Jennifer, Dartmouth College
Jost, Christine, Harvard Medical School
Juneja, Renu, Population Council

Kelly, Mary, Syracuse University
Kipke, Daryl R., Syracuse University
Klein, Kathryn, Emory University School of Medicine
Knudsen, Knud D., U.S. Food and Drug Administration
Kowtha, Vijay, NINDS/NIH
Krause, Todd L., University of Texas, Austin
Kuhns, William, The Hospital for Sick Children
Kumar, Sanjay, University of Pennsylvania

Latorre, Ramon, Fac. Ciencias Universidad de Chile, Chile
Leighdigh, Christopher, Brown University
Leonard II, Edward E., University of Pittsburgh
Levy, Daniel, University of Pennsylvania
Lewis, Laura, Brandeis University
Liang, Zhi-quo, Population Council
Lin, Jen-Wei, NYU Medical Center
Liu, Dongjie, Institute for Basic Research
Ljubetic, Cecilia, Children's Hospital and Harvard Medical School
Locke, Rachel, Washington University School of Medicine
Loeffler, Cornelia, Technical University Munich, Germany
Lorenzoni, Patrizia, Friedrich Miescher Institut
Luca, Frank, Harvard Medical School

Malik, Fady, University of California, San Francisco
Malinowska, Danuta H., University of Cincinnati College of Medicine
Martin, Rainer, Universitat of Ulm, Germany
McNally, Francis J., University of California, San Francisco
McPhie, Donna, NINDS/NIH
Menichini, Enrico, University of Naples, Italy
Misevic, Gradimir N., University Hospital of Basel, Switzerland
Mitchison, Timothy, University of California
Miyakawa, Hiroyoshi, Yamagata University School of Medicine, Japan
Miyazawa, Atsuo, Waseda University, Japan
Moczydlowski, Edward, Yale University
Modean, Carrie Ann, University of Southern California
Montgomery, John D., University of Auckland, New Zealand
Morales, Lissette, Lehman College-City University of New York
Moreira, Jorge E., NINDS/NIH
Morrell, Candy M., University of Maryland Eastern Shore
Moshiach, Simon, NIH

Nelson, Heather, Bowdoin College
Niclas, Joshua, University of California, San Francisco

Olds, James, NINDS/NIH

Papaconstandinou, Eleni, University Hospital
Paxson, Cheryl L., University of Health Sciences, Chicago Medical School
Perozo, Eduardo, University of California, Los Angeles
Perrone-Capano, Carla, University of Naples, Italy
Plant, Charles P., Tufts Medical School
Powers, Maureen, Vanderbilt University

Rafferty, Keen A., University of Illinois
Rebhun, Lionel I., University of Virginia
Regehr, Wade, University of Pennsylvania
Rodriguez, Katrin, University of Illinois, Champaign-Urbana
Rose, Andrew, Washington University Medical School
Rosenkranz, Margalit, NYU Medical Center
Ross, Paul E., University of California, Irvine
Rusciano, Dario, Friedrich Miescher Institut

Sagar, Anjali, University of Health Sciences, Chicago Medical School
Sagi, Amir, Hebrew University, Israel

Sakakibara, Manabu, Toyohashi University of Technology, Japan
Sanchez, Ivelisse, Hunter College
Sanchez-Andres, Juan V., NINDS/NIH
Schreurs, Bernard, NIH
Sheetz, Jonathan, Bates College
Sheller, Rebecca, University of Texas
Shibuya, Ellen, Harvard Medical School
Sivaramakrishnan, Shobhana, University of Southern California
Sormani, Maria Pia, Italy
Spivack, Warren, Institute for Basic Research
Stokes, Darrell, Emory University
Stoyanovsky, Detcho, University of Connecticut Health Center
Sugimori, Mutsuyuki, NYU Medical Center
Sung, Yeng Je, New York State Institute for Basic Research
Sung, Ying Ju, New York Institute for Basic Research
Swank, Douglas, University of Pennsylvania
Sweet, Hyla C., Union College

Takagi, Hiroshi, Waseda University, Japan
Terada, Hirotoshi, Hamamatsu Photonics, K.K., Japan
Terasaki, Mark, NIH

Varela, Manuel F., University of New Mexico School of Medicine Cancer Center
Vargas, Fernando, U.S. Food and Drug Administration
Viswanath, Dilip B., NINDS/NIH

Wache, Susanne C., University of Connecticut
Walker, John E., Illinois Institute of Technology
Wheeler, Robert B., University Rochester School of Medicine & Dentistry
Wikswo, John B., Vanderbilt University
Williams, Donna, National Marine Fisheries Service and University of Maryland Eastern Shore
Wooden, Jason M., University of Washington
Wu, Jian-young, Yale University School of Medicine

Yang, Zhaohui, University of Pennsylvania

Zakevicius, Jane, University of Illinois College of Medicine
Zecevic, Dejan, Institute for Biological Research, Yugoslavia
Zhong, Nan, Institute for Basic Research in Developmental Disabilities
Zigman, Bunnie R., University of Rochester School of Medicine

Library Readers: General

Baccetti, Baccio M., Institute of General Biology, Italy
Baur, Susan, North Falmouth, Massachusetts

Carriere, Rita, SUNY Health Center, Brooklyn
Child, Frank M., Trinity College
Chinard, Francis, New Jersey Medical School
Cobb, Jewel P., California State University
Cohen, Leonard A., American Health Foundation
Collin, Pete, Coastside Group
Conner, Carol Scott-, University of Mississippi
Conner, Harold F., The Johns Hopkins University

Duncan, Thomas, Nichols College

Edds, Louise Luckenbill, Ohio University
Eisen, Herman N., Massachusetts Institute of Technology
Epstein, Herman T., Brandeis University

Farmanfarmaian, A., Rutgers University
Frenkel, Krystyna, NYU Medical Center
Friedler, Gladys, Boston University School of Medicine
Friend, Daniel S., University of California, San Francisco

Gabriel, Mordecai L., Brooklyn College
German, James L., The New York Blood Center
Gilbert, Daniel L., NIH
Goldstein, Moise H., The Johns Hopkins University
Goodman, Dewitt S., Columbia University
Guttenplan, Joseph, NYU Dental Center

Hill, Richard W., Michigan State University
Humphreys, Tom, Kewalo Marine Laboratory

Ilan, Joseph, Case Western Reserve University

Judith, Ilan, Case Western Reserve University
Jothy, Serge, McGill University

Kaltenbach, Jane C., Mount Holyoke College
Klemow, Kenneth M., Wilkes University

Laderman, Aimlee D., Yale University
Lee, John J., City College of CUNY
Levitz, Mortimer, NYU School of Medicine
Luster, Peter R., New Canaan, CT

Marine Research, Falmouth, Massachusetts
May, Ronald, Concord Chemists, New York, NY
Mooseker, Mark S., Yale University

Nicaise, Hernandez-, University of Nice, France

Ohki, Shinpei, SUNY, Buffalo
Olins, Ada, University of Tennessee, Oak Ridge
Olins, Donald, University of Tennessee, Oak Ridge

Pierson, Beverly K., University of Puget Sound
Pleasure, David, Childrens Hospital of Philadelphia
Pleasure, Jeanette, Childrens Hospital of Philadelphia
Prosser, C. Ladd, University of Illinois
Prusch, Robert T., Gonzaga University

Rakieten, Nathan, SUNY
Rasmussen, Howard, Yale School of Medicine
Robinson, Denis, MBL
Rose, Birgit, University of Miami School of Medicine
Roth, Lorraine, Woods Hole, MA
Rounds, Donna J., Yale University
Russell-Hunter, W. D., Syracuse University
Ruttner, Zoltan, National Institute of Alcohol Abuse

Schippers, Jay M., New York, New York
Shapley, Robert, NYU
Shepro, David, Boston University
Shriftman, Mollie Starr, North Nassau Mental Health Center
Speigel, Evelyn, Dartmouth College
Spotte, Stephen, University of Connecticut
Stephenson, William K., Earlham College
Stracher, Alfred, SUNY, Health Science Center
Sweet, Frederick, Washington University School of Medicine
Szent-Gyorgyi, Andrew, Brandeis University
Szulman, Aron E., MaGee Womens' Hospital

Trager, William, The Rockefeller University

Wangh, Lawrence J., Brandeis University
Warren, Leonard, Wistar Institute
Weir, Gary, Naval Historical Center
Wilbur, Charles G., Colorado State University
Wittenberg, Jonathan B., Albert Einstein College of Medicine
Worgul, Basil V., Columbia University

Young, Lily Y., NYU Medical Center
Young, Wise, NYU Medical Center

Zaragoza, Salvador R., UNAM, Mexico

Library Readers: Desks

Aizawa, Kenneth, Central Michigan University
Allen, Garland E., Washington University
Anderson, Everett, Harvard Medical School
Avioli, Louis V., Washington University

Boyer, John F., Union College

Candelas, Graciela C., University of Puerto Rico
Clark, Arnold M., Woods Hole, MA
Cohen, Seymour S., MBL
Collier, Marjorie M., Saint Peters' College
Copeland, D. Eugene, MBL
Costa, Joseph E., Buzzards Bay Project

Gross, Paul R., University of Virginia
Grossman, Albert, NYU Medical Center

Herskovits, Theodore, Fordham University

Inoue, Sadayuki, McGill University

Katz, George M., Merck Sharp & Dohme Research Laboratories
King, Kenneth, Children's Hospital
Krane, Stephen, Harvard Medical School
Kravitz, Edward A., Harvard Medical School

Leighton, Joseph, Peralta Cancer Research Institute
Levy, Robert Galatzer, University of Chicago
Lorand, Laszlo, Northwestern University

Marshall, Bryan, University of Pennsylvania
Mauzerall, David, The Rockefeller University
Metuzalls, Janis, University of Ottowa
Mizell, Merle, Tulane University

Nagel, Ronald L., Albert Einstein College of Medicine
Narahashi, Toshio, Northwestern University Medical School
Nickerson, Peter A., SUNY, Buffalo

Pappas, George D., University of Illinois
Person, Philip, Research Testing Lab
Pierce, Sidney K., University of Maryland

Rickles, Frederick R., University of Connecticut Health Center
Roth, Jay S., Woods Hole, MA

Schweitzer, A. Nicola, Imperial College of Science, London
Shephard, Frank C., East Falmouth, MA
Sonnenblick, Benjamin P., Rutgers University
Spector, Abraham, Columbia University
Spiegel, Melvin, Dartmouth College
Sundquist, Eric, U.S. Geological Survey
Sydlik, Mary Ann, Western Michigan University

Tilney, Lewis, University of Pennsylvania
Tweedel, Kenyon S., University of Notre Dame

Van Holde, Kensal E., Oregon State University

Webb, Marguerite H., Woods Hole, MA
Wittenberg, Beatrice A., Albert Einstein College of Medicine

Library Readers: Rooms

Churchill, Frederick B., Indiana University
Cohen, Stanley N., Stanford University School of Medicine
Filley, Woody, Filley & Co., Inc., Bedminster, NJ
Hines, Michael, Duke University Medical Center
Malbon, Craig C., SUNY, Stony Brook
Moore, John W., Duke University Medical Center
Rabinowitz, Michael, Harvard Medical School
Reynolds, George T., Princeton University
Stuart, Ann E., University of North Carolina
Tykocinski, Mark L., Case Western Reserve University
Weidner, Earl, Louisiana State University
Weissman, Gerald, NYU Medical Center
Zweig, Ronald, Ecologic, North Falmouth, MA

Domestic Institutions Represented

A T & T Laboratories
Alabama, University of, at Birmingham
Albert Einstein College of Medicine
American Bionetics, Inc.
American Psychological Association
Ames Laboratory
Analytical Luminescence Laboratory
Applied Biosystems
Arizona Research Laboratory
Arizona, University of
Arizona, University of, School of Medicine
Atlantex & Zieler Instrument Corporation
Axon Instruments, Inc.

Bates College
Baruch College of City University of New York
Baylor College of Medicine
Beckman Instruments, Inc.
Becton Dickinson IS
Belmont Abbey College
Bethesda Research Labs
Bio-Rad Laboratories, Microscience Division
Bodega Marine Station
Boston Biomedical Research Institute
Boston University
Boston University School of Medicine
Bowling Green State University
Brandeis University
Brigham & Women's Hospital
Brinkmann Instruments, Inc.
Brookhaven National Laboratory

Brooklyn College of City University of New York
Brown University
Bryn Mawr College
Bunton Instrument Co[illegible]nc.

California Institu[illegible]nology
California State [illegible]sity
California, University of, Berkeley
California, University of, Davis
California, University of, Irvine
California, University of, Los Angeles
California, University of, Riverside
California, University of, San Diego
California, University of, San Francisco
California, University of, Santa Barbara
California, University of, Santa Cruz
Cambridge Instruments
Cambridge Technology
Case Western Reserve University
Case Western Reserve University School of Medicine
Carnegie Institute of Washington
Carnegie-Mellon University
Case Western Reserve University
Center for Great Lakes Studies
Center for Marine Science Research
Center for Neurobiology and Behavior
Chicago Medical School
Chicago, University of
Children's Hospital and Harvard Medical School
Ciba Corning Diagnostics Corp.
Cincinnati, University of
City College of New York
City University of New York
City University of New York, Lehman College
City University of New York Medical School
Clark University
Cleveland Veterans Affairs Medical College
Colgate University
Colorado College
Colorado State University
Colorado, University of, Boulder
Colorado, University of, Health Sciences
Columbia University
Columbia University College of Physicians and Surgeons
Connecticut, University of
Connecticut, University of, Health Center
Cornell University
Cornell University, N.Y. State College of Veterinary Medicine
Costar Corporation
Coy Laboratory Products
Crimson Camera Technical Sales

Dage MTI, Inc.
Dana-Farber Cancer Institute
Dartmouth College
Dawson Company
Delaware, University of
Diamond General Corporation
Digital Equipment Corporation
Donsanto Corporation
Duke University
Duke University
Duke University Medical School

E. I. duPont de Nemours & Co., (Inc.)
East Tennessee State University
Eastman Kodak Company
E.G. & G., Inc.
Emory University
Emory University School of Medicine
Eppendorf, Inc.
Ericomp, Inc.

FDA-Bethesda
Falmouth Hospital
Finnegan, Henderson, Farabow Law Firm
Fisher Scientific
Florida State University
Florida, University of
Flow Laboratories
Fotodyne, Inc.

General Scanning, Inc.
General Valve Corporation
George Washington University
Georgetown University Medical School
Georgia Institute of Technology
Georgia, University of
Gerontonlogy Research Institute
GIBCO/BRL Life Technologies, Inc.
Gilson Medical Electronics, Inc.
Gonzaga University
Grass Instrument Company

Hamamatsu Photonics Systems
HHMI, Johns Hopkins Medical School
HHMI, Massachusetts General Hospital
Hacker Instruments, Inc.
Frederick Haer & Company
Hahnemann Medical College
Hahnemann University
Hampshire College
Harbor-University of California Los Angeles Medical Center
Harvard Medical School
Harvard University
Hawaii, University of
Health Sciences, University of
Health Sciences, University of,/Chicago Medical School
Hoefer Scientific
Holy Cross College
Honeywell Corporation
Hopkins Marine Station
Hospital for Sick Children
Houston, University of
Howard Hughes Medical Institute
Howard University
Hutchinson Cancer Research Center
Hunter College
Hunter College and City University of New York Graduate Center

IBI - A Kodak Co.
I.B.M.-T.J. Watson Research Center
ICN Radiochemicals
Illinois Natural History Survey
Illinois State University
Illinois, University of
Illinois, University of, Urbana-Champaign
Indec Systems Corporation
Inovision Corporation
Indiana University
Indiana University School of Medicine
Institute for Basic Research
Institute for Basic Research in Developmental Disabilities
International Biotechnologies, Inc.
Iowa State University
Iowa, University of
Institute for Basic Research in Developmental Disabilities
Institute of Neuroscience
ISCO, Inc.

JEOL
Johns Hopkins Hospital, The
Johns Hopkins Medical Institute, The
Johns Hopkins Medical School, The
Johns Hopkins School of Medicine, The
Johns Hopkins University, The
Johns Hopkins University School of Medicine, The
Jouan, Inc.

Kansas, University of
Kent State University
Kentucky, University of
Kentucky, University of, Medical School
Kinetic Systems
Kipp & Zonen
Kodak Research Laboratory
David Kopf Instruments
Kramer Scientific Corporation

Lab Line Instruments, Inc.
Lab Systems
Laser Science
Lehman College of City University of New York
Leica, Inc.
Lindberg Enterprises
Living State Physics Group, Vanderbilt University
Los Alamos National Laboratories
Louisiana State University
Louisiana State University Medical Center
Loyola University
Ludlum Measurements, Inc.

Marine Biological Laboratory (MBL)
Marine Biomedical Institute, Galveston
Marquette University
Maryland, University of
Maryland, University of, Baltimore
Maryland, University of, Center of Marine Biotechnology

Maryland, University of, Eastern Shore
Maryland, University of, School of Medicine
Massachusetts General Hospital
Massachusetts Institute of Technology
Massachusetts, University of
Massachusetts, University of, Amherst
Massachusetts, University of, Boston
Massachusetts, University of, Medical Center
Massachusetts, University of, Medical School
Mayo Clinic
Medical College of Georgia
Medical College of Ohio
Medical Systems Corporation
Meiji Techno America
Memorial Sloan Kettering Cancer Center
Merck & Company
Merck, Sharp & Dohme Research Laboratory, New Jersey
Miami, University of
Miami, University of, School of Medicine
Michigan State University
Michigan State University, Center for Microbial Ecology
Michigan Technological University
Michigan, University of
Michigan, University of, Ann Arbor
Millipore Corporation
Minnesota, University of
Missouri-Columbia, University of
MJ Research
Molecular Dynamics
Molecular Probes
Moravian College
Mount Holyoke College
Mt. Sinai School of Medicine
Murray State University

NEC Research Institute
NIH/NIDDK/MDB
National Heart, Lung and Blood Institute
National Institutes of Health
National Institutes of Health/NCI
National Institutes of Health/NHLBI
National Institutes of Health/NICHD
National Institutes of Health/NINDS
National Institutes of Health/NIEHS
National Institutes of Health/NIDDK
National Institutes of Mental Health/NIH
National Jewish Center for Immunology & Respiratory Medicine
National Marine Fisheries Service/University Maryland Eastern Shore
National Multiple Sclerosis Society
National Science Foundation
Naval Medical Research Institute
Naval Research Laboratory
Neslab Instruments, Inc.
Neuro Data Instrument Corporation
New Brunswick Scientific Company, Inc.
New England Medical Center
New Hampshire, University of
New Jersey Medical School
New Jersey Medical School and Fordham University
New Mexico, University of, School of Medicine Cancer Center
New York Medical College
New York State Department of Health
New York State Institute for Basic Research
New York University
New York University Medical Center
New York University School of Medicine
Newport Corporation
Nikon Corp.
Nikon, Inc.
Noran Instruments
North Carolina State University
North Carolina, University of, Chapel Hill
North Dakota University
Northfield Mount Hermon School
Northwestern University
Northwestern University Medical School

Oberlin College
Office of Naval Research
Ohio State College
Ohio State University
Oklahoma, University of
Olympus Corporation
Oregon Health Sciences University
Oregon State University
Oregon, University of
Oregon, University of, Institute of Neuroscience
Owl Scientific

Panasonic Communications and Systems Company
Parmly Hearing Institute, Loyola University of Chicago
Pennsylvania State University
Pennsylvania, University of
Pennsylvania, University of, School of Medicine
Perceptics Corporation
Perkin-Elmer Corporation
Pharmacia, Inc.
Pharmacia LKB Nuclear, Inc.
Photometrics, Ltd.
Photonic Microscopy, Inc.
Photon Technology International
Pittsburgh, University of
Pittsburgh, University of, Medical School
Polaroid Corporation
Pomona College
Ponce School of Medicine
Population Council
Population Council-CBR, The
Portland State University
Presbyterian University Hospital
Princeton University
Puget Sound, University of
Princeton University

Radiomatic Instruments & Chemical Company, Inc.
Reed College
RMC
Roche Institute of Molecular Biology
Rochester, University of
Rochester, University of, School of Medicine
Rochester, University of, School of Medicine & Dentistry
Rockefeller University, The
Rockefeller University, Howard Hughes Medical Institute
Rowland Institute for Science
Rutgers University

Salk Institute
San Francisco General Hospital
San Francisco State University
Sarastro, Inc.
Savant Instruments, Inc.
Scientific Systems
Scott and White Clinic
Scripps Clinic and Research Foundation
Scripps Institute of Oceanography
Sequoia Turner
Shimadzu Scientific Instruments, Inc.
Silicon Graphics, Inc.
Smithsonian Institution
Sony Medical Electronics
South Carolina, University of
Southern California, University of
St. Mary-of-the-Woods College
Stanford University
Stanford University Medical Center
State University of New York
State University of New York, Albany
State University of New York, Buffalo
State University of New York Health Science Center, Brooklyn
State University of New York, Purchase
State University of New York, Stony Brook
State University of New York, Syracuse
Stratagene
Strong Memorial Hospital
Supercomputing Research Center, Applications Research
Sutter Instrument Company
Swarthmore College
Swift Instruments, Inc.
Syntex Research
Syracuse University

Technical Manufacturing Corporation
Technical Products International, Inc.
Technical Video, Ltd.
Temple University
Texas A & M University
Texas Christian University
Texas Tech. University
Texas, University of, Austin
Texas, University of, Health Science Center, Houston
Texas, University of, Medical Branch
Texas, University of, Medical Branch-Galveston
Texas, University of, Medical School
Thomas Jefferson University Hospital
Tremont Research Institute

Tufts University
Tufts University School of Medicine
Tufts University School of Veterinary Medicine
Tulane University
Turner Designs

Union College
United States Department of Agriculture
United States Food & Drug Administration
Universal Imaging Corporation
University Hospitals of Cleveland
University Press of Kansas
U. S. Biochemical Corporation
Utah, University of

Vanderbilt University
Vassar College
Vaytek, Inc.
Veterans Affairs Medical Center
Video Scope International, Ltd.
Virginia Commonwealth University
Virginia, University of
Virginia, University of, School of Medicine
Vital Images

Wake Forest University
Wake Forest University/Bowman Gray Medical School
Warner Instrument Corporation
Washington, University of
Washington University Medical School
Washington, University of, St. Louis
Washington University School of Medicine
Waters Chromatography Division
Wesleyan University
West Florida, University of
West Virginia University
Wheaton College
Whitehead Institute
Wild Leitz USA, Inc.
Williams College
Wisconsin, University of
Woods Hole Oceanographic Institution
Worcester Foundation for Experimental Biology
Worcester Polytechnic Institute

Xybion Corporation

Yale University
Yale University School of Medicine

Carl Zeiss, Inc.

Foreign Institutions Represented

AA Bogomoletz Institute of Physiology, USSR
Academy of Sciences, Institute of Cytology, USSR
Alberta, University of, Canada
Auckland, University of, New Zealand

Basel, University of, Switzerland
Belgrade, University of, Yugoslavia
Bernhard Nocht Institut fur Tropenmedizin, Germany
Bergen, University of, Norway
Bielefeld, University of, Germany
Biozentrum, Basel, Switzerland
Bonn, University of, Germany
Botanisches Institut, Germany
British Columbia, University of, Canada
British Museum of Natural History, United Kingdom

Calgary, University of, Canada
Cambridge, University of, United Kingdom
CAS in Marine Biology-Portonovo, India
Catania, University of, Italy
Center for Research & Advanced Studies-IPN, Mexico
Chiba University, Japan
Chiba University School of Medicine, Japan
Chile, University of, C.E.C.S., Chile
Chile, Universidad de, Chile
CINEVESTAV-IPN, Mexico City, Mexico
Cologne, University of, Germany
Concordia University, Canada
Curtin, John, School of Medical Research, Australia
Cyprus Institute of Neurology & Genetics, Cyprus

Dalhousie University, Canada
Dalhousie University Medical School, Canada
Dublin City University, Ireland
Fac. de Ciencias Universidad de Chile, Chile
Federal University of Pernambuco, Brazil
Federal University, Rio de Janeiro, Brazil
FIDIA Research Laboratories, Italy
Freie Universitat, Berlin, Germany
Friedrich Miescher Institut, Switzerland

Goettingen, University of, Germany
GSF-Forschungszentrum, Germany

Hamamatsu Photonics, KK, Japan
Hebrew University, Israel
Helsinki, University of, Finland
Herlev University Hospital, Denmark

Imperial College of Science & Technology, United Kingdom
Institute for Biological Research, Yugoslavia
Institute of Histology & Embryology, Austria
Instituto M.y.M. Ferreyra, Argentina
Instituto Oswaldo Cruz, Brazil
I.V.I.C., Venezuela

Katholieke Universiteit-Leuven, Belgium
Kobe University, Japan
Koln, University of, Germany
Konstanz, University of, Germany

Life Sciences Institute, Israel
London School of Hygiene & Tropical Medicine, United Kingdom
London School of Hygiene, Brazil
London, University of, Egham, United Kingdom
Ludwig Institute for Cancer Research, United Kingdom
Lund, University of, Sweden

Max-Planck-Institut-fur-Biophysikalische Chemie, Nikolausberg, Germany
Max Planck-Institut fur Biologie, Germany
Max Planck-Institut fur Biologische Kybernetick, Germany
Max Planck-Institut fur Entwicklungsbiologie, Germany
Manitoba Institute of Cell Biology, Canada
McGill University, Canada
Medical Research Council, United Kingdom
Medical Research Council, Laboratory of Molecular Biology, United Kingdom
Milan, University of, Italy
Montreal Chest Hospital Centre, Canada
Montreal Neurological Institute, Canada
Montreal, University of, Canada
Moscow State University, USSR
Mueller Institute, University of Basel, Switzerland
Munich, University of, Germany

Naples, University of, Italy
Naples Zoological Station, Italy
Nottingham, University of, England, United Kingdom
National Institute for Medical Research, United Kingdom
National Research Center for Biotechnology, Germany

Osnabruch, University of, Germany
Ottawa, University of, Canada
Oxford University, United Kingdom

Philipps-Universitat, Germany
Philipps-Universitat, Marburg, Germany
Pisa, University of, Italy

Queens College, United Kingdom
Queens University, Canada
Queensland, University of, Australia

Ruhr-University of Bochun, Germany

St. Andrews University, Scotland
Seoul National University, Korea

Sienna, University of, Italy
Simon Bolivar, University of, Venezuela
Simon Fraser University, Canada
Southampton, University of, United Kingdom
State University of Utrecht, The Netherlands
Stazione Zoologica, Italy
Stockholm, University of, Sweden
Swiss Federal Institute, Switzerland
Swiss Federal Institute of Technology, Switzerland

Technische Universitat, Munchen, Germany
Tokyo, University of, Japan
Toronto, University of, Canada
Tubingen, University of, Germany
TNO Medical Biological Laboratory, The Netherlands

Umea, University of, Sweden
Ulm, University of, Germany
University College, London, United Kingdom
Universita di Palermo, Italy
University Hospital of Basel, Switzerland
Uppsala University, Sweden
Utrecht, University of, The Netherlands

Vienna, University of, Austria
Vrije Universiteit Brussels, Belgium

Waseda University, Japan
Wellcome Research Laboratories, United Kingdom
Western Ontario, University of, Canada
Wolfson College, United Kingdom

Yamagata University School of Medicine, Japan
Yoido St. Mary's Hospital, Korea

Zimbabwe, University of, Zimbabwe
Z.L.F. Kantonsspital, Basel, Switzerland

Year-Round Research Programs

Boston University Marine Program

Faculty

Atema, Jelle (Professor of Biology, Program Director)
Humes, Arthur G. (Professor of Biology Emeritus)
Tamm, Sidney L. (Professor of Biology)
Valiela, Ivan (Professor of Biology)

Staff

Hahn, Dorothy (Senior Administrative Secretary)
Kean, Kristen (Program Assistant)
Schillizzi, Cynthia (Program Manager)

Visiting faculty and investigators

D'Avanzo, Charlene (Hampshire College)
Gunderson, Robert (Vanderbilt University)
Herlands, Louis (New England Aquarium)
Hinga, Kenneth (University of Rhode Island)
Horridge, Adrian (Australia National University, Canberra)
Huber, Robert (Harvard Medical School)
Kaufman, Les (Edgerton Research Lab, New England Aquarium)
Kremer, James (University of Southern California)
Lavalli, Kari (Northeastern University Marine Station)
Peckol, Paulette (Smith College)
Raiswell, Robert (University of Leeds, UK)
Rhoads, Donald (Boston University)
Rietsma, Carol (SUNY, New Paltz)
Sardet, Christian (Villefranche-sur-Mer, France)
Seeler, Jacob (University of Texas Southwestern Medical Center)
Simmons, William ([illegible] versity)
Tranter, Martyn (University of Southampton, UK)
Wainright, Sam (University of Southern California)
Webb, Jacqueline (New York State College of Veterinary Medicine, Cornell)

Research staff

Dudley, Judy (Visiting Research Assistant)
Foreman, Kenneth (Research Associate)
Karnofsky, Elisa (Research Assistant)
Tamm, Signhild (Senior Research Associate)
Voigt, Rainer (Research Associate)

Teaching assistants

Alber, Merryl (Course Assistant)
Beck, John (Course Assistant)
Bushman, Paul (Course Assistant)
Bryden, Cynthia (Course Assistant)
Cowan, Diane (Course Assistant)
Farley, Lynda (Course Assistant)
Gomez, George (Course Assistant)
Hersh, Douglas (Course Assistant)
Karavanich, Christy (Course Coordinator)

Graduate students

Alber, Merryl
Bohachevsky, Boris
Bryden, Cynthia
Bushman, Paul
Cowan, Diane
Elskus, Adria
Farley, Lynda
Gomez, George
Hersh, Douglas
Karavanich, Christy
Katz, Andrea
LaMontagne, Michael
Lavalli, Kari
Lowe, Brian
Mazel, Charles
Mosiach, Simon
Portnoy, John
Tamse, Armando
Usup, Gires
White, David

Undergraduate students Fall 1991

Barak, Jeri (San Jose State)
Borg, Tracey

Borges, Christopher
Brayer, Kathryn
Burtner, Jason
Bussey, Kimberly
Callahan, Sean (Lawrence University)
Chapman, Christine
Coyne, David
Davila, Diego
Economakis, Alistair
Flick, Kevin
Fox, Pamela
Frantzman, Julia
Fricke, Julia
Geer, Thomas
Gettel, Gretchen
Gibson, Rachel
Gibbs, Leslie (Trinity University)
Gooss, Kevin
Hall, Brian
Herr, Barbara
Himmerick, Sarah
Hsieh, Penny
Johnson, Jacqueline
Jones, Deborah (Kent State)
Kane, Elizabeth (Boston College)
Kantor, Shanyn
Kasirsky, Jessica
Krolick, Amy Jo
Laffler, Karen
Linde, Emily
Maier, Michele
Mativi, Karen
Ndow, Sallimatta
Oliff, Daniel
Pimental, Helena
Pinzon, Ronald
Quigley, Wendolyn
Ritenburg, Katherine (University of Rochester)
Rogers, Francine
Sauer, Keith
Seman, Eileen
Sheinke, Sara
Sher, Talia (University of Rochester)
Singer, Joshua
Steenburg, Eric
Streelman, Todd (Bucknell)
Sweitzer, Julie
Tatham, Holl
Washurn, Ericka
Wiens, Louise
Williamson, Sarah

Summer undergraduate interns

Baden, Sara
Cherry, Bryan (Michigan State University)
Christman, Laurie (Boston University)
Collins, Beth
Collins, Glynnis
Deiner, Michael (Louisiana State University)
Du, Jun (UMass Dartmouth)
Gettel, Gretchen (Boston University)
Harris, Matthew (Boston University)
Kinkade, Christopher (Boston University)
Klotz, Darrell (Bucknell)
Kriger, Andrew
O'Brien, Maille (University of Massachusetts, Dartmouth)
Reischauer, Alyssa (University of Southern California)
Waggett, Caryl (Brown)
Wells, Victoria
White, Klane
Ziemba, Robert (Boston University)

Laboratory of Jelle Atema

Organisms use chemical signals as their main channel of information about the environment. These signals are transported in the marine environment by turbulent currents, viscous flow, and molecular diffusion. Receptor cells extract signals through various filtering processes. Currently, the lobster with its exquisite sense of taste and smell, is our major model to study the signal filtering capabilities of the whole animal and its narrowly tuned receptor cells. Research focuses on amino acids (food signals) and pheromones (courtship and dominance) neurophysiology of receptor cells, behavior guided or modulated by chemical signals, and computational models of odor plumes and neural filters.

Laboratory of Arthur G. Humes

Research interests include systematics, development, host specificity, and geographical distribution of copepods associated with marine invertebrates. Current research is on taxonomic studies of copepods from invertebrates in the tropical Indo-Pacific area, and poecilostomatoid and siphonostomatoid copepods from deep-sea hydrothermal vents and cold seeps.

Laboratory of Sidney Tamm

Research interests include cell physiology and motility, cytoskeleton, ciliary and flagellar motion, and trophic ecology of gelatinous zooplankton. Current research is on neural and ionic control of ciliary feeding and escape behaviors of marine invertebrates, distribution of calcium channels and calcium sensors in ctenophore cilia, geotactic mechanisms and sensory receptors in ctenophores, jellies with jaws (macrociliary teeth and actin bundles in *Beröe*), and rotary motors and fluid membranes in symbiotic protozoa.

Laboratory of Ivan Valiela

Our major research activity involves the Waquoit Bay Land Margin Ecosystems Research Project. This work examines how human activity in coastal watersheds (including landscape use and urbanization) increases nutrient loading to groundwater and streams. Nutrients in groundwater are transported to the sea, and, after biogeochemical transformation, enter coastal waters. There, increased nutrients bring about a series of changes. The Waquoit Bay LMER is designed to help us to understand and model the coupling of land use and consequences to receiving waters, and to study the processes involved.

A second long-term research topic is the structure and function of salt marsh ecosystems, including the processes of predation, herbivory, decomposition, and nutrient cycles.

The Ecosystems Center

The Center was established in 1975 to promote research and education in ecosystems ecology. Twelve senior scientific staff and 43

research assistants and support [illegible] the terrestrial and aquatic ecology of a wide variety of [illegible] ranging from Brazil (carbon cycling and trace gas emi[illegible]opical forests and pastures) to the Alaskan Arctic [illegible]s of the response of tundra, lake and stream biota [illegible] Harvard Forest (long-term studies of the effects of [illegible]orest ecosystems) to Massachusetts Bay (rates of denitri[illegible]y projects, such as those dealing with sulfur transformations in lakes and nitrogen cycling in the forest floor, investigate the movements of nutrients and make use of the Center's mass spectrometry laboratory (directed by Brian Fry) to measure the stable isotopes of carbon, nitrogen, and sulfur. The research results are applied wherever possible to questions of the successful management of the natural resources of the earth. In addition, the ecological expertise of the staff is made available to public affairs groups and government agencies who deal with such problems in acid rain, ground water contamination, and possible carbon dioxide-caused climate change.

Staff and consultants

Hobbie, John E., Co-Director
Melillo, Jerry M., Co-Director
Bahr, Michele
Banta, Gary
Bauman, Carolyn
Bowles, Francis
Bowles, Margaret
Chapman, Jonathan
Deegan, Linda
Donovan, Suzanne
Dornblaser, Mark
Downs, Martha
Drummey, Todd
Fahnski, Stephen
Fry, Brian
Garritt, Robert
Geyer, Heidi
Giblin, Anne
Griffin, Elisabeth
Helfrich, John
Hopkinson, Charles
Hullar, Meredith
Jesse, Martha
Jones, David
Kicklighter, David
Kling, George
Kracko, Karen
Laundre, James
Michmerhuizen, Catherine
Miliefsky, Michelle
Moller, Bernard
Nadelhoffer, Knute
Newkirk, Kathleen
Padien, Daniel J.
Pallant, Julie
Parmentier, Nancy
Peterson, Bruce
Rastetter, Edward
Regan, Kathleen
Ricca, Andrea
Schwamb, Carol
Schwarzman, Elisabeth
Shaver, Gaius
Steudler, Paul
Tholke, Kristin
Tucker, Jane

Postdoctorals

Castro, Mark
McKane, Robert
Neill, Christopher
Peterjohn, William
Wainright, Sam

Visiting scholars

McGuire, A. David, U.S.D.A. Forest Service
Normann, Bosse, University of Umeå, Sweden

Laboratory for Marine Animal Health

The laboratory provides diagnostic, consultative research, and educational services to the institutions and scientists of the Woods Hole community concerned with marine animal health. Diseases of wild, captive, and cultured animals are investigated.

Staff

Abt, Donald A., Director and The Robert R. Marshak Term Professor of Aquatic Animal Medicine and Pathology, School of Veterinary Medicine, University of Pennsylvania
Bullis, Robert A., Research Assistant Professor of Microbiology, University of Pennsylvania
Lawrence, Wade B., Research Assistant Professor of Pathology, University of Pennsylvania
Leibovitz, Louis, Director Emeritus
McCafferty, Michelle, Histology Technician, University of Pennsylvania
Moniz, Priscilla C., Secretary
Smolowitz, Roxanna M., Research Associate in Pathology, University of Pennsylvania
Wadman, Elizabeth A., Microbiology Technician, University of Pennsylvania

Laboratory of Aquatic Biomedicine

This laboratory investigates leukemias of soft shell clams. Monoclonal antibodies developed by this laboratory and techniques in molecular biology are used to investigate the differences between normal and leukemic cells and their ontogeny. The impact of pollutants on leukemogenesis is currently being studied with an emphasis on regional superfund sites.

Staff

Reinisch, Carol L., Investigator, MBL, and Chairperson Department of Comparative Medicine, Tufts University School of Veterinary Medicine

Ecosystems Center Research Assistant Carolyn Bauman and MBL Science Writing Fellow David Baron set up a fish wier at Toolik Lake, Alaska, field site.

Miosky, Donna, Laboratory Technician
White, Marja, Postdoctoral Fellow

Laboratory of Cell Biochemistry

This laboratory studies developmental, metabolic, and environmental influences on the genetic regulation of cellular enzymes. Current emphasis is on the gene products involved in hepatic heme biosynthesis and utilization in marine fish. These processes are responsive to hormonal and nutritional signals as well as to environmental pollutants and carcinogens. This work is being conducted with fish liver *in vivo*, with primary cultures of normal hepatocytes, and with cultured hepatoma cells isolated from a fish tumor. Gene activity is quantitated with cDNA probes, and the relevant genes are being cloned in bacteria to define better the actions of chemical inducers. Other research is concerned with translocation of proteins between various subcellular compartments both in fish hepatocytes and in invertebrate eggs before and after fertilization.

Staff

Cornell, Neal W., Senior Scientist
Bruning, Grace, Research Assistant

Visiting scientist

Fox, T. O., Harvard Medical Center

Laboratory of Developmental Genetics

This research group studies the early gene control of cellular differentiation pathways (cell lineage determination) in the embryos of tunicates and other marine invertebrate species.

Staff

Whittaker, J. Richard, Senior Scientist
Crowther, Robert, Research Associate
Loescher, Jane L., Research Assistant
Meedel, Thomas H., Assistant Scientist

Visiting investigators

Collier, J. R., Brooklyn College
Lee, James J., Columbia University, College of Physicians & Surgeons

Laboratory of Judith P. Grassle

Studies on the population genetics and ecology of marine invertebrates living in disturbed environments, especially of sibling species in the genus Capitella (Polychaeta).

Staff

Grassle, Judith P., Senior Scientist
Feinsilber, Sigalit, Research Assistant
Mills, Susan W., Research Assistant

Laboratory of Haryln O. Halvorson

Over the past year, we have isolated a large number of sporeformers from various marine environments like deep sea cores and sediments. Our intention is to characterize these bacteria at the molecular level, with emphasis on genes associated with sporulation and germination. Protocols based on DNA fingerprinting and quantitative hybridizations have been developed to differentiate these bacteria from one another, as well from terrestrial sporeformers. The hybridization data has shown that the bacterial isolates are not closely related to one another.

Numerical taxonomic methods are also being used to cluster the various isolates. The physiologically interesting sporeformers will also be characterized by physical mapping using rare-cutting restriction endonucleases.

Staff

Halvorson, Harlyn O., Principal Investigator
Chikarmane, Hemant, Assistant Scientist
Glick, Beatriz, Research Assistant
VanLooy, Lori, Research Assistant

Visiting investigators

Anderson, Porter, University of Rochester
Keynan, Alex, Hebrew University, Jerusalem, Israel
Kornberg, Hans, Christ's College, Cambridge, UK
Vincent, Walter, University of Delaware
Yashphe, Jacob, Hebrew University, Jerusalem, Israel

Laboratory of Shinya Inoué

Study of the molecular mechanism and control of mitosis, cell division, cell motility, and cell morphogenesis, with emphasis on biophysical studies made directly on single living cells, especially developing eggs in marine invertebrates. Development of biophysical instrumentation and methodology, such as polarization optical and video microscopy and digital image processing techniques, and exploration of their underlying theory are an integral part of the laboratory's effort.

Staff

Inoué, Shinya, Distinguished Scientist
Knudson, Robert, Instrument Development Engineer
Oldenbourg, Rudolf, Assistant Scientist
Stukey, Jetly, Research Assistant
Woodward, Bertha M., Laboratory Manager

Visiting investigator

Stemmer, Andreas, University of Basel, Switzerland

Laboratory of Alan M. Kuzirian

The research explores the functional morphology and ultrastructure of various organ systems in opisthobranch mollusks. The program includes mariculture of the nudibranch, Hermissenda crassicornis, with emphasis on developing reliable culture methods for rearing and maintaining the animal as a research resource. Studies include optimization of adult and larval nutrition, control of facultative pathogens and disease, and development of morphologic criteria for staging larvae and juveniles. These morphologic studies stress the ontogeny of neural and sensory structures. Concurrent with these studies is the development of a new technique to obtain and reconstruct serial block face images (SBFI) of epoxy embedded tissue actually sectioned inside an SEM by an in situ miniature ultramicrotome. Additional collaborative research includes histochemical investigations on strontium's role in initiating calcification in molluscan embryos (shell and statoliths), as well as immunocytochemical labelling of cell-surface and secretory product antigens of neurosecretory neurons in the eye of Aplysia.

Staff

Kuzirian, Alan M., Assistant Scientist
Tamse, Catherine T., Research Assistant

Visiting investigator

Leighton, Stephen, Biomedical Engineering & Instrumentation Branch, National Center for Research Resources, NIH

Laboratory of Molecular Evolution

The major research effort of this laboratory is the structure analysis of ribosomal RNA. Similarities between small subunit ribosomal RNA sequences are used to infer the evolutionary history of eukaryotic microorganisms and to design molecular probes for studies in marine ecology.

Staff

Sogin, Mitchell L., Director
Bhattacharya, Debashish, Postdoctoral Fellow
Bibeau, Claude, Research Assistant
Gunderson, John, Research Associate
Hinkle, Greg, Postdoctoral Fellow
Leipe, Detlev, Postdoctoral Fellow
Stickel, Shawn, Research Assistant
Wainwright, Patricia, Postdoctoral Fellow

Laboratory of Neuroendocrinology

This laboratory studies the molecular and cellular bases of two neural programs that regulate different important behaviors in the model mollusk Aplysia. Research is conducted on the mechanisms of the neuronal circadian oscillators located in the eyes. These circadian oscillators drive the circadian activity rhythm of the animal, which is concerned with the daily timing of food gathering and of prolonged rest. Additional research is conducted on a group of neuroendocrine cells that produce a peptide, "egg-laying hormone," that initiates egg laying and associated behaviors. The laboratory is interested in how the three-dimensional shape of this peptide hormone allows a highly specific interaction with its receptor and the intracellular processes that are triggered by it. In another project, the laboratory has discovered and is continuing research on a novel second messenger enzyme, an NADase, in the oocytes of Aplysia, that generates cyclic ADPR, a Ca^{2+}-mobilizing product.

Staff

Strumwasser, Felix, Director
Cox, Rachel L., Senior Research Assistant
Glick, David, Senior Postdoctoral Fellow
Hellmich, Mark, Postdoctoral Fellow
Lewis, Karen, Laboratory Assistant
Rainville, Carol, Research Assistant
Vogel, Jackie, Research Assistant

Laboratory of Robert E. Palazzo

This laboratory studies the biochemical regulation of cellular events during meiosis and mitosis. An integral part of the research effort is the design of reconstitution systems that faithfully execute cell cycle dependent events under defined conditions. Current cell biological, immunochemical, biochemical, and microscopic methodologies are employed. Using marine eggs as a material source, assays have been developed that allow the study of germinal vesicle breakdown (GVBD), aster formation, and reactivation of isolated mitotic apparatus *in vitro*. Current focus of the laboratory is on the identification of cell cycle dependent regulatory events with major emphasis on protein phosphorylation and other post-translational modifications. The ultimate goal is the identification of key enzymes and target substrates that are involved in the regulation of cell division and are highly conserved during evolution.

Staff

Palazzo, Robert E., Assistant Scientist
Ferreira, Adriana, Postdoctoral Associate
Gong, Lei, Research Assistant
Hellmich, Helen, Postdoctoral Associate
Vogel, Jacalyn, Research Assistant

Visiting investigators

Browne, Carol, Wake Forest University
Eckberg, William R., Howard University
Rieder, Conly, Wadsworth Center

Laboratory of Monica Riley

Research in this laboratory focuses on the molecular evolution and gene expression in the bacterium Escherichia coli. In a collaborative effort, a database containing information on the intermediary metabolism and biochemical pathways of E. coli is being developed. When completed, this database is expected to contain information on each metabolic reaction, the enzyme, the reactants, products, cofactors, activators, inhibitors, kinetics, equilibrium constants, binding constants, etc.

Related research is on the evolution of the E. coli DNA and organization of the genes in the chromosome. Comparative nucleotide and amino acid sequence data provide information on the evolutionary relationships of E. coli genes to homologous genes in related bacteria.

Laboratory of Sensory Physiology

Since 1973, the laboratory has conducted research on various aspects of vision. Current studies focus on photoreceptor cells, on their light-absorbing pigments, and on their biochemical reactions initiated by light stimulation. Microspectrophotometric and biochemical techniques are used to study the receptors of both vertebrates (amphibia, fish, and mammals) and invertebrates (horseshoe crab and squid).

Staff

Harosi, Ferenc, Director, Associate Scientist, MBL, and Boston University School of Medicine
Szuts, Ete, Associate Scientist, MBL, and Boston University School of Medicine

Visiting investigators

Evans, Barbara I., University of Oregon, Eugene
Kleinschmidt, Jochen, NYU Medical Center
Singarajah, Kandar, V., Federal University of Paraiba, Brazil

Laboratory of Osamu Shimomura

Biochemical studies of the various types of bioluminescent systems. Preparation of the improved forms of aequorin for measuring intracellular free calcium.

Staff

Shimomura, Osamu, Senior Scientist, MBL, and Boston University School of Medicine
Shimomura, Akemi, Research Assistant

Visiting investigator

Nakamura, Hideshi, Harvard University

Laboratory of Raquel Sussman

We investigate the molecular mechanism of DNA damage-inducible functions in E. coli. Present studies deal with novel genes that affect radiation-induced mutagenesis and analysis of RecA functions.

Staff

Sussman, Raquel, Associate Scientist
Dudley, Karen, Research Assistant
Chikarmane, Hemant, Postdoctoral Research Associate

National Vibrating Probe Facility

We are exploring the roles of ionic currents, gradients, and waves in controlling development. We focus on controls of pattern and controls by calcium ions.

Staff

Jaffe, Lionel, Senior Scientist and Facility Director
Kuhtreiber, Willem, Physiologist
McLaughlin, Jane, Research Assistant
Miller, Andrew, Assistant Scientist
Sanger, Richard, Senior Electronics Technician
Shipley, Alan, Research Associate
Smith, Peter J. S., Research Associate

Visiting investigators

Alexander, Stephen, Wadsworth Center, Albany
Arnold, John, University of Hawaii
Bearer, Elaine, Brown University
Bi, Yu, Zhejiang University, China
Browne, Carole, Wake Forest College
Buonano, Mark, Massachusetts Institute of Technology
Cullander, Christopher, University of California, San Francisco
Felle, Hubert, Botanical Institute, Giessen, Germany
Fishman, Harvey, University of Texas, Medical Branch, Galveston
Fluck, Richard, Franklin & Marshall
Hill, Susan, Michigan State University
Hoch, Harvey, Cornell University
Isaacs, Hugh, Brookhaven National Laboratories
Keith, David, Yale University
Kinnamon, Sue, Colorado State University
Koshian, Leon, Cornell University
Krause, Todd, University of Texas, Medical Branch, Galveston
Leech, Colin, Cambridge University
Lucas, William, University of California, Davis
Ryan, Peter, Cornell University
Sardet, Christian, Station Zoologique, Villefranche-sur-mer, France
Schiefelbein, John, University of Michigan
Shapiro, James, University of Chicago
Smith, Peter, Cambridge University, UK
van Egeraat, Jan, Vanderbilt University
Wang, Rui, University of Alberta
Woodruff, Richard, West Chester State, Pennsylvania

Other Year-Round Investigators and Staff

Stephens, Raymond E., Principal Investigator
Szent-Gyorgyi, Gwen, Research Assistant
Tilney, Lewis G., University of Pennsylvania
Tilney, Molly S., University of Pennsylvania

Honors

Friday E[illegible], Lectures

Mimi Koe[illegible]rsity of California, Berkeley, 28 June "*Biomec[illegible] of Morphogenesis: Developing Notochords*"
Howard Berg, Harvard University, 5 July "*Some of My Best Friends are Bacteria*"
Leon Rosenberg, Yale University School of Medicine, 12 July "*Constructing a National Agenda for Biomedical Research*"
Theodore Holmes Bullock, University of California, San Diego, 18, 19 July (Forbes Lectures) "*What's Better About More Complex Brains*" (18 July) "*The Morphology of Activity in Complex Brains*" (19 July)
Thomas Eisner, Cornell University, 26 July "*Molecular Basis of Mate Assessment: The Insect's Way*"
Ronald Calabrese, Emory University, 2 August (Lang Lecture) "*Messenger Molecules in the Brain*"
Ursula Goodenough, Washington University of Saint Louis, 9 August "*Flagellar Surface Motility and Sexual Signalling in* Chlamydomonas"
Sir Hans Kornberg, University of Cambridge, 16 August (Monsanto Lecture) "*How Sugars Enter the Cell: What is True for* E. coli *Is Also Largely True for* E. lephants"
Lionel Jaffe, Marine Biological Laboratory, 23 August "*Calcium Oscillations, Waves and Gradients*"
Jane Lubchenco, Oregon State University, 30 August "*Ecological Challenges: Biodiversity and Global Change*"

Fellowships

Robert Day Allen Fellowship

Sergei A. Kuznetsov, Moscow State University, USSR

Frederik B. Bang Fellowship Fund

Fraser Shilling, University of Southern California, Los Angeles
Gary M. Wessel, Brown University

Frank A. Brown Memorial Readership

Kenneth Aizawa, Central Michigan University

Jean & Katsuma Dan Fellowship

Tatsuma Mohri, Tokyo Institute of Technology, Japan

Bernard Davis Fellowship

Raul Saavedra, Ch[illegible]'s Hospital and Harvard Medical School

M. G[illegible] Fuortes Fellowship

Arturo Hernandez-Cruz, Un[illegible]d de la Republica, Uruguay

Doreen Grace Fund Fellowship

Robert Paul Malchow, University of Illinois College of Medicine
Stephen J. Moorman, University of Michigan
William F. Wonderlin, West Virginia University

William Randolph Hearst Fellowship

Michael Figdor, Institute of Histology & Embryology, Austria
Danielle Hamill, University of Kansas

Stephen W. Kuffler Fellowship

Sara S. Garber, University of Alabama, Birmingham

Frank R. Lillie Fellowship

Frank Boess, Cambridge University, UK
Heidi Browning, University of Indiana
Stefanie Kaech, Friedrich Miescher-Institut, Switzerland
Kathy Ann Miller, University of Puget Sound
Aileen Morse, University of California, Santa Barbara
Donna Senger, University of Alberta, Canada
Robert Wilson, National Institute for Medical Research, UK

Jacques Loeb Fellowship

Paris Ataliotis, Ludwig Institute for Cancer Research, UK

Nikon, Inc. Fellowship

Ronald D. Vale, University of California, San Francisco

Nikon International Fellowship

Stephen J. Smith, Stanford University School of Medicine

Herbert W. Rand Fellowship

Sara S. Garber, University of Alabama, Birmingham
Arturo Hernandez-Cruz, Universidad de la Republica, Uruguay
Avram Hershko, Technion-Faculty of Medicine, Israel
Sergei A. Kuznetsov, Moscow State University, USSR
Robert Paul Malchow, University of Illinois College of Medicine
Mary Kate Worden, Harvard Medical School

Science Writing Fellowships

Sandra Ackerman, Freelance
Pamela Adkins, Merck & Co.
David Baron, WBUR-FM, Boston, MA
Sandra Blakeslee, Freelance
David Bulloch, Freelance
Doron Dagani, *Chemical & Engineering News*
Blake Edgar, *Pacific Discovery*
Nancy Ehrlich, *Scientific American Medicine*
Lew Frederick, KGW-TV, Portland, OR
Rebecca Kolberg, United Press International
Susan Laughlin, Chedd-Angier Production Co.
David Schwartz, Freelance

H. Burr Steinbach Memorial Fellowship

Kathleen King Siwicki, Swarthmore College

Steps Toward Independence—MBL Summer Fellowship

Arturo Hernandez-Cruz, Universidad de la Republica, Uruguay
Stephen J. Moorman, University of Michigan

Walter Steffen, University of Minnesota
Patricia Wadsworth, University of Massachusetts, Amherst
Mary Kate Worden, Harvard Medical School

Universal Imaging Fellowship

Andreas C. Stemmer, MRC Laboratory of Molecular Biology, UK

Scholarships

ASCB Fellows

Barry N. Bates, Purdue University
Elizabeth P. Garcia, University of Maryland
Graciela A. Unguez Monoz, University of California, Los Angeles
Homero L. Rey, University of California, Berkeley
Brian K. Romias, University of California, Los Angeles

Biology Club of CUNY

Dake Zheng, Duke University Medical Center

Father Arsenius Boyer Scholarship Fund

Dake Zheng, Duke University Medical Center

C. Lalor Burdick Scholarship

Barbara Maclay, Duke University

Gary N. Calkins Memorial Scholarship

Elizabeth Butler, University of Southampton, UK

Frances S. Claff Memorial Scholarship

Elizabeth Butler, University of Southampton, UK

Edwin Grant Conklin Memorial Scholarship

Elizabeth Butler, University of Southampton, UK

Lucretia Crocker Endowment Fund

Lori Buchholz, Center for Great Lakes Studies
Patricia Schulte, Stanford University
Tara Toolan, Harvard University

Bernard Davis Scholarship

Brenda W. Bennison, Florida State University
Francisco Calderon, University of Puerto Rico
Heike Jager, Universitat Osnabruck, Germany
Mark Johnson, University of Alabama
Gudrun Karsten, Ruhr-University of Bochun, Germany
Monika Kern, University of Bonn, Germany
Daniel Miller, Cornell University
R. Mohanraju, CAS, Marine Biology, Portonovo, India
Sergei Ostroumov, SUNY, Stony Brook
Sylvia Schnell, University of Tubingen, Germany
Tara Toolan, Harvard University
Gunter Wallner, Technische Universitat, Munchen, Germany

William F. and Irene Diller Scholarship Fund

Ann Greig, University of North Carolina, Chapel Hill

Caswell Grave Scholarship

Debra Fadool, University of Florida
Kobei Hatta, University of Oregon
Thomas Otis, Stanford University

Aline D. Gross Scholarship

Barbara Maclay, Duke University

Merkel H. Jacobs Scholarship

Meredith Levine-Lazaroff, Tufts University
Dake Zheng, Duke University Medical Center

Arthur Klorfein Fund Scholarship

Ann Greig, University of North Carolina, Chapel Hill
Rulang Jiang, Wesleyan University
Michael Laidlaw, Brown University
Elena Levine, University of California, San Francisco
Ralf Sommer, University of Munich, Germany

S. O. Mast Founders Scholarship

Thomas Otis, Stanford University

Allen R. Memhard Scholarship

Ann Greig, University of North Carolina, Chapel Hill
Meridith Levine-Lazaroff, Tufts University

Center for Microbial Ecology Fellow, Michigan State Scholarship

Yvonne Boldt, University of Minnesota

Faith Miller Scholarship

William F. Wonderlin, West Virginia University

Alberto Monroy Fellow

Massimiliano Andreazzoli, University of Pisa, Italy

James S. Mountain Memorial Fund Scholarship

Eugene Kim, University of Pennsylvania
Mark Pirner, University of Minnesota
Penny Post, Carnegie Mellon University
Karen Schnetzer, Georgia Institute of Technology
David Sherwood, Duke University

Planetary Biology Internship

Thomas P. Pitta, University of Connecticut

William Townsend Porter Foundation Fellowship

Barry Bates, Purdue University
John Cooper, SUNY, Buffalo

Elizabeth Garcia, University of Maryland, Baltimore
Domingo Rivera, University of California
Graciela Unguez-Munoz, University of California, Los Angeles

A. W. Rand Scholarship

Olga Alexandrova, Institute of Cytology, Academy of Science, USSR
Mark Barrey, Wesleyan University
Susan Burden, Case Western Reserve University
Seresh Jesuthasan, University of Oxford, UK
Alexander McDougall, University College, UK
Maura A. McGrail, University of Minnesota
Robert Morris, Harvard University
Martin Murphy, University of Cambridge, UK
Puneet Opal, Northwestern University
Mark Pirner, University of Minnesota
Penny Post, Carnegie Mellon University
Evelyn Rider, University of California, Los Angeles, Medical Center
Susan Safley, Emory University
Karen Schnetzer, Georgia Institute of Technology
David Sherwood, Duke University
Elizabeth Smith, Emory University
Richard Sucgang, Columbia University
James Swanson, Memorial Sloan Kettering Cancer Center
Julia Wulfkuhle, Purdue University
Hana Yaari, Memorial Sloan Kettering Cancer Center

Society for General Physiologists Scholarships

Helen J. Doyle, Max Planck Institut, Germany
Debra A. Fadool, University of Florida
Ashok N. Hegde, Columbia University, HHMI
Homero L. Rey, University of California, Berkeley

Marjorie W. Stetten Fund

Paris Ataliotis, Ludwig Institute for Cancer Research, UK

Surdna Foundation Scholarship

Joan Bernhard, New York State Department of Health
Richard Blakemore, University of New Hampshire
Lori Buchholz, Center for Great Lakes Studies
Douglas Campbell, University of Western Ontario, Canada
Julie Dutcher, Center for Marine Science Research
Marie Antoinette Juinio, University of Rhode Island
Kathy Ann Miller, University of Puget Sound

William Morton Wheeler Family Founders' Scholarship

Meredith Levine-Lazaroff, Tufts University

Awards

Lewis Thomas Award

Robert Cooke, *Newsday*

Board of Trustees and Committees

Corporation Officers and Trustees

Ex officio

Honorary Chairman of the Board of Trustees, Denis M. Robinson, Key Biscayne, FL
Chairman of the Board of Trustees, Sheldon J. Segal, The Population Council, New York, NY
Vice Chairman of the Board of Trustees, Robert E. Mainer, The Boston Company, Boston, MA
President of the Corporation, James D. Ebert, Chesapeake Bay Institute, Baltimore, MD
Director of the Corporation, Harlyn O. Halvorson, Marine Biological Laboratory, Woods Hole, MA
Treasurer, Robert D. Manz, Helmer & Associates, Waltham, MA
Clerk of the Corporation, Kathleen Dunlap, Tufts University School of Medicine, Boston, MA

Class of 1995

Clay Armstrong, University of Pennsylvania Medical School, Philadelphia, PA
Eric Davidson, California Institute of Technology, Pasadena, CA
Judith Grassle, Institute of Marine & Coastal Sciences, Rutgers University, New Brunswick, NJ
Mary J. Greer, Cambridge, MA
Franklin M. Loew, Tufts University School of Veterinary Medicine, North Grafton, MA
Brian Salzberg, University of Philadelphia School of Medicine, PA
Robert Silver, Cornell University, Ithaca, NY
J. P. Trinkaus, Yale University, New Haven, CT

Class of 1994

Frederick Bay, The Bay Foundation, New York, NY
Mary-Ellen Cunningham, Grosse Pointe Farms, MI
Robert D. Goldman, Northwestern University Medical School, Chicago, IL
Rodolfo R. Llinás, New York University Medical Center, New York, NY
Robert W. Pierce, Boca Grande, FL
Thomas D. Pollard, Johns Hopkins University, Baltimore, MD
Irving W. Rabb, University Place at Harvard Square, Cambridge, MA
Joan V. Ruderman, Harvard University School of Medicine, Boston, MA
Joseph Sanger, University of Pennsylvania School of Medicine, Philadelphia, PA
Ann E. Stuart, University of North Carolina, Chapel Hill, NC

Class of 1993

Garland E. Allen, Washington University, St. Louis, MO
Jelle Atema, Marine Biological Laboratory, Woods Hole, MA
William L. Brown, Weston, MA
Alexander W. Clowes, University of Washington School of Medicine, Seattle, WA
Barbara Ehrlich, University of Connecticut, Farmington, CT
Richard E. Kendall, East Falmouth, MA
Edward A. Kravitz, Harvard Medical School, Boston, MA
Jerry A. Melillo, Marine Biological Laboratory, Woods Hole, MA
Roger D. Sloboda, Dartmouth College, Hanover, NH

Class of 1992

Norman Bernstein, Diane and Norman Bernstein Foundation, Washington, DC
Ellen R. Grass, Grass Foundation, Quincy, MA
Neil Jacobs, Hale & Dorr, Boston, MA
Sir Hans Kornberg, Christ's College, Cambridge, UK
George Langford, Dartmouth College, Hanover, NH
Jack Levin, V.A. Medical Center, San Francisco, CA
Evelyn Spiegel, Dartmouth College, Hanover, NH
Andrew G. Szent-Györgyi, Brandeis University, Waltham, MA
Kensal E. VanHolde, Oregon State University, Corvallis, OR
Stanley W. Watson, Associates of Cape Cod, Inc., Falmouth, MA

Emeriti

Edward Adelberg, Yale University, New Haven, CT
John B. Buck, Sykesville, MD
Seymour S. Cohen, Woods Hole, MA
Arthur L. Colwin, Key Biscayne, FL
Laura Hunter Colwin, Key Biscayne, FL
D. Eugene Copeland, Marine Biological Laboratory, Woods Hole, MA
Sears Crowell, Indiana University, Bloomington, IN
Alexander T. Daignault, Boston, MA
William T. Golden, New York, NY
Teru Hayashi, Woods Hole, MA
Ruth Hubbard, Cambridge, MA
Lewis Kleinholz, Reed College, Portland, OR
Maurice E. Krahl, Tucson, AZ
Charles B. Metz, Miami, FL
Keith R. Porter, University of Pennsylvania, Philadelphia, PA
C. Ladd Prosser, University of Illinois, Urbana, IL
S. Meryl Rose, Waquoit, MA
W. D. Russell-Hunter, Syracuse University, Syracuse, NY
John Saunders, Jr., Waquoit, MA
Mary Sears, Woods Hole, MA
Homer P. Smith, Woods Hole, MA
W. Randolph Taylor, Ann Arbor, MI
D. Thomas Trigg, Wellesley, MA
Walter S. Vincent, Woods Hole, MA
George Wald, Cambridge, MA

Executive Committee of the Board of Trustees

Sheldon J. Segal, Chairman
Robert B. Barlow Jr., 1991
Mary-Ellen Cunningham, 1994
James D. Ebert*
Ray L. Epstein*
Robert D. Goldman, 1994
Harlyn O. Halvorson*
Robert E. Mainer, Vice Chairman
Robert D. Manz*
Jerry A. Melillo, 1993
Irving W. Rabb, 1991
Joseph W. Sanger, 1992

Trustee Committees 1991

Audit

Robert Mainer
Ray L. Epstein
Robert D. M...
Joan V. P...
Gaius Shaver
Andrew G. Szent-Györgyi
D. Thomas Trigg
Stanley W. Watson

Compensation

Sheldon J. Segal, Chairman
Robert E. Mainer
Robert D. Manz
Irving W. Rabb
D. Thomas Trigg

Development

Frederick Bay
Mary-Ellen Cunningham
James D. Ebert*
Harlyn O. Halvorson*
Luigi Mastroianni
Robert Pierce
Sheldon J. Segal*

Investment

William L. Brown, Chairman
Ray L. Epstein*
William T. Golden
Maurice Lazarus
Werner R. Loewenstein
Robert D. Manz*
Irving W. Rabb
W. Nicholas Thorndike
D. Thomas Trigg

Long-Range Planning Committee

Robert Manz, Chairman
Dieter Blennemann
Ray Epstein*
Rodolfo Ilinás
Robert Mainer
John Speer*
Andrew Szent-Györgyi

Standing Committees for the Year 1991

Buildings & Grounds

Kenyon Tweedell, Chairman
Alfred B. Chaet
Lawrence B. Cohen
Richard D. Cutler*
Ferenc Harosi
Donald B. Lehy*
Thomas Meedel
Evelyn Spiegel

Fellowships

Thoru Pederson, Chairman
Martha Constantine-Paton
Ray L. Epstein*
Leslie D. Garrick*
Ann Giblin
George M. Langford
Eduardo Macagno
Carol L. Reinisch
J. Richard Whittaker

Housing, Food Service, and Child Care

Thomas Reese, Chairman
Jelle Atema
Andrew Bass
Susan Barry
Donald Chang
Richard Cutler*
Stephen Highstein
LouAnn King*

*ex officio

Institutional Animal Care and Use

Leslie D. Garrick, Chairman
Robert A. Bullis
Alfred Chaet
Ray L. Epstein
Edward Jaskun
Alan Kuzirian
Andrew Mattox

Instruction

Roger D. Sloboda, Chairman
George Augustine
Ray L. Epstein*
Leslie D. Garrick*
Leah T. Haimo
Susan Hill
Hans Laufer
Joan V. Ruderman
Robert B. Silver
Raymond Stephens
John Waterbury

Library Joint Management

Harlyn O. Halvorson, Chairman
Craig Dorman, WHOI
Ray L. Epstein
Robert B. Gagosian, WHOI
John W. Speer*
David Stonehill
Gary Walker, WHOI

Library Joint Advisory

David Shepro, Chairman
Werner Deuser, WHOI
Henry J. B. Dick, WHOI
Kevin Freidland, US Marine Fisheries
John Hobbie
Henry Stommel, WHOI
Page Valentine, USGS
Gerald Weissman

Marine Resources

Robert Goldman, Chairman
Donald Abt
William Cohen
Richard Cutler*
Donald B. Lehy*
Toshio Narahashi
George Pappas
Roger Sloboda
Melvin Spiegel
Antoinette Steinacher

Radiation Safety

Ete Z. Szutz, Chairman
David W. Borst
Richard L. Chappell
Sherwin J. Cooperstein
Louis M. Kerr
Andrew Mattox*
Robert Rakowski
Walter Vincent

Research Services

Brian D. Noe, Chairman
Peter Armstrong
Robert B. Barlow Jr.

Richard Cutler*
Barbara Ehrlich
Kenneth Foreman
Joseph Ilan
Ehud Kaplan
Samuel S. Koide
Aimlee Laderman
Jack Levin
Andrew Mattox*
Robert Palazzo
Paul Steudler

*ex officio

Research Space

Joseph W. Sanger, Chairman
Paul De Weer
Ray L. Epstein*
Leslie D. Garrick*
David Landowne
Hans Laufer
Eduardo Macagno
Jerry A. Melillo
Robert Silver
Steven Treistman
Ivan Valiela
Richard Vallee

Safety

John Hobbie, Chairman
Lee Bourgoin
Richard Cutler*
Edward Enos*
Susan Goux
Louis M. Kerr
Alan Kuzirian
Donald B. Lehy*
Andrew Mattox*
Gerald Phillabaum
Paul Steudler

Laboratory Support Staff*

Biological Bulletin
Clapp, Pamela L., Managing Editor
Ready, Beth
Showalter, Christine M.

Computer Services
Tollios, Constantine D., Manager
Cserny, Mary
Schmidt, Valerie

Controller's Office
Speer, John W., Controller
Accounting Services
Binda, Ellen F.
Campbell, Ruth B.
Davis, Doris C.
Ghetti, Pamela M.
Gilmore, Mary F.
Hobbs, Roger W., Jr.
Hough, Rose A.
Poravas, Maria
Riley, Janis E.

Chem Room
Miller, Lisa A.
Schorer, Timothy M.

Purchasing
Hall, Lionel E., Jr.
Schorer, Timothy M.

Copy Service Center
Mountford, Rebecca J., Supervisor
Jackson, Jacquelyn F.
Ridley, Sherie

Including persons who joined or left the staff during 1991

Development Office
Ayers, Donald E., Director
Aspinwall, Duncan P.
Berthel, Dorothy
Faxon, Wendy P.
Lessard, Kelley J.

Director's Office
Halvorson, Harlyn O., Director
Epstein, Ray L., Associate Director
Burrhus, I. Elaine
Catania, Didia

Gray Museum
Backus, Richard H., Curator
Armstrong, Ellen P.
Montiero, Eva

Housing
King, LouAnn D., Conference Center and Housing Manager
Barnes, Susan M.
Collins, Paul J.
Johnson, Frances N.
Krajewski, Viola I.
Kuil, Elisabeth
Mancevice, Denise M.
Mancini, Mary
McNamara, Noreen

Telephone Office
Baker, Ida M.
Geggatt, Agnes L.
Ridley, Alberta W.

Human Resources
Goux, Susan P., Manager
Donovan, Marcia H.

Library
Stonehill, David L., Director, MBL/WHOI Library Center
Ashmore, Judith A.
Baker, John D.
Costa, Marguerite E.
Dvorak, John M.
Fisher, Susan
Goux, Randal
Keenan, Patrick M.
Kogelnik, Andreas
Lanahan, Paul
Mirra, Anthony J.
Monahan, A. Jean
Mountford, Rebecca J.
Nelson, Heidi
Norton, Catherine N.
Paszek, Aaron
Pratson, Patricia G.
Remsen, David
Showalter, Christine M.
deVeer, Joseph M.
Wright, Rosemary

MBL Associates Liaison
Scanlon, Deborah
Price, F. Carol
Wilkes, Jennifer

Public Information Office
Liles, George W., Jr., Director
Anderson, Judith L.
Ashmore, Lynne E.
Kaye-Peterson, Amy

Safety Services
Mattox, Andrew H., Safety Officer

Apparatus
Barnes, Franklin D.
Haskins, William A.

Martin, Lowell V.
Nichols, Francis H., Jr.

Shipping and Receiving
Geggatt, Richard E.
Illgen, Robert F.

Services, Projects and Facilities

Cutler, Richard D., Manager
Enos, Joyce B.
Kurland, Charles I.
Philbin, Linda M.

Buildings and Grounds
Lehy, Donald B., Superintendent
Baldic, David P.
Blumsack, Jeffrey J.
Blunt, Hugh F.
Bourgoin, Lee E.
Carini, Robert J.
Fish, David L., Jr.
Fuglister, Charles K.
Gonsalves, Paul J.
Gonsalves, Walter W., Jr.
Hathaway, Peter J.
Justason, C. Scott
Lochhead, William M.
Lunn, Alan G.
MacLeod, John B.
McAdams, Herbert M. III
Mills, Stephen A.
Olive, Charles W., Jr.
Rattacasa, Frank D.
Schoepf, Claude
deVeer, Robert L.

Electron Microscopy Lab
Kerr, Louis M.

Housekeeping Services
Phillabaum, Gerald, General Supervisor
Allen, Wayne D.
Anderson, Lewis B.
Boucher, Richard L.
Collins, Paul J.
Conlin, Henry P.
Dorris, John J.
Gibbons, Roberto G.
Krajewski, Chester J.
Lynch, Henry L.
Quelle, Arthur III

Instrument Development Lab
Knudson, Robert

Machine Shop
Sylvia, Frank E.

Marine Resources Center
Enos, Edward G., Jr., Superintendent
Cipoletta, Charles D.
Elder, Peggy
Fisher, H. Thomas, Jr.
Hanley, Janice S.
Moniz, Priscilla C.
Monteiro, Dana
Sullivan, Daniel A.
Tassinari, Eugene
Torres, Sophie J.

Photolab
Golder, Linda M.
Golder, Robert J.

Sponsored Programs

Garrick, Leslie D., Administrator
Ainsworth, Janet
Chrysler, Dorianne
Dwane, Florence
Huffer, Linda
Lynch, Kathleen F.

Animal Care Facility
Shephard, Jennifer

Summer Support Staff

Amon, Tyler C.
Anderson, Penny
Ashmore, Lynne E.
Balmer, Ethan
Boyer, Cynthia
Brereton, Richard
Brown, I. Justin
Cadwalader, George, Jr.
Capobianco, James A.
Charlton, Bernie
Chin, Hong
Connor, John H.
Cutler, Laura
Diachun, Peter
Donovan, Jason P.
Geishecker, Loriann
Gomes, Edwina
Goux, Randal
Hainfeld, Colleen
Hamilton, Elizabeth R.
Hibbitt, Karen
Hobbie, David B.
Huguenin, J. Sanders
Huguenin, Suzanne
Hullum, Rebekah
Illgen, Robert C.
Just, Thomas
Kessler, Anne P.
Klein, Jill
Lacey, Rebekah
Langford, George M. III
Langton, Lori
Llinás, Alexander
Lowrance, David III
McLean, Suzanne
Monteiro, Ann
Moorhouse, Laura
Noe, Eric
Nolan, Nancy L.
O'Connor, Patricia M.
O'Hara, Aqua
Peal, Richard W.
Pettit, Antonia
Phillips, Daniel
Rajan, Supritha
Remsen, Andrew S.
Rickles, Jason
Sayers, Scott
Sheetz, Jennifer
Sheffield, James
Shephard, Jennifer
Shephard, Jillian
Smith, Kelli M.
Snyder, Rebecca
Sofferman, Rebecca
Swope, John G.
Tamm, Ingrid
Tang, Can
Thompson, Nuala
Torres, Sophie J.
Ulbrich, Ciona
VanEgeraat, Lisbeth
Varao, John
Wetzel, Ernest D.
White, Zoe A.

Members of the Corporation*

Life Members

Abbott, Marie, c/o Vaughn Abbott, Flyer Rd., East Hartland, CT 06027 (deceased)

Bang, Betsy G., 76 F.R. Lillie Road, Woods Hole, MA 02543
Bartlett, James H., Department of Physics, University of Alabama, Box 870324, Tuscaloosa, AL 35487-0324
Beams, Harold W., Department of Biology, University of Iowa, Iowa City, IA 52242
Bernheimer, Alan W., Department of Microbiology, New York University Medical Center, 550 First Ave., New York, NY 10016
Bertholf, Lloyd M., Westminster Village #2114, 2025 E. Lincoln St., Bloomington, IL 61701
Bodian, David, 4100 North Charles St., #913, Baltimore, MD 21218
Bridgman, A. Josephine, 715 Kirk Rd., Decatur, GA 30030
Buck, John B., 7200 Third Ave., #C020, Sykesville, MD 21784
Burbanck, Madeline P., Box 15134, Atlanta, GA 30333
Burbanck, William D., Box 15134, Atlanta, GA 30333

Carpenter, Russell L., 60-H Lake St., Winchester, MA 01890 (deceased)
Clark, Arnold M., 53 Wilson Rd., Woods Hole, MA 02543
Cohen, Adolph I., Department of Ophthalmology, Washington University School of Medicine, St. Louis, MO 63110
Cohen, Seymour S., 10 Carrot Hill Rd., Woods Hole, MA 02543-1206
Colwin, Arthur, 320 Woodcrest Rd., Key Biscayne, FL 33149
Colwin, Laura Hunter, 320 Woodcrest, Key Biscayne, FL 33149
Copeland, D. E., 41 Fern Lane, Woods Hole, MA 02543
Corliss, John O., P. O. Box 53008, Albuquerque, NM 87153
Costello, Helen M., Carolina Meadows, Villa 137, Chapel Hill, NC 27514
Crouse, Helen, Address unknown

Dudley, Patricia L., Department of Biological Sciences, Barnard College, Columbia University, 3009 Broadway, New York, NY 10027

Edwards, Charles, University of Southern Florida College of Medicine, MDC Box 40, 12901 Bruce B. Downs Blvd., Tampa, FL 33612

Failla, Patricia M., 2149 Loblolly [illegible] Johns Island, SC 29455

Ferguson, James K. W., 56 Clarkehaven St., Thornhill, Ontario L4J 2B4 Canada

Glusman, Murray, 50 E. 72nd St., New York, NY 10021
Goldman, David, 63 Loop Rd., Falmouth, MA 02540
Graham, Herbert, 36 Wilson Rd., Woods Hole, MA 02543
Green, James W., 409 Grant Ave., Highland Park, NJ 08904
Grosch, Daniel S., 1222 Duplin Road, Raleigh, NC 27607

Hamburger, Viktor, Department of Biology, Washington University, St. Louis, MO 63130
Hamilton, Howard L., Department of Biology, University of Virginia, 238 Gilmer Hall, Charlottesville, VA 22901
Harding, Clifford V., Jr., Wayne State University School of Medicine, Department of Ophthalmology, Detroit, MI 48201
Haschemeyer, Audrey E. V., 21 Glendon Road, Woods Hole, MA 02543
Hauschka, Theodore S., FD1, Box 781, Damariscotta, ME 04543
Hisaw, F. L., 5925 SW Plymouth Drive, Corvallis, OR 97330
Hubbard, Ruth, 21 Lakeview Avenue, Cambridge, MA 02138
Humes, Arthur G., Marine Biological Laboratory, Woods Hole, MA 02543
Hurwitz, Charles, Veterans Administration Hospital, Basic Science Research Laboratory, Albany, NY 12208

Johnson, Frank H., Department of Biology, Princeton University, Princeton, NJ 08540 (deceased)
Jones, Meredith L., Division of Worms, Museum of Natural History, Smithsonian Institution, Washington, DC 20560

Kaan, Helen W., Royal Megansett Nursing Home, Room 205, P. O. Box 408, N. Falmouth, MA 02556 (deceased)
Karush, Fred, Department of Microbiology, University of Pennsylvania School of Medicine, Philadelphia, PA 19104-6076
Kille, Frank R., 1111 S. Lakemont Ave. #444, Winter Park, FL 32782
Kingsbury, John M., Department of Plant Biology, Cornell University, Ithaca, NY 14853
Kleinholz, Lewis, Department of Biology, Reed College, 3203 SE Woodstock Blvd., Portland, OR 97202

Laderman, Ezra, Yale University, School of Music, New Haven, CT 06520
Lauffer, Max A., Address unknown
LeFevre, Paul G., 15 Agassiz Road, Woods Hole, MA 02543
Levine, Rachmiel, 2024 Canyon Rd., Arcadia, CA 91006

* Including action of the 1991 Annual Meeting

Lochhead, John H., 49 Woodlawn Rd., London SW6 6PS, England, UK
Loewus, Frank A., Washington State University, Institute of Biological Chemistry, Pullman, WA 99164
Loftfield, Robert B., Department of Chemistry, University of New Mexico School of Medicine, Albuquerque, NM 87131

Magruder, Samuel R., 270 Cedar Lane, Paducah, KY 42001
Malkiel, Saul, Allergic Diseases, Inc., 130 Lincoln St., Worcester, MA 01609
Mathews, Rita W., Box 131, Southfield, MA 01259
Miller, James A., 307 Shorewood Drive, E. Falmouth, MA 02536
Moore, John A., Department of Biology, University of California, Riverside, CA 92521
Moscona, Arthur A., University of Chicago, Department of Molecular Genetics and Cell Biology, 920 East 58th Street, Chicago, IL 60637
Mullins, Lorin J., University of Maryland School of Medicine, Department of Biophysics, Baltimore, MD 21201

Nasatir, Malmon, P. O. Box 379, Ojai, CA 93024-0379

Page, Irving H., Box 516, Hyannisport, MA 02647 (deceased)
Pollister, A. W., 8 Euclid Ave., Belle Mead, NJ 08502
Prosser, C. Ladd, Department of Physiology and Biophysics, Burrill Hall 524, University of Illinois, Urbana, IL 61801
Provasoli, Luigi, Via Stazione 43, 21025 Comerio (VA), Italy
Prytz, Margaret McDonald, Address unknown

Ratner, Sarah, Department of Biochemistry, Public Health Research Institute, 455 First Ave., New York, NY 10016
Renn, Charles E., Address unknown
Richards, A. Glenn, 942 Cromwell Ave., St. Paul, MN 55114
Rice, Robert V., 30 Burnham Dr., Falmouth, MA 02540
Rockstein, Morris, 600 Biltmore Way, Apt. 805, Coral Gables, FL 33134
Ronkin, Raphael R., 3212 McKinley St., NW, Washington, DC 20015
Rose, S. Meryl, 32 Crosby Ln., E. Falmouth, MA 02536

Sanders, Howard, Woods Hole Oceanographic Institution, Woods Hole, MA 02543
Sato, Hidemi, Faculty of Social Science, Nagano University, Shiminogo, Ueda, Nagano 386-12, Japan
Scharrer, Berta, Department of Anatomy, Albert Einstein College of Medicine, 1300 Morris Park Avenue, Bronx, NY 10461
Schlesinger, R. Walter, University of Medicine and Dentistry of New Jersey, Department of Molecular Genetics and Microbiology, Robert Wood Johnson Medical School, Piscataway, NJ 08854-5635
Schmitt, F. O., Room 16-512, Massachusetts Institute of Technology, Cambridge, MA 02139
Scott, Allan C., 1 Nudd St., Waterville, ME 04901
Shemin, David, 33 Lawrence Farm Rd., Woods Hole, MA 02543 (deceased)
Silverstein, Arthur M., The Johns Hopkins Hospital Wilmer Institute, Baltimore, MD 21205
Smith, Homer P., 8 Quissett Ave., Woods Hole, MA 02543
Smith, Paul F., P. O. Box 264, Woods Hole, MA 02543
Sonnenblick, B. P., 515A Heritage Hill, Southbury, CT 06488
Steinhardt, Jacinto, 1508 Spruce St., Berkeley, CA 94709
Stephens, Grover C., Department of Ecology & Evolutionary Biology, School of Biological Sciences, University of California, Irvine, CA 92717

Taylor, Robert E., 20 Harbor Hill Rd., Woods Hole, MA 02543
TeWinkel, Lois E., Rockridge, 25 Coles Meadow Road, Northampton, MA 01060 (deceased)
Trager, William, The Rockefeller University, 1230 York Ave., New York, NY 10021

Villee, Claude A., Harvard Medical School, Parcel B/Room 122, 25 Shattuck Street, Boston, MA 02115
Vincent, Walter S., 16 F.R. Lillie Rd., Woods Hole, MA 02543

Wald, George, 21 Lakeview Ave., Cambridge, MA 02138
Waterman, T. H., Yale University, Biology Department, Box 6666, New Haven, CT 06511
Weiss, Paul A., (deceased)
Wichterman, Ralph, 31 Buzzards Bay Ave., Woods Hole, MA 02543
Wiercinski, Floyd J., 36 James St., Woods Hole, MA 02543
Wigley, Roland L., 35 Wilson Rd., Woods Hole, MA 02543
Wilber, Charles G., Department of Biology, Colorado State University, Fort Collins, CO 80523

Zinn, Donald J., Department of Zoology, University of Rhode Island, Kingston, RI 02881
Zorzoli, Anita, 18 Wilbur Blvd., Poughkeepsie, NY 12603
Zweifach, Benjamin W., 8811 Nottingham Place, La Jolla, CA 92037

Regular Members

Abt, Donald A., Marine Biological Laboratory, Woods Hole, MA 02543
Acheson, George H., 25 Quissett Ave., Woods Hole, MA 02543
Adams, James A., Department of Natural Sciences, University of Maryland, Princess Anne, MD 21853
Adelberg, Edward A., Provost's Office, 115 Hall of Graduate Studies, Yale University, New Haven, CT 06520
Adelman, William J., Jr., 160 Locust St., Falmouth, MA 02540
Afzelius, Bjorn, Wenner-Gren Institute, University of Stockholm, Stockholm, Sweden
Alberte, Randall S., Department of Molecular Genetics and Cell Biology, University of Chicago, 1103 E. 57th Street, Chicago, IL 60637
Alkon, Daniel, NINCDS/NIH, Dept. LMNC, Bldg. Park, Rm. 431, Bethesda, MD 20852
Allen, Garland E., Department of Biology, Washington University, St. Louis, MO 63130
Allen, Nina S., Department of Biology, Wake Forest University, Box 7325, Winston-Salem, NC 27109
Amatniek, Ernest, 4797 Boston Post Rd., Pelham Manor, NY 10803
Anderson, Everett, Department of Anatomy & Cell Biology, LHRBB, Harvard Medical School, 45 Shattuck St., Boston, MA 02115
Anderson, J. M., 110 Roat St., Ithaca, NY 14850
Anderson, Porter W., Department of Pediatrics, University of Rochester Medical Center, Box 690, 601 Elmwood Ave., Rochester, NY 14642
Armett-Kibel, Christine, Department of Biology, University of Massachusetts, Boston, MA 02125
Armstrong, Clay M., Department of Physiology, University of Pennsylvania Medical School, Philadelphia, PA 19104
Armstrong, Peter B., Department of Zoology, University of California, Davis, CA 95616
Arnold, John M., Pacific Biomedical Research Center, 209 Snyder Hall, University of Hawaii, Honolulu, HI 96822
Arnold, William A., 102 Balsam Rd., Oak Ridge, TN 37830
Ashton, Robert W., Bay Foundation, 99 Wall St., New York, NY 10005
Atema, Jelle, Boston University Marine Program, Marine Biological Laboratory, Woods Hole, MA 02543

Atwood, Kimball C., III, P. O. Box [illegible], Woods Hole, MA 02543
Augustine, George J., Section of [illegible]obiology, Department of Biological Sciences, Univers[illegible] Southern California, Los Angeles, CA 90089-0371
Ayers, Donald F., Mar[illegible]al Laboratory, Woods Hole, MA 02543

Baccetti, Baccio, [illegible]te of General Biology, 53100 Siena, Italy
Baker, Robert G., Department of Physiology and Biophysics, New York University Medical Center, 550 First Ave., New York, NY 10016
Baldwin, Thomas O., Department of Biochemistry and Biophysics, Texas A&M University, College Station, TX 77843
Barlow, Robert B., Jr., Institute for Sensory Research, Syracuse University, Merrill Lane, Syracuse, NY 13244-5290
Barry, Daniel T., Department of Physical Medicine and Rehabilitation, ID204, University of Michigan Hospital, Ann Arbor, MI 48109-0042
Barry, Susan R., Department of Physical Medicine and Rehabilitation, ID204, University of Michigan Hospital, Ann Arbor, MI 48109-0042
Bartell, Clelmer K., 2000 Lake Shore Drive, New Orleans, LA 70122
Bass, Andrew H., Seely Mudd Hall, Department of Neurobiology, Cornell University, Ithaca, NY 14853
Battelle, Barbara-Anne, Whitney Laboratory, 9505 Ocean Shore Blvd., St. Augustine, FL 32086
Bauer, G. Eric, Department of Anatomy, University of Minnesota, Minneapolis, MN 55455
Bay, Frederick, Bay Foundation, 99 Wall St., New York, NY 10005
Baylor, Edward R., P. O. Box 93, Woods Hole, MA 02543
Baylor, Martha B., P. O. Box 93, Woods Hole, MA 02543
Beams, Harold W., Department of Biology, University of Iowa, Iowa City, IA 52242
Bearer, Elaine L., Division of Biology & Medicine, Department of Pathology, Brown University, Box G, Providence, RI 02912
Beauge, Luis Alberto, Department of Biophysics, Instituto M.y.M. Ferreyra, Casilla de Correo 389, 5000 Cordoba, Argentina
Beck, L. V., School of Experimental Medicine, Department of Pharmacology, Indiana University, Bloomington, IN 47401
Begenisich, Ted, Department of Physiology, University of Rochester, Medical Center, Box 642, 601 Elmwood Ave., Rochester, NY 14642
Begg, David A., LHRRB, Harvard Medical School, 45 Shattuck St., Boston, MA 02115
Bell, Eugene, Organogenesis, Inc., 83 Rogers St., Cambridge, MA 02142
Benacerraf, Baruj, Dana-Farber Cancer Institute, 44 Binney Street, Boston, MA 02115 (resigned)
Benjamin, Thomas L., Department of Pathology, Harvard Medical School, 25 Shattuck St., Boston, MA 02115
Bennett, M. V. L., Albert Einstein College of Medicine, Department of Neuroscience, 1410 Pelham Pkwy. S., Bronx, NY 10461
Bennett, Miriam F., Department of Biology, Colby College, Waterville, ME 04901
Berg, Carl J., Jr., P. O. Box 769, Kilauea, Kauai, HI 96754-0769
Berlin, Suzanne T., 3 Marsh St., Gloucester, MA 01930
Berne, Robert M., Departm[illegible]ent of Physiology, University of Virginia, School of Medicine, Charlottesville, VA 22908
Bernstein, Norman, Diane and Norman Bernstein Foundation, Inc., 5301 Wisconsin Ave., #600, Washington, DC 20015-2015
Bezanilla, Francisco, Department of Physiology, University of California, Los Angeles, CA 90024
Biggers, John D., Department of Physiology, Harvard Medical School, Boston, MA 02115
Bishop, Stephen H., Department of Zoology, Iowa State University, Ames, IA 50010
Blaustein, Mordecai P., Department of Physiology, School of Medicine, University of Maryland, 655 W. Baltimore Street, Baltimore, MD 21201
Blennemann, Dieter, Carl Zeiss, Inc., One Zeiss Drive, Thornwood, NY 10594
Bloom, George S., Department of Cell Biology and Neuroscience, The University of Texas Southwestern Medical Center, 5223 Harry Hines Blvd., Dallas, TX 75235-9039
Bloom, Kerry S., Department of Biology, University of North Carolina, Wilson Hall, CB#3280, Chapel Hill, NC 27599-3280
Bodznick, David A., Department of Biology, Wesleyan University, Lawn Avenue, Middletown, CT 06457
Boettiger, Edward G., 29 Juniper Point, Woods Hole, MA 02543
Boolootian, Richard A., Science Software Systems, Inc., 3576 Woodcliff Rd., Sherman Oaks, CA 91403
Borgese, Thomas A., Department of Biology, Lehman College, CUNY, Bronx, NY 10468
Borisy, Gary G., Laboratory of Molecular Biology, University of Wisconsin, Madison, WI 53706
Borst, David W., Jr., Department of Biological Sciences, Illinois State University, Normal, IL 61761-6901
Bosch, Herman F., Box 617, Woods Hole, MA 02543
Bowles, Francis P., P. O. Box 674, Woods Hole, MA 02543
Boyer, Barbara C., Department of Biology, Union College, Schenectady, NY 12308
Brandhorst, Bruce P., Department of Biological Sciences, Simon Fraser University, Barnaby, BC V5A 156 Canada
Brehm, Paul, Department of Neurobiology and Behavior, SUNY at Stony Brook, Stony Brook, NY 11794 (resigned)
Brinley, F. J., Neurological Disorders Program, NINCDS, 812 Federal Building, Bethesda, MD 20892
Brown, Joel E., Department of Ophthalmology, Box 8096 Sciences Center, Washington University, 660 S. Euclid Ave., St. Louis, MO 63110
Brown, Stephen C., Department of Biological Sciences, SUNY, Albany, NY 12222
Brown, William L., Bank of Boston (01-23-11), 100 Federal St., Boston, MA 02106-2016
Browne, Carole L., Department of Biology, Wake Forest University, Winston-Salem, NC 27109
Browne, Robert A., Department of Biology, Wake Forest University, Box 7325, Winston-Salem, NC 27109
Bryant, Shirley H., Department of Pharmacology and Cell Biophysics, University of Cincinnati, Cincinnati, OH 45267
Bucklin, Anne C., Marine Biological Laboratory, Woods Hole, MA 02543
Bullis, Robert A., Marine Biological Laboratory, Woods Hole, MA 02543
Burd, Gail Deerin, Department of Molecular and Cell Biology, University of Arizona, Tucson, AZ 85721
Burdick, Carolyn J., Department of Biology, Brooklyn College, Bedford Avenue & Avenue H, Brooklyn, NY 11210
Burger, Max, Freidrich Miesner Institut Bau 1060 Postfach 2543, Basel 4002, Switzerland
Burgos, Mario, IHEM Medical School, UNC 5500 Mendoza, Argentina
Burky, Albert, Department of Biology, University of Dayton, Dayton, OH 45469
Burstyn, Harold Lewis, Melvin and Melvin, 700 Merchants Bank Bldg., Syracuse, NY 13202-1686
Bursztajn, Sherry, Harvard Medical School, Mailman Research Center, 115 Mill St., Belmont, MA 02178
Bush, Louise, 7 Snapper Lane, Falmouth, MA 02540 (deceased)

Calabrese, Ronald L., Department of Biology, Emory University, 1555 Pierce Drive, Atlanta, GA 30322
Callaway, Joseph C., Department of Physiology, New York Medical College, Basic Sciences Bldg., Valhalla, NY 10595
Candelas, Graciela C., Department of Biology, University of Puerto Rico, Rio Piedras, PR 00931
Carew, Thomas J., Department of Psychology, Yale University, P. O. Box 11A, Yale Station, New Haven, CT 06520
Cariello, Lucio, Biochemistry Department, Stazione Zoologica, Villa Comunale, 80121 Naples, Italy
Carlson, Francis D., Biophysics Department, The Johns Hopkins University, N. Charles St., Baltimore, MD 21218
Carriere, Rita M., Department of Anatomy and Cell Biology, Box 5, SUNY Health Science Center, 450 Clarkson Ave., Brooklyn, NY 11203
Case, James, Office of Research Development, Cheadle Hall, University of California, Santa Barbara, CA 93111
Cassidy, Rev. J. D., St. Stephen Priory, Spiritual Life Center, 20 Glen St., Box 370, Dover, MA 02030-0370
Cebra, John J., Department of Biology, Leidy Labs, G-6, University of Pennsylvania, Philadelphia, PA 19174
Chaet, Alfred B., University of West Florida, Pensacola, FL 32504
Chambers, Edward L., Department of Physiology and Biophysics, University of Miami, School of Medicine, P. O. Box 016430, Miami, FL 33101
Chang, Donald C., Department of Physiology, Baylor College of Medicine, One Baylor Plaza, Houston, TX 77030
Chappell, Richard L., Department of Biological Sciences, Hunter College, Box 210, 695 Park Ave., New York, NY 10021
Chauncey, Howard H., 30 Falmouth St., Wellesley Hills, MA 02181 (deceased)
Chen, Thomas T., Center for Marine Biotechnology, University of Maryland, 600 E. Lombard St., Baltimore, MD 21202
Chikarmane, Hemant M., Marine Biological Laboratory, Woods Hole, MA 02543
Child, Frank M., III, Department of Biology, Trinity College, Hartford, CT 06106
Chisholm, Rex L., Department of Cell Biology and Anatomy, Northwestern University Medical School, 303 E. Chicago Avenue, Chicago, IL 60611
Citkowitz, Elena, 410 Livingston St., New Haven, CT 06511
Clark, Eloise E., Academic Affairs, Bowling Green State University, Bowling Green, OH 43403
Clark, Hays, 26 Deer Park Drive, Greenwich, CT 06830
Clark, James M., 210 Emerald Lane, Palm Beach, FL 33480
Clark, Wallis H., Jr., Bodega Marine Laboratory, P. O. Box 247, Bodega Bay, CA 94923
Claude, Philippa, Primate Center, Capitol Court, Madison, WI 53706
Clay, John R., Laboratory of Biophysics, NIH, Building 9, Room 1E-124, Bethesda, MD 20892
Clowes, Alexander W., Department of Surgery RF-25, University of Washington School of Medicine, Seattle, WA 98195
Clutter, Mary, Office of the Director, Room 518, National Science Foundation, Washington, DC 20550
Cobb, Jewel Plummer, California State University, 800 State College Boulevard, Fullerton, CA 92634
Cohen, Avis H., Section of Neurobiology and Behavior, Mudd Hall, Cornell University, Ithaca, NY 14853-2702
Cohen, Carolyn, Rosenstiel Basic Medical Sciences Research Center, Brandeis University, Waltham, MA 02254
Cohen, Lawrence B., Department of Physiology, Yale University School of Medicine, 333 Cedar Street, New Haven, CT 06510-8026
Cohen, Maynard, Department of Neurological Sciences, Rush Medical College, 600 South Paulina, Chicago, IL 60612
Cohen, Rochelle S., Department of Anatomy, University of Illinois, 808 W. Wood Street, Chicago, IL 60612
Cohen, William D., Department of Biological Sciences, Hunter College, 695 Park Ave., Box 79, New York, NY 10021
Coleman, Annette W., Division of Biology and Medicine, Brown University, Providence, RI 01912
Collier, Jack R., Department of Biology, Brooklyn College, Bedford & Avenue H, Brooklyn, NY 11210
Collier, Marjorie McCann, Biology Department, Saint Peter's College, 2641 Kennedy Boulevard, Jersey City, NJ 07306
Cook, Joseph A., The Edna McConnell Clark Foundation, 250 Park Ave., New York, NY 10017
Cooperstein, S. J., University of Connecticut Health Center, Department of Anatomy, Farmington Ave., Farmington, CT 06032
Cornell, Neal W., Marine Biological Laboratory, Woods Hole, MA 02543
Cornwall, Melvin C., Jr., Department of Physiology L714, Boston University School of Medicine, 80 E. Concord St., Boston, MA 02118
Corson, David Wesley, Jr., 1034 Plantation Lane, Mt. Pleasant, SC 29464
Corwin, Jeffrey T., Department of Otolaryngology, University of Virginia Medical Center, Box 430, Charlottesville, VA 22908
Costello, Walter J., Department of Zoology, College of Medicine, Ohio University, Athens, OH 45701
Couch, Ernest F., Department of Biology, Texas Christian University, Fort Worth, TX 76129
Cremer-Bartels, Gertrud, Universitats Augenklinik, 44 Munster, Germany
Crow, Terry J., Department of Neurobiology and Anatomy, University of Texas Medical School, Houston, TX 77225
Crowell, Sears, Department of Biology, Indiana University, Bloomington, IN 47405
Crowther, Robert, Marine Biological Laboratory, Woods Hole, MA 02543
Cunningham, Mary-Ellen, 62 Cloverly Road, Grosse Pointe Farms, MI 48236
Currier, David L., P. O. Box 2476, Vineyard Haven, MA 02568
Cutler, Richard, Marine Biological Laboratory, Woods Hole, MA 02543

Daignault, Alexander T., 280 Beacon St., Boston, MA 02116
Dan, Katsuma, Tokyo Metropolitan Union, Meguro-ku, Tokyo, Japan
D'Alessio, Giuseppe, Department of Organic & Biological Chemistry, University of Naples, Via Mezzocannone 16, Naples, Italy 80134
D'Avanzo, Charlene, School of Natural Science, Hampshire College, Amherst, MA 01002
David, John R., Seeley G. Mudd Building, Room 504, Harvard Medical School, 250 Longwood Ave., Boston, MA 02115
Davidson, Eric H., Division of Biology, 156-29, California Institute of Technology, Pasadena, CA 91125
Davis, Bernard D., Bacterial Physiology Unit, Harvard Medical School, Boston, MA 02115
Davis, Joel P., Seapuit, Inc., P. O. Box G, Osterville, MA 02655
Daw, Nigel W., 78 Aberdeen Place, Clayton, MO 63105
Deegan, Linda A., The Ecosystems Center, Marine Biological Laboratory, Woods Hole, MA 02543
DeGroof, Robert C., 145 Water Crest Dr., Doylestown, PA 18901
DeHaan, Robert L., Department of Anatomy and Cell Biology, Emory University School of Medicine, Atlanta, GA 30322
DeLanney, Louis E., Institute for Medical Research, 2260 Clove Drive, San Jose, CA 95128
Dentler, William L., Department of Physiology & Cell Biology, University of Kansas, 4011 Haworth Hall, Lawrence, KS 66044

DePhillips, Henry A., Jr., Department of Chemistry, Trinity College, 300 Summit Street, Hartford, CT 06106
DeSimone, Douglas W., Department of Anatomy and Cell Biology, Box 439, Health Sciences Center, University of Virginia, Charlottesville, VA
DeToledo-Morrell, L., Department of Neurological Sciences, Rush Medical College, Chicago, IL 60614
Dettbarn, Wolf-Dietrich, Department of Pharmacology, School of Medicine, Vanderbilt University, Nashville, TN 37127
De Weer, Paul J., Department of Physiology, University of Pennsylvania School of Medicine, Philadelphia, PA 19104-6085
Dixon, Keith E., School of Biological Sciences, Flinders University, Bedford Park, 5042, South Australia, Australia
Dowdall, Michael J., Department of Zoology, School of Biological Sciences, University of Nottingham, University Park, Nottingham NG7 2RD, England, UK (dropped)
Dowling, John E., The Biological Laboratories, Harvard University, 16 Divinity St., Cambridge, MA 02138
DuBois, Arthur Brooks, John B. Pierce Foundation Laboratory, 290 Congress Ave., New Haven, CT 06519
Duncan, Thomas K., Department of Environmental Sciences, Nichols College, Dudley, MA 01570
Dunham, Philip B., Department of Biology, Syracuse University, Syracuse, NY 13244
Dunlap, Kathleen, Department of Physiology, Tufts University Medical School, Boston, MA 02111
Dunlap, Paul V., Department of Biology, Woods Hole Oceanographic Institution, Redfield 316, Woods Hole, MA 02543
Dworkin, Martin, Department of Microbiology, University of Minnesota, 1460 Mayo Bldg., Box 196 UMHC, Minneapolis, MN 55455-0312

Ebert, James D., Chesapeake Bay Institute, The Johns Hopkins University, c/o Department of Biology, Mudd 114, Baltimore, MD 21218
Eckberg, William R., Department of Zoology, Howard University, Washington, DC 20059
Edds, Kenneth T., Department of Anatomical Sciences, SUNY, Buffalo, NY 14214
Eder, Howard A., Albert Einstein College of Medicine, 1300 Morris Park Ave., Bronx, NY 10461
Edstrom, Joan, 2515 Milton Hills Dr., Charlottesville, VA 22901
Egyud, Laszlo G., 18 Skyview, Newton, MA 02150
Ehrlich, Barbara E., Division of Cardiology, University of Connecticut Health Center, 263 Farmington Avenue, Farmington, CT 06030
Eisen, Arthur Z., Division of Dermatology, Washington University, St. Louis, MO 63110
Eisenman, George, Department of Physiology, University of California Medical School, Los Angeles, CA 90024 (resigned)
Elder, Hugh Young, Institute of Physiology, University of Glasgow, Glasgow, Scotland G12 8QQ
Elliott, Gerald F., The Open University Research Unit, Foxcombe Hall, Berkeley Rd., Boars Hill, Oxford, England OX1 5HR
Englund, Paul T., Department of Biological Chemistry, Johns Hopkins School of Medicine, Baltimore, MD 21205
Epel, David, Hopkins Marine Station, Pacific Grove, CA 93950
Epstein, Herman T., Lawrence Farm Road, Woods Hole, MA 02543
Epstein, Ray L., Marine Biological Laboratory, Woods Hole, MA 02543
Erulkar, Solomon D., 318 Kent Rd., Bala Cynwyd, PA 19004
Essner, Edward S., Kresge Eye Institute, Wayne State University, 540 E. Canfield Ave., Detroit, MI 48201

Farb, David H., Department of Pharmacology L603, Boston University School of Medicine, Boston, MA 02118
Farmanfarmaian, A., Department of Biological Sciences, Nelson Biological Laboratory, Rutgers University, Piscataway, NJ 08855
Fein, Alan, Department of Physiology, University of Connecticut Health Center, Farmington, CT 06032
Feinman, Richard D., Box 8, Department of Biochemistry, SUNY Health Science Center, 450 Clarkson Avenue, Brooklyn, NY 11203
Feldman, Susan C., Department of Anatomy, University of Medicine and Dentistry of New Jersey, New Jersey Medical School, 100 Bergen St., Newark, NJ 07103
Fessenden, Jane, Marine Biological Laboratory, Woods Hole, MA 02543
Festoff, Barry W., Neurology Service (127), Veterans Administration Medical Center, 4801 Linwood Blvd., Kansas City, MO 64128
Fink, Rachel D., Department of Biological Sciences, Clapp Laboratory, Mount Holyoke College, South Hadley, MA 01075
Finkelstein, Alan, Albert Einstein College of Medicine, 1300 Morris Park Ave., Bronx, NY 10461
Fischbach, Gerald, Department of Neurobiology, Harvard Medical School, 220 Longwood Ave., Boston, MA 02115
Fishman, Harvey M., Department of Physiology and Biophysics, University of Texas Medical Branch, Galveston, TX 77550
Flanagan, Dennis, 12 Gay St., New York, NY 10014
Fluck, Richard Allen, Department of Biology, Franklin & Marshall College, Box 3003, Lancaster, PA 17604-3003
Foreman, K. H., Boston University Marine Program, Marine Biological Laboratory, Woods Hole, MA 02543
Fox, Thomas Oren, Division of Medical Sciences, Harvard Medical School, 260 Longwood Ave., Boston, MA 02115
Franzini-Armstrong, Clara, Department of Biology G-3, School of Medicine, University of Pennsylvania, Philadelphia, PA 19143
Frazier, Donald T., Department of Physiology, University of Kentucky Medical Center, Lexington, KY 40536
French, Robert J., Health Sciences Center, University of Calgary, Calgary, Alberta, T2N 4N1, Canada
Freygang, Walter J., Jr., 6247 29th St., NW, Washington, DC 20015
Friedler, Gladys, Boston University School of Medicine, 80 East Concord Street, Boston, MA 02118
Fry, Brian, Marine Biological Laboratory, Woods Hole, MA 02543
Fukui, Yoshio, Department of Cell Biology and Anatomy, Northwestern University Medical School, Chicago, IL 60201 (resigned)
Fulton, Chandler M., Department of Biology, Brandeis University, Waltham, MA 02254
Furshpan, Edwin J., Department of Neurophysiology, Harvard Medical School, Boston, MA 02115
Futrelle, Robert P., College of Computer Science, Northeastern University, 360 Huntington Avenue, Boston, MA 02115

Gabriel, Mordecai, Department of Biology, Brooklyn College, Brooklyn, NY 11210
Gadsby, David C., Laboratory of Cardiac Physiology, The Rockefeller University, 1230 York Avenue, New York, NY 10021
Gainer, Harold, Section of Functional Neurochemistry, NIH, Bldg. 36, Room 4D-20, Bethesda, MD 20892
Galatzer-Levy, Robert M., 180 N. Michigan Avenue, Chicago, IL 60601
Gall, Joseph G., Carnegie Institution, 115 West University Parkway, Baltimore, MD 21210
Gallant, Paul E., NIH, Bldg. 36, Rm. 2A-29, Bethesda, MD 20892
Garber, Sarah S., Department of Physiology & Biophysics, University of Alabama, Birmingham, BHSB 768 UAB Station, Birmingham, AL 35294-0005

Gascoyne, Peter, Department of Experimental Pathology, Box 85E, University of Texas System Cancer Center, M. D. Anderson Hospital and Tumor Institute, Texas Medical Center, 6723 Bertner Avenue, Houston, TX 77030

Gelperin, Alan, Department of Biophysics, AT&T Bell Labs, Room 1C464, 600 Mountain Avenue, Murray Hill, NJ 07974

German, James L., III, Lab of Human Genetics, The New York Blood Center, 310 East 67th St., New York, NY 10021

Gibbs, Martin, Institute for Photobiology of Cells and Organelles, Brandeis University, Waltham, MA 02254

Giblin, Anne E., Ecosystems Center, Marine Biological Laboratory, Woods Hole, MA 02543

Gibson, A. Jane, Wing Hall, Cornell University, Ithaca, NY 14850

Gifford, Prosser, 540 N Street, SW, S-903, Washington, DC 20024

Gilbert, Daniel L., Laboratory of Biophysics, NIH/NINDS, Bldg. 9, Room 1E-124, Bethesda, MD 20892

Giudice, Giovanni, Dipartimento di Biologia Cellulare e Dello Sviluppo, I-90123, Via Archirafi 22, Universita di Palermo, Palermo, Italy

Giuditta, Antonio, Department of General Physiology, University of Naples, Via Mezzocannone 8, Naples, Italy 80134

Glynn, Paul, Hunter College of CUNY, Department of Biological Sciences, 695 Park Avenue, New York, NY 10021

Golden, William T., American Museum of Natural History, 40 Wall St., Room 4201, New York, NY 10005

Goldman, Robert D., Department of Cell, Molecular and Structural Biology, Northwestern University, 303 E. Chicago Ave., Chicago, IL 60611

Goldsmith, Paul K., NIH, Bldg. 10, Room 9C-101, Bethesda, MD 20892

Goldsmith, Timothy H., Department of Biology, Yale University, New Haven, CT 06510

Goldstein, Moise H., Jr., ECE Department, Barton Hall, Johns Hopkins University, Baltimore, MD 21218

Goodman, Lesley Jean, Department of Biological Sciences, Queen Mary College, Mile End Road, London, E1 4NS, England, UK

Goudsmit, Esther M., Department of Biology, Oakland University, Rochester, MI 48309 (resigned)

Gould, Robert Michael, Institute for Basic Research in Developmental Disabilities, 1050 Forest Hill Rd., Staten Island, NY 10314

Gould, Stephen J., Museum of Comparative Zoology, Harvard University, Cambridge, MA 02138

Govind, C. K., Life Sciences Division, University of Toronto, 1265 Military Trail, West Hill, Ontario, M1C 1A4, Canada

Graf, Werner, Rockefeller University, 1230 York Ave., New York, NY 10021

Grant, Philip, 2939 Van Ness Street, N.W., Apt. 302, Washington, DC 20008

Grass, Albert M., The Grass Foundation, 77 Reservoir Rd., Quincy, MA 02170 (deceased)

Grass, Ellen R., The Grass Foundation, 77 Reservoir Rd., Quincy, MA 02170

Grassle, Judith, Institute of Marine & Coastal Studies, Rutgers University, Box 231, New Brunswick, NJ 08903

Graubard, Katherine, Department of Zoology, NJ-15, University of Washington, Seattle, WA 98195

Greenberg, Everett Peter, Department of Microbiology, College of Medicine, Iowa City, IA 52242

Greenberg, Michael J., Whitney Laboratory, 9505 Ocean Shore Blvd., St. Augustine, FL 32086

Greer, Mary J., 16 Hillside Ave., Cambridge, MA 02140

Griffin, Donald R., Concord Field Station, Harvard University, Old Causeway Road, Bedford, MA 01730

Gross, Paul R., Center for Advanced Studies, University of Virginia, 444 Cabell Hall, Charlottesville, VA 22903

Grossman, Albert, New York University Medical Center, 550 First Ave., New York, NY 10016

Grossman, Lawrence, Department of Biochemistry, Johns Hopkins University, 615 North Wolfe Street, Baltimore, MD 21205

Gruner, John, Department of Neurosurgery, New York University Medical Center, 550 First Ave., New York, NY 10016

Gunning, A. Robert, P. O. Box 165, Falmouth, MA 02541

Gwilliam, G. P., Department of Biology, Reed College, Portland, OR 97202

Haimo, Leah, Department of Biology, University of California, Riverside, CA 92521

Hall, Linda M., Department of Biochemistry and Pharmacology, SUNY, 317 Hochstetter, Buffalo, NY 14260

Hall, Zack W., Department of Physiology, University of California, San Francisco, CA 94143

Halvorson, Harlyn O., Marine Biological Laboratory, Woods Hole, MA 02543

Hamlett, Nancy Virginia, Department of Biology, Swarthmore College, Swarthmore, PA 19081

Hanna, Robert B., College of Environmental Science and Forestry, SUNY, Syracuse, NY 13210

Haneji, Tatsuji, Chiba University Medical School, 1-8-1, Inohana, Chiba, 280, Japan

Harosi, Ferenc I., Laboratory of Sensory Physiology, Marine Biological Laboratory, Woods Hole, MA 02543

Harrigan, June F., 7415 Makaa Place, Honolulu, HI 96825

Harrington, Glenn W., Division of Cell Biology and Biophysics, 403 Biological Sciences Building, University of Missouri, Kansas City, MO 64110

Harris, Andrew L., Department of Biophysics, Johns Hopkins University, 34th & Charles Sts., Baltimore, MD 21218

Hastings, J. W., The Biological Laboratories, Harvard University, 16 Divinity Street, Cambridge, MA 02138

Hayashi, Teru, 7105 SW 112 Place, Miami, FL 33173

Haydon-Baillie, Wensley G., Porton Int., 2 Lowndes Place, London, SW1X 8DD, England, UK

Hayes, Raymond L., Jr., Department of Anatomy, Howard University, College of Medicine, 520 W St., NW, Washington, DC 20059

Hepler, Peter K., Department of Botany, University of Massachusetts, Amherst, MA 01003

Herndon, Walter R., University of Tennessee, Department of Botany, Knoxville, TN 37996-1100

Herskovits, Theodore T., Department of Chemistry, Fordham University, John Mulcahy Hall, Room 638, Bronx, NY 10458

Hiatt, Howard H., Department of Medicine, Brigham and Women's Hospital, 75 Francis Street, Boston, MA 02115

Highstein, Stephen M., Department of Otolaryngology, Washington University School of Medicine, St. Louis, MO 63110

Hildebrand, John G., Arizona Research Laboratories, Division of Neurobiology, 603 Gould-Simpson Science Building, University of Arizona, Tucson, AZ 85721

Hill, Richard W., Department of Zoology, Michigan State University, E. Lansing, MI 48824

Hill, Susan D., Department of Zoology, Michigan State University, E. Lansing, MI 48824

Hillis-Colinvaux, Llewellya, Smithsonian Tropical Research Institute, Unit 0948 APO-AA, Miami, FL 34002-0948

Hillman, Peter, Department of Biology, Life Sciences & Neurobiology, Hebrew University, Jerusalem 91904, Israel

Hinegardner, Ralph T., Division of Natural Sciences, University of California, Santa Cruz, CA 95064

Hines, Michael, Department of Neurobiology, Duke University Medical Center, Box 3209, Durham, NC 27710

Hinsch, Gertrude, W., Dep[illegible] of Biology, University of South Florida, Tampa, FL 33[illegible]
Hobbie, John E., Ecos[illegible]ter, Marine Biological Laboratory, Woods Hole, M[illegible]
Hodge, Alan J., [illegible]ckburn Ave., San Diego, CA 92111
Hoffman, Joseph, [illegible]ent of Physiology, School of Medicine, Yale Univers[illegible] Haven, CT 06515
Hollyfield, Joe G., Baylor School of Medicine, Texas Medical Center, Houston, TX [illegible]030
Holtzman, Eric, Department of Biological Sciences, Columbia University, New York, NY 10017
Hopkinson, Jr., Charles S., Marine Biological Laboratory, Woods Hole, MA 02543
Hoskin, Francis C. G., Department of Biology, Illinois Institute of Technology, Chicago, IL 60616
Houghton, Richard A., III, Woods Hole Research Center, P. O. Box 296, Woods Hole, MA 02543
Hoy, Ronald R., Section of Neurobiology and Behavior, Cornell University, Ithaca, NY 14853
Hufnagel, Linda A., Department of Microbiology, University of Rhode Island, Kingston, RI 02881
Hummon, William D., Department of Zoology, Ohio University, Athens, OH 45701
Humphreys, Susie H., Research & Development, Kraft, Inc., 801 Waukegan Rd., Glenview, IL 60025
Humphreys, Tom D., University of Hawaii, PBRC, 41 Ahui St., Honolulu, HI 96813
Hunt, Richard T., ICRF, Clare Hall Laboratories, South Mimms Potter's Bar, Herts EN6-3LD, England
Hunter, Robert D., Department of Biological Sciences, Oakland University, Rochester, MI 48309-4401
Hunter, W. Bruce, Box 321, Lincoln Center, MA 01773
Hurwitz, Jerard, Sloan Kettering Institute for Cancer Research, 1275 York Avenue, New York, NY 11021
Huxley, Hugh E., Department of Biology, Rosenstiel Center, Brandeis University, Waltham, MA 02154
Hynes, Thomas J., Jr., Meredith and Grew, Inc., 160 Federal Street, Boston, MA 02110-1701

Ilan, Joseph, Department of Developmental Genetics and Anatomy, Case Western Reserve University School of Medicine, Cleveland, OH 44106
Ingoglia, Nicholas, Department of Physiology, New Jersey Medical School, 100 Bergen St., Newark, NJ 07103
Inoué, Saduyki, Department of Anatomy, McGill University Cancer Centre, 3640 University St., Montreal, PQ, H3A 2B2, Canada
Inoué, Shinya, Marine Biological Laboratory, Woods Hole, MA 02543
Isselbacher, Kurt J., Massachusetts General Hospital, 32 Fruit Street, Boston, MA 02114
Issidorides, Marietta, R., Department of Psychiatry, University of Athens, Monis Petraki 8, Athens, 140 Greece
Izzard, Colin S., Department of Biological Sciences, SUNY, 1400 Washington Ave., Albany, NY 12222

Jacobs, Neil, Hale & Dorr, 60 State St., Boston, MA 02109
Jacobson, Antone [illegible], Department of Zoology, University of Texas, Austin, TX 78712 (resigned)
Jaffe, Lionel, Marine B[illegible]al Laboratory, Woods Hole, MA 02543
Jannasch, Holger W., Depar[illegible]ent of Biology, Woods Hole Oceanographic Institution, Woods Hole, MA 02543
Jeffery, William R., Bodega Marine Laboratory, Box 247, Bodega Bay, CA 94923
Johnston, Daniel, Division of Neuroscience, Baylor College of Medicine, Baylor Plaza, Houston, TX 77030
Josephson, Robert K., Department of Biological Sciences, University of California, Irvine, CA 92717

Kabat, E. A., Department of Microbiology, College of Physicians and Surgeons, Columbia University, 630 West 168th St., New York, NY 10032
Kaczmarek, Leonard K., Department of Pharmacology, Yale University School of Medicine, 333 Cedar St., New Haven, CT 06510
Kaley, Gabor, Department of Physiology, Basic Sciences Building, New York Medical College, Valhalla, NY 10595
Kaltenbach, Jane, Department of Biological Sciences, Mount Holyoke College, South Hadley, MA 01075
Kaminer, Benjamin, Department of Physiology, School of Medicine, Boston University, 80 East Concord St., Boston, MA 02118
Kane, Robert E., PBRC, University of Hawaii, 41 Ahui St., Honolulu, HI 96813
Kaneshiro, Edna S., Department of Biological Sciences, University of Cincinnati, Cincinnati, OH 45221
Kao, Chien-yuan, Department of Pharmacology, Box 29, SUNY, Downstate Medical Center, 450 Clarkson Avenue, Brooklyn, NY 11203
Kaplan, Ehud, Department of Biophysics, The Rockefeller University, 1230 York Ave., New York, NY 10024
Karakashian, Stephen J., Apt. 16-F, 165 West 91st St., New York, NY 10024
Karlin, Arthur, Department of Biochemistry and Neurology, Columbia University, 630 West 168th St., New York, NY 10032
Katz, George M., Fundamental and Experimental Research Labs, Merck Sharp and Dohme, P. O. Box 2000, Rahway, NJ 07065
Kelly, Robert E., Department of Anatomy, College of Medicine, University of Illinois, P. O. Box 6998, Chicago, IL 60680
Kemp, Norman E., Department of Biology, University of Michigan, Ann Arbor, MI 48109
Kendall, John P., Faneuil Hall Associates, 176 Federal Street, 2nd Floor, Boston, MA 02110
Kendall, Richard E., Commissioner of Environmental Management, 100 Cambridge Street, Room 1905, Boston, MA 02202
Kerr, Louis M., Marine Biological Laboratory, Woods Hole, MA 02543
Keynan, Alexander, Hebrew University, Jerusalem, Israel
Khan, Shahid M. M., Department of Anatomy & Structural Biology, Albert Einstein College of Medicine, 1300 Morris Park Ave., Bronx, NY 10461
Kiehart, Daniel P., Department of Cellular and Developmental Biology, Harvard University, 16 Divinity Street, Cambridge, MA 02138
Kirk, Mark D., Division of Biological Sciences, University of Missouri, Columbia, MO 65211
Klein, Morton, Department of Microbiology, Temple University Medical School, Philadelphia, PA 19103 (dropped)
Klotz, Irving M., Department of Chemistry, Northwestern University, Evanston, IL 60201
Knudson, Robert A., Marine Biological Laboratory, Woods Hole, MA 02543
Knide, Samuel S., Population Council, The Rockefeller University, 1230 York Avenue, New York, NY 10021
Kornberg, Sir Hans, The Master's Lodge, Christ's College, Cambridge CB2 3BU, England, UK
Kosower, Edward M., Ramat-Aviv, Tel Aviv, 69978 Israel
Krahl, M. E., 2783 W. Casas Circle, Tucson, AZ 85741
Krane, Stephen M., Arthritis Unit, Massachusetts General Hospital, Fruit Street, Boston, MA 02114
Krauss, Robert, FASEB, 9650 Rockville Pike, Bethesda, MD 20814

Kravitz, Edward A., Department of Neurobiology, Harvard Medical School, 220 Longwood Ave., Boston, MA 02115
Kriebel, Mahlon E., Department of Physiology, SUNY Health Science Center, Syracuse, NY 13210
Kristan, William B., Jr., Department of Biology B-022, University of California San Diego, La Jolla, CA 92093
Kropinski, Andrew M. B., Department of Microbiology/Immunology, Queen's University, Kingston, Ontario K7L 3N6, Canada
Kuhns, William J., Hospital for Sick Children, Department of Biochemistry Research, Toronto, Ontario M5G 1X8, Canada
Kuhtreiber, Willem M., Marine Biological Laboratory, Woods Hole, MA 02543
Kusano, Kiyoshi, NIH, Bldg. 36, Room 4D-20, Bethesda, MD 20892
Kuzirian, Alan M., Marine Biological Laboratory, Woods Hole, MA 02543

Laderman, Aimlee, Yale University School of Forestry, New Haven, CT 06511
LaMarche, Paul H., Eastern Maine Medical Center, 489 State St., Bangor, ME 04401
Landis, Dennis M. D., Department of Developmental Genetics and Anatomy, Case Western Reserve University School of Medicine, Cleveland, OH 44106
Landowne, David, Department of Physiology, P. O. Box 016430, University of Miami School of Medicine, Miami, FL 33101
Langford, George M., Department of Biological Sciences, Dartmouth College, 6044 Gilman Laboratory, Hanover, NH 03755
Lasser-Ross, Nechama, Department of Physiology, New York Medical College, Valhalla, NY 10595
Laster, Leonard, University of Massachusetts Medical School, 55 Lake Avenue, North, Worcester, MA 01655
Laufer, Hans, Department of Biological Science, Molecular and Cell Biology, Group U-125, University of Connecticut, Storrs, CT 06268
Lazarow, Paul B., Department of Cell Biology and Anatomy, Mount Sinai Medical School, Box 1007, 5th Avenue & 100th Street, New York, NY 10021
Lazarus, Maurice, Federated Department Stores, Inc., Sears Cresent, City Hall Plaza, Boston, MA 02108
Leadbetter, Edward R., Department of Molecular and Cell Biology, U-131, University of Connecticut, Storrs, CT 06268
Lederberg, Joshua, The Rockefeller University, 1230 York Ave., New York, NY 10021
Lee, John J., Department of Biology, City College of CUNY, Convent Ave. and 138th St., New York, NY 10031
Lehy, Donald B., Marine Biological Laboratory, Woods Hole, MA 02543
Leibovitz, Louis, 3 Kettle Hole Road, Woods Hole, MA 02543
Leighton, Joseph, 2324 Lakeshore Avenue, #2, Oakland, CA 94606
Leighton, Stephen, NIH, Bldg. 13 3W13, Bethesda, MD 20892
Leinwand, Leslie Ann, Department of Microbiology and Immunology, Albert Einstein College of Medicine, 1300 Morris Park Ave., Bronx, NY 10461
Lerman, Sidney, Eye Research Lab, Room 41, New York Medical College, 100 Grasslands Ave., Valhalla, NY 10595
Lerner, Aaron B., Yale University, School of Medicine, New Haven, CT 06510
Lester, Henry A., 156-29 California Institute of Technology, 156-29, Pasadena, CA 91125
Levin, Jack, Veterans Administration Medical Center, 113A, 4150 Clement St., San Francisco, CA 94121
Levinthal, Francoise, Department of Biology, Columbia University, Fairchild Bldg., Room 1013, New York, NY 10026
Levitan, Herbert, Department of Zoology, University of Maryland, College Park, MD 20742
Levitan, Irwin B., Department of Biochemistry, Brandeis University, Waltham, MA 02254
Linck, Richard W., Department of Anatomy, Jackson Hall, University of Minnesota, 321 Church Street, S. E., Minneapolis, MN 55455
Lipicky, Raymond J., Department of Cardio-Renal/Drug Prod. Div., FDA, Rm. 16B-45, 5600 Fishers Lane, Rockville, MD 20857
Lisman, John E., Department of Biology, Brandeis University, Waltham, MA 02254
Liuzzi, Anthony, 55 Fay Rd., Box 184, Woods Hole, MA 02543
Llinás, Rodolfo R., Department of Physiology and Biophysics, New York University Medical Center, 550 First Ave., New York, NY 10016
Loew, Franklin M., Tufts University School of Veterinary Medicine, 200 Westboro Rd., N. Grafton, MA 01536
Loewenstein, Birgit R., Department of Physiology and Biophysics, R-430, University of Miami School of Medicine, Miami, FL 33101
Loewenstein, Werner R., Department of Physiology and Biophysics, University of Miami, P. O. Box 016430, Miami, FL 33101
London, Irving M., Massachusetts Institute of Technology, E-25-551, Cambridge, MA 02139
Longo, Frank J., Department of Anatomy, University of Iowa, Iowa City, IA 52442
Lorand, Laszlo, Department of Biochemistry and Molecular Biology, Northwestern University, 2153 Sheridan Road, Evanston, IL 60208
Luckenbill-Edds, Louise, 155 Columbia Ave., Athens, OH 45701

Macagno, Eduardo R., 1003B Fairchild, Department of Biosciences, Columbia University, New York, NY 10027
MacNichol, E. F., Jr., Department of Physiology, Boston University School of Medicine, 80 E. Concord St., Boston, MA 02118
Maglott-Duffield, Donna R., American Type Culture Collection, 12301 Parklawn Drive, Rockville, MD 20852-1776
Maienschein, Jane Ann, Department of Philosophy, Arizona State University, Tempe, AZ 85287-2004
Mainer, Robert, The Boston Company, One Boston Place, OBP-15-D, Boston, MA 02168
Malbon, Craig Curtis, Department of Pharmacology, Health Sciences Center, SUNY, Stony Brook, NY 11794-8651
Manalis, Richard S., Department of Biological Sciences, Indiana University—Purdue University at Fort Wayne, 2101 Coliseum Blvd., E. Fort Wayne, IN 46805
Mangum, Charlotte P., Department of Biology, College of William and Mary, Williamsburg, VA 23185
Manz, Robert D., Helmer and Associates, Suite 1310, 950 Winter St., Walthan, MA 02154
Margulis, Lynn, Botany Department, University of Massachusetts, Morrill Science Center, Amherst, MA 01003
Marinucci, Andrew C., 102 Nancy Drive, Mercerville, NJ 08619
Marsh, Julian B., Department of Biochemistry and Physiology, Medical College of Pennsylvania, 3300 Henry Ave., Philadelphia, PA 19129
Martin, Lowell V., Marine Biological Laboratory, Woods Hole, MA 02543
Martinez, Jr., Joe L., Department of Psychology, University of California, Berkeley, 3210 Tolman Hall, Berkeley, CA 94720
Martinez-Palomo, Adolfo, Seccion de Patologia Experimental, Cinvesav-ipn, 07000 Mexico, D.F. A.P., 140740, Mexico
Maser, Morton, Woods Hole Education Assoc., P. O. Box EM, Woods Hole, MA 02543
Mastroianni, Luigi, Jr., Department of Obstetrics and Gynecology, Hospital of the University of Pennsylvania, 106 Dulles, 3400 Spruce Street, Philadelphia, PA 19104-4283
Matteson, Donald R., Department of Biophysics, University of Maryland School of Medicine, 660 Redwood Street, Baltimore, MD 21201

Mautner, Henry G., Department of Biochemistry, Tufts University School of Medicine, 136 Harrison Ave., Boston, MA 02111
Mauzerall, David, The Rockefeller University, 1230 York Ave., New York, NY 10021
McCann, Frances, Department of Physiology, Dartmouth Medical School, Hanover, NH 03755
McLaughlin, Jane A., Marine Biological Laboratory, Woods Hole, MA 02543
McMahon, Robert F., Department of Biology, Box 19498, University of Texas, Arlington, TX 76019
Meedel, Thomas, Marine Biological Laboratory, Woods Hole, MA 02543
Meinertzhagen, Ian A., Department of Psychology, Life Sciences Center, Dalhousie University, Halifax, Nova Scotia B3H 451, Canada
Meiss, Dennis E., 462 Soland Avenue, Hayward, CA 94541
Melillo, Jerry A., Ecosystems Center, Marine Biological Laboratory, Woods Hole, MA 02543
Mellon, DeForest, Jr., Department of Biology, Gilmer Hall, University of Virginia, Charlottesville, VA 22903
Mellon, Richard P., P. O. Box 187, Laughlintown, PA 15655
Metuzals, Janis, Department of Pathology, University of Ottawa, Ottawa, Ontario, K1H 8M5 Canada
Metz, Charles B., 7220 SW 124th St., Miami, FL 33156
Miledi, Ricardo, Department of Psychobiology, University of California, Irvine, CA 92717
Milkman, Roger, Department of Biology, University of Iowa, Iowa City, IA 52242
Miller, Andrew L., Marine Biological Laboratory, Woods Hole, MA 02543
Mills, Robert, 10315 44th Avenue, W 12 H Street, Bradenton, FL 33507-1535
Misevic, Gradimir, Department of Research, University Hospital of Basel, Mebelstrasse 20, CH-4031, Basel, Switzerland
Mitchell, Ralph, DAS, Harvard University, 29 Oxford Street, Cambridge, MA 02138
Miyakawa, Hiroyoshi, Department of Physiology, Yamagata University School of Medicine, Yamagata 990-23, 7990-23 Japan
Miyamoto, David M., Department of Biology, Drew University, Madison, NJ 07940
Mizell, Merle, Laboratory of Tumor Cell Biology, Tulane University, New Orleans, LA 70118
Moore, John W., Department of Neurobiology, Box 3209, Duke University Medical Center, Durham, NC 27710
Moore, Lee E., Department of Physiology and Biophysics, University of Texas Medical Branch, Galveston, TX 77550
Morin, James G., Department of Biology, University of California, Los Angeles, CA 90024
Morrell, Frank, Department of Neurological Science, Rush Medical Center, 1753 W. Congress Parkway, Chicago, IL 60612
Morse, M. Patricia, Marine Science Center, Northeastern University, Nahant, MA 01908
Morse, Robert W., Box 574, N. Falmouth, MA 02556 (resigned)
Morse, Stephen Scott, The Rockefeller University, 1230 York Ave., Box 2, New York, NY 10021-6399
Mote, Michael I., Department of Biology, Temple University, Philadelphia, PA
Mountain, Isabel, Virginia #112, 6251 Old Dominion Drive, McLean, VA 22101
Muller, Kenneth J., Department of Physiology and Biophysics, University of Miami School of Medicine, Miami, FL 33101
Murray, Andrew W., Department of Physiology, University of California, Box 0444, San Francisco, CA 94143-0444
Murray, Sandra Ann, Department of Neurology, Anatomy and Cell Science, University of Pittsburgh School of Medicine, Pittsburgh, PA 15261
Musacchia, Xavier J., Department of Physiology and Biophysics, University of Louisville School of Medicine, Louisville, KY 40292

Nabrit, S. M., 686 Beckwith St., SW, Atlanta, GA 30314
Nadelhoffer, Knute, Marine Biological Laboratory, Woods Hole, MA 02543
Naka, Ken-ichi, 2-9-2 Tatsumi Higashi, Okazaki, Japan 444
Nakajima, Shigehiro, Department of Pharmacology and Cell Biology, University of Illinois College of Medicine at Chicago, 808 S. Wolcott Street, Chicago, IL 60612
Nakajima, Yasuko, Department of Anatomy and Cell Biology, University of Illinois College of Medicine at Chicago, M/C 512, Chicago, IL 60612
Narahashi, Toshio, Department of Pharmacology, Northwestern University Medical School, 303 East Chicago Ave., Chicago, IL 60611
Nasi, Enrico, Department of Physiology, Boston University School of Medicine, R-406, 80 E. Concord St., Boston, MA 02118
Nealson, Kenneth H., Great Lakes Research Center, University of Milwaukee, 600 E. Greenfield Ave., Milwaukee, WI 53204
Nelson, Leonard, Department of Physiology, CS10008, Medical College of Ohio, Toledo, OH 43699
Nelson, Margaret C., Section of Neurobiology and Behavior, Cornell University, Ithaca, NY 14850
Nicholls, John G., Biocenter, Klingelbergstrasse 70, Basel 4056, Switzerland
Nickerson, Peter A., Department of Pathology, SUNY, Buffalo, NY 14214
Nicosia, Santo V., Department of Pathology, University of South Florida, College of Medicine, Box 11, 12901 North 30th St., Tampa, FL 33612
Noe, Bryan D., Department of Anatomy and Cell Biology, Emory University School of Medicine, Atlanta, GA 30322
Northcutt, R. Glenn, Department of Neuroscience, A-001, Scripps Institution of Oceanography, La Jolla, CA 92093-0201
Norton, Catherine N., Marine Biological Laboratory, Woods Hole, MA 02543
Nushaum, Michael P., Neurobiology Research Center, University of Alabama, Birmingham, Wolker Hall, G878S, Birmingham, AL 35294

Obaid, Ana Lia, Department of Physiology and Pharmacy, University of Pennsylvania School of Medicine, B-400 Richards Bldg., Philadelphia, PA 19104-6085
Oertel, Donata, Department of Neurophysiology, University of Wisconsin, 281 Medical Science Bldg., Madison, WI 53706
O'Herron, Jonathan, 45 Swifts Lane, Darien, CT 06820
Ohki, Shinpei, Department of Biophysical Sciences, SUNY at Buffalo, 224 Cary Hall, Buffalo, NY 14214
Oldenbourg, Rudolf, Marine Biological Laboratory, Woods Hole, MA 02543
Olds, James L., NIH, 911W125, Bldg. 9, Bethesda, MD 20892
Olins, Ada L., University of Tennessee-Oak Ridge, Graduate School of Biomedical Sciences, Biology Division ORNL, P. O. Box 2009, Oak Ridge, TN 37831-8077
Olins, Donald E., University of Tennessee-Oak Ridge, Graduate School of Biomedical Sciences, Biology Division ORNL, P. O. Box 2009, Oak Ridge, TN 37831-8077
O'Melia, Anne F., 16 Evergreen Lane, Chappaqua, New York 10514
Oschman, James L., 31 Whittier Street, Dover, NH 03820

Palazzo, Robert E., Marine Biological Laboratory, Woods Hole, MA 02543
Palmer, John D., Department of Zoology, University of Massachusetts, Amherst, MA 01002

Palti, Yoram, Rappaport Institution, Technion, POB 9697, Haifa, 31096 Israel

Pant, Harish C., NINCDS/NIH, Laboratory of Neurochemistry, Bldg. 36, Roonr 4D-20, Bethesda, MD 20892

Pappas, George D., Department of Anatomy, College of Medicine, University of Illinois, 808 South Wolcott St., Chicago, IL 60612

Pardee, Arthur B., Department of Pharmacology, Harvard Medical School, Boston, MA 02115

Pardy, Roosevelt L., School of Life Sciences, University of Nebraska, Lincoln, NE 68588

Parmentier, James L., Becton Dickinson Research Center, P. O. Box 12016, Research Triangle Park, NC 27709

Passano, Leonard M., Department of Zoology, Birge Hall, University of Wisconsin, Madison, WI 53706

Pearlman, Alan L., Department of Physiology, School of Medicine, Washington University, St. Louis, MO 63110

Pederson, Thoru, Worcester Foundation for Experimental Biology, Shrewsbury, MA 01545

Perkins, C. D., 400 Hilltop Terrace, Alexandria, VA 22301

Person, Philip, Research Testing Labs, Inc., 167 E. 2nd St., Huntington Station, NY 11746

Peterson, Bruce J., Ecosystems Center, Marine Biological Laboratory, Woods Hole, MA 02543

Pethig, Ronald, School of Electronic Engineering Science, University College of N. Wales, Dean St., Bangor, Gwynedd, LL57 IUT, UK

Pfohl, Ronald J., Department of Zoology, Miami University, Oxford, OH 45056

Pierce, Robert W., 4851 Shore Lane, P. O. Box 1404, Boca Grande, FL 33921

Pierce, Sidney K., Jr., Department of Zoology, University of Maryland, College Park, MD 20742

Poindexter, Jeanne S., Science Division, Long Island University, Brooklyn Campus, Brooklyn, NY 11201

Pollard, Harvey B., NIH, NIDDKD, Bldg. 8, Rm. 401, Bethesda, MD 20892

Pollard, Thomas D., Department of Cell Biology and Anatomy, Johns Hopkins University, 725 North Wolfe St., Baltimore, MD 21205

Poole, Alan F., Academy of Natural Sciences of Philadelphia, 19th and the Parkway, Philadelphia, PA 19103

Porter, Beverly H., 13617 Glenoble Drive, Rockville, MD 20853

Porter, Keith R., Department of Biology, Leidy Laboratories, Rm. 303, University of Pennsylvania, Philadelphia, PA 19104-6018

Porter, Mary E., Department of Cell Biology and Neurology, University of Minnesota, 4-147 Jackson Hall, Minneapolis, MN 55455

Potter, David, Department of Neurobiology, Harvard Medical School, Longwood Avenue, Boston, MA 02115

Potts, William T., Department of Biology, University of Lancaster, Lancaster, England, UK

Powers, Dennis A., Hopkins Marine Station, Stanford University, Pacific Grove, CA 93950

Powers, Maureen K., Department of Psychology, Vanderbilt University, Nashville, TN 37240

Pratt, Melanie M., Department of Anatomy and Cell Biology, University of Miami School of Medicine (R124), P. O. Box 016960, Miami, FL 33101

Prendergast, Robert A., Wilmer Institute, Johns Hopkins Hospital, 601 N. Broadway, Baltimore, MD 21205

Presley, Phillip H., Carl Zeiss, Inc., 1 Zeiss Drive, Thornwood, NY 10594

Price, Carl A., Waksman Institute of Microbiology, Rutgers University, P. O. Box 759, Piscataway, NJ 08854

Prior, David J., Department of Biological Sciences, NAU Box 5640, Northern Arizona University, Flagstaff, AZ 86011

Prusch, Robert D., Department of Life Sciences, Gonzaga University, Spokane, WA 99258

Purves, Dale, Department of Neurobiology, Duke University Medical School, Box 3209, Durham, NC 27710

Quigley, James, Department of Pathology, SUNY Health Science Center, BHS Tower 9, Rm. 140, Stony Brook, NY 11794

Rabb, Irving W., 1010 Memorial Drive, Cambridge, MA 02138

Rabin, Harvey, DuPont Co., CRD, Exp. Station 328/358, Wilmington, DE 19880

Rabinowitz, Michael B., Marine Biological Laboratory, Woods Hole, MA 02543

Rafferty, Nancy S., Department of Anatomy, Northwestern University Medical School, 303 E. Chicago Avenue, Chicago, IL 60611

Rakowski, Robert F., Department of Physiology and Biophysics, UHS/The Chicago Medical School, 3333 Greenbay Rd., N. Chicago, IL 60064

Ramon, Fidel, Dept. de Fisiologia y Biofisca, Centro de Investigacion y de Estudius Avanzados del ipn, Apurtado Postal 14-740, D.F. 07000, Mexico

Ranzi, Silvio, Sez Zoologia Sc Nat, Via Coloria 26, 120133, Milano, Italy

Rastetter, Edward B., Ecosystems Center, Marine Biological Laboratory, Woods Hole, MA 02543

Rebhun, Lionel I., Department of Biology, Gilmer Hall, University of Virginia, Charlottesville, VA 22901

Reddan, John R., Department of Biological Sciences, Oakland University, Rochester, MI 48309-4401

Reese, Barbara F., NINCDS/NIH, Bldg. 36, Room 3B26, 9000 Rockville Pike, Bethesda, MD 20892

Reese, Thomas S., NINCDS/NIH, Bldg. 36, Room 2A27, 9000 Rockville Pike, Bethesda, MD 20892

Reiner, John M., 111 Emerson St., Apt. 623, Denver, CO 80218 (deceased)

Reinisch, Carol L., Tufts University School of Veterinary Medicine, 136 Harrison Avenue, Boston, MA 02111

Reynolds, George T., Department of Physics, Jadwin Hall, Princeton University, Princeton, NJ 08544

Rich, Alexander, Department of Biology, Massachusetts Institute of Technology, Cambridge, MA 02139

Rickles, Frederick R., Department of Medicine, Division of Hematology-Oncology, University of Connecticut Health Center, Farmington, CT 06032

Riley, Monica, Marine Biological Laboratory, Woods Hole, MA 02543

Ripps, Harris, Department of Ophthalmology, University of Illinois College of Medicine, 1855 W. Taylor Street, Chicago, IL 60611

Ritchie, Murdoch, Department of Pharmacology, Yale University School of Medicine, 333 Cedar St., New Haven, CT 06510

Robinson, Denis M., 200 Ocean Lane Drive #908, Key Biscayne, FL 33149

Rome, Lawrence C., Department of Biology, University of Pennsylvania, Philadelphia, PA 19104

Rosenbaum, Joel L., Department of Biology, Kline Biology Tower, Yale University, New Haven, CT 06520

Rosenberg, Philip, School of Pharmacy, Division of Pharmacology, University of Connecticut, Storrs, CT 06268 (resigned)

Rosenbluth, Jack, Department of Physiology, New York University School of Medicine, 550 First Ave., New York, NY 10016

Rosenbluth, Raja, Department of Biological Sciences, Simon Fraser University, Burnaby, BC, V5A 1S6, Canada

Roslansky, John, Box 208, Woods Hole, MA 02543

Roslansky, Priscilla F., Box 208, Woods Hole, MA 02543

Ross, William N., Department of Physiology, New York Medical College, Valhalla, NY 10595

Roth, Jay S., 18 Millfield Street, P. O. Box 285, Woods Hole, MA 02543

Rowland, Lewis P., Neurological Institute, 710 West 168th St., New York, NY 10032

Ruderman, Joan V., Department of Anatomy and Cell Biology, Harvard University School of Medicine, Boston, MA 02115

Rushforth, Norman B., Department of Biology, Case Western Reserve University, Cleveland, OH 44106

Russell-Hunter, W. D., Department of Biology, Lyman Hall 012, Syracuse University, Syracuse, NY 13244

Saffo, Mary Beth, Institute of Marine Sciences, 272 Applied Sciences, University of California, Santa Cruz, CA 95064

Sager, Ruth, Dana Farber Cancer Institute, 44 Binney St., Boston, MA 02115

Sagi, Amir, Department of Biological Chemistry, Hebrew University, Jerusalem 91904, Israel

Salama, Guy, Department of Physiology, University of Pittsburgh, Pittsburgh, PA 15261

Salmon, Edward D., Department of Biology, Wilson Hall, CB3280, University of North Carolina, Chapel Hill, NC 27599

Salzberg, Brian M., Department of Physiology, University of Pennsylvania, B-400 Richards Bldg., Philadelphia, PA 19104-6085

Sanborn, Richard C., 11 Oak Ridge Road, Teaticket, MA 02536

Sanger, Jean M., Department of Anatomy, School of Medicine, University of Pennsylvania, 36th and Hamilton Walk, Philadelphia, PA 19174

Sanger, Joseph, Department of Anatomy, School of Medicine, University of Pennsylvania, 36th and Hamilton Walk, Philadelphia, PA 19174

Sattelle, David B., AFRC Unit-Department of Zoology, University of Cambridge, Downing St., Cambridge CB2 3EJ, England, UK

Saunders, John W., Jr., P. O. Box 381, Waquoit Station, Waquoit, MA 02536

Saz, Arthur K., Department of Immunology, Georgetown University Medical School, Washington, DC 20007

Schachman, Howard K., Department of Molecular Biology, University of California, Berkeley, CA 94720

Schatten, Gerald P., Integrated Microscopy Facility for Biomedical Research, University of Wisconsin, 1117 W. Johnson St., Madison, WI 53706

Schatten, Heide, Department of Zoology, University of Wisconsin, Madison, WI 53706

Schiff, Jerome A., Institute for Photobiology of Cells and Organelles, Brandeis University, Waltham, MA 02254

Schmeer, Arline C., Mercenene Cancer Research Institute, Hospital of Saint Raphael, New Haven, CT 06511

Schmidek, Henry H., Henry Ford Neurosurgical Institute, Henry Ford Hospital, Detroit, MI 48202

Schnapp, Bruce J., Department of Physiology, Boston University Medical School, 80 East Concord Street, Boston, MA 02118

Schneider, E. Gayle, Department of Obstetrics and Gynecology, Yale University School of Medicine, 333 Cedar St., New Haven, CT 06510 (dropped)

Schuel, Herbert, Department of Anatomical Sciences, SUNY, Buffalo, Buffalo, NY 14214

Schuetz, Allen W., School of Hygiene and Public Health, Johns Hopkins University, Baltimore, MD 21205 (dropped)

Schwartz, James H., Center for Neurobiology and Behavior, New York State Psychiatric Institute—Research Annex, 722 W. 168th St., 7th Floor, New York, NY 10032

Schweitzer, Andrea Nicola, Laboratory of Parasitic Diseases, NIH, NIAID, Bldg. 4, Room 126, Bethesda, MD 20892

Scofield, Virginia Lee, Department of Microbiology and Immunology, UCLA School of Medicine, Los Angeles, CA 90024

Sears, Mary, P. O. Box 152, Woods Hole, MA 02543

Segal, Sheldon J., The Population Council, One Dag Hammarskjold Plaza, New York, NY 10036

Selman, Kelly, Department of Anatomy, College of Medicine, University of Florida, Gainesville, FL 32601

Shanklin, Douglas R., Department of Pathology, Room 584, University of Tennessee College of Medicine, 800 Madison Avenue, Memphis, TN 38163

Shapiro, Herbert, 6025 North 13th St., Philadelphia, PA 19141 (deceased)

Shashoua, Victor E., Ralph Lowell Labs, Harvard Medical School, McLean Hospital, 115 Mill St., Belmont, MA 02178

Shaver, Gaius R., Ecosystems Center, Marine Biological Laboratory, Woods Hole, MA 02543

Shaver, John R., 18 Las Parras, Cayey, PR 00633

Sheetz, Michael P., Department of Cell Biology and Physiology, Washington University Medical School, 606 S. Euclid Ave., St. Louis, MO 63110

Shepard, David C., P. O. Box 44, Woods Hole, MA 02543

Shepro, David, Department of Microvascular Research, Boston University, 5 Cummington St., Boston, MA 02215

Sher, F. Alan, Immunology and Cell Biology Section, NIAID/NIH, Laboratory of Parasitic Disease, Building 5, Room 114, Bethesda, MD 20892 (resigned)

Sheridan, William F., Biology Department, University of North Dakota, Box 8238, University Station, Grand Forks, ND 58202-8238

Sherman, I. W., Department of Biology, University of California, Riverside, CA 92521

Shimomura, Osamu, Marine Biological Laboratory, Woods Hole, MA 02543

Siegel, Irwin M., Department of Ophthalmology, New York University Medical Center, 550 First Avenue, New York, NY 10016

Siegelman, Harold W., Department of Biology, Brookhaven National Laboratory, Upton, NY 11973

Silver, Robert B., Department of Physiology, Cornell University, 822 Veterinary Research Tower, Ithaca, NY 14853-6401

Siwicki, Kathleen K., Biology Department, Swarthmore College, 500 College Ave., Swarthmore, PA 19081

Sjodin, Raymond A., Department of Biophysics, University of Maryland, Baltimore, MD 21201

Skinner, Dorothy M., Oak Ridge National Laboratory, P. O. Box 2009, Biology Division, Oak Ridge, TN 37831

Sloboda, Roger D., Department of Biological Sciences, Dartmouth College, Hanover, NH 03755

Sluder, Greenfield, Worcester Foundation for Experimental Biology, 222 Maple Ave., Shrewsbury, MA 01545

Smith, Michael A., Jl Sinabung, Buntu #7, Semarang, Java, Indonesia (dropped)

Smith, Peter J. S., Marine Biological Laboratory, Woods Hole, MA 02543

Smith, Ralph I., Department of Zoology, University of California, Berkeley, CA 94720

Smith, Stephen J., Department of Molecular & Cellular Physiology, Stanford University School of Medicine, Stanford, CA 94305-5426

Smolowitz, Roxanne M., Laboratory of Marine Animal Health, Marine Biological Laboratory, Woods Hole, MA 02543

Sogin, Mitchell, Marine Biological Laboratory, Woods Hole, MA 02543

Sorenson, Martha M., Depto de Bioquimica-RFRJ, Centro de Ciencias da Saude-I. C. B., Cidade Universitaria-Fundad, Rio de Janeiro, Brasil 21.910

Speck, William T., Department of Pediatrics, Case Western Reserve University, Cleveland, OH 44106

Spector, Abraham, College of Physicians and Surgeons, Columbia University, 630 West 168th Street, New York, NY 10032
Speer, John W., Marine Biological Laboratory, Woods Hole, MA 02543
Speksnijder, Johanna E., Department of Experimental Zoology, University of Utrecht, Padualaan 8 3584 CH Utrecht, The Netherlands
Sperelakis, Nicholas, Department of Physiology & Biophysics, University of Cincinnati, Cincinnati, OH 45267-0576
Spiegel, Evelyn, Department of Biological Sciences, Dartmouth College, Hanover, NH 03755
Spiegel, Melvin, Department of Biological Sciences, Dartmouth College, Hanover, NH 03755
Spray, David C., Albert Einstein College of Medicine, Department of Neurosciences, 1300 Morris Park Avenue, Bronx, NY 10461
Steele, John Hyslop, Woods Hole Oceanographic Institution, Woods Hole, MA 02543
Steinacker, Antoinette, Dept. of Otolaryngology, Washington University, School of Medicine, Box 8115, 4566 Scott Avenue, St. Louis, MO 63110
Steinberg, Malcolm, Department of Biology, Princeton University, Princeton, NJ 08540
Stephens, Raymond E., Marine Biological Laboratory, Woods Hole, MA 02543 (resigned)
Stemmer, Andreas C., MRC Laboratory of Molecular Biology, Hills Rd., Cambridge CB2 2QH, England
Stetten, Jane Lazarow, 4701 Willard Ave., Chevy Chase, MD 20815
Steudler, Paul A., Ecosystems Center, Marine Biological Laboratory, Woods Hole, MA 02543
Stokes, Darrell R., Department of Biology, Emory University, Atlanta, GA 30322
Stommel, Elijah W., Marine Biological Laboratory, Woods Hole, MA 02543
Stracher, Alfred, Department of Biochemistry, SUNY Health Science Center, 450 Clarkson Ave., Brooklyn, NY 11203
Strehler, Bernard L., 2310 Laguna Circle Dr., Agoura, CA 91301-2884
Strickler, J. Rudi, Center for Great Lakes Studies, 600 East Greenfield Ave., Milwaukee, WI 53204
Strumwasser, Felix, Marine Biological Laboratory, Woods Hole, MA 02543
Stuart, Ann E., Department of Physiology, Medical Sciences Research Wing 206H, University of North Carolina, Chapel Hill, NC 27599-7545
Sugimori, Mutsuyuki, Department of Physiology and Biophysics, New York University Medical Center, 550 First Avenue, New York, NY 10016
Summers, William C., Huxley College of Environmental Studies, Western Washington University, Bellingham, WA 98225
Suprenant, Kathy A., Department of Physiology and Cell Biology, 4010 Haworth Hall, University of Kansas, Lawrence, KS 66045
Sussman, Maurice, 72 Carey Lane, Falmouth, MA 02540
Sussman, Raquel B., Marine Biological Laboratory, Woods Hole, MA 02543
Sweet, Frederick, Box 8064, Washington University School of Medicine, 499 South Euclid, St. Louis, MO 63110
Sydlik, Mary Anne, Department of Biology, Geneseo, SUNY, Geneseo, NY 14454
Szent-Györgyi, Andrew, Department of Biology, Brandeis University, Bassine 244, 415 South Street, Waltham, MA 02254
Szuts, Ete Z., Laboratory of Sensory Physiology, Marine Biological Laboratory, Woods Hole, MA 02543

Tabares, Lucia, AVDA. Department of Physiology, Sanchez, Pizjuan 4, 411009 Seville, Spain
Tamm, Sidney L., Boston University Marine Program, Marine Biological Laboratory, Woods Hole, MA 02543 (dropped)
Tanzer, Marvin L., Department of Oral Biology, Medical School, University of Connecticut, Farmington, CT 06032
Tasaki, Ichiji, Laboratory of Neurobiology, NIMH/NIH, Bldg. 36, Rm. 2B-16, Bethesda, MD 20892
Taylor, Douglass L., Center for Fluorescence Research, Carnegie Mellon University, 440 Fifth Avenue, Pittsburgh, PA 15213
Teal, John M., Department of Biology, Woods Hole Oceanographic Institution, Woods Hole, MA 02543
Telfer, William H., Department of Biology, University of Pennsylvania, Philadelphia, PA 19104
Telzer, Bruce, Department of Biology, Pomona College, Claremont, CA 91711
Thorndike, W. Nicholas, Wellington Management Company, 28 State St., Boston, MA 02109
Townsel, James G., Department of Physiology, Meharry Medical College, Nashville, TN 37208
Travis, D. M., Veterans Administration Medical Center, 2101 Elm Street, Fargo, ND 58102
Treistman, Steven N., Worcester Foundation for Experimental Biology, 222 Maple Avenue, Shrewsbury, MA 01545
Trigg, D. Thomas, 125 Grove St., Wellesley, MA 02181
Trinkaus, J. P., Department of Biology, Box 6666, Yale University, New Haven, CT 06511
Troll, Walter, Department of Environmental Medicine, College of Medicine, New York University, New York, NY 10016
Troxler, Robert F., Department of Biochemistry, School of Medicine, Boston University, 80 East Concord St., Boston, MA 02118
Tucker, Edward B., Department of Natural Sciences, Baruch College, CUNY, 17 Lexington Ave., New York, NY 10010
Turner, Ruth D., Mollusk Department, Museum of Comparative Zoology, Harvard University, Cambridge, MA 02138
Tweedell, Kenyon S., Department of Biological Sciences, University of Notre Dame, Notre Dame, IN 46656
Tykocinski, Mark L., Institute of Pathology, Case Western Reserve University, 2085 Adelbert Rd., Cleveland, OH 44106
Tytell, Michael, Department of Anatomy, Bowman Gray School of Medicine, Wake Forest University, Winston-Salem, NC 27103

Ueno, Hiroshi, Department of Medical Chemistry, Osaka Medical College, 2-7 Daigaku-machi, Takatsuki, Osaka 569, Japan

Valiela, Ivan, Boston University Marine Program, Marine Biological Laboratory, Woods Hole, MA 02543
Vallee, Richard, Cell Biology Group, Worcester Foundation for Experimental Biology, Shrewsbury, MA 01545
Valois, John, Marine Biological Laboratory, Woods Hole, MA 02543
Van Holde, Kensal, Department of Biochemistry and Biophysics, Oregon State University, Corvallis, OR 97331-6503
Vogel, Steven S., LBM, NIDDK/NIH, Bldg. 10, Rm. 9B04, Bethesda, MD 20894

Waksman, Byron, Foundation for Microbiology, 300 East 54th St., New York, NY 10022
Wall, Betty, 9 George St., Woods Hole, MA 02543
Wallace, Robin A., Whitney Laboratory, 9505 Ocean Shore Blvd., St. Augustine, FL 32086
Wang, Ching Chung, Department of Pharmaceutical Chemistry, University of California, San Francisco, CA 94143
Wang, Hsien-yu, Department of Biochemistry, National Defense Medical Center, Taipei, Taiwan, Republic of China
Wangh, Lawrence J., Department of Biology, Brandeis University, 415 South St., Waltham, MA 02254

Warner, Robert C., Department of Molecular Biology and Biochemistry, University of California, Irvine, CA 92717
Warren, Kenneth S., Maxwell Communications Corp., 866 Third Avenue, New York, NY
Warren, Leonard, Wistar Institute, 36th and Spruce Streets, Philadelphia, PA
Waterbury, John B., Department of Biology, Woods Hole Oceanographic Institution, Woods Hole, MA 02543
Watson, Stanley, Associates of Cape Cod, Inc., P. O. Box 224, Woods Hole, MA 02543
Waxman, Stephen G., Department of Neurology, LCI 708, Yale School of Medicine, 333 Cedar Street, New Haven, CT 06510
Webb, H. Marguerite, Marine Biological Laboratory, Woods Hole, MA 02543
Weber, Annemarie, Department of Biochemistry and Biophysics, School of Medicine, University of Pennsylvania, Philadelphia, PA 19066
Weidner, Earl, Department of Zoology and Physiology, Louisiana State University, Baton Rouge, LA 70803
Weiss, Dieter G., Institut fur Zoologie, Technische Universitat Munchen, 8046 Garching, FRG
Weiss, Leon P., Department of Animal Biology, School of Veterinary Medicine, University of Pennsylvania, Philadelphia, PA 19104
Weissmann, Gerald, New York University Medical Center, 550 First Avenue, New York, NY 10016
Werman, Robert, Neurobiology Unit, The Hebrew University, Jerusalem, Israel
Westerfield, R. Monte, The Institute of Neuroscience, University of Oregon, Eugene, OR 97403
Whittaker, J. Richard, Marine Biological Laboratory, Woods Hole, MA 02543
Wilson, Darcy B., Medical Biology Institute, 11077 North Torrey Pines Road, La Jolla, CA 92037
Wilson, T. Hastiogs, Department of Physiology, Harvard Medical School, Boston, MA 02115
Witkovsky, Paul, Department of Ophthalmology, New York University Medical Center, 550 First Ave., New York, NY 10016
Wittenberg, Beatrice, Department of Physiology & Biophysics, Albert Einstein College of Medicine, Bronx, NY 10461
Wittenberg, Jonathan B., Department of Physiology and Biophysics, Albert Einstein College, 1300 Morris Park Ave., Bronx, NY 01461
Wolfe, Ralph, Department of Microbiology, 131 Burrill Hall, University of Illinois, Urbana, IL 61801 (resigned)
Wolken, Jerome J., Department of Biological Sciences, Carnegie Mellon University, 440 Fifth Ave., Pittsburgh, PA 15213
Wonderlin, William F., Department of Pharmacology & Toxicology, West Virginia University, Morgantown, WV 26506
Worden, Mary Kate, Department of Neurobiology, Harvard Medical School, 220 Longwood Ave., Boston, MA 02115
Worgul, Basil V., Department of Ophthalmology, Columbia University, 630 West 168th St., New York, NY 10032
Wu, Chau Hsiung, Department of Pharmacology, Northwestern University Medical School, Chicago, IL 60611
Wyttenbach, Charles R., Department of Physiology and Cell Biology, University of Kansas, Lawrence, KS 66045

Yashphe, Jacob, Mevasseret Zion A, 11 Yasmin St., P. O. Box 1150, Jerusalem, Israel
Yeh, Jay Z., Department of Pharmacology, Northwestern University Medical School, Chicago, IL 60611

Zigman, Seymour, School of Medicine and Dentistry, University of Rochester, 260 Crittenden Blvd., Rochester, NY 14620
Zigmond, Richard E., Center for Neurosciences, School of Medicine, Case Western Reserve University, Cleveland, OH 44106 (resigned)
Zimmerberg, Joshua J., NIH, Bldg. 12A, Room 2007, Bethesda, MD 20892
Zottoli, Steven J., Department of Biology, Williams College, Williamstown, MA 01267
Zucker, Robert S., Neurobiology Division, Department of Molecular and Cellular Biology, University of California, Berkeley, CA 94720
Zukin, Ruth Suzanne, Department of Neuroscience, Albert Einstein College of Medicine, 1300 Morris Park Ave., Bronx, NY 10461

Associate Members

Ackroyd, Dr. Frederick W.
Adams, Dr. Paul
Adelberg, Mrs. Edward A.
Ahearn, Mr. and Mrs. David
Albers, Mr. Henry
Alden, Mr. John M.
Allard, Mrs. Constance M.
Allard, Dr. Dean C., Jr.
Allen, Ms. Camilla K.
Allen, Dr. Nina S.
Allison, Mr. and Mrs. Douglas F.
Amon, Mr. Carl H., Jr.
Anderson, Mr. [illegible]egory
Anderson, Drs. [illegible] and Helene M.
Anderson, Mr. and Mr[illegible]neca
Andrews, Dr. Edwin J.
Antonucci, Dr. Robert V.
Aristide, Ms. Tracy
Armstrong, Dr. and Mrs. Richard A.
Armstrong, Dr. and Mrs. Samuel C.
Arnold, Mrs. Lois
Arvin, Ms. Kara L.
Ashworth, Mr. and Mrs. Henry
Aspinwall, Mr. and Mrs. Duncan
Atwood, Dr. and Mrs. Kimball C., III
Ayers, Mrs. Elizabeth
Backus, Ms. Nell
Bagley, Mr. Everett E.
Baker, Mrs. C. L.
Ball, Mrs. Eric G.
Ball, Mrs. Grace Snavely
Ballantine, Mrs. Elizabeth E.
Bang, Mrs. Betsy G.
Bang, Ms. Molly
Banks, Ms. Jamie
Banks, Mr. and Mrs. William L.
Barlow, Mr. and Mrs. R. Chaning
Barlow, Dr. and Mrs. Robert B. Jr.
Barrows, Mrs. Mary Prentice
Bator, Ms. Frances B.
Baum, Mr. Richard T.
Baylor, Drs. Edward and Martha
Beckman, Mrs. Barbara
Beers, Mrs. Dorothy
Belesir, Mr. Tasos
Bennett, Drs. Michael and Ruth
Berg, Mr. and Mrs. C. John
Bernheimer, Drs. Alan W. and Harriet P.
Bernstein, Mr. and Mrs. Norman
Bicker, Mr. Alvin
Bigelow, Mr. and Mrs. Robert O.
Bihrle, Dr. William
Bird, Mr. William R.
Bishop, Mrs. John
Bissonnette, Mrs. Carol L.
Bleck, Dr. Thomas P.
Blumenfeld, Dr. Olga
Boche, Mr. Robert D.
Bodeen, Mr. and Mrs. George H.
Boettiger, Dr. and Mrs. Edward G.
Boettiger, Ms. Julie
Bolton, Mr. and Mrs. Thomas C.
Bonn, Mr. Theodore A.
Borg, Dr. and Mrs. Alfred F.
Borgese, Dr. and Mrs. Thomas
Bowles, Dr. and Mrs. Francis P.
Bradley, Dr. and Mrs. Charles C.
Bradley, Mr. Richard
Brown, Ms. Cornelia
Brown, Mrs. Jennie P.
Brown, Mr. James
Brown, Mrs. Neil
Brown, Mr. and Mrs. T. A.
Brown, Dr. and Mrs. Thornton
Brown, Mr. Walter B.
Browne, Dr. John M.
Broyles, Dr. Robert H.
Buck, Dr. and Mrs. John B.
Buckely, Mr. George D.
Bunts, Mr. and Mrs. Frank E.
Burghauser, Dr. Alan H.
Burwell, Dr. and Mrs. E. Langdon

Butler, Dr. Dore
Buxton, Mr. and Mrs. Bruce E.
Buxton, Mr. E. Brewster
Cadwalader, Mr. George
Calkins, Mr. G. N., Jr.
Campbell, Mrs. David G.
Canney, Ms. Paula
Carlson, Dr. and Mrs. Francis
Carlton, Mr. and Mrs. Winslow G.
Case, Mrs. Barbara L.
Case, Mrs. Patricia A.
Chandler, Mr. Robert
Chase, Mr. Thomas H.
Chevalier, Mr. Randall H.
Child, Dr. and Mrs. Frank M., III
Chisholm, Dr. Sallie W.
Claff, Mr. and Mrs. Mark
Clark, Dr. and Mrs. Arnold M.
Clark, Mr. and Mrs. Hays
Clark, Mr. James McC.
Clark, Mr. and Mrs. John
Clark, Mr. and Mrs. Leroy, Jr.
Clark, Dr. Peter L.
Clark, Mrs. Roberta
Clarke, Dr. Barbara J.
Clement, Mrs. Octavia
Cloud, Dr. Laurence P.
Clowes Fund, Inc.
Clowes, Dr. and Mrs. Alexander W.
Clowes, Mr. Allen W.
Clowes, Mrs. Margaret
Cobb, Dr. Jewel P.
Coburn, Mr. and Mrs. Lawrence H.
Cohen, Dr. and Mrs. Seymour S.
Coleman, Drs. John and Annette
Collum, Mrs. Peter
Collier, Mr. Christopher
Colt, Dr. LeBaron C., Jr.
Connell, Mr. and Mrs. W. J.
Cook, Dr. and Mrs. Joseph
Cook, Dr. and Mrs. Paul W., Jr.
Copel, Mrs. Marcia N.
Copeland, Dr. and Mrs. D. Eugene
Copeland, Mr. Frederick C.
Copeland, Mr. and Mrs. Preston S.
Corbett, Mr. James J.
Costello, Mrs. Helen M.
Coughlin, Dr. John F.
Cowan, Mr. and Mrs. James F., III
Cowan, Ms. Stacy
Cowling, Mr. John
Cowling, Dr. Vincent
Crabb, Mr. and Mrs. David L.
Crain, Mr. and Mrs. Melvin C.
Cramer, Mr. and Mrs. Ian D. W.
Crane, Mrs. Sylvia E.
Crane, Josephine B., Foundation
Crane, Mr. Thomas S.
Crosby, Miss Carol
Cross, Mr. and Mrs. Norman C.
Crossley, Miss Dorothy
Crossley, Miss Helen
Crowell, Dr. and Mrs. Sears
Currier, Mr. and Mrs. David L.
Daignault, Mr. and Mrs. Alexander T.
Daniels, Mr. and Mrs. Bruce G.
Davidson, Dr. Morton
Davis, Mr. and Mrs. Joel P.
Day, Mr. and Mrs. Pomeroy
Decker, Dr. Raymond F.
DeMello, Mr. John
DiBerardino, Dr. Marie A.
DiCecca, Dr. and Mrs. Charles A.
Dickson, Dr. William A.
Dierolf, Dr. Shirley H.
Donnette, Mr. and Mrs. Joseph
Donovan, Mr. David L.
Dorman, Dr. and Mrs. Craig
Douglas, Ms. Jean
Dreyer, Mrs. Mary R.
Droban, Ms. Suzanne
Drummey, Mr. and Mrs. Charles E.
Drummey, Mr. Todd A.
DuBois, Dr. and Mrs. Arthur B.
Dudley, Dr. Patricia
Dugan, Mr. and Mrs. William P.
Duplaix, Dr. Nicole
DuPont, Mr. A. Felix, Jr.
Dutton, Mr. and Mrs. Roderick L.
Ebert, Dr. and Mrs. James D.
Egloff, Dr. and Mrs. F. R. L.
Eliott, Mr. Raymond
Engles, Mr. and Mrs. George
Enos, Mr. Edward, Jr.
Eppel, Dr. and Mrs. Dudley
Epstein, Mr. and Mrs. Ray L.
Estabrooks, Mr. Gordon C.
Eustis, Mr. and Mrs. Jack
Evans, Mr. and Mrs. Dudley
Farley, Miss Joan E.
Farmer, Miss Mary
Farnham, Ms. Elizabeth
Faull, Mr. J. Horace, Jr.
Fausch, Mr. and Mrs. David
Ferguson, Dr. and Mrs. James J., Jr.
Fisher, Mrs. Bruce C.
Fisher, Mr. and Mrs. Frederick S., III
Fisher, Dr. and Mrs. Saul H.
Fluck, Dr. Richard A.
Folino, Mr. John W., Jr.
Forbes, Mr. John M.
Ford, Mr. John H.
Fowlkes, Mr. Aaron
Francis, Mr. Lewis W., Jr.
Frenkel, Dr. Krystyna
Fribourgh, Dr. James H.
Friendship Fund
Frosch, Dr. and Mrs. Robert A.
Funkhouser, Dr. John J.
Fye, Mrs. Paul M.
Gabriel, Dr. and Mrs. Mordecai L.
Gagnon, Mr. Michael
Gaiser, Mrs. Mary Jewett
Gallagher, Mr. Robert O.
Garcia, Dr. Ignacio
Garfield, Miss Eleanor
Gault, Ms. Christine
Gellis, Dr. and Mrs. Sydney
Gephard, Mr. Stephen
Gerhard, Ms. Sylvia K.
German, Dr. and Mrs. James L., III
Gewecke, Mr. and Mrs. Thomas H.
Gifford, Mr. and Mrs. Cameron F.
Gifford, Dr. and Mrs. Prosser
Gilbert, Drs. Daniel L. and Claire
Gildea, Dr. Margaret C. L.
Gillette, Mr. and Mrs. Robert S.
Glad, Mr. Robert
Glass, Dr. and Mrs. H. Bentley
Glazebrook, Mr. James G.
Glazebrook, Mrs. Rebeckah D.
Glenn, Mr. Gary
Gmeiner, Mr. and Mrs. John
Goldman, Mrs. Mary L.
Goldring, Mr. Michael P.
Goldstein, Dr. and Mrs. Moise H., Jr.
Goodgal, Dr. Sol H.
Goodwin, Mr. and Mrs. Charles
Gould, Miss Edith
Grace, Miss Priscilla B.
Grant, Mrs. Rose
Grassle, Mr. and Mrs. John
Greene, Mrs. Davis Crane
Greenberg, Noah and Mosher, Diane
Greer, Mr. and Mrs. W. H., Jr.
Griffin, Mrs. Robert W.
Griffith, Dr. and Mrs. B. Herold
Grosch, Dr. and Mrs. Daniel S.
Gross, Mrs. Mona
Gunning, Mr. and Mrs. Robert A.
Haakonsen, Dr. Harry O.
Hadamard, Dr. Antoine F.
Haigh, Mr. and Mrs. Richard H.
Hall, Mr. Peter A.
Hall, Mr. Warren C.
Halvorson, Dr. and Mrs. Harlyn O.
Hamstrom, Miss Mary Elizabeth
Harrington, Mr. Robert B.
Harrington, Mr. Robert D., Jr.
Harvey, Dr. and Mrs. Richard B.
Hassett, Mr. and Mrs. Charles
Hastings, Dr. and Mrs. J. Woodland
Hathaway, Ms. Elizabeth E.
Haubrich, Dr. Robert R.
Hay, Mr. John
Hays, Dr. David S.
Hayward, Mr. and Mrs. Gary G.
Heaney, Mr. John D.
Hedberg, Mrs. Frances M.
Hedberg, Dr. Mary
Hersey, Mrs. Jane M.
Hiatt, Dr. and Mrs. Howard
Hibbitt, Mrs. H. D.
Hichar, Dr. Barbara
Hill, Mrs. Bertha V.
Hirschfeld, Mrs. Eleanor M.
Hobbie, Dr. and Mrs. John
Hocker, Mr. and Mrs. Lon
Hodge, Dr. and Mrs. Stuart
Hodosh, Mrs. Helen
Hokin, Mr. Richard
Holmes, Mrs. George
Hornor, Mr. Townsend
Horwitz, Dr. and Mrs. Norman H.
Hoskin, Dr. and Mrs. Francis C. G.
Hough, Mr. John T.
Houston, Mr. and Mrs. Howard E.
Howard, Mrs. Mary Jean
Hoyle, Dr. Merrill C.
Huekle, Mrs. Eleanor L.
Huettner, Dr. and Mrs. Robert J.
Huettner, Ms. Susan A.
Hutchinson, Mr. Alan D.
Hyde, Mrs. Pauline
Hynes, Mr. and Mrs. Thomas J., Jr.
Inoué, Dr. and Mrs. Shinya
Issokson, Mr. and Mrs. Israel
Jackson, Miss Elizabeth B.
Jaffe, Dr. and Mrs. Ernst R.
Janney, Mrs. Mary D.
Jewett, G. F., Foundation
Jewett, Mr. and Mrs. G. F., Jr.
Jewett, Mr. and Mrs. Raymond L.
Jones, Mrs. Barbara W.
Jones, Mr. and Mrs. DeWitt C., III
Jones, Mr. and Mrs. Frederick, II
Jones, Mr. Frederick S., III
Jordan, Dr. and Mrs. Edwin P.
Juterbock, Ms. Barbara J.
Kahn, Dr. Harry S.
Kaminer, Dr. and Mrs. Benjamin
Kanellopoulos, Mrs. Barbara
Kanwisher, Mrs. Joan T.
Karplus, Mrs. Alan K.
Karush, Mrs. Sally
Katz, Mrs. Marcella
Kavaru, Dr. Madhav
Kelleher, Mr. and Mrs. Paul R.
Kendall, Mr. and Mrs. Richard E.

Keosian, Mrs. Jessie
Keoughan, Miss Patricia E
Ketchum, Mrs. Nancy
Kirschenbaum, Mrs
Kissam, Mr. and M
M.
Kivy, Dr
Koller, Dr.
Korgen, Dr
Kracl, M
Kravitz, Dr and Mrs. Edward A.
Kroll, Dr. Peter
Kuffler, Mrs. Phyllis
Kutner, Dr. Lawrence
LaVigne, Mrs. Margaret M.
Laderman, Mr. Ezra and Dr. Aimlee
Lafferty, Ms. Nancy
Lahner, Mrs. Alta S.
Lakian, Mr. and Mrs. John
Larmon, Mr. Jay
Lash, Ms. Rebecca
Laster, Dr. and Mrs. Leonard
Latham, Mrs. Eunice
Laufer, Dr. and Mrs. Hans
Laufer, Ms. Jessica, and Weiss, Mr. Malcolm
Laufer, Dr. Marc R.
La Vigne, Mrs. Richard J.
Lawrence, Mr. Frederick V.
Lawrence, Mr. William
Leach, Dr. and Mrs. Berton J.
LeBlond, Mr. and Mrs. Arthur
Leeson, Mr. and Mrs. A. Dix
LeFevre, Dr. Marian E.
Leffler, Dr. Charles W.
Lehman, Miss Robin
Lenher, Dr. and Mrs. Samuel
Leprohon, Mr. Joseph
Levine, Mr. Joseph
Levine, Dr. and Mrs. Rachmiel
Levitz, Dr. Mortimer
Levy, Mr. and Mrs. Stephen R.
Libbin, Mr. Edwin M.
Light, Mr. and Mrs. Donald W.
Lindner, Mr. Timothy P.
Little, Mrs. Barbara C.
Livingstone, Mr. and Mrs. Robert
Lloyd, Mr and Mrs. James E.
Loeb, Mrs
Loessel, Mr
Londergan, M
Lovell, Mr. and M Hollis R.
Lovering, Mr. Ru
Low, Miss Doris I
Lowe, Dr. and Mrs
Mackey, Mr. and Mrs K.
MacLeish, Mrs. Margaret M
MacNary, Mr. B. Glenn
MacNichol, Dr. and Mrs. Edward F., Jr.
Maddigan, Mr. Thomas A.
Magee, Ms. Chris
Maher, Ms. Anne Camille
Mahler, Mrs. Annemarie E.
Mahler, Mrs. Suzanne D.
Maini, Dr. William L.
Maloof, Mr. Sam
Mansworth, Miss Marie
Manual, Dr. Isabelle
Maples, Dr. and Mrs. Philip B.
Marken, Mrs. Madeline
Marsh, Dr. and Mrs. Julian B.
Martyna, Mr. and Mrs. Joseph C.
Mason, Mr. and Mrs. Appleton
Mastroianni, Dr. and Mrs. Luigi, Jr.
Mather, Mr. and Mrs. Frank J., III
Matherly, Mr. and Mrs. Walter
Matthiessen, Dr. and Mrs. G. C.
Mauzerall, Mrs. Miriam J.
McClane, Mrs. Louise
McCusker, Mr. and Mrs. Paul T.
McElroy, Mrs. Nella W.
McGonigle, Mr. Paul
McIlwain, Dr. Susan G.
McMurtrie, Mrs. Cornelia Hanna
Meigs, Mr. and Mrs. Arthur
Meigs, Dr. and Mrs. J. Wister
Melillo, Dr. and Mrs. Jerry A.
Mellon, Mr. and Mrs. Richard P.
Mendelson, Dr. Martin
Metz, Dr. and Mrs. Charles B.
Meyers, Mr. and Mrs. Richard
Milbury, Mr. Edwin van. R.
Miller, Dr. Daniel G.
Miller, Mr. and Mrs. Paul
Mills, Mrs. Margaret A.
Mirro, Dr. Robert
Mixer, Mrs. Florence E.
Mizell, Dr. and Mrs. Merle
Monroy, Mrs. Anna
Montgomery, Dr. and Mrs. Charles H.
Montgomery, Mrs. Mary E.
Moore, Drs. John and Betty
Morgan, Miss Amy
Morse, Mrs. Jane Nolan
Morse, Dr. M. Patricia
Moul, Mrs. Hazel
Munson, Mr. William
Murchelano, Dr. Robert
Murray, Mr. David M.
Myles-Tochko, Drs. Christina J. and John
Nace, Ms. Eleanor M.
Nace, Mr. Paul F., Jr.
Naugle, Mr. John E.
Neall, Mr. William G.
Nelson, Dr. and Mrs. Leonard
Nelson, Dr. Pamela
Netsky, Dr. Martin
Newton, Mr. William E.
Nickerson, Mr. and Mrs. Frank I.
Norman, Mr. and Mrs. Andrew E.
Norman Foundation
Norris, Mr. and Mrs. Barry
Norris, Mr. and Mrs. John A.
Norris, Mr. William
Norton, Mrs. Catherine N.
O'Connell, Dr. and Mrs. Clifford
Offenback, Dr. Jack A.
O'Herron, Mr. and Mrs. Jonathan
Olszowka, Dr. Janice S.
O'Neil, Mr. and Mrs. Barry T.
O'Neil, Mr. Thomas
O'Rand, Mr. and Mrs. Michael
O'Sullivan, Dr. Renee Bennett
Ott, Drs. Philip and Karen
Palmer, Mr. and Mrs. David
Pappas, Dr. and Mrs. George D.
Park, Mr. and Mrs. Malcolm S.
Parkinson, Mr. and Mrs. Robert
Parmenter, Miss Carolyn L.
Parmenter, Dr. Charles
Pearce, Dr. John B.
Pearson, Mrs. Helen M.
Peltz, Dr. and Mrs. William L.
Pendergast, Mrs. Claudia R.
Pendleton, Dr. and Mrs. Murray E.
Peri, Mr. and Mrs. John B.
Perkins, Dr. and Mrs. Courtland D.
Person, Dr. and Mrs. Philip
Peters, Mr. and Mrs. Frederick S
Peterson, Mr. and Mrs. E. Gunnar
Peterson, Mr. and Mrs. E. Joel
Peterson, Mr. Raymond W.
Petty, Mr. Richard F.
Pfeiffer, Mr. and Mrs. John
Pires, Dr. and Mrs. Anthony
Plough, Ms. Frances
Plough, Mr. and Mrs. George H.
Pointe, Mr. Albert
Pointe, Mr. Charles
Porter, Dr. and Mrs. Keith R.
Pothier, Dr. and Mrs. Aubrey, Jr.
Press, Dr. Frank
Proskauer, Mr. Joseph H.
Proskauer, Mr. Richard
Prosser, Dr. and Mrs. C. Ladd
Psaledakis, Mr. Nicholas
Psychoyos, Dr. Alexandre
Putnam, Mr. and Mrs. Allan Ray
Putnam, Mr. and Mrs. William A., III
Rankin, Mrs. Julia S.
Raphael, Ms. Ellen S.
Raymond, Dr. Samuel
Reese, Ms. Bonnie
Regan, Reverend Msgr. John J.
Regis, Ms. A. Kathy
Reingold, Mr. Stephen C.
Reynolds, Mrs. George
Reynolds, Dr. John L.
Reynolds, Mr. and Mrs. Robert M.
Ricca, Dr. and Mrs. Renato A.
Righter, Mr. and Mrs. Harold
Riina, Mr. John R.
Riley, Dr. Monica
Ripple, Mr. and Mrs. John
Ripps, Mrs. Jeanne
Robb, Mrs. Alison A.
Robbins, Ms. Ann
Roberts, Ms. Jean
Roberts, Mr. Mervin F.
Robertson, Mrs. Lola E.
Robinson, Dr. Denis M.
Robinson, Mr. John G.
Robinson, Mr. and Mrs. Marius A.
Roose, Ms. Elayne
Root, Mrs. Pauline
Rosenthal, Ms. Hilde
Roslansky, Drs. John and Priscilla
Ross, Dr. and Mrs. Donald
Ross, Dr. Robert
Ross, Dr. Virginia S.
Roth, Dr. Stephen
Rowan, Mr. Edward
Rowe, Dr. Don
Rowe, Mrs. Martha P.
Rubinow, Mrs. Shirley
Rugh, Mrs. Harriett S.
Ryder, Mr. Francis C.
Sager, Dr. Ruth
Sallet, Mrs. Grace W.
Sallop, Ms. Linda and Fenlon, Mr. Michael
Sanidas, Dr. and Mrs. Dennis J.
Sardinha, Mr. George J.
Saunders, Dr. and Mrs. John W.
Saunders, Mrs. Lawrence
Saunders, Lawrence, Fund
Sawyer, Mr. and Mrs. John E.
Saz, Mrs. Ruth L.
Scheffler, Ms. Astrid
Schlesinger, Dr. and Mrs. R. Walter
Schwamb, Mr. and Mrs. Peter
Schwartz, Dr. Lawrence
Scott, Mrs. Elsie M.
Scott, Mr. and Mrs. Norman E.
Sears, Mr. Clayton C.
Sears, Mr. and Mrs. Harold B.
Sears, Mr. Harold H.
Seaver, Mr. George A.
Seder, Mr. John
Segal, Dr. and Mrs. Sheldon J.
Selby, Dr. Cecily
Seliger-Egelson, Ms. Pauline
Senft, Mrs. Deborah G.
Shanklin, Dr. and Mrs. D. R.
Shapiro, Mr. and Mrs. Howard
Shapley, Dr. Robert
Sharp, Mr. and Mrs. Robert W.
Sheehy, Mr. David
Shemin, Mrs. Charlotte

Shepro, Dr. and Mrs. David
Sheprow, Mrs. Marilyn
Sherblom, Dr. James P.
Sichel, Dr. Enid
Sidie, Dr. James
Siegel, Mr. and Mrs. Alvin
Silver, Mr. and Mrs. Bertram R.
Simmons, Mr. Tim
Simon, Mr. and Mrs. Stephen A.
Singer, Mr. and Mrs. Daniel M.
Smith, Drs. Frederick E. and Marguerite A.
Smith, Mr. and Mrs. Homer P.
Smith, Mrs. Janice R.
Smith, Mr. Van Dorn C.
Snyder, Mr. Robert M.
Solomon, Dr. and Mrs. A. K.
Sonnenblick, Mrs. Perle
Specht, Mr. and Mrs. Heinz
Speck, Dr. William T.
Spiegel, Drs. Melvin and Evelyn
Spotte, Mr. Stephen
Steele, Mrs. M. Evelyn
Steele, Dr. Robert E.
Stein, Mr. Ronald
Steinbach, Mrs. Eleanor
Steingard, Mr. Sol
Stern, Ms. Ann
Stetson, Mrs. Judith G.
Stetten, Dr. Gail
Stetten, Mrs. Jane Lazarow
Stracher, Dr. Dorothy
Stump, Mr. Robert
Sudduth, Dr. William W.
Sussman, Dr. and Mrs. Maurice
Swain, Mr. Albert H.
Swanson, Dr. and Mrs. Carl P.
Swift, Mr. and Mrs. F. Kent
Swope, Mrs. Marjorie P.
Swope, Mr. and Mrs. Gerard L.
Szent-Györgyi, Dr. Andrew
Taber, Mr. George H.
Talamas-Rohana, Dr. Eduardo
Taylor, Mr. James K.
Taylor, Mrs. Jean G.
Tebbetts, Mr. and Mrs. Edwin H.
Tietje, Mr. Emil D., Jr.
Timmins, Mrs. Linda L.
Todd, Mr. and Mrs. Gordon F.
Tolkan, Mr. and Mrs. Norman N.
Trager, Mrs. Ida
Trigg, Mr. and Mrs. D. Thomas
Troll, Dr. and Mrs. Walter
Trousof, Miss Natalie
Tucker, Miss Ruth
Tully, Mr. and Mrs. Gordon F.
Ulbrich, Ms. Ciona
Ulbrich, Mr. and Mrs. Volker
Valois, Mr. and Mrs. John
Vancouver Public Aquarium
Van Buren, Mrs. Alice H.
Van Holde, Mrs. Barbara
Veeder, Mrs. Alice
Veeder, Ms. Susan
Villee, Drs. Claude and Dorothy
Vincent, Mr. and Mrs. Samuel W.
Vincent, Dr. Walter S.
Vonderhaar, Dr. William
Wagner, Mr. Mark
Waksman, Dr. and Mrs. Byron H.
Walter, Mr. and Mrs. Henry
Ward, Dr. Robert T.
Ware, Mr. and Mrs. J. Lindsay
Warren, Dr. Henry B. and Ms. Cornelia Brown
Warren, Mrs. Eve
Watt, Mr. and Mrs. John B.
Weeks, Mr. and Mrs. John T.
Weiffenbach, Dr. and Mrs. George
Weinstein, Miss Nancy B.
Weisberg, Mr. and Mrs. Alfred M.
Weissmann, Dr. and Mrs. Gerald
Wessel, Dr. Gary
Wheeler, Dr. and Mrs. Paul S.
Wheeler, Dr. William M.
Whitehead, Mrs. Barbara
Whitney, Mr. and Mrs. Geoffrey G., Jr.
Wichterman, Dr. and Mrs. Ralph
Wickersham, Mrs. Joan
Wiese, Dr. Konrad
Wigley, Mrs. Roland
Wigley, Ms. Susan
Wilber, Mrs. Clare M.
Wilhelm, Dr. Hazel S.
Willis, Mr. Herbert F.
Wilson, Mr. and Mrs. Leslie J.
Wilson, Dr. and Mrs. T. Hastings
Winn, Dr. William M.
Winsten, Dr. Jay A.
Witting, Miss Joyce
Woitkoski, Miss Nancy
Wolfinsohn, Mrs. Sarah A.
Woodwell, Dr. and Mrs. George M.
Wrigley, Mrs. Roland
Yntema, Mrs. Elizabeth S.
Young, Miss Nina L.
Zimmerli, Mr. and Mrs. Bruce
Zinn, Dr. and Mrs. Donald J.
Zipf, Dr. Elizabeth

Gift Shop Volunteers

Marion Adelberg
Barbara Atwood
Pat Barlow
Harriet Bernheimer
Glorie Borgese
Jennie Brown
Elizabeth Buck
Pat Case
Shirley Chaet
Vera Clark
Peggy Clowes
Jewell Cobb
Villa Crowell
Betsy Daignault
Janet Daniels
Alma Ebert
Ellie Gabriel
Rose Grant
Silvia Green
Edie Grosch
Barbara Grossman
Sandea Hadamard
Jean Halvorson
Elizabeth Hamstrom
Helen Hodosh
Sally Karush
Brookie Ketchum
Ruth Ann Laster
Evelyn Laufer
Barbara Little
Sally Loessell
Vinnie Mackey
Connie Martyna
Mariam Mauzerall
Phyllis Myers
Florence Mixer
Lorraine Mizell
Eleanor Nace
Bertha Person
Margareta Pothier
Elizabeth Price
Kathryn Price
Julia Rankin
Virginia Reynolds
Erika Righter
Elsie Scott
Marilyn Shepro
Fran Silverstein
Marcia Simmons
Cynthia Smith
Peggy Smith
Louise Specht
Jane Stetten
Dorothy Stracher
Natalie Trousof
Mary Ulbrich
Barbara Van Holde
Alice Veeder
Barbara Whitehead
Clare Wilber

MBL Tour Guides

Betsy Bang
John Buck
Sears Crowell
Teru Hayashi
Isabel Mountain
Julie Rankin
Lola Robertson
Donald Zinn
Margery Zinn

Certificate of Organization
Articles of Amendment
Bylaws of the MBL

Certificate of Organization

(On File in the Office of the Secretary of the Commonwealth)

No. 3170

We, Alpheus Hyatt, President, William Stanford Stevens, Treasurer, and William T. Sedgwick, Edward G. Gardiner, Susan Mims and Charles Sedgwick Minot being a majority of the Trustees of the Marine Biological Laboratory in compliance with the requirements of the fourth section of chapter one hundred and fifteen of the Public Statutes do hereby certify that the following is a true copy of the agreement of association to constitute said Corporation, with the names of the subscribers thereto:

We, whose names are hereto subscribed, do, by this agreement, associate ourselves with the intention to constitute a Corporation according to the provisions of the one hundred and fifteenth chapter of the Public Statutes of the Commonwealth of Massachusetts, and the Acts in amendment thereof and in addition thereto.

The name by which the Corporation shall be known is
THE MARINE BIOLOGICAL LABORATORY.

The purpose for which the Corporation is constituted is to establish and maintain a laboratory or station for scientific study and investigations, and a school for instruction in biology and natural history.
The place within which the Corporation is established or located is the city of Boston within said Commonwealth.
The amount of its capital stock is none.
In Witness Whereof, we have hereunto set our hands, this twenty seventh day of February in the year eighteen hundred and eighty-eight, Alpheus Hyatt, Samuel Mills, William T. Sedgwick, Edward G. Gardner, Charles Sedgwick Minot, William G. Farlow, William Stanford Stevens, Anna D. Phillips, Susan Mims, B. H. Van Vleck.
That the first meeting of the subscribers to said agreement was held on the thirteenth day of March in the year eighteen hundred and eighty-eight.
In Witness Whereof, we have hereunto signed our names, this thirteenth day of March in the year eighteen hundred and eighty-eight, Alpheus Hyatt, President, William Stanford, Treasurer, Edward G. Gardiner, William T. Sedgwick, Susan Mims, Charles Sedgwick Minot.
(Approved on March 20, 1888, as follows:
I hereby certify that I have made an examination of the within written certificate and the records of the corporation duly submitted to my inspection, that the requirements of sections one, two, three and four of chapter one hundred and fifteen, and sections eighteen, twenty and twenty-one of chapter one hundred and six, of the Public Statutes, have been complied with, and I hereby approve said certificate this twentieth day of March A.D. eighteen hundred and eighty-eight.

Charles Endicott
Commissioner of Corporations)

Articles of Amendment

(On File in the Office of the Secretary of the Commonwealth)

We, James D. Ebert, President, and David Shepro, Clerk of the Marine Biological Laboratory, located at Woods Hole, Massachusetts 02543, do hereby certify that the following amendment to the Articles of Organization of the Corporation was duly adopted at a meeting held on August 15, 1975, as adjourned to August 29, 1975, by vote of 444 members, being at least two-thirds of its members legally qualified to vote in the meeting of the corporation:

Voted: That the Certificate of Organization of this corporation be and it hereby is amended by the addition of the following provisions:
"No Officer, Trustee or Corporate Member of the corporation shall be personally liable for the payment or satisfaction of any obligation or liabilities incurred as a result of, or otherwise in connection with, any commitments, agreements, activities or affairs of the corporation.
"Except as otherwise specifically provided by the Bylaws of the corporation, meetings of the Corporate Members of the corporation may be held anywhere in the United States.
"The Trustees of the corporation may make, amend or repeal the Bylaws of the corporation in whole or in part, except with respect to any provisions thereof which shall by law, this Certificate or the bylaws of the corporation, require action by the Corporate Members."

The foregoing amendment will become effective when these articles of amendment are filed in accordance with Chapter 180, Section 7 of the General Laws unless these articles specify, in accordance with the vote adopting the amendment, a later effective date not more than thirty days after such filing, in which event the amendment will become effective on such later date.

In Witness whereof and Under the Penalties of Perjury, we have hereto signed our names this 2nd day of September, in the year 1975, James D. Ebert, President; David Shepro, Clerk.
(Approved on October 24, 1975, as follows:
I hereby approve the within articles of amendment and, the filing fee in the amount of $10 having been paid, said articles are deemed to have been filed with me this 24th day of October, 1975.

Paul Guzzi
Secretary of the Commonwealth)

Bylaws of the Corporation of the Marine Biological Laboratory

(Revised August 17, 1990; February 16, 1991; June 30, 1991; and August 16, 1991)

ARTICLE I—THE CORPORATION

A. *Name and Purpose* The name of the Corporation shall be The Marine Biological Laboratory. The Corporation's purpose shall be to establish and maintain

a laboratory or station for scientific study and investigation and a school for instruction in biology and natural history.

B. *Nondiscrimination.* The Corporation shall not discriminate on the basis of age, religion, color, race, national or ethnic origin, sex or sexual preference in its policies on employment and administration or in its educational and other programs.

ARTICLE II—MEMBERSHIP

A. *Members.* The Members of the Corporation ("Members") shall consist of persons elected by the Board of Trustees (the "Board"), upon such terms and conditions and in accordance with such procedures, not inconsistent with law or these Bylaws, as may be determined by the Board. At any regular or special meeting of the Board, the Board may elect new Members. Any Member may vote at any meeting of the Members in person only and not by proxy. Members shall serve until their death or resignation unless earlier removed with or without cause by the affirmative vote of two-thirds of the Trustees then in office. Any Member who has retired from his or her home institution may, upon written request to the Corporation, be designated a Life Member. Life Members shall not have the right to vote and shall not be assessed for dues.

B. *Meetings.* The annual meeting of the Members shall be held on the Friday following the first Tuesday in August of each year, at the Laboratory of the Corporation in Woods Hole, Massachusetts, at 9:30 a.m. The Chairperson of the Board shall preside at meetings of the Corporation. If no annual meeting is held in accordance with the foregoing provision, a special meeting may be held in lieu thereof with the same effect as the annual meeting, and in such case all references in these Bylaws, except in this Article II.B., to the annual meeting of the Members shall be deemed to refer to such special meeting. Members shall transact business as may properly come before the meeting. Special meetings of the Members may be called by the Chairperson or the Trustees, and shall be called by the Clerk, or in the case of the death, absence, incapacity or refusal by the Clerk, by any other officer, upon written application of Members representing at least ten percent of the smallest quorum of Members required for a vote upon any matter at the annual meeting of the Members, to be held at such time and place as may be designated.

C. *Quorum.* One hundred (100) Members shall constitute a quorum at any meeting. Except as otherwise required by law or these Bylaws, the affirmative vote of a majority of the Members voting in person at a meeting attended by a quorum shall constitute action on behalf of the Members.

D. *Notice of Meetings.* Notice of any annual meeting or special meeting of Members, if necessary, shall be given by the Clerk by mailing notice of the time and place and purpose of such meeting at least 15 days before such meeting to each Member at his or her address as shown on the records of the Corporation.

E. *Waiver of Notice.* Whenever notice of a meeting is required to be given a Member, under any provision of the Articles or Organization or Bylaws of the Corporation, a written waiver thereof, executed before or after the Meeting by such Member, or his or her duly authorized attorney, shall be deemed equivalent to such notice.

F. *Adjournments.* Any meeting of the Members may be adjourned to any other time and place by the vote of a majority of those Members present at the meeting, whether or not such Members constitute a quorum, or by any officer entitled to preside at or to act as Clerk of such meeting, if no Member is present or represented. It shall not be necessary to notify any Members of any adjournment unless no Member is present or represented at the meeting which is adjourned, in which case, notice of the adjournment shall be given in accordance with Article II.D. Any business which could have been transacted at any meeting of the Members as originally called may be transacted at an adjournment thereof.

ARTICLE III—ASSOCIATES OF THE CORPORATION

Associates of the Corporation. The Associates of the Marine Biological Laboratory shall be an unincorporated group of persons (including associations and corporations) interested in the Laboratory and shall be organized and operated under the general supervision and authority of the Trustees. The Associates of the Marine Biological Laboratory shall have no voting rights.

ARTICLE IV—BOARD OF TRUSTEES

A. *Powers.* The Board of Trustees shall have the control and management of the affairs of the Corporation. The Trustees shall annually elect a Chairperson of the Board who shall serve until his or her successor is selected and qualified. They shall annually elect a President of the Corporation. They shall annually elect a Vice Chairperson of the Board who shall be Vice Chairperson of the meetings of the Corporation. They shall annually elect a Treasurer. They shall elect a Clerk, who shall be a resident of Massachusetts and shall serve a term of four years. Eligibility for re-election of the Clerk shall be in accordance with the content of this Article IV as applied to Corporate or Board Trustees. They shall elect Trustees-at-Large as specified in this Article IV. They shall appoint a Director of the Laboratory for a term not to exceed five years, provided the term shall not exceed one year, if the candidate has attained the age of 65 years prior to the date of the appointment. They shall choose such other officers and agents as they shall think best. They may fix the compensation of all officers and agents of the Corporation and may remove them at any time. They may fill vacancies occurring in any of the offices. The Board shall have the power to choose an Executive Committee from their own number as provided in Article V, and to delegate to such Committee such of their own powers as they may deem expedient in addition to those powers conferred by Article V. They shall, from time to time, elect Members to the Corporation upon such terms and conditions as they shall have determined, not inconsistent with law or these Bylaws.

B. *Composition and Election.* There shall be four groups of Trustees:

(1) Trustees ("the Corporate Trustees") elected by the Members according to such procedures, not inconsistent with these Bylaws, as the Trustees shall have determined. Except as provided below, such Trustees shall be divided into four classes of six, one class to be elected each year to serve for a term of four years. Such classes shall be designated by the year of expiration of their respective terms.

(2) Trustees ("Trustees-at-Large"). Nominees for Trustees-at-large shall be introduced at the annual meeting of the Corporation for subsequent election by the Board according to such procedures, not inconsistent with these Bylaws, as the Trustees shall have determined. Such Trustees-at-Large shall be divided into four classes of four Trustees, one class to be elected each year to serve for a term of four years. Such classes shall be designated by the year of expiration of their respective terms. It is contemplated that, unless otherwise determined by the Trustees for good reason, Trustees-at-Large, shall be individuals who have not been considered for election as Corporate Trustees.

(3) Trustees *ex officio* shall be the Chairperson, the Vice Chairperson, the President, the Treasurer, the Clerk and the Director of the Laboratory.

(4) Trustees emeriti shall include any Member who has retired from his or her home institution and has requested to serve as a Trustee emeritus provided he or she has served a full elected term as a regular Trustee. A Trustee *ex officio* is eligible to serve as a Trustee emeritus provided he or she has served as Trustee ex officio for at least four years. Trustees *ex officio* and emeriti shall have all the rights of the Trustees, except that Trustees emeriti shall not have the right to vote.

(5) The total number of Corporate Trustees and Trustees-at-Large elected in any year (excluding Trustees elected to fill vacancies which do not result from expiration of a term) shall not exceed ten. The number of Trustees-at-Large so elected shall not exceed four and, unless otherwise determined by vote of the Trustees, the number of Corporate Trustees so elected shall not exceed six. Corporate Trustees shall always constitute a majority on the Board of those elected or approved by the Members.

(6) Newly elected Trustees shall take office at the February meeting of the Board, but may participate in discussions at intervening meetings following their election, without voting rights.

(7) The Trustees and officers shall hold their respective offices until their successors are chosen and qualified.

C. *Eligibility.* A Corporate Trustee or a Trustee-at-Large who has been elected to an initial four-year term or remaining portion thereof, of which he/she has served at least two years, shall be eligible for re-election to a second four-year term, but shall be ineligible for re-election to any subsequent term until two years have elapsed after he/she has last served as a Trustee.

D. *Removal.* Any Trustee may be removed from office at any time with or without cause, by vote of a majority of the Members entitled to vote in the election of Trustees; or for cause, by vote of two-thirds of the Trustees then in office. A Trustee may be removed for cause only if notice of such action shall have been given to all of the Trustees or Members entitled to vote, as the case may be, prior to the meeting at which such action is to be taken and if the Trustee to be so removed shall have been given reasonable notice and opportunity to be heard before the body proposing to remove him or her.

E. *Vacancies.* Any vacancy in the Board, unless and until filled by the Members at any annual or special meeting of the Members, may be filled by vote of a majority of the remaining Trustees present at a meeting of Trustees at which a quorum is present or by appointment of all of the Trustees if less than a quorum shall remain in office.

F. *Meetings.* The annual meeting of the Trustees shall be held promptly after the annual meeting of the Members at the Laboratory in Woods Hole, Massachusetts. Special meetings of the Trustees may be called by the Chairman, the President or by any seven Trustees to be held at such time and place as may be designated. The Chairperson of the Board, when present, shall preside over all meetings of the Trustees. Written notice shall be sent to a Trustee's usual or last known place of

residence at least two weeks bef[illegible]ing. Notice of a meeting need not be given to any Trustee if a writt[illegible]otice executed by such Trustee before or after the meeting is filed [illegible] of the meeting, or if such Trustee shall attend the meeting with[illegible] prior thereto or at its commencement the lack of notice given to [illegible].

G. *Transfers of In[illegible]* There shall be no transfer of title nor long-term lease of rea[illegible] the Corporation without prior approval of not less than two-third[illegible]rustees. Such real property transactions shall be finally acted upon at a meeting of the Board only if presented and discussed at a prior meeting of the Board. Either meeting may be a special meeting and no less than four weeks shall elapse between the two meetings. Any property acquired by the Corporation after December 1, 1989 may be sold with the prior approval of not less than two-thirds of the Trustees (other than any Trustee or Trustees with a direct or indirect financial interest in the transaction being considered for approval) who are present at a regular or special meeting of the Board at which there is a quorum.

ARTICLE V—COMMITTEES

A. *Executive Committee.* The Executive Committee is hereby designated to consist of not more than eleven (11) Trustees, including the *ex officio* Trustees (Chairperson of the Board, Vice Chairperson of the Board, President, Treasurer, and Director of the Laboratory); and six additional Trustees, two of whom shall be elected by the Board each year, to serve for a three-year term.

Newly elected Executive Committee Members shall take office at the February meeting of the Board, but may participate in discussions at intervening meetings following their election, without voting rights.

Beginning with the Members elected for terms ending in 1990, one of the Trustees elected to serve on the Executive Committee shall be a Trustee-at-Large. Beginning with the Members elected for terms ending in 1991, the Trustees will elect, to the Executive Committee, Trustees to ensure that the Committee includes four Corporate Trustees and two Trustees-at-Large.

The Chairperson of the Board shall act as Chairperson of the Executive Committee and the Vice Chairperson as Vice Chairperson. The Executive Committee shall meet at such times and places and upon such notice and appoint such subcommittees as the Committee shall determine.

The Executive Committee shall have and may exercise all the powers of the Board during the intervals between meetings of the Board except those powers specifically withheld, from time to time, by vote of the Board or by law. The Executive Committee may also appoint such committees, including persons who are not Trustees, as it may, from time to time, approve to make recommendations with respect to matters to be acted upon by the Executive Committee or the Board.

The Executive Committee shall keep appropriate minutes of its meetings, which shall be reported to the Board. Any actions taken by the Executive Committee shall also be reported to the Board.

The elected Members of the Executive Committee shall constitute a Standing Committee for the Nomination of Officers, responsible for making nominations at each annual meeting of the Members and of the Board for candidates to fill each office as the respective terms of office expire (Chairperson of the Board, Vice Chairperson of the Board, President, Treasurer, Clerk and Director of the Laboratory).

B. *Board Committees Generally.* The Board shall have the power, by vote of a majority of the Trustees in attendance at the meeting, to elect an Investment Committee, a Nominating Committee and any other committee and, by like vote, to delegate thereto some or all of the powers of the Board except those which by law, the Articles of Organization or these Bylaws they are prohibited from delegating. The members of any such committee shall have such tenure and duties as the Trustees shall determine. The Investment Committee, which shall oversee the management of the Corporation's endowment funds and marketable securities shall include as *ex officio* members, the Chairperson of the Board, the Treasurer and the Chairperson of the Audit Committee, together with such Trustees as may be required for not less than two-thirds of the Investment Committee to consist of Trustees. Except as oth[illegible]rovided by these Bylaws or determined by the Trustees, any such committee [illegible] rules for the conduct of its business, but, unless otherwise provided by the [illegible]n such rules, its business shall be conducted as nearly as possible in the [illegible]er as is provided by these Bylaws for the Trustees.

C. *Actions Without a Meeting.* [illegible] required or permitted to be taken at any meeting of the Executive Com[illegible] any other committee elected by the Trustees may be taken without a meeti[illegible] members of such committees consent to the action in writing and such writte[illegible] consents are filed with the records of meetings. Members of the Executive Committee or any other committee elected by the Trustees may also participate in any meeting by means of a telephone conference call, or otherwise take action in such a manner as may, from time to time, be permitted by law.

D. *Manual of Procedures.* The Board of Trustees, on the recommendation of the Executive Committee, shall establish guidelines and modifications thereof to be recorded in a Manual of Procedures. Guidelines shall establish procedures for: 1) Nomination and election of members of the Corporation, Board of Trustees and Executive Committee; 2) Election of Officers; 3) Formation and Function of Standing Committees.

ARTICLE VI—OFFICERS

A. *Enumeration.* The officers of the Corporation shall consist of a President, a Treasurer and a Clerk, and such other officers having the powers of President, Treasurer and Clerk as the Board may determine, and a Director of the Laboratory. The Corporation may have such other officers and assistant officers as the Board may determine, including (without limitation) a Chairperson of the Board, Vice Chairperson and one or more Vice-Presidents, Assistant Treasurers or Assistant Clerks. Any two or more offices may be held by the same person. An officer need not be a Member or Trustee of the Corporation. If required by the Trustees, any officer shall give the Corporation a bond for the faithful performance of his or her duties in such amount and with such surety or sureties as shall be satisfactory to the Trustees.

B. *Tenure.* Except as otherwise provided by law, by the Articles of Organization or by these Bylaws, the President, Treasurer, and all other officers shall hold office until the first meeting of the Board following the annual meeting of Members and thereafter, until his or her successor is chosen and qualified.

C. *Resignation.* Any officer may resign by delivering his or her written resignation to the Corporation at its principal office or to the President or Clerk and such resignation shall be effective upon receipt unless it is specified to be effective at some other time or upon the happening of some other event.

D. *Removal.* The Board may remove any officer with or without cause by a vote of a majority of the entire number of Trustees then in office, at a meeting of the Board called for that purpose and for which notice of the purpose thereof has been given, provided that an officer may be removed for cause only after having an opportunity to be heard by the Board at a meeting of the Board at which a quorum is personally present and voting.

E. *Vacancy.* A vacancy in any office may be filled for the unexpired balance of the term by vote of a majority of the Trustees present at any meeting of Trustees at which a quorum is present or by written consent of all of the Trustees if less than a quorum of Trustees shall remain in office.

F. *Director.* The Director shall be the chief operating officer and, unless otherwise voted by the Trustees, the chief executive officer of the Corporation. The Director shall, subject to the direction of the Trustees, have general supervision of the Laboratory and control of the business of the Corporation. At the annual meeting, the Director shall submit a report of the operations of the Corporation for such year and a statement of its affairs, and shall, from time to time, report to the Board all matters within his or her knowledge which the interests of the Corporation may require to be brought to its notice.

G. *Deputy Director.* The Deputy Director, if any, or if there shall be more than one, the Deputy Directors in the order determined by the Trustees, shall, in the absence or disability of the Director, perform the duties and exercise the powers of the Director and shall perform such other duties and shall have such other powers as the Trustees may, from time to time, prescribe.

H. *President.* The President shall have the powers and duties as may be vested in him or her by the Board.

I. *Treasurer and Assistant Treasurer.* The Treasurer shall, subject to the direction of the Trustees, have general charge of the financial affairs of the Corporation, including its long-range financial planning, and shall cause to be kept accurate books of account. The Treasurer shall prepare a yearly report on the financial status of the Corporation to be delivered at the annual meeting. The Treasurer shall also prepare or oversee all filings required by the Commonwealth of Massachusetts, the Internal Revenue Service, or other Federal and State Agencies. The account of the Treasurer shall be audited annually by a certified public accountant.

The Assistant Treasurer, if any, or if there shall be more than one, the Assistant Treasurers in the order determined by the Trustees, shall, in the absence or disability of the Treasurer, perform the duties and exercise the powers of the Treasurer, shall perform such other duties and shall have such other powers as the Trustees may, from time to time, prescribe.

J. *Clerk and Assistant Clerk.* The Clerk shall be a resident of the Commonwealth of Massachusetts, unless the Corporation has designated a resident agent in the manner provided by law. The minutes or records of all meetings of the Trustees and Members shall be kept by the Clerk who shall record upon the record book of

the Corporation minutes of the proceedings at such meetings. He or she shall have custody of the record books of the Corporation and shall have such other powers and shall perform such other duties as the Trustees may, from time to time, prescribe.

The Assistant Clerk, if any, or if there shall be more than one, the Assistant Clerks in the order determined by the Trustees, shall, in the absence or disability of the Clerk, perform the duties and exercise the powers of the Clerk and shall perform such other duties and shall have such other powers as the Trustees may, from time to time, prescribe.

In the absence of the Clerk and an Assistant Clerk from any meeting, a temporary clerk shall be appointed at the meeting.

K. *Other Powers and Duties.* Each officer shall have in addition to the duties and powers specifically set forth in these Bylaws, such duties and powers as are customarily incident to his or her office, and such duties and powers as the Trustees may, from time to time, designate.

ARTICLE VII—AMENDMENTS

These Bylaws may be amended by the affirmative vote of the Members at any meeting, provided that notice of the substance of the proposed amendment is stated in the notice of such meeting. As authorized by the Articles of Organization, the Trustees, by a majority of their number then in office, may also make, amend or repeal these Bylaws, in whole or in part, except with respect to the (a) the provisions of these Bylaws governing (i) the removal of Trustees and (ii) the amendment of these Bylaws and (b) any provisions of these Bylaws which by law, the Articles of Organization or these Bylaws, requires action by the Members.

No later than the time of giving notice of meeting of Members next following the making, amending or repealing by the Trustees of any Bylaw, notice thereof stating the substance of such change shall be given to all Members entitled to vote on amending the Bylaws.

Any Bylaw adopted by the Trustees may be amended or repealed by the Members entitled to vote on amending the Bylaws.

ARTICLE VIII—INDEMNITY

Except as otherwise provided below, the Corporation shall, to the extent legally permissible, indemnify each person who is, or shall have been, a Trustee, director or officer of the Corporation or who is serving, or shall have served at the request of the Corporation as a Trustee, director or officer of another organization in which the Corporation directly or indirectly has any interest as a shareholder, creditor or otherwise, against all liabilities and expenses (including judgments, fines, penalties, and reasonable attorneys' fees and all amounts paid, other than to the Corporation or such other organization, in compromise or settlement) imposed upon or incurred by any such person in connection with, or arising out of, the defense or disposition of any action, suit or other proceeding, whether civil or criminal, in which he or she may be a defendant or with which he or she may be threatened or otherwise involved, directly or indirectly, by reason of his or her being or having been such a Trustee, director or officer.

The Corporation shall provide no indemnification with respect to any matter as to which any such Trustee, director or officer shall be finally adjudicated in such action, suit or proceeding not to have acted in good faith in the reasonable belief that his or her action was in the best interests of the Corporation. The Corporation shall provide no indemnification with respect to any matter settled or comprised unless such matter shall have been approved as in the best interests of the Corporation, after notice that indemnification is involved, by (i) a disinterested majority of the Board of the Executive Committee, or (ii) a majority of the Members.

Indemnification may include payment by the Corporation of expenses in defending a civil or criminal action or proceeding in advance of the final disposition of such action or proceeding upon receipt of an undertaking by the person indemnified to repay such payment if it is ultimately determined that such person is not entitled to indemnification under the provisions of this Article VIII, or under any applicable law.

As used in the Article VIII, the terms "Trustee," "director" and "officer" include their respective heirs, executors, administrators and legal representatives, and an "interested" Trustee, director or officer is one against whom in such capacity the proceeding in question or another proceeding on the same or similar grounds is then pending.

To assure indemnification under this Article VIII of all persons who are determined by the Corporation or otherwise to be or to have been "fiduciaries" of any employee benefits plan of the Corporation which may exist, from time to time, this Article VIII shall be interpreted as follows: (i) "another organization" shall be deemed to include such an employee benefit plan, including without limitation, any plan of the corporation which is governed by the Act of Congress entitled "Employee Retirement Income Security Act of 1974," as amended, from time to time, ("ERISA"); (ii) "Trustee" shall be deemed to include any person requested by the Corporation to serve as such for an employee benefit plan where the performance by such person of his or her duties to the Corporation also imposes duties on or otherwise involves services by, such person to the plan or participants or beneficiaries of the plan; (iii) "fines" shall be deemed to include any excise tax plan pursuant to ERISA; and (iv) actions taken or omitted by a person with respect to an employee benefit plan in the performance of such person's duties for a purpose reasonably believed by such person to be in the interest of the participants and beneficiaries of the plan shall be deemed to be for a purpose which is in the best interests of the Corporation.

The right of indemnification provided in this Article VIII shall not be exclusive of or affect any other rights to which any Trustee, director or officer may be entitled under any agreement, statute, vote of Members or otherwise. The Corporation's obligation to provide indemnification under this Article VIII shall be offset to the extent of any other source of indemnification of any otherwise applicable insurance coverage under a policy maintained by the Corporation or any other person. Nothing contained in the Article shall affect any rights to which employees and corporate personnel other than Trustees, directors or officers may be entitled by contract, by vote of the Board or of the Executive Committee or otherwise.

ARTICLE IX—DISSOLUTION

The consent of every Trustee shall be necessary to effect a dissolution of the Marine Biological Laboratory. In case of dissolution, the property shall be disposed of in such a manner and upon such terms as shall be determined by the affirmative vote of two-thirds of the Trustees then in office in accordance with the laws of the Commonwealth of Massachusetts.

ARTICLE X—MISCELLANEOUS PROVISIONS

A. *Fiscal Year.* Except as otherwise determined by the Trustees, the fiscal year of the Corporation shall end on December 31st of each year.

B. *Seal.* Unless otherwise determined by the Trustees, the Corporation may have a seal in such form as the Trustees may determine, from time to time.

C. *Execution of Instruments.* All checks, deeds, leases, transfers, contracts, bonds, notes and other obligations authorized to be executed by an officer of the Corporation in its behalf shall be signed by the Director or the Treasurer except as the Trustees may generally or in particular cases otherwise determine. A certificate by the Clerk or an Assistant Clerk, or a temporary Clerk, as to any action taken by the Members, Board of Trustees or any officer or representative of the Corporation shall as to all persons who rely thereon in good faith be conclusive evidence of such action.

D. *Corporate Record.* The original, or attested copies, of the Articles of Organization, Bylaws and records of all meetings of the Members shall be kept in Massachusetts at the principal office of the Corporation, or at an office of the Corporation's Clerk or resident agent. Said copies and records need not all be kept in the same office. They shall be available at all reasonable times for inspection by any Member for any proper purpose, but not to secure a list of Members for a purpose other than in the interest of the applicant, as a Member, relative to the affairs of the Corporation.

E. *Articles of Organization.* All references in these Bylaws to the Articles of Organization shall be deemed to refer to the Articles of Organization of the Corporation, as amended and in effect, from time to time.

F. *Transactions with Interested Parties.* In the absence of fraud, no contract or other transaction between this Corporation and any other corporation or any firm, association, partnership or person shall be affected or invalidated by the fact that any Trustee or officer of this Corporation is pecuniarily or otherwise interested in or is a director, member or officer of such other corporation or of such firm, association or partnership or in a party to or is pecuniarily or otherwise interested in such contract or other transaction or is in any way connected with any person or person, firm, association, partnership, or corporation pecuniarily or otherwise interested therein; provided that the fact that he or she individually or as a director, member or officer of such corporation, firm, association or partnership in such a party or is so interested shall be disclosed to or shall have been known by the Board of Trustees or a majority of such Members thereof as shall be present at a meeting of the Board of Trustees at which action upon any such contract or transaction shall be taken; any Trustee may be counted in determining the existence of a quorum and may vote at any meeting of the Board of Trustees for the purpose of authorizing any such contract or transaction with like force and effect as if he/she were not so interested, or were not a director, member or officer of such other corporation, firm, association or partnership, provided that any vote with respect to such contract or transaction must be adopted by a majority of the Trustees then in office who have no interest in such contract or transaction.

Reference: *Biol. Bull.* **183:** 70–77. (August, 1992)

High Calcium Zones at the Poles of Developing Medaka Eggs

R. A. FLUCK[2], A. L. MILLER[1], AND L. F. JAFFE[1]

[1]*Marine Biological Laboratory, Woods Hole, Massachusetts 02543 and* [2]*Department of Biology, Franklin & Marshall College, Lancaster, Pennsylvania 17604*

Abstract. We have injected medaka fish zygotes with recombinant aequorin and visualized the resulting patterns of luminescence to reveal patterns of free calcium during early development. We have co-injected fluorescein-labeled aequorin to correct for nonuniformities in aequorin (as opposed to calcium) distributions by visualizing the resulting patterns of fluorescence as opposed to luminescence. We have also coinjected a calcium buffer to facilitate calcium diffusion, dissipate apparent calcium gradients, and thus confirm their reality.

An exploratory study shows zones of elevated free calcium at the vegetal as well as the animal pole during the first day of development and thus up to the beginning of gastrulation. A closer study during the first 6 h, and thus through ooplasmic segregation and early cleavage, shows a steady zone of high calcium at the vegetal pole and a slowly oscillating one at the animal pole. The latter is particularly strong during ooplasmic segregation and cytokinesis. This report contains the first unambiguous evidence of relatively steady zones of high cytosolic calcium during the development of an animal egg.

Introduction

Pattern formation starts at the poles—particularly at the vegetal pole—of animal eggs. One striking example of this general statement is in the ascidian egg. Here the unfertilized egg is so free of pattern that any half will form a tadpole; yet after fertilization and the resultant contraction of the cortex toward a region near the vegetal pole, only vegetal fragments will form tadpoles (Reverberi, 1971; Jeffery, 1984; Speksnijder *et al.*, 1990a). Another example is the frog, in which pattern starts as the mitochondrial cloud, the germ plasm, and one or more potent m-RNAs all attach to the vegetal pole of the very young oocyte; in which the zygote's animal half is still totipotent; and in which early blastula cells derived from the vegetal pole plasm induce formation of both the embryonic mesoderm and the dorsal axis (Capco and Jeffery, 1982; Nieuwkoop, 1985; Wylie *et al.*, 1985; Forristall *et al.*, 1991; Melton, 1991). Yet another example is the *Drosophila* egg, in which early pattern is organized from both poles and in which certain key m-RNAs, as well as the germ plasm, move within the maturing oocyte to the insect equivalent of the vegetal pole (Nüsslein-Volhard and Roth, 1989; Ephrussi *et al.*, 1991).

In all three of these eggs—ascidian, frog, and fly—early patterning involves a striking movement of key materials to, or near, the vegetal pole. In these animal eggs, more is known about these key materials than about the mechanisms that establish this pole and drive them to it; the reverse is true in the fucoid egg. Little is known of the key materials in this plant egg; however there is strong evidence that the establishment of a steady subsurface zone of elevated calcium is essential to the mechanism that establishes the first—in this case rhizoidal—developmental pole. Moreover, such a zone has been directly visualized at a stage when localization of the rhizoidal pole is still reversible (Jaffe, 1990a, b).

The role of high calcium zones in the polarizing fucoid egg suggests that they may play a comparable one in animal eggs. Indeed, there is interesting evidence for just such a role in *Xenopus* oocytes (Robinson, 1979; Larabell and Capco, 1988) as well as in *Drosophila* follicles (Overall and Jaffe, 1985) and in ascidian zygotes (Jeffery, 1982). Moreover, in aequorin-loaded medaka eggs, persistent polar zones of high luminescence were visualized more than six years ago. However their meaning has been uncertain because of the possibility that the aequorin rather than free calcium was concentrated at these eggs' poles

Received 4 February 1992; accepted 18 May 1992.

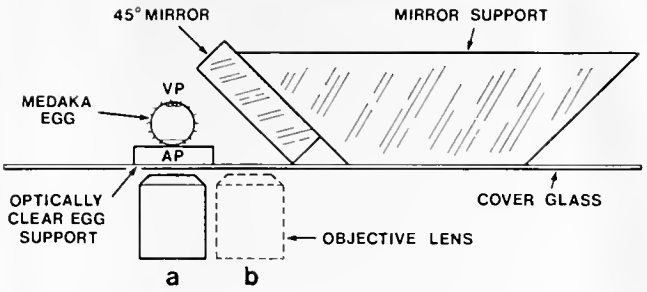

Figure 1. Method of observing an undisturbed medaka egg from either the animal pole (position a) or the side (position b). The stage is moved to attain these two views. VP = vegetal pole; AP = animal pole.

(Jaffe, 1986). In this report we finally show that it is indeed the pattern of free calcium rather than its indicator that creates the observed zones of polar luminescence in such eggs.

Materials and Methods

To obtain gametes, gonads were removed from breeding medaka and placed in a balanced saline solution (BSS: 111 m*M* NaCl; 5.37 m*M* KCl; 1.0 m*M* $CaCl_2$; 0.6 m*M* $MgSO_4$; 5 m*M* HEPES, pH 7.3). To prepare unfertilized eggs for microinjection, we transferred them through five successive washes of Ca^{2+}/Mg^{2+}-free BSS over a period of 1 h. Approximately 1.0 nl of a 0.62% solution of recombinant aequorin (Shimomura *et al.*, 1990) in 100 m*M* KCl, 5 m*M* HEPES, and 0.05 m*M* EDTA was injected equatorially using micropipettes of ≤5 μm tip diameter. To correct for nonuniformities in the distribution of aequorin, we injected other eggs with 1.0 nl of a mixture of 0.45% unmodified recombinant aequorin and 0.15% recombinant that was labeled with one fluorescein per aequorin molecule (Shimomura, 1991). The injection technique employed was Hiramoto's quantitative low-pressure method (Hiramoto, 1962). Details of a procedure used to introduce a micropipette into the thin peripheral cytoplasmic layer of the medaka egg were those described by Gilkey (1983). After microinjection, the eggs were transferred to BSS containing 0.2 m*M* Ca^{2+} for 30 min, transferred to BSS for 30 min, fertilized, transferred to the microscope stage, and observed at 16–17°C.

Two methods were used to observe chorionated eggs. In the first, eggs were placed on a 1-mm thick platform of Dow Corning high vacuum grease and observed in their normal, blastodisc-down orientation with a Zeiss IM-35 inverted microscope, a Nikon Planapo 10/0.45 objective and a 75 mm optical doublet, which together produced a 6× magnified image on the photocathode of an imaging photon detector or IPD made by Imaging Technology Ltd., East Sussex, UK. This device consists of a microchannel plate intensifier with a resistive anode as the positional encoder (Speksnijder *et al.*, 1990b). Eggs were viewed either directly (Fig. 1, lens position "a") or via a mirror (Fig. 1, lens position "b"). The indirect (or side) view enabled us to simultaneously observe both the animal and vegetal poles of the egg. External illumination of the egg for bright field and dark field viewing was achieved with a condenser and a fiber optic cable, respectively. In the second method used to observe the eggs, they were flattened slightly between a coverglass and slide, held with their animal-vegetal axis parallel to the slide, and viewed directly.

To facilitate calcium diffusion and thus dissipate calcium gradients in the ooplasm, we injected eggs with dibromo-BAPTA as follows: a high-pressure system (Medical Systems Corp. PLI-100) was used to microinject 1.5 nl of a solution of dibromo-BAPTA (50 m*M* dibromo-BAPTA; 150 m*M* KCl; 5 m*M* HEPES, pH 7.0) into the equatorial region of an unfertilized egg that had already been injected with aequorin. This egg was then inseminated within 30 s, before the injected buffer had time to block fertilization. [A comparable volume of KCl (150 m*M* KCl; 5 m*M* HEPES, pH 7.0) was injected into control eggs.] If the volume of the ooplasm (except for oil globules) is 46 nl (Fluck, unpub.) and we assume that 60% of the cytosol is water (Bolender, 1978), then we can calculate an accessible ooplasmic volume of 27.6 nl. Thus the dibromo-BAPTA was diluted about 18-fold, to a final concentration in the cytosol of about 2.7 m*M*. At this concentration, this calcium buffer will substantially facilitate the diffusion of Ca^{2+} away from any zones of elevated $[Ca^{2+}]$ which are in the micromolar range (Speksnijder *et al.*, 1989).

The raw data from the IPD system consist of a sequential record of photon positions and times, measured one at a time. This system will record up to around 100,000 photons/s. Because we never encountered more than about 30 photons/s, system saturation was never a problem. Images were generated by accumulating data over any desired interval and representing multiple pho-

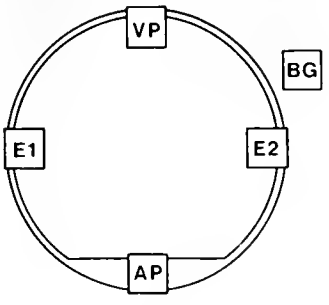

Figure 2. Regions of an aequorin loaded medaka egg's image that were used for a quantitative analysis of its patterns of luminescence and fluorescence. VP = vegetal pole; AP = animal pole; E = equator; BG = background.

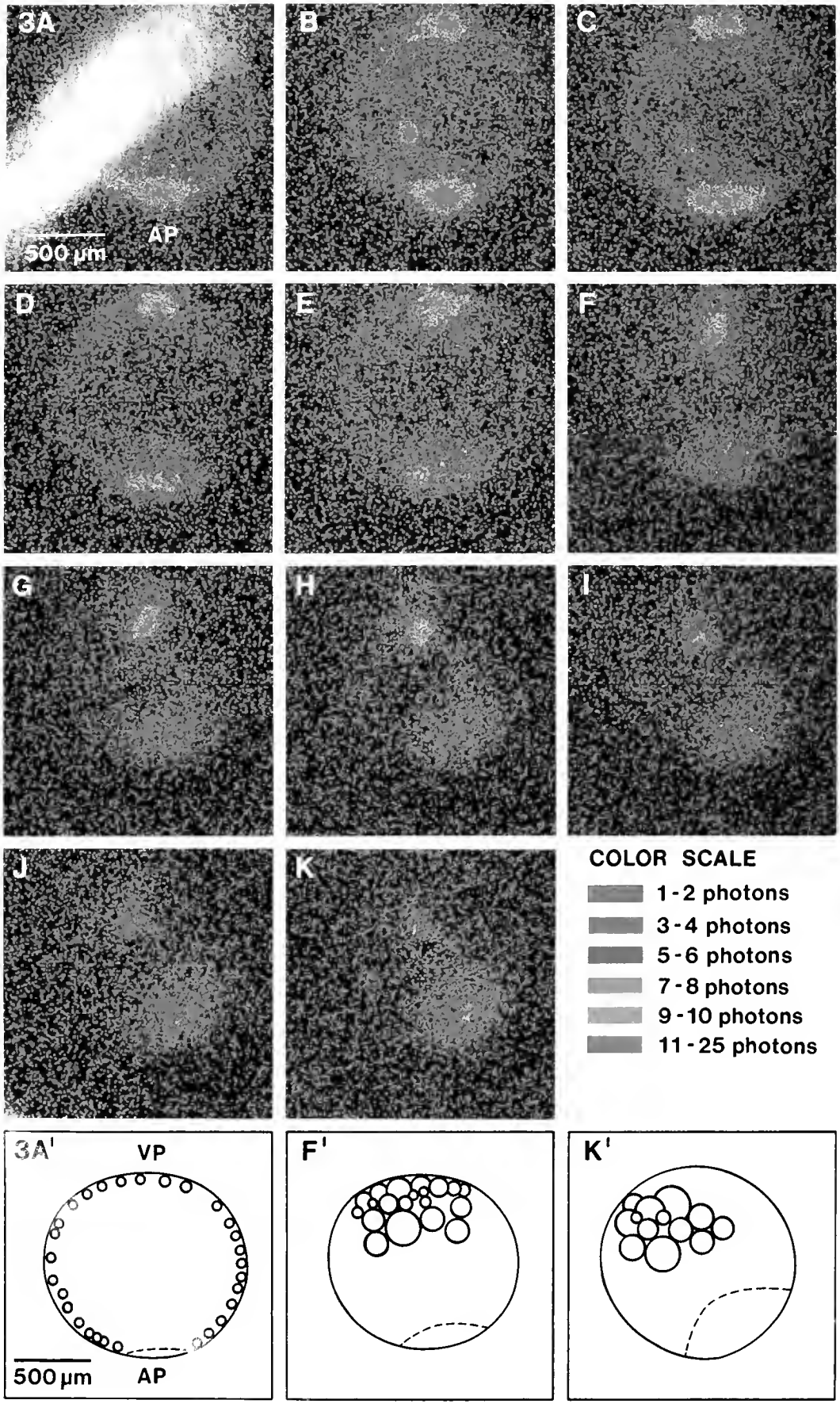
3A
B
C
500 µm
AP
D
E
F
G
H
I
J
K
COLOR SCALE
1-2 photons
3-4 photons
5-6 photons
7-8 photons
9-10 photons
11-25 photons
3A'
VP
500 µm
AP
F'
K'

tons per pixel with a color scale. Photon collection was briefly (10 s) interrupted at appropriate intervals to record brightfield images of the eggs. This allowed us to compare luminescent and brightfield images as the relatively slow processes of ooplasmic segregation and cytokinesis proceeded.

We used the IPD system to observe the fluorescence emitted by fluorescein-labeled aequorin in the eggs. Appropriate excitation filters (two 485 DF22 filters in series) and a 530-DF30 barrier filter were obtained from Omega Optical, Inc. (Brattleboro, Vermont). The latter was supplemented with two Schott OG 530 filters.

Our quantitative analysis consisted of measuring luminescence in 150 μm wide square boxes placed at either the vegetal or animal poles and then dividing these values by the mean of those collected from two similar boxes placed at the equator of the egg (Fig. 2). Each resulting luminescence ratio was divided by a corresponding fluorescence ratio (from fluorescein aequorin) to correct for differences in aequorin concentration. All raw light intensity values were corrected for background.

Results and Discussion

Color Figure 3 displays the pattern of luminescence in a representative aequorin injected medaka egg during the first 22 h of development, up to the early to mid gastrula stage. Striking zones of high luminescence persist at both poles throughout this period.

The blastodisc seems to roughly correspond to the animal zone of high luminescence. However, no known structure corresponds to the remarkable, 150 to 300 μm wide vegetal zone of luminescence. Moreover, we do not yet know if the gradual, overall decline in luminescence during the first day of development represents a slow fall in aequorin or in free calcium concentration. However, the observed pattern of luminescence should somehow represent a natural, developmental pattern because medaka eggs, which are loaded with recombinant aequorin, regularly hatch into swimming fish. While roughly consistent with the preliminary results reported earlier (Jaffe, 1986), these new ones should be more reliable because the natural aequorin used in the older studies somehow inhibited development beyond the blastula stage (Ridgway *et al.*, 1977).

Color Figure 4 displays this pattern during the first 2 h, almost to first cleavage; while Figure 7 provides quantitative information as well as temporal detail from fertilization through the first few cleavages. A strong vegetal zone of luminescence appears as soon as the fertilization wave reaches the vegetal pole and remains relatively constant in both intensity and diameter for at least 6 h. However, a distinct animal zone of luminescence does not appear until well after the fertilization wave has subsided. It then slowly oscillates so as to largely disappear and then reappear three times during the first 6 h. These reappearances presumably represent the slow calcium waves that accompany cytokinesis during the first three cleavages (Fluck *et al.*, 1991).

However, the biological role of the first, precleavage zone of animal pole calcium is less clear. The additional examples displayed in Figure 6 indicate that this precleavage zone is a real one that is present between about 20% and 50% of the period between fertilization and first cleavage. The presence of this precleavage zone of animal pole calcium may be somehow connected to the process of ooplasmic segregation because this process is largely completed while this zone is present. Ooplasmic segregation comprises the roughly simultaneous movement of the oil droplets toward the vegetal pole and of the bulk of the cytoplasm to the animal pole. Both oil droplet movement and the thickening of the blastodisc, which indicates cytoplasmic flow, start at about 20% of the precleavage period and are largely over by 70% of it (Fluck *et al.*, unpublished).

Polar luminescence represents foci of calcium not aequorin

Color Figure 5 displays representative patterns of fluorescence coming from eggs injected with fluorescein-aequorin during the precleavage period. No sign of a vegetal focus of aequorin fluorescence can be seen.

Figure 3. Representative patterns of luminescence from an aequorin-loaded medaka egg during the first day of development. Each colored panel shows the luminescence accumulated during two successive hours. Thus panel 3A shows luminescence accumulated for 2 h starting at 5 min after fertilization; 3B shows the luminescence accumulated from 2 to 4 h; 3C, from 4 to 6 h, etc. Panels 3A′, F′, and K′ show sketches of the slowly rotating egg made from brief transmitted light observations carried out just after the corresponding luminescent images were obtained. The persistent antipodal zones of high luminescence remain at the egg's poles.

The luminescence seen in the left hand hemisphere of 3A represents a faint residue of the intense fertilization wave described by Gilkey *et al.* (1978) and by Yoshimoto *et al.* (1986). It is scarcely seen on the right because the aequorin had not yet fully diffused to the right half at this time. The interpolar spot of decreasing luminescence in the left half of panels 3A–C represents calcium leaking in through the slowly healing injection site. It is wound calcium.

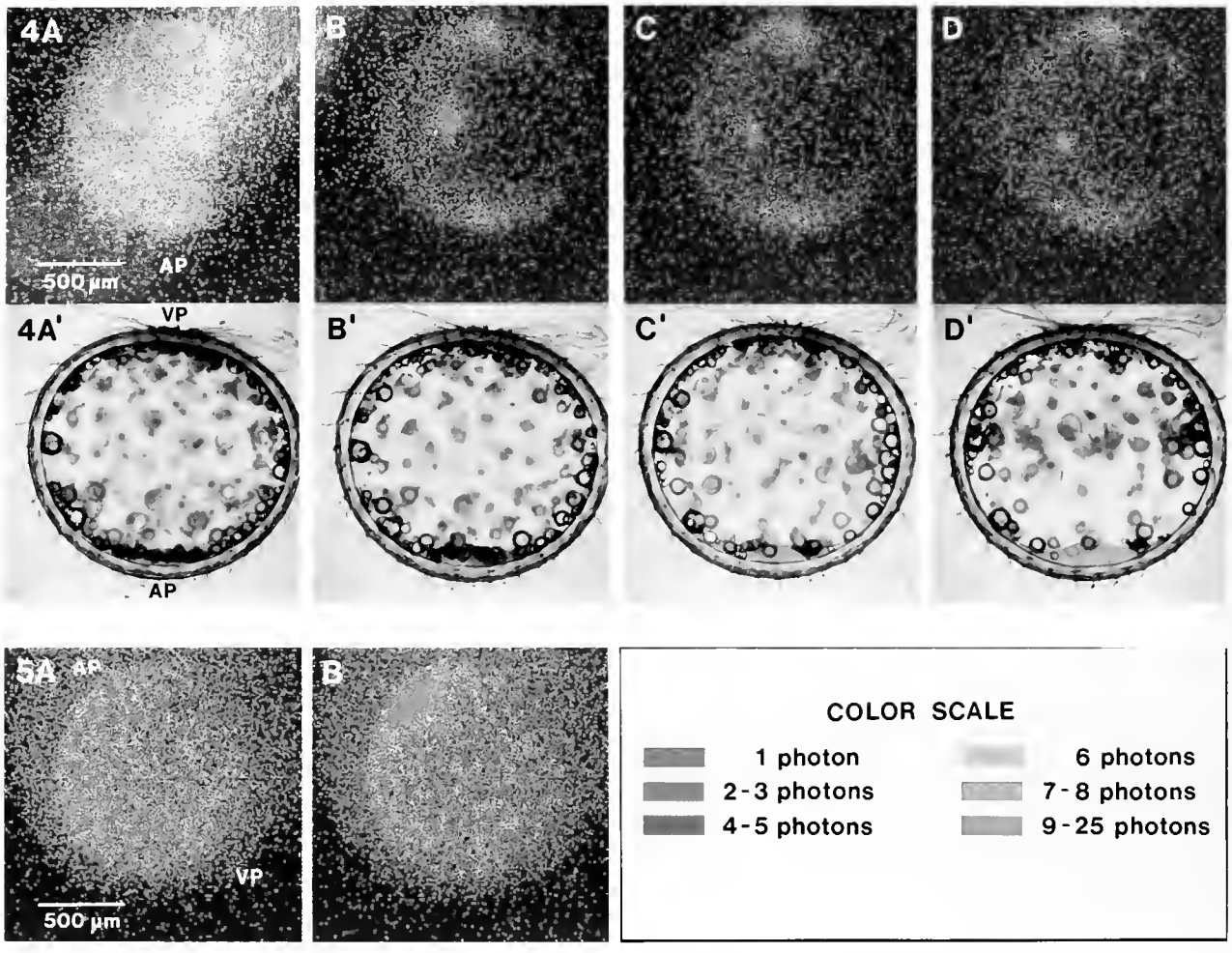

Figure 4. Patterns of luminescence during the first 2 h of development of the same egg shown in Figure 3. Each colored panel represents luminescence accumulated over successive 30-min periods: while each black and white image was obtained via brief transmitted light exposure soon after the corresponding luminescent one. The growing blastodisc's images have been tinted yellow to make them easier to see.

Figure 5. Patterns of fluorescence from a representative medaka egg coinjected with both aequorin and fluorescein-labeled aequorin so as to indicate the distribution of aequorin. A. Observed at 30 min after fertilization, a stage right after accumulation of the image shown in Figure 4A. Note the absence of foci of fluorescence at either pole. The faint, apparent fluorescence seen outside of the egg's boundary is an artifact resulting from incomplete absorption of the exciting light by the barrier filter. (B) Observed 90 min after fertilization, a stage after accumulation of the image shown in Figure 4C. A focus of fluorescence has now appeared at the animal pole because of the accumulation of cytoplasm in the blastodisc during ooplasmic segregation.

In uninjected control eggs, autofluorescence is so low that the egg appears as a black hole against the dim extracellular glow produced by that exciting light that traverses the barrier filter. So a vegetal focus of fluorescence from aequorin is not hidden by autofluorescence. Aequorin is simply not concentrated at the vegetal pole.

Hence the vegetal zone of luminescence must represent a standing zone of high free calcium, not aequorin. The data in Table I confirm this inference quantitatively. Vegetal luminescence remains three times more intense than equatorial or background luminescence when the luminescence ratio is divided by the corresponding ratio of fluorescence coming from coinjected fluorescein-aequorin in the two regions. This inference was further confirmed by the results of experiments in which the eggs were injected with enough of the calcium buffer, dibromo-BAPTA to substantially facilitate the diffusion of Ca^{2+} away from any zones of high $[Ca^{2+}]$, which are in the micromolar range. As Table II shows, such injections halve the relative intensity of the vegetal zone of luminescence.

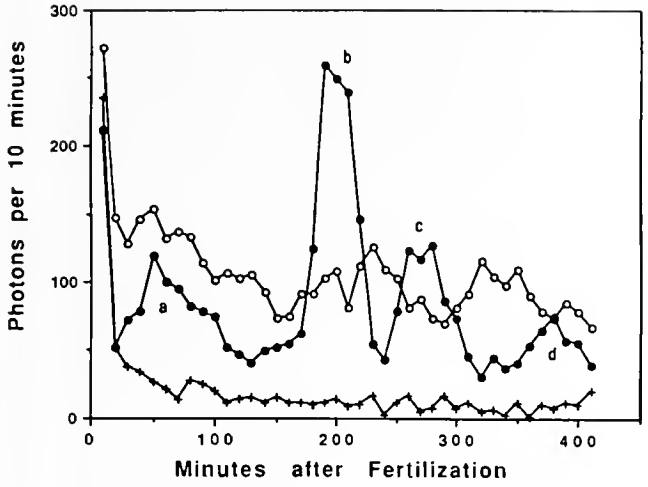

Figure 6. Luminescent intensities observed at the vegetal (○), animal (●), and equatorial (+) regions at various times after fertilization. While the focus of luminescence at the vegetal pole is clearly due to a steady zone of high calcium there, the focus at the animal pole is only clearly above that due to more cytoplasm and hence more aequorin there at the precleavage peak (a) and during each of the first three cleavages (b–d).

Color Figure 5 also displays the pattern of fluorescence coming from fluorescein-aequorin in the animal hemisphere. Here an obvious focus of fluorescence appears at the animal pole together with the precleavage zone of luminescence. So the development of a precleavage zone of high animal calcium is not qualitatively obvious. However, Table I shows that when the ratio of animal pole to equatorial luminescence is corrected for the corresponding fluorescence ratio, it remains about five-fold and thus clearly represents a second zone of high free calcium at the animal pole. Moreover, as Table II and Figure 8 show, the reality of this second, animal zone is also confirmed by the results of coinjecting a calcium buffer. When enough is introduced to substantially facilitate the diffusion of Ca^{2+} away from any zone in the micromolar range, the luminescence at the animal pole falls steadily to a level which is far below the control level.

Significance of the results

This report shows that the zones of high luminescence seen at the poles of aequorin-injected medaka eggs are indeed zones of high free calcium. A preliminary report is available of a similar, if less continuous, high calcium zone at the vegetal pole of *Xenopus* eggs (Miller *et al.*, 1991). Moreover, in ascidian zygotes, striking, periodic calcium waves are regularly seen to start at or near the vegetal pole during the period between fertilization and first polar body formation (Speksnijder *et al.*, 1990b). Because these waves are attenuated en route to the animal pole, they correspond to a high calcium zone at the vegetal pole when averaged over time. This raises the question of how generally high calcium zones appear at the vegetal poles of developing oocytes and eggs.

It also raises a number of other questions. Thus what are the sources (and sinks) which maintain the high calcium zones—particularly the vegetal one—in the medaka egg? To what extent does this calcium come from the medium, from the yolk compartment or from the endoplasmic reticulum? A related question concerns the radial location of these zones. Are they restricted to a very shallow region just under the plasma membrane as they seem to be in fucoid eggs (Jaffe, 1990a) and in medaka cleavage furrows (Fluck *et al.*, 1991)? Above all, what is their role

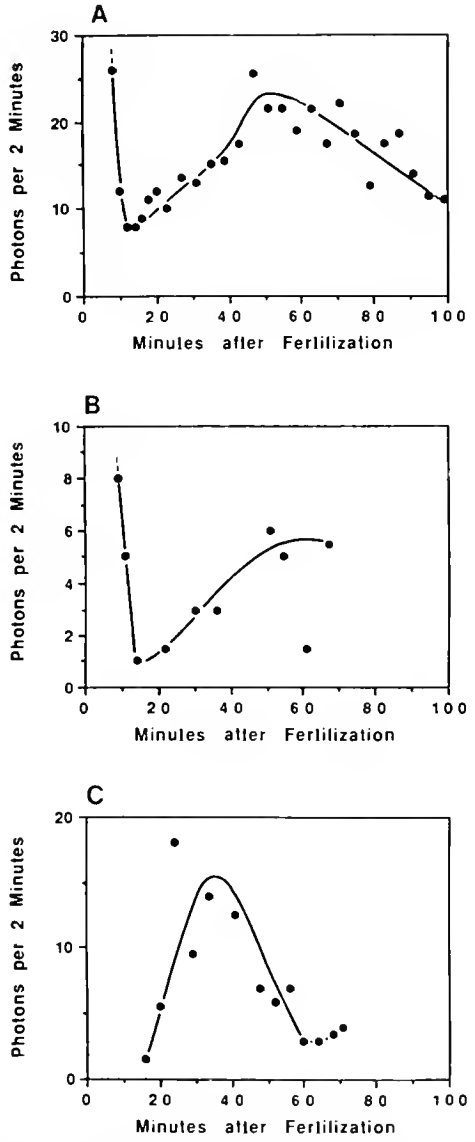

Figure 7. Luminescent intensity observed at the animal pole *versus* time after fertilization in three eggs. (A) The first 100 min of data shown in Figure 7. (B, C) Data from two other eggs.

Relative luminescence [illegible] the equator of aequorin-loaded medaka eggs in the [illegible]od[a]

	N	Luminescence ratio pole/equator ± SEM	
		Vegetal	Animal
Uncorrected:	11	3.0 ± 0.7	8.7 ± 3.4
Corrected for Aequorin Ratio[b]	9	3.4 ± 1.4	4.9 ± 1.6

[a] Luminescence was accumulated between about 15 and 100 min after fertilization at 16°C and thus between 10 and 60% of the period before cleavage.

[b] This was done in a separate group of eggs coinjected with fluorescein-labeled aequorin by dividing the luminescence ratio by the fluorescence ratio.

in development? In particular, what is their role in ooplasmic segregation? Here some evidence is already available. Long ago, Yoshi Sakai reported some striking effects of prick activation on the loci of ooplasmic segregation in medaka eggs (Sakai, 1964). In particular, if vegetal halves are strongly prick-activated, then the cytoplasm accumulates (to form what would normally be the blastodisc) at the point of activation and the oil droplets migrate towards the opposite pole. Such pricking undoubtedly both initiated an activation wave of calcium and established an enduring region of high calcium at the wound (compare Fig. 3 and Fig. 4). It is true that the organization of animal halves proved to be less sensitive to the pricking site. Nevertheless, these old experiments suggest that calcium zones may play at least a reinforcing role in normal ooplasmic segregation. Recently, we have observed that ooplasmic segregation in the medaka egg can be markedly inhibited by injecting enough of the calcium buffer, dibromo-BAPTA, to inhibit the formation of high calcium zones (Miller *et al.*, unpub.).

Table II

Dibromo-BAPTA reduces aequorin luminescence at the animal and vegetal poles of the medaka egg[a]

Injectate(s)	N	Luminescence ratios pole/equator ± SEM	
		Vegetal	Animal
Aequorin	11	3.0 ± 0.7	8.7 ± 3.4
Aequorin + KCl	4	3.0 ± 0.5	7.8 ± 1.9
Aequorin + dbBAPTA	10	1.6 ± 0.3	3.6 ± 0.8

[a] The buffer was injected to a final cytosolic concentration of 2.7 m*M*. Luminescence was accumulated between about 15 and 100 min after fertilization at 16°C and thus between 10 and 60% of the period before cleavage.

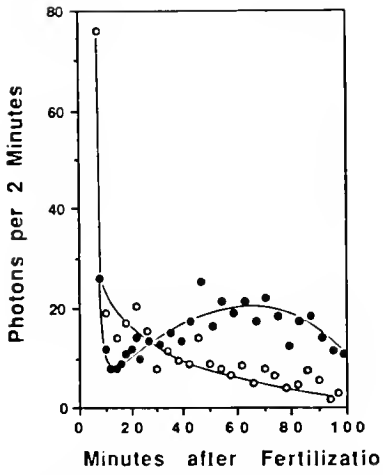

Figure 8. Effect of dibromo-BAPTA injection on the time course of luminescence at the animal pole. Control curve (●) shows data from a single representative egg. Experimental curve (○) shows data pooled from 10 separate eggs.

Aeknowledgments

We thank Dr. Osamu Shimomura for generously providing both the unlabeled recombinant aequorin and the fluorescein-labeled aequorin used in this work. This work was financially supported by NSF grant DCB 9017210 to RAF and DCB 9103569) to LFJ.

Literature Cited

Bolender, R. P. 1978. Correlation of morphometry and stereology with biochemical analysis of cell fractions. *Int. Rev. Cytol.* **55:** 247–289.

Capco, D. G., and W. R. Jeffery. 1982. Transient localizations of messenger RNA in *Xenopus laevis* oocytes. *Dev. Biol.* **89:** 1–12.

Ephrussi, A., L. K. Dickinson, and R. Lehmann. 1991. *oskar* organizes the germ plasm and directs localization of the posterior determinant *nanos*. *Cell* **66:** 37–50.

Fluck, R. A., A. L. Miller, and L. F. Jaffe, 1991. Slow calcium waves accompany cytokinesis in medaka fish eggs. *J. Cell Biol.* **115:** 1259–1265.

Forristall, C., L. Mosquera, and M. L. King. 1991. A cytoskeletal fraction from *Xenopus laevis* oocytes contains two new vegetally localized mRNAs. *J. Cell. Biol.* **115:** 47a.

Gilkey, J. C. 1983. Roles of calcium and pH in activation of eggs of the medaka fish, *Oryzias latipes*. *J. Cell Biol.* **97:** 669–678.

Gilkey, J. C., L. F. Jaffe, E. B. Ridgway, and G. T. Reynolds. 1978. A free calcium wave traverses the activating egg of the medaka, *Oryzias latipes*. *J. Cell Biol.* **76:** 448–466.

Hiramoto, Y. 1962. Microinjection of the live spermatazoa into sea urchin eggs. *Exp. Cell Res.* **27:** 416–426.

Jaffe, L. F. 1986. Calcium and morphogenetic fields. *CIBA Symp.* **122:** 271–288.

Jaffe, L. F. 1990a. The roles of intermembrane calcium in polarizing and activating eggs. Pp. 389–417 in *Mechanisms of Fertilization*, B. Dale, ed. Springer, Berlin.

Jaffe, L. F. 1990b. Calcium ion currents and gradients in fucoid eggs. Pp. 120–126 in *Calcium in Plant Growth and Development*, R. T. Leonard and P. K. Hepler, eds. American Society Plant Physiologists, Rockville, MD.

Jeffery, W. R. 1982. Calcium ionophore polarizes ooplasmic segregation in ascidian eggs. *Science* **216:** 545–547.

Jeffery, W. R. 1984. Pattern formation by ooplasmic segregation in ascidian eggs. *Biol. Bull.* **166:** 277–298.

Larabell, C. A., and D. G. Capco. 1988. Role of calcium in the localization of maternal poly $(A)^+$ RNA and tubulin mRNA in *Xenopus* oocytes. *Roux's Arch. Dev. Biol.* **197:** 175–183.

Melton, D. A. 1991. Pattern formation during animal development. *Science* **252:** 234–241.

Miller, A. L., J. A. McLaughlin, and L. F. Jaffe. 1991. Imaging free calcium in *Xenopus* eggs during polar pattern formation and cytokinesis. *J. Cell Biol.* **115:** 280a.

Nieuwkoop, P. D. 1985. Inductive interactions in early amphibian development and their general nature. *J. Embryol. Exp. Morphol.* **895:** 333–347.

Nüsslein-Volhard, C., and S. Roth. 1989. Axis determination in insect embryos. *CIBA Symp.* **144:** 37–55.

Overall, R., and L. F. Jaffe. 1985. Patterns of ionic current through *Drosophila* follicles and eggs. *Dev. Biol.* **108:** 102–119.

Reverberi, G. 1971. Ascidians. Pp. 529–532 in *Experimental Embryology of Marine and Freshwater Invertebrates*, G. Reverberi, ed. North Holland, Amsterdam.

Ridgway, E. B., J. C. Gilkey, and L. F. Jaffe. 1977. Free calcium increases explosively in activating medaka eggs. *Proc. Natl. Acad. Sci. USA* **74:** 623–627.

Robinson, K. R. 1979. Electrical currents through full-grown and maturing *Xenopus* oocytes. *Proc. Natl. Acad. Sci. USA* **76:** 837–841.

Sakai, Y. T. 1964. Studies on the ooplasmic segregation in the egg of the fish, *Oryzias latipes* I. *Embryologia* **8:** 129–134.

Shimomura, O. 1991. Preparation and handling of aequorin solutions for measurement of cellular Ca^{2+}. *Cell Calcium* **12:** 635–643.

Shimomura, O., S. Inouye, B. Musick, and Y. Kishi. 1990. Recombinant aequorin and recombinant semi-synthetic aequorins. *Biochem. J.* **270:** 309–312.

Speksnijder, J. E., A. L. Miller, M. H. Weisenseel, T-H. Chen, and L. F. Jaffe. 1989. Calcium buffer injections block fucoid egg development by facilitating calcium diffusion. *Proc. Natl. Acad. Sci. USA* **86:** 6607–6611.

Speksnijder, J. E., C. Sardet, and L. F. Jaffe. 1990a. The activation wave of calcium in the ascidian egg and its role in ooplasmic segregation. *J. Cell Biol.* **110:** 1589–1598.

Speksnijder, J. E., C. Sardet, and L. F. Jaffe. 1990b. Periodic calcium waves cross ascidian eggs after fertilization. *Dev. Biol.* **142:** 246–249.

Wylie, C. C., D. Brown, S. F. Godsave, J. Quarmby, and J. Heasman. 1985. The cytoskeleton of *Xenopus* oocytes and its role in development. *J. Embryol. Exp. Morphol.* **895:** 1–15.

Yoshimoto, Y., T. Iwamatsu, K-I. Hirano, and Y. Hiramoto. 1986. The wave pattern of free calcium release upon fertilization in medaka and sand dollar eggs. *Dev. Growth Differ.* **28:** 583–596.

Reference: *Biol. Bull.* **183:** 78–83. (August, 1992)

Localization of Laminin in the Subepidermal Basal Lamina of the Planarian *Dugesia japonica*

ISAO HORI

Department of Biology, Kanazawa Medical University, Uchinada, Ishikawa 920-02, Japan

Abstract. The planarian subepidermal basal lamina consists of three structural elements: namely, an electronlucent zone, a limiting layer, and a microfibrillar layer. Ultrastructural observations following ruthenium red staining were in agreement with previously published reports. The staining clearly revealed positive material on the limiting layer and the individual microfibrils. The limiting layer was continuous and separated the electronlucent zone from the microfibrillar layer. The distribution of laminin, a noncollagenous basal lamina glycoprotein, was determined for the planarian basal lamina using various methods of immunocytochemistry. The reactive substance appeared only on the limiting layer and in the electronlucent zone along the limiting layer. The reactive products on the limiting layer appeared discontinuous. They were also present in the regenerated basal lamina, though the reactivity was a little weaker than in that of intact animals. Localization of laminin in the planarian subepidermal basal lamina is discussed in comparison with that of the basal lamina of vertebrates.

Introduction

The basal lamina or basement membrane is responsible for the maintenance of epithelial integrity, and its condition determines cell behavior during wound repair (Schittny *et al.*, 1988). Consequently, a variety of studies have been carried out with regard to each component of the basal lamina. In view of current knowledge, its molecular components are type IV collagen, sulfated proteoglycans, fibronectin, and laminin, and their distribution can be associated with the function of the epithelial cells (Farquhar, 1981; Leblond *et al.*, 1982; Newgreen, 1984; Simo *et al.*, 1991).

Received 21 October 1991; accepted 18 May 1992.

The subepidermal basal lamina of planarians is structurally quite different from that of higher animals. The planarian basal lamina is characterized by an electronlucent zone of irregular shape and a microfibrillar layer (Pedersen, 1966; Bedini and Papi, 1974; Rieger, 1981; Tyler, 1984). Extracellular matrix components are concentrated mainly in the subepidermal basal lamina. Our previous studies using electron microscopy and autoradiography have shown that the basal lamina is regenerated by interaction between the wound epidermis and differentiating myoblasts (Hori, 1979, 1980). Although the morphological changes and behavior of regenerative cells have been studied well in planarians, cytochemical information about its molecular components is not readily available. This study examines by immunocytochemistry the localization of laminin, a kind of extracellular glycoprotein, in the planarian basal lamina and compares it with the results of ruthenium red staining.

Materials and Methods

Animals

The freshwater planarian *Dugesia japonica* was used in this study. Healthy worms (10–15 mm in length) were selected and maintained without food for a week in our laboratory. Intact tissues from the region between the auricles and pharynx were dissected from six worms. Regenerates of six other worms were obtained by decapitation. Specimens were allowed to regenerate for 4 or 6 days in tap water at 18°C.

Electron microscopy for ruthenium red staining

For the detection of extracellular proteoglycans, tissues were processed for ruthenium red (RR) staining according to Luft (1971). They were fixed for 60 min in 1.2% glutaraldehyde at 4°C, and postfixed for 3 h in 1% osmium

tetroxide at room temperature. Both fixatives were buffered with 0.1 *M* sodium cacodylate (pH 7.4) containing 0.1% ruthenium red (TAAB). Fixation was carried out in a dark room. Specimens were dehydrated with a graded ethanol series and embedded in Epon 812. Thin sections were counterstained with uranyl acetate and lead citrate, and then photographed with a Hitachi H-500 electron microscope.

Immunohistochemistry

Tissues were fixed in Zamboni fixative (Zamboni and DeMartino, 1967) for 4 h at 4°C. After being rinsed for 30 min with cold TBS (pH 7.5), they were dehydrated with graded ethanols and embedded in paraffin. The immunoreaction was carried out according to the AB Complex method (Hsu *et al.*, 1981). Deparaffinized sections (3–5 μm thick) were incubated for 5 min with 3% hydrogen peroxide and incubated for 20 min with bovine serum (normal) diluted 1:5 in TBS. The sections were then incubated overnight at 4°C with rabbit anti-laminin antibody (Sanbio) diluted 1:50 in TBS. For controls, sections were incubated with TBS. All the sections were then incubated for 30 min with biotinylated swine anti-rabbit immunoglobulins (DAKO) diluted 1:300 in TBS, and then again for 30 min with avidin and biotinylated horseradish peroxidase reagents (AB Complex/HRP, DAKO). After being rinsed with TBS they were incubated for 5 min with 3,3 diaminobenzidine tetra-hydrochloride (DAB).

Tissue processing for immunoelectron microscopy

Tissues were fixed for 2 h in 1% glutaraldehyde and 2% paraformaldehyde in 0.1 *M* phosphate buffer (pH 7.4) at 0°C. Tissue pieces were rinsed for 30 min in the buffer, dehydrated in graded ethanols at progressively lowered temperature (down to −25°C), and embedded in Lowicryl HM20 according to Carlemalm *et al.* (1982). The samples were transferred to pure resin at −35°C and maintained overnight. Capsules filled with fresh precooled resin were polymerized for at least 24 h under UV light at −35°C. They were then further hardened at room temperature for 2 days. Thin sections were mounted on collodion-supported nickel grids and immunostained by the following two methods.

(1) ABC method. The sections were preincubated for 30 min with TBS containing 1% bovine serum albumin (BSA). Then they were incubated overnight with polyclonal rabbit anti-laminin antibody (Sanbio) diluted 1:50–1:200 in TBS at 4°C. For controls, sections were incubated with TBS. After being rinsed with TBS, they were incubated for 30 min with affinity-isolated, biotinylated swine anti-rabbit immunoglobulins (DAKO) diluted 1:300 in TBS, followed by incubation with AB Complex/HRP for 2 h. Then they were treated for one minute with DAB. After being rinsed with TBS and distilled water, they were observed without counterstaining.

(2) PAG method. Another group of sections were immunostained by Protein A-gold (PAG) reagents according to Roth *et al.* (1978). Thin sections were rinsed for 5 min with PBS and preincubated for 20 min with PBS BSA (1%). They were then incubated overnight with polyclonal rabbit anti-laminin antibody (Sanbio) diluted 1:50–1:500 in PBS BSA at 4°C. After being rinsed with PBS, they were incubated for 45 min with Protein A-gold colloids (Funakoshi) diluted 1:10 in PBS. They were rinsed with PBS and distilled water and stained with uranyl acetate and lead citrate.

Results

Morphological aspects of the basal lamina

The general architecture of the subepidermal basal lamina stained with ruthenium red is shown in Figure 1. The basal lamina separates the single-layered epidermis from underlying muscle fibers. It is divided into three structural elements; namely, an electronlucent zone surrounded by the basal cytoplasmic processes of epidermal cells, a microfibrillar layer including a number of microfibrils, and a limiting layer separating these elements.

The electronlucent zone changes its shape according to basal alterations of the epidermal cells. In most areas, specific filaments are seen producing a meshwork within this zone. In the cross-sectioned basal lamina, these filaments often run parallel to the limiting layer (Fig. 1). The limiting layer is linear and uniform, identical to the lamina densa of the vertebrate basal lamina. The limiting layer had a strong affinity for RR (Fig. 1), and this dye revealed the continuous nature of the layer. Each basal process of an epidermal cell characteristically develops a hemidesmosome at its tip, and the epidermal cells come in contact with the limiting layer through such hemidesmosomes. When RR-treated specimens were viewed at a higher magnification, the RR-positive material was particularly evident at the hemidesmosomal regions (Fig. 1, inset). The microfibrillar layer constitutes most of the basal lamina. It is underlain with plasma membranes of muscle cells. Its thickness varies from 1 to 4 μm. Viewed in cross section, most of microfibrils were coated with RR-positive material (Fig. 1, inset).

The cytoplasmic portions of some kind of parenchymal gland cells are often seen intruding into the epidermal layer. Therefore their cytoplasmic portions, including secretory granules, can also be seen within the microfibrillar layer (Fig. 1).

Immunohistochemical observations

The distribution of laminin was first investigated at the light microscopic level by indirect immunohistochem-

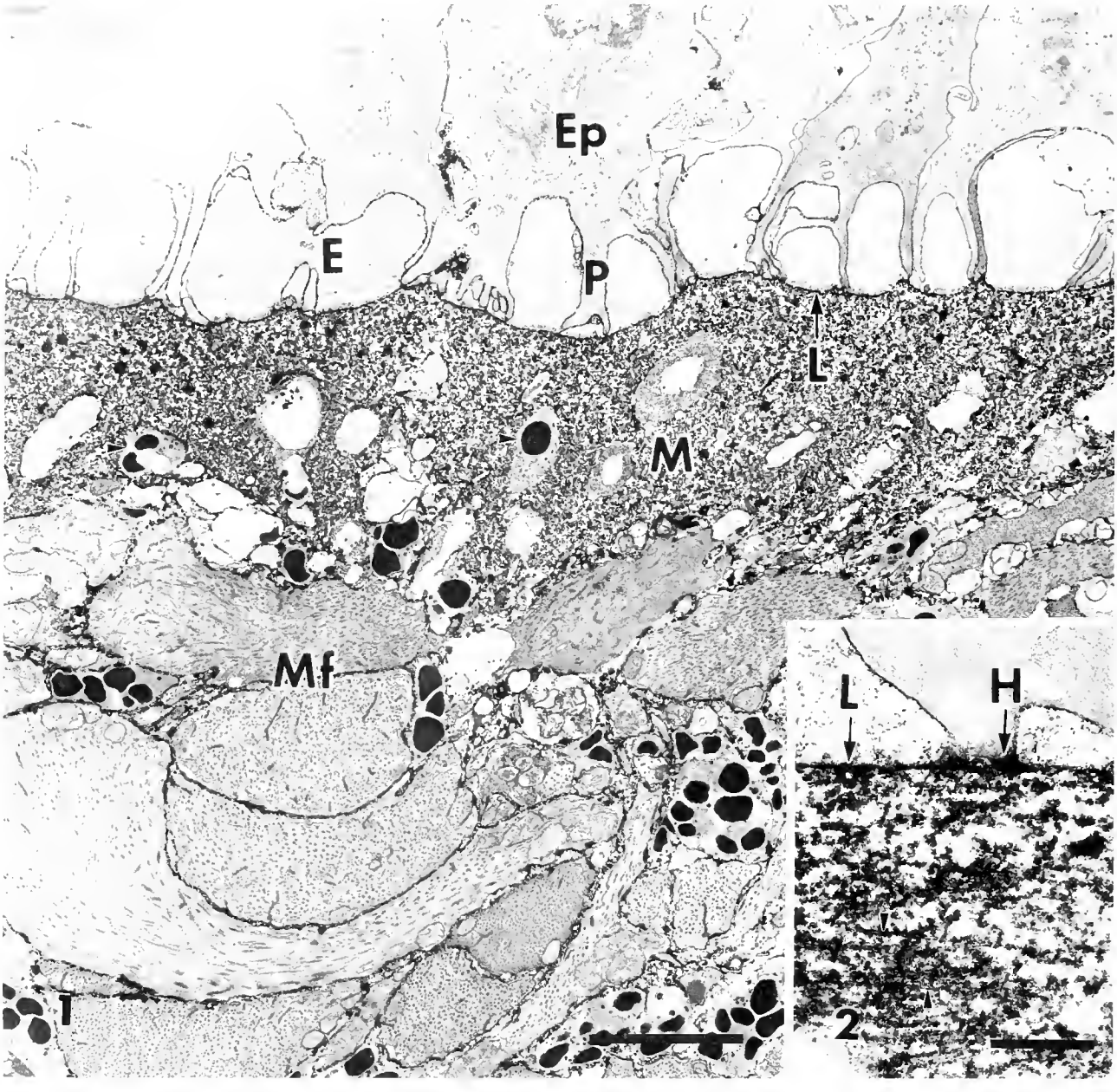

Figure 1. Low magnification view to demonstrate ruthenium red-positive areas in the subepidermal basal lamina. Three structural elements of the basal lamina are evident. Arrowheads indicate the cytoplasmic portion of a gland cell. Scale bar = 2 μm. Inset: High magnification view of the hemidesmosomal region. Ruthenium red staining. The limiting layer is stained clearly. Arrowheads indicate positive material surrounding microfibrils. Scale bar = 0.5 μm. Abbreviations: Ep, epidermal cell; P, cytoplasmic process; E, electronlucent zone; L, limiting layer; M, microfibrillar layer; Mf, muscle fiber; H, hemidesmosome.

istry. Dense its, indicating binding of the antibody to laminin, served on the basal lamina. The deposits were es prominent on its epidermal side (Fig. 2). Simila were also seen in the same region of the 6-day rege g. 4). The control sections incubated with TBS showed no reactive deposits in the basal lamina (Fig. 3).

Immunoelectron microscopic observations

To resolve the localization of laminin in the basal lamina, immunoelectron microscopy was applied to Lowicryl-embedded thin sections. The ABC method showed dense immunoreactivity on the limiting layer and on a part of the electronlucent zone along the limiting layer (Fig. 5).

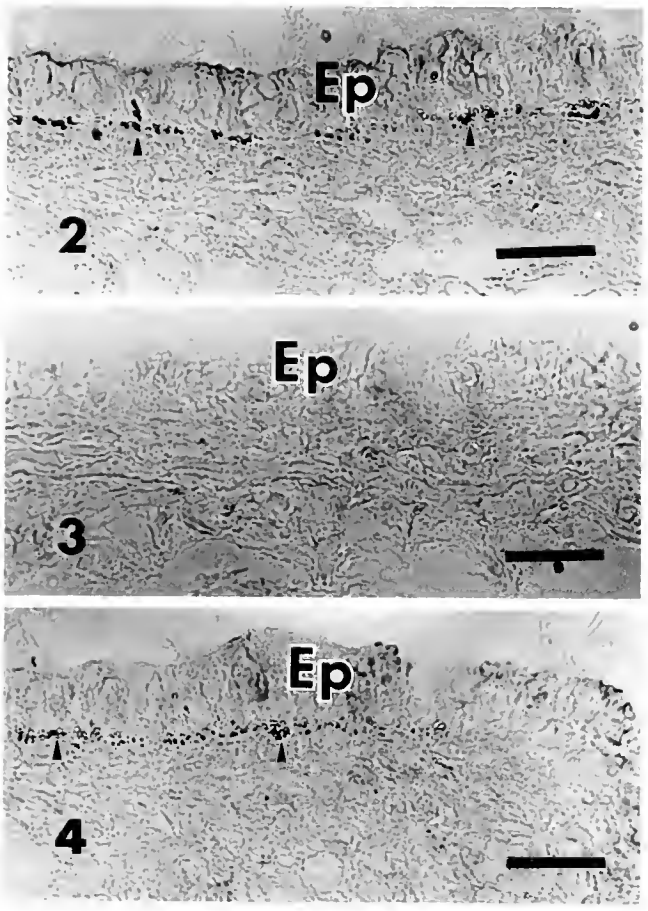

Figures 2–4. Immunohistochemical localization of laminin in the basal lamina. Reactive products are distributed along the basal lamina (arrowheads). Scale bar = 20 μm. **Figure 2.** Intact. **Figure 3.** Intact; control. **Figure 4.** Six-day regenerate. Ep, epidermal cell.

In control sections, no reactive substances were seen in the basal lamina (Fig. 6). The stained material on the limiting layer appeared discontinuous. In the 6-day regenerate, when newly formed basal lamina appeared, the reactivity of the limiting layer was also evident, though the staining was slightly weak (data not shown). In both cases, there were no reactive products in the microfibrillar layer.

The localization of laminin in the basal lamina of intact and regenerating worms was compared by the PAG method. The labeling of laminin resulted in significant deposits in the limiting layers of both intact and regenerated tissues (Figs. 7, 8). Fewer gold particles were in the microfibrillar layer than in the limiting layer.

Discussion

The planarian subepidermal basal lamina has varying degrees of development in different species (Bedini and Papi, 1974). The occurrence and constitution of the planarian basal lamina may not reflect the phylogenetic position of animals, but rather unique functional significance of the basal lamina (Lindroos, 1991). Variations in thickness mainly relate to the extent to which the microfibrillar layer is developed (Sluys, 1989). For example, Rhabdocoela have no microfibrils (Holt and Metrick, 1975), whereas some species of marine triclad have well-organized microfibrillar layer (MacRae, 1965). The basal lamina of the former is similar to that of mammals, and the basal lamina of the latter is similar to that of amphibian larvae (Hay and Revel, 1963). In spite of such variations, the limiting layer can be seen in the basal laminae of most turbellarians.

The results of RR staining provide additional information about the structure and chemical nature of the basal lamina. Because we could demonstrate the RR-positive material in the planarian basal lamina, the limiting layer probably includes sulfated proteoglycans. This is in agreement with the results of experiments on human basement membranes (Horiguchi *et al.*, 1989). The electronlucent zone is occupied by reticular filaments. In our samples, these filaments appear as a meshwork running parallel to the limiting layer. Such a meshwork is, however, not always seen in the planarian basal lamina (Skaer, 1961; Rieger, 1981). The variation in the structure of reticular filaments may depend, not only on their chemical properties, but also on methods of tissue preparation.

Laminin is one of the main components of basal laminae. Its distribution has been examined in many vertebrates (Jacob *et al.*, 1991). Because the antigenic determinants of laminin are not species-specific (Foidart *et al.*, 1980), we have used rabbit anti-laminin antibodies to detect the localization of laminin in the planarian basal lamina. Immunohistochemical staining demonstrated that the distribution of laminin is restricted to the limiting layer and a part of the electronlucent zone. In contrast to the RR-positive proteoglycans, laminin is distributed on the limiting layer discontinuously. This finding is in accord with the observations of Lindroos and Still (1988), who noted irregular deposits of laminin beneath the epithelium of *Polycelis nigra*.

The localization of laminin on vertebrate basement membranes differs from one report to the next: *i.e.*, it is localized in the entire region of the basal lamina (Inoué, 1989); in the lamina densa (Laurie *et al.*, 1982); in the lamina lucida (Foidart *et al.*, 1980; Madri *et al.*, 1980); and at the junction between the lamina densa and lamina lucida (Schittny *et al.*, 1988). Laminin is known to play many important roles in various phenomena, but nothing has been reported about the significance of such varied distributions.

Planarian epidermal cells have no ability to proliferate mitotically so that certain parenchymal cells migrate into the epidermis to produce its cellular succession. In my

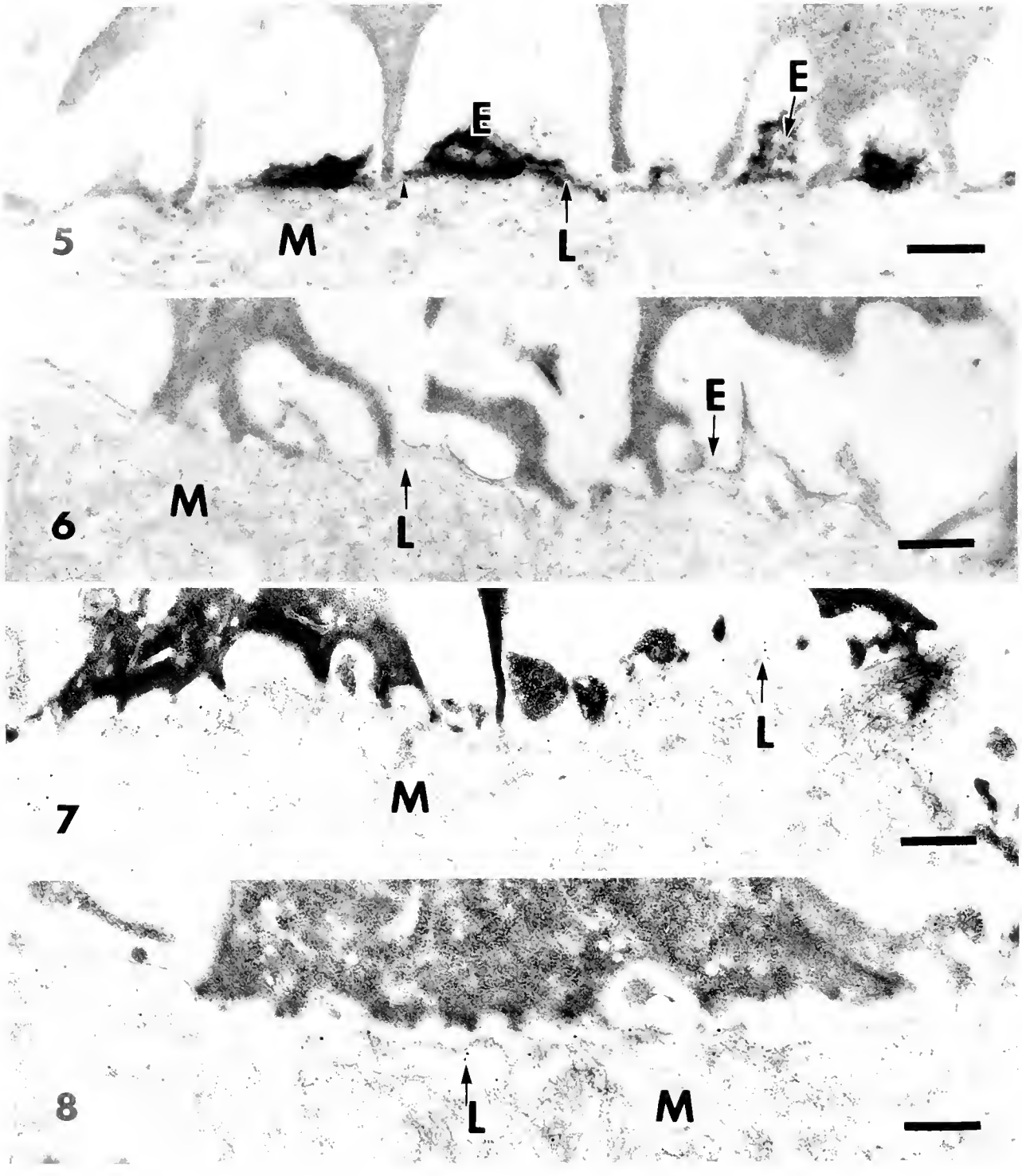

Figures 5–6. Localization of laminin by ABC method of Lowicryl-embedded sections. The limiting [illegible] and a part of the electronlucent zone are stained. Arrowhead indicates a discontinuous portion of reaction products. **Figure 5.** Intact. Scale bar = 0.5 μm. **Figure 6.** Control. Scale bar = 0.5 μm.

Figures 7–8. Localization of laminin by immunogold labeling of Lowicryl-embedded sections. Gold particles are seen associated with the limiting layer. **Figure 7.** Intact. Scale bar = 1 μm. **Figure 8.** Four-day regenerate. Scale bar = 0.5 μm. E, electronlucent zone; L, limiting layer; M, microfibrillar layer.

previous study, I ascertained that rhabdite-forming cells are differentiated from regenerative cells and contribute to the cellular succession, both in intact and regenerating planarians (Hori, 1978). Moreover, other kinds of parenchymal gland cells usually extend their cytoplasmic processes, which contain secretory granules, into the epidermal layer (Tyler, 1984). Thus one can assume that the planarian basal lamina probably provides a microenvironment that guides such cell movement from the parenchyma to the epidermis. Recent studies suggest that changes of laminin accumulation affect various cell behaviors, such as cell movement (Simo *et al.*, 1991), cell differentiation (Kubota *et al.*, 1988), interaction between epithelial and underlying cells (Richoux *et al.*, 1989), and cell proliferation (Hogan, 1981). Planarian regeneration is also a complex process including extracellular matrix components. In an earlier study, I reported that fibronectin, another extracellular glycoprotein, is detected around migrating cells within the planarian blastema (Hori, 1991), but the data were based only on the immunocytochemistry of fixed and resin-embedded tissues. Further analysis will require that experiments be carried out *in vitro* to examine the roles of such glycoproteins in cell behavior during planarian regeneration.

Literature Cited

Bedini, C., and F. Papi. 1974. Fine structure of the turbellarian epidermis. Pp. 108–147 in *Biology of Turbellaria*, N. W. Riser, and M. P. Morse, eds. McGraw-Hill Book Co., New York.

Carlemalm, E., R. M. Garavito, and W. Villinger. 1982. Resin development for electron microscopy and an analysis of embedding at low temperature. *J. Microsc.* **126:** 123–143.

Farquhar, M. G. 1981. The glomerular basement membrane: a selective macromolecular filter. Pp. 335–378 in *Cell Biology of Extracellular Matrix*, E. D. Hay, ed. Plenum Press, New York.

Foidart, J. M., E. W. Bere, M. Yaar, S. I. Rennard, M. Gullino, G. R. Martin, and S. I. Katz. 1980. Distribution and immunoelectron microscopic localization of laminin, a noncollagenous basement membrane glycoprotein. *Lab. Invest.* **42:** 336–342.

Hay, E. D., and J. P. Revel. 1963. Autoradiographic studies of the origin of the basement lamella in *Ambrystoma. Dev. Biol.* 7: 152–168.

Hogan, B. 1981. Laminin and epithelial cell attachment. *Nature* **290:** 737–738.

Holt, P. A., and D. F. Mettrick. 1975. Ultrastructural studies of the epidermis and gastrodermis of *Syndesmis franciscana* (Turbellaria: Rhabdocoela). *Can. J. Zool.* **53:** 536–549.

Hori, I. 1978. Possible role of rhabdite-forming cells in cellular succession of the planarian epidermis. *J. Electron Microsc.* **27:** 89–102.

Hori, I. 1979. Structure and regeneration of the planarian basal lamina: an ultrastructural study. *Tissue Cell* **11:** 611–621.

Hori, I. 1980. Localization of newly synthesized precursors of basal lamina in the regenerating planarian as revealed by autoradiography. *Tissue Cell* **12:** 513–521.

Hori, I. 1991. Role of fixed parenchyma cells in blastema formation of the planarian *Dugesia japonica*. *Int. J. Dev. Biol.* **35:** 101–108.

Horiguchi, Y., J. R. Couchman, A. V. Ljubimov, H. Yamasaki, and J-D. Fine. 1989. Distribution, ultrastructural localization, and ontogeny of the core protein of a human sulfate proteoglycan in human skin and other basement membranes. *J. Histochem. Cytochem.* **37:** 961–970.

Hsu, S-M., L. Raine, and H. Fanger. 1981. A comparative study of the peroxidase-antiperoxidase method and an avidin-biotin complex method for studying polypeptide hormones with radioimmunoassay antibodies. *Am. J. Clin. Pathol.* **75:** 734–738.

Inoué, S. 1989. Ultrastructure of basement membranes. *Int. Rev. Cytol.* **117:** 57–98.

Jacob, M., B. Christ, H. J. Jacob, and R. E. Poelmann. 1991. The role of fibronectin and laminin in development and migration of the avian Wolffian duct with reference to somitogenesis. *Anat. Embryol.* **183:** 385–395.

Kubota, Y., H. K. Kleinman, G. R. Martin, and T. J. Lawley. 1988. Role of laminin and basement membrane in the morphological differentiation of human endothelial cells into capillary-like structures. *J. Cell Biol.* **107:** 1589–1598.

Laurie, G. W., C. P. Leblond, and G. R. Martin. 1982. Localization of type IV collagen, laminin, heparan sulfate proteoglycan, and fibronectin to the basal lamina of basement membranes. *J. Cell Biol.* **95:** 340–344.

Lindroos, P. 1991. Aspects on the extracellular matrix and protonephridia in flatworms, with special reference to the tapeworm *Diphyllobothrium dendriticum*. Pp. 6–53 in Thesis. Åbo Akademis Kopieringscentral, Åbo.

Lindroos, P., and M. J. Still. 1988. Extracellular matrix components in *Polycelis nigra* (Turbellaria, Tricladida). *Fortsch. Zool.* **36:** 157–162.

Luft, J. H. 1971. Ruthenium red and violet II. Fine structural localization in animal tissues. *Anat. Rec.* **171:** 369–416.

MacRae, E. K. 1965. Fine structure of the basement lamella in a marine turbellarian. *Am. Zool.* **5:** 247.

Madri, J. A., F. J. Roll, H. Furthmayr, and J. M. Foidart. 1980. Ultrastructural localization of fibronectin and laminin in the basement membranes of the murine kidney. *J. Cell Biol.* **86:** 682–687.

Newgreen, D. 1984. Spreading of explants of embryonic chick mesenchymes and epithelia on fibronectin and laminin. *Cell Tissue Res.* **236:** 265–277.

Pedersen, K. J. 1966. The organization of the connective tissue of *Discocelides langi* (Turbellaria, Polycladida). *Z. Zellforsch.* **71:** 94–117.

Richoux, V., T. Darribère, J-C. Boucaut, J. E. Elèchon, and J-P. Thiery. 1989. Distribution of fibronectins and laminin in the early pig embryo. *Anat. Rec.* **223:** 72–81.

Rieger, R. M. 1981. Morphology of the turbellaria at the ultrastructural level. *Hydrobiologia* **84:** 213–229.

Roth, J., M. Bendayan, and L. Orci. 1978. Ultrastructural localization of intracellular antigens by the use of protein A-gold complex. *J. Histochem. Cytochem.* **26:** 1074–1081.

Schittny, J. C., R. Timpl, and J. Elgel. 1988. High resolution immunoelectron microscopic localization of functional domains of laminin, nidogen, and heparan sulfate proteoglycan in epithelial basement membrane of mouse cornea reveals different topological orientations. *J. Cell Biol.* **107:** 1599–1610.

Simo, P., P. Simon-Assmann, F. Bouziges, C. Leberquier, M. Kedinger, P. Ekblom, and L. Sorokin. 1991. Changes in the expression of laminin during intestinal development. *Development* **112:** 477–487.

Skaer, R. J. 1961. Some aspects of the cytology of *Polycelis nigra*. *Q. J. Microsc. Sci* **102:** 295–317.

Sluys, R. 1989. *A Monograph of the Marine Triclads*. Pp. 1–5. A. A. Belkema, Rotterdam.

Tyler, S. 1984. Turbellarian platyhelminths. Pp. 112–132 in *Biology of the Integument Vol. 1 Invertebrates*, J. Bereiter-Hahn, ed. Springer-Verlag, Berlin.

Zamboni, L., and C. DeMartino. 1967. Buffered picric acid-formaldehyde: a new, rapid fixative for electron microscopy. *J. Cell Biol.* **35:** 148A.

Reference: *Biol. Bull.* **183**: 84–93. (August, 1992)

Assembly of the Hatching Envelope Around the Eggs of *Trachypenaeus similis* and *Sicyonia ingentis* in a Low Sodium Environment

JOHN W. LYNN[1], PATRICIA S. GLAS[1], AND JEFFREY D. GREEN[2]

[1]*Department of Zoology and Physiology, Louisiana State University, Baton Rouge, Louisiana 70803 and* [2]*Department of Anatomy, Louisiana State University School of Medicine, New Orleans, Louisiana 70112*

Abstract. The eggs of many penaeoidean shrimp undergo two dramatic morphological events when spawned into normal seawater (Lynn *et al.*, 1991). Following the initial release of jelly precursor from crypts in the cortex of the egg, an extracellular envelope elevates and transforms into a substantial "hatching envelope" (HE) 30–40 min after spawning. The HE's of *Sicyonia ingentis* and *Trachypenaeus similis* eggs have distinct laminar morphologies and range from 90 to 110 nm thick. The HE elevates approximately 80 μm from the egg in *T. similis* and 40 μm from the egg in *S. ingentis*. Although eggs spawned into low Na^+ artificial seawater (with choline chloride or Tris-HCl substituted for the NaCl) underwent normal release and formation of the jelly layer, the HE failed to develop normally. The HE retained a 100-nm thickness, but lacked the distinctive inner flocculent zone and dense outer covering. The HE collapsed to the egg surface, reducing the perivitelline space. Assembly of the HE resembles the formation of the sea urchin fertilization envelope and demonstrates a similar sensitivity to the lack of Na^+ in the ambient environment.

Introduction

The eggs of penaeoidean shrimp (Crustacea: Decapoda) undergo two dramatic morphological changes following their release from the female, at spawning, into the surrounding seawater (Lynn *et al.*, 1991). These changes have best been characterized in *Penaeus japonicus*, *P. setiferus*, *P. aztecus*, and *Sicyonia ingentis* and sequentially comprise: (1) the dramatic release of the jelly precursor from the extracellular cortical crypts; (2) transformation of the precursor material into a layer of jelly that forms around the egg; and (3) the elevation and assembly of the hatching envelope (HE) following the exocytosis of at least two types of vesicles from the egg cytoplasm (Clark *et al.*, 1980, 1990; Pillai and Clark, 1988, 1990). These events are initiated by contact of the egg with seawater and are independent of sperm-egg interaction (Pillai and Clark, 1987; Lynn *et al.*, 1991).

Release of the jelly precursor from eggs of at least two penaeid species, *P. aztecus* and *P. setiferus*, has been demonstrated to be dependent on the presence of Mg^{+2} in the seawater (Clark and Lynn, 1977). Once released, the heterogeneous jelly precursor is transformed into a homogeneous, translucent material surrounding the entire egg. This transformation is also reported to be dependent on extracellular Mg^{+2} (Clark and Lynn, 1977) and appears to be mediated by one or more proteolytic enzymes (Clark and Lynn, 1977; Lynn and Clark, 1987; Green *et al.*, 1990).

The next major morphological change during egg activation, assembly of the hatching envelope, has been reported in detail for *S. ingentis* by Pillai and Clark (1988). The assembly of the HE proceeds in two sequential phases at approximately 45 min post-spawning and comprises: (1) exocytosis of a group of dense vesicles that combine with a thin fluffy surface coat to produce the nascent or "thin" HE; and (2) a second exocytosis of vesicles which releases ring granules that combine with the nascent HE to form a laminar structure composed of a dense outer

Received 19 February [illegible] cepted 18 May 1992.

Abbreviations: HE—hat[illegible]velope; FE—fertilization envelope; ASW—artificial seawater; V[illegible]ine envelope; ChCl—choline chloride; TEM—transmission electro[illegible]croscopy; SEM—scanning electron microscopy.

stratum and a more flocculent inner layer. Although the morphological characteristics of HE formation have been described elegantly for *S. ingentis,* little is known about the underlying mechanisms of its assembly around the egg. At present, no information is available concerning ion requirements or enzymatic processes involved in the transformation of the surface coat into the HE as described by Pillai and Clark (1988).

In this paper, we report the effects of Na^+ ion depletion on the morphology of HE formation in the eggs of *S. ingentis* and *Trachypenaeus similis* when sodium in the seawater is replaced with choline, Tris, or potassium. In addition, we also provide a brief comparative description of the morphological events associated with the jelly layer formation in the spawned eggs of *T. similis.*

Materials and Methods

Animals

Specimens of *Trachypeneaus similis* were collected in the Gulf of Mexico off the Louisiana coast by otter trawl and gravid females were transported to the laboratory at ambient temperature in aerated tanks under constant light. *Sicyonia ingentis* were obtained from the laboratory of W. H. Clark at the Bodega Marine Laboratory. These animals were collected off San Pedro in southern California by standard otter trawl and transported to the laboratory in chilled (4–10°C) aerated tanks. For both species, spawning was induced by placing the animals in darkness (Pillai *et al.,* 1988).

Media

Artificial normal (480 m*M* sodium) seawater (ASW) was prepared according to the formulae of Chambers and De Armendi (1979) and buffered to pH 8.3 with 10 m*M* TAPS (N-Tris[hydroxymethyl]methyl-3-amino-propanesulfonic acid). Reduced sodium seawaters (approximately 26 m*M* sodium) were prepared by substituting choline chloride in a 1:1 ratio for sodium chloride (Chambers and De Armendi, 1979), or, in some experiments, substituting either potassium chloride or Tris-HCl [tris(hydroxymethyl)aminomethane] for sodium (Gould-Somero *et al.,* 1979).

Gametes

Eggs were collected by placing a spawning female directly on top of a small beaker (30 ml beaker for *T. similis*) or crystallizing dish (30 × 75 mm) containing either control or experimental media. The cells were gently swirled to prevent sticking and clumping during the first 15–20 min after spawning. Eggs were monitored for normal elevation and appearance of HE before fixation in both controls and experimentals. In some cases, eggs originally spawned into reduced Na^+ seawater were transferred back into normal seawater at 10-min intervals through 60 min post-spawning and observed for HE formation and cleavage until 120 min post-spawning.

Hardening of the HE under different experimental conditions was evaluated by the resistance of the envelope to collapse and extraction when treated with 1.0 *M* urea (Schuel *et al.,* 1982) at 4 min and 15 min time points after the beginning of HE elevation. Eggs were observed for the beginning of the HE elevation. After the HE was first detected in 50% of the eggs observed, they were transferred at either 4 or 15 min post HE appearance into urea and were incubated for 5 min. At 5 min, the urea was aspirated off the eggs, replaced with normal seawater, and the eggs were immediately fixed for electron microscopy. Subsamples of eggs were then scored with a light microscope for the presence of elevated HEs and the remainder were processed for transmission electron microscopy for further observations.

Light and electron microscopy

Eggs were observed with light microscopy (phase and brightfield) on either a Nikon Diaphot or Nikon Optiphot microscope. A petroleum jelly ring was placed on microscope slides to prevent the coverslip from crushing the eggs placed within the ring and to reduce the effects of desiccation. Diameters of eggs and elevated HEs were measured with a calibrated filar eyepiece micrometer.

Samples for electron microscopy were fixed in either 2% glutaraldehyde in ASW, or a 1.2% paraformaldehyde/3% glutaraldehyde combination in ASW. After a 2–4 h fixation, the samples were rinsed twice in ASW followed by two rinses in 0.2 *M* cacodylate buffer, pH 7.4. Eggs were postfixed in 1% osmium in 0.2 *M* cacodylate, pH 7.4, for 1 h. Following two rinses in cacodylate buffer, the samples were dehydrated in either a graded acetone or ethanol series and embedded in Spurr's (1969) low viscosity epoxy resin or Embed 812 (EMS), respectively, for sectioning.

Samples were sectioned using a Porter Blum MT-2B or a Reichert Ultracut E ultramicrotome using either glass or diamond knives. Thick sections (1 μm) were stained with 0.5% toluidine blue and observed with a light microscope. Thin sections were stained with methanolic uranyl acetate and aqueous lead citrate and observed with a JEOL 100-CX transmission electron microscope (TEM).

For scanning electron microscopy (SEM), eggs were processed as described above for transmission electron microscopy except that after dehydration with the graded acetone series, the eggs were critical point dried, mounted on SEM stubs with double stick tape, and coated with 10 nm gold. Samples were then viewed with either a Hitachi HS-500 or a Cambridge StereoScan 260 SEM.

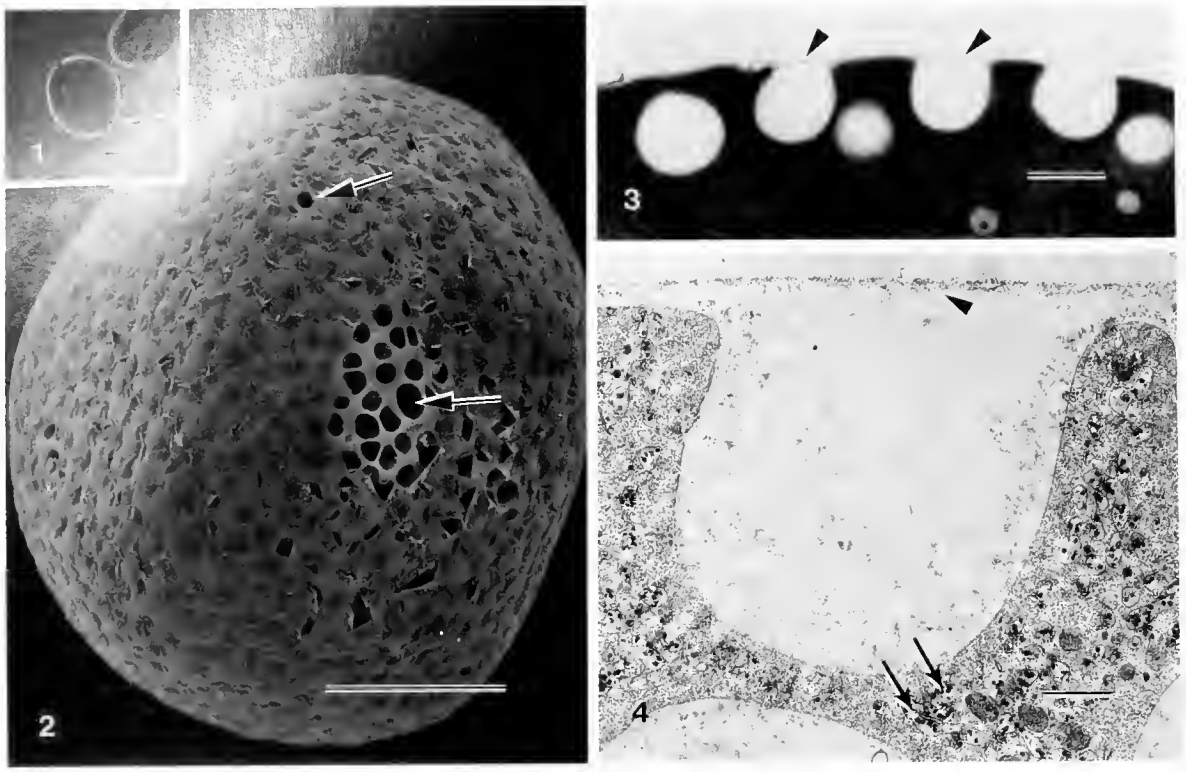

Figure 1. A phase micrograph of a *Trachypenaeus similis* egg spawned directly into seawater containing fixative. Note birefringence of the cortical region of the egg (arrowhead) and the irregular egg shape. Bar = 100 μm.

Figure 2. The vitelline envelope overlying the egg plasma membrane and cortical crypts of *T. similis* are apparent in this SEM. Note the openings of the underlying crypts where the vitelline envelope has been disturbed (arrow) and their non-uniform diameters. Bar = 50 μm.

Figure 3. The relationship between the thin vitelline envelope (arrowheads) and the underlying cortical crypts can be observed in light micrographs of thick plastic sections. Bar = 10 μm.

Figure 4. In this TEM of a *T. similis* egg crypt, the jelly precursor material appears as a diffuse fibrillar material. The egg cytoplasm contains cisternae (arrows) with electron-dense material. The vitelline envelope is a thin, fluffy material overlying the crypts (arrowhead). Bar = 1 μm.

Statistical analysis

Comparisons of dimensional changes of total egg + hatching envelope diameter between control and experimental samples were performed using Instat (Graphpad Software, Inc.) for the Student's *t*-test using a two-tailed test with test for significance of $P < 0.001$. Number of trials for each comparison are given as n.

Results

Morphology of T. similis egg activation

Although the morphology of the early activational events observed in spawned eggs of *Trachypenaeus similis* is very similar to that described in *Penaeus sp.* and *Sicyonia ingentis* (i.e., Clark *et al.*, 1980, 1990; Lynn *et al.*, 1991), a description is provided here for the first time to illustrate the similarities and the minor differences. Eggs of *T. similis* spawned into seawater and fixed within 1 min are approximately 220 μm in diameter. A bright refractile ring in the cortex of the egg corresponds to the cortical crypts that contain the jelly precursor material (Fig. 1). Release of the jelly precursor from the cortical crypts and transformation of the precursor into a homogeneous jelly layer around the egg of *T. similis* closely resembles that of *P. aztecus* and *S. ingentis*. The crypts are separated from the external environment only by a thin investment coat, the vitelline envelope (VE) (Figs. 2, 3, 4). It should be noted, however, that the jelly precursor in *T. similis* does not appear to have the small feathery elements previously described for other penaeid species (Clark *et al.*, 1980, 1990; Clark and Lynn, 1977; Lynn and Clark, 1987; Lynn *et al.*, 1991). Each crypt is partially encompassed by a granular cytoplasmic zone devoid of yolk platelets (Fig. 4). The peripheral cytoplasm also includes

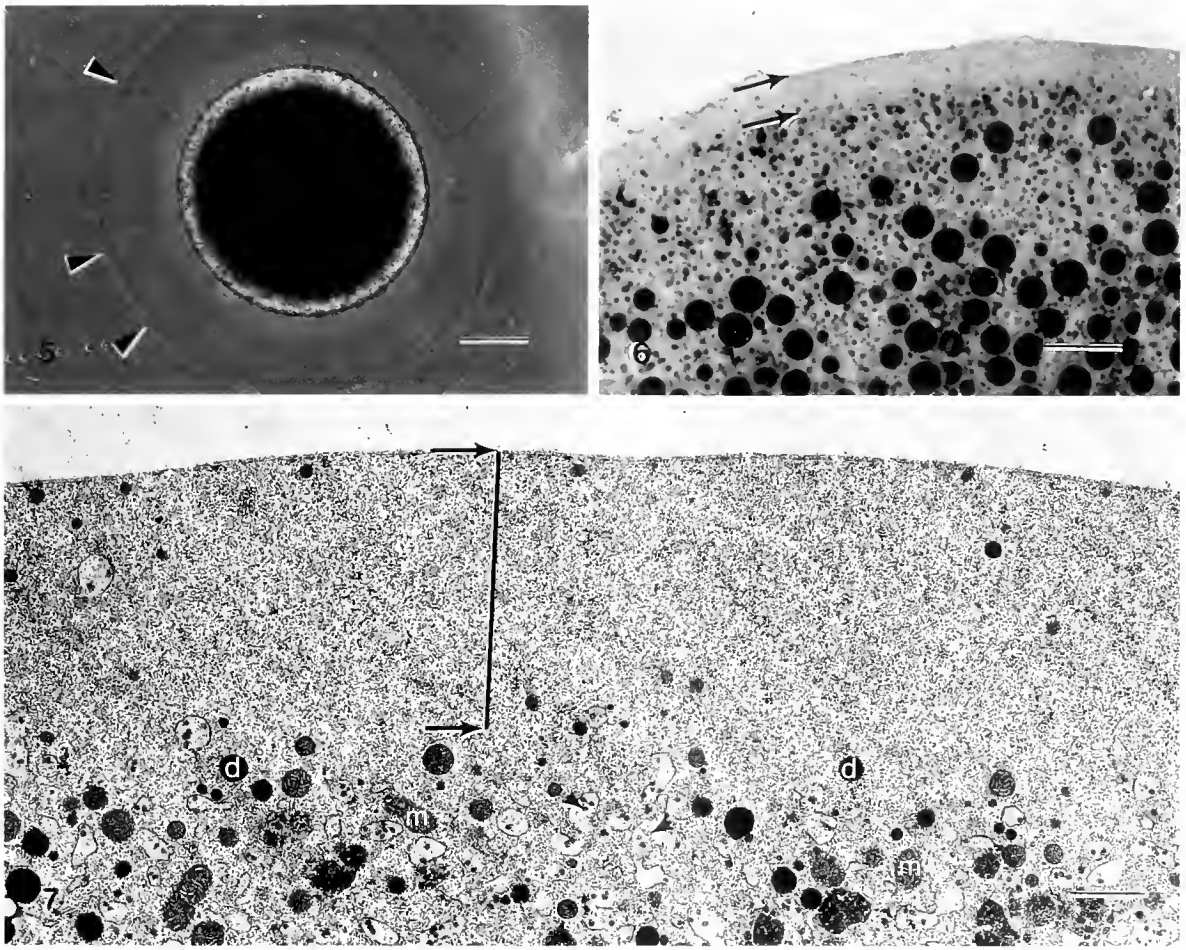

Figure 5. A phase micrograph of a living *Trachypenaeus similis* egg 6 min post-spawning reveals the translucent jelly layer (arrowheads) formed from the cortical crypt material. Bar = 50 μm.

Figure 6. At 30 min, the *T. similis* egg has a distinct cortical cytoplasmic band (delimited by arrows) observable in light micrographs of thick plastic sections. This band separates the cell membrane of the egg from the central cytoplasm which contains yolk platelets and darkly staining vesicles. Bar = 10 μm.

Figure 7. As observed at higher magnifications in TEM micrographs, the cytoplasmic band (delimited by arrows with bar) in the cortex is devoid of major large organelles. The underlying cytoplasm contains mitochondria (m), dense vesicles (d), and cisternal elements (arrowheads) with densely staining granules. Bar = 1 μm.

large numbers of cisternae which contain granules. These vesicles extend into the deeper cytoplasm as well.

Immediately upon contact of the eggs with seawater, the jelly precursor is released from the crypts and, within a few minutes, is transformed into a translucent, homogeneous layer around the egg (Fig. 5). The release of the jelly precursor from the crypts occurs within 1–2 min, but its transformation into a homogeneous layer may require up to 5 min at 21–22°C. The precursor material released from the cortical crypts is granular and heterogeneous as reported for the dispersal phases of other penaeid species, even though *T. similis* lacks the distinct feathery elements as noted above. During this time the surface of the egg rounds up and smooths out (Fig. 5). A granular band of cytoplasm remains evident in the cortex for 30–35 min post spawning and contains no major organelles (Figs. 6, 7). As also reported for *S. ingentis* (Pillai and Clark, 1987), the *T. similis* egg is spawned in first meiotic metaphase arrest. Between 25 and 30 min, the first polar body is released (not shown) and precedes the elevation of the HE.

The translucent jelly layer remains around the egg for an extended period of time and is still visible when the HE is elevated between 35 and 45 min post-spawning. The elevation of the envelope is virtually simultaneous around the entire egg and does not appear to proceed in

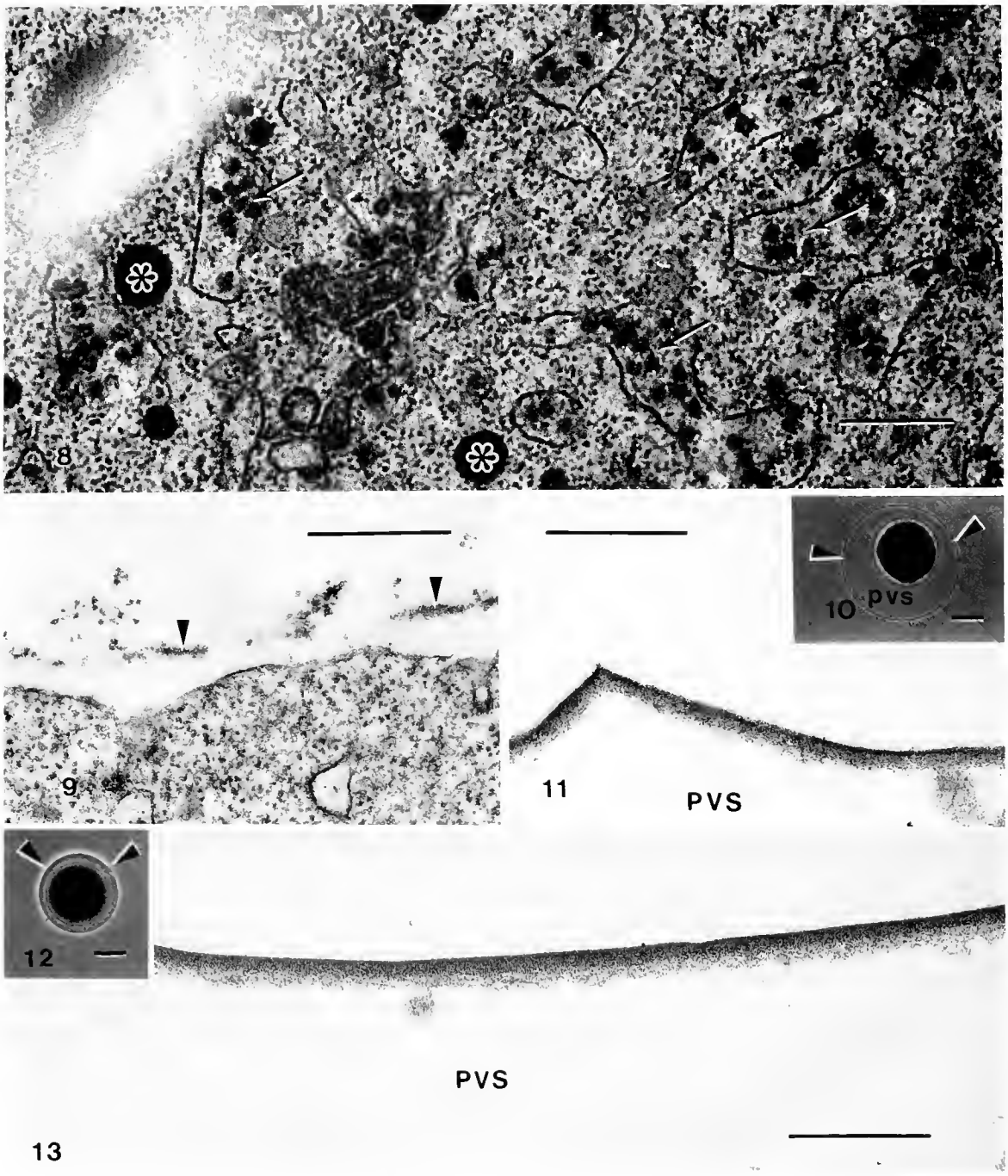

Figure 8. Both ring-like inclusions (arrows) sequestered in cisternal elements and dense granules (asterisks) are observed in higher magnification TEM micrographs of the deeper non-cortical cytoplasm of *Trachypenaeus similis* eggs. Bar = 0.5 μm.

Figure 9. In this TEM micrograph of a *T. similis* egg, an early HE has an amorphous structure (arrowheads) prior to the release of the ring vesicles from the cisternal elements. Bar = 0.5 μm.

Figure 10. By about 60–75 min, the formation of the HE is complete in *T. similis*. A phase micrograph shows the large perivitelline space (pvs) that is formed and the refractile character of the elevated HE (arrowheads). Bar = 100 μm.

Figure 11. A late or "tanned" HE of *T. similis* observed with TEM shows a distinct laminar structure consisting of a flocculent inner layer facing the perivitelline space (PVS), and a dense outer layer. Bar = 0.5 μm.

Figure 12. A phase micrograph of an *S. ingentis* egg with HE (arrowheads) at 60 min. Bar = 100 μm.

Figure 13. A TEM of the "tanned" HE of *S. ingentis* demonstrating the distinct laminar structure. As in the *T. similis* HE, a flocculent inner layer faces the perivitelline space (PVS) and lies beneath a dense outer covering. Bar = 0.5 μm.

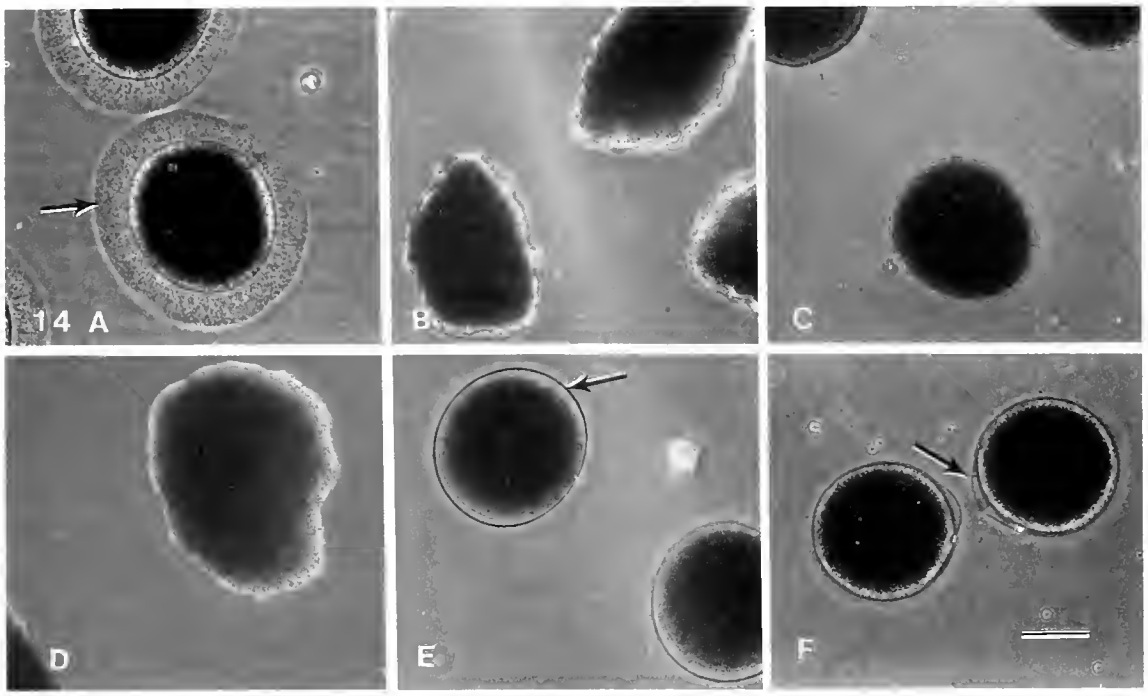

Figure 14 A–F. A series of phase micrographs of living eggs showing the altered formation of the HE in both *Trachypenaeus similis* and *Sicyonia ingentis* in reduced Na^+ seawater. (A) A *T. similis* egg with jelly coat (arrow) in ChCl-substituted seawater at 4–5 min post spawning. (B) A crenated *S. ingentis* egg in ChCl-substituted seawater at 12 min. (C) A *S. ingentis* egg has rounded up in ChCl-substituted seawater by 35 min showing a typical morphology for both species. (D) A phase micrograph at 20 min of a *S. ingentis* egg spawned into Tris-substituted seawater showing the prolonged irregular morphology of eggs in this media. (E) The collapsed HE (arrow) around the *S. ingentis* egg in ChCl-substituted seawater at 65 min. (F) Collapsed HEs (arrow) around *T. similis* eggs in ChCl-substituted seawater at 65 min. Bar = 100 μm for all phase micrographs.

a wave-like fashion. Two populations of granules also have been identified in the *T. similis* egg (Fig. 8) and appear similar to the dense and ring vesicles in the *S. ingentis* egg (Pillai and Clark, 1988; Lynn *et al.*, 1991). The dense vesicles migrate to the cortex and line up just beneath the plasmalemma by 30 min post spawning. This population of vesicles is the first to undergo exocytosis. Subsequently, the ring vesicles contained in cisternal elements migrate to the cortical cytoplasm and undergo exocytosis at a slightly later time.

The morphology of the HE formation around *S. ingentis* eggs has been previously reported by Pillai and Clark (1988). The formation of the HE around *T. similis* eggs is similar. It progresses from a fibrous, non-laminar structure (Fig. 9) to a well defined bilayered structure (Fig. 11). By 60 min post-spawning, the HE consists of a dense outer stratum covering a thicker more flocculent inner layer (Fig. 11) similar to that observed in *S. ingentis* (Fig. 13). A space between the oolemma and the elevated, hardened HE is distinct and defines the perivitelline space (Figs. 10, 12).

Effect of low sodium seawater on HE formation

Eggs of both *T. similis* and *S. ingentis* spawned into and held in seawater with choline chloride replacing sodium chloride underwent normal, early morphological changes as described above. The egg jelly precursor was released from the crypts and transformed into a translucent jelly layer as in normal seawater (Fig. 14A). In contrast to control eggs in normal seawater, the egg surface remained crenated in *S. ingentis* eggs (Fig. 14B), and the overall morphology was irregular and flattened. The eggs eventually rounded up by approximately 25 min in the choline chloride-substituted seawater (Fig. 14C). First polar body formation was delayed by approximately 10 min in both *T. similis* and *S. ingentis*.

The elevation of the HE characterizing the later morphological events was significantly reduced in eggs of both *T. similis* and *S. ingentis* spawned into ChCl-substituted seawater. Observed with light microscopy, the HE did not fully elevate in either species and remained conspicuously close to the surface of the egg (Fig. 14E, F). Measurement of the total diameter of the egg and

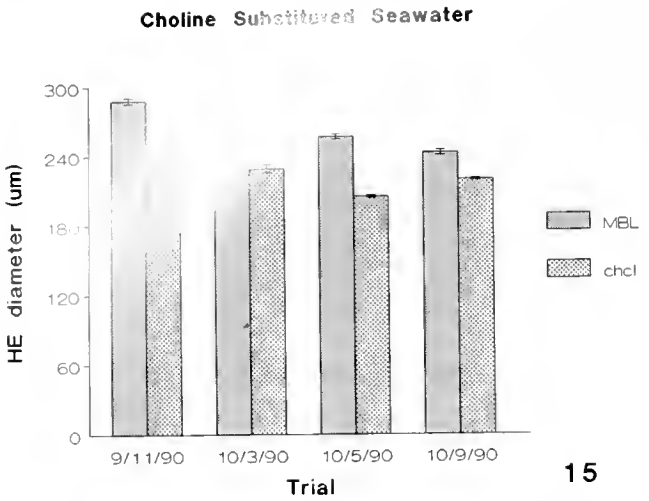

Figure 15. Comparison of hatching envelope diameters of eggs spawned into ASW or choline chloride substituted seawater. In each of the four trials, HE diameters were significantly less in choline chloride substituted seawaters (error bars are standard error; $P < 0.001$; Student t-test).

HE in either ASW or ChCl-substituted seawater revealed a statistically significant difference ($P < 0.001$, Student *t*-test between controls and experimentals (Fig. 15). In addition, the perivitelline space was not as well defined as in eggs spawned into normal seawater (compare Figs. 10, 12 and 14E, F). The thickness of the HE as observed with transmission electron microscopy remained approximately the same, but the definitive bilayered appearance was absent even as late as 70 min after spawning (Figs. 16, 17).

Tris-HCl-substituted seawater prevented the irregular egg surface from smoothing out for an extended period of time in *S. ingentis* (Figs. 14D, 18). Although jelly transformation appeared normal, polar bodies were not observed and the HE did not elevate as late as 90 min post spawning. Envelopes were not detected with TEM, and numerous ring vesicles remained in the cytoplasm as late as 60 min post-spawning.

In contrast, potassium-substituted seawater had little, if any, effect on the spawned eggs of *S. ingentis*. Jelly precursor release was normal, and transformation to a translucent layer was complete. Polar bodies were observed and the HE elevated with no delay as in the normal seawater controls. The bilayered appearance of the envelope in electron micrographs was similar to that observed in the control eggs (Fig. 19).

Transfer from choline chloride-substituted seawater back to normal seawater rescues HE formation

S. ingentis eggs spawned into ChCl-substituted seawater and transferred to normal seawater at varying times, elevated a normal HE as long as the transfer preceded the beginning of HE formation. In *S. ingentis*, transfers between 30 and 45 min post-spawning resulted in eggs with HE elevations not significantly different from controls ($P < .001$, 7 of 9 trials). Although results were assayed only at the light microscopic level, elevated envelopes appeared identical to control eggs in normal seawater. Hatching envelopes of eggs transferred back into ASW once HE elevation had begun (times greater than 50 min post-spawning) were not significantly different from eggs held chronically in ChCl-substituted seawater ($P < .001$, 3 of 3 trials).

In reciprocal experiments, eggs initially spawned into ASW and transferred into ChCl-substituted seawater at times earlier than approximately 45 min (prior to the initial observation of an elevating HE), all had HE's which were significantly reduced in their elevation compared to control counterparts (n = 3 trials). Later transfers did not appear to affect HE elevation.

Urea disperses HEs elevated in low sodium but not those in normal seawater

Eggs of *S. ingentis* spawned into ASW were subsequently treated for 5 min with urea at either 4 or 15 min after the initial elevation of the HE was detected at the light level. At 4 min, the HE's were noticeably less birefringent, more wrinkled in appearance, and of lower elevation when observed with light microscopy. Observations with TEM revealed that at 4 min the outer dense stratum was still present, but the inner flocculent layer was not present (Fig. 20). By 15 min, the envelopes were still wrinkled, although the birefringence of the envelope appeared similar to controls when observed with light microscopy. TEM observations demonstrate that a distinct laminar structure had developed although the inner layer was slightly more flocculent in appearance (Fig. 22) than eggs spawned into normal seawater.

The HEs of eggs spawned into ChCl-substituted seawater were significantly affected when treated with urea at both 4 and 15 min after the elevation of the envelope was first detected. The envelopes in both cases were almost always indistinguishable from the surface of the eggs in phase contrast microscopy. In electron micrographs, the HEs appeared as broken investments with a fluffy irregular morphology (Fig. 21). Those envelopes treated with urea at the 15 min time point were less irregular but retained a distinct fluffy appearance (Fig. 23). In neither case was a laminar morphology ever observed.

Discussion

Eggs of several species of penaeoidean shrimp undergo similar morphological events associated with egg activation following the release of the eggs into normal seawater.

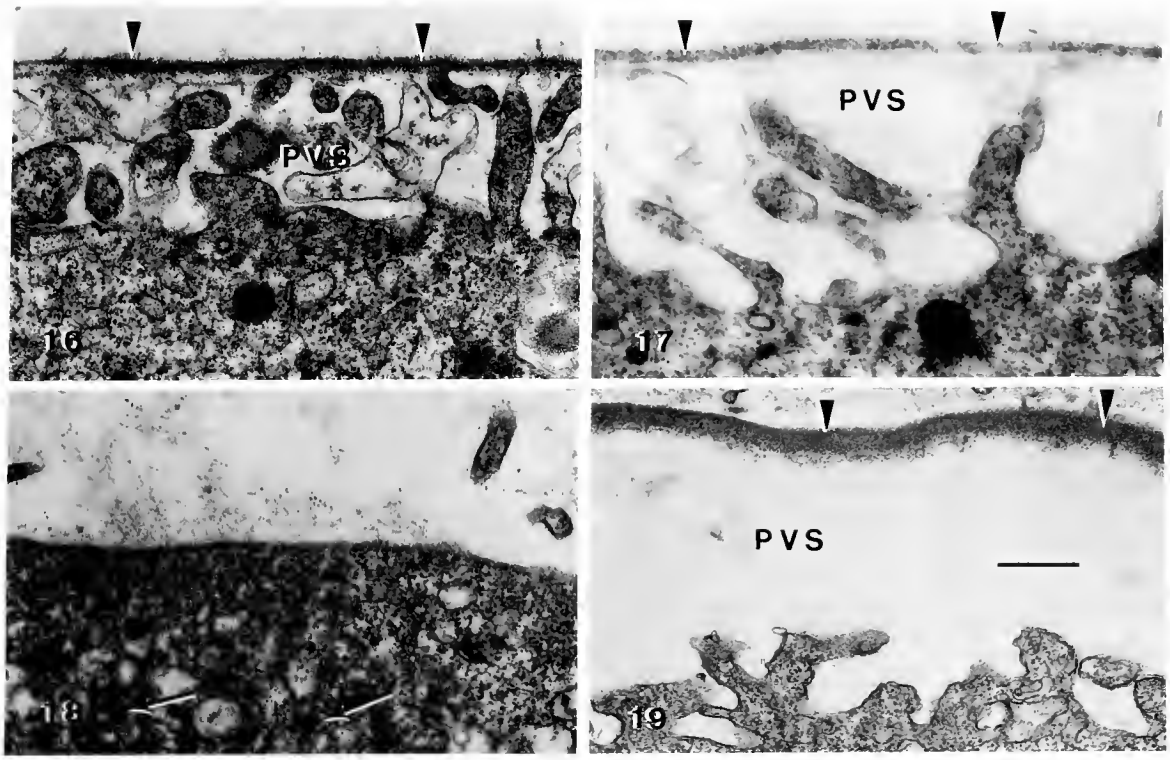

Figures 16–19. A series of TEM micrographs showing effects of various substitutions on HE formation. Arrowheads = HE; PVS = perivitelline space. Bar = 0.5 μm for all.

Figure 16. A *Trachypenaeus similis* egg at 60 min showing the fluffy appearance of an incomplete HE in ChCl-substituted seawater.

Figure 17. A *Sicyonia ingentis* egg at 70 min showing the fluffy appearance of an incomplete HE in ChCl-substituted seawater.

Figure 18. A *S. ingentis* egg at 60 in Tris-substituted seawater. Note the ring vesicles (arrows) in the peripheral cytoplasm. HEs were not detected in any samples.

Figure 19. A *S. ingentis* egg at 60 min in KCl-substituted seawater. The morphology for these HEs appears normal.

Particularly notable are two dramatic and distinct extracellular events resulting in the assembly of new coats around the egg (Clark *et al.*, 1980, 1990; Lynn and Clark, 1987; Pillai and Clark, 1988). The results reported here are the first to demonstrate a role for sodium in the elevation or hardening of the hatching envelope in the penaeoidean shrimp species *T. similis* and *S. ingentis*. Sodium can be replaced by potassium but not by Tris or choline, classic substitutes for sodium (*e.g.*, Chambers and De Armendi, 1979; Schuel *et al.*, 1982). The major effect on the morphology of the HE related to the deficiency of sodium appeared to be the incomplete transformation of the nascent envelope into a definitive bilayered pattern. Particularly interesting is the fact that both of these penaeoid species show a similar dependence on the presence of sodium ions for the assembly of the HE.

A sodium dependency is also observed in the elevation and hardening of the sea urchin fertilization envelope (FE) (Nishioka and Cross, 1978; Schon and Decker, 1981; Schuel *et al.*, 1982; Schuel, 1985; Cheng *et al.*, 1991). The HE of the shrimp and the FE of the sea urchin are similar in that they are formed as the result of the exocytosis of cortical granules, both envelopes are built on a template of a preexisting "surface coat," and both serve a protective function during later developmental stages (Schuel, 1978). During assembly of the FE in the sea urchin, *Strongylocentrotus purpuratus*, the microvillar casts in the vitelline envelope are transformed from a blunt shape to an angular shape apparently by the insertion of structural proteins into the fertilization envelope during the hardening process (Carroll and Baginski, 1978; Chandler and Heuser, 1980; Kay and Shapiro, 1985).

Crosslinking of the components in the hatching envelope were assayed by solubility of the envelope or its components in urea. These assays were similar to those performed by Schuel *et al.* (1982) on sea urchin fertilization envelopes. Several differences between these two systems were apparent from our current observations. First, in the

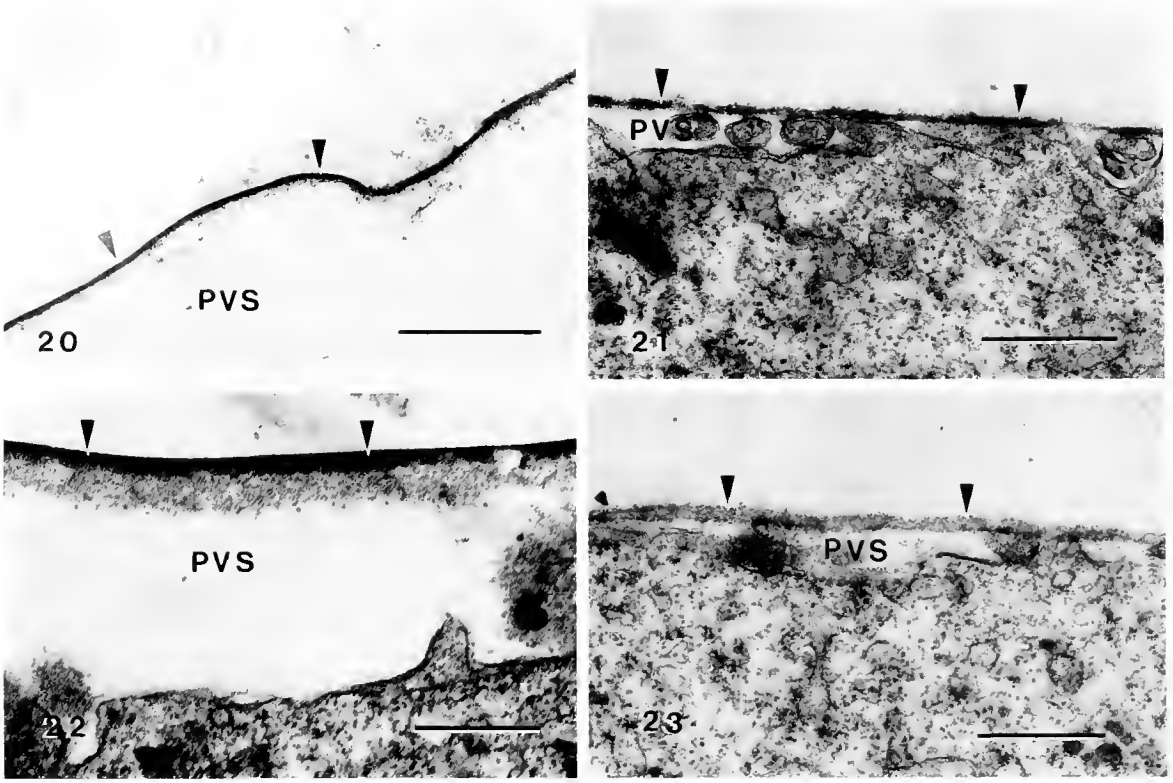

Figures 20–23. A series of TEM micrographs of *Sicyonia ingentis* eggs spawned into ASW or ChCl-substituted seawater, treated at either 4 or 15 min post HE elevation with 1 *M* urea for 5 min, washed and prepared for EM. Arrowheads = HE; PVS = perivitelline space; Bar = 0.5 μm for all.

Figure 20. ASW at 4 min. Dense outer layer remains, but inner flocculent layer is absent (compare to Fig. 13).

Figure 21. ChCl-substituted seawater at 4 min. The HE is fluffier than the dense outer layer remaining in Figure 20 and collapsed onto the egg surface.

Figure 22. ASW at 15 min. The HE retains the normal morphology of a dense outer stratum over an inner flocculent layer.

Figure 23. ChCl-substituted seawater at 15 min. The HE remains fluffy and collapsed onto the egg surface. There is no distinct morphological difference between the ChCl-substituted, urea-treated HE at 4 min and this later time point.

shrimp egg, the envelope was not completely removed with urea in either normal or ChCl-substituted seawater. Therefore, the exocytosis of the dense granules combining with the pre-existing surface coat formed a very stable HE template ("thin HE" of Pillai and Clark, 1988) within 4 min of its appearance. This initial stage of HE formation, then, appears to be independent of the absence of sodium or the presence of choline. In contrast, the fertilization envelope of sea urchins remains labile to urea solubilization for up to 10 min in both normal and sodium-depleted seawaters, indicating the time required for effective crosslinking (Schuel *et al.*, 1982).

Second, HEs of shrimp eggs in normal seawater at 15 min were not affected by urea. Both the outer dense and inner flocculent layer appeared to be intact, implying that the insertion and crosslinking of ring vesicle material into the outer dense layer was completed (Pillai and Clark, 1988). In contrast, the inner layer of HEs in sodium-depleted seawater did not form. In sodium-depleted seawater the thin HEs appeared similar whether treated with urea or not. This suggests that insertion of the ring vesicle material depends upon the presence of sodium (or potassium).

These observations (consistent with those of Schuel *et al.*, 1982, 1985) implicate sodium in the integration of structural proteins into the HE of shrimp eggs. Moreover, in the sea urchin system, quaternary amines affect the elevation of the fertilization envelope, possibly by interfering with protein insertion into the nascent envelope (see Kay and Shapiro, 1985, for review). Although quaternary amines have not been investigated systematically for their effects on the elevation and hardening of the HE around penaeoid eggs, we cannot rule out the possibility of similar effects of the amine-containing compounds, Tris

and choline. It should be pointed out that in the present studies, of the substitutes used, only choline is a quaternary amine. In addition, in experiments with a partial choline chloride substitution for sodium HE elevation was not statistically different from control eggs. These data suggest that concentrations of choline chloride as high as 240 m*M* did not have an observable effect. Conversely, it may be interpreted that the requirement for sodium in HE formation in these experiments was satisfied.

A second possibility might be inhibition of exocytotic processes responsible for the formation of the HE. However, there is currently no evidence to suggest that the exocytosis of the cortical vesicles associated with the elevation and transformation of the HE was inhibited in choline substituted seawater. When Tris was used as a sodium substitute, ring vesicle exocytosis was inhibited, as evidenced by the number of vesicles remaining in the cortical cytoplasm. On the other hand, the dense vesicles, which are the first to undergo exocytosis, were not observed in the egg cortex. Because the first phase of HE assembly was not observed in Tris-treated eggs, the fate of the dense vesicles is unclear.

Our data here demonstrate a significant effect of the ionic composition of seawater on the formation of the HE in *S. ingentis* and *T. similis*. These observations on HE assembly and elevation in the penaeoidean shrimp are consistent with data from the sea urchin system suggesting a role for sodium in the regulated assembly of an extracellular matrix.

Acknowledgments

We wish to express our thanks to Drs. Wallis H. Clark and Fred Griffin at the Bodega Marine Laboratory in Bodega Bay, California, for supplying animals (*Sicyonia ingentis*) and the many long discussions regarding egg activation in penaeid shrimp. *Trachypenaeus similis* females were kindly provided through the cooperation of Jim Hanifen and his colleagues from the Coastal Ecology Section of the Louisiana Department of Wildlife and Fisheries. We also thank Carol Thouron and Michele St. Onge for their technical assistance at Louisiana State University Medical Center in preparing sections and Susan Hughes at LSU for her general laboratory help and cheerful attention to the drudgery of tedious details. This research was supported in part by funding from NOAA, National Sea Grant Program, U.S. Dept. of Commerce, under grant #NA89AA-D-SG226 project #R/SA-1 through the Louisiana Sea Grant College Program at Louisiana State University.

Literature Cited

Carroll, E. J., Jr., and R. M. Baginski. 1978. Sea urchin fertilization envelope: isolation, extraction and characterization of a major protein fraction from *Strongylocentrotus purpuratus* embryos. *Biochemistry* **17:** 2605–2612.

Chambers, E. L., and J. De Armendi. 1979. Membrane potential, action potential and activation potential of eggs of the sea urchin, *Lytechinus variegatus*. *Exp. Cell Res.* **122:** 203–218.

Chandler, D. E., and J. Heuser. 1980. The vitelline layer of the sea urchin egg and its modifications during fertilization: a freeze fracture study using quick freeze and deep-etching. *J. Cell Biol.* **84:** 618–632.

Cheng, S-d., P. S. Glas, and J. D. Green. 1991. Abnormal sea urchin fertilization envelope assembly in low sodium seawater. *Biol. Bull.* **180:** 346–354.

Clark, W. H., Jr., J. W. Lynn, A. I. Yudin, and H. O. Persyn. 1980. Morphology of the cortical reaction in the eggs of *Penaeus aztecus*. *Biol. Bull.* **158:** 175–186.

Clark, W. H., Jr., and J. W. Lynn. 1977. A Mg^{++} dependent cortical reaction in the eggs of Penaeid shrimp. *J. Exp. Zool.* **200:** 177–183.

Clark, W. H., A. I. Yudin, J. W. Lynn, F. J. Griffin, and M. C. Pillai, 1990. Jelly layer formation in penaeoidean shrimp eggs. *Biol. Bull.* **178:** 295–299.

Gould-Somero, M., L. A. Jaffe, and L. Z. Holland. 1979. Electrically mediated fast polyspermy block in eggs of the marine worm. *Urechis caupo*. *J Cell Biol.* **82:** 426–440.

Green, J. D., P. S. Glas, and J. W. Lynn. 1990. Jelly release in shrimp eggs is suppressed by trypsin inhibitors. *Am. Zool.* **30:** 39a.

Kay, E. S., and B. M. Shapiro. 1985. The formation of the fertilization membrane of the sea urchin egg. Pp. 45–80 in *Biology of Fertilization*, C. B. Metz and A. Monroy, eds. Academic Press, Orlando, FL.

Lynn, J. W., M. C. Pillai, P. S. Glas, and J. D. Green. 1991. Comparative morphology and physiology of egg activation in selected Penaeoidea. Pp. 47–64 in *Frontiers of Shrimp Research*, P. De Loach, ed. Elsevier, NY.

Lynn, J. W., and W. H. Clark, Jr. 1987. Physiological and biochemical investigations of the egg jelly release in *Penaeus aztecus*. *Biol. Bull.* **173:** 451–460.

Nishioka, D., and N. Cross. 1978. The role of external sodium in sea urchin fertilization. *ICN-UCLA Symp. Mol. Cell. Biol.* **12:** 403–412.

Pillai, M. C., and W. H. Clark, Jr. 1987. Oocyte activation in the marine shrimp, *Sicyonia ingentis*. *J. Exp. Zool.* **244:** 325–329.

Pillai, M. C., and W. H. Clark, Jr. 1988. Hatching envelope formation in shrimp (*Sicyonia ingentis*) ova: origin and sequential exocytosis of cortical vesicles. *Tissue Cell* **20:** 941–952.

Pillai, M. C., and W. H. Clark, Jr. 1990. Development of cortical vesicles in *Sicyonia ingentis* ova: their heterogeneity and role in elaboration of the hatching envelope. *Mol. Reprod. Dev.* **26:** 78–89.

Pillai, M. C., F. J. Griffin, and W. H. Clark, Jr. 1988. Induced spawning of the decapod crustacean *Sicyonia ingentis*. *Biol. Bull.* **174:** 181–185.

Schon, E. A., and G. L. Decker. 1981. Ion-dependent stages of the cortical reaction in surface complexes isolated from *Arbacia punctulata* eggs. *J. Ultrastruc. Res.* **76:** 191–201.

Schuel, H. 1985. Functions of egg cortical granules. Pp. 1–43 in *Biology of Fertilization*, C. B. Metz and A. Monroy, eds. Academic Press, Orlando, FL.

Schuel, H. 1978. Secretory functions of egg cortical granules in fertilization and development: a critical review. *Gamete Res.* **1:** 299–382.

Schuel, H., R. Schuel, P. Dandekar, J. Boldt, and R. G. Summers. 1982. Sodium requirements in hardening of the fertilization envelope and embryonic development in sea urchins. *Biol. Bull.* **162:** 202–213.

Spurr, A. R. 1969. A low viscosity epoxy resin embedding medium for electron microscopy. *J. Ultrastruct. Res.* **26:** 31–43.

Reference: *Biol. Bull.* **183:** 94–98. (August, 1992)

Tolerance of Infaunal Benthic Foraminifera for Low and High Oxygen Concentrations

LEON MOODLEY AND CHRISTOPH HESS

Netherlands Institute for Sea Research, P. O. Box 59, 1790 AB, Den Burg, Texel, The Netherlands

Abstract. *Ammonia beccarii* is irregularly distributed in the subtidal sediment of the southern North Sea, with substantial numbers occurring as deep as 35 cm below the water-sediment interface. Deep infaunal specimens are insensitive to high oxygen concentrations (±225 μM), and all specimens isolated from different depth intervals continued their normal activities (feeding and growth) when exposed to dysaerobic oxygen content (<12.5 μM). Specimens of *E. excavatum*, *Q. seminulum*, and *E. scabra*, when subjected to the same conditions, behave similarly to *A. beccarii*. These benthic foraminifera have very low oxygen requirements.

The chambers of *A. beccarii* that are formed *in situ* at different depth intervals in the sediment have a wide range in the porosity (*i.e.*, % of area occupied by pores) which is adequate for gas exchange under both high and low oxygen conditions. However, chambers formed in the laboratory under dysaerobic conditions have a significantly higher porosity (mainly due to larger pores) than do chambers constructed in well oxygenated water.

Foraminifera live at the oxic-anoxic boundary throughout the sediment and therefore must occasionally be subjected to completely anoxic conditions. *A. beccarii*, *E. excavatum*, and *Q. seminulum* actively survived at least 24 h without oxygen, indicating that they are capable of facultative anaerobic metabolism.

Introduction

Benthic foraminifera occur epiphytically, epizoically, epifaunally, and infaunally (*e.g.*, Buzas, 1974; Thiel, 1975; Coull *et al.*, 1977; Alexander and DeLaca, 1987; Bernhard, 1989; Lutze and Thiel, 1989). They evidently exploit all benthic marine environments, and some soft-shelled forms also inhabit empty foraminiferal tests (Gooday, 1986; Moodley, 1990a).

There seem to be two general trends in the vertical distribution of benthic foraminifera in soft sediments. In deep-sea environments, certain species have their maximum densities in deeper sediment layers (below the upper two centimeters) and appear to prefer the associated low oxygen concentrations (Corliss, 1985; Mackensen and Douglas, 1989). The advantage of active migration to these deeper layers would be less competition and predation (Gooday, 1986; Mackensen and Douglas, 1989). There is some evidence that infaunal species are adapted to their habitats, having greater pore densities evenly distributed over most of the test (in response to low oxygen content); their tests have rounded edges and planispiral coiling or have ovate or cylindrical shapes. In contrast, epifaunal species (that live on and within the upper centimeter; Corliss, 1985) are biconvex or plano-convex and either lack pores or have large surface pores on only one side of the test (Corliss and Emerson, 1990).

In shallow subtidal and intertidal areas, the vertical distribution of benthic foraminifera is irregular without a consistent stratification of species. The occurrence of Foraminifera in deeper layers has been attributed to passive transport resulting from bioturbation (*e.g.*, Collison, 1980; Langer *et al.*, 1989), and substantial numbers are often encountered below the oxygenated layer (Bernhard, 1989; Moodley, 1990b). When food is abundant throughout the sediment, there seems to be no need for foraminifera to concentrate at any particular level or for species to partition their habitat vertically (Thiel, 1983). Further, the extent to which they can maintain a desired depth depends on the physical (water movement) and biological (macrofaunal activities) stability of the sediment.

The availability of food determines the maximum habitat depth in deep-sea sediment, which varies from 6 to 15 cm (Coull *et al.*, 1977; Corliss, 1985). Oxygen avail-

Received 2 October 1991; accepted 18 May 1992.

ability may set the limits in shallow areas, which generally have a larger supply of organic matter (Gooday, 1986): Foraminifera have been reported to be living at core depths of 30–35 cm in such areas (Goldstein, 1988; Moodley, 1990b). Although Foraminifera sampled from below the oxic layer have been reported to be alive (as assessed by cytoplasmic stainability or cytoplasmic streaming), actual activity under dysaerobic or anoxic conditions has not been demonstrated.

In a shallow, organically enriched zone in the southern North Sea, oxygen penetration in May 1990, excluding the local subduction by macrofauna, was only 4.5 mm, yet the majority of the foraminiferan population was encountered below this depth. The differences in infaunal densities of foraminifera in this area have been related to the type of bioturbation (Moodley, 1990b). *Ammonia beccarii* (Linné), like all other foraminifera, had maximum numbers within the upper 5 cm, but remained common down to 35 cm (Moodley, 1990b).

Deep infaunal specimens are exposed to low oxygen concentrations. Therefore, to test whether infaunal and epifaunal specimens of *A. beccarii* differ in their sensitivity to different oxygen concentrations, specimens were isolated from different depth intervals and exposed to both high and low oxygen concentrations. Some species, like *A. beccarii*, have pores both on the dorsal and ventral side. To search for further variation in the response to low oxygen concentrations, pores in *A. beccarii* were counted and pore diameters measured, for chambers constructed under different conditions. Specimens of *Elphidium excavatum* (Terquem), *Quinqueloculina seminulum* (Linné) and *Eggerella scabra* (Williamson) were also exposed to the same conditions but were not examined in detail.

Because they occur at the oxic-anoxic boundary throughout the sediment, a few species of foraminiferans were maintained totally without oxygen, and their fate under these conditions was determined. *A. beccarii* was examined for methanogenic bacteria because anaerobic protozoans sometimes certain symbiotic methanogenic bacteria that take up the protons formed when the protozoans remove reduction equivalents as hydrogen (Van Bruggen *et al.*, 1983; Fenchel, 1987).

Material and Methods

Sediment samples were collected several times during 1989 and 1990 with a Reineck box-corer from the Frisian Front area in the southern North Sea (Moodley, 1990b). This area (40 m water depth) is characterized by a fine grained sediment with a high POC content (1.29% in June and 0.55% in February; Moodley, 1990b). Subsamples were taken from the box-cores with a PVC pipe (Ø 9.5 cm). On boards centimeter slices of the cores were immediately made; the slices were kept in glass jars with seawater and maintained at ambient temperature until the initiation of the experiments. The following intervals were sampled: 0–1, 4–5, 9–10, 14–15, 19–20, 29–30, and 34–35 cm.

Benthic foraminifera occurring in soft sediments feed by first concentrating particles around the aperture or test, forming a food cyst; the presence of empty cysts, or of particles attached to the tests, would indicate that the protozoans were active under the maintenance conditions. In polythalamous (multi-chambered) species, growth is achieved by the construction of a new chamber, and an increase in the number of chambers is also used as an indicator of activity under the different conditions. Just before the beginning of every experiment, each foraminiferan specimen was cleaned under the dissecting microscope (all attached particles were removed from the test with a brush). The maximum diameter of the test was then measured and the number of chambers counted under the inverted microscope. Every foraminiferan used in the experiments was isolated from field samples that had been collected no more than three days before the start of the experiments.

The sensitivity of *A. beccarii* to high oxygen levels was examined as follows. Specimens of the same size range were isolated from different depth intervals (n = 21, 1–5 specimens per depth interval) and maintained with fresh detritus as food, at 15°C and without light, until they built a new chamber. The detritus was either the <50 μm fraction removed from surface sediment or heat-killed *Chlorella*. These benthic foraminifera, maintained only with detritus as a food source, have been observed to grow and reproduce in the laboratory (Moodley, unpub.). High oxygen concentrations (±225 μM, monitored with an oxygen meter) were maintained by frequently replacing the seawater with well oxygenated seawater. Specimens of *E. excavatum* (n = 3), *E. scabra* (n = 4), and *Q. seminulum* (n = 4) were also included in this experiment.

To examine their behavior under low oxygen conditions, another set of foraminiferans isolated from different depth intervals (n = 12, 1–2 specimens per depth interval) were maintained with less than 12 μM O_2. The low oxygen content was obtained by extensively flushing the seawater in the maintenance vessel with nitrogen (N_2 type 6.0, that was guaranteed to contain <12.5 μM O_2, Air Products, Nederland BV) until the reading on the oxygen meter passed the zero value. Zero calibration was done with a zero-oxygen solution (HI 7040, Hanna Instruments USA). The maintenance vessel, constructed especially for these experiments, was hermetically sealed and kept for 6 days without any increase in oxygen content, as registered by constant monitoring. Specimens of *E. excavatum* (n = 6), *E. scabra* (n = 7), and *Q. seminulum* (n = 4) were also exposed to low oxygen concentrations.

Table I

Sensitivity of specimens from [illegible] intervals (cm) in the sediment to different [illegible] trations

Depth interval	High ox (±225				Low oxygen (<12 μM)				Anoxic[a]			
	A	Eg	[illegible]	Q	A	Eg	El	Q	A	Eg	El	Q
0–1	++	+	nd	nd	++	+	nd	nd	+	nd	+	+
4–5	++	+	+	nd	++	nd	+	nd				
9–10	+	nd	++	nd	++	+	+	nd				
14–15	++	nd	nd	nd	+	+	+	nd				
19–20	++	nd	nd	+	++	nd	nd	+				
29–30	++	+	+	nd	++	+	+	nd				
34–35	++	nd	nd	nd	++	+	+	nd				

[a] For the anoxic experiment, only specimens isolated from upper cm of the sediment were used (n = 8). The number of specimens of each species from different depth intervals exposed to high or low oxygen varied from 1 to 5 specimens. A = *A. beccarii*, El = *E. excavatum*, Eg = *E. scabra*, Q = *Q. seminulum*. (+) = active, (++) = active and growing, nd = no data.

Morphological variation in *A. beccarii* in response to different oxygen concentrations was also examined. The pore characteristics of the chambers constructed under maintenance conditions were measured. Individuals maintained under high oxygen and individuals maintained under low oxygen were compared.

Specimens were isolated from different depths in the sediment, and the pore characteristics of the tests were evaluated. Because a few specimens had aberrant last chambers, the penultimate chamber was used for this analysis of *in situ* test formation at different depths.

The pores on the dorsal side of the chambers (visualized on SEM micrographs) were counted and a standard area calculated. The pore diameters were also measured and considered together with pore density as porosity (*i.e.*, % of chamber area occupied by pores), as calculated by Frerichs *et al.* (1972). The significance of the differences were tested with the Mann-Whitney *U* Test.

In the third experiment, specimens of *A. beccarii* (n = 1), *E. excavatum* (n = 2) and *Q. seminulum* (n = 5), isolated from surficial sediment, were exposed to anoxic conditions for 24 h with detritus as food. The maintenance vessel was kept at room temperature (±20°C) without light. Anoxic conditions were obtained by first extensively flushing with nitrogen and then removing traces of oxygen with ascorbic acid (a strong reducing agent; 0.13%), and then immediately hermetically sealing off the vessel. The above treatment also results in a color change of resazurin and methylene blue; these redox indicators were individually added to control vessels lacking foraminifera, verifying the reduced conditions of the maintenance medium which was buffered with 30 mM sodium bicarbonate.

Methanogenic bacteria are characterized by fluorescent coenzymes that are easily detected by epifluorescence microscopy (Van Bruggen *et al.*, 1983; Fenchel, 1987), so this method was used to search for symbiotic methanogenic bacteria in *A. beccarii*.

Results

Deep infaunal specimens proved to be insensitive to high oxygen concentration, for they continued feeding and growing (Table I). All of the specimens examined continued to be active even at extremely low oxygen concentrations (<12 μM). Activity was not restricted to feeding; six specimens of *A. beccarii* also continued growing at low oxygen levels (Table I).

There is a wide range in the porosity of chambers of *A. beccarii* constructed *in situ* at different depth intervals in the sediment (Fig. 1). But the porosity of the chambers constructed in the laboratory under dysaerobic conditions is significantly higher than that of the chambers formed under well oxygenated conditions (±225 μM; Table II). This difference is mainly due to a significant difference in pore diameter, and not in pore density (Table II).

All specimens actively endured 24 h without oxygen (Table I), as implied by the presence of particles around the test or aperture. In one of the trial experiments (not included in Table I) inadequate buffering resulted in a drop in pH (to <6) causing the almost total decalcification of the foraminifera; nevertheless they were still alive and active under anoxic conditions.

No methanogenic bacteria were detected in *A. beccarii*. This is not strange since methanogens are considered to be extremely sensitive to oxygen.

Discussion

With an oxygenated layer only a few millimeters thick, infaunal specimens are totally dependent on the burrow-

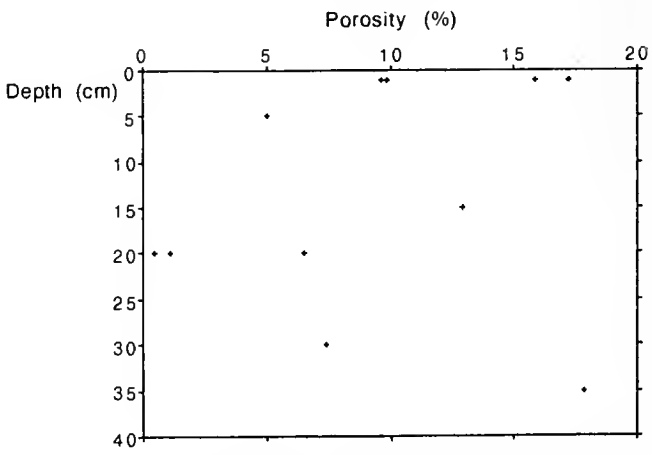

Figure 1. Porosity of the penultimate chambers of *Ammonia beccarii* formed *in situ* at different depth intervals in the sediment.

Table II

Comparison of pore characteristics in chambers of Ammonia beccarii *formed under different oxygen concentrations*

	Pore density		Pore diameter		Porosity	
	H	L	H	L	H	L
	1284	559	1	1.8	10.1	14.2
	1083	410	1.13	1.6	10.9	8.2
	715	653	1.08	2	6.5	20.5
	1391	84	0.8	0.7	7	0.3
	1001	221	1.08	2.37	9.2	9.7
	235	842	1.08	1.76	2.2	20.5
	144	780	0.3	1.35	0.1	11.2
	841	905	0.67	1.35	3	12.9
	671		0.7		2.6	
Mean	815	557	0.87	1.62	5.73	12.19
SD	430	297	0.28	0.5	3.9	6.62
Statistical difference	ns		$P > 0.005$***		$0.025 > P > 0.01$**	

Pore densities (#/10^4 μm^2), pore diameters (μm) and porosity (%) of the chambers formed in maintenance under high (±225 μM = H) and low (<12.5 μM = L) oxygen concentrations with statistical differences (Mann-Whitney U Test).

ing activities and irrigation of macrofauna for their oxygen supply. Depending on the type of bioturbation, foraminifera are transported to deeper layers and, at the same time, are provided with food and oxygen or are simply buried and then subjected to anoxic conditions. They generally exhibit negative geotaxis (Richter, 1964; Lee *et al.*, 1969; Severin and Erskian, 1981; Moodley, 1990b), and this behavior ensures, to a certain extent, their position in more favorable layers with respect to food and oxygen availability. When the supply of oxygen is cut off, *e.g.*, because the burrower has moved, they are subjected to anoxia that they can endure for at least 24 h. The presence of particles around the test or aperture indicates pseudopodial activity under anoxic and dysaerobic conditions, so they are capable of migrating to more favorable layers, permitting aerobic metabolism with a higher ATP-yield. Bolivinids and buliminids burrow into oxygen-depleted layers (Kitazato, 1981) and may be able to endure anoxic conditions for even longer periods.

Facultative anaerobiosis is not uncommon in free-living Protozoa (Fenchel, 1987; Anderson, 1988) and in marine infaunal invertebrates: *e.g.*, various bivalve mollusks (see Zwaan, 1977), polychaete worms *Arenicola marina* (see Zebe, 1975), and *Nereis diversicolor* (see Schöttler, 1978). In all cases, some sort of fermentation process provides metabolic energy. Considering the environment these benthic foraminifera inhabit and their very slow movement (0.84–30.0 mm/h; Kitazato, 1988), facultative anaerobiosis would seem to be necessary for their survival. Although no symbiotic methanogenic bacteria were found in *A. beccarii* from the southern North Sea with well-oxygenated bottom water, foraminifera living in sediment below anoxic waters (*i.e.*, exposed to prolonged anoxic conditions) may very well have symbionts, as earlier suggested by Kitazato (1989) for infaunal species. However, under constant, totally anoxic conditions benthic foraminifera are absent (Murray, 1991).

A wide range in porosity in *A. beccarii* (Fig. 1) is apparently adequate for gas exchange under both low and high oxygen conditions (Table I). But gas exchange is increased when pores are larger (Table II). Indeed, foraminiferan gas exchange is enhanced by the concentration of their mitochondria under pore openings (Leutenegger and Hansen, 1979), which would be maximized by larger pores. Hofker (1968) noted that the pore diameter of Cretaceous gavelinellid species increases progressively with test volume and attributed this phenomenon to greater respiratory requirements. However, the function of pores in gas exchange does not exclude other functions (Leutenegger and Hansen, 1979).

Benthic foraminifera evidently have very low oxygen requirements and respiration rates (Bradshaw, 1961; Lee and Muller, 1973). They belong to the subphylum Sarcodina that, as a group, also seems to have lower metabolic rates when compared to flagellates and ciliates of the same size (Fenchel, 1987). Benthic foraminifera have also been reported to grow and reproduce slightly below the oxidized zone (Matera and Lee, 1972). That low oxygen concentration is not a limiting factor for their existence is also corroborated by field observations. For example, as a result of a depressed oxygen level (0.21 ml l^{-1} or 9.24 μM O_2) in the winter of 1979-80 in the deep basin (115 m) of the Gullmar Fjord, Sweden, the macrofaunal component of the fauna disappeared. In contrast, the meiofauna exhibited no clear signs of being affected and, of all the meiofaunal taxa, the foraminifera seemed to withstand these conditions best (Josefson and Widbom, 1988). Deep-sea benthic environments with *continuous* dysaerobic conditions (oxygen-depleted bottom waters) support large standing stocks, but a low diversity of benthic foraminifera (*e.g.*, Phleger and Soutar, 1973; Douglas *et al.*, 1980; see Mackensen and Douglas, 1989). This could probably be explained in terms of different tolerance levels of oxygen concentrations for survival and reproduction. Additionally, assemblages that predominate during prolonged or continuous dysaerobic conditions consist mainly of flattened (shapes with a high surface area/volume ratio), unornamented, highly perforate, and thin walled forms (Bernhard, 1986).

Acknowledgments

We thank J. E. van Hinte and G. C. Cadée for their critical review and valuable suggestions. R. P. M. Bak and

J. H. Vosjan are gratefully acknowledged for their comments. Many thanks to E. Epping and C. G. N. de Vooys for essential discussions on the subject of anaerobic culture. The paper benefited from criticism by two anonymous reviewers. All maintenance vessels were constructed by the technical staff of the NIOZ (The Netherlands Institute for Sea Research).

Literature Cited

Alexander, S. P., and T. E. DeLaca. 1987. Feeding adaptations of the foraminiferan *Cibcides refugens* living epizoically and parasitically on the Antarctic scallop *Adamussium colbecki*. *Biol. Bull.* **173:** 136–155.

Anderson, O. R. 1988. *Comparative Protozoology.* Springer-Verlag, New York, 482 pp.

Bernhard, J. M. 1986. Characteristic assemblages and morphologies of benthic Foraminifera from anoxic, organic-rich deposits: Jurassic through Holocene. *J. Foram. Res.* **16:** 207–215.

Bernhard, J. M. 1989. The distribution of benthic foraminifera with respect to oxygen concentration and organic carbon levels in shallow-water Antarctic sediments. *Limnol. Oceanogr.* **34:** 1131–1141.

Bradshaw, J. S. 1961. Laboratory experiments on the ecology of Foraminifera. *Cushman Found. Foram. Res. Contr.* **12:** 87–106.

Buzas, M. A. 1974. Vertical distribution of *Ammobaculites* in the Rhode River, Maryland. *J. Foram. Res.* **7:** 144–147.

Collison, P. 1980. Vertical distribution of foraminifera off the coast of Northumberland, England. *J. Foram. Res.* **10:** 75–78.

Corliss, B. H. 1985. Microhabitats of benthic foraminifera within deep-sea sediments. *Nature* **314:** 435–438.

Corliss, B. H., and S. Emerson. 1990. Distribution of Rose Bengal stained benthic foraminifera from the Nova Scotia continental margin and Gulf of Maine. *Deep-Sea Res.* **37:** 381–400.

Coull, B. C., R. L. Ellison, J. W. Fleeger, R. P. Higgins, W. D. Hope, W. D. Hummon, R. M. Rieger, W. E. Strerer, H. Thiel, and J. H. Thiel. 1977. Quantitative estimates of the meiofauna from the deep-sea of North Carolina, USA. *Mar. Biol.* **39:** 233–240.

Douglas, R. G., J. Liestman, C. Walch, G. Blake, and M. L. Cotton. 1980. The transition from live to sediment assemblage in benthic foraminifera from the southern California borderland. Pp. 257–280 in *Quarternary Depositional Environments of the Pacific Coast* M. E. Field, A. H. Bouma, I. P. Colburn, R. G. Douglas, and J. C. Ingle, eds. Pacific Coast Paleogeography Symposium 4, Pacific Section S. E. P. M., Los Angeles.

Fenchel, T. 1987. *Ecology of Protozoa.* Science Tech. Publishers, Madison, WI. 197 pp.

Frerichs, W. E., M. E. Heiman, L. E. Borgman, and A. W. H. Bé. 1972. Latitudinal variations in planktonic foraminiferal test porosity: Part 1. Optical studies. *J. Foram. Res.* **2:** 6–13.

Goldstein, S. T. 1988. Foraminifera of relict salt marsh deposits, St. Catherines Island, Georgia: taphonomic implications. *Palaios* **3:** 327–334.

Gooday, A. 1986. Meiofaunal foraminiferans from the bathyal Porcupine Seabight (north east Atlantic): size structure, standing stock, taxonomic composition, species diversity and vertical distribution in the sediment. *Deep-Sea Res.* **33:** 1135–1373.

Hofker, J. 1968. Studies of foraminifera. Part 1—General problems. *Publ. Natuurhistorisch Genoot. Limburg* **18:** 1–135.

Josefson, A. B., and B. Widbom. 1988. Differential response of benthic macrofauna and meiofauna to hypoxia in the Gullmar fjord basin. *Mar. Biol.* **100:** 31–40.

Kitazato, H. 1981. Observations of behaviour and mode of life of benthic foraminifers in laboratory. *Geosci. Rep. Shizuoka Univ.* **6:** 61–71.

Kitazato, H. 1988. Locomotion of some benthic foraminifera in and on sediments. *J. Foram. Res.* **18:** 344–349.

Kitazato, H. 1989. Vertical distribution of benthic foraminifera within sediments (Preliminary Report). *Benthos Research* (Bull. Jpn. Assoc. Benthology) **35/36:** 41–51.

Langer, M., L. Hottinger, and B. Huber. 1989. Functional morphology in low-diverse benthic foraminiferal assemblages from tidal flats of the North Sea. *Senckenberg. Marit.* **20:** 81–90.

Lee, J. J., W. A. Muller, R. J. Stone, M. E. McEnery, and W. Zucker. 1969. Standing crop of foraminifera in sublittoral epiphytic communities of Long Island salt marsh. *Mar. Biol.* **4:** 44–61.

Lee, J. J., and W. A. Muller. 1973. Trophic dynamics and niches of salt marsh foraminifera. *Am. Zool.* **13:** 215–223.

Leutenegger, S., and H. J. Hansen. 1979. Ultrastructural and radiotracer studies of pore function in foraminifera. *Mar. Biol.* **54:** 11–16.

Lutze, G. F., and H. Thiel. 1989. Epibenthic foraminifera from elevated microhabitats: *Cibicidoides wuellerstorfi* and *Planula arminensis*. *J. Foram. Res.* **19:** 153–158.

Mackensen, A., and R. G. Douglas. 1989. Down-core distribution of live and dead deep-water benthic foraminifera in box-cores from the Weddell Sea and the California continental borderland. *Deep-Sea Res.* **36:** 879–900.

Matera, N. J., and J. J. Lee. 1972. Environmental factors affecting the standing crop of foraminifera in sublittoral and psammolittoral communities of a Long Island salt marsh. *Mar. Biol.* **14:** 89–103.

Moodley, L. 1990a. "Squatter" behaviour in soft-shelled foraminifera. *Mar. Micropaleontol.* **16:** 149–153.

Moodley, L. 1990b. Southern North Sea seafloor and subsurface distribution of living benthic foraminifera. *Neth. J. Sea. Res.* **27:** 57–71.

Murray, J. W. 1991. *Ecology and Palaeoecology of Benthic Foraminifera.* Longman Scientific and Technical, England. 397 pp.

Phleger, F. B., and A. Soutar. 1973. Production of benthic foraminifera in three east Pacific oxygen minima. *Micropaleontology* **19:** 110–115.

Richter, G. 1964. Zur Ökologie der Foraminiferen. II. Lebensraum und Lebensweise von *Nonion depressulum, Elphidium excavatum* und *E. selseyense*. *Natur. Museum* **94:** 421–430.

Schottler, U. 1978. Investigations of the anaerobic metabolism of the polychaete worm *Nereis diversicolor*. *M. J. Comp. Physiol.* **125:** 185–189.

Severin, K. P., and M. G. Erskian. 1981. Laboratory experiments on the vertical movements of *Quinqueloculina impressa* Reuss through sand. *J. Foram. Res.* **11:** 133–136.

Thiel, H. 1975. The size structure of the deep-sea benthos. *Intern. Rev. Ges. Hydrobiologie* **60:** 575–606.

Thiel, H. 1983. Meiobenthos and nanobenthos of the deep-sea. Pp. 167–230 in *The Sea*, vol. 8. G. T. Rowe, ed. John Wiley, New York.

Van Bruggen, J. J. A., C. K. Stumm, and G. D. Vogels. 1983. Symbiosis of methanogenic bacteria and sapropelic protozoa. *Arch. Mikrobiol.* **136:** 89–96.

Zebe, E. 1975. *In vivo*-Untersuchungen über den Glucose-Abbau bei *Arenicola marina* (Annelida, Polychaeta). *J. Comp. Physiol.* **101:** 135–145.

Zwaan, A de. 1977. Anaerobic energy metabolism in bivalve molluscs. *Oceanogr. Mar. Biol. Ann. Rev.* **15:** 103–187.

Reference: *Biol. Bull.* **183**: 99–112. (August, 1992)

Pathologic Cuticular Changes of Winter Impoundment Shell Disease Preceding and During Intermolt in the American Lobster, *Homarus americanus*

ROXANNA M. SMOLOWITZ, ROBERT A. BULLIS, AND DONALD A. ABT

Laboratory for Marine Animal Health, School of Veterinary Medicine, University of Pennsylvania, Marine Biological Laboratory, Woods Hole, Massachusetts, 02543

Abstract. Cuticular lesions from twenty-four market sized lobsters (*Homarus americanus*) with winter impoundment shell disease were examined. Histological descriptions of cuticular lesions were correlated with the substage of molt for each lobster, because cuticle components and inflammatory mechanisms vary in each. A lesion severity grading system was developed and applied to four specific substages of the five-stage (A–E) molting cycle. Lesions present in substage C_4, in which the membranous layer is deposited, and D_0 (passive premolt) were divided into five grades, ranging from mild erosions (Grade I) to severe ulceration (Grade V) of the cuticle. Cuticular lesions from lobsters in C_4/D_0 were compared with cuticular lesions from lobsters in substages C_2/C_3. Defensive mechanisms exhibited by animals in all substages were epicuticle deposition, melanization, inflammatory cell infiltration, and pseudomembrane formation. In addition, animals in C_4 and D_0 showed proliferation of the membranous layer in affected foci. The lesion grading scheme presented in this paper can be used to describe and compare both inter- and intraspecies crustacean shell lesions.

Introduction

After their capture, and until their sale, many American lobsters, *Homarus americanus*, are held in tidal impoundments. These impoundment populations can be maintained for up to six months, a period sufficient to span closed seasons and times of adverse weather. The impoundments, built by damming off coves or suitable sections of beach, must be located where the rise and fall of the tides are great enough to ensure adequate flushing of the pound. Ideally, impoundments should be cool in summer, seldom freeze in winter, and be in an area of relatively high and constant inshore salinity. Conditions in a pound primarily depend on the number and health of the lobsters impounded, the quality of the water supply, and the extent to which it is replaced at high tide. Even in excellent locations, unfavorable conditions may develop in pounds, particularly during neap tides (McLeese and Wilder, 1964).

A commonly recognized problem of lobsters held in impoundments during the winter months is an increase in shell disease. This unsightly condition, characterized by blackened (melanized) erosions into the cuticle, affects marketability and can spread through a population leading to widespread losses and decreased profitability. Winter mortalities due to shell disease have historically been a particular problem in Nova Scotia (Hess, 1937; Taylor, 1948; Malloy, 1978; Bullis, 1989; Getchell, 1989). Previous reports provide minimal information about the inflammatory mechanisms and pathogenesis of this disease, especially with regard to the differences apparent during various stages of the molting cycle. Malloy (1978) briefly described progressive cuticular erosions resulting from the establishment of mixed populations of bacteria, with chitinolytic ability, within the lesions. But he did not describe the inflammatory mechanisms or the effects of the molting cycle on the histological appearance of the erosions. Any description of progressive cuticular lesions must be related to the histological appearance of the normal cuticle during the several phases of the molting cycle. Such information is essential to an understanding of lesion development and its effect upon the animals.

Received 3 January 1992; accepted 5 May 1992.

Table I

Histological appearance of [illegible] during stages of the normal molting cycle [illegible] lobsters (Aiken, 1980; Travis, 19[illegible]ner, 1962)

Stage of molt	Changes in the integument	Layers of cuticle present*
Stage A	Mineralization of the postecdysial cuticle	Epicuticle[1] Exocuticle[1]
Stage B	Striated endocuticle is deposited	Epicuticle[1] Exocuticle[1] Striated endocuticle[1]
Stage C		
Substage C_1	Decreased height of cuticular epithelium	Epicuticle[1] Exocuticle[1] Striated endocuticle[1]
Substages C_2 and C_3	Thin lamellar endocuticle is deposited in the carapace	Epicuticle[1] Exocuticle[1] Striated endocuticle[1] Thin-lamellar-endocuticle[1]
Substage C_4	Intermolt. Membranous layer is deposited	Epicuticle[1] Exocuticle[1] Striated endocuticle[1] Thin-lamellar-endocuticle[1] Membranous layer[1]
Stage D		
Substage D_0	Passive premolt. Transition period from intermolt to premolt.	Epicuticle[1] Exocuticle[1] Striated endocuticle[1] Thin-lamellar-endocuticle[1] Membranous layer[1]
Substage D_1	Retraction of the epidermis from the cuticle with dissolution of the inner portion of the membranous layer (apolysis) and deposition of a new epicuticle	Old cuticle[1] Apolytic space Epicuticle[2]
Substage D_2	Deposition of exocuticle in the new cuticle	Old cuticle[1] Apolytic space Epicuticle[2] Exocuticle[2]
Substage D_3	Extensive reabsorption of minerals from the endocuticles of the old cuticle	Epicuticle[1] Exocuticle[1] Dissolution of the endocuticles[1] Apolytic space Epicuticle[2] Exocuticle[2]
Stage E	Ec[illegible]	Epicuticle[2] Exocuticle[2]

* The superscript[1] identifies those cuticular layers (old cuticle) which will be eliminated at ecdysis (Stage E). The superscript[2] designates cuticular layers that will remain as part of the postecdysial (new) cuticle.

The crustacean molting cycle is divided into five major stages (A through E) (Table I), with most stages further divided into substages (Travis, 1955; Dennell, 1960; Skinner, 1962; Aiken, 1980). In this study, lesions occurring principally in four substages of the molt cycle were examined (C_2, C_3, C_4, and D_0). Substages C_2 and C_3 (of Stage C) are not readily divisible by histological examination in homarids, but they span the time of thin-lamellar-endocuticle deposition (Fig. 1) (Table I).

In C_4, passive intermolt, the normal decapod cuticle is made up of four layers: epicuticle, exocuticle, endocuticle, and membranous layer (Fig. 2) (Table I) (Aiken, 1980). The endocuticle is divided into two parts, the striated endocuticle and the thin-lamellar-endocuticle. In homarids, the thin-lamellar-endocuticle does not contain vertical striations but does contain calcium; but both of these are features of the striated endocuticle. The membranous layer is a thin, dense band that is deposited during C_4 internal to the thin-lamellar-endocuticle by epithelial cells. Passive premolt, D_0, is described as a time of slow, gradual tran-

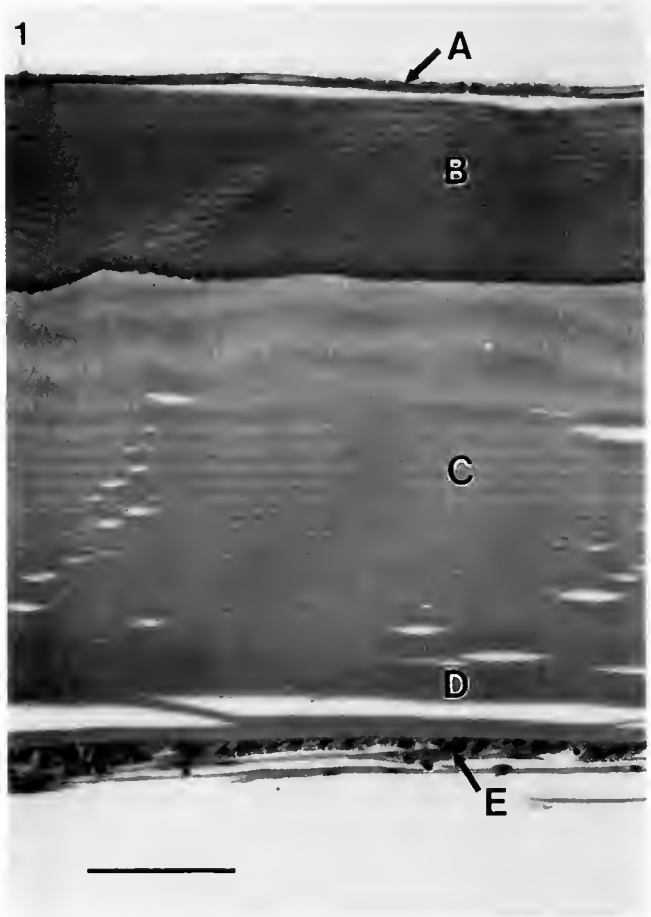

Figure 1. Normal cuticle of a lobster in C_2/C_3. Epicuticle (A), exocuticle (B), striated endocuticle (C), thin-lamellar-endocuticle (D), cuticular epithelium (E). Bar represents 60 μm.

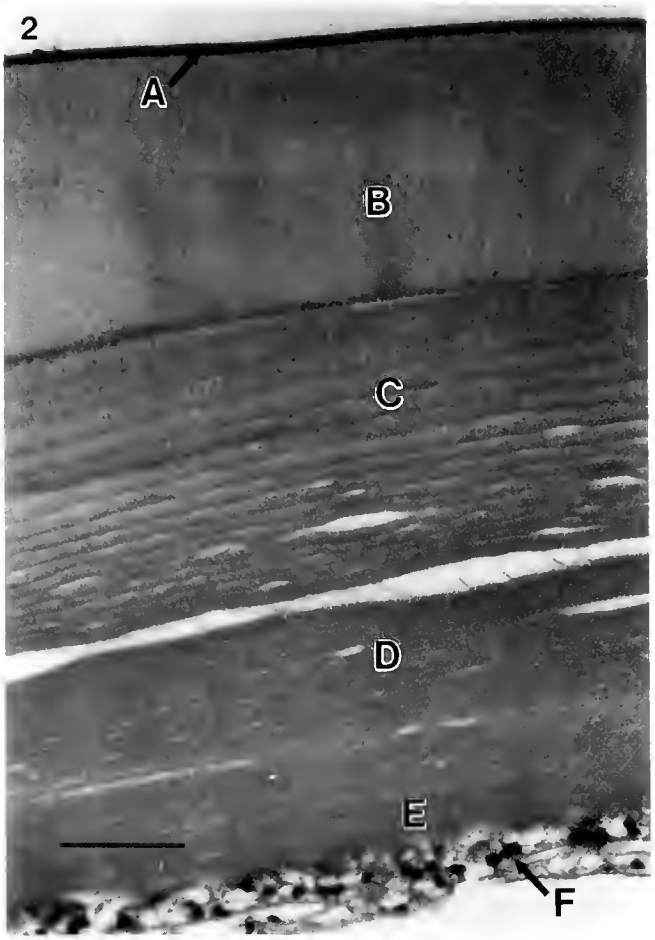

Figure 2. Normal cuticle of a lobster in C_4/D_0. Epicuticle (A), exocuticle (B), striated endocuticle (C), thin-lamellar-endocuticle (D), membranous layer (E), cuticular epithelium (F). Bar represents 60 μm.

sition between C_4 and D_1. The inner portion of the membranous layer dissolves in D_1 to form a fracture line between the old cuticle and the new (apolysis) (Aiken, 1980). Some authors include the membranous layer as part of the thin-lamellar-endocuticle (Dennell, 1960; Aiken, 1980). The function of the membranous layer before dissolution (and that which the thin-lamellar-endocuticle shares in homarid lobsters) is exhibited by the broken-cuticle test, in which the flexible membranous layer prevents a clean breakage of the cuticle and holds the two edges together (Aiken, 1980). Substage C_4, and D_0, which follows it, are histologically indistinguishable in the general cuticle. Together, the duration of these two substages makes up approximately 56% of the molt cycle (Aiken, 1980).

In this paper we describe the histological changes associated with the progressive cuticular erosions in lesions of winter impoundment shell disease as seen in a non-randomly selected group of 24 lobsters held in a winter impoundment facility for several months. Lobsters were predominately in either C_2/C_3 or C_4/D_0 of the molting cycle, and descriptions were therefore limited to these substages.

Materials and Methods

Twenty-four market size lobsters (450–500 g) were obtained through Paul's Lobster Co. (Boston, Massachusetts) from their winter impoundment on Gran Manan Island, Nova Scotia, Canada. Lobsters were collected during a disease outbreak and were chosen to provide a spectrum of lesions from grossly normal to severely eroded. The severity of the cuticular lesions on each lobster varied, but the number of foci and the severity of the erosions were graded in each individual, with a few animals containing numerous deep erosions.

Winter impoundment associated cuticular lesions were prepared for histological study. Tissues were fixed in 10% formalin in seawater (3.7% active formaldehyde), decal-

Figure 3. Dorsal view of *Homarus americanus* showing severe signs of shell disease characterized by diffuse pitting erosions (arrows) of the chelipeds, carapace, and abdominal segments.

Figure 4. Ventral view of *Homarus americanus* showing the characteristic hyperpigmentation (arrow) usually associated with naturally acquired abrasions and scratches.

Figure 5. Traumatic cracking (arrow) of the exoskeleton resulting from aggressive behavior. Crushing lesions are common in impounded lobster populations.

cified in formic acid/sodium citrate, embedded in paraffin, and stained with hematoxylin and eosin using standard techniques. The nomenclature proposed by Aiken (1980) was used to describe the layers of the cuticle. These lobsters were subsequently identified histologically as being in substages C_2/C_3 or C_4/D_0 of the molting cycle. In this paper, cuticular lesions from lobsters in substages C_2 and C_3 are described together, as are lobsters in substages C_4 and D_0. After examination, representative samples were selected and a grading system was developed based on the depth and severity of the erosions.

Results

Gross examination of affected animals revealed diffuse pitting erosions covering the entire exoskeleton, but most prominent on the carapace and dorsal abdominal segments (Fig. 3). The appearance of individual erosions varied greatly in the amount of melanization (abnormal black discoloration) and the depth of the erosion. No attempt was made in this study to correlate the gross appearance of individual erosions with their histological appearance. Other types of shell lesions noted were: lesions of the ventral surface characterized by linear foci of hyperpigmentation associated with abrasions and scratches (Fig. 4); and crushing injuries manifested by cracking of the exoskeleton and severe blackening of underlying tis-

Table II

Shell disease grading system for homarid molting substages C_4/D_0 and C_2/D_3

Grade I. Epicuticular erosion.
Grade II. Erosion into the exocuticle.
Grade III. Erosion into the striated endocuticle and the thin-lamellar-endocuticle.
Grade IV. Erosion into the pseudomembrane.
Grade V. Total erosion of the cuticle and ulceration of the underlying cuticular epithelium.

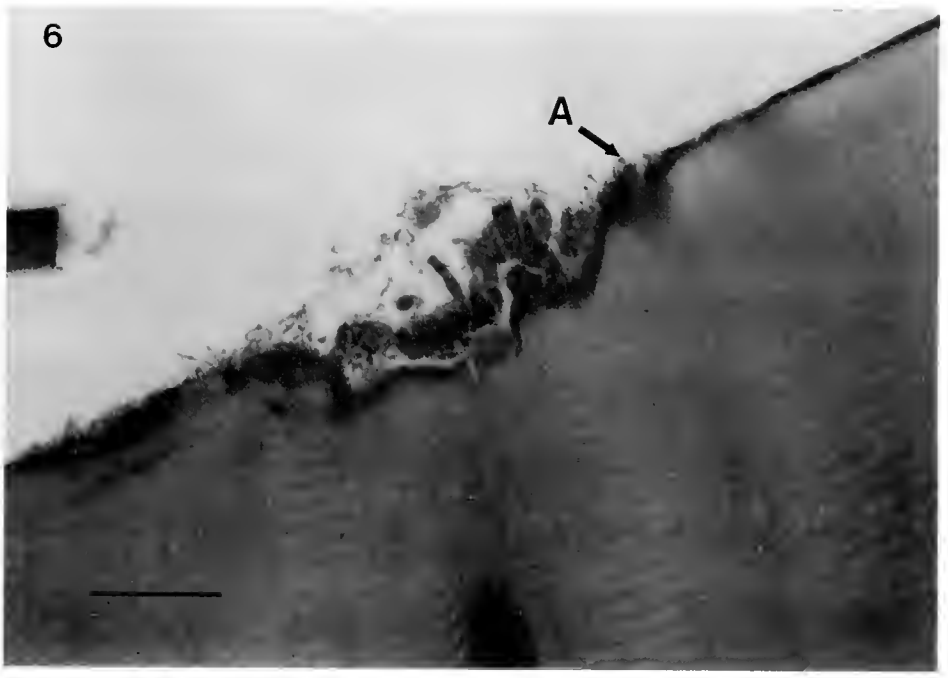

Figure 6. C_4/D_0. Grade I. Erosion of the epicuticle (A) and colonization of the setal pit by various organisms. Bar represents 44 μm.

sues (Fig. 5). These last two types are representative of other common lesions present in lobster cuticles both in impoundments and in the wild. These two lesion types will be described in subsequent papers.

Histopathology of shell lesions

Because the majority of the homarid molt cycle is spent in C_4/D_0, lesions will be first described for these substages, followed by comparative descriptions of C_2/C_3 lesions.

Histopathology of shell lesions from lobsters in C_4/D_0 (Table II)

Histological examination of cuticles from lobsters in the final intermolt stage (C_4/D_0) demonstrated a membranous layer present in both inflamed and normal cuticle. The cuticular lesions were divided into five progressive grades of severity and were described as follows:

Grade I. Epicuticular erosion in the perisetal cuticle (Fig. 6) and tegmental pore cuticle. Seta are normally present within shallow, regular pits in the cuticle. Erosions through the epicuticle appeared to first occur at foci in the shoulders and sides of setal pits and were characterized by necrosis and melanization. Occasionally there was melanization of the innervating neuronal core within the cuticular canals in the epicuticle and exocuticle. Only rarely was cuticle around setal pores necrotic and melanized. In a few affected foci, a very mild increase in the thickness of the outer layer of the epicuticle was seen. The dermal tegmental glands in these animals were large and prominent, indicating the early portion of the C_4/D_0 period. In late C_4/D_0, dermal tegumental glands were greatly reduced in size. The flora within the setal pits were mixed but often were dominated by filamentous algae. The underlying cuticular epithelium was mildly hypertrophic.

Grade II. Erosion into the exocuticle (Fig. 7). Erosions extended into the exocuticle with necrosis, and loss of cuticular matrix, resulting in the formation of shallow craters in the carapace. Mild to moderate melanization of the exposed exocuticular border occurred. Tissue decalcification, however, produced variably bleached shades of melanin (Smolowitz *et al.*, 1992) associated with the inflammatory response that consisted of granulocytes, agranulocytes, and semigranulocytes. Epidermal hypertrophy, in varying amounts, was evident at the base of the erosions. There was a mild influx of granulocytes and agranulocytes with occasional diapedesis of these inflammatory cells between epidermal cells. In some animals, significant thickening of the inner thin-lamellar-endocuticle/membranous layer was noted, especially in Grade II lesions adjacent to more severely graded foci. Grade II appeared rarely in Stage C_4/D_0 of the molt cycle and most Grade II lesions were adjacent to Grade III lesions.

Grade III. Erosion into the striated endocuticle and the thin-lamellar-endocuticle (Figs. 8, 9). Most erosions examined in this grade extended into the striated endocuticle

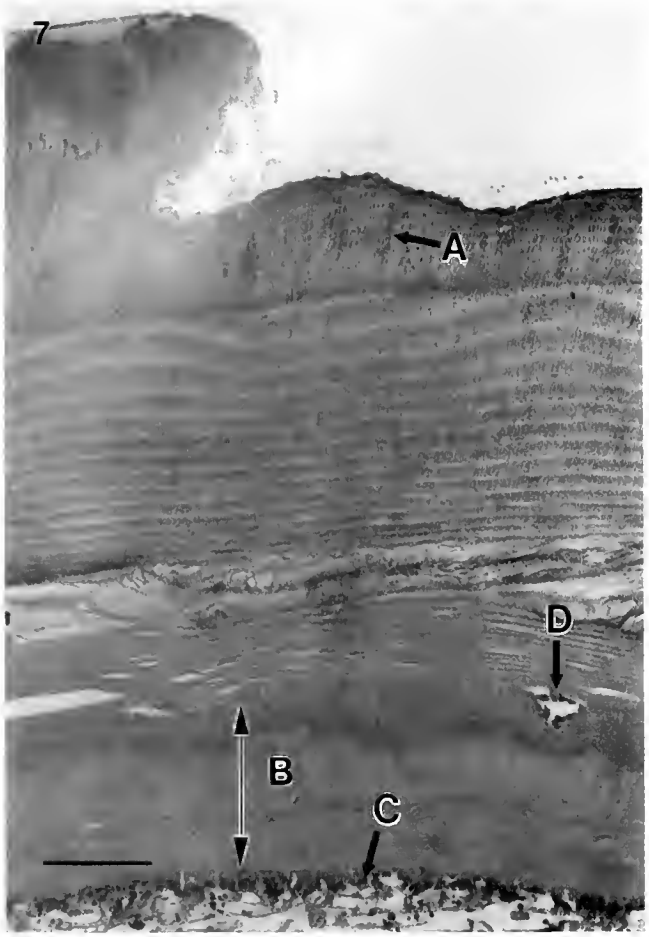

Figure 7. C_4/D_0. Grade II. Erosion into the exocuticle with melanization (A). Thickened thin lamellar/membranous layer (B). Mildly hypertrophic epithelium (C). Focus of inflammatory cell accumulation between the outer thin-lamellar-endocuticle and the inner thin-lamellar-endocuticle/membranous layer (D). Bar represents 100 μm.

and only rarely into the outer thin-lamellar-endocuticle. Melanization of the surface of these erosions was moderate to severe and occasionally extended vertically into the thin-lamellar-endocuticle. The inflammatory cell population was increased from Grade II, and diapedesis of cells through the epidermis and into the cuticular canals was noted. Puckering of the membranous layers occasionally formed pockets predominately containing granulocytes. These pockets often appeared to be associated with cuticular canals. Accumulations of inflammatory cells were present multifocally at the junction of the striated endocuticle with the thin-lamellar-endocuticle, between layers of the thin-lamellar-endocuticle, at the junction of the thin-lamellar-endocuticle with the membranous layer and within layers of the membranous layer. In some instances, loosely attached pseudomembranes were formed in these same areas. The pseudomembranes, varying between 5 to 25 cells in thickness, were composed predominately of layers of spindle shaped, transformed inflammatory cells primarily oriented parallel to the surface epithelium. Other non-transformed inflammatory cells were found in lesser numbers within the pseudomembranes.

In several inflamed foci, the normal sequential and orderly change in the histological appearance between the thin-lamellar-endocuticle and the membranous layer no longer was present. Instead, an abnormal section of cuticle indistinctly began at the inner side of the thin lamellar cuticle and continued to the surface of the cuticular epithelium. This unusual section of cuticle appeared histologically to be composed of repetitive alternations of the thin-lamellar-endocuticle and the membranous layer. In such inflamed areas, this combination of inner thin-lamellar-endocuticle and membranous layer had increased in depth, sometimes greatly, when compared to adjacent unaffected cuticle.

Rarely in the inflamed areas, cuticular pearl formation was present in the dermis (Fig. 9). These structures were composed of thin-lamellar-endocuticle secreted by dermal nests of displaced cuticular epithelial cells. Such nests were formed by focal invagination or detachment of cuticular epithelial cells. Multifocal, mild to severe, tegmental adenitis and setal cell inflammation were characterized predominately by encapsulation and melanization. The cuticular epithelium was hypertrophic and often vacuolated at its cuticular surface.

Grade IV. Erosion into the pseudomembrane (Fig. 10). Lesions of this grade were characterized by erosions through the striated endocuticle and outer layers of the thin-lamellar-endocuticle, thus exposing a pseudomembrane which protected the otherwise exposed inner combined thin-lamellar-endocuticle/membranous layer below. The pseudomembrane appeared as described in Grade III, but varied between 25 to 150 cells in thickness, and the necrotic surface of the pseudomembrane was melanized to varying depths. The inner thin-lamellar-endocuticle/membranous layer below the pseudomembrane was often thickened. Other dermal changes were as described in Grade III.

Grade V. Total erosion of the cuticle and ulceration of the underlying cuticular epithelium (Fig. 11). Lesions of Grade V were focal necrosis and sloughing of the cuticle with ulceration of the epithelium. The resulting ulcers were covered by a thick pseudomembranous crust consisting of alternating layers composed of predominately horizontally aligned, transformed inflammatory cells between layers of edematous necrotic tissue. One to two layers of transformed inflammatory cells were firmly attached to, and formed the surface of, the dermis. Hyperplastic and hypertrophic epithelium were present at the edges of the ulcers. The severe dermatitis was characterized superficially by a great influx of inflammatory cells and by transformed inflammatory cells randomly oriented to-

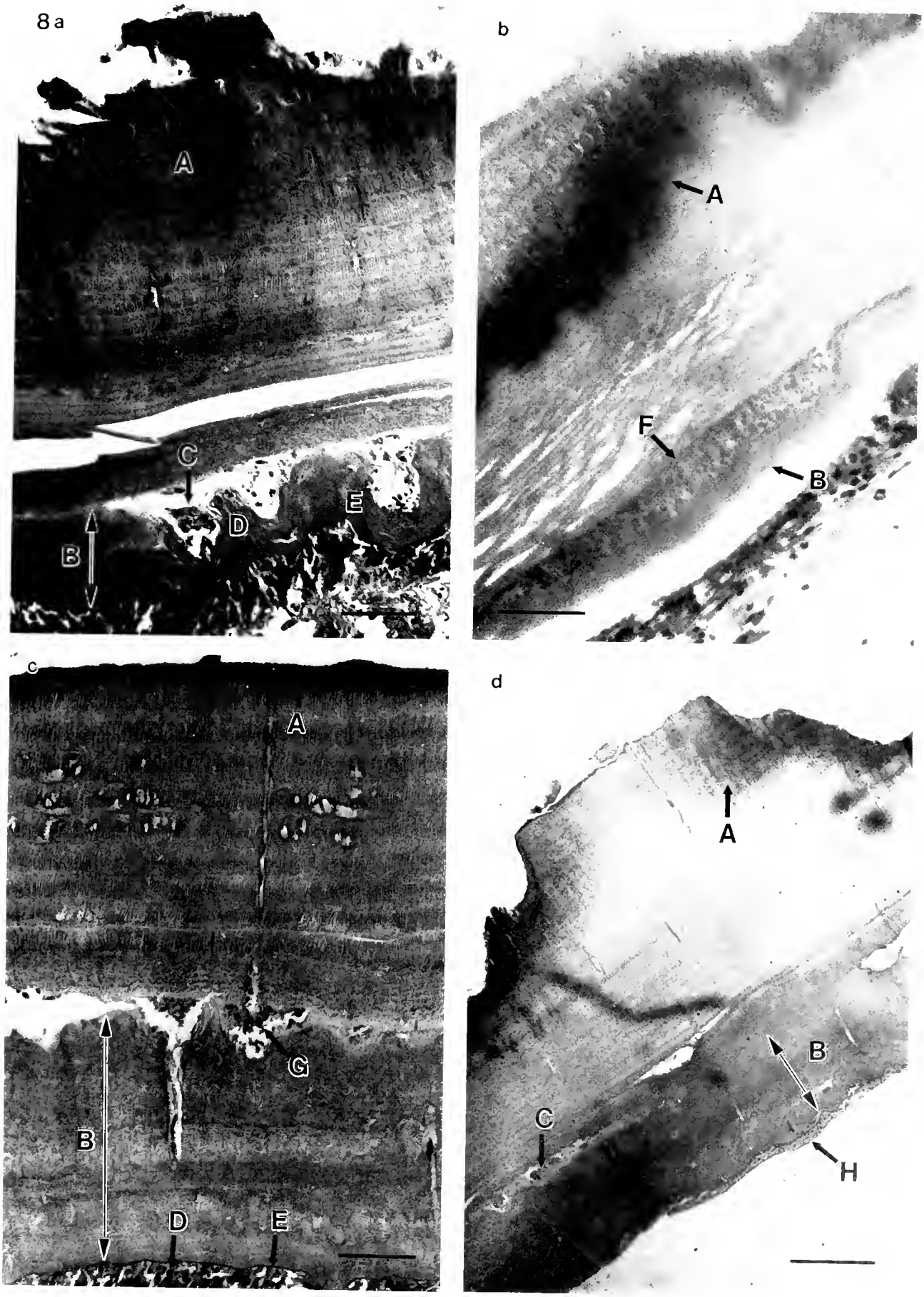
8 a
A
C
D
E
B
b
A
F
B
c
A
G
B
D
E
d
A
B
C
H

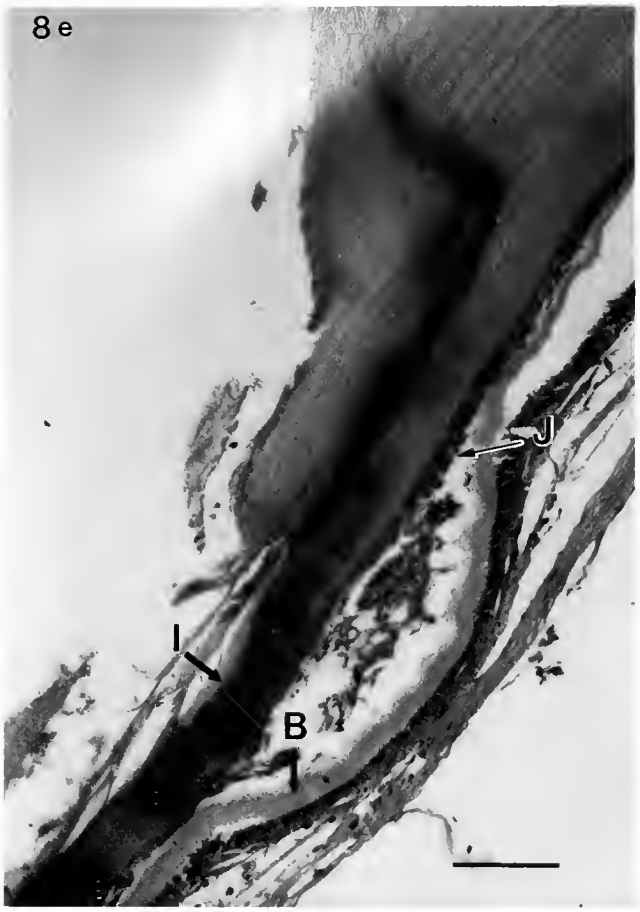

Figure 8. C_4/D_0, Grade III. 8a–d: Erosion into the striated endocuticle with melanization (A). Proliferation of the inner thin-lamellar-endocuticle/membranous layer (B). 8a. Puckering of the thin-lamellar-endocuticle/membranous layer with accumulation of granulocytes in pockets (C). Diapedesis of inflammatory cells (D) through hypertrophic epithelium (E) Bar represents 100 μm. 8b. Focal large accumulation of inflammatory cells (F) between the outer thin-lamellar-endocuticle and the inner thin-lamellar-endocuticle/membranous layer. Bar represents 60 μm. 8c. Accumulation of granulocytes in pockets associated with cuticular canals between layers of the thin-lamellar-endocuticle (G). Bar represents 100 μm. 8d. Molted cuticle showing the ecdysial separation line (H). Bar represents 230 μm. 8e. Increased depth of the inner thin-lamellar-endocuticle/membranous layer (B). Erosion into the outer thin-lamellar-endocuticle with melanization (I). Formation of a pseudomembrane between the outer thin-lamellar-endocuticle and the inner thin-lamellar-endocuticle/membranous layer (J) in late grade III. Bar represents 100 μm.

ward the surface layers of transformed cells. Within the deeper dermis, myoblastic proliferation was present as evidenced by bundles of myoblastic cells occurring at angles (somewhat perpendicular) to the surface. Melanized encapsulations (granulomas), many of which represented foci of tegmental gland and setal cell inflammation as well as thrombi within the open circulatory system, were scattered throughout the dermis. Edema, vascular dilation, margination of inflammatory cells in vessels, and multifocal severe necrotizing myositis of the underlying muscles were also noted.

The individual from the study group of 24 lobsters that demonstrated with Grade V lesions was in late D_1/early D_2 of the molt cycle as determined by examining areas of the cuticle away from the lesions. However, the description of the lesion is completely applicable to C_4/D_0 because: as evidenced by gross observation, the lesion initially developed during the intermolt or early premolt time period (before new cuticle developed); there was a lack of new cuticle in the area of the lesion; and substages D_1 and D_2 occur very quickly and would not have allowed sufficient time for this lesion to develop.

Pathology of shell lesions from lobsters in C_2/C_3 (Table II)

In C_2/C_3, cuticular lesions were also divided into five grades that were comparable to those in C_4/D_0. In C_2/C_3 the membranous layer had not yet been formed and proliferation of the inner thin-lamellar-endocuticle/membranous layer had not occurred.

Grade I. Epicuticular erosion in the perisetal cuticle and tegmental pore cuticle. In contrast to C_4/D_0, dermal tegmental glands were large and prominent throughout these substages of the molting cycle. Other changes, including colonization of the setal pits by a mixed flora often predominated by filamentous algae (Fig. 12), were as described for Grade I of C_4/D_0.

Grade II. Erosion into the exocuticle (Fig. 13). The eroded cuticular surface appeared as in Grade II of C_4/D_0. Epithelial hypertrophy with diapedesis of inflammatory cells was noted as above, but interestingly and characteristically, this stage of molt exhibited accumulations of inflammatory cells between the epithelium and the base of the cuticle. These foci were from two to four cells thick and consisted of a mixture of inflammatory cells, often predominated by granulocytes.

Grade III. Erosion into the striated endocuticle and the thin-lamellar-endocuticle (Fig. 14). Early Grade III lesions were characterized by erosions into the upper levels of the striated endocuticle. However, at the epithelial-cuticular border, an accumulation of a mixed population of inflammatory cells formed a pseudomembrane populated predominately by transformed cells oriented parallel to the surface of the epithelium and base of the cuticle. This pseudomembrane was from 5 to 30 cells thick. The cuticular epithelium was hypertrophic and hyperplastic and displaced ventrally from the cuticle to a position below the pseudomembrane. The inner thin-lamellar-endocuticle/membranous layer was not present between the pseudomembrane and the epithelium. Tegmental adenitis was present multifocally in the dermis.

Grade IV. Erosion into the pseudomembrane. This grade was not applicable to C_2/C_3 because the membra-

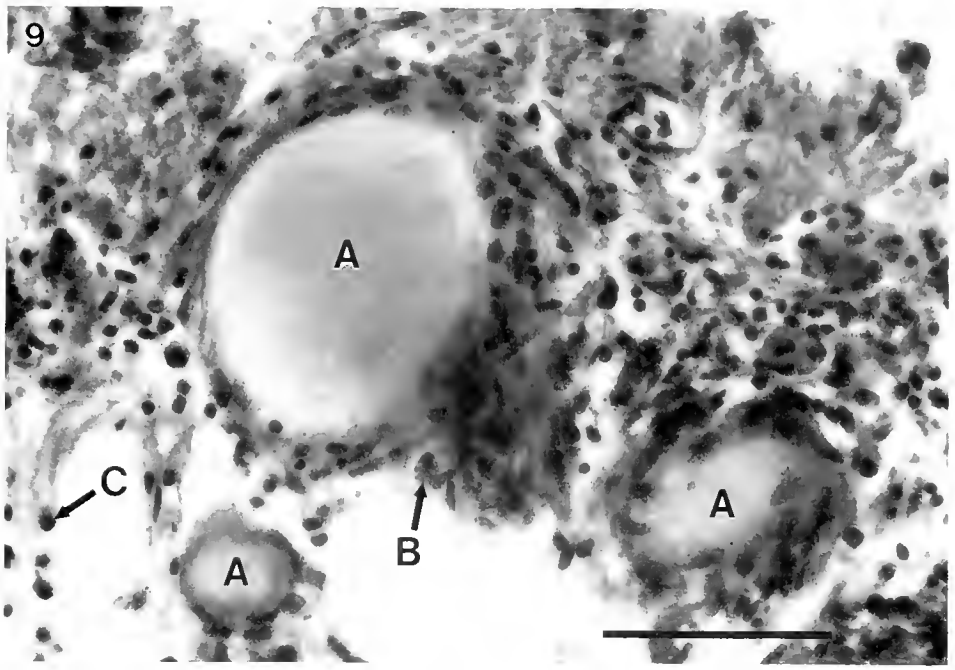

Figure 9. C_4/D_0, Grade III. Cuticular pearls (A) in the dermis of inflamed cuticle containing granulocytes (B) and agranulocytes (C). Bar represents 64 μm.

nous layer was not yet formed and there was no proliferation of the inner thin-lamellar-endocuticle/membranous layer as in C_4/D_0.

Grade V. Total erosion of the cuticle and ulceration of the underlying cuticular epithelium. No Grade V lesions were seen from lobsters in C_2/C_3 of the molt cycle but would be very similar to those of Grade V in C_4/D_0 lobsters. Evidence for this conclusion is provided by examination of a severe shell lesion from an animal in C_2/C_3 of the molt cycle that showed a late grade III/early grade

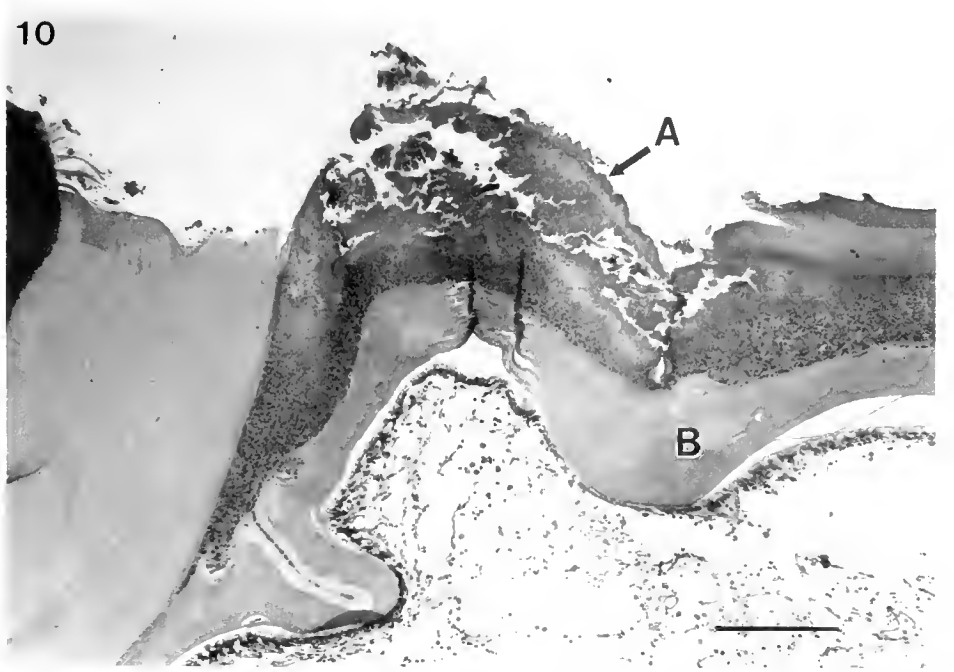

Figure 10. C_4/D_0, Grade IV. Melanization and necrosis of the exposed pseudomembrane (A). Increased depth of the inner thin-lamellar-endocuticle/membranous layer (B). Bar represents 220 μm.

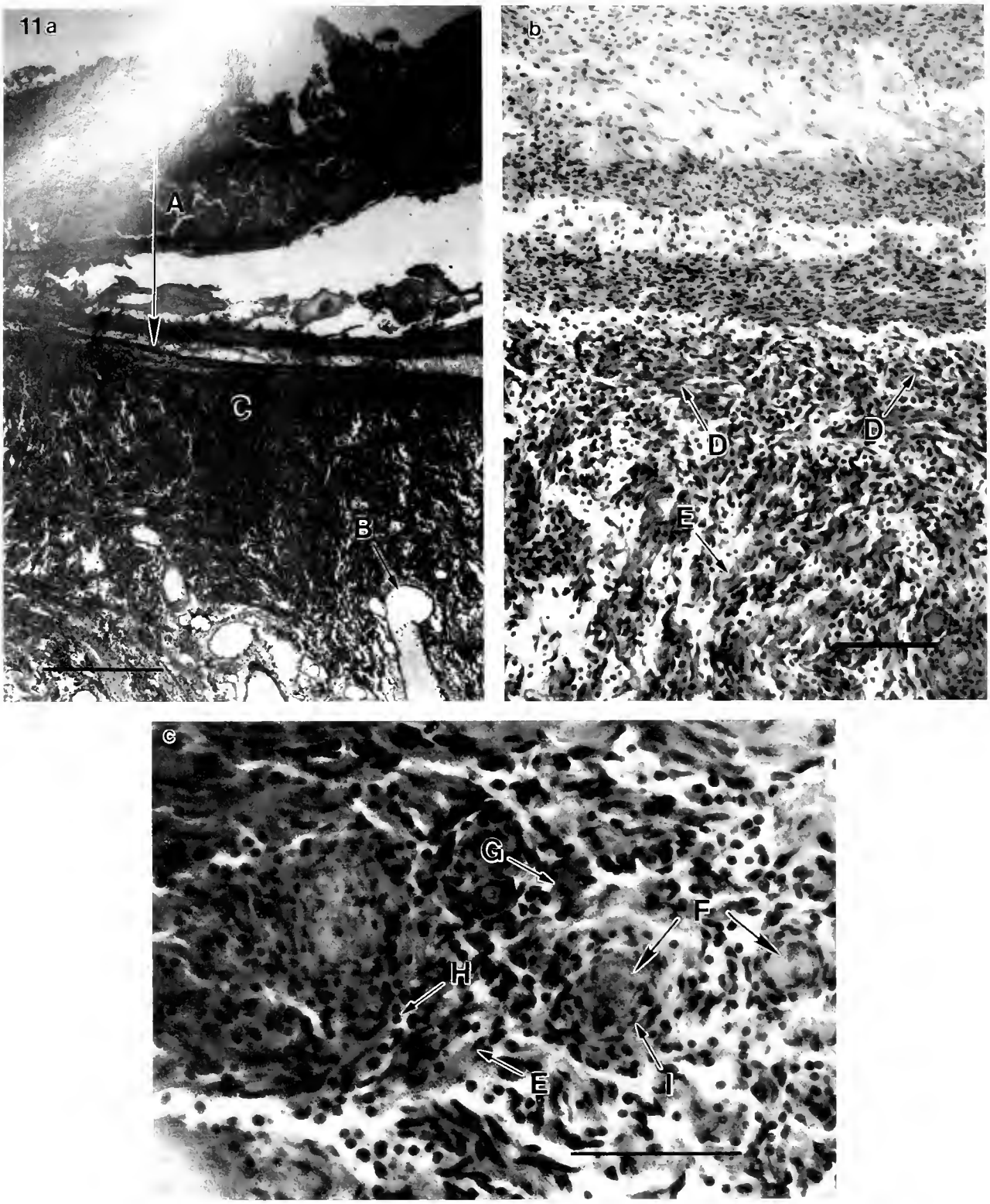

Figure [illegible], D_0, Grade V. 11a. Lamellae of transformed inflammatory cells alternating with necrotic debris at the surface (A) of the cuticular ulcer. Dilated vascular channels (B). Increase in cellularity of the dermis (C). [illegible] represents 620 μm. 11b. Transformed agranulocytes (D) occur at various angles to the ulcerated surface. Fibroblastic proliferation is present in the deeper dermis (E). Bar represents 70 μm. 11c. Encapsulations (granulomas) (F) are present at various levels within the inflamed dermis containing untransformed inflammatory cells consisting of granulocytes (G) and agranulocytes/semigranulocytes (H) as well as transformed encapsulating inflammatory cells (I). Bar represents 64 μm

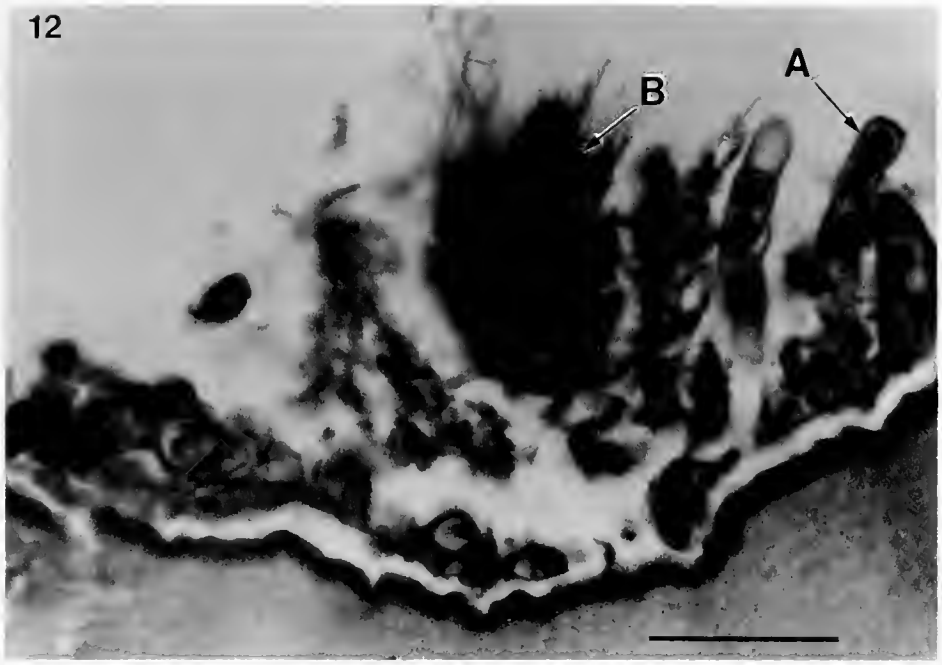

Figure 12. C_2/C_3, Grade I. Filamentous algae predominate (A) in the perisetal depression around the hair-fan organ (B). Bar represents 38 μm.

V lesion. In this lesion, a thick pseudomembrane, 100 or more cells in thickness, occurred below a necrotic, but still attached, thin-lamellar-endocuticle. No cuticular epithelium was present and the erosion was accompanied by deeper dermal inflammation similar to Grade V of C_4/D_0.

Discussion

Examination of homarid cuticular inflammation in winter impoundment shell disease revealed some important histological inflammatory mechanisms in all substages examined including: epicuticular deposition; melanization; inflammatory cell infiltration; and pseudomembrane formation. Proliferation of the membranous layer was seen only in those animals in C_4/D_0 of the molting cycle. Cuticular erosion development in the two molting substage groups, C_2/C_3 and C_4/D_0, was progressive. The erosions in both groups were divisible into grades, each of which demonstrated characteristic protective mechanisms.

In Grade I of C_2/C_3 and early C_4/D_0, epicuticle continued to be deposited, both within setal pits and throughout the cuticle, in an attempt to maintain the epicuticular layer and prevent erosion into the exocuticle. Although the continued production of epicuticle was only rarely confirmed histologically in this study, post-ecdysial production of this shellac-like cement layer by dermal tegmental glands has been previously confirmed in arthropods (Neville, 1975). However, the extent to which epicuticle was deposited varied with the activity of the tegmental glands as determined by the substage of the molting cycle (Arsenault *et al.*, 1979).

Filamentous algae predominated in early epicuticular erosions. The role these organisms play in the initial penetration of the epicuticle is not immediately obvious. Breaching of the epicuticle often occurred first at the shoulders and sides of the setal pits. In general, setal pits provided a protected cuticular microenvironment for colonization by fungi, and other organisms (Malloy, 1978). Erosions of higher grades were filled with a variety of microbes including fungi, bacteria, amoebae, and other protozoa. Chitinolytic and lipolytic bacteria were isolated in shell lesions from lobsters in all stages of the disease.

The cause of impoundment shell disease is not due to any single etiological agent, but rather results from the aggregate effects of epicellular enzymes produced by the mixture of various types of organisms present on the surface of the lesions (Sindermann, 1990). Swarming vibrios, pseudomonads, and *Flavobacter* spp. were cultured from the blood of five of eight lobsters. Bacteria of these types have previously been implicated in shell disease from a variety of marine crustacea (Sindermann *et al.*, 1989). Hemolymph infection by ciliated protozoa resembling *Mugardia* sp. (Sherburne and Bean, 1991) were noted histologically in sections of some severely affected animals. Indeed, severe shell lesions may have allowed for dehabilitation of the lobsters, which increased the animals'

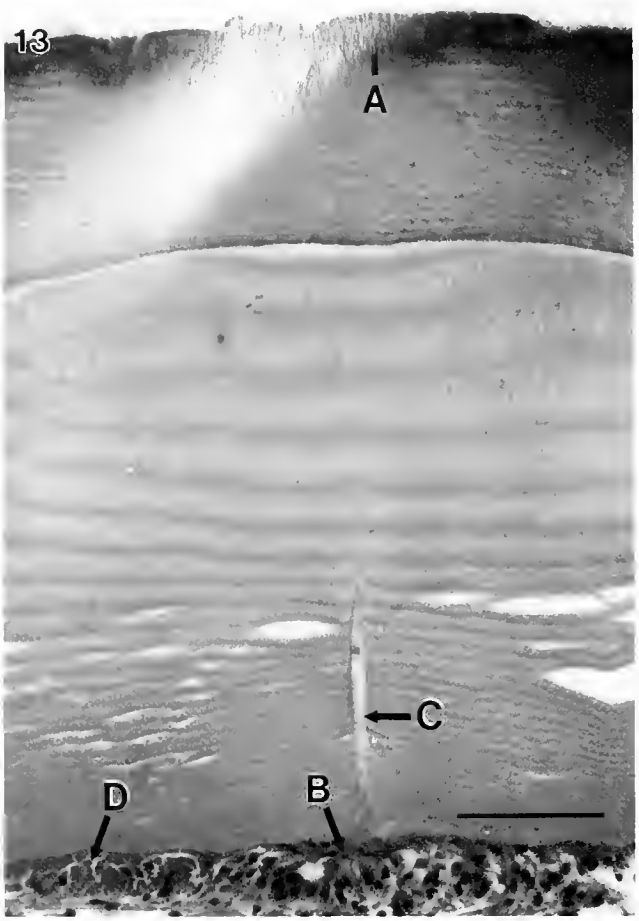

Figure 13. C_2/C_3, Grade II. Erosion and melanization (A) of the exocuticle is present. Mild accumulation of inflammatory cells (B) which appear to be predominately granulocytes at the base of the cuticle are often centered around cuticular canals (C). The epithelium is necrotic in one focus (D). Bar represents 60 μm.

susceptibility to opportunistic infections, such as that by ciliated protozoans.

Melanization was an important and prominent part of the inflammatory response and was seen in Grades I–V of both Stages C_4/D_0 and C_2/D_0. However, it was especially prominent in the striated cuticle of Grade III erosions. Melanized foci were bleached to varying degrees by the decalcification process and so appeared much lighter in sections than when viewed grossly (Smolowitz *et al.*, 1992).

Increased depth of the inner thin-lamellar-endocuticle/membranous layer in C_4/D_0 provided an excellent method for increasing the depth of the protective cuticular barrier between the cuticular epithelium and the environment. Interestingly, in addition to an increase in thickness of these layers, there is often a loss of the orderly deposition and distinctiveness of these two layers, which can be seen in histologically normal cuticle. The lack of orderly deposition is probably an indication of the similarity of the two layers and may reflect a vacillating cuticular secretory response by the cuticular epithelial cells to toxins, degradation products, etc. from the inflamed cuticle above or bacterial or protozoal septicemia. Proliferation of the inner thin-lamellar-endocuticle/membranous layer appeared to be distinct from new cuticle formation because dissolution of an ecdysial membrane [with retraction of the epithelium and formation of a molting space between the old cuticle and the cuticular epithelium (apolysis) and production of new epicuticle and exocuticle] was not evident (Travis, 1955; Skinner, 1962). In Stage C_2/C_3 of the molting cycle, the membranous layer was not present and the thin-lamellar-endocuticle alone did not proliferate in response to the inflammatory stimulus. This difference from substage C_4/D_0 may have been a result of the normal effects on the epithelial cells by the molting hormones (Neville, 1975).

Pathologic epithelial hypertrophy was noted in several lesions but was most consistently found from Grades III to V of all substages. In early C_2/C_3 and after late C_4/D_0, epithelial cells were physiologically hypertrophic diffusely throughout the cuticle indicating active cuticular secretion due to normal molting cycle activity. Thus in early C_2/C_3 and late C_4/D_0, pathological epithelial hypertrophy could not be differentiated from adjacent normal activity.

Formation of a pseudomembrane in Grade III of C_2/C_3 represents an important protective effort to prevent ulceration of the cuticular epithelium. Additionally, it is probable that continued secretion of cuticle would occur beneath the pseudomembrane by the still-intact epithelial cells upon appropriate stimulation perhaps by molting hormones. Thus, the inflammatory process could progress from Grade III of C_2/C_3 to Grade IV of C_4/D_0.

In C_4/D_0, the pseudomembrane is necessary for protection of the inner layers of the thin-lamellar-endocuticle/membranous layer so that separation of the epithelium at apolysis can still occur and prevent focal adhesion between the old and new shells. Pseudomembranes appear to develop progressively from foci that were at first identified as primarily granulocytic. However, the transformed cells responsible for formation of pseudomembranes appeared to originate from an influx of semigranulocytes or agranulocytes (Johnson, 1980; Johansson and Söderhäll, 1989). Inflammatory cell identification and function *in vivo* warrants further study. *In toto*, pseudomembranes probably represent the cuticular "clots" referred to in the literature (Bang, 1983; Sindermann *et al.*, 1989). The formation of pseudomembranes in Grade V of C_4/D_0 to shield the underlying dermis after epithelial ulceration, affords an additional method of inflammatory protection.

Dermal foci of encapsulation and melanization were common and probably reflected the vulnerability of teg-

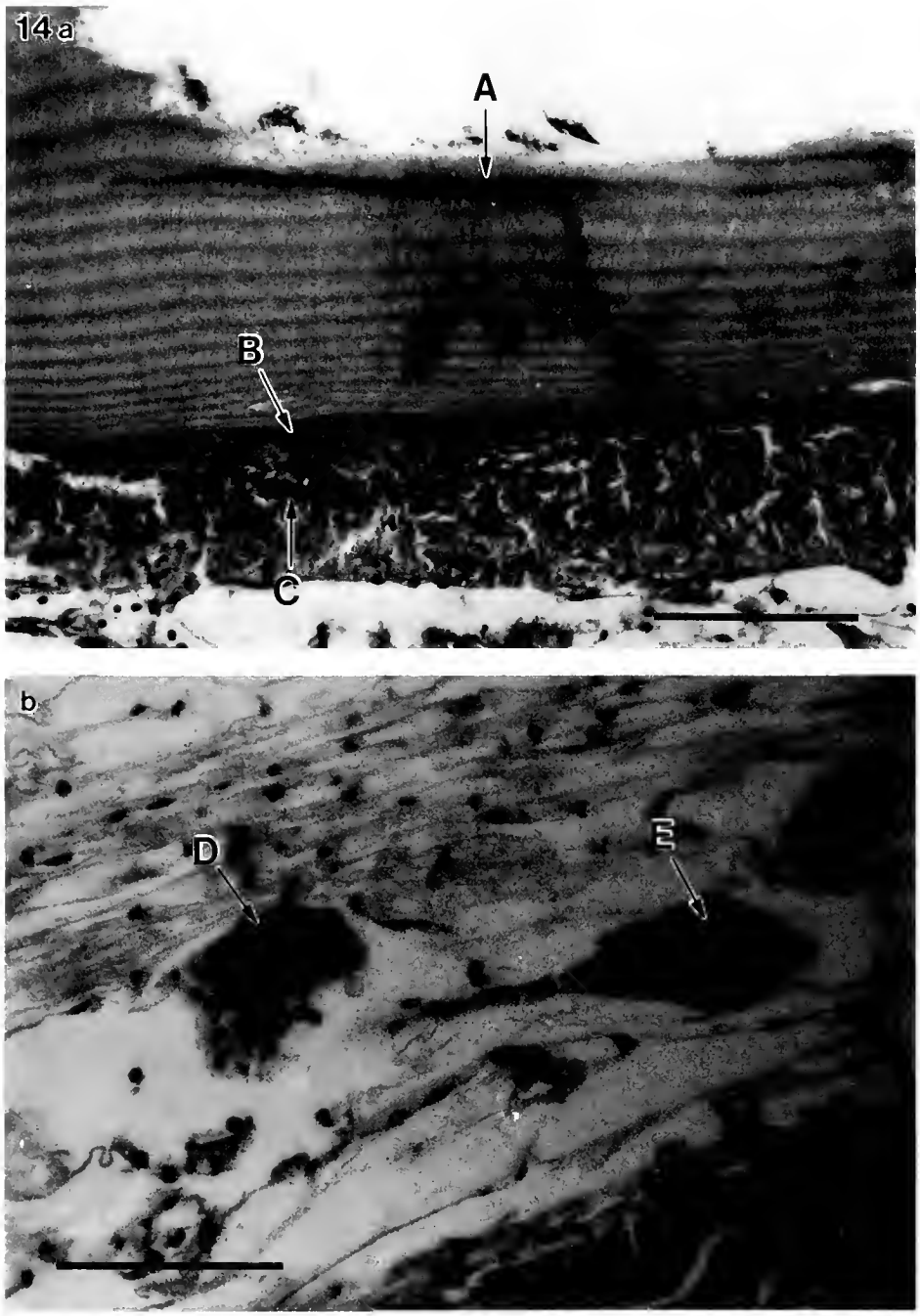

Figure 14. C_2/C_3, Grade III. 14a. Erosion into the striated endocuticle with melanization (A). Formation of a pseudomembrane (B) between the cuticular epithelium (C) and the base of the cuticle. Bar represents 120 μm. 14b. Inflamed tegmental gland with invading inflammatory cells (D) and adjacent normal tegmental gland (E). Bar represents 71 μm.

mental glands and setal cells to infection because they provide direct conduits to the surface by way of the cuticular canals. Other melanized encapsulations in the open portion of the circulatory system may have been related to stimulation of inflammatory cells by bacteremia or toxic products (Johansson and Söderhäll, 1989).

Examination of Grade III lesions in a molted shell and the postmolt cuticle demonstrate that molting can effectively eliminate lesions confined to the upper levels of the cuticle. However, molting is not completely effective if erosions through the pseudomembrane into the inner thin-lamellar-endocuticle/membranous layer have occurred or

cuticle has ulcerated. At this point, the ability to survive depends on a balance between numbers of infective organisms, husbandry conditions, and effectiveness of the inflammatory and immune responses.

The inflammatory defense mechanisms of melanization, inner thin-lamellar-endocuticle/membranous layer proliferation, pseudomembrane proliferation, and molting provide homarids varied and extremely effective methods for preventing or inhibiting shell disease in their natural environment. However, inflammatory defense mechanisms do not seem as effective in protecting animals confined in stress-producing impoundment areas.

The classification scheme and description of cuticular inflammatory responses presented herein for winter impoundment shell disease can be used generally in situations with gradually developing cuticular lesions such as those due to pollution and overcrowding. Overlap between substages and grades should be expected because cuticle formation is not a static process and foci of erosion in cuticles can span several substages. However, this scheme provides a framework with which to begin the classification and further the understanding of these cuticular lesions. The function of inflammatory cells that seem to predominate in these erosions requires further study, especially in relation to the mediators produced and definite identification of the cells responsible for *in vivo* pseudomembrane formation and encapsulation. Future studies in our laboratory will include descriptions of the inflammatory responses in these and other stages of the molt cycle in relation to animals of varying ages, and development of a macroscopic impoundment shell disease grading system based on the histological grading system described in this paper. We also will study the differences between impoundment shell disease lesions and those due to other causes such as demonstrated in Figures 4 and 5. Comparative studies of cuticular inflammatory responses in other Crustacea are ongoing.

Acknowledgments

We thank Elizabeth Wadman for clinical technical assistance, Michelle McCafferty for the histological preparations, Polly Moniz for secretarial help, and the generosity of Paul's Lobster Co. This study was supported in part by a grant from the National Center for Research Resources, National Institutes of Health (P40-RR1333-11).

Literature Cited

Aiken, D. E. 1980. Molting and growth. Pp. 103–110, 178–182, and 321–329 in *The Biology and Management of Lobsters,* Vol. 1, J. S. Cobb and B. F. Phillips, eds. Academic Press, New York.

Arsenault, A. L., R. E. Clattenburg, and D. E. Aiken. 1979. The morphology and secretory transport mechanism of the tegumental glands of the lobster (*Homarus americanus*) as related to the molt cycle. *J Submicrosc. Cytol.* **11:** 193–207.

Bang, F. B. 1983. Crustacean disease responses. Pp. 118 and 143–144 in *The Biology of Crustacea,* Vol. 6, *Pathobiology,* A. J. Provenzano, Jr., ed. Academic Press, New York.

Bullis, R. A. 1989. Shell disease in impounded American lobsters, *Homarus americanus, Biol. Bull.* **177:** 327.

Dennell, R. 1960. Integument and exoskeleton. Pp. 449–472 in *The Physiology of Crustacea,* Vol. 1, T. H. Waterman, ed. Academic Press, New York.

Getchell, R. G. 1989. Bacterial shell disease in crustaceans: a review. *J. Shellf. Path.* **8:** 1–6.

Hess, E. 1937. A shell disease in lobsters (*Homarus americanus*) caused by chitinivorous bacteria. *J. Biol.* **3:** 358–362.

Johansson, M. W., and K. Soderhall. 1989. Cellular immunity in crustaceans and the proPo system. *Parasitol. Today* **5:** 171–176.

Johnson, P. T. 1980. *Histology of the Blue Crab, Callinectes sapidus. A model for the Decapoda.* Praeger Publishers, New York. 440 pp.

Malloy, S. C. 1978. Bacteria induced shell disease of lobsters (*Homarus americanus*). *J. Wildl. Dis.* **14:** 2–10.

McLeese, D. W., and D. G. Wilder. 1964. Lobster storage and shipment. Fisheries Research Board of Canada. Bulletin #147.

Neville, A. C. 1975. Biology of the arthropod cuticle. Pp. 10–27 and 46 in *Zoophysiol. Ecol.,* Vol. 4/5, D. S. Farnes, ed. Springer-Verlag, New York.

Sherburne, S. W., and L. L. Bean. 1991. Mortalities of impounded and feral maine lobsters, *Homarus americanus* H. Milne-Edwards, 1837, caused by the protozoan ciliate *Mugardia* (Formerly *Anophrys = Paranophrys*), with initial prevalence data from ten locations along the Maine coast and one offshore area. *J. Shellf. Res.* **10:** 315–326.

Sindermann, C. J., F. Csulak, T. K. Sawyer, R. A. Bullis, D. W. Engel, B. T. Estrella, E. J. Noga, J. B. Pearce, J. C. Rugg, R. Runyon, J. A. Tiedemann, and R. R. Young. 1989. *Shell Disease of Crustaceans in the New York Bight.* NOAA Tech. Memo., F/NEC-74.

Sindermann, C. J. 1990. Diseases of marine shellfish. Pp. 48–52 in *Principal Diseases of Marine Fish and Shellfish,* Vol. 2. Academic Press, New York.

Skinner, D. M. 1962. The structure and metabolism of a crustacean integumentary tissue during a molt cycle. *Biol. Bull* **123:** 634–647.

Smolowitz, R. M., R. A. Bullis, and D. A. Abt. 1992. Mycotic branchitis in laboratory maintained hermit crabs (Pagurus spp.). *J. Crustacean Biol* **12(2):** 161–168.

Taylor, C. C. 1948. Shell disease as a mortality factor in the lobster (*Homarus americanus*). *Maine Dept. of Seashore Fish. Circ.* **4:** 1–8.

Travis, D. F. 1955. The molting cycle of the spiny lobster, *Panulirus argus* Latreille. I. Molting and growth in laboratory-maintained individuals. *Biol. Bull.* **108:** 88–112.

Reference: *Biol. Bull.* **183**: 113–122. (August, 1992)

Identified *Helix* Neurons: Mutually Exclusive Expression of the Tetrapeptide and Heptapeptide Members of the FMRFamide Family

G. A. COTTRELL[1], D. A. PRICE[2], K. E. DOBLE[2], S. HETTLE[1], J. SOMMERVILLE[1], AND M. MACDONALD[1,*]

[1]*School of Biological and Medical Sciences, University of St. Andrews, Fife, KY16 9TS, U.K. and*
[2]*The Whitney Laboratory, University of Florida, 9505 Ocean Shore Blvd., St. Augustine, Florida 32086-8623*

Abstract. Extracts were prepared from selected neurons taken from the central ganglia of the pulmonate snail *Helix aspersa*, and parallel radioimmunoassay (RIA) and high pressure liquid chromatography (HPLC) were used to analyze for FMRFamide-related peptides (FaRPs). Some neurons (*e.g.*, the cerebral C3 neuron) contained only the tetrapeptides related to FMRFamide (tetra-FaRPs), whereas two clusters of neurons in the parietal ganglia contain a preponderance of the hepta-FaRPs. Using cloned cDNA probes in molecular hybridization studies, we showed that the C3 neuron (and some other large neurons) contain the mRNA species that encodes the tetra-FaRPs. In contrast, the neurons of the parietal clusters predominantly express the mRNA that encodes the hepta-FaRPs. These results were confirmed by *in situ* hybridization with antisense RNA on whole mount ganglia. Each type of experiment supports the view that FaRP-containing *Helix* neurons express either the tetra-FaRPs *or* the hepta-FaRPs, but not both.

Introduction

The ganglia of molluscs contain several pharmacologically active peptides related to FMRFamide. These peptides have been referred to as the FaRPs and include FLRFamide, FMRFamide itself, and several N-terminally extended forms, most of which are heptapeptides (Price and Greenberg, 1989). In *Helix aspersa*, the hepta-FaRPs are: pQDPFLRFamide, NDPFLRFamide, SDPFLRFamide, NDPYLRFamide, and SEPYLRFamide (Price *et al.*, 1990). Analyses of cDNAs from *H. aspersa* suggest that one species of mRNA encodes both of the tetra-FaRPs (*i.e.*, FMRFamide and FLRFamide), whereas another encodes all of the hepta-FaRPs together with the base sequence for another peptide, pQDPFLRIamide (Lutz *et al.*, 1990; Lutz *et al.*, 1992). Evidence that this latter peptide occurs in *H. aspersa* ganglia had previously been obtained by fast atom bombardment mass spectroscopy (see Bradley, 1982), and it has recently been sequenced (Lesser and Greenberg, pers. comm.).

FaRPs have potent pharmacological actions on peripheral and cardiac muscle cells and neurons. Often considerable differences in potencies are observed between the tetra- and the hepta-FaRPs; in some cases tetra-FaRPs produce opposing actions to the hepta-FaRPs (*e.g.*, Cottrell and Davies, 1987; Lehman and Greenberg, 1987). Such observations have led to the suggestion that there is more than one type of FaRP receptor in molluscan species.

Immunohistochemical studies with different antisera prepared against FMRFamide and related peptides provide evidence for an exclusively neuronal localization of FaRPs (Boer *et al.*, 1980; Schot and Boer, 1982). But we cannot always assume that such antisera stain only FaRPs. A better way to establish the presence of FaRPs in a particular neuron is to analyze extracts of the isolated neuron by RIA. The use of more than one antiserum can be useful in helping to distinguish the different related peptides. Even more information can be gained by subjecting extracts to high pressure liquid chromatography (HPLC), provided that sufficient material is available.

Received 27 March 1992; accepted 18 May 1992.

* Present address: Beatson Institute for Cancer Research, Glasgow, UK.

Immunohistochemistry of *H. aspersa* ganglia has shown that many cells possess FMRFamide-like immunoreactivity. One such neuron in each cerebral ganglion, the C3 neuron, contains an estimated 300 fmoles of FMRFamide (Cottrell *et al.*, 1988). Moreover, a parallel RIA procedure with two antisera revealed that neuron C3 is rich in FMRFamide itself, but contains none of the N-terminally extended forms (Bewick *et al.*, 1990). These observations are in accord with molecular genetics studies suggesting that, in *H. aspersa*, the tetra-FaRPs and hepta-FaRPs are encoded on different species of mRNA (Lutz *et al.*, 1990, 1992).

We wondered whether the tetra-FaRPs and hepta-FaRPs would generally be expressed in different cells, and therefore decided to reinvestigate the distribution of FaRP-containing neurons in *H. aspersa*. Unfortunately, no detailed map of such neurons has been made for this species. Recently, however, Elekes and Nässel (1990) used a commercially supplied FMRFamide antiserum to make a detailed immunohistochemical study of the ganglia of *Helix pomatia*. This species is closely related to *H. aspersa*. For example, Lutz *et al.* (1992) found that the tetra-FaRP precursors are 95% identical at the nucleotide level. Moreover, the ganglia of *H. aspersa* are very similar to those of *H. pomatia*, large neurons and clusters having identical locations in each species. For example, Elekes and Nässel (1990) detected FaRP-immunoreactivity in the *H. pomatia* C3 neuron and in clusters of smaller neurons in the parietal ganglia, which has also been observed in *H. aspersa* (Cottrell *et al.*, 1988). We began this study by assuming that neurons located similarly in the two species contain the same peptides and have therefore used the detailed information provided for *H. pomatia* to investigate *H. aspersa*. We have also undertaken some experiments to investigate the mRNA species that encode the different FaRPs in some of the identified neurons.

Materials and Methods

Specimens of *H. aspersa*, kindly supplied by Dr. R. Koch (Fullerton, California) were used for the peptide analysis experiments. *H. aspersa* collected in Scotland in the locality of St. Andrews were used for the mRNA hybridization experiments.

Radioimmunoassays

Individual specified neurons or small cluster of neurons were dissected from desheathed ganglia and transferred to small Eppendorf tubes containing 50 or 100 μl of acetone. The acetone containing the cells was left at −20°C until assayed, but for at least 16 h. The cellular debris was then spun down, the supernatant removed to a clean tube and dried in a Speed-Vac. The residue was resuspended in RIA buffer (100 μl) for immediate assay or in 0.1% TFA for HPLC fractionation. HPLC fractionations were done as previously described (Price *et al.*, 1990) on a Brownlee Aquapore Octyl column (2.1 × 220 mm), and 0.5 min (about 250 μl) fractions were collected. Aliquots (5 μl) were used directly in the RIA; alternatively the fractions were dried in a Speed-Vac, resuspended in RIA buffer, and 25 μl taken for assay. The radioimmunoassays were performed as described previously (Lehman and Price, 1987), using antiserum S253 at a 1/25,000 final dilution, or antiserum Q2 at a 1/600 final dilution. An antiserum developed against EFLRIamide was also used in some experiments at a final concentration of 1/25,000.

Hybridization analysis of mRNA in different neuronal cell types

Individual neurons or small clusters of neurons were dissected from isolated desheathed ganglia, placed in microcentrifuge tubes containing 0.25 ml of lysis buffer [50 m*M* Tris, pH 8.0, 10 m*M* EDTA, pH 8.0, 0.5% sodium dodecyl sulphate (SDS) and 0.5 mg/ml proteinase K] and incubated at room temperature (about 22°C) for 4 h. The entire tube contents were then loaded onto nitrocellulose filters that had been inserted in a slot-blot apparatus. The filters were air-dried and baked for 2 h at 80°C in a vacuum oven. The filters were hybridized, according to standard techniques (Maniatis *et al.*, 1982), to ^{32}P random-primer labeled DNA probes prepared from either the tetra-FaRP cDNA or hepta-FaRP cDNA isolated from *H. aspersa* (Lutz *et al.*, 1992). After hybridization, the filters were washed stringently (final wash: 0.25 × SSC, 0.1% SDS, 65°C, 2 h [1X SSC contains 0.15 *M* sodium chloride, 0.015 *M* trisodium citrate]), and the bands were visualized by autoradiography; 'Agfa Curix' film was used and exposed for four days at −70°C.

Hybridization to mRNA in situ

Two sets of RNA probes were synthesized: those complimentary to mRNA sequences encoding tetra-FaRPs, and those complementary to mRNA sequences encoding hepta-FaRPs. These antisense probes were transcribed from cDNA cloned in BlueScript plasmids (Lutz *et al.*, 1992) using T7 RNA polymerase as described previously (Kreig and Melton, 1987). The probes were labeled with digoxigenin-11-uridine-5'-triphosphate as a component of the synthesis reaction, as recommended (Boehringer-Mannheim data sheet).

Whole mounts of the cerebral ganglia, and also the suboesophageal ganglia from which the pedal ganglia had been removed, were prepared for *in situ* hybridization according to the method of Tautz and Pfeifle (1989). The preparations were fixed for 20 min, hybridized with the antisense RNA (5 ng/ml in 4 × SSC for 18 h at 37°C), washed for 30 min, and finally stained with FITC-labeled

antibody to digoxigenin (Boehringer-Mannheim) for 2 h. The antibody was diluted 1 in 100 in phosphate buffered saline containing 0.05% Tween 20 (PBS/T) plus 2% bovine serum albumin. The preparations were then washed extensively in PBS/T and mounted in glycerol/PBS (9:1) for viewing on a scanning confocal-laser microscope (Bio-Rad MRC 600). N-propyl gallate (Sigma) was added to the PBS (2.5 g/10 ml) as an antifade agent.

Results

Survey of Single and Clusters of Immunoreactive Neurons detected Histochemically

Refer to Figure 1 for locations of neurons used and Table I for a summary of the results.

Cerebral ganglia

As a test of the dissection and RIA procedures, experiments were first made on the C1 neuron, which contains 5-hydroxytryptamine but does not stain positively with FMRFamide antisera. The level of immunoreactivity in this neuron was lower than the limit of detection, *i.e.*, less than 0.01 pmole/cell (see Table I). This result suggests that general contamination of samples during cell isolation did not pose a problem.

C3 neuron. Previous histochemical and RIA data suggest that this neuron contains one or more FaRPs (Cottrell *et al.*, 1982), and most probably only FMRFamide and FLRFamide (Bewick *et al.*, 1990). Assays of single C3 cells in the present study indicate levels of FMRFamide equivalent to about 0.2 pmole/cell.

Right mesocerebral cluster. The experiments of Elekes and Nässel (1990) showed that a mass of cells in the mesocerebral area of the right cerebral ganglion were stained with the FMRFamide antiserum. Because they are so abundant, we subjected extracts of these cells to HPLC before RIA (see data below).

Pleural ganglia

Neurons equivalent to LPL1 and RPL1. Two large cells, which have the same location as LPL1 and RPL1 detected immunocytochemically in *H. pomatia* by Elekes and Nässel (1990), were isolated from *H. aspersa* pleural ganglia. The level of immunoreactivity assessed by RIA in these *H. aspersa* neurons was low (0.02; 0.08 pmole). When levels in large cells (*i.e.*, those greater than 160 μ in diameter) are less than 0.1 pmole, they are considered low in contrast to the 0.2 pmole detected in the C3 neuron. The C3 neuron has a diameter of about 80 μ, and its volume is therefore only about 1/8th of that of the larger cells. Whether the low levels detected in the large pleural neurons represent contamination from adhering neuropil, or low cellular content of peptide, was not investigated further.

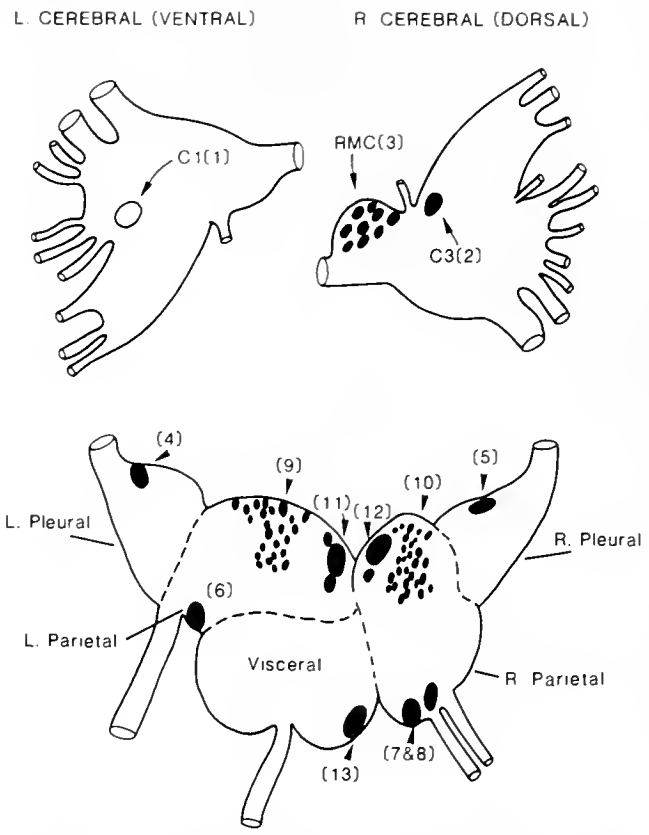

Figure 1. The locations of the neurons taken for RIA from the cerebral, pleural, parietal, and visceral ganglia. The ventral surface of the left cerebral ganglion is shown to indicate the location of the C1 neuron, whereas all of the other ganglia are viewed from the dorsal aspect. The designations that have been given to these different neurons, numbered in brackets, for both *H. pomatia* and *H. aspersa*, are listed in Table I. Immunohistochemical evidence suggests that those neurons marked in black may contain FaRPs (see text).

Parietal ganglia

Neurons equivalent to LPa1, RPa1, and RPa2. The neurons LPa1, RPa1, and RPa2 in *H. pomatia* are all immunoreactive to FaRP-antisera (Elekes and Nässel, 1990), but extracts prepared from neurons in the same locations in *H. aspersa* did not contain appreciable levels of FaRP when tested by RIA (see Table I).

Left and right parietal FaRP-clusters. Histochemical studies in both *H. pomatia* and *H. aspersa* suggest that there are relatively large numbers of small to medium sized FaRP-immunoreactive neurons located rostro-marginally and rostro-centrally in both parietal ganglia. Clusters of cells from these regions were cut out en masse. As shown in Table I, RIA with S253 antiserum provides evidence that such clusters are rich in FMRFamide or related peptides.

Table I

RIA survey of Fa-IR n[illegible] in the central ganglia of Helix aspersa *or* Helix pomatia

Ganglia		*H. pomatia*	*H. aspersa*	Content with S253
Cerebral			C1	<0.01; <0.01
	2	C3*	C3*	0.20; 0.25
	3	R. Dorso-marginal* rostral mesocerebral cells	R. mesocerebral cells	See Fig. 1
Pleural	4&5	L.PL1* & R.PL1*	Large cells in identical position	0.08; 0.02
Parietal	6	L.Pa1*	D5	0.02; 0.04
	7	R.Pa1*	F1 or F2	<0.01 (2); <0.01
	8	R.Pa2*	F2 or F3	
	9	L. Rostro-marginal* & Rostro-central cells	L. Parietal* Fa-cluster	15.9 (50), 10.8 (50)
	10	R. Rostro-marginal* & Rostro-central cells	R. Parietal* Fa-cluster	9.8 (40), 16.6 (40)
	11	L.Pa3* & associated cells	D1, D2 & D2a	1.22 (2); 0.6 (3)
	12	R.Pa3* & associated cells	F76, F77 & F78	0.26 (2); 0.3 (2)
Visceral	13	V16*	E2 or E4	<0.01 (3)
Pedal	14	Large caudal* cells	Neurons in same location	<0.01; <0.01

The nomenclature of Elekes and Nässel (1990) is used for *H. pomatia* neurons and that of Kerkut *et al.* (1975) for *H. aspersa* neurons. The cells that have been identified histochemically as immunoreactive against FMRFamide antisera (Fa-IR) are marked with an asterisk; they were observed by Elekes and Nässel (1990) in *H. pomatia*, or in *H. aspersa* by Cottrell *et al.* (1982) or Cottrell *et al.* (1988). The values are given in pmole equivalents of FMRFamide, either per cell when an individual neuron was assayed alone, or for a number of cells (number in brackets) assayed together.

In an attempt to determine whether these cells contain a preponderance of either the tetra- or hepta-FaRPs, parallel assays were made using two antisera: (a) Q2, which shows a high sensitivity to the hepta-FaRPs but a comparatively low sensitivity to FMRFamide itself; and (b) S253, with which FMRFamide and the hepta-FaRPs are approximately equipotent (see Bewick *et al.*, 1990, for exact values). With this assay system, extracts rich in FMRFamide should appear to have a higher FaRP-content when tested with S253 than with Q2. On the other hand, extracts rich in the hepta-FaRPs should yield about the same quantitative result with either assay (*i.e.*, the ratio of the two values should be close to 1). The results of two such experiments yielded the following ratios: 0.92 (2.93 pmole/3.11 pmole) and 0.59 (9.28 pmole/15.70 pmole) for the left parietal FaRP-cluster; and 1.03 (16.50 pmole/15.9 pmole) and 0.94 (10.2 pmole/10.81 pmole) for the right parietal FaRP-cluster.

These data suggest that both the left and right parietal clusters are rich in the hepta-FaRPs, an observation substantiated for the right FaRP-parietal cluster by HPLC and for both the left and right clusters by *in situ* hybridization (see below).

Large rostro-medial cells. Elekes and Nässel (1990) provided histochemical evidence that these neurons (LPa3 and RPa3) in *H. pomatia* contain FaRPs. RIAs with antiserum S253 indicated that neurons located in the same position in *H. aspersa* also contain FaRPs (Table I). Several other assays were undertaken on these cells, attempts being made to distinguish between the three large neurons that occur in this location in each ganglion in *H. aspersa* (*i.e.*, D1, D2, and D2a; F76, F77, and F78). In spite of repeated dissections, however, these neurons could not be identified individually by appearance alone. Nevertheless, each member of both groups (left and right) was successfully isolated and assayed (Table II). These experiments showed that each of these cells was immunoreactive

Table II

Analyses of the large rostrally located cells of the left and right parietal ganglia in the position of LPa3 and RPa3 of H. pomatia

	D1, D2, and D2a		F76, F77, and F78	
A	i	0.34	i	0.08
	ii	0.28	ii	0.16
			iii	0.26
B	i	0.24	i	0.2
			ii	0.1
			iii	0.08
C	i	0.32	i	0.12
D	i	0.14	i	0.14
	ii	0.26	ii	0.46
	iii	0.3	iii	0.22
E	i	0.38	i	0.3
	ii	0.26	ii	0.1
	iii	0.42	iii	0.46
Avs		0.29		0.206
(min = 0.14, max = 0.42)			(min = 0.08, max = 0.46)	

Three large cells could usually be observed at each location (D1, D2, and D2a of the left, and F76, F77, and F78 of the right parietal ganglion of *H. aspersa*), but they could not be reliably distinguished by appearance. Individual cells were dissected from five preparations (A to E), but only in preparations D and E were all of the separate cells successfully isolated and assayed. The results suggest that most if not all of these large neurons contain FaRPs. Values are given in pmole equivalents of FMRFamide per cell.

to antiserum S253 and that, of all the *single* cells assayed in the different ganglia, they had the highest level of immunoreactivity.

Parallel RIAs were made on many single cell extracts prepared from individual neurons in this rostro-medial location. Of 26 cell extracts, 21 had Q2/S253 ratios ranging from 0.05 to 0.35; 3 had values in the range of 0.36 to 0.86; and the remaining two had values of 1.0 and 1.7. These data suggest that most of the large cells in this region contain FMRFamide, but not appreciable levels of the hepta-FaRPs. This conclusion was substantiated by HPLC and also by analysis of the mRNA in these large cells (see below). The significance of the finding that a few cell extracts yielded Q2/S253 ratios close to 1 is not clear. It could have resulted from contamination by some of the surrounding parietal cluster neurons, from inaccurate assays, or possibly from the existence, with the region, of an unidentified heptapeptide-containing neuron. Estimates of the FMRFamide content of all the cells analyzed in this location, based on assays using the S253 antiserum, varied from about 0.02 to 0.2 pmole per cell.

Visceral and pedal ganglia

Large visceral and the large caudal pedal neurons. Histochemical evidence in *H. pomatia* obtained by Elekes and Nässel (1990) suggests that specified neurons in the visceral and pedal ganglia may contain FaRPs. RIAs of individual neurons dissected from the same locations in *H. aspersa* ganglia, however, indicated that these cells do not contain FaRPs (see Table I).

RIA of Extracts Prepared by High Pressure Liquid Chromatography

Right parietal FaRP-cluster

Extracts of these cells yielded large peaks with S253 that correspond to the heptapeptides pQDPFLRFamide, NDPFLRFamide, and SDPFLRFamide (see Fig. 2). There was also a small peak corresponding to FLRFamide and an even smaller one in the position of FMRFamide. The presence of the heptapeptides was confirmed by assays of the fractions with the Q2 antiserum, which also detected a strong peak corresponding to the NDPYLRFa and SEPYLRFamide heptapeptides that were not detected with the S253 antiserum. Analysis of aliquots of the same fractions with yet another antiserum developed against EFLRIamide showed that the right parietal FaRP-cluster also contains pQDPFLRIamide which—together with all the above heptapeptides—is also encoded on the *H. aspersa* mRNA (see Lutz *et al.*, 1992).

These data therefore confirm those from the parallel RIA and support the notion that the neurons of the right FaRP-cluster are rich in the hepta-FaRPs. The ratio of each of the hepta-FaRPs to FMRFamide in the extracts

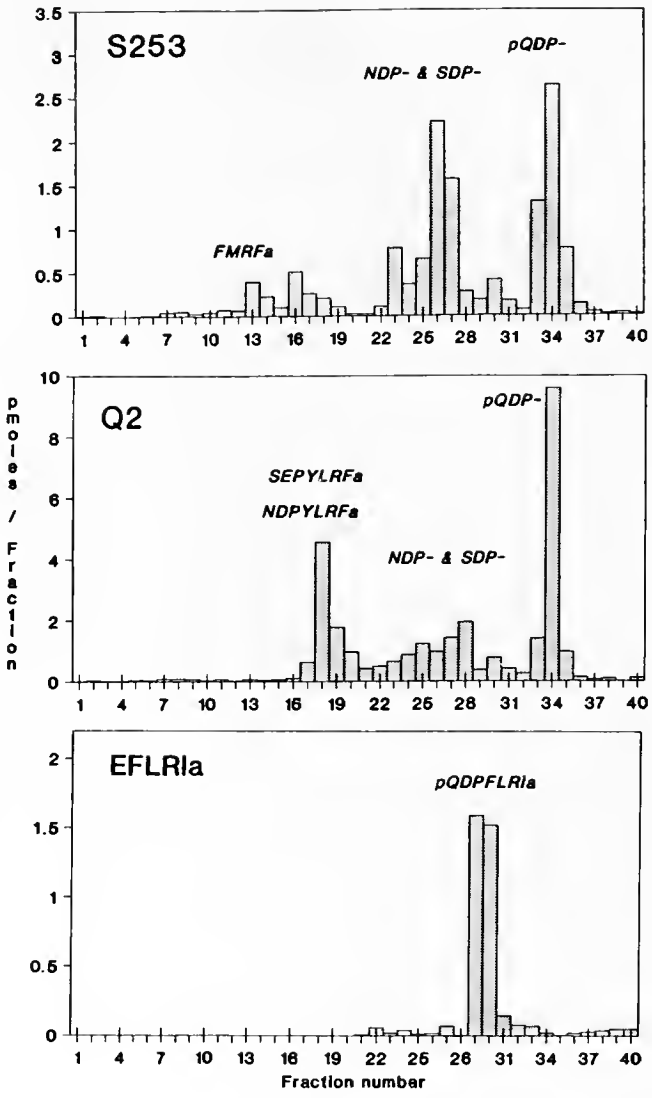

Figure 2. HPLC fractionation of an extract prepared from the parietal cluster of neurons. The fractions were assayed with three antisera: (a) S253, which reacts equally well with both the tetra- and hepta-FaRPs (excluding SEPYLRFamide and NDPYLRFamide); (b) Q2, which is most sensitive to the hepta-FaRPs; and (c) anti-EFLRIa, which selectively reacts with pQDPFLRIamide. For NDP-, SDP-, and pQDP-, the C-terminal is -FLRFa; a = amide. The hepta-FaRPs predominate in the parietal cluster neurons. There is, however, a small peak at the location of FMRFamide; this probably represents some contamination of the sample.

was about 10 to 1. Whether any of the neurons enclosed within the dissected cluster contained any authentic FMRFamide is questionable, because some neuropil, which is rich in FMRFamide, would probably have been included in the sample of cells that were removed en masse.

Right mesocerebral cell cluster

Analysis of HPLC fractions with the more selective S253 antiserum indicated, against our expectations, that

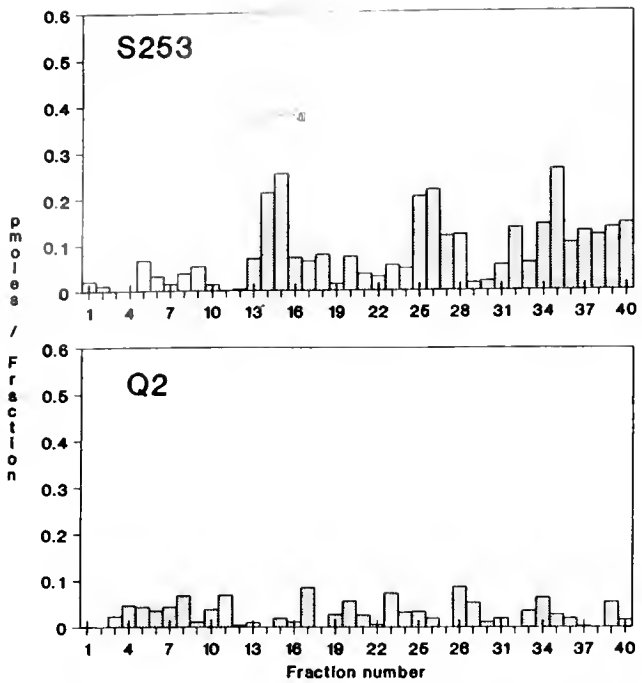

Figure 3. HPLC fractionation of two *Aplysia* giant R2 neurons showing a clear peak with the S253 antiserum corresponding to FMRFamide, a shoulder at the location of FLRFamide (fractions 16 and 17), and two other peaks (at fractions 25/26 and 34). The identity of the latter peaks is not known, but could represent intermediates in the processing of the prohormone for FMRFamide and FLRFamide.

these cells contained neither FMRFamide nor any FaRP. The absence of the hepta-FaRPs was confirmed with the Q2 antiserum. No peak corresponding to pQDPFLRI-amide was detected with the EFLRIamide antiserum.

Aplysia *R2 cell*

An extract of two of the large R2 *Aplysia* neurons known to contain FMRFamide (Schaeffer *et al.*, 1985) was fractionated and assayed with the S253 and Q2 antisera (Fig. 3). Available evidence indicates that *Aplysia* ganglia do not contain hepta-FaRPs. With S253, the major peak corresponded to FMRFamide with a shoulder corresponding to FLRFamide in fractions 16 and 17 predicted from what is known of the structure of the precursor peptide. Unexpectedly, some other peaks corresponding to higher molecular weight peptides, as yet unidentified, were also observed with S253. These peptides were not detected when the Q2 antiserum was used. Further, there was no peak corresponding to the position of pQDPFLRIamide.

Cerebral C3 neurons

The C3 neurons are much smaller than the *Aplysia* R2 neurons and more were required for HPLC. Eight cells were isolated over a period of 19 days. Fractionation of the extract of these cells and RIA with S253 showed several peaks. The first corresponded to oxidized FMRFamide (Fig. 4). The presence of the oxidized form of the peptide was probably related to the relatively long period taken to amass sufficient cells. Oxidized FMRFamide is only

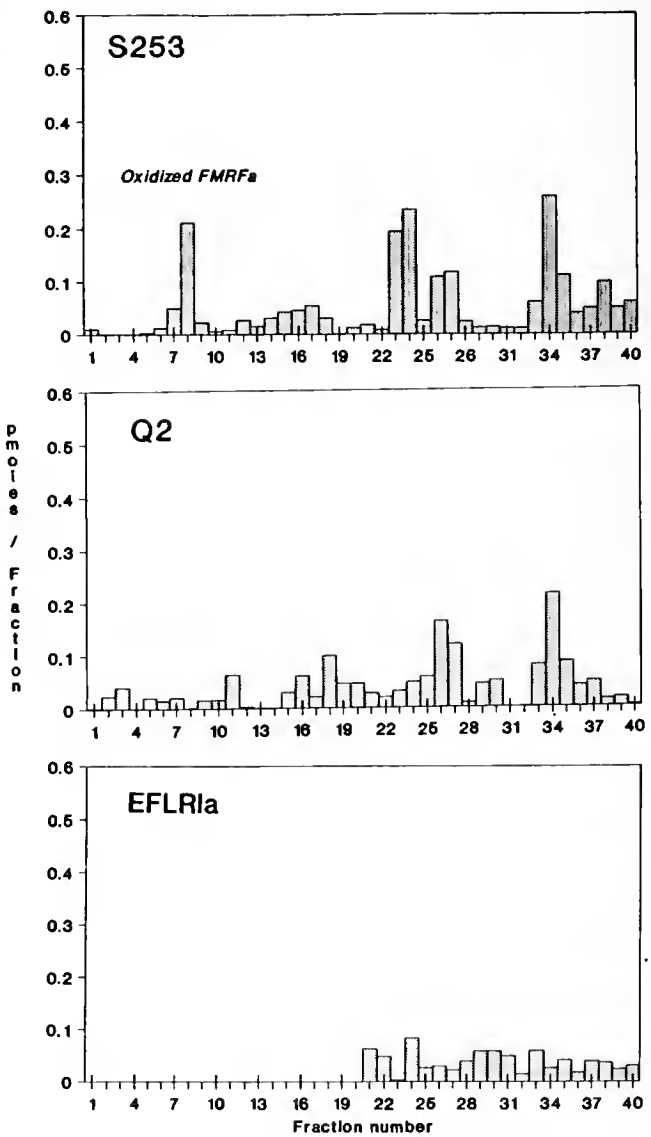

Figure 4. HPLC fractionation of an extract of eight C3 neurons. The C3 neuron is only about 100 μ in diameter and occurs singly in each cerebral ganglion. Several are required to provide sufficient material to detect the peptides by HPLC. The peak at fraction 8, with S253 antiserum, corresponds to oxidized FMRFamide. As S253 reacts about four times less intensely with oxidized FMRFamide that with FMRFamide itself, FMRFamide must be the most abundant FaRP in the extract. A small peak at fractions 16 and 17 corresponds to FLRFamide. Other peaks corresponding to higher molecular weight peptides are also seen, as with the *Aplysia* R2 neuron (Fig. 3). These unknown peptides could also be processing intermediates.

about one quarter as reactive with S253 as the unoxidized form. Thus FMRFamide is the predominant peptide in the C3 neuron, as previous experiments have shown. A small peak corresponding to FLRFamide was also observed in fractions 16 and 17; and three other peaks indicative of higher molecular weight peptides appeared, two of them eluting in positions similar to those of the unidentified peptides seen in the extract of the *Aplysia* R2 neuron. The identity of none of these peaks is known, although at least one of them (at fraction 34) does appear to react with the Q2 antiserum. Neither SEPYLRFamide nor NDPYLRFamide were observed with the Q2 antiserum, nor was pQDPFLRIamide with the EFLRIamide antiserum.

Large cells in the location of LPa3 and RPa3

Extracts were prepared from three preparations, each containing eight large neurons that are located in the vicinity of LPa3 and RPa3 of *H. pomatia* (Elekes and Nässel, 1990): *i.e.*, D1, D2, D2a, F76, F77, and F78 of *H. aspersa* (Kerkut *et al.*, 1975). RIA of HPLC fractions provided clear evidence that at least some of the neurons in this group contain FMRFamide (see Fig. 5). At present, we cannot distinguish between these large cells based on their appearance alone.

Analysis of mRNA from Single Neurons and Small Clusters of Neurons

The mRNA contents of the following cell types were examined by hybridization, as described above: C3 neurons; cells from the right parietal FaRP cluster; and the group comprising the D1, D2, D2a and the F76, F77, F78 neurons, which corresponds to the large neurons in the region of LPa3 and RPa3 of *H. pomatia* (see Elekes and Nässel, 1990).

Two filters were prepared. Onto each were loaded both the contents of about 35 cells from the right parietal FaRP cluster and the contents of about 15 cells of the D1-D2a and F76-78 groups. Additionally, onto only one of the filters (because of the difficulty in isolating large numbers of intact C3 neurons) we loaded the contents of five C3 neurons (see lane C in Fig. 6a). The filter with the C3 neuron sample was hybridized to the tetra-FaRP cDNA of *H. aspersa*, and the other filter to the hepta-FaRP cDNA. The results of this experiment are shown in Figure 6. A strongly hybridizing band appears in the D1-D2a/F76-F78 sample when it is probed with the tetra-FaRP cDNA, while only a very faint band is produced when it is probed with the hepta-FaRP cDNA. Conversely, the sample from the cells of the right parietal FaRP cluster shows hardly any hybridization to the tetra-FaRP cDNA, but very strong hybridization to the hepta-FaRP cDNA. The extract of C3 neurons, though small in volume, shows a moderate amount of hybridization to the tetra-FaRP cDNA.

Subsequent to these hybridizations, the DNA probes were stripped from both the filters (by placing them in a solution of 20 m*M* Tris, pH 7.5 at boiling point and then allowing the solution to cool), and the filters were then reciprocally re-probed—*i.e.*, the filter with the C3 sample was hybridized to the hepta-FaRP cDNA and the second filter to the tetra-FaRP cDNA. The results of this second round of hybridization were exactly as described above for the cells of the right parietal FaRP cluster and those of the D1-D2a/F76-F78 group; but no hybridization to the C3 cell sample was detected with the heptapeptide-cDNA (data not shown).

Thus, the C3 neurons do contain mRNA for the tetra-FaRPs (as anticipated), but not for the hepta-FaRPS. Also, the cells of the D1-D2a/F76-F78 group contain, in great predominance, mRNA for the tetra-FaRPS; and those of the right parietal FaRP cluster contain, again in great predominance, mRNA for the hepta-FaRPS. These results

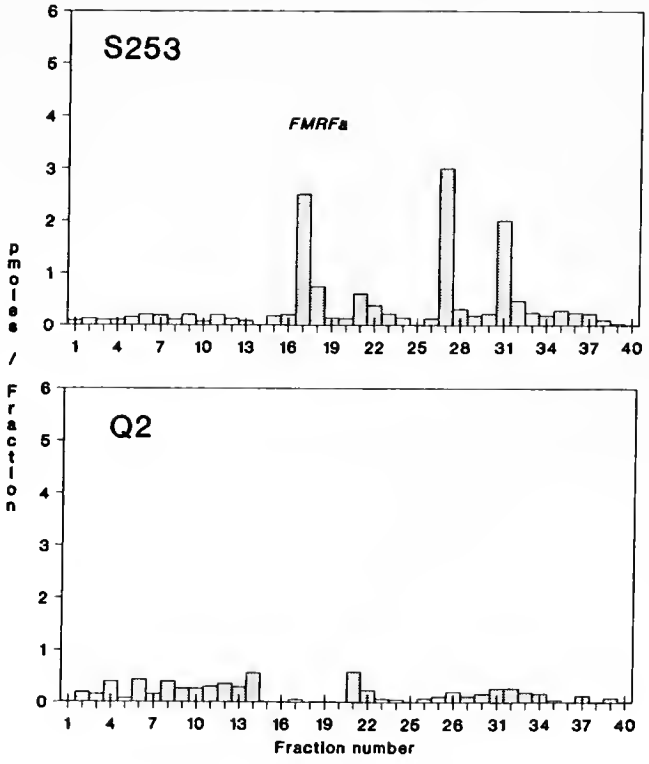

Figure 5. HPLC fractionation of the large parietal neurons, taken from three ganglion preparations, in the location of D1, D2, D2a, F76, F77, F78. This extract was run on a new column that retained FMRFamide slightly more effectively than the column used for the other extracts. A major peak corresponding to FMRFamide is seen, as are two other peaks reflective of higher molecular weight peptides of unknown identity.

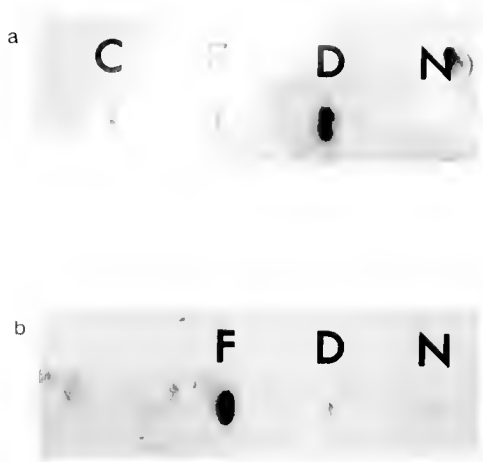

Figure 6. Autoradiographs of filters with various cell extracts hybridized with either (top) tetra-, or (bottom) hepta-FaRP cDNA probes of *H. aspersa* (Lutz *et al.*, 1992). The cells analyzed were: C, C3 neurons; F, the right parietal cell cluster; and D, neurons from the groups D1-D2a, F76-F78. The control, N, was a sample of physiological solution taken from the organ bath during dissection of the cells. Neither of the probes hybridized with the control sample, while the tetra-FaRP cDNA hybridized strongly to the sample from the cells of the D1-D2a/F76-F78 groups (D), and moderately to the C3 cell sample (C). The cells of the parietal cluster (F) reacted much more strongly with the hepta-FaRP cDNA probe than with the tetrapeptide probe. No reaction with the heptapeptide probe was seen with the C3 neuron sample, and only a weak reaction was seen with sample D. Subsequent stripping of the probes from the filters, followed by reciprocal re-probing gave exactly the same result, with the additional observation that no hybridization to the C3 sample was seen with the hepta-FaRP cDNA.

are consistent with the immunohistological and HPLC data described above.

Detection of FaRP-Encoding mRNA in Neurons by In Situ *Hybridization with Whole-Mounted Ganglia*

The C3 neuron and the parietal cell clusters were examined directly for tetra- and hepta-FaRP mRNA by *in situ* hybridization. Antisense RNA probes were synthesized in the presence of digoxigenin-labeled UTP, one specific for tetrapeptide encoding mRNA, the other specific for heptapeptide encoding mRNA, (*cf.*, Lutz *et al.*, 1992). The probes were hybridized to whole-mount preparations of cerebral and suboesophageal ganglia and were subsequently detected by means of a fluorescein-labeled antibody to digoxigenin (Fig. 7). Cells in the left and right parietal ganglia that react intensely with the probe detecting heptapeptide mRNA are shown in Figure 7a. These cell clusters correspond to ones that are rich in hepta-FaRPs and that do not react with the probe detecting the tetrapeptide mRNA (data not shown). In contrast, the C3 neuron reacted with the probe detecting the tetrapeptide mRNA (Fig. 7b), but not with the probe for the heptapeptide mRNA (data not shown).

Discussion

Identification of FaRP-containing neurons in H. aspersa

Some of the neurons in *H. aspersa*, in the same locations as cells in *H. pomatia* that react immunocytochemically with FMRFamide antiserum, contain detectable levels of FaRPs, but others do not. The absence of FaRPs in some of these cells may be due to the species difference, or because some of the neurons detected immunocytochemically do not contain FaRPs. Certainly, FMRFamide antisera have been used to identify non-FMRFamide peptides in neurons of, for instance, coelenterates (see Grimmelikhuijzen and Graff, 1986) and echinoderms (Elphick *et al.*, 1991).

Differential localization of the tetra- and the hepta-FaRPs

Helix neurons that possess FaRPs appear to be of two sorts. Either they contain the tetrapeptide FMRFamide (and also presumably FLRFamide, although this is difficult to detect because of its lower concentration), as in the C3 neuron, and some of the large parietal neurons (D1, D2, D2a, F76, F77 and F78), *or* they contain the hepta-FaRPs, as in the right and left parietal clusters. This conclusion, suggested by earlier studies with the C3 neurons (Bewick *et al.*, 1990), is supported by the HPLC data and also by the parallel R1As of the parietal clusters and the large parietal neurons (D1, D2, D2a, F76, F77, F78) reported here.

Differential localization of mRNAs for the tetra- and the hepta-FaRPs

Two mRNA species encode the FaRPs in *Helix* (Lutz *et al.*, 1990, 1992). One species encodes FMRFamide and FLRFamide, and the other encodes all the hepta-FaRPs and pQDPFLRIamide. The C3 neurons and the some of the large parietal neurons (D1, D2, D2a, F76, F77, F78) possess mRNA encoding the tetra-FaRPs, whereas neurons of the parietal clusters are abundant in mRNA encoding the hepta-FaRPs. Bearing in mind the technical problem of isolating the different neurons uncontaminated with other cell types and neuropil, especially with the relatively large amount of tissue taken for the parietal cluster samples, the differential distribution of the mRNA, and also of the peptides, is striking.

The data suggest that either one of the mRNAs or the other is expressed, at least in the neurons studied here. This view is supported by hybridization of antisense RNA probes to mRNA *in situ*. In whole-mount ganglia, we saw that the C3 neuron expresses the mRNA encoding the tetra-FaRPs, whereas the parietal clusters express the mRNA encoding the hepta-FaRPs. The results of recent *in situ* hybridization experiments on *Lymnaea stagnalis*

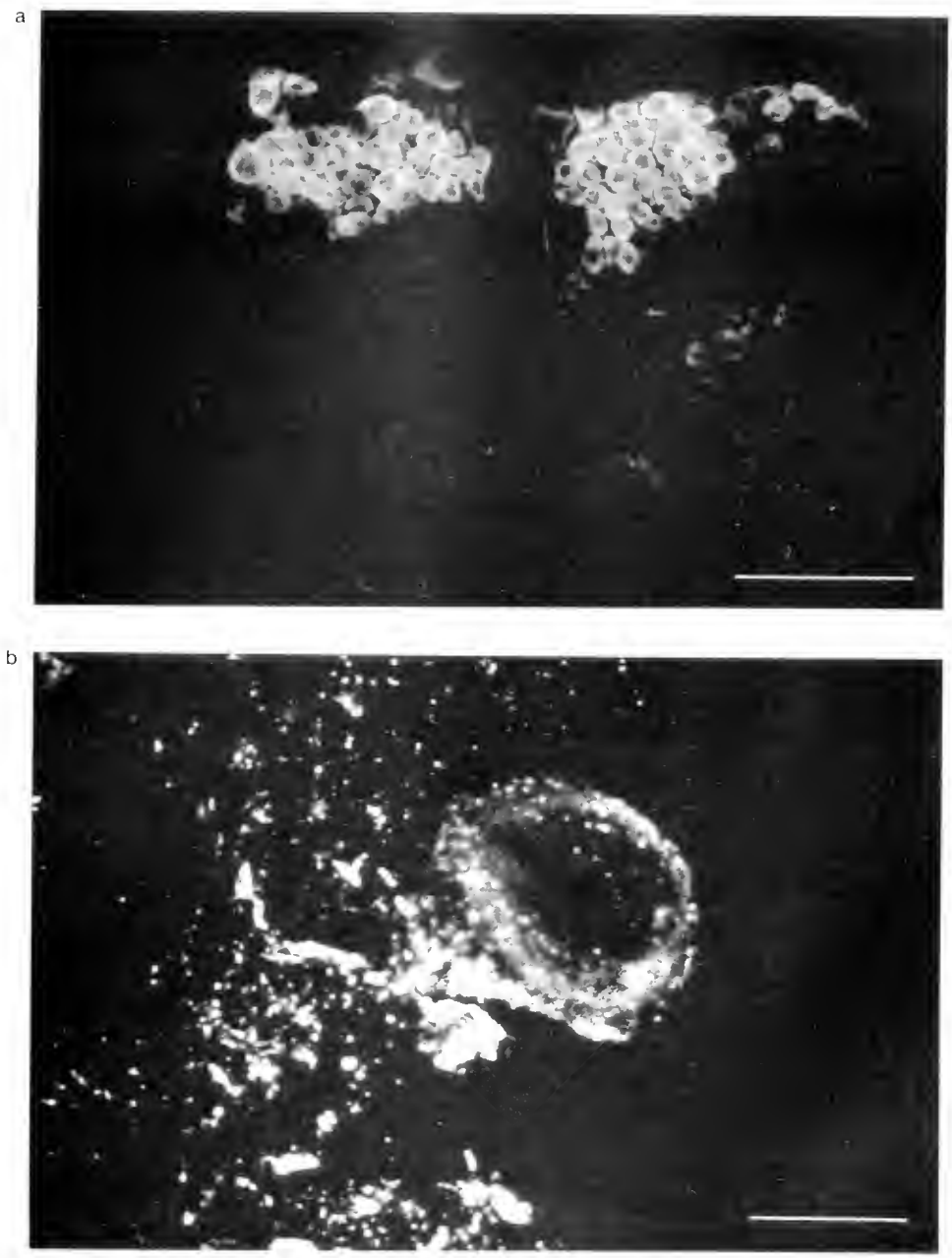

Figure 7. Hybridization of specific antisense probes *in situ* to mRNA encoding either tetra- or hepta-FaRPs. Hybridized mRNA is detected using fluorescein-labeled antibodies directed against the probes. (a) Whole mount of the visceral and left and right parietal ganglia hybridized with the probe specific for heptapeptide-encoding mRNA. The left and right parietal cell clusters are seen to fluoresce strongly; cf. with Figure 1. (b) Whole mount of a cerebral ganglion hybridized with the probe specific for tetrapeptide-encoding mRNA. Only the C3 neuron is seen to fluoresce. Note the higher magnification and the presence of some punctate fluorescence, some of which was non-specific, close to the axon hillock of the C3 neuron. Hepta-FaRP mRNA is not detected in the C3 neuron, nor is tetra-FaRP mRNA detected in the parietal cell clusters (not shown here). The scale bar corresponds to 250 μm in (a) and 50 μm in (b).

provide good evidence that, in this species too, the tetra-FaRPs are expressed in some neurons and the hepta-FaRPs in others (Saunders *et al.*, 1992).

The use of the antisense RNA probe for the heptapeptide mRNA defines most clearly the number of neurons comprising the heptapeptide-containing clusters, their packing together, and their topography in the parietal ganglia of *H. aspersa*. Because none of the cells within these clusters stained with the probe for the tetra-mRNA, they would appear to provide a homogeneous source of

neurons for further studies on the synthesis of the hepta-FaRPs carried out with a range of biochemical and molecular biological techniques.

Acknowledgments

We wish to thank Dr. Metter Morgensen for assistance with the confocal microscopy and Ms. Niovi Santama, Neuroscience Interdisciplinary Research Centre, University of Sussex, Falmer, BN1 1QG, UK, for antiserum against EFLRIamide. Work at the Whitney Laboratory was supported by NIH grant HL28440 (to DAP).

Literature Cited

Bewick, G. S., D. A. Price, and G. A. Cottrell. 1990. The fast response mediated by the C3 motoneurone of *Helix* is not attributable to the contained FMRFamide. *J. Exp. Biol.* **148:** 201–219.

Boer, H. H., L. P. C. Schot, J. A. Veenstra, and D. Reichelt. 1980. Immunocytochemical identification of neural elements in the central nervous system of a snail, some insects, a fish and a mammal with an antiserum to the molluscan cardio-excitatory tetrapeptide FMRFamide. *Cell Tissue Res.* **213:** 21–27.

Bradley, C. V. 1982. Structural studies on bioactive organic compounds. PhD Thesis, University of Cambridge, UK.

Cottrell, G. A., L. P. C. Schot, and G. J. Dockray. 1982. Identification and probable role of a single neurone containing the neuropeptide *Helix* FMRFamide. *Nature* **304:** 638–640.

Cottrell, G. A., and N. W. Davies. 1987. Multiple receptors for a molluscan peptide (FMRFamide) and related peptides in *Helix*. *J. Physiol.* **382:** 51–68.

Cottrell, G. A., N. W. Davies, and J. Turner. 1988. Actions and roles of the FMRFamide peptides in *Helix*. Pp. 283–298 in *Neurohormones in Invertebrates*. Society for Experimental Biology series volume 33, M. C. Thorndyke and G. J. Goldsworthy, eds. Cambridge University Press, Cambridge, UK.

Elekes, K., and D. R. Nässel. 1990. Distribution of FMRFamide-like immunoreactive neurons in the central nervous system of the snail *Helix pomatia*. *Cell Tissue Res.* **262:** 177–190.

Elphick, M. R., D. A. Price, T. D. Lee, and M. C. Thorndyke. 1991. The SALMFamides: a new family of neuropeptides isolated from an echinoderm. *Proc. R. Soc. Lond. B* **243:** 121–127.

Grimmelikhuijzen, C. J. P., and D. Graff. 1986. Isolation of ⟨Glu-Gly-Arg-Phe-NH_2 (Antho-RFamide), a neuropeptide from sea anemones. *Proc. Natl. Acad. Sci. USA* **83:** 9817–9821.

Kerkut, G. A., J. D. C. Lambert, R. J. Gayton, J. E. Locker, and R. J. Walker. 1975. Mapping of nerve cells in the suboesophageal ganglion of *Helix aspersa*. *Comp. Biochem. Physiol.* **50A:** 1–25.

Krieg, P. A., and D. A. Melton. 1987. *In vitro* RNA synthesis with SP6 RNA polymerase. *Meth. Enzymol.* **155:** 397–415.

Lehman, H. K., and M. J. Greenberg. 1987. The actions of FMRFamide-like peptides on visceral and somatic muscles of the snail *Helix aspersa*. *J. Exp. Biol.* **131:** 55–68.

Lehman, H. K., and D. A. Price. 1987. Localization of FMRFamide-like peptides in the snail *Helix aspersa*. *J. Exp. Biol.* **131:** 37–53.

Lutz, E. M., W. Lesser, M. Macdonald, and J. Sommerville. 1990. Novel peptides revealed by cDNAs cloned from *Helix aspersa* nervous system. *Soc. Neurosci. Abstr.* **16:** 549.

Lutz, E. M., M. Macdonald, S. Hettle, D. A. Price, G. A. Cottrell, and J. Sommerville. 1992. Structure of cDNA clones and genomic DNA encoding FMRFamide related peptides (FaRPs) in *Helix*. *Mol. Cell. Neurosci.* (in press).

Maniatis, T., E. F. Fritsch, and J. Sambrook. 1982. *Molecular Cloning—A Laboratory Manual.* Cold Spring Harbor Laboratory Publications.

Price, D. A., and M. J. Greenberg. 1989. The hunting of the FaRPs: the distribution of FMRFamide-related peptides. *Biol. Bull.* **177:** 198–205.

Price, D. A., W. Lesser, T. D. Lee, K. E. Doble, and M. J. Greenberg. 1990. Seven FMRFamide-related and two SCP-related cardioactive peptides from *Helix*. *J. Exp. Biol.* **154:** 421–437.

Saunders, S. E., E. Kellett, K. Bright, P. R. Benjamin, and J. F. Burke. 1992. Cell-specific alternative RNA splicing of an FMRFamide gene transcript in the brain. *J. Neurosci.* **12:** 1033–1039.

Schaeffer, M., M. R. Picciotto, T. Kreiner, R. R. Kaldany, R. Taussig, and R. H. Scheller. 1985. *Aplysia* neurons express a gene encoding multiple FMRFamide neuropeptides. *Cell* **41:** 457–467.

Schot, L. P. C., and H. H. Boer. 1982. Immunocytochemical demonstration of peptidergic cells in the pond snail *Lymnaea stagnalis* with an antiserum to the molluscan cardioactive tetrapeptide FMRFamide. *Cell Tissue Res.* **225:** 347–354.

Tautz, D., and C. Pfeifle. 1989. A non-radioactive *in situ* hybridization method for the localization of specific RNAs in *Drosophila* embryos reveals translational control of the segmentation gene *hunchback*. *Chromosoma* **98:** 81–85.

Reference: *Biol. Bull.* **183**: 123–137. (August, 1992)

Characterization of a Cystine-Rich Polyphenolic Protein Family from the Blue Mussel *Mytilus edulis* L.[1]

LESZEK M. RZEPECKI[1], KAROLYN M. HANSEN, AND J. HERBERT WAITE

College of Marine Studies, University of Delaware, 700 Pilottown Road, Lewes, Delaware 19958

Abstract. Marine bivalve mollusks synthesize, in the phenol and accessory glands of the foot, proteins that integrate the post-translationally hydroxylated amino acid 3,4-dihydroxyphenylalanine (DOPA) into their primary sequence. These polyphenolic proteins serve as structural and adhesive components of the byssal threads which form the extraorganismic holdfast. One family of byssal precursors, previously characterized in a number of mytiloid species, consists of proteins between 70–130 kDa containing 8–18 mol % DOPA. The high molecular weight precursor isolated from the foot of the blue mussel (*Mytilus edulis* Linnaeus, 1758) is here designated as Mefp-1. We now present evidence for the occurrence, in *M. edulis*, of a second, structurally unrelated, family of DOPA proteins (Mefp-2) of about 42–47 kDa. These novel proteins contain 2–3 mol % DOPA and, in startling contrast to Mefp-1, are also enriched in the disulphide-containing amino acid cystine (6–7 mol %). Consideration of the amino acid compositions of Mefp-1 and 2 and of the terminal adhesive plaques of byssal threads suggests that Mefp-2 makes up about 25% of plaque protein, whereas Mefp-1 content is about 5%. The Mefp-2 family exhibits electrophoretic microheterogeneity, but members share similar N- and C-terminal amino acid sequences. Analysis of peptides isolated after tryptic hydrolysis suggests that the primary sequence of Mefp-2 is tandemly repetitive, with at least three types of motif. The sequence degeneracy of the motifs is greater than in Mefp-1. Mefp-2 has minimal sequence homology with known structural proteins and may be a structural element of the plaque matrix.

Received 27 March 1992; accepted 20 May 1992.

Abbreviations: DOPA, 3,4-dihydroxyphenylalanine; Mefp-1 & -2, *Mytilus edulis* foot protein 1 and 2; CAMC; S-carbamidomethylcysteine; COMC, S-carboxymethylcysteine; NBA, Na/Borate/Ascorbate buffer; DTT, dithiothreitol; HPLC, high pressure liquid chromatography; EDTA, ethylenediaminetetraacetic acid; SDS- or AU-PAGE, sodium dodecylsulphate or acetic acid-urea polyacrylamide gel electrophoresis; IEF, isoelectric focussing; PAS, periodic acid-Schiff stain; NBT, nitroblue tetrazolium.

[1] Corresponding author.

Introduction

Mussels make a secure adhesive holdfast (byssus) that bonds tightly to wet and irregular surfaces without the extraordinary preparative treatments required when humans try their hand at similar tasks (Waite, 1987). The byssus, a collagenous extraorganismic tendon, is a bundle of threads that terminate in an adhesive plaque. The byssus is synthesized by a muscular organ, the mussel foot (see schematic diagram in Fig. 1). The thread coalesces from the secretions of various glands lining the ventral groove of the foot, while the plaque forms at the distal depression. The collagenous core of the thread is secreted by the collagen gland (Vitellaro-Zuecarello, 1980), and a protective varnish, made of an *o*-diphenolic resin coupled with a curing enzyme, is secreted by the accessory gland and applied to the thread cortex (Brown, 1952; Pujol, 1967; Vitellaro-Zuccarello, 1981). The resin is known to be a 130 kDa, tandemly repetitive protein (here called Mefp-1, *Mytilus edulis* foot protein), which incorporates into its primary structure a high proportion of 3,4-dihydroxyphenylalanine (DOPA), synthesized post- or co-translationally through the action of a tyrosyl hydroxylase (Waite, 1983; Benedict and Waite, 1986a). The curing enzyme is a catecholoxidase, activated after secretion of the resin, which converts the peptidyl DOPA residues into peptidyl DOPA-quinone, a probable cross-linking agent during sclerotization (Waite, 1990; Rzepecki and Waite, 1991, for reviews).

The plaque is formed from glandular secretion at the distal depression, and the main gland involved appears to be the phenol gland, so called because of its intense affinity for phenol in histological reagents (Tamarin *et al.*, 1976). Antibodies to Mefp-1 bind strongly to phenol and accessory glands (Benedict and Waite, 1986a), and Mefp-1 has been isolated from dissected phenol glands (Waite, 1983). Mefp-1 has also been identified as the adhesive at the interface between plaque and substratum (Benedict and Waite, 1986a), and its physicochemical properties are consistent with such a role (Filpula *et al.*, 1990).

Little is known, however, about the components of the plaque matrix. We have now characterized another potential ingredient of phenol gland secretion, Mefp-2, which may be a structural element of plaque matrix. Mefp-2 incorporates some DOPA, but is distinct from Mefp-1 in composition, sequence, and physicochemical properties, and hence probably serves a different role in byssal structure.

Materials and Methods

Purification of DOPA proteins

Cultured blue mussels (*Mytilus edulis* L.) were obtained via Rehoboth Seafood Market (Rehoboth Beach, Delaware) after being shipped live from Maine on ice. Feet were excised within two days of original shipment and stored in 30-g lots at −70°C.

The DOPA proteins were extracted and purified, as described by Pardo *et al.* (1990) and modified by Rzepecki *et al.* (1991). Briefly, 30 g of mussel feet were homogenized in a Waring blendor in 300 ml 0.7% perchloric acid, and the homogenate was sedimented at 31,000 × *g* to remove particulate matter. The DOPA proteins precipitated upon the addition of acetone to 66% final volume. The precipitate was resolubilized in 5–7 ml 5% acetic acid and then fractionated, in the same buffer, on a 2.5 × 90 cm column of Sephadex G-200 or G-150 (Pharmacia LKB Biotechnology Inc., Piscataway, New Jersey). The eluate was monitored at 280 nm. The final purification of Mefp-2 was achieved as follows. The lyophilized Sephadex fractions were chromatographed in 5% acetic acid on a 2.5 × 90 cm column of Sephacryl S-300 or S-400 (Pharmacia) monitored at 280 nm. This step was followed by high pressure liquid chromatography (HPLC) on a 0.7 × 25 cm semi-preparative Brownlee Aquapore RP-300 (C_8) reverse phase column (Rainin Instrument Co., Woburn, Massachusetts) with a Rabbit HPX solvent delivery system (Rainin); monitoring was at 280 nm with a Model 116 dual wavelength detector (Gilson Medical Electronics Inc., Middleton, Wisconsin). The acetonitrile/water solvent gradients contained 0.1% trifluoracetic acid.

In all of the chromatography procedures, the separation of Mefp-1 and Mefp-2 was assessed by gel electrophoresis (see below). Proteins were lyophilized after HPLC purification and stored dry at −20°C. DOPA concentrations were determined by the Arnow (1937) method (Waite and Tanzer, 1981), and the protein concentrations were determined according to Bradford (1976), with a Bio-Rad (Richmond, California) reagent kit.

The localization of Mefp-2 was studied in specimens of *M. edulis* that were collected locally (Roosevelt Inlet, Lewes, Delaware), kept in flowing seawater at 12–15°C, and allowed to deposit byssal threads on to plexiglass plates. In one set of experiments, some mussel feet were excised and serially sectioned, as illustrated in Figure 1a. The acid-urea soluble protein was extracted from each section by homogenization in a small glass homogenizer containing 200–300 μl of 5% acetic acid, 8 *M* urea. The particulate matter was sedimented at 13,000 × *g* for 5 min and was then analyzed for acid-soluble proteins by electrophoresis. In a second set of experiments, byssi were collected 24 h after their synthesis and rinsed in water; the plaques and threads were then separated with a scalpel. About 110–140 mg and 150–175 mg wet weight of plaques and threads, respectively, were homogenized, with a little silica powder (Silica Gel G, 250 μm Analtech, Newark, Delaware) to provide abrasion, in either 400 μl 5% acetic acid with 8 *M* urea, or in 200 μl of the sample buffer used for SDS-PAGE (Laemmli, 1970); the particulate matter was removed as above. Polyclonal anti-Mefp-2 rabbit antibodies were contractually prepared by Cambridge Research Biochemicals (Cambridge, Great Britain), and were used to determine the immunoreactivity of thread and plaque extracts and control Mefp-2 (Blake *et al.*, 1984). Dot blots on nitrocellulose were exposed for 1 h to a 10^{-5} dilution of serum, or a 10^{-4} dilution of pre-immune serum. Binding was detected with goat anti-rabbit IgG-coupled alkaline phosphatase (Boehringer-Mannheim, Indianapolis, Indiana).

S-Alkylation of Mefp-2

S-Alkylation of Mefp-2 to *S*-carbamidomethyl-Mefp-2 (CAMC-Mefp-2) or *S*-carboxymethyl-Mefp-2 (COMC-Mefp-2) was effected after the cystine residues had been reduced by a modification of a procedure of Hollecker's (1990). Stock solutions of Mefp-2 (10 mg/ml) were freshly prepared in H_2O. To 80 μl Mefp-2 was added 20 μl of 0.1 *M* EDTA, pH 7.0, which caused precipitation. After the addition of 400 μl of NBA buffer (0.5 *M* boric acid, 0.5 *M* ascorbic acid, brought to pH 8.0 with 6 *N* NaOH), the precipitate redissolved: 20 μl of fresh 1 *M* dithiothreitol (DTT) together with 1.15 ml of 8 *M* urea were then added, and the reaction mixture was incubated for 40 min at room temperature. After the reduction, the cyteines were

S-alkylated by the addition of fresh iodoacetamide or iodoacetate (300 μl of a 0.25 *M* stock in a 1:4 dilution of the NBA buffer for iodoacetamide, or, for iodoacetate, undiluted NBA buffer containing 0.6 μl of 6 *N* NaOH per mg iodoacetate), and the reaction mixture was incubated for a further 30 min. The reaction was terminated by the addition of 20 μl glacial acetic acid, and the proteins were immediately separated from the low molecular weight solutes by HPLC, as described. Control alkylations of Mefp-2 in buffers with urea, but no DTT, were also performed. Protein fractions were lyophilized, redissolved in H_2O, and stored at 4°C for up to 1 week before use.

Peptide preparation and purification

Native Mefp-2 or its alkylated derivatives were incubated (in 100 m*M* Tris, 100 m*M* ascorbate, pH 7.5, for 7 h at room temperature) with trypsin (Boehringer Mannheim, Indiana), at a trypsin to protein weight ratio of 1:25 or 1:50 for native and alkylated Mefp-2, respectively. Mefp-2 concentrations were about 1 mg/ml. The incubation was terminated by the addition of glacial acetic acid to 5% final volume, and the peptides were resolved directly by HPLC on a 0.46 × 25 cm Microsorb C_{18} reverse phase column (Rainin), as described above. In an effort to recover the DOPA peptides specifically, Mefp-2 (0.5 mg/ml) was treated with trypsin in 400 μl of a 1:2 dilution of the above buffer for 6 h, then loaded on a small column containing 0.4 ml of phenyl boronate agarose (PBA-30, Lot # JM-2134D with 37.8 μMoles boron/ml; Amicon Corp., Danvers, Massachusetts) which had been equilibrated in a 1:5 dilution of the above buffer. Bound peptides were washed twice with 0.4 ml of the diluted buffer, twice more with 0.4 ml of deionized water, and eluted with three washes of 5% acetic acid. Eluted peptides were separated by HPLC.

Amino acid analysis and peptide sequencing

The amino acid compositions of the hydrolyzed proteins and peptides were determined on a Beckman System 6300 Autoanalyzer (Beckman Instruments, Palo Alto, California) using the ninhydrin reaction for detection (Waite, 1991). Polypeptides were usually hydrolyzed by the rapid method of Tsugita *et al.*, in 5 *N* HCl with 8% trifluoracetic acid and 8% phenol *in vacuo* at 158°C for 22 min, except that hydrolysis was effected in the bulk phase, rather than the vapor phase as in the original method. Unfortunately, the high concentrations of phenol required for quantitative yields of DOPA caused the reaction of phenol and cystine to give an unidentified product which co-migrated with histidine on the amino acid analyzer. Consequently, the amino acid compositions of native (non-alkylated) Mefp-2 were determined after hydrolysis in 6 *N* HCl, for 24 h at 105°C, in the presence or absence of 10% phenol. DOPA, tyrosine, serine, and threonine values were recovered from phenolic hydrolysates, while cystine and histidine values were obtained from aphenolic hydrolysates; we deduced a corrected composition from both data sets using the lysine value as a common factor. In the case of reduced and alkylated Mefp-2, alkylated cysteine was recovered after hydrolysis as *S*-carboxymethylcysteine (*S*-COMC) which co-migrated on the amino acid analyzer with 3-hydroxyproline. Because native Mefp-2 contained no 3-hydroxyproline, the content of *S*-COMC was simply determined by applying a correction factor of 2.23 to the reported 3-hydroxyproline values. This correction factor was empirically determined by running a concentration series of *S*-COMC standards (Sigma) on the analyzer. Peptides and proteins were sequenced on a microsequenator (Porton Instruments, Tarzana, California) using automated Edman degradation. PTH-amino acid derivatives were resolved and quantitated by HPLC as previously described (Waite, 1991). Additional N-terminal analysis was performed on 4.6 mg/ml Mefp-2 in a buffer consisting of 46 m*M* sodium phosphate, 18 m*M* sodium borate, and 18 m*M* sodium ascorbate, pH 7.0. Incubations were performed at room temperature for different time intervals and the released amino acids were analyzed directly. The hog kidney aminopeptidase M (Boehringer Mannheim) used in this N-terminal analysis was prepared by dialysis against 50 m*M* sodium phosphate, pH 7.0, at a nominal concentration of 0.09 mg/ml.

Gel electrophoresis and isoelectric focussing

Acetic acid-urea polyacrylamide gel electrophoresis (AU-PAGE) was performed according to Panyim and Chalkley (1969) with 5% polyacrylamide, 5% acetic acid and 8 M urea, pH 2.7 (Rzepecki *et al.*, 1991). Discontinuous sodium dodecylsulphate polyacrylamide gel electrophoresis (SDS-PAGE) was performed according to Laemmli (1970), except that various concentrations of DTT were used in the sample treatment buffer. Low molecular mass protein standards ranged from 14.4–97.4 kDa (Bio-Rad, California). Gels were stained for protein in 0.001% Coomassie Blue R-250 in 7.5% acetic acid, 40% methanol.

The DOPA proteins were visualized by staining the gels with the Arnow (1937) method, as described by Waite and Tanzer (1981). We also used a new redox cycling method involving the production of formazan from nitroblue tetrazolium (NBT) in the presence of glycine at pH > 10 (Paz *et al.*, 1991), but at a small cost in sensitivity, did not usually transfer the proteins electrophoretically to nitrocellulose as recommended by the authors. For Arnow assays, SDS gels were first acidified by equilibration in 5% acetic acid; for NBT stain, all gels were washed twice in 50–100 ml of 0.2 *M* sodium borate, pH 8.5, to

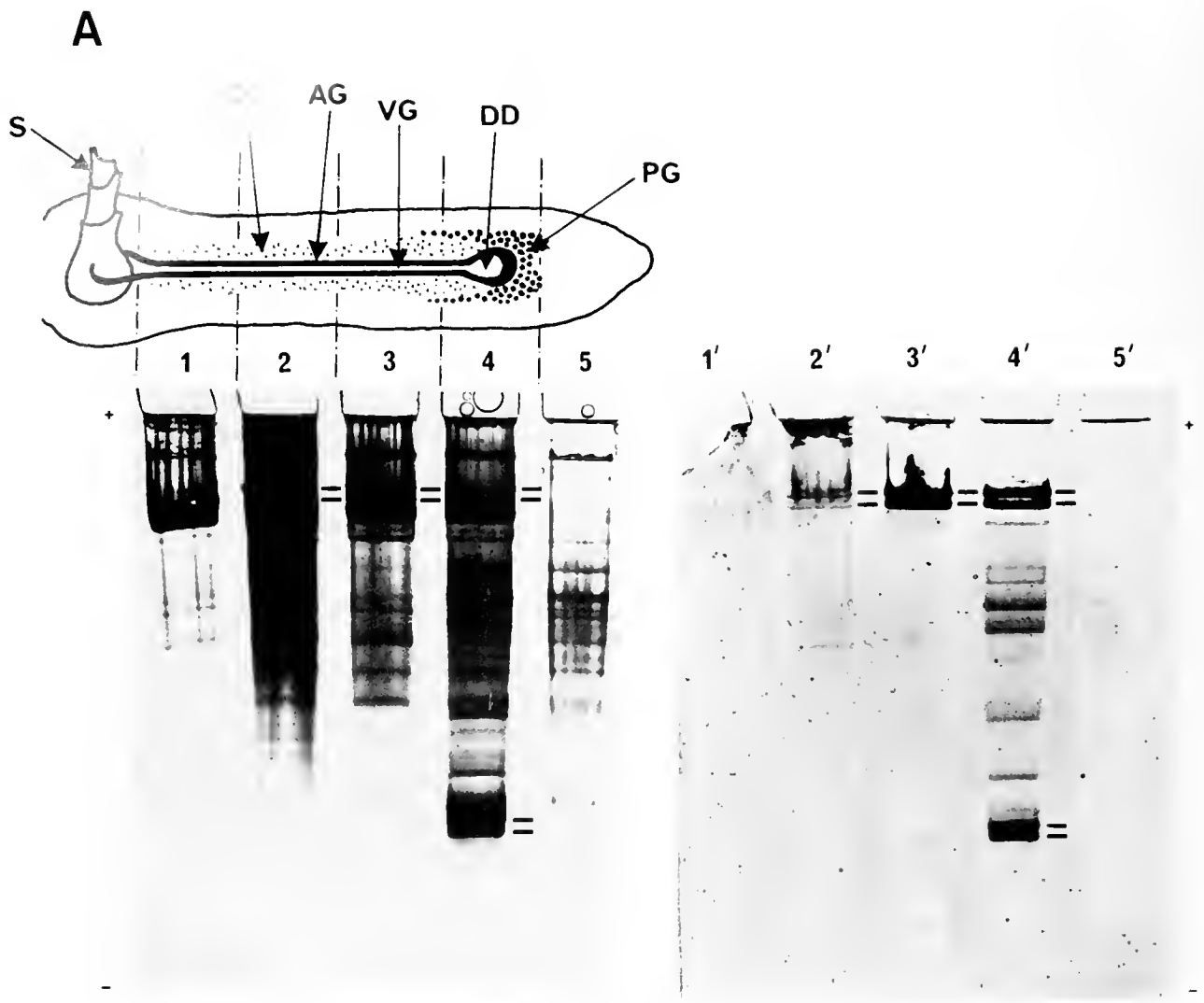

Figure 1. Localization of Mefp-2 in *Mytilus edulis* foot and byssus. (A) AU-PAGE analysis of acid-urea soluble proteins from a serially sectioned mussel foot. Lanes 1–5 correspond to the indicated foot sections and were stained with Coomassie Blue. Lanes 1′–5′ correspond to the same sections run on a parallel gel stained by the NBT redox cycling assay. The drawn parallel bars indicate position of Mefp-1 (upper) and Mefp-2 (lower) proteins. Schematic codes are: S, stem of the byssus; CG, collagen gland; AG, accessory gland; VG, ventral groove; DD, distal depression; and PG, phenol gland. (B) SDS-PAGE (15% polyacrylamide) of proteins extracted from threads and plaques in SDS and neutral buffer. Gels stained as indicated; symbols P, T, M-2 and St refer to: plaque extract, thread extract, pure Mefp-2, and molecular weight standards, respectively; arrows indicate Mefp-2. (C) AU-PAGE analysis of acetic acid-urea soluble proteins from threads and plaques. Gels stained as indicated; symbols are as in (B); arrows indicate Mefp-2. The higher molecular weight aggregates apparent in pure Mefp-2 in (B) and (C) were artefactual results of prolonged storage in water at −20°C and were never found in freshly isolated protein. Arnow tests were not performed in (B) and (C). (D) Dot blots of pure DOPA proteins, and thread and plaque acetic acid-urea soluble proteins, stained as indicated. The amount of total protein blotted is given in the center; symbols are as in (B).

remove the electrophoresis buffers before adding the NBT redox cycling reagent. Use of the NBT redox cycling assay was prefered in this study since, though it is somewhat less specific than the Arnow assay in detecting *o*-diphenols, it is considerably more sensitive, and the stain lasts indefinitely, once the gels have been washed first in alkaline borate and then in 5% acetic acid. Unless specified, however, the presence of DOPA in electrophoretic protein species was confirmed at least once by the Arnow stain before routine use of the NBT assay.

Glycoproteins were detected by the periodic acid-Schiff (PAS) stain (Segrest and Jackson, 1972), with bovine α_1-

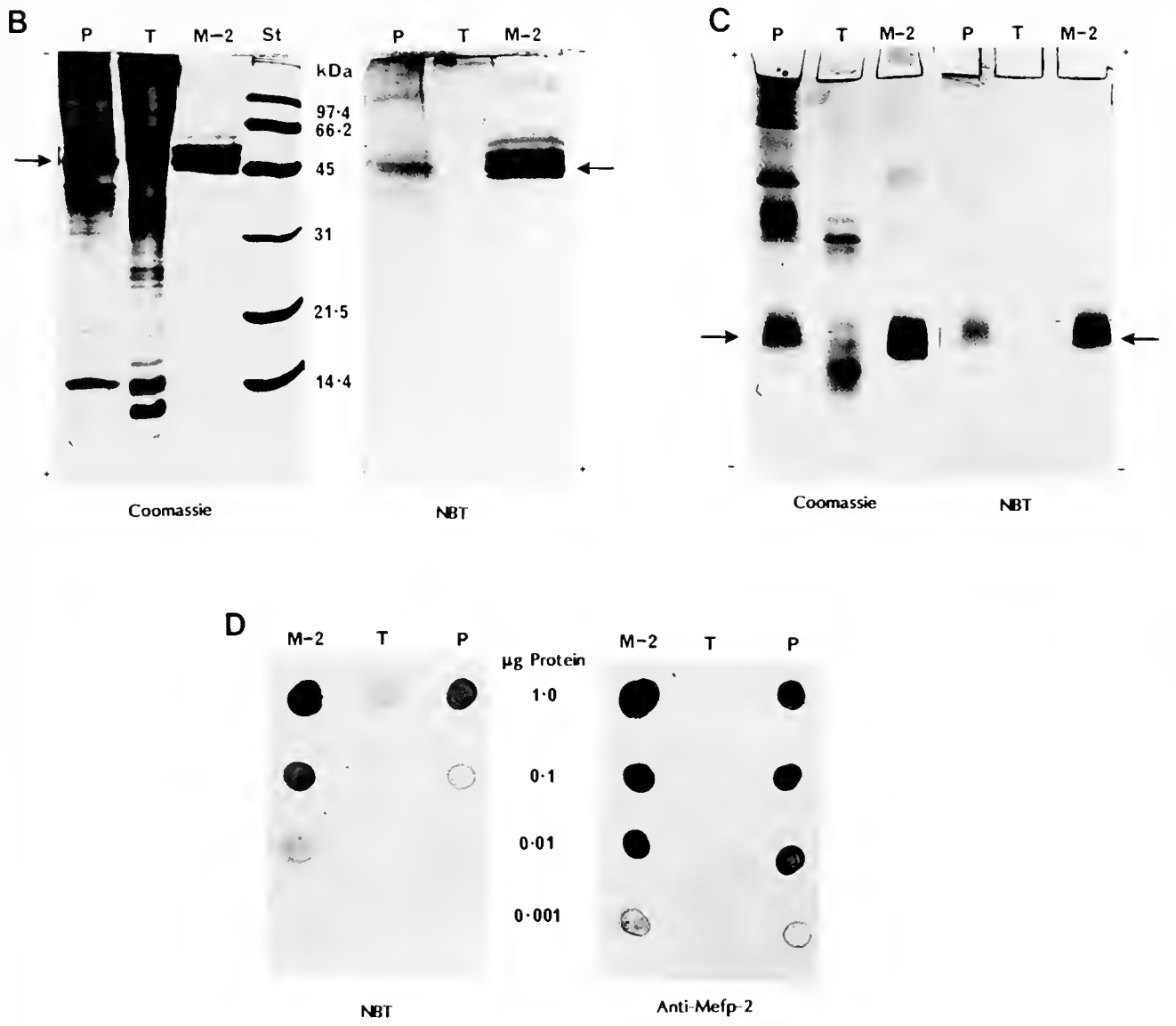

Figure 1. *(Continued)*

acid glycoprotein (Sigma Chemical Co., St. Louis, Missouri) and collagen (type II calf skin) serving as positive controls.

Denaturing isoelectric focussing (IEF) was performed with pH 3–10 ampholytes (FMC Bioproducts, Rockland, Maryland) in 8 *M* urea, 10% glycerol, 6% triton X-100, using 0.02 *M* acetic acid and 1 *N* NaOH as the anolyte and catholyte, respectively (Guilian *et al.*, 1984). Gels were pre-equilibrated (200 V, 15 min; 500 V, 30 min; 800 V, 30 min) before samples (in the above buffer with 15 mg/ml DTT) were applied to the gel under the anolyte. Proteins were focussed for 2–3 h at 1000 V, and a lane was removed for pH gradient determination (by incubation of 0.5 cm gel slices overnight in 1 ml of 0.1% NaCl) before the gel was stained.

Results and Discussion

Localization of Mefp-2 in M. edulis *byssus*

DOPA proteins extracted from serially sectioned mussel feet and electrophoretically resolved by AU-PAGE were detected by the NBT redox cycling assay and with Coomassie Blue (Fig. 1a). Mefp-1 migrated as a doublet identical to the previously characterized 130 kD DOPA protein (Waite, 1983), and it was found in foot sections throughout the length of the ventral groove corresponding to accessory and phenol glands. Mefp-2 was exclusively associated with the distal foot section that encompasses the phenol gland involved in plaque secretion. Several minor NBT-positive proteins of intermediate electrophoretic

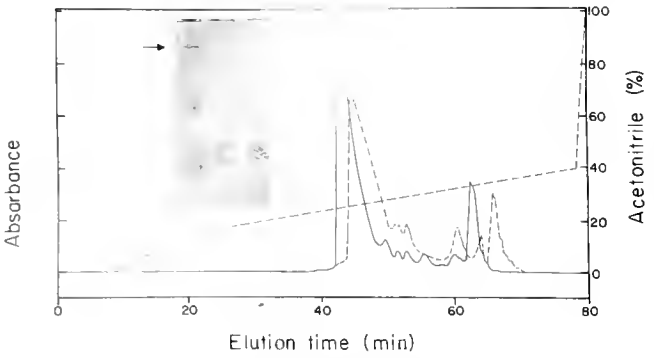

Figure 2. HPLC chromatography profiles of Mefp-2 (———) and Mefp-1 (-----) monitored at 280 nm. Proteins were resolved on a 0.7 × 25 cm semi-preparative C_8 column with an acetonitrile gradient, as indicated by the inclined dashed line. *Inset:* AU-PAGE of purified Mefp-2 at three concentrations, stained with Coomassie Blue. The arrow indicates the position of trace Mefp-1 contaminants.

mobility were also observed in this distal segment, but their origin and nature were not investigated further. To obtain a better separation between phenol and accessory glands, we micro-dissected phenol and accessory glands from thin foot sections and again, Mefp-2 was exclusively detected in the phenol gland, whereas Mefp-1 appeared in both glands. No other byssal glands are known to contain DOPA proteins.

Extraction of byssal plaques in either acetic acid-urea or neutral SDS buffers yielded a polypeptide that co-migrated with Mefp-2 during both SDS- and AU-PAGE and stained positively with NBT (Fig. 1b, c); miscellaneous electrophoretic species that stained with Coomassie Blue, but not NBT, also appeared. Preliminary amino acid analysis following HPLC purification of this NBT-positive plaque polypeptide revealed a composition very similar to authentic Mefp-2 (Diamond and Waite, unpub.). No polypeptide extracted from byssal threads alone exhibited NBT reactivity or electrophoretic behavior akin to Mefp-2, and no polypeptides corresponding to intact Mefp-1 were detected in plaque or thread extracts. Dot blots confirmed that a considerable proportion (*ca.* 10%) of acid-soluble plaque protein was NBT-sensitive, and immunoreactivity assays demonstrated that the extracted material that reacted with anti-Mefp-2 antibodies was specific to plaques (Fig. 1d). Pre-immune serum was unreactive in these assays. These observations are complicated by some cross-reactivity between the as yet unpurified polyclonal anti-M[illegible]-2 and pure Mefp-1, but the electrophoresis and dot bl[illegible]sults together strongly suggest that, because Mefp-1 [illegible]ved to occur in both threads and plaques (Benedict [illegible]aite, 1986a), Mefp-2 is an important component [illegible]of the plaque.

Purification and comp[illegible] of Mefp-2

Considerable separation of Mefp-1 and -2 was obtained by chromatography of the proteins on Sephadex G-150 or G-200 in 5% acetic acid (G-200 gave better separation but was not reuseable). Mefp-2, the predominant component of the trailing Sephadex fractions, was rechromatographed on Sephacryl S-300 or S-400, because HPLC alone failed to separate Mefp-2 from residual Mefp-1. Although the difficulty of assessing the relative contributions of either DOPA protein to an unknown mixture preclude presentation of a quantitative purification table, final yields of pure Mefp-2 ranged between 1–5 mg from 30 g wet mussel feet, depending on the season of the year in which the mussels were collected (mussels collected in winter gave better yields than in other seasons). Mefp-2 was resolved by AU-PAGE into two predominant electrophoretic bands (Fig. 2, inset), although minor bands

Table I

Amino acid composition of Mefp-2 and related proteins[a]

Amino acid, symbol	Mefp-2	CAMC-Mefp-2	Mefp-1[b]	Plaques[c]
3-Hyp	0.0	0.0	42–27	1.6
4-Hyp	0.0	0.0	161–120	28.4
Asp, D or Asn, N	127.0	115.1	12	88.3
Thr, T	42.2	38.8	113	32.6
Ser, S	73.9	65.8	93	66.5
Glu, E or Gln, Q	49.2	43.7	5	50.0
Pro, P	111.9	91.8	41–82	44.0
Gly, G	141.5	132.6	10	219.9
Ala, A	38.6	35.3	81	89.2
Hcys	68.2	1.8	0	20.5
Cys, C	0.0	155.3	—	—
Val, V	43.4	37.3	5	34.0
Met, M	1.9	1.0	2	5.9
Ile, I	9.0	8.2	8	20.3
Leu, L	12.6	11.7	trace	44.6
Dopa, Y* (or ¥)	28.6	25.8	181–110	14.8
Tyr, Y	56.0	51.7	31–73	46.2
Phe, F	9.6	9.0	0	10.0
His, H	8.0	10.1	3	46.0
Lys, K	134.7	124.7	214	51.8
Arg, R	43.7	40.2	3	61.0

[a] Amino acid compositions are given as residues per thousand (RPT) and are averaged from several preparations with a standard deviation of approximately 5%. The Mefp-2 composition was derived as described in Materials and Methods to obtain both DOPA and cystine values. CAMC-Mefp-2 was generally hydrolyzed by the rapid hydrolysis method, and cysteine was quantitated as *S*-carboxymethylcysteine. Ranges of values for certain amino acids in the Mefp-1 composition were derived from successive fractions under the peak of HPLC purified protein, and reflect differing degrees of hydroxylation of Pro and Tyr. Few such differences were apparent in Mefp-2. Cys, Lys and DOPA values are underlined for convenience.

[b] Rzepecki *et al.* (1991).

[c] Benedict and Waite (1986b).

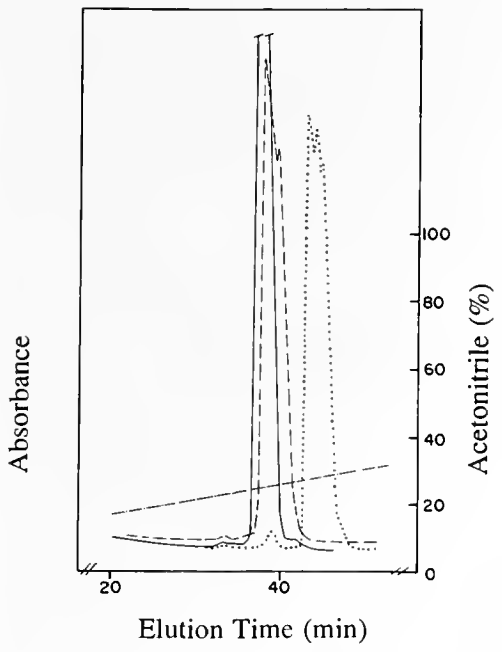

Figure 3. HPLC chromatography profiles of control Mefp-2 (———), and CAMC-Mefp-2 (-----) and COMC-Mefp-2 (· · · · · · · ·), reduced and alkylated as indicated in Materials and Methods, and monitored at 280 nm. Proteins were resolved on a 0.46 × 25 cm analytical C_8 column using the same gradient program as shown in Figure 2 (inclined dashed line). Concentration of control Mefp-2 was half that of the alkylated derivatives, but the detector attenuation was halved.

of similar mobility were often apparent. All reacted positively with the NBT and *o*-diphenol-specific Arnow stains (not shown), consistent with presence of DOPA in the amino acid composition. Mefp-2, resolved by SDS-PAGE (see below), did not stain with the PAS procedure for *cis*-diol sugars, though control proteins in the same gel were PAS-positive, suggesting that Mefp-2, in common with Mefp-1, is not a glycoprotein.

The most dramatic compositional difference between Mefp-1 and -2 (Table I) is the occurrence of cystine exclusively in Mefp-2 and at remarkably high levels (6–7 mol %). A comparison of native Mefp-2 with reduced and *S*-carbamidomethylated protein (CAMC-Mefp-2), together with the exceedingly low levels of *S*-carboxymethylcysteine in the acid hydrolysates of native Mefp-2 that had been treated with iodoacetamide in 4.8 or 6 *M* urea without prior reduction by DTT, shows that most of the *S*-alkylated cysteine (*ca.* 15 mol %) had originally been in the disulphide form. The DOPA content of Mefp-2 (2–3 mol %) was much lower than that of Mefp-1 (11–18%) and, unlike other molluscan DOPA proteins (Rzepecki *et al.*, 1991), the Lys:DOPA ratio far exceeded unity. Both contained proline, but no hydroxylation to 3- and 4-Hyp occurred in Mefp-2. Glycine, rare in Mefp-1, made up about 14 mol % of Mefp-2. Elevated levels (about 5-fold) of Asx and Glx, and lower levels of Ser and Thr, were also found in Mefp-2, in addition to other significant differences.

A comparison of the Mefp-1, Mefp-2, and byssal plaque amino acid compositions allows a crude estimate of the contributions of the two DOPA proteins to the overall plaque composition. Assuming that Mefp-1 is the only source of 3-hydroxyproline in byssus (Waite, 1983), the amount of Mefp-1 in the plaque may be estimated from the plaque 3-Hyp value (Benedict and Waite, 1986b) to be 4–5 mol % of plaque protein, and the proportion of DOPA residues belonging to Mefp-1 can be calculated. On the further assumption that all the remaining DOPA belongs to Mefp-2, a round figure of 25 mol % may be calculated for the plaque content of Mefp-2. At this postulated concentration, Mefp-2 would account for about 90% of plaque cystine and 70% of plaque lysine residues. Although these precise numbers should be taken *cum grano salis* [since (i) 3-Hyp occurs at low levels (<0.2 mol %) in the plaque and is difficult to quantitate; (ii) the content of the readily oxidized DOPA residues is easily underestimated, even in fresh byssus; and (iii) minor proteins containing DOPA or 3-Hyp may occur], they are consistent with the apparent proportion of Mefp-2 extractable from plaque and foot (Fig. 1). These considerations thus establish an upper limit to the content of Mefp-2 in the plaque.

HPLC and electrophoretic characterization of Mefp-2

HPLC and electrophoretic analyses of native, as well as reduced and *S*-alkylated Mefp-2 revealed a challenging complexity in chromatographic and electrophoretic behavior. The alkylated Mefp-2 derivatives eluted more slowly than control protein on HPLC, with the *S*-carboxymethylated protein (COMC-Mefp-2) unexpectedly the slower of the two (Fig. 3). Mefp-2 that had been reduced with DTT, but not alkylated, eluted with a delay comparable to COMC-Mefp-2 (not shown). Denaturing AU-PAGE profiles of fractions under the chromatographic peaks of Figure 3 showed that the two major bands exhibited by native Mefp-2 had been converted, upon reduction and alkylation, into multiplets with four or more components (Fig. 4a). Both COMC- and CAMC-Mefp-2 migrated considerably more slowly than the native polymer, with COMC-Mefp-2 again the slower of the pair. Mefp-2 that had been reduced by DTT, but not alkylated, migrated with intermediate mobility, but upon storage in water at 4°C, partially regained the faster mobility characteristic of native Mefp-2 (not shown). All electrophoretic species stained positively for DOPA with both NBT and Arnow tests (not shown).

Electrophoretic mobility on denaturing AU-PAGE systems depends both on molecular weight and charge density (Hollecker, 1990). Although alkylation of Mefp-2

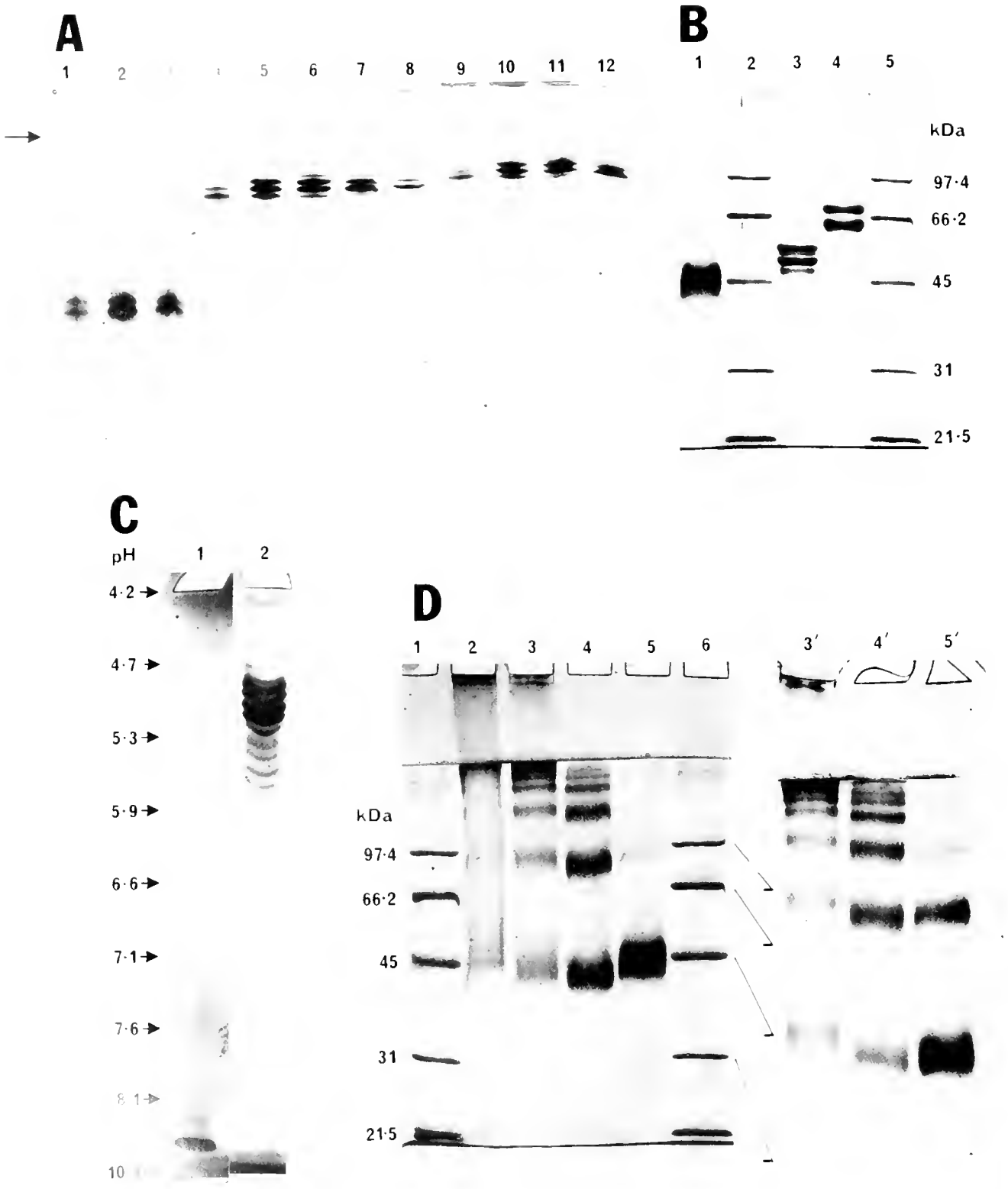

Figure [illegible] CAM AU-PAGE analysis of sequential HPLC fractions under the chromatographic peaks of Figure [illegible] lanes 1–3, native Mefp-2; lanes 4–8, CAMC-Mefp-2; lanes 9–12, COMC-Mefp-2. The arrow indicates the expected position of Mefp-1. Gel stained with Coomassie Blue. (B) SDS-PAGE (12% poly-

would increase the molecular mass of the protein by some 3–3.5 kDa (assuming about 56–62 alkylated cysteines per protein of 42–47 kDa with 360–400 amino acids), this increase alone seems insufficient to account for the reduced mobility under AU-PAGE, so modified charge density and alterations in protein conformation induced by disulphide reduction and alkylation undoubtedly contributed to the electrophoretic differences. The overall similarity between the relative mobilities of CAMC- and COMC-Mefp-2, which have widely different pI values (see below), together with their common difference from native Mefp-2, which has the same pI as CAMC-Mefp-2, argue for the pre-eminence of conformational changes. A transformation from a compact to an extended configuration upon reduction and alkylation is consistent with the observed anomalous electrophoretic and chromatographic migration.

Analysis of Mefp-2 and its alkylated derivatives by SDS-PAGE, following reduction in 50 m*M* DTT, was similarly complex (Fig. 4b). In contrast to Mefp-1, which precipitates in SDS, native Mefp-2 usually exhibited two electrophoretic bands (at low loading concentrations) with apparent molecular masses in the range 42–47 kDa, although minor NBT-positive bands migrating in the same range were frequently present. Electrophoretic migration was, however, somewhat variable within that range and appeared dependent on the protein concentration and degree of reduction. Several electrophoretic bands [which exhibited positive NBT and Arnow reactions (not shown)] were resolved for CAMC- and COMC-Mefp-2, with apparent molecular masses in the ranges 48–54 kDa and 63–71 kDa, respectively. The decreased mobility of CAMC-Mefp-2 was almost, yet not quite, explained by the molecular mass increment (3–3.5 kDa, see above) resulting from alkylation, but COMC-Mefp-2 migrated considerably more slowly. *S*-Alkylation with iodoacetate is well known to induce electrophoretic anomalies (Lane, 1978).

Isoelectric focussing (IEF) studies in highly reducing and denaturing media (Fig. 4c) showed that the apparent pI of native Mefp-2 lay between 9 and 10 pH units (*i.e.*, largely beyond the resolving power of available ampholytes), similar to that for Mefp-1. CAMC-Mefp-2, which theoretically has the same net charge as native Mefp-2, migrated identically (not shown). COMC-Mefp-2, with a greatly decreased net positive charge owing to the additional carboxyl moieties, migrated as a family of at least ten distinct members, with pI values in the range 4.7–5.9. Analogous electrophoretic heterogeneity occurs in the DOPA proteins of *Fasciola hepatica* (Waite and Rice-Ficht, 1989).

The variable migration of native Mefp-2 during SDS-PAGE caused us to investigate further the effects of DTT on electrophoretic behavior in this system. In the absence of DTT, Mefp-2 could barely be induced to enter even the stacking gel of discontinuous SDS-PAGE systems (Fig. 4d). As the DTT concentration was increased to 50 m*M*, progressively more Mefp-2 entered the resolving gel and migrated in a ladder-like pattern consistent with the presence of higher molecular weight aggregates of 2, 3, 4 or more polypeptide chains. At the highest DTT concentrations, most of the Mefp-2 migrated as an apparent monomer (*cf.* Fig. 4b). The obvious explanation for this observation, that the oligomeric Mefp-2 resulted from intermolecular disulphide bonds, does not seem tenable, since significant high molecular weight aggregates were rarely observed upon resolution of the same protein preparations by denaturing AU-PAGE (although they sometimes occurred on prolonged storage when frozen in water—*cf.* also Figs. 1b, e and 2, with Fig. 4a, d). Apparently, then, conditions exist for the aggregation of native, but not reduced, Mefp-2 in solution, although the precise contribution, if any, of SDS to this phenomenon remains to be determined. This is consistent with the precipitation frequently noted in concentrated neutral solutions of Mefp-2, and with preliminary X-ray scattering data (Trumbore, pers. comm.).

Primary structure of Mefp-2

Despite the apparent electrophoretic heterogeneity of Mefp-2, N-terminal sequencing of pure protein revealed a single detectable N-terminus, H_2N-Thr-Ser-Pro-Xaa-Yaa-Dop-Asp-Asp-Asp-Glu . . . , where Xaa and Yaa

acrylamide) analysis of Mefp-2 and derivatives. Lane 1, native Mefp-2; lane 3, CAMC-Mefp-2; lane 4, COMC-Mefp-2; lanes 2 and 5, molecular weight standards. Gel stained with Coomassie Blue. (C) IEF analysis of Mefp-2. Lane 1, native Mefp-2; lane 2, COMC-Mefp-2; CAMC-Mefp-2 migrated identically to native Mefp-2 and is not shown. Proteins were focussed on separate gels in parallel, and the gels were stained with the NBT redox cycling assay. The pH gradient is indicated on the left. (D) Effects of DTT on native Mefp-2 migration during SDS-PAGE (12% polyacrylamide). Lanes 1 and 6 are molecular weight standards. DTT concentrations: lane 2, 0 m*M*; lane 3, 0.5 m*M*; lane 4, 5 m*M*; lane 5, 50 m*M*. The gel was stained with Coomassie Blue. Lanes 3′–5′ are from a gel run in parallel, but stained with the NBT redox cycling assay, and correspond to lanes 3–5 in the gel on the left.

were predominantly P[illegible] Arg, though Tyr, Gly, Thr and Gln were also [illegible] Table II). Treatment of Mefp-2 with aminopep[illegible] released low levels of Thr, Ser, Pro, DOPA [illegible] consistent with the sequenator analysis. [illegible]ical combination of variability and constancy at the N-terminus might be explicable in terms of multiple genes or alternate mRNA splicing mechanisms (*cf.* Bobek *et al.*, 1988; Pihlajaniemi and Tamminen, 1990), but analysis of Mefp-2 from an individual organism has not yet been possible.

Native Mefp-2 (unlike Mefp-1) was relatively resistant to a variety of proteases, including trypsin, chymotrypsin, pepsin, *Staphylococcus aureus* V8, and collagenase, even at unusually high protease:Mefp-2 ratios (up to 1:1) in the presence of urea, although increases in electrophoretic mobility and heterogeneity were often apparent upon electrophoresis (see Fig. 5a, inset, for AU-PAGE of trypsin-treated Mefp-2). SDS-PAGE in the presence of DTT showed that, upon trypsin treatment, the apparent molecular mass decreased from about 45 kDa to 30–35 kDa with some increase in heterogeneity (not shown). HPLC of trypsin-treated native Mefp-2 resolved some minor peptides (Fig. 5a), but reduction and alkylation of the residual disulphide bonded protein did not result in the recovery of any new peptides upon rechromatography, confirming that little internal nicking had occurred. Trypsin digestion of both COMC- and CAMC-Mefp-2 converted both alkylated derivatives to their component peptides (Fig. 5). These results suggest that trypsin trimmed native Mefp-2 at the N- or C-terminus, or both, leaving the residual disulphide bonded core protein largely intact.

Peptides obtained by HPLC chromatography of trypsin-treated native and alkylated Mefp-2 fell generally into three major classes, all containing either tyrosine or DOPA (Figs. 6, 7). All three types were isolated from alkylated Mefp-2, but only Type II peptides were identified in digests of native Mefp-2. Owing to the chromatographic complexity of the peptide mixture, the relative content of the three classes was rather difficult to determine with any precision. Most fractions contained two major peptides (usually in unequal proportions), and sequences for peptides in various HPLC fractions were assigned by consideration of relative yields of amino acids in successive sequenator cycles. Fortunately, sequence consistencies became readily apparent, and a consideration of Figures 5–7, assuming that UV absorbance at 230 nm broadly reflects peptide concentration, suggests that the majority (at least 80%) of Mefp-2 can probably be accounted for by the identified motifs.

Type I peptides. This type of motif appeared to predominate in Mefp-2, with identified peptides accounting for perhaps 40–50% of the 230 nm absorbance of Figure 5b, although no individual peptide contributed more than 5–10%. It was highly enriched in Cys, Gly, and Pro, and was basic due to the excess of Lys and Arg over Glu and Asp. Significantly, we found no evidence that the Tyr residues were hydroxylated to DOPA in this type of motif. For convenience, we have subdivided the Type I motif into six submotifs (Fig. 6), which combine variously to

Table II

N-terminal analysis of Mefp-2[a]

	Sequenator analysis Amino acid (yield, pMoles × 10^3)		Aminopeptidase analysis
Cycle #	Fraction 5	Fraction 6	Amino acid (RPT)
1	T (2.0)	T (1.5)	S (225, 219)
2	S (1.8)	S (1.4)	T (185, 178)
3	P (2.2)	P (1.8)	P (171, 187)
4	R (2.1)	P (1.1) R (0.6) Y (0.5) G (0.5)	R (70, 88)
5	P (1.0) T (0.5) Y (0.5) Q (0.4)	P (1.2) Q (0.9)	Y* (64, 48)
6	Y* (1.7)	Y* (1.4)	D/N (32, 25)
7	D (1.5)	D (1.6)	[G (93, 87)]
8	D (1.6)	D (2.1)	
9	D (2.3) G (1.2)	D (2.1)	
10	several amino acids detected in significant quantities (D, E, G, K, Y)		

[a] N-Terminal sequences and [illegible]opeptidase M analyses were obtained as described in Materials and Methods. Sequences were derived from two adjacent fractions under the peak [illegible] an HPLC elution profile of Mefp-2, similar to that of Figure 2. In the aminopeptidase analysis, amino acid compositions from two individual [illegible]riments (with aminopeptidase incubation times of 2.5 and 16 h), are reported as residues per thousand (RPT) for the most abundant amino acids, the remainder ranging between 0–30 RPT. The yields were low, perhaps due to protein aggregation, adsorption in neutral buffer, or both; thus the gly[illegible]ne detected probably reflected background contamination of the vessels or protein preparations. One letter amino acid codes are given in Table I.

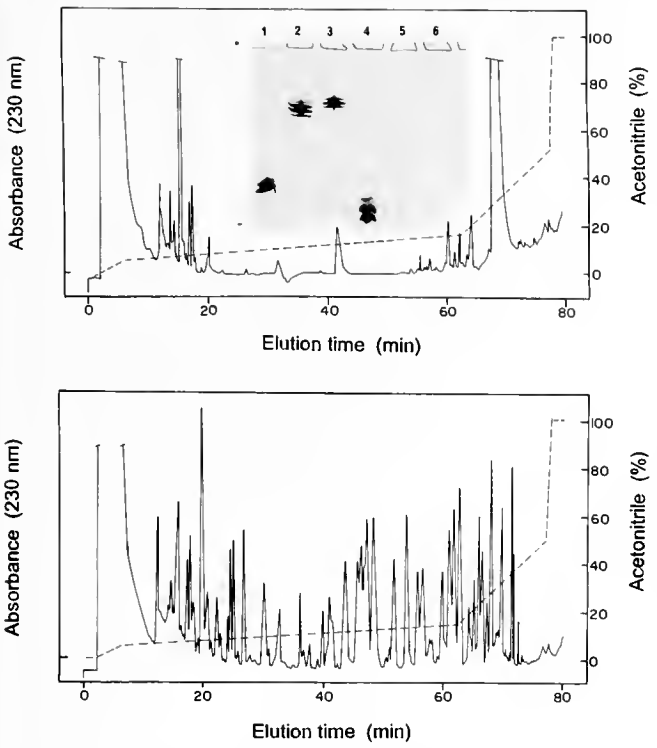

Figure 5. HPLC chromatography profiles of Mefp-2 and derivatives following proteolytic digestion with trypsin. Peptides were resolved on a 0.46 × 25 cm C_{18} column using acetonitrile gradients as indicated by the dashed lines. Fractions of 1 ml were collected at a flow rate of 1 ml/min. (A) Peptides and undigested core protein (fractions 68–72) derived from native Mefp-2. *Inset:* AU-PAGE analysis of native Mefp-2, CAMC-Mefp-2 and COMC-Mefp-2 before (lanes 1–3, respectively), and after (lanes 4–6, respectively) proteolysis with a trypsin:protein weight ratio of 1:50, or 1:25 in the case of native Mefp-2. Equivalent concentrations of protein were run in each lane, and the gel was stained with Coomassie Blue. (B) Peptides derived from COMC-Mefp-2. The peptide map derived from CAMC-Mefp-2 was qualitatively similar to that shown in (B).

Cystine Enriched Tryptic Peptides

Oligopeptide Submotifs

Peptide # COMC	CAMC	Sequence	1	2	3	4	5	6
		Consensus (*Type I*):	[CY]	CV	GGYSG	PTC	QENAC	KPNPC [X]K
			T	L			GV V	A
		Type I peptides						
38	32b	*C APLGK*						
50b		VNVC KPN...						
64b	53b	*YIC APNPC* K						
57a	46b	*YVC APNPC K*						
48a		C GENVC KPNPC QNK						
							V A	
49a		C QVHAC KPNPC N{N/T}K						
52a		C GVNAC NPNPC K						
62a	51b	*GGYSG PTC GENVC APNPC QCK*						
63a	52b	*GGYSG PTC GVNAC KPNPC QNR*						
							F	
63b	51a	*CS GGYSG PTC NVNAC KPNP-* NK						
64a	53a	*CV GGYSG PTC QENAC KPNPC* K						
66a		CTCV GGYSG PTC QENAC KPNPC SN...						
69a		CL GGYIG PTC -ED— KPNPC N...						
68		CL GGYKG PTC -ED— KPNPC NIK						
		V					NV	
	54b	CYCV GGYSG FQ...						
71		CYCT GGYCG LT...						
58	54a	*CYHD NSDDG* PTC QENAC KPNPC N...						
55b	52b	*CYHD K*						
31	27/28	*CYHD GK*						
34	32a	*GGYSG P*(K)						
53	48	*[S]GYYG PEC* ...						
		Q						
49b		GTGYVGYIG R						
55a		GSSYN- --C ---IC K						
		Others						
73a		[CSADK]FGDYTCDFRPGYFGPE{C/Q}...						
69b		GGYGKFNDYLE...						

Figure 6. Cystine-enriched tryptic peptide sequences derived from alkylated Mefp-2. Numbers under the COMC heading correspond to fractions obtained from the HPLC chromatogram depicted in Figure 5b (*i.e.*, peptides from COMC-Mefp-2); those under CAMC correspond to HPLC fractions of peptides from CAMC-Mefp-2 (not shown). Letters after the numbers indicate whether the peptide was a major (a) or minor (b) component of the HPLC fraction. In cases of ambiguity, where more than one peptide was found in the fraction, sequences were assigned by consideration of relative PTC-amino acid yields in successive sequenator cycles. Sequences in *italics* are those obtained from both COMC- and CAMC-Mefp-2 preparations. DOPA and alkylated cysteine residues are emphasized, and sequences are spaced as submotifs for convenience only. Residues in parentheses () were inferred from composition data, or were difficult to assign owing to low yields or ambiguous results in a sequenator cycle. Residues in brackets [ ] are optional sequence extensions in peptide variants. Residues separated in braces {/} are alternative amino acids found in that position of the sequence; in other cases, alternative amino acids are shown below the main peptide sequence. Ellipses (. . .) indicate probable continuation of a peptide beyond the last residue clearly resolved on the sequenator; dashes (– – –) indicate gaps introduced into the sequence to optimize putative alignment. The symbol X in the consensus sequence indicates one or two optional small polar amino acids.

form both complete and truncated motifs. Tyrosine typically occurs in submotif #2, GGYSG, in the company of small residues. This propinquity of Tyr and small residues is common in tyrosine- or DOPA-containing structural proteins from species in various phyla (*e.g.*, Johnson *et al.*, 1987; Waite and Rice-Ficht, 1987, 1989; Bobek *et al.*, 1988; Mehrel *et al.*, 1990; Aggeli *et al.*, 1991; Rzepecki *et al.*, 1991); it has been attributed in part to the hypothetical steric requirements of 3-tyrosyl hydroxylases (Rzepecki *et al.*, 1992), although this feature is clearly insufficient for tyrosine hydroxylation in Mefp-2. Tyrosine also occurred in submotif #1 with vicinal Cys residues; this relationship has never been observed in a protein where tyrosine is known to be hydroxylated to DOPA, but occurs infrequently in other glycine, cystine, and tyrosine enriched structural proteins, although replacement of Tyr by Cys in $(G)_nY/C$ sequences is more usual (*e.g.*, Bobek *et al.*, 1988; Mehrel *et al.*, 1990; Aggeli *et al.*, 1991).

Submotifs #3 (PTC) and [illegible] (KPNPC) are enriched in Cys and Pro and are [illegible] to the GGYSG submotif, the most conser[illegible]. Submotif #4 is relatively variable, with [illegible]s of Gly for Gln, Val for Glu, and Ala for [illegible] the terminal Cys residue appears invariant. The [illegible]minal submotif (#6) consists of 0–2 small polar residues (Asn, Gln, etc.) with a C-terminal Lys or Arg. A search of the SWISS-PROT Protein Sequence Data Bank [release 19 (August 1991) with 21,795 entries] failed to identify any remarkable homologies between the Type I motif and any other known sequence. [Note, however, the conceptual similarity between Type I motifs and conotoxin sequences. Conotoxins, isolated from the venomous marine cone snails (*Conus*), are small (10–30 amino acid) multiply disulphide bonded peptides, with 2–4 highly variable loops of 1–6 amino acids between adjacent Cys residues, and are potent antagonists of various neuromuscular receptors (Olivera *et al.*, 1990)]. The Cys-rich nature of Type I motifs, as well as their relative abundance, suggests that they are derived from the core of Mefp-2, which is resistant to trypsin digestion in the non-alkylated state. If they are thus concentrated, then such an arrangement would result in a quasi-periodic distribution of Cys and Tyr residues over much of the protein.

Type II peptides. These motifs were enriched in Pro and Ser, and were highly acidic, containing almost palindromic runs of Asp and Glu bracketed by DOPA residues (Fig. 7). The first DOPA was often found at the C-terminus of a PPSY* (Y* = DOPA) sequence, analogous to a submotif of the Mefp-1 tandem repeat (AKP*SY*P*P*TY*K where P* = hydroxyproline; Waite, 1983). The second DOPA had Asp as its N-terminal partner with, frequently, Thr at its C-terminus; similar arrangements occur in the high molecular weight DOPA proteins from other molluscan species, but are foreign to Mefp-1 (Rzepecki *et al.*, 1991). No Cys or Gly residues were found, thus sealing the distinction between Type I and Type II sequences. The Mefp-2 N-terminus, TSPxxY*DDD(E) . . . (Table II and Fig. 7), is a Type II sequence, and was the only N-terminus detected (see above). The C-terminal sequence (K)SPPSY*NDDDEY* was identified in several independent peptide preparations by the close [illegible]respondence between the observed amino acid compos[illegible] which lacked Lys or Arg (in trypsin derived prepa[illegible]) but had equimolar DOPA, Ser, and Pro contents, a[illegible] expected composition calculated from the sequen[illegible]ltimate DOPA residue was inferred largely fro[illegible]sition data, since sequenator yields of C-terminal [illegible]ere greatly reduced, though still marginally eviden[illegible]c cases. No other peptides were reliably identified a[illegible]terminal. Thus the DOPA rich N- and C-terminal sequences of Mefp-2 are probably structurally similar and, in contrast to the basic Type I

Dopa Enriched Tryptic and Chymotryptic Peptides

COMC	Peptide # CAMC	Native	Sequences	Comments
			Type II peptides	
		†Untreated	TSPxx**Y**DDD (E) . . .	N-Terminus
66b			TSPDP**Y**DDDEDD**Y**TPPV (R)	
62b			T----**Y**DDDEDD**Y**TPPV (R) K	
		†Trypsin	TSP----DDEDD?TPPV (K)	Dopa prominent in
			D P DE	composition but not
			Q	detected in sequence.
		16	TSP (R) . . ?	
		†Chymotrypsin	KSPPS**Y**NDDDE (**Y**)	C-Terminus?
		†Trypsin	SPPS**Y**NDDDE (**Y**)	C-Terminus?
45a		43/44	*SPPS**Y**NDDDE (**Y**)*	C-Terminus?
		†Chymotrypsin	KSPPSNNDD . . .	
			Type III peptides	
52b			A**Y**--NP**C**FKR	
47a			A**Y**KPNP**C**ASR[PGYR]	
48a*			A**Y**KPNP**C**ASG-P**C**KK	
			Y N . . .	
49*			A**Y**KPNP**C**ASS-P**C** (K)	
58*			A**Y**KPNP**C**VVSKP**C** (**C**) . . .	
			Others	
70*			**Y**FP**C**CPS**Y**NG . . .	
48b			NT**C**I**C**G**Y**NGSGG**Y**R	
50a	46a		*Y**N**GV**C**KP{N/S}GGS**Y**K*	
47b			**Y**NGV . . .	
			Y	
48b*			SNGV**C**K (F) SG . . .	
			Y	
19		†Trypsin	G**Y**SGR	
			Y K	
62*			**Y**?PVNP**C**LKK	
		70	**Y**SPVN . . .	Core Protein N-Terminus??
			Y	
68*			GG**YY**G**Y**N**C**N . . .	

Figure 7. DOPA-enriched tryptic peptides from native Mefp-2 and alkylated derivatives. Numbers under the Native heading correspond to fractions from Figure 5a, those under COMC and CAMC headings are as in Figure 6. Numbers marked with an asterisk (*) correspond to peptides isolated by phenyl boronate affinity chromatography prior to HPLC purification (not shown). The symbol (†) indicates data from earlier preliminary experiments using Mefp-2 prepared from different batches of mussels. "Untreated" Mefp-2 refers to the N-terminal analysis. Peptides from native Mefp-2 specifically labeled as "trypsin" derived were obtained by digestion of Mefp-2 in 100 m*M* Tris, 50 m*M* ascorbate buffer, pH 8.0 for 24 h at room temperature with a trypsin:protein weight ratio of 1:10, then isolated by HPLC on a 0.46 × 25 cm C_8 column with the same elution gradient as used for protein isolation. Peptides were detected at 280 nm. Peptides specifically labeled as "chymotrypsin" derived were obtained by digestion of Mefp-2 in 150 m*M* Tris, 150 m*M* ascorbate buffer, pH 7.5, at room temperature for 6 h with a chymotrypsin:protein ratio of 1:1, then resolved by HPLC, following lyophilization and resuspension in 5% acetic acid, on a 0.46 × 25 cm Vydac C_{18} column with a 0–25% gradient of acetonitrile in water, incorporating 0.1% trifluoracetic acid. Because few peptides were obtained by either of these protocols, the HPLC profiles have been omitted. Other symbols and protocols are as described in Figure 6, except Y which is a symbol for DOPA to facilitate peptide alignment.

motifs and the DOPA-containing motifs from other DOPA proteins, are highly acidic.

Type III peptides. This last major type contained both DOPA and Cys residues, in addition to Pro, Lys, and Ala. The DOPA residue was found in the sequence AY*KPNPC . . . , where the KPNPC segment is identical to submotif #5 of the Type 1 motif. Although there is some compositional similarity to the Mefp-1 consensus motif, the only sequence identity is in the dipeptide Y*K, which is a common feature of many molluscan DOPA proteins (Rzepecki *et al.*, 1991). The distribution of Type III peptides within the Mefp-2 sequence is unknown.

Minor peptide sequences were apparent, including some unusual vicinal YY and Y*Y dipeptides previously found in DOPA proteins from the mussels *Modiolus modiolus* and *Trichomya hirsuta* (Rzepecki *et al.*, 1991), and certain tunicates (C. Hawkins, pers. comm.). Although variation in Mefp-2 is considerable, the domination of the heterogeneous Mefp-2 family by a limited number of motif variants indicates that it is tandemly repetitive. However, unlike most DOPA proteins, the motif degeneracy is quite marked, and the sequences often diverge markedly from those expected on the basis of previously analyzed DOPA proteins (Rzepecki *et al.*, 1991; Rzepecki and Waite, 1991). Moreover, Mefp-2 exhibits no sequence homologies with any previously characterized cysteine- or cystine-containing proteins, including disulphide bonded collagens (Dublet and Rest, 1991), high sulphur keratins (Fraser *et al.*, 1972), zinc-binding proteins (DuBois *et al.*, 1990; Opipari *et al.*, 1991), metallothioneins (Lerch, 1980; Nemer *et al.*, 1985), keratinocyte loricrins (Mehrel *et al.*, 1990), proteoglycans such as perlecan (Noonan *et al.*, 1991), and adhesive laminins of the neuromuscular junction (Hunter *et al.*, 1989). Mefp-2 thus appears to be a novel class of structural protein, and any short sequence similarities to other classes may be stochastic or result from common structural features related to function.

Conclusions

The blue mussel, *Mytilus edulis*, incorporates at least two distinct DOPA proteins into its byssus. The first of these to be characterized (Waite, 1983), Mefp-1, forms a protective varnish at the interface between byssus and environment, and may also be the adhesive agent at the interface between plaque and substratum (Benedict and Waite, 1986a). The second major DOPA protein of the blue mussel, Mefp-2, appears to be a structural component exclusively of the plaque, contributing up to 25% of plaque protein. (About 90–95% of the dry weight of the *M. edulis* plaque is proteinaceous; Diamond and Waite, unpublished.) Mefp-2 seems to be a tandemly repetitive, multidomain protein, with short, acidic, DOPA-containing N- and C-terminal regions, and a large central domain constrained by quasi-periodic internal disulphide bridges to a compact conformation resistant to proteolytic degradation. The peptide motifs of Mefp-2 are quite unlike those of any other known structural proteins. Speculations about secondary structure are premature, because in tandemly repetitive proteins, the correct order of short peptide motifs over an entire protein cannot be deduced by standard peptide mapping techniques, and it is debatable whether all members of the heterogeneous Mefp-2 family share identical subsets of motifs. Nevertheless, the sequence of the Type 1 motif (Fig. 6) of Mefp-2 contains proline and/or glycine rich segments that alternate with sequences containing none of these β-turn associated residues, and it is therefore consistent with conformational models, such as the β-meander postulated for certain glycine and tyrosine rich *Schistosoma* eggshell proteins (Rodrigues *et al.*, 1989).

The composition of Mefp-2, incorporating cystine and DOPA, implies some role involving the stabilization of the plaque matrix by covalent disulphide and quinone-derived cross-links. *In vitro*, Mefp-2 can form oligomeric aggregates that might, in time, be stabilized by rearrangement of disulphide bonds to form inter-molecular cross-links. If Mefp-2 indeed constitutes 25% of plaque protein, then it would incorporate 90% of the plaque cystine residues and thus would be virtually its own sole potential disulphide cross-link partner. The DOPA residues might then serve to cross-link the resulting disulphide-linked Mefp-2 homopolymer to other protein components of the plaque, although the apparent extractability of Mefp-2 from day-old plaques suggests that, if such cross-links are real, they form slowly. Much of the internal volume of the blue mussel plaque is occupied by a microscopic foam which does not bind anti-Mefp-1 polyclonal antibodies strongly (Benedict and Waite, 1986a). Disulphide-rich proteins (Kitabatake and Doi, 1987; Okumura *et al.*, 1989), and rigid proteins in general (Graham and Phillips, 1976; Halling, 1981), are known to stabilize foams, and we had previously noted that Mefp-1 should be a good foam stabilizer by virtue of its cross-linking potential (Rzepecki and Waite, 1991). Mefp-2 also appears suited for such a role, although until it can be precisely localized within the plaque matrix, its function will remain conjectural. [Preliminary attempts to extract acid-soluble proteins analogous to Mefp-2 from the foot of the ribbed mussel *Geukensia demissa*, which secretes a high molecular weight DOPA protein (Gdfp) analogous to Mefp-1, but lacks a distinctive foam structure in its plaque (Waite *et al.*, 1989), have failed to detect significant quantities of any putative Gdfp-2 (Rzepecki, unpub. data): a correlation of habitat and plaque ultrastructure with DOPA protein variants in other mussel species should be informative.]

Many questions, however, remain unresolved. The apparent localization of Mefp-2 to the phenol gland is somewhat equivocal. The phenol gland is an apparent site of Mefp-1 synthesis and storage (Waite, 1983; Benedict and Waite, 1986b), but the true nature of the phenol gland secretions is still puzzling—do they contain one or both DOPA proteins? The sequence differences between DOPA-containing motifs in Mefp-1 and Mefp-2 raise questions about the specificity and number of the putative tyrosyl hydroxylases responsible for conversion of peptidyl tyrosine to DOPA, and also about the nature of the catecholoxidase responsible for peptidyl quinone production (although curiously, no catecholoxidase activity has yet been detected in the phenol gland). The reproducibility of specific disulphide bonds, and thus the degree of conservation of secondary and tertiary structure, is unknown. Finally, although we still require a full representative sequence from the Mefp-2 family, data obtained from cDNA or genomic sequences must be interpreted with caution, because the Mefp-2 family of proteins may prove to be a multigene family and may also be subject to alternative splicing of mRNA. The association of such phenomena with many repetitive structural proteins is well documented (*e.g.,* Bobek *et al.,* 1988; Pihlajaniemi and Tamminen, 1990).

Acknowledgments

We thank Dr. Mark Trumbore for helpful discussions and the computer search of the SWISS-PROT Protein Sequence Data Bank, and Tom Diamond for sharing his studies on byssal plaque protein compositions. This work was funded by a grant from the Office of Naval Research.

Literature Cited

Aggeli, A., S. J. Hamodrakas, K. Koitopoulou, and M. Konsolaki. 1991. Tandemly repeating peptide motifs and their secondary structure in *Ceratitis capitata* eggshell proteins Ccs36 and Ccs38. *Int. J. Biol. Macromol.* **13:** 307–315.

Arnow, L. 1937. Colorimetric determination of components of 3,4-dihydroxyphenyl-L-alanine/tyrosine mixtures. *J. Biol. Chem.* **118:** 531–537.

Benedict, C. V., and J. H. Waite. 1986a. Location and analysis of byssal structural proteins of *Mytilus edulis*. *J. Morphol.* **189:** 171–18

Benedict, C. V., and J. H. Waite. 1986b. Composition and ultrastructure of the [illegible] of *Mytilus edulis*. *J. Morphol.* **189:** 261–270.

Blake, M. S., K. [illegible]nston, G. J. Russel-Jones, and E. C. Gotschlich. 1984. A rapid, sensitive method for detection of alkaline phosphatase-conjugated [illegible]body on Western blots. *Anal. Biochem.* **136:** 175–176.

Bobek, L. A., D. M. K[illegible]nd P. T. LoVerde. 1988. Small gene family encoding an egg[illegible]orion) protein of the human parasite *Schistosoma mansoni*. *Mol. Biol.* **8:** 3008–3016.

Bradford, M. M. 1976. A rapid and sensitive method for the quantitation of microgram quantities of protein utilizing the principle of protein dye binding. *Anal. Biochem.* **72:** 248–254.

Brown, C. H. 1952. Some structural proteins of *Mytilus edulis*. *Q. J. Microsc. Sci.* **93:** 487–502.

Dublet, B., and M. van der Rest. 1991. Type XIV collagen, a new homotrimeric molecule extracted from fetal bovine skin and tendon with a triple helical disulfide-bonded domain homologous to type IX and type XII collagens. *J. Biol. Chem.* **266:** 6853–6858.

DuBois, R. N., M. W. McLane, K. Ryder, L. F. Lau, and D. Nathans. 1990. A growth factor-inducible nuclear protein with a novel cysteine/histidine repetitive sequence. *J. Biol. Chem.* **265:** 19185–19191.

Filpula, D. R., S.-M. Lee, R. P. Link, S. L. Strausberg, R. L. Strausberg. 1990. Structural and functional repetition in a marine mussel adhesive protein. *Biotechnol. Prog.* **6:** 171–177.

Fraser, R. D. B., T. P. MacRae, G. E. Rogers. 1972. *Keratins: Their Composition, Structure and Biosynthesis.* C. C. Thomas, Springfield, IL.

Graham, D. E., and M. C. Phillips. 1976. The conformation of proteins at the air-water interface and their role in stabilizing foams. Pp. 237–253 in *Foams,* Akers, R. J., ed. Academic Press, London.

Guilian, G. G., R. L. Moss, and M. Greaser. 1984. Analytical isoelectric focussing using a high-voltage vertical slab polyacrylamide gel system. *Anal. Biochem.* **142:** 421–436.

Halling, P. J. 1981. Protein-stabilized foams and emulsions. *CRC Crit. Rev. Food Sci. Nutr.* **15:** 155–203.

Hollecker, M. 1990. Counting integral numbers of residues by chemical modification. Pp. 145–153 in *Protein Structure,* T. E. Creighton, ed. IRL Press, Oxford.

Hunter, D. D., V. Shah, J. P. Merlie, and J. R. Sanes. 1989. A laminin-like adhesive protein concentrated in the synaptic cleft of the neuromuscular junction. *Nature* **338:** 229–234.

Johnson, K. S., D. W. Taylor, and J. S. Cordingley. 1987. Possible eggshell protein gene from *Schistosoma mansoni*. *Mol. Biochem. Parasitol.* **22:** 89–100.

Kitabatake, N., and E. Doi. 1987. Conformational change of hen egg ovalbumin during foam formation detected by 5,5′-dithiobis(2-nitrobenzoic acid). *J. Agric. Food Chem.* **35:** 953–957.

Laemmli, U. K. 1970. Cleavage of structural proteins during the assembly of the head of bacteriophage T4. *Nature* **227:** 680–685.

Lane, L. C. 1978. A simple method for stabilizing protein-sulfhydryl groups during SDS-gel electrophoresis. *Anal. Biochem.* **86:** 655–664.

Lerch, K. 1980. Copper metallothionein, a copper-binding protein from *Neurospora crassa*. *Nature* **284:** 368–370.

Mehrel, T., D. Hohl, J. A. Rothnagel, D. B. Longley, C. Cheng, U. Lichti, M. E. Bisher, A. C. Steven, P. M. Steinert, S. H. Yuspa, and D. Roop. 1990. Identification of a major keratinocyte cell envelope protein, Loricrin. *Cell* **61:** 1103–1112.

Nemer, M., D. G. Wilkinson, E. C. Travaglini, E. J. Sternberg, and T. R. Butt. 1985. Sea urchin metallothionein sequence: key to an evolutionary diversity. *Proc. Natl. Acad. Sci. USA* **82:** 4992–4994.

Noonan, D. M., A. Fullet, P. Valente, S. Cai, E. Horigan, M. Sasaki, Y. Yamada, and J. R. Hassell. 1991. The complete sequence of Perlecan, a basement membrane heparan sulfate proteoglycan, reveals extensive similarity with laminin A chain, low density lipoprotein-receptor, and the neural cell adhesion molecule. *J. Biol. Chem.* **266:** 22939–22947.

Okumura, K., Y. Miyaki, H. Taguchi, and Y. Shimabayashi. 1989. Enhanced stability of protein foam due to disulfide bond formation just after foaming. *Agric. Biol. Chem.* **53:** 2029–2030.

Olivera, B. M., J. Rivier, C. Clark, C. A. Ramilo, G. P. Corpuz, F. C. Abogadie, E. E. Mena, S. R. Woodward, D. R. Hillyard, and L. J. Cruz. 1990. Diversity of *Conus* neuropeptides. *Science* **249:** 257–263.

Opipari, A. W., M. S. Boguski, V. M. Dixit. 1991. The A20 cDNA induced by tumor necrosis factor α encodes a novel type of zinc finger protein. *J. Biol. Chem.* **265:** 14705–14708.

Panyim, S., and G. R. Chalkley. 1969. High resolution acrylamide gel electrophoresis of histones. *Arch. Biochem. Biophys.* **130:** 337–346.

Pardo, J., E. Gutierrez, C. Saez, M. Brito, and L. O. Burzio. 1990. Purification of adhesive proteins from mussels. *Prot. Express. Purif.* **1:** 147–150.

Paz, M. A., R. Flückiger, A. Boak, H. M. Kagan, and P. M. Gallop. 1991. Specific detection of quinoproteins by redox-cycling staining. *J. Biol. Chem.* **266:** 689–692.

Pihlajaniemi, T., and M. Tamminen. 1990. The a1 chain of type XIII collagen consists of three collagenous and four noncollagenous domains, and its primary transcript undergoes complex alternative splicing. *J. Biol. Chem.* **265:** 16922–16928.

Pujol, J. P. 1967. Le complex byssogène des mollusques bivalves. Histochimie comparée des sécrétions chez *Mytilus edulis* L. et *Pinna nobilis*. *Bull. Soc. Linn. Normandie* **8:** 308–332.

Rodrigues, V., M. Chaudri, M. Knight, H. Meadows, A. E. Chambers, W. R. Taylor, C. Kelly, and A. J. G. Simpson. 1989. Predicted structure of a major *Schistosoma mansoni* eggshell protein. *Mol. Biochem. Parasitol.* **32:** 7–14.

Rzepecki, L. M., and J. H. Waite. 1991. Dopa proteins: versatile varnishes and adhesives from marine fauna. Pp. 119–148 in *Bioorganic Marine Chemistry*, Vol. 4, P. J. Scheuer, ed. Springer-Verlag, Berlin.

Rzepecki, L. M., S.-S. Chin, J. H. Waite, and M. F. Lavin. 1991. Molecular diversity of marine glues: polyphenolic proteins from five mussel species. *Mol. Mar. Biol. Biotechnol.* **1:** 78–88.

Rzepecki, L. M., K. M. Hansen, and J. H. Waite. 1992. Bioadhesives: DOPA and phenolic proteins as components of organic composite materials. In *Principles of Cell Adhesion*, P. D. Richardson, and M. Steiner, eds. CRC Press, Inc., Boca Raton, FL.

Segrest, J. P., and R. L. Jackson. 1972. Molecular weight determination of glycoproteins by polyacrylamide gel electrophoresis in sodium dodecyl sulfate. *Meth. Enzymol.* **28:** 54–63.

Tamarin, A., P. Lewis, and J. Askey. 1976. The structure and formation of the byssal attachment plaque-forming region in *Mytilus californianus*. *J. Morphol.* **149:** 199–221.

Tsugita, A., T. Uchida, H. W. Mewes, and T. Ataka. 1987. Rapid vapor phase acid hydrolysis of peptide and protein. *J. Biochem.* **102:** 1595–1597.

Vitellaro-Zuccarello, L. 1981. Ultrastructural and cytochemical study on the enzyme gland of the foot of a mollusc. *Tiss. Cell* **13:** 701–713.

Vitellaro-Zuccarello, L. 1980. The collagen gland of *Mytilus galloprovincialis*: an ultrastructural and cytochemical study on secretory granules. *J. Ultrastruct. Res.* **73:** 135–147.

Waite, J. H. 1987. Nature's underwater adhesive specialist. *Int. J. Adhesion Adhesives* **7:** 9–14.

Waite, J. H. 1990. The phylogeny and chemical diversity of quinone-tanned glues and varnishes. *Comp. Biochem. Physiol.* **97B:** 19–29.

Waite, J. H. 1991. Detection of peptidyl-DOPA by amino acid analysis and microsequencing techniques. *Anal. Biochem.* **192:** 429–433.

Waite, J. H. 1983. Evidence for a repeating 3,4-dihydroxyphenylalanine- and hydroxyproline-containing decapeptide in the adhesive protein of the mussel, *Mytilus edulis* L. *J. Biol. Chem.* **258:** 2911–2915.

Waite, J. H., D. C. Hansen, and K. T. Little. 1989. The glue protein of ribbed mussels (*Geukensia demissa*): a natural adhesive with some features of collagen. *J. Comp. Physiol.* **159B:** 517–525.

Waite, J. H., and A. C. Rice-Ficht. 1987. Presclerotized eggshell protein from the liver fluke *Fasciola hepatica*. *Biochemistry* **26:** 7819–7825.

Waite, J. H., and A. C. Rice-Ficht. 1989. A histidine-rich protein from the vitellaria of the liver fluke *Fasciola hepatica*. *Biochemistry* **28:** 6104–6110.

Waite, J. H., and M. L. Tanzer. 1981. Specific colorimetric detection of *o*-diphenols and 3,4-dihydroxyphenylalanine-containing peptides. *Anal. Biochem.* **111:** 131–136.

Reference: *Biol. Bull.* **183**: 138–142. (August, 1992)

Measurement of Microscale Patchiness in a Turbulent Aquatic Odor Plume Using a Semiconductor-Based Microprobe

PAUL A. MOORE[1]*, RICHARD K. ZIMMER-FAUST[2], SPENCER L. BEMENT[3], MARC J. WEISSBURG[2], J. MICHAEL PARRISH[1], AND GREG A. GERHARDT[1]

[1]*Departments of Psychiatry and Pharmacology, Neuroscience Training Program, and Rocky Mountain Center for Sensor Technology, University of Colorado Health Sciences Center, Denver, Colorado 80262;* [2]*Department of Biology and Marine Sciences Program, University of South Carolina, Columbia, South Carolina 29208; and* [3]*Department of Electrical Engineering and Computer Science, University of Michigan, Ann Arbor, Michigan 48019*

The distribution of chemical signals within aquatic environments is highly patchy and heterogeneous due to dispersion by turbulent eddies. We aimed to quantify the smallest spatial scales associated with chemical patches, and therefore measured the structure of chemical signals under turbulent flow simultaneously at two chemical sensors spaced from 200 to 800 μm apart. Measurements were done under controlled stimulus and flow conditions with a novel semiconductor-based, multisite, microelectrochemical electrode (5–2000 μm² surface area sensors) and a high-speed computer-based recording system. The chemical signals received at the sensor were intermittent, with wide fluctuations in concentration. Patchiness in signal structure was found at spatial scales as small as 200 μm. Significant differences in signal height were found between recordings made at probes spaced 200, 400, 600, and 800 μm apart. These data demonstrate that sub-millimeter patches occur in aquatic turbulent odor plumes. Such differences in chemical signal structure over small spatial scales might be important for marine animals that employ olfactory orientation. We propose alternative ways by which organisms might deal with these fine scale differences in odor concentration. Animals much larger than microscale patches may have evolved elongated olfactory organs that integrate signals, thereby smoothing variations in sensory input. Animals about the same size as microscale patches may be able to capitalize on microscale variation by extracting directional information from turbulent odor plumes.

Aquatic animals use chemical signals in identifying food and mates, selecting and colonizing substrates, and detecting and avoiding predators. One of the most demanding uses of chemical signals is in the spatial orientation to an odor source. Over the years, there has been considerable debate about the role played by chemical signals in guiding search patterns (1–4). Some of the debate has been due to misunderstanding of the structure of environmental odor signals at the spatial and temporal scales used by receptor cells and behaving animals. In previous studies, time-averaged models have been used to estimate odor concentration gradients along the plume (5, 6). These models are appropriate only for animals sampling odor signals for many minutes before making a decision (7). Because animals often operate at shorter time scales, these models are generally poor in predicting animal behavioral responses (8). Recent advances in technology and theory have shown that distributions of chemical signals are highly patchy at behaviorally relevant time and space scales (See reviews 4, 9, 10). As a result of turbulence, animals located down current of an odor source experience periods well above and below the mean odor concentration (3, 11, 12, 13). It is from these spatial and temporal fluctuations that animals extract spatial information during orientation to an odor source.

Received 2 April 1992; accepted 30 May 1992.

* Present address and correspondence: Paul A. Moore, Monell Chemical Senses Center, 3500 Market Street, Philadelphia, PA 19104-3308.

Many aquatic animals extract spatial information from odor plumes using either chemosensory appendages, such as crustacean antennules and catfish barbels, or solitary chemoreceptor cells scattered along body surfaces (14). Both types of receptor populations play important roles in chemosensory orientation within turbulent odor plumes (15–17). The distance and directional information necessary for orientation toward an odor source is influenced by the spatial and temporal fluctuations within an odor plume. Therefore, knowledge of chemical signal variation within the plume is critical to determining neural and behavioral mechanisms governing chemosensory orientation.

The purpose of this study was to measure microscale chemical signal structure under turbulent conditions, to analyze the signal for potential spatial information available to orienting animals, and to determine the lower size limit of odor patches. We constructed an odor delivery system that simulates the release of chemicals from a suspension feeding clam (a common prey item for many marine predators, including crustaceans and fishes). The resulting microscale chemical signals were quantified by electrochemical recordings at 200 Hz using a novel, multisite semiconductor-based microelectrode. This sensor had five recording sites, each spaced 200 μm apart along the electrode shank. Odor signals were measured simultaneously from two sensors spaced 200, 400, 600, or 800 μm apart.

The chemical tracer (2 m*M* dopamine with 0.01 m*M* ascorbic acid as an anti-oxidant) was introduced into the carrier flow through the excurrent siphon of a model clam. The clam was designed on the basis of principles and procedures applied previously (18). The size and pumping rate of our model corresponded to a small hard clam, *Mercenaria mercenaria,* common in estuaries along the Atlantic and Gulf of Mexico coasts of the United States. The model clam consisted of a pair of plastic tubes that simulated the excurrent (3.1 mm I.D.) and incurrent (4.7 mm I.D.) siphons. The tubes were placed contiguously, with the tips set 3 mm above the substrate and the excurrent siphon positioned downstream. The excurrent flow was supplied from a small, constant-head tank, while the incurrent flow was taken by gravity feed from the flume. Flow rates of 0.51 ± 0.02 ml/s were determined with a flowmeter. The Reynolds number of the jet flowing at the excurrent siphon was ≈42, indicating that flow was laminar at the excurrent exit (18).

Chemical measurements were made in a fully developed boundary layer flow created in a 10 × 0.75 × 0.15 m recirculating flume (Weissburg and Zimmer-Faust, in prep.). The free-stream current speed was 3.8 ± 0.2 cm/s; shear velocity was 0.33 cm/s, and roughness Reynolds number was ≈1.8. The working section (1 × 0.45 m) was located 7.5 m downstream of the entry and 1.5 m upstream of the exit weir. The entire bottom of the flume was layered to a uniform depth with sand (351 ± 10 μm diameter, n = 100). The seawater had a salinity of 25 ppt and a temperature of 25.0 ± 0.5°C during experiments.

The multichannel (5 recording sites per sensor), semiconductor-based electrodes were fabricated by the Center for Integrated Sensors and Circuits, University of Michigan, Ann Arbor, using high-yield approaches (19). Each sensor site was sputter-coated with 500 nm of iridium, and then wire bonded to a circuit board carrier. The electrode recording sites were positioned 200 μm apart (center to center of site distance; Fig. 1). The individual sites were oval in shape, each having a surface area of 2000 μm^2. The shank was 150 μm wide and 15 μm thick.

Recordings were made at 200 Hz using IVEC-5 (In Vivo Electrochemistry Computer System; Medical Systems Corp.) and a customized recording program (available on request). The basic principles used in applying this technique to aquatic chemical detection can be found elsewhere (20). During each 5-ms epoch, 20 data points were collected (10 points per sensor). Each sensor was sampled alternately (*i.e.,* during any 5-ms epoch, points 1, 3, 5, 7, 9, . . . were sampled from channel 1; points 2, 4, 6, 8, 10, . . . from channel 2). The ten points were summed and stored as the final 200 Hz data point. The electrode was held at a fixed voltage of +0.55 V (*vs.* Ag/AgCl reference) during the whole recording sequence. A micromolar/count calibration factor could not be determined for the sensor prior to the experiment because of the prototypical nature of the two channel 200 Hz recording technique. Post-experiment calibration showed a typical linear response relationship between concentration and counts for all five sensors (21). Typical calibration factors for 2000 μm^2 sensors range from 100 to 300 counts/micromolar.

We placed the electrode 31 cm downstream of the excurrent siphon and 6 cm above the sand bed, with the face of the electrode directed perpendicular to the flow. The Reynolds number generated by the probe was ≈3,

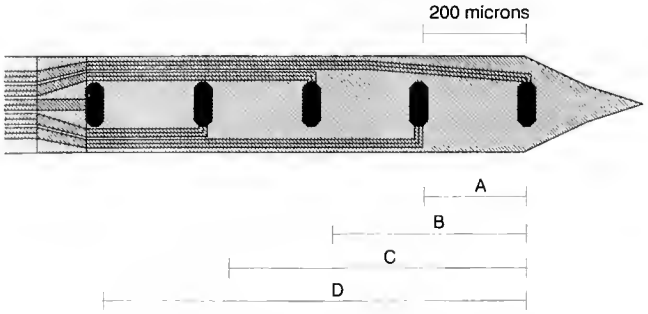

Figure 1. *Diagram of multichannel semiconductor-based sensor showing five, 2000 μm^2 recording sites. Recording sites were spaced 200 μm apart (center to center distance). Sites are numbered consecutively starting from the tip (#1) to the last site up the shank (#5).*

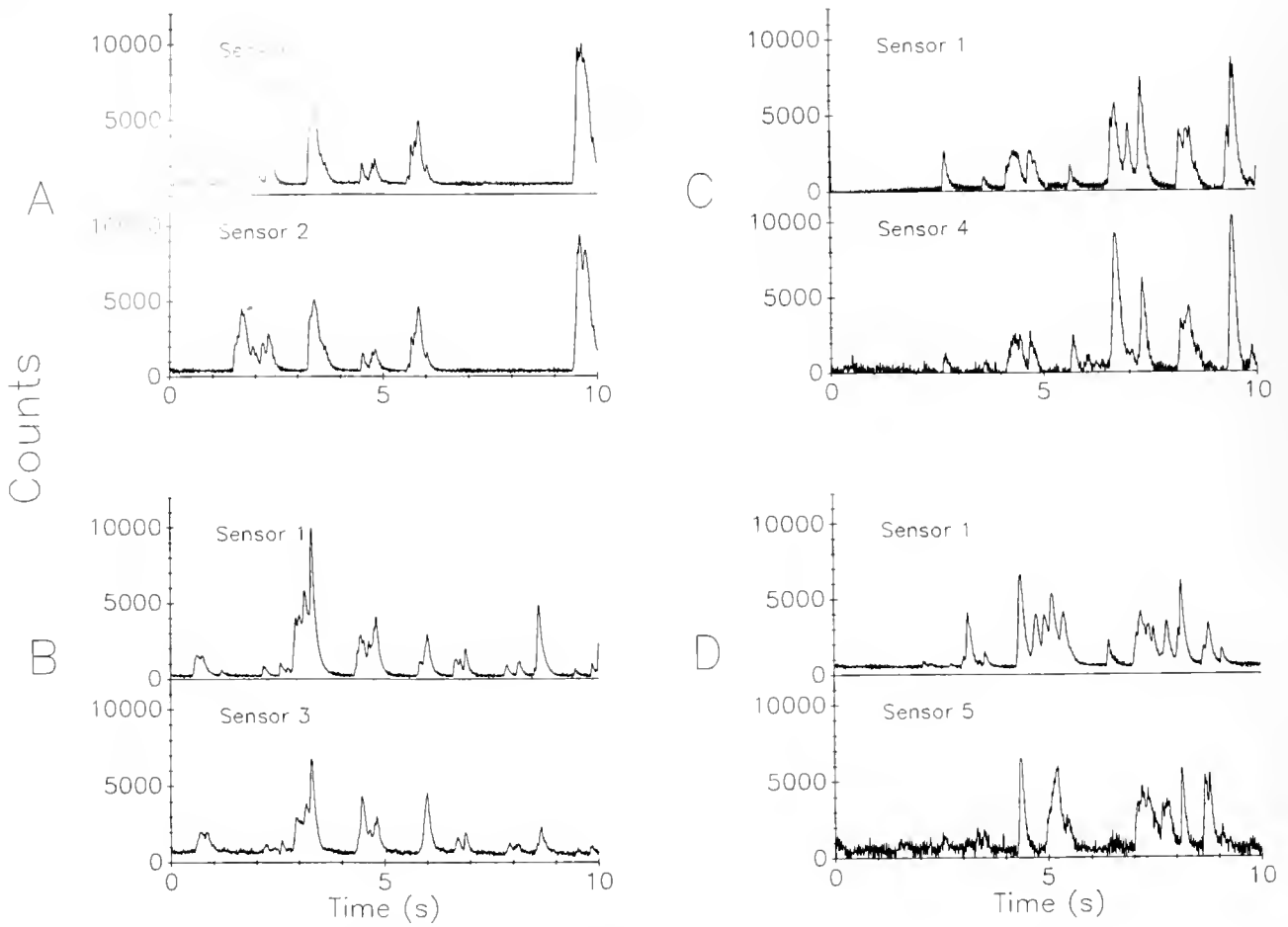

Figure 2. *Examples of 10-s odor profiles measured at each of the four sensor pairs. Sensor #1 was used in all paired recordings as the reference point. Distances are Sensor 1-2, 200 μm (A); Sensor 1-3, 400 μm (B); Sensor 1-4, 600 μm (C); Sensor 1-5, 800 μm (D). Paired recordings were made simultaneously. X-axis tick marks represent 1-s intervals and Y-axis tick marks represent 1000 counts (See text for explanation of counts)*

indicating little separation for the flow around the sensor. A total of ten 10-s periods and one 20-s period were recorded for each pair of recording sites.

We digitally filtered the recordings with a 40 Hz low-pass filter. Construction of this filter was based on C-language algorithms (22). All signal analysis procedures (except filters) were performed with a commercial signal processing program (DADiSP Worksheet). Frequency spectra showed electronic noise spikes at 60 Hz and several harmonics of this frequency. Spectra also showed that most of the chemical signal data was below 10 Hz.

Each recording was set to a baseline determined by averaging signals over a 2-s period. Profiles that were set to a baseline were analyzed for pulse height, defined previously as peak concentration level above background associated with a microscale patch (See Methods in 3). Pulse height can potentially provide directional information to animals during chemical orientation within an odor plume (3, 4, 11, 12, 23). We compared the pulse height recorded simultaneously at two sensors by taking the absolute value of the difference. We repeated this procedure for all of the pulses within an entire data set. The differences were then averaged, the value serving as the 'mean difference' in pulse height between sensor pairs. Statistical significance was determined using ANOVAs and *post-hoc* Tukey-Kramer multiple comparisons (24).

Although dopamine was released continuously, the electrochemical signals were very heterogeneous in space and time (Fig. 2). The chemical signal measured here is similar to those previously recorded in the laboratory (3, 13) and in the field (11, 14, 25). Heterogeneity in chemical signals (Fig. 2) resulted from turbulent eddies. Mechanical forces act within a moving fluid to create large scale eddies (compared to the initial size of the odor plume) that transfer their energy to successively smaller eddies until energy is dissipated as heat. This cascade (the Kolmogorov scale) has a lower size limit below which molecular diffusion determines the distribution of odor molecules.

The smallest size at which patchiness in chemical signal structure occurs can be estimated from the differences in pulse heights at different sensor spacings (Fig. 3). The mean difference in pulse heights between sensors spaced 200 μm apart was significantly less than sensors spaced: 400, 600, 800 μm apart ($P < 0.01$). The difference in pulse height at 200 μm (900 counts, 10–50% of any pulse height) is less than half that at the other sensor spacings. Results indicate that the minimum size of the turbulent eddies and spatial patchiness in the chemical signals was about 200 to 400 μm. When the distance between recording sites increases, there are periods during which only one sensor detects an odor pulse, as seen in Figure 2D (3–4 s). Therefore, chemosensory receptors located only hundreds of μm apart on an animal's olfactory appendage can apparently receive very different signal inputs.

The observed minimum spatial scale of concentration fluctuation can be compared to the theoretically derived values for turbulent flow η (26). The minimum scale of turbulent eddies is:

$$\eta = (\kappa z \nu^3 / U^{*3})^{1/4} \quad (1)$$

where κ is 0.40 (von Karman's constant), z = 6 cm (distance above the sand bed), ν = 0.01 cm^2/s (kinematic viscosity of water), and U* = 0.33 cm/s (shear velocity). The minimum scale of concentration fluctuations (ηc) is:

$$\eta c = \eta (D/\nu)^{1/2} \quad (2)$$

where D = 10^{-5} cm^2/s (molecular diffusion coefficient). Applying equations 1 and 2, we find $\eta \approx 1000$ μm and $\eta c \approx 30$ μm for the conditions of our experiments. These order of magnitude estimates approximate the spatial fluctuations measured in our study.

The interaction between the size of the turbulent eddies and that of the odor plume determines the properties of concentration fluctuations within the plume (27, 28, 29). At the sub-millimeter scale, odor patchiness depends greatly on the lower size limit of turbulent eddies. Knowledge of fine-scale turbulence may therefore provide further insights into the form of odor signals and the evolution of the sensory systems designed to extract information from them.

In the present study, differences in odor signals occurred at spatial scales as small as 200–400 μm. One mechanism used by aquatic animals to orient to odor sources involves the comparison of chemosensory input at paired bilateral appendages (15–17). In this case, orientation requires that microscale differences within odor patches be averaged or integrated along each receptor organ so that differences between organs may be fully resolved. The spatial integration along a chemosensory appendage would have to occur at spatial scales larger than the spatial scale of differences in odor signals to reduce the "chemical noise" caused by small scale concentration fluctuations.

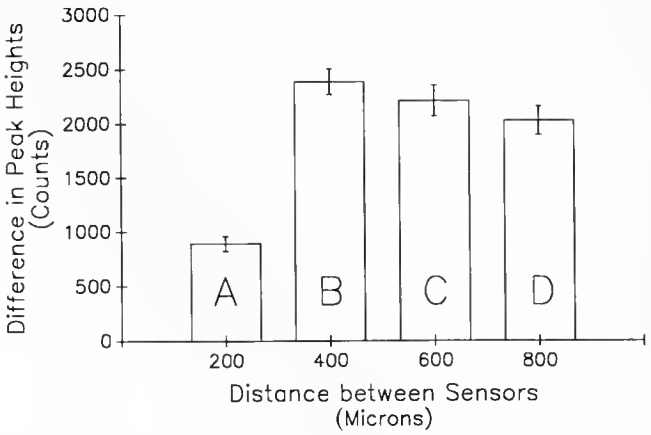

Figure 3. *Mean differences (±S.E.M.) between peak heights in simultaneously recorded odor profiles at distances of 200 (A, n = 200), 400 (B, n = 159), 600 (C, n = 195), and 800 μm (D, n = 230). Mean difference for 400, 600, and 800 μm distances were significantly different from 200 μm (P < 0.01), but not significantly different from each other.*

Conversely, if significant spatial differences in chemical signal structure consistently occur at the scales shown here, then directional and distance information from odor plumes could potentially be derived via differential sensory input along a single chemosensory appendage for larger animals, or between paired sensors for smaller animals, *e.g.*, copepods. In these cases, discrete spatial innervation along a chemosensory appendage would be required to preserve the integrity of spatial differences in odor signals. Spatial integrity of chemosensory innervation has been shown for the catfish taste organs (30, 31), but the innervation at the sub-millimeter spatial scales mentioned here have not been studied.

In summary, our measurements have shown that differences in chemical signal structure can exist at sub-millimeter spatial scales in benthic boundary layers. Further work is now needed to determine the relationship between hydrodynamics and the spatio-temporal structure of odor plumes, and to test whether microscale patchiness is used by animals to exact directional and distance information about odor sources. In addition to the results gathered here, the multisite electrode provided excellent sensitivity to dopamine under prolonged exposure to seawater and advective conditions. Continued studies on microscale patchiness can help to define the patterns of spatial innervation in chemosensory appendages that are necessary to preserve information enabling animals to orient in turbulent odor plumes.

Acknowledgments

This work was supported by USPHS grant #'s AG00441, AG06434, and NSF grant # BNS 9110308 to GAG; NSF grant #'s RII-8996152, DIR-8954231, DIR-

9013187 to RZ-F; and [illegible] Drug Abuse Training Fellowship # AA074[illegible]

Literature Cited

1. **Bell, W. J. [illegible]** no-orientation in walking insects. Pp. 93–106 in [illegible]*ogy of Insects*, W. J. Bell, and R. T. Cardé, eds. Sinauer Associates, Inc., MA.
2. **Kennedy, J. S. 1986.** Some current issues in orientation to odour sources. Pp. 11–25 in *Mechanisms in Insect Olfaction*, T. L. Payne, M. C. Birch, and C. E. J. Kennedy, eds. Clarendon Press, Oxford.
3. **Moore, P. A., and J. Atema. 1991.** Spatial information in the three-dimensional fine structure of an aquatic odor plume. *Biol. Bull.* **181:** 408–418.
4. **Murlis, J., J. S. Elkinton, and R. T. Cardé. 1992.** Odor plumes and how insects use them. *Ann. Rev. Entomol.* **37:** 505–532.
5. **Bossert, W. H., and E. O. Wilson. 1963.** The analysis of olfactory communication among animals. *J. Theor. Biol.* **5:** 443–469.
6. **Zimmer-Faust, R. K., and J. F. Case. 1983.** A proposed dual role of odor in foraging by the California spiny lobster, *Panulirus interruptus* (Randall). *Biol. Bull.* **164:** 341–353.
7. **Gibson, G., and J. Brady. 1988.** Flight behavior of tsetse flies in host odour plumes: the initial response to leaving or entering odour. *Physiol. Entomol.* **13:** 29–42.
8. **Elkinton, J. S., R. T. Cardé, and C. J. Mason. 1984.** Evaluation of time-average dispersion models for estimating pheromone concentration in a deciduous forest. *J. Chem. Ecol.* **10:** 1081–1108.
9. **Atema, J. 1988.** Distribution of chemical stimuli. Pp. 29–56 in *Sensory Biology of Aquatic Animals*, J. Atema, A. N. Popper, R. R. Fay, and W. N. Tavolga, eds. Springer-Verlag, NY.
10. **Zimmer-Faust, R. K. 1989.** The relationship between chemoreception and foraging behavior in crustaceans. *Limnol. Oceanogr.* **34:** 1367–1374.
11. **Murlis, J., and C. D. Jones. 1981.** Fine-scale structure of odour plumes in relation to insect orientation to distant pheromone and other attractant sources. *Physiol. Entomol.* **6:** 71–86.
12. **Moore, P. A., and J. Atema. 1988.** A model of a temporal filter in chemoreception to extract directional information from a turbulent odor plume. *Biol. Bull.* **174:** 355–363.
13. **Zimmer-Faust, R. K., J. M. Stanfill, and S. B. Collard, III. 1988.** A fast, multichannel fluorometer for investigating aquatic chemoreception and odor trails. *Limnol. Oceanogr.* **33:** 1586–1595.
14. **Laverack, M. S. 1988.** The diversity of chemoreceptors. Pp. 287–312 in *Sensory Biology of Aquatic Animals*, J. Atema, A. N. Popper, R. R. Fay, and W. N. Tavolga, eds. Springer-Verlag, NY.
15. **Reeder, P. B., and B. W. Ache. 1980.** Chemotaxis in the Florida spiny lobster, *Panulirus argus*. *Anim. Behav.* **28:** 831–839.
16. **Johnsen, P. B., and J. H. Teeter. 1980.** Spatial gradient detection of chemical cues by catfish. *J. Comp. Physiol.* **140:** 95–99.
17. **Devine, D. V., and J. Atema. 1982.** Function of chemoreceptor organs in spatial orientation of the lobster, *Homarus americanus:* differences and overlap. *Biol. Bull.* **163:** 144–153.
18. **Monismith, S. G., J. R. Koseff, J. K. Thompson, C. A. O'Riordan, and H. M. Nepf. 1990.** A study of model bivalve siphonal currents. *Limnol. Oceanogr.* **35:** 680–696.
19. **Najafi, N., and K. D. Wise. 1985.** A high-yield IC-compatible multichannel recording array. *IEEE Trans. Electron Devices* **32:** 1206–1211.
20. **Moore, P. A., G. A. Gerhardt, and J. Atema. 1989.** High resolution spatio-temporal analysis of aquatic chemical signals using microelectrochemical electrodes. *Chem. Senses* **14:** 829–840.
21. **Van Horne, C. G., S. BeMent, B. J. Hoffer, and G. A. Gerhardt. 1990.** Multichannel semiconductor-based electrodes for *in vivo* electrochemical and electrophysiological studies in rat CNS. *Neurosci. Letters* **120:** 249–252.
22. **Embree, P. M., and B. Kimble. 1991.** C-language algorithms for digital signal processing. Prentice Hall, Englewood, NJ.
23. **Murlis, J. 1986.** The structure of odour plume. Pp. 27–38 in *Mechanisms in Insect Olfaction*, T. L. Payne, M. C. Birch, and C. E. J. Kennedy, eds. Clarendon Press, Oxford.
24. **Sokal, R. D., and F. J. Rohlf. 1981.** *Biometry.* W. H. Freeman and Company, San Francisco.
25. **Atema, J., P. A. Moore, L. Madin, and G. A. Gerhardt. 1991.** Subnose-I: tracking odor plumes at 900 meters beneath the ocean surface. *Mar. Ecol. Prog. Ser.* **74:** 303–306.
26. **Tennekes, H., and J. L. Lumley. 1972.** *A First Course in Turbulence,* MIT Press, Cambridge, MA. 300 pp.
27. **Aylor, D. E. 1976.** Estimating peak concentrations of pheromones in the forest. Pp. 177–188 in *Perspectives in Forest Entomology*, J. E. Anderson and M. K. Kaya, eds. Academic Press, NY.
28. **Aylor, D. E., J-Y. Parlange, and J. Granett. 1976.** Turbulent dispersion of disparlure in the forest and male gypsy moth response. *Env. Entomol.* **10:** 211–218.
29. **Miksad, R. W., and J. Kittredge. 1979.** Pheromone aerial dispersion: a filament model. 14th Conf. *Agric. For. Met., Am. Met. Soc.* **1:** 238–243.
30. **Hayama, T., and J. Caprio. 1989.** Lobule structure and somatotopic organization of the medullary facial lobe in the channel catfish, *Ictalurus punctatus*. *J. Comp. Neurol.* **285:** 9–17.
31. **Marui, T., J. Caprio, S. Kiyohara, and Y. Kasahara. 1988.** Topographical organization of taste and tactile neurons in the facial lobe of the sea catfish, *Plotosus lineatus*. *Brain Res.* **446:** 178–182.

Reference: *Biol. Bull.* **183:** 143–146. (August, 1992)

Recurring Themes and Variations: An Overview and Introduction

WILLIAM E. S. CARR

The Whitney Laboratory, University of Florida, 9505 Ocean Shore Boulevard, St. Augustine, Florida 32086-8623

A Recurring Theme With Variations

For several years, investigators have noted that the external chemoreceptors on olfactory organs of marine animals respond to some chemicals identical to those activating receptors on neurons and other internal cell types. For example, our studies with the spiny lobster, *Panulirus argus,* revealed that the olfactory organ possessed distinct populations of chemoreceptor cells that are differentially activated by exogenous adenosine-5′-monophosphate (AMP), ATP, L-glutamate, glycine, or taurine. All of these substances are putative neurotransmitters or modulators in internal cells and tissues where, except for taurine, distinct receptor types have been characterized (reviewed by Carr *et al.,* 1987, 1989). Certainly the chemoreceptors cited above, and the complementary receptors on internal nerve or muscle cells, have obvious parallels; *i.e.,* each has a membrane binding site for specific chemicals appearing in an extracellular aqueous milieu, and each receptor is coupled to a transmembrane transduction mechanism affecting membrane excitability.

Earlier suspicions that the similarities between external and internal "chemoreceptors" were only superficial are now largely dispelled. Applications of modern gene cloning and sequencing techniques have revealed that the external cAMP chemoreceptor of slime molds and the internal β-adrenergic receptor of mammals belong to the same family of G protein coupled receptors (Fig. 1). All members of this large receptor family are integral membrane proteins with seven transmembrane segments, an intracellular C-terminus, an extracellular N-terminus, plus other homologies including partial amino acid sequence identity and similar topographical organization in the membrane (see Sibley *et al.,* 1987; Klein *et al.,* 1988).

Received 13 March 1992; accepted 18 May 1992.

The homologies described above for an external chemoreceptor of a microbe, and a receptor in mammalian internal tissues extend far beyond the structure of the receptor protein itself to include a multi-molecular system that is broadly adapted to transmembrane signaling. These signaling systems all include transduction components using a related family of dissociable G-proteins that couple receptor activation to molecular cascades including second messenger enzymes, second messengers, protein kinases, and other components affecting membrane excitation or other intracellular events (see Fig. 2).

The occurrence, in organisms ranging from microbes to man, of receptors, G proteins, and intracellular effectors indicative of a closely related family of transmembrane signaling systems, strongly suggests that this system first evolved in unicellular progenitors and was genetically conserved and modified during the course of metazoan evolution (for review, see Carr, 1990). Hence we now see the molecular components of this signaling system broadly deployed and modified as one type of "recurring theme with variations" (Fig. 2) that performs broad functions, ranging from light reception (*e.g.,* Hall, 1987) to the recognition of chemical signals from other cells, tissues, organisms, or the environment.

A Summary of Topics

The participants in this Symposium have made original, seminal discoveries strongly reinforcing our awareness that recurring themes and variations are both broadly expressed and integral to future developments in marine biotechnology. The first paper by Gregory Baxter and Daniel Morse shows that certain marine larvae are induced to settle and metamorphose in response to specific chemical cues on the surface of a habitat suitable for the next stage of the life cycle. The chemical cues are recog-

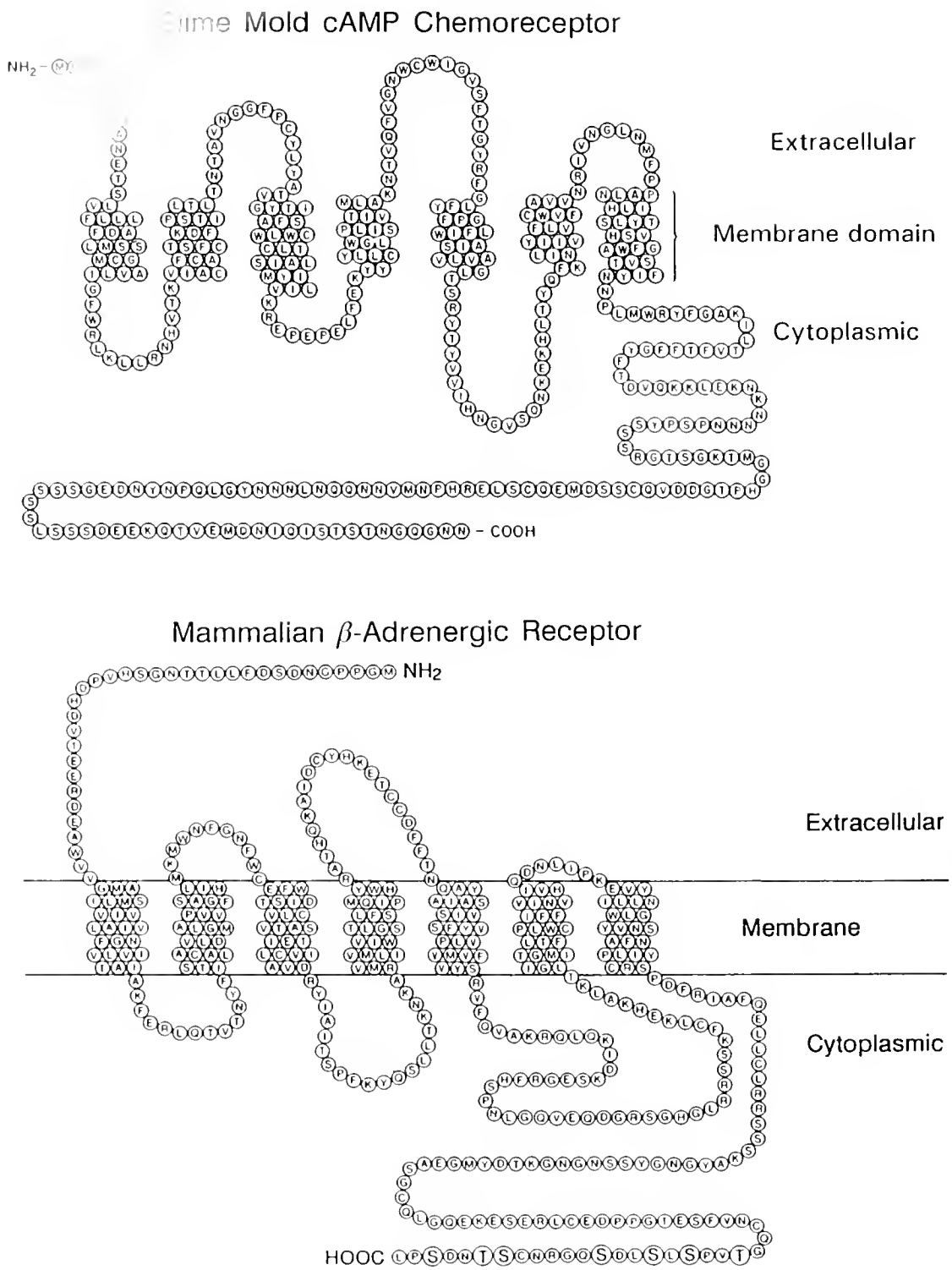

Members of a recurring gene family. Deduced amino acid sequences and proposed structure of t[illegible] hemoreceptor of slime mold, *Dictyostelium discoideum*, (from Klein *et al.*, 1988) and a mamm[illegible]renergic receptor (from Sibley *et al.*, 1987). Further details are given in text.

nized in part by G protein-coupled receptors belonging to the same large, recurring family of transmembrane signaling systems described above.

Stephanie Schulz and David Garbers describe guanylyl cyclase receptors, which are major components of an entirely different type of transmembrane signaling system.

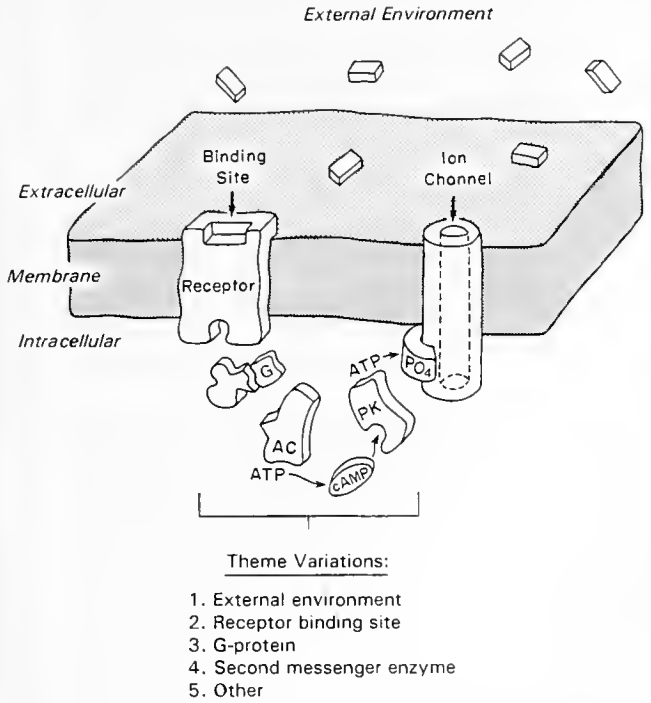

Figure 2. A recurring theme for transmembrane signaling: generalized structure of a G protein-coupled system. Binding of an extracellular ligand activates the receptor which is coupled to a dissociable G protein (G) that links receptor activation to a cascade of subsequent transduction components depicted as: the second messenger enzyme, adenylate cyclase (AC); the second messenger, cAMP; and a protein kinase (PK) that phosphorylates an ion channel. Examples of variations in the depicted theme include: (1) an *external environment* composed of seawater for a chemoreceptor of a marine organisms, or of the fluid in a synaptic cleft for an internal synaptic receptor; (2) a *binding site* affecting receptor activation after binding specific ligands that may range from small catecholamines to a 28 kd glycoprotein hormone (Kobilka, 1992); (3) a dissociable *G protein* yielding α and $\beta\gamma$ subunits which may stimulate or inhibit a second messenger enzyme, or directly affect an ion channel (*e.g.*, Birnbaumer, 1990; Simon *et al.*, 1991). (4) other *second messenger enzymes: e.g.*, phospholipase C that yields diacylglycerol and inositol trisphosphate (*ibid;* Berridge and Irvine, 1989), or phospholipase A_2 yielding arachidonic acid and its metabolites (Shimizu and Wolfe, 1990; Simon *et al.*, 1991).

This latter system recurs in such disparate forms as the external chemoreceptors of sea urchin sperm and the internal receptors for atrial natriuretic peptides in mammals and fish.

In the next paper, Baldomero Olivera and colleagues reveal that cone snails produce families of small peptide venoms that cause debilitating effects by disrupting specific, recurring transmembrane signaling systems of both prey and non-prey organisms.

Sherry Painter explains that *Aplysia,* the sea hare, produces a family of peptides, structurally and genetically related to egg laying hormone (ELH). Whereas ELH functions internally to regulate ovulation and egg-laying behavior, other members of the family are released externally as sex pheromones affecting the reproductive behavior of neighboring individuals.

Peter Sorensen next describes a somewhat analogous recurring theme wherein similar molecules have evolved dual functions as internal hormones and external sex pheromones in fish. In particular, specific steroids and prostaglandins function internally as hormones regulating egg development and spawning in female fish; but when released into the water, these same substances, or metabolically related ones, serve as sex pheromones detected by the male olfactory system to stimulate milt production and coordinate synchronous spawning by the two sexes.

In the final paper, Herbert Waite describes the recurring mechanisms whereby invertebrates, while completely submerged in seawater, produce strong waterproof adhesives from unique proteins containing dihydroxyphenylalanine (DOPA) and DOPA quinone moieties which contribute to strong cross-linked matrices. Interestingly, the recurring theme of adhesive production described by Waite adjoins that of larval recognition of substrate developed in the initial presentation by Baxter and Morse. The DOPA moieties present in the protein cement used for tube construction by certain gregarious polychaete worms may contribute to the chemical signal that induces settlement and metamorphosis by larvae of conspecifics (Jensen and Morse, 1990).

Knowledge of Recurring Themes: Opportunities for New Research Strategies

Each of the symposium presentations describes how basic research may be applied to the development of useful products. Product development is an important outgrowth of the current "biotechnology age" where the sequencing of genes and gene products, and the biochemical identification of new hormones, pheromones, and other natural products is occurring at a rapid pace. In addition to useful products, however, the current techniques of molecular biology, combined with our awareness of the widespread occurrence of recurring themes, provide opportunities to investigate basic questions not readily addressed with earlier technologies. Examples of probing, yet "approachable," questions generated by the symposium presentations are as follows:

1. In addition to G protein-coupled receptor systems, do some larvae employ other known types of transmembrane signaling systems to recognize substrate-specific morphogens, or to detect entirely different types of chemical signals, such as feeding stimulants or deterrents? Do the molecular components of larval chemosensory systems persist and function in later developmental stages as either external or internal receptor systems?

2. In mammals, one form of osmotic imbalance causing diarrhea results from activation of guanylyl cyclase (GC) receptors by [illegible]ic peptides of bacteria (Schulz *et al.*, 1990). [illegible] pathological condition recur in aquatic vert[illegible] such as fish and reptiles, which must maintain internal body fluids in a state of osmotic disequilibrium with the environment?

3. Do the genes that encode cone snail venoms (conotoxins) express significant homology with other genes of cone snails, or those of other mollusks or even members of different phyla? Because many conotoxins have high affinities for, or may even activate, defined receptors or ion channels, could these peptides have evolved initially as neurotransmitters or modulators which later became adapted to serve as venoms?

4. In mollusks and fishes, do homologies exist between receptors present within the ovary, and externally on the olfactory organ, because both are activated by identical or structurally similar hormones and pheromones?

5. The genomes of some protozoa include genes that express enzymes for synthesizing catechol precursors, catechols, quinones, and products of "quinone-tanning" (Van Houten *et al.*, 1981; Waite, 1990). Because this genetic information still exists in contemporary unicells, what genomic changes contributed to the divergence of DOPA pathways creating products as disparate as neurotransmitters, odor blockers (Kittredge *et al.*, 1974), antimicrobial agents (Azumi *et al.*, 1990), and waterproof adhesives and varnishes (*e.g.*, Waite, 1990)?

Answers to questions such as those above will bring us closer to understanding the origins, utility, and evolutionary divergence of recurring themes. These same answers may also provide insight into the confluence of disparate recurring themes that were subjected to unique selection pressures as a result of co-evolving together in the same, or in competing, organisms.

Acknowledgments

This Symposium and its publication were funded in part by NSF Grant DCB-9107729. The author's studies are partially funded by NSF Grant BNS-8908340.

Literature Cited

Azumi, K., H. Yokosawa, and S. Ishii. 1990. Halocyamines: novel antimicrobial tetrapeptide-like substances isolated from the hemocytes of the solitary ascidian *Halocynthia roretzi*. *Biochemistry* **29:** 159–165.

Berridge, M. J., and R. F. Irvine. 1989. Inositol phosphates and cell signalling. *Nature* **341:** 197–205.

Birnbaumer, L. 1990. Transduction of receptor signal into modulation of effector activity by G proteins: the first 20 years or so. *FASEB J.* **4:** 3178–3188.

Carr, W. E. S. 1990. Chemical signaling systems in lower organisms: a prelude to the evolution of chemical communication in the nervous system. Pp. 81–94 in *Evolution of the First Nervous System*, P.A.V. Anderson, ed. Plenum Press, New York.

Carr, W. E. S., B. W. Ache, and R. A. Gleeson. 1987. Chemoreceptors of crustaceans: similarities to receptors for neuroactive substances in internal tissues. *Environ. Health Perspect.* **71:** 31–46.

Carr, W. E. S., R. A. Gleeson, and H. G. Trapido-Rosenthal. 1989. Chemosensory systems in lower organisms: correlations with internal receptor systems for neurotransmitters and hormones. *Adv. Environ. Comp. Physiol.* **5:** 25–52.

Hall, Z. W. 1987. Three of a kind: the β-adrenergic receptor, the muscarinic acetylcholine receptor, and rhodopsin. *Trends Neurosci.* **10:** 99–101.

Jensen, R. A., and D. E. Morse. 1990. Chemically induced metamorphosis of polychaete larvae in both the laboratory and ocean environment. *J. Chem. Ecol.* **16:** 911–930.

Kittredge, J. S., F. T. Takahashi, J. Lindsey, and R. Lasker. 1974. Chemical signals in the sea: marine allelochemics and evolution. *Fishery Bull.* **72:** 1–11.

Klein, P. S., T. J. Sun, C. L. Saxe, III, A. R. Kimmel, R. L. Johnson, and P. N. Devreotes. 1988. A chemoattractant receptor controls development in *Dictyostelium discoideum*. *Science* **241:** 1467–1472.

Kobilka, B. 1992. Adrenergic receptors as models for G protein-coupled receptors. *Annu. Rev. Neurosci.* **15:** 87–114.

Schulz, S., C. K. Green, P. S. T. Yuen, and D. L. Garbers. 1990. Guanylyl cyclase is a heat-stable enterotoxin receptor. *Cell* **63:** 941–948.

Shimizu, T., and L. S. Wolfe. 1990. Arachidonic acid cascade and signal transduction. *J. Neurochem.* **55:** 1–15.

Sibley, D. R., J. L. Benovic, M. G. Caron, and R. J. Lefkowitz. 1987. Regulation of transmembrane signaling by receptor phosphorylation. *Cell* **48:** 913–922.

Simon, M. I., M. P. Strathmann, and N. Gautam. 1991. Diversity of G proteins in signal transduction. *Science* **252:** 802–808.

Van Houten, J., D. C. R. Hauser, and M. Levandowsky. 1981. Chemosensory behavior in protozoa. Pp. 67–124 in *Biochemistry and Physiology of Protozoa*, 2nd ed., Vol 4, M. Levandowsky and S. H. Hutner, eds. Academic Press, New York.

Waite, J. H. 1990. The phylogeny and chemical diversity of quinone-tanned glues and varnishes. *Comp. Biochem. Physiol.* **97B:** 19–29.

Reference: *Biol. Bull.* **183**: 147–154. (August, 1992)

Cilia from Abalone Larvae Contain a Receptor-Dependent G Protein Transduction System Similar to that in Mammals

GREGORY T. BAXTER AND DANIEL E. MORSE*

Department of Biological Sciences and the Marine Biotechnology Center, University of California, Santa Barbara, California 93106

Abstract. Lysine and related diamino acids amplify (facilitate) the response to inducers of metamorphosis in larvae of the marine mollusk *Haliotis rufescens*. Previous studies showed that a cholera toxin-sensitive G protein transduces the lysine signal via a diacylglycerol-dependent pathway. We have isolated and partially purified larval cilia that may be involved in recognizing the facilitating chemical signals. These isolated cilia provide an open or porous membrane-associated sensory system that is uniquely tractable for *in vitro* analyses of chemosensory signal transduction. The cilia contain receptors that exhibit sodium-independent binding of the facilitating diamino acids. The binding strength for lysine and related diamino acids *in vitro* is correlated with the effectiveness of these ligands as facilitators *in vivo*. The cilia contain a cholera toxin-sensitive G protein functionally coupled to the lysine receptor. The receptor and the G protein reciprocally regulate one another, suggesting that the chemosensor may be a member of the rhodopsin-like, G protein-coupled transmembrane receptor superfamily. Previous analyses of mRNAs from the larval cilia revealed a sequence coding for a G protein with high homology to G_q from mammalian brain, and another sequence coding for a protein homologous to G_i/G_o. Similarities between this system, other chemosensory signal transduction pathways, and mechanisms of neuronal long-term potentiation are evident. Because the receptors and transducers controlling settlement and metamorphosis in *Haliotis* and other marine invertebrate larvae appear homologous to components controlling neuronal activity, cellular proliferation, and differentiation in mammals, characterization of the molecules controlling metamorphosis may help in the design of new regulators useful in medicine.

Received 30 March 1992; accepted 18 May 1992.

Abbreviations: G protein, guanine nucleotide binding protein; GABA, γ-aminobutyric acid; GppNHp, guanosine 5′ (β,γ-imido) triphosphate; PKC, protein kinase C; ASW, artificial seawater; SDS, sodium dodecyl sulfate; PAGE, polyacrylamide gel electrophoresis; DAPA, L-α,β-diaminopropionic acid; GDP-β-S, guanosine 5′-0-[β-thio] diphosphate; PLC, phospholipase C; Tris, tris-hydroxymethylaminomethane.

* Author to whom all correspondence should be addressed.

Introduction

The molecular components and mechanisms controlling the settlement and metamorphosis of marine invertebrate larvae in response to chemical signals from the environment are strikingly similar, in some cases, to those that mediate responses to hormones, transmitters, and other signals regulating neuronal activity, behavior and cellular differentiation in mammals. These processes in the larvae, like their counterparts in mammals, also exhibit far greater complexity than first realized. We present here recent findings on one such system from a molluscan larva, and discuss these data in the context of recently discovered sequence homologies and other evidence for relatedness to mammalian receptor-transducer pathways in molluscan and coral larval systems.

Larvae of the marine gastropod mollusk *Haliotis rufescens* (red abalone) are induced to settle from the plankton and metamorphose in response to exogenous γ-aminobutyric acid (GABA)[1]-mimetic peptides found on the surfaces of specific algae; GABA and GABA analogs also induce this metamorphosis (Morse *et al.*, 1979, 1980; Morse and Morse, 1984; Morse, 1985, 1990). These morphogenic inducers are recognized by externally accessible chemosensory receptors that have been characterized by radioligand binding and competition studies (Trapido-Rosenthal and Morse, 1986a). The induction of meta-

morphosis of *Haliotis* larvae by low concentrations of these inducers can be potentiated, or amplified, by lysine and structurally related diamino acids (Trapido-Rosenthal and Morse, 198[illegible]). Experiments *in vivo* showed that transduction of the facilitating diamino acid signal is mediated by a regulatory pathway that is separate from the morphogenetic pathway (Trapido-Rosenthal and Morse, 1986a, b; Baxter and Morse, 1987).

From experiments conducted with *Haliotis* larvae *in vivo*, we concluded that a cholera toxin-sensitive G protein transduces the facilitating diamino acid signal, and that this G protein may control a phospholipase C-diacylglycerol-protein kinase C cascade (Baxter and Morse, 1987). We report here the purification of epithelial cilia from *Haliotis* larvae, and the finding that a chemosensory diamino acid (lysine) receptor is located on these isolated cilia. These cilia also contain a cholera toxin-sensitive G protein functionally coupled to the lysine receptor. These observations, and the recent discovery of mRNAs coding for G proteins in the isolated cilia (Wodicka and Morse, 1991), support the suggestion that some of these cilia may have a chemosensory function. The lysine receptor and G protein reciprocally regulate one another in the isolated cilia, in a manner similar to that observed for transmembrane receptor-controlled G proteins in mammalian systems. In conjunction with the recently reported high sequence homology between one of the ciliary G proteins and a G protein from mammalian brain (Wodicka and Morse, 1991), these results indicate that similar signal transduction pathways and components may be central to regulation in both larval metamorphosis and mammalian neuronal function and cell differentiation.

Materials and Methods

Larvae and materials

Haliotis rufescens larvae were produced and cultured at 15°C at a density of 10^5 larvae per liter, as described previously (Morse *et al.*, 1979, 1980). Under these conditions, larvae become competent for metamorphosis 7 days post-fertilization (Morse *et al.*, 1980). Forty-eight hours prior to use, competent larvae were transferred to fresh 5 μm filtered ultraviolet sterilized seawater containing 2 μg/ml rifampicin, at a density of 10^5 larvae/liter at 15°C. The radiochemicals [^{32}P]-NAD, [^{3}H]-L-lysine, [^{3}H]-L-alanine and [^{3}H]-L-leucine were purchased from DuPont/NEN. Electrophoresis reagents were purchased from Bio-Rad Laboratories. All other chemicals were purchased from Sigma. Artificial seawater media (see below) were aerated [illegible]16 h at 15°C before use.

Cilia isolation

Abscission of cilia was induced by a modification of the calcium/ethanol procedure developed by Watson and Hopkins (1962). Prior to removal of cilia, 10^6 larvae at 7 days post-fertilization were incubated at 15°C in 18 l of a calcium-free artificial seawater (ASW) solution (420 m*M* NaCl, 9.0 m*M* KCl, 52 m*M* $MgSO_4$, 23 m*M* $MgCl_2$, 2.0 m*M* $NaHCO_3$, 9.0 m*M* Tris-HCl, and 2 μg/ml rifampicin; final pH = 7.8) for 24 h, and then transferred to normal ASW (Cavanaugh, 1956) containing rifampicin (2 μg/ml) for a further 24 h incubation at 15°C to allow equilibration to normal conditions. This treatment effectively removes the larval shell, thus exposing the epithelial cilia (located primarily on the head). Approximately 10^6 treated larvae then were placed in 135 ml ASW to which ethanol was added to a final concentration of 10% (v/v); this mixture was gently stirred for 1 min at room temperature. $CaCl_2$ was added to a final concentration of 10 m*M* over that in ASW, and the sample stirred for an additional 17 min at room temperature. After filtration through a 95 μm nylon mesh (Nitex brand) to remove deciliated larvae, the suspension of shed cilia was centrifuged at 1500 × *g* for 5 min at 4°C to precipitate debris; the cilia then were collected by centrifugation at 10,000 × *g* for 10 min at 4°C. The resulting cilia pellet was washed three times by resuspension in 30 ml buffer [20 m*M* Tris-HCl (pH 7.6), 10 m*M* $MgCl_2$, 1 m*M* EGTA] and centrifugation at 10,000 × *g* for 10 min at 4°C. The final washed pellet was resuspended in buffer (as specified below). Protein was measured spectrophotometrically (Bradford, 1976) after alkaline digestion.

Scanning electron microscopy

The cilia pellet was suspended in water and applied to poly-L-lysine-treated glass cover slips. After 30 min, the cover slips with affixed cilia were washed with water, subjected to critical-point drying, sputtercoated with gold, and examined with an ISI Model Alpha-9 scanning electron microscope.

Radioligand binding assays

Binding of (^{3}H)-L-lysine was analyzed as a function of concentration with minor modifications of the method previously described (Trapido-Rosenthal and Morse, 1986a). Cilia were apportioned at a final protein concentration of 50 μg/ml in 250 μl final volume of binding buffer (20 m*M* Tris-HCl pH 7.6, 10 m*M* $MgCl_2$), and incubated with radioactive ligand for 1 h at 2°C. Assays were terminated by filtration through 0.2 μm nitrocellulose membrane filters (Millipore HAWP; 25 mm diam.) that had been presoaked in buffer at 0°C for 20 min. Filters were rinsed rapidly with two successive 3-ml portions of ice-cold buffer and dissolved in scintillation fluid; radioactivity was determined by liquid scintillation. Scatchard analyses of binding data were performed with the non-linear curve fitting programs EBDA/LIGAND of

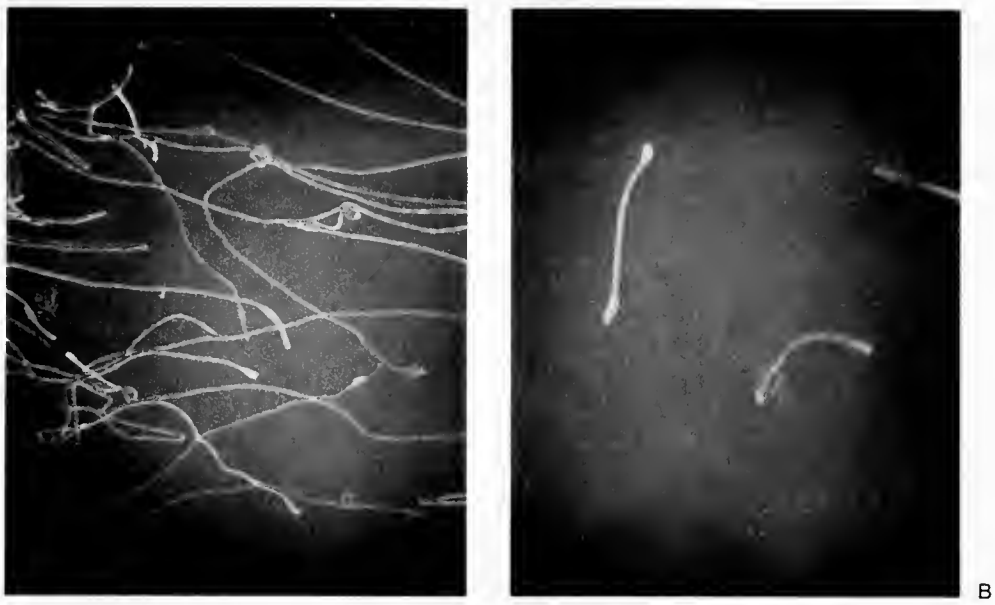

Figure 1. Scanning electron micrographs of the cilia purified from *Haliotis* larvae. (A) Scanning electron micrograph of cilia preparation (2400×). Contour lengths of the long propulsive cilia ≥ 5.0 μm. (B) Isolated view of smaller proposed sensory cilia (length *ca.* 0.5 μm) in the same preparation (4500×).

Rodbard and Munson (McPherson, 1985). Competition for binding by unlabelled L-lysine, L-ornithine, or L-α,β-diaminopropionic acid was analyzed similarly, with the same program.

ADP-ribosylation

Cholera toxin-catalyzed ADP-ribosylation for the labeling of G protein was performed as described by Pace and Lancet (1986), using cholera toxin preactivated by incubation with 20 m*M* dithiothreitol at room temperature for 15 min. Cilia (200 μg/ml protein) were incubated at room temperature in a buffer containing 20 m*M* Tris-HCl (pH 7.6), 30 m*M* thymidine, 1 m*M* ATP, 0.1 m*M* GTP, 5 m*M* $MgCl_2$, 1 m*M* EDTA, 3 m*M* phosphoenolpyruvate, 5 units/ml pyruvate kinase, 0.05% Triton X-100, 1 m*M* dithiothreitol, 5 μ*M* [^{32}P]-NAD (10–20 Ci/mmol), and preactivated cholera toxin at a final concentration of 10 μg/ml in a final volume of 200 μl. The reaction was terminated after 30 min by adding an equal volume of 2× electrophoresis sample buffer (100 m*M* Tris-HCl pH 6.8, 20% glycerol, 2% SDS, 100 m*M* dithiothreitol, and 0.004% bromophenol blue) and boiling for 20 min. ADP ribosylation of cilia for G protein activation was conducted under similar conditions without radioisotope (Pace and Lancet, 1986), using a 1-h incubation. Cilia then were centrifuged at 15,000 × *g* for 10 min at 4°C, resuspended in buffer, and assayed as described.

Gel electrophoresis and autoradiography

Proteins were separated by one-dimensional SDS polyacrylamide gel electrophoresis (SDS-PAGE) (Laemmli, 1970) with a 10% separating gel. Molecular weight standards were included on each gel. Gels were dried and exposed to Kodak X-OMAT x-ray film with intensifying screens at −70°C. Bands were quantified by densitometric scanning of the autoradiogram with an LKB Ultra Scan XL.

Results

Isolation of larval cilia

Cilia were purified from *Haliotis rufescens* larvae as described above; the yield was about 0.8 g wet weight/10^6 larvae. The resulting preparation contained cilia recognizably derived from externally accessible structures, apparently including the propulsive swimming cilia from cells of the velum and sensory cilia from the cephalic apical tuft and other sensory structures (Bonar, 1978; Yool, 1985). The deciliated larvae remained alive and largely intact, indicating that the cilia obtained were removed from external epithelia. Scanning electron microscopy revealed a highly purified but heterogeneous population of cilia with no apparent contamination by other cellular material (Fig. 1). Two distinct classes are seen: elongated cilia (≥5 μm length), apparently the swimming cilia from the velum, and short cilia (*ca.* 0.5 μm long), each with an enlarged process at one end (Fig. 1B); these apparently include the paddle cilia of the apical tuft and other sensory tissues. [Although the distal enlargement is clearly an artifact of fixation, its distribution in any organism is limited to particular body regions (Short and Tamm, 1991). In

larval *Haliotis refescens* (cf. [illegible]ol, 1985)—as in marine turbellaria (Ehlers and Ehl[illegible] 1978)—paddle cilia are found only on sens[illegible] reflecting, presumably, a unique specializatio[illegible]% gel electrophoresis confirmed the substantial p[illegible]ion of the larval cilia (Baxter, 1991); a domi[illegible]otein with molecular mass identical to that of α and β tubulin was found in the cilia preparation, whereas this was only a minor constituent of the proteins from the whole larvae.

Lysine receptors

The purified cilia exhibit specific and saturable binding of [^{3}H]-L-lysine that reaches equilibrium within 15 min at 2°C (Baxter, 1991). Scatchard analysis of the specific equilibrium binding (Fig. 2) formally resolves a high affinity binding site ($K_d \leq 0.1\ \mu M$) and a low affinity site ($K_d \geq 10\ \mu M$). The maximal binding (B_{max}) of lysine is on the order of 10 femtomoles/μg cilia protein at the high affinity site and *ca.* 100 femtomoles/μg protein at the low affinity site. Although exhibiting some variation from one preparation of cilia to another, these binding parameters proved highly reproducible within each preparation. The presence or absence of sodium had no significant effect on these parameters for lysine binding (Baxter, 1991).

The abilities of the unlabeled facilitating diamino acids L-α,β-diaminopropionic acid (DAPA), L-lysine and L-ornithine to compete for the specific binding of [^{3}H]-L-lysine to the cilia are correlated with the activities of these compounds as facilitators of larval metamorphosis (Fig. 3). The rank order of binding strength and biological effectiveness is DAPA > L-lysine > ornithine.

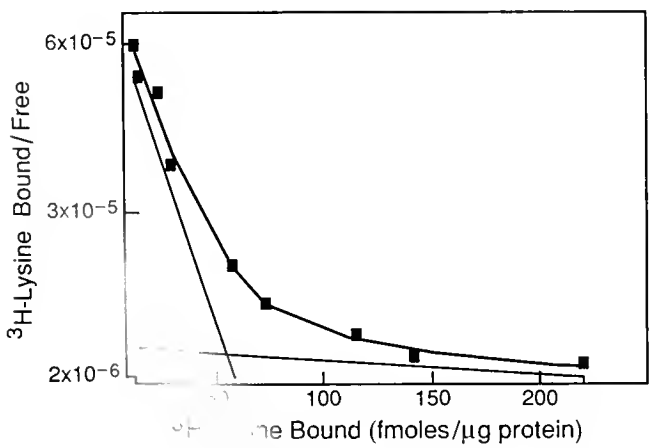

Figure 2. Binding [illegible]-lysine to cilia purified from *Haliotis* larvae. Scatchard analysis [illegible]librium specific binding data. Data were analyzed with the computer assisted non-linear curve fitting programs EBDA/LIGAND (McPherson, 1985); each point represents the mean of three determinations. Details as described in Materials and Methods.

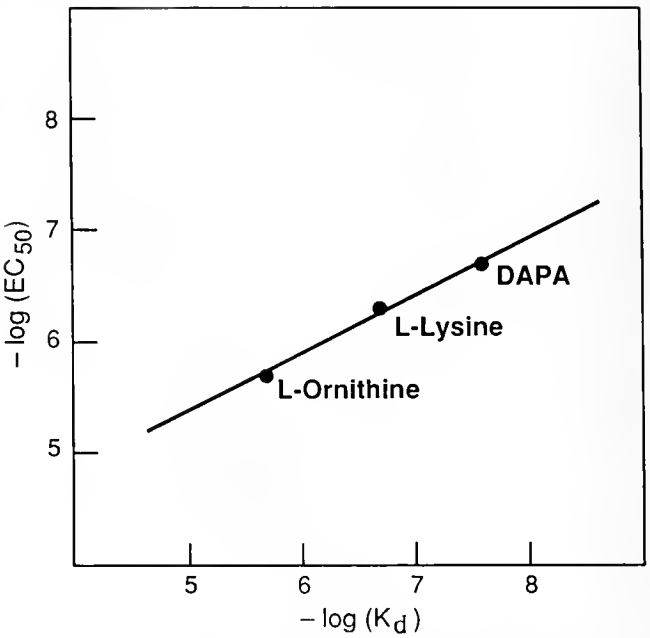

Figure 3. Comparison of the ciliary binding affinities of DAPA, L-lysine and L-ornithine to the relative biological effectiveness of these compounds as facilitators of the larval morphogenetic response. The apparent dissociation constants were determined by competition binding studies with [^{3}H]-L-lysine and analyses of data using the computer programs EBDA/LIGAND as described in Materials and Methods. The EC_{50} value is the concentration of diamino acid that produces 50% of the maximal amplification of the morphogenetic response induced by 0.1 μM GABA. This was determined using the biological assay of settlement and metamorphosis described in detail elsewhere (Trapido-Rosenthal and Morse, 1985).

Receptor coupled to G protein

We previously reported that cholera toxin and the nonhydrolyzable GTP analog 5'-guanylylimidodiphosphate (GppNHp), both activators of G proteins, facilitate the morphogenetic response of *Haliotis* larvae to GABA in a manner similar to that of the diamino acids, thus implicating G protein in this control (Baxter and Morse, 1987). Labeling with cholera toxin, which catalyzes ADP-ribosylation of susceptible G protein α subunits (Schleifer *et al.*, 1980), reveals this protein in the isolated cilia. A major polypeptide substrate for this reaction was found with an apparent molecular mass of 45 kDa (Baxter, 1991), in the range reported for the α subunits of cholera toxin-sensitive G proteins from a variety of sources (Schleifer *et al.*, 1980; Hurley *et al.*, 1984; Gilman, 1987). We show here that this ADP-ribosylation of the ciliary protein catalyzed by cholera toxin is stimulated as much as 10-fold by the nonhydrolyzable GTP analog, GppNHp, in a concentration-dependent manner (Fig. 4).

Direct activation of G protein in the cilia with GppNHp reciprocally affects the lysine receptors, increasing the K_d of the high affinity lysine receptor 17-fold, with little effect

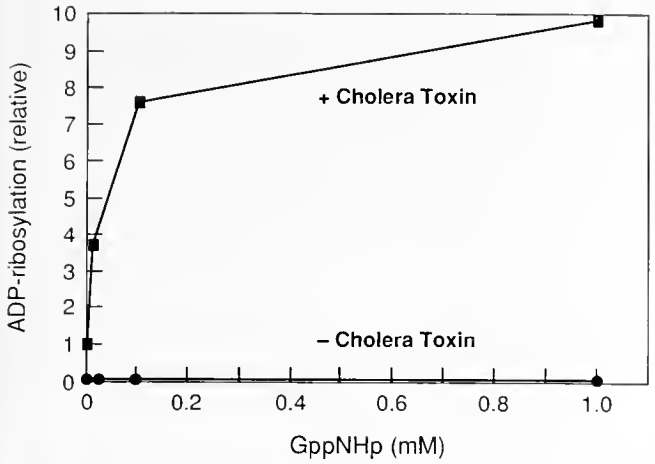

Figure 4. Stimulation of cholera toxin-dependent ADP-ribosylation by GppNHp. Isolated cilia were incubated with [^{32}P]-NAD in the presence and absence of 10 μg/ml cholera toxin and increasing concentrations of GppNHp. The treated cilia then were solubilized by boiling in SDS-PAGE sample buffer and proteins were separated on 10% SDS polyacrylamide gels followed by autoradiography. The values presented were determined from densitometric scans of the 45 kDa bands of the autoradiogram; relative ADP-ribosylation was normalized to ^{32}P-ADP-ribose incorporation in the absence of added GppNHp.

on total binding (Table I). Pretreatment of the cilia with cholera toxin produces a similar effect (14-fold increase in K_d; Table I). Thus we conclude that both GppNHp and cholera toxin, agents that facilitate the larval response *in vivo* (Baxter and Morse, 1987) and interact with a ciliary G protein *in vitro* (Fig. 4; *cf.* Baxter, 1991), reciprocally modulate the affinity of the ciliary lysine receptor *in vitro*.

Discussion

Facilitation and long-term potentiation

Lysine and its analogs facilitate the response of *Haliotis* larvae to low concentrations of morphogenetic stimuli, apparently increasing the sensitivity or output of the morphogenetic pathway without affecting the K_d or B_{max} of the receptors that bind the morphogenetic GABA analogs (Trapido-Rosenthal and Morse, 1985, 1986a, b; Morse, 1990). The receptors and signal transducers of the lysine-dependent regulatory or amplifier pathway prove to be distinct from those of the morphogenetic pathway (Baxter and Morse, 1987; Morse, 1990). In *Haliotis* larvae, the facilitation (amplification) of responsiveness to morphogenetic stimuli is long-lived, persisting for at least several days (Trapido-Rosenthal and Morse, 1986b). This facilitation is thus similar, both functionally and biochemically, to mechanisms of long-term potentiation and classical conditioning (learning) in other systems (*cf.* Greenberg *et al.*, 1987; Malenka *et al.*, 1987; Malinow *et al.*, 1989; Sweatt and Kandel, 1989; Nelson *et al.*, 1990). The possible adaptive significance of this system for the dual regulation of larval site-selection and metamorphosis by convergent chemosensory pathways may include the capacity for fine-tuning site selection behavior in response to chemical characteristics of the environment, with enhanced selection of sites for metamorphosis (irreversible commitment to a sessile habit) in potentially favorable areas (Trapido-Rosenthal and Morse, 1986b; Baxter and Morse, 1987; Morse, 1990).

Functional coupling of ciliary receptor and G protein

Evidence obtained *in vivo* demonstrated that the regulatory pathway is controlled by chemosensory receptors specific for lysine and lysine analogs, and that the lysine binding signal is transduced by a receptor-regulated G protein-dependent cascade (Baxter and Morse, 1987). The findings that (1) the effect of lysine binding is mimicked by G protein activators, including cholera toxin and GppNHp, and by PKC activators such as diacylglycerol, and (2) the facilitation by lysine is blocked by the G protein inhibitor, GDP-β-S, while facilitation by the direct PKC activator, diacylglycerol, is not inhibited, suggested that the facilitation by lysine is obligatorily transduced by a G protein, and that the action of diacylglycerol and PKC occur downstream from the GDP-β-S inhibitable G protein (Baxter and Morse, 1987). These observations thus indicated that the lysine receptor, G protein, and PKC act in a sequential cascade, possibly involving the G protein-dependent generation of the PKC-specific second messenger, diacylglycerol. Figure 5 schematically illustrates the suggested sequence of signal transduction events mediating the facilitation by lysine, and indicates the sites of activation and inhibition by the G protein effectors.

Cilia isolated from the larval epithelium contain sodium-independent receptors for lysine, and lysine binding to these receptors can be modulated by treatment of the cilia with G protein effectors. The sodium independence

Table I

Effect of G protein activators on lysine binding

	Treatment		
Parameter	Control	GppNHp	Cholera toxin
K_d (μM)	.07 ± .05	1.2 ± .05	1.0 ± 0.6
B_{max} (fmol/μg)	9.3 ± 2.9	9.5 ± 0.4	10.0 ± 1

Radioligand binding analyses were performed with cilia, and K_d and B_{max} values determined for the high affinity binding site by Scatchard analysis of the equilibrium binding data as described. Binding studies were performed in the presence and absence of 0.1 m*M* GppNHp and with cilia pretreated with cholera toxin and NAD, as described in Materials and Methods.

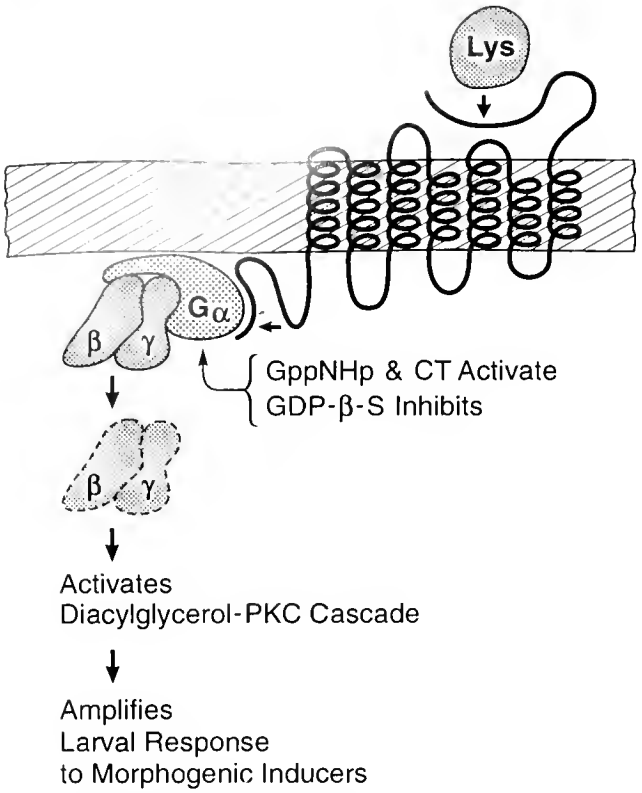

Figure 5. Schematic diagram of the hypothetical signal transduction pathway suggested to mediate the facilitation by lysine. Binding of lysine to an extracellular domain of the receptor protein (drawn here as a transmembrane protein) activates dissociation of the intracellular trimeric G protein. The released β and γ subunits of the G protein then activate the downstream cascade (apparently including a diacylglycerol-dependent activation of PKC) that results in the facilitation of larval settlement and metamorphosis. GppNHp and cholera toxin (CT) directly activate the G protein and mimic the facilitating effect of lysine. GDP-β-S inhibits the G protein and inhibits facilitation by lysine, but does not inhibit facilitation by diacylglycerol (*cf.* Baxter and Morse, 1987).

of the lysine receptors on the isolated cilia (Baxter, 1991) suggests that they may be true chemosensory receptors, as the binding of amino acids to transporters generally is sodium-dependent (Boge and Rigal, 1981; *cf.* Jaeckle and Manahan, 1989). Because the purified cilia are predominantly free of other cell structures, we can exclude the binding of lysine to synaptic receptors in this preparation.

Baxter (1991) first observed that cholera toxin-catalyzed labelling of the putative G protein α-subunit in the isolated cilia is stimulated significantly by the diamino acid receptor ligand lysine. This result, analogous to the direct increase in susceptibility to labelling caused by GppNHp (Fig. 4), suggests that the lysine receptor is functionally coupled to a cholera toxin-sensitive G protein in the purified cilia. Transmembrane receptors coupled to G proteins display a marked decrease in their affinity (increased K_d) for ligand in the presence of GTP analogs and other G protein activators (Stadel *et al.*, 1982). This effect is thought to result from the activation-induced dissociation of G protein from the receptor, reciprocally altering the receptor's binding affinity for ligand. Our observation of this effect on the ciliary lysine receptor in response to both GppNHp and cholera toxin (Table I), which interact with the ciliary G protein *in vitro* (Fig. 4) and can replace lysine as an amplifier of larval sensitivity to morphogen *in vivo* (Baxter and Morse, 1987), thus further supports the suggestion that the receptor is functionally coupled to a cholera toxin-sensitive G protein, and that the receptor and G protein reciprocally regulate one another. These results suggest that the lysine receptor on the larval cilia may be a member of the G-coupled transmembrane receptor superfamily (*cf.* Fig. 5).

G protein-dependent pathways of chemosensory signal transduction have been characterized in cilia from several vertebrates, including fish, amphibians, and mammals (Chen and Lancet, 1984; Pace *et al.*, 1985; Huque and Bruch, 1986; Pace and Lancet, 1986; Anholt *et al.*, 1987; Huque *et al.*, 1987; Jones and Reed, 1989). Other receptor-coupled G protein-dependent signal transduction cascades, similar to that involved in the lysine-stimulated amplifier pathway of the *Haliotis* larvae (Baxter and Morse, 1987), are common mediators of hormonal and other chemical signals controlling cell function and differentiation in a wide variety of systems, including mammals (Gilman, 1987; Freissmuth *et al.*, 1989; Bourne *et al.*, 1990).

Other similarities between larval and mammalian systems

Recently, cilia isolated from the *Haliotis* larvae have been found to contain mRNAs coding for two G protein α subunits. One is highly homologous to members of the G_q subfamily, while the other is closely related to the G_i/G_o group (Wodicka and Morse, 1991). It is striking that in the region of the deduced protein sequence corresponding to the two guanosine nucleotide binding domains, 50 of the 51 amino acid residues of the larval $G_q\alpha$ are identical to those in the protein from mammalian brain.

Other strong similarities have been found between receptor–transducer systems controlling neuronal activity and cellular differentiation in mammals and those controlling the settlement and metamorphosis of marine invertebrate larvae (Morse, 1985, 1990). The inducer recognized by the *Haliotis* larvae is a GABA-mimetic peptide produced by the algae on which the larvae are induced to settle (Morse and Morse, 1984). This peptide also binds strongly and specifically to GABA receptors purified from mammalian brain (H. Trapido-Rosenthal and A. N. C. Morse, in prep.). Similarly, we have found that the inducer of settlement and metamorphosis recognized by larvae of

the coral, *Agaricia humilis,* is a sulfated glycosaminoglycan that also is mitogenic for mammalian lymphocytes (Morse and Morse, 1991). Thus: (1) for larvae from two invertebrate phyla, the natural inducers of settlement and metamorphosis cross-react with mammalian receptors controlling cell proliferation, differentiation or function; and (2) the larval receptors and transducers thus far characterized in these pathways are functionally and structurally related to those in mammals. These findings suggest (beyond the probable evolutionary relatedness of the larval and mammalian systems) that characterization of the molecules controlling larval settlement and metamorphosis may point to the design of new regulators of mammalian cell function with usefulness in biotechnology and medicine.

Acknowledgments

This work was supported by grants from the National Institutes of Health (1-RO1-RR06640), the National Science Foundation (DCB87-18224), and the Neuroscience Institute of the University of California at Santa Barbara. We are grateful to Neal Hooker for production and cultivation of the *Haliotis* larvae.

Literature Cited

Anholt, R. R. H., S. M. Mumby, D. A. Stoffers, P. R. Girard, J. F. Kuo, and S. H. Snyder. 1987. Transduction proteins of olfactory receptor cells: identification of guanine nucleotide binding proteins and protein kinase C. *Biochemistry* **26:** 788–795.

Avenet, P., F. Hofmann, and B. Lindemann. 1988. Transduction in taste receptor cells requires cAMP-dependent protein kinase. *Nature* **331:** 351–354.

Baloun, A. J., and D. E. Morse. 1984. Ionic control of settlement and metamorphosis in larval *Haliotis rufescens* (Gastropoda). *Biol. Bull.* **167:** 124–138.

Barrowman, M. M., S. Cockcroft, and B. D. Gomperts. 1986. Two roles of guanine nucleotides in the stimulus-secretion sequence of neutrophils. *Nature* **319:** 504–507.

Baxter, G. 1991. Signal transduction controlling larval metamorphosis. Ph.D. Thesis, University of California, Santa Barbara. 87 pp.

Baxter, G., and D. E. Morse. 1987. G Protein and diacylglycerol regulate metamorphosis of planktonic molluscan larvae. *Proc. Natl. Acad. Sci. USA* **84:** 1867–1870.

Boge, G., and A. Rigal. 1981. Na^+-dependent amino acid transport by brush border membrane vesicles isolated from the intestine of a Mediterranean teleost (*Boops salpa*). *Biochem. Biophys. Acta* **649:** 455–461.

Bonar, D. B. 1978. Ultrastructure of a cephalic sensory organ in larvae of the gastropod *Phestilla sibogae*. *Tissue Cell* **10:** 153–165.

Bourne, H. R., D. A. Sanders, and F. McCormick. 1990. The GTPase superfamily: a conserved switch for diverse cell functions. *Nature* **348:** 125–132.

Bradford, M. A. 1976. A rapid sensitive method for the quantitation of microgram quantities of protein utilizing the principle of protein-dye binding. *Anal. Biochem.* **72:** 248–254.

Cavanaugh, G. M. 1956. *Formula and Methods IV of the Marine Biological Laboratory Chemical Room.* Marine Biol. Lab., Woods Hole, MA.

Chen, Z., and D. Lancet, 1984. Membrane proteins unique to vertebrate olfactory cilia: candidates for sensory receptor molecules. *Proc. Natl. Acad. Sci. USA* **81:** 1859–1863.

Ehlers, U., and B. Ehlers. 1978. Paddle cilia and discocilia—genuine structures? *Cell Tissue Res.* **192:** 489–501.

Freissmuth, M., P. J. Casey, and A. G. Gilman. 1989. G proteins control diverse pathways of transmembrane signaling. *FASEB J.* **3:** 2125–2131.

Gilman, A. G. 1987. G proteins: transducers of receptor generated signals. *Ann. Rev. Biochem.* **56:** 615–649.

Greenberg, S. M., V. F. Castellucci, H. Bayley, and J. H. Schwartz. 1987. A molecular mechanism of long-term sensitization in *Aplysia*. *Nature* **329:** 62–65.

Huque, T., and R. C. Bruch. 1986. Odorant-and guanine nucleotide-stimulated phosphoinositide turnover in olfactory cilia. *Biochem. Biophys. Res. Commun.* **137:** 36–42.

Huque, T., J. G. Brand, J. L. Rabinowitz, and D. L. Bailey. 1987. Phospholipid turnover in catfish barbel (taste) epithelium with special reference to phosphatidylinositol-4,5-bisphosphate. *Chem. Senses* **12:** 666–667.

Hurley, J. B., M. I. Simon, D. B. Teplow, J. D. Robishaw, and A. G. Gilman. 1984. Homologies between signal transducing G proteins and ras gene products. *Science* **226:** 860–862.

Jaeckle, W. R., and D. T. Manahan. 1989. Feeding by nonfeeding larvae: uptake of dissolved amino acids from seawater to lecithotrophic larvae of the gastropod *Haliotis rufescens*. *Mar. Biol.* **103:** 87–94.

Jones, D. T., and R. R. Reed. 1989. G_{olf}: An olfactory neuron specific-G protein involved in odorant signal transduction. *Science* **244:** 790–795.

Laemmli, U. 1970. Cleavage of structural proteins during assembly of the head of bacteriophage T4. *Nature* **227:** 680–685.

Malenka, R. C., D. V. Madison, and R. A. Nicoll. 1986. Potentiation of synaptic transmission in the hippocampus by phorbol esters. *Nature* **321:** 175–177.

Malinow, R., H. Schulman, and R. W. Tsien. 1989. Inhibition of postsynaptic PKC or CaMK II blocks induction but not expression of LTP. *Science* **245:** 862–865.

McCloskey, M. A. 1988. Cholera toxin potentiates IgE-coupled inositol phospholipid hydrolysis and mediator secretion by RBL-2H3 cells. *Proc. Natl. Acad. Sci. USA* **85:** 7260–7264.

McPherson, G. A. 1985. *Kinetic, EBDA, Ligand, Lowry. A Collection of Radioligand Binding Analysis Programs.* Elsevier Science Publishers. BV, UK.

Morse, A. N. C., and D. E. Morse. 1984. Recruitment and metamorphosis of *Haliotis rufescens* larvae are induced by molecules uniquely available at the surfaces of crustose red algae. *J. Exp. Mar. Biol. Ecol.* **75:** 191–215.

Morse, D. E. 1985. Neurotransmitter-mimetic inducers of settlement and metamorphosis of marine planktonic larvae. *Bull. Mar. Sci.* **37:** 697–706.

Morse, D. E. 1990. Recent progress in larval settlement and metamorphosis: closing the gaps between molecular biology and ecology. *Bull. Mar. Sci.* **46:** 465–483.

Morse, D. E., and A. N. C. Morse. 1991. Enzymatic characterization of the morphogen recognized by *Agaricia humilis* (scleractinian coral) larvae. *Biol. Bull.* **181:** 104–122.

Morse, D. E., H. Duncan, N. Hooker, A. Baloun, and G. Young. 1980. GABA induces behavioral and developmental metamorphosis in planktonic molluscan larvae. *Fed. Proc. Fed. Am. Soc. Exp. Biol.* **39:** 3237–3241.

Morse, D. E., N. Hooker, H. Duncan, and L. Jensen. 1979. γ-Aminobutyric acid, a neurotransmitter, induces planktonic abalone larvae to settle and begin metamorphosis. *Science* **204:** 407–410.

Nelson, T. J., C. Collin, and D. L. Alkon. 1990. Isolation of a G protein that is modified by learning and reduces potassium currents in *Hermissenda*. *Science* **247:** [illegible]

Pace, U., and D. Lancet. 19[illegible] ry GTP-binding protein: signal transducing polyper[illegible]rate chemosensory neurons. *Proc. Natl. Acad. Sci.* [illegible]-4951.

Pace, U., E. Hanski, [illegible]an, and D. Lancet. 1985. Odorant-sensitive adenylate cyclase may mediate olfactory reception. *Nature* **316:** 255–258.

Rothenberg, P. L., and C. R. Kahn. 1988. Insulin inhibits pertussis toxin-catalysed ADP-ribosylation of G proteins. *J. Biol. Chem.* **263.** 15546–15552.

Schleifer, L. S., J. C. Garrison, P. C. Sternweis, J. Northup, and A. G. Gilman. 1980. The regulatory component of adenylate cyclase from uncoupled S49 lymphoma cells differs in charge from the wild type protein. *J. Biol. Chem.* **255:** 2641–2644.

Short, G., and S. L. Tamm. 1991. On the nature of paddle cilia and discocilia. *Biol. Bull.* **180:** 466–474.

Stadel, J. M., A. DeLean, and R. J. Lefkowitz. 1982. Molecular mechanisms of coupling in hormone receptor-adenylate cyclase systems. *Adv. Enzymol.* **53:** 1–43.

Sweatt, J. D., and E. R. Kandel. 1989. Persistent and transcriptionally-dependent increase in protein phosphorylation in long-term facilitation of *Aplysia* sensory neurons. *Nature* **339:** 51–54.

Trapido-Rosenthal, H. G. 1985. Initial characterization of receptors for molecules that induce the settlement and metamorphosis of *Haliotis rufescens* larvae. Doctoral Dissertation, University of California, Santa Barbara, CA. 131 pp.

Trapido-Rosenthal, H., and D. E. Morse. 1985. L-α, ω-diamino acids facilitate GABA induction of larval metamorphosis in a gastropod mollusc (*Haliotis rufescens*). *J Comp. Physiol. B* **155:** 403–414.

Trapido-Rosenthal, H., and D. E. Morse. 1986a. Availability of chemosensory receptors is down-regulated by habituation of larvae to a morphogenetic signal. *Proc. Natl. Acad. Sci. USA* **83:** 1603–1607.

Trapido-Rosenthal, H. G., and D. E. Morse. 1986b. Regulation of receptor-mediated settlement and metamorphosis in larvae of a gastropod mollusc (*Haliotis rufescens*). *Bull. Mar. Sci.* **39:** 383–392.

Watson, M. R., and J. M. Hopkins. 1962. Isolated cilia from *Tetrahymena pyriformis*. *Exp. Cell Res.* **28:** 280–295.

Wodicka, L., and D. E. Morse. 1991. cDNA sequences reveal mRNAs for two Gα signal transducing proteins from larval cilia. *Biol. Bull.* **180:** 318–327.

Xuan, Y-T., Y-F. Su, K-J. Chang, and W. D. Watkins. 1987. A pertussis/cholera toxin sensitive G-protein may mediate vasopressin-induced inositol phosphate formation in smooth muscle cell. *Biochem. Biophys. Res. Comm.* **146:** 898–906.

Yool, A. J. 1985. Physiological analysis of the induction of metamorphosis in larvae of *Haliotis rufescens*. Doctoral Dissertation, University of California, Santa Barbara, CA. 111 pp.

Reference: *Biol. Bull.* **183**: 155–158. (August, 1992)

Guanylyl Cyclase: A Cell-Surface Receptor Throughout the Animal Kingdom

STEPHANIE SCHULZ

Howard Hughes Medical Institute and Department of Pharmacology, University of Texas Southwestern Medical Center, Dallas, Texas 75235-9050

Abstract. The enzyme guanylyl cyclase occurs in both soluble and membrane-associated forms, and catalyzes the formation of the second messenger cyclic GMP. The membrane forms of guanylyl cyclase encompass a family of cell-surface receptors that mediate the biological activity of a variety of peptide ligands. Representatives of this receptor family have been identified in such diverse species as rats and sea urchins. In echinoderm spermatozoa, guanylyl cyclase is a receptor for egg-associated peptides, eliciting species-specific effects, including changes in sperm respiration and motility, and a chemotactic response. In mammals, the family of guanylyl cyclases includes receptors for natriuretic peptides, as well as the target of bacterial heat-stable enterotoxins. The identification of natriuretic peptides in amphibians, birds, and fish suggests that guanylyl cyclase receptors play a role in osmotic balance in a variety of organisms. Molecular cloning evidence implies that homologs of the mammalian guanylyl cyclase receptors exist in other vertebrates, and perhaps even in invertebrates. Guanylyl cyclases thus represent an example of receptors that have diversified to serve both as external chemoreceptors and as internal hormone receptors.

Introduction

The production of cyclic GMP, an intracellular second messenger, is catalyzed by guanylyl cyclases. This enzyme family includes both soluble and particulate forms, and is widely distributed in various cell types throughout the animal kingdom. The soluble and particulate forms of the enzyme are distinctly different in both their structure and their mode of regulation. The soluble enzyme is a heterodimer composed of α and β subunits; tissue-specific isoforms of each subunit are known to exist (Schulz *et al.*, 1991). The activity of the soluble enzyme is regulated by diffusable substances, nitric oxide for example (Schulz *et al.*, 1991). The particulate enzyme, in contrast, is monomeric (although the active conformation may be multimeric), with a single transmembrane domain (Yuen and Garbers, 1992). A variety of studies have demonstrated that members of the particulate guanylyl cyclase family are receptors for such diverse ligands as echinoderm egg peptides, natriuretic peptides, and *Escherichia coli* heat-stable enterotoxin. Cyclic GMP generated in response to such stimuli is implicated in the regulation of ion channel function, and the modulation of cyclic nucleotide-dependent phosphodiesterase and protein kinase activity. This review will focus on the current understanding of the receptor guanylyl cyclases in mammals, and their counterparts in other species.

Received 24 April 1992; accepted 29 May 1992.

Receptor Guanylyl Cyclases in Echinoderms

Particulate guanylyl cyclase was first characterized in, and purified from, the spermatozoa of sea urchins. This cell type is a rich source of the particulate form of the enzyme, and apparently contains no soluble enzyme. Studies of sea urchin spermatozoa were among the first to suggest that guanylyl cyclase might serve as a receptor for extracellular signals. Peptides were purified from sea urchin egg-conditioned medium that would elicit several biochemical and behavioral changes in spermatozoa of the homologous species. Exposure of spermatozoa to the peptides resact or speract (purified from *Arbacia punctulata* or *Strongylocentrotus purpuratus*, respectively, Table 1) increases respiration and motility, elevates intracellular pH, alters ion fluxes, and elevates cyclic nucleotide levels (Garbers, 1989). In addition, resact is a potent chemoattractant for *Arbacia* spermatozoa (Ward *et al.*, 1985). Crosslinking studies demonstrated that resact apparently

Table I

Amino acid sequences of peptides known to activate particulate guanyly cyclases. Longer circulating forms of brain and C-type natriuretic peptide have been identified

I. Atrial Natriuretic Peptide	
Human/Porcine	S L R R S S C F G G R M D R I G A Q S G L G C N S F R Y
Rat	S L R R S S C F G G R I D R I G A Q S G L G C N S F R Y
Eel	S K S S S P C F G G K L D R I G S Y S G L G C N S R K
Bullfrog	S S D C F G S R I D R I G A Q S G M G C – G R R F
II. Brain Natriuretic Peptide	
Human	S P K M V Q G S G C F G R K M D R I S S S S G L G C K V L R R H
Porcine	S P K T M R D S G C F G R R L D R I G S L S G L G C N V L R R Y
Rat	N S K M A H S S S C F G Q K I D R I G A V S R L G C D G L R L F
Chicken	M M R D S G C F G R R I D R I G S L S G M G C N G S R K N
III. C-Type Natriuretic Peptide	
Porcine	G L S K G C F G L K L D R I G S M S G L G C
Killifish	G W N R G C F G L K L D R I G S M S G L G C
Eel	G W N R G C F G L K L D R I G S L S G L G C
IV. Heat-Stable Enterotoxins and Gastrointestinal Peptides	
Guanylin	P N T C E I C A Y A A C T G C
Escherichia coli ST_h	N S S N Y C C E L C C N P A C T G C Y
Escherichia coli ST_p	N T F Y C C E L C C N P A C A G C Y
Yersinia enterocolitica ST	V S S D W D C C D V C C N P A C A G C
Vibrio cholerae non-01 ST	I D C C E I C C N P A C F G C L N
V. Echinoderm Egg Peptides	
Speract (*Strongylocentrotus purpuratus*)	G F D L N G G G V G
Resact (*Arbacia punctulata*)	C V T G A P G C V G G G R L – NH_2
Mosact (*Clypeaster japonicus*)	D S D S A Q N L I G

binds to a 160,000 molecular weight protein that was shown to be guanylyl cyclase (Shimomura *et al.*, 1986). Speract, on the other hand, could be crosslinked to a 77,000 molecular weight protein (Dangott *et al.*, 1989). The relationship between the two crosslinked binding proteins is unclear, because both sea urchin species contain both proteins. The functional receptor may be composed of multiple subunits, only one of which is labeled by chemical crosslinking. The respective guanylyl cyclases and 77 kDa proteins have been cloned from both *Arbacia* and *Strongylocentrotus* (Singh *et al.*, 1988; Dangott *et al.*, 1989; Thorpe and Garbers, 1989; L. J. Dangott, pers. comm.). However, none of the clones conferred peptide binding or cyclase activity upon transfected mammalian cells. Incorrect processing of echinoderm transcripts may be responsible for the lack of functional expression in COS cells, or both proteins may be necessary for the expression of a peptide-binding complex.

Receptor Guanylyl Cyclases in Mammals

The cloning of sea urchin guanylyl cyclase provided a valuable probe for cloning mammalian forms of the enzyme. The amino acid sequence predicted by the sea urchin guanylyl cyclase cDNA contained a single putative transmembrane domain, suggesting a topography like that of the growth factor receptors: an extracellular ligand binding domain, and an intracellular regulatory/catalytic domain. The cDNA encoding the intracellular, presumably conserved, regulatory/catalytic domain was used as a probe to screen various cDNA libraries, and the first mammalian guanylyl cyclase (GC-A) was cloned from rat and human (Chinkers *et al.*, 1989; Lowe *et al.*, 1989). Reports in the literature had demonstrated the stimulation of guanylyl cyclase activity by atrial natriuretic peptide (ANP), and the copurification of ANP binding and guanylyl cyclase activities (reviewed in Schulz *et al.*, 1989a). Expression of cloned GC-A allowed direct testing of the hypothesis that guanylyl cyclase was an ANP receptor, and this was shown to be the case (Chinkers *et al.*, 1989; Lowe *et al.*, 1989). A number of natriuretic peptides have now been discovered, and the cloning of a second mammalian guanylyl cyclase (GC-B) has demonstrated the diversity within this receptor-enzyme family (Chang *et al.*, 1989; Schulz *et al.*, 1989b). GC-B also binds and is activated by natriuretic peptides. But although GC-A preferentially binds and responds to ANP, GC-B preferentially responds to C-type natriuretic peptide (CNP) (Koller *et al.*, 1991). Whether additional natriuretic peptide receptors exist is not yet known, but the existence of brain natriuretic peptide (BNP) suggests that at least one additional member of the family remains to be identified.

Heat-stable enterotoxins (ST) produced by several strains of pathogenic bacteria have long been known to

Table II

Alignment of partial-length guanylyl cyclase-receptor sequences with the homologous regions of the mammalian natriuretic and heat-stable enterotoxin receptors

Speract Receptor	AYMLVSGLPLRNGDRHAGQIASTAHHLLESVKGFIVPHKPRVFLKLRIGIHSGSGVAGVVGLT
Natriuretic Peptide and Related Receptors	
Rat GC-A	AYMVVSGLPVRNGQLHAREVARMALALLDAVRSFRIRHRPQEQLRLRIGIHTGPVGAGVVGLK
Rat GC-B	AYMVVSGLPGRNGQRHAPEIARMALALLDAVSSFRIRHRPHDQLRLRIGVHTGPVCAGVVGLK
Fish	AYMVVSGLPVRNGKLHAREIAGMSLALLEQVKTFKIRLRPNDQLRLRIGIHTGP
Xenopus	AYMVVSGLPVRNGKLHAREIARMSLALLDAVKSFKIRHRPDQQLGLRIGI
Sea urchin	AYMCVSGLPIRNGDFHAREIARMSLALLHEITSFRIRHRPEERLRLRIGVHTG
Earthworm	AYMVVSGLPVRNGKLHAREIARMSLALLDAVRSFKIRHRPNQQLRLRIGIHTGPVCAGVVGLK
Heat-Stable Enterotoxin and Related Receptors	
Rat GC-C	AYVVASGLPMRNGNRHAVDISKMALDILSFMGTFELEHLPGLPVWIRIGVHSGPCAAGVVGIK
Fish	AYMVASGLPKRNGDRHAVDIALMALDMLAGVGTFELQHLPGIPLWIRIGVHSGPGAAGVVGNK
Xenopus	AYMVVSGLPNRNGNNHAVDISRMALDILCFMGSFELRHLPGLPVWIRIGIHSGPCAAGVVGIK

Sequences obtained using the polymerase chain reaction. The degenerate primers were used in the PCR to amplify amino acids 894-956, 890-952, and 854-916 in the catalytic domains of GC-A, GC-B, and GC-C, respectively.

increase the activity of a particulate guanylyl cyclase in the intestinal brush-border. Elevated cyclic GMP is correlated with increased intestinal secretion, which results in the diarrhea associated with enterobacterial infection (Field *et al.*, 1978). Reports in the literature suggested that toxin binding and guanylyl cyclase activities reside in separate molecules, but chromatographic separation of the two activities was not complete. To determine whether a guanylyl cyclase is the ST receptor, degenerate primers were designed based on conserved sequences in the catalytic domain of all cloned guanylyl cyclases. These primers were used in the polymerase chain reaction (PCR) to amplify guanylyl cyclase sequences in the cDNA from rat small intestine. A new member of the cyclase family (GC-C) was identified by this method, and its cDNA subsequently cloned (Schulz *et al.*, 1990). GC-C conferred both ST binding and guanylyl cyclase activity on transfected COS cells (Schulz *et al.*, 1990). Recently, a 15 residue peptide, guanylin, was purified from acid extracts of rat small intestine (Currie *et al.*, 1992). Guanylin is 47% identical with the active portion of ST, and elevated cyclic GMP levels in T84, an intestinal cell-line rich in GC-C (Currie *et al.*, 1992). While the effects of guanylin on cloned GC-C have not yet been assessed, this peptide may, in fact, be its endogenous ligand.

Guanylyl Cyclase-Linked Receptors in Other Organisms

Natriuretic peptides have been identified in such diverse organisms as amphibians, fish, and birds (Table I), suggesting that receptors for these ligands are also present throughout the animal kingdom. We have used a PCR approach to identify guanylyl cyclases in a variety of species representing several phyla. RNA was prepared from various tissues of frog, fish, sea urchin, and earthworm. RNA was reverse transcribed to cDNA which was used as a PCR template with degenerate primers similar to those used to identify GC-C. These primers amplify a 250 base pair region in the highly conserved cyclase catalytic domain. Natriuretic peptide receptor-like sequences (homology > 70%) were amplified from frog, fish, and sea urchin; sequences homologous with GC-C were amplified from frog and fish (Table II). Additional sequences with homology to the membrane guanylyl cyclases, but with no strong homology to any particular receptor type, were amplified from both sea urchin and fish. Additional members of the receptor family may yet remain to be identified in mammals. Several guanylyl cyclase sequences were also amplified from earthworm. Although none of these sequences was strongly homologous with a particular mammalian cyclase, they were clearly of the membrane, rather than of the soluble type. An ANP-like peptide has been identified in earthworm heart by immunological cross-reactivity with mammalian ANP (Vesely and Giordano, 1992). This suggests that a homolog of GC-A may exist in invertebrates outside the Deuterostomia. Crustacean hyperglycemic hormone (CHH) seems to activate membrane guanylyl cyclase (Goy, 1990). CHH is a large peptide without apparent sequence homology to the natriuretic peptides or guanylin, although it does contain multiple cysteine residues. Thus, the Protostomia may have evolved an independent set of guanylyl cyclase receptors and ligands.

Summary

Guanylyl cyclase is a receptor for diverse intracellular and extracellular signalling molecules. A growing body of evidence suggests that multiple forms of this receptor-enzyme exist throughout the animal kingdom. Some receptor types are apparently conserved across species, oth-

ers may be unique. Studying the interaction between the guanylyl cyclases and their respective ligands will be valuable in defining the role of cyclic GMP in cellular function.

Acknowledgments

I am grateful to David L. Garbers in whose laboratory this work was done. I thank Cecelia Green and Rustico Ramos for performing the PCR and sequence analysis of the fish, frog, earthworm, and sea urchin samples.

Literature Cited

Chang, M. S., D. G. Lowe, M. Lewis, R. Hellmiss, E. Chen, and D. V. Goeddel. 1989. Differential activation by atrial and brain natriuretic peptides of two different receptor guanylate cyclases. *Nature* **341:** 68–72.

Chinkers, M., D. L. Garbers, M. S. Chang, D. G. Lowe, H. Chin, D. V. Goeddel, and S. Schulz. 1989. A membrane form of guanylate cyclase is an atrial natriuretic peptide receptor. *Nature* **338:** 78–83.

Currie, M. G., K. F. Fok, J. Kato, R. J. Moore, F. K. Hamra, K. L. Duffin, and C. E. Smith. 1992. Guanylin: an endogenous activator of intestinal guanylate cyclase. *Proc. Natl. Acad. Sci. USA* **89:** 947–951.

Dangott, L. J., J. E. Jordan, R. A. Bellet, and D. L. Garbers. 1989. Cloning of the mRNA for the protein that crosslinks to speract. *Proc. Natl. Acad. Sci. USA* **86:** 2128–2132.

Field, M., L. H. Graf Jr., W. J. Laird, and P. L. Smith. 1978. Heat-stable enterotoxin of *Escherichia coli*: *in vitro* effects on guanylate cyclase activity, cyclic GMP concentration, and ion transport in small intestine. *Proc. Natl. Acad. Sci. USA* **75:** 2800–2804.

Garbers, D. L. 1989. Molecular basis of fertilization. *Annu. Rev. Biochem.* **58:** 719–742.

Goy, M. F. 1990. Activation of membrane guanylyl cyclase by an invertebrate peptide hormone. *J. Biol. Chem.* **265:** 20220–20227.

Koller, K. J., D. G. Lowe, G. L. Bennett, N. Minamino, K. Kangawa, H. Matsuo, and D. V. Goeddel. 1991. Selective activation of the B natriuretic peptide receptor by C-type natriuretic peptide (CNP). *Science* **252:** 120–123.

Lowe, D. G., M. S. Chang, R. Hellmiss, E. Chen, S. Singh, D. L. Garbers, and D. V. Goeddel. 1989. Human atrial natriuretic peptide receptor defines a new paradigm for second messenger signal transduction. *EMBO J.* **8:** 1377–1384.

Schulz, S., M. Chinkers, and D. L. Garbers. 1989a. The guanylate cyclase/receptor family of proteins. *FASEB J.* **3:** 2026–2035.

Schulz, S., C. K. Green, P. S. T. Yuen, and D. L. Garbers. 1990. Guanylyl cyclase is a heat-stable enterotoxin receptor. *Cell* **63:** 941–948.

Schulz, S., S. Singh, R. A. Bellet, G. Singh, D. J. Tubb, H. Chin, and D. L. Garbers. 1989b. The primary structure of a plasma membrane guanylate cyclase demonstrates diversity within this new receptor family. *Cell* **58:** 1155–1162.

Schulz, S., P. S. T. Yuen, and D. L. Garbers. 1991. The expanding family of guanylyl cyclases. *TIPS* **12:** 116–120.

Shimomura, H., L. J. Dangott, and D. L. Garbers. 1986. Covalent coupling of a resact analogue to guanylate cyclase. *J. Biol. Chem.* **261:** 15778–15782.

Singh, S., D. G. Lowe, D. S. Thorpe, H. Rodriguez, W. J. Kuang, L. J. Dangott, M. Chinkers, and D. L. Garbers. 1988. Membrane guanylate cyclase is a cell-surface receptor with homology to protein kinases. *Nature* **334:** 708–712.

Thorpe, D. S., and D. L. Garbers. 1989. The membrane form of guanylate cyclase: homology with a subunit of the cytoplasmic form of the enzyme. *J. Biol. Chem.* **264:** 6545–6549.

Vesely, D. T., and A. T. Giordano. 1992. The most primitive heart in the animal kingdom contains the atrial natriuretic peptide hormonal system. *Comp. Biochem. Physiol.* **101C:** 325–329.

Ward, G. E., C. J. Brokaw, D. L. Garbers, and V. D. Vacquier. 1985. Chemotaxis of *Arbacia punctulata* spermatozoa to resact, a peptide from the egg jelly layer. *J. Cell Biol.* **101:** 2324–2329.

Yuen, P. S. T., and D. L. Garbers. 1992. Guanylyl cyclase-linked receptors. *Annu. Rev. Neurosci.* **15:** 193–225.

Reference: *Biol. Bull.* **183:** 159–164. (August, 1992)

Conus Peptides: Phylogenetic Range of Biological Activity

LOURDES J. CRUZ[1,2], CECILIA A. RAMILO[1]*, GLORIA P. CORPUZ[1], AND BALDOMERO M. OLIVERA[2]

[1]*Marine Science Institute, University of the Philippines, Diliman, Quezon City 1101, Philippines, and* [2]*Department of Biology, University of Utah, Salt Lake City, Utah, 84112*

Abstract. The major function of the venoms of the predatory marine snails belonging to the genus *Conus* is to paralyze prey. Thus, the venom of each *Conus* species acts on receptors and ion channels of the prey; previous studies suggested much less activity on homologous receptor targets in more distant taxa. In this article, we address the question of whether some peptide components of *Conus* venoms ("conopeptides") have "cross-phylum" biological activity.

We examined the venom of *Conus textile*, a mollusk-hunting *Conus*, using a mammalian biological activity assay. We purified a 23 amino acid "convulsant peptide" with potent activity in the mammalian CNS, even though it comes from the venom of a snail-hunting *Conus* species. A survey of *Conus textile* venom fractions indicates that, in addition to the convulsant peptide, many other components of this venom will exhibit "cross-phylum" biological activity. Conopeptides with broad-range phylogenetic specificity should be useful tools for studying the evolution of receptors and ion channels, and of nervous systems.

Introduction

The small peptides present in the venoms of the predatory marine snails that belong to the genus *Conus* (cone snails) are proving to be of great interest in molecular neuroscience. This large and diverse family of highly constrained peptides ("conopeptides") are 10–30 amino acids in length and exhibit exquisite specificity towards cell surface receptors and ion channels (for recent overviews see Olivera *et al.*, 1990, 1991). Some of the peptides are now choice research tools in neurobiology. Because they are relatively rigid, their three-dimensional structures can be determined; the structures of several conopeptides have been solved by multidimensional NMR techniques. Given their small size and constrained conformation, the *Conus* peptides have great potential as lead compounds for drug development.

In this introduction, we will briefly review the biology and biochemistry of conopeptides. Furthermore, we describe results on a peptide that has "cross-phylum" biological activity. Such conopeptides may be useful tools for examining how certain receptors and ion channels have been used by various phyla in the course of evolution.

Biology and biochemistry of conopeptides

The cone snails are believed to be the most venomous of all molluscs. Many human fatalities have been caused by cone snail envenomation. There are about 500 *Conus* species; all are predators, and all use venom as the primary means for subduing prey. The venom is injected into the prey with a hollow harpoon-like tooth. The species of *Conus* can be divided into three major groups on the basis of the animals they feed on, *i.e.*, the worm-hunting, mollusk-hunting and fish-hunting Conidae. The venom of at least one species of each of these groups has been analyzed.

A major factor that contributes to the success of *Conus* is the remarkable biochemistry of their venoms. The biologically active components of *Conus* venoms are an exceptionally diverse family of small, conformationally constrained peptides. A single *Conus* venom may well have over fifty different such peptides, with varied pharmacological specificities. From the numerous peptides that have been purified from various *Conus* species, certain general concepts have emerged.

Each natural conopeptide appears to be specifically targeted to a macromolecular receptor, interfering with its

Received 7 April 1992; accepted 29 May 1992.

* Present address: Department of Chemistry, Washington State University, Pullman, Washington.

normal function. The conopeptides can have very high affinity for their receptors; ω-conotoxin GVIA, for example, targets to neuronal voltage-sensitive calcium channels and has picomolar affinities for the high affinity targets. The high affinity and specificity of conopeptides is dependent on their highly constrained, relatively rigid conformations. In the majority of conopeptides, Cys residues, which are involved in forming multiple disulfide bonds, constitute 20–50% of all amino acids (for an overview, see Olivera *et al.*, 1990).

Peptides in the size range of the conopeptides would not normally have a specific conformation, but would equilibrate between many alternative conformations under physiological conditions. Usually, about 50 amino acid residues would be required before a polypeptide assumed a specific conformation. The sum of noncovalent forces (hydrogen bonds, hydrophobic interactions, and the like) in a small peptide are insufficient to stabilize a single conformation. But in most conopeptides the covalent crosslinking through multiple disulfide bonding presumably stabilizes the biologically active conformation. Indeed, conopeptides have some of the highest known densities of disulfide bonding found in any biological system; one 12 amino acid peptide isolated from a *Conus* venom has three disulfide bonds (see Olivera *et al.*, 1990).

A recent examination of cDNA clones encoding various conopeptides has revealed how the cone snails may have evolved the complex pharmacological cocktails of conopeptides that are their venoms. As will be described elsewhere (D. R. Hillyard, unpub. results), an "antibody-like evolutionary strategy" probably generated the array of small *Conus* peptides with diverse ligand specificity, but relatively conserved folding pathways and structural frameworks. The net result is that every species has its own characteristic mixture of peptides, and this conopeptide cocktail is highly potent on the particular prey type on which the species specializes. Thus, not only has a rather unusual biochemical strategy been used for paralyzing prey (*i.e.*, small, highly constrained peptides), but to generate the wide diversity of peptides in cone snail venom, a novel genetic and evolutionary strategy is employed by the genus as well.

Phylogenetic specificity of conopeptides

Pharmacological experiments carried out on crude venom by Endean and Rudkin (1963 and 1965) revealed that venom samples from *Conus* species that specifically prey on fish had no effect on mollusks or worms, and vice versa. These early studies suggested that the venom of a particular *Conus* species is presumably strongly selected to act on protein targets in the prey, and that the more unrelated the taxa to the prey, the more unlikely that it would have targets for the biologically active components in the venom.

Studies of individually isolated conopeptides have supported this general picture of the phylogenetic specificity of *Conus* venoms. A conopeptide from the venom of a particular species is generally specific for targets in the phylum to which the prey belongs. The conopeptides from the fish-hunting *Conus* venoms have been particularly well studied. Although in all cases specifically tested, the peptides have been inactive in invertebrate systems, they vary in how broadly they act. For example, α-conotoxins GI and MI from *Conus geographus* and *magus*, respectively, are broadly active in vertebrate systems, and appear to act at nicotinic acetylcholine receptors, not only in fish, but also in all mammalian systems tested. In contrast, α-conotoxin SI seems much more phylogenetically narrow in its biological activity: this peptide will inhibit nicotinic acetylcholine receptors in fish and in elasmobranchs (*Torpedo*), but its activity in mammalian systems is orders of magnitude less. Although the sequence changes are not very great, there are apparently strikingly different conformations assumed by these two peptides (Pardi *et al.*, 1990; Christensen *et al.*, 1991). The ω-conotoxins and μ-conotoxins, which target voltage-sensitive calcium channels and sodium channels, respectively, are also inactive in invertebrate systems. Considerable variation in the activity of the ω-conotoxins in different vertebrate systems has also been observed (see Ramilo *et al.*, 1992).

Thus, the general view of *Conus* venoms and conopeptides from studies on the fish-hunting species is that the agents to be found are likely to be vertebrate-specific. The studies on crude venoms suggest that worm-hunting species are likely to have conopeptides specific to annelids, and snail-hunting cones are likely to have conopeptides that are mollusk-specific. The one invertebrate-specific peptide tested so far, the King-Kong (KK) peptide from the snail-hunting species, *Conus textile*, is inactive in mammalian systems (Hillyard *et al.*, 1989).

However, peptides with broad phylogenetic specifity are desirable as tools for investigating the role of their receptor targets over a long period of evolutionary time. The present evidence from cloning suggests that most receptors and ion channels evolved early in eukaryotic evolution, and are widely used by all of the higher eukaryotic taxa. If a highly specific peptide ligand were able to inhibit the activity of such a receptor over a broad range of different phyla, the various uses to which that cell surface receptor had been put in the different taxa could be much more easily investigated. Thus, it is of interest to determine whether there are any conopeptides that have a broader specificity than those already characterized. In this article, we will show that a significant complement of conopeptides probably exhibit broad phylogenetic specificity.

Materials and Methods

Materials

Specimens of *Conus textile* were collected from the sea around the islands of Marinduque, Philippines. Venom

was extracted from the specimens as described previously (Cruz *et al.*, 1976).

Preparation of the venom extract

About one gram of the lyophilized venom was suspended in 10 ml of 1.1% acetic acid, placed on ice for 10 min with occasional stirring, then centrifuged at 12,000 × *g* in a Sorvall refrigerated centrifuge. The residue was extracted twice with 5 ml 1.1% acetic acid. Each time, the suspension was sonicated seven times at 65 watts (Sonifier, Heat Systems Ultrasonics, Inc.) for 10 s at 15-s intervals before centrifugation. The supernates were pooled and lyophilized.

Gel filtration chromatography

Lyophilized venom extract was dissolved in 5 ml of 1.1% acetic acid. The dissolved extract was chromatographed at 4°C on a column (110 × 2.5 cm) of Sephadex G-25 (fine), with 1.1% HAc as the eluent. The fractions corresponding to the chromatographic peaks were pooled, lyophilized, bioassayed, and stored at −20°C for further separation by HPLC.

High performance liquid chromatography

The lyophilized Sephadex G-25 fraction was redissolved in 2.0 ml of 0.1% trifluoroacetic acid (TFA), filtered, then chromatographed in several batches on a semi-preparative C18 column (TSK-ODS 120T, 7.8 × 300 mm, fully capped, 10 μm particle size). Subsequent fractionations were done on an analytical VYDAC reverse-phase C_{18} column (4.6 × 250 mm, 5 μm) and a Brownlee Spheri-5 ODS column (4.6 × 220 mm, 5 μm). The solvent system used for all HPLC runs consisted of 0.1% TFA as buffer A, and 0.1% TFA in 60% acetonitrile as buffer B.

Amino acid analysis

Peptide samples were hydrolyzed *in vacuo* with 6 *N* HCL/1% phenol for 18 h at 105°C. Amino acid analysis was done by reverse-phase HPLC of phenylthiocarbamyl derivatives (Bidlingmeyer *et al.*, 1984; Heinrikson and Meredith, 1984).

Peptide sequencing

The purified convulsant peptide was reduced and carboxymethylated as previously described (Cruz *et al.*, 1987) and then analyzed in a spinning-cup sequencer according to the method of Tarr *et al.* (1978). Phenylthiohydantoin derivatives were identified by HPLC using a gradient slightly modified from that of Hunkapiller and Hood (1978).

Results

Assay of a venom from a snail-hunting Conus *species for mammalian activity*

To examine whether components of a particular *Conus* venom are restricted in their activity to the phylum of its prey, we investigated the biological activities present in the venom of *Conus textile*. *Conus textile* is a common molluscivorous cone, and is one of the more highly successful large species in the genus. It is widely distributed from the Hawaiian Islands to the Red Sea, and is abundant in much of the Indo-Pacific. This species is of particular interest because it has been reported to be fatal to humans. However, when the venom was initially examined by Endean and Rudkin (1963), they did not find that it was active when tested in vertebrate systems.

We decided to re-examine the activity of *Conus textile* venom components for activity on mammalian receptors. Our laboratory has developed a sensitive assay for conopeptides that display activity in mammals. Direct injection of a venom component into the central nervous system of mice (i.c. injection) has proven to be an effective method for identifying vertebrate-active components (see Olivera *et al.*, 1990). The components of *Conus textile* venom were therefore assayed by i.c. injection into mice.

In this assay, both crude *Conus textile* venom, and all crude fractions assayed, had potent activity when injected intra-cranially into mice. Crude *Conus textile* venom causes seizure-like symptoms and death in mice. To determine the identity of a vertebrate-active component of the venom, we purified and characterized one venom component using biological activity in the mouse CNS as an assay.

Purification and characterization of a convulsant peptide from Conus textile *venom*

Conus textile venom was first fractionated according to size, as shown in Figure 1A. A major peptide fraction was then subfractionated by reverse-phase HPLC as shown in Figure 1B. The earliest eluting fraction from the first HPLC column caused paralysis and death in mice. This fraction was then rerun on reverse-phase HPLC. Two fractions in Figure 1C characteristically caused sudden jumping activity shortly after injection, and this was followed by convulsions, stretching of limbs, and jerking behavior. After these initial symptoms, the mouse would lie on its side and after approximately 25 min would tend to recover from the most severe symptoms. This general type of behavior was elicited by more than one peak in the chromatogram in Figure 1C, but only the indicated peak was further purified to homogeneity. Further HPLC purification finally yielded a homogeneous peptide with a convulsant activity (Fig. 1D). There may be, however, several isoforms of the convulsant peptide in *Conus textile* venom; this is being further investigated.

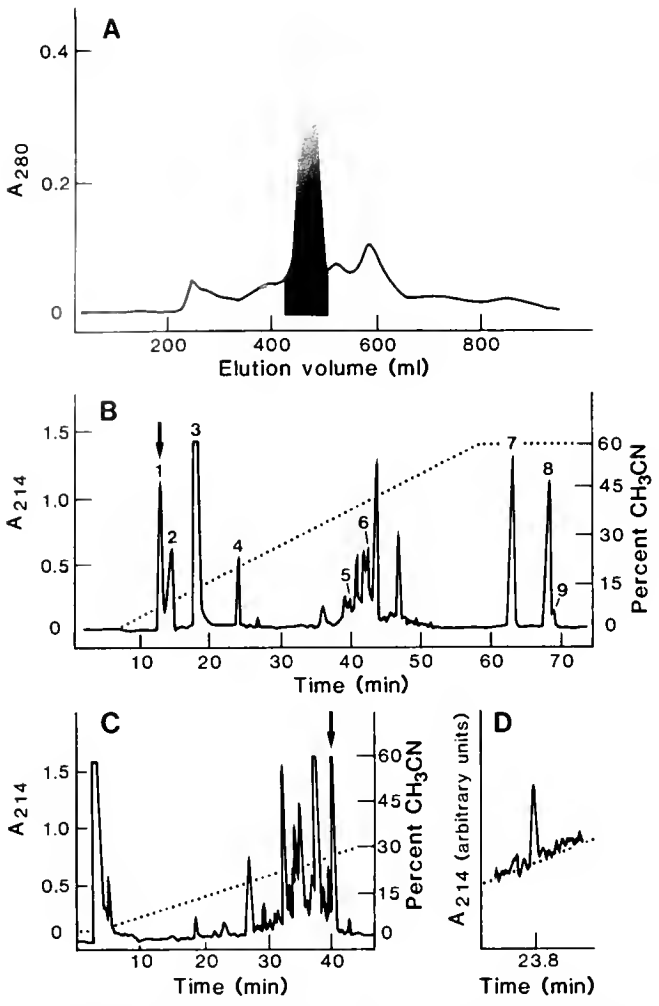

Figure 1. Purification of a convulsant peptide from *Conus textile* venom. Details of the procedure are described in Materials and Methods. (A) Column chromatography of crude venom extract on Sephadex G-25 with 1.1% acetic acid as eluent. (B) HPLC of pooled fractions from the shaded peak of Panel A on semi-preparative reversed phase C18 column at a gradient of 1.2% CH_3CN/min in 0.1% TFA. (C) The peak indicated by an arrow in B was further fractionated by HPLC on an analytical C18 column at 0.6% CH_3CN/min in 0.1% TFA. The peak corresponding to the convulsant peptide is indicated by an arrow. This was rerun on HPLC to remove impurities. (D) HPLC of purified convulsant peptide on a Brownlee C18 column using a 0.6% CH_3CN/min gradient in 0.1% TFA (23.8 min corresponds to 29.3% CH_3CN). The peaks indicated by numbers in panel B produced the following behavioral effects when injected intracranially in two-week old mice: (1) twitching, jerking, and paralysis; (2) jerking and stretching; (3) hyperactivity followed by weakness; (4) circular motion and jerking; (5) jumping, jerking, and running; (6) scratching and hyperactivity; (7) jumping and circular motion; (8) stretching; and (9) running and rolling over. Peaks 1, 3, 5, 6 and 9 are lethal.

The purified peptide was then subjected to amino acid analysis, as well as Edman sequencing. The results of these analyses are shown in Table I. The data are consistent with the convulsant peptide being a 23 amino acid peptide with the sequence:

NCPYCVVYCCPPAYCEASGCRPP.

To confirm the sequence and to determine whether the peptide was blocked at the carboxyl terminus, a fast atom bombardment (FAB) mass spectrometric analysis was carried out. The observed mass value of the convulsant peptide was 2487.90 mass units. The calculated value, if the peptide were amidated at the C-terminus, is 2487.95. These data therefore confirm the peptide sequence given

Table I

Determination of the primary structure of the convulsant peptide

A. Amino acid analysis

Amino acid*	pmol	Mole ratio**
Asp	57.9	0.7 (1)
Glu	149.9	1.9 (1)
Ser	87.1	1.1 (1)
Gly	107.3	1.3 (1)
Arg	83.5	1.0 (1)
Ala	137.7	1.7 (2)
Pro	390.6	4.9 (5)
Tyr	126.5	1.6 (3)
Val	71.9	0.9 (2)
Cys	153.5	1.9 (6)

B. Sequence analysis

Step	Assigned residues	Yield (pmol of PTH amino acid)
1	Asn	390
2	Cys*	400
3	Pro	270
4	Tyr	500
5	Cys*	320
6	Val	520
7	Val	560
8	Tyr	380
9	Cys*	300
10	Cys*	270
11	Pro	140
12	Pro	150
13	Ala	190
14	Tyr	240
15	Cys*	110
16	Glu	120
17	Ala	150
18	Ser	150
19	Gly	90
20	Cys*	77
21	Arg	30.5

Molecular weight: MH+ = 2487.90 Calc. MW = 2487.95

Sequence: NCPYCVVYCCPPAYCEASGCRPP*

* Cys residues were analyzed as the carboxymethyl adduct.

** Values in parenthesis indicate the number of amino acid residues found by sequence analysis as verified by FAB mass spectrometry.

The first step yielded a significant amount of glutamic acid as a contaminant. No residues were assigned for residues 22 and 23 since the yields for these steps were very low.

Table II

Major conopeptide structural frameworks

Four-loop conopeptides	(C---C---CC---C---C)
Example: ω-conotoxin GVIA	CKSPGSSCSPTSYNCCRSCNPYTKRCY*
Three-loop conopeptides	(CC---C---C---CC)
Example: μ-conotoxin GIIIA	RDCCTPPKKCKDRQCKPQRCCA*
Two-loop conopeptides	(CC---C---C)
Example: α-conotoxin GI	ECCNPACGRHYSC*

P = hydroxyproline; * denotes an amidated C-terminus.

above, and suggest that the convulsant peptide is amidated at the C-terminus, as is common among conopeptides.

Multiple peptides active in mammalian systems from Conus textile *venom*

During the purification of the convulsant peptide, we found that many other fractions exhibited activity in the mammalian central nervous system. Thus, the fractions from the first HPLC step were assayed for activity by the mouse i.c. injection assay. Many of the fractions (indicated by numbers in Fig. 1B) induce dramatic and diverse symptomatology in mice, and some fractions are lethal. Although the proportion of active fractions may be significantly lower than in a fish-hunting *Conus* venom, a very significant proportion of the total that were assayed still showed biological activity in the mammalian CNS.

These results indicate that many components of *Conus textile* venom have potent activity on receptors present in the mammalian central nervous system. Since the one component that was purified and characterized was a typical disulfide-rich conopeptide, we think it likely that *Conus* venoms will yield many such peptides with cross-phylum biological activity.

Discussion

The convulsant peptide described above has a number of interesting pharmacological and structural features. It defines a new subclass of conopeptides. As we have described previously, although the peptides in *Conus* venoms exhibit remarkable pharmacological diversity, the cysteine framework of these peptides is, in fact, highly conserved. Three major conopeptide classes of disulfide frameworks have been characterized so far, *i.e.*, the 2-loop, 3-loop, and 4-loop structural frameworks, as indicated in Table II (see Olivera *et al.*, 1990, 1991). The convulsant peptide clearly belongs to the class of conopeptides with four-loop structural frameworks.

But, within each structural framework class, rather distinctive subclasses emerge. For the four-loop conotoxin frameworks in particular, two distinctive subclasses were previously characterized; they are designated as Group I (the ω-conotoxin subclass) and Group II (the KK peptide subclass) in Table III. These subclasses are distinguishable by the overall biochemical characteristics of their peptides; in the case of the ω-conotoxins, the amino acids are overwhelmingly hydrophilic, and the peptides have a high net positive charge. In the case of the KK peptides, the intercysteine amino acids are considerably more hydrophobic, with a net negative charge.

The convulsant peptide differs from these two classes in having a very different number of amino acids present in each of the four amino acid loops between Cys residues. Between the first and second cysteine residues, and the second and third Cys, both the King-Kong peptides and the ω-conotoxins have 5–6 amino acids; in the convulsant peptide, the first two loops are extremely short with only two and three amino acids, respectively. A peptide with the same length distribution as the convulsant peptide has also been found in a worm-hunting cone, *Conus quercinus* (Abogadie *et al.*, 1990). The convulsant peptide and this latter conopeptide will probably define a new subclass within the four-loop structural framework class, distinct from either the KK peptide or the ω-conotoxin subclasses.

We are especially interested in determining the prepropeptide structure of the convulsant peptide. The prepro regions of the KK conopeptides and the ω-conotoxins have recently been found to be homologous but clearly divergent from each other (Colledge and Hillyard, 1992; D. Hillyard, unpub. results). In contrast, all KK peptides are highly homologous in the sequences of the prepro regions of the precursor molecule. If, as we postulate, the convulsant peptide defines a new subclass of four-loop conopeptides, we expect that the prepro sequences will exhibit some homology, but also considerable divergence from the KK and ω-conotoxin subclasses of precursors. It should then become possible to quickly identify other

Table III

Four-loop conopeptides; proposed subclasses

Name		Charge
Group I		
ω-Conotoxin GVIA	CKSPGSSCSPTSYNCCRSCNPYTKRCY*	+5
ω-Conotoxin MVIIA	CKGKGAKCSRLMYDCCTGSCRSGKC*	+6
Group II		
KK-0 peptide	WCKQSGEMCNLLDQNCCDGYCIVLVCT	−2
KK-1 peptide	CIEQFDPCEMIRHTCCVGVCFLMACI	−1.5
Group III		
Convulsant peptide	NCPYCVVYCCPPAYCEASGCRPP*	+1

The ω-conotoxins were described in Olivera *et al.*, 1985; the KK peptides in Woodward *et al.*, 1990. P stands for hydroxyproline; * means that the peptide is amidated at the C-terminus.

members of the convulsant peptide subclass by a molecular genetic approach specific for the prepro regions should permit identification of new conopeptides that are similarly within the convulsant peptide subclass.

The potent activity of this peptide in mammalian systems might not have been predicted from earlier data on crude venoms and well-characterized conopeptides from fish-hunting cone snails. Because the convulsant peptide is found in the venom of *Conus textile*, which clearly specializes in hunting other gastropod mollusks, finding a conopeptide that is highly potent in the mammalian central nervous system raises a number of interesting questions. Are there some biological reasons why *Conus textile* might have evolved a peptide that is active in mammalian systems? We think it more likely that the peptide has a receptor target that is highly conserved in both mammals and mollusks, and that this peptide will prove to have a particularly broad phylogenetic range.

The experiments described above provide a paradigm for quickly identifying a subset of peptides in a *Conus* venom that are likely to have a broad phylogenetic range, *i.e.*, assaying for biological activity in a phylum totally unrelated to the prey. Such peptides are probably not uncommon. In the preliminary survey of a *Conus textile* venom fraction shown in Figure 1B, we found a very significant proportion of all components in the venom active when injected into the central nervous system of mammals. The convulsant peptide is thus only the first of many such cross-phylum peptides to be characterized in detail.

It will be of interest to determine whether the subset of receptors targeted by such "broad-range" conopeptides is different from the subset of receptors targeted by narrow range conopeptides. However, further investigation into these issues will require the identification of the molecular targets of the convulsant peptide and other broad range conopeptides. We believe that the availability of "broad-range" conopeptides will be important in elucidating, not only the evolution of various ion channels and receptors, but ultimately the evolution of nervous systems in higher eukaryotes.

Acknowledgments

This work was supported by NIH grants GM 22737 (to BMO) and NS 27219 (to LJC), and by grants from the Marine Science Institute and the International Foundation for Science (Stockholm, Sweden). Amino acid analysis and sequencing were done in the laboratory of Dr. W. R. Gray, Dept. of Biology, University of Utah and mass spectrophotometry was done Dr. Terry Lee of the Beckman Research Institute of the City of Hope, California.

Literature Cited

Abogadie, F. C., C. A. Ramilo, G. P. Corpuz, and L. J. Cruz. 1990. Biologically active peptides from *Conus quercinus*, a worm-hunting species. *Trans. Natl. Acad. Sci. & Tech. (Philippines)* **12:** 219–232.

Bidlingmeyer, B. A., S. A. Cohen, and T. L. Tarvin. 1984. Rapid analysis of amino acids using pre-column derivatization. *J. Chromatogr.* **336:** 93–104.

Christensen, D. J., C. D. Poulter, R. A. Myers, and B. M. Olivera. 1992. Determination of the solution conformation of conotoxin SI by two-dimensional NMR. *Abstracts of Papers, 203rd National Meeting of the American Chemical Society.* Abstr. No. 331.

Colledge, C. J., J. P. Hunsperger, J. S. Imperial, and D. R. Hillyard. 1992. Precursor structure of ω-conotoxin GVIA determined from a cDNA clone. *Toxicon* (in press).

Cruz, L. J., G. Corpuz, and B. M. Olivera. 1976. A preliminary study of *Conus* venom protein. *Veliger* **18:** 302–308.

Cruz, L. J., V. de Santos, G. C. Zafaralla, C. A. Ramilo, R. Zeikus, W. R. Gray, and B. M. Olivera. 1987. Invertebrate vasopressin/oxytocin homologs. Characterization of peptides from *Conus geographus* and *Conus striatus* venoms. *J. Biol. Chem.* **262:** 15821–15824.

Endean, R., and C. Rudkin. 1963. Studies of the venoms of some Conidae. *Toxicon* **1:** 49–64.

Endean, R., and C. Rudkin. 1965. Further studies of the venoms of Conidae. *Toxicon* **2:** 225–249.

Heinrikson, R. L., and S. C. Meredith. 1984. Amino acid analysis by reverse-phase high-performance liquid chromatography: precolumn derivatization with phenylisothiocyanate. *Anal. Biochem.* **136:** 65–74.

Hunkapiller, M. W., and L. E. Hood. 1978. Direct microsequence analyses of polypeptides using an improved sequenator, a nonprotein carrier (polybrene) and high pressure liquid chromatography. *Biochemistry* **17:** 2124–2133.

Olivera, B. M., W. R. Gray, R. Zeikus, J. M. McIntosh, J. Varga, J. Rivier, V. de Santos, and L. J. Cruz. 1985. Peptide neurotoxins from fish-hunting cone snails. *Science* **230:** 1338–1343.

Olivera, B. M., J. Rivier, C. Clark, C. A. Ramilo, G. P. Corpuz, F. C. Abogadie, E. E. Mena, S. R. Woodward, D. R. Hillyard, and L. J. Cruz. 1990. Diversity of *Conus* neuropeptides. *Science* **249:** 257–263.

Olivera, B. M., J. Rivier, J. K. Scott, D. R. Hillyard, and L. J. Cruz. 1991. Conotoxins. *J. Biol. Chem.* **33:** 22067–22070.

Pardi, A., A. Goldes, J. Florance, and D. Maniconte. 1989. Solution structures of α-conotoxins determined by two-dimensional NMR spectroscopy. *Biochemistry* **28:** 5494–5501.

Ramilo, C. A., G. C. Zafaralla, L. Nadasdi, L. G. Hammerland, D. Yoshikami, W. R. Gray, J. Ramachandran, G. Miljanich, B. M. Olivera, and L. J. Cruz. 1992. Novel α- and ω-conotoxins from *Conus striatus* venom. *Biochemistry* (in press).

Tarr, G. E., J. F. Beecher, M. Bell, and D. J. McKean. 1978. Polyquarternary amines prevent peptide loss from sequenators. *Anal. Biochem.* **84:** 622–627.

Woodward, S. R., L. J. Cruz, B. M. Olivera, and D. R. Hillyard. 1990. Constant and hypervariable regions in conotoxin polypeptides. *EMBO J.* **9:** 1015–1020.

Reference: *Biol. Bull.* **183:** 165–172. (August, 1992)

Coordination of Reproductive Activity in *Aplysia:* Peptide Neurohormones, Neurotransmitters, and Pheromones Encoded by the Egg-Laying Hormone Family of Genes

SHERRY D. PAINTER

The Marine Biomedical Institute and The Department of Anatomy and Neurosciences, University of Texas Medical Branch, Galveston, Texas 77555-0843

Abstract. Pheromones play a significant role in coordinating reproductive activity in the marine opisthobranch mollusk *Aplysia.* Although solitary during most of the year, these simultaneous hermaphrodites gather into breeding aggregations during the reproductive season. The aggregations contain both mating and egg-laying animals, and are associated with masses of recently deposited egg cordons. Behavioral studies suggest that cordon-derived pheromonal factors are primarily responsible for establishing and maintaining the aggregations. Egg-laying animals are more attractive than sexually mature, but nonlaying, conspecifics and have a shorter mean latency to mating; egg cordons and egg-cordon eluates, when placed in the surrounding seawater, enhance the attractiveness of nonlaying animals and reduce their mean latency to mating. Similar effects are observed when extracts of the atrial gland are placed in the seawater, suggesting that secretory products of this oviductal exocrine organ may function as sexual pheromones. Biochemical analyses indicate that there may be multiple attractants in atrial gland extracts, and that at least one of these (A-NTP) is a peptide encoded by the A gene. The A gene belongs to a small family of structurally related genes that are expressed in a tissue-specific manner. Another member of the family, the egg-laying hormone (ELH) gene, is expressed in the neuroendocrine bag cells. Peptide products of the ELH gene act as neurohormones and nonsynaptic neurotransmitters, initiating egg laying and coordinating its associated behaviors. Peptide products of a family of genes may thus act internally and externally to coordinate both male and female reproductive activities.

Received 30 March 1992; accepted 29 May 1992.

Abbreviations: AG, atrial gland; ASW, artificial seawater; BCP, bag-cell peptide; ELH, egg-laying hormone; NTP, N-terminal peptide; RHD, red hemiduct; WHD, white hemiduct.

Introduction

The neuroendocrine regulation of reproductive activity in the marine opisthobranch mollusk *Aplysia* has been widely studied for over 25 years. Attention has focused primarily on the induction of egg laying and the regulation of its associated behaviors. Although pheromones play a significant role in coordinating reproductive activity in this genus, relatively little is known about the pheromonal factors or their specific activities.

Field studies of both *A. californica* (Kupfermann and Carew, 1974; Audesirk, 1979) and *A. fasciata* (Susswein *et al.,* 1983, 1984) indicate that, although *Aplysia* is a solitary animal during most of the year, it gathers into breeding aggregations or "brothels" during the summer reproductive season. The aggregations, containing both mating and egg-laying animals, are usually associated with masses of recently deposited egg cordons, often laid one on top of another. Most of the egg-laying animals simultaneously mate as females, even though mating does not cause reflex ovulation (*A. brasiliana,* Blankenship *et al.,* 1983), suggesting that egg laying may precede mating in the aggregations rather than resulting from it. Similar observations have been made in the laboratory when animals have not been individually caged (*A. californica,* Audesirk, 1977; *A. fasciata,* Susswein *et al.,* 1983, 1984; *A. brasiliana,* Blankenship *et al.,* 1983).

Behavioral studies suggest that the egg cordon is a source of pheromonal factors that attract conspecifics and induce

mating activity (*A. brasiliana*, Aspey and Blankenship, 1976; Jahan-Parwar, 1977; Painter *et al.*, 1989, 1991; *A. californica*, Jahan-Parwar, 1976; Audesirk, 1977); they may also induce egg-laying activity (*A. californica*, Audesirk, 1977) and may be responsible for the masses of egg cordons associated with breeding aggregations. Because mating does not enhance the attractiveness of a nonlaying animal (*A. dactylomela*, Lederhendler *et al.*, 1977), and mating does not cause reflex ovulation (*A. brasiliana*, Blankenship *et al.*, 1983), egg cordons are likely to be the primary sources of pheromonal factors that establish and maintain the aggregations.

Behavioral studies further suggest that the atrial gland, an exocrine organ secreting into the oviduct (*A. californica*, Arch *et al.*, 1980; Beard *et al.*, 1982; Painter *et al.*, 1985), may be a tissue source of the "cordon-derived" pheromonal activity (Painter *et al.*, 1989, 1991; also see Susswein and Benny, 1985). Extracts of other regions of the reproductive tract have not been examined, however, and the active atrial gland factors have not been identified.

The experiments described in this report demonstrate that extracts of the atrial gland specifically enhance the attractiveness of nonlaying animals, that the activity is found predominantly in the low and intermediate molecular weight fractions examined, and that A-NTP (N-terminal peptide encoded by the A gene) is one of the active factors. The A gene belongs to a small family of structurally related genes that are expressed in a tissue-specific manner in the animal (*A. californica*, Scheller *et al.*, 1983; Mahon *et al.*, 1985). Another member of the family, the egg-laying hormone (ELH) gene, is expressed in the neuroendocrine bag cells; products of the ELH gene appear to act as neurohormones and nonsynaptic neurotransmitters to induce ovulation (*A. californica*, Chiu *et al.*, 1979; Rothman *et al.*, 1983b; *A. brasiliana*, Nagle *et al.*, 1988a), regulate packaging and transport of the eggs through the reproductive tract (*A. californica*, Nagle *et al.*, 1990; Alevizos *et al.*, 1991), and (presumably) coordinate a stereotypical series of behaviors that accompany egg deposition. Thus, peptide products of a family of genes may act both internally and externally to coordinate male and female reproductive activities, ensuring propagation of the species.

Materials, Methods, and Results

Animals

Specimens of *Aplysia brasiliana* (Rang), weighing from 95 to 400 g, were collected from South Padre Island, Texas, and were used in experiments between June and September, the normal reproductive season for this species. *Aplysia brasiliana* was selected as the experimental animal for T-maze experiments because it has lower levels of chance attraction than *A. californica* (*i.e.*, it is less likely to enter one of the arms and stop locomoting when no attractant is present; Painter, 1991), and it can be collected in large numbers from the south Texas coast during the reproductive season. The animals were housed in individual cages in one of five large aquaria containing recirculating artificial seawater (ASW; Instant Ocean, Aquarium Systems, Mentor, Ohio) at room temperature (20 ± 2°C); the salinity ranged from 30 to 32 ppt. A 14:10 light:dark cycle was maintained, with the light period starting at 6 am; animals were fed dried laver in the late afternoon (4–6 pm) after the experiments were completed.

Specimens of *Aplysia californica* (Cooper) were purchased from Alacrity Marine Biological Services (Redondo Beach, California) and were maintained as described above for *A. brasiliana*, except that the ASW was cooled to 14 ± 2°C. *Aplysia californica* was used as the source of tissues for biochemical analyses because the exocrine organs associated with the egg-laying portion of the reproductive tract are larger and more well-defined than in *A. brasiliana* (Painter *et al.*, 1985). Note that pheromonal attractants do not appear to be species-specific in *Aplysia* (Kupfermann and Carew, 1974).

Only sexually mature individuals were used as experimental animals or as sources of tissues for biochemical studies. Sexual maturity was defined as the ability to lay eggs spontaneously or in response to injections of atrial gland extract. The extract was prepared as follows. Atrial glands were removed from sexually mature specimens of *Aplysia californica* (approximately 100 mg wet weight per animal) and stored at −70°C until use. Ten glands were homogenized in 20 ml of ice-cold filtered ASW in a hand-held glass-on-glass homogenizer. The homogenate was centrifuged at 48,000 × *g* for 20 min at 4°C, the supernatant collected and frozen at −20°C until use. Egg deposition was induced by injecting 0.1 ml of the thawed extract through the foot into the hemocoel; egg laying began approximately 30 min later. Most animals were injected two to five days after arriving in the lab. Immature animals were injected at weekly intervals thereafter until they responded to the injections.

Bioassay

Apparatus. As previously described (Painter *et al.*, 1991), a T-maze was constructed of clear Plexiglas (0.62 cm thick) and sealed with clear aquarium cement; it was cured for several days in ASW before use. Its overall dimensions were: height (base to top of T), 40.7 cm; width (distance between ends of arms), 101 cm; width of pathway, 10.2 cm; and depth, 10.2 cm. Removable stimulus cages (12.7 cm × 10 cm; depth, 10.2 cm) were placed in both arms for each experiment.

Experimental protocol and statistical analyses. Experiments were performed in a room adjacent to the aquar-

ium facility with overhead fluorescent lighting; the maze was positioned so that the lighting was uniform throughout the apparatus. As previously described (Painter *et al.*, 1991), 6 l of aerated ASW that had not previously contacted an *Aplysia* was placed in a cleaned and air-dried maze. A sexually mature "stimulus" animal was placed in a stimulus cage in one arm and a potential attractant added to the adjacent seawater. A sexually mature "test" animal was placed in the base of the maze 5 min later. Both the stimulus and test animals were briefly rinsed in fresh ASW before being introduced into the maze. In most cases, the test animal moved directly to the top of the maze and exhibited one of two general types of behavior: (1) it stopped, moved its head from side to side, then moved into one arm or returned to the base of the maze and stayed; or (2) it swam back and forth between arms, sometimes returning to the base, until it decided to stop. A response was considered to be positive if the test animal travelled to the stimulus within 20 min and maintained contact with the stimulus cage for 5 min, negative if it travelled to the opposite arm and maintained contact with the cage for 5 min, and no choice if it did neither. Animals were choosing between a stimulus and no stimulus in these experiments, rather than between two qualitatively or quantitatively different stimuli. Fifteen experiments were performed for each potential attractant, and the attractant was alternated between arms in consecutive experiments. Statistical significance was assessed by χ^2 analyses.

Four criteria were used to select animals for each experiment: (1) the animal must not have laid eggs during the preceding 24 h; (2) the animal must not have participated in a behavioral experiment during the preceding 24 h; (3) the animal must not have served as a test animal for the attractant being examined; and (4) the test and stimulus animals must have been housed in the same aquarium.

Tissue sources of pheromonal attractants

Tissue extracts for bioassay. Reproductive tracts were removed from sexually mature animals that had not laid eggs during the preceding 24 h. They were dissected into 6 components: the albumen gland, mucous gland, winding gland, atrial gland, red hemiduct (RHD), and white hemiduct (WHD) (Fig. 1). The albumen, mucous and winding glands are components of the accessory genital mass, and are responsible for packaging the eggs into a cordon (*A. californica*, Coggeshall, 1972). The RHD and atrial gland are components of the functional oviduct, through which the egg cordon is transported to the exterior of the animal. The WHD is the copulatory portion of the tract and does not contribute directly to egg deposition (*A. californica*, Painter *et al.*, 1985). Tissues were stored at −70°C until use.

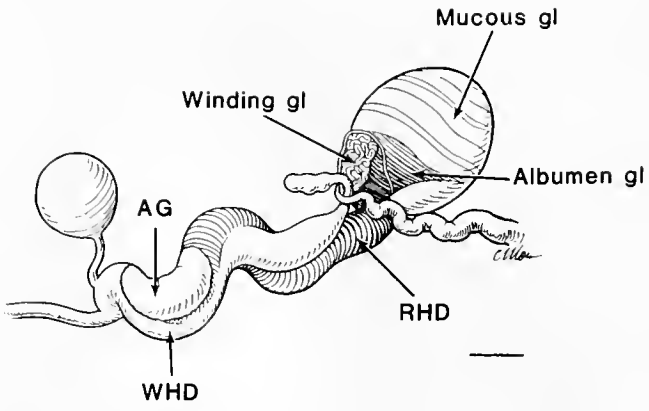

Figure 1. Schematic diagram of the reproductive tract of *Aplysia californica* anterior to the ovotestis. Extracts were made of each of the labeled organs, and the extracts bioassayed for pheromonal activity in T-maze experiments. RHD: red hemiduct; WHD: white hemiduct.

Prior to extraction, the tissues were thawed and weighed. They were then homogenized in ice-cold filtered ASW (3 cycles, final volume: 1 ml/50 mg wet weight) in a hand-held glass-on-glass homogenizer, and the homogenate centrifuged at 48,000 × *g* for 20 min at 4°C. The supernatant was collected, distributed into 1-ml aliquots, and the aliquots frozen at −20°C until used in a bioassay (3–6 days for each tissue).

Animals. Ninety-five *Aplysia brasiliana* were used in these experiments.

Results. To assess directional bias and chance levels of attraction in the maze, 15 experiments were performed in which no stimulus was placed in either arm. Four animals (26.7%) moved to the left and remained, two (13.3%) moved to the right and remained, while 9 (60%) did neither. These results demonstrate that there is no directional bias in the maze and establish chance levels of attraction at three animals (20%).

A similar level of attraction (2 animals; 13.3%) and pattern of responses was obtained when the stimulus was a nonlaying animal (Fig. 2). The two sets of responses were not significantly different [$\chi^2(2) = 0.92$, $0.50 < P < 0.75$], consistent with results obtained in earlier studies using this bioassay system (Painter *et al.*, 1991).

In subsequent experiments, aimed at enhancing the attractiveness of a nonlaying stimulus animal, extracts of various reproductive tract organs were placed in the adjacent ASW. Extracts of either the albumen gland or the atrial gland increased the number of animals attracted to the nonlayer and decreased the number of animals making no choice responses (Fig. 2). The pattern of responses obtained with the atrial gland extract differed significantly from that obtained with the nonlayer alone ($\chi^2 = 8.91$, $0.01 < P < 0.025$); the changes in pattern obtained with the albumen gland extract were less significant [$\chi^2(2) = 3.98$, $P = 0.20$].

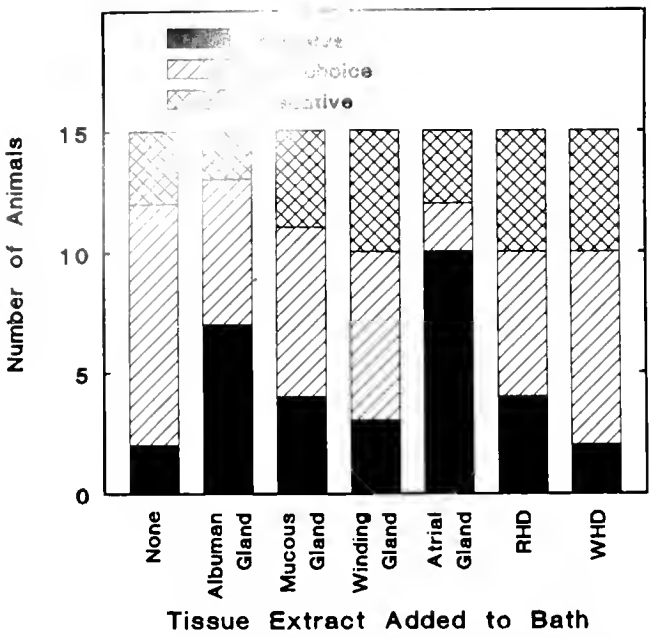

Figure 2. Secretory products of both the *Aplysia californica* albumen gland and atrial gland may be pheromonal attractants. The number of *A. brasiliana* attracted to a nonlaying conspecific was increased when an extract of either the albumen gland or atrial gland was placed in the adjacent ASW; only the atrial gland significantly altered the pattern of responses. Extracts of other *A. californica* reproductive organs did not affect the attractiveness of a nonlaying animal or significantly affect the pattern of responses. This bar graph is based on 105 single-arm experiments, 15 per stimulus; in each experiment, animals chose between a stimulus in one arm and no stimulus in the other.

Extracts of other reproductive tract organs did not affect the number of animals attracted to the nonlayer or the number of animals making no choice responses (Fig. 2). In each case, the pattern of responses did not differ significantly from that obtained with the nonlayer alone [$\chi^2(2) = 1.08$, $0.50 < P < 0.75$ for the mucous gland; $\chi^2(2) = 0.46$, $0.75 < P < 0.90$ for the winding gland; $\chi^2(2) = 2.16$; $0.25 < P < 0.50$ for the RHD; $\chi^2(2) = 0.72$, $0.50 < P < 0.75$ for the WHD]. These results suggest that the enhanced attractiveness of the nonlaying animal was specifically associated with the atrial gland extracts, and that it may be a physiological source of "cordon-derived" pheromonal attractants.

Extracts and column chromatography. In this case, six atrial glands (800 mg wet weight) were homogenized in 10 ml of 1 *M* acetic acid containing 20 m*M* HCl (4°C) in a hand-held glass-on-glass homogenizer. The homogenate was centrifuged at 48,000 × *g* for 20 min at 4°C, the supernatant removed and immediately applied to a 2.5 cm × 49 cm column of Sephadex G-50 superfine (4°C). The column had been calibrated with the following molecular weight standards: bovine serum albumin (66,200), cytochrome *c* (12,300), bacitracin (1500), and cobalt chloride (660). The eluting material was pooled into three fractions (I, >10 kDa; II, 1.5–10 kDa; III, <1.5 kDa); each fraction was then distributed into 16 aliquots and lyophilized. The lyophilized aliquots were resuspended in distilled water, relyophilized, and frozen at −20°C until use. Each was resuspended in 1 ml of distilled water immediately before addition to the maze.

Results. Sephadex G-50 elution profiles of acidic extracts of the atrial gland have been published previously (see, *e.g.,* Nagle *et al.,* 1988b) and are not shown here. Each of the molecular weight fractions increased the number of animals attracted to the nonlayer and decreased the number of animals making no choice responses (Fig. 3), but only fraction II significantly altered the pattern of responses from that obtained with the nonlayer alone [I, $\chi^2(2) = 1.76$, $0.25 < P < 0.50$; II, $\chi^2(2) = 9.34$, $P < 0.01$; III, $\chi^2(2) = 5.60$, $P = 0.06$]. The pattern of responses to fraction III did not differ significantly from that to fraction II [$\chi^2(2) = 1.45$, $0.25 < P < 0.50$] and none of the patterns differed significantly from the pattern obtained with a nonlayer and unfractionated atrial gland extract [I, $\chi^2(2) = 3.58$; $0.10 < P < 0.25$; II, $\chi^2(2) = 1.15$; $0.50 < P < 0.75$; III, $\chi^2(2) = 3.06$, $0.10 < P < 0.25$]. These results suggest that the atrial gland attractants have a wide range of molecular weights.

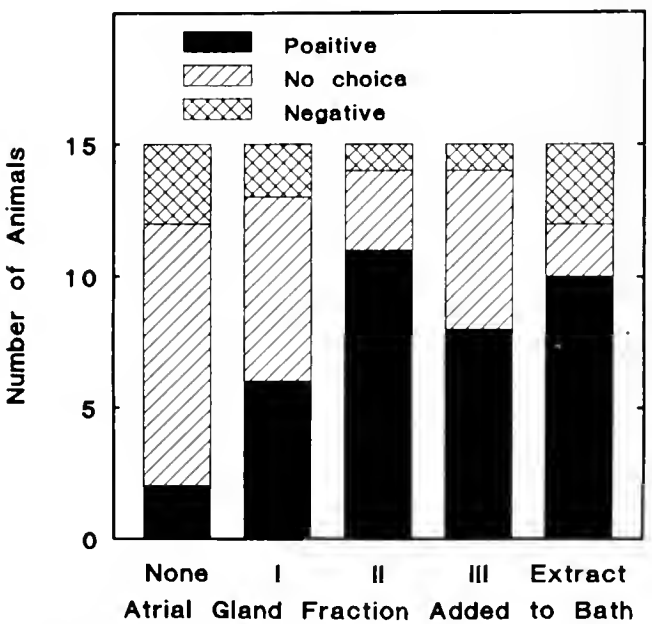

Figure 3. Atrial gland attractant activity is distributed over a range of molecular weights: the number of *A. brasiliana* attracted to a nonlaying conspecific was increased by placing fraction I (>10 kDa), II (1.5–10 kDa) or III (<1.5 kDa) in the adjacent ASW. The patterns of responses were not significantly different from that to a nonlayer with unfractionated atrial gland extract. This bar graph is based on 75 single-arm experiments, 15 per stimulus; in each experiment, animals chose between a stimulus in one arm and no stimulus in the other.

Identification of A-NTP as a potential attractant

Previous studies (Nagle *et al.*, 1988b) have shown that the low molecular weight fraction III contains two predominant peptide species, corresponding to A-NTP (N-terminal peptide encoded by the A gene) and B-NTP (N-terminal peptide encoded by the B gene). These peptides are each 13 residues in length, differing in sequence at only 3 positions, and have blocked amino termini (Fig. 4). Because amino acid compositional and microsequence analyses indicate that A-NTP is present in significantly larger quantities than B-NTP (Nagle *et al.*, 1988b), we decided to synthesize A-NTP for bioassay and future egg-cordon elution experiments.

Peptide synthesis. A-NTP was synthesized at the Biomolecular Synthesis Facility at the University of Texas Medical Branch and purified by C18 reversed-phase HPLC. The identity of the peptide was confirmed, and the amount of material quantified by amino acid compositional analysis. Microsequence analyses (as described in Nagle *et al.*, 1988b) yielded no amino acid residues, confirming that the amino terminus was blocked.

Bioassay. Three stimuli were examined in this series of experiments: (1) a nonlayer with nothing added to the ASW; (2) a nonlayer with a recently deposited conspecific egg cordon (laid by another animal following injection of atrial gland extract; deposition completed within the preceding 30 min; mean volume, 2.0 ml); and (3) a nonlayer with 100 μg of synthetic A-NTP (60% of the amount of A-NTP and B-NTP in one gland; Nagle *et al.*, 1988b).

Animals. Animals were selected from a pool of 183.

Results. Because of the larger population of animals used in these experiments, directional bias and chance levels of attraction were reassessed. Four of 15 animals (26.7%) travelled to the left when there was no stimulus in either arm, three of 15 (20%) travelled to the right, and eight (53.3%) did neither. The pattern of responses was not significantly altered when a nonlayer was the stimulus [$\chi^2(2) = 1.70$, $0.25 < P < 0.50$] (Fig. 5).

The number of animals attracted to a nonlayer was increased, and the number of animals making negative or no choice responses decreased, by placing either a conspecific egg cordon or synthetic A-NTP in the adjacent seawater (Fig. 5), but only the egg cordon significantly altered the pattern of responses obtained with nonlaying animals [egg cordon, $\chi^2(2) = 6.92$, $0.025 < P < 0.05$; A-NTP, $\chi^2(2) = 5.64$, $P = 0.06$]. The patterns of responses to these two stimuli did not differ significantly from each other [$\chi^2(2) = 0.09$, $0.95 < P < 0.975$], however. This suggests that pheromonal attractants are highly conserved in the two species of *Aplysia*.

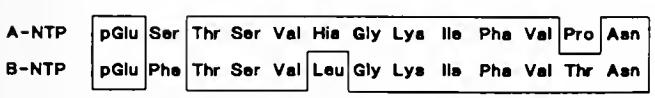

Figure 4. Amino acid sequences of A-NTP and B-NTP, as predicted from nucleotide sequence analyses of the A and B genes (Scheller *et al.*, 1983) and confirmed by biochemical analyses of purified peptides (Nagle *et al.*, 1988b).

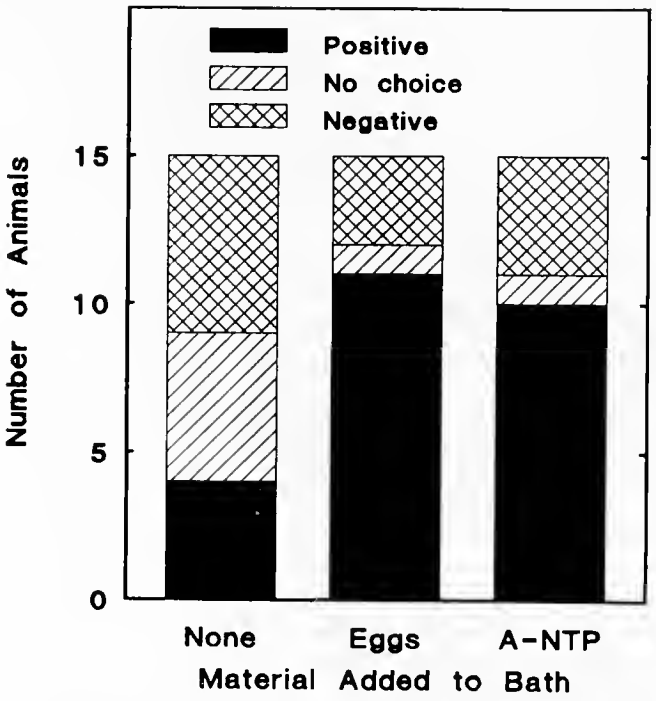

Figure 5. A-NTP is one of the attractive atrial gland factors: the number of *Aplysia brasiliana* individuals attracted to a nonlaying conspecific was increased by placing A-NTP in the adjacent ASW. The response pattern differed significantly from that to a nonlayer alone but not from that to a nonlayer with a recently deposited *A. brasiliana* egg cordon. This bar graph is based on 60 single-arm experiments, 15 per stimulus; in each experiment, animals were choosing between a stimulus in one arm and no stimulus in the other.

Discussion

These experiments show that extracts of the albumen gland and atrial gland enhance the attractiveness of nonlaying animals when placed in the adjacent seawater, but that the pattern of responses is significantly altered only by the atrial gland extracts. This suggests that atrial gland products may play the more significant role in pheromonal attraction. The relative locations of the glands within the reproductive tract would seem to support such a conclusion. The albumen gland is a component of the accessory genital mass and is one of the first exocrine organs contacted by the eggs (*A. californica*, Coggeshall, 1972); the atrial gland, in contrast, is a component of the oviduct and is the last major exocrine organ contacted by the egg cordon before deposition (*A. californica*, Painter *et al.*, 1985). Nevertheless, the material assayed in these exper-

iments was extracted f[illegible]ng wet weight of tissue. This corresponds to [illegible]y 40–50% of the material in an atrial gland [illegible]ay mature animal, but only 10–20% of the [illegible]an albumen gland. Dose-response experi[illegible]not been performed for extracts of either orga[illegible]t is possible that extracts of 40–50% of the albumen gland would yield more significant changes in response pattern.

Extracts of other portions of the reproductive tract, including the mucous gland, winding gland, RHD, and WHD, did not affect the attractiveness of a nonlaying animal, suggesting that the attractant activity is specifically associated with the atrial gland (and perhaps the albumen gland) rather than being broadly distributed throughout the egg-laying portion of the tract.

The <1.5 kDa and 1.5–10 kDa fractions increased the number of animals attracted to a nonlayer in the maze, demonstrating that attractant activity occurs over a broad range of molecular weights and suggesting that there may be multiple attractants in the gland. One of these is A-NTP, the predominant component of the low molecular weight fraction (Nagle *et al.*, 1988b). The second (and only other) major component of this fraction is B-NTP, a 13-residue peptide that is identical to A-NTP at 10 of the 13 positions (Fig. 4). Although B-NTP has not been tested in the bioassay, it is likely to be attractive as well, and probably contributes to the attractiveness of both the low molecular weight fraction and the unfractionated atrial gland extract.

The amount of A-NTP tested in the bioassay is equivalent to 60% of the material in a single atrial gland and is probably an unphysiologically high dose. This raises the possibility that the attraction is a pharmacological rather than a physiological effect. We have not as yet performed dose-response experiments to determine where this dose falls on the curve, or analyzed egg cordon eluates to determine the amounts of material that might be recovered from an egg cordon. These experiments are in progress, however.

The attractive components of the intermediate molecular weight fraction have not yet been identified. The activity is unlikely to result from complexing of a single low molecular weight species (*e.g.*, A-NTP or B-NTP), since previous studies suggest that complexing is minimized under the acidic conditions used in our experiments (Heller *et al.*, 1980; Kelner *et al.*, 1984). More importantly, complexes have not been identified in biochemical analyses of the 1.5–10 kDa fraction of acidic atrial gland extracts (Nagle *et al.*, 1986, 1988b). The fraction may contain novel factors with attractant activity, but the processing intermediates A-NTP-peptide A and B-NTP-peptide B also elute in this fraction (Nagle *et al.*, 1988b). Experiments are in progress to identify the attractive factors in this fraction.

The small amount of attractant activity associated with the high molecular weight fraction may reside in the A or B prohormones, which elute in this fraction, but this has not been demonstrated. The fraction may also contain novel attractants.

Neuroendocrine regulation of egg laying

Much more is known about the neuroendocrine regulation of egg laying in *Aplysia* than is known about pheromonal attraction or pheromonal induction of mating and egg laying. Ovulation is preceded by a prolonged and synchronous burst of electrical activity in the normally quiescent bag cells (*A. brasiliana*, Dudek *et al.*, 1979), two clusters of neuroendocrine cells located in the abdominal ganglion (*A. californica*, Frazier *et al.*, 1967; *A. brasiliana*, Blankenship and Coggeshall, 1976). The stimulus that normally elicits bag-cell activity is not known, but it appears to originate in the cerebral or pleural ganglia (*A. californica*, Haskins and Blankenship, 1979; Painter *et al.*, 1988; Brown *et al.*, 1989; Ferguson *et al.*, 1989) and to be at least partially under pheromonal control (*A. californica*, Audesirk, 1979).

Ovulation is induced by ELH (*A. californica*, Rothman *et al.*, 1983b), one of approximately nine peptides released during bag-cell activity (*A. californica*, Stuart *et al.*, 1980). Seven of these peptides have been purified from bag-cell extracts or releasates, and chemically characterized. Some of the peptides [*e.g.*, the α-, β-, and γ-bag-cell peptides (BCPs)] have autocrine activities in *in vitro* assays, affecting bag-cell excitability in a temperature-dependent manner (*A. californica*, Rothman *et al.*, 1983a; Redman and Berry, 1991). Others have neurohormonal activities, inducing ovulation (ELH, *A. californica*, Rothman *et al.*, 1983b) and regulating the packaging of eggs into a cordon (δ-BCP, *A. californica*, Nagle *et al.*, 1990). All of the bag-cell peptides that have been examined in an *in vitro* neuroassay system have additional local hormonal activities. These actions appear to be important for transporting the egg cordon through the oviduct (*A. californica*, Alevizos *et al.*, 1991) and for regulating characteristic egg-laying behaviors, although this has not been directly demonstrated *in vivo*.

The bag-cell products that have been characterized to date are encoded by the ELH gene (*A. californica*, Scheller *et al.*, 1983). This gene belongs to a small family of structurally related genes, each of which contains a sequence homologous to ELH and one or more sequences homologous to α-BCP. Members of the ELH family are expressed in a tissue-specific manner in the animal (*A. californica*, Scheller *et al.*, 1983; Mahon *et al.*, 1985), with the ELH gene being expressed in the bag cells and in small populations of neurons in the cerebral and pleural ganglia. Electrophysiological evidence suggests that the cerebral

and pleural cells provide excitatory input onto the bag cells (*A. californica,* Brown *et al.,* 1989; Ferguson *et al.,* 1989); they may, therefore, play a role in regulating egg-laying activity.

Other members of the ELH gene family, the A and B genes, are expressed in the atrial gland (*A. californica,* Scheller *et al.,* 1983; Mahon *et al.,* 1985). Although peptide products of the atrial gland induce egg laying when injected into sexually mature and receptive animals (*A. californica,* Arch *et al.,* 1978), the exocrine nature of atrial gland secretory activity (*A. californica,* Arch *et al.,* 1980; Beard *et al.,* 1982) precludes a hormonal function for these peptides. The present studies and others on pheromonal induction of mating (Painter *et al.,* 1989; also see Susswein and Benny, 1985) suggest that they may serve as sexual pheromones, attracting animals to breeding aggregations and inducing them to mate.

Thus, peptide products of a small family of genes may act to induce and coordinate both male and female reproductive activities: peptide products of the ELH gene, expressed in the neuroendocrine bag cells, act as neurohormones to induce ovulation and, presumably as non-synaptic neurotransmitters, to regulate the activities and behaviors that accompany egg laying; peptide products of the A gene, expressed in the exocrine atrial gland and secreted onto the egg cordon during deposition, may act as sexual pheromones to attract animals into the aggregation and induce them to mate. Experiments now in progress are aimed at identifying the other attractive atrial gland products and determining whether one or more actually reach the environment to act as sexual pheromones. Dose-response characteristics of the attractants found in eluates will also be examined.

Acknowledgments

We thank Bret Clough for collecting and maintaining the animals, Dr. Sherman Pernia for synthesizing A-NTP, Mr. Steve Smith for performing compositional and microsequence analyses of the purified synthetic peptide, Dr. Mae Huang for advice on statistical analyses, and Debbie Pavlu for preparing the manuscript. This work was supported by NIH grants NS22079 and HD28500, and by NSF grant BBS 87 11368. The Florence and Marie Hall Endowment for Excellence in the Biomedical Sciences provided support for the computer facilities used in these studies.

Literature Cited

Alevizos, A., K. R. Weiss, and J. Koester. 1991. Synaptic actions of identified peptidergic neuron R15 in *Aplysia.* III. Activation of the large hermaphroditic duct. *J. Neurosci.* **11:** 1282–1290.

Arch, S., J. Lupatkin, T. Smock, and M. Beard. 1980. Evidence for an exocrine function of the *Aplysia* atrial gland. *J. Comp. Physiol.* **151:** 131–137.

Arch, S., T. Smock, R. Gurvis, and C. McCarthy. 1978. Atrial gland induction of the egg-laying response in *Aplysia californica. J. Comp. Physiol.* **128:** 67–70.

Aspey, W. P., and J. E. Blankenship. 1976. *Aplysia* behavioral biology: II. Induced burrowing in swimming *A. brasiliana* by burrowed conspecifics. *Behav. Biol.* **17:** 301–312.

Audesirk, T. E. 1977. Chemoreception in *Aplysia californica.* III. Evidence for pheromones influencing reproductive behavior. *Behav. Biol.* **20:** 235–243.

Audesirk, T. E. 1979. A field study of growth and reproduction in *Aplysia californica. Biol. Bull.* **157:** 407–421.

Beard, M., L. Millechia, C. Masuoka, and S. Arch. 1982. Ultrastructure of secretion in the atrial gland of a mollusc (*Aplysia*). *Tissue Cell* **14:** 297–308.

Blankenship, J. E., and R. E. Coggeshall. 1976. The abdominal ganglion of *Aplysia brasiliana:* a comparative morphological and electrophysiological study, with notes on *A. dactylomela. J. Neurobiol.* **7:** 383–405.

Blankenship, J. E., M. K. Rock, L. C. Robbins, C. A. Livingston, and H. K. Lehman. 1983. Aspects of copulatory behavior and peptide control of egg laying in *Aplysia. Fed. Proc.* **42:** 96–100.

Brown, R. O., S. M. Pulst, and E. Mayeri. 1989. Neuroendocrine bag cells of *Aplysia* are activated by bag cell peptide-containing neurons in the pleural ganglion. *J. Neurophysiol.* **61:** 1142–1152.

Chiu, A. Y., M. W. Hunkapiller, E. Heller, D. K. Stuart, L. E. Hood, and F. Strumwasser. 1979. Purification and primary structure of the neuropeptide egg-laying hormone of *Aplysia californica. Proc. Natl. Acad. Sci. USA* **76:** 6656–6660.

Coggeshall, R. E. 1972. The structure of the accessory genital mass in *Aplysia californica. Tissue Cell* **4:** 105–127.

Dudek, F. E., J. S. Cobbs, and H. M. Pinsker. 1979. Bag cell electrical activity underlying spontaneous egg laying in freely behaving *Aplysia brasiliana. J. Neurophysiol.* **42:** 804–817.

Ferguson, G. P., A. ter Maat, and H. M. Pinsker. 1989. Egg laying in *Aplysia.* II. Organization of central and peripheral pathways for initiating neurosecretory activity and behavioral pathways. *J. Comp. Physiol., pt. A* **164:** 849–857.

Frazier, W. T., E. R. Kandel, I. Kupfermann, R. Waziri, and R. E. Coggeshall. 1967. Morphological and functional properties of identified neurons in the abdominal ganglion of *Aplysia californica. J. Neurophysiol.* **30:** 1288–1351.

Haskins, J. T., and J. E. Blankenship. 1979. Interactions between bilateral clusters of neuroendocrine cells in *Aplysia. J. Neurophysiol.* **42:** 356–367.

Heller, E., L. K. Kaczmarek, M. W. Hunkapillar, L. E. Hood, and F. Strumwasser. 1980. Purification and primary structure of two neuroactive peptides that cause bag cell afterdischarge and egg-laying in *Aplysia. Proc. Natl. Acad. Sci. USA* **77:** 2328–2332.

Jahan-Parwar, B. 1976. Aggregation pheromone from the egg-mass of *Aplysia. The Physiologist* **19:** 240.

Kelner, K. L., G. T. Nagle, S. D. Painter, and J. E. Blankenship. 1984. Biosynthesis of peptides in the atrial gland of *Aplysia californica. J. Comp. Physiol., pt. B* **154:** 435–442.

Kupfermann, I., and T. Carew. 1974. Behavior patterns of *Aplysia californica* in its natural environment. *Behav. Biol.* **12:** 317–337.

Lederhendler, I. I., K. Herriges, and E. Tobach. 1977. Taxis in *Aplysia dactylomela* (Rang, 1828) to water-borne stimuli from conspecifics. *Anim. Learning Behav.* **5:** 355–358.

Mahon, A. C., J. R. Nambu, R. Taussig, M. Shyamala, A. Roach, and R. Scheller. 1985. Structure and expression of the egg-laying hormone gene family in *Aplysia. J. Neurosci.* **5:** 1872–1880.

Nagle, G. T., M. de Jong-Brink, S. D. Painter, M. M. J. Bergamin-Sassen, J. E. Blankenship, and A. Kurosky. 1990. Delta-bag cell peptide from the egg-laying hormone precursor of *Aplysia:* processing,

primary structure, and bio[illegible]y. *J. Biol. Chem.* **265:** 22329–22335.

Nagle, G. T., S. D. Pain[illegible]ship, J. V. A. Choate, and A. Kurosky. 1988a. [illegible]aying hormones of *Aplysia brasiliana* and *Ap[illegible]*re identical. *Peptides* **9:** 867–872.

Nagle, G. T., S. [illegible]E. Blankenship, J. D. Dixon, and A. Kurosky. 19[illegible] for the expression of three genes encoding homologo[illegible]nd peptides that cause egg laying in *Aplysia*. *J. Biol. Che[illegible]* 26[illegible]853–7859.

Nagle, G. T., S. D. Painter, J. E. Blankenship, and A. Kurosky. 1988b. Proteolytic processing of egg-laying hormone-related precursors in *Aplysia:* identification of peptide regions critical for biological activity. *J. Biol. Chem.* **263:** 9223–9237.

Painter, S. D. 1991. Pheromonal attraction and induction of mating behavior in *Aplysia.* Pp. 67–71 in *Molluscan Neurobiology,* K. S. Kits, H. H. Boer, and J. Joose, eds. North Holland Press, New York.

Painter, S. D., M. G. Chong, M. A. Wong, A. Gray, J. Cormier, and G. T. Nagle. 1991. Relative contributions of the egg layer and egg cordon to pheromonal attraction and the induction of mating and egg-laying activity in *Aplysia. Biol. Bull.* **181:** 81–94.

Painter, S. D., A. R. Gustavson, V. K. Kalman, G. T. Nagle, and J. E. Blankenship. 1989. Induction of copulatory behavior in *Aplysia:* atrial gland factors mimic the excitatory effects of recently deposited egg cordons. *Behav. Neural Biol.* **51:** 222–236.

Painter, S. D., V. K. Kalman, G. T. Nagle, R. A. Zuckerman, and J. E. Blankenship. 1985. The anatomy and functional morphology of the large hermaphroditic duct of three species of *Aplysia,* with special reference to the atrial gland. *J. Morphol.* **186:** 167–194.

Painter, S. D., M. K. Rock, G. T. Nagle, and J. E. Blankenship. 1988. Peptide B induction of bag-cell activity in *Aplysia:* localization of sites of action to the cerebral and pleural ganglia. *J. Neurobiol.* **19:** 695–706.

Redman, R. S., and R. W. Berry. 1991. Temperature modulates the regulatory actions of alpha bag cell peptide. *Soc. Neurosci. Abstr.* **16:** 909.

Rothman, B. S., E. Mayeri, R. O. Brown, P.-M. Yuan, and J. E. Shively. 1983a. Primary structure and neuronal effects of α-bag cell peptide, a second candidate neurotransmitter encoded by a single gene in bag cell neurons of *Aplysia. Proc. Natl. Acad. Sci. USA* **80:** 5753–5757.

Rothman, B. S., G. Weir, and F. E. Dudek. 1983b. Egg-laying hormone: direct action on the ovotestis of *Aplysia. Gen. Comp. Endocrinol.* **52:** 134–141.

Scheller, R. H., J. F. Jackson, L. B. McAllister, B. S. Rothman, E. Mayeri, and R. Axel. 1983. A single gene encodes multiple neuropeptides mediating a stereotyped behavior. *Cell* **32:** 7–22.

Stuart, D. K., A. Y. Chiu, and F. Strumwasser. 1980. Neurosecretion of egg-laying hormone and other peptides from electrically active bag cell neurons of *Aplysia. J. Neurophysiol.* **43:** 488–498.

Susswein, A. J., and M. Benny. 1985. Sexual behavior in *Aplysia fasciata* induced by homogenates of the large hermaphroditic duct. *Neurosci. Lett.* **59:** 325–330.

Susswein, A. J., S. Gev, Y. Achituv, and S. Markovitch. 1984. Behavioral patterns of *Aplysia fasciata* along the Mediterranean coast of Israel. *Behav. Neural Biol.* **41:** 7–22.

Susswein, A. J., S. Gev, E. Feldman, and S. Markovitch. 1983. Activity patterns and time budgeting of *Aplysia fasciata* under field and laboratory conditions. *Behav. Neural Biol.* **39:** 203–220.

Reference: *Biol. Bull.* **183:** 173–177. (August, 1992)

Hormonally Derived Sex Pheromones in Goldfish: A Model for Understanding the Evolution of Sex Pheromone Systems in Fish

PETER W. SORENSEN

Department of Fisheries and Wildlife, University of Minnesota, St. Paul, Minnesota 55108

Abstract. It is now well established that female goldfish release unmodified and metabolized sex hormones to the water and that some of these compounds function as potent sex pheromones detected by the male's olfactory sense. In goldfish, both olfactory pheromonal receptors and their corresponding hormonal receptors appear to be transmembrane-domain receptors coupled with G proteins. Recent studies of other teleost fish indicate that fish commonly use 'hormonal-pheromones.' Taken together, these data suggest that fish pheromone systems may have evolved as a consequence of a chance expression of hormone receptor molecules on olfactory receptor cells. Isolation and identification of olfactory and hormonal receptors may be the next step in resolving this question.

Introduction

Pheromones have been defined as "substances that are excreted to the outside by an individual and received by a second individual of the same species, in which they release a specific reaction, for example a definite behaviour or developmental process" (Karlson and Luscher, 1959). Living in an aquatic environment generally devoid of visual cues but rich in dissolved compounds, fish have evolved highly developed chemosensory and pheromonal signalling systems. Where studied, these pheromonal systems have been found to play fundamental roles promoting reproductive synchrony, and there are many examples of the odor of sexually mature fish stimulating either a physiological process or a behavior (Liley, 1982; Stacey and Sorensen, 1991). However, until our recent serendipitous discovery that ovulatory female goldfish, *Carassius auratus*, release the steroidal sex hormone 17α,20β-dihydroxy-4-pregnen-3-one (17,20βP) to the water where it then functions as a pre-ovulatory sex pheromone (Dulka *et al.*, 1987), not a single fish sex pheromone had been clearly identified. Although our discovery that an unmodified hormone functioning as a pheromone seemed surprising at the time, Kittredge *et al.* (1971) had predicted almost 20 years earlier that aquatic organisms commonly use hormonal compounds as pheromones. Kittredge *et al.* (1971) based this prediction on the apparent evolutionary ease with which such a system might evolve: hormonal cues are both naturally released and inherently meaningful, and their recognition might require only one step (mutation), the chance expression of hormonal receptors on chemosensory receptor cells.

Recent investigations indicate that fish may commonly use 'hormonal-pheromones.' In addition to 17,20βP, the goldfish uses at least one other major class of hormonal compounds, the F prostaglandins (PGFs), as sex pheromones (Sorensen *et al.*, 1988). Additionally, at least a dozen examples of other fish species whose olfactory systems are acutely and specifically sensitive to hormonal compounds are now known (Stacey and Sorensen, 1991; Sorensen *et al.*, 1992). These findings in fish are not the first to document a parallel between internal and external chemical signalling systems. Almost 40 years ago, Haldane (1954) noted that acetylcholine and epinephrine altered protozoan swimming patterns and hypothesized that the internal signalling systems found in metazoa may have evolved from external (pheromonal) systems used by their unicellular ancestors. Today at least a dozen neuroactive substances from vertebrates are known to stimulate invertebrate chemosensory responses. Reviewing the biochemical mechanisms underlying the internal and chemosensory receptor systems for these substances, Carr *et al.* (1989) conclude that enough similarities exist to 'provide strong support for Haldane's (1954) hypothesis.' Do similarities also exist between hormonal and pheromonal

Received 2 April 1992; accepted 19 May 1992.

receptor systems in t[illegible] And if they do, is Haldane's (1954) hypo[illegible]ptor 'internalization,' or Kittredge *et al.*'s [illegible]esis of receptor 'externalization,' the [illegible]on? This paper will address these questi[illegible]oldfish hormonal-pheromone system.

A Brief Overview of the Goldfish Hormonal-Pheromone System

Because we have recently published several reviews on the goldfish hormonal-pheromone system (Stacey and Sorensen, 1991; Sorensen *et al.*, 1991; Stacey, 1991; Sorensen, 1992), I will only review the most pertinent elements here. Briefly, female goldfish ovulate in the early morning when light levels are low and, like other oviparous teleosts, become sexually receptive at the time of ovulation (Stacey, 1987). Because ovulated eggs remain viable for but a few hours within the female, females must, and generally do, spawn (release their eggs) within a few hours; male-female reproductive physiology and behavior must be tightly synchronized. This synchrony appears mediated by at least two hormonal-pheromones released in a sequential manner by ovulatory females. Although there is evidence for a third steroidal pheromone resembling androstenedione which has inhibitory actions on male gonadotropin (GtH) release (Stacey, 1991; Sorensen *et al.*, 1991), we will not discuss it here because it is still poorly understood.

In goldfish, as in the vast majority of externally fertilizing fish, oocyte final maturation (resumption of meiosis) is stimulated by a surge in GtH release which in turn stimulates synthesis of the steroidal maturational hormone 17,20βP by ovarian follicles (Stacey, 1987). Circulating levels of immunoreactive-17,20βP increase dramatically during the 10–12 h period preceding ovulation in goldfish and then collapse at the time of ovulation, which coincides with spawning (Stacey *et al.*, 1989). Circulating 17,20βP is rapidly cleared to the water (by unknown means) where it then functions as a potent odorant with pheromonal actions (Dulka *et al.*, 1987). Although much of the blood-borne 17,20βP is released unmodified as a free steroid, considerable quantities are conjugated with either glucuronic acid (17,20βP-G) or sulfate (17,20βP-S), and this mixture is accompanied by a variety of non-pheromonally active steroids (Sorensen *et al.*, 1991); it is unclear whether 17,20βP release reflects a specialized female signaling system. As assayed by electro-olfactogram (EOG) recording from the olfactory epithelium, and confirmed by whole-animal bioassays, the goldfish olfactory system is acutely sensitive to 17,20βP and 17,20βP-S, but not 17,20βP-G (Sorensen *et al.*, 1991). Although 17,20βP and 17,20βP-S appear to be detected by different receptor mechanisms, both stimulate male GtH release (Sorensen *et al.*, 1991), and evoke increased sperm production by the time of spawning (Dulka *et al.*, 1987). Because neither steroid appears to have immediate dramatic influences on male behavior, this pre-ovulatory pheromone is considered a 'primer' (Sorensen *et al.*, 1989).

At the time of ovulation (when final maturation is complete) female goldfish become sexually receptive and release another pheromone which is derived from circulating prostaglandin $F_{2\alpha}$ ($PGF_{2\alpha}$). In goldfish, and presumably many other fish, $PGF_{2\alpha}$, or a compound closely resembling it, appears to have both a paracrine function modulating ovulation (Stacey and Goetz, 1982), and a hormonal function stimulating female spawning behavior (Stacey, 1987). Evidence for these roles is extensive but somewhat indirect. As in most vertebrates, $PGF_{2\alpha}$ stimulates follicular rupture in goldfish oocytes both *in vitro* and *in vivo* (see Goetz *et al.*, 1991), and $PGF_{2\alpha}$ is measurable in cultures of goldfish oocytes (Goetz, 1991). Additionally, exposure to indomethacin, a prostaglandin synthetase inhibitor, blocks ovulation both *in vitro* and *in vivo* (Stacey and Goetz, 1982). Evidence that $PGF_{2\alpha}$ functions as a behavioral hormone stimulating female sexual behavioral receptivity comes from the discovery that interperitoneal injections of $PGF_{2\alpha}$ elicit apparently normal sexual receptivity in non-ovulated females within minutes (Stacey, 1976). Because $PGF_{2\alpha}$ injection is most effective if injected directly into the cranium (Stacey and Peter, 1979), direct actions on the brain are strongly suspected. These findings receive support from the observation that PGF titers increase dramatically in the blood of recently ovulated goldfish (Bouffard, 1979) and the fact that females exhibit sexual behavior only when holding ovulated eggs (Stacey and Goetz, 1982).

Recent evidence now suggests that circulating $PGF_{2\alpha}$ associated with the presence of ovulated eggs is rapidly metabolized and cleared to the water where it then functions as a pheromone stimulating male sexual behavior. PGFs may thus synchronize ovulation, female sexual behavior, and male arousal. Indications of this possibility first arose with the observation that non-ovulated goldfish injected with $PGF_{2\alpha}$ release an odor which elicits male reproductive behavior (Sorensen *et al.*, 1986). Recently we discovered that as measured by EOG recording, the goldfish olfactory system is acutely and specifically sensitive to waterborne $PGF_{2\alpha}$ and a mammalian metabolite 15-keto-prostaglandin $F_{2\alpha}$ (15k-$PGF_{2\alpha}$) (Sorensen *et al.*, 1988). The relevance of this was confirmed by the finding that males exposed to waterborne PGFs become sexually active, and that ovulated females release immunoreactive PGFs to the water (Sorensen *et al.*, 1988). Most recently, we have injected goldfish with radiolabeled $PGF_{2\alpha}$ and established that they release substantial quantities of at least three unknown metabolites of $PGF_{2\alpha}$ but not 15K-$PGF_{2\alpha}$ suggesting that the pheromone is a mixture of several novel PGF metabolites (unpub.).

Comparing Hormonal and Pheromonal Functions of 17,20βP and PGFs in Goldfish

Although not a single vertebrate olfactory receptor molecule has been identified, a preponderance of evidence suggests that olfactory receptors are members of a superfamily of surface receptors that cross the cellular membrane seven times and are associated with guanine nucleotide-binding proteins (G proteins) (Anholt *et al.*, 1991). The most direct evidence for this possibility comes from Buck and Axel (1991) who constructed oligonucleotide probes to demonstrate the existence of an extremely large family of genes encoding for G protein-linked transmembrane proteins expressed exclusively in olfactory tissue isolated from rats. Although this superfamily of transmembrane proteins appears to meet all of the criteria of olfactory receptors, direct proof is still lacking. Buck and Axel (1991) note that 'the detection of odors at the surface in the periphery is therefore likely to involve signaling mechanisms shared by other hormone or neurotransmitter systems.' They also note that 'members of this family of olfactory proteins are conserved in lower vertebrates and . . . presumably extended over evolutionary time.' Here I examine the goldfish hormonal-pheromone system to determine whether hormonal and pheromonal receptor mechanisms share the same biochemical/biophysical mechanisms, keeping in mind that if they do, this might reflect common evolutionary origins.

Ligand-binding studies using goldfish olfactory epithelium have clearly established that binding activity for 17,20βP is associated with neural membranes (Rosenblum *et al.*, 1991)—as is the case for all vertebrate olfactory binding activity studied to date (Anholt *et al.*, 1991), including that for feeding attractants (amino acids) in fish (see Bruch and Rulli, 1988). Ligand-binding studies have not been conducted for PGFs, but electrical responses elicited by PGFs are extremely similar to those elicited by amino acids and 17,20βP—there is every reason to suspect that they are also associated with the cell membrane. Signal transduction mechanisms associated with 17,20βP and PGF olfactory responsiveness have not yet been studied, but signal transduction mechanisms have been extensively investigated in fish in association with the olfactory responsiveness of catfish (*Ictalurus punctatus*) to amino acids. The mechanisms described are similar to those found in higher vertebrates (see Anholt *et al.*, 1991). Briefly, the catfish studies indicate that amino acid olfactory receptors are coupled to G protein(s) which may activate either cAMP-gated cation channels (Bruch and Teeter, 1989), or inositol triphosphate (IP3)-gated calcium channels (Restrepo *et al.*, 1990). Although fish olfactory G protein(s) have not been identified, it is fascinating that a mammalian olfactory G protein has been (G_{olf}), and it has a high degree of homology (88%) with conventional $G_{s\alpha}$ (Jones and Reed, 1989).

It is striking that the hormonal actions of both 17,20βP and $PGF_{2\alpha}$ also appear to be mediated by membrane receptors associated with G proteins. 17,20βP appears to exert its actions on the fish oocyte via a membrane receptor, a scenario resembling the actions of progesterone on the amphibian oocyte (see Jalabert *et al.*, 1991). Direct evidence for this possibility in the goldfish comes from the observation that 17,20βP stimulates final maturation when applied to the oocyte surface, but is ineffective if injected directly into the oocyte cytoplasm (data reported by Nagahama, 1987). Indirect support comes from other species of fish in which ligand-binding studies have demonstrated a high level of specific binding activity for 17,20βP-related steroids to oocyte membranes (see Patino and Thomas, 1990). Additionally, although no direct evidence of G protein involvement in 17,20βP-induced final maturation has been reported, it is quite clear that adenylate cyclase and cAMP are involved because administration of either cAMP or forskolin to oocytes blocks maturation. The latter finding is thought to indicate that 17,20βP exerts its actions by reducing cAMP, thereby reducing the phosphorylation of an inhibitory substrate by cAMP-dependent protein kinase (see Jalabert *et al.*, 1991). These findings suggest that the 17,20βP membrane receptor might be coupled to an inhibitory G protein. Unfortunately, $PGF_{2\alpha}$ binding has not been studied in either the fish ovary or brain. However, where studied in mammals, $PGF_{2\alpha}$ binding activity has been found associated with cell membranes in both the ovary (Rao, 1976) and brain (Watanabe *et al.*, 1985). Additionally, in goldfish there is strong evidence that G proteins are associated with ovulation—orthovanadate, a G-protein stimulator, evokes both IP_3 production and ovulation (Ranjan and Goetz, 1990). Signal transduction mechanisms associated with the behavioral effects of $PGF_{2\alpha}$ have not been studied.

Existing evidence suggests that both pheromonal (olfactory) and hormonal receptors for 17,20βP and PGF in goldfish are transmembranal and linked to G proteins—supporting the possibility that these systems might be evolutionarily related. But what about the relative specificities and sensitivities of goldfish olfactory and hormonal receptors? As measured by EOG recording (Sorensen *et al.*, 1990) and radio-receptor assay (Rosenblum *et al.*, 1991), olfactory structure-activity relationships for 17,20βP binding appear quite similar to those described by hormonal studies assaying the effects of steroids on final maturation (Jalabert, 1976). However, although not measured, it seems quite unlikely that the pheromonally active metabolite 17,20βP-S has hormonal activity. A similar scenario exists for the PGFs—the pheromonally active metabolite 15K-$PGF_{2\alpha}$ has little ability to stimulate female sexual behavior (Sorensen *et al.*, 1987). Do these differences in olfactory and hormonal receptor binding characteristics negate the possibility that these systems are related? Not necessarily, at least if Kittredge *et al.*'s

(1971) hypothesis is ... seems quite reasonable that olfactory hormon... receptors should quickly diversify in ac... speciation events and the pressures for ... ecies-isolation mechanisms that must accom... Hormone metabolism and release mechanisms ... also be expected to exhibit diversification. The existence of both 17,20βP and 17,20βP-S binding activity in the goldfish epithelium may be an example of pheromonal-evolutionary divergence.

A final consideration is whether it is conceivable that a transmembranal hormonal receptor expressed in an olfactory membrane could interact functionally with olfactory G proteins to transduce a response. Although this experiment has not been performed, receptor proteins have been transferred to foreign cell membranes and remained functional (Citri and Schramm, 1980). Furthermore, G_{olf} is apparently similar enough to $G_{s\alpha}$ that it will stimulate adenylate cyclase activity when expressed in lymphoma cells (Jones and Reed, 1989). In summary, what little we know about pheromonal receptor mechanisms and their hormonal counterparts in goldfish suggest they are strikingly similar, perhaps similar enough that they be evolutionarily related.

Hormonal-Pheromones in Other Species of Fish: The Question of Species-Specificity and Its Relevance to the Evolution of Hormonal-Pheromones

It is important to understand the diversity (species-specificity) of hormonal-pheromone systems because it reflects on how these systems may have evolved. This is especially the case because fish hormonal systems are thought to be highly similar ('conserved'); 17,20βP, or a very closely related steroid, has been found to serve as the maturational hormone in all fish examined to date (Scott and Canario, 1987). Although paracrine and hormonal $PGF_{2\alpha}$ function is less well understood, evidence suggests that it too is used by many fishes (Stacey, 1987; Goetz *et al.*, 1991). In contrast, surveys of EOG sensitivity of various fishes increasingly indicate that hormonal-pheromones might be species-specific (Sorensen *et al.*, 1992). For instance, EOG recording has now been used to describe the olfactory sensitivities of at least half a dozen members of the family Cyprinidae to almost 20 hormonal compounds. Of these species, only the goldfish and the closely related common carp, *Cyprinus carpio*, detect either 17,20βP or 17,20βP-S; the rest detect 17,20βP-G. Perhaps even more striking, the olfactory sensitivity of three species from the family Catastomidae, a family in the same order as the Cyprinidae, have now been tested and no sensitivity to any sex steroids has been measured (Sorensen *et al.*, 1992). Similarly, although all members of the Cyprinidae and Catastomidae tested respond to PGFs, there are clear differences in relative responsiveness. In spite of the fact that these data must be interpreted cautiously because of the small number of species and individuals tested, uncertainties about the meaning of EOG recording, and our poor understanding of hormone metabolism and excretion in fish—it seems safe to conclude that fish pheromone systems are more diverse than the hormone systems from which they are metabolically derived.

As previously mentioned, species-specificity in hormonal-pheromone system function may not be surprising, but when associated with a highly conserved hormonal system, as appears to be the case in fish, it strongly suggests that if one of these systems is evolutionarily derived from the other, the hormonal system is the likely predecessor. It is a simple matter to imagine how a common hormonal-pheromone system might come to exhibit evolutionary radiation, but nearly impossible to imagine how and why a highly conserved hormone system could evolve from a pre-existent, diverse pheromone system. An alternative possibility that I have not yet considered is that hormonal and pheromonal receptor systems may be independently derived from common, extremely ancient, and unknown chemoreceptor systems. However, I presently know of no data that support this possibility. In conclusion, existing evidence from the goldfish hormonal-pheromone system, and fish in general, supports Kittredge *et al.*'s (1971) hypothesis that pheromonal signaling systems may reflect an externalization of internal hormonal signalling systems. Definitive proof of this hypothesis awaits receptor identification, a project I hope this treatise will encourage.

Acknowledgments

I thank Dr. William Carr for organizing the symposium and Drs. Norm Stacey, Rick Goetz, and Sandy Scott for their enthusiastic assistance. Mr. Weiming Li, Ms. Gail Sorensen, and two anonymous reviewers kindly reviewed the manuscript and made many helpful suggestions. My research has been supported by the Alberta Heritage Foundation for Medical Research, the National Science Foundation, and the Minnesota Agricultural Experiment Station (Contribution number 19,813).

Literature Cited

Anholt, R. H. R. 1991. Odor recognition and olfactory transduction: the new frontier. *Chem Senses* **16:** 421–427.

Bouffard, R. E. 1979. The role of prostaglandins during sexual maturation, ovulation, spermiation, in the goldfish, *Carassius auratus*. Unpublished M.Sc. Thesis, University of British Columbia.

Bruch, R. C., and R. D. Rulli, 1988. Ligand binding specificity of a neutral L-amino acid olfactory receptor. *Comp. Biochem. Physiol.* **91B:** 535–540.

Bruch, R. C., and J. H. Teeter. 1989. Receptor events and transduction in taste and olfaction. Pp. 283–298 in *Chemical Senses: Receptor Events and Transduction in Taste and Olfaction*, J. G. Brand, J. H. Teeter, R. H. Cagan, and M. R. Kare, eds. Deeker, New York.

Buck, L., and R. Axel. 1991. A novel multigene family may encode odorant receptors: a molecular basis for odorant recognition. *Cell* **65:** 175–187.

Carr, W. E. S., R. A. Gleesen, and H. G. Tapedo-Rosenthal. 1989. Chemosensory systems in lower organisms: correlations with internal receptor systems for neurotransmitters and hormones. *Adv. Comp. Environ. Physiol.* **5:** 25–52.

Citri, Y., and M. Schramm. 1980. Resolution, reconstitution, and kenetics of the primary action of a hormone receptor. *Nature* **287:** 297–300.

Dulka, J. G., N. E. Stacey, P. W. Sorensen, and G. J. Van Der Kraak. 1987. Sex steroid pheromone synchronizes male-female spawning readiness in the goldfish. *Nature* **325:** 251–253.

Goetz, F. W. 1991. Compartmentalization of prostaglandin synthesis within the fish ovary. *Am. J. Physiol.* **260:** R462–R865.

Goetz, F. W., A. K. Berndtson, and M. Ranjan. 1991. Ovulation: mediators at the ovarian level. Pp. 127–202 in *Vertebrate Endocrinology: Fundamentals and Biomedical Applications, Vol. 4A,* P. K. T. Pang and M. Schreibmann, eds. Academic Press, New York.

Haldane, J. B. S. 1954. La signalisation animale. *Annee Biol.* **58:** 89–98.

Jalabert, B. 1976. *In vitro* oocyte maturation and ovulation in rainbow trout (*Salmo gairdneri*), northern pike (*Essox lucius*) and goldfish (*Carassius auratus*). *J. Fish Res. Board Can.* **33:** 974–988.

Jalabert, B., A. Fostier, B. Breton, and C. Weil. 1991. Oocyte maturation in vertebrates. Pp. 23–90 in *Vertebrate Endocrinology: Fundamentals and Biomedical Applications, Vol 4A,* P. K. T. Pang and M. Schreibmann, eds. Academic Press, New York.

Jones, D. T., and R. R. Reed. 1989. G_{olf}: an olfactory neuron specific-G protein involved in odorant signal transduction. *Science* **244:** 790–795.

Karlson, P., and M. Luscher. 1959. "Pheromones": a new term for a class of biologically active substances. *Nature* **183:** 55–56.

Kittredge, J. S., M. Terry, and F. J. Takahashi. 1971. Sex pheromone activity of the moulting hormone, crustecdysone, on male crabs (*Pachygrapsus crassipes, Cancer antennarius,* and *C. anthonyi*). *Fish. Bull.* **69:** 337–343.

Liley, N. R. 1982. Chemical communication in fish. *Can. J. Fish. Aquat. Sci.* **39:** 22–35.

Nagahama, Y. 1987. 17α,20β-dihydroxy-4-pregnen-3-one: a teleost maturation-inducing hormone. *Dev. Growth Differ.* **29:** 1–12.

Patino, R., and P. Thomas. 1990. Characterization of membrane receptor activity for 17α,20β,21-trihydroxy-4-pregnen-3-one in ovaries of the spotted seatrout (*Cynosion nebulosus*). *Gen. Comp. Endocrinol.* **78:** 204–217.

Ranjan, M., and F. W. Goetz. 1990. Orthovanadate and fluoroaluminbate stimulate inositol phosphate production and in vitro ovulation in goldfish (*Carassius auratus*). *Biol. Reprod.* **43:** 323–334.

Rao, C. V. 1976. Inhibition of ^{3}H prostaglandin $F_{2\alpha}$ binding to its receptors by progesterone. *Steroids* **27:** 831–843.

Restrepo, D., T. Miyamoto, B. P. Bryant, and J. H. Teeter. 1990. Odor stimuli trigger influx of calcium into olfactory neurons of the channel catfish. *Science* **249:** 1166–1168.

Rosenblum, P. M., P. W. Sorensen, N. E. Stacey, and R. E. Peter. 1991. Binding of the steroidal pheromone 17α,20β-dihydroxy-4-pregnen-3-one to goldfish, *Carassius auratus,* olfactory epithelium membrane preparations. *Chem. Senses* **16:** 143–154.

Scott, A. P., and A. V. M. Canario. 1987. Status of oocyte maturation-inducing steroids in teleosts. Pp. 224–234 in *Proceedings of the Third International Symposium on the Reproductive Physiology of Fish,* D. R. Idler, L. W. Crim, and J. M. Walsh, eds. Memorial University Press, St. John's, Newfoundland.

Sorensen, P. W. 1992. Hormones, pheromones, and chemoreception. Chapter 11 in *Fish Chemoreception,* T. J. Hara, ed. Chapman and Hall, London (in press).

Sorensen, P. W., N. E. Stacey, and K. J. Chamberlain. 1989. Differing behavioral and endocrinological effects of two female sex pheromones on male goldfish. *Horm. Behav.* **23:** 317–332.

Sorensen, P. W., N. E. Stacey, and P. Naidu. 1986. Release of spawning pheromone(s) by naturally ovulated and prostaglandin-injected non-ovulated female goldfish. Pp. 149–154 in *Chemical Signals in Vertebrates IV,* D. Duvall, D. Muller-Schwarze, and D. Silverstein, eds. Plenum Press, New York.

Sorensen, P. W., K. J. Chamberlain, N. E. Stacey, and T. J. Hara. 1987. Differing roles of prostaglandin $F_{2\alpha}$ and its metabolites in goldfish reproductive behavior. P. 164 in *Proceedings of the Third International Symposium on the Reproductive Physiology of Fish,* D. R. Idler, L. W. Crim, and J. M. Walsh, eds. Memorial University Press, St. John's, Newfoundland.

Sorensen, P. W., F. W. Goetz, A. P. Scott, and N. E. Stacey. 1991. Recent studies of the goldfish indicate both unmodified and modified hormones function as sex pheromones. Pp. 191–193 in *Proceedings of the Fourth International Symposium on the Reproductive Physiology of Fish,* A. P. Scott, J. P. Sumpter, D. E. Kime, and M. S. Rolfe, eds. Fishsymp, Sheffield, UK.

Sorensen, P. W., T. J. Hara, N. E. Stacey, and J. G. Dulka. 1990. Extreme olfactory specificity of male goldfish to the preovulatory steroidal pheromone 17α,20β-dihydroxy-4-pregnen-3-one. *J. Comp. Physiol. A* **166:** 373–383.

Sorensen, P. W., T. J. Hara, N. E. Stacey, and F. W. Goetz. 1988. F prostaglandins function as potent olfactory stimulants comprising the postovulatory female sex pheromone in goldfish. *Biol. Reprod.* **39:** 1039–1050.

Sorensen, P. W., I. A. S. Irvine, A. P. Scott, and N. E. Stacey. 1992. Electrophysiological measures of olfactory sensitivity suggest that goldfish and other fish use species-specific mixtures of hormones and their metabolites as sex pheromones. In *Chemical Signals in Vertebrates VI,* R. Doty and D. Muller-Schwarze, ed. Plenum Press, New York (in press).

Stacey, N. E. 1976. Effects of indomethacin and prostaglandins on the spawning behaviour of female goldfish. *Prostaglandins* **12:** 113–126.

Stacey, N. E. 1987. Roles of hormones and pheromones in fish reproductive behavior. Pp. 28–69 in *Psychobiology of Reproductive Behavior,* D. Crews, ed. Prentice-Hall, New York.

Stacey, N. E. 1991. Hormonal pheromones in fish: status and prospects. Pp. 177–181 in *Proceedings of the Fourth International Symposium on the Reproductive Physiology of Fish,* A. P. Scott, J. P. Sumpter, D. E. Kime, and M. S. Rolfe, eds. Fishsymp, Sheffield, UK.

Stacey, N. E., and F. W. Goetz. 1982. Role of prostaglandins in fish reproduction. *Can. J. Fish. Aquat. Sci.* **39:** 92–98.

Stacey, N. E., and R. E. Peter. 1979. Central action of prostaglandins in spawning behavior in the goldfish. *Physiol. Behav.* **30:** 621–628.

Stacey, N. E., and P. W. Sorensen. 1991. Function and evolution of fish hormonal pheromones. Pp. 109–135 in *Biochemistry and Molecular Biology of Fishes,* Vol. 1, P. L. Hochachka and T. P. Mommsen, eds. Elsevier, Toronto.

Stacey, N. E., P. W. Sorensen, J. G. Dulka, and G. J. Van Der Kraak. 1989. Direct evidence that 17α,20β-dihydroxy-4-pregnen-3-one functions as the preovulatory pheromone in goldfish. *Gen. Comp. Endocrinol.* **75:** 62–70.

Watanabe, Y., H. Tokumoto, A. Yamahita, S. Natramiya, N. Mizuno, and O. Hayaishi. 1985. Specific binding of prostaglandin D_2, E_2, $F_{2\alpha}$ in postmortem human brain. *Brain Res.* **342:** 110–116.

Reference: *Biol. Bull.* **183:** 178– August, 1992)

The DOPA Ephemera: A Recurrent Motif in Invertebrates

J. HERBERT WAITE

Marine Biology–Biochemistry Program, College of Marine Studies, University of Delaware, Lewes, Delaware 19958

Abstract. 3,4-Dihydroxyphenylalanine (DOPA) occurs transiently in nature as a free or peptide-bound amino acid. It is probably universally distributed in tissues and fluids of invertebrates. DOPA is a highly versatile metabolite, participating in neuroendocrine, immune, and reproductive functions, as well as in the formation of such products as bioadhesives, silks, integuments, and pigments. The mechanism by which DOPA is formed from tyrosine or peptidyl tyrosine remains to be determined in most cases. Future advances in DOPA chemistry may lead to a better understanding of the resonance between structural and sensory functions in animals.

Introduction

3,4-Dihydroxyphenyl-L-alanine (DOPA) is a biochemical ephemera in the sense that it is rarely an end product and is a highly transient intermediate to boot. Its presence in living matter was established at the beginning of the 1900s (Bloch, 1917) and is, in the minds of most, intimately associated with the biosynthesis of neurotransmitters, hormones, and pigments in higher organisms (Nagatsu, 1973). In the blissfully arcane literature on invertebrates, however, DOPA finds a much more extensive functional distribution. Its metabolism affects everything from egg capsules to silks, integuments, immunity, and feeding. DOPA, the free amino acid, is invariably derived from tyrosine by a number of pathways that will be briefly discussed below. But there is another form, which I shall refer to as peptidyl-DOPA, that is widely distributed in nonarthropod invertebrates and generally associated with the formation of sclerotized structures (Waite, 1990). There is but a single known exception to its functional association with sclerotization, and that is the apparent role of peptidyl-DOPA in the biosynthesis of quinoprotein enzyme cofactors in eukaryotes (Janes *et al.*, 1990). In this case, a redox cofactor, peptidyl 6-hydroxy-DOPA, serves in the catalytic oxidation of amines.

Are tyrosine and peptidyl-tyrosine hydroxylated to their DOPA counterparts by the same suite of enzymes? Do they share similar functions? Do any of their functions overlap? Although there has been some speculation on these subjects, there are no clear answers yet. The aims of the present essay are: to describe the known enzymic origins of DOPA; to set out the phyletic distribution of DOPA and related metabolites; and to offer some thoughts on the significance of DOPA-containing pathways.

Origins of DOPA

To date, there are three known types of enzymes that form DOPA from tyrosine. Enzymes of the first type (type I) are found in the adrenal medulla of the kidney and sympathetic ganglia of the nervous system (or their equivalents) in higher animals (Nagatsu, 1973). The key enzyme here is tyrosine hydroxylase (TH; E.C. 1.14.16.2). TH is an iron-containing mixed-function oxidase that catalyzes the specific *o*-hydroxylation of tyrosine in the presence of pteridine cofactors:

$$\text{I. tyrosine} + O_2 + \text{tetrahydrobiopterin} \rightarrow \text{DOPA} + H_2O + \text{dihydrobiopterin.}$$

Dihydrobiopterin (DHP) is recycled as tetrahydrobiopterin by a NADPH-coupled DHP reductase (E.C. 1.6.99.7). TH is important as the rate-limiting step in catecholaminergic pathways (Nagatsu, 1973). The enzyme appears to be a tetramer of identical subunits weighing 60 kD each. Recent molecular studies suggest that, although a single gene encodes TH, several tissue-specific forms of TH mRNA may be produced by alternative splicing (Grima *et al.*, 1987). The role of heterogeneity in translated products is not known. The DOPA formed by

Received 30 March 1992; accepted 18 May 1992.

this enzyme is strictly transient and goes on to become dopamine followed by noradrenaline or adrenaline (adrenal medulla). The enzymatic hydroxylation of tyrosine in insect hemolymph is enhanced by the addition of tetrahydropteridine, a close relative of tetrahydrobiopterin (Pau and Kelly, 1975), but no one has yet suggested this enzyme activity to be that of TH. Although the enzyme is presumed to be ubiquitous, the actual distribution of TH in animals other than a few vertebrates and fruit flies, has not been rigorously demonstrated. TH is not capable of hydroxylating peptidyl-tyrosine (Waite and Marumo, unpublished studies).

The second enzymatic pathway, involving DOPA (type II), must be presented cautiously to avoid confusion. Indeed, if the multiplicity of names for the reaction pathway is any indication (*i.e.*, monophenolase, phenolase, phenoloxidase, tyrosinase, *o*-diphenolase, *o*-diphenoloxidase, polyphenoloxidase, DOPA oxidase, catecholase, or catecholoxidase), confusion already reigns. Two points can be made about type II enzymes: (1) enzyme-substrate specificity in various organisms, and even in tissues from the same organism, is highly diverse; and (2) these enzymes are capable, in principle, of catalyzing two distinct but not necessarily punctuated reactions. The first reaction is the *o*-hydroxylation of monophenols (such as tyrosine) to diphenols or catechols (such as DOPA). The recommended name for this activity is monophenol monooxygenase (E.C. 1.14.18.1). Note that the reaction must be primed by a catechol (Hearing *et al.*, 1978). Reaction stoichiometry for the conversion of the monophenol, tyrosine, is shown below[1]:

IIA. tyrosine + DOPA + O_2 → DOPA + DOPA-quinone + H_2O.

The second activity is the oxidative dehydrogenation of a catechol (such as DOPA) to an *o*-quinone. The Nomenclature Committee of the International Union of Biochemistry (1984) recommends catechol oxidase (E.C. 1.10.3.1) as the most appropriate name for this step:

IIB. DOPA + ½ O_2 → DOPA-quinone + H_2O.

Few, if any, of the enzymes in this class catalyze the two reactions equally well. The two rates are roughly comparable in the frog and human skin enzymes (Barisas and McGuire, 1974; Nishioka, 1978), while in fungal and microbial enzymes, IIB has a turnover number 10–20 times greater than IIA (Lerch and Ettlinger, 1972; Vanni and Gastaldi, 1990). Enzymes in insect cuticle rarely have detectable monophenol monoxygenase activity. This is also characteristic of enzymes involved in the tanning of various other sclerotized structures (Table I). Moreover, in a number of invertebrate structures, DOPA-derived metabolites may actually be oxidized by an enzyme activity more akin to laccase (E.C. 1.10.3.2), in which there is removal of only one electron at a time:

IIC. 4 DOPA + O_2 → 4 DOPA-semiquinone + $2H_2O$.

This can have the effect of shifting chemical reactivity from the ring to the sidechain of DOPA or related metabolites (Sugumaran, 1988; Hopkins and Kramer, 1992).

Considering the diversity of forms and roles that this class of enzymes encompasses, it is pointless to attempt to generalize its molecular properties. Thus far, the enzymes appear to contain binuclear copper in which the metals are often ferromagnetically silent (Jolley *et al.*, 1974). Sequence homologies around the active site of the enzymes appear to be high, especially with respect to histidines (Watters *et al.*, 1992; Müller *et al.*, 1988). In other respects, such as molecular weight, amino acid composition, and isoelectric point, enzymes from different organisms, even different tissues, vary greatly. Some of the fungal enzymes have demonstrated activity towards peptidyl-tyrosine (Marumo and Waite, 1986; Lissitzky and Rolland, 1962), but to the best of my knowledge, invertebrate catechol oxidases that have any effect on proteins prefer peptidyl-DOPA (Watters *et al.*, 1992; Waite, 1985).

The third enzyme-catalyzed pathway (type III) for producing DOPA from tyrosine involves peroxidase, but in an untypical setting. Peroxidases (from horseradish or milk) hydroxylate tyrosine to DOPA, *in vitro*, at temperatures near 0°C, when supplied with an electron donor such as dihydroxyfumarate (Klibanov *et al.*, 1981):

III. tyrosine + O_2 + dihydroxyfumarate → DOPA + oxalooxalate + H_2O.

This reaction is intriguing in that it requires oxygen instead of peroxide. Yields of DOPA can be as high as 70%, although at temperatures above 0°C, many byproducts are formed. It is unknown whether the peroxidase formation of DOPA has any biological basis, or whether peptidyl tyrosine can be converted to peptidyl-DOPA.

Distribution of DOPA Pathways

Reaction pathways involving DOPA and related products are widely distributed throughout the Invertebrata. The composite creature in Figure 1 represents an integration of all the DOPA pathways with known functions. Probably no single organism possesses all of these pathways, although certain arthropods may come close. Tyrosine and DOPA are involved in the cephalopod ink sac where an enzyme of category II (with both monophenol monoxygenase and catecholoxidase activities) converts the two amino acids to melanin (Prota *et al.*, 1981). When ejected into the environment, the black ink serves as a defensive olfactory and visual cloaking device. Aphids se-

[1] N.B. When tyrosine is the only substrate, the enzyme is termed a tyrosinase.

Table I

A functional menagerie [illegible] pathways in invertebrate animals. Enzyme activity is subdivided into monophenol mo[illegible] catecholoxidase (IIB)

Tissue	Enzyme	Native substrate	Refs
Proto[illegible]			
Spore[illegible]	IIB	?	1
Hap[illegible]sporidia			
Ctenophora			
Nervous system	II?	DOPA/cysteinylDOPA	2
Cnidaria			
Nervous system	II?	DOPA/tyrosine	3
Coelenterate hydrozoa			
Gorgonin	?	Peptidyl-DOPA	4
Sea fans			
Perisarc	IIB	Dopamine (?)	5
Hydroids			
Platyhelminthes			
Eggshell	IIA & B	Peptidyl-DOPA	6
Trematodes, turbellarians			
Metacercarial cyst	IIB	?	7
Trematodes			
Annelida			
Cocoon	IIB	Peptidyl-DOPA	8
Leech			
Coelomic fluid	IIB	?	9
Earthworm			
Cement	IIB	Peptidyl-DOPA	10
Sabellarid polychaetes			
Mollusca			
Ink sac	IIA & B	D-DOPA/tyrosine	11
Various cephalopods			
Byssus	IIB	Peptidyl-DOPA	12
Mussels			
Hemolymph	IIB	?	13
Various bivalves			
Periostracum	IIB	Peptidyl-DOPA	14
Mussels			
Shell Matrix	IIA & B	Peptidyl-DOPA	15
Clams, oysters, mussels			
Arthropods			
Silk	IIB	N-3,4-dihydroxyphenyllactyl DOPA	16
Silkworm moths			
Saliva	IIB	DOPA; catechin	17
Aphids, wasps			
Cuticle	IIA, B & C	N-acetyldopamine	18
Various insects			
Blood cells	I, IIA & B	Tyrosine, DOPA ?	19
Crayfish, cockroaches			
Ootheca	IIB	Protocatechuic acid; N-acyldopamine	20
Cockroach, mantids			
Wing pigment	IIB	N-β-alanyldopamine, L-kynurenine	21
Butterflies			
Echinodermata			
Brown bodies	IIB	DOPA ?	22
Sea cucumbers			
Urochordata			
Blood cells	IIB	Peptidyl-DOPA	23
Ascidians			

[1]Varndell (1981); [2]Carlberg (1988); [3]Carlberg and Elofsson (1987); [4]Tidball (1982); Holl *et al.* (1992); [5]Knight (1968); [6]Waite and Rice-Ficht (1987); Smyth and Clegg (1959); Nollen (1971); [7]Campbell (1960); [8]Knight and Hunt (1974); [9]Valembois *et al.* (1988); [10]Vovelle (1965); Jensen and Morse (1988); [11]Prota *et al.* (1985), [12]Waite (1985); Rzepecki *et al.* (1991); [13] Belyayeva (1981); [14]Waite and Wilbur (1976); Waite and Andersen (1978); [15]Wheeler *et al.* (1988); Samata *et al.* (1980); [16]Kawasaki and Sato (1985); Przibram and Schmalfuss (1927); Kramer *et al.* (1989); [17]Peng and Miles (1988); [18]Hopkins and Kramer (1992); [19]Johansson and Söderhäll (1989); [20]Kramer *et al.* (1989); Kawasaki and Yagi (1983); Whitehead *et al.* (1960); Yago *et al.* (1990), [21]Yago (1989); [22]Canicatti and Seymour (1991); [23]Azumi *et al.* (1990); Watters *et al.* (1992); Chaga (1980); Dorsett *et al.* (1987); Smith *et al.* (1991).

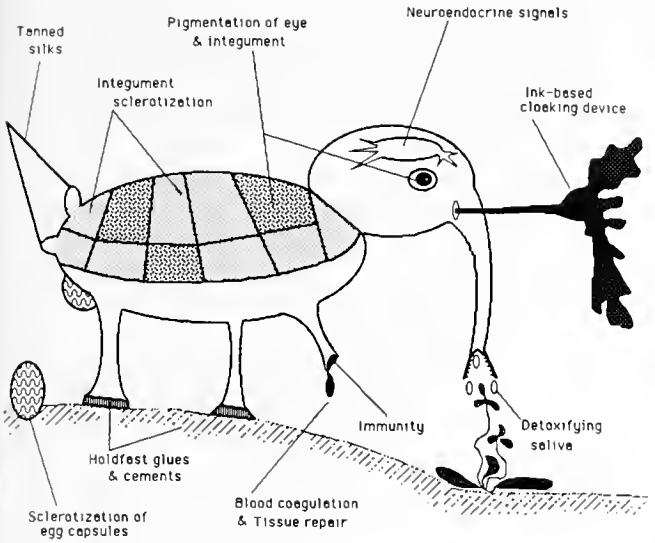

Figure 1. DOPA and enzymes that metabolize DOPA are phylogenetically and organismically scattered throughout the invertebrates. This illustration attempts to integrate all reported functions of DOPA chemistry in a single fantastical chimaera. See text and Table 1 for specific details.

crete a catechol oxidase into their meals to detoxify plant tissues rich in phenols (Peng and Miles, 1988). DOPA and related metabolites in plants and seeds pose an effective chemical barrier against many herbivores lacking in such salivary activity (Rehr *et al.,* 1973). Insects (Nappi *et al.,* 1991), crustaceans (Johansson and Söderhäll, 1988), holothuroids (Canicatti and Seymour, 1991), molluscs (Belyayeva, 1981), annelids (Valembois *et al.,* 1988), and tunicates (Watters *et al.,* 1992) have type II enzyme activity in body fluids, where it functions in a cell-mediated immunity leading to the encapsulation of foreign material and often the repair of injured tissue. In arthropods, the enzyme is present as a zymogen and activated by a pathogen-sensitive protease (Aspan and Söderhäll, 1991). Both monophenol monoxygenase and catechol oxidase activities are present in arthropods, while in ascidians and holothuroids only catechol oxidase is detectable (Canicatti and Seymour, 1991; Watters *et al.,* 1992). There are very few data on the molecular kinetics of these enzymes, and fewer still on the identity of the physiological substrates of such enzymes. Nappi *et al.* (1991) observed that blood tyrosine levels increased during parasite infection of *Drosophila melanogaster,* and tyrosine would be an appropriate substrate if melanin production were the chief aim of the enzyme. Perhaps the DOPA-containing peptides of morula cells (Dorsett *et al.,* 1987; Azumi *et al.,* 1990; Smith *et al.,* 1991) serve as substrates for catecholoxidase in ascidians.

Quinone-tanned adhesives and cements are especially common among marine mussels and sabellariid polychaetes. Precursors of these materials include catechol oxidases and DOPA-containing proteins, many of which have been sequenced (Vovelle, 1965; Waite, 1985; Jensen and Morse, 1988; Rzepecki *et al.,* 1991). Catechol oxidase activity has been histochemically detected in barnacle cement, but the native substrate acted upon is unknown (Yule and Walker, 1987). DOPA-containing proteins and catecholoxidases are also implicated in the sclerotization of trematode and turbellarian egg capsules and cysts (Smyth and Clegg, 1959; Nollen, 1971; Ishida and Teshirogi, 1986; Waite and Rice-Ficht, 1987). In insect ootheca, the DOPA derivatives are not protein-bound, but rather DOPA-derived metabolites of low molecular weight; *e.g.,* protocatechuic acid in cockroach ootheca (Whitehead *et al.,* 1960), and N-acyldopamines in mantid ootheca (Kawaski and Yago, 1983). The same situation seems pertinent in many insect silks, which are tanned by the action of DOPA metabolites and catechol oxidase (Przibram and Schmalfuss, 1927; Kawasaki and Sato, 1985; Kramer *et al.,* 1989).

The most extensive exploitation of DOPA chemistry has undoubtedly occurred in the development of exoskeletal integuments. This includes the ubiquitous cuticles of insects (Hopkins and Kramer, 1992), molluscan shells (Degens *et al.,* 1967), coelenterate exoskeletons such as gorgonin and perisarc (Knight, 1968; Holl *et al.,* 1992), tunicates (Robinson *et al.,* 1986) and, possibly, some of the infinitely varied packaging strategies of creatures like tardigrades, loricates, bryozoans, *etc.* (Waite, 1990). Sclerotization of insect cuticles has come to mean at least two different pathways involving oxidases and DOPA-derived metabolites (Brunet, 1980; Sugumaran, 1988). In β-sclerotization, protein cross-linking activity is localized on the N-acetylethyl side chain of N-acetyldopamine (NADA) (Andersen, 1974). The cross-linked products are colorless *in vivo* but as yet chemically uncharacterized. The more classical pathway dubbed "quinone-tanning" (which probably doubles in melanization) involves a direct attack on the aromatic ring by nucleophilic groups, presumably from the protein-chitin components (Hopkins and Kramer, 1992). Details about the chemical transformations occuring during sclerotization are still controversial (Sugumaran, 1988) and beyond the scope of this article. Crustaceans and insects may share many of the same features of cuticle sclerotization, but this is not the case for other arthropods such as arachnids, chelicerates, and chilopodes, nor for other invertebrates such as mollusks and coelenterates (especially gorgonians). In at least some of these instances, sclerotization, although still ostensibly based on quinone-tanning, appears to involve the action of catecholoxidase on DOPA-containing proteins. How widespread this strategy really is remains unclear (Waite, 1990).

The function of pigmentation by melanin formation is still debated (Hill, 1992). It may protect underlying tissues from ultraviolet light, to scavenge radicals, or to provide

adaptive colorations, *e.g.* camouflage or adornment. In contrast to vertebrate pigmentation is largely an intracellular event in skin, eyes, and hair bulb cells, invertebrates secrete the granular organelles containing and substrate precursors directly into acellular (Riley, 1977; Hiruma and Riddiford, 1988). The two most common melanins, eumelanin and pheomelanin, are formed by the catalytic oxidation and polymerization of DOPA, or DOPA and cysteine, respectively (Prota and Thompson, 1976). Insect pigments such as papilliochrome (Table I), derived from other DOPA-derived co-reactants, are also possible (Yago, 1989) and probably common.

In the neuroendocrine systems of higher organisms, DOPA is formed from tyrosine by tyrosine hydroxylase (type I). Not until its further transformation to dopamine, noradrenaline or adrenaline, however, is the *o*-diphenol endowed with neuroendocrine function. Subsequent transformations, involving *O*-methylation, sulfation, or oxidation to pigments, may just be ways of terminating the signal function (Nagatsu, 1973). That dopamine and noradrenaline are *not* universally employed as neurotransmitters is suggested by the discovery that only DOPA and related metabolites (5-hydroxyDOPA and cysteinylDOPA) occur in the nervous systems of some cnidarians and ctenophores (Carlberg and Elofsson, 1987; Carlberg, 1988). If a type II enzyme is responsible for the formation of DOPA and cysteinyl-DOPA in these organisms, then it would be intriguing to know how melanins are prevented from forming. Indeed, perhaps there is a suggestion here that neurotransmitters and pigments-sclerotins may have had a common evolutionary origin in the ectoderm of primitive organisms.

Significance of DOPA

Table I is, alas, a bitter pill for those wishing to discover the origin of DOPA in invertebrates. With the exception of the neuroendocrine catecholamines and melanization pathways (inks, host encapsulation of pathogens, and pigmentation), pathetically little is known about the formation of DOPA and peptidyl-DOPA. Is the hydroxylation brought about by a tetrahydropterin-linked tyrosine hydroxylase, a type IIA monophenol monoxygenase, or even a prolyl hydroxylase (E.C.1.14.11.2)-like activity directed instead toward peptidyl-tyrosyl residues? Nothing at present detracts from or advocates any of these. Many organisms go to considerable lengths to separate, even compartmentalize, the tyrosine-to-DOPA and DOPA-to-quinone steps into discrete, non-continuous biochemical transformations. Why should this be, when a bifunctional type II enzyme could have done it in one fell swoop? The answer may be that transient DOPA has unique functions that cannot be properly discharged when the tyrosine to quinone conversion is unpunctuated. Waite (1987) has suggested that peptidyl-DOPA may have important metal chelating roles during adhesion in DOPA-containing marine glues. Another suggestive function is emerging in the area of larval settlement cues. The larvae of gregariously sessile invertebrates, such as barnacles, sabellariid polychaetes, mussels, oysters, and others, are attracted with varying degrees of fastidiousness by conspecific cues arising from such materials as shell (Crisp, 1967), cement (Jensen and Morse, 1984), byssal threads (Eyster and Pechenik, 1987), and body extracts (Crisp and Meadows, 1962). Some of these effects on settlement are ostensibly mimicked by exposing the larvae to DOPA (Jensen and Morse, 1984; Coon *et al.*, 1985), DOPA-metabolites (Chevolot *et al.*, 1991; Pires and Hadfield, 1991), and DOPA-derived microbial exopolymers (Fitt *et al.*, 1990). The biological relevance of free DOPA as a marine cue has been vigorously debated and with good cause (Jensen and Morse, 1990; Pawlik, 1990; Johnson *et al.*, 1991). DOPA is notoriously unstable in seawater. Moreover, the *specific* appeal of many cue-containing materials would seem to militate against their reliance on metabolites as common as free DOPA. Crisp (1974) first proposed that, because of the nature of lamellar-turbulent flow, effective settlement cues were only to be found following physical contact with the surface. This suggests that larvae have sensors (receptors) for immobilized cues present on settlement surfaces. Perhaps then peptidyl-DOPA (or one of its metabolites) present in natural settlement-inducing materials, such as shell, byssus, or cement, is the cue. This would satisfy two observations: that free DOPA can mimic settlement cues to some extent, and that settlement cues are highly selective. The latter would be fulfilled, for example, if larvae sensed some form of DOPA, as well as primary flanking sequences in the protein.

Postscript

The potential number and diversity of DOPA-producing and oxidizing enzymes in invertebrates casts a pall on strategies that involve their purification and characterization after the whole organism has been disrupted. Although such studies are still commonplace (*e.g.*, Oshima and Nagayama, 1980; Simpson *et al.*, 1987; Maruyama *et al.*, 1991), they will have very little to offer biology until at last they address the functions and distribution of the enzymes *in vivo*. The DOPA ephemera is unique in that it seems to be pivotal in the seesaw between structural and sensory biochemistry. A better understanding of the evolutionary and physiological resonance between these two would undoubtedly scintillate any number of sclerotized minds, including mine.

Acknowledgments

There are too many researchers to whom I owe a debt of gratitude for advancing or assiduously working the field.

I thank them all and make my apologies in advance to those who feel slighted at not being properly represented in the cited literature. I never intended to write an exhaustive review of this subject, simply a probing overview. Bill Carr deserves credit for tempting me to step into this morass.

Literature Cited

Andersen, S. O. 1974. Evidence for two mechanisms of sclerotization in insect cuticle. *Nature* **251:** 507–508.

Aspan, A., and K. Söderhäll. 1991. Purification of prophenoloxidase from crayfish blood cells and its activation by an endogenous serine proteinase. *Insect Biochem.* **21:** 363–371.

Azumi, K., H. Yokosawa, and S. Ishii. 1990. Presence of 3,4-dihydroxyphenylalanine-containing peptides in hemocytes of the ascidian *Halocynthia roretzi*. *Experientia* **46:** 1020–1023.

Barisas, B. G., and J. S. McGuire. 1974. Proteolytically activated tyrosinase from frog epidermis. *J. Biol. Chem.* **249:** 3151–3156.

Belyayeva, T. G. 1981. Fenoloksidaza u morskikh dvustvorchatykh mollyuskov *Crenomytilus grayanus* i *Modilous difficilis*. *Zhur. Obsh. Biol.* **42:** 771–779.

Bloch, B. 1917. Chemische Untersuchung über das specifische pigmentbildende Ferment der Haut, die DOPA-oxidase. *Hoppe-Seylers Z. Physiol. Chem.* **98:** 226–254.

Brunet, P. C. J. 1980. The metabolism of the aromatic acids concerned in the cross-linking of insect cuticle. *Insect Biochem.* **10:** 467–500.

Campbell, W. C. 1960. Presence of phenolase in the fasciolid metacercarial cyst. *J. Parasitol.* **46:** 848.

Canicatti, C., and J. Seymour. 1991. Evidence for phenoloxidase activity in *Holothuria tubulosa* (Echinodermata) brown bodies and cells. *Parasitol. Res.* **77:** 50–53.

Carlberg, M. 1988. Localisation of catechol compounds in the ctenophore *Mnemiopsis leidyi*. *Comp. Biochem. Physiol.* **91C:** 69–74.

Carlberg, M., and R. Elofsson. 1987. Presence of DOPA and TOPA in coelenterate nervous system. *Neurochem. Intern.* **11:** 161–167.

Chaga, O. Y. 1980. Orto-difenoloksidaznaya sistema of astsidii. *Tsitologiya* **22:** 619–625.

Chevolot, L., J. C. Cochard, and J. C. Yvin. 1991. Chemical induction of larval metamorphosis of *Pecten maximus* with a note on the nature of naturally occurring triggering substances. *Mar. Ecol. Prog. Ser.* **74:** 83–89.

Coon, S. L., D. B. Bonar, and R. M. Weiner. 1985. Induction of settlement and metamorphosis of the pacific oyster, *Crassostrrea gigas* (Thunberg) by L-DOPA and catecholamines. *J. Exp. Mar. Biol. Ecol.* **94:** 211–221.

Crisp, D. J. 1974. Surface chemistry and life in the sea. *Chemistry & Industry* **5:** 187–193.

Crisp, D. J. 1967. Chemical factors inducing settlement in *Crassostrea virginica* (Gmelin). *J. Animal Ecol.* **36:** 329–335.

Crisp, D. J., and P. S. Meadows. 1962. Adsorbed layers—the stimulus to settlement in barnacles. *Proc. R. Soc. B.* **158:** 364–387.

Degens, E. T., D. W. Spencer, and R. H. Parker. 1967. Paleobiochemistry of molluscan proteins. *Comp. Biochem. Physiol.* **20:** 553–579.

Dorsett, L. C., C. J. Hawkins, J. A. Grice, M. F. Lavin, P. M. Merefield, D. L. Parry, and I. L. Ross. 1987. Ferreascidin: A highly aromatic protein containing 3,4-dihydroxyphenylalanine from the blood cells of a stolidobranch ascidian. *Biochemistry* **26:** 8078–8082.

Eyster, L. S., and J. A. Pechenik. 1987. Attachment of *Mytilus edulis* larvae on algal and byssal filaments is enhanced by water agitation. *J. Exp. Mar. Biol. Ecol.* **114:** 99–110.

Fitt, W. K., S. L. Coon, M. Walch, R. M. Weiner, R. R. Colwell, and D. B. Bonar. 1990. Settlement behavior and metamorphosis of oyster larvae (*Crassostrrea gigas*) in response to bacterial supernatants. *Mar. Biol.* **106:** 389–394.

Grima, B., A. Lamouroux, C. Boni, J. F. Julien, F. Javoy-Agid, and J. Mallet. 1987. A single human gene encoding multiple tyrosine hydroxylases with different predicted functional characteristics. *Nature* **326:** 707–711.

Hearing, V. J., T. M. Ekel, P. M. Montague, E. D. Hearing, and J. M. Nicholson. 1978. Mammalian tyrosinase: isolation by a simple new procedure and characterization of its steric requirements for cofactor activity. *Arch. Biochem. Biophys.* **185:** 407–418.

Hill, H. Z. 1992. The function of melanin or six blind people examine an elephant. *BioEssays* **14:** 49–56.

Hiruma, K., and L. M. Riddiford. 1988. Granular phenoloxidase involved in cuticular melanization in the tobacco hornworm. *Dev. Biol.* **130:** 87–97.

Holl, S. M., J. Schaefer, W. M. Goldberg, K. J. Kramer, T. D. Morgan, and T. L. Hopkins. 1992. Comparison of black coral skeleton and insect cuticle by a combination of C-13 NMR and chemical analyses. *Arch. Biochem. Biophys.* **292:** 107–127.

Hopkins, T. L., and K. J. Kramer. 1992. Insect cuticle sclerotization. *Annu. Rev. Entomol.* **37:** 87–97.

Ishida, S., and W. Teshirogi. 1986. Eggshell formation in polyclads (Turbellaria). *Hydrobiologia* **132:** 127–135.

Janes, S. M., D. Wemmer, A. J. Smith, S. Kaur, D. Maltby, A. L. Burlingame, and J. P. Klinman. 1990. A new redox cofactor in eukaryotic enzymes: 9-hydroxyDOPA at the active site of serum amine oxidase. *Science* **248:** 981–987.

Jensen, R. A., and D. E. Morse. 1990. Chemically induced metamorphosis of polychaete larvae in both the laboratory and ocean environment. *J. Chem. Ecol.* **16:** 911–930.

Jensen, R. A., and D. E. Morse. 1988. The bioadhesive of *Phragmatopoma californica* tubes: a silk-like cement containing L-DOPA. *J. Comp. Physiol. B* **158:** 317–328.

Jensen, R. A., and D. E. Morse. 1984. Intraspecific facilitation of larval recruitment: gregarious settlement of polychaete *Phragmatopoma californica*. *J. Exp. Mar. Biol. Ecol.* **83:** 107–126.

Johansson, M. W., and K. Söderhäll. 1989. Cellular immunity in crustaceans and the prophenoloxidase system. *Parasitol. Today* **5:** 171–176.

Johnson, C. R., D. G. Muir, and A. L. Reysenbach. 1991. Characteristic bacteria associated with surfaces of coralline algae: a hypothesis for bacterial induction of marine invertebrate larvae. *Mar. Ecol. Prog. Ser.* **74:** 281–294.

Jolley, R. L., L. H. Evans, N. Makino, and H. S. Mason. 1974. Oxytyrosinase. *J. Biol. Chem.* **249:** 335–345.

Kawasaki, H., and M. Yago. 1983. The identification of 2 N-acyldopamine glucosides in the left colleterial gland of the praying mantid *Tenodera aridifolia* and their role in oothecal sclerotization. *Insect Biochem.* **13:** 267–271.

Kawasaki, H., and H. Sato. 1985. The tanning agent of the Japanese giant silkmoth *Dictyoploca japonica* Butler. *Insect Biochem.* **15:** 681–684.

Klibanov, A. M., Z. Berman, and B. N. Alberti. 1981. Preparative hydroxylation of aromatic compounds catalyzed by peroxidase. *J. Am. Chem. Soc.* **103:** 6263–6264.

Knight, D. P., and S. Hunt. 1974. Molecular and ultrastructural characterization of the egg capsule of the leech *Erpobdella octoculata* L. *Comp. Biochem. Physiol.* **47A:** 871–880.

Knight, D. P. 1968. Cellular basis for quinone tanning of the perisarc in the thecate hydroid *Campanularia (Obelia) flexuosa* Hinks. *Nature* **218:** 584–586.

Kramer, K. J., V. Bork, J. Schaefer, T. D. Morgan, and T. L. Hopkins. 1989. Solid state 13C NMR and chemical analyses of insect noncuticular sclerotized support structures: mantid oothecae and cocoon silks. *Insect Biochem.* **19:** 69–77.

Lerch, K., and L. Ettlinger. 1972 ...tion and characterization of a tyrosinase from *Strepto* ...*cens*. *Eur. J. Biochem.* **31:** 427–437.

Lissitzky, S., and M. R... ...oxydation de la tyrosine et de peptides ou prote... ...ut, par la polyphenoloxydase de champignon *b*... ...*ta* **56:** 95–110.

Maruno, K., and J. U... ...1986. Optimization of the hydroxylation of tyrosine and ...ontaining peptides by mushroom tyrosinase. *Btochim. Biophys. Acta* **872:** 98–103.

Maruyama, N., H. Etoh, K. Sakata, and K. Ina. 1991. Studies on the phenoloxidase from *Mytilus edulis* associated with adhesion. *Agric. Biol. Chem.* 55: 2887–2889.

Muller, G., S. Ruppert, E. Schmid, and G. Schütz. 1988. Functional analysis of alternatively spliced tyrosinase gene transcripts. *EMBO J.* 7: 2723–2730.

Nagatsu, T. 1973. *Biochemistry of Catecholamines.* University Park Press, Baltimore.

Nappi, A. J., Y. Carton, and F. Frey. 1991. Parasite-induced enhancement of hemolymph tyrosinase activity in a selected immune reactive strain of *Drosophila Melanogaster*. *Arch. Insect Biochem. Physiol.* **18:** 159–168.

Nishioka, K. 1978. Particulate tyrosinase of human malignant melanoma. *Eur. J. Biochem.* **85:** 137–148.

Nollen, P. M. 1971. Digenetic trematodes: quinone tanning system in eggshells. *Exp. Parasitol* **30:** 64–72.

Nomenclature Committee of IUB 1984. *Enzyme Nomenclature.* Academic Press, Orlando.

Oshima, T., and F. Nagayama. 1980. Purification and properties of catecholoxidase from krill. *Bull. Jpn. Soc. Sci Fish.* **46:** 1036–1042.

Pau, R. N., and C. Kelly. 1975. The hydroxylation of tyrosine by and enzyme from the 3rd instar larvae of the blowfly *Calliphora erythrocephala Biochem J* **147:** 565–573.

Pawlik, J. R. 1990. Natural and artificial induction of metamorphosis of *Phragmatopoma lapidosa californica* (Polychaeta: sabellariidae), with a critical look at the effects of bioactive compounds on marine invertebrate larvae. *Bull. Mar Sci.* **46:** 512–536.

Peng, Z., and P. W. Miles. 1988. Studies of the salivary physiology of plant bugs: function of the catecholoxidase of rose aphids. *J Insect Physiol.* **34:** 1027–1033.

Pires, A., and M. G. Hadfield. 1991. Oxidation breakdown products of catecholamines and H_2O_2 induce partial metamorphosis in the nudibranch *Phestilla sibogae* Bergh. *Biol. Bull.* **180:** 310–317.

Prota, G., and R. H. Thompson. 1976. Melanin pigmentation in mammals. *Endeavour* **35:** 32–39.

Prota, G., J. P. Ortonne, C. Voulot, C. Khatchadourian, G. Nardi, and A. Palumbo. 1981. Occurrence and properties of tyrosinase in the ejected ink of cephalopods. *Comp. Biochem. Physiol. B* **68:** 415–419.

Przibram, H., and H. Schmalfuss. 1927. Das Dioxyphenylalanin in den Kokons des Nachtpfauenauges *Samia cecropia* L. *Biochem. Z.* **187:** 467–469.

Rehr, S. S., D. H. Janzen, and P. P. Feeny. 1973. L-DOPA in legume seeds: a chemical barrier to insect attack. *Science* **181:** 81–82.

Riley, P. A. 1977. The mechanism of melanogenesis in comparative biology of skin. *Symp. Zool. Soc. Lond.* **39:** 77–95.

Robinson, W. E., K. Kustin, and R. A. Cloney. 1986. The influence of tunichrome and other reducing compounds on tunic and fin formation in embryonic *Ascidia callosa* Stimpson. *J Exp. Zool* **237:** 63–72.

Rzepecki, L. M., S. S. Chin, J. H. Waite, and M. A. Lavin. 1991. Molecular diversity of marine glues: polyphenolic proteins from five mussel species. *Mol. Mar. Biol. Biotechnol* **1:** 78–88.

Samata, T., P. Sanguansri, C. Cazaux, M. Hamm, J. Engels, and G. Krampitz. 1980. Biochemical studies on the components of mollusk shells. Pp. 37–47 in *Mechanisms of Biomineralisation in Animals and Plants.* M. Omori, and N. Watabe, eds. Tokai University Press, Tokyo.

Simpson, B. K., M. R. Marshall, and W. S. Otwell. 1987. Phenoloxidase from shrimp (*Penaeus setiferus*) Purification and some properties. *J. Agric. Food Chem* **35:** 918–921.

Smith, M. J., D. Kim, B. Horenstein, K. Nakanishi, and K. Kustin. 1991. Unraveling the chemistry of tunichrome. *Acc. Chem. Res.* **24:** 117–124.

Smyth, J. D., and J. A. Clegg. 1959. Egg shell formation in trematodes and cestodes. *Exp. Parasitol.* **8:** 286–323.

Sugumaran, M. 1988. Molecular mechanisms for cuticular sclerotization. *Adv. Insect Physiol.* **21:** 179–231.

Tidball, J. G. 1982. Ultrastructural and cytochemical analysis of the cellular basis for tyrosine derived collagen cross-links in *Leptogorgia virgulata* (Cnidaria). *Cell. Tiss. Res.* **222:** 635–645.

Valembois, P. P., P. Roche, and P. Götz. 1988. Phenoloxidase activity in the coelomic fluid of earthworms. *Dev. Comp. Immunol.* **13:** 429–430.

Vanni, A., and D. Gastaldi. 1990. Kinetic investigations on the double enzymic activity of the tyrosinase mushroom. *Ann. Chim.* **80:** 35–60.

Varndell, I. M. 1981. Catecholoxidase activity associated with sporogenesis in *Haplosporidium malacobdellae*. *Z. Parasitenkd.* **65:** 153–162.

Vovelle, J. 1965. Le tube de *Sabellaria alveolata* (L.) annelide polychete Hermellidae et son ciment etude ecologique, experimentale, histologique et histochimique. *Arch. Zool. Exp. Gen* **106:** 1–187.

Waite, J. H. 1990. Phylogeny and chemical diversity of quinone-tanned glues and varnishes. *Comp Biochem. Physiol. B* **97:** 19–29.

Waite, J. H. 1987. Nature's underwater adhesive specialist. *Int. J. Adhes Adhesion* 7: 9–14.

Waite, J. H. 1985. Catechol oxidase in the byssus of the common mussel *Mytilus edulis*. *J Mar. Biol Assoc. UK* **65:** 359–371.

Waite, J. H., and S. O. Andersen. 1978. DOPA in an insoluble shell protein of *Mytilus edulis*. *Biochim. Biophys. Acta* **541:** 107–114.

Waite, J. H., and K. M. Wilbur. 1976. Phenoloxidase in the periostracum of the marine mollusc *Modiolus demissus* Dillwyn. *J. Exp. Zool.* **195:** 359–367.

Waite, J. H., and A. C. Rice-Ficht. 1987. Presclerotized eggshell protein from the liver fluke *Fasciola hepatica*. *Biochemistry* **26:** 7819–7825.

Watters, D., I. Ross, B. Garrone, M. McEwan, W. Finlayson, C. Hawkins, and M. Lavin. 1992. A catechol oxidase from the blood cells of the ascidian *Pyura stolonifera* is a member of the tyrosinase family. *Mol., Mar. Biol. Biotechnol.* (in press.)

Wheeler, A. P., K. W. Rusenko, D. M. Swift, and C. S. Sikes. 1988. Regulation of *in vitro* and *in vivo* of $CaCO_3$ crystallization by fractions of oyster shell matrix. *Mar. Biol* **98:** 71–80.

Whitehead, D. L., P. C. J. Brunet, and P. W. Kent. 1960. Specificity *in vitro* of a phenoloxidase from *Periplaneta americana*. *Nature* **185:** 610.

Yago, M. 1989. Enzymic synthesis of papiliochrome II, a yellow pigment in the wings of papilionid butterflies. *Insect Biochem.* **19:** 673–678.

Yago, M., H. Sato, S. Oshima, and H. Kawasaki. 1990. Enzymic activities involved in the oothecal sclerotization of the praying mantid *Tenodera aridifolia sinensis*. *Insect Biochem.* **20:** 745–750.

Yule, A. B., and G. Walker. 1987. Adhesion in barnacles. Pp. 389–404 in *Crustacean Issues Barnacle Biology*, A. J. Southward, ed. Balkema, Rotterdam.

CONTENTS

Volume 183 Number 2

THE BIOLOGICAL BULLETIN

OCTOBER, 1992

Published by the Marine Biological Laboratory

Future Classics

Marine Ecology of the Arabian Region

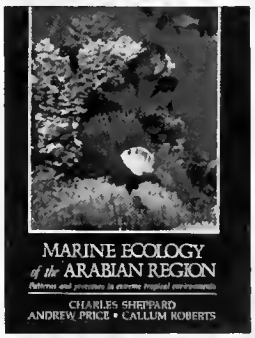

Patterns and Processes in Extreme Tropical Environments

Charles Sheppard, Andrew Price, and Callum Roberts

This book summarizes the available information on the Arabian region, then reviews the processes shaping the various marine and coastal systems. Some of the world's poorest and richest nations border these seas, making diverse claims on fisheries and other natural resources. The Gulf War was a recent example of the wide range of impacts affecting the region.

May 1992, 368 pp., $64.00/ISBN: 0-12-639490-3

Dynamic Aquaria

Building Living Ecosystems

Walter H. Adey and Karen Loveland

The book presents exciting new concepts that will provide scientists, professional aquarists, and hobbyists with the opportunity to learn how to closely approximate natural ecosystems in closed, artificial environments.

1991, 643 pp., $39.95/ISBN: 0-12-043790-2

The Ecology of Fishes on Coral Reefs

edited by
Peter F. Sale

From the Foreword

"**The Ecology of Fishes on Coral Reefs** can provide a foundation on which to build future research."

—PAUL R. EHRLICH
Stanford University, California

1991, 754 pp., $69.95/ISBN: 0-12-615180-6

Artificial Habitats for Marine and Freshwater Fisheries

edited by
William Seaman Jr. and Lucian M. Sprague

This book provides a comprehensive review of the facts, issues, and global trends emerging from the use of artificial habitats in aquatic ecosystems.

1991, 285 pp., $39.95/ISBN: 0-12-634345-4

Ecology and Classification of North American Freshwater Invertebrates

edited by
James H. Thorp and Alan P. Covich

Ecology and Classification of North American Freshwater Invertebrates, written by experts in the ecology of various freshwater invertebrate groups, is the most up-to-date and informative text of its kind. The coverage includes all freshwater invertebrate phyla with an emphasis on ecological information.

1991, 911 pp., $59.95/ISBN: 0-12-690645-9

Order from your local bookseller or directly from

ACADEMIC PRESS
HBJ Order Fulfillment Department #17915
6277 Sea Harbor Drive, Orlando, FL 32887

CALL TOLL FREE
1-800-321-5068
FAX **1-800-336-7377**

THE BIOLOGICAL BULLETIN

PUBLISHED BY
THE MARINE BIOLOGICAL LABORATORY

OCTOBER, 1992

Printed and Issued by
LANCASTER PRESS, Inc.
3575 HEMPLAND ROAD
LANCASTER, PA

THE BIOLOGICAL BULLETIN

THE BIOLOGICAL BULLETIN is published six times a year by the Marine Biological Laboratory, MBL Street, Woods Hole, Massachusetts 02543.

Subscriptions and similar matter should be addressed to Subscription Manager, THE BIOLOGICAL BULLETIN, Marine Biological Laboratory, Woods Hole, Massachusetts 02543. Single numbers, $30.00. Subscription per volume (three issues), $77.50 ($155.00 per year for six issues).

Communications relative to manuscripts should be sent to Michael J. Greenberg, Editor-in-Chief, or Pamela L. Clapp, Managing Editor, at the Marine Biological Laboratory, Woods Hole, Massachusetts 02543. Telephone: (508) 548-3705, ext. 428. FAX: 508-540-6902. E-mail: pamcl@hoh.mbl.edu.

POSTMASTER: Send address changes to THE BIOLOGICAL BULLETIN, Marine Biological Laboratory, Woods Hole, MA 02543.

Second-class postage paid at Woods Hole, MA, and additional mailing offices.
ISSN 0006-3185

INSTRUCTIONS TO AUTHORS

The Biological Bulletin accepts outstanding original research reports of general interest to biologists throughout the world. Papers are usually of intermediate length (10–40 manuscript pages). A limited number of solicited review papers may be accepted after formal review. A paper will usually appear within four months after its acceptance.

Very short, especially topical papers (less than 9 manuscript pages including tables, figures, and bibliography) will be published in a separate section entitled "Research Notes." A Research Note in *The Biological Bulletin* follows the format of similar notes in *Nature*. It should open with a summary paragraph of 150 to 200 words comprising the introduction and the conclusions. The rest of the text should continue on without subheadings, and there should be no more than 30 references. References should be referred to in the text by number, and listed in the Literature Cited section in the order that they appear in the text. Unlike references in *Nature*, references in the Research Notes section should conform in punctuation and arrangement to the style of recent issues of *The Biological Bulletin*. Materials and Methods should be incorporated into appropriate figure legends. See the article by Lohmann *et al.* (October 1990, Vol. **179:** 214–218) for sample style. A Research Note will usually appear within two months after its acceptance.

The Editorial Board requests that regular manuscripts conform to the requirements set below; those manuscripts that do not conform will be returned to authors for correction before review.

1. ***Manuscripts.*** Manuscripts, including figures, should be submitted in triplicate. (Xerox copies of photographs are not acceptable for review purposes.) The original manuscript must be typed in no smaller than 12 pitch, using double spacing (*including* figure legends, footnotes, bibliography, etc.) on one side of 16- or 20-lb. bond paper, 8½ by 11 inches. Please, no right justification. Manuscripts should be proofread carefully and errors corrected legibly in black ink. Pages should be numbered consecutively. Margins on all sides should be at least 1 inch (2.5 cm). Manuscripts should conform to the *Council of Biology Editors Style Manual*, 5th Edition (Council of Biology Editors, 1983) and to American spelling. Unusual abbreviations should be kept to a minimum and should be spelled out on first reference as well as defined in a footnote on the title page. Manuscripts should be divided into the following components: Title page, Abstract (of no more than 200 words), Introduction, Materials and Methods, Results, Discussion, Acknowledgments, Literature Cited, Tables, and Figure Legends. In addition, authors should supply a list of words and phrases under which the article should be indexed.

2. ***Title page.*** The title page consists of: a condensed title or running head of no more than 35 letters and spaces, the manuscript title, authors' names and appropriate addresses, and footnotes listing present addresses, acknowledgments or contribution numbers, and explanation of unusual abbreviations.

3. ***Figures.*** The dimensions of the printed page, 7 by 9 inches, should be kept in mind in preparing figures for publication. We recommend that figures be about 1½ times the linear dimensions of the final printing desired, and that the ratio of the largest to the smallest letter or number and of the thickest to the thinnest line not exceed 1:1.5. Explanatory matter generally should be included in legends, although axes should always be identified on the illustration itself. Figures should be prepared for reproduction as either line cuts or halftones. Figures to be reproduced as line cuts should be unmounted glossy photographic reproductions or drawn in black ink on white paper, good-quality tracing cloth or plastic, or blue-lined coordinate paper. Those to be reproduced as halftones should be mounted on board, with both designating numbers or letters and scale bars affixed directly to the figures. All figures should be numbered in consecutive order, with no distinction between text and plate figures. The author's name and an arrow indicating orientation should appear on the reverse side of all figures.

4. ***Tables, footnotes, figure legends, etc.*** Authors should follow the style in a recent issue of *The Biological Bulletin* in preparing table headings, figure legends, and the like. Because of the high cost of setting tabular material in type, authors are asked to limit such material as much as possible. Tables, with their headings and footnotes, should be typed on separate sheets, numbered with consecutive Roman numerals, and placed after

the Literature Cited. Figure legends should contain enough information to make the figure intelligible separate from the text. Legends should be typed double spaced, with consecutive Arabic numbers, on a separate sheet at the end of the paper. Footnotes should be limited to authors' current addresses, acknowledgments or contribution numbers, and explanation of unusual abbreviations. All such footnotes should appear on the title page. Footnotes are not normally permitted in the body of the text.

5. ***Literature cited.*** In the text, literature should be cited by the Harvard system, with papers by more than two authors cited as Jones *et al.*, 1980. Personal communications and material in preparation or in press should be cited in the text only, with author's initials and institutions, unless the material has been formally accepted and a volume number can be supplied. The list of references following the text should be headed Literature Cited, and must be typed double spaced on separate pages, conforming in punctuation and arrangement to the style of recent issues of *The Biological Bulletin*. Citations should include complete titles and inclusive pagination. Journal abbreviations should normally follow those of the U. S. A. Standards Institute (USASI), as adopted by BIOLOGICAL ABSTRACTS and CHEMICAL ABSTRACTS, with the minor differences set out below. The most generally useful list of biological journal titles is that published each year by BIOLOGICAL ABSTRACTS (BIOSIS List of Serials; the most recent issue). Foreign authors, and others who are accustomed to using THE WORLD LIST OF SCIENTIFIC PERIODICALS, may find a booklet published by the Biological Council of the U.K. (obtainable from the Institute of Biology, 41 Queen's Gate, London, S.W.7, England, U.K.) useful, since it sets out the WORLD LIST abbreviations for most biological journals with notes of the USASI abbreviations where these differ. CHEMICAL ABSTRACTS publishes quarterly supplements of additional abbreviations. The following points of reference style for THE BIOLOGICAL BULLETIN differ from USASI (or modified WORLD LIST) usage:

A. Journal abbreviations, and book titles, all underlined (for *italics*)

B. All components of abbreviations with initial capitals (not as European usage in WORLD LIST *e.g., J. Cell. Comp. Physiol.* NOT *J. cell. comp. Physiol.*)

C. *All* abbreviated components must be followed by a period, whole word components *must not* (*i.e., J. Cancer Res.*)

D. Space between all components (*e.g., J. Cell. Comp. Physiol.*, not *J.Cell.Comp.Physiol.*)

E. Unusual words in journal titles should be spelled out in full, rather than employing new abbreviations invented by the author. For example, use *Rit Vísindafjélags Islendinga* without abbreviation.

F. All single word journal titles in full (*e.g., Veliger, Ecology, Brain*).

G. The order of abbreviated components should be the same as the word order of the complete title (*i.e., Proc.* and *Trans.* placed where they appear, not transposed as in some BIOLOGICAL ABSTRACTS listings).

H. A few well-known international journals in their preferred forms rather than WORLD LIST or USASI usage (*e.g., Nature, Science, Evolution* NOT *Nature, Lond., Science, N.Y.: Evolution, Lancaster, Pa.*)

6. ***Reprints, page proofs, and charges.*** Authors receive their first 100 reprints (without covers) free of charge. Additional reprints may be ordered at time of publication and normally will be delivered about two to three months after the issue date. Authors (or delegates for foreign authors) will receive page proofs of articles shortly before publication. They will be charged the current cost of printers' time for corrections to these (other than corrections of printers' or editors' errors). Other than these charges for authors' alterations, *The Biological Bulletin* does not have page charges.

Reference: *Biol. Bull.* **183:** 185–199. (October, 1992)

Patterns of Hemocyte Production and Release Throughout the Molt Cycle in the Penaeid Shrimp *Sicyonia ingentis*

JO ELLEN HOSE*, GARY G. MARTIN, SAM TIU, AND NANCY McKRELL

Biology Department, Occidental College, 1600 Campus Road, Los Angeles, California 90041

Abstract. The production and release of hemocytes was evaluated throughout the molt cycle in the shrimp *Sicyonia ingentis*. Hematopoiesis occurs in paired epigastric hematopoietic nodules (HPN) which consist of an extensive network of vessels. Hemocytes are produced within the walls of these tubules and released into the vessel lumens. During molt stage C (intermolt), few cells were present in the tubule wall; most of these were hematopoietic stem cells. Elevated mitotic rates during stages C to D_{1-2} (2–4%) led to the production and rapid release of individual hemocytes, primarily granulocytes. Although the mitotic rate progressively declined from stage D_{3-4} until after ecdysis (stage A_1), the maturing hemocytes accumulated within the tubule walls. Around ecdysis, production of hyaline hemocytes exceeded that of granulocytes. Large groups of these hemocytes were channeled into the vessel lumens immediately after molting. Mitotic rates increased again during stages A_2 and B with the number of hemocytes in the tubules reaching seven times that of stage C.

Morphological stages in the transition of hematopoietic stem cells into hyaline hemocytes and granulocytes are described, and a model of decapod hemocyte maturation is presented.

Introduction

Decapod hemocytes are produced within specialized hematopoietic tissue, the location and architecture of which vary greatly, even within close taxonomic groups. In lobsters, crabs, and crayfish, a sheet-like hematopoietic tissue covers the cardiac stomach or the heart, and maturing hemocytes are organized into small lobules of variable thickness (Cuénot, 1893, 1905; Kollman, 1908; Demal, 1953; Ghiretti-Magaldi *et al.*, 1977). Stem cells line the apical border of each lobule and maturing hemocytes migrate toward the hemal space (Johnson, 1980). Young hemocytes are liberated into adjacent hemal spaces and then into the general circulation. Paired epigastric hematopoietic nodules (HPN) are present in penaeid shrimps, (Oka, 1969; Martin *et al.*, 1987) and some species may have ancillary sites of hematopoietic tissue surrounding the antennal artery, and at the base of the maxillipeds (Bell and Lightner, 1988). For this study, a penaeid shrimp (*Sicyonia ingentis*) was chosen because it has a simple hematopoietic system; hematopoiesis occurs only within the HPN as ancillary sites have not been demonstrated. The HPN is formed by extensive branching of the ophthalmic artery, and hemocytes are produced within the wall of these vessels, termed hematopoietic tubules. The lumen of each tubule is lined by endothelial cells, through which most hemocytes enter the peripheral circulation. Hemocytes and stem cells are located within the fibrillar extracellular matrix, which comprises the wall of the tubule. The outside of the tubule is surrounded by capsular cells, which apparently secrete a dense meshwork of collagen fibrils. Hemocytes exit through the outer wall into the open circulatory system less frequently (Martin *et al.*, 1987).

The regulation of hematopoiesis in decapod crustaceans is poorly understood, but is probably influenced by physiological processes such as molting, reproduction, and disease status, as well as by environmental conditions like temperature and water quality (Bauchau and Plaquet, 1973; Johnson, 1980; Bauchau, 1981). Detailed information on the effect of the molt cycle on hemocyte production and release is not available. Two studies (Marrec,

Received 15 July 1991; accepted 22 July 1992.

* To whom correspondence should be addressed. Current address: 405 Indio Dr., Shell Beach, CA 93449.

1944; Charmantier [illegible] showed that mitotic activity in hematopoietic ti[illegible]bs was high during the intermolt period (st[illegible] and early C) and low immediately after e[illegible]. The major release of hemocytes o[illegible] the ecdysial interval (stages D through [illegible] 1944; Johnson, 1980).

Studie[illegible]ied on hematopoiesis have not attempted to classi[illegible]e maturing hemocytes and stem cells. Such distinctions are essential because the different categories of hemocytes perform different functions (Hose *et al.*, 1990). Most researchers divide decapod hemocytes into two major groups, hyaline hemocytes and granulocytes (Bauchau, 1981; Hose *et al.*, 1990). Hyaline hemocytes initiate coagulation of the hemolymph (Omori *et al.*, 1989) and are thought to be involved in hardening (tanning) of the exoskeleton after molting (Vacca and Fingerman, 1983). In contrast, granulocytes are responsible for defense against foreign materials (Ratner and Vinson, 1983; Söderhäll *et al.*, 1988; Hose *et al.*, 1990) and may liberate proteins which contribute to formation of the exoskeleton (Vacca and Fingerman, 1983). Identification of early maturation stages can enhance our understanding of hemocyte genesis particularly regarding whether granulocytes and hyaline hemocytes constitute a single line or two separate lines of maturation.

The dynamics of hemocyte production and release were followed throughout the molt cycle in the shrimp *Sicyonia ingentis*. Hematopoietic nodules were removed at various stages of the molt cycle, and, mitotic activity, hemocyte maturation, and release were quantified. Hemopoietic cells were categorized using morphological criteria corresponding to cytochemical and physiological properties of shrimp hemocytes (Martin and Hose, in press). The production and release of granulocytes could, therefore, be differentiated from that of hyaline hemocytes. In addition, the ultrastructure of stem cells and maturing hemocytes were described, contributing morphologic evidence for a model of decapod hemocyte maturation. The information presented here is expected to form a basis for future studies utilizing physiological and biochemical techniques.

Materials and Methods

Animal collection

Shrimp were collected in 160 m of water off Huntington Beach, California and maintained in aquaria with flow-through seawater at 18°C. They were fed *ad libitum* on a commercial shrimp diet.

Molt staging

Molt stage was determined by observing the retraction of epithelium within setae of the antennal scales (Anderson, 1985). Shrimp were categorized into one of the following molt stages: A_1, A_2, B, C, D_0, D_{1-2}, and D_{3-4}.

HPN preparation

Hematopoietic nodules (Martin *et al.*, 1987) were dissected and immediately fixed in 2.5% glutaraldehyde in a 0.1 *M* solution of sodium cacodylate at pH 7.8 containing 12% glucose for 2–3 hrs at 20°C. Tissues were washed in a 0.1 *M* solution of sodium cacodylate at pH 7.8 containing 24% sucrose for > 10 min and then post-fixed for 1 h in 1% OsO_4 in a 0.1 *M* solution of sodium cacodylate at pH 7.8. The nodules were stained *en bloc* for 1 h in 3% uranyl acetate, then dehydrated, infiltrated and embedded in Spurrs' (1969) resin and sectioned. Thick sections (0.5 μm) were routinely stained in methylene blue for examination under an Olympus light microscope (LM). Thin sections (90 nm) were stained in Reynolds lead citrate for 5 min and viewed using a Zeiss EM 109 transmission electron microscope (TEM). Five animals were processed and analyzed for each molt stage.

LM analyses

Tubule counts. Cells for each shrimp were counted and identified in cross sections of four tubules. Lumen diameter and tubule wall width were measured using an ocular micrometer. Cell counts could be directly compared because mean widths of the lumen and wall did not differ significantly throughout the molt cycle or between animals. In one half of each tubule and the corresponding lumen, all of the hemocytes and stem cells were counted and categorized into one of the following: hyaline stem cells, hyaline hemocyte, granulocyte stem cell, small granule stem cell, small granule hemocyte, or large granule hemocyte. The basic characteristic used to distinguish between cells of the hyaline and granulocyte lines was the relatively darker cytoplasmic staining of the former (greater electron density for TEM evaluations); this characteristic was visible in every cell regardless of the angle of sectioning. Stem cells had boundaries that were difficult to resolve using LM; on TEM examination, this appeared to result from their tight apposition to other cells. In contrast, hemocytes were separated from adjacent cells, usually by fibrillar extracellular matrix (Fig. 1c, d, f) (Martin *et al.*, 1987). Hemocytes had rounded contours or were migrating through the tubule wall. Morphological descriptions were based on examination of at least 50 oblique sections of cells with a nucleus. Longest axes were measured in at least 20 of these cells.

Hyaline hemocytes were distinguished from hyaline stem cells on the basis of their smaller size, higher N:C ratio, and their densely basophilic nucleus. Hyaline stem cells were separated from granulocyte stem cells because the former were smaller, had cytoplasm, which stained

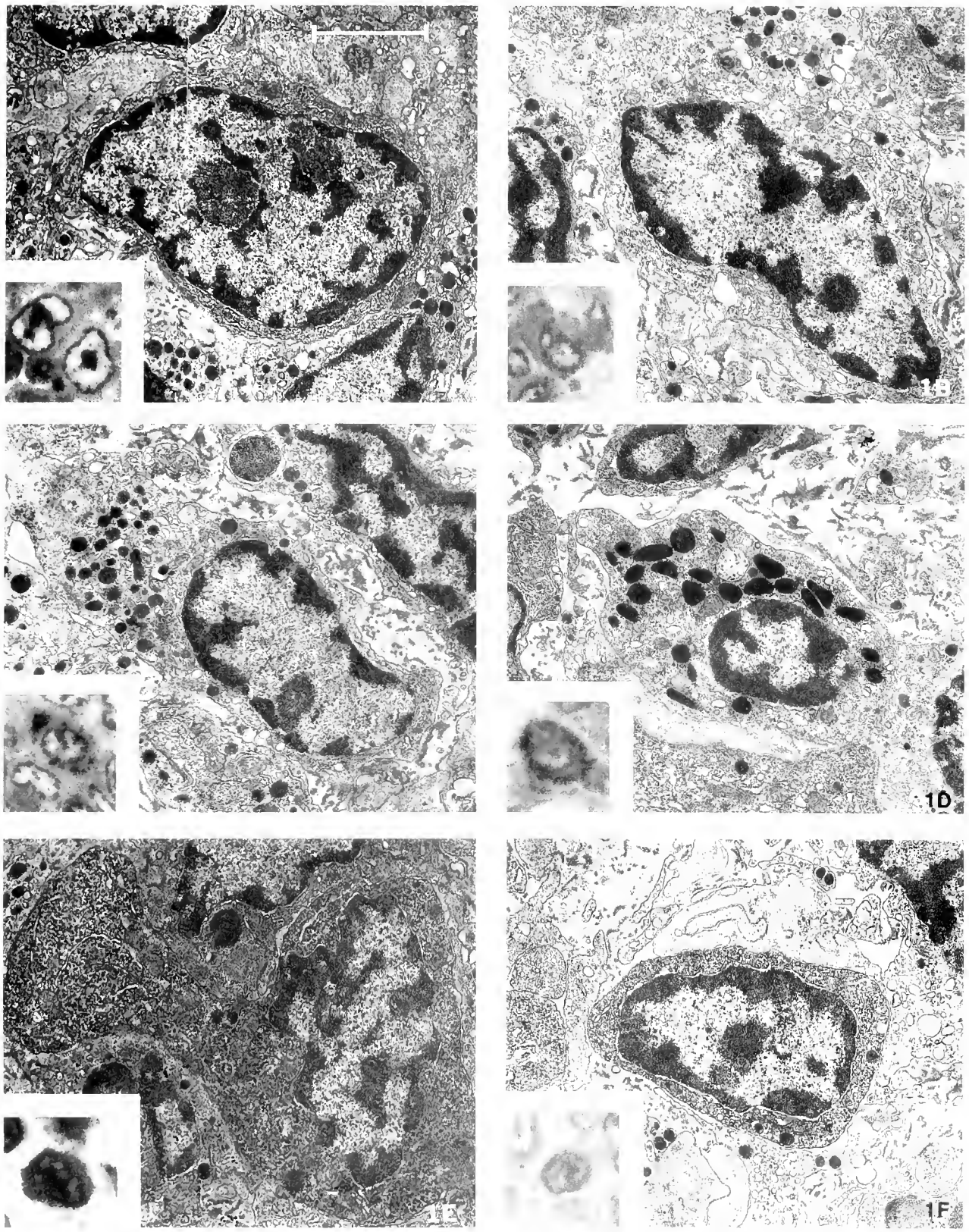

Figure 1. Transmission electron micrographs and light micrographs (inserts) of cells from the hematopoietic tissue of shrimp. (A) Early granulocyte stem cell. (B) more mature granulocyte stem cell. (C) small granule hemocyte. (D) large granule hemocyte. (E) hyaline stem cell, and (F) hyaline hemocyte. All figures at 8000×, scale bar = 2.5 μm. Light micrographs—methylene blue, 1800×.

darkly with methylene [illegible] and contained at most two cytoplasmic granules [illegible] M level, granulocyte stem cells possessed [illegible] plasm with zero to two obvious granules [illegible] ve nucleus containing finely granular [illegible] one or two large nucleoli. The small granule [illegible] cells had a lower N:C ratio than the granulocyte [illegible] cells, their nuclei were more basophilic with small nucleoli, and they contained between three and ten granules. Small granule hemocytes were separated from the granulated stem cells on the basis of their oval shape, numerous small (0.4 μm diameter) dark cytoplasmic granules, and lower N:C ratio. Large granule hemocytes had, in addition to small cytoplasmic granules, large cylindrical (0.8 μm in longest diameter) granules and the lowest N:C ratio of any cell type observed. Only nucleated cells were counted. Hemocytes exiting the tubule via the endothelium or outer margin were recorded. Capsular cells on the outside of the tubule were not enumerated.

Cell counts from four tubules were averaged to obtain profiles for each animal. Numbers and proportions of hyaline stem cells, hyaline hemocytes, granulocyte and small granule stem cells, and small and large granule hemocytes were calculated, and values from the five animals were averaged. Longest axes of stem cells were measured using an ocular micrometer. Hemocytes within the tubule wall were not measured because many were irregularly shaped as they migrated into the lumen. Cells within the lumen were similarly evaluated, and diameters of hyaline and small granule hemocytes were measured. Means of these parameters were compared throughout the molt cycle. Where appropriate, data were evaluated for differences using *t*-tests or analysis of variance with a significance level set at $P = 0.05$.

Mitotic index. Dividing cells were recorded and identified during LM anlaysis of the tubules. Hematopoietic cells were considered mitotic from the disappearance of the nuclear membrane during prophase to its reappearance during telophase. The absence of the nuclear membrane was observed at both the LM and TEM levels. Nuclear characteristics were not used to identify dividing cells because of nuclear changes occurring during mitosis. Instead, cells of the hyaline and granulocyte lines were distinguished by the relatively darker cytoplasm of the hyaline cells using LM (greater cytoplasmic electron density using TEM). To further strengthen the assignment of a cell as hyaline or granulocyte, the darkness of its cytoplasm was usually compared to that of non-dividing cells adjacent to it which could be identified as hyaline or granulocyte based on characteristics of the nucleus and cytoplasmic granules. Using criteria described in the previous section, a dividing cell was considered to be a stem cell if its plasma membrane was contiguous with other cells, and a hemocyte if it was detached. To determine the mitotic index, the number of mitotic hemocytes/precursors was divided by the total number of hematopoietic cells examined within the tubule. Endothelial cells and hemocytes within the lumen were not included in these calculations although mitotic activity was recorded. Percentages of mitotic hemocytes in each category were then calculated.

TEM analyses

Transmission electron microscopy (TEM) was used to (1) verify the identity of cells tentatively identified using LM, (2) describe the ultrastructure of maturing hemocytes, and (3) determine nucleocytoplasmic (N:C) ratios of stem cells and maturing hemocytes. Nucleocytoplasmic ratios on longitudinal sections of cells were determined by dividing the area of the nucleus by the area of the cell. Measurements were made using electron micrographs placed on a digitizing tablet and were analyzed by Sigma-Scan@ computer software (Jandel Scientific).

Results

Description of stem cells and maturing hemocytes

Cells that were sectioned through the nucleus could be classified into one of six categories: granulocyte stem cell, small granule stem cell, small granule hemocyte, large granule hemocyte, hyaline stem cell, and hyaline hemocyte (Fig. 1). Granulocyte stem cells (Fig. 1a) were large, averaging between 7.1 and 9.9 μm in longest diameter (Table 1). The cell outline was irregular and the plasma membrane often difficult to discern. These cells had a very high N:C ratio (65.8% ± 8.8%, n = 10; $\bar{X} \pm SD$) and the nucleus was frequently oval with only a thin rim of marginated chromatin visible. The single large nucleolus (1.5 μm diameter) was the most distinctive feature visible at the LM level. In methylene blue-stained thick sections, the cytoplasm was light blue and featureless and contained zero to two granules. In TEM sections, from two to ten mitochondria were present as well as abundant rough endoplasmic reticulum (RER) and up to two homogeneous, electron dense cytoplasmic granules (0.5 μm diameter). In addition to these larger granules, up to five smaller granules (~0.15–0.20 μm diameter), which appeared to be coalescing, could be found upon ultramicroscopic examination. The nucleus contained mostly euchromatin with a narrow border of heterochromatin. In Martin *et al.*'s (1987) classification of shrimp hematopoietic cells, these were termed stromal cells. We now consider them to be the earliest granulocyte stem cells based on the transition of granules in the cytoplasm which presumably form a continuum with small granule stem cells (described in the following paragraph) and with small granule hemocytes.

Table I

Diameters of shrimp stem cells from hematopoietic tissue and hemocytes from the lumens of hematopoietic vessels

	Molt stage							
	C	D_0	D_{1-2}	D_{3-4}	A_1	A_2	B	C
Stem cells								
Granulocyte	9.8 ± 2.0 (90)	9.9 ± 1.8 (95)	8.9 ± 1.9 (100)*	7.1 ± 1.7 (99)*	7.9 ± 1.8 (149)*	7.9 ± 1.8 (205)	7.4 ± 1.8 (202)*	9.8 ± 2.0 (90)
Small granule	9.5 ± 1.6 (83)	9.3 ± 1.8 (94)	9.0 ± 2.1 (55)	9.0 ± 1.5 (27)	8.7 ± 1.8 (33)	8.9 ± 1.9 (114)	8.3 ± 1.8 (94)*	9.5 ± 1.6 (83)
Hyaline	8.6 ± 1.4 (44)	7.9 ± 1.4 (79)*	7.6 ± 1.5 (62)	7.6 ± 1.9 (71)	7.1 ± 1.6 (123)*	7.0 ± 1.7 (86)	7.1 ± 1.5 (74)	8.6 ± 1.4 (44)
Hemocytes								
Small granule	7.6 ± 1.3 (47)	8.0 ± 0.9 (68)	8.0 ± 0.8 (60)	6.5 ± 0.7 (33)*	8.2 ± 0.8 (66)*	8.2 ± 1.0 (75)	7.9 ± 1.6 (26)*	7.6 ± 1.3 (47)
Hyaline	6.6 ± 0.3 (20)	6.7 ± 0.8 (45)	6.6 ± 0.8 (43)	5.5 ± 0.8 (45)*	5.8 ± 0.7 (79)*	6.8 ± 0.7 (75)*	6.7 ± 1.0 (27)	6.6 ± 0.3 (20)

* Denotes values which are statistically different from values of preceding molt stage, *t*-test, $P < 0.05$.
X ± SD (n) in μm.

Small granule stem cells were distinguished by the presence of many (3–10), small (0.33 μm diameter), ovoid granules in the cytoplasm. These stem cells were usually larger (from 8.3 to 9.5 μm in largest diameter) than the early granulocyte stem cells at identical molt stages (Table 1), and their outlines were irregular (Fig. 1b). The N:C ratio (49.0% ± 8.3%, n = 10) was significantly less than that of the early granulocyte stem cell. The nucleus had a variable shape, ranging from a smooth oval to indented or irregular. One or two nucleoli were present and they were smaller than those of the early granulocyte stem cells. The chromatin pattern was also different from that of the early granulocyte stem cell with a thicker marginal chromatin band and heterochromatin bands radiating from the one or two central nucleoli. The cytoplasm was light blue and featureless at the LM level except for the small homogeneous granules which were often a lighter blue than those of small granule hemocytes. In TEM preparations, the granules appeared to be newly formed by the coalescence of smaller vesicles. Numerous mitochondria and free ribosomes were present.

Small granule hemocytes were followed from various stages of maturation into large granule hemocytes; the transition was accompanied by progressively lower N:C ratios and by increasing numbers and sizes of the cytoplasmic granules. The youngest small granule hemocytes had >10 cytoplasmic granules with diameters of approximately 0.35 μm. Mature small granule hemocytes (Fig. 1c) closely resembled those within the peripheral circulation with round to oval cell contours and >15 0.4 μm diameter granules. However, their mean N:C ratio of 42.2% (SD = 9.6%, n = 10) was higher than that of circulating small granule hemocytes (Martin and Hose, in press). The small granule hemocytes could be distinguished from hyaline cells by their small (6 × 3 μm), ovoid nuclei containing a single, dense, central nucleolus. The marginal chromatin was thicker than those found in granulocyte stem cells, and frequently appeared as a continuous ring or in regularly spaced clumps. Initially, these cells were described as small granule hemocytes lacking cytoplasmic deposits (Martin *et al.*, 1987). They were later identified as small granule granulocytes (Hose and Martin, 1989; Hose *et al.*, 1990). Large granule hemocytes (Fig. 1d) were similar to their circulating counterparts (Martin and Hose, in press) and were distinguished from small granule hemocytes by very low N:C ratios (22.2% ± 5.1%, n = 5) and numerous large (0.8 μm) and smaller cytoplasmic granules.

Hyaline stem cells (Fig. 1e) were the smallest type of stem cell (7.0–8.6 μm diameter, Table 1) with a mean N:C ratio of 45.9% (SD = 8.3%, n = 10). The nucleus was usually oval to oblong, sometimes indented but never angular. The chromatin was denser than those found in granulocyte stem cells. Nucleoli were seldom discernible, even using TEM. A thin rim of dark blue cytoplasm encircling the nucleus conformed to the nuclear contours. Cytoplasmic granules were rarely visible at the LM level. TEM examination revealed a distinctive nuclear characteristic; the presence of thick heterochromatin bands spanning the nucleus. Very little euchromatin was observed. The cytoplasm was filled with tiny spherical (50 nm diameter), electron dense deposits which frequently formed larger clumps measuring up to 186 nm. These deposits were identical to those previously described from a subgroup of granulated hematopoietic cells (Martin *et al.*, 1987) and from circulating hyaline hemocytes (Omori *et al.*, 1989) of the shrimp. The stem cells possessed a Golgi apparatus and numerous mitochondria. Hyaline stem cells lacking cytoplasmic granules were common; these were termed agranular hemocytes in our previous study (Martin *et al.*, 1987). These stem cells sometimes either contained a few small (0.25 μm diameter), homogeneous electron dense granules or their presumptive precursors which were three times larger, having a granular substructure and containing the electron dense core. Up to seven granules with a striated substructure (0.4 μm

diameter) could be f[illegible] esc appeared identical to the striated granules [illegible] circulating hyaline hemocytes (Omori

Hyaline [illegible]) ranged in appearance as a continu[illegible] me stem cells to mature cells indistin[illegible] those within the peripheral circulatio[illegible] lls matured, the mean length diminished [illegible] 5.5 and 6.8 μm (Table I) and the N:C ratio increased (61.6% ± 6.2%, n = 10). More heterochromatin was present, often as a dense marginal band in addition to the thick transverse bands present in hyaline stem cells. In methylene blue-stained LM sections, the cytoplasm of hyaline cells frequently appeared featureless, staining metachromatic or intensely basophilic. However, at the EM level the cytoplasm contained large clumps of electron dense deposits, striated granules, a few homogeneous electron dense granules, and several mitochondria.

Hemocyte production

Mitotic index. Mitotic activity within the hematopoietic nodules was cyclical, with the lowest levels bracketing the ecdysial interval (stages D_{3-4} through B) and highest during intermolt and early pre-molt (stages C–D_{1-2}) (Table II). Mitotic activity during stage C was about 2.2% and nearly doubled to a maximum of 4.2% at stage D_0. The mitotic index progressively decreased thereafter until stage A_1, when it reached its lowest level of 0.2%. A secondary burst of mitotic activity occurred during stage A_2 in which 2.0% of the cells were dividing. In stage B, the mitotic rate declined to 0.8% and then increased again to the stage C level.

Most of the dividing cells were granulocyte stem cells and hyaline stem cells (Fig. 2, Table II). Two-thirds of dividing hyaline cells were stem cells; the remainder were hyaline hemocytes. Division of small granule hemocytes was rarely observed, as was division of hemocytes within the lumens of the hematopoietic tubules. Mitotic rates of the granulocyte stem cells contributed the bulk of the total mitotic activity and were responsible for producing the observed cyclic pattern. In contrast, the mitotic index of hyaline stem cells remained essentially constant throughout the molt cycle, exhibiting a modest increase from stage A_1 to D_{3-4}. Like that of granulocytes, the mitotic activity of hyaline cells was lowest during stage A_1 with a subsequent pulse during stage A_2, then a decrease during stage B.

Tubule differential counts. A molt cycle-related trend was observed in which the number of cells in the hematopoietic tubules was least during stage C and had almost tripled by stage B (Table III). This observation, along with the cyclic hemocyte release ending in stage B (see following section), makes stage C the most convenient portion of the molt cycle to begin this description of hemocyte production.

During stage C, a mean of 46 stem cells was present per cross section of tubule (Table III). A maximum value of 111 stem cells was recorded in stage D_{3-4}, which declined to 89 in stage B. Of the stage C stem cells, 80% were stem cells in the granulocyte line and 20% were hyaline stem cells. The proportions of granulocyte stem cells remained high until stage A_1, when hyaline stem cells comprised about 40% of the total. During stages A_2 and B, the proportion of hyaline stem cells increased to around 80%. Diameters for all stem cell types were greatest in stage C, then decreased throughout the cycle by 1 to 2 μm (Table I). The smallest diameters were most frequently recorded in stage B tubules.

Very few mature hemocytes were observed in the tubule wall from stage C until just before ecdysis (stage D_{3-4}), with means ranging from 12 to 18 cells (Table III). Hem-

Table II

Mitotic activity (% of cells dividing) in shrimp hematopoietic tubules

	Molt stage							
	C	D_0	D_{1-2}	D_{3-4}	A_1	A_2	B	C
Hyaline cells								
Stem cells	0.27	0.42	0.43	0.54	0.11	0.36	0.09	0.27
Hemo[illegible]	0.13	0.08	0.08	0.04	0.02	0.16	0.05	0.13
Total h[illegible]	0.40	0.50	0.51	0.58	0.13	0.52	0.14	0.40
Granulocyte								
Stem cells	1.68	3.53	1.42	0.51	0.12	1.34	0.60	1.68
Small granu[illegible]tes	0.09	0.17	0.04	0.02	0.00	0.12	0.06	0.09
Total granuloc[illegible]	1.77	3.70	1.46	0.53	0.12	1.46	0.66	1.77
Total mitotic activit[illegible]	2.17 ± 0.40*	4.20 ± 0.89	1.97 ± 0.49	1.11 ± 0.33*	0.25 ± 0.18*	1.98 ± 1.12	0.80 ± 0.27*	2.17 ± 0.40*

* Denotes values significa[illegible]tly different from molt stage D_0, analysis of variance and Student-Newman-Keuls, $P = 0.05$.
Values for total mitotic activity are the mean and standard error for five individuals.

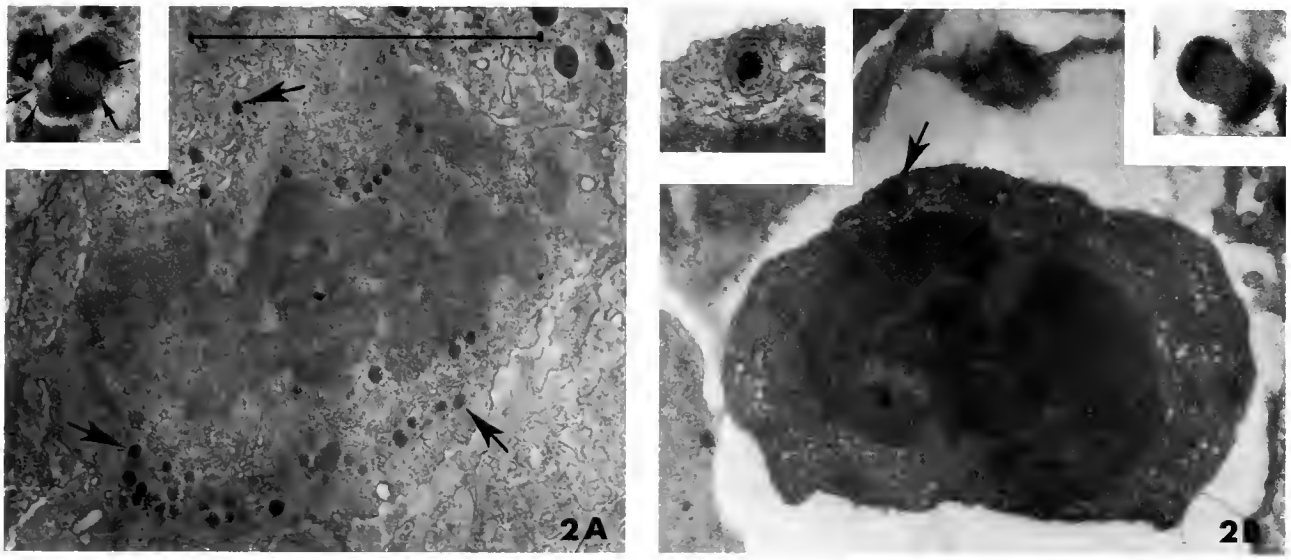

Figure 2. Transmission electron micrographs and light micrographs (inserts) of dividing cells. Spindle microtubules and centrioles are not visible in the electron micrographs, but both cells lack nuclear envelopes. (A) Granulocyte stem cell in metaphase; insert shows a cell in anaphase (arrows = granules). (B) Hyaline cell in prophase or metaphase. Right insert shows a cell in telophase and left insert same cell at a higher magnification (17,600×) of a typical granule with a striated substructure from the hyaline cell. Granulocyte and hyaline stem cells may be distinguished by differences in the electron density of the cytoplasm (note the darker cytoplasm of the hyaline cell) and the substructure of the cytoplasmic granules (arrows). Note the homogeneous substructure of the electron dense granules in the granulocyte stem cell. Electron micrographs 9600×; scale bar = 5 μm. Light micrographs—methylene blue, 1800×.

ocytes constituted only 12–20% of the total hematopoietic cells during these stages. After molting, the number of hemocytes almost tripled to 42. Throughout the post-ecdysial stages (A_1 to B), their numbers doubled as maturing hemocytes accumulated within the tubules. In stage B, 48% of the hematopoietic cells were hemocytes.

Cells of the granulocyte line predominated within the intermolt and early pre molt hematopoietic tissue (stages C through D_{1-2}). Mitotic activity progressively increased from stage A_1 to a peak at stage D_0. Numbers of granulocyte stem cells were lowest during stage C, and increased to a maximum during stage D_{3-4} (Fig. 3). During stages B and C, granulocyte stem cells were usually the earliest forms with zero or only a few coalescing granules and a distinctive large central nucleolus. Stem cells in stage C tubules were the largest of any molt stage, averaging 9.8 μm in diameter (Table I). More mature, smaller stem cells were typical of stage D tubules; these contained numerous electron dense granules. Small granule hemocytes were the most prominent hemocyte type during stages D_{0-2}, after which they declined in abundance (Fig. 4). Large granule hemocytes first appeared in stage C tubules and, although they became more abundant until stage D_{1-2}, they were infrequently observed. Despite the high mitotic rate of granulocytes (Fig. 3a) and the increasing numbers of stem cells in the granulocyte line during stages C

Table III

Numbers of hemocytes, stem cells, and total cells per hematopoietic tubule

	Molt stage							
	C	D_0	D_{1-2}	D_{3-4}	A_1	A_2	B	C
Hemocytes	12.0 ± 3.9	11.0 ± 1.4	18.4 ± 5.2	14.8 ± 3.2	41.8 ± 19.9	38.4 ± 9.9	83.0 ± 17.7	12.0 ± 3.9
Stem cells	46.2 ± 3.0	60.8 ± 11.1	97.0 ± 9.7	111.4 ± 8.6	97.2 ± 18.5	90.8 ± 23.2	88.6 ± 11.5	46.2 ± 3.0
Total cells	58.2 ± 4.3	71.8 ± 11.9	115.4 ± 6.1	126.0 ± 11.7	139.0 ± 29.7	129.2 ± 26.5	171.6 ± 27.5	58.2 ± 4.3

* Denotes total cell counts significantly different from those of molt stage B, analysis of variance and Student-Newman-Keuls, $P = 0.05$.
Values are mean and standard error from five individuals.

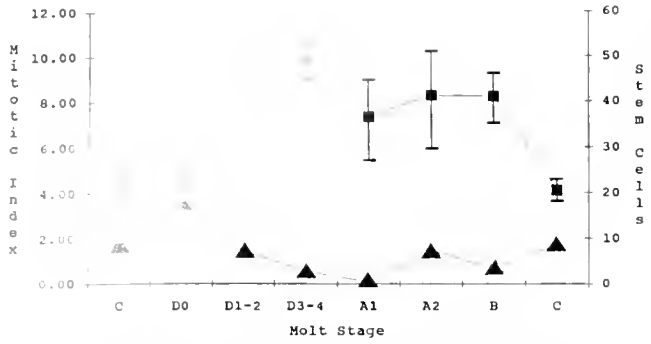

Figure 3. Mitotic index of granulocytes (% of cells in mitosis) (▲) and numbers of granulocyte stem cells (■) in the hematopoietic tissue of shrimp throughout the molt cycle. Error bars are ± 1 standard deviation. Numbers of granulocyte stem cells were significantly higher during molt stages D_{1-4}.

through D_{3-4} (Fig. 3b), surprisingly few maturing granulocytes were observed within the wall of the hematopoietic tubules (Fig. 4a). They were apparently released soon after production (see next section). A secondary, post-ecdysial burst of granulocyte production reflected the enhanced mitotic activity of stage A_2. Hemocytes produced during stages A_2 through B accumulated within the tubules. The fluctuating numbers of hemocytes within the tubules reflect differences in release rates of maturing granulocytes and will be discussed in the section on hemocyte release.

In contrast to granulocyte production, which occurred primarily in stages C through D_{1-2}, hyaline hemocytes were produced at comparatively low rates during these stages. Most hyaline hemocytes were instead produced during the stages bracketing ecdysis (D_{3-4} through A). Mitotic activity in the hyaline stem cells increased from a low level during stage B to a maximum during stage D_{3-4} (Fig. 5). The numbers of hyaline stem cells and hyaline hemocytes within the tubules peaked shortly thereafter, in stage A_1 (Fig. 6). Although numbers of hyaline stem cells then decreased to reach their lowest level at stage C, numbers of hyaline hemocytes remained elevated throughout stage B, apparently aided by a pulse of hyaline stem cell division during stage A_2. Hyaline stem cell sizes were greatest during molt stage C, with a mean diameter of 8.6 μm (Table I). They then declined to 7.6 μm during stage D_{3-4} and attained their minimum size of approximately 7.1 μm from stage A_1 through stage B.

Hemocyte maturation. Observations of cells within hematopoietic tubules suggest that granulocytes and hyaline hemocytes progress along two separate lines of maturation. Because stage C tubules contained the earliest granulocyte stem cells recognizable at the LM level, electron micrographs of tubules from the previous stage (B) were examined for cells that might be precursors to the granulocyte stem cell or, possibly, a common progenitor of both hemocyte lines. Stem cells in stage B tubules were of two types—those that possessed coalescing cytoplasmic granules and that lacked the deposits (granulocyte stem cells) and those which contained the distinctive cytoplasmic deposits of the hyaline cell line. No stem cell could be found that possessed ultrastructural features common to both lines of hemocytes.

Granulocytes arose from an undifferentiated cell type typical of stem cells with its large size, a nucleus containing predominantly euchromatin, and a high N:C ratio. Its cytoplasm lacked specialized organelles. This cell was common in stage A_2 and B specimens (Fig. 1a). As maturation of granulocyte stem cells progressed, cells developed a few small granules which were in various stages of coalescence (Fig. 1b); these were frequently observed in stage B tubules (Fig. 7). Although they occasionally appeared larger than the undifferentiated forms, maturing stem cells had a progressively lower N:C ratio and condensed electron dense granules were present. As granulocyte stem cells matured into small granule hemocytes and then into large granule hemocytes, the number of cytoplasmic granules increased, the granules became larger, and the N:C ratio further decreased (Fig. 1c, d). Clusters of granulocytes in various stages of maturation were present in stage C and D_0 tubules; they frequently contained one to several granulocyte stem cells and small granule stem cells as well as small granule and occasional large granule hemocytes (Fig. 8). The clusters sometimes appeared to be bounded by a thin basal lamina.

Hyaline stem cells resembled undifferentiated granulocyte stem cells except for their lower N:C ratio, the lack of a prominent central nucleolus, the predominant heterochromatin within the nucleus, and the more electron-dense cytoplasm. Early hyaline stem cells lacking cytoplasmic granules were most readily observed in stage C tubules. As the hyaline stem cell matured, it became smaller (Table I), the cytoplasmic deposits organized into large, dense clumps, and the nucleus became more condensed. In these stem cells, abundant in stage D tubules, the cytoplasm also contained coalescing granules with an obvious striated substructure as well as a few small, homogeneous electron dense granules. Hyaline hemocytes were smaller than the stem cells (Table I) and the cytoplasmic granules resembled those present in their circulating counterparts. Clusters of maturing hyaline stem cells and hemocytes usually contained fewer cells than did the granulocyte clusters; they were most readily observed in late stage D tubules (Fig. 9). Like the granulocyte clusters, hyaline clusters occasionally appeared to be enclosed by a basal lamina.

Hemocyte release

Lumen counts. Release of hyaline cells and granulocytes into the lumen of the hematopoietic tubules occurred at

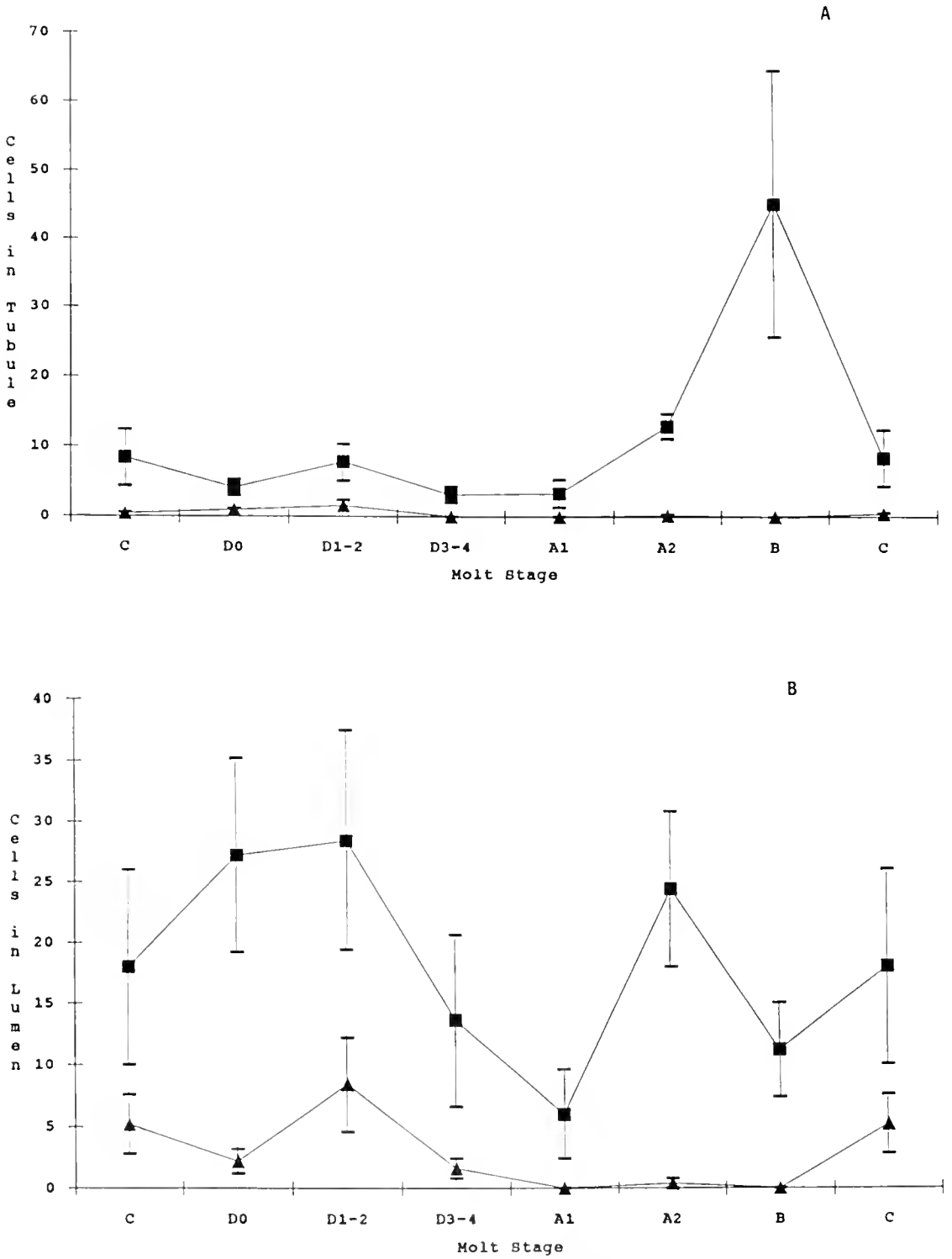

Figure 4. Numbers of small (■) and large (▲) granule hemocytes within shrimp hematopoietic tubules (A) and the lumens of the tubules (B) throughout the molt cycle. Mean of five shrimp, four tubules/shrimp. Error bars are ±1 standard deviation. Significantly more small granule hemocytes were present in the tubules during molt stage B, probably reflecting increased mitotic activity during stage A_2. The only significant difference in the numbers of small granule hemocytes released into the lumen was an elevation during stage D_{1-2} corresponding to the surge in mitotic activity during stage D_0. Mean tubule diameters remained similar throughout the molt cycle, so cell counts could be directly compared

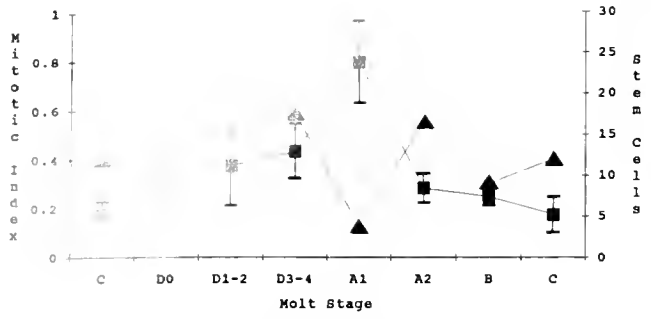

Figure 5. Mitotic index of hyaline cells (% of cells in mitosis) (▲) and numbers of hyaline stem cells (■) in the hematopoietic tissue of shrimp throughout the molt cycle. Mean of five shrimp, four tubules/shrimp. Error bars are +1 standard deviation. The number of hyaline stem cells was significantly higher only during molt stage A_1.

different times during the molt cycle. Granulocytes appeared to be released soon after production during intermolt and early D stages (Fig. 4). However, a second, smaller pulse of granulocyte production occurred during stage A_2 with some of the cells apparently released during this stage and the rest accumulated in the tubules during stage B and released during stage C. Characteristics of the released cells supported these inferences. Sizes of released granulocytes during stages D_{0-2} were large (Table I) and they more closely resembled small granule stem cells (*i.e.*, fewer granules and a higher N:C ratio than most circulating small granule hemocytes), suggesting that they were indeed released soon after production. Similarly, small granule cells released during stage A were larger and more immature compared to those released during B and C, which were smaller and contained more granules.

Production of hyaline hemocytes peaked during the ecdysial period (stage D_{3-4} through A). Hyaline cells appeared to be released soon after their production during stages C through D_{1-2}. Many of these cells appeared to be maturing hyaline stem cells since their size approximated that of the stem cells (Table I), the N:C ratio was lower than that of circulating hyaline hemocytes, and the cytoplasm was frequently agranular. During stages D_{3-4} and A_1, however, the size of released cells significantly declined, and they appeared more like circulating hyaline hemocytes with heavily condensed chromatin and clumped cytoplasmic deposits, suggesting that further maturation occurred while they accumulated in the tubules for post-ecdysial release. There was a second pulse of hyaline hemocyte production during stage A_2 with the apparent rapid release of these relatively large, immature hyaline cells occurring during stages A_2 and B.

Occasionally, dividing cells were present inside the lumen of the hematopoietic tubules. These were most frequently cells intermediate between small granule stem cells and hemocytes, in addition to a few large, immature hyaline hemocytes. No relationship to molt stage could be detected due to the rarity of mitotic cells in the lumen.

Release through endothelium. Most hemocytes exited the tubules through the endothelium. During stages C and early D, diapedesis of individual hemocytes (usually granulocytes) was most common, with the endothelial barrier remaining intact (Fig. 10a). Around the ecdysial period, however, endothelial channels were observed through which groups of maturing hemocytes, usually hyaline hemocytes, were released into the lumen (Fig. 10b). By stage B, the endothelial lining was difficult to distinguish since it appeared to be composed of isolated cells detached from the underlying stroma and interspersed with groups of exiting hemocytes.

Regeneration of the endothelium began during stages C and D_0, as evidenced by the presence of cells undergoing mitosis, thickening of the endothelial cells, and the continuous appearance of the basal lamina. The regenerated endothelium seen in pre-ecdysial tubules appeared continuous save for isolated diapedesis by individual hemocytes. However, during stage D_{3-4}, groups of emigrating hemocytes formed channels between individual endothelial cells. The endothelial barrier was progressively destroyed by the hyaline hemocytes released during the ecdysial interval. By stage A_2, the endothelial cells appeared attenuated and were frequently detached from the underlying collagenous stroma. In stage B, large channels separating the endothelial cells were visible in electron micrographs (Fig. 11), and some of the endothelial cell nuclei appeared to be degenerating. Also in stage B, many circular formations resembling myelin figures were dispersed through the collagenous stroma. We could not identify any cell type involved in production or repair of the collagenous matrix forming the stroma of the hematopoietic tubules.

Release through capsule. A small percentage (<5%) of hemocytes was released via migration through the outer capsule of the tubule into the adjacent hemal space. In each tubule, only one or two hemocytes were usually present in the capsular network of collagen fibrils. This percentage did not change considerably throughout the molt cycle except for stage D_{3-4} in which 12% of the hemocytes were observed to be migrating through the capsule. There were no obvious differences between the categories of hemocytes exiting the capsule and those released via the endothelium.

Discussion

Our study shows that changes in hematopoietic activity of the shrimp *Sicyonia ingentis* are related to the molt cycle. Hemocyte production and release correspond with the known physiological roles of hemocytes. Hyaline hemocytes initiate hemolymph coagulation (Omori *et al.*,

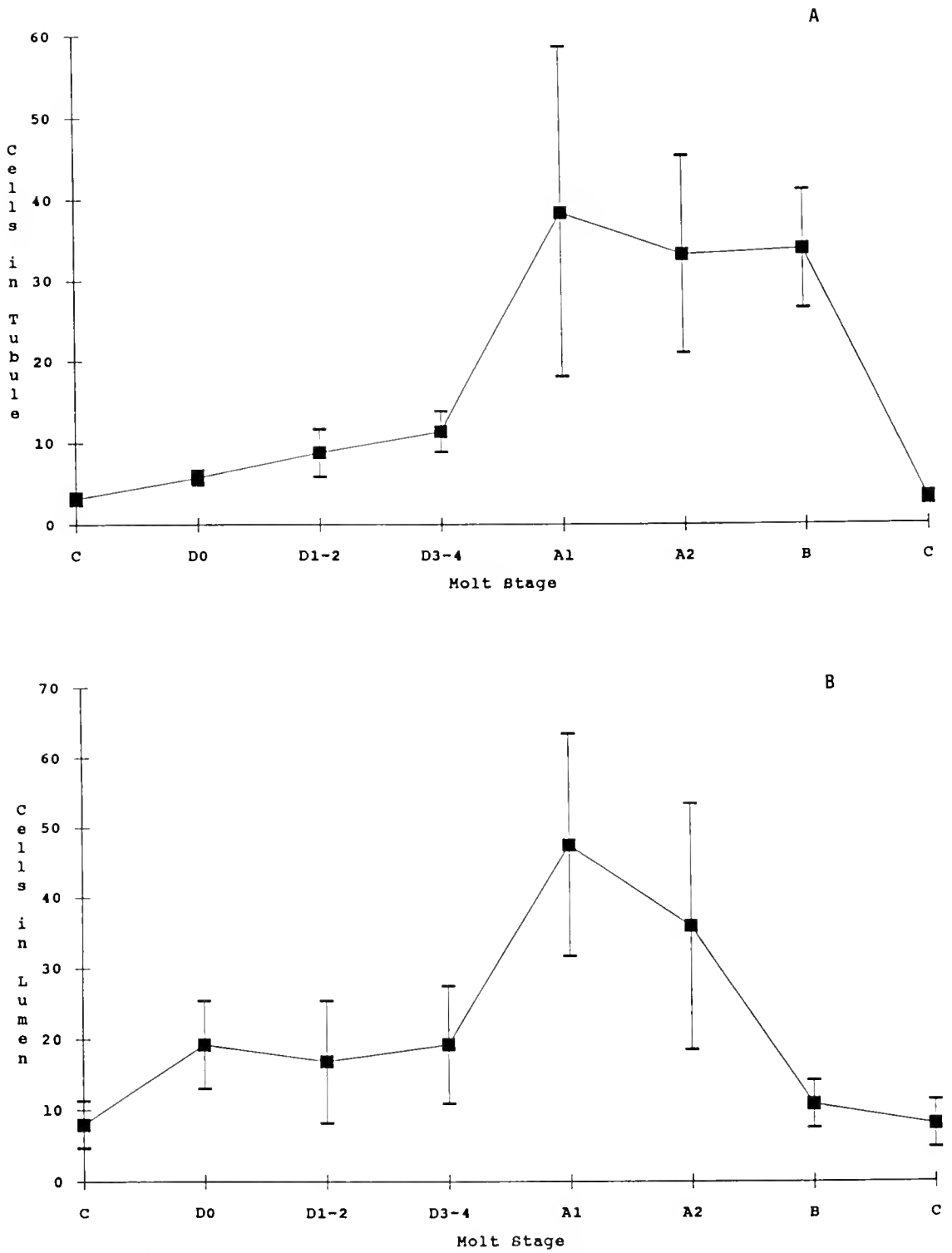

Figure 6. Numbers of hyaline hemocytes within shrimp hematopoietic tubules (A) and the lumens of the tubules (B) throughout the molt cycle. Mean of five shrimp, four tubules/shrimp. Error bars are ±1 standard deviation. The number of hyaline hemocytes inside the tubules was significantly elevated during molt stages A_1–B (post-ecdysis), concurrent and following the increased number of hyaline stem cells during stage A_1 as shown in Figure 5. Although a similar pattern of hyaline hemocyte release was observed during stages A_1–B, differences between the numbers of hyaline hemocytes inside the lumen were not significant due to high variability among the counts. Mean tubule diameters remained similar throughout the molt cycle, so cell counts could be directly compared.

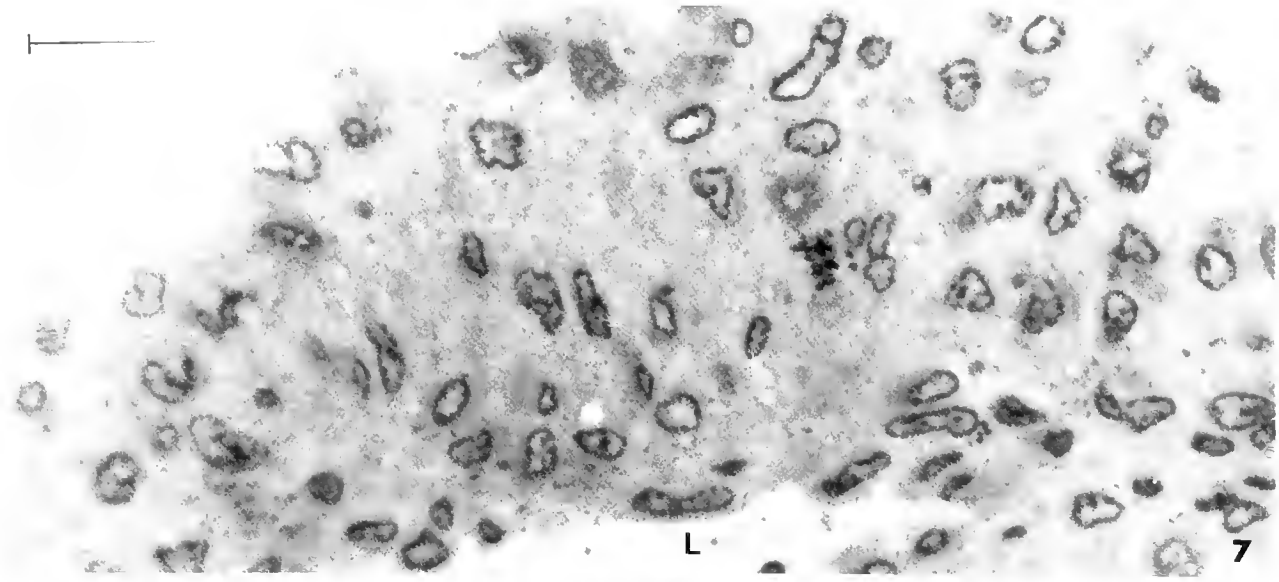

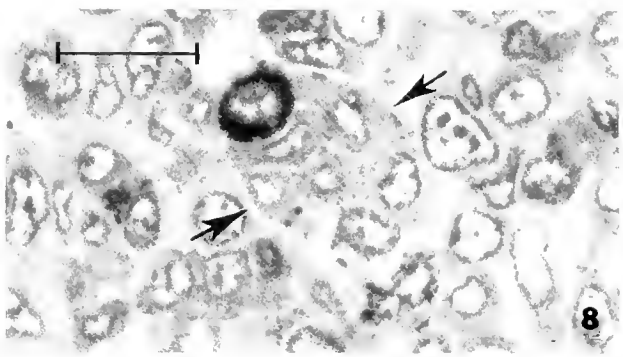

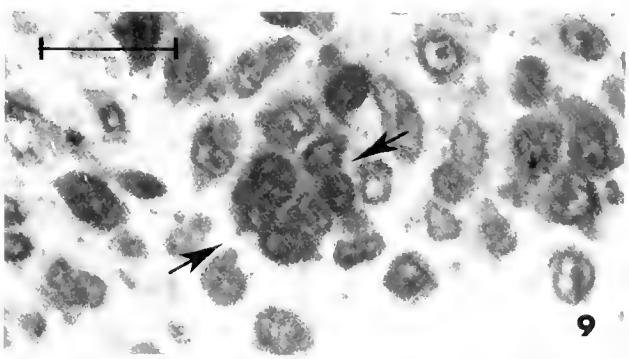

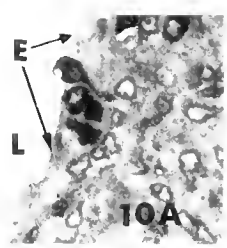

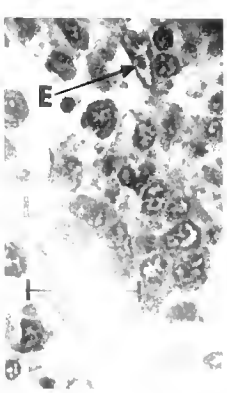

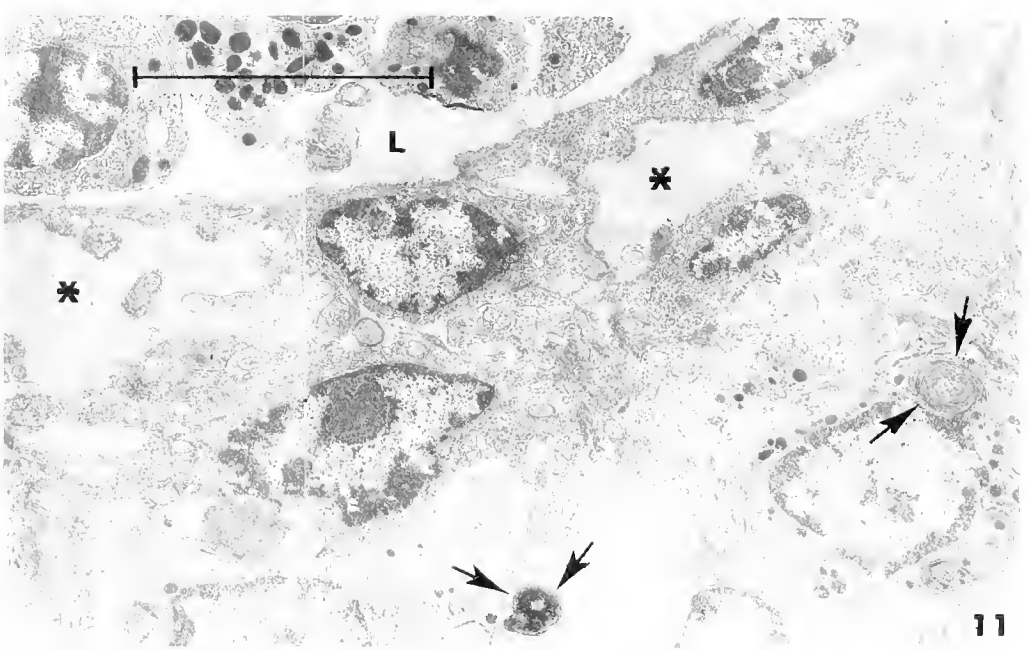

Figure 7. Light micrograph of stage V_2 tubule containing mostly stem cells. Hemocytes appeared to [illegible] already released from this tubule. Contrast the relative acellularity here with the more abundant hemocytes and large stem cells present in Figures 8 and 9. L, lumen. Methylene blue. 1430×; scale bar 20 μm.

1989) and contribute to formation of the pre-ecdysial procuticle and sclerotinization of the endocuticle at postecdysis (Vacca and Fingerman, 1983); they are thus essential throughout the molt cycle but also figure importantly during ecdysis. Hyaline hemocytes are produced at fairly constant levels from early intermolt (stage C) until immediately before molting (stage D_{3-4}). Some release occurs throughout this period, but many accumulate within the HPN until a large burst is released at postecdysis (stages A–B). Elevated numbers of hyaline hemocytes have previously been reported around ecdysis in the hemolymph (Kollman, 1908). Despite the use of slightly different molt stages in their analysis, Tsing *et al.* (1989) reported a similar pattern for their "lysing hemocytes," which undoubtedly are hyaline hemocytes. Not only have elevated numbers of circulating hyaline cells been noted around the time of ecdysis, but they have been observed migrating into the epidermis (Vacca and Fingerman, 1983). The latter investigators found that cross-linking of the endocuticle protein matrix is accomplished by diphenolic metabolites apparently synthesized or carried by the hyaline hemocyte. They further speculated that during molting, lysis of hyaline hemocytes liberates diphenols into the hemolymph which are translocated into the soft cuticle. We have also observed the accumulation of hyaline hemocytes beneath the forming cuticle but have been unable to duplicate Vacca and Fingerman's (1983) demonstration of diphenolic intermediates within these cells.

Granulocytes are primarily responsible for defense against foreign particles (Söderhäll *et al.*, 1988; Hose and Martin, 1989). Studies combining ultrastructural and cytochemical cell identification demonstrate that small granule hemocytes phagocytose small particles like bacteria (Hose *et al.*, 1990), although another group claims that hyaline hemocytes are also phagocytic, albeit at extremely low rates (Söderhäll *et al.*, 1988). In contrast, the role of large granule hemocytes is undisputed in the encapsulation of large foreign bodies such as metazoan parasites (Hose *et al.*, 1990). Although other cellular components may be involved, the prophenoloxidase system located in the granules and secretory vesicles of large granule hemocytes is considered to be the primary defense against most foreign molecules (Söderhäll *et al.*, 1986). Granulocytes, therefore, are essential to the host throughout the molt cycle. Small granule hemocytes are produced at the highest rate and released during intermolt and early premolt. Maturation of small granule hemocytes into large granule hemocytes occurs both in the hematopoietic tissue as well as in the peripheral circulation. This would ensure the constant production of large granule hemocytes, which eventually must become senescent and apparently lose the phagocytic portion of their defensive ability (Hose and Martin, 1989). The present study demonstrated that a minor pulse of granulocytes is produced and liberated during the postecdysial stage A_2 although available studies indicate that the duration of this stage is only a few hours (Skinner, 1962; Anderson, 1985). Similar results were reported by Tsing *et al.* (1989), where total granulocyte counts increased in the hemolymph from stage C to a maximum at stage D_{3-4}, followed by a large decline during the period immediately prior to ecdysis (stage D_4). A secondary increase was observed during stages $A–B_1$, followed by a decrease during stage B_2. Granulocytes may also participate in hardening of the exoskeleton. According to Vacca and Fingerman (1983), granulocytes cooperate in producing the procuticle and hardening the endocuticle by contributing formative proteins to be cross-linked by diphenols released by hyaline hemocytes. Granulocytes predominated in the cuticle prior to ecdysis and appeared to be degranulated by postecdysis. They speculated that release of granules into the hemolymph liberated proteins which may be involved in tanning, basement membrane formation, and wound healing. Other studies have suggested that granulocytes may activate an alternate pathway of hemolymph coagulation (Ravindranath, 1980; Durliat, 1985; Söderhäll *et al.*, 1988). Certainly the abundance of granulocytes as well as hyaline cells to repair the exoskeleton and fight infection is advantageous during ecdysis when the newly formed exoskeleton is soft and most susceptible to damage.

The only other study providing morphologic information on hematopoiesis throughout the molt cycle is Johnson's (1980) description of the hematopoietic tissue in the blue crab *Callinectes sapidus*. These photomicro-

Figure 8. Light micrograph of stage D_0 tubule showing granulocyte cluster (arrows). Methylene blue. 1700×; scale bar = 12 μm.

Figure 9. Light micrograph of stage D_{1-2} tubule showing a hyaline cell cluster (arrows). Methylene blue. 1700×; scale bar = 12 μm.

Figure 10. Light micrographs of hemocytes exiting from the wall of the hematopoietic tubule into the lumen (L). (A) Diapedesis of three hemocytes through the intact endothelium (E) of an intermolt shrimp. (B) During molting, the endothelial barrier is discontinuous; a single endothelial cell (E) is present at the top. A large group of hemocytes enters the lumen through a channel in the endothelium. Methylene blue. 1066 ×; scale bar = 15 μm.

Figure 11. Transmission electron micrograph of subendothelial spaces (*) and myelin figures (arrows) in the stroma of a stage B tubule. 5250×; scale bar = 8 μm.

graphs show hemo[illegible]bling granulocytes and corresponding ste[illegible] the intermolt tissues. Most of the stem c[illegible]ominent cytoplasmic granules and nucle[illegible]s (large central nucleolus) typical of the g[illegible]e. These cells appear similar to the granul[illegible]cells described here in the shrimp and also ar[illegible]vident in stages B through D_{1-2} tissue. In the crab, granulocytes produced during intermolt apparently were released soon after production since no increase in intermolt tissue thickness was noted despite the enhanced mitotic activity occurring from stages B_2 to late C (Johnson, 1980). Pre- and post-molt hematopoietic tissue appeared to be filled with smaller (5–6 μm diameter) hemocytes with a high N:C ratio, which may be hyaline stem cells and hemocytes. Johnson described a second type of stem cell with densely basophilic, homogeneous nuclei which lack distinct nucleoli. These characteristics are typical of the hyaline stem cells described in the shrimp which predominate in the pre- and post-molt hematopoietic tissue.

In both Johnson's (1980) study and ours, some individual variability was noted (1) in the types of hemocytes produced, (2) in the mitotic indices, and (3) between different portions of the hematopoietic tissue. Individual variability would be expected to result from differences in health status and environmental conditions. For example, increased production of granulocytes should occur in response to infectious disease. Studies have documented enhanced hematopoiesis in decapods infected with a virus (Lightner *et al.*, 1983) and a fungus (Hose *et al.*, 1984), although they did not categorize the types of hemocytes produced. Johnson (1980) noted the presence of mature granulocytes in the hematopoietic tissue of blue crabs infected with certain viruses, bacteria, and protozoa. However, stimulation of hematopoiesis may only be a transient response to an overwhelming acute infection, as has been shown for the fungus *Fusarium solani*. In early stages of the disease, mitosis is enhanced, but in advanced cases, the circulating hemocyte count drops and the hematopoietic tissue becomes necrotic (Hose *et al.*, 1984). Investigations are underway in our laboratory to quantify mitotic rates and hemocyte production in bacteria-infected shrimp.

Environmental stress can also modulate hematopoiesis. For instance, mitotic activity is greatly reduced in overwintering blue crabs, and degenerating hematopoietic cells are con[illegible]n (Johnson, 1980). Developing granulocytes routinely [illegible]ur in the hematopoietic tissue only at this time. Hem[illegible]te production becomes enhanced as spring water tem[illegible]atures increase. Long-term laboratory maintenance of blue crabs resulted in a similar increase in mitotic activity. Other factors with virtually undescribed effects on hematopoiesis include reproductive status, diet (Bauchau and Plaquet, 1973), and environmental pollution.

Although the observations of hemocyte maturation described here support our previous theory that the hyaline hemocytes and granulocytes comprise two separate lines (Martin *et al.*, 1987; Hose *et al.*, 1990), the scheme may be incomplete. Is there a common pluripotential stem cell which gives rise to the hyaline and granulocyte stem cells, and if so, where is it located? We were unable to find any cells within the hematopoietic tubules which possessed shared characteristics, such as the presence of striated granules or cytoplasmic deposits in a cell with numerous homogeneous granules, a large central nucleolus, or a nucleus containing predominately euchromatin. Such a cell might be detected in *in vivo* autoradiography experiments or in long-term *in vitro* maintenance of hematopoietic tissue using the culture methods described by Brody and Chang (1989). However, in their study, no mitosis was observed in contrast to earlier experiments where mitosis continued through the 12-day culture period (Fischer-Piette, 1931). Advances or modification of culture techniques and appropriate selection of mitotically active molt stages may yield sufficient material to follow the maturation of individual cells.

Any understanding of decapod hematopoiesis must recognize its interdependence upon a multiplicity of physiological and pathological states. Knowledge of the influences of normal physiology and disease status are essential before hematopoiesis can be effectively modulated to combat infectious disease or alleviate health problems arising in mariculture situations.

Acknowledgments

We thank Laura Targgart and Greg Omori for their efforts in collecting shrimp at the necessary molt stages. Technical assistance was supplied by Julia While. The project was supported by NSF grant DCB-8502150 to GM and JEH.

Literature Cited

Anderson, S. L. 1985. Multiple spawning and molt synchrony in free spawning shrimp (*Sicyonia ingentis*: Penaeoidea). *Biol. Bull.* **168:** 377–394.

Bauchau, A. G. 1981. Crustaceans. Pp 386–420 in *Invertebrate Blood Cells*, Vol. 2, Academic Press, New York.

Bauchau, A. G., and J. C. Plaquet. 1973. Variation du nombre des hémocytes chez les crustacés brachyoures. *Crustaceana* **24:** 215–223.

Bell, T., and D. V. Lightner. 1988. *A handbook of Normal Penaeid Shrimp Histology*. World Aquaculture Society, Allen Press, Kansas. 114 pp.

Brody, M. D., and E. S. Chang. 1989. Ecdysteroid effects on primary cell cultures. *Int. J. Invertebr. Reprod. Dev.* **16:** 141–147.

Charmantier, M. 1972. Étude préliminaire de la leucopoièse chez *Pachygrapsus marmoratus* (Crustacé, Decapode) au cours du cycle d'intermue. *C. R. Acad. Sci.*, Ser. D, **275:** 683–686.

Cuénot, L. 1893. Études physiologiques sur les Crustacés Decapodes. *Arch. Biol. Lieges* **13**:245–303.

Cuénot, L. 1905. L'organe phagocytaire des Crustacés Decapodes. *Arch. Zool. Exp. Gen.*, Ser. 4, **3**: 1–16.

Demal, J. 1953. Genèse et différenciation d'hémocytes chez *Palaemon varians* Leach. *Cellule* **56**: 87–103.

Durliat, M. 1985. Clotting processes in Crustacea Decapoda. *Biol. Rev.* **60**: 473–498.

Fischer-Piette, E. 1931. Culture de tissus de Crustacés. La glande lymphatique du Homard. *Arch. Zool. Exp. Gen.* **74**: 33–52.

Ghiretti-Magaldi, A., C. Milanese, and G. Tognon. 1977. Hemopoiesis in Crustacea Decapoda: origin and evolution of hemocytes and cyanocytes of *Carcinus maenas*. *Cell Differ.* **6**: 167–186.

Hose, J. E., D. V. Lightner, R. M. Redman, and D. A. Danald. 1984. Observations of the pathogenesis of the imperfect fungus, *Fusarium solani*, in the California brown shrimp, *Penaeus californiensis*. *J. Invertebr. Pathol.* **44**: 292–303.

Hose, J. E., G. G. Martin, and A. S. Gerard. 1990. A decapod hemocyte classification scheme integrating morphology, cytochemistry, and function. *Biol. Bull.* **178**: 33–45.

Hose, J. E., and G. G. Martin. 1989. Defense functions of granulocytes in the ridgeback prawn *Sicyonia ingentis* Burkenroad 1938. *J. Invertebr. Pathol.* **53**: 335–346.

Johnson, P. T. 1980. *Histology of the Blue Crab, Callinectes sapidus: A Model for the Decapoda.* Praeger, New York. 440 pp.

Kollman, M. 1908. Récherches sur les leucocytes et le tissue lymphoide des Invertébrés. *Ann. Sci. Nat. Zool.*, Ser. 9, **8**: 1–240.

Lightner, D. V., R. M. Redman, and T. A. Bell. 1983. Infectious hypodermal and hematopoietic necrosis, a newly recognized virus disease of penaeid shrimp. *J. Invertebr. Pathol.* **42**: 62–70.

Marrec, M. 1944. L'organe lymphocytogène des Crustacés décapodes. Son activité cyclique. *Bull. Inst. Oceanogr. Monacograph* 867, 4 pp.

Martin, G. G., and J. E. Hose. in press. Vascular elements and blood (hemolymph), in *Microscopic Anatomy of Invertebrates.* Vol. X, Decapod Crustacea. F. W. Harrison, ed. Wiley-Liss, New York.

Martin, G. G., J. E. Hose, and J. J. Kim. 1987. Structure of hematopoietic nodules in the ridgeback prawn *Sicyonia ingentis*: light and electron microscopic observations. *J. Morphol.* **192**: 193–204.

Oka, M. 1969. Studies on *Penaeus orientalis* Kishinouye. VIII. Structure of newly found lymphoid organ. *Bull. Jpn. Soc. Sci. Fish.* **35**: 245–250.

Omori, S. A., G. G. Martin, and J. E. Hose. 1989. Morphology of hemocyte lysis and clotting in the ridgeback prawn, *Sicyonia ingentis*. *Cell Tissue Res.* **255**: 117–123.

Ratner, S., and S. B. Vinson. 1983. Phagocytosis and encapsulation: cellular immune responses in Arthropoda. *Am. Zool.* **23**: 185–194.

Ravindranath, M. H. 1980. Haemocytes in haemolymph coagulation of arthropods. *Biol. Rev.* **55**: 139–170.

Skinner, D. M. 1962. The structure and metabolism of a crustacean integumentary tissue during a molt cycle. *Biol. Bull.* **123**: 635–647.

Söderhäll, K., M. W. Johansson, and V. J. Smith. 1988. Internal defense mechanisms. Pp. 213–235 in *Freshwater Crayfish: Biology, Management and Exploitation.* D. M. Holdich and R. S. Lowery, eds. Croom Helm, London.

Söderhäll, K., V. J. Smith, and M. W. Johansson. 1986. Exocytosis and uptake of bacteria by isolated haemocyte populations of two crustaceans: evidence for cellular co-operation in the defense reactions of arthropods. *Cell Tissue Res.* **245**: 43–49.

Spurrs, A. 1969. A low viscosity epoxy embedding medium for electron microscopy. *J. Ultrastruct. Res.* **26**: 31–43.

Tsing, A., J.-M. Arcier, and M. Brehélin. 1989. Hemocytes of penaeid and palaemonid shrimps: Morphology, cytochemistry, and hemograms. *J. Invertebr. Pathol.* **53**: 64–77.

Vacca, L. L., and M. Fingerman. 1983. The roles of hemocytes in tanning during the molting cycle: A histochemical study of the fiddler crab, *Uca pugilator*. *Biol. Bull.* **165**: 758–777.

Reference: *Biol. Bull.* **183**: 200–210. (October, 1992)

Particulate Tubulin in Interphase and Metaphase Extracts of Oocytes of *Spisula*

KATHY A. SUPRENANT*

Department of Physiology and Cell Biology, University of Kansas, Lawrence, Kansas 66045–2106 and Marine Biological Laboratory, Woods Hole, Massachusetts 02543*

Abstract. In 1972 Weisenberg reported that surf clam oocytes contained a particulate and sedimentable pool of tubulin that could be isolated in buffers containing hexylene glycol. This "interphase particulate tubulin" (IPT) copurified with 10-20 μm granular spheres, which were identified as the "tubulin-containing structures" (TCS). Approximately one TCS per oocyte was isolated and the TCS disappeared after nuclear envelope breakdown. Weisenberg postulated that the TCS was comprised of a stored form of tubulin or a microtubule-assembly intermediate.

To characterize this intriguing form of stored tubulin, IPT was isolated in hexylene glycol-containing buffers as described by Weisenberg (1972, *J. Cell Biol.* 54, 266–278) and the amount of sedimentable tubulin was quantitated by immunoblotting during the first meiotic cell cycle. Approximately 10% of the total tubulin in *Spisula* oocytes sediments at g forces that are too small to pellet tubulin dimers or even single microtubules. Granular spheres, approximately 15 μm in diameter, are present in the sedimentable tubulin fractions. During the first cell cycle, the granular spheres disappear while the sedimentable tubulin levels gradually decrease. Although the disappearance of the spheres corresponds with the loss of sedimentable tubulin, the spheres do not contain tubulin. An initial centrifugation of the oocyte homogenates at 650g leaves most of the tubulin in the supernatant and the granular spheres in the pellet. The tubulin-containing fractions are composed of membranes and an amorphous unidentified material associated with short microtubules. Sedimentable tubulin is not detected in homogenates prepared at 0°C or in the absence of hexylene glycol, conditions that favor microtubule disassembly. It is likely that sedimentable tubulin is composed of hexylene glycol-induced polymers and not unique particulate structures that sequester tubulin. Finally, the granular spheres that contaminate the tubulin preparations are identified as nucleoli. They are morphologically identical to the nucleoli of the intact oocyte and they fluoresce brightly when stained with the Hoechst DNA dye 22358.

Received 6 May 1992; accepted 22 July 1992.

Abbreviations: IPT—interphase particulate tubulin; TCS—tubulin-containing structure; MFNSW—millipore-filtered natural seawater; hexylene glycol—2-methyl-2,4-pentanediol; HGL—hexylene glycol-containing phosphate buffer; GV—germinal vesicle; PIPES—piperazine-N,N-bis(2-ethane-sulfonic acid); EGTA—ethylene glycol-bis(β-aminoethyl ether) N,N,N′,N′-tetraacetic acid.

* Address for correspondence

Introduction

The regulation of microtubule length and spatial organization is important for diverse cellular processes such as axoplasmic transport and chromosome movements. Since microtubules are in a dynamic equilibrium with their tubulin subunits (Inoué, 1981; Mitchison and Kirschner, 1984), factors that perturb the free tubulin concentration can radically change microtubule performance (Mitchison and Kirschner, 1987; DeBrabander *et al.*, 1986; Avila 1990). In many cells, the polymer-monomer equilibrium is checked and balanced by regulating tubulin biosynthesis (Lefebvre and Rosenbaum, 1986; Cleveland *et al.*, 1988). Levels of unpolymerized tubulin subunits can censor their own synthesis as well as regulate microtubule assembly dynamics.

The mechanism for maintaining unassembled tubulin within the cytoplasm is not understood. *In vitro* studies have shown that a significant amount of unassembled tubulin is found in cellular fractions obtained by low speed centrifugation. In neuroblastoma cells, for example,

6–10% of the total tubulin is present in an insoluble, non-microtubular form (Hiller and Weber, 1978; Nath and Flavin, 1979; Olmsted, 1981). A membrane-associated or membrane-bound tubulin is also a common finding in neuronal cells and tissues (Stephens, 1986, 1990). Whether these fractions represent a unique unassembled form of tubulin is not established.

One of the most provocative studies of sedimentable tubulin was described by Weisenberg (1972). A particulate and sedimentable form of tubulin was found in surf clam oocytes and named "interphase-particulate tubulin" (IPT). Interphase-particulate tubulin was operationally defined as a colchicine-binding activity that sedimented at extremely low g forces and it was suggested that IPT is either a storage form of tubulin or a microtubule assembly intermediate. Spherical structures (10–20 μm in diameter) were identified as the particulate tubulin-containing structure or TCS. There was only one such TCS per oocyte. Moreover, the TCS disappeared and the level of IPT decreased during the first meiotic cell cycle. The tantalizing implication from these experiments was that an insoluble form of tubulin contained within a specific structure might regulate microtubule polymerization during the cell cycle. In this report, the presence and identity of the TCS and IPT is reexamined in order to characterize a potentially unique form of tubulin that may play an important role in microtubule dynamics during the embryonic cell cycle.

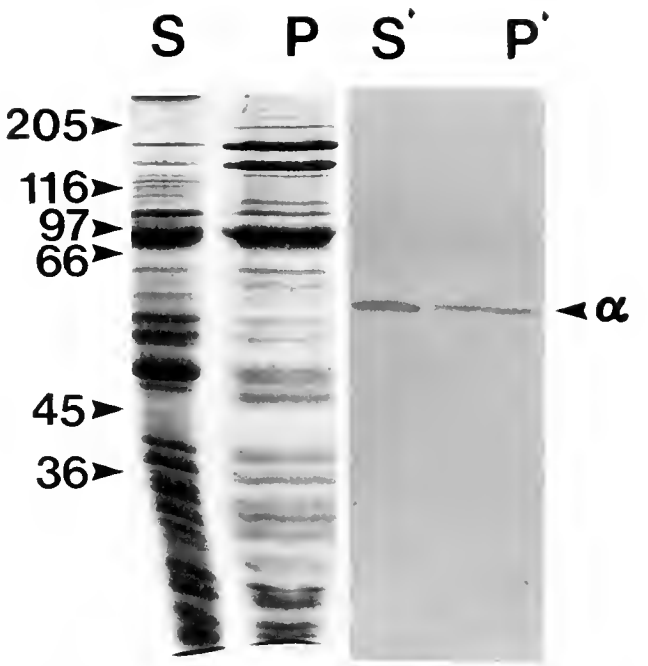

Figure 1. Identification of particulate tubulin extracts of oocytes of *Spisula* by Western blotting. The left panel illustrates the protein composition of the 2500g supernatant (S) and pellet (P) analyzed by SDS-PAGE and stained with Coomassie blue. Duplicate protein samples were separated by SDS-PAGE and electrophoretically transferred to nitrocellulose. A monoclonal antibody (DM 1A) against α-tubulin was used to probe an immunoblot of the 2500g supernatant (S') and pellet (P). DM1A is a commercially available mouse monoclonal antibody prepared against chick brain α-tubulin (Blose *et al.*, 1984). The epitope for this antibody is located at the acidic C-terminal domain of the α-subunit (Serrano *et al.*, 1986; Breitling and Little, 1986). The position of α-tubulin is noted. Relative molecular mass standards are in kilodaltons.

Materials and Methods

Particulate tubulin isolation

Individuals of *Spisula solidissima* were provided by the Department of Marine Resources at the Marine Biological Laboratory (Woods Hole, MA). Ovaries were dissected and minced into Millipore-filtered (0.22 μm) natural seawater (MFNSW) and filtered through several layers of cheesecloth to obtain free oocytes. Oocytes were washed once in MFNSW and three times in Ca^{++}-free artificial seawater (Salmon, 1982). Oocytes were washed and kept at room temperature (21–22°C) for no longer than one hour. Oocytes were parthenogenetically activated by the addition of 14 ml of 0.5 M KCl in distilled water to a dilute suspension of oocytes (5 ml oocytes in 86 ml seawater) (Allen, 1953). Particulate tubulin was isolated at room temperature from an equal volume of oocytes at 0, 3, 6, 9, 12, 15, 18, and 21 min following activation. At each time point a small sample was immediately fixed in 1 ml of 75% ethanol and 25% acetic acid and later stained with lacto-orcein to visualize the chromosomes and accurately stage the cell cycle progression (Westendorf *et al.*, 1989).

Particulate tubulin was isolated from germinal vesicle stage oocytes and from parthenogenetically activated oocytes during the first meiotic cell cycle. One ml of packed oocytes was suspended at room temperature in ten volumes of HGL solution containing 1 M 2-methyl-2,4-pentanediol (hexylene glycol), and 0.01 *M* potassium phosphate at pH 6.2. The oocytes were homogenized with a Wheaton Dura-Grind Stainless Steel Dounce homogenizer with a 0.0005″ wall clearance. It was not necessary to remove or soften the vitelline envelop when using this homogenizer, so homogenates could be prepared rapidly at 3-min intervals. Homogenates were also prepared with a teflon pestle-glass homogenizer used by Weisenberg (1972); identical results were obtained with this instrument even though it was necessary to first soften the vitelline layer with glycerol before cell lysis (Rebhun and Sharpless, 1964). The homogenate was underlayed with a 5 ml cushion of 10% (w/v) sucrose in HGL and centrifuged at 4°C in a low-speed swinging bucket rotor at 5000rpm for 30 min (Beckman JS-13.1) (2500g at r_{av}). The 2500g

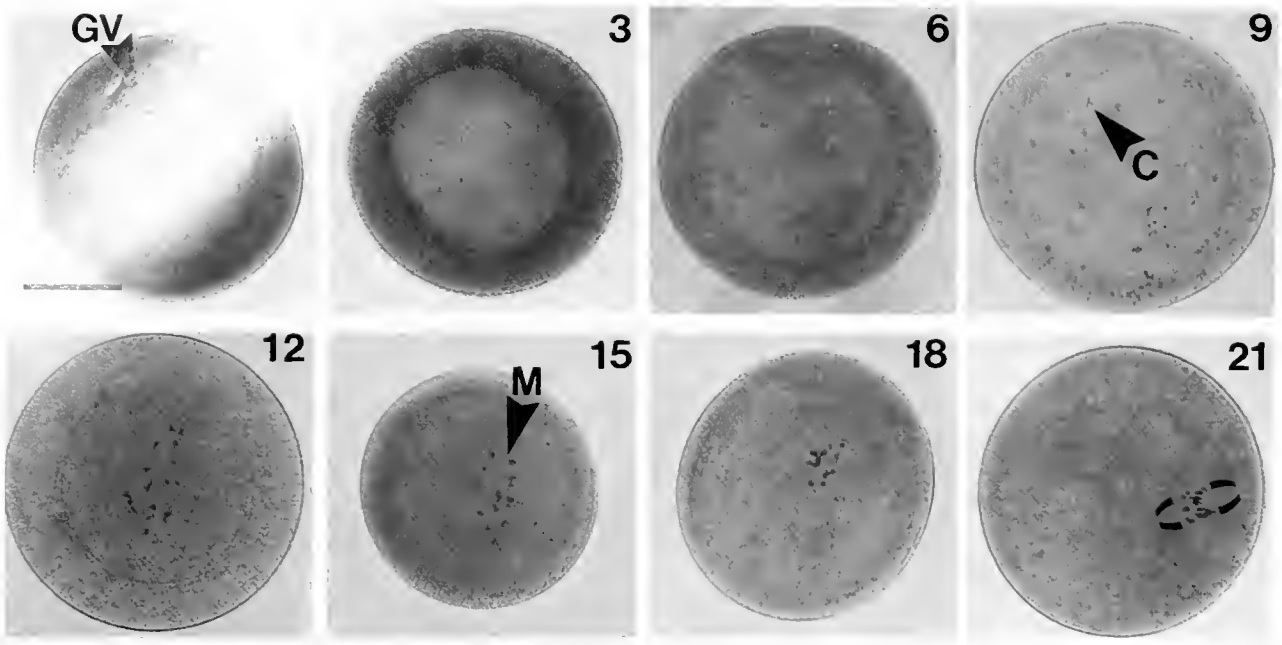

Figure 2. Oocyte development in *Spisula* following parthenogenetic activation visualized by brightfield light microscopy. Oocytes were fixed with ethanol-acetic acid and stained with lacto-orcein to visualize the chromosomes. The germinal vesicle (GV) present in the unactivated oocyte breaks down 9–10 min after activation. The chromosomes (C) are easily visualized after staining with lactoorcein as minute tetrads. The chromosomes congress towards the metaphase plate (M) as the first meiotic spindle forms in the center of the oocyte by 15′ post-activation. Chromosomes begin to separate as the first meiotic spindle (position indicated by brackets) moves to the cortex at 21′. The oocytes were flattened to different extents in these micrographs. Bar = 30 μm.

supernatant and sucrose cushion were removed, mixed together, and placed on ice. The 2500g pellet was resuspended stoichiometrically in 16 ml of ice cold HGL (volume equal to total homogenate volume plus sucrose cushion). Both supernatant and pellet fractions were frozen for later analysis.

Measurement of protein concentration

Protein concentrations were determined by the method of Lowry *et al.* (1951). Bovine serum albumin (BSA) was used as a protein standard.

Polyacrylamide gel electrophoresis

Proteins were analyzed on 0.75 mm SDS-polyacrylamide gels with the discontinuous buffer formulation of Laemmli (1970). The separating gel contained 8% acrylamide and 4 *M* urea. Gels were stained for protein with Coomassie blue in a concentrated methanol/acetic acid solution (Sambrook *et al.*, 1989).

Immunoblotting

For immunoblot analysis, unstained SDS-polyacrylamide gels were electrophoretically transferred to nitrocellulose (BA-45, Schleicher and Schuell, Keene, NH) as described by Towbin *et al.* (1979). The nitrocellulose blot was air-dried for 1–3 h and then blocked with Tris-buffered saline (TBS) (10 m*M* Tris-HCl, pH 7.4, 0.15 *M* NaCl) containing 5% (w/v) Carnation's non-fat dry milk for 45–60 min at room temperature. After blocking, the blot was incubated for 18–24 h (4°C) with a monoclonal antibody specific for α-tubulin (DM1A) (ICN Immunobiologicals, Lisle, IL) diluted 1:500 in TBS with 5% milk. After washing (4 times, 10 min each in TBS), the blot was blocked again for 15 min in TBS with 5% milk then incubated in a 1:2000 dilution of horseradish peroxidase-conjugated goat anti-mouse IgG (Hyclone Laboratories, Logan, UT) in TBS-milk for 2–3 h at room temperature. The blot was washed again in TBS (4 times, 10 min) and incubated 5–15 min in freshly prepared developer (20 ml TBS, 4 ml of 3 mg/ml 4-chloro-1-napthol in methanol, 20 μl of 30% hydrogen peroxide) (Hawkes *et al.*, 1982). The blots were rinsed in deionized water, air-dried, and photographed.

Light and electron microscopy

Preparations were examined with a Nikon Optiphot equipped with phase and fluorescence light optics. Images

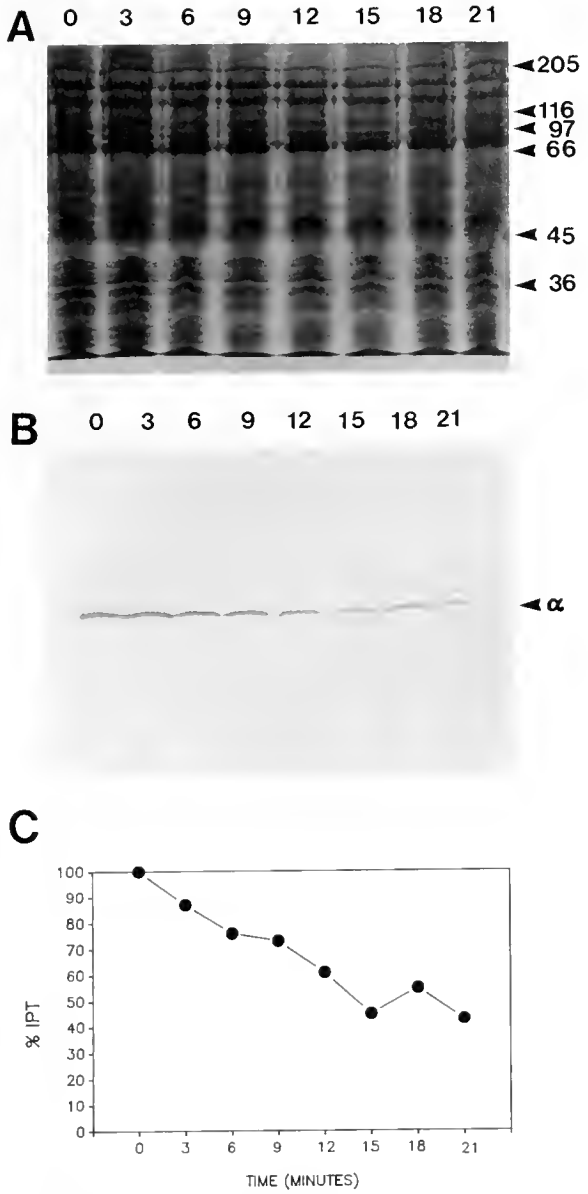

Figure 3. Quantitation of IPT during the first meiotic cell cycle in extracts of oocytes of *Spisula*. Particulate tubulin fractions were isolated from equal volumes of oocytes at 3′ intervals following parthenogenetic activation. An equal volume of each particulate tubulin fraction was separated by SDS-PAGE and stained with Coomassie blue (A). Identical samples were blotted to nitrocellulose and probed with a monoclonal antibody against α-tubulin (B). The blots were scanned with an Apple OneScanner interfaced to an Apple IIcx computer and analyzed with the public domain software program IMAGE. The amount of sedimentable tubulin obtained at each interval is expressed as a percent of the total interphase particulate tubulin (IPT) detected in the oocyte (C).

were recorded on TMAX 100 and 400 film developed in TMAX developer. For electron microscopy, samples were negatively stained with uranyl acetate on glow discharged, carbon-coated formvar grids.

Results

Interphase particulate tubulin (IPT) and the tubulin-containing structure (TCS)

A significant fraction (>10%) of the total detectable tubulin in surf clam oocytes sediments at very low centrifugal forces (Fig. 1). This tubulin corresponds to the interphase particulate tubulin (IPT) described by Weisenberg (1972). Following oocyte activation, the level of particulate tubulin decreases steadily during the time course of nuclear envelop breakdown and formation of the first meiotic spindle (Figs. 2, 3). The decrease in sedimentable tubulin following parthenogenesis suggests that the interphase particulate tubulin (IPT) may be a storage form of tubulin that becomes solubilized.

Tubulin dimers (Mr 100,000) alone or single microtubules cannot pellet at 2500g's. There are, however, large 15 μm spherical particles present in unactivated oocyte homogenates that might be associated with the particulate tubulin (Fig. 4); these particles are conspicuously absent from homogenates prepared 10 min after parthenogenetic activation. In addition, these large particles pellet with the particulate tubulin (Fig. 5). After centrifugation through sucrose, the particles frequently take on an ovoid profile and become more granular in appearance. These large particles are actually composed of two tandemly arranged spheres. The smaller 3–5 μm spheres are frequently detached from the larger 12–13 μm spheres (Fig. 5C–F). These spherical particles bear a striking resemblance to the nucleolus and nucleolinus of the intact germinal vesicle stage oocytes (Fig. 5A). To confirm their identity, these structures were incubated with Hoechst 33258 and examined by fluorescence light microscopy (Fig. 6). Both the large and small particle fluoresce brightly revealing their DNA content.

The nucleolus is not a tubulin-containing structure

To determine if any sedimentable tubulin was associated with the nucleoli, the nucleoli were separated from the tubulin by centrifugation. Oocytes were homogenized in HGL, underlayed with a sucrose cushion and centrifuged at 650g (2500 rpm) for 5 min in a clinical centrifuge. Four fractions were obtained—the uppermost supernatant S1, the sucrose interface S2, the sucrose cushion S3, and the pellet (Fig. 7A). Each fraction was resuspended stoichiometrically in 11 ml of HGL (starting volume of homogenate) and small aliquots were examined by phase microscopy (Fig. 7C). Under these centrifugation conditions the nucleoli pellet to the bottom of the tube and are not detected in any of the supernatant fractions.

Sedimentable tubulin is detected in all fractions (Fig. 7B). Each 11 ml fraction was underlayed with 10% sucrose

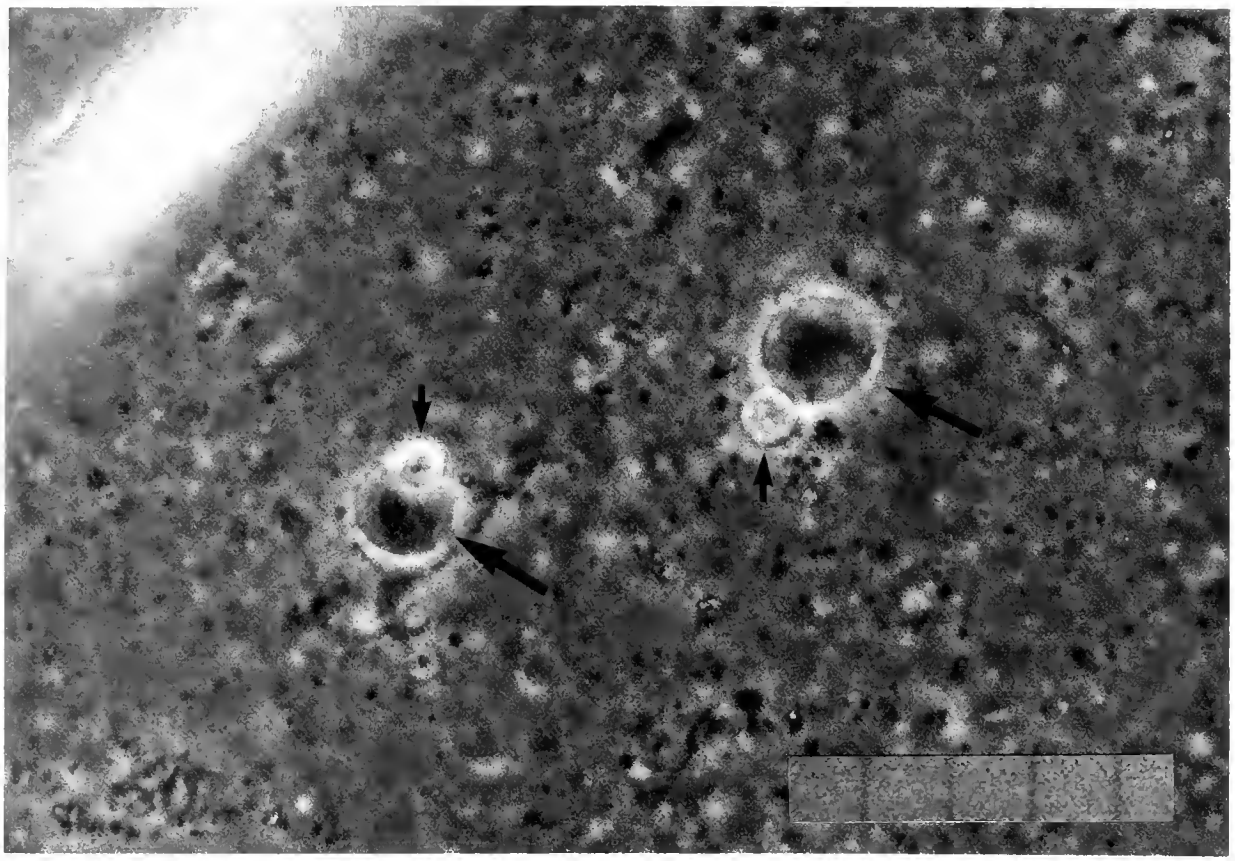

Figure 4. Homogenates of unactivated surf clam oocytes contain large, tandemly arranged, globular structures. In phase microscopy, a large, phase-dark sphere (large arrows) is associated with a small, round, phase-light particle (small arrows). These tandemly arranged particles are frequently associated with a phase-dark membrane-like structure (see particle on the left). A magnification bar with 10 μm spacing is shown.

in HGL and centrifuged at 2500g to pellet the particulate tubulin. An equal volume of each resuspended pellet was analyzed and compared by SDS-PAGE and immunoblotting (Fig. 7B). Each 650g fraction—S1, S2, S3, and P—contained tubulin that sedimented at 2500g. The largest amount of particulate tubulin was found in the fractions farthest away from the nucleoli (Table I). This does not rule out the possibility that a small amount of sedimentable tubulin still might be associated with the nucleoli. However, no nucleolar tubulin was detected by immunofluorescence with the DM 1A antibody. The levels of nucleolar fluorescence were indistinguishable from the controls in which no first antibody was added.

To identify the source of the particulate tubulin, a small sample of each resuspended pellet (2500g) was negatively stained with uranyl acetate for transmission electron microscopy (Fig. 7D). The bottom three fractions contain numerous short microtubules which are associated with membranes and densely staining, amorphous aggregates. No microtubules are detected in the uppermost fraction (S1), which also contained numerous membranes, granular aggregates, and the largest fraction of particulate tubulin.

The abundance of membranes in all fractions suggested that the sedimentable tubulin might be membrane-bound. The amount of IPT that was detergent-soluble was examined before and 5 min after parthenogenetic activation. Homogenates were prepared in HGL in the presence and absence of 0.5% Triton-X-100 and the amount of tubulin in the 2500g pellets was compared by immunoblotting. Inclusion of this non-ionic detergent has no effect on the amount of sedimentable tubulin detected before or after activation, indicating that the sedimentation of this tubulin is not dependent upon membrane integrity.

The presence of microtubules in three of the four fractions suggests that microtubule assembly may have taken place in the homogenates prepared *in vitro*. The hexylene glycol used in this and the previous study (Weisenberg, 1972) may have promoted the assembly of microtubules and their association with the denser and more massive

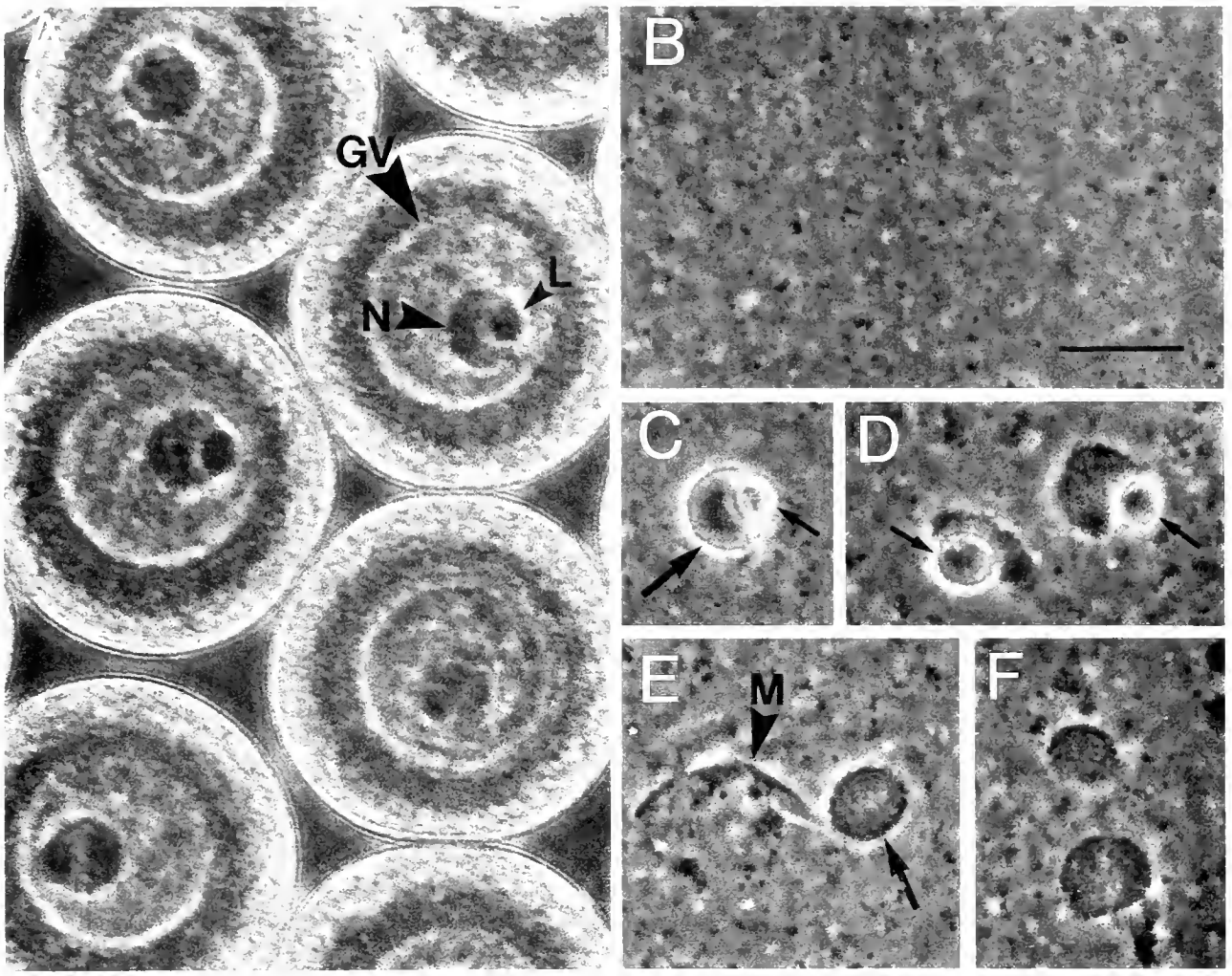

Figure 5. Phase microscopy of particulate tubulin fractions in extracts of oocytes of *Spisula*. Unactivated oocytes (A), were homogenized and centrifuged as described in the Materials and Methods to yield a 2500 g supernatant (B) and 2500g pellet that contains the interphase particulate tubulin (C–F). Tandemly arranged large spheres (large arrows) and small particles (small arrows) are absent from the supernatant fractions. After centrifugation, the small particle is frequently lost and only the larger sphere is observed. Membrane-like (M) structures are frequently associated with the larger sphere. Compare the morphology of the tandemly arranged particles to the nucleolus (N) and nucleolinus (L) of the intact oocyte (5A). Within the germinal vesicle (GV) lie a tandemly arranged structure indistinguishable from the structures in the 2500g pellet. Bar 20 μm.

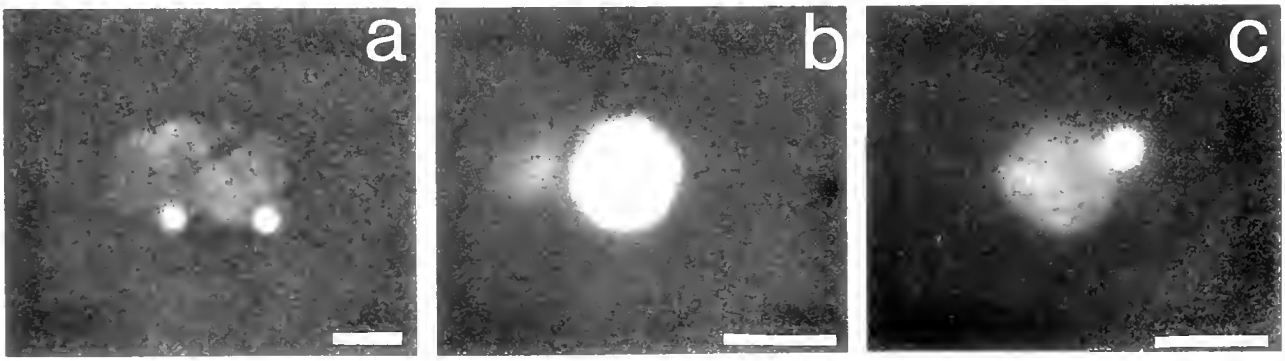

Figure 6. Hoechst DNA staining of the 2500g pellet fraction. Pellets were resuspended in HGL, incubated for 10 min on poly-L-lysine coated coverslips, rinsed twice with HGL, and finally with HGL containing 2 μg/ml Hoechst 22358. The magnification bar is 10 μm.

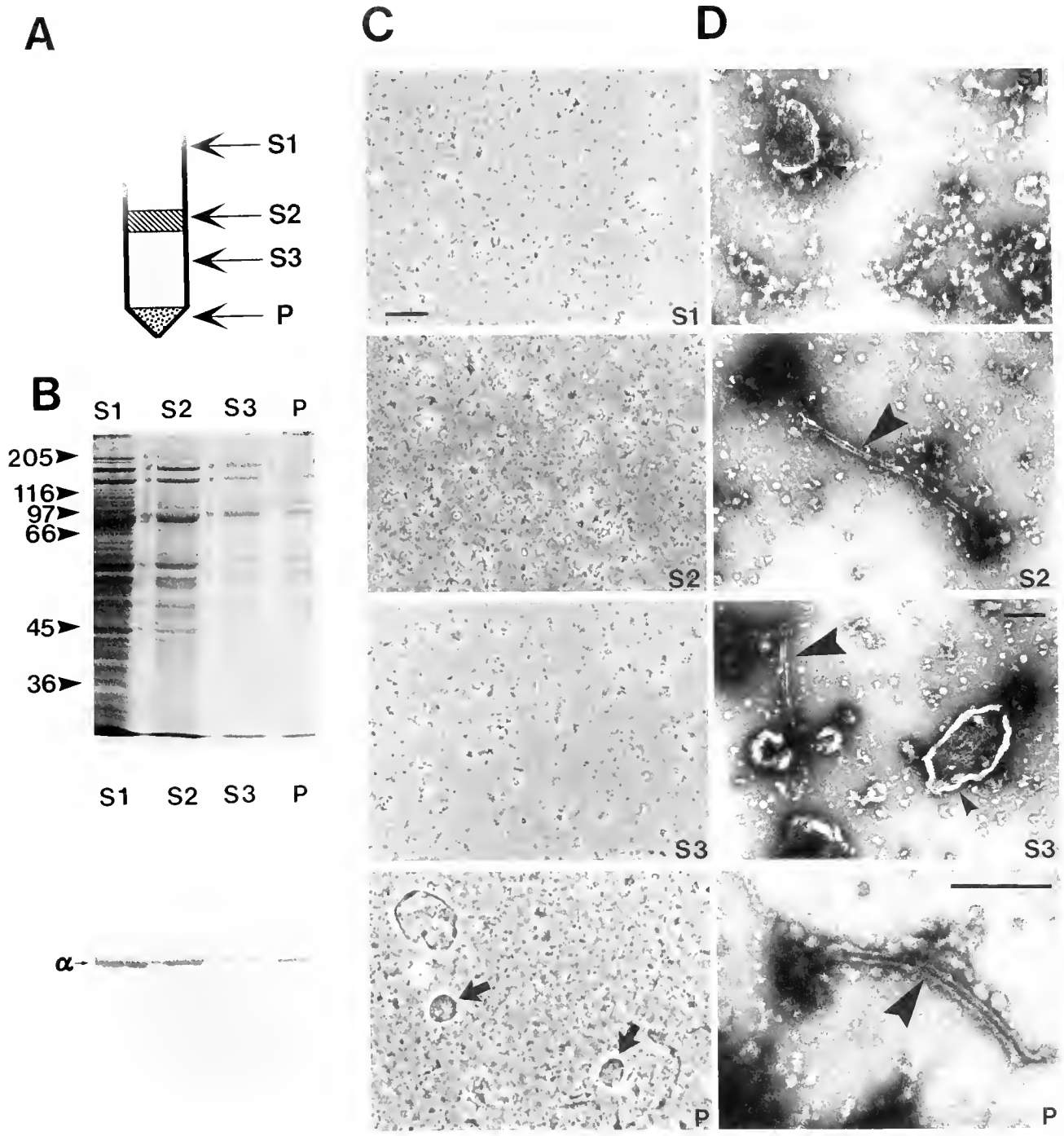

Figure 7. Separation of the nucleoli from the particulate tubulin-containing fractions in extracts of oocytes of *Spisula* by low speed centrifugation. Panel A. Diagram illustrating the four fractions obtained after a 650g centrifugation (see Results). Each 650g fraction was diluted in HGI and examined by phase microscopy (Panel C). The nucleoli are only detected in 650g pellet (P). Each 650g fraction was centrifuged again to obtain a 2500g pellet. SDS-PAGE analysis of each 2500g pellet is shown in Panel B (top). Identically prepared samples were blotted to nitrocellulose and probed with the DM1A antibody against α-tubulin. Each 650g fraction contains a significant amount of tubulin that sediments at 2500g. Each 2500g pellet was resuspended in HGI and negatively stained with uranyl acetate for electron microscopy (Panel D). Membranes (small arrowheads) are present in every fraction while microtubules were detected in the three heaviest fractions—S2, S3, and P. Magnification bar is equal to 20 μm in panel C and 0.25 μm in panel D.

Table I

Amount of particulate tubulin in each 650g fraction expressed as a percentage of the total interphase particulate tubulin (IPT) found in all four fractions in extracts of oocytes of Spisula

Fraction	% Total IPT
S1	47.2
S2	33.3
S3	5.4
P	14.1

cytoplasmic aggregates and organelles. To examine this possibility, experiments were carried out under conditions that favored microtubule disassembly. Homogenates were prepared in either ice cold HGL or in phosphate buffers at room temperature in the absence of hexylene glycol. There is no detectable tubulin in the 2500g pellets under either of these conditions. Finally, homogenates were prepared at pH 6.6, 6.9, and 7.2 in ice-cold microtubule-reassembly buffer that contained PIPES, $MgSO_4$, EGTA, GTP, DTT, protease inhibitors, and no hexylene glycol. Several pH values were tested, because it was shown recently that microtubule assembly in surf clam oocyte extracts is favored at alkaline pH (Suprenant 1989; 1991). Under these isolation conditions, all the tubulin is detected in the supernatant fluids (Fig. 8). There is no sign of interphase particulate tubulin on these heavily overloaded gels. These results indicate that the microtubules found in the particulate tubulin preparation are either stabilized or induced to assemble by the hexylene glycol.

Discussion

Fertilization of surf clam oocytes results in a major reorganization of the cytoplasm that ultimately results in syngamy and the first mitotic cleavage division (Allen, 1953; Rebhun, 1959; Longo and Anderson, 1970a, b; Dan and Itoh, 1984). During the 75 min following fertilization, microtubules of two meiotic and one mitotic apparatus are assembled and disassembled. The regulatory events that are responsible for these transitions in microtubule polymerization are not known. The unfertilized clam oocyte does contain up to 30 μM tubulin (Burnside *et al.*, 1973; Suprenant, 1991), none of which appears to be assembled into microtubules (Kuriyama *et al.*, 1986). Weisenberg (1972) proposed that this unpolymerized tubulin was sequestered in discrete spherical, tubulin-containing structures (TCS).

In this study, the particulate and sedimentable pool of tubulin, first described by Weisenberg (1972) as "interphase-particulate tubulin" or IPT, was isolated from surf clam oocytes. Every attempt was made to duplicate the isolation conditions described by Weisenberg. The only substantive change was the assay used to identify and quantitate the IPT. Instead of a colchicine-binding assay, tubulin was solubilized, separated from other oocyte proteins by electrophoresis, and quantitated by Western blotting with a monoclonal antibody, DM 1A, generated against chick brain microtubules (Blose *et al.*, 1984). An immunoassay is more advantageous than a colchicine-binding assay because it is very sensitive and highly specific for tubulin even in a total cellular homogenate and it avoids the thermal inactivation or decay of the colchicine-binding reaction.

This study and Weisenberg's (1972), have shown that over 10% of the total tubulin in surf clam homogenates is "particulate" and sediments at very low g forces. Because the amount of IPT decreases following activation, Weisenberg (1972) suggested the exciting possibility that IPT was a stored form of tubulin or microtubule-assembly intermediate. The results from this study indicate that this hypothesis is probably not true because both the microtubule-associated and aggregated forms of IPT are dependent upon hexylene glycol. High concentrations of solvents (1–4 M) such as glycerol (Lee and Timasheff, 1977), DMSO (Himes *et al.*, 1976), polyethylene glycol (Herzog and Weber, 1978), and hexylene glycol (Kane, 1962; Rebhun and Sharpless, 1974) can promote the polymerization of tubulin and stabilize microtubules against disassembly.

It is likely that the decrease in IPT following oocyte activation reflects the *in vitro* cytoplasmic assembly conditions. For example, recent studies have examined nucleated-microtubule growth at defined cell cycle states in *Xenopus* cell-free extracts (Gard and Kirschner, 1987a, b; Belmont *et al.*, 1990; Verde *et al.*, 1990; Gotoh *et al.*, 1991). Visualization of microtubules in real-time and in fixed preparations reveals that microtubules assembled in mitotic extracts are shorter and more dynamic than those in interphase extracts. If microtubules in surf clam extracts behave similarly, the transition from interphase to mitosis would be accompanied by an increase in microtubule turnover and a decrease in the steady state mass of assembled polymer.

Similar to the previous report (Weisenberg, 1972), unactivated surf clam homogenates contain large granular particles as well as a form of tubulin that sediments at low g forces. In this study, the granular particle is identified as the nucleolus, not the tubulin-containing structure. The nucleolus is not the source of the interphase particulate tubulin since it can be separated from the bulk of the sedimentable tubulin and tubulin cannot be detected within the nucleolus by immunofluorescence. The granular particle is identified as the nucleolus because it: (1) is present at only one copy per cell, (2) is morphologically

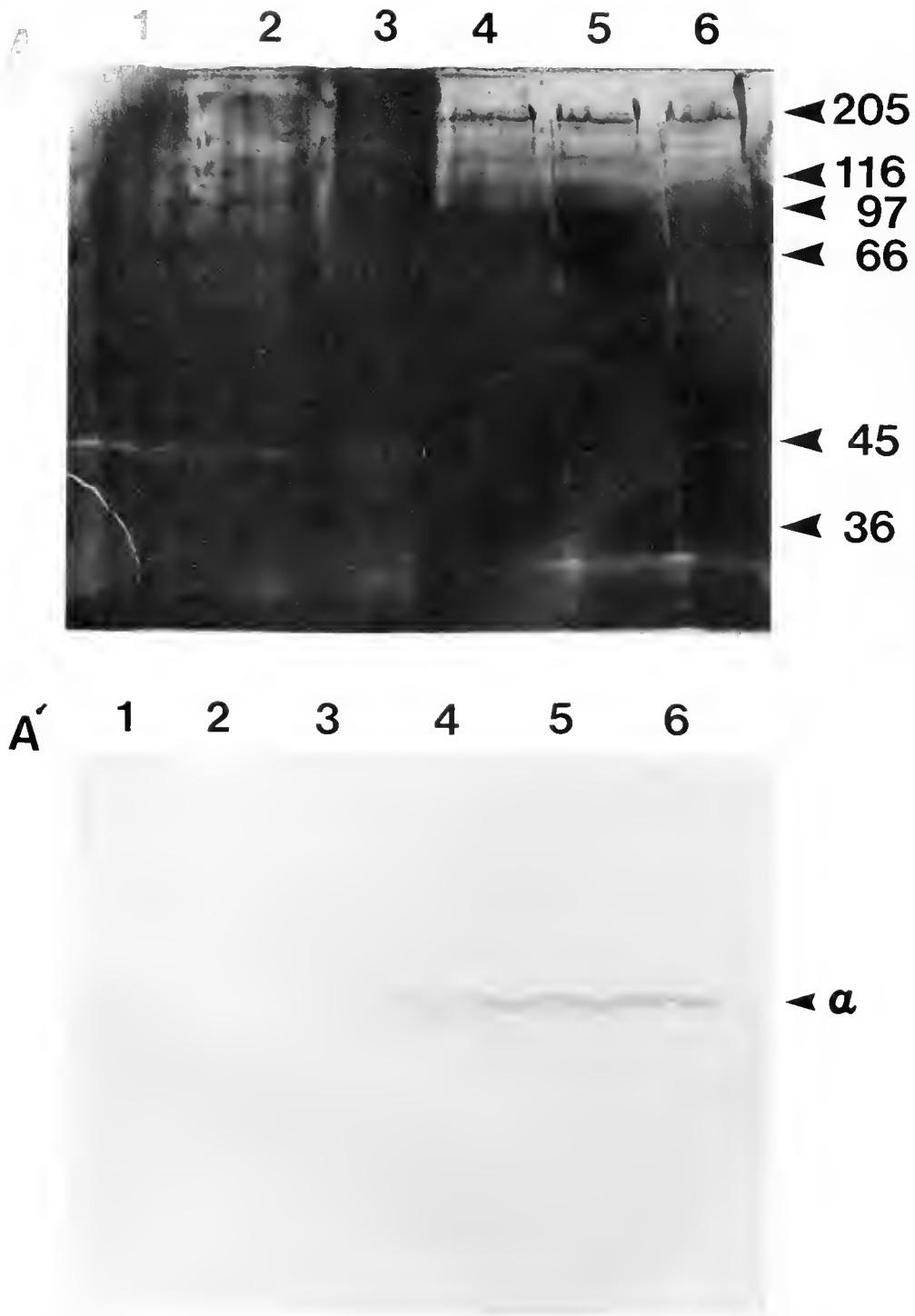

Figure 8. Sedimentable tubulin was absent from homogenates prepared in a microtubule assembly buffer without hexylene glycol. Surf clam oocytes were homogenized in a buffer containing 100 m*M* K-PIPES, 4 m*M* EGTA, 1 m*M* $MgSO_4$, 1 m*M* DTT, 0.2 m*M* PMSF, 10 μg/ml leupeptin, and 1 m*M* GTP, at either pH 6.6, 6.9, or 7.2. Homogenates were centrifuged at 2500g through a 10% sucrose cushion prepared at the appropriate pH. Proteins in the supernatant and pellet were separated by SDS-PAGE and electroblotted to nitrocellulose. Panel A is Western blot stained for total protein with India ink (Hughes *et al.*, 1988). Panel A′ is the corresponding immunoblot with the DM1A anti-α-tubulin antibody. Lanes 1, 2, and 3 are the 2500g pellets from the pH 6.6, 6.9, and 7.2 homogenates and Lanes 4, 5, and 6 are the corresponding supernates at pH 6.6, 6.9, and 7.2. Note the absence of pelletable tubulin in all three pellets.

identical to the nucleolus in the intact cell, (3) stains intensely with Hoechst, and (4) disappears at the time of breakdown of the nuclear envelop.

Finally, it is important to note that a significant fraction of the particulate tubulin is not associated with any detectable microtubules. Whether this particulate tubulin represents a functional form of tubulin that is able to form microtubules has not been established. In this study, all attempts to reassemble microtubules from the aggregated particulate tubulin fractions were unsuccessful. As the ionic strength of the oocyte cytoplasm is normally quite high, it is likely that some of this tubulin is denatured by the low ionic strength potassium phosphate buffer used throughout most of this study. Particulate tubulin was not detected in a higher ionic strength, PIPES-buffered microtubule-assembly solution, nor was it detected in Buffer T (Westendorf *et al.*, 1989). Buffer T is formulated to mimic the known constituents of molluscan cytoplasm and contains 0.3 *M* glycine, 0.12 *M* K-gluconate, 0.1 *M* taurine, 40 m*M* NaCl, 10 m*M* EGTA, 2.5 m*M* $MgCl_2$, and 0.1 *M* HEPES at pH 7.2. Thus, it appears that a large fraction of the "interphase-particulate tubulin" is artifactual or at least is operationally dependent upon the isolation conditions.

Acknowledgments

K.A.S. is grateful to Bill Dentler for providing the electron micrographs. This work was supported by a R.D. Allen Summer Fellowship (1988) at the Marine Biological Laboratory and by grants NSF-DCB9003544 and CTR-2874.

Literature Cited

Allen, R. D. 1953. Fertilization and artificial activation in the egg of the surf-clam, *Spisula solidissima*. *Biol. Bull.* **105:** 213–238.

Avila, J. 1990. Microtubule dynamics. *FASEB J.* **4:** 3284–3290.

Belmont, L. D., A. Hyman, K. E. Sawin, and T. J. Mitchison. 1990. Real-time visualization of cell cycle-dependent changes in microtubule dynamics in cytoplasmic extracts. *Cell* **62:** 579–589.

Blose, S. H., D. I. Meltzer, and J. R. Feramisco. 1984. 10-nm filaments are induced to collapse in living cells microinjected with monoclonal and polyclonal antibodies against tubulin. *J. Cell Biol.* **98:** 847–858.

Burnside, B., C. Kozak, and F. C. Kafatos. 1973. Tubulin determination by an isotope dilution-vinblastine precipitation method. The tubulin content of *Spisula* eggs and embryos. *J. Cell Biol.* **59:** 755–762.

Breitling, F., and M. Little. 1986. Carboxy-terminal regions on the surface of tubulin and microtubules. Epitope locations of YOL1/34, DM1A and DM1B. *J. Mol. Biol.* **189:** 367–370.

Cleveland, D. W. 1988. Autoregulated instability of tubulin mRNAs: a novel eukaryotic regulatory mechanism. *TIBS* **13:** 339–343.

Dan, K., and S. Itoh. 1984. Studies of unequal cleavage in molluscs: I. Nuclear behavior and anchorage of a spindle pole to cortex as revealed by isolation technique. *Dev. Growth & Differ.* **26:** 249–262.

DeBrabander, M., G. Geuens, R. Nuydens, K. A. S. Willebrords, F. Aerts, J. DeMey, and J. R. McIntosh. 1986. Microtubule dynamics during the cell cycle: the effects of taxol and nocodazole on the microtubule system of PtK2 cells at different stages of the mitotic cycle. *Int. Rev. Cytol.* **101:** 215–274.

Gard, D. L., and M. W. Kirschner. 1987a. Microtubule assembly in cytoplasmic extracts of *Xenopus* oocytes and eggs. *J. Cell Biol.* **105:** 2191–2201.

Gard, D. L., and M. W. Kirschner. 1987b. A microtubule-associated protein from *Xenopus* eggs that specifically promotes assembly at the plus-end. *J. Cell Biol.* **105:** 2203–2215.

Gotoh, Y., E. Nishida, S. Matsuda, N. Shiina, H. Kosako, K. Shiokawa, T. Akiyama, K. Ohta, and H. Sakai. 1991. *In vitro* effects on microtubule dynamics of purified *Xenopus* M-phase-activated MAP kinase. *Nature* **349:** 251–254.

Hawkes, R., E. Niday, and J. Gordon. 1982. A dot-immunobinding assay for monoclonal and other antibodies. *Anal. Biochem.* **119:** 142–147.

Herzog, W., and K. Weber. 1978. Microtubule formation by pure brain tubulin *in vitro*: the influence of dextran and poly(ethylene glycol). *Eur. J. Biochem.* **94:** 249–254.

Hiller, G., and K. Weber. 1978. Radioimmunoassay for tubulin: a quantitative comparison of the tubulin content of different established tissue culture cells and tissues. *Cell* **14:** 795–804.

Himes, R. H., P. R. Burton, and J. M. Gaito. 1976. Dimethyl sulfoxide-induced self-assembly of tubulin lacking associated proteins. *J. Biol. Chem.* **252:** 6222–6228.

Hughes, J. H., K. Mack, and V. V. Hamparian. 1988. India ink staining of proteins on nylon and hydrophobic membranes. *Anal. Biochem.* **173:** 18–25.

Inoué, S. 1981. Cell division and the mitotic spindle. *J. Cell Biol.* **91:** 131s–147s.

Kane, R. E. 1962. The mitotic apparatus: Isolation by controlled pH. *J. Cell Biol.* **12:** 47–55.

Kuriyama, R., G. G. Borisy, and Y. Masui. 1986. Microtubule cycles in oocytes of the surf clam, *Spisula solidissima*, an immunofluorescence study. *Dev. Biol.* **114:** 151–160.

Laemmli, U. K. 1970. Cleavage of structural proteins during the assembly of the head of bacteriophage T4. *Nature* **227:** 680–685.

Lee, J. C., and S. N. Timasheff. 1977. *In vitro* reconstitution of calf brain microtubules: effects of solution variables. *Biochemistry* **16:** 1754–1764.

Lefebvre, P. A., and J. L. Rosenbaum. 1986. Regulation of the synthesis and assembly of ciliary and flagellar proteins during regeneration. *Annu. Rev. Cell Biol.* **2:** 517–546.

Longo, F. J., and E. Anderson. 1970a. An ultrastructural analysis of fertilization in the surf clam, *Spisula solidissima* I. Polar body formation and development of the female pronucleus. *J. Ultrastruct. Res.* **33:** 495–514.

Longo, F. J., and E. Anderson. 1970b. An ultrastructural analysis of fertilization in the surf clam, *Spisula solidissima*. II. Development of the male pronucleus and the association of the maternally and paternally derived chromosomes. *J. Ultrastruct. Res.* **33:** 515–527.

Lowry, O. H., N. J. Rosebrough, A. L. Farr, and R. J. Randall. 1951. Protein measurements with the Folin-phenol reagent. *J. Biol. Chem.* **193:** 265–275.

Mitchison, T., and M. Kirschner. 1984. Dynamic instability of microtubule growth. *Nature* **312:** 237–242.

Mitchison, T., and M. Kirschner. 1987. Some thoughts on the partitioning of tubulin between monomer and polymer under conditions of dynamic instability. *Cell Biophys.* **11:** 35–55.

Nath, J., and M. Flavin. 1979. Tubulin tyrosylation *in vivo* and changes accompanying differentiation of cultured neuroblastoma-glioma hybrid cells. *J. Biol. Chem.* **254:** 11505–11510.

Olmsted, J. B. 1981. [illegible] in differentiating neuroblastoma cells. *J. Cell Biol.* [illegible]

Rebhun, L. I. 1959. [illegible] cleavage in the surf clam, *Spisula solidissima* [illegible] and toluidine blue as vital stains. *Biol. Bull.* [illegible]

Rebhun, L. [illegible] pless. 1964. Isolation of spindles from the [illegible] *solidissima*. *J. Cell Biol.* **22:** 488–492.

Salmon, [illegible] 1989. Mitotic spindles isolated from sea urchin eggs with [illegible] buffers. *Methods in Cell Biol.* **25:** 69–105.

Sambrook, [illegible] E. Fritsch, and T. Maniatis. 1989. *Molecular Cloning. A Laboratory Manual* Second Edition. Cold Spring Harbor Laboratory Press, New York.

Serrano, L., F. Wandosell, and J. Avila. 1986. Location of the regions recognized by five commercial antibodies on the tubulin molecule. *Anal. Biochem.* **159:** 253–259.

Stephens, R. E. 1986. Membrane Tubulin. *Biol. Cell* **57:** 95–110.

Stephens, R. E. 1990. *Ciliary and Flagellar Membranes.* R. A. Bloodgood, ed. Plenum Press, New York. Pp. 217–240.

Suprenant, K. A. 1989. Alkaline pH favors microtubule self-assembly in surf clam *Spisula solidissima* oocyte extracts. *Exp. Cell Res.* **184:** 167–180.

Suprenant, K. A. 1991. Unidirectional microtubule assembly in cell-free extracts of *Spisula solidissima* oocytes is regulated by subtle changes in pH. *Cell Motil. Cytoskeleton* **19:** 207–220.

Towbin, H., T. Stachelin, and J. Gordon. 1979. Electrophoretic transfer of proteins from polyacrylamide gels to nitrocellulose sheets: Procedure and some applications. *Proc. Natl. Acad. Sci. USA* **76:** 4350–4354.

Verde, F., J.-C. Labbe, M. Doree, and E. Karsenti. 1990. Regulation of microtubule dynamics by cdc2 protein kinase in cell-free extracts of *Xenopus* eggs. *Nature* **343:** 233–238.

Weisenberg, R. C. 1972. Changes in the organization of tubulin during meiosis in the eggs of the surf clam, *Spisula solidissima*. *J. Cell Biol.* **54:** 266–278.

Westendorf, J. M., K. I. Swenson, and J. V. Ruderman. 1989. The role of cyclin B in meiosis I. *J. Cell Biol.* **108:** 1431–1444.

Reference: *Biol. Bull.* **183**: 211–219. (October, 1992)

Cell Cooperation During Host Defense in the Solitary Tunicate *Ciona intestinalis* (L)

VALERIE J. SMITH* AND CLARE M. PEDDIE

School of Biology and Medical Sciences, Gatty Marine Laboratory, University of St Andrews, Fife, KY16 8LB, Scotland

Abstract. Phagocytosis in the solitary ascidian *Ciona intestinalis* was investigated using mixed and separated populations of blood cells *in vitro*. Only the vacuolar and granular amoebocytes were seen to ingest bacteria, and when the serine protease inhibitors, STI, or benzamidine were added to monolayers of mixed cell types, uptake was significantly reduced. Analyses carried out with isolated cells revealed that phagocytosis was enhanced by incubation of the bacteria in blood cell lysate supernatants (CLS) that had been pre-treated with LPS. By contrast, pre-incubation of the bacteria in CLS preparations that were inhibited by benzamidine produced lower levels of phagocytosis. Treatment of the bacteria with plasma also failed to promote uptake, and there was no detectable agglutination of the bacteria by CLS. As lysate supernatants made from morula cells, but not other cell types, were effective in promoting phagocytosis, we propose that opsonins are derived from the morula cells, and that phagocytosis involves cooperation between different cell populations. Moreover, as the morula cells are the principal repositories of prophenoloxidase and an associated serine protease (factors which are activated by LPS but blocked by STI or benzamidine), prophenoloxidase or the protease may be involved in the opsonic phenomenon in a similar way to that previously reported for arthropods.

Introduction

The recognition of non-self is a fundamental aspect of an animal's immune network and a major determinant of the host's ability to survive microbial infection or parasitization. Invertebrates lack specific immunoglobulins and specialized T lymphocytes in their defense repertoires, but are able to mount highly efficient cellular and humoral defense strategies against foreign agents (Ratcliffe *et al.*, 1985; Smith, 1991). An understanding of the biochemical basis for recognition and blood cell activation in these animals is important in tracing the evolution of immune capability and in the identification of suitable non-vertebrate models for experimental study. The deuterostomes, and especially the ascidians, are a particularly significant group because of their phylogenetically strategic position close to the vertebrates (Bone, 1979).

Several workers have examined the cellular responses of ascidians using both *in vivo* (Smith, 1970; Anderson, 1971; Parrinello *et al.*, 1977; Raftos and Cooper, 1991) and *in vitro* methods (Rowley, 1981; 1982a) (see also review by Pestarino, 1991). However, the responses of the cells to foreign onslaught, particularly *in vitro*, have been studied only with mixed blood cell populations. There have been no investigations of separated cells or attempts to assess the extent of interaction between the various cell types.

Although immune reactivity in vertebrates entails cooperation between the different leucocyte groups, the importance of cell-cell cooperation in invertebrate host defense has only been demonstrated for the arthropods (Söderhäll *et al.*, 1986; Persson *et al.*, 1987; Anggraeni and Ratcliffe, 1991). In both crustaceans and insects, the granular-type cells appear to mediate cell cooperation by providing the opsonins necessary for efficient uptake of bacteria by the phagocytes (Söderhäll *et al.*, 1986; Anggraeni and Ratcliffe, 1991). In crayfish, they also donate factors which promote encapsulation (Persson *et al.*, 1987). As yet, the cell signals involved have not been fully characterized, but the prophenoloxidase activating (proPO) system, contained within the granular and se-

Received 4 March 1992; accepted 7 July 1992.

* To whom reprint requests and correspondence should be addressed.

Abbreviations: STI, Soyabean trypsin inhibitor; LPS, Lipopolysaccharide; CLS, whole blood cell lysate supernatant; MAC, marine anticoagulent; MS, marine saline; CAC I, citrated cacodylate buffer; CAC II, cacodylate buffer; proPO, prophenoloxidase; L-dopa L-hydroxyophenylanaline; MLS, morula cell lysate supernatant; CcLS, cell lysate supernatant excluding morula cells; pNA, p-nitroaniline.

migranular cells or t[illegible]alent, has been implicated in the phenome[illegible]äll *et al.*, 1986; Anggraeni and Ratcliffe, [illegible]roPO system in crustaceans and insect[illegible]ascade of serine proteases and other fac[illegible]pecifically triggered by microbial carboh[illegible]ely lipopolysaccharides (LPS) or β 1,3-glucans [illegible]ews by Söderhäll, 1982; Söderhäll and Smith, 1986a, b; Smith and Söderhäll, 1986; Johansson and Söderhäll, 1989; Smith, 1991). Because phenoloxidase activity occurs exclusively in the granular type cells, it also represents a useful marker for the purity of separated cells in functional evaluations of immune reactivity (Söderhäll and Smith, 1983; Söderhäll *et al.*, 1986; Smith and Söderhäll, 1991; Chisholm and Smith, 1992). So far, few suitable markers have been identified for the cell populations in other invertebrate phyla.

Recently, however, the separation technique devised for crustacean hemocytes has been successfully applied to the solitary ascidian, *Ciona intestinalis* (Smith and Söderhäll, 1991). Five cell bands were obtained, and the enzyme prophenoloxidase was found to reside primarily in the morula cells (Smith and Söderhäll, 1991). Further analyses have established that phenoloxidase activity also occurs in the morula cells of several ascidian species and in individuals of *C. intestinalis*, as in arthropods, it exists as a proenzyme which is activated by proteases or LPS but not other carbohydrates (Jackson *et al.*, in press). Furthermore, the enzyme is blocked by the serine protease inhibitors, STI and benzamidine, (Jackson *et al.*, in press) and seems to be associated with an LPS-sensitive protease contained within the blood cells (Jackson and Smith, unpubl. obs.).

The present investigation was conducted to examine the cellular defenses of urochordates and, by using separated cell populations, to assess the extent of any cell cooperation involved. We chose to examine phagocytosis because it is a universal process which serves in surveillance against invading micro-organisms in nearly all animals. We show that uptake of bacteria is achieved only by the phagocytic amoebocytes and is strongly influenced by factors (opsonins) derived from the morula cells. In addition, by treating the cells or opsonizing preparations with LPS or serine protease inhibitors, we explored the possibility of a link between the opsonic effect and the phenoloxidase and protease activities contained within the morula cells.

Materials and Methods

Animals

Specimens of *C. intestinalis* were collected from the west coast of Scotland and maintained in aerated circulating seawater (32 ± 2‰; 10 ± 2°C) until use. The animals were blotted dry to remove any excess seawater and bled by removal of the tunic and puncture of the pericardium. The blood was drained from the perivisceral and pericardial cavities, care being taken not to contaminate the blood with pyrogens from the gut. The blood (usually 1–2 ml per animal) was diluted 1:1 with ice-cold marine anticoagulant (MAC) (0.1 *M* glucose; 15 m*M* trisodium citrate; 13 m*M* citric acid; 10 m*M* EDTA; 0.45 *M* NaCl; pH 7.0) and processed immediately.

Cell separation

The blood cell populations of *C. intestinalis* were separated by a modification of the density gradient centrifugation method described by Söderhäll and Smith (1983) and Smith and Söderhäll (1991). Briefly, freshly collected blood (approximately 2 ml), diluted 1:1 in MAC was spun through preformed continuous gradients of 60% Percoll (Pharmacia, Uppsala, Sweden) in 3.2% NaCl, at 1900 g for 10 min, at 4°C. The cell types were identified according to the criteria given by Rowley (1981). The phagocytes and morula cells were then further purified by a second centrifugation on preformed gradients of 40% Percoll, while the pigment cells and stem cells were enriched on secondary gradients of 80% Percoll.

The separated cell populations were removed from the gradients and washed once in 10 ml of marine saline (MS) (12 m*M* $CaCl_2 \cdot 6H_2O$; 11 m*M* KCl; 26 m*M* $MgCl_2 \cdot 6H_2O$; 45 m*M* tris; 38 m*M* HCl; 0.45 *M* NaCl; pH 7.4) before resuspension in 800 μl MS. Phenoloxidase and protease activities in the blood cell suspensions were determined for each cell band; L-dopa or S-2337 were used as described below.

Preparation of blood cell monolayers

Blood cell monolayers from individuals of *C. intestinalis* were prepared by a modification of the methods given in Smith and Ratcliffe (1978) and Söderhäll *et al.* (1986). For the mixed cell monolayers, 1.2 ml of freshly collected blood, diluted 1:1 with MAC, was washed once with 5 ml of MS, and resuspended in 1.2 ml MS. Two hundred microlitres of this mixed cell suspension was laid onto each clean, pyrogen-free, glass coverslip in tissue culture grade sterile six-well trays (Sterilin, Feltham, England), and the coverslips were incubated at 20°C for 60 min to allow the cells to settle, attach and spread on the glass surface. Each coverslip was then washed twice with 1 ml of MS and moistened with a fresh 0.5 ml volume of MS.

For separated blood cell monolayers, the cells were removed from the gradients with a pasteur pipette, washed once in MS, and resuspended in fresh MS at a concentration of ca 1×10^8 ml^{-1}. To each coverslip was added 200 μl of the cell suspension and the cells were incubated and washed as above.

Preparation of blood cell lysate supernatants

The diluted blood (about 5 ml) from 4–5 large (7.5–14 cm long) animals was pooled, and the cells were pelleted

by gentle centrifugation (800 g, 10 min, 4°C). The supernatant was discarded, and the cells were washed twice in ice-cold citrated cacodylate buffer (CAC I) (10 m*M* sodium cacodylate, 100 m*M* trisodium citrate, 0.45 *M* NaCl; pH 7.0) before homogenization with a glass piston tissue grinder in citrate-free cacodylate buffer (CAC II) (10 m*M* sodium cacodylate; 50 m*M* $MgCl_2 \cdot 6H_2O$; 50 m*M* $CaCl_2 \cdot 6H_2O$; 0.45 *M* NaCl; pH 7.0). The homogenate was then spun (40,000 g, 20 min, 4°C) and the resulting supernatant, designated CLS, used as enzyme source.

For some phagocytosis experiments (see below), cell lysate supernatants were prepared from separated cells. One, designated MLS, was prepared from the morula cell band, while a second, the control (CcLS), was made from all the cell bands excluding the morula cell band. In both cases, the cell bands were removed from the gradients, pooled where necessary, washed in 10 ml of MAC, and resuspended in 1 ml aliquots of fresh citrated CAC I buffer. The two suspensions were spun at 800 g for 10 min at 4°C, resuspended in 600 μl of CAC II, and homogenized with a glass piston tissue grinder (8 min, 4°C) before centrifugation at 14,500 g for 20 min (4°C). Protein in the CcLS was adjusted to match that of the MLS, and phenoloxidase and protease activities in each of the lysate supernatants were determined as below.

Preparation of plasma

Undiluted blood (approximately 2 ml per animal) was collected from individual medium sized animals (4–7 cm long) and placed into ice-cold polycarbonate tubes. The samples were immediately centrifuged (800 g, 10 min), the supernatants decanted and used as plasma.

Measurement of enzyme activities

Phenoloxidase activity was determined spectrophotometrically at 490 nm after treatment with trypsin or, for controls, CAC II buffer; L-dopa was used as substrate as in Smith and Söderhäll (1983a, 1991). Enzyme activity was expressed as the change in absorbance at 490 nm per min per mg protein.

Protease activity was assayed according to the method of Söderhäll (1983). Briefly, 100 μl of blood cell lysate supernatants of *C. intestinalis* were pre-incubated with an equal volume of lipopolysaccharide (LPS) (from *Escherichia coli* 0111:B4, phenolic extraction), at a concentration of 1 mg ml^{-1} in tris buffer (0.1 *M* tris; 50 m*M* HCl; 10 m*M* $CaCl_2 \cdot 6H_2O$; pH 8.0). For controls, CLS was mixed with 100 μl of tris buffer. After 10 min at 20°C, 200 μl of tris buffer, and 100 μl of the chromogenic substrate, Bz-Ile-Glu (-O-piperidyl) Gly-Arg-pNA · HCl (S-2337) (Kabi-Vitrum, Stockholm, Sweden) (1 mg ml^{-1} in tris buffer) were added to each tube, and the samples were incubated for a further 60 min. The reaction was terminated by the addition of 100 μl of 50% acetic acid, the samples spun at 2500 g (10 min), and the absorbances read against a blank, consisting of buffer, substrate and elicitor, at 405 nm. Enzyme activity was calculated as nmol p-nitroaniline (pNA) released per minute per mg protein.

Protein

Protein in the various cell lysates and plasma was determined by the method of Bradford (1976); bovine serum albumin was used as standard.

Preparation of bacteria

The bacterium, *Psychrobacter immobilis*, formerly *Moraxella sp.* (NCMB 308), was cultured and prepared as described in Smith and Ratcliffe (1978). Washed bacteria were suspended in MS at a concentration of 5×10^8 ml^{-1} and either used immediately or pretreated with various cell lysate supernatants, as described below, before presentation to the cells.

Phagocytosis assays in vitro

The optimal incubation time for bacterial uptake by blood cells of *C. intestinalis* was investigated by challenging monolayers prepared from mixed cells with 100 μl of washed bacteria in MS (*i.e.*, 5×10^7 per monolayer). Controls received 100 μl of MS, and all cultures were incubated on a rocking platform for time intervals ranging from 30 min to 3 h at 20°C. On the basis of this experiment (see Results below), the cell:bacteria cultures in all subsequent experiments were incubated for 2 h.

To examine the effect of serine protease inhibitors on the phagocytic response, monolayers of mixed cells were incubated with either 100 μl of STI in MS (to give a final concentration of 0.143 mg ml^{-1}) or 100 μl of benzamidine (final concentration 14.3 m*M* in MS) before addition of the bacteria. Controls received 100 μl MS, and all cultures, except one of the controls which was given 100 μl of MS, were overlaid with 100 μl of bacteria and incubated as above.

The uptake of bacteria by individual cell types was studied with monolayers prepared from separated cells as described above. To determine whether the uptake of bacteria by isolated phagocytes is influenced by factors present in the cells and entails cell cooperation, monolayers of separated phagocytic amoebocytes were challenged with bacteria pre-incubated in different blood cell lysate supernatants.

Firstly, the bacteria were pre-treated in CLS by incubating 100 μl of washed bacteria (5×10^8 ml^{-1} in CAC II) in 4 ml of CLS (protein concentration of approximately 0.01 mg ml^{-1}). Previously, the CLS had been reacted with 100 μl of LPS (1 mg ml^{-1} in CAC II) (10 min, 20°C).

Further 100 μl sam[illegible] bacteria were incubated in CLS that had be[illegible] with 100 μl CAC II instead of LPS. Secon[illegible] bacteria were incubated in CLS that h[illegible]ed with benzamidine. For this, 4 ml of C[illegible] with 1 ml of 100 m*M* benzamidine in CAC [illegible] nal concentration of 20 m*M*) before addition [illegible] and incubation with bacteria as above. Tubes [illegible]ch CAC II buffer was substituted for the benzamidine were run in parallel as positive controls. Other bacterial samples (100 μl) were incubated in 4 ml of freshly prepared plasma for comparison with the CLS treatments. Finally, bacteria were pre-incubated either in morula cell lysate supernatants (MLS) or in lysate supernatants made from all cell types excluding the morula cells (CcLS). In each case, 500 μl of the respective cell lysate supernatant, pre-treated with 50 μl of LPS, were incubated with 50 μl of bacteria.

All bacteria:lysate, bacteria:buffer, or bacteria:plasma mixtures were incubated for 1 h at 20°C. The bacteria were then washed three times in MS, resuspended in 0.5 ml of fresh MS, and incubated with the phagocytes as above. In every case, controls received bacteria pre-incubated in CAC II buffer only. Protease activities in the lysate supernatants were determined as above. Protease, rather than phenoloxidase, activity was used as a marker for morula cell products because the activity of this enzyme generally shows less variation between animals (data not shown). Cell viability was checked by trypan blue exclusion in all experiments, and bacterial uptake was determined as described below.

Evaluation of bacterial uptake

After incubation, the monolayers were gently washed with three 1 ml changes of MS, fixed in 2 ml of 10% seawater formalin, and observed under phase contrast optics of a Leitz Diaplan microscope. Intracellular bacteria were distinguished from extracellular forms according to the criteria given in Smith and Ratcliffe (1978), and the percentage of blood cells containing one or more ingested bacteria was determined by counting at least 200 cells per coverslip. For each experiment, phagocytosis was determined on duplicate monolayers for each animal, and with the opsonization assays, uptake was assessed for 12 animals using six different lysate supernatants.

Titration of agglutinins

The p[illegible]nce of bacterial agglutinins in blood cells of *C. intestina[illegible]* was investigated as follows. Serial two fold dilutions of [illegible] of CLS in CAC II were made in U-bottomed microlitre trays (Sterilin). Control wells received 50 μl of CAC II instead of the CLS samples, and 50 μl of *P. immobilis* (ca 5×10^8 ml^{-1} in CAC II) was added to every well. The trays were incubated at 20°C for 24 h, and the titers were recorded as the reciprocal of the last CLS dilution showing unequivocal agglutination. The titer was assessed visually and also at 570 nm using an agglutination program on a microplate reader (Dynatech).

Statistical analyses

Differences in levels of uptake of the bacteria by the cells between treatments, and differences in enzyme activities in the cell lysate supernatants between controls and experimentals, were analysed by the Students *t*-test. Differences were considered significant when $P \leq 0.05$.

Results

Cell separation

The blood cells of *C. intestinalis* were separated by density gradient centrifugation, yielding six distinct bands of cells (Table I). Scrutiny of these cells under phase contrast optics revealed eight, morphologically different cell types. They were identified, according to the terminology given by Rowley (1981, 1982a), as signet ring cells (band 1), non-vacuolar hyaline amoebocytes (band 2), vacuolar amoebocytes (band 3), granular amoebocytes (band 3), morula cells (band 4), compartment cells (band 4), pigment cells (band 5), and small, undifferentiated cells (band 6) that resemble vertebrate lymphocytes, and that we designate stem cells because of their similarity to the progenitor cells of other invertebrate species (Table I). We were unable to distinguish a band of cells corresponding to the refractile amoebocytes described by Rowley (1981, 1982a, b), although the reasons for this are unknown.

Only the vacuolar and the granular amoebocytes occupying band 3 were seen to ingest bacteria *in vitro*, so all the cells collected from this band are classified as phagocytic amoebocytes (see below). Likewise, as the morula and compartment cells differed from each other only in terms of their degree of vacuolation, they are referred to collectively as morula cells. The relative proportion of each cell type in whole blood is shown in Table I. These are unlikely to represent absolute values, however, as a number of factors, including body size, season, and allogeneic stimulation, are known to affect differential blood cell counts in ascidians (Smith, 1970; Biggs and Swinehart, 1979; Raftos and Cooper, 1991).

Phenoloxidase and protease activities significantly above control values were found only in the morula cell band ($P = 0.016$ and 0.045, respectively). Slightly enhanced protease activities were detectable in the phagocytic cell band although these were not significantly higher than the controls ($P = 0.461$, Table I). Whether this was a result of contamination by products released by the morula cells during bleeding or separation is not clear. In general, enzyme activities in the morula cell band were approximately three times higher than in the other cell bands or the controls (Table I). Measurement of phe-

noloxidase and protease activities in the signet ring cell band was prevented by low protein yields. Spot assays on this band, performed as described by Söderhäll and Smith (1983), indicated that enzyme activity was not detectable (data not shown).

Phagocytosis by mixed cell monolayers of C. intestinalis in vitro

Cell viability remained at about 96% for 2 h and at over 90% for 3 h under all the experimental conditions (Fig. 1). Uptake of the bacterium *P. immobilis* on mixed cell monolayers increased from about 7% in the first 30 min to a maximum of 36% at 2 h (Fig. 1). Thereafter, uptake declined to about 23% at 3 h (Fig. 1). This perceived drop in phagocytic activity may represent the detachment of phagocytes from the monolayers over prolonged incubation. Accordingly, 2 h was taken to be the optimal incubation time in terms of both cell viability and uptake in all subsequent experiments.

Treatment of the mixed cell monolayers with the serine protease inhibitor, STI, significantly depressed the level of uptake of bacteria from 39 to 16.6% over 2 h ($P = 0.029$) (Table II). A similar effect was observed with benzamidine, where the level of phagocytosis was reduced to 13.4% over the same time period ($P = 0.009$) (Table II). Again, cell viability remained at about 96% or better.

Phagocytosis by separated phagocytes of C. intestinalis in vitro

The *in vitro* phagocytic ability of each of the separated cell types is shown in Table I. Uptake of the bacteria *P.*

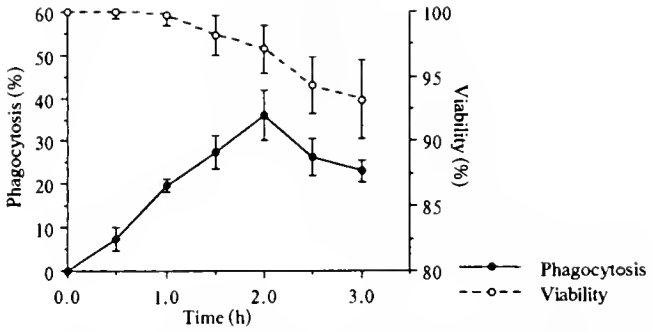

Figure 1. Viability and phagocytosis in mixed blood cell monolayer cultures from *Ciona intestinalis*. The experiments were repeated five times. The values represent mean with bars representing SE. Phagocytosis of the bacteria *Psychrobacter immobilis* was determined under phase contrast optics as described in Materials and Methods. Viability was determined by trypan blue exclusion.

immobilis was achieved only by the phagocytic amoebocytes collected from band 3 of the Percoll gradients. Under these culture conditions, about 5% of the cells were seen to ingest bacteria (Table III), whereas about 39% of the cells were seen to contain intracellular bacteria in the mixed cell cultures (Table II). There did not appear to be preferential phagocytosis either by the non-vacuolar amoebocytes over the granular cells or vice versa (data not shown).

When the phagocytic amoebocytes were challenged with bacteria pre-incubated with LPS-treated CLS, uptake was significantly increased from 5.12 to 42.82%

Table I

Phenoloxidase and protease activities in different blood cell types of Ciona intestinalis

[a] Band	[b] Cell type	[c] Cell count	[d] Phenoloxidase activity (ΔA_{490} min^{-1} mg protein^{-1})	[e] Protease activity (nmol pNA released min^{-1} mg protein^{-1})	[f] n
1	Signet ring cells	*ca.* 9%	NT	NT	6
2	Hyaline leucocytes	*ca.* 16%	0.168 ± 0.045	8.33 ± 3.69	6
3	Phagocytic amoebocytes	*ca.* 37%	0.149 ± 0.052	11.35 ± 2.13	6
4	Morula cells	*ca.* 7%	0.454 ± 0.109*	25.09 ± 4.24*	6
5	Pigment cells	*ca.* 10%	0.130 ± 0.021	7.40 ± 1.49	6
6	Stem cells	*ca.* 19%	0.157 ± 0.025	7.91 ± 3.77	6
—	[g] Control	—	0.148 ± 0.018	6.79 ± 1.34	6

[a] Band on gradients, as counted from the meniscus.

[b] Cell type as identified under phase-contrast optics.

[c] The proportion of each cell type was determined from differential counts of whole blood. A minimum of 600 cells per animal were scored under phase-contrast optics.

[d] The cells from each band were removed from the gradients and pre-incubated with trypsin before the addition of L-dopa. Phenoloxidase activity was then determined spectrophotometrically at 490 nm. NT = not tested.

[e] The cells from each band were removed from the gradients and pre-incubated with LPS before the addition of the chromogenic substrate S-2337. Released p-nitroaniline was determined spectrophotometrically at 405 nm. NT = not tested.

[f] n = number of animals tested.

[g] Controls consisted of cells collected from each cell band pre-incubated with CAC II instead of the elicitor before addition of the enzyme substrate. Control values for both enzyme activities were similar for all bands.

* Significantly different compared with control ($P \leq 0.05$).

[illegible] III

Phagocytosis in m[illegible] monolayer cultures from individuals [illegible]

[a] Treatment	[b] Percentage phagocytosis	[c]n
Benzam[illegible] M)	13.48 ± 4.50*	5
STI (0.[illegible]	16.60 ± 2.51*	5
MS (co[illegible]	39.00 ± 4.68	5

[a] Mixed cell monolayers were treated with 100 μl of STI (final concentration 0.143 mgml^{-1}) or benzamidine (final concentration 14.3 m*M*), or, for controls, 100 μl MS, before the addition of bacteria.

[b] Proportion of phagocytes containing one or more intracellular bacterium of *P. immobilis*, as determined under phase-contrast optics as in Materials and Methods. Values are means ± SE.

[c] n = number of experimental runs.

* Significantly different compared with control ($P \leq 0.05$).

($P < 0.001$) (Table III). Significantly enhanced uptake was also recorded with the bacteria pre-incubated in CLS without LPS ($P < 0.001$), although this was substantially lower at 20.57% (Table III). Related enzyme assays of the lysates showed that protease activity was significantly higher in the LPS-activated CLS than in the CLS alone ($P = 0.05$). Pre-treatment of the CLS with benzamidine significantly reduced the subsequent uptake to 12.58% ($P = 0.048$), and the enzyme activities in this CLS were similar to those in the CLS alone ($P = 0.871$, Table III). Pre-incubation of the bacteria in plasma also produced no significant increase in uptake over the controls, with only 4.8% of the cells containing one or more bacteria ($P = 0.974$, Table III).

The opsonic effect of the CLS seems to be due, at least in part, to factors contained within the morula cells, since lysate supernatants made from these cells (MLS) were effective in raising the level of phagocytosis from 4.2% in the controls to 26.1% ($P < 0.001$, Table IV). Lysate supernatants made from all the other cell types, excluding the morula cells, (CcLS) were, on the other hand, ineffective in promoting uptake which remained at 8.6%, a value close to that obtained with the controls (Table IV). Again, protease activities in the MLS were significantly higher than in the controls ($P < 0.001$), whereas protease activities in the CcLS were not significantly different to control values ($P = 0.143$). Thus, *in vitro* phagocytosis of bacteria by individuals of *C. intestinalis* appears to entail cooperation between different blood cell types, and the opsonic effect may be linked to the presence of high protease activity in the morula cells.

Titration of agglutinins

Agglutination towards the bacterium *P. immobilis* was not observed in any of the CLS samples, indicating that the opsonic effect seen in the preparations described above was not due to aggregation of the bacteria in the CLS fractions.

Discussion

Previous studies of phagocytosis by urochordate blood cells have used *in vitro* methods with mixed cell cultures. While this approach overcomes some of the complications inherent *in vivo*, the failure to use purified populations of cells may obscure any interactive events between the different cell types. With mixed cell monolayers, Rowley (1981) has reported that phagocytosis in individuals of *C. intestinalis* is carried out by the hyaline and granular amoebocytes. However, he was only able to distinguish phagocytic activity in the vacuolar, as opposed to the non-vacuolar, hyaline amoebocytes through ultrastructural analysis (Rowley, 1982a). In the present study of separated cell populations, we have been able to confirm that uptake is achieved only by the vacuolar hyaline and granular cells (*i.e.*, phagocytic amoebocytes) *in vitro*, and to show that phagocytosis in separated cell cultures is much lower than in mixed cell monolayers. More importantly, we have shown that phagocytic vigor is restored by pre-treating the bacteria with blood cell lysate supernatants. Thus, we have demonstrated for the first time that factors (opsonins) that promote phagocytosis by the amoebocytes reside in the blood cells of *C. intestinalis*.

By pre-treatment of the test bacteria with lysate supernatants of separated cell populations, we have also established that these opsonic factors in *C. intestinalis* appear

Table III

The effect of pre-treatment of Psychrobacter immobilis *on uptake by separated phagocytes from* Ciona intestinalis

[a] Treatment of *P. immobilis*	[b] Percentage phagocytosis	[c] Protease activity (nmol pNA released min^{-1} mg protein^{-1})	[d]n
CLS + buffer	20.57 ± 1.13*	7.90 ± 0.48	6
CLS + LPS + buffer	42.82 ± 4.79*	15.45 ± 2.67**	6
CLS + LPS + benzamidine	12.58 ± 1.21*	8.24 ± 1.94	6
Plasma	4.81 ± 2.10	NT	3
Buffer control	5.12 ± 0.49	—	6

[a] Cultures of *P. immobilis* were incubated for 1 h in each of the media, as in Materials and Methods. The buffer was CAC II. After pre-treatment, each bacterial suspension was washed twice in MS and resuspended in fresh MS before the cells were challenged.

[b] Proportion of phagocytes with one or more intracellular bacterium of *P. immobilis*, as determined under phase-contrast optics. Values are means ± SE.

[c] Each CLS was pre-incubated with buffer, LPS or benzamidine (final concentration 20 mM) as appropriate before the addition of the chromogenic substrate S-2337. Released p-nitroaniline was determined spectophotometrically at 405 nm after 60 min. Values are means ± SE. NT = not tested.

[d] n = number of experimental runs.

* Significantly different compared with control ($P \leq 0.05$).

** Significantly different compared with CLS + buffer ($P \leq 0.05$).

Table IV

The effect of pre-treatment of Psychrobacter immobilis *with different cell lysate supernatants on uptake by separated phagocytes from* Ciona intestinalis

[a] Treatment of *P. immobilis*	[b] Percentage phagocytosis	[c] Protease activity (nmol pNA released min^{-1} mg protein $^{-1}$)	[d]n
[e] MLS + LPS	26.08 ± 1.79*	[f] 29.61 ± 1.68**	6
[e] CeLS + LPS	8.62 ± 1.42*	[f] 13.41 ± 1.01	6
Buffer control	4.23 ± 0.52	—	6

[a] Cultures of *P. immobilis* were incubated for 1 h in MLS, CeLS or, for controls, CAC II buffer. They were then washed in MS before addition to the monolayers.

[b] Proportion of phagocytes containing one or more intracellular bacterium of *P. immobilis*, as determined under phase-contrast optics. Values are means ± SE.

[c] Protease activities in the MLS and CeLS were determined spectrophotometrically at 405 nm. Each lysate was incubated with LPS before the addition of the chromogenic substrate S-2337. Released p-nitroaniline was determined spectrophotometrically at 405 nm. Values are means ± SE.

[d] n = number of experimental runs.

[e] MLS = morula cell lysate supernatant; CeLS = cell lysate supernatant from all the cell types excluding the morula cells.

[f] Controls for protease activity comprised CeLS or MLS incubated with buffer instead of LPS before the addition of S-2337. Values were similar for both controls.

* Significantly different compared with buffer incubated bacteria (control) ($P \leq 0.05$).

** Significantly different compared with protease activity in controls (8.12 ± 1.45; mean ± SE; n = 6; $P \leq 0.05$).

to be contributed principally by the morula cells. In other ascidians, the morula cells participate in many phases of the cellular defenses. For example, they migrate to, and break down at sites of tunic injury (Smith, 1970), form multilayered capsules around foreign implants (Anderson, 1971), and infiltrate sites of non-fusion reactions between incompatible colonies (Taneda and Watanabe, 1982). The present paper provides substantial evidence that they play an indirect role in phagocytosis and mediate cell cooperation during host defense responses.

Cooperation between blood cell types occurs during phagocytosis in crustaceans (Söderhäll *et al.*, 1986) and insects (Anggraeni and Ratcliffe, 1991), but equivalent events have not previously been found for deuterostome invertebrates. At present, it is unknown whether similar cooperation takes place in related groups (hemichordates and cephalochordates), or the extent to which it accompanies the other defense processes in ascidians. Certainly, cooperative interaction of the blood cells is an important feature of cellular immunoreactivity in fish and other vertebrates, although it is probably mediated through a different pathway to that in invertebrates.

The enhanced uptake recorded in the present study was probably not due to a 'protein effect', as the protein concentrations of the lysate supernatants were carefully adjusted to comparable levels within each experiment. Moreover, an opsonic effect was not seen after pre-treatment of the bacteria with plasma. Nor can the results be explained by bacterial agglutination, as micro-titer assays failed to show detectable bacterial agglutination in the presence of CLS from *C. intestinalis*.

As inclusion of STI or benzamidine in the mixed cell cultures was found to reduce uptake of bacteria without loss of cell viability, and pre-treatment of the CLS with benzamidine before opsonization of the test bacteria impaired its stimulatory effect, we propose that the enhanced uptake recorded in the present study was mediated through serine protease activity. The occurrence of serine protease activity, stimulated by LPS and reduced by benzamidine or other protease inhibitors, in the blood cells of *C. intestinalis* has been reported by Jackson and Smith (unpub. obs.). Furthermore, it co-exists with prophenoloxidase (Smith and Söderhäll, 1991; Jackson *et al.*, in press) and appears to be involved in the activation of phenoloxidase by LPS (Jackson and Smith, unpub. obs.). In the present study, we clarify that protease and phenoloxidase activities in *C. intestinalis* are located in the morula cells and demonstrate that enhanced phagocytosis *in vitro* correlates with high protease activities in the opsonizing CLS or MLS preparations. Since the bacteria were washed extensively after opsonization before challenging the cells, enhanced uptake of the bacteria incubated in LPS-treated CLS or MLS samples cannot be attributed to a direct action of LPS on the phagocytes. Moreover, LPS-treatment of lysate supernatants (CeLS) made from all the blood cell types except the morula cells only weakly promoted phagocytosis above control levels. We therefore propose that the opsonic effect observed with morula cells of *C. intestinalis* is associated with the activation of prophenoloxidase or protease by LPS. A parallel situation has been described for arthropods (Smith and Söderhäll, 1983a; Ratcliffe *et al.*, 1984; Söderhäll *et al.*, 1986; Anggraeni and Ratcliffe, 1991), but, until the opsonin is purified from individuals of *C. intestinalis*, the precise role of phenoloxidase and protease activities in phagocytosis by this animal remains speculative.

As yet, we are uncertain how the opsonins in *C. intestinalis* may be donated by the morula cells *in vivo*, but it is reasonable to predict that in the mixed cell cultures *in vitro*, the opsonin is generated *in situ* by discharge from the morula cells. In this way, it would be available on the coverslips to coat the test bacteria and promote uptake by the cells. An equivalent process has already been described for arthropods (Smith and Söderhäll, 1983a; Leonard *et al.*, 1985), and LPS-induced exocytosis of prophenoloxidase activating proteins from the granular and semi-granular hemocytes *in vitro* has been observed in crayfish (Smith and Söderhäll, 1983b; Johansson and Söderhäll, 1985). Whether the opsonin in *C. intestinalis*

is exocytosed from [illegible]ula cells in a similar way has not been determi[illegible]gh LPS-stimulated release of proteases fro[illegible]cells (of undefined type) has been reported f[illegible]ascidian *Halocynthia roretzi* by Azumi [illegible]. Further work is necessary to clarify the situ[illegible]e solitary ascidian *C. intestinalis*.

Fin[illegible]extent to which phenoloxidase and protease activities are linked to other host defense responses in individuals of *C. intestinalis* is unknown. In crustaceans, the proPO system has been shown to participate in clotting (Söderhäll, 1981), mediate encapsulation (Persson *et al.*, 1987), generate cell adhesion molecules (Johansson and Söderhäll, 1988; Kobayashi *et al.*, 1990), and have antimicrobial activity (Söderhäll and Ajaxon, 1982; Söderhäll and Smith, 1986a). While urochordates share with arthropods a reliance upon such defense strategies for protection against microbial exploitation, more research is necessary to discover the underlying biochemical pathways in deuterostomes.

Acknowledgments

We thank the various sports divers, principally from Cupar Sub-Aqua Club (BSAC 1094) and UMBSM Special Branch (BSAC 902), for their voluntary assistance with the collection of specimens. We are grateful to Dr. Alan Jackson and Mrs. June Chisholm for helpful discussion. The work was supported by grants from SERC, the Nuffield Foundation, and the Royal Society.

Literature Cited

Anderson, R. S. 1971. Cellular responses to foreign bodies in the tunicate *Molgula manhattensis*. *Biol. Bull.* **141:** 91–98.

Anggraeni, T., and N. A. Ratcliffe. 1991. Studies on cell-cell co-operation during phagocytosis by purified haemocyte populations of the wax moth, *Galleria mellonella*. *J. Insect Physiol.* **37:** 453–460.

Azumi, K., H. Yokosawa, and S. Ishii. 1991. Lipopolysaccharide induces release of a metallo-protease from the hemocytes of the ascidian, *Halocynthia roretzi*. *Dev. Comp. Immunol.* **15:** 1–7.

Biggs, W. R., and J. H. Swinehart. 1979. Studies of the blood of *Ascidia ceratodes*. Total blood counts, differential blood cell counts, hematocrit values, seasonal variations and fluorescent characteristics of blood cells. *Experientia* **35:** 1047–1049.

Bone, Q. 1979. *The Origin of Chordates.* 2nd ed., Carolina Biol. Suppl. Co., North Carolina.

Bradford, M. M. 1976. A rapid and sensitive method for the quantitation of microgram quantities of protein utilizing the principle of protein-dye binding. *Anal. Biochem.* **72:** 248–254.

Chisholm, J. R. S., and V. J. Smith. 1992. Antibacterial activity in the hemocytes of the shore crab, *Carcinus maenas* (L). *J. Mar. Biol. Assoc. U.K.* **72:** 529–542.

Jackson, A. D., V. J. Smith, and C. M. Peddie. In Press. *In vitro* phenoloxidase activity in the blood of *Ciona intestinalis* and other ascidians. *Dev. Comp. Immunol.*

Johansson, M. W., and K. Söderhäll. 1985. Exocytosis of the proPO activating system from crayfish haemocytes. *J. Comp. Physiol.* **156B:** 175–181.

Johansson, M. W., and K. Soderhäll. 1988. Isolation and purification of a cell adhesion factor from crayfish blood cells. *J. Cell Biol.* **106:** 1795–1803.

Johansson, M. W., and K. Söderhäll. 1989. A cell adhesion factor from crayfish haemocytes has degranulating activity towards crayfish granular cells. *J. Cell Biol.* **106:** 1795–1804.

Kobayashi, K., M. W. Johansson, and K. Söderhäll. 1990. The 76kD cell-adhesion factor from crayfish haemocytes promotes encapsulation *in vitro*. *Cell Tissue Res.* **260:** 13–18.

Leonard, C. M., N. A. Ratcliffe, and A. F. Rowley. 1985. The role of prophenoloxidase activation in non-self recognition and phagocytosis by insect blood cells. *J. Insect Physiol.* **13:** 789–799.

Parrinello, N., E. Patricolo, and C. Canicatti. 1977. Tunicate immunobiology. I. Tunic reaction of *Ciona intestinalis* L. to erythrocyte injection. *Boll. Zool.* **44:** 373–381.

Persson, M., A. Vey, and K. Söderhäll. 1987. Encapsulation of foreign particles *in vitro* by separated blood cells from crayfish, *Astacus leptodactylus*. *Cell Tissue Res.* **247:** 409–415.

Pestarino, M. 1991. The neuroendocrine and immune systems in Protochordates. *Adv. Neuroimmunol.* **1:** 114–123.

Raftos, D. A., and E. L. Cooper. 1991. Proliferation of lymphocyte-like cells from the solitary tunicate, *Styela clava*, in response to allogenic stimuli. *J. Exp. Zool.* **260:** 391–400.

Ratcliffe, N. A., C. M. Leonard, and A. F. Rowley. 1984. Prophenoloxidase activation: nonself recognition and cell co-operation in insect immunity. *Science* **226:** 557–559.

Ratcliffe, N. A., A. F. Rowley, S. W. Fitzgerald, and C. P. Rhodes. 1985. Invertebrate immunity: basic concepts and recent advances. *Int. Rev. Cytol.* **97:** 183–350.

Rowley, A. F. 1981. The blood cells of the sea squirt *Ciona intestinalis*: morphology, differential counts, and *in vitro* phagocytic activity. *J. Invertebr. Pathol.* **37:** 91–100.

Rowley, A. F. 1982a. Ultrastructural and cytochemical studies on the blood cells of the sea squirt, *Ciona intestinalis*. I. Stem cells and amoebocytes. *Cell Tissue Res.* **223:** 403–414.

Rowley, A. F. 1982b. The blood cells of *Ciona intestinalis*: an electron probe X-ray study. *J. Mar. Biol. Assoc. U.K.* **62:** 607–620.

Smith, M. J. 1970. The blood cells and tunic of the ascidian *Halocynthia aurantium* (Pallas). I. Haemotology, tunic morphology, and partition of cells between blood and tunic. *Biol. Bull.* **138:** 354–378.

Smith, V. J. 1991. Invertebrate immunology: phylogenetic, ecotoxicological and biomedical implications. *Comp. Haematol. Int.* **1:** 61–76.

Smith, V. J., and N. A. Ratcliffe. 1978. Host defense reactions of the shore crab *Carcinus maenas* (L) *in vitro*. *J. Mar. Biol. Assoc. U.K.* **58:** 367–379.

Smith, V. J., and K. Söderhäll. 1983a. β-1,3 glucan activation of crustacean hemocytes *in vitro* and *in vivo*. *Biol. Bull.* **164:** 299–314.

Smith, V. J., and K. Söderhäll. 1983b. Induction of degranulation and lysis of haemocytes in the freshwater crayfish, *Astacus astacus* by components of the prophenoloxidase activating system *in vitro*. *Cell Tissue Res.* **233:** 295–303.

Smith, V. J., and K. Söderhall. 1986. Cellular immune mechanisms in the Crustacea. In: *Immune Mechanisms in Invertebrate Vectors*, A. M. Lackie, ed. *Proc. Symp. Zool. Soc. Lond.* **56:** 59–79.

Smith, V. J., and K. Söderhäll. 1991. A comparison of phenoloxidase activity in the blood of marine invertebrates. *Dev. Comp. Immunol.* **15:** 251–261.

Söderhäll, K. 1981. Fungal cell wall β-1,3 glucans induce clotting and phenoloxidase attachment to foreign surfaces of crayfish haemocyte lysate. *Dev. Comp. Immunol.* **5:** 566–573.

Söderhäll, K. 1982. Prophenoloxidase activating system and melanization—a recognition system of arthropods?—A review. *Dev. Comp. Immunol.* **6:** 601–611.

Soderhall, K. 1983. β-1,3-glucan enhancement of protease activity in crayfish hemocyte lysate. *Comp. Biochem. Physiol.* **74B:** 221–224.

Söderhall, K., and R. Ajaxon. 1982. Effect of quinones and melanin on mycelial growth of *Aphanomyces* spp. and extracellular protease

of *Aphanomyces astaci*, a parasite on crayfish. *J. Invertebr. Pathol.* **39:** 105–109.

Söderhäll, K., and V. J. Smith. 1983. Separation of the haemocyte population of *Carcinus maenas* and other marine decapods, and prophenoloxidase distribution. *Dev. Comp. Immunol.* **7:** 229–239.

Söderhäll, K., and V. J. Smith. 1986a. The prophenoloxidase activating cascade as a recognition and defence system in arthropods. Pp. 251–285 in *Humoral and Cellular Immunity in Arthropods*, A. P. Gupta, ed. John Wiley and Sons Ltd., New York.

Söderhäll, K., and V. J. Smith. 1986b. The prophenoloxidase activating system: the biochemistry of its activation and role in arthropod cellular immunity, with special reference to crustaceans. Pp. 208–223 in *Immunity in Invertebrates*, M. Bréhélin, ed. Springer Verlag, Berlin.

Söderhäll, K., V. J. Smith, and M. W. Johannson. 1986. Exocytosis and uptake of bacteria by isolated populations of two crustaceans: evidence for cellular co-operation in the defence reactions of arthropods. *Cell Tissue Res.* **245:** 43–49.

Taneda, Y., and H. Watanabe. 1982. Studies on colony specificity in the compound ascidian, *Botryllus primigenus* oka. I. Initiation of "non-fusion" reaction with special reference to blood cell infiltration. *Dev. Comp. Immunol.* **6:** 43–52.

Reference: *Biol. Bull.* **183**: 220–232 (October, 1992)

Biological Consequences of Topography on Wave-swept Rocky Shores: I. Enhancement of External Fertilization

MARK DENNY, JEFF DAIRIKI[1], AND SANDRA DISTEFANO

Department of Biological Sciences, Stanford University, Hopkins Marine Station, Pacific Grove, California, 93950

Abstract. Surge channels on wave-swept rocky shores are characterized by the violent hydrodynamic mixing that accompanies broken waves. It has been suggested that this mixing rapidly dilutes gametes shed into the surf zone, thereby severely reducing the fraction of eggs that can be fertilized externally. Although surge channels are well mixed within themselves, field experiments show that the exchange of water between these small embayments and the adjacent mainstream is surprisingly slow. Thus, surge channels may act as "containment vessels," limiting the rate at which gametes are diluted, and thereby enhancing the efficacy of external fertilization. Indeed, a mathematical model of fertilization in surge channels suggests that given a sufficient population of adult males within a surge channel, 80–100% of eggs may be fertilized. This result must be tempered, however, by the possibility that the small-scale shears induced by turbulence interfere with fertilization.

Introduction

Recent field experiments with marine organisms have demonstrated that the fraction of eggs externally fertilized during spawning can be adversely affected by water motion. For example, when water velocity is 0.1–0.2 m s^{-1} and an individual male is separated from a female by more than 5 m, studies of sea urchins (Pennington, 1985; Levitan, 1991) and a hydroid (Yund, 1990) show that only 5–15% of eggs are fertilized. This low rate of fertilization is attributed to the dilution of gametes by turbulent mixing in flow. The percentage of eggs fertilized can be somewhat higher (approximately 30–50%) if multiple males are present, but is lower at higher velocities (Pennington, 1985; Levitan *et al.*, 1992). Even in fish that actively pair to spawn, the fraction of eggs fertilized can be low (40–50%) when the flow exceeds 0.1 m s^{-1} and wave-induced turbulence disperses the gametes (Petersen, 1991; Petersen, *et al.* 1992).

These studies (and the low rates of fertilization they report) raise important questions about the role of water motion in external fertilization and the consequences it may have in the evolution of reproductive strategies. However, flow during these experiments was relatively benign. How effective can external fertilization be under more extreme hydrodynamic conditions?

As ocean waves break upon rocky shores they generate water velocities as high as 15 m s^{-1} (Denny, 1988; Vogel, 1981), twenty to 100-fold faster than those in the studies cited above. These high velocities are accompanied by much more violent mixing of water. The "white water" characteristic of the surf zone is visual evidence of the extreme turbulence in breaking waves, and Denny and Shibata (1989) proposed that turbulence in the benthic boundary layer of the surf zone reduces the effectiveness of external fertilization well below even the low values measured subtidally. They estimate that only about 0.01–0.1% of eggs released into the surf zone are fertilized by a single adult male under typical conditions, and a maximum of only about 3% are fertilized when multiple males spawn synchronously. These predicted rates of fertilization are one to two orders of magnitude lower than those measured in subtidal flows, and suggest even more dramatic consequences for intertidal plants and animals than those proposed for subtidal organisms.

Denny and Shibata (1989) note, however, that the fraction of eggs fertilized in the surf zone could be sub-

Received 11 April 1992; accepted 27 July 1992.

[1] Present address: School of Oceanography WB-10, University of Washington, Seattle, Washington, 98195.

stantially higher than they predict if the volume into which gametes can be diluted is limited. Experiments described here show that blind-ended surge channels (the small-scale embayments typical of rocky shores) can act to limit the dilution volume for gametes of benthic organisms. Shoreline topography may thereby enhance the effectiveness of external fertilization in the surf zone, and the fraction of eggs fertilized in surge channels may actually be similar to that found in subtidal habitats.

Materials and Methods

Field experiments were conducted on the shoreline adjacent to Hopkins Marine Station, Pacific Grove, California. Four blind-ended surge channels (essentially, small-scale bays) were chosen to span the size typical of this coastline. Each was surveyed with a surveyor's level, tape measure, and stadial rod to provide the location (in cylindrical coordinates) of 100–150 points, and these points were analyzed (Surfer, Golden Software, Inc.) to produce a topographic map of each surge channel (Fig. 1). From these maps, the volume of each channel was estimated as a function of still water level (Fig. 2). Volume (at approximately the mean still-water level present during this study) ranged from 3.5 to 45 m^3.

The residence time of water in these channels was measured at high tide as follows. A control sample of water in the center of the channel was taken with a test tube attached to a wooden pole. For this and all subsequent samples, the tube was filled and emptied once before sampling to minimize the effects of any contaminants in the tube. Thirty grams of water-soluble fluorescein dye was dissolved in a liter of seawater, and 100–200 ml of the solution was introduced into the surge channel. The dye was allowed to mix throughout the channel until it appeared uniform, a process resulting from the entry of one to three breaking waves into the channel (10–30 s). Dipped samples were then taken at intervals of 15 or 30 s (depending on the rate of exchange between surge channel and mainstream) until the dye was no longer visible in the channel. Typically 15–30 samples were taken in each trial. Two trials were conducted for each channel on each sampling day. Trials were alternated between sites to allow dye to be thoroughly dispersed from each site prior to the second trial. Sample tubes were capped and kept in the dark until analyzed (usually the next day).

Markers were glued to one wall of each surge channel at 25 cm vertical intervals, allowing us to estimate visually (to within approximately 10 cm) the maximal and minimal height of the water's surface during each surge. Measurements were recorded in each channel, for each surge, during a 5 min period both before the first trial and after the last trial. The average of each 5-min series of readings provided an estimate of the mean, or still-water, level in the channel during the trial. The average of minimal heights provided an estimate of the mean low water level. The number of surges encountered, divided by the 5-min duration of the recording session, provided an estimate of the average period of the surge. Periods ranged from about 9–14 s. The height of each surge was estimated as the maximal height minus the subsequent minimal height. Heights recorded in each 5-min period were averaged to provide an estimate, H_{avg}, of the sea state during each trial. Average surge heights varied from 0.14 m to 0.74 m.

The concentration of dye in each sample was measured with an Aminco model SPF 500 spectrofluorometer and a standard series of dilutions from the stock dye solution. Concentrations were corrected for any background fluorescence present in the control sample, and were expressed as a fraction, C_r, of the concentration in the initial experimental sample. A model of the time series of relative concentrations from each trial was then determined by fitting the data to the equation:

$$C_r(t) = a \exp(-kt) + c; \qquad \text{(Eq. 1)}$$

a simplex algorithm (Caceci and Cacheris, 1984) was used to estimate the least-squares fit. The parameter c represents the quasi-equilibrium concentration of dye at the end of each trial when the concentration in the surge channel is equal to that in the adjacent mainstream flow. In all cases, c is small (typically <0.0001 a). The *exchange parameter* k represents the fraction of dye escaping from the surge channel in each interval of time t, and is thus a measure of the rate of exchange of water between surge channel and mainstream. The expected residence time, T_r, of a dye particle in the surge channel is

$$T_r = 1/k. \qquad \text{(Eq. 2)}$$

A total of 73 trials were conducted between October, 1988 and June, 1990. In three trials (4.1%), the measured concentrations in a surge channel appeared to increase substantially for one or more samples in the middle of the trial. These increases occurred too late in each trial to be attributed to incomplete initial mixing, and were due either to contamination in the sample tubes or to the accidental introduction of concentrated dye into the surge channel from an undetected "refuge" (a high tide pool, for example). Data from these anomalous trials were not included in the analysis.

A mixing model for blind-ended surge channels

As a means for examining our data, we formulated a simple model of the exchange between a surge channel and the mainstream. For the purposes of this model, the topography of a surge channel is represented by its volume versus still-water-level curve as shown in Figure 2. At the mean low water level determined for a trial, the channel holds a volume V_0. When a surge enters

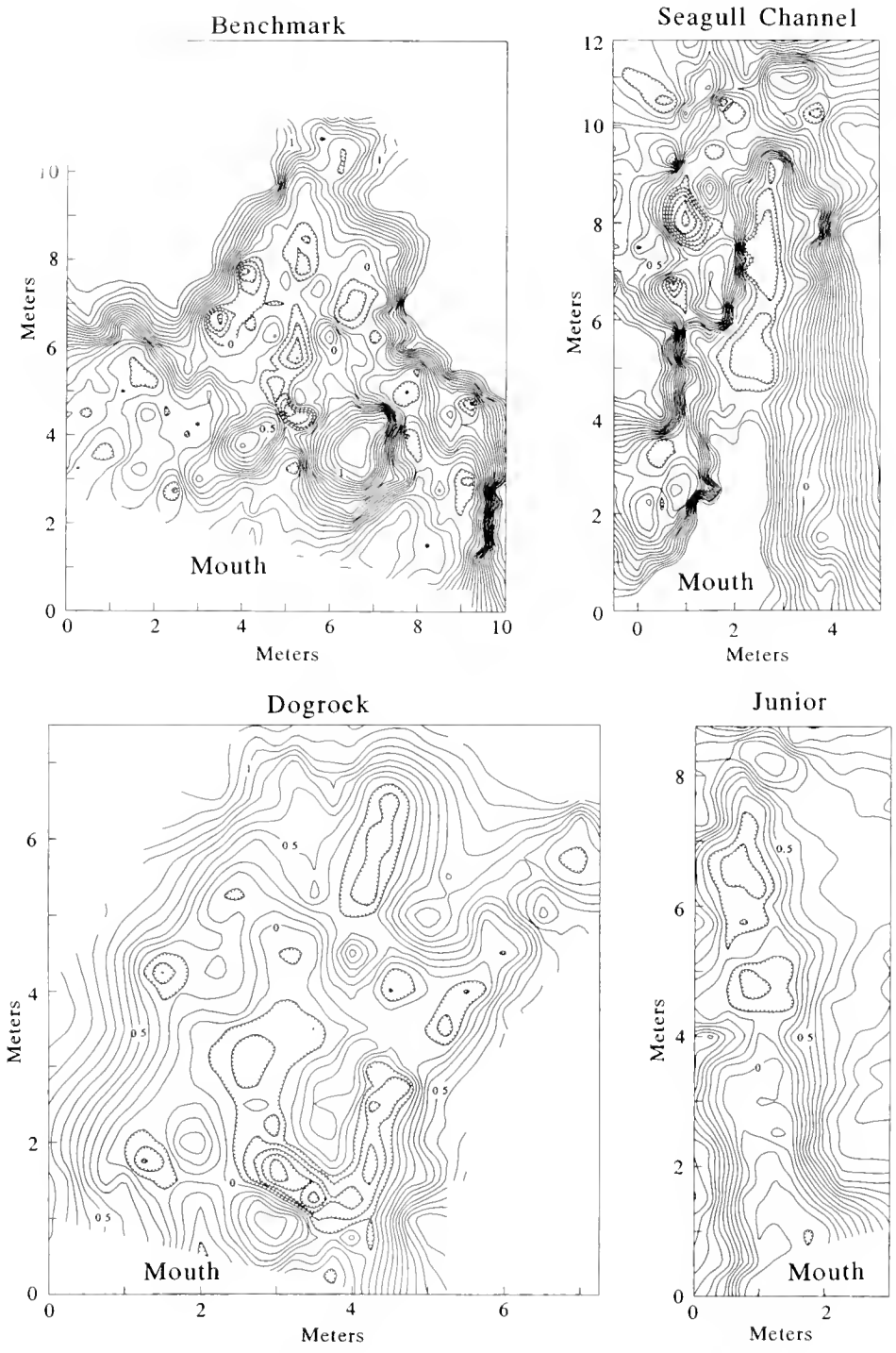

Figure 1. Topographical maps of the four embayments used in this study. Vertical gradations are 0.1 m; hachures denote local depressions.

the channel the water level rises, increasing the channel's volume by an amount ΔV. If the initial volume (V_0) and added volume (ΔV) are thoroughly mixed, the probability that a particle is carried out of the channel as the surge subsides and the water returns to its original level is

$$\text{Probability per surge} = \frac{\Delta V}{(V_0 + \Delta V)}. \quad \text{(Eq. 3)}$$

But the mixing of initial and added volumes may not be complete; in such a case the probability of escape from the channel is only a fraction, m, ($0 \leq m \leq 1$) of this

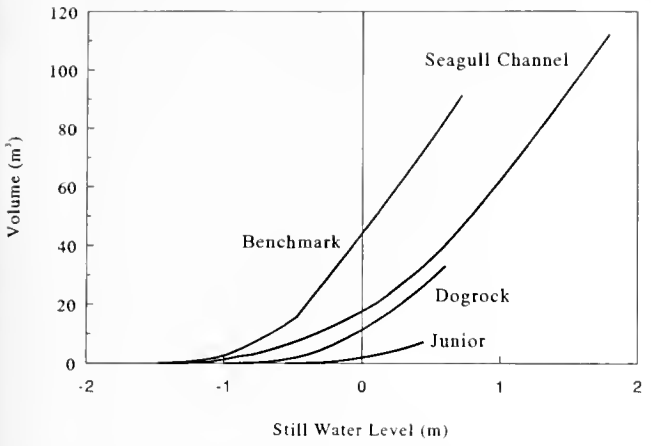

Figure 2. The relation between still water level and surge channel volume for the four embayments used in this study. These curves were calculated using the topographical maps of Figure 1.

maximal probability. If the average period between surges is T seconds, the probability that a dye particle is carried out of the channel in one second is thus

$$k = m \frac{\Delta V}{(V_0 + \Delta V)T}, \qquad \text{(Eq. 4)}$$

where k is again the exchange parameter of Eq. 1.

V_0, ΔV, T, and k can be determined experimentally, allowing us to calculate the *mixing parameter* m:

$$m = \frac{k(V_0 + \Delta V)T}{\Delta V}. \qquad \text{(Eq. 5)}$$

Abundance of surge channels

The abundance of surge channels on a shore is strongly dependent on the local topography, and therefore may vary greatly from site to site. Due to the fractal nature of shorelines (Mandelbrot, 1982; Denny, in press), it is difficult to quantify precisely the abundance of surge channels for even a single site, because the exact location of the shoreline varies with the scale at which the shore is examined. An estimate of the abundance of surge channels on the shores at Hopkins Marine Station was made, however, using the following technique (Fig. 3).

An aerial photograph of the shore was traced onto paper to provide a two-dimensional representation of the shoreline with accurate detail present at a scale smaller than that used in the analysis. A point was chosen at random on this trace, and a caliper placed with one tip at this point. The caliper was then "walked" down the trace, and the distance between the tips of the caliper set the scale at which the shoreline was measured. The series of contiguous lines joining points where the caliper intersected the trace defined one realization of the "average" shoreline at that particular scale (Fig. 3). Segments of the actual shore that lie shoreward of this average were defined to be surge channels; segments seaward of the average shoreline were promontories. At each scale, the fraction of the average shoreline that comprised the mouths of surge channels, A, was then taken as a measure of relative surge channel abundance. This procedure was repeated for several starting points and the results averaged. The abundance of surge channels was measured at scales ranging from 2.2 to 22.4 m.

The shore at Hopkins Marine Station is formed from granite, and is not atypical of rocky shores on the west coast of North America.

Theory of external fertilization

If the exchange between water in surge channels and that in the adjacent mainstream is slow, then surge channels may function as "containment vessels" for gametes, thereby allowing for the effective fertilization of eggs. This possibility can be examined mathematically.

In this analysis, we follow the model of Denny and Shibata (1989), based primarily on data from sea urchins. Males are assumed to release sperm into a surge channel at a constant rate Q_s per second resulting in a concentration of sperm C_s (with units of m^{-3}) that may vary through time. Denny and Shibata (1989) also allowed C_s to vary in space, but for present purposes we assume that sperm are thoroughly mixed, ensuring that C_s is the same everywhere within the surge channel. Sperm (like dye particles) have a probability k in each second of passively escaping from the surge channel into the adjacent mainstream, and we assume that sperm that escape from the surge channel do not re-enter.

Sperm can swim and, under certain conditions, can move preferentially toward eggs (*e.g.*, Miller, 1985). The speed of sperm locomotion is very slow, however, a few tens of $\mu m\ s^{-1}$. In contrast, the motion of neutrally buoy-

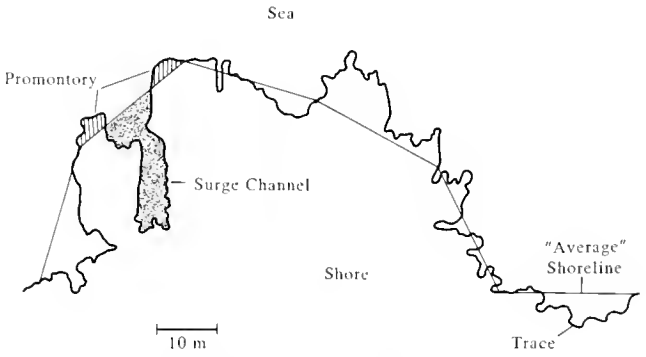

Figure 3. An example showing the traced shoreline (thick line), "average" shoreline at a particular scale (thin line segments), and the surge channel and promontory portions for a single segment of the average shore. This shoreline was traced from an aerial photograph of the shore at Hopkins Marine Station.

ant particles in turb[illegible]w can be characterized by a velocity u_* (the [illegible]ocity), a measure of the intensity of tur[illegible]ow (Schlichting, 1979; Denny, 1988; Den[illegible]ta, 1989). For the intensely turbulent fl[illegible] the surf zone of wave-swept shores, u_* is app[illegible]ately equal to 0.1 u_{avg}, where u_{avg} is the ensemble average velocity of the water (see Denny, 1988; Denny and Shibata, 1989). Water velocities in the surf zone vary from approximately 1–15 m s^{-1} (Denny, 1988), suggesting that u_* is 0.1–1.5 m s^{-1}. Thus, the velocity imposed by turbulence is four to five orders of magnitude faster than a sperm's swimming speed, and we assume that the swimming speed of sperm can be safely neglected in the present context.

Given these assumptions, we see that the rate of change of sperm concentration is equal to the difference between the rate at which concentration increases due to the release of sperm and the rate at which concentration decreases due to the passive escape of sperm to the mainstream:

$$\frac{dC_s(t)}{dt} = \frac{Q_s}{V} - kC_s(t), \qquad \text{(Eq. 6)}$$

where V is the still-water volume of the surge channel.

If we assume that $C_s(0) = 0$, we calculate that

$$C_s(t) = \frac{Q_s}{kV}[1 - \exp(-kt)]. \qquad \text{(Eq. 7)}$$

At infinite time C_s reaches a steady-state concentration, $C_{s,\infty}$:

$$C_{s,\infty} = \frac{Q_s}{kV}. \qquad \text{(Eq. 8)}$$

We assume that females release eggs at the constant rate Q_e per second, and that eggs are mixed and exchanged as for sperm. Thus,

$$\frac{dC_e(t)}{dt} = \frac{Q_e}{V} - kC_e(t), \qquad \text{(Eq. 9)}$$

$$C_e(t) = \frac{Q_e}{kV}[1 - \exp(-kt)], \qquad \text{(Eq. 10)}$$

$$C_{e,\infty} = \frac{Q_e}{kV}, \qquad \text{(Eq. 11)}$$

where C_e is the instantaneous concentration of eggs (m^{-3}) and $C_{e,\infty}$ is the steady-state concentration.

We assume that the rate at which sperm fertilize eggs is governed by the co-occurring concentrations of both sperm and eggs and by a "reaction" parameter, ϕ.

$$\text{Rate of fertilization} = \phi C_{s,v}(t)C_{e,v}(t). \qquad \text{(Eq. 12)}$$

Here, $C_{s,v}$ and $C_{e,v}$ are the concentrations of unattached sperm and virgin eggs, respectively.

The reaction parameter is the product of the effective speed at which sperm are mixed through the water (here assumed to be the friction velocity u_*) and the effective "collision cross section" of an egg (Denny and Shibata, 1989), and has units $m^3\ s^{-1}$.

If an egg could be fertilized by the first sperm that contacted any point on its surface, the "collision cross section" would be the same as the projected area of the egg. For sea urchin eggs with a diameter of 10^{-4} m this is 7.85×10^{-9} m^2. Laboratory measurements suggest, however, that sea urchin eggs behave as if only a small fraction of their surface area is fertilizable. The reason for this reduced cross section is unclear. Vogel *et al.* (1982) suggest that apparent fertilizable area is only about 1% of the overall area for *Paracentrotus lividus*. More recent experiments with *Strongylocentrotus fransiscanus* (Levitan *et al.*, 1991) suggest an apparent fraction of 3%. Using this latter value, we find that

$$\phi = u_*(2.4 \times 10^{-10}\ m^2), \qquad \text{(Eq. 13)}$$

and because $u_* \approx 0.1u_{avg}$,

$$\phi \approx u_{avg}(2.4 \times 10^{-11}\ m^2). \qquad \text{(Eq. 14)}$$

Given that average water velocities in the surf zone vary from approximately 1 to 15 m s^{-1}, ϕ is likely to vary from 2.4×10^{-11} to 3.5×10^{-10} $m^3\ s^{-1}$.

Denny and Shibata (1989) calculated that an individual urchin extrudes sperm at approximately $10^7\ s^{-1}$ or eggs at $10^4\ s^{-1}$, and these values are used here. Due to the vast overabundance of sperm it seems safe to assume that the concentration of sperm is minimally affected by the attachment of sperm to eggs; thus

$$C_{s,v} = C_s. \qquad \text{(Eq. 15)}$$

Given these assumptions, we can describe the flux of virgin eggs through a surge channel. Virgin eggs are added to the local population as they are released by females and are removed either by escaping to the mainstream or by fertilization. Thus:

$$\frac{dC_{e,v}(t)}{dt} = \frac{Q_e}{V} - kC_{e,v}(t) - \phi C_s(t)C_{e,v}(t). \qquad \text{(Eq. 16)}$$

At this point the mathematics can be simplified if we convert each of the variables of interest to a dimensionless form. In the present context, time is important primarily as it relates to the residence time of gametes in a surge channel. Thus we may specify a dimensionless time τ,

$$\tau = t/T_r = kt. \qquad \text{(Eq. 17)}$$

Note that

$$\frac{dg}{d\tau} = \frac{dg}{dt}\frac{dt}{d\tau} = \frac{1}{k}\frac{dg}{dt} \qquad \text{(Eq. 18)}$$

for any function g.

The instantaneous concentration of eggs can be expressed in dimensionless form by dividing by the steady-state concentration of eggs. Thus,

$$e(\tau) \equiv \frac{C_e(\tau)}{C_{e,\infty}} = \frac{C_e(\tau)}{(Q_e/kV)}. \qquad \text{(Eq. 19)}$$

Similarly, the instantaneous concentration of virgin eggs is:

$$v(\tau) \equiv \frac{C_{e,v}(\tau)}{C_{e,\infty}} = \frac{C_{e,v}(\tau)}{(Q_e/kV)}. \qquad \text{(Eq. 20)}$$

The instantaneous concentration of sperm is made dimensionless by expressing it as a fraction of the steady-state concentration of sperm:

$$s(\tau) \equiv \frac{C_s(\tau)}{C_{s,\infty}} = \frac{C_s(\tau)}{(Q_s/kV)}. \qquad \text{(Eq. 21)}$$

Finally, we devise a dimensionless fertilization parameter Θ that incorporates several of the variables that govern the rate of fertilization:

$$\Theta \equiv \frac{\phi}{k} C_{s,\infty} = \frac{\phi Q_s}{k^2 V} = \frac{\phi Q_s T_r^2}{V}. \qquad \text{(Eq. 22)}$$

Inserting these dimensionless variables into our previous results (Eqs. 7, 8, 10, 11, and 16), we find that:

$$s(\tau) = e(\tau) = 1 - \exp(-\tau), \qquad \text{(Eq. 23)}$$

$$s_\infty = e_\infty = 1, \qquad \text{(Eq. 24)}$$

$$\frac{dv(\tau)}{d\tau} = 1 - v(\tau) - \Theta s(\tau) v(\tau). \qquad \text{(Eq. 25)}$$

Thus, at steady state (that is, when $dv(\tau)/d\tau = 0$),

$$v_\infty = 1/(1 + \Theta). \qquad \text{(Eq. 26)}$$

In other words, the larger Θ is, the lower the steady-state fraction of virgin eggs, v_∞. A large Θ can result from a large rate of sperm release (for example, due to the presence of multiple males), a small surge channel volume, an intense level of turbulence, or a long residence time (Eq. 22). Thus, any combination of these factors produces a lowered fraction of virgin eggs. Note, however, that Θ scales with the square of residence time, so v_∞ is especially sensitive to T_r (or, equivalently, to k).

Now, the concentration of fertilized eggs is equal to the difference between the total concentration of eggs and the concentration of virgin eggs. By analogy, the *fraction* of all eggs that are fertilized, $f(\tau)$, is equal to $1 - v(\tau)$. From Equation 26 we see that at steady-state

$$f_\infty = \Theta/(1 + \Theta). \qquad \text{(Eq. 27)}$$

Non-steady-state conditions

This result applies to surge channels once they have reached a steady-state concentration of gametes. Is it realistic to apply these steady-state results to the real world? To answer this question, we solved Equation 25 for v as a function of τ using an implicit trapazoidal finite difference technique:

$$v([i+1]\delta\tau) = v(i\delta\tau)\frac{\{1 - (\delta\tau/2)[1 + \Theta - \Theta\exp - (i\delta\tau + \tfrac{1}{2}\delta\tau)]\}}{\{1 + (\delta\tau/2)[1 + \Theta - \Theta\exp - (i\delta\tau + \tfrac{1}{2}\delta\tau)]\}} + \frac{\delta\tau}{\{1 + (\delta\tau/2)[1 + \Theta - \Theta\exp - (i\delta\tau + \tfrac{1}{2}\delta\tau)]\}}, \qquad \text{(Eq. 28)}$$

where $\delta\tau$ is the time step and i is a counter (i = 0, 1, 2, 3, . . .). At $\tau = 0$, all eggs are assumed to be virgin so that $v(0) = 1$.

We again set $f = 1 - v$ and follow f as a function of dimensionless time.

Results

Mixing in surge channels

The decrease in dye concentration within a surge channel is modeled accurately by the exponential decrease of Equation 1 (Fig. 4). The average coefficient of determination (r^2) for the 70 trials is 0.955 (with a standard deviation of 0.054), indicating that, to a first approximation, each dye particle can be regarded as having a fixed probability of escaping from the surge channel in a given interval.

Exchange between surge channel and mainstream water is surprisingly slow. The exchange parameter k varies from approximately 0.001 to 0.04, implying average residence times, T_r, of 25 to 1000 s.

The mixing parameter, m, varies from about 0.05 to 0.9. When data from all four surge channels are combined, m is found to be an increasing function of average surge height (Fig. 5), but variation in H_{avg} explains only 17% of the variation in m. The mixing parameter is not significantly correlated with the average fractional change in volume during a downsurge, $\Delta V/(V_0 + \Delta V)$ ($r = 0.0619$, 68 df, $P > 0.5$).

When data from all four surge channels are combined, the exchange parameter k is found to be an increasing function of average surge height (Fig. 6), and the relationship explains 51% of the variation in k. The exchange parameter is also positively correlated with the fractional change in volume in the surge channel, which is itself a direct function of H_{avg}, but the correlation ($k = 0.179\ H_{avg} + 0.0023$, $r = 0.431$, 68 df) explains much less of the variation than does surge height alone (19 *vs.* 51%).

Abundance of surge channels

Surge channels form about 46% of the shoreline at Hopkins Marine Station (Table 1). The fractional abundance of surge channels is not correlated with the scale at which the shoreline is measured ($r = 0.134$, 3 df, $P > 0.5$), at least for the range of scales examined here.

Predicted fraction of eggs fertilized

At a realistic value of Θ (that is, a realistic combination of k, V, ϕ, and Q_s), a substantial fraction of eggs is expected

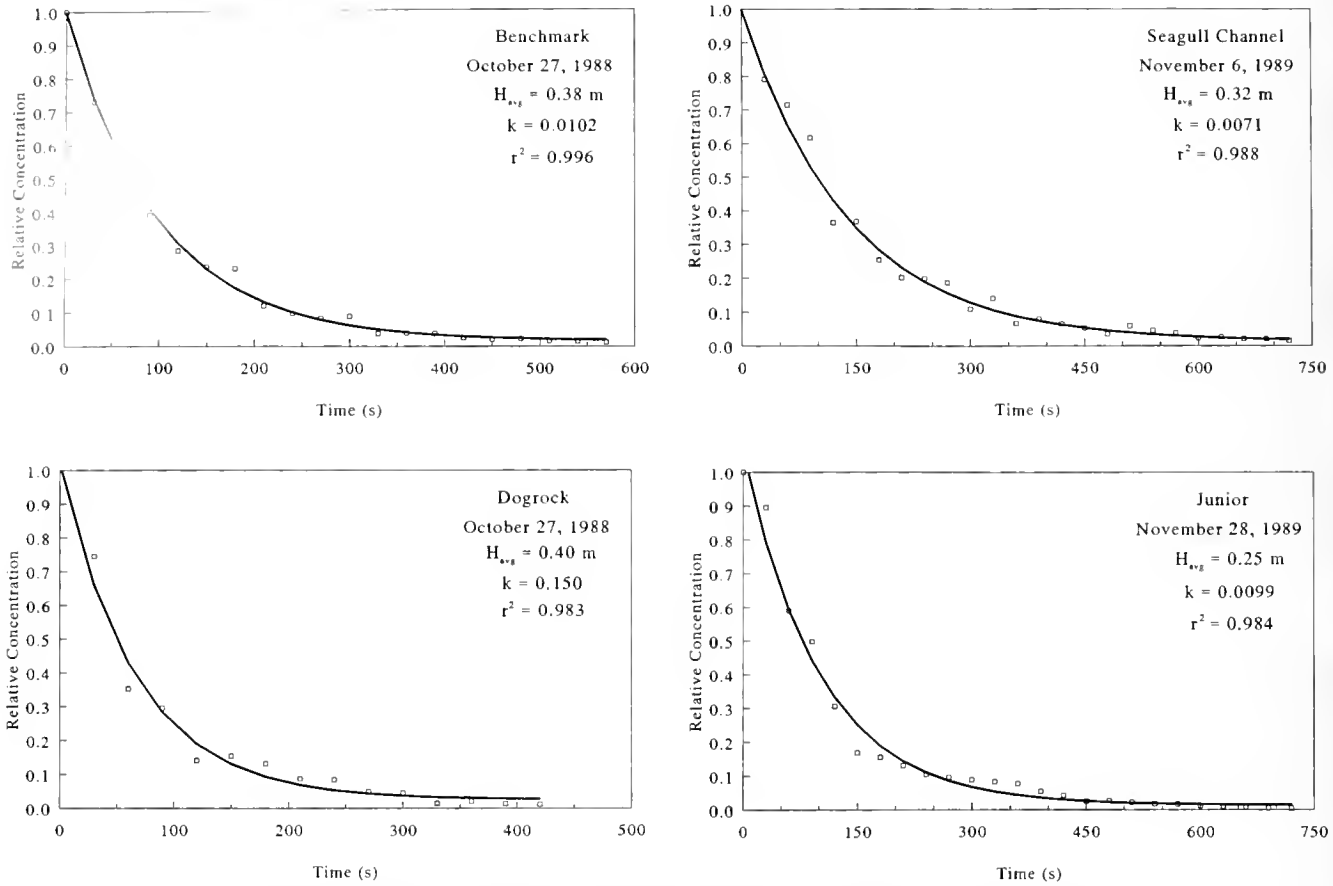

Figure 4. Representative examples of the temporal decay in dye concentration in the experimental embayments. The solid curves are least-squares fits to the data using the model of Equation 1.

to be fertilized (Fig. 7). For example, if ϕ is 10^{-10} m^3 s^{-1}, and the residence time is 50 s ($k = 0.02$ s^{-1}) for a surge channel with a volume of 10 m^3 (typical values for the shore at Hopkins Marine Station), about 20% of eggs can be fertilized by a single male. This is two to three orders of magnitude larger than the fraction predicted by Denny and Shibata (1989) for flow outside of surge channels.

Multiple males

Increasing the number of males present in a surge channel increases Q_s, with a concomitant increase in Θ, and thereby an increase in the fraction of eggs fertilized (Fig. 8). Consider, for instance, a surge channel with the same residence time as that cited above ($k = 0.02$ s^{-1}), but with five times the volume (50 m^3). If this channel has an average still water depth of 1 m, it has approximately 70 m^2 of substratum area. Even given the fivefold increase in volume, if only 3 males are present per square meter of substratum (210 males total, a realistic value for wave-swept shores), 90% of eggs are expected to be fertilized.

Smaller channels will have a larger ratio of substratum area to channel volume. Thus, given the same spatial density of male urchins, smaller channels will have a higher fraction of eggs fertilized.

Time dependence of fertilization

The time-dependent fraction of eggs fertilized is shown in Figure 9a. For realistic values of Θ, values of f within 10% of steady-state values are obtained within a period of 5 T_r. For a typical residence time of 50–120 s, this implies that the steady-state estimate of fertilization fraction is reached within 4–10 minutes. Given that an individual urchin in the laboratory releases gametes for approximately 1 h, equilibrium conditions are likely to apply to most gametes released.

Note that Figure 9a shows the fraction of eggs fertilized relative to the steady-state fraction. The absolute fraction fertilized is shown as a function of dimensionless time in Figure 9b. The fraction fertilized decreases with decreasing Θ as expected.

Discussion

Mixing in small surge channels

The rate of exchange between small, well-mixed surge channels and mainstream waters is both a simple and a

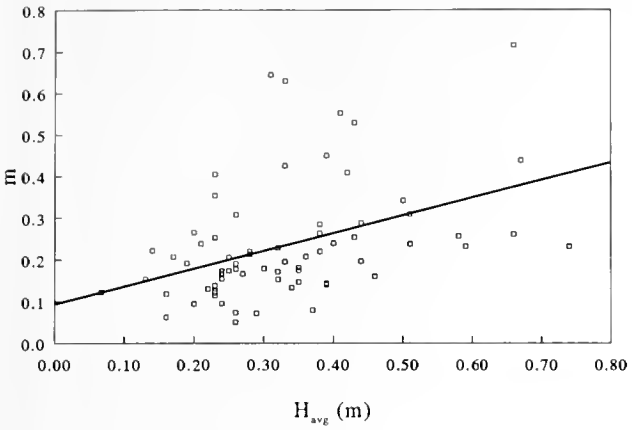

Figure 5. The relation between average surge height (H_{avg}) and the dimensionless mixing parameter, m. The linear regression (solid line) explains approximately 17% of the variation in m: $m = 0.424 \times H_{avg} + 0.094$ ($r^2 = 0.173$), where H_{avg} is measured in m.

complex process. Our data indicate that the probability per time that a small, inanimate, neutrally buoyant particle will escape from a surge channel is constant for at least a few tens of minutes, and that this probability can be predicted with reasonable accuracy from the height of the surge present in the surge channel. In this respect the results of the process are simple to predict as shown in Figure 6.

It is more difficult to account for these predictions on a mechanistic basis, primarily because of the variability of the mixing parameter, m. At present, m cannot be predicted accurately, from either average surge height (Fig. 4) or fractional change in volume. Probably, m is affected by the local topography of each surge channel and by chance variation in the shape of each breaking wave, rendering it of little value as a general predictive tool.

Note that the relationship measured here between surge height and exchange parameter (Fig. 6) can be applied

Table I

Fraction of the average shoreline that comprises the mouths of surge channels at Hopkins Marine Station

Scale (m)	Fraction, A
2.2	0.446
4.5	0.440
9.0	0.508
22.4	0.455

only to a relatively narrow range of channel sizes. There is a lower limit to the size at which a local indentation in the shoreline can be considered a surge channel for our purposes. If the still-water depth in the indentation is less than the amplitude of the surge ($=H_{avg}/2$), the indentation is completely emptied by an average downsurge, and the probability of a particle re-entering the channel on the subsequent upsurge is set more by mainstream mixing and advection than by mixing within the indentation itself. In this case, the indentation is not a surge channel in the sense that we have used the term here.

The upper limit to the size of this relationship is set by the size at which a surge channel is no longer well mixed within itself. Only if the channel is well mixed can Equation 1 accurately model residence time. We have noticed distinct advective patterns in bays in excess of the size studied here—particles that enter a larger bay at one portion of its mouth predictably exit at another specific region. In this case, the probability of exchange for a particle depends in part on its history, and the simple model of Equation 1 cannot be expected to hold. Thus, the predictions implicit in Figure 6 should not be applied to surge channels larger than approximately 100 m^3.

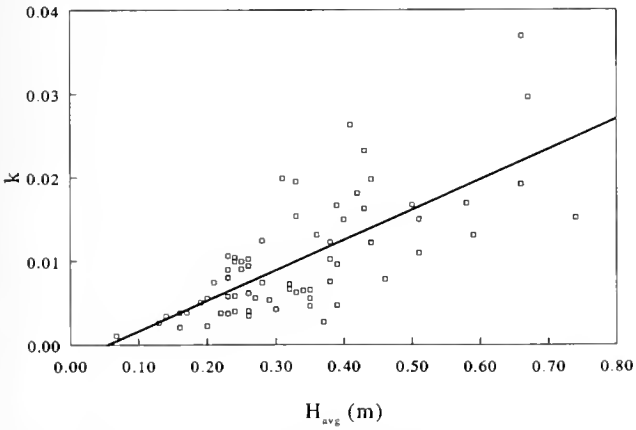

Figure 6. The relation between average surge height (H_{avg}) and the exchange parameter k. The linear regression (solid line) explains approximately 51% of the variation in k: $k = 0.036 \times H_{avg} + 0.002$ ($r^2 = 0.514$), where H_{avg} is measured in m, and k has the units s^{-1}.

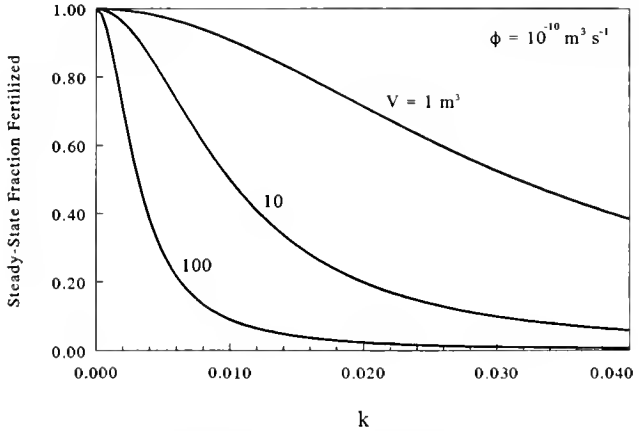

Figure 7. As the probability of gametes escaping from a surge channel increases, the equilibrium fraction of eggs fertilized decreases. The larger the volume of the surge channel (V), the lower the fraction of eggs fertilized.

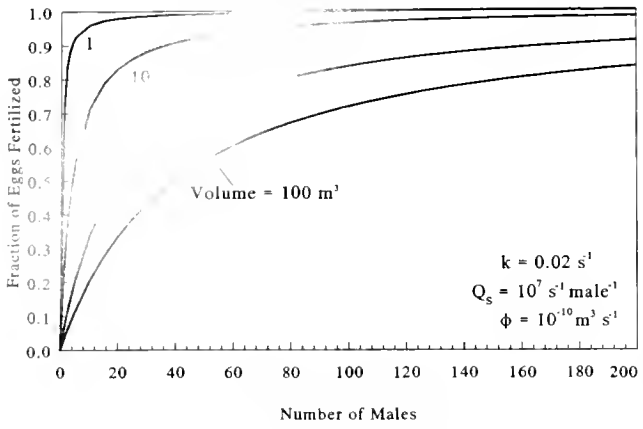

Figure 8. The fraction of eggs fertilized increases with the number of males present in a surge channel.

The fraction of eggs fertilized

The predictions made here suggest that external fertilization in surge channels may be quite effective, with fertilization fractions comparable to or exceeding those measured for benthic invertebrates in relatively benign subtidal flows (Pennington, 1985; Yund, 1990; Levitan, 1991; Levitan *et al.*, 1992). If these predictions are valid, fertilization may be much less of a limiting process than suggested by the model of Denny and Shibata (1989), at least within surge channels.

Furthermore, about 46% of the shoreline at Hopkins Marine Station is formed of surge channels (Table II). If we assume that the fraction of eggs fertilized within the surf zone, but outside of surge channels, is equal to the maximal fraction predicted by Denny and Shibata (1989) (3%), and that individuals are randomly distributed along the shore, then the overall fraction of eggs fertilized is approximately

$$\text{Overall fraction} = (f - 0.03)A + 0.03, \quad \text{(Eq. 29)}$$

where f is again the steady-state fraction of eggs fertilized in surge channels, and A is the fraction of shoreline that comprises the mouths of channels. For f = 0.9 and A = 0.46, the overall fraction of eggs fertilized is thus 43%, suggesting that external fertilization in the surf zone, taken as a whole, may be considerably higher than that suggested by Denny and Shibata (1989).

The role of shoreline topography in controlling the overall rate of external fertilization is clear in Equation 29. If the shore is constructed of rocks that are not susceptible to the formation of surge channels, A will be small, and the overall fraction of eggs fertilized will be similarly small. Conversely, on a shore where surge channels are abundant, external fertilization may be quite effective.

Localized fertilization

Denny and Shibata (1989) concluded that, as long as there is no practical limit to the volume into which eggs and sperm are mixed, dilution of gametes is so rapid that those few eggs that are fertilized are likely to be fertilized by sperm from the nearest males. In this fashion, rapid dilution insures the localization of fertilization.

As a corollary to the effectiveness of fertilization in surge channels, we note the implication that the long residence time of water in channels can again lead to localization of fertilization. Once gametes escape from a channel they are subject to the infinite dilution described by Denny and Shibata (1989), and subsequent fertilization becomes highly unlikely. Eggs released in a surge channel are therefore very likely to be fertilized by males in the same channel. Thus both infinite dilution and the limitation of dilution result in localized fertilization, leading us to suppose that, as a general rule, external fertilization in the surf zone can be effective only over short distances.

The effect of localized fertilization due to surge channels on the population genetics of a species is unclear. Although the residence time of small surge channels is surprisingly long, it is still short compared to the larval lifetime of most species, which vary from a few hours to several

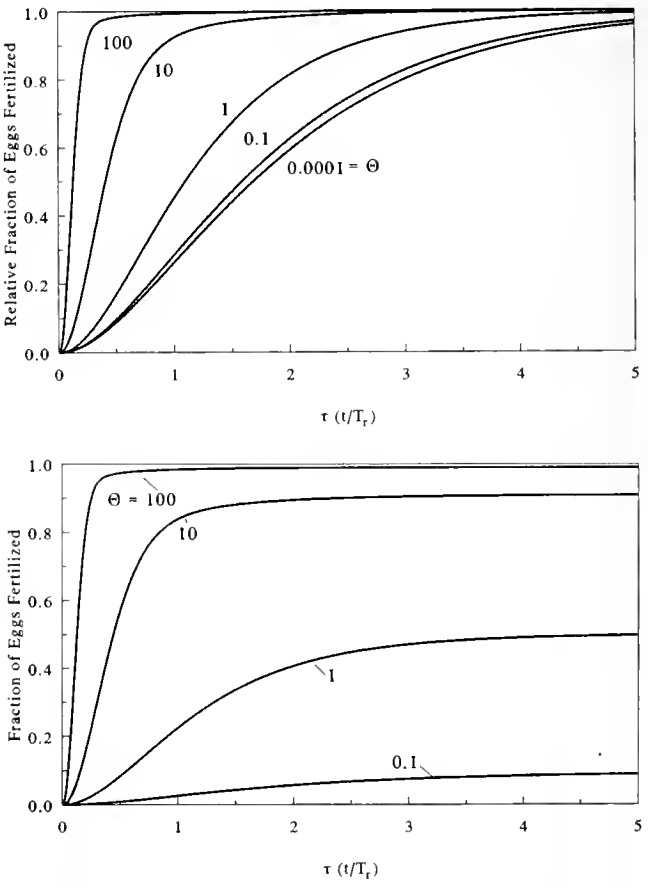

Figure 9. (A) Steady-state conditions are approached within a period equal to 5 times the retention time ($\tau = 5$). The fraction of eggs fertilized is expressed as a fraction of the steady-state value. (B) The actual fraction of eggs fertilized is plotted without being normalized to the fraction at steady state.

months. As a result, although fertilization may be localized, the resulting larvae are free to participate in the larger-scale dynamics of the population. We recognize that the long residence time of surge channels may have important implications for the spatial pattern of settlement of larvae, as well as for the probability that newly fertilized embryos will be consumed by benthic suspension feeders, but these implications will not be developed here.

Instantaneous mixing, shear stress, and a note of caution

We foresee two factors that could affect the results presented here.

First, the model of external fertilization assumes that gametes are instantaneously mixed throughout a surge channel. As noted, however, thorough mixing within a channel requires the entry of one to three breaking waves. In the brief period prior to the arrival of the first wave, local high concentrations of gametes may be present, and if eggs encounter an area of high sperm concentration, the probability of fertilization may be very high. Note, however, that any momentary reduction in mixing that allows a high concentration of sperm to be maintained also reduces the probability that an egg will be delivered, by chance, to that area of high concentration. Quantitative analysis of the dynamics of fertilization over times shorter than the period of the surge will require a more complete understanding of the structure of turbulence within surge channels than is currently available.

Second, the calculations made here are based on the assumption that sperm and eggs interact in a fashion akin to molecules in a gas. If a sperm happens to be in the vicinity of an egg and aimed in the right direction, it impacts on the egg, sticks, and (perhaps) fertilization follows. However, this simple view ignores the small-scale hydrodynamics relevant to sperm and eggs, and as a result may overestimate the probability of fertilization.

To see why, we explore flow in the surf zone at the spatial scale of a gamete. This exploration is carried out in two steps. First, we examine the rate at which turbulent kinetic energy is dissipated in the surf zone. Next, we use these results to estimate the average velocity gradient to which gametes are subjected. The biological consequences of this gradient can then be discussed.

Ocean waves carry energy with them as they approach the shore. The rate, P, at which wave energy is transported across the mouth of a surge channel M meters wide is

$$P \approx (1/8)\rho g H^2 M (2gH)^{1/2}$$
$$\approx 0.177 \rho g^{3/2} H^{5/2} M, \qquad \text{(Eq. 30)}$$

where ρ is the density of seawater (approximately 1025 kg m^{-3}), g is the acceleration due to gravity (9.81 m s^{-1}), and H is wave height (Denny, 1988). Thus, the power per meter of surge channel mouth, P′, is

$$P' \approx 0.177 \rho g^{3/2} H^{5/2}. \qquad \text{(Eq. 31)}$$

In making this calculation we have assumed that wave height at breaking is equal to water depth (Denny, 1988), and that waves at breaking move at the speed predicted by solitary wave theory (in this case, $(2gH)^{1/2}$ [Denny, 1988]).

Some of this incident wave energy may be carried back out of the surge channel if the wave reflects from the shore. If the height of the reflected wave is a fraction R of the incoming wave height ($0 \le R < 1$), the net power delivered to the channel (per meter of channel mouth) is

$$P'_n \approx 0.177 \rho g^{3/2} H^{5/2} (1 - R^{5/2}). \qquad \text{(Eq. 32)}$$

On rocky shores, R (the *reflection coefficient*) is typically small. For example, the R for a rubble breakwater (similar in topography to a rocky shore) is less than 0.29 when the slope of the breakwater is 1:5 (U.S. Army Corps of Engineers, 1984). If the slope is 1:10, the reflection coefficient is less than 0.13. If energy is transported inshore by waves but only a small fraction is carried back out by waves, most of the incident wave power must either be dissipated in the surf zone or transported out by other means (*e.g.*, kinetic energy associated with an undertow, acoustic energy). Effective transport by these other mechanisms appears unlikely, and we assume here that most wave energy is dissipated in the surf zone.

The magnitude of this rate of energy dissipation can be estimated from a simple example. The bottom of a surge channel has a slope α, as shown in Figure 10, and the wave height at the mouth of the channel is equal to the depth at the mouth of the channel. Given these conditions, waves break near the channel mouth, and the entire net energy of the waves is dissipated within the channel.

The still-water volume of the surge channel per width of mouth is

$$V'_{swl} \approx \frac{H^2}{2 \tan \alpha}. \qquad \text{(Eq. 33)}$$

As a breaking wave moves into the channel, its height decreases as wave energy is first converted to tubulent kinetic energy and then dissipated. Thornton and Guza (1983) have shown that the average (root mean square)

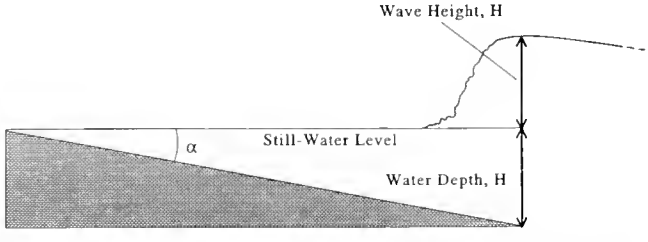

Figure 10. A schematic cross section through a surge channel illustrating the relation between bottom slope (α) and water depth, and showing the typical shape of a broken wave.

height of waves after breaking on a given shore is a constant fraction of water depth. For a sandy beach, this fraction is 0.4 and it is likely to be similar on rocky shores. For purposes of computation, however, we use a value of 1.0 as the broken wave propagates into the channel. We assume that its shape approximates that of a turbulent bore; that is, it has a steep leading face, and the water level behind the face is nearly equal to that of the wave crest (Fig. 10). Given these assumptions, the broken wave increases the volume of water in the surge channel by maximally ¼ the channel's still-water value. Thus, the maximal effective volume of water in which the wave energy is dissipated is

$$V' \approx \frac{5H^2}{8 \tan \alpha} \qquad \text{(Eq. 34)}$$

The minimal rate at which wave energy is dissipated per unit of effective water volume (W′) in the surge channel is thus,

$$W' = P_n'/V' \approx 0.283\rho g^{3/2}H^{1/2}(1 - R^{5/2}) \tan \alpha. \qquad \text{(Eq. 35)}$$

Now, the turbulent kinetic energy due to wave breaking is ultimately dissipated as heat via the action of viscosity. This mechanism is elegantly described by Lazier and Mann (1989): at small spatial scales, turbulent eddies in the broken wave are damped by the water's viscosity, forming in their stead a linear velocity gradient (or shear) within the fluid that varies randomly in direction and strength. It is the interaction of this shear with viscosity that converts turbulent kinetic energy to heat.

The scale at which the chaotic motion of turbulent eddies is effectively damped can be estimated from the Kolmogorov length scale, L_v:

$$L_v = \left(\frac{\mu^3}{\rho^3 \epsilon}\right)^{1/4}, \qquad \text{(Eq. 36)}$$

where μ is the dynamic viscosity of seawater (1 to 2 $\times 10^{-3}$ Pa s, depending on temperature), ρ is again the water's density, and ϵ is the rate at which turbulent kinetic energy is dissipated per mass of fluid (W kg^{-1}). The largest shears are found in eddies with a diameter equal to approximately 40 L_v. Smaller eddies are much less energetic, and few eddies have a diameter less than 5–10 L_v (Lazier and Mann, 1989).

The fact that wave energy is dissipated via small-scale velocity gradients provides a method for examining the characteristics of flow on the spatial scale of eggs and sperm. Consider a small cubic volume of water with its top face moving relative to its bottom face such that a linear velocity gradient β (with units of s^{-1}) is established within the cube. As a result, the water in the cube is sheared. From Newton's law of viscosity (Vogel, 1981), we know that the shear stress (force per area) required to deform water at this rate is

$$\sigma = \mu\beta. \qquad \text{(Eq. 37)}$$

If the cube has sides of length dx, the force required to shear the cube is thus

$$F = dx^2\mu\beta. \qquad \text{(Eq. 38)}$$

The power, P, dissipated by this force is equal to the product of force and velocity. The velocity at the top of the cube differs from that at the bottom by $dx\beta$. Therefore,

$$P = dx^3\mu\beta^2. \qquad \text{(Eq. 39)}$$

The power dissipated per volume (dx^3) is thus

$$W' = \mu\beta^2, \qquad \text{(Eq. 40)}$$

and the power dissipated per mass is

$$\epsilon = \mu\beta^2/\rho. \qquad \text{(Eq. 41)}$$

Equating Equations 35 and 40 and solving for β, we find that the average velocity gradient in the fluid in a surge channel is:

$$\beta_{avg} \approx 0.532\rho^{1/2}g^{3/4}H^{1/4}(1 - R^{5/2})^{1/2}(\tan \alpha)^{1/2}\mu^{-1/2}, \qquad \text{(Eq. 42)}$$

and (from Eq. 37) the average shear stress in the fluid is

$$\sigma_{avg} \approx 0.532\rho^{1/2}g^{3/4}H^{1/4}(1 - R^{5/2})^{1/2}(\tan \alpha)^{1/2}\mu^{1/2}. \qquad \text{(Eq. 43)}$$

Note that these are *average* values for shear and shear stress. At any point in the fluid, instantaneous values likely vary through time. For each interval where the shear stress is lower than average, however, there must be a compensating interval in which stress is larger than average.

We are now in a position to evaluate directly the small-scale flow regime in surge channels and to explore its biological consequences.

For a slope of 1:5, a breaking wave height of 1 m, a reflection coefficient of 0.29, and a dynamic viscosity of 1 $\times$ 10^{-3} Pa s, the average rate of energy dissipation within a surge channel is 1.66 W kg^{-1} (Eqs. 40 and 41). From this value we estimate that the eddies associated with maximal shear stresses are approximately 1094 μm in diameter, 11–14 times the diameter of sea urchin eggs (80–100 μm). The smallest eddies likely to be found in surf-zone flow are about 137–273 μm in diameter. Even these small eddies are larger than typical gametes, suggesting that gametes in the surf zone experience a flow regime characterized primarily by linear shears rather than by turbulent eddies.

Note that the heat capacity of water is about 4200 J kg^{-1} K^{-1} (Weast, 1977). At the dissipation rate in this example, water is heated by only 0.0004°C s^{-1}. Thus, the energy dissipation within a surge channel is not sufficient to raise the temperature substantially, even for retention times of 100–1000 s.

For the typical conditions cited above, the average shear stress in the water is about 1.30 Pa, and the average mi-

croscale velocity gradient is 1304 s^{-1}. The presence of this gradient means that the velocity at one side of an egg is quite different from that at the opposite side, which causes the egg to rotate. The rate of rotation (in cycles per second) is (Happel and Brenner, 1983; Kessler, 1986)

$$\frac{\beta}{4\pi}. \qquad \text{(Eq. 44)}$$

In other words, an egg in a typical surf zone rotates on average about 104 times per second! Sperm oriented parallel to the velocity gradient (*i.e.*, the velocity at the tip of their flagellum is maximally different from that at their head) will also be rotated by the shear, but because sperm are elongated rather than spherical, rotation is likely to cease once the sperm lies perpendicular to the instantaneous gradient (*i.e.*, with its head and tail in flow at the same speed).

The practical results of the rapid rotation of eggs, the rapid re-orientation of sperm, and the large shear stresses in the fluid are difficult to estimate. Certainly the egg, as a solid object, will entrain fluid with it as it rotates, creating a complex, 3-dimensional, temporally variable boundary layer that must be crossed by sperm. Whether the rotation itself can affect contact between egg and sperm is less clear. Also unclear is whether surf-zone shear stresses are sufficient to dislodge sperm from the egg once they have attached, or to damage the sperm or egg directly, although Denny and Shibata (1989) note preliminary evidence that even low shear stresses can reduce the fraction of eggs fertilized in the laboratory.

While the precise effects of the small-scale flow regime are unclear, the motions of sperm and egg will surely be complex and highly dynamic in turbulent flow which may also impede effective contact and subsequent fertilization and development. As long as the effects of shear stress and egg rotation remain unknown, the calculations made here concerning the effectiveness of fertilization in surge channels must be taken with a grain of salt. If turbulence inhibits the contact and subsequent attachment of sperm to eggs, or if the rapid rotation of eggs is detrimental to their survival, the calculations made here may overestimate the effectiveness of fertilization.

Acknowledgments

We thank E. C. Bell, B. Gaylord, K. Mead, H. Lasker, C. Petersen, and an anonymous reviewer for helpful suggestions. This study was funded by NSF grant OCE-87-11688 to M. Denny.

Literature Cited

Caceci, M. S., and W. P. Cacheris. 1984. Fitting curves to data. *Byte* **9:** 340–362.

Denny, M. W. 1988. *Biology and the Mechanics of the Wave-Swept Environment.* Princeton University Press, Princeton, NJ. 329 pp.

Denny, M. W. in press. Roles of hydrodynamics in the study of life on wave-swept shores, in *Ecomorphology,* P. C. Wainwright and S. Reilly, eds. University of Chicago Press, Chicago, IL.

Denny, M. W., and M. F. Shibata. 1989. Consequences of surf-zone turbulence for settlement and external fertilization. *Am. Nat.* **134:** 859–889.

Happel, J., and H. Brenner. 1983. *Low Reynolds Number Hydrodynamics.* Martinus Nijhoff Publishers, Dordrecht. 553 pp.

Kessler, J. O. 1986. The external dynamics of swimming micro-organisms. Pp. 257–307 in *Progress in Phycological Research,* Vol. 4, F. E. Round and D. J. Chapman, eds. Biopress Ltd., Bristol.

Lazier, J. R. N., and K. H. Mann. 1989. Turbulence and diffusive layers around small organisms. *Deep-Sea Res.* **36:** 1721–1733.

Levitan, D. R. 1991. Influence of body size and population density on fertilization success and reproductive output in a free-spawning invertebrate. *Biol. Bull.* **181:** 261–268.

Levitan, D. R., M. A. Sewell, and F.-S. Chia. 1991. Kinetics of fertilization in the sea urchin *Strongylocentrotus franciscanus:* interaction of gamete dilution, age, and contact time. *Biol. Bull.* **181:** 371–378.

Levitan, D. R., M. A. Sewell, and F.-S. Chia. 1992. How distribution and abundance influence success in the sea urchin *Strongylocentrotus franciscanus. Ecology* **73:** 248–254.

Mandelbrot, B. B. 1982. *The Fractal Geometry of Nature.* W. H. Freeman and Co, New York. 460 pp.

Miller, R. 1985. Sperm chemo-orientation in the metazoa. Pp. 275–337 in *The Biology of Fertilization,* Vol. 2, C. B. Metz and A. Monroy, eds. Academic Press, New York.

Pennington, J. T. 1985. The ecology of fertilization of echinoid eggs: the consequences of sperm dilution, adult aggregation, and synchronous spawning. *Biol. Bull.* **169:** 417–430.

Petersen, C. W. 1991. Variation in fertilization rate in the tropical reef fish, *Halichores bivattus:* correlates and implications. *Biol. Bull.* **181:** 232–237.

Petersen, C. W., R. R. Warner, S. Cohen, H. C. Hess, and A. T. Sewell. 1992. Variable pelagic fertilization success: implications for mate choice and spatial patterns of mating. *Ecology* **73:** 391–401.

Schlichting, H. 1979. *Boundary Layer Theory.* 7th ed. McGraw Hill, New York. 817 pp.

Thornton, E. B., and R. T. Guza. 1983. Transformation of wave height distributions. *J. Geophys. Res.* **88:** 5925–5938.

U. S. Army Corps of Engineers. 1984. *Shore Protection Manual.* U. S. Government Printing Office, Washington, DC.

Vogel, H., G. Czihak, P. Chang, and W. Wolf. 1982. Fertilization kinetics of sea urchin eggs. *Math. Biosci.* **58:** 189–216.

Vogel, S. 1981. *Life in Moving Fluids.* Willard Grant Press, Boston, Massachusetts. 352 pp.

Weast, R. C. 1977. *Handbook of Chemistry and Physics.* Chemical Rubber Company, Cleveland, Ohio.

Yund, P. O. 1990. An *in situ* measurement of sperm dispersal in a colonial marine hydroid. *J. Exp. Zool.* **253:** 102–106.

Appendix I

s used in the text and the equation where each is defined or first used

Symbol	Definition	Units	Equation
A	Relative abundance of channels		29
$C_e(t)$	Concentration of eggs at time t	m^{-3}	9
$C_{\cdot}$	Concentration of virgin eggs	m^{-3}	16
$C_{e,x}$	Steady-state egg concentration	m^{-3}	11
$C_t(t)$	Relative dye concentration		1
$C_s(t)$	Concentration of sperm at time t	m^{-3}	6
$C_{s,v}$	Concentration of unattached sperm	m^{-3}	15
$C_{s,x}$	Steady-state sperm concentration	m^{-3}	8
$e(\tau)$	Dimensionless egg concentration		19
e_x	Steady-state e		24
$f(\tau)$	Fraction of eggs fertilized		
f_x	Steady-state fraction of fertilized eggs		27
F	Force	N	38
g	Acceleration due to gravity	$m\ s^{-2}$	30
H	Surge height	m	31
k	Exchange parameter	s^{-1}	1
L_v	Kolmogorov length scale	m	35
m	Mixing parameter		4
P	Energy flux into a surge channel	W	30
P′	Energy flux per meter of channel mouth	$W\ m^{-1}$	31
P'_n	Net P′	$W\ m^{-1}$	32
Q_e	Rate of egg release	s^{-1}	9
Q_s	Rate of sperm release	s^{-1}	6
R	Reflection coefficient		32
$s(\tau)$	Dimensionless sperm concentration		21
s_x	Equilibrium s		24
t	Time	s	1
T	Period of the surge	s	4
T_r	Expected residence time (1/k)	s	2
u_{avg}	Mean water velocity	$m\ s^{-1}$	14
u_*	Friction velocity	$m\ s^{-1}$	13
$v(\tau)$	Dimensionless concentration of virgin eggs		20
v_x	Equilibrium v		26
V	Channel volume at still water level	m^3	3
V_0	Surge channel volume at mean low water	m^3	3
V′	Maximal volume per meter of channel mouth	m^2	34
V'_{swl}	Volume per meter channel mouth at SWL	m^2	33
Δ V	Surge-induced increase in channel volume	m^3	3
W′	P'_n/V'	$W\ m^{-3}$	35
α	Bottom slope		33
β	Velocity gradient	s^{-1}	37
β_{avg}	Average velocity gradient	s^{-1}	42
ϵ	Rate of energy dissipation	$W\ kg^{-1}$	36
Θ	Dimensionless interaction parameter		22
μ	Dynamic viscosity of water	Pas	36
ρ	Water density	$kg\ m^{-3}$	30
σ	Shear stress	Pa	37
σ_{avg}	Average shear stress	Pa	43
τ	Dimensionless time		17
ϕ	Reaction parameter	$m^3\ s^{-1}$	12

Reference: *Biol. Bull.* **183**: 233–241. (October, 1992)

Is There Extraovarian Synthesis of Vitellogenin in Penaeid Shrimp?

M. FAINZILBER[1], M. TOM[1], S. SHAFIR[1], S. W. APPLEBAUM[2], AND E. LUBZENS[1,*]

[1]*Israel Oceanographic and Limnological Research, P.O. Box 8030, Haifa 31080, Israel, and*
[2]*Department of Entomology, Faculty of Agriculture, Hebrew University of Jerusalem, Rehovot, Israel*

Abstract. Extraovarian synthesis of vitellogenin (Vg), has been reported for several crustaceans, mainly in the subepidermal adipose tissue (SAT) or the hepatopancreas (HEP). The precise site(s) of Vg synthesis in penaeid shrimp is hitherto unknown and was investigated in a large local species *Penaeus semisulcatus* de Haan. Protein synthesis was determined in SAT and HEP tissue pieces incubated *in vitro*. Incubations were at 25°C for eight hours in an oxygen enriched atmosphere, under sterile conditions in a physiological medium, containing ^{14}C-leucine. At the end of the incubation period, tissue homogenates and medium samples were analyzed for *de novo* protein synthesis. Total protein synthesis was determined by trichloroacetic acid precipitation. Specific vitellin (Vt) synthesis was determined by radioimmunoprecipitation with a polyclonal Vt-specific antiserum. Characterization of other *de novo* synthesized proteins was carried out by fluorography from polyacrylamide gels. Subepidermal adipose tissues removed from females at all stages of ovarian development did not synthesize Vt-specific proteins, in spite of the fact that total protein synthesis levels were high. The major protein synthesized *de novo* in the SAT of males and females is a protein with an identical electrophoretic mobility as hemocyanin in polyacrylamide gels. *In vitro* protein synthesis in HEP tissues was low compared to SAT or ovary systems. Vt-specific *de novo* synthesized protein was identified in HEP's from early vitellogenic females, but constituted less than 15% of total protein synthesis. We have previously shown that ovarian tissues from vitellogenic females incubated *in vitro* exhibited high levels of protein synthesis, an average of 38% of which is Vt-specific (Browdy *et al.*, 1990, *J. Exp. Zool.* **255**: 205–215). The calculated Vt synthesis rates in ovaries were up to 23 times higher than in HEP. We conclude that the extraovarian contribution to vitellogenesis in *P. semisulcatus* is low.

Received 26 August 1991; accepted 1 June 1992.
* To whom correspondence should be sent.

Introduction

Vitellogenesis is associated with the formation of yolk globuli within the developing oocytes in the ovary. Proteins and lipids are the main constituents of yolk, and vitellin (Vt) is the major protein that accumulates within the ovary during this process (Adiyodi and Subramoniam, 1983; Meusy and Payen, 1988). Vitellogenesis is an endocrine-regulated process, and is therefore of interest as a central part of the female reproductive cycle (Quackenbush, 1986; Fingerman, 1987; Charniaux-Cotton and Payen, 1988). It has been intensively studied in the lower vertebrates (Tata, 1976; Lam *et al.*, 1978; Huang *et al.*, 1979) and in various groups of insects (Kanost *et al.*, 1990). There has been increasing interest in crustacean vitellogenesis, due to the growing commercial importance of crustaceans in aquaculture and the interest in new models for basic research (Laufer and Downer, 1988). A critical prerequisite for studying vitellogenesis at the endocrine and cellular levels is identification of the tissues that participate in the synthesis of yolk and its precursors.

The sites of synthesis of Vt or its precursor molecules have not yet been fully established for penaeid shrimps. A protein which reacts immunologically to antiserum prepared against purified Vt was found in the haemolymph of vitellogenic females. This protein, known as vitellogenin (Vg), has been reported in all species studied so far (Kerr, 1968; Ceccaldi, 1970; Wolin *et al.*, 1973; Fyffe and O'Connor, 1974; Caubere *et al.*, 1976; Meusy, 1980; Dehn *et al.*, 1983; Ferrero *et al.*, 1983; Marzari *et al.*, 1986; Tom *et al.*, 1987a; Suzuki, 1987; Nelson *et al.*, 1988; Quackenbush and Keeley, 1988; Quackenbush,

1989a). The presence in the haemolymph raises the question of possible extraovarian sites for synthesis of Vt or its precursor.

Previous studies on crustacean vitellogenesis have focused on two tissues as possible sites for Vg synthesis; ovarian follicular tissues, and hepatopancreases (HEP). *De novo* synthesis of Vt in the ovaries has been shown for one isopod (Gohar *et al.*, 1985) and several decapods (Lui and O'Connor, 1976; Eastman-Reks and Fingerman, 1985), including three species of penaeid shrimps (Yano and Chinzei, 1987; Quackenbush, 1989a, b; Browdy *et al.*, 1990). However, there is also convincing proof for extraovarian synthesis of Vg in the adipose tissues of isopods and amphipods (Picaud, 1980; Souty and Picaud, 1981; Junera and Meusy, 1982). Vt-positive immunoreactivity has been reported for the adipose tissue of *Parapenaeus longirostris* (Tom *et al.*, 1987a) and in the HEP of two brachyuran decapods (Paulus and Laufer, 1987). Different groups have reported conflicting results for *in vitro* Vg synthesis by the HEP in penaeids. Yano and Chinzei (1987) and Rankin *et al.* (1989) were unable to show *de novo* Vg synthesis in HEP of *Penaeus japonicus* and *Penaeus vannamei*, respectively. In contrast, Quackenbush (1989a, b) has reported *in vitro* synthesis of proteins immunoreactive with antibodies to yolk in cultures of the HEP of *Penaeus vannamei*. There have been no studies so far on *de novo* synthesis of Vg in penaeid adipose tissues.

Although there is sufficient evidence to support a role for the ovary in Vt synthesis in penaeids, the quantitative contribution of ovarian versus extraovarian synthesis is not clear. We have tried to clarify this question by studying protein synthesis *in vitro* in the three putative vitellogenic tissues of *Penaeus semisulcatus*. We have recently shown that the ovaries of this species synthesize Vt *in vitro*, and that the portion of Vt-specific synthesis from total-protein synthesis varies in accordance with ovarian developmental stages (Browdy *et al.*, 1990). In this report, we summarize our studies on protein and Vg synthesis in the adipose and hepatopancreatic tissues of this marine shrimp species.

Materials and Methods

Chemicals

Amino acids, HEPES, Bis-Tris, vitamins and supplements for media were cell-culture tested grade and were obtained from Sigma. [^{14}C(U)]leucine (308 mCi/m*M*) was purchased from New England Nuclear. All other reagents were of analytical grade.

Seawater

Mediterranean seawater (salinity 40‰) was pumped onshore into a central reservoir and used immediately. For *in vitro* cultures it was filtered through sieves and a 0.45 μm-membrane filter, and finally sterilized by filtering through a heat sterilized 0.22 μm-membrane filter. Dilutions were performed using deionized water (Ionex, Israel) prior to sterilization.

Animals

Adults of *P. semisulcatus* were collected in Haifa Bay, Israel. They were held in 3 m^3 running seawater tanks, at a density of 20 specimens per tank. Water was changed at a rate of 300% per day. Salinity was constant at 40‰, and temperature ranged from 18°C (winter) to 27°C (summer). The animals were fed once a day on a mixture of frozen fish, squid, shrimp, and *Artemia*. Females were individually marked by clipping of the uropods, and ovarian development was monitored externally, according to the methods of Browdy and Samocha (1985).

Polyacrylamide gel electrophoresis (PAGE) and electroblotting

Electrophoresis in non-denaturating conditions was performed according to Davis (1964) in 5% polyacrylamide gels. Coomassie Blue stains for proteins and dithiooxamide stains for copper-conjugated proteins were performed according to Hames and Rickwood (1981).

Western blots from PAGE were done using a Bio-Rad electroblotting apparatus at 400 mA for 4–5 h at 4°C. Proteins were transferred to nitrocellulose papers, dried, and stored at 4°C until staining. Immunostaining was according to Browdy *et al.* (1990).

Purification of Vt and preparation of rabbit specific antiserum

Vitellin was identified as the main constituent of ripe ovaries by comparing the electrophoretic profiles in non-denaturing polyacrylamide gels (PAGE) of ripe and undeveloped ovarian homogenates. It was purified from homogenates of ripe ovaries by two steps of column chromatography and one of preparative PAGE as described by Browdy *et al.* (1990). Anti-Vt serum was prepared in rabbits after injection of 0.5 mg Vt as described by Tom *et al.* (1987b). The specificity of the antiserum was verified by immunoblotting (Bio-Rad immunoblot assay system) against all the fractions obtained during the purification as shown in Browdy *et al.* (1990). The antiserum reacted only with the Vt fraction.

Determination of oocyte diameter

Prior to *in vitro* incubations, a piece of tissue was removed from each ovary tested then fixed in 4% formalin in seawater. The average oocyte diameter was determined as described by Shlagman *et al.* (1986).

In vitro *incubation experiments*

Subepidermal adipose tissues (SAT's) were excised from females at different stages of vitellogenesis and from intermolt males. The SAT from each animal was divided into four pieces and each was incubated in Landureau's medium modified for penaeid tissues as described in Fainzilber *et al.* (1989). ^{14}C-leucine was added to a final concentration of 0.25 μCi/ml. Cold leucine level in the media was 0.11 m*M*.

Incubations were at 25°C with gentle shaking and an oxygen enriched atmosphere. Following the incubation period, tissues were removed and homogenized in 0.1 *M* phosphate buffer. Homogenates were centrifuged at 14,000 rpm for 10 min in an Eppendorf Microfuge at 4°C. *De novo* synthesized proteins were determined by TCA precipitation. Samples of tissue homogenates, supernatant, and the incubation media were pipetted onto Whatman 3 mm filter paper discs, dried, precipitated in 10% TCA, and washed according to Mans and Novelli (1961). Discs were counted in scintillation vials with 5 ml Aquasol-2 (New England Nuclear) in a Kontron Betamatic liquid scintillation counter, and quenching was monitored by measuring sample channels ratio (SCR). The specific activities of the media (cpm/μg leucine) were calculated from samples prepared on filter paper discs, and final results were calculated as μg leucine incorporated into TCA precipitable protein. Control incubations were carried out with media containing labelled leucine but lacking tissue and with tissue incubated without labelled leucine. Tissue protein was determined by the method of Bradford (1976).

Radioimmunoprecipitation (RIP) was carried out by taking 50 μl samples from tissue homogenates, supernatants and media. These samples were mixed with precalibrated volumes of anti-Vt serum after the addition of 0.1 mg purified Vt, to ensure maximum precipitation. Reaction volumes were adjusted to 1 ml with 0.4 *M* NaCl. Incubation was for 1 h at room temperature, after which vials were further incubated at 4°C for 24 h. Normal rabbit serum (NRS) was added instead of anti-Vt serum in control vials. Additional controls included NRS with a calibrated amount of goat-anti-rabbit serum, to obtain a large non-specific pellet. Following the incubation at 4°C, samples were centrifuged and the pellet washed three times with 0.4 *M* NaCl. Finally the pellet was dissolved in 75 μl of 0.5 *M* NaOH and incubated with vigorous shaking for 1 h at 37°C. The dissolved pellet was neutralized with 2 *M* HCl and the complete sample was applied to Whatman 3 mm paper discs, dried, and counted as described above.

The hepatopancreas was excised from previtellogenic and vitellogenic females and intermolt males, weighed, and each cut into 8–12 pieces. Each piece was weighed separately. They were prewashed for 1 h with frequent changes of media and each piece was incubated separately. Pieces of HEP were homogenized in their incubation media, centrifuged, and supernatants taken for analysis. Protease inhibitors (0.2 m*M* PMSF, 1 m*M* Aprotinin, 1 m*M* Leupeptin) were added, and the samples were analyzed as described above. All controls were as described for SAT incubations, with the addition of a zero time incubation control. Pieces of HEP were immersed in incubation media containing ^{14}C-leucine and were immediately homogenized and processed for analysis. Zero-time controls and background counts were similar. There was no difference between incubations with or without protease inhibitors. A number of different media compositions were tried and the best composition was found to be the modified Landureau medium buffered with Bis-Tris to pH 6.5.

All incubations and RIP were performed in culture plates or tubes coated with Sigmacote (Sigma Chemical Co.).

For fluorography from PAGE, incubations were as described above, except that media contained 2.5 μCi/ml ^{14}C-leucine and no cold leucine. Samples from these incubations were separated on PAGE. Gels were fixed in 7.5% acetic acid for 1 h, washed, and immersed in Amplify (Amersham, U.K.) for 30 min. Afterwards, gels were dried at 60°C under vacuum and exposed to Kodak XAR5 films at −70°C.

Collection of hemolymph and identification of hemocyanin

Hemolymph was removed from shrimp by cutting the rostrum and bleeding into 1 ml of a 10% sodium citrate solution. The hemolymphs of several females or several males were pooled and placed separately into test tubes. Hemocyanin was identified as the main constituent of whole hemolymph, which stained positively for copper (Horn and Kerr, 1963, 1969).

Results

Protein synthesis in in vitro *incubated SAT*

De novo protein synthesis and secretion to the medium were measured at regular time intervals during the incubation of the adipose tissues, and were found to increase linearly after an initial lag period of about 4 h, with a similar rate of protein synthesis in a male control (Fig. 1). Over 90% of the *de novo* synthesized TCA precipitable proteins were found in the medium fraction. A comparison of levels of total protein synthesis in SAT's of 13 females at different stages of vitellogenesis showed a large variability between females at the same vitellogenic stage, but failed to show any correlation between the vitellogenic

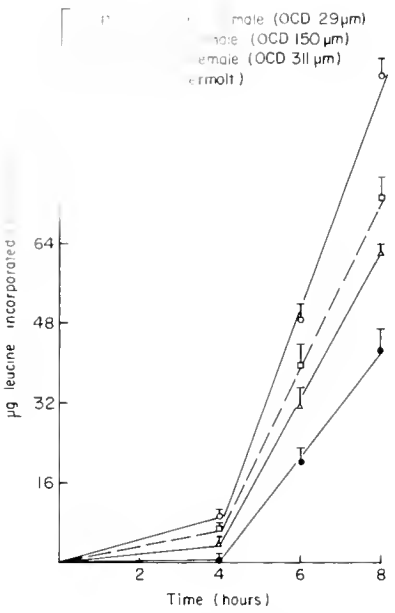

Figure 1. The incorporation rate of leucine into protein secreted by *in vitro* incubated subepidermal adipose tissue (SAT) in *Peneaus semisulcatus*. Tissues were removed from a male, and previtellogenic and vitellogenic females. Results were calculated for whole SAT. The mean ± S.D. for four replicates are given in each case. The average oocyte diameter (OCD) in ovaries is indicated (in μm) for each female.

stage and the synthesis of proteins in the adipose tissues (Table I). In excess antibody precipitations of all the samples, no Vt-specific proteins were detected. Ovaries from the same females all produced Vt *in vitro*, at levels averaging 38% of the total *de novo* synthesized protein (Browdy *et al.*, 1990; Table I).

SAT proteins were separated in non-denaturating polyacrylamide gels. Total proteins were visualized with Coomassie Blue (Fig. 2A), while incorporation of radiolabel into *de novo* synthesized SAT proteins was visualized by fluorography (Fig. 2B). Vt-specific immunological staining was performed on Western blots (Fig. 2C) and copper conjugated proteins by dithio-oxamide staining (Fig. 2D). Samples from previtellogenic and vitellogenic females and control males were run on each gel. Figure 2C shows that samples from SAT's of vitellogenic females stained positive for Vt. However, Vt was not visualized in the fluorographic exposures (Fig. 2B). One major radioactive band is seen in the fluorography of all the samples, including the male control. Based on the position of this band versus the position of hemocyanin (Fig. 2A), and on a positive reaction with the copper stain (Fig. 2D), the main *de novo* synthesized protein in adipose tissues appears to be hemocyanin or a copper containing protein with a similar electrophoretic mobility in non-denaturating polyacrylamide gels.

Protein synthesis in in vitro *incubated HEP*

Protein synthesis was measured in HEP incubated *in vitro* in a number of media and culture conditions, including those of Quackenbush (1989a, b). Protein synthesis in these cultures was low, and typically only 4–7% of the available label was incorporated into TCA precipitable proteins. This compares to 14–23% for ovarian

Table I

In vitro *protein synthesis in tissues of female (F) and male (M)* Penaeus semisulcatus

Tissue	Sex	Vitellogenic stage and oocyte diameter (μm)	Number of replicates[a]	Total protein synthesis[b]	Vt specific fraction[c] (%)
SAT	F	previtellogenic (≤100)	4	39.8 ± 15	0
	F	vitellogenic (100–300)	6	25.2 ± 9.2	0
	F	late vitellogenic (300–380)	3	28.2 ± 6.6	0
	M	—	4	26.6 ± 8.4	0
HEP	F	previtellogenic (≤100)	4	2.6 ± 1.3	5.2 ± 2.9
	F	vitellogenic (130–200)	4*	4.6 ± 1.6	14.4 ± 1.1
	F	vitellogenic (247–299)	5	0.4 ± 0.2	3.7 ± 2.0
	M	—	5	0.8 ± 0.3	0.8 ± 0.6
Ovary[d]	F	previtellogenic (≤100)	5	11.2 ± 3.1	5.0 ± 3.2
	F	vitellogenic (110–200)	4	55.2 ± 10.8	34.3 ± 4.7
	F	vitellogenic (220–281)	4	39.1 ± 4.5	42.3 ± 7.6

[a] Each replicate represents 2–3 pieces of tissue from a single animal, except where marked *. In this case, two pieces each from two animals were used.

[b] μg leucine incorporated into TCA precipitable protein per whole organ after 6 h of incubation (mean ± S.D.).

[c] Fraction of Vt specific immunoprecipitable protein from total *de novo* synthesized TCA precipitable protein (mean ± S.D.).

[d] Ovary data are based on Browdy *et al* (1990; Figs. 5, 6) and are shown for comparison.

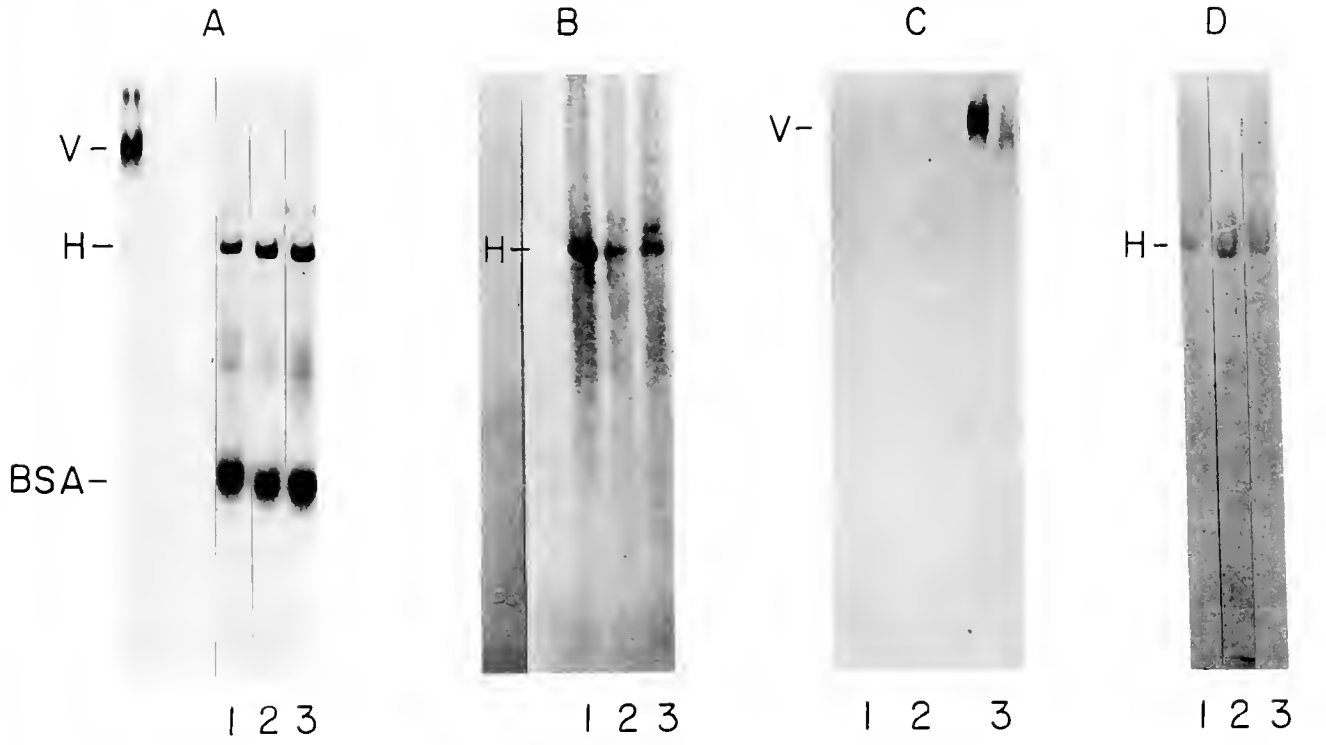

Figure 2. Non-denaturing polyacrylamide gel electrophoresis (5%) of protein synthesized *in vitro* by subepidermal adipose tissue (SAT) in *Peneaus semisulcatus*. Medium fractions only shown. (A) Coomassie blue stained gels. (B) Fluorography after 9 days of exposure. (C) Vt-specific immunological stain after Western blotting. (D) Copper-conjugated protein stain. Lanes: (1) male; (2) previtellogenic female (40 μm OCD); and (3) vitellogenic female (164 μm OCD). The positions of vitellin (V) and hemocyanin (H), which were run in separate lanes in the same gels, is indicated. Bovine serum albumin (BSA) was included in the culture media. Each lane in A, C, and D was run with 25 μl aliquots. In gels visualized by fluorography each lane was loaded with a sample containing 15,000–30,000 cpm of TCA precipitable protein.

cultures and 50–61% for SAT. The best conditions were found to be incubation in Landureau's medium modified for penaeid tissue (Fainzilber *et al.*, 1989) at pH 6.5 with 20 m*M* Bis-Tris. Protein synthesis rates in HEP from 11 females under these conditions differed according to the stage of vitellogenesis (Fig. 3, Table I), and were highest for females at an early stage of vitellogenesis (OCD 130–200 μm). Excess antibody precipitations revealed Vt-specific label ranging from 3.7% of total proteins synthesized in late vitellogenic females to 14.4% in early vitellogenesis (Table I). Male HEP cultures were also found to contain Vt-specific label, at near-background levels of 0.8%.

Comparison between different tissues

To evaluate the possible quantitative significance of the Vt synthesis in HEP cultures, leucine incorporation results were translated into Vt synthesis rates, calculated from the molar ratio of leucine in purified *Penaeus semisulcatus* Vt (Tom *et al.*, in press). These calculated Vt synthesis values were corrected to allow for the 2 h lag in protein synthesis observed in HEP incubations of early vitellogenic females (Fig. 3), and the final values obtained represent synthesis rates during the linear phase. Similar calculations were performed for ovaries incubated *in vitro*, from the data of Browdy *et al.* (1990). Ovarian Vt synthesis rates ranged from 1.2 μg Vt/whole ovary/h in previtellogenic females to 36.4 μg Vt/whole ovary/h in vitellogenic females (Fig. 4). These values were 3–23 times higher than the corresponding Vt synthesis rates in HEP cultures (0.34–1.6 μg Vt/whole HEP/h in previtellogenic and early vitellogenic females, Fig. 4).

Fluorography of TCA precipitates from female HEP samples run on polyacrylamide gels failed to show radioactivity in the region of the Vt band, which is clearly seen in the parallel lane of an ovary sample (Fig. 5). One of the main bands seen in fluorography of samples from HEP incubations has the same position as does the putative hemocyanin band from SAT samples (Fig. 5).

Discussion

The results shown above and those of Browdy *et al.* (1990) strongly suggest that the ovary is the main site of

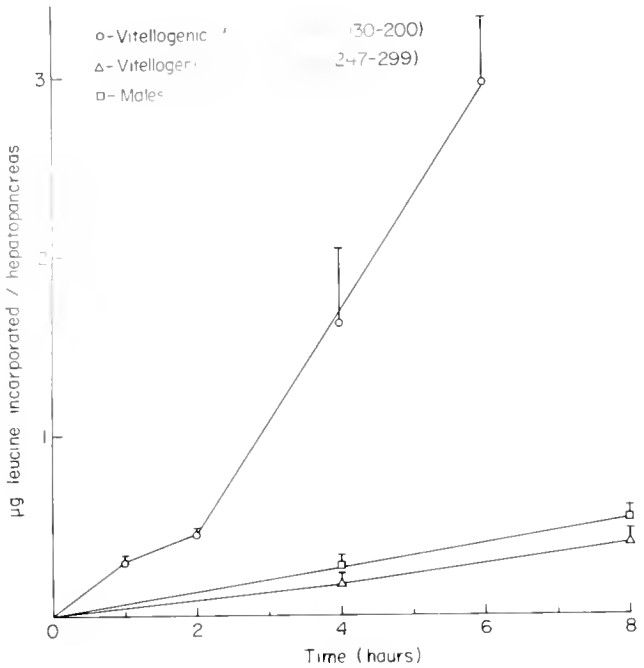

Figure 3. The incorporation rate of leucine into protein by *in vitro* incubated hepatopancreas pieces in *Peneaus semisulcatus*. Results (mean ± S.D.) were calculated per whole hepatopancreas and are presented for males and early and late vitellogenic females. Mean ± S.D. for four replicates at each time point are shown. The average oocyte diameters (OCD) in the ovaries of the females are indicated in µm.

Vt synthesis in *Penaeus semisulcatus* and that the SAT has no role in this process. These conclusions are based on Vt-specific immunoprecipitations (Table I) and fluorography of samples on PAGE (Fig. 2). The main protein synthesized in *in vitro* incubations of SAT appears to be hemocyanin or a related protein based on its positive copper stain and position in PAGE (Fig. 2). The fact that the SAT-synthesized protein has the same position in PAGE as the main HEP product (Fig. 5) is noteworthy, since the HEP is a well characterized hemocyanin synthesizing tissue in decapod crustaceans (Senkbeil and Wriston, 1981; Bielefeld *et al.*, 1986; Preaux *et al.*, 1986). There are no previous reports of hemocyanin synthesis in adipose tissues of Crustacea.

Hemocyanin accounts for 90–95% of the hemolymph serum proteins in crustaceans (Horn and Kerr, 1969; Rochu and Fine, 1978; Ferrero *et al.*, 1983; Hagerman, 1983; de Fur *et al.*, 1985). Most of the copper found in the hemolymph (about 95%) was found to be bound to hemocyanin (Horn and Kerr, 1963). Evidence in the literature strongly suggests the midgut gland (HEP) as a site of synthesis of hemocyanin in several crustacean species (see review of Mangum, 1983). However, Ghiretti-Magaldi *et al.* (1977) postulated a "lymphocytogluic" organ associated with the gizzard, and Senkbeil and Wriston (1981) observed synthesis on the "intestinal wall". The high levels of synthesis found in the present report suggest that the SAT may be a major hemocyanin synthesizing tissue in penaeid shrimp, and should motivate additional research into the role of adipose tissues in this process.

The quantitative significance of the HEP in Vg synthesis in penaeid shrimp is still unclear. The data shown above (Table I, Fig. 4), suggest that this tissue synthesizes a Vt-immunoreactive protein in previtellogenic and early vitellogenic females. However, it seems that quantitatively the contribution of the HEP is low. Previous studies of protein synthesis *in vitro* in HEP of *Penaeus japonicus* and *Penaeus vannamei* have reported conflicting results. Yano and Chinzei (1987) did not detect synthesis of Vt-specific proteins in *in vitro* incubated HEP of *P. japonicus*. However, their incubations were performed in salts ringer without buffer, vitamins and sugar supplements, that we have found to be essential for cultures of HEP, and the total protein synthesis they reported was very low. Rankin *et al.* (1989) reported that incorporation of radiolabelled leucine in *in vitro* incubated HEP of *P. vannamei* was relatively high early in the cycle of ovarian development. They did not observe changes in the SDS-PAGE peptide pattern during ovarian development, and did not use antibodies or other means of identifying Vg specific synthesis. The synthesis of yolk proteins reported by

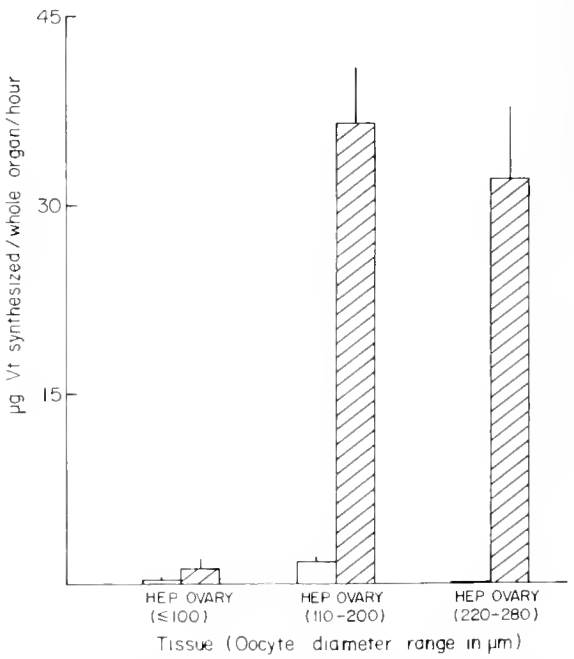

Figure 4. Vitellin synthesis rates in hepatopancreases (HEP) versus ovaries incubated *in vitro*, in females of *Peneaus semisulcatus* at different stages of vitellogenesis. Ovary data are calculated from the results of Browdy *et al.* (1990). Synthesis rates are calculated for the whole organ, and represent the linear phase of protein synthesis, after the lag period (see Fig. 1).

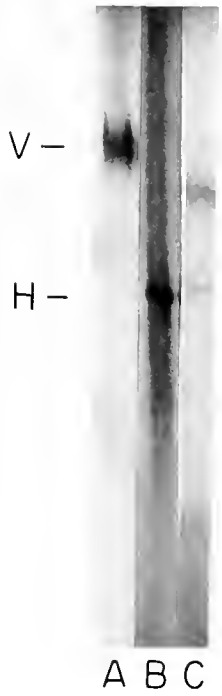

Figure 5. Comparative fluorography of proteins synthesized *de novo* in the ovary (A), subepidermal adipose tissue (B), and hepatopancreas (C), during *in vitro* incubations of tissues from vitellogenic females of *Penaeus semisulcatus*. The positions of vitellin (V) and hemocyanin (H) are shown. 15,000 cpm of TCA precipitable proteins were loaded in each lane.

Quackenbush (1989a, b) for HEP of *Penaeus vanammei* is not clearly attributable to Vg synthesis. This is due to the use of an antigen for antibody production which does not represent the whole Vt. This antigen was a 97 kD protein resolved from SDS-PAGE (and therefore in denaturated form) and found in both ovaries and HEP. The antibody to this antigen reacted with three different ovarian proteins and one hepatopancreatic protein. The levels of immunoreactive proteins in ovaries of *P. vannamei*, when measured with this antibody, reached a maximum level of 8% of total tissue protein (Quackenbush, 1989b), much lower than the expected levels for the main storage protein of a mature penaeid ovary (Rankin *et al.*, 1989).

Our comparison of the Vt synthesis rates per whole organ in HEP versus ovary (Fig. 4) clearly shows that there is a difference of one order of magnitude in Vt synthesis rates in these two organs incubated *in vitro*. We cannot rule out the possibility that this difference is less extreme *in vivo*. However, Vg hemolymph levels and turnover were found to be low in both previtellogenic and vitellogenic *P. semisulcatus* females (Shafir *et al.*, 1992 and unpub. obs.). These results lead us to the conclusion that although the HEP may be involved in the synthesis of some ovarian proteins, its quantitative significance is probably low. The possibility that the HEP may be involved in synthesis of an exclusively extraovarian Vt component has yet to be shown.

Vitellin-specific immunoreactivity has been found in SAT samples of *Penaeus semisulcatus* (Fig. 2C), *P. japonicus* (Vazquez-Boucard, 1985) and *Parapenaeus longirostris* (Tom *et al.*, 1987a). Vitellin-positive reactions have also been observed in the immunohistological preparations of HEP from two brachyuran decapods (Paulus and Laufer, 1987). These results show the presence of Vt immunoreactive compounds, but do not provide evidence for active synthesis of these compounds in the tissues examined. A high molecular weight Vt immunoreactive compound has been found in the hemolymph of several crustaceans. The Vt positive reactions in tissues may be due to absorption of hemolymph in the incubated tissues, or may suggest a role for these tissues in the catabolism of Vt following resorption of oocytes. Oocyte resorption provides one of the explanations for the presence of Vt immunoreactivity in the hemolymph. It is also possible that such immunoreactivity results from Vg synthesis in ovarian follicle cells, secretion of the Vg into the hemolymph, and subsequent uptake into developing oocytes (Yano and Chinzei, 1987).

It should be noted that most of the data supporting the ovary as a single or main site of Vt synthesis in penaeids have been obtained from *in vitro* systems. Such systems, although possessing many advantages for subsequent endocrinological studies, might not provide the necessary conditions for a specific tissue to function as it does *in vivo*. Conversely, an *in vivo* experimental approach does not allow the clear isolation of a specific tissue's contribution. Identification of yolk protein mRNA from tissues of females at different stages of vitellogenesis, using *in vitro* translation systems could clarify this issue. These techniques have been used with success for the study of hemocyanin synthesis in crayfish (Bielefeld *et al.*, 1986). The feasibility of this approach is currently under examination in our laboratory.

To summarize, our results and other recent publications suggest that the ovary is the most prominent site for Vt synthesis in penaeid shrimp. This is in contrast to the extraovarian synthesis of Vg in Isopoda and Amphipoda (Meusy and Payen, 1988). It seems that different groups of crustaceans use different strategies for the synthesis of their yolk proteins. In this respect, crustaceans are apparently similar to insects, in which at least three different strategies of yolk protein synthesis have been characterized (Kanost *et al.*, 1990). It is noteworthy that insects with different strategies of yolk synthesis also differ in various aspects of the endocrine regulation of this process, a fact with interesting implications for future studies of endocrine regulation of vitellogenesis in crustaceans.

Acknowledgments

This research was supported by grants from the Israeli Ministry of Energy and Infrastructure, the Binational Agricultural Research and Development Fund (Project No. I-147-[illegible]), and the Basic Research Fund of the Israeli National Academy of Sciences (Project No. 231/91). We thank Dr. Craig Browdy for helpful discussions, and two anonymous reviewers for their constructive criticism.

Literature Cited

Adiyodi, R. G., and T. Subramoniam. 1983. Oogenesis, Oviposition, and Oosorption. Pp. 443–495. In *Reproductive Biology of Invertebrates*, Vol. 1., K. G. Adiyodi and R. G. Adiyodi, eds. Wiley, New York.

Bielefeld, M., G. Gellissen, and K. D. Spindler. 1986. Protein production and the moulting cycle in the crayfish *Astacus leptodactylus*. *Insect Biochem.* **16:** 175–180.

Bradford, M. M. 1976. A rapid and sensitive method for the quantitation of microgram quantities of protein utilizing the principle of protein dye binding. *Anal. Biochem.* **72:** 248–254.

Browdy, C. L., and T. M. Samocha. 1985. The effect of eyestalk ablation on spawning, molting and mating of *Penaeus semisulcatus* de Haan. *Aquaculture* **49:** 19–29.

Browdy, C. L., M. Fainzilber, M. Tom, Y. Loya, and E. Lubzens. 1990. Vitellin synthesis in relation to oogenesis in *in vitro* incubated ovaries of *Penaeus semisulcatus* (Crustacea, Decapoda, Penaeidae). *J. Exp. Zool.* **255:** 205–215.

Caubere, J. L., R. Lafon, F. Rene, and C. Sales. 1976. Maturation et ponte chez *Penaeus japonicus* en captivite, essai de controle de cette reproduction a Maguelonne dans les cotês Françaises. FAO Tech. Conf. on Aquaculture, Kyoto, Japan. FIR:AQ/Conf/76/E.49. 18 pp.

Ceccaldi, H. J. 1970. Evolution des proteines de l'hemolymphe de *Penaeus kerathurus* femelle durant la vitellogenese. *C.R. Seances Soc. Biol. Fil.* **164:** 2572–2575.

Charniaux-Cotton, H., and G. Payen. 1988. Crustacean reproduction. Pp. 279–303 in *Endocrinology of Selected Invertebrate Types*, vol. 2. H. Laufer, and R. G. H. Downer, eds. Alan R. Liss Inc., New York.

Davis, B. J. 1964. Disc electrophoresis. II. Method and application to human serum proteins. Ann. N.Y. Acad. Sci. **121:** 404–427.

De Fur, P. L., C. P. Mangum, and B. R. McMahon. 1985. Cardiovascular and ventilatory changes during ecdysis in the blue crab *Callinectes sapidus* Rathbun. *J. Crust. Biol.* **5:** 207–215.

Dehn, P. F., D. E. Aiken, and S. L. Waddy. 1983. Aspects of vitellogenesis in the lobster *Homarus americanus*. *Can. Tech. Rep. Fish. Aquat. Sci.* **1161:** iv + 24 pp.

Eastman-Reks, S., and M. Fingerman. 1985. *In vitro* synthesis of vitellin by the ovary of the fiddler crab *Uca pugilator*. *J. Exp. Zool.* **233:** 111–116.

Fainzilber, M., C. L. Browdy, M. Tom, E. Lubzens, and S. W. Applebaum. 1989. Protein synthesis *in vitro* in cultures of the subepidermal adipose tissue and the ovary of the shrimp *Penaeus semisulcatus*. *Tissue Cell* **21:** 911–916.

Ferrero, E. A., G. Graziosi, R. Marzari, and A. Mosco. 1983. Protein pattern variability of the hemolymph of mantis shrimp, *Squilla mantis* L. (Crustacea, Stomatopoda). *J. Exp. Zool.* **225:** 341–345.

Fingerman, M. 1987. The endocrine mechanisms of crustaceans. *J. Crust. Biol.* **7:** 1–24.

Fyffe, W. E., and J. D. O'Connor. 1974. Characterization and quantification of a crustacean lipovitellin. *Comp. Biochem. Physiol.* **47B:** 851–867.

Ghiretti-Magaldi, A., C. Milanesi, and G. Tognon. 1977. Hemopoiesis in Crustacea Decapoda: origin and evolution of hemocytes and cyanocytes of *Carcinus maenas*. *Cell Diff.* **6:** 167–186.

Gohar, M., C. Souty-Grosset, and R. Juchault. 1985. Rhythme nycthemeral de la synthese proteique ovarienne chez le crustacé oniscoide *Porcellio dilatatus* Brandt et rôle du protocerebron. *Can. J. Zool.* **63:** 799–803.

Hagerman, L. 1983. Haemocyanin concentration of juvenile lobsters (*Homarus gammarus*) in relation to moulting cycle and feeding conditions. *Mar. Biol.* **77:** 11–17.

Hames, B. D., and D. Rickwood. 1981. *Gel Electrophoresis of Proteins. A Practical Approach.* IRL Press, Oxford, 290 pp.

Horn, E. C., and M. S. Kerr. 1963. Hemolymph protein and copper concentrations of adult blue crabs (*Callinectes sapidus* Rathbun). *Biol. Bull.* **125:** 499–507.

Horn, E. C., and M. S. Kerr. 1969. The hemolymph proteins of the blue crab, *Callinectes sapidus*. I. Hemocyanins and certain other major protein constituents. *Comp. Biochem. Physiol.* **29:** 493–508.

Huang, E. S., K. J. Kao, and A. V. Nalbandov. 1979. Synthesis of sex steroids by cellular components of chicken follicles. *Biol. Reprod.* **20:** 454–461.

Juncra, H., and J. J. Meusy. 1982. Vitellogenin and lipovitellins in *Orchestia gammarellus* (Pallas) (Crustacea, Amphipoda); labelling of subunits after *in vivo* administration of ^{3}H-leucine. *Experientia* **38:** 252–253.

Kanost, M. R., J. K. Kawooya, J. H. Law, R. O. Ryan, M. C. Van Heusden, and R. Ziegler. 1990. Insect haemolymph proteins. Pp. 299–396 in *Advances in Insect Physiology*, vol. 22. Academic Press, New York.

Kerr, M. S. 1968. Protein synthesis by the hemocytes of *Callinectes sapidus*: a study of *in vitro* incorporation of ^{14}C-leucine. *J. Cell. Biol.* **39:** 72a–73a.

Lam, T. J., S. Pandey, Y. Nagahama, and W. S. Hoar. 1978. Endocrine control of oogenesis, ovulation and oviposition in goldfish. Pp. 55–64 in *Comparative Endocrinology*. P. J. Gaillard, and H. H. Boer, eds. Elsevier, Amsterdam.

Laufer, H., and R. G. H. Downer. 1988. *Endocrinology of Selected Invertebrate Types.* Alan R. Liss Inc., New York, 500 pp.

Lui, C. W., and J. D. O'Connor. 1976. Biosynthesis of lipovitellin by the crustacean ovary. II. Characterization and *in vitro* incorporation of amino acids into the purified subunits. *J. Exp. Zool.* **195:** 41–52.

Mangum, C. P. 1983. Oxygen transport in the blood. Pp. 373–429 in *The Biology of Crustacea*, vol. 5. D. E. Bliss, ed. Academic Press, New York.

Mans, R. J., and G. D. Novelli. 1961. Measurement of the incorporation of radioactive amino acids into protein by a filter paper disk method. *Arch. Biochem. Biophys.* **94:** 48–53.

Marzari, R., E. Ferrero, A. Mosco, and A. Savoini. 1986. Immunological characterization of the vitellogenic proteins in *Squilla mantis* hemolymph (Crustacea, Stomatopoda). *Exp. Biol.* **45:** 75–80.

Meusy, J. J. 1980. Vitellogenin, the extraovarian precursor of the protein yolk in Crustacea: a review. *Reprod. Nutr. Develop.* **20:** 1–21.

Meusy, J. J., and G. G. Payen. 1988. Female reproduction in malacostracan Crustacea. *Zool. Sci.* **5:** 217–265.

Nelson, K., B. Heyer, E. Johnson, D. Hedgecock, and E. S. Chang. 1988. Photoperiod-induced changes in hemolymph vitellogenins in female lobsters (*Homarus americanus*). *Comp. Biochem. Physiol.* **90B:** 809–821.

Paulus, J. E., and H. Laufer. 1987. Vitellogenocytes in the hepatopancreas of *Carcinus maenas* and *Libinia emarginata* (Decapoda Brachyura). *Int. J. Invertebr. Reprod. Develop.* **11:** 29–44.

Picaud, J. L. 1980. Vitellogenin synthesis by the fat body of *Porcellio dilatatus* Brandt (Crustacea, Isopoda). *Int. J. Invertebr. Reprod.* **2:** 347–349.

Preaux, G., A. Vandamme, B. de Bethune, M. P. Jacobs, and R. Lontie. 1986. Hemocyanin-mRNA-rich fractions of Cephalopodan Decabranchia and of Crustacea, their *in vivo* and *in vitro* translation. Pp. 485–488 in *Invertebrate Oxygen Carriers*. B. Linzen, ed. Springer-Verlag, Berlin.

Quackenbush, L. S. 1986. Crustacean endocrinology, a review. *Can. J. Fish. Aquat. Sci.* **43:** 2271–2282.

Quackenbush, L. S. 1989a. Vitellogenesis in the shrimp, *Penaeus vannamei: in vitro* studies of the isolated hepatopancreas and ovary. *Comp. Biochem. Physiol.* **94B:** 253–261.

Quackenbush, L. S. 1989b. Yolk protein production in the marine shrimp *Penaeus vannamei*. *J. Crust. Biol.* **9:** 509–516.

Quackenbush, L. S., and L. L. Keeley. 1988. Regulation of vitellogenesis in the fiddler crab, *Uca pugilator*. *Biol. Bull.* **175:** 321–331.

Rankin, S. M., J. Y. Bradfield, and L. L. Keeley. 1989. Ovarian protein synthesis in the South American white shrimp, *Penaeus vannamei*, during the reproductive cycle. *Invertebr. Reprod. Dev.* **15:** 27–33.

Rochu, D., and J. M. Finc. 1978. Antigenic structure of the hemocyanin in six species of decapod Crustacea. *Comp. Biochem. Physiol.* **59A:** 145–150.

Senkbeil, E. G., and J. C. Wriston. 1981. Hemocyanin synthesis in the American lobster *Homarus americanus*. *Comp. Biochem. Physiol.* **68B:** 163–171.

Shafir, S., M. Tom, M. Ovadia, and E. Lubzens. 1992. Protein, vitellogenin and vitellin levels in the haemolymph and ovaries during ovarian development in *Penaeus semisulcatus* (de Haan). *Biol. Bull.* **183:** (in press).

Shlagman, A., C. Lewinsohn, and M. Tom. 1986. Aspects of the reproductive activity of *Penaeus semisulcatus* de Haan along the southeastern coast of the Mediterranean. *Mar. Ecol.* **7:** 15–22.

Sooty, C., and J. L. Picaud. 1981. Vitellogenin synthesis in the fat body of the marine crustacean Isopoda *Idotea balthica baoteri* during vitellogenesis. *Reprod. Nutr. Dev.* **21:** 95–101.

Suzuki, S. 1987. Vitellins and vitellogenins of the terrestrial isopod, *Armadillidium vulgare*. *Biol. Bull.* **173:** 345–354.

Tata, J. R. 1976. The expression of the vitellogenin gene. *Cell* **9:** 1–14.

Tom, M., M. Goren, and M. Ovadia. 1987a. Localization of the vitellin and its possible precursors in various organs of *Parapenaeus longirostris* (Crustacea, Decapoda, Penaeidae). *Int. J. Invertebr. Reprod. Dev.* **12:** 1–12.

Tom, M., M. Goren, and M. Ovadia. 1987b. Purification and partial characterization of vitellin from the ovaries of *Parapenaeus longirostris* (Crustacea, Decapoda, Penaeidae). *Comp. Biochem. Physiol.* **87B:** 17–23.

Tom, M., M. Fingerman, T. K. Hayes, V. Johnson, B. Kerner, and E. Lubzens. in press. A comparative study of the ovarian proteins from two penaeid shrimps, *Penaeus semisulcatus* (De Haan) and *Penaeus vannamei* (Boone). *Comp. Biochem. Physiol.*

Vazquez-Boucard, C. 1985. Identification preliminaire du tissu adipeux chez le crustacé Decapode *Peneus japonicus* Bate, a l'aide de anticorps antilipoistellene. *C R. Acad. Sci. Ser. III Sci. Vie* **300:** 95–97.

Wolin, E. M., H. Laufer, and D. F. Albertini. 1973. Uptake of the yolk protein, lipovitellin, by developing crustacean oocytes. *Dev. Biol.* **35:** 160–170.

Yano, I., and Y. Chinzei. 1987. Ovary is the site of vitellogenin synthesis in kuruma prawn, *Penaeus japonicus*. *Comp. Biochem. Physiol.* **86B:** 213–218.

Reference: *Biol. Bull.* 183: 242–247. (October, 1992)

In vivo Incorporation of Labeled Methionine into Proteins, Vitellogenin, and Vitellin in Females of the Penaeid Shrimp *Penaeus semisulcatus* de Haan

SHAI SHAFIR[1,2], MICHAEL OVADIA[2], AND MOSHE TOM[1]

[1]*Israel Oceanographic and Limnological Research, P.O. Box 8030, Haifa, 31080, Israel, and* [2]*Tel Aviv University, G. S. Wise Faculty of Life Sciences, Department of Zoology, Tel Aviv 69978, Israel*

Abstract. [^{35}S]-Methionine was injected into 11 intact vitellogenic females of the penaeid shrimp *Penaeus semisulcatus* de Haan. Levels of radiolabeled methionine, total protein and vitellogenin/vitellin (Vg/Vt) were measured in the hemolymph during 24 h following methionine injections. The same parameters were measured 24 h after injection, in the hepatopancreas and ovaries of sacrificed females. Proteins were precipitated by trichloroacetic acid and Vg/Vt was immunoprecipitated by anti-Vt serum.

Hemolymphatic protein and Vg/Vt levels were constant throughout the 24 h of the experiment starting from the first sampling of hemolymph, two h after injection. Similar amounts of Vg/Vt were found in the hepatopancreas compared to the ovary 24 h after injection, and 10% of the labeled protein in the ovary and 6.4% in the hepatopancreas were Vg/Vt. Free-labeled methionine was still present in all tissues examined after 24 h. The labeled protein and Vg/Vt in the ovary and the hepatopancreas could not be explained by the hemolymphatic content of the two organs. The hemolymphatic Vg is 24-fold labeled over the ovarian Vt, 24 h after injection. The results indicate more intense involvement of the hepatopancreas in the vitellogenic process than can be deduced from earlier *in vitro* studies. This study confirms the earlier definition of the oogenic stage of rapid Vt accumulation in the ovary (AOD range of 150–250 μm) and also indicates a role for the hemolymph in transporting Vg between its processing sites.

Received 4 February 1992; accepted 2 July 1992.

Abbreviations: AOD—Average oocyte diameter; dpm—disintegrations per minute; Mw—Molecular weight; SAT—Subepidermal adipose tissue; TCA—Trichloroacetic acid; Vg—Vitellogenin; Vt—Vitellin.

Introduction

Crustacean vitellin (Vt) is a lipoglycoprotein that accumulates in the oocyte cytoplasm. Vt is used later for the nutrition of the non-feeding embryo and larval stages. Vitellogenin (Vg), a vitellin-immunoidentical protein, is a female-specific protein found in crustacean extraoocytic tissues and hemolymph (Meusy and Payen, 1988). Vg is produced by the subepidermal adipose tissue (SAT) of anostracan (Van Beek *et al.*, 1987), isopod (Picaud, 1980; Souty and Picaud, 1981; Picaud *et al.*, 1989), and amphipod (Junera and Croisille, 1980; Croisille and Junera, 1980) crustaceans before it is transported by the hemolymph into the developing oocytes.

Decapod Vg is present in the SAT (Meusy *et al.*, 1983; Vazquez-Boucard, 1985; Tom *et al.*, 1987), hepatopancreas (Paulus and Laufer, 1987; Quackenbush and Keeley, 1988; Quackenbush, 1989a, b; Fainzilber *et al.*, 1992) and hemolymph (Kerr, 1969; Cecalldi, 1970; Wolin *et al.*, 1973; Fylfe and O'Connor, 1974; Caubere *et al.*, 1976; Dehn *et al.*, 1983; Durliat, 1984; Marzari *et al.*, 1986; Tom *et al.*, 1987; Yano, 1987; Quackenbush, 1989a; Shafir *et al.*, in prep.). A major source of decapod yolk is Vt synthesis by the ovary itself (Lui *et al.*, 1974; Lui and O'Connor, 1976, 1977; Dehn *et al.*, 1983; Eastman-Reks and Fingerman, 1985; Yano and Chinzei, 1987; Quackenbush, 1989a; Browdy *et al.*, 1990). The site of Vt synthesis in *Penaeus japonicus* was suggested to be the follicle cells (Yano and Chinzei, 1987). No Vg synthesis occurred in *in vitro* incubated SAT of *Penaeus semisulcatus* (Fainzilber *et al.*, 1992); however, three studies have reported Vg synthesis in the decapod hepatopancreas: Quackenbush and Keeley (1988) in *Uca pugilator;* Quackenbush (1989a) in *Penaeus vannamei* and Fainzilber *et al.* (1992) in *Penaeus semisulcatus.*

Vt endocytosis by the ovaries of several decapod species, including penaeids has been reported by Beams and Kessel, 1963; Hinsch and Cone, 1969; Wolin *et al.*, 1973; Duronslet *et al.*, 1975; Zerbib, 1979; Schade and Shivers, 1980; Zerbib and Mustel, 1984; and Jugan and Soyez, 1985. Vg receptors were found and isolated from the oocytic cytoplasm membrane of two decapod species (Jugan, 1985; Laverdure and Soyez, 1988; Jugan and Van Herp, 1989).

The penaeid ovary is a well established major synthetic site of Vt compared to the minor quantitative contribution of the penaeid hepatopancreas to Vg production, as was revealed by *in vitro* incubations of penaeid hepatopancreas and ovaries in the presence of labeled amino acids. Yano and Chinzei (1987) found no Vg synthesis at all in *P. japonicus* hepatopancreas in contrast to a high Vt synthesis in the ovary. Two additional studies, carried out in *P. vannamei* (Quackenbush, 1989a) and in *P. semisulcatus* (Browdy *et al.*, 1990; Fainzilber *et al.*, 1992) revealed lower rates of yolk synthesis in the hepatopancreas compared to the respective ovarian rates. The rate of Vg production, normalized per mg protein, in the hepatopancreas of *P. vannamei* was around 10% of the ovarian value at early and mid vitellogenesis. An apparent increase of this percentage to 50% at late vitellogenesis of *P. vannamei*, is an artifact caused by the normalization method, as the accumulation of yolk in the ovary during vitellogenesis adds protein that does not contribute to Vt synthesis but reduces the rate of synthesis per mg protein. A further reduction of the contribution of the whole hepatopancreas *versus* the whole ovary is due to its smaller protein content. The Vg rate of synthesis in the whole hepatopancreas of *P. semisulcatus* reached 4.35% of the Vt rate of synthesis in the whole ovary. The percentages of synthesized Vg from total protein synthesis in the hepatopancreas were also low in both *P. vannamei* and *P. semisulcatus* (1 and 14.4%, respectively) compared to similar percentages in the ovary (8 and 40%, respectively).

The small contribution of the *in vitro* incubated hepatopancreas to Vg synthesis should be further established by complementary *in vivo* methods, having better resemblance to the natural vitellogenic process. An appropriate method for examination of the hepatopancreas share in yolk synthesis is the identification of Vg-mRNA in the penaeid hepatopancreas and ovary, a study yet to be done. Another approach, the one taken by the present research, includes determination of the presence of radioactively labeled Vg and Vt in the hemolymph, hepatopancreas, and the ovary of vitellogenic penaeid females following injection of labeled amino acid. It is aimed at validating the overall involvement of the hepatopancreas and the ovary (not distinguishing between production and processing of Vg/Vt) and at examining the dynamics of circulating Vg.

Materials and Methods

Animals

Adults of *Peneaus semisulcatus* were collected in Haifa Bay, Israel. Thirty shrimp were held in a 3000-liter seawater tank. Water temperature ranged from 18°C (winter) to 27°C (summer). Water was replaced at a rate of 300% per day. Animals were fed daily with defrosted *Artemia* and a mixture of defrosted shrimp, fish, and squid. Females were individually tagged by clipping their uropods. Their oogenic stage was monitored periodically by visual examination of the ovaries according to the method of Browdy and Samocha (1985). Ovarian developmental stages were determined more accurately after sacrificing the females, by measuring the average oocyte diameter (AOD) as described by Shlagman *et al.* (1986). Molting of individual females was recorded daily by identification of the clipped cods on the uropods of the collected exuviae.

Chemicals

[^{35}S]–Methionine, 300 mCi/mMol was purchased from Amersham, U.K. All other reagents were of analytical grade.

[^{35}S]–methionine labeling and sampling of labeled tissues

Labeled methionine was injected through the thin cuticle connecting the thorax and the abdomen using 1 ml disposable syringes. Samples of hemolymph from live individuals were collected from the same site with 1 ml syringes containing a premeasured volume of the anticoagulant 10% tri-sodium citrate. Hemolymph from sacrificed females was collected in a premeasured volume of 10% tri-sodium citrate through an excision cut in the anterior part of the cephalothorax, at the base of the eyestalk.

The ovary and hepatopancreas were dissected from each of the sacrificed females and weighed before a portion of the ovary was fixed in 4% formaldehyde in seawater for the measurement of oocyte diameters. The remaining part of the ovary was then weighed again. The hepatopancreas and ovary from each of the females were homogenized separately in 0.1 *M* phosphate buffer, pH 7.4. Hemolymph samples and homogenized tissues were centrifuged and the supernatants were used for the TCA precipitation and radioimmunoprecipitation (RIP).

TCA precipitation and measurement of total labeled methionine

Four 50 μl aliquots taken from each supernatant were pipetted onto Whatman 3 mm filter paper discs and dried. The proteins were precipitated onto two of the discs in 10% TCA according to Mans and Novelli (1961), and all

four discs were radioactively counted in scintillation vials with 4 ml Aquasol-2 (NEN) in a Kontron Betamatic liquid scintillation counter.

Radioimmunoprecipitation (RIP)

Radioimmunoprecipitation was carried out by mixing 25 μl samples of each supernatant with unlabeled purified vitellin (75 μg in 25 μl) and 200 μl of anti-Vt serum. The anti-Vt serum was prepared and examined for Vt specificity according to Browdy *et al.* (1990) and Tom *et al.* (1992). Control samples contained normal rabbit serum (NRS) instead of anti-Vt serum. The total volume in the reaction tube was adjusted to 0.5 ml with 0.4 *M* NaCl and was mixed thoroughly before overnight incubation at 4°C. Following incubation, samples were centrifuged and the pellets washed three times with 0.4 *M* NaCl. Finally, each pellet was dissolved in 75 μl of 0.5 *M* NaOH by vigorous shaking for ½ h at room temperature and was neutralized with 25 μl of 2 *M* HCl before it was counted.

Complete immunoprecipitation of the labeled antigen was achieved with an adequate antigen-antibody ratio. The determination of suitable amounts of reactants was carried out by reacting fixed amounts of unlabeled Vt and labeled sample with increasing amounts of anti-Vt serum, followed by washing and counting the pellets.

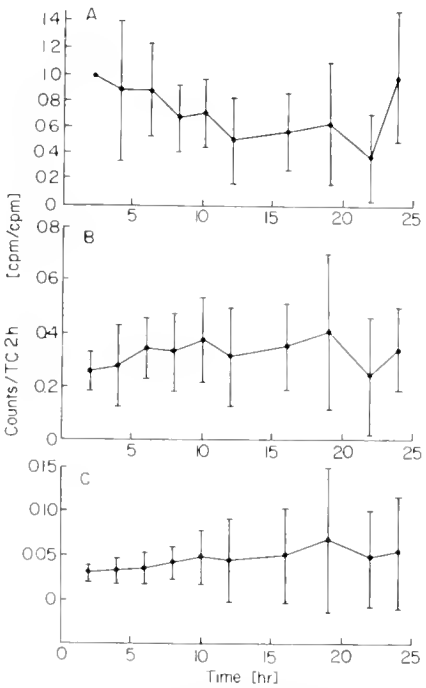

Figure 1. Twenty-four h time course presentation of (A) hemolymph total-labeled methionine, (B) labeled protein, and (C) labeled Vg normalized by the counts of total-labeled methionine in the hemolymph 2 h after injection (TC2h) in *Penaeus semisulcatus*. Vertical lines show standard deviations.

Table I

Incorporation of [^{35}S]*-methionine into TCA precipitable proteins and Vg/Vt in the hepatopancreas and ovary of* Penaeus semisulcatus *24 h after injection*

Parameters [*]	Ovary	Hepatopancreas
Total [^{35}S]-methionine	0.0573 ± 0.0450	0.2954 ± 0.1693
TCA precipitable protein	0.0278 ± 0.0260	0.0501 ± 0.0289
Immunoprecipitable Vt	0.0028 ± 0.0058	0.0032 ± 0.0021

[*]—dpm/total dpm in the hemolymph 2 h after injection/g dry weight of the organ (n = 11).

Results

Eleven vitellogenic females with AOD ranging from 180 to 350 μm were injected with 127 μCi of [^{35}S]-methionine dissolved in 20 μl of distilled water. The regular feeding, temperature, and water circulation regimes were maintained during the 24 h experiment. Hemolymph samples were taken every two h for the first 12 h. Samples were taken at longer intervals during the last 12 h of the incubation period to avoid stressing the sampled females. The females were sacrificed after 24 h, their hemolymph bled and their ovaries and hepatopancreas homogenized separately in a measured volume of 0.1 *M* phosphate buffer, pH 7.4. A piece of each ovary was taken for AOD measurement. The concentration of labeled methionine counted in the hemolymph 2 h after injection served as the normalization index, with the assumption that the injected methionine was evenly dissolved in the hemolymph following that period, as was previously found for [^{3}H]-inulin collected in the hemolymph (Shafir *et al.*, in prep.). Normalizing of protein and Vg/Vt counts by this index compensates for differences in hemolymph volume and for the amounts of injected methionine which entered the hemolymph.

Three values of radioactivity were counted in each hemolymphatic sample: total labeled methionine, labeled TCA precipitable proteins and labeled immunoprecipitated Vg (Fig. 1). There is no significant difference in the concentration of either labeled protein or Vg in the hemolymph during the entire experiment, starting from the first sampling two hours after injection. The standard deviations of the levels of labeled protein and Vg increase with time.

Incorporation of methionine into total protein and Vg/Vt in the hepatopancreas and in the ovary, 24 h after injection, is presented in Table I. The level of labeled Vg in the examined tissues could not be explained by the labeled Vg found in its hemolymphatic component alone, even if the whole tissue is considered replaced by an equal volume of hemolymph, assuming 1 g wet weight of tissue is approximately equivalent to 1 ml of hemolymph (Table II).

Table II

Average ratio (n = 11) of labeled proteins in the hepatopancreas or ovary to labeled proteins found in an identical hemolymph volume in Penaeus semisulcatus

Ratios [dpm/dpm]	TCA	RIP
Hepatopancreas/hemolymph	5.07 ± 2.13	4.08 ± 3.34
Ovary/hemolymph	4.82 ± 3.21	2.71 ± 1.33

Tissue volume was estimated by assuming 1 gm wet weight equals 1 ml of hemolymph. The hepatopancreas and the ovary were dissected 24 h after *in vivo* [^{35}S]-methionine injection. Protein labeling was determined from radioactive counting of the TCA-precipitable proteins (TCA) and the immunoprecipitated Vg/Vt (RIP).

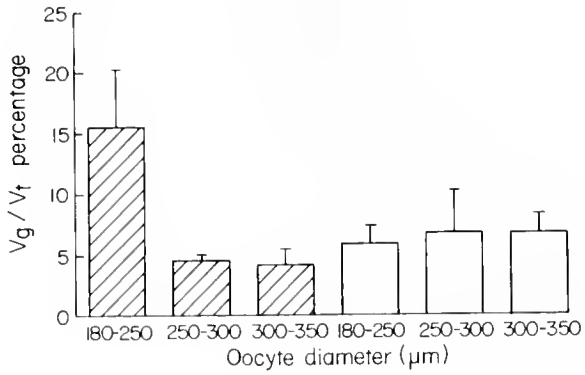

Figure 2. Percentage of labeled Vg/Vt from the labeled proteins in the ovary (filled bars) and hepatopancreas (white bars) 24 h after [^{35}S]-methionine injection. Vertical lines show standard deviations.

The percentages of synthesized Vg/Vt from total protein synthesized in the ovary and hepatopancreas are presented in Figure 2, which shows a decrease of relative methionine incorporation into ovarian Vt as oogenesis proceeds, while the value in the hepatopancreas was constant.

Comparison of the levels of total-labeled methionine and TCA precipitable labeled protein in the examined tissues (Fig. 1a, b, and Table I) shows that free-labeled methionine was present in the female even 24 h after injection. Free-labeled methionine was also present in the above tissues with reduced amounts of injected methionine (results not shown).

The molar ratio (P, in percents) of labeled methionine incorporated into Vg or Vt from the total methionine in the Vg or Vt was calculated using the parameters described in Table III. Molar amounts of methionine are given per gram body weight.

$$P = \frac{\text{Moles of labeled methionine}}{\text{Moles of total methionine}} \times 100$$

For the hemolymphatic Vg the result was:

$$P = \frac{28210/2.2 \times 10^6/300}{177 \times 0.03/131.2} \times 100 = 0.1056\%$$

and for the ovarian Vt the result was:

$$P = \frac{30590/2.2 \times 10^6/300}{4550 \times 0.03/131.2} \times 100 = 0.0044\%$$

The results show that 24 h after injection of labeled methionine, the ratio between labeled Vg in the hemolymph and labeled Vt in the ovary is 24 (0.1056/0.0044).

Discussion

The possible roles of the ovary, hepatopancreas and hemolymph of female penaeid shrimp in the vitellogenic process were investigated. This objective was accomplished in part by determining whether [^{35}S]-methionine had become incorporated into Vg/Vt present in these organs 24 h after its injection into the hemolymph of vitellogenic females.

Free-labeled methionine was found in the hemolymph, ovary and hepatopancreas 24 h after injection even when an extremely small quantity of radioactive methionine was injected. This observation indicates high levels of endogeneous methionine, competing with the incorporation of labeled methionine into proteins, preventing pulse labeling of proteins. The absence of a pulse of labeled proteins and Vg did not allow determination of Vg turnover in the hemolymph. Injection of labeled Vg into vitellogenic females might be a more suitable method to achieve its pulse labeling in the hemolymph.

A relatively high percentage of *in vivo* labeled protein in the ovaries at early vitellogenesis (AOD = 180–250 μm, Fig. 2) was Vt (15.5%), which is in agreement with

Table III

Parameters used for calculating molar ratio of labeled methionine incorporated into Vg or Vt, from total methionine in Vg or Vt in Penaeus semisulcatus

Parameter	Value	Source
Percentage of methionine in Vt	3% (w/w)	Tom *et al.* (1992)
Mw of methionine residue	131.2	—
Maximum level of hemolymph Vg	177 μg/g body weight	Shafir *et al.* (in prep.)
Maximum level of ovarian Vt	4550 μg/g body weight	Shafir *et al.* (in prep.)
Specific activity of labeled methionine	300 μCi/μMol	NEN, U.S.A.
Maximum level of hemolymph labeled Vg	28210 dpm/g body weight	Present study
Maximum level of ovarian labeled Vt	30590 dpm/g body weight	Present study

the data of Shafir *et al.* (in prep.) who showed that oocytes of this size are not accumulating Vt. The reduced percentage of labeled protein found in the present study vitellogenesis (4.4%, Fig. 2) when combined with slow increase of accumulated Vt in ovaries at the same AOD range (Shafir *et al.*, in prep.) indicates inhibition of Vt accumulation in the ovary of the intact female at AOD > 250 μm. In contrast, ovaries incubated *in vitro* showed no inhibition of Vt synthesis at any stage of vitellogenesis although a decrease in the percentage of synthesized Vt was observed at AOD > 350 μm, presumably due to increased synthesis of other proteins (Browdy *et al.*, 1990).

The amount of labeled Vg and its percentage of the total labeled protein in the hepatopancreas were similar to the corresponding values of labeled Vt in the ovary after the 24 h experiment (Table I and Fig. 2). These labeled Vg/Vt amounts can not be explained by the hemolymphatic Vg component of the two organs alone (Table II). They are probably the result of an equilibrium between the influx of circulating Vg and the contribution of *in situ* produced Vg and Vg secretion during the 24 h of the experiment. These findings strongly suggest that the hepatopancreas has a more prominent role in the vitellogenic process than could be deduced from the results of earlier comparable *in vitro* incubations (Browdy *et al.*, 1990; Fainzilber *et al.*, 1992) (see also Introduction). The *in vitro* studies favor the penaeid ovary as the major Vt synthetic site, a conclusion supported by other studies (Yano and Chinzei, 1987; Quackenbush, 1989a). The differences between the *in vivo* and *in vitro* studies can be attributed to a more efficient Vg synthesis by the intact *in vivo* hepatopancreas, or to its functioning as a Vg processing site. This processing might involve addition of a polypeptide subunit which would explain the small amount of synthesis of a Vg-immunoidentical substance, or binding of a lipid component to the Vg molecule.

Absorption in penaeid ovaries of non-spawned ovulated oocytes immediately after spawning and in developing oocytes at the commencement of the premolt stage was reported by Browdy (1988). The absorption of ovulated oocytes is correlated with a relatively high Vg level in the hemolymph of recently spawned females (Shafir *et al.*, in prep.). Consequently, secretion of Vt into the hemolymph is postulated for females with normally developing ovaries and is suggested as one explanation for the presence of Vg in the hemolymph. This Vg is assumed to be either newly synthesized Vt that will be further processed in extraovarian sites, prior to its reuptake by the developing oocytes or a degradation product of previously synthesized Vt. The 24-fold more intensive labeling of Vg compared with the Vt labeling found in the present study argues against the possibility of unselected secretion of ovarian Vt, because if this were the case, similar Vg/Vt labeling should have been seen in both the ovary and the hemolymph.

In conclusion, evidence from this and previous studies supports the hypothesis that the hepatopancreas has a more intense involvement in the vitellogenic process than could be deduced from earlier *in vitro* studies, but is not necessarily the only site of Vg synthesis. The rapid accumulation of Vt that occurs early in vitellogenesis (AOD range of 150–250 μm) and the arrest of Vt accumulation later (AOD > 250 μm), first found by Shafir *et al.* (in prep.), is confirmed by the present findings. Furthermore, the present study shows that circulating Vg is not a degraded Vt which is secreted unselectively from the ovary.

Acknowledgments

We thank Ms. Alisa Hadani for her dedicated technical assistance. This study was supported by the Israeli Ministry of Energy and Infrastructure through their support of research projects in mariculture at IOLR and also by grant No. I-1435-88 to Dr. M. Tom from the U. S.—Israel Binational Agricultural Research and Development Fund (BARD).

Literature Cited

Beams, H. W., and R. G. Kessel. 1963. Electron microscopy studies on developing crayfish oocytes with special references to the origin of yolk. *J. Cell Biol.* **18:** 621–649.

Browdy, L. C. 1988. Aspects of the reproductive biology of *Penaeus semisulcatus* de Haan (Crustacea; Decapoda; Penaeidae). Ph.D. Thesis, Univ. of Tel Aviv, 138 pp.

Browdy, C. L., M. Fainzilber, M. Tom, Y. Loya, and E. Lubzens. 1990. Vitellin synthesis in relation to oogenesis in *in vitro* incubated ovaries of *Penaeus semisulcatus* (Crustacea, Decapoda, Penaeidae). *J. Exp. Zool.* **255:** 205–215.

Browdy, C. L., and T. M. Samocha. 1985. The effect of eyestalk ablation on spawning, molting and mating of *Penaeus semisulcatus* de Haan. *Aquaculture* **49:** 19–29.

Caubere, J. J., R. Lafon, F. Rene, and C. Sales. 1976. Maturation et ponte chez *Penaeus japonicus* en captivite essai de controle de cette reproduction a maguelone sur les côtes françaises. *FAO Tech. Conf. on Aquacult.*, Kyoto, Japan. AQ/Conf/76/E.49: 1–17.

Ceccaldi, H. J. 1970. Evolution des proteines de l'hemolymphe de *Penaeus kerathurus* femelle durant la vitellogenese. *C. R. Sean. Soc. Biologie* **164:** 2572.

Croisille, Y., and H. Junera. 1980. Site of vitellogenin synthesis in *Orchestia gammarella* (Crustacea, amphipoda). Immunohistological demonstration of appreciable amounts of vitellogenin in the subepidermal adipose tissue of females in which secondary vitellogenesis is taking place. C. R. *Hebd. Seances Acad. Sci.* Ser. D. **290:** 1487–1490.

Dehn, P. F., P. E. Aiken, and S. L. Waddy. 1983. Aspects of vitellogenesis in the lobster *Homarus americanus*. *Can. Tech. Rep. Fish. Aquat. Sci. D* **(1161):** i–iv, 1–24.

Durliat, M. 1984. Occurrence of plasma proteins in ovary and egg extracts from *Astacus leptodactylus*. *Comp. Biochem. Physiol.* **78B:** 745–754.

Dunnslet, M. J., I. A. Yudin, R. S. Wheeler, and W. H. Clark, Jr. 1975. Light and fine structural studies of natural and artificially

induced egg growth of penaeid shrimp. *Proc. World Maricult. Soc.* **6:** 105–122.

Eastman-Reks, S. B., and M. Fingerman. 1985. *In vitro* synthesis of vitellin by the ovary of the fiddler crab *Uca pugilator*. *J. Exp. Zool.* **233:** 111–116.

Fainzilber, M., M. Tom, S. Shafir, S. W. Applebaum, and E. Lubzens. 1992. Is there extraovarian synthesis of vitellogenin in penaeid shrimp? *Biol. Bull.* **183:** 233–241.

Fyffe, W. E., and J. D. O'Connor. 1974. Characterization and quantification of a crustacean lipovitellin. *Comp. Biochem. Physiol.* **47B:** 851–867.

Hinsch, G. W., and M. V. Cone. 1969. Ultrastructural observations of vitellogenesis in the spider crab *Libinia emarginata*. *J. Cell Biol.* **40:** 336–342.

Jugan, P. 1985. Regulation de la croissance ovocytaire chez la crustacé *Macrobrachium rosenbergii* (De Man). Demonstration d'une endocytose par recepteurs et approché du mode d'action de la neurohormone inhibitrice de la vitellogenese. Ph.D. Thesis, P. and M. Curie University, Paris. 68 pp.

Jugan, P., and D. Soyez. 1985. *In vitro* inhibitory effect of a sinus gland extract on oocyte endocytosis in the prawn *Macrobrachium rosenbergii*. *C. R. Acad. Sc.* Paris Ser. III **300:** 705–709.

Jugan, P., and F. Van Herp. 1989. Introductory study of an oocyte membrane protein that specifically binds vitellogenin in the crayfish *Orconetes limosus*. *Invert. Reprod. Dev.* **16:** 149–154.

Junera, H., and Y. Croisille. 1980. Recherche du lieu de synthese de la vitellogenine chez le crustacé amphipode *Orchestia gammarella* (Pallas). Mise en evidance d'une activation de la synthese proteique dans le tissu adipeus sous-epidermique en liaison avec la production de vitellogenine. *C. R. Acad. Sc.* Paris **290:** 703–706.

Kerr, M. S. 1969. The hemolymph proteins of the blue crab, *Callinectes sapidus* II: a lipoprotein seroligically identical to oocyte lipovitellin. *Dev. Biol.* **20:** 1–17.

Laverdure, A. M., and D. Soyez. 1988. Vitellogenin receptors from lobster oocyte membrane, solubilization and characterization by a solid phase binding assay. *Int. J. Invert. Reprod. Dev.* **13:** 251–266.

Lui, C. W., and J. D. O'Connor. 1976. Biosynthesis of lipovitellin by the crustacean ovary. II. Characterization and *in vitro* incorporation of amino acids into the purified subunits. *J. Exp. Zool.* **195:** 41–52.

Lui, C. W., and J. D. O'Connor. 1977. Biosynthesis of crustacean lipovitellin. III. The incorporation of labeled amino acids into the purified lipovitellin of the crab *Pachygrapsus crassipes*. *J. Exp. Zool.* **199:** 105–108.

Lui, C. W., B. A. Sage, and J. D. O'Connor. 1974. Biosynthesis of lipovitellin by the crustacean ovary. *J. Exp. Zool.* **188:** 289–296.

Mans, R. J., and G. D. Novelli. 1961. Measurement of the incorporation of radioactive amino acids into protein by a filter-paper disk method. *Arch. Biochem. Biophys.* **94:** 48–53.

Marzari, R., E. Ferrero, A. Mosco, and A. Savoini. 1986. Immunological characterization of the vitellogenic proteins in *Squilla mantis* hemolymp, Crustacea Stomatopoda. *Exp. Biol.* (Berl.) **45:** 75–80.

Meusy, J. J., and G. P. Payen. 1988. Female reproduction in malacostracan crustacea. *Zool. Sci.* **5:** 217–265.

Meusy, J. J., H. Junera, P. Cledon, and M. Martin. 1983. Vitellogenin in a decapod crustacean *Palaemon serratus*, identification, immunological similarity to vitellin synthesis and role of the eyestalks. *Reprod. Nutr. Dev.* **23:** 625–640.

Paulus, J. P., and H. Laufer. 1987. Vitellogenocytes in the hepatopancreas of *Carcinus maenas* and *Libinia emarginata* (Decapoda, Brachyura). *Int. J. Inv. Reprod. Dev.* **11:** 29–44.

Picaud, J. L. 1980. Vitellogenin synthesis by the fat-body of *Porcellio dilatatus* Brandt (Crustacea, Isopoda). *Int. J. Inv. Reprod.* **2:** 341–349.

Picaud, J. L., C. Souty-Grosset, and G. Martin. 1989. Vitellogenesis in terrestial isopods: Female specific proteins and their control. *Monitore Zool. Ital. (N.S.) Monogr.* **4:** 305–331.

Quackenbush, L. S. 1989a. Yolk protcins production in the marine shrimp *Penaeus vannamei*. *J. Crustacean Biol.* **9:** 509–516.

Quackenbush, L. S. 1989b. Vitellogenesis in the shrimp *Penaeus vannamei: in vitro* studies of the isolated hepatopancreas and ovary. *Comp. Biochem. Physiol.* **94B:** 253–261.

Quackenbush, L. S., and L. L. Keeley. 1988. Regulation of vitellogenesis in the fiddler crab *uca pugilator*. *Biol. Bull.* **175:** 321–331.

Schade, M. L., and R. R. Shivers. 1980. Structural modulation of the surface and cytoplasm of oocytes during vitellogenesis in the lobster *Homarus americanus*. *J. Morphol.* **163:** 13–26.

Shlagman, A., C. Lewinsohn, and M. Tom. 1986. Aspects of the reproductive activity of *Penaeus semisulcatus* de Haan along the southeastern coast of the Mediterranean. *P.S.Z.N.I. Mar. Ecol.* **7:** 15–22.

Souty, C., and J-L Picaud. 1981. Vitellogenin synthesis in the fat body of the marine crustacean Isopoda *Idotea balthica basteri* during vitellogenesis. *Reprod. Nutr. Dev.* **21:** 95–102.

Tom, M., M. Fingerman, T. K., Hayes, V. Johnson, B. Kerner, and E. Lubzens. 1992. A comparative study of the ovarian proteins from two penaeid shrimps, *Penaeus semisulcatus* De Haan and *Penaeus vannamei* (Boone). *Comp. Biochem. Physiol.* **102B:** 483–490.

Tom, M., M. Goren, and M. Ovadia. 1987. Localization of the vitellin and its possible precursors in various organs of *Parapenaeus longirostris* (Crustacea, Decapoda, Penaeidae). *Int. J. Invert. Reprod. Dev.* **12:** 1–12.

Van Beek, E., M. Van Brussel, G. Criel, and A. De Loof. 1987. A possible extra-ovarian site for synthesis of lipovitellin during vitellogenesis in *Artemia* sp., Crustacea, Anostraca. *Int. J. Invert. Reprod. Dev.* **12:** 227–240.

Vazquez-Boucard, C. 1985. Identification preliminaire du tissu adipeux chez le crustacé decapode *Penaeus japonicus* bate a l'aide d'antilipouitelline. *C. R. Acad. Sc.* Paris **300:** 95–97.

Wolin, E. M., H. Laufer, and D. F. Albertini. 1973. Uptake of the yolk protein, lipovitellin, by developing crustacean oocytes. *Dev. Biol.* **35:** 160–170.

Yano, I. 1987. Effect of 17α-hydroxy-progesterone on vitellogenin secretion in the Kuruma prawn *Penaeus japonicus*. *Aquaculture* **61:** 49–57.

Yano, I., and Y. Chinzei. 1987. Ovary is the site of vitellogenin synthesis in kuruma prawn, *Penaeus japonicus*. *Comp. Biochem. Physiol.* **86B:** 213–218.

Zerbib, C. 1979. Ultrastructural study of the oocyte during vitellogenesis in the crabs *Astacus astacus* and *A. leptodactylus*. *Int. J. Invert. Reprod.* **1:** 289–296.

Zerbib, C., and J. J. Mustel. 1984. Incorporation of tritiated vitellogenin into the oocytes of the crustacean amphipod *Orchestia gammarelus*. *Int. J. Invertebr. Reprod. Dev.* **7:** 63–68.

Reference: *Biol. Bull.* 183: 248–257. (October, 1992)

Development of the Infusoriform Embryo of *Dicyema japonicum* (Mesozoa: Dicyemidae)

HIDETAKA FURUYA, KAZUHIKO TSUNEKI, AND YUTAKA KOSHIDA

Department of Biology, College of General Education, Osaka University, Toyonaka, 560, Japan

Abstract. The cleavage pattern and cell lineage of the infusoriform embryo of the dicyemid mesozoan *Dicyema japonicum* were studied in fixed material with the aid of a light microscope. The early cleavages are holoblastic and spiral. At the 16-cell stage, the animal pole consists of four mesomeres, the equatorial region consists of four macromeres with four alternating sub-macromeres, and the vegetal pole is composed of four micromeres. At around the 20- to 24-cell stage, cleavage becomes asynchronous and its pattern changes from spiral to bilateral. The four micromeres, namely, the presumptive germinal cells, do not divide further and are finally incorporated into the cytoplasm of four urn cells, which are generated after divisions of the sub-macromeres. The blastomeres situated in the animal hemisphere give rise to ciliated cells that cover the posterior part of the embryo. Two blastomeres ($2a^2$ and $2d^2$) undergo extremely unequal divisions and the much smaller sister blastomeres degenerate and ultimately disappear during embryogenesis. The fully formed embryo consists of 37 cells. These cells are produced after only four to eight rounds of cell division. The cell lineage appears to be invariant among embryos, apart from the derivation of the lateral cells.

Introduction

The bodies of dicyemid mesozoans consist of only 20 to 40 cells and are organized in a very simple fashion (Nouvel, 1948; McConnaughey, 1951). Although Hyman (1940, 1956) considered dicyemids to be truly primitive multicellular animals, until some twenty years ago many zoologists regarded the simple body organization of dicyemids as the result of degeneration due to parasitism in the cephalopod kidney (Nouvel, 1948; McConnaughey, 1951; Stunkard, 1954; Ginetsinskaya, 1988). However, recent studies on the base compositions and sequences of their nucleic acids have suggested that dicyemids are somewhat closer to ciliate protozoans than to flatworms (Lapan and Morowitz, 1974; Hori and Osawa, 1987).

In any attempt to evaluate the phylogenetic position of an organism, a knowledge of the normal development of the organism can be crucial. In the case of dicyemids, such information may also attract the attention of developmental biologists because, in the animal kingdom, the development of dicyemids may represent one of the simplest patterns of cell differentiation that occurs during embryogenesis. Nevertheless, the development of the infusoriform embryo of dicyemids has been minimally studied (McConnaughey, 1951; Sponholtz, 1964; Lapan and Morowitz, 1975) and the details of the cell lineage during embryogenesis remain to be determined.

In this report, we describe the pattern of cleavage and the cell lineage during the development of the infusoriform embryo of *Dicyema japonicum*. In the complex life cycle of dicyemids, the vermiform embryo and the infusorigen each develop asexually from an axoblast (agamete) and the stem nematogen is believed to develop asexually from a germinal cell of the infusoriform embryo (McConnaughey, 1951; Lapan and Morowitz, 1975; Hochberg, 1982, 1983). The infusoriform embryo is the only form that develops from a fertilized egg and the development that we discuss herein is that of infusoriform embryos. In individuals of *Dicyema japonicum*, they are ultimately composed of 37 cells.

Materials and Methods

Seventeen host octopuses, *Octopus vulgaris*, were purchased or collected personally in the western part of Japan. Although, in this region, four species of dicyemids are found in the kidneys of *Octopus vulgaris* (Furuya *et al.*,

Received 6 April 1992; accepted 22 July 1992.

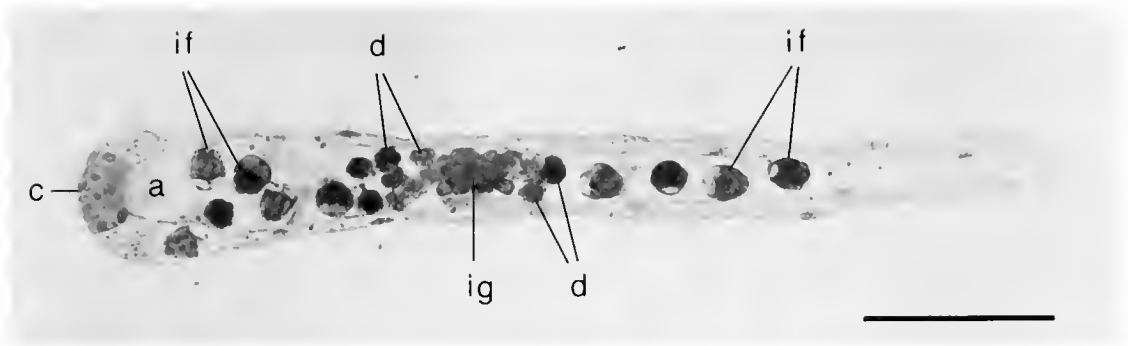

Figure 1. Light micrograph of a rhombogen of *Dicyema japonicum* a, axial cell; c, calotte; d, developing infusoriform; if, infusoriform embryo; ig, infusorigen (hermaphroditic gonad). Scale bar = 100 μm.

1992), only those of *Dicyema japonicum* Furuya et Tsuneki, 1992 were examined throughout this study. After the octopus had been sacrificed, its kidneys were taken out and smeared directly on glass slides. Smeared dicyemids were immediately fixed with Carnoy's fixative or alcoholic Bouin's solution (absolute ethanol saturated with picric acid: formalin: acetic acid, 15:5:1). Specimens fixed with Carnoy's fixative were stained with Feulgen's stain or by the PAS method and were poststained with Ehrlich's hematoxylin and light green. Some specimens were treated with saliva before the PAS staining. Specimens fixed with alcoholic Bouin's solution were stained with Ehrlich's hematoxylin and light green only. The embryos in the axial cell of rhombogens were observed with the aid of a light microscope under an oil-immersion objective at a magnification of 2000 diameters. Blastomeres were identified by criteria such as position within the embryo, size of nucleus and cell, and stainability of nucleus and cell. By paying careful attention, we identified each swollen nucleus that was about to divide and each metaphase figure in terms of the blastomere that was going to divide and the resulting two daughter blastomeres. Each developing embryo with or without dividing blastomeres was sketched at three different optical depths and a three-dimensional diagram was reconstructed from these sketches. The fully formed embryo consisted of only 37 cells and special techniques such as injection of a tracer and videoscopy were not required for determination of the cell lineage. The early cleavages of *Dicyema japonicum* were spiral and, therefore, the terminology of blastomeres that is generally used for embryos with spiral cleavages was adopted in designating the blastomeres. The cells of the infusoriform were named according to the earlier authors (Nouvel, 1948; McConnaughey, 1951; Short and Damian, 1966; Ridley, 1969; Matsubara and Dudley, 1976).

Results

In individuals of *Dicyema japonicum*, there is usually only one infusorigen, which is functionally a hermaphroditic gonad, and it is located in the center of the axial cell of a rhombogen (Fig. 1). A sperm enters the oocyte, which is located around the axial cell of the infusorigen. Then the oocyte undergoes meiosis and produces the polar bodies, and the two-pronucleus stage follows (Fig. 2a–d). Fertilized eggs are about 12.3 μm in diameter. As development proceeds from the 2-cell to the 4-cell stage and beyond (Fig. 2e–h), the embryo leaves the infusorigen and moves toward the anterior or posterior end of the axial cell of the rhombogen. In large specimens, there are more than 20 embryos, including fully formed infusoriforms, in a single rhombogen. In some cases, therefore, nearly the entire series of developmental stages can be observed in a single fixed rhombogen.

Cleavage is holoblastic and early cleavages proceed spirally. The first cleavage is meridional and equal, and produces two blastomeres, AB and CD (Figs. 2e, 3a). The second cleavage is latitudinal and equal, and produces four blastomeres, A, B, C, and D (Figs. 2f, 3b). Blastomeres A and C are in contact with each other at the animal pole, and blastomeres B and D are in contact at the vegetal pole. The third cleavage is again equal and four blastomeres, 1a, 1b, 1c, and 1d, are formed at the animal hemisphere (Figs. 2g, 3c). When viewed from the animal pole, these blastomeres are organized spirally clockwise to their sister blastomeres (1A, 1B, 1C, 1D), which form the vegetal hemisphere. The 8-cell embryo, thus, consists of two tiers of four cells (quartet). The descendants of blastomeres A and 1B are destined to form the left side of the infusoriform and the descendants of blastomeres C and 1D form the right side of the embryo.

The fourth cleavage is unequal and results in the 16-cell embryo (Figs. 2i, 3d). Four blastomeres, 1a, 1b, 1c, and 1d, divide and produce the mesomeres $1a^1$, $1b^1$, $1c^1$, and $1d^1$ at the animal pole, and the macromeres $1a^2$, $1b^2$, $1c^2$, and $1d^2$ in the equatorial region. These divisions are not typically spiral. Blastomeres $1a^1$, $1b^1$, $1c^1$, and $1d^1$ undergo no further division. Blastomeres $1a^1$ and $1c^1$ become the dorsal caudal cells (DC) of the left and right

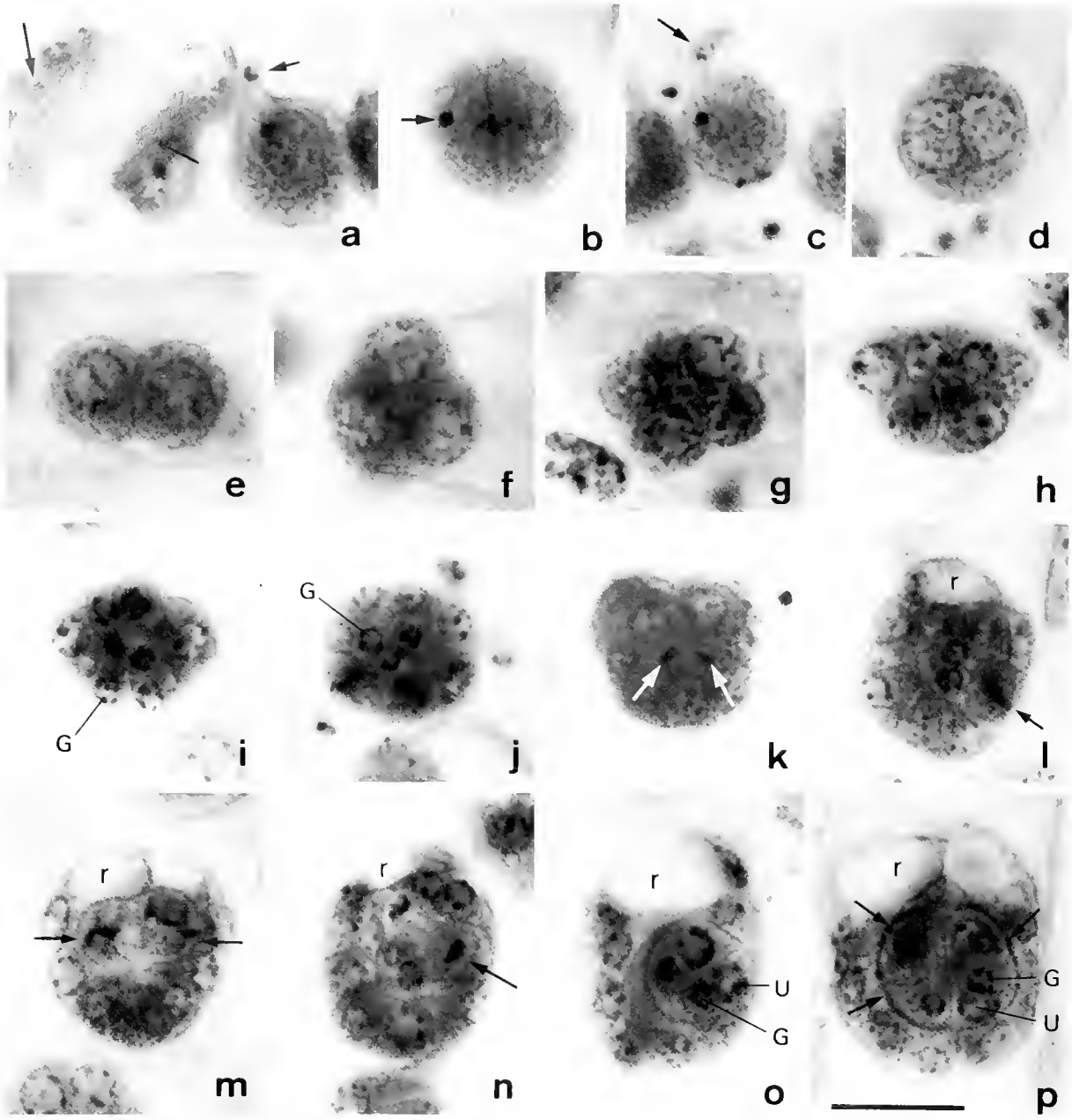

Figure 2. Light micrographs of eggs, developing infusoriform embryos, and fully formed infusoriform embryos of *Dicyema japonicum*. Photomicrographs were taken at magnifications of 2000 diameters under an oil-immersion objective. Scale bar = 10 μm. **a.** An infusorigen (left) and an oocyte undergoing meiosis (right). The short arrow indicates the first polar body and the long arrows indicate spermatozoa. **b.** An oocyte undergoing the second meiotic division. The arrow indicates a spermatozoon. **c.** An oocyte finishing meiosis (center). The arrow indicates the second polar body. **d.** A fertilized egg at the 2-pronucleus stage. **e.** Two-cell embryo. **f.** Four-cell embryo. One blastomere is out of focus. **g.** Eight-cell embryo. An axial cell nucleus is seen in the lower left corner. **h.** Twelve-cell embryo (optical section). **i.** Sixteen-cell embryo (optical section). **j.** Twenty-four-cell embryo (optical section). **k.** Twenty-nine-cell embryo (ventral view). The arrows indicate degenerating cells produced after extremely unequal divisions. **l.** Twenty-nine-cell embryo (sagittal optical section). The arrow indicates a metaphase figure of $2d^2$. Two small nuclei in the center are those of germinal cells. r = refringent body. **m.** Thirty-three-cell embryo (horizontal optical section). Arrows indicate metaphase figures of $2b^{211}$ and $2c^{211}$. r = refringent body. **n.** Thirty-six-cell embryo (sagittal optical section). The arrow indicates a telophase figure of $2c^{212}$. r = refringent body. **o.** Fully formed embryo (sagittal optical section). r = refringent body. **p.** Fully formed embryo (horizontal optical section). Arrows indicate granules in capsule cells. r = refringent body.

side of the embryo, respectively. Blastomeres $1b^1$ and $1d^1$ become the median dorsal cell (MD) and the ventral caudal cell (VC), respectively. Macromere $1d^2$ also does not divide further and ultimately becomes the couvercle cell (C). These three cells (MD, VC, C) are located in the midline of the embryo and, thus, are not paired. Among the other macromeres, $1a^2$ and $1c^2$ usually undergo no further divisions and become the lateral caudal cell (LC) of the left and right side, respectively. Macromere $1b^2$ subsequently divides once more (Fig. 3j). The resultant sister blastomeres gradually accumulate a refringent body in the cytoplasm and finally become the apical cells (A).

The fourth division in the vegetal hemisphere generates four sub-macromeres, 2a, 2b, 2c, and 2d, in the subequatorial region, and four micromeres, 2A, 2B, 2C, and 2D, at the vegetal pole. Micromeres 2A, 2B, 2C, and 2D do not divide further and they ultimately become the germinal cells (G). After the fourth division, the cleavages are not synchronized among the blastomeres (Figs. 2j–n, 3e–l, 4).

The 20-cell stage is achieved by the unequal division of blastomeres 2a, 2b, 2c, and 2d (Fig. 3e). When the embryo is viewed from the vegetal pole, the daughter blastomeres $2a^1$, $2b^1$, $2c^1$, and $2d^1$ occupy the left side of $2a^2$, $2b^2$, $2c^2$, and $2d^2$, respectively. At around this stage, the four micromeres 2A, 2B, 2C, and 2D (the presumptive germinal cells) are incorporated into the inside of the embryo as the other blastomeres grow and rearrange themselves. Blastomeres $2a^1$ and $2d^1$ undergo no further divisions and eventually they become the posteroventral lateral cells (PVL) of the left and right side, respectively.

The cleavage pattern beyond the 20-cell stage is not spiral but bilateral. Beyond this stage, the order of divisions of blastomeres is not necessarily identical among developing embryos and the subsequent developmental stages, such as the 24-cell stage and so on, become increasingly less well defined. For example, in the embryo shown in Figure 3f (23-cell stage), blastomere $2c^{22}$ has already divided into its daughter cells while, in the embryo shown in Figure 3h (24-cell stage), the same blastomere is still intact.

Blastomeres $2b^1$ and $2c^1$ usually divide once more and generate the paired dorsal cells (PD) and lateral cells (L) on the left and right side, respectively. In some individuals, however, these blastomeres ($2b^1$ and $2c^1$) do not divide further and simply become the paired dorsal cells. In these embryos, macromeres $1a^2$ and $1c^2$ divide once more and produce the lateral cells and the lateral caudal cells. In every case, the embryos become slightly oval in shape.

Blastomeres $2a^2$, $2b^2$, $2c^2$, and $2d^2$ exhibit complex patterns of cleavages. Blastomere $2a^2$ usually undergoes extremely unequal division (Fig. 2k); the much smaller sister blastomere (not named here) becomes pycnotic and is destined sooner or later to degenerate. The much larger sister blastomere soon divides again and produces $2a^{21}$ and $2a^{22}$. Blastomere $2a^{21}$ becomes the capsule cell (CA), while blastomere $2a^{22}$ divides once more and produces the anterior lateral cell (AL; $2a^{221}$) and the second ventral cell (V2; $2a^{222}$). The capsule cell has a large nucleus and later accumulates PAS-positive granules in the cytoplasm. These granules are PAS-positive even after the saliva-test is applied. The second ventral cell later extends a long cytoplasmic process medially. The cleavage pattern and cell lineage of blastomere $2d^2$ are the same as those of blastomere $2a^2$, although $2d^2$ produces the cells that occupy the right side of the embryo.

Blastomere $2b^2$ first divides into $2b^{21}$ and $2b^{22}$, and blastomere $2b^{22}$ soon divides again. The resultant blastomere $2b^{221}$ becomes flattened (Fig. 4d); it covers the anterior region of the embryo and eventually it is transformed into the enveloping cell (E). The sister blastomere $2b^{222}$ becomes the first ventral cell (V1). The blastomeres generated from $2b^{21}$ are gradually incorporated into the inside of the embryo as the blastomeres derived from the animal hemisphere grow and rearrange themselves. Blastomere $2b^{211}$ then divides (Fig. 2m) to produce blastomeres $2b^{2111}$ and $2b^{2112}$. Blastomere $2b^{2111}$ becomes transparent apart from its nucleus and it is ultimately designated the dorsal internal cell (DI). Blastomere $2b^{2112}$ eventually projects cilia into a small cavity, the urn cavity, and becomes the ventral internal cell (VI). The urn cavity is a cleft formed between the ventral internal cells and the urn that is composed of four urn cells. Blastomere $2b^{212}$ finally divides and produces two urn cells (U) of the left side. The cleavage pattern and cell lineage of blastomere $2c^2$ are the same as those of blastomere $2b^2$: the descendants of $2c^2$ ultimately contribute to the right side of the embryo's body. The urn itself apparently rotates as a mass and, thus, it cannot be determined for each urn cell whether it was originally the right one or left one.

After all cells of the embryo have been laid down, one germinal cell is incorporated into the cytoplasm of each of the four urn cells (Fig. 5d). In individuals of *Dicyema japonicum*, the nucleus of each urn cell does not divide and each urn cell contains only one nucleus throughout. As the infusoriform matures, the nuclei of most of the cells tend to become pycnotic. Nuclear pycnosis takes place first in the second ventral cell. However, the nuclei of the germinal cells and the urn cells do not become pycnotic, even in the mature infusoriform.

The cell lineage of the infusoriform embryo of *Dicyema japonicum* is summarized in Figure 6. Blastomeres A and D follow exactly the same pattern of cleavages. Blastomeres B and C follow a very similar pattern of cleavages. A difference is found only in blastomeres $1b^2$ and $1c^2$: the former divides once to produce the apical cells but the latter does not. Even in the A and D series, however, corresponding blastomeres do not necessarily produce the

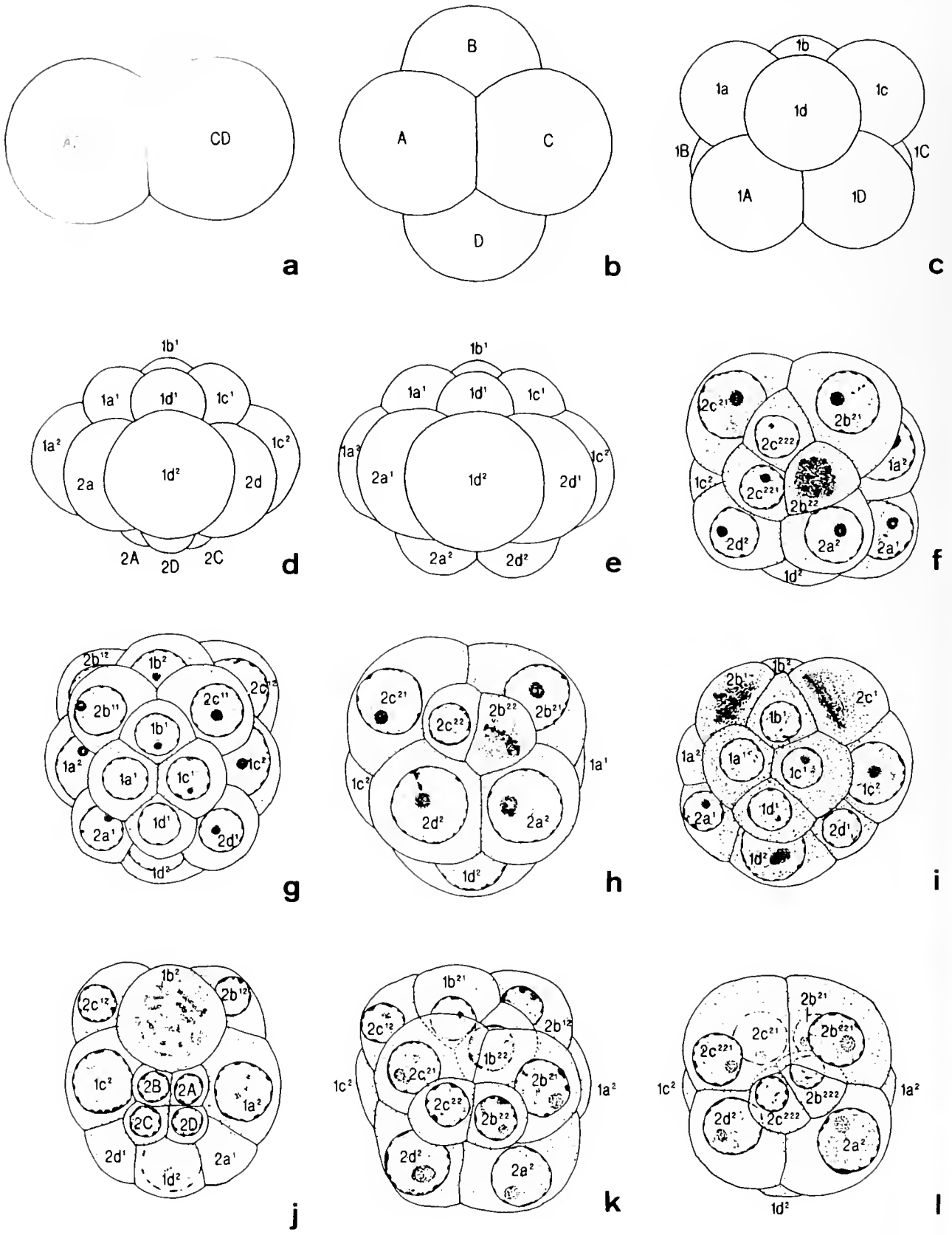

Figure 3. Sketches of early embryos of *Dicyema japonicum*. Blastomeres are named according to the notation system for spiral cleavages. Scale bar = 10 μm. **a.** Two-cell stage (from the animal pole). **b.** Four-cell stage (from the animal pole). **c.** Eight-cell stage (lateral view). **d.** Sixteen-cell stage (lateral view).

same types of cell. For example, blastomere $1a^1$ becomes the dorsal caudal cell of the left side, while blastomere $1d^1$ produces the ventral caudal cell in the midline. Ultimately, four to eight rounds of cell division take place, excluding extremely unequal divisions, until each cell is established (Table I). Germinal cells are one type of cell that is determined early in embryogenesis. The cell lineage is invariant, apart from the derivation of the lateral cell. As mentioned above, it is usually derived from $2b^1$ and $2c^1$ (see Fig. 6), but in some embryos it is derived from $1a^2$ and $1c^2$. Extremely unequal divisions, accompanied by degeneration of the much smaller daughter blastomeres, usually occur in blastomeres $2a^2$ and $2d^2$. However, it remains to be determined whether the unequal divisions occur consistently in these blastomeres in every embryo, and whether such divisions never occur in the $2b^2$ and $2d^2$ series.

The fully formed embryo consists of 37 cells (Fig. 5). Two enveloping cells (E) are flat and enclose the anterior half of the embryo; these cells are not depicted in Figure 5. Two apical cells (A) are completely enclosed by these cells and each contains one large refringent body in the cytoplasm. The nucleus is in the dorsocaudal part of each apical cell. The refringent body is known to contain magnesium inositol hexaphosphate, at least in individuals of *Dicyema typus* (Lapan, 1975). The external cells that are distinctly ciliated are as follows: two paired dorsal cells (PD), a median dorsal cell (MD), two dorsal caudal cells (DC), two lateral caudal cells (LC), a ventral caudal cell (VC), two lateral cells (L), and two posteroventral lateral cells (PVL). The cells forming the ventral surface of the embryo do not have cilia. They include two first ventral cells (V1), two second ventral cells (V2), two anterior lateral cells (AL), and a couvercle cell (C) which covers up the urn. Five cell types constitute the interior of the embryo. Two ventral internal cells (VI) have cilia that project into the urn cavity. Two dorsal internal cells (DI) and two capsule cells (CA) are not ciliated. The dorsal internal cells were once called glycogen cells (McConnaughey, 1951), but they appear to be PAS-negative. By contrast, the capsule cells have PAS-positive granules in their cytoplasm. Each of the four urn cells encloses a germinal cell in its cytoplasm. The body length, excluding cilia, of the fully formed embryo is about 24 μm and the body width is about 19 μm.

Discussion

The processes of fertilization and extrusion of the polar body in dicyemid mesozoans were studied in detail by Short and Damian (1967). However, the development of the infusoriform embryo, which is the only organism that is produced directly after fertilization, has only been studied to a limited extent (McConnaughey, 1951; Sponholtz, 1964; Lapan and Morowitz, 1975). The pattern of development in *Dicyema japonicum*, which is described herein in detail, is very different from that briefly described for *Dicyemennea adscita* and some other species by McConnaughey (1951) and from the cursory depiction in the case of unspecified species by Lapan and Morowitz (1975), although these earlier reports indicated that the early cleavages followed a spiral pattern, as we observed in this study. A spiral pattern of early cleavages appears to be universal among dicyemids.

Spiral cleavage in dicyemids is reminiscent of that in flatworms (Platyhelminthes) and this similarity may be used as an argument for a phylogenetic relationship between dicyemids and flatworms. In acoels, however, cleavages proceed by duets and small blastomeres are not produced at the vegetal pole (Apelt, 1969; Henley, 1974). In polyclads, early cleavages proceed by quartets as in dicyemids, but four small macromeres produced at the vegetal pole of the polyclad embryo are later absorbed during embryogenesis (Hyman, 1951; Kato and Minegishi, 1983). Details of developmental patterns, thus, are different between dicyemids and flatworms. In sponges (Porifera), the early cleavages are usually radial and, in coelenterates (Cnidaria), it is radial, bilateral, or partly spiral (Uchida and Yamada, 1983). The cleavage patterns of these primitive invertebrates are so diverse that a similarity in cleavage pattern *per se* may not necessarily reflect a phylogenetic relationship between the organisms concerned. Development of placozoans, *Trichoplax adhaerens*, has been only partly described (Grell, 1972), and development of fertilized eggs of the Orthonectida has never been described. Detailed comparative studies on the development of these "mesozoan" animals are necessary if we are to gain any insight into details of the evolution of these animals.

In the infusoriform embryos of dicyemids, there is no germ layer and groups of cells are roughly distinguished only as outer cells and inner cells. The outer cells, which

e. Twenty-cell stage (lateral view). Blastomeres 2A–D have been incorporated inside the embryo and, thus, they are not seen from outside. **f.** Twenty-three-cell stage (ventral view). Note a prophase figure in $2b^{22}$. **g.** Twenty-four-cell stage (dorsal view). **h.** Twenty-four-cell stage (ventral view). Note a metaphase figure in $2b^{22}$. **i.** Twenty-four-cell stage (dorsal view). Note prophase to metaphase figures in $2b^1$ and $2c^1$. **j.** Twenty-five-cell stage (horizontal optical section). Note an early prophase figure in $1b^2$. **k.** Twenty-five-cell stage (ventral view). **l.** Twenty-six-cell stage (ventral view).

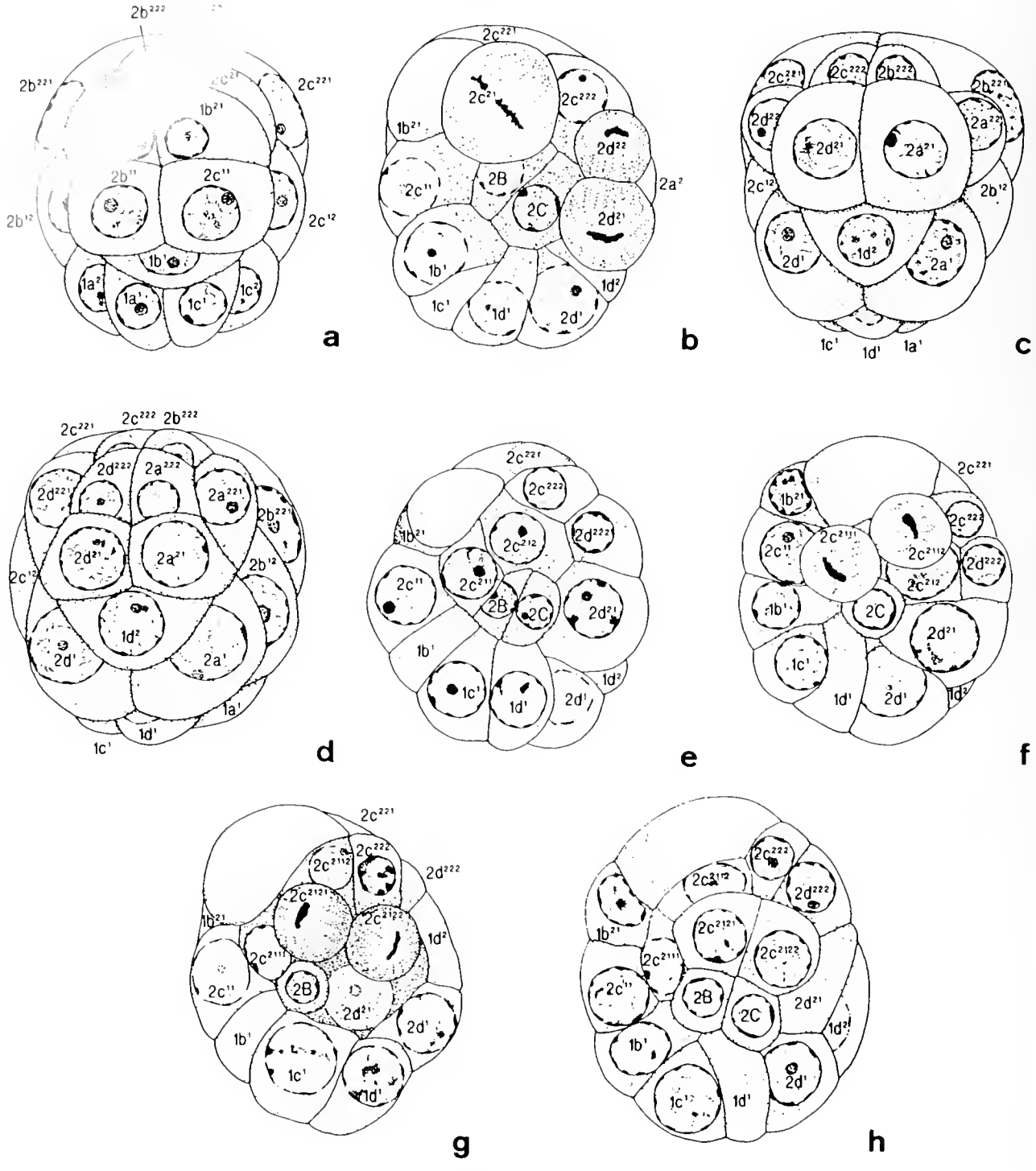

Figure 4. Sketches of late embryos of *Dicyema japonicum*. Scale bar = 10 μm. **a.** Twenty-nine-cell stage (dorsal view). **b.** Twenty-nine-cell stage (sagittal optical section). Note a metaphase figure in $2c^{21}$ and a telophase figure in $2d^{2}$. **c.** Twenty-nine-cell stage (ventral view). **d.** Thirty-three-cell stage (ventral view). Large capsule cells ($2a^{21}$ and $2d^{21}$) are still situated on the ventral surface. **e.** Thirty-three-cell stage (sagittal optical section). **f.** Thirty-three-cell stage (sagittal optical section). Note a telophase figure in $2c^{211}$ that is dividing to produce dorsal and ventral internal cells ($2c^{2111}$ and $2c^{2112}$). **g.** Thirty-six-cell stage (sagittal optical section). Note a telophase figure in $2c^{212}$ that is dividing to produce two urn cells ($2d^{2121}$ and $2d^{2122}$). **h.** Early 37-cell stage (sagittal optical section). Cell divisions have been completed, but germinal cells (2B and 2C) have not yet been incorporated into the cytoplasm of urn cells ($2c^{2121}$ and $2c^{2122}$).

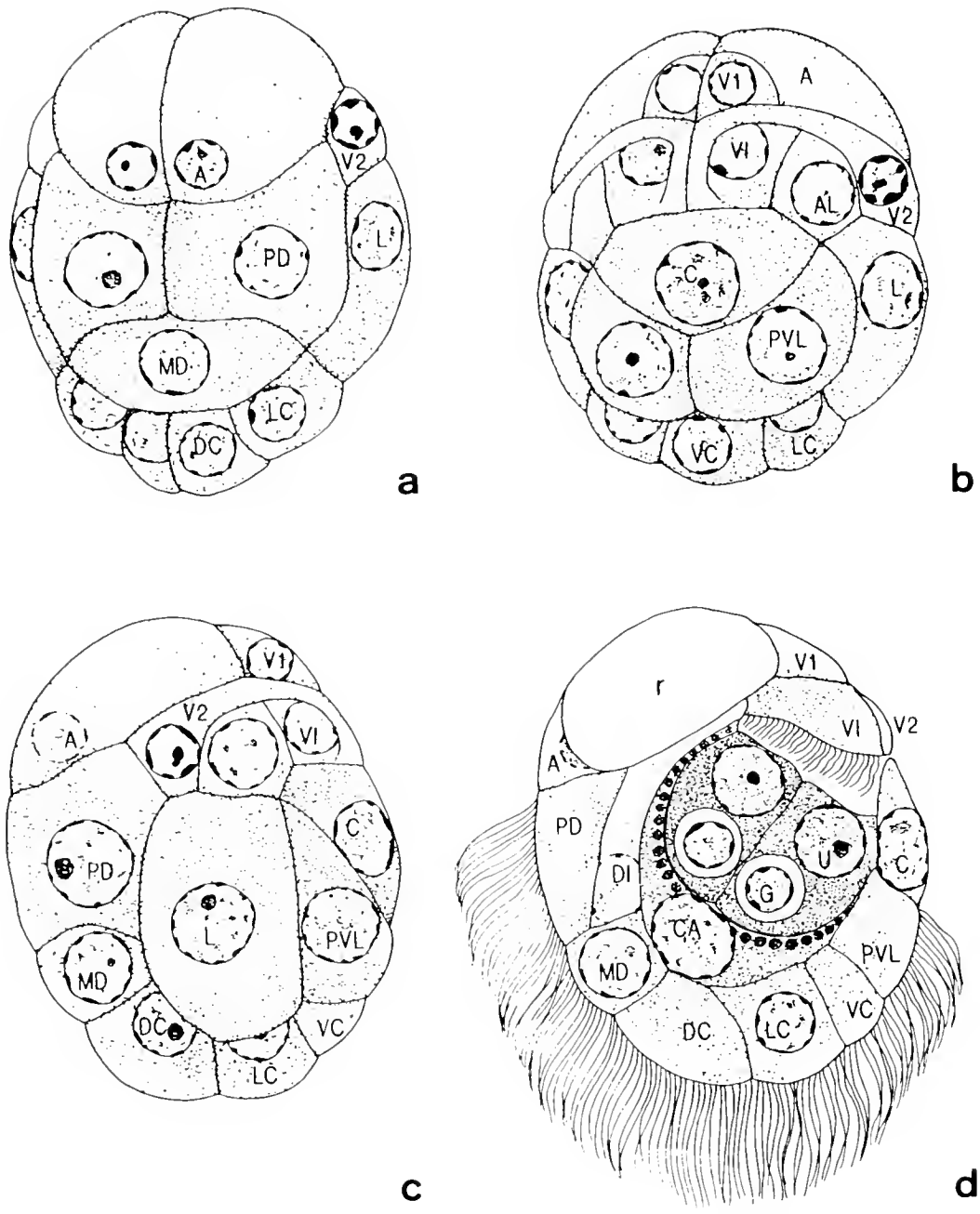

Figure 5. Sketches of a fully formed infusoriform embryo. Scale bar = 10 μm. **a.** Dorsal view. **b.** Ventral view. **c.** Lateral view. **d.** Sagittal optical section. Enveloping cells are not depicted. Cilia are omitted in **a**, **b**, and **c**. r = refringent body.

occupy the dorsal and caudal surfaces of the embryo, are ciliated and are derived from the blastomeres of the animal hemisphere of the embryo, and the inner cells are derived from the blastomeres of the vegetal hemisphere. The innermost germinal cells are derived from the cells that form the vegetal pole. These processes of cellular rearrangement are observed in many other groups of animals and appear to represent the basic pattern of the early development of animals. It is also apparent that the outer ciliated cells differentiate much earlier than the inner cells, with the exception of the germinal cells (Fig. 6 and Table I). In infusoriform embryos, the cells of the vegetal hemisphere are apparently incorporated passively into the interior of the embryo as the cells of the animal hemisphere

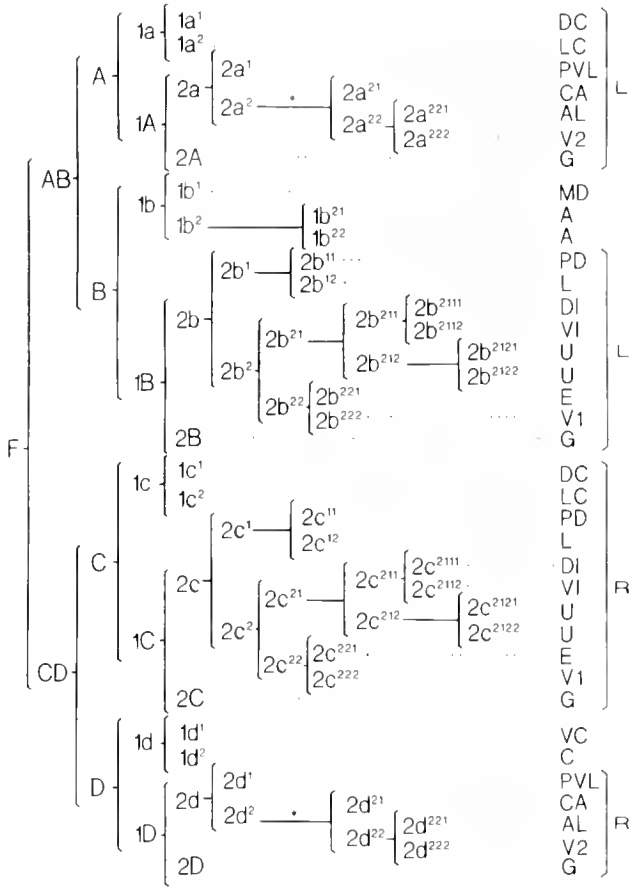

Figure 6. Cell lineage of the infusoriform embryo of *Dicyema japonicum*. Blastomeres are named according to the notation system generally used for spiral cleavage. F implies a fertilized egg. L implies the left side of the embryo and R implies the right side. See the text for explanations of abbreviations in the right column. Blastomeres $2a^2$ and $2d^2$ usually undergo extremely unequal divisions at the points marked by asterisks. The much smaller daughter blastomeres degenerate and do not contribute to the formation of the embryo. In some embryos, $1a^2$ and $1c^2$ divide once more and produce lateral cells and lateral caudal cells. In these embryos, $2b^1$ and $2c^1$ do not divide further and simply become paired dorsal cells.

proliferate. This type of development is similar to the epiboly seen in the stereoblastulae of some invertebrates including flatworms (Hyman, 1951; Henley, 1974). In dicyemids, a cavity called the urn cavity appears between the ventral internal cells and the urn, but this slit-like space is certainly formed secondarily and cannot be taken to represent a blastocoel.

In many species of dicyemid including *Dicyema japonicum*, the infusoriform finally consists of 37 cells, but in some species belonging to the genus *Dicyema* or *Dicyemennea* the infusoriforms consist of 39 cells (Short, 1971). In these latter species, there is a pair of third ventral cells in addition to the standard 37 cells. In peculiar cases such as in *Dicyema knoxi*, the infusoriform is composed of 37 cells, but there is a pair of postcapsular cells instead of a pair of anterior lateral cells (Short, 1971). In these cases, clearly, the last part of the cell lineage of the embryos is different from that of *Dicyema japonicum*. In individuals of *Dicyema japonicum*, the two blastomeres $2a^2$ and $2d^2$ usually undergo extremely unequal divisions and the resultant, much smaller daughter cells degenerate without contributing to the formation of the embryo. In his short description of the development of infusoriforms, McConnaughey (1951) noted the occurrence of chromosome elimination during embryogenesis. In individuals of *Dicyema japonicum*, at least, what takes place is not chromosome elimination, but an unequal division that results in the pycnotic degeneration of the smaller blastomere. We can offer no explanation, at present, for the production of blastomeres that are destined to die. Programmed cell death is also noted in the embryogenesis of the nematode, *Caenorhabditis elegans* (Sulston *et al.*, 1983).

In summary, the infusoriforms of dicyemids are consistently composed of only 37 or 39 cells. These cells, with more or less clear evidence of specific differentiation, such as dense cilia, PAS-positive granules, refringent bodies, and so on, are produced after only a very few rounds of cell division. The development of the infusoriform embryos of dicyemids appears to be the simplest type of development seen in the animal kingdom. Thus, these infusoriform embryos might be useful as the simplest model system for the study of cell differentiation and morphogenesis in animals, especially if a method for culture of these embryos outside the axial cell becomes available and mutants can be generated.

Table I

*The number of cleavage divisions that precede formation of each type of cell**

Number of divisions	Type of cell
Four	Dorsal caudal cells (DC), lateral caudal cells (LC), median dorsal cell (MD), ventral caudal cell (VC), couvercle cell (C), and germinal cells (G)
Five	Posteroventral lateral cells (PVL), apical cells (A), paired dorsal cells (PD), and lateral cells (L)
Six	Capsule cells (CA)
Seven	Anterior lateral cells (AL), first ventral cells (V1), second ventral cells (V2), and enveloping cells (E)
Eight	Dorsal internal cells (DI), ventral internal cells (VI), and urn cells (U)

* Extremely unequal divisions are not counted. In some embryos, paired dorsal cells are formed after four rounds of division and lateral caudal cells after five rounds of division (see text).

Acknowledgments

We express our sincere thanks to Ms. Kikuko Kurihara for her valuable assistance during the preparation of this manuscript.

Literature Cited

Apelt, G. 1969. Fortpflanzungsbiologie, Entwicklungszyklen und vergleichende Frühentwicklung acoeler Turbellarien. *Mar. Biol.* **4:** 267–325.

Furuya, H., K. Tsuneki, and Y. Koshida. 1992. Two new species of the genus *Dicyema* (Mesozoa) from octopuses of Japan with notes on *Dicyema misakiense* and *Dicyema acuticephalum*. *Zool. Sci.* **9:** 423–437.

Ginetsinskaya, T. A. 1988. *Trematodes, Their Life Cycles, Biology and Evolution.* Amerind Publishing Co. Pvt. Ltd., New Dehli. (Translation of the original Russian edition, 1968).

Grell, K. G. 1972. Eibildung und Furchung von *Trichoplax adhaerens* F. E. Schulze (Placozoa). *Z. Morphol. Tiere* **73:** 297–314.

Henley, C. 1974. Platyhelminthes (Turbellaria). Pp. 267–343 in *Reproduction of Marine Invertebrates, Vol. 1* A. C. Giese and J. S. Pearse, eds., Academic Press, New York.

Hochberg, F. G. 1982. The "kidneys" of cephalopods: a unique habitat for parasites. *Malacologia* **23:** 121–134.

Hochberg, F. G. 1983. The parasites of cephalopods: a review. *Mem Nat. Mus. Vic.* **44:** 109–145.

Hyman, L. 1940. *The Invertebrates, Vol. I* McGraw Hill, New York.

Hyman, L. 1951. *The Invertebrates, Vol. II* McGraw Hill, New York.

Hyman, L. 1956. *The Invertebrates, Vol. V* McGraw Hill, New York.

Hori, H., and S. Osawa. 1987. Origin and evolution of organisms as deduced from 5S ribosomal RNA sequences. *Mol. Biol. Evol.* **4:** 445–472.

Kato, K., and H. Minegishi. 1983. Turbellaria. Pp. 145–158 in *Invertebrate Embryology, Vol. I* K. Dan, K. Sekiguchi, Y. Ando, H. Watanabe, eds., Baifukan, Tokyo (in Japanese).

Lapan, E. A. 1975. Magnesium inositol hexaphosphate deposits in mesozoan dispersal larva. *Exp. Cell Res.* **94:** 277–282.

Lapan, E. A., and H. J. Morowitz. 1974. Characterization of mesozoan DNA. *Exp. Cell Res.* **83:** 143–151.

Lapan, E. A., and H. J. Morowitz. 1975. The dicyemid Mesozoa as an integrated system for morphogenetic studies. 1. Description, isolation and maintenance. *J. Exp. Zool.* **193:** 147–160.

Matsubara, J. A., and P. L. Dudley. 1976. Fine structural studies of the dicyemid mesozoan, *Dicyemennea californica* McConnaughey. II. The young vermiform stage and the infusoriform larva. *J. Parasitol.* **62:** 390–409.

McConnaughey, B. H. 1951. The life cycle of the dicyemid Mesozoa. *Univ. Calif. Publ. Zool.* **55:** 295–336.

Nouvel, H. 1948. Les Dicyémides. 2e partie: infusoriforme, tératologie, spécificité du parasitisme, affinités. *Arch. Biol.* **59:** 147–223.

Short, R. B. 1971. Three new species of *Dicyema* (Mesozoa: Dicyemidae) from New Zealand. *Biology of the Antarctic Seas* **IV:** 231–249.

Short, R. B., and R. T. Damian. 1966. Morphology of the infusoriform larva of *Dicyema aegira* (Mesozoa: Dicyemidae). *J. Parasitol.* **52:** 746–751.

Short, R. B., and R. T. Damian. 1967. Oogenesis, fertilization, and first cleavage of *Dicyema aegira*. *J. Parasitol.* **53:** 185–195.

Sponholtz, G. M. 1964. The early embryology and morphology of the infusoriform larva of a species of *Dicyema* (Mesozoa: Dicyemidae). Master Thesis, Florida State University.

Stunkard, H. W. 1954. The life history and systematic relations of the Mesozoa. *Q. Rev. Biol.* **29:** 230–244.

Sulston, J. E., E. Schierenberg, J. G. White, and J. N. Thomson. 1983. The embryonic cell lineage of the nematode *Caenorhabditis elegans*. *Dev. Biol.* **100:** 64–119.

Uchida, T., and M. Yamada. 1983. Cnidaria. Pp. 103–133 in *Invertebrate Embryology, Vol. I.* K. Dan, K. Sekiguchi, Y. Ando, H. Watanabe, eds., Baifukan, Tokyo (in Japanese).

Reference: *Biol. Bull.* **183**: 258–268. (October, 1992)

Cell Movements during Gastrulation of Starfish Larvae

RITSU KURAISHI AND KENZI OSANAI

Marine Biological Station of Asamushi, Tohoku University, Asamushi, Aomori 039-34, Japan

Abstract. Archenteron formation was monitored by measurement of cellular volume, injection of tracer enzyme, and vital staining. The cellular volume of the whole embryo did not change significantly from the start of gastrulation to the beginning of the mesenchyme-migration stage; the archenteron increased from about 10–20% during these stages. Tracer injection revealed that the boundary between the progenies of the veg1 and veg2 blastomeres of 32-cell-stage embryos was in the outer layer at the early gastrula stage, and at the rear end of the stomach at the bipinnaria stage. These results demonstrate a migration of cells from the outer layer to the archenteron wall during starfish gastrulation. Vital staining marks around the blastopore showed that the presumptive esophagus, stomach, and intestine area were added to the archenteron at the start of gastrulation, during the early to late gastrula stage, and thereafter, respectively. Tracer injection also indicated that the presumptive zone of the cardiac sphincter was twisted about 180° clockwise around the axis of the archenteron after the late gastrula stage, dragging the cells in the presumptive zone of the esophagus and stomach.

Introduction

Gastrulation is a striking event in the early development of echinoderms. It involves a dynamic morphological change from a monolayered to a multilayered embryo, accompanied by differentiation of the mesendoderm from the ectoderm.

Starfish embryos are good materials for investigation of the mechanism of gastrulation because both oocytes and embryos of starfish have markers for the presumptive site of archenteron formation (Schroeder, 1985; Kuraishi and Osanai, 1989) and, because the oocytes, embryos, and blastomeres are larger than those of sea urchins. This provides an advantage in microsurgery. In addition, both oocyte fragments and blastomeres derived from the animal hemisphere have little capacity for archenteron formation (Maruyama and Shinoda, 1990; Zhang *et al.*, 1990), unlike those of sea urchins (Henry *et al.*, 1989; Khaner and Wilt, 1990). They would be good recipients for implantation experiments to investigate cytoplasmic determinants responsible for archenteron formation.

Despite such advantages, little is known about the morphogenetic movements of archenteron formation in normal starfish larvae. Thus, we traced the movement of cells into the archenteron wall by measuring the volume of the archenteron wall, tracer enzyme injection, and vital staining.

Received 28 January 1992; accepted 1 June 1992.

Materials and Methods

Materials

Adult individuals of *Asterina pectinifera* were collected during their breeding season at Asamushi, Aomori prefecture, and at Hashirimizu, Kanagawa prefecture (Japan). Gametes were prepared as described elsewhere (Kuraishi and Osanai, 1988). Oocyte maturation was induced by treatment with 1 μm 1-methyl adenine (1-MeAde). The oocytes were fertilized about 45 min after the start of 1-MeAde treatment. The fertilized eggs were washed with filtered seawater and allowed to develop at about 19°C.

Measurement of cellular volume in gastrulae

The cellular volume of the archenteron and the outer layer was calculated based on the practically rotationally symmetrical shape around the animal-vegetal axis. The larvae were photographed through a plane including the animal-vegetal axis. The boundary between the archenteron and outer layer was determined tentatively in the plane as a line running parallel to the axis and passing the most posterior point of the basal surface of the

embryonic wall. An imaging, two-dimensional coordinate system was prepared on the photographic print where the animal pole and animal-vegetal axis were defined as the origin and x-axis, respectively. Then the grids that were perpendicular to the x-axis were settled at every micrometer along the x-axis. The shape of the archenteron and outer layer was recorded by establishing the coordinates where these outlines crossed the grids, using an electronic digitizer. The volume was measured by calculating that of the solid of revolution obtained by rotating the shape around the animal-vegetal axis. In order to photograph the gastrulae through the mid-sagittal optical plane with minimum deformation resulting from immobilization, ciliary movement of the gastrulae was inhibited with 100 m*M* sodium azide in 80% filtered seawater, and the gastrulae were transferred to a wedge-shaped "egg holder" (Kishimoto, 1986). The holder was placed narrow side down for a few minutes, to allow most of the gastrulae to settle in the wedge with their lateral side against the wall. Then optical sections of the gastrulae including the anteroposterior axis were photographed. The concentration of sodium azide required for inhibition of ciliary movement was much higher than that for the sea urchin, *Hemicentrotus pulcherrimus* (Kominami, 1988). However, no unfavorable influence was observed after this treatment, providing the duration was less than 15 min.

Intracellular injection of horseradish peroxidase

A tracer enzyme, horseradish peroxidase (HRP), was injected into blastomeres iontophoretically following the procedure of Nishida (1987). The equipment used for micro-manipulation was set up according to Maruyama *et al.* (1986). The electrodes were made by pulling out glass capillary tubes with inner fibers (GD-1, Narishige Sci. Inst. Lab.) using a microelectrode puller (PG-1, Narishige Sci. Inst. Lab.). They were filled with 2% HRP in 0.2 *M* KCl at the tip, and then backfilled with 0.2 *M* KCl by sandwiching a small amount of silicone oil. The resistance of each electrode was adjusted to 15–30 MΩ by breaking the tip. HRP was introduced into the blastomere with a positive current of 10–15 nA for 30–90 s. The embryos were then transferred separately into individual holes of a 24-hole culture plate.

To examine the distribution of descendant cells of the injected blastomere, they were fixed in 1% glutaraldehyde in filtered seawater overnight at 4°C. The fixed specimens were also stained histochemically according to Nishida (1987), and observed as whole mounts using light microscopy.

Vital staining of larvae

Gastrulae were suspended in 0.05% Nile blue sulfate in filtered seawater for 30–60 s and washed thoroughly with filtered seawater to mark the outer layer. This treatment only stained deeply the Nile blue-positive granules (Kuraishi and Osanai, 1989) of cells in the outer layer.

Larvae were first held in an egg holder to individually mark the blastopore lip and the archenteron of the gastrulae. A fine glass capillary with a 1 μm diameter tip filled with 1% Nile blue sulfate in distilled water was pushed against the area to be stained and the Nile blue solution was ejected gradually for about 30 s by pressure. Because the position of the stained region differed among the larvae, the stained larvae were photographed and reared individually in each hole of the 24-well culture plate. For observation and microphotography of the swimming larvae at later stages, their ciliary movement was inhibited by 100 mM sodium azide in 80% filtered seawater and then they were mounted in an egg holder. The orientation of the larvae was adjusted by micromanipulation.

Results

Morphological aspects of gastrulation

The larvae started gastrulation about 17–18 h after onset of 1-MeAde treatment. Hereafter, the developmental time referred to represents the time after 1-MeAde treatment. At the beginning of gastrulation, the vegetal plate covering about half of the larva's diameter invaginated at the posterior end (vegetal pole) of the larva (Fig. 1A). The gastrula stage was divided into five substages according to Dan-Sohkawa *et al.* (1986).

The early gastrula stage extended from the start of gastrulation to 22 h, during which the blastopore gradually decreased in diameter (Fig. 1A, B). At the end of this stage, the length of the archenteron had reached about ⅓ that of the whole larva.

The mesenchyme differentiation stage extended from 22–27 h. The body of the larva elongated along the anteroposterior axis, and the length of the archenteron reached half that of the whole larva by the end of this stage. The tip of the archenteron appeared spherical and swelled to ½ of the larva's diameter. The cell layer of this region became thinner than that of the other parts of the embryo. The rest part of the archenteron appeared cylindrical, with an outer diameter about ¼ that of the outer layer (Fig. 1C).

The mesenchyme migration stage extended from 27 to 35 h. The appearance of the larvae was almost the same as that at the mesenchyme differentiation stage, except for the presence of mesenchyme cells in the blastocoel, having ingressed from the tip of the archenteron.

The late gastrula stage extended from 35 to 40 h. The mesenchyme cells spread all over the blastocoel, and the

Figure 1. Normal larvae of *Asterina pectinifera*. (A) start of gastrulation; (B) early gastrula stage; (C) mesenchyme-differentiation stage; (D) late gastrula stage; (E, F) mouth-formation stage; and (G, H) bipinnaria stage. (E, G) Observed from dorsal side. (F, H) Observed from right side. ac = anterior coelom, pc = posterior coelom, e = esophagus, s = stomach, i = intestine. Scale bar = 100 μm.

outer layer became flattened slightly in a dorso-ventral direction (Fig. 1D).

Mouth-formation stage extended from 40 to 48 h, during which time the body became much more flattened in a dorso-ventral direction. The blastopore decreased in diameter and moved to the ventral side (Fig. 1F). A pair of coelomic rudiments projected to the lateral side from the tip of the archenteron (Fig. 1E). The outer diameter of the posterior $\frac{1}{3}$ of the rest of the archenteron started to increase gradually. A rudiment of the left posterior coelom projected into the blastocoel from the dorsal wall of this widening region and began to migrate to the left side (Fig. 1F). The archenteron began to bend toward the ventral side, where invagination of the stomodaeum had already begun.

Larvae reached the early bipinnaria stage at about 72 h. The digestive tract had differentiated into the esophagus, stomach, and intestine. The boundary between the esophagus and stomach was sharply constricted by the cardiac sphincter. The boundary between the stomach and intestine was not so obviously constricted by the pyloric sphincter compared to that of sea urchins. Coeloms existed on both sides of the esophagus and by the left side of the stomach (Fig. 1G).

Cellular volume of archenteron

In sea urchins, translocation of cells from the outer layer into the archenteron wall occurs only in the first few hours of gastrulation (Horstadius, 1973; Hardin, 1989; Burke *et al.*, 1991). To clarify whether this also occurs in

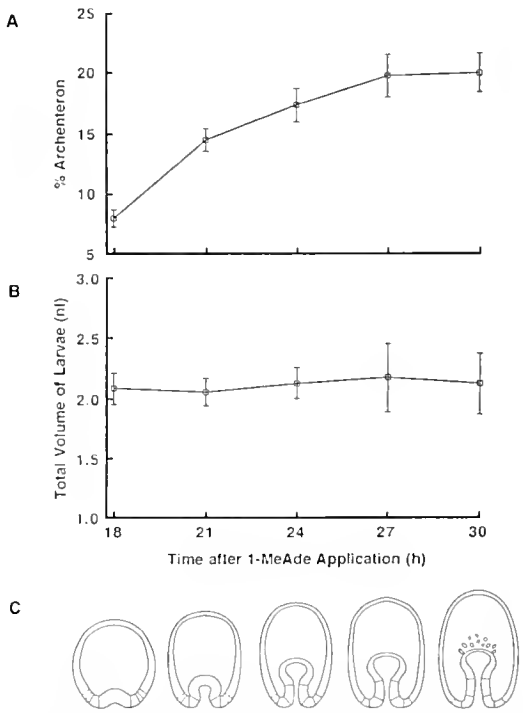

Figure 2. (A, B) Change in the total volume of the embryonic wall of normal gastrulae (B) and relative volume of the archenteron wall against the total (A) in a typical batch of *Asterina pectinifera*. (C) Outlines of typical gastrulae at the start of gastrulation (18 h), early gastrula stage (21 h), mesenchyme-differentiation stage (24 h, 27 h), and mesenchyme-migration stage (30 h) shown with calculated 10, 15, 20, and 25% relative volume lines. The volumes were measured in more than 10 individuals for each data point in A and B. The error bar represents the 99% confidence interval. The volume of the mesenchyme cells was neglected in volume measurement at 30 h.

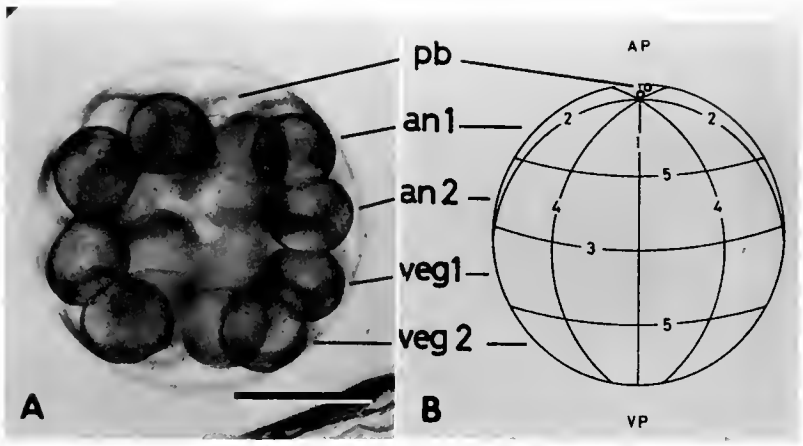

Figure 3. A 32-cell-stage embryo of *Asterina pectinifera* (A) and a schematic illustration showing the position of cleavage planes up to the 5th cleavage (B). AP = animal pole, VP = vegetal pole, pb = polar bodies, 1 = first cleavage plane, 2 = second cleavage plane, 3 = third cleavage plane, 4 = fourth cleavage plane, 5 = fifth cleavage plane. Though each cleavage divides the blastomere almost equally, the axis of animal-vegetal polarity is detectable by the position of the polar bodies. Scale bar = 100 μm.

starfish gastrulation, the volume of the embryonic wall in both the archenteron and the outer layer was measured. Since the volume was calculated assuming that the body of the larva was rotationally symmetrical around the antero-posterior axis, only larvae younger than the mesenchyme migration stage were used.

The relative volume of the vegetal plate, which invaginated at the start of gastrulation, ranged from 8 to 10% of the whole volume of the embryonic wall in the three batches used (Fig. 2A). The volume ratio of the wall of the archenteron increased to about 15% by the end of the early gastrula stage, and to about 20% by the end of the mesenchyme differentiation stage (Fig. 2A). In spite of the increase in the relative volume of the archenteron wall, the cellular volume of the whole embryo did not change significantly, and was almost identical to that of immature oocytes. This suggests that translocation of cells into the archenteron continues at least until the mesenchyme differentiation stage.

The areas having volume ratios of 10, 15, 20, and 25% from the tip of the archenteron were also calculated in each of the larvae used for volume measurement. Figure 2C shows outlines of typical specimens in the batch used to plot Figure 2A and B, with the 10, 15, 20, and 25% lines indicated.

Intracellular injection of HRP

In sea urchins, descendants of veg2 cells invaginate as the vegetal plate during the primary phase of gastrulation and form most of the archenteron (Horstadius, 1973; Davidson, 1989). To clarify if this occurs in starfish gastrulae, a tracer enzyme, HRP, was injected into cells in the tiers occupying the vegetal or subequatorial quarter of the embryo. The labeling pattern was then observed at the early gastrula and bipinnaria stages. A typical embryo of *A. pectinifera* showed almost equal orthoradial cleavage (Fig. 3B). At the 32-cell stage, the embryo consisted of four tiers, each containing eight cells. These tiers were named an1, an2, veg1, and veg2 from the animal pole to the vegetal pole (Fig. 3A). HRP was injected into one of the veg1 or the veg2 blastomeres at this stage. When one of the veg1 blastomeres was injected with HRP, the labeled cells were distributed only in the posterolateral region of the outer layer at the early gastrula stage (Fig. 4A, B). At the bipinnaria stage, the labeled cells were distributed not only in the posterior part of the ectoderm but also in the intestine and the rear end of the stomach (Fig. 4D). However, when one of the veg2 blastomeres was injected, the labeled cells were distributed from the tip of the archenteron to the posterior end of the outer layer at the early gastrula stage (Fig. 4C), and from the esophagus to the rear end of the stomach at the bipinnaria stage (Fig. 4E). This shows that the boundary area between veg1 and veg2 was added to the archenteron after the early gastrula stage.

The band of labeled cells was twisted torsionally in the esophagus and in the stomach (Fig. 4E). The results of careful observation of this aspect are described later.

Vital staining with Nile blue

To observe the movement of involuting cells during the gastrula stage more precisely, cells in either the outer layer or the archenteron were vitally stained with Nile

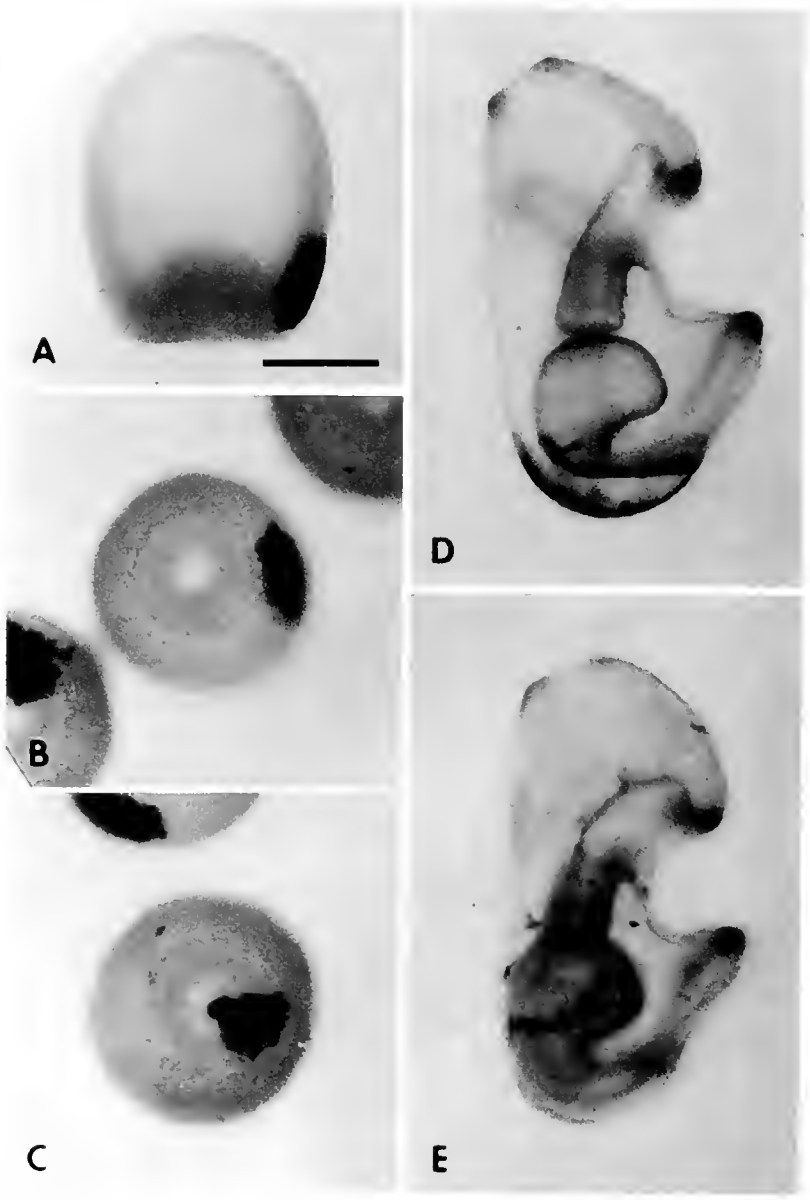

Figure 4. Larvae of *Asterina pectinifera* following injection of HRP into one of the veg1 blastomeres (A, B, D) and veg2 blastomeres (C, E) at the 32-cell stage, observed at the early gastrula stage (A–C), and the bipinnaria stage (D, E). A, D, E shown in lateral view, B in rear view of the same larva as that in A1, and C in rear view. The boundary between the labeled regions is located in the outer layer at the early gastrula stage (A–C), but at the rear end of the stomach at the bipinnaria stage (D, E). Scale bar = 100 μm.

blue. When the outer layer was stained at the early gastrula stage (Fig. 5A2), the cylindrical part of the archenteron consisted of stained cells from the mesenchyme differentiation stage to the late gastrula stage (Fig. 5B2, C2). After the mouth-formation stage, the outer diameter of the stained region of the archenteron increased (Fig. 5D2). At the bipinnaria stage, the stomach, the intestine, and the left posterior coelom consisted of stained cells (Fig. 5E2). In bipinnariae which were stained at the mesenchyme differentiation stage, the posterior part of the stomach and the intestine consisted of stained cells (Fig. 6A1, A2). When the outer layer was stained at the late gastrula stage, the area of Nile blue was observed all over the intestine other than the ectoderm (Fig. 6B1, B2). When the posterior end of the archenteron near the blastopore or the blastopore lip was stained as a control to check

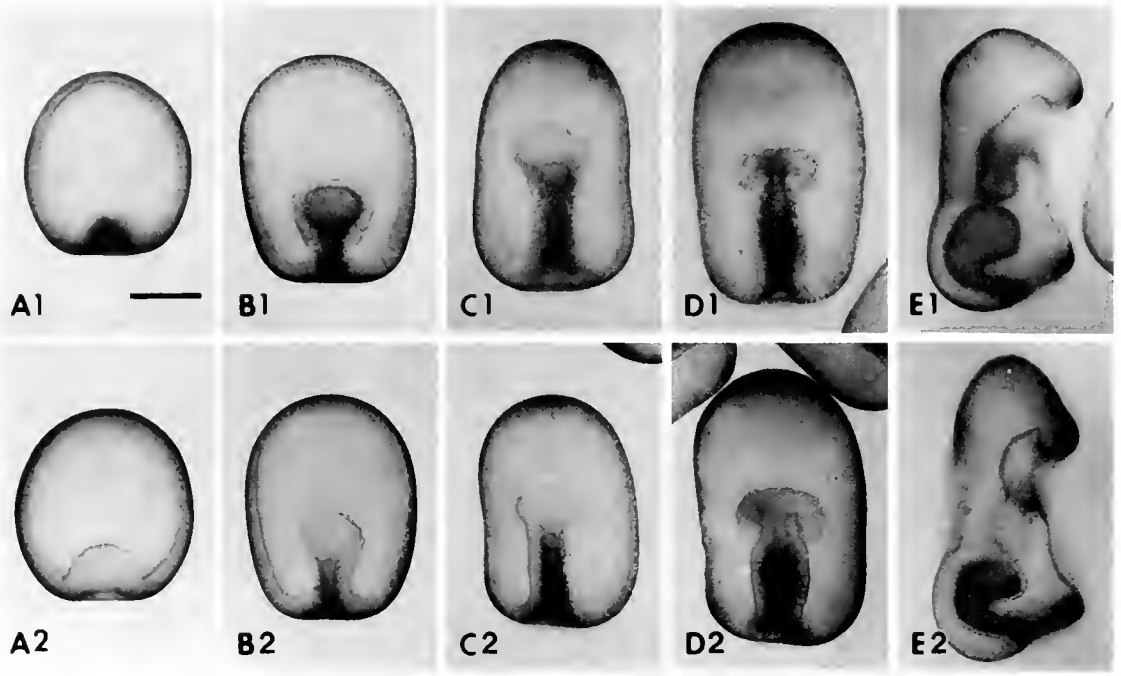

Figure 5. Larvae of *Asterina pectinifera* stained with Nile blue at the blastula stage (1) and at the early gastrula stage (2). (A) early gastrula stage, (B) mesenchyme-differentiation stage, (C) late gastrula stage, (D) mouth-formation stage, (E) bipinnariae stage. When larvae were stained at the early gastrula stage, stained Nile blue-positive granules were not observed in the archenteron (A2), tip of the archenteron (B2–D2), or the esophagus (E2). Scale bar = 100 μm. Since the larvae are flattened due to pressure from the coverslips in 1–4, they appear larger than usual.

dispersal of the dye, unstained cells became detectable behind the stained region in the archenteron in the later stages (Fig. 7).

The boundary between the stained and unstained regions in larvae that were stained at the early gastrula stage almost coincided with the position of the 10% line in Figure 2C at both the early gastrula and mesenchyme differentiation stages (Fig. 5A2, B2). This confirms that vital staining is a reliable method for monitoring cellular movement during the gastrulation process.

Lateral movement of archenteron cells

When HRP was injected into one of the veg2 blastomeres in a 32-cell-stage embryo, the band of labeled cells appeared twisted torsionally in the digestive tract at the bipinnaria stage (Fig. 4D, E). To examine this twisting more precisely, one of the blastomeres in the vegetal hemisphere of an 8- or 16-cell-stage embryo was injected with HRP and the distribution of labeled cells was observed at the bipinnaria stage. Figure 8 shows four complementary patterns in which left ventral (A), left dorsal (B), right dorsal (C), and right ventral (D) regions in the posterior part of the ectoderm were labeled. In all cases, the band of labeled cells was parallel to the axis of the digestive tract from the anus to the posterior end of the stomach, sharing the same orientation as the ectoderm relative to the dorso-ventral axis. However, the band was twisted torsionally about 180° clockwise from the posterior end of the stomach to the cardiac sphincter, and about the same degree counterclockwise from the cardiac sphincter to the stomodaeum.

To determine when the digestive tract (or the archenteron) became twisted, the distribution of labeled cells was also observed at earlier stages. From the early gastrula stage to the mesenchyme differentiation stage, the bands of the labeled cells were not twisted (Fig. 9A). At the late gastrula stage, the band was twisted slightly clockwise at the anterior part of the cylindrical region of the archenteron and counterclockwise at the posterior half of the inflated region (Fig. 9B). At the mouth formation stage, the band was twisted much more evidently (Fig. 9C). These results show that the presumptive region of the cardiac sphincter rotated about 180° clockwise around the longitudinal axis of the archenteron, dragging the presumptive zone of the esophagus and stomach, after the mesenchyme-differentiation stage.

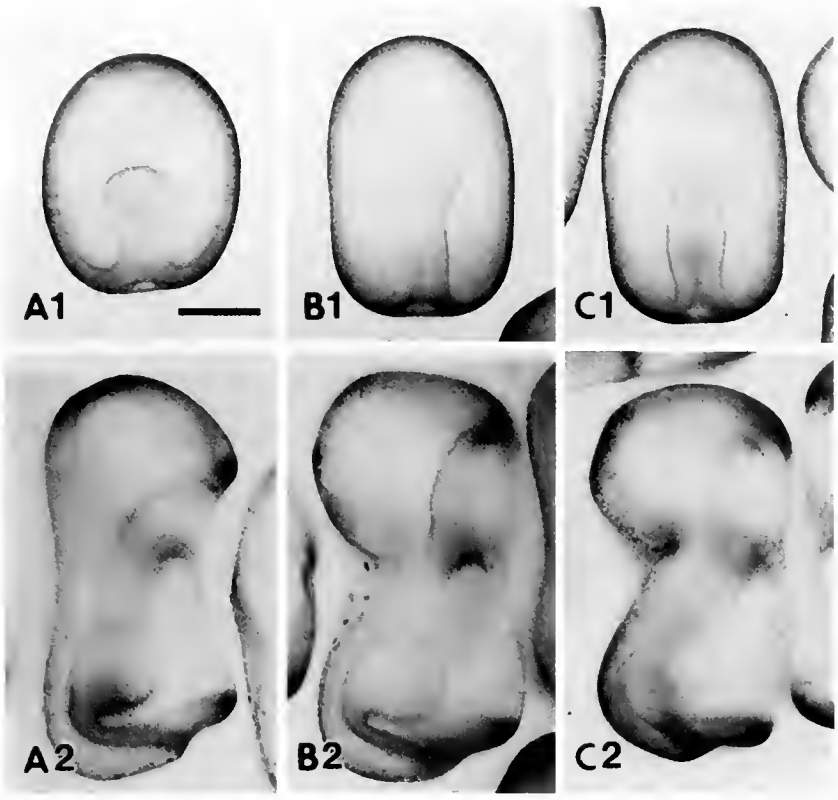

Figure 6. Larvae of *Asterina pectinifera* stained with Nile blue at the mesenchyme-differentiation stage (A), the late gastrula stage (B), and the mouth-formation stage (C), observed just after staining (1) and at the bipinnaria stage (2). The whole archenteron (A–C), esophagus and anterior half of the stomach (A2–C2), posterior half of the stomach (B2, C2), and anterior half of the intestine (C2) are constructed of unstained cells. Scale bar = 100 μm.

When the left dorsal side of the ectoderm was labeled, labeled cells distributed only in the anterior region in the left posterior coelom (Fig. 8B2). In contrast, when the right dorsal side of the ectoderm was labeled, the labeled cells distributed only in the posterior region in the left posterior coelom (Fig. 8C2).

Discussion

The present study demonstrates that in gastrulae of *A. pectinifera*, cells at the rear end of the outer layer are added to the archenteron throughout the gastrula stage, constructing the posterior part of the archenteron. The volume ratio of the archenteron was 8–10% at the start of gastrulation, increasing to 15% at the early gastrula stage and reaching 20% at the start of the mesenchyme migration stage. Kominami (1984) showed that the relative volume of the archenteron wall ranges from 20 to 25% at the early to mid gastrula stage (= mesenchyme migration stage in this study) in *A. pectinifera*. This result is almost consistent with our result obtained from 30-h embryos. He considered that the vegetal quarter of the embryos would differentiate into the mesendoderm, provided that the amount of cellular material in the archenteron did not increase afterward. However, the result of vital staining shows that translocation of cells into the archenteron wall continued thereafter.

Evidence from HRP-injection in the present study indicate that the coeloms, mesenchyme cells, esophagus, and the stomach are formed of veg2 descendants. The result of the vital staining shows that the presumptive area of these organs are added to the archenteron from the start of gastrulation to the late gastrula stage. Since cleavage in *A. pectinifera* is almost equal, the volume of each tier is about 25% of the whole volume of the embryo at the 32-cell stage. Thus, the increase in the volume of the archenteron during the mesenchyme-migration and late-gastrula stage is calculated to be about 5% (25 − 20%) of the whole volume of the larvae. The intestine is mainly formed of veg1 descendants (Fig. 4D), which are added to the archenteron after the late gastrula stage (Fig. 6C). The length and the outer and inner diameter of the

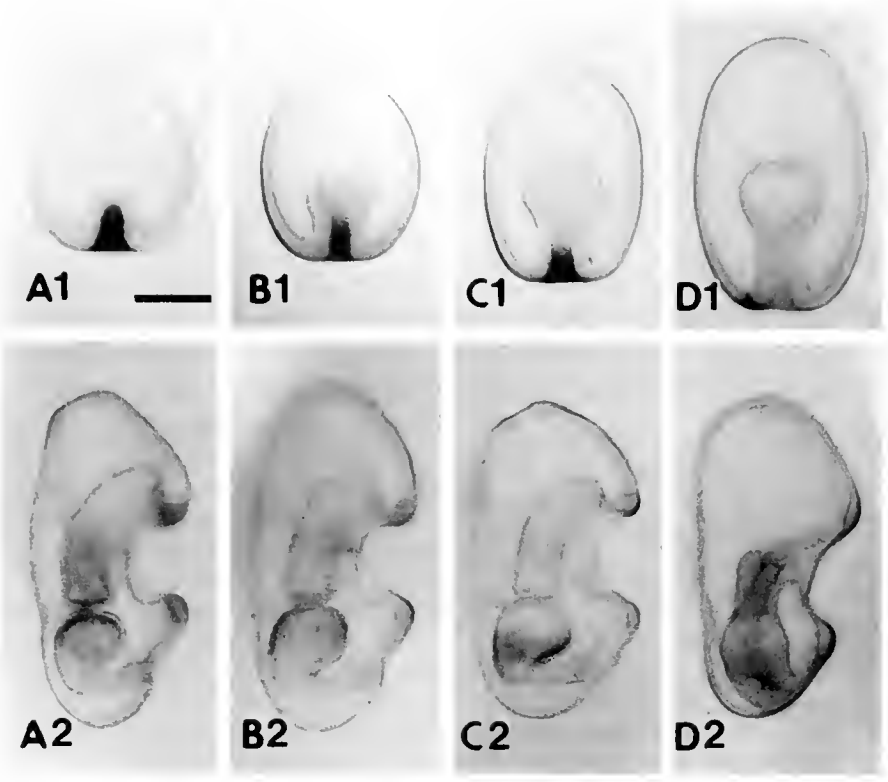

Figure 7. Larvae of *Asterina pectinifera* in which the posterior part of the archenteron near the blastopore (A–C) or the blastopore lip (D) was stained with Nile blue. Row 1 shows larvae just after staining. (A) early gastrula stage, (B) mesenchyme differentiation stage, (C) late gastrula stage, and (D) mesenchyme migration stage. Row 2 shows the same larvae as those in row 1 observed at the bipinnaria stage (A–C) or at the end of the mouth formation stage (D). Scale bar = 100 μm.

intestine of the bipinnaria in Figure 2H are 150 μm, 30 μm, and 10 μm, respectively. The volume is calculated to be about 0.1 nl (about 5% of the whole volume of the larvae before the mesenchyme-migration stage), assuming that it is a simple tube. Thus, volume increase of the archenteron wall continues after the mesenchyme-migration stage, though the rate decreases considerably.

In sea urchins, cellular materials are also added to the archenteron wall from the outer layer during the primary phase of gastrulation (Ettensohn, 1984; Burke *et al.*, 1991), while the apico-basal length of the cells around the vegetal pole decreased only slightly. These facts indicate that the buckling of the cell sheet is not the result of cell rounding, as suggested by Gustafson and Wolpert (1963, 1967) (Ettensohn, 1984). Our results shows that this is also the case in starfish.

In sea urchin embryos, however, translocation of cells from the outer layer to the archenteron wall only lasts for the first few hours of gastrulation (Hardin, 1989; Burke *et al.*, 1991) and the active cell rearrangement is proposed to be the major mechanism for the archenteron elongation thereafter (secondary phase of gastrulation) (Ettensohn, 1985; Hardin and Cheng, 1986; Hardin, 1989). Hardin (1989) showed that the cell number and the volume of the archenteron did not change significantly during the secondary phase of gastrulation, though the definition of the archenteron area is not clearly demonstrated in his report. The volume of the boundary region is relatively large because the thickness of the larval wall and the distance from the axis of symmetry is greater than in other parts of the archenteron. Cell number and calculated volume would thus vary widely depending on where the boundary is determined. It might be possible that different definition in the archenteron area lead to the different conclusion. However, the evidences from the vital staining at the rear end of the larvae also indicate that the cell addition from the outer layer occurs only in starfish in later stages of gastrulation (Hardin, 1984; Burke *et al.*, 1991; Figs. 6, 7). On the other hand, the band of HRP-labeled cells in the gastrula appeared narrow in later stages (Fig. 9) suggesting that rearrangement of cells may also be the mechanism of archenteron elongation in starfish. The change in the mechanism of gastrulation appears to progress rather more gradually in starfish than sea urchins.

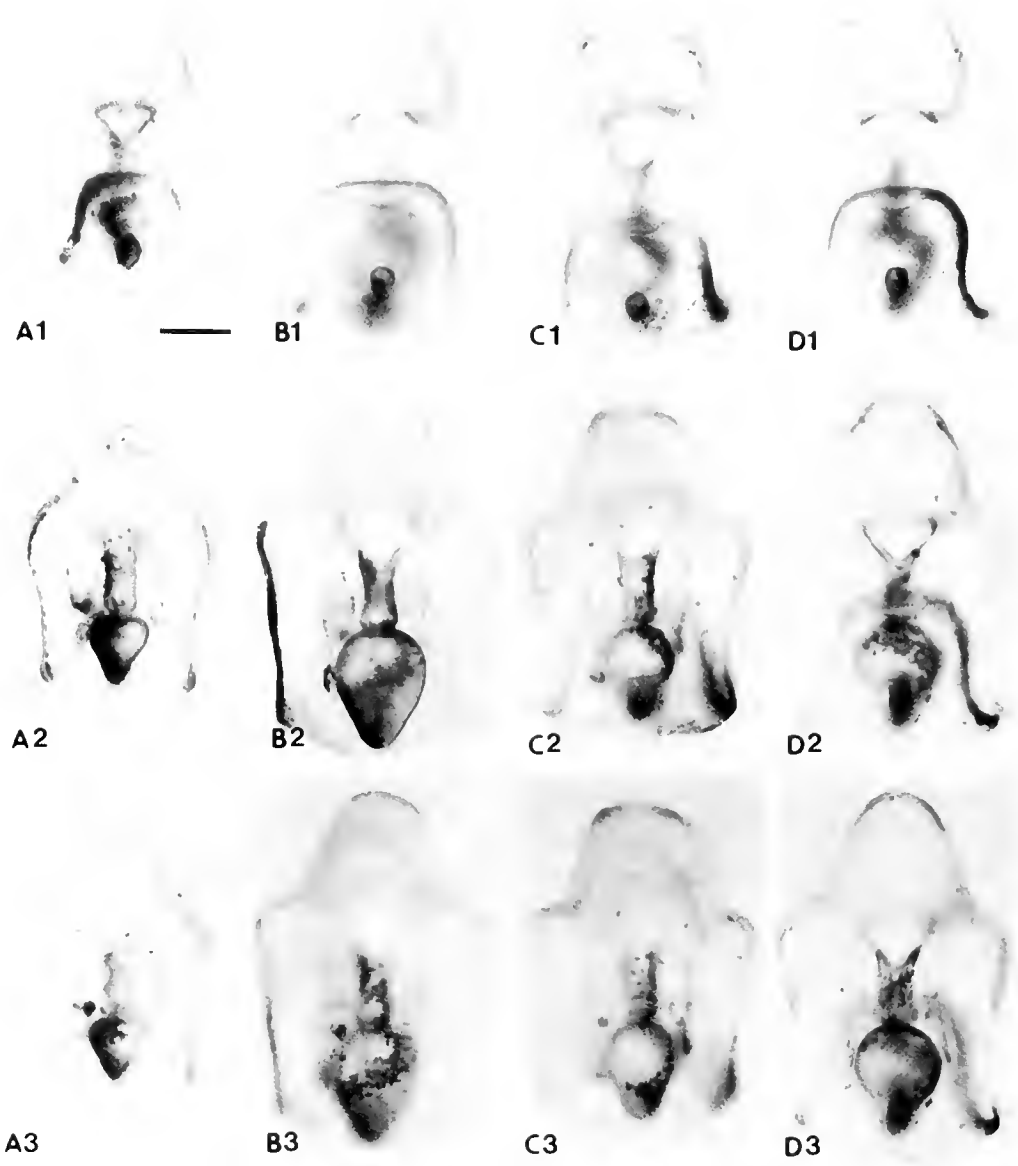

Figure 8. Bipinnariae in which one of the vegetal-half blastomeres was injected with HRP at the 8-cell stage. The left ventral (A), left dorsal (B), right dorsal (C), and right ventral (D) parts of the posterior ectoderm and part of the digestive tract are stained, respectively. Scale bar = 100 μm. All photographs are printed to allow observation from the dorsal side. A1–D1 are focused at the anus; C2 and D2 are focused at the ventral surface of the stomach; A2, B2, and D3 are focused at the axis of the esophagus; and A3, B3, and C3 are focused at the dorsal surface of the stomach. The band of labeled cells is twisted clockwise in the stomach, and counterclockwise in the esophagus in all cases. The anterior and posterior halves of the left posterior coelom are labeled in B2 and C2, respectively.

The movements of mesendoderm cells in larvae of *A. pectinifera* are shown in Figure 10. The cellular volume of the vegetal plate which invaginated at the start of gastrulation is 8–10% of the total volume of the embryo. Later, this region becomes the swelled region at the tip of the archenteron and sheds mesenchyme cells into the blastocoel. The anterior half of this region begins to project laterally at the mouth-formation stage, and becomes the anterior coelom of the bipinnaria. The posterior half of this region differentiates into the esophagus. The cells in the presumptive stomach and left posterior coelom area are added to the archenteron from the early gastrula stage

Figure 9. Gastrulae of *Asterina pectinifera* in which one of the vegetal blastomeres was injected with HRP at the 8- or 16-cell stage. (A) mesenchyme-differentiation stage, (B) late gastrula stage, and (C) mouth-formation stage. The front ectoderm is removed in (A) to show the labeled cells in the archenteron more clearly. The band of labeled cells in the archenteron is twisted in (B) and (C), but not in (A). Scale bar = 100 μm.

to the end of the late gastrula stage. The coeloms, esophagus, and stomach are formed mainly from veg2–descendants. Since cleavage in *A. pectinifera* embryos is almost equal, the volume ratio of each tier may be about 25% of the whole volume. Thus, the volume ratio of the stomach is calculated to be about 15% (25 − 10%). The presumptive intestine area is generally originated from the veg1 tier and added to the archenteron after the late gastrula stage. The volume of this area is calculated to be about 5% of that of the whole larvae. Thus, the total volume of the mesendoderm finally reaches about 30% of the whole volume of the larvae before the mesenchyme-migration stage.

After the late gastrula stage, the cells in the presumptive zone of the cardiac sphincter began to migrate laterally clockwise on the archenteron wall, dragging the cells in the presumptive esophagus and stomach zone. The rest of the archenteron maintained its original orientation in relation to the dorso-ventral axis. The significance and the mechanism of this torsional twisting of the archenteron was not examined in this study. However, it is possible that this twisting may be related to the mechanism of the constriction of this region, since the twisting occurs at the same area and about the same time as the constriction.

The labeling pattern of the left posterior coelom in HRP-injected larvae showed that the cells in the anterior and the posterior region of this vesicle originated from the left dorsal and right dorsal region, respectively. The rudiment of the left posterior coelom projected into the

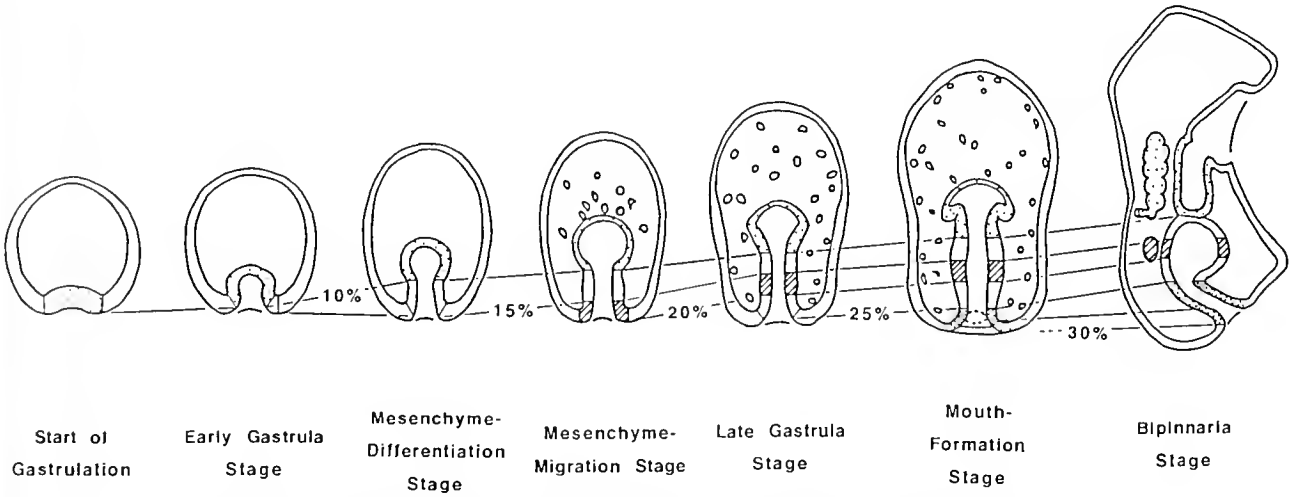

Figure 10. Schematic illustration of the gastrulation process of *Asterina pectinifera*. Lines between each of the profiles link the points that are involuted at the same point of development.

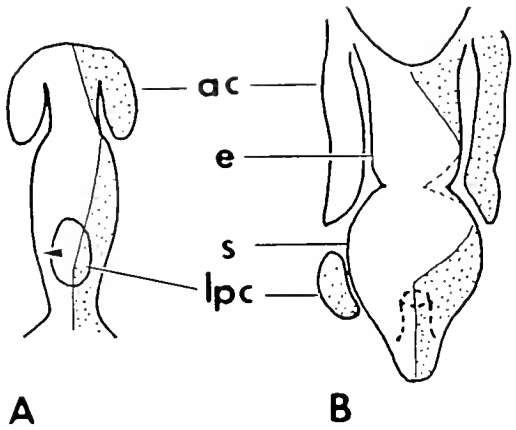

Figure 11. Schematic illustration of formation of the left posterior coelom. (A) mouth-formation stage. (B) bipinnaria stage. ac = anterior ceoloms, e = esophagus, s = stomach, lpc = left posterior coelom. Dotted region consists of cells from the original right side.

blastocoel from the dorsal side of the archenteron at the mouth formation stage, when the twisting had already been initiated. The anterior region of this rudiment projected from the twisting area where the original left dorsal cells had migrated, while the posterior region consisted of cells of the mid dorsal region. The rudiment then migrates to the left side during the mouth formation stage. As a result, the anterior and posterior halves of the left posterior coelom consist of cells from different longitudes (Fig. 11).

Acknowledgments

We thank Dr. H. Nishida of the Tokyo Institute of Technology for his advice on methods of microinjection. We also thank Messrs. T. Mayama, S. Tamura, and M. Washio of Asamushi Marine Biological Station for their assistance in collecting and rearing the animals.

Literature Cited

Burke, R. D., R. L. Myers, T. L. Sexton, and G. Jackson. 1991. Cell movements during the initial phase of gastrulation in the sea urchin embryo. *Dev. Biol.* **146:** 542–557.

Dan-Sohkawa, M., H. Yamanaka, and K. Watanabe. 1986. Reconstruction of bipinnaria larvae from dissociated embryonic cells of the starfish, *A. pectinifera*. *J. Embryol. Exp. Morphol.* **94:** 47–60.

Davidson, E. H. 1989. Lineage-specific gene expression and the regulative capacities of the sea urchin embryo: a proposed mechanism. *Development* **105:** 421–445.

Ettensohn, C. A. 1984. Primary invagination of the vegetal plate during sea urchin gastrulation. *Am. Zool.* **24:** 571–588.

Ettensohn, C. A. 1985. Gastrulation in the sea urchin embryo is accompanied by the rearrangement of invaginating epithelial cells. *Dev. Biol.* **112:** 383–390.

Hardin, J. D., and L. Y. Cheng. 1986. The mechanisms and mechanics of archenteron elongation during sea urchin gastrulation. *Dev. Biol.* **115:** 490–501.

Hardin, J. 1989. Local shifts in position and polarized motility drive cell rearrangement during sea urchin gastrulation. *Dev. Biol.* **136:** 430–445.

Henry, J. J., S. Amemiya, G. A. Wray, and R. A. Raff. 1989. Early inductive interactions are involved in restricting cell fates of mesomeres in sea urchin embryos. *Dev. Biol.* **136:** 140–153.

Horstadius, S. 1973. *Experimental Embryology in Echinoderms.* Clarendon Press, Oxford. 192 pp.

Khaner, O., and F. Wilt. 1990. The influence of cell interactions and tissue mass on differentiation of sea urchin mesomeres. *Development* **109:** 625–634.

Kishimoto, T. 1986. Microinjection and cytoplasmic transfer in starfish oocytes. *Methods Cell Biol.* **27:** 379–394.

Kominami, T. 1984. Allocation of mesendodermal cells during early embryogenesis in the starfish, *Asterina pectinifera*. *J. Embryol. Exp. Morphol.* **84:** 177–190.

Kominami, T. 1988. Determination of dorso-ventral axis in early embryos of the sea urchin, *Hemicentrotus pulcherrimus*. *Dev. Biol.* **127:** 187–196.

Kuraishi, R., and K. Osanai. 1988. Determination of antero-posterior axis in starfish larvae. *Bull. Mar. Biol. Stn. Asamushi* **18:** 67–76.

Kuraishi, R., and K. Osanai. 1989. Structural and functional polarity of starfish blastomeres. *Dev. Biol.* **136:** 304–310.

Maruyama, Y. K., K. Yamamoto, I. Mita-Miyazawa, T. Kominami, and S. Nemoto. 1986. Manipulative methods for analyzing embryogenesis. *Methods Cell Biol* **27:** 326–343.

Maruyama, Y. K., and M. Shinoda. 1990. Archenteron-forming capacity in blastomeres isolated from eight-cell stage embryos of the starfish, *Asterina pectinifera*. *Dev. Growth Differ* **32:** 73–84.

Nishida, H. 1987. Cell lineage analysis in ascidian embryos by intracellular injection of a tracer enzyme. III. Up to the tissue restricted stage. *Dev. Biol.* **121:** 526–541.

Schroeder, T. E. 1985. Cortical expressions of polarity in the starfish oocyte. *Dev. Growth Differ.* **27:** 311–321.

Zhang, S., X. Wu, J. Zhou, R. Wang, and S. Wu. 1990. Cytoplasmic regionalization in starfish oocyte occurrence and localization of cytoplasmic determinants responsible for the formation of archenteron and primary mesenchyme in starfish (*Asterias amurensis*) oocytes. *Chin J Oceanogr Limnol.* **8:** 263–272.

Reference: *Biol. Bull.* **183**: 269–277. (October, 1992)

Growth Rates and Growth Strategy in a Clonal Marine Invertebrate, the Caribbean Octocoral *Briareum asbestinum*

DANIEL A. BRAZEAU[1] AND HOWARD R. LASKER

Department of Biological Sciences, State University of New York, Buffalo, NY 14260

Abstract. Colony form directly effects colony reproductive output among colonial benthic invertebrates. The relationship between reproductive effort, colony form, and growth rate in colonies of the Caribbean octocoral *Briareum asbestinum* were examined by measuring the growth rates of 118 tagged colonies on Pinnacles and House Reef in the San Blas Islands, Panama. Colony growth rates, individual branch growth rates, and branch addition rates were measured over six month intervals from July 1986 to July 1988.

Colonies grew at a net rate of 16.6 cm/year and added 1.2 branches/year. Individual branch measurements yielded a net rate of growth of 2.02 cm/year/branch. Positive growth rates, which provide a measure of minimum potential growth, were 71.3 cm/year, and 8.7 branches/year for colonies and 6.21 cm/year for individual branches. Net growth rates and branch addition rates were 76 and 85% less than potential growth rates indicating large losses to fragmentation and predation. Calculated mean longevity of individual colonies (ramets) is short (10.6 years), given observed rates of growth and loss. However, since fragmented branches can reattach and initiate new colonies, losses due to fragmentation contribute to the asexual expansion of the genet.

In July 1987, 783 branches on the tagged colonies were individually mapped in order to characterize the relationship between branch size and the number of bifurcations (tips), and growth rates. The best predictor of growth rate was the number of tips per branch ($r^2 = 0.46$; $P < .0001$). No relationship was found between branch growth and branch size, consequently branch growth per unit length decreased as branch size increased. The independence of branch growth and size may reflect the diversion of energy away from growth toward reproduction. As a consequence of this pattern, bifurcating growth forms will, on a colony basis, grow more rapidly and amass more reproductive tissue than simple linear extension. However, the short longevity of ramets of *Briareum asbestinum* limits the advantage to be gained from accumulating reproductive tissue by rapid branch bifurcation.

Received 16 September 1991; accepted 7 July 1992.

[1] Present address: Department of Biology, University of Houston, Houston, TX 77204–5513.

Introduction

One of the fundamental components of the interaction between an organism and its environment is the organism's morphology. Among colonial invertebrates "form" takes on multiple interpretations corresponding to the multiple levels of individuality. The individual zooid or polyp, the colony which those polyps form, and the collection of genetically identical colonies can all be considered to have a form that to differing degrees contributes to the fitness of the genotype (or genet). In this paper we examine growth of a Caribbean gorgonian coral and show how the pattern of growth generates colony form and how that affects one element of fitness: colony reproductive output.

Colony form among benthic invertebrates influences virtually all aspects of the organism's interaction with the environment. Colony morphology affects resistance to wave and current action (Wainwright and Dillon, 1969; Chamberlain and Graus, 1975; Velimirov, 1976; Graus, *et al.*, 1977; Tunnicliffe, 1982; Vosberg, 1982), feeding (Leversee, 1976; McKinney, 1981; Ryland and Warner, 1986), competitive interactions, and even the susceptibility to predation (Kaufmann, 1973; Jackson, 1979). All of these factors should have clear repercussions on fitness, but perhaps the most direct effect of colony morphology

is on reproduction [illegible] benthic invertebrates grow by adding new [illegible] (*i.e.*, polyps or zooids) to the colony. Among [illegible] species, each of these individuals is capable [illegible] gametes. However, in many cases individuals near the growing colony edge or tip are either [illegible] productive or produce fewer gametes than individuals further removed from the growing edge (Rinkevich and Loya, 1979; Wallace, 1985; Chornesky and Peters, 1987; Brazeau and Lasker, 1990). Thus, both total colony size and colony form determine gamete production. Many benthic species also propagate via fragmentation, thus colony growth rate and form also affects the size, survivability, and generation rate of asexual propagules (Walker and Bull, 1983; Lasker, 1984, 1990). Since the pattern and rate of growth of a colony effects both colony size and form, the pattern of growth becomes a key element in the reproductive strategies of benthic species.

In this paper we use data on the form and growth rates of the arborescent form of the Caribbean gorgonian *Briareum asbestinum* to examine the relationship between growth and reproduction. Among arborescent colonies growth can be partitioned into three components, the generation of new branches, extension of existing branch tips, and the production of gametes. Polyps of *B. asbestinum* that are near the growing branch tip produce fewer gametes than those five cm or more behind the growing tip (Brazeau and Lasker, 1990). Thus the distribution of growth between extension of existing branches and the formation of new branches will have key effects on the colony's reproductive output. *Briareum asbestinum* is an excellent species for such a study as it has a sufficiently simple morphology to allow accurate assessments of form and growth.

Materials and Methods

Colonies of *Briareum asbestinum* are common throughout the Caribbean and occur over a wide depth range (1–20 m). Colonies consist of moderate sized polyps (1 mm diameter) that grow in encrusting and/or simple branching morphologies. Reproductive colonies of *B. asbestinum* are gonochoric brooders (Brazeau and Lasker, 1990). Sexual maturity is determined by size (branch length) for both sexes. All branches greater than 20 cm in length contain gametes prior to spawning.

Data on colony growth were collected as part of a larger study examining fecundity and reproductive success of colonies of *B. asbestinum* at Pinnacles and House Reef in the San Blas Point area near the Smithsonian Tropical Research Institute field station in the San Blas Islands, Panama (Fig. 1). House Reef is a shallow reef rising from *Thallassia* beds at a depth of 6 m to <0.5 m. The reef slope consists almost entirely of the stony corals, *Agarcia*

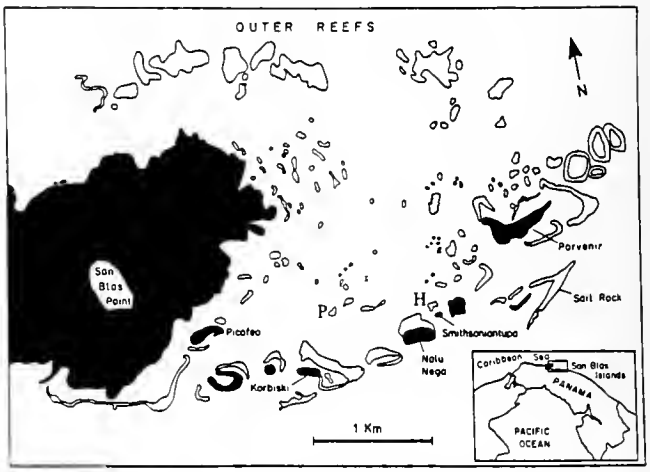

Figure 1. San Blas point region in the San Blas Islands, Panama. Open areas designate reefs: P-Pinnacles Reef and H-House Reef.

spp. and *Porites furcata*, and the hydrocoral, *Millepora complanata*. Colonies of *B. asbestinum* are common along the entire depth gradient. Pinnacles is a patch reef complex extending from 0.5 to 8 m depth. It has higher coral and gorgonian diversity than House. Unlike House Reef, the hard substrate at Pinnacles Reef is broken by many sand patches and channels. Colonies of *B. asbestinum* are found throughout the patch reef, but are most common at depths of 5–8 m.

In July of 1986, 46 colonies at Pinnacles and 60 colonies at House Reef were tagged by attaching aluminum tags to the substratum at the base of each colony. Colonies were chosen haphazardly, the only requirement being that colonies be of reproductive size (have at least one branch 20 cm in length). The length of all branches for each colony were measured to the nearest 0.5 cm. Approximately every six months (Jan 7–Feb 13; May 31–July 29, 1987; Jan 19–Feb 16; May 22–Aug 26, 1988) all colonies that could be positively identified (tags could be found) were remeasured. In July of 1987, 31 colonies at Pinnacles were added to the colonies remaining from the previous year. In all, 118 colonies on the two reefs were monitored for at least one six-month interval. For 65 of these colonies, there are measurements for all four six-month intervals.

In July of 1987 it became apparent that colony size was highly variable due to the loss of branches due to colony fragmentation. In order to obtain a more accurate measure of colony growth, 45 colonies at each reef were arbitrarily selected from the tagged colonies and the lengths of each branch individually recorded on colony diagrams. The individual branches were then identified and measured in subsequent surveys. These data provide more accurate growth measurements for 783 individually identified branches. To determine if there is a lateral or horizontal component to colony growth in *B. asbestinum*,

all branches that had been knocked down, but were still attached to the colonies, were also recorded on colony diagrams and measured over each interval.

Whole colony measurements were used to calculate two measures of colony growth rates: (1) branch specific colony growth, that is total colony growth divided by the number of branches per colony present at the end of each interval (cm/branch/year); and (2) change in number of branches/colony. Sample variances were large and heterogeneous despite log or cubic transformation therefore differences in colony and individual branch growth data were tested using the nonparametric Mann-Whitney U test (SPSS-X release 2.2; Hull and Nie, 1981). In order to reduce the probability of a type I error due to the multiple statistical tests, significance levels were determined using the Bonferroni procedure (for L tests the corrected significance level $\{\alpha'\}$ is, $\alpha' = \alpha/L$).

Results

General colony characteristics

Mean colony size and number of branches/colony for the tagged colonies of *B. asbestinum* of reproductive size on Pinnacles and House Reef increased in each year of the study (Fig. 2). At the beginning of the study the average colony had 9.5 branches (S.E. = 0.7, n = 101) and a total length of 176.7 cm (S.E. = 14.0, n = 101). Mean branch length was 19.1 cm (S.E. = 0.6, n = 716). Colonies had an average of 0.67 (S.E. = 0.09, n = 119) horizontal branches, 14.3 cm (S.E. = 2.3, n = 119) in length. Colonies at Pinnacles were significantly larger than colonies at House Reef in total length (Mann-Whitney U test, P = .003, n = 101). There were no significant differences in the number of branches/colony, though branch size at Pinnacles was significantly larger than at House Reef (Mann-Whitney U test, P = .001, n = 709).

Colony growth

There was no distinct horizontal component to colony growth for colonies of *B. asbestinum*. Of 119 horizontal branches, none grew horizontally in length, though many turned upward and grew or gave rise to new branches which then grew vertically. Consequently, colony growth can be characterized entirely in terms of branch addition or loss, and changes in total colony height.

Losses in colony size were caused by: (1) fragmentation, (2) predation, primarily by the snail *Cyphoma gibbosum* and the polychaete *Hermodice carunculata* (pers. obs.), and (3) death. Fragmentation was particularly important, resulting in the loss of whole branches or sections of colony. These losses caused much of the variation seen in colony growth. In order to obtain a more accurate estimate of colony growth rates, positive growth rates were calculated by excluding from the data set all colonies that decreased in size. The growth rates calculated in this way provide a minimum estimate of colony growth potential when free of losses due to predation and fragmentation.

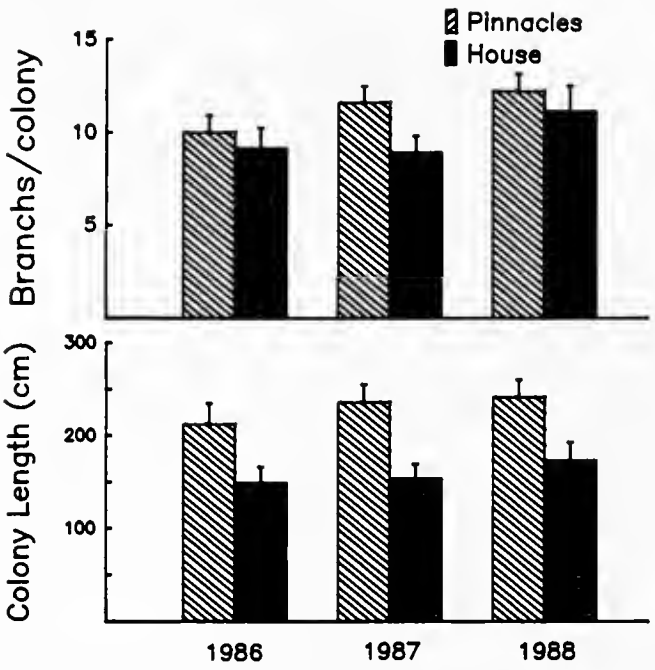

Figure 2. Bar graphs of mean colony size and number of branches/colony of *Briareum asbestinum* for the years 1986, 1987, and 1988. Error bars designate one standard error.

During the period from July 1986 to July 1988 colonies of *B. asbestinum* increased in total size by 14.3 cm/year (S.E. = 1.0, n = 89) and added 1.23 branches/year (S.E. = 0.4, n = 89) in the two populations studied (Table I). Excluding cases of negative growth yields positive growth rates of 71.3 cm/year/colony (S.E. = 9.2, n = 59) and 8.7 branches/year/colony (S.E. = 0.7, n = 59). Figure 3 shows colony growth in terms of specific growth and addition rates of branches. There were no significant differences between reefs in net colony growth rates for any of the three measures (Table II). There were, however, significant differences in positive growth rates between reefs, indicating that during some intervals potential growth rates were higher at House Reef than at Pinnacles (Table II).

Growth rates of individual branches

Growth rates of individual branches, for both net and positive growth, from 1987 to 1988 are shown in Table III. There were significant differences in growth rates of branches between reefs. Net branch growth rate was significantly higher at House Reef in Jul. 87–Jan. 88 and Jan.–Jul. 1988 (Table III). Similarly, positive growth rates of branches at House Reef were significantly higher than those at Pinnacles over both interval (Table III).

Table I

Net and positive mean growth rates for Briareum asbestinum *for each six-month period from July 1986 through July 1987*

Reef site	n	Colony growth rates cm/month: Net mean	S.E.	n	Positive mean	S.E.
Pinnacles						
Jul 86–Jan 87	33	1.48	1.3	25	4.98	0.6
Jan 87–Jul 87	28	2.28	1.1	18	5.55	1.1
Jul 87–Jan 88	64	2.81	1.3	44	7.30	0.9
Jan 88–Jul 88	72	−1.10	1.2	42	3.56	1.1
House						
Jul 86–Jan 87	35	1.85	0.8	23	4.51	0.7
Jan 87–Jul 87	32	2.30	1.7	21	7.65	1.2
Jul 87–Jan 88	47	2.15	1.9	30	8.88	1.7
Jan 88–Jul 88	46	−0.60	1.6	29	5.40	0.9
Both						
Jul 86–Jan 87	68	1.66	0.7	48	4.75	0.4
Jan 87–Jul 87	60	2.30	1.0	39	6.71	0.8
Jul 87–Jan 88	111	2.53	1.1	74	7.96	0.9
Jan 88–Jul 88	118	−0.90	0.9	71	4.31	0.7

Growth rates are for vertical growth only. Negative numbers indicate tissue or branch loss.

One of the advantages of following the growth of individual branches is that it allows one to examine the relationship between branch growth (and, therefore, colony growth) and branch characteristics like initial length and number of bifurcations (branch tips). Positive growth rates of branches were independent of branch size ($r^2 = 0.005$; $P > 0.153$), indicating that small and large branches had similar growth rates (Fig. 4). Positive growth rates of branches were positively correlated with the number of branch tips ($r^2 = 0.455$; $P < 0.0001$). Thus, growth rates of branches are determined by the number of growing tips, not by branch size (Fig. 5). The slope of the regression line for positive branch growth *versus* number of branch tips, yields a growth rate of 5.93 cm/year/tip (S.E. = 0.39).

Discussion

Rate of growth

The best estimate of growth rate of colonies of *B. asbestinum* comes from the measurement of individual branches. These data yield a net growth rate of 2.02 cm/year/branch. This value is less than the branch growth rates reported by Gladfelter *et al.* (1978) for scleractinians with branching morphologies (*Acropora cervicornis*, 7.1 cm/year; *A. prolifera*, 5.9–8.2 cm/year; and *A. palmata*,

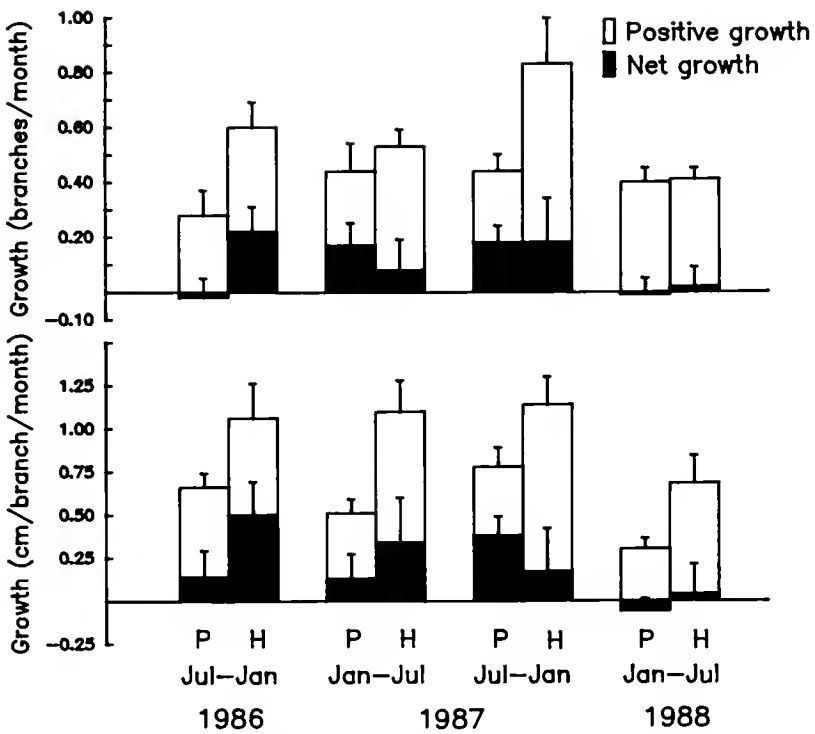

Figure 3. Mean growth rates in cm/branch and branches/colony for colonies of *Briareum asbestinum* on Pinnacles (P) and House Reef (H). Growth rates are shown for each six-month period beginning July 1986 to July 1988. Values for n are given in Table I. Error bars designate one standard error.

Table II

Results of Mann-Whitney U test comparing net and positive growth rates of colonies of Briarium asbestinum *between Pinnacles and House Reefs for each six-month interval*

			Colony growth measures					
			cm/month		cm/branch/month		branches/month	
Factor	n_1	n_2	U	SL	U	SL	U	SL
Net growth:								
Jul 86–Jan 87	33	35	524.5	0.515	563.0	0.859	428.0	0.765
Jan 87–Jul 87	28	32	448.0	0.692	387.0	0.208	466.5	0.892
Jul 87–Jan 88	64	47	1448.0	0.385	1559.0	0.815	1520.0	0.646
Jan 88–Jul 88	72	46	1467.0	0.162	1423.5	0.103	1624.0	0.566
Positive growth:								
Jul 86–Jan 87	25	23	259.5	0.563	226.0	0.204	75.7	**0.010**
Jan 87–Jul 87	18	21	154.0	0.232	92.0	**0.004**	96.0	0.145
Jul 87–Jan 88	44	30	684.0	0.833	501.5	0.033	340.0	0.061
Jan 88–Jul 88	42	29	362.5	**0.004**	282.5	**<0.001**	201.5	0.496

U-statistic and significance level shown for each colony growth measure. Significant differences ($\alpha' = 0.05/3 = 0.016$) indicated by bold print. SL = level of significance.

4.7–9.9 cm/year), though the positive individual branch growth rates of colonies of *B. asbestinum* (6.21 cm/year) are similar to scleractinian growth rates. Growth rates of branches for colonies of *B. asbestinum* appeared similar to those reported for other Caribbean gorgonians (Kinzie, 1970; Lasker, 1990; Yoshioka and Yoshioka, 1991). However, it should be noted that these studies reported growth rates based upon changes in colony height (not true branch growth) and in one case (Kinzie, 1970) were given as the means of positive growth only. The most comparable value from this study would be the branch specific growth rates of positive colony growth. This value for colonies of *B. asbestinum* (9.25 cm/year, Fig. 3) is greater than that reported for most gorgonians.

Average colony size of colonies of *B. asbestinum* increased over both years of the study on both reefs, though both populations experienced very low or negative growth in the period from January to July of 1988. Total colony length and number of branches/colony increased 20 and 24%, respectively, from July 1986 to July 1988. However, positive colony growth rates, which provide an estimate of the minimum growth potential of colonies, indicate that colonies of *B. asbestinum* can potentially increase 71.3 cm/year in length and add 8.7 branches/year. This is a potential yearly increase of 40% in colony length and 91% in branch number relative to mean colony size. A similar comparison of net and positive growth rates of individual branches indicated that net growth rates were only 32.5% of positive growth rates. This disparity between the minimum potential growth and the realized or net growth suggests that colonies (ramets) of *B. asbestinum* sustain large losses due to predation, colony fragmentation, and disease. Because fragmentation often results in the establishment of new colonies, the loss to the genet is certainly less. Lasker (1983) found that 24–60% of the colonies of *B. asbestinum* at nearby Marsarkantupo reef in the San Blas Islands originated from nearby colonies. Similarly 18–67% of the colonies of *B. asbestinum* examined at Carrie Bow Cay, Belize resulted from colony fragmentation (Lasker, 1983). In this study, 62% of the colonies of *B. asbestinum* monitored had at least one branch that had been knocked down and reattached to the substrate. Thus, colony fragmentation (*i.e.* branch loss), while detrimental to the ramet, potentially increases clonal spread to the benefit of the genet.

While genet longevity may be increased by routine colony fragmentation, ramets will be relatively transitory given this strategy. Ramet age can be estimated from the data collected here by dividing total colony size by the net colony growth rate to yield an age of 10.6 years for an average reproductive colony (largest colony estimated age, 50.1 years). This value over estimates average ramet age because colonies too small to be reproductive were not included in this study. This suggests that most ramets of *B. asbestinum* are short-lived when compared to scleractinians (Connell, 1973; Buddemeir and Kinzie, 1976) and some gorgonians (Grigg, 1977; Lasker, 1990). While individual mean ramet longevity may have little importance when considered from the level of the genet it is important from the standpoint of sexual reproduction in that ramet longevity must be sufficient to allow ramets to reach reproductive size. In this regard, the small size of colonies of *Briareum asbestinum* at first reproduction, as compared to other scleractinians and gorgonians (Brazeau and Lasker, 1990), agrees well with the transitory nature of ramets.

Table III

Net and positive ... branches of Briareum asbestinum *for the period July ... 88*

Reef	n	Jul 88–Jan 88 (cm/month) Mean	S.D	Jan 88–Jul 88 (cm/month) Mean	S.D.	Jul 87–Jul 88 (cm/year) Mean	S.D.
Net growth							
Pinnacles	424	0.31	0.74	−0.04	1.11	1.64	1.27
House	359	0.41	1.30	0.01	1.18	2.46	10.57
Both	783	0.36	1.04	−0.02	1.15	2.02	9.11
Mann-Whitney U Tests: Pinnacles *vs.* House Reef							
N_1:N_2		424:359		424:359		424:359	
U		63626.5		69599.0		65483.0	
SL		<0.00001		0.038		0.0008	

Reef	Jul 87–Jan 88 (cm/month) n	Mean	S.D.	Jan 88–Jul 88 (cm/month) n	Mean	S.D.	Jul 87–Jul 88 (cm/year) n	Mean	S.D.
Positive growth									
Pinnacles	307	0.62	0.43	253	0.48	0.40	285	5.43	3.61
House	259	0.93	0.67	222	0.58	0.41	262	7.05	5.03
Both	566	0.76	0.57	475	0.53	0.41	547	6.21	4.41
Mann-Whitney U Tests: Pinnacles *vs.* House Reef									
N_1 N_2		307:259			253:222			285:262	
U		27090.0			22891.5			30212.0	
SL		<0.00001			0.0005			0.0001	

Growth rates determined from measurements of individually mapped branches. Mann-Whitney U test results show a significant difference in net branch growth rates between reefs for all intervals. SL = level of significance.

Net rates of colony growth were on average 18% (per 6-month interval) greater on House Reef than at Pinnacles. Growth rates of individual branches were 33% higher on House Reef. While this study design cannot address the cause of these differences, these data do indicate that growth rates of some clonal marine invertebrates may be extremely site specific. Given the high growth rates at House Reef, it is interesting that colony size was greater at Pinnacles. These data show that colony size tells very little about a colony's growth rate, and that the factors that cause tissue and/or branch loss are higher at House Reef than at Pinnacles. However, as noted above, branches lost *via* fragmentation may reattach. Thus, whereas ramets may decrease in size or disappear entirely, the genet may potentially increase in areal extent *via* this process. This is particularly important for colonies of *B. asbestinum* on reefs like House Reef where success at sexual reproduction at least locally seems to be very low (as measured by the number of embryos released, Brazeau and Lasker, in press). In contrast, growth rates at Pinnacles are lower, but success at sexual reproduction is higher (Brazeau and Lasker, in press). These differences between reefs (low sexual reproduction with high potential for asexual reproduction *vs.* higher success at sexual reproduction with low potential for asexual reproduction) may result in populations with greatly different levels of genetic diversity. Interestingly, the factors that presumably enhance fragmentation (*i.e.*, high turbulence) may also greatly reduce sexual reproduction in populations of *B. asbestinum* (Brazeau and Lasker, in press).

Pattern of growth

The ability to measure the entire colony allows one to examine the nature of growth in ramets of *B. asbestinum*. Growth rates in ramets of *B. asbestinum* are independent of colony or branch size. This seems to be the rule for many scleractinians (Bak *et al.*, 1977; Hughes and Jackson, 1985) and at least one other gorgonian (Wahle, 1983), though Chornesky and Peters (1987) have found that rates of vertical and lateral growth in colonies of *Porites astreoides* increases with colony surface area. Growth in colonies of *B. asbestinum* was found to be determined by the number of branch tips. This suggests that most of the polyps on a branch are not involved with branch growth, only those near the tip. This agrees with the reproductive biology of colonies of *B. asbestinum*. Reproductive effort (number and volume of gonads/polyp) increases away from the tip and base of the branch (Brazeau and Lasker, 1990). Thus as branch size and, therefore, the number of polyps away from the tip increases, growth rates remain the same while average reproductive effort per polyp increases.

The relationship between reproductive effort and branch growth and its implications for clonal growth strategies are shown in Figure 6. The graph shows that by bifurcating, branches increase reproductive tissue exponentially compared to the linear rate of increase for a branch with a single growing tip. This relationship stems from the exponential rate of increase of tissue in continually branching systems and in this regard is not too surprising. However, the graph illustrates two important points: (1) upright branching colonies should be arborescent, and (2) the benefit of arborescent growth becomes most important with age (colony or ramet longevity). The model agrees well with the growth forms observed among gorgonians. Unlike many gorgonians, however, ramets of *B. asbestinum* are not highly arborescent. Sixty-two percent of all branches measured in this study had a single tip. This incongruity is resolved by considering overall growth strategy of colonies of *B. asbestinum*. Site tenacity of ramets of *B. asbestinum* is low. Most branches never reach a size where the reproductive benefits of an arborescent strategy greatly exceed that of a single growing tip.

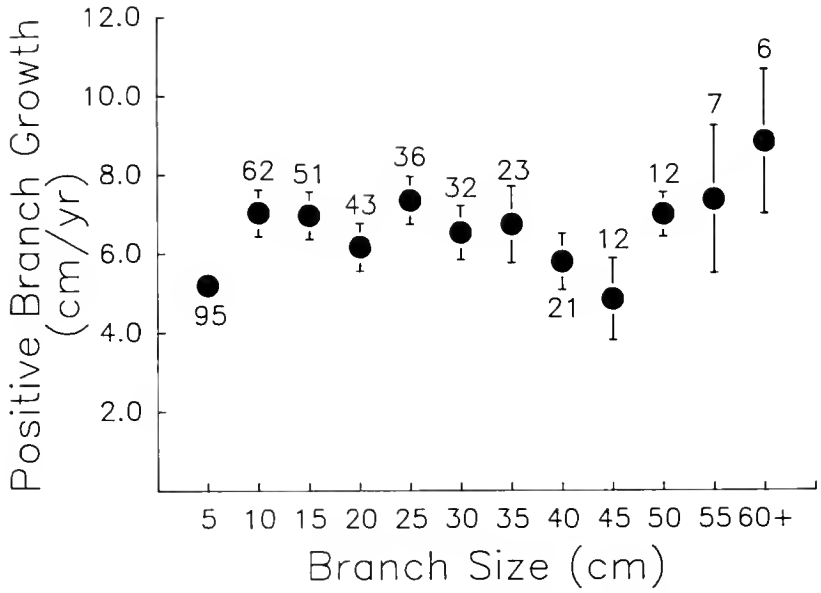

Figure 4. The relationship between positive branch growth and initial branch size ($r^2 = 0.005$; $P = 0.153$). Number of branches in each size class indicated above points. Error bars are ± one standard error. In a number of cases the error bars are smaller than the dots.

Average branch size in ramets of *B. asbestinum* is 19.1 cm, which corresponds to 3–5 years of age. As shown in Figure 6, the difference between the growth strategies in this period is slight. In addition, the arborescent growth strategy would increase drag forces on the branches and further increase the probability of branches being lost. This simple graphical model predicts that branching species with high site tenacity will be arborescent. Species like *B. asbestinum* with low site tenacity, will reach reproductive age early, and should have branches with few bifurcations.

Acknowledgments

We thank the Kuna Indians and the Republic of Panama for permission to work in the San Blas Islands and the Smithsonian Tropical Research Institute for the use of its facilities. M. A. Coffroth assisted with the fieldwork

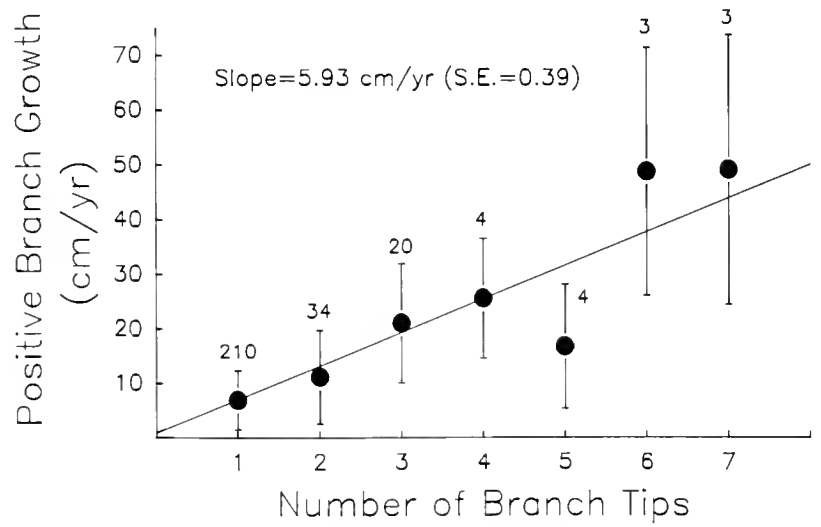

Figure 5. The relationship between positive branch growth and the number of tips/branch ($r^2 = 0.455$; $P < 0.0001$). Number of branches in each class indicated above points. Error bars are ± one standard error.

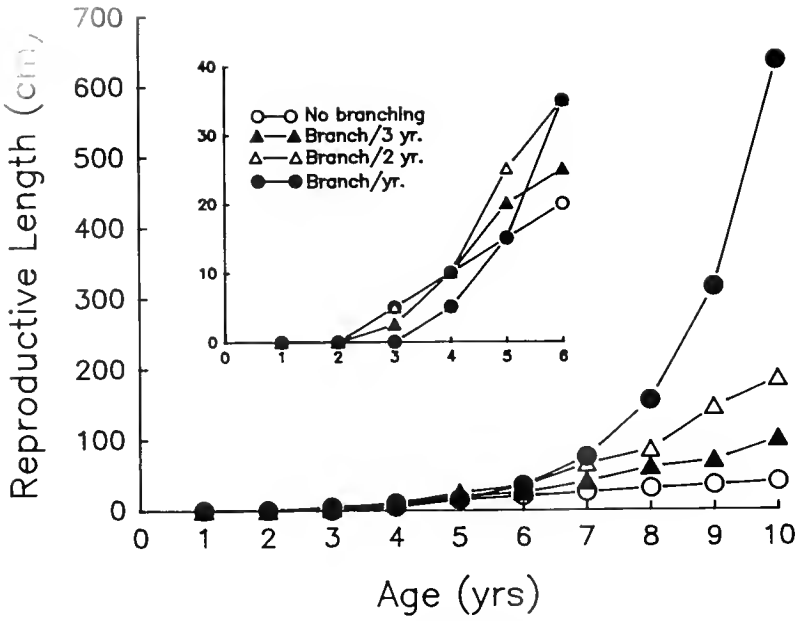

Figure 6. Increase in reproductive tissue for different growth strategies ranging from colonies whose branches never bifurcate to colonies with branches that bifurcate every year. Growth rate and amount of reproductive tissue follow the growth pattern of colonies of *Briareum asbestinum*. Growth rate is tip dependent (5.9 cm/tip/year). Reproductive tissue is calculated assuming losses of 5 cm to base and each growing tip. Inset shows an expanded view of the first six years.

and provided comments on the manuscript. This research was supported by NSF grant OCE-8521684.

Literature Cited

Bak, R. P., J. J. Brouns, and F. M. Heys. 1977. Regeneration and aspects of spatial competition in the scleractinian corals *Agaricia agaricites* and *Montastrea annularis*. *Proc. Third Int. Coral Reef Symp.* **1**: 143–148.

Brazeau, D. A., and H. R. Lasker. 1990. Sexual reproduction and external brooding by the Caribbean gorgonian, *Briareum asbestinum*. *Mar. Biol.* **104**: 465–474.

Brazeau, D. A., and H. R. Lasker. in press. Reproductive success in a marine benthic invertebrate, the Caribbean octocoral *Briareum asbestinum*. *Mar. Biol.* **000**: 000–000.

Buddemeir, R. W., and R. A. Kinzie. 1976. Coral growth. *Oceanogr. Mar. Biol. Annu. Rev.* **14**: 183–225.

Chamberlain, J. A., and R. R. Graus. 1975. Water flow and hydromechanical adaptations of branched reef corals. *Bull. Mar. Sci.* **25**: 112–125.

Chornesky, E. A., and E. C. Peters. 1987. Sexual reproduction and colony growth in the scleractinian coral *Porites astreoides*. *Biol. Bull.* **172**: 161–177.

Connell, J. H. 1973. Population ecology of reef-building corals. Pp. 205–245 in *Biology and Geology of Coral Reefs*, Vol II. O. A. Jones and R. Endean eds. Academic Press, New York.

Gladfelter, E. H., R. K. Monahan, and W. B. Gladfelter. 1978. Growth rates of five reef-building corals in the northeastern Caribbean. *Bull. Mar. Sci.* **28**: 728–734.

Graus, R. R., J. A. Chamberlain, J. A., and A. M. Boker. 1977. Structural modification of corals in relation to waves and currents. Pp. 135–153 in *Reefs and Related Carbonates—Ecology and Sedimentology. Studies in Geology 4*, S. H. Frost, M. P. Weiss, and J. B. Saunders, eds. Am. Assoc. Petrol. Geol. Tulsa, Oklahoma.

Grigg, R. W. 1977. Population dynamics of two gorgonian corals. *Ecology* **58**: 278–290.

Hughes, T. P., and J. B. C. Jackson. 1985. Population dynamics and life histories of foliaceous corals. *Ecol. Monogr.* **55**: 141–166.

Hull, C. H., and N. H. Nie. 1981. *SPSS Update 7–9. New Procedures and Facilities for Release 7–9*. McGraw-Hill Book Co. New York.

Jackson, J. B. C. 1979. Morphological strategies of sessile animals. Pp. 499–555 in *Biology and Systematics of Colonial Organisms*, G. Larwood and B. R. Rosen, eds. Syst. Assoc. Spec. vol. 11. Academic Press, London.

Kaufmann, K. W. 1973. The effect of colony morphology on the life-history parameters of colonial animals. In *Animal Colonies*, R. S. Boardman, A. H. Cheetham, and W. A. Oliver, eds. Dowden, Hutchinson and Ross. Pennsylvania.

Kinzie, R. A. 1970. *The ecology of the gorgonians (Cnidaria, Octocorallia) of Discovery Bay, Jamaica*. Ph.D. Thesis, Yale University.

Lasker, H. R. 1983. Vegetative reproduction in the octocoral, *Briareum asbestinum* (Pallas). *J. Exp. Mar. Biol. Ecol.* **72**: 157–169.

Lasker, H. R. 1984. Asexual reproduction, fragmentation, and skeletal morphology of a plexaurid gorgonian. *Mar. Ecol. Prog. Ser.* **19**: 261–268.

Lasker, H. R. 1990. Clonal propagation and population dynamics of a gorgonian coral. *Ecology* **71**: 1578–1589.

Leversee, G. J. 1976. Flow and feeding in fan-shaped colonies of the gorgonian coral, *Leptogorgia*. *Biol. Bull.* **151**: 344–356.

McKinney, F. K. 1981. Planar branch systems in colonial suspension feeders. *Paleobiology* 7: 344–354.

Rinkevich, B., and Y. Loya. 1979. The reproduction of the Red Sea coral *Stylophora pistillata*. II. Synchronization in breeding and seasonality of planulae shedding. *Mar. Ecol. Prog. Ser.* **1**: 145–152.

Ryland, J. S., and G. F. Warner. 1986. Growth and form in modular animals: ideas on the size and arrangement of zooids. *Philos. Trans. R. Soc. Lond. Ser. B Biol. Sci.* **313:** 53–76.

Tunnicliffe, V. 1982. The effects of wave induced flow on a reef coral. *J. Exp. Mar. Biol. Ecol.* **64:** 1–10.

Velimirov, B. 1976. Variations in growth forms of *Eunicella cavolini* Koch (octocorallia) related to intensity of water movement. *J. Exp. Mar. Biol.* **21:** 109–117.

Vosberg, F. 1982. *Acropora reticulata* structure, mechanics, and ecology of a reef coral. *Proc. R. Soc. Lond. Ser. B* **214:** 481–499.

Wahle, C. M. 1983. The roles of age, size and injury in sexual reproduction among Jamaican gorgonians. *Am. Zool.* **23:** 961.

Wainwright, S. A., and J. R. Dillon. 1969. On the orientation of sea fans (Genus *Gorgonia*). *Biol. Bull.* **136:** 130–139.

Walker, T. A., and G. D. Bull. 1983. A newly discovered method of reproduction in gorgonian coral. *Mar. Ecol. Prog. Ser.* **12:** 137–143.

Wallace, C. C. 1985. Reproduction, recruitment and fragmentation in nine sympatric species of the coral genus *Acropora*. *Mar. Biol.* **88:** 217–233.

Yoshioka, P. M., and B. B. Yoshioka. 1991. A comparison of the survivorship and growth of shallow-water gorgonians species of Puerto Rico. *Mar. Ecol. Prog. Ser.* **69:** 253–260.

Reference: *Biol. Bull.* **183**: 278–296. (October, 1992)

Characteristics of Carbonates of Gorgonian Axes (Coelenterata, Octocorallia)

J. C. LEWIS, T. F. BARNOWSKI, AND G. J. TELESNICKI

Department of Biological Sciences, Brock University, St. Catharines, Ontario, Canada L2S 3A1

Abstract. Axial skeletons of 13 species of gorgonians were examined by SEM, X-ray diffraction, and polarizing microscopy. Calcite, though occasionally amorphous is the major biogenic carbonate of axes. Non-biogenic mineralization may be calcitic, amorphous, or aragonitic. Axes of *Plexaurella* contain numerous, lenticular, calcitic loculi of spherulitic prismatic crystals. Mineralization in *Ellisella barbadensis* is in the form of concentric layers of perpendicularly oriented, lath-shaped crystals that extend through the annulations. Numerous longitudinally oriented collagen fibers perforate the crystals. Mineralization in *Lophogorgia cardinalis* is in the form of crescentic, shield-shaped, flat, laminated plates composed of alternating layers of calcified (sheathed) and uncalcified collagen fibers. The fibrous component in all species is oriented parallel to the longitudinal axis of axes. Fine striae on transversely fractured crystals of species of *Plexaurella* and *E. barbadensis* probably represent daily growth banding. The functional associations of mineral forms with stiffness, resistance to twist, and water movement zones are discussed.

Introduction

The gross morphology of a gorgonian colony is primarily the product of its variably branching axial skeleton (Muzik and Wainwright, 1977), which is composed primarily of a collagenous matrix called gorgonin (Barnes, 1980; Goldberg, 1976). The function of the axis as a mechanical support system is based on octocorals being passive suspension feeders that collect particulate food from flowing water. The axis must be rigid enough to hold the fragile polyps off the substratum and must be able to withstand the total water velocities for the particular habitat or zone inhabited (Muzik and Wainwright, 1977). The mechanical properties of the axis can vary (Jeyasuria and Lewis, 1987) with the sclerotization of the gorgonin (Goldberg, 1976) and calcification (Kingsley and Watabe, 1987). Usually the major component of the axial skeleton is the gorgonin, composed mainly of collagen fibers in a proteinaceous matrix (Leversee, 1969). The protein matrix is largely uncharacterized, but the collagen, though modified (Goldberg, 1973, 1976; Wainwright *et al.*, 1982), is characterized as collagen.

Gorgonin is deposited extracellularly in concentric layers around a central, hollow, chambered canal that seldom exceeds 100 μm in diameter. Goldberg's (1973) micrographs of fractured surfaces show that these layers are made of collagen fibers. The fibers appear to be lath-shaped not round as is mammalian tendon (Weise, 1988). The three-dimensional fibrous texture of gorgonin is complex, but shows a preferred axial orientation (Goldberg, 1973). The axis is thus flexible (when wet) and has a high tensile strength. The mechanical properties of collagens vary widely. Different chemical and macromolecular composition as well as the organization of collagen fibers (Goldberg, 1976), profoundly influence their mechanical properties.

Though flexibility can apparently be controlled or modulated by sclerotization of the collagen within the axial skeleton, a widely used method of stiffening axes in gorgonians is extracellular deposition of carbonates within the collagen interstitial spaces (Lowenstam, 1964; Jeyasuria and Lewis, 1987). Jeyasuria and Lewis (1987) determined the Young's modulus of the axial skeletons of thirteen species of holaxonian octocorals representing twelve genera and found that they range from 0.2 Gdynes/cm^2 to 90 Gdynes/cm^2; axial stiffness also correlated well with zone-related water movement. Relative quantities of calcareous material in the axial skeletons were strongly correlated with Young's modulus, suggesting an important role for calcareous material in modulating the mechanical

Received 16 August 1991; accepted 2 July 1992.

properties of the axial skeleton. Modulation of axial stiffness through calcification would be an effective mechanism for dealing with the different hydrodynamic forces encountered at various depths.

The two major calcium salts used in skeletal structures are calcium phosphates and calcium carbonates. Usually, phosphates occur in conjunction with collagen, and carbonates in conjunction with glycoproteins. Phosphates tend to be the major form in vertebrates and brachiopods; carbonates in most other invertebrates (Vincent, 1981) including gorgonians. Jeyasuria and Lewis (1987) compared the mole percent $MgCO_3$ in $Mg/Ca(CO_3)$ of thirteen species of octocorals. Three distinct groups were found: 14–18 mole percent $MgCO_3$, 33–42 mole percent $MgCO_3$, and 71–85 mole percent $MgCO_3$. X-ray diffraction patterns for *E. barbadensis*, from the first group, showed high magnesium calcite as the crystallographic form of the carbonate mineral. The higher percentages are chemically indicative of dolomite and magnesite respectively, but crystallographic mineral type was not determined by X-ray diffraction. The substitution of smaller ions such as magnesium, carrying the same charge as calcium into a calcium carbonate matrix, increases the density of the ionic packing. This results in both higher densities and greater hardness (Vincent, 1981).

The process of biomineralization can be biogenic and mediated by the organic matrix, in which case the precipitation process is controlled by a biological system, or it can be nonbiogenic and simply biologically induced, but not controlled. The calcified loculi evident in some species of octocorals are the result of a biogenic process (Wainwright, 1988). Crystal formation by organisms is commonly controlled by an array of extracellular proteins and polysaccharides. In skeletal mineralization, these macromolecules generally form a mold or framework in which the crystals grow. The macromolecules on the surface of this organic matrix are most directly involved in regulating crystal nucleation and growth (Addadi *et al.*, 1987). The polysaccharides are generally sulfated and carboxylated (Weiner *et al.*, 1983). The type of mineral nucleated may reflect the molecular structure of the nucleation site. Weiner *et al.* (1983) have proposed that the mineral crystal form (*i.e.*, calcite or aragonite) is dependent on the nucleation site.

In this study, the morphology of the axial skeleton was examined in representatives of ten genera of gorgonians. The 12 species chosen represent an axial mineral gradient in which the value calcium + magnesium/dry weight varies from 0.15–25% (Esford and Lewis, 1990), and the mineral form based on atomic absorption spectroscopy could be aragonite, calcite, dolomite or magnesite (Jeyasuria and Lewis, 1987; Esford and Lewis, 1990). Light microscopy, polarizing microscopy, scanning electron microscopy, and X-ray diffraction were used to perform intra- and interspecific comparisons of collagen fiber orientation, calcified loculus orientation, and mineral crystallographic form within the axis, and to describe in detail the calcified aggregates in several species.

Materials and Methods

The specimens of octocorals used for this study were obtained during field trips to the reefs of Tobago, West Indies. Most of the samples were collected from the northeastern tip of the island between 1984 and 1988. The 13 species used were chosen from ten genera so as to represent a broad array of octocorallian morphological and compositional characteristics. Whole colonies were collected intact, dipped in 10% formalin, air dried, and transported to Brock University for dry storage.

Species were identified with the aid of Bayer's (1961) guide "The Shallow Water Octocorallia of the West Indian Region". They are all in the phylum Cnidaria, class Anthozoa, subclass Octocorallia, order Gorgonacea, and suborder Holaxonia. Those in the family Plexauridae include the species *Plexaura flexuosa, Plexaurella grisea, Plexaurella fusifera, Plexaurella nutans, Eunicea tourneforti, Pseudoplexaura porosa,* and *Muricea muricata;* and in the family Gorgonidae are the species *Lophogorgia cardinalis, Gorgonia ventalina, Leptogorgia virgulata, Pseudopterogorgia acerosa,* and *Pseudopterogorgia bipinnata;* and in the family Ellisellidae is the species *Ellisella barbadensis.*

Cortex and adherent material were removed and the axis exposed. Sections were then cut from the axis, either with a jeweler's saw or a fine-toothed, circular, Drommel blade. Samples meant to show cross-sectional and longitudinal surfaces were taken from bases, mid-sections, and tips of each colony. Three series were cut. The first set was dipped in a sodium hypochlorite solution, which dissolved the organic matrix and exposed calcified inclusions. The second series was etched in 12% trichloroacetic acid, dissolving the calcified aggregates. The third series of samples were buffed with an emery board. Each species was then examined under dissecting and compound microscopes.

Measurements on those samples containing substantial calcified aggregates were made with an optical micrometer. The proportions of organic matrix to calcified structure were derived from cross sections: the amount of calcified material was compared with the amount of organic matrix along a series of radial lines.

Alizarin red S staining was also done to indicate the extent of mineralization. Samples were etched in bleach for up to 30 min, then washed in deionized water. They were then placed in a vial with an Alizarin Red S stain for 7–10 min and rinsed with deionized water. This stain colors calcite and aragonite red, and dolomite blue. The

procedure was also used for thin translucent shavings cut from unetched axes with a #10 scalpel blade. Shavings were examined with a light microscope at a magnification of 1000×.

Small axial samples, about 1.5 cm^3, were stripped of all adherent matter and immersed in sodium hypochlorite solution until all of the organic matter dissolved. The remaining particulate matter was then rinsed several times with deionized water. The mineral was then filtered and collected on #1 Whatman filter paper. With a mortar and pestle, the residual powder was ground to a fine consistency. A Picker 2087 generator was used to diffract an X-ray beam through the powder, which had been affixed to a glass plate with silicon vacuum gel. A graphical readout representing theta angles was produced. Diffraction peaks were then compared to standards so that the mineralized crystal lattice of each of the samples could be identified.

No diffraction pattern was generated from some of the samples. Powder from these samples was packed into a 0.03 mm capillary tube, and an X-ray beam was passed through the specimen using a Nonius CAD–4 automated, single crystal X-ray diffractometer. The X-ray beams are diffracted directly on to a film plate as diffraction rings. From the spacing between rings, the theta angles were calculated for comparison to known mineral standards.

Scanning electron microscopy (SEM)

Various preparative techniques were utilized to expose the outer, inner, lateral, longitudinally fractured, and the transversely fractured surfaces of the axial skeleton. Fractured transverse surfaces were obtained with a fine handsaw, or by bending or twisting the axial skeleton perpendicular to the longitudinal axis until it fractured. Longitudinal surfaces were exposed by splitting cross-sectional specimens with a scalpel blade. The fractured specimens were examined untreated or after further treatment. To remove the gorgonin and collagen fibres and to expose the calcareous matrix, specimens were treated with concentrated hypochlorite bleach (Chlorox® or Javex®) for various periods, from 30 s to 20 min, depending upon the amounts of organic matrix to be removed. To expose organic matrix and remove the calcareous components, specimens were treated with 10% HCl or 2% ascorbic acid. To remove large amounts of the calcareous material relatively rapidly or to free collagen fibres from the gorgonin, concentrated HCl was used for intervals ranging from a few minutes to several hours. When only a relatively light etching of a fractured or exposed calcareous surface was desired, dilute 2% ascorbic acid was used for short periods, 30–240 s. Combinations of these treatments were also used to determine relationships between calcareous and organic matrices. Powder residue was also examined.

Specimens were mounted on aluminum SEM stubs with double-sided mounting tape, gold sputter-coated (Polaron PS-3) for 60–120 s, and examined in a Hitachi S-570 scanning electron microscope.

Results

The gorgonian axes examined were morphologically diverse. They ranged from axes that were white and heavily calcified, through those with white, crystalline aggregates embedded in brown gorgonin, to those with no apparent mineralization and with gorgonin that varied from brown and fibrous to almost glassy black. Dried axes exhibit some artifacts due to dehydration. There is often some longitudinal checking or cracking of the gorgonin, but it is usually not severe. Heavily mineralized axes exhibit the least artifactual splitting. Axes with what appears to be amorphous, dense gorgonin show moderate checking. Axes that are readily distinguishable as fibrous usually show the greatest degree of artifactual splitting. Measurements taken with calipers revealed no significant differences in axis diameter between fresh, dehydrated, and rehydrated samples. The 12 species examined can be readily separated into 3 groups on the basis of mineralization.

Species with high Ca + Mg values (*i.e.*, 10–25% Ca + Mg/dry wt; Jeyasuria and Lewis, 1987; Esford and Lewis, 1990) contain easily distinguishable calcified aggregates. The species making up this group include *Ellisella barbadensis, Plexaurella nutans, Plexaurella grisea,* and *Plexaurella fusifera.* With the exception of *E. barbadensis,* the mineralized loculi in cross-sectional aspect are semi-lunate and oriented so their concave surfaces face the central core of the axis. In longitudinal aspect, loculi are lenticular in shape. The number of loculi per unit area is greatest near the central region of the axis. Individuals of *E. barbadensis* have a mineralized central rod surrounded by mineralized cylinders reminiscent of a single bone osteon. As with the species of *Plexaurella,* the proportion of calcified material to organic matrix decreases distal to the axis center. The cylinders near the axial periphery deform into sickle-shaped aggregates.

The percentage of cross-sectional area occupied by mineralized aggregates varies with species and longitudinal position along the axis. The approximate percentages of mineral aggregate are: *E. barbadensis*—tip 94%, mid-colony 81%, base 46%; *P. grisea*—tip 89%, mid-colony 63%, base 29%; and *P. nutans*—tip 85%, mid-colony 57%, base 32%; and *P. fusifera*—tip 75%, mid-colony 53%, base 37%. In all cases, the proportion of gorgonin to mineral increases toward the base.

Those species with a moderate amount of Ca + Mg (*i.e.*, 2–10% Ca + Mg/dry wt) (Jeyasuria and Lewis, 1987; and Esford and Lewis, 1990) include *Leptogorgia virgulata, Lophogorgia cardinalis, Pseudopterogorgia bipinnata,* and *Pseudopterogorgia acerosa.* These species

contain bundles of relatively large collagen fibers. Mineral is associated with the fiber bundles of *Pseudopterogorgia bipinnata* and *Pseudopterogorgia acerosa* (Fig. 1a). Whether the collagen fibers themselves are mineralized, or are encased by mineral, is not clear. Bleach etching reveals thin, cylindrical, calcified sheets between the layers of organic matrix of both *Leptogorgia virgulata* and *Lophogorgia cardinalis*.

In contrast, those octocorals with Ca + Mg contents of 1–<0.1% Ca + Mg/dry wt (Jeyasuria and Lewis, 1987; Esford and Lewis, 1990) appear in cross-section to be composed of fibrous gorgonin. No mineral aggregates are apparent. Included in this group are *Plexaura flexuosa, Muricea muricata,* and *Eunicea tourneforti*. Though *Gorgonia ventalina* has a Ca + Mg content within the moderate range (2–10%) of the previous group, it is morphologically similar to this group. Despite apparent lack of mineralization, when all organic material is removed by hypochlorite digestion, a fine, crystalline residue remains. Most of these are similar to crystals noted in the hollow core of axes on SEM examination. Crystals separated from the matrix are highly variable in shape (Fig. 1b, c, d). Individuals of *M. muricata* exhibit crystals roughly scalenohedron in shape, an alternate habit or form of calcite (Fig. 1b). In *Plexaura flexuosa* (Fig. 1c) and many other species, crystals with sharp edges and regular geodesic forms characteristic of both nonbiogenic mineral deposition and calcite can be found. Some of the crystals in *Eunicea tourneforti* (Fig. 1d) are needle-like and characteristic of aragonite.

In every species, the points of light extinction as determined from polarizing microscopy with crossed Nicholls' filters, indicate a fibril orientation parallel to the long axes of the colony. The extent of extinction was high, and the angles of light extinction occurred at consistent angles of horizontal stage rotation at 0° and 90°. In crossed Nicholls' polarizing microscopy, polarizing filters are positioned above and below the specimen and are oriented at 90° to each other. Parallel-oriented polarizing elements in the specimen will cause light extinction when aligned with the polarizing planes of either filter. These trends were equally apparent in all species, and the interlocular organic fibrillae of the heavily calcified samples also show a distinct uniform orientation.

The X-ray diffraction patterns indicate high magnesium calcite as the crystallographic mineral form in *Plexaurella fusifera, Plexaurella nutans, Plexaurella grisea, Ellisella barbadensis, Pseudopterogorgia acerosa, Pseudopterogorgia bipinnata,* and *Muricea muricata*. Amorphous mineral, that which does not produce a clear diffraction pattern, was found in *Lophogorgia cardinalis, Leptogorgia virgulata, Plexaura flexuosa,* and *Gorgonia ventalina*. The mineral from *Eunicea tourneforti* was found to be aragonitic (Table 1).

Aliziran red staining of heavily calcified species, such as *Plexaurella fusifera, Plexaurella nutans, Plexaurella grisea,* and *Ellisella barbadensis,* showed good differentiation. The high magnesium calcite loculi stained red, and the interstitial matrix remained unstained (Table 1). The moderately calcified species, such as *Leptogorgia virgulata, Lophogorgia cardinalis, Pseudopterogorgia bipinnata, Pseudopterogorgia acerosa,* and *Gorgonia ventalina* contain calcified, lath-like sheets rather than discrete loculi. They stained with less differentiation. It appears that the mineral is contained within or around the collagenous fibers, producing the impression of widespread mineralization in low concentration. Axes of *Plexaura flexuosa, Muricea muricata,* and *Eunicea tourneforti* did not stain with Aliziran red, an indication that no mineralization occurs in these species. Powder, collected as a residue after the organic matrix was digested, yielded crystals from each species. All stained positively (red); but species such as *M. muricata* and *Eunicea tourneforti* produced limited amounts of crystal, little of which stained.

Detailed scanning electron microscopic examination was done on the calcareous components of axes of several heavily mineralized species.

Plexaurella nutans, P. grisea *and* P. fusifera

Because the carbonate deposits in the axes of these three species showed only minor differences, they are treated as a single group.

Axial skeletons of species of *Plexaurella* are composed of fibrous gorgonin and calcareous loculi. In a bleach-etched cross section of an axis of *Plexaurella nutans,* the large number of loculi and their tight packing are clearly evident, and they form a substantial component of the axis (Fig. 2a). Elongate loculi are semi-lunate, through anvil, to kidney-shaped in cross section (Fig. 2b). Widths vary from about 40 μm to more than 250 μm. Inner (toward the hollow core), outer and lateral surfaces of loculi are morphologically distinct (Figs. 2b, c). Surfaces of transversely fractured loculi exhibit fan-shaped, crystal patterns that radiate peripherally (Figs. 2c, d). At high magnification, after light ascorbic-acid etching, fine lateral striations that vary in width from 0.3–0.5 μm are visible in all three species (Fig. 2d).

Individual loculi are elongate, pallisade-shaped, longitudinally oriented with respect to the axis, and occasionally branch (Fig. 3a). The outer surface of a loculus is composed of the ends of the crystal plates (Fig. 3b), horizontally oriented and irregularly fusiform. Exposed ends of crystals appear as small, thin, narrow transverse plates that terminate at the outer surface of the loculus (Fig. 3b). Localized groups of plates exhibit similar orientations slightly different from adjacent groups (Fig. 3b). The inner surfaces of loculi exhibit longitudinally oriented

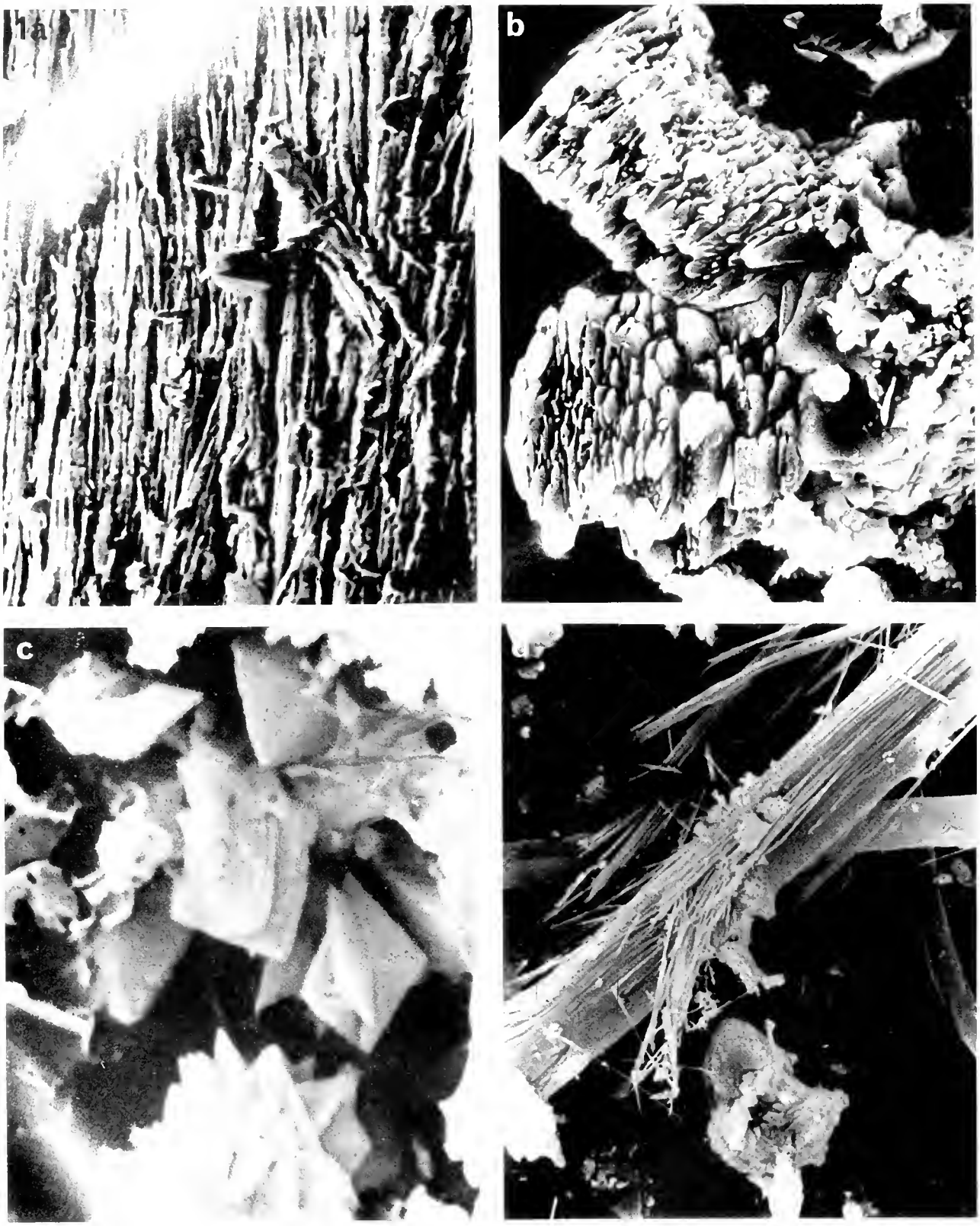

Figure 1. (a) Surface of collagen fiber layer of *Muricea muricata*. X-ray diffraction pattern indicates calcite. 2000×. (b) Mineral aggregate from the hollow axial core of *Muricea muricata*. X-ray diffraction pattern indicates calcite. Crystal forms are scalenohedral, an alternate calcite form characteristic of non-biogenic deposition. 1300×. (c) Calcareous crystals from the hollow axial core of *Plexaura flexuosa* of geodesic form indicative of typical, non-biogenic calcite deposition. X-ray diffraction pattern is amorphous. 3800×. (d) Mineral aggregates from the hollow core of *Lamellaria tourneforti*. The needle-like crystal form is characteristic of non-biogenic aragonite deposition. X-ray diffraction pattern indicates aragonite. 1200×.

Table I

Staining properties, compositional, and morphological characteristics of investigated species of octocorallians relative to water movement zones

Species	Aliziran red stain	Carbonate crystal type	Gross mineral form	Axis matrix	Water movement zone	Colony size and branch form
Ellisella barbadensis	+	Calcite	heavily calcified cylinders	fibrous	current, deep	large, whip
Plexaurella nutans	+	Calcite	lenticular loculi semi-	fibrous,	surge,	large, long thick branches
Plexaurella grisea	+	Calcite	lunate in cross section	homogeous	moderate	large, long moderate branches
Plexaurella fusifera	+	Calcite				medium, moderate branches
Leptogorgia virgulata	+	Amorphous	thin crescentic platelets	fibers in layers	surge,	small, elongate thin branches
Lophogorgia cardinalis	+	Amorphous	between fiber layers		deep current, deep	small, planar, highly branched
Pseudopterogorgia acerosa	+	Calcite	small aggregates interspersed with fibers	bundles of fibers in regular	surge, moderate	large, plumose, feathery
Pseudopterogorgia bipinnata	+	Calcite	and in hollow core	layers	surge, deep	large, bipinnately plumose
Gorgonia ventalina	+	Amorphous	small aggregates	sheet-like cylinders	breaker, shallow	large, fan, reticulum
Muricea muricata	−	Calcite	no mineral in matrix,	heavily fibrous	surge,	moderate, bottle brush
Plexaura flexuosa	−	Amorphous	crystals in hollow core	cylinders	moderate to shallow	moderate, elongate branches
Eunicea tourneforti	−	Aragonite				moderate, candelabra, thick branches

grooves relative to the axis (Fig. 3c). These vertical striae are sometimes punctuated with fine granular areas. In all species, inner locular and lateral surfaces show similar longitudinal grooves, their widths ranging from 0.4–0.8 μm. Layers of gorgonin surround the individual loculi and are 8–50 μm thick. Longitudinally oriented collagen fibers approximately 0.4–8.0 μm in diameter are similar in diameter to the longitudinal grooves found on the inner locular surfaces in all 3 species (Fig. 3d). A longitudinally fractured loculus of *Plexaurella* reveals radiating crystal plates that extend from the inner surface to the outer edge of the loculus (Fig. 3e). Secondary branching of the individual crystal plates occurs. The apices of the crystal aggregates occur on or in the inner surface layer as distinct spherulitic units with the crystal plates radiating outward from the inner surface layer.

A classification of molluscan shell microstructure was created by integration of the nomenclature for brachiopods with that of mollusks (Carter and Clark, 1985). This was done to eliminate the considerable overlap and inconsistencies in the application of microstructural terminology found even within single molluscan classes. The classification system integrated by Carter and Clark (1985) will be used to describe the microstructure of Gorgonian axial skeleton calcification because of its relevance to invertebrates, though other authors (Vincent, 1982; Simkiss and Wilbur, 1989) have used other terminologies in their descriptions of similar microstructural types found in vertebrates.

Ellisella barbadensis

When bleach-etched, the cross-sectional surface of the axis shows extensive calcareous material and distinct concentric annulations, about 20–60 μm wide (Fig. 4a). The acid-etched cross-sectional surface (Fig. 4b) from which the calcareous material has been removed shows the high density of collagen fibers that compose a major portion of the axial skeleton. The collagen fibers freed from the calcareous material mat together and form protruding ridges (Fig. 4b). Large numbers of longitudinally oriented collagen fibers penetrate the calcareous material of the annulations (Fig. 4c). Annulations are composed of individual, tightly packed crystals or aggregates oriented perpendicular to the longitudinal axis of the colony (Fig. 4d). Crystals or crystal aggregates are elongate, lath-shaped, and extend entirely across an annulation. In cross section or end-on view, they are usually square and approximately 3×3 μm (Fig. 4e).

Numerous longitudinally oriented collagen fibers (Fig. 5a) are 0.2–0.4 μm in diameter. They perforate the carbonate aggregates (Fig. 5b, c). Figure 5b shows the ends of the collagen fibers protruding through the carbonate structure. Figure 5c shows the perforations remaining in the carbonate subsequent to collagen removal by bleach. A light ascorbic acid etch subsequent to transverse fracture and bleach etching reveals a series of fine, transverse striae 0.2–0.4 μm wide on the crystalline surface (Fig. 5c).

Outer and inner vertical surfaces of annulations display a multilaminar layer of fine-grained, longitudinally

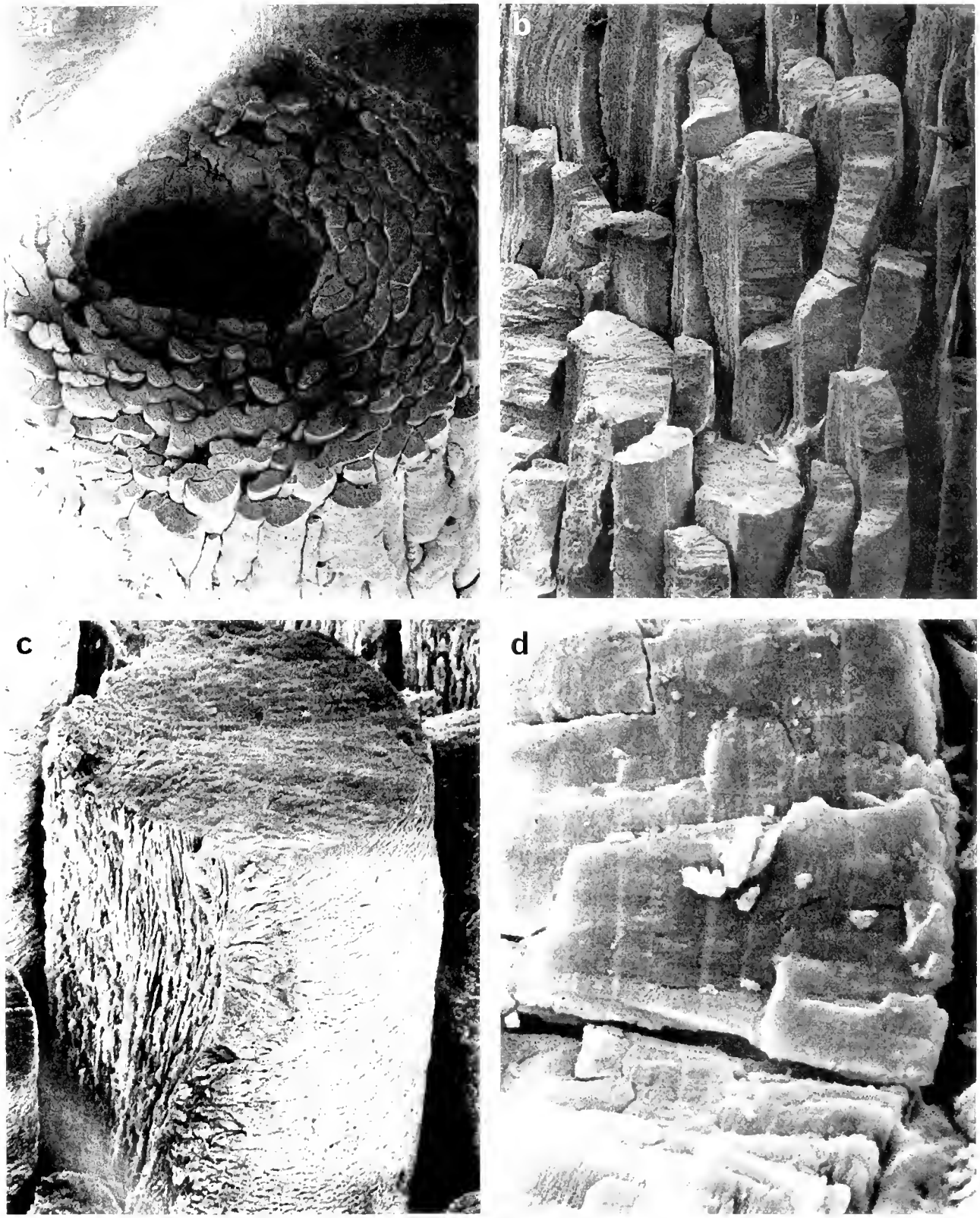

Figure 2. (a) Cross section of a bleach-etched (gorgonin removed) axis of *Plexaurella nutans*. Note the hollow core and numerous, tightly packed semi-lunate calcareous loculi. ×25. (b) Bleach-etched (gorgonin removed), transversely fractured loculi of *Plexaurella nutans*. Inner, outer, and lateral locular surfaces are apparent. Note radiating, fan-like pattern on both transversely and longitudinally fractured surfaces. 160×. (c) Bleach-etched single loculus of *Plexaurella grisea*. Note the fibroid pattern on the inner locular surface, the stacked, fusiform, crystal plate ends of the outer locular surface, and the radiating fan pattern on the transversely cleaved surface. 950×. (d) Lightly ascorbic-acid etched, transversely cleaved loculus surface of *Plexaurella fusifera*. Note the fine, vertical striae with a periodicity of about 0.3 μm that may represent episodic carbonate deposition. 4700×.

oriented crystals (Fig. 5d). There are usually a minimum of two sublayers on each surface of an annulation.

Lophogorgia cardinalis

Numerous, crescentic, lamellar, calcareous plate loculi are a major component of the axial skeleton (Fig. 6a). Removal of gorgonin and collagen by bleach etching eliminates the overlying support for the calcareous components of the loculi. Subsequent dehydration, necessary for examination in the SEM, introduces artifactual fractures in the plates and breaks them into smaller, irregular blocks (Fig. 6b). The shield-like loculi are irregular in outline and have connections with neighboring locular plates (Fig. 6c). The outer surface of locular plates is composed of fine-grained, generally longitudinally oriented crystals or aggregates (Fig. 6d). The interlocular gorgonin contains longitudinally oriented, layered collagen fibers (Fig. 6e) 0.1–0.3 μm in diameter.

Viewed edge-on, the longitudinally fractured plates are seen to branch laterally in a pattern reminiscent of cardiac muscle fibers and to form fused connections with adjacent plate loculi (Fig. 7a). The loculi are also laminated (Fig. 7a, b) with alternating layers of smooth, fine, longitudinally oriented crystals, or aggregates, and gorgonin-collagen (Fig. 7b). A transverse fracture of a loculus clearly reveals the lamination (Fig. 7c). The centers of many crystals are hollow (Fig. 7c). Acid etching, to remove the carbonate, leaves the fused and melted ends of the dense gorgonin-collagen layers of the lamellar plate as readily apparent layers in Fig. 7d.

Discussion

Octocoral axes are composed of a limited number of structural elements. Principally they contain variable amounts of flexible collagen fibers, embedded in a pliant, proteinaceous matrix, and minerals that exist in a variety of crystal forms and aggregate shapes (Kingsley and Watabe, 1984). These components are assembled in a surprisingly large range of forms (Telesnicki, 1990; Barnowski, 1991), the functional significance of which is dimly known at present. Functional relationships can be better understood if structure is known and can be used to complement, explain, and infer functional interaction. Detailed SEM examination of the carbonate inclusions in three genera has revealed three substantively different mineralization types from which some functional inferences may be derived.

Genus Ellisella

The axis of individuals of *Ellisella barbadensis* is extensively mineralized (about 30%/dry weight) by high magnesium calcite (Jeyasuria and Lewis, 1987; Esford and Lewis, 1990). Only when it is decalcified does the large collagen fiber content become evident. The axis consists of numerous, smooth concentric annular layers reminiscent of a single osteon from bone. The principal individual crystalline components of the annulations are elongate, lath-shaped, perpendicularly oriented with respect to the axis, and they extend across the entire width of the annulus. Whether these are single crystals or multiple crystal composites was not determined. These units, stacked like two-by-fours in a lumber yard, are highly resistant to compressional forces, but like bricks in a wall held only by mortar, provide little resistance to tensional forces which would tend to lift them apart. Tensional forces are accommodated by the numerous, high tensile strength, uncalcified, collagen fibers (Moss, 1964) that perforate the laths. These longitudinally oriented fibers are surrounded by calcareous material and appear tightly incorporated into it. Individual collagen fibers extend through a minimum of several laths, if not the entire length of the annulus. They can be thought of as analogous to the effectively non-extendible, iron reinforcing rods in concrete that strengthen it in tension. This construction produces the stiffest, shallow-water gorgonian axis (Jeyasuria and Lewis, 1987; Esford and Lewis, 1990) that has been recorded to date. It also has a comparatively high torsion modulus (Jeyasuria and Lewis, 1987) despite the flexibility of the collagen fibers. That is probably a result of the manner in which the lath-like, crystal aggregates are stacked, but this was not examined extensively.

The elongate, whip-like individuals of *Ellisella barbadensis* generally occur well below wave base in areas of current-generated water movement only. Forces generated by such currents are high (Roberts *et al.*, 1975), and this is one reason for the high stiffness of the axis. The other is as follows. The majority of shallow water gorgonians occur in the surge zone where wave action returns them through the upright position approximately every 12 s (open ocean wave period). Below wave base, where *Ellisella barbadensis* occurs, currents can be anywhere from constant and unidirectional through intermittent and multidirectional. In most tidal locations, bidirectional currents alternating about twice per day could be expected. In any case, the current is comparatively constant for relatively long periods (a few h). A comparatively stiff axial skeleton is required to maintain the polyps in a feeding position in the water column, and to keep the colony off the substratum under these conditions.

Fine striae, approximately 0.3 μm in width, evident on cross sections lightly etched with ascorbic acid probably represent episodic carbonate accretion. No data have been published on the rate of elongation of *Ellisella barbadensis*, let alone on the rate of increase in its diameter. The striae could represent daily accretion rates; in which case, the yearly increase in diameter would be about 0.25 mm. If they represented growth associated with different tidal

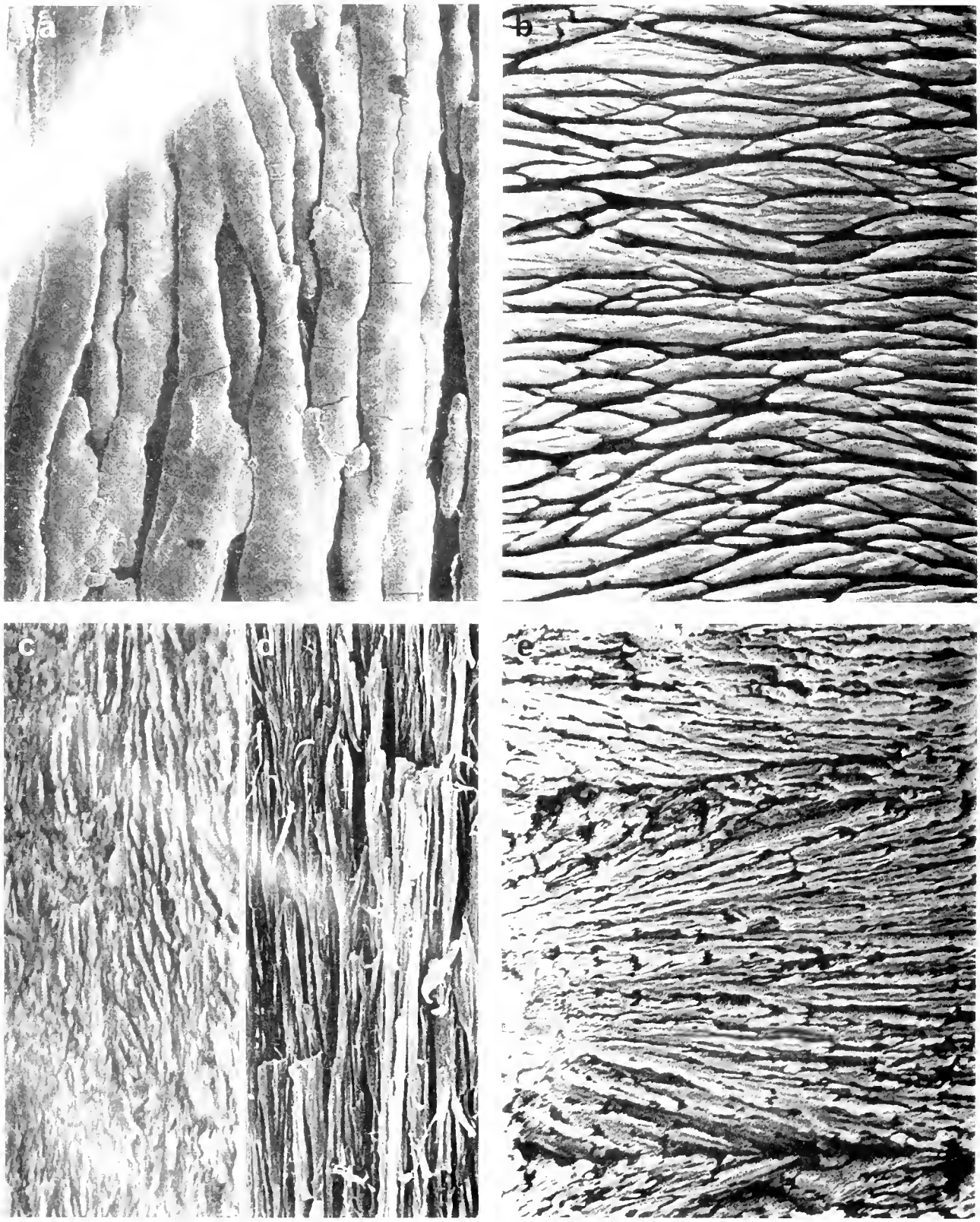

Figure 3. (a) Bleach-etched outer loculi of *Plexamella grisea* are elongate, pallisade-shaped, longitudinally oriented, occasionally branch, and fuse with other loculi. Note in lower left corner the spherical, crystalline units that have not yet fused completely into a mature loculus. 100×. (b) Bleach-etched outer locular surface of *Plexamella luteola* composed of outer ends of the crystal plates. Most are fusiform. 4700×. (c) Bleach-

current regimes, of which there would be about four per day, the increase in diameter would be approximately 1 mm/year. It could be that only currents from one direction carry enough nutrient to permit carbonate deposition, or that nocturnal currents do so. In those cases there would be two striae per day deposited and an accretion rate of 0.5 mm/year. These are ahermatypic organisms (Goldberg, 1973), therefore they are dependent on "captured" prey for nutrients. Other scenarios could also account for the striae. If the diameter, including that at the base, accretes at a constant rate that does not change with age, then an individual with a basal thickness of 1 cm (not uncommon) could be somewhere between 10 and 40 years of age. This is, of course, a very crude estimate.

A series of micrographs of randomly taken specimens cannot be used to prove that dynamic processes occur in a particular sequence. Nevertheless, many micrographs of annuli in various stages of development have been examined, and we are now confident that annulus formation can be outlined. The formation of an annular layer begins with the deposition of fine, "seed crystals" over the smooth outer surface of a previous, inner annulation. The fine crystals initially have a random, granular appearance. As collagen fibers are synthesized and encapsulated within the fine seed crystals, the layer becomes longitudinally striated with impressions of the collagen fibers. It is on the outer surface of this "seed-crystal" layer that the thin perpendicularly oriented annulation crystals nucleate. Small, 'initial', annular crystals nucleate on the surfaces of the fine crystals. As the fine annular crystals grow outward, they become oriented perpendicularly by lateral interference from adjacent crystals. These fine crystals merge to form the larger, lath-shaped, perpendicularly oriented crystal aggregates that span the annulus. Collagen fiber synthesis and deposition must occur prior to crystal growth, since the longitudinally oriented collagen fibers are incorporated within the crystalline material. When annular crystal growth ceases, the skeletogenic cells of the axial epithelium secrete another layer of fine, capping crystals.

Genus Plexaurella

Axes of *Plexaurella nutans, P. grisea* and *P. fusifera* are extensively mineralized (about 20%/dry weight) by calcite of the high magnesium variety (Jeyasuria and Lewis, 1987; Esford and Lewis, 1990). In these species, crystalline aggregates (loculi), which are lenticular and fusiform, can be up to 5 mm in length and are semi-lunate in cross section. They are embedded longitudinally in the gorgonin. As in all the gorgonians examined, the collagen fibers course longitudinally through the proteinaceous matrix of the gorgonin, but do not penetrate the crystalline aggregates. The loculi are solid, crystalline structures composed of regular, spherulitic, prismatic units similar to those of molluscan shell (Carter and Clark, 1985).

Species of *Plexaurella* occur in the surge zone where they are subjected to both wave and current-generated water movements that produce high forces in storm conditions. Normally, forces generated in the surge zone are lower than those encountered either in deeper water (produced by current only), or in the shallower breaker zone (Roberts *et al.*, 1975). In addition to the back and forth sway from wave action, there is also a twisting motion that is amplified by current. Species of *Plexaurella* are generally large (some up to 2 m in height) with comparatively long, thick branches. The moderately high stiffness and moderate torsion resistance of these species accommodate them to the forces in the surge zone. Separation of the collagenous and mineral phases, with the retention of approximately similar proportions of carbonate (Jeyasuria and Lewis, 1987; Esford and Lewis, 1990), may lower the stiffness from that of *Ellisella barbadensis*. The lenticular crystalline loculi probably also stiffen the axis in the manner of filler particles (Koehl, 1982) and maintain stiffness in a moderately high (for gorgonians) range. The semi-lunate, cross-sectional shape of the loculi probably allows species of *Plexaurella* to rotate somewhat in response to twisting forces and results in a moderately low torsion modulus (Jeyasuria and Lewis, 1987).

Fine striae, about 0.4 μm in width, evident on lightly ascorbic acid-etched cross sections of loculi, again probably represent episodic carbonate accretion. No data have been published on growth rates of species of *Plexaurella*, but they appear to be very slow growing (circa 1 cm/year; Paul Yoshioka, pers. comm.). If these striae are comparable to those from *Ellisella barbadensis*, and assuming that one stria represents accretion over the same time period in both species (which may well not be the case),

---

etched inner locular surface of *Plexaurella nutans* with longitudinal grooves between fine crystals. Irregular, rosette-like patterns are thought to represent nucleation sites for spherulitic crystal aggregates of the loculus. 2300×. (d) Surface of the longitudinally-fractured gorgonin layer between loculi of *Plexaurella nutans* with longitudinally oriented collagen fibres. Note that the diameters of the collagen fibers correspond to the groove diameters in 3c. 2300×. (e) Lightly ascorbic-acid etched, longitudinally fractured loculus of *Plexaurella nutans*. Several spherulitic crystal units are evident with crystal plates radiating fan-like from an inner nucleation site out to the outer edge of the loculus. Note that some crystal plates branch and the series of cavities where adjacent plates interfere with plate growth. X-ray diffraction pattern indicates crystalline calcite. 3750×.

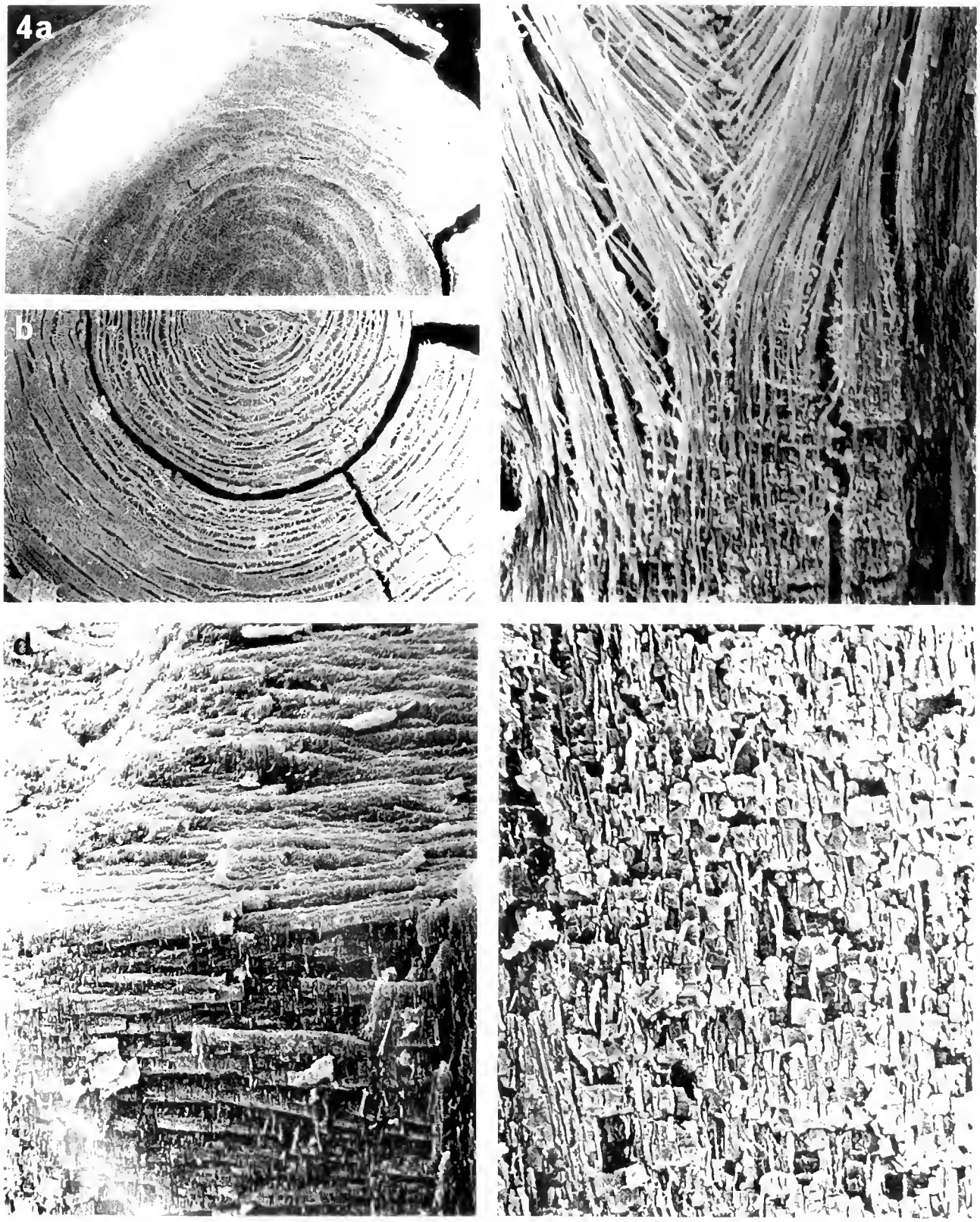

Figure 4. (a) Bleach-etched (gorgonin removed) cross section of the axis of *Ellisella barbadensis*. Note the heavily calcified annular rings of uneven diameters. 25×. (b) Acid-etched (calcareous matter removed) cross section of the axis of *Ellisella barbadensis*. Note the concentric ridges formed by extensive collagen fibers matted together. 25×. (c) Acid-etched, longitudinally fractured annular ring showing longitudinally

then the growth rate of the species of *Plexaurella* is about 25% faster. Species of *Plexaurella* are hermatypic (Ramsaroop, 1977) and contain symbiotic zooxanthellae principally in the tissues of their polyps. Hermatypic forms may gain additional nutrition and therefore increased growth potential from this symbiotic relationship between them (Pearse and Muscatine, 1971). Though the exact mechanisms of crystal growth, induction and cessation are not known, growth has been related to diurnal cycles. Chalker and Taylor (1978) and Gladfelter (1984) reported that calcification in scleractinian corals is directly proportional to photosynthesis. Daily variations in skeletogenesis are due, not only to daily changes in solar irradiance, but also to daily changes in the efficiency of the symbiotic algal photosynthesis. Zooxanthellae of *Gymnodinium microadriaticum* exhibit an endogenous circadian rhythm (Chalker and Taylor, 1978). Reduced organic carbons produced by algal photosynthesis are used as a substrate for the formation of an organic matrix upon which crystal growth occurs (Kingsley and Watabe, 1984). Narrow lines produced by capping proteins that halt crystal growth in response to a variety of factors in scleractinians are similar to those noted in this species (Chalker and Taylor, 1978).

Again, knowing the pitfalls, we feel that enough loculi in various stages of formation have been examined to permit an outline of loculus formation. It probably begins with deposition of fine, granular crystals over and around loose collagen fibers. The collagen fibers do not appear to be calcified, but are surrounded by the fine-grained crystals. This forms a thin, seed crystal layer. Deposition of the fine seed crystal layer could be induced by coating the collagen fibers with glycosaminoglycans (GAGs) which are known to concentrate calcium, creating the supersaturation necessary for nucleation on the collagen fibers (Addadi *et al.*, 1987). Within the thin seed-crystal layer, spherulitic nucleation sites occur at various points. Crystal growth initially radiates in all directions, but interference is encountered in most directions. The inner surface, seed-crystal layer, and adjacent nucleation sites restrict most of the crystal plate elongation to a direction perpendicular to the initiation layer. This method of crystal plate elongation initially results in the nodular appearance of loculi in the early stages of formation, with each nodule representing crystal plate growth from a single nucleation site. As locular thickness increases through crystal plate elongation and secondary branching, the radiating crystal plate ends of the individual nodules become increasingly interdigitated and more difficult to distinguish. When the loculus is near the final stage of formation, the outer surface loses the nodular texture and forms a relatively smooth, rounded, outer surface. At this stage, the rounded outer locular surface is composed of the sharp-pointed, lath-shaped (Carter and Clark, 1985) crystal plate ends.

The transversely fractured surface has a fan-like crystal pattern which radiates outwards only from the inner surface nucleation sites. This radiating pattern is due to the outward growth of the crystal plates, the ends of which create the outer surface.

On longitudinally fractured surfaces of individual loculi the fan-like crystal plate growth is readily apparent. Again, the radiating pattern from the inner surface occurs only from discrete nucleation sites. Secondary branching of the crystal plates occurs at regular intervals along the edges of the elongating crystal plates. The vertical rows of holes evident in the ascorbic acid-etched longitudinally fractured surfaces are located where there is interference between the secondarily branching plates. These secondary interference edges appear as 3.0 μm wide bands in the transversely fractured surfaces.

Biomineralization requires four conditions: (1) fluid supersaturation, (2) crystal nucleation, (3) crystal growth, and (4) a mechanism for controlling crystal growth so it can be structurally useful to an organism (Simkiss and Wilbur, 1989). Little is known about the calcium-carbonate secreting skeletogenic cells of gorgonian axes or of their ability to control crystal deposition. Kingsley and Watabe's (1984) work on *Leptogorgia virgulata* (a related gorgonian), showed that calcium ions are transported from the external environment to the axis. Calcium ion transport out of the axis through the axial epithelium was mediated by Ca-ATPase (Kingsley and Watabe, 1984). In 1987, Kingsley and Watabe isolated carbonic anhydrase activity adjacent to calcifying structures in the axis. Thus, a mechanism for fluid supersaturation exists in gorgonians. The mineral crystals probably grow on a framework of extracellular proteins and polysaccharides (Weiner *et al.*, 1983). Addadi *et al.* (1987) demonstrated that sulphates and beta-sheet structured carboxylates from the acidic matrix macromolecules cooperate in oriented calcite crystal nucleation.

oriented collagen fibers. Thin horizontal plates are remnants of calcareous plates. 1900×. (d) Annular ring with transverse and longitudinal fracture surfaces. Crystal aggregates oriented horizontally are tightly stacked (like lumber), elongate, lath-shaped and extend entirely across the annular ring. Thin vertical fibers are broken collagen fibers. X-ray diffraction pattern indicates calcite. 950×. (e) Outer surface of a fractured annulation. Crystal aggregates are oriented in end-on view and are perpendicular to the longitudinal axis of the colony. In cross section most are square (3 × 3 μm). Vertical fibers are collagen fibers, many of which are broken. 950×.

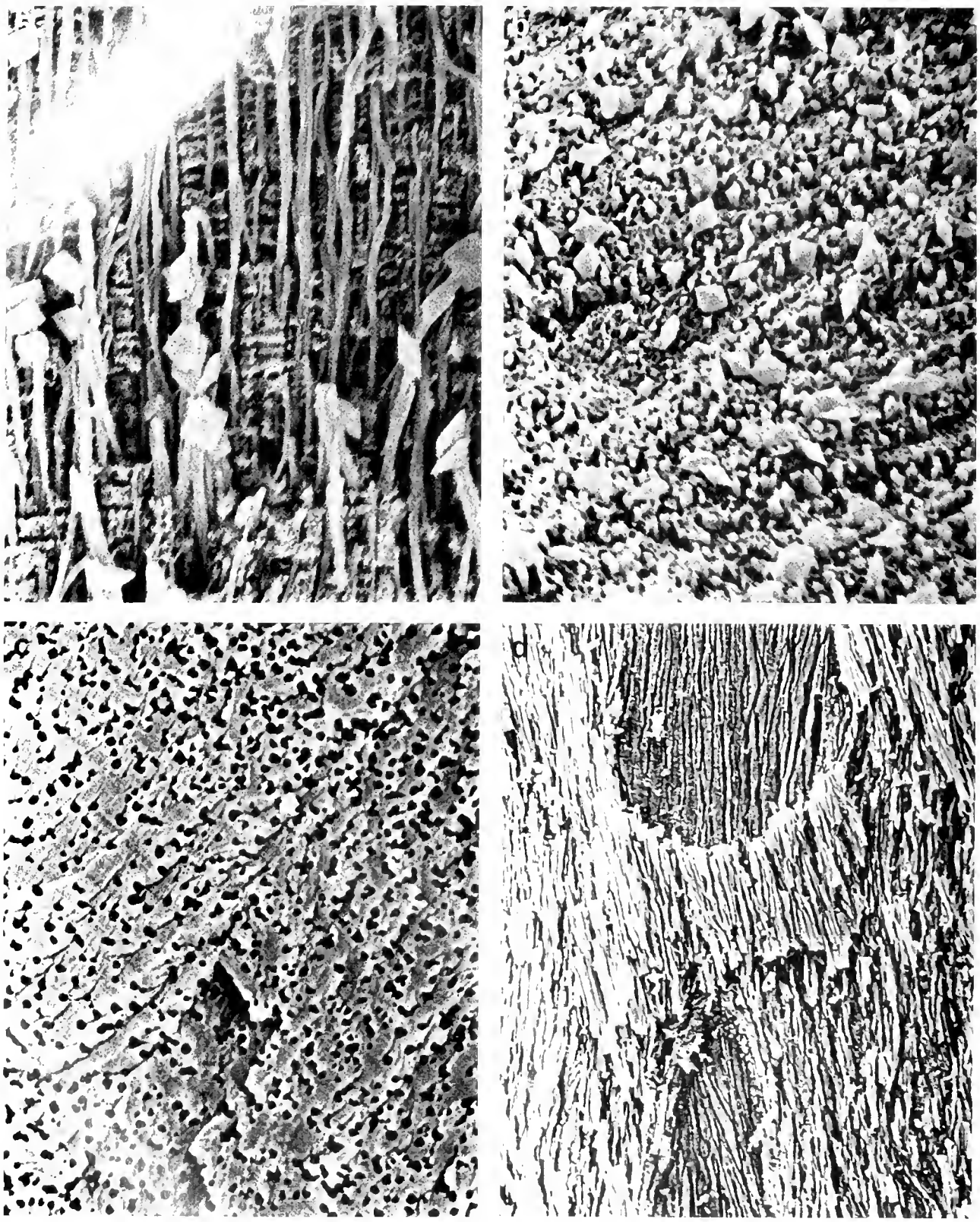

Figure 5. *Urechis barbadensis*. (a) Ascorbic-acid etched, longitudinal fracture of an annulus with longitudinally oriented collagen fibers 0.2–0.4 μm diameter. Fibers have been freed from eroded crystal aggregates (horizontal bars). Bipyramidal shapes are crystal flakes. ×4700. (b) Ascorbic-acid etched surface of a transversely cleaved annulus. Short, protruding, slightly smoothed ends of collagen fibers protrude from the

Genus Lophogorgia

The axis of individuals of *Lophogorgia cardinalis* is moderately mineralized (about 10%/dry weight) by a carbonate with a high magnesium content (Jeyasuria and Lewis, 1987; Esford and Lewis, 1990). The X-ray diffraction pattern is that of an amorphous material, but it produces a faint calcite diffraction pattern. That this carbonate is probably a high magnesium calcite is supported by atomic absorption spectrometric determinations of mole percentages of magnesium in the calcium/magnesium carbonate. Mineral deposits occur as plate loculi that are crescentic, multilaminar, branched plates of irregular outline. Simplistically, the laminae of the plates are formed by alternating high and low density (fibers per unit area of gorgonin) layers of longitudinally oriented collagen fibers. The dense collagen fiber layers are lightly mineralized; the sparsely fibered layers, heavily mineralized. The mineral, in the form of tiny mineral bodies (crystals?), occurs in the matrix between and around collagen fibers. Collagen fibers in the low density laminae are usually heavily calcified, to the point they are individually sheathed by mineral, and often several adjacent collagen fibers may be incorporated into one, usually plate-like mass. Extensive mineralization of these laminae effectively produces very thin mineral sheets. Densely fibered laminae contain tiny mineral bodies (crystals) in the matrix. Ledger and Franc (1987) found that, in the axial skeleton of the sea pen *Veretillum cynomorium*, calcite deposits initially nucleate extracellularly between collagen fibers. They grow, push aside the collagen fibers, and eventually surround and encapsulate them. Significantly, mineral does not form within the collagen fibril, and collagen is not involved in the nucleation process. The same process may be occurring here. That the high magnesium calcite deposits in *Leptogorgia virgilata*, *Lophogorgia cardinalis*, and *Gorgonia ventalina* are amorphous is not surprising, if all of the mineral is in a form similar to that noted in *Lophogorgia cardinalis*. Crystals surrounding the collagen fibers are very small at about 0.1 μm thick and a few microns long. They are not arranged in a sufficiently regular pattern to produce a strong calcite diffraction pattern, but a faint diffraction pattern typical of calcite is barely detectable on the negatives. Randomly oriented proteoglycan molecules within a highly hydrated gel matrix between cell layers may cause the precipitation of crystals in an amorphous form (Kingsley and Watabe, 1984). Another possible explanation for the amorphous nature of calcareous matrix of *Lophogorgia cardinalis* is that the collagen fibers have nucleation sites on their surface. In Goldberg's (1976) analysis of the chemistry of gorgonian axial skeletons, the presence of large amounts of glycosaminoglycans (GAGs) was observed in a heavily mineralized gorgonian. The GAGs may coat the individual collagen fibers and thus initiate nucleation of the fine granular crystals (Addadi *et al.*, 1987). This method of crystal deposition and nucleation on individual collagen fibers could account for the fine, granular, amorphous nature of the mineral in *Lophogorgia cardinalis*.

Lateral to the calcified laminae are relatively thick layers of gorgonin containing a high density of collagen fibers. The structure of the laminated plate loculi is reminiscent of the laminated safety glass of automobile windshields.

Lophogorgia cardinalis, like *Ellisella barbadensis*, occurs below wave base where it is subject to current only. These small (circa 15 cm), relatively highly branched, planar, almost fan-like organisms require considerable stiffness to resist the current and maintain the polyps in feeding position in the water column. Their axial skeletons are among the stiffest found in Caribbean gorgonians (Esford and Lewis, 1990), and their torsion moduli are also high (Jeyasuria and Lewis, 1987). Laminated structures are often stiffer than comparable uniform composites, but it is the interconnectedness of the shield loculi that influences the stiffness. The extent and thickness of interconnections between individual plates probably also modulates resistance to twisting forces. Individual, separated, plate loculi embedded in gorgonin would not impart much resistance to compression. Interconnections between large numbers of them, effectively forming a mineral reticulum, would probably be quite resistant to compression. Such a reticulum would also produce considerable resistance to torsional forces.

SEMS of the axis of individuals of *Lophogorgia cardinalis* exhibit considerable artifactual disruption. Splits, cracks, and gaping spaces are common. Almost any treatment aimed at revealing one of the mineral or organic components of the axis will cause major structural perturbation. Removing the mineral phase with acids causes collagen to swell. This swelling disrupts structural integrity particularly along planes of weakness. Since the organic

eroded carbonate crystal surface. Carbonate forms irregular ring patterns around some of the collagen fibers. Bipyramidal shapes are crystal flakes. 4700 ·. (c) Bleach-etched surface of a transversely cleaved annulus. Collagen has been removed and reveals perforations in the carbonate crystal plates through which the fibers extend. Note the high density of the perforations and the fine diagonal striae with a period of about 0.2 μm that probably represent episodic carbonate deposition. 4700 ·. (d) Bleach-etched, longitudinally fractured outer surface layers of an annulus. The multilaminar layer of fine-grained, longitudinal crystals caps the annular crystal aggregates and forms nucleation sites for subsequent annulus formation. 1900 ·.

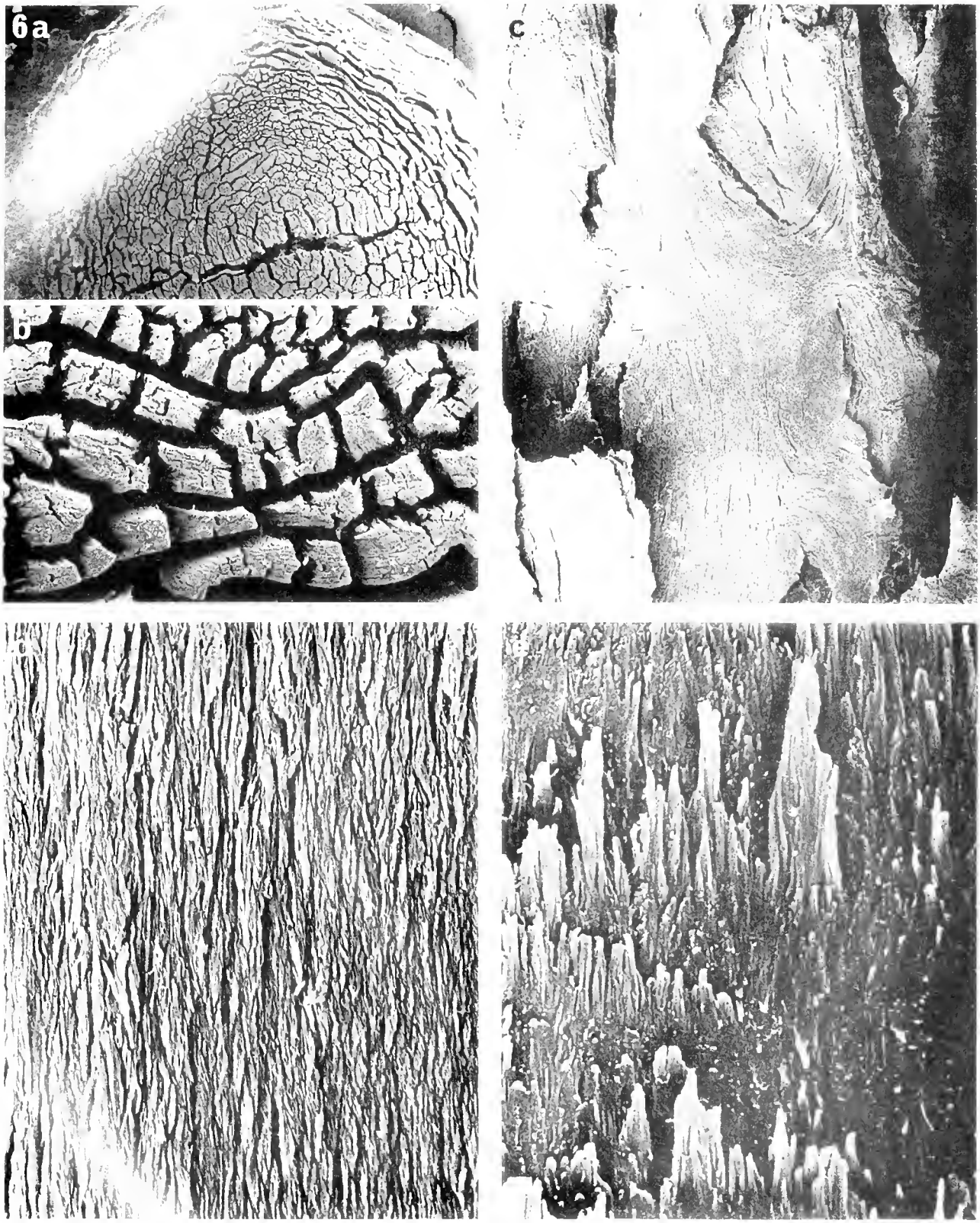

Figure 6. (a) Bleach-etched (gorgonin removed) cross section of the axis of *Lophogorgia cardinalis*. Numerous, radially crescentic calcareous loculi form a major component of the axis. 33×. (b) Bleach-etched cross section showing crescentic loculi with artifactual fractures caused by removal of gorgonin support, rehydration and dehydration. 470×. (c) Bleach-etched, longitudinally fractured axis of *L. cardinalis* showing the outer surface of a plate loculus. Note its irregular outline and connections with neighbouring locular plates. 160×. (d) Bleach-etched, outer surface of a plate loculus with fine-grained, longitudinally oriented crystals. 2400×. (e) Interlocular gorgonin with layered, longitudinally oriented collagen fibers. 2400×.

phase is so large, about 90% (Esford and Lewis, 1990), its removal with hypochlorite also eliminates support for the mineral phase. Since the mineral is in the form of delicate plates and single, free-standing, carbonate-sheathed collagen fibers, this undermining has rather drastic effects. These are further exacerbated by the swelling caused by hypochlorite and the subsequent dehydration required for examination by SEM. Fortunately, the deleterious effects of these treatments do not appear to be uniformly distributed. They appear to be limited to the large checks, cracks and gaps, and large areas of axis remain in what appears to be the "original" condition, with one phase or another removed.

All species

Polarized microscopy of thin longitudinal sections indicates that the 12 species examined have a fibrillar component oriented in parallel with the longitudinal axis of the colony only.

Calcareous material could also be extracted from the axes of all species examined, though in some species the minute amounts of carbonate extracted were probably from the hollow core of the axis and are possibly nonbiogenic in origin. X-ray diffraction indicates that the major form of carbonate occurring in these gorgonian axes is calcite. Positive Aliziran red staining, in combination with calcium and magnesium proportions derived from atomic absorption spectroscopy (Jeyasuria and Lewis, 1987; Esford and Lewis, 1990), indicate that the carbonate is in the form of high magnesium calcite. This also applies to those crystal forms that produced an amorphous X-ray diffraction pattern.

Ellisella barbadensis and the three species of *Plexaurella* have large, regular crystalline, high magnesium calcite aggregations in their axes. In these species, visible mineralization was highest in the cross sections of tips and lowest in bases. This correlates well with the findings of Esford and Lewis (1990) that the Young's modulus or stiffness of axial skeletons was higher in the tips than in the bases of *Ellisella barbadensis* and the species of *Plexaurella* that they examined.

Axes of *Lophogorgia cardinalis* and *Leptogorgia virgilata* contain thin carbonate plates that produce amorphous X-ray diffraction patterns. Mole percentages of magnesium in the carbonate (Jeyasuria and Lewis, 1987) are indicative of high magnesium calcite. Atomic absorption spectroscopy also indicates high magnesium calcite as the mineral form for the amorphously diffracting small crystalline aggregates from *Gorgonia ventalina*.

Species of *Pseudopterogorgia* have calcitic fibroids between or around collagen bundles. Fibroid mineralization probably occurs between collagen bundles which act as templates. This results in the fibrous appearance of the mineral.

In the preceding genera, mineralization is biologically controlled. The organic matrix acts to constrain the exterior surface of the mineralized aggregate, making a finite variety of shapes possible. This biogenic process is characterized by a mineralization site sealed off from the environment by a barrier through which ions cannot freely diffuse (Lowenstam and Weiner, 1989). Space delineation is a fundamental part of the cellular machinery that controls mineralization (Wilbur, 1984). Biological control of the type and form of mineral deposited is undoubtedly important for structural reasons.

In the remaining species, mineralization is thought to be nonbiogenic and occurs in an open environment such as the hollow central region of the axis. The physical characteristics of nonbiogenic mineralization include a morphological structure analogous to their organic counterparts, as well as randomly clumped aggregates of varying sizes (Lowenstam and Weiner, 1989). These diagnostic features are readily observed in the scanning electron micrographs of *Eunicea tourneforti*, *Muricea muricata*, and *Plexaura flexuosa*. Nonbiogenic mineralization may be induced by a relatively minor perturbation, such as the introduction of biologically produced metabolic endproducts, the release of particular cations by the cell, or even by the construction of a charged surface such as a cell wall (Wainwright, 1988). Basically, no specialized cellular or macromolecular mechanism regulates this precipitation.

A characteristic of nonbiogenic mineralization is that the type of mineral formed is a function of the environmental conditions in which the organism occurs, as much as of the biological processes involved in its formation (Wainwright, 1988). Thus, the same organism in a different environment can form different minerals (Lowenstam and Weiner, 1989). A mineral shift, whereby a species may precipitate different mineral forms in response to external stimuli, was demonstrated by Lowenstam (1964), who found that temperature and salinity were the dependent variables in the ratios of aragonite to calcite in certain (*Octocorallia*) species of *Holaxonia*. He concluded that, at mean seawater salinity, the aragonite/calcite ratio of the carbonate skeleton increased with the ambient temperature.

In this study, species exhibiting what we regard as nonbiogenic mineralization that probably occurs only in the hollow core of the axis, contain minute quantities of carbonate and less than ½ of 1% total Ca + Mg/dry wt of axis (Jeyasuria and Lewis, 1987; Esford and Lewis, 1990). X-ray diffraction patterns from minute quantities of mineral reveal calcite in *Muricea muricata*, aragonite in *Eunicea tourneforti*, and amorphous in *Plexaura flexuosa*. Here, "amorphous" means only that no recognizable diffraction pattern is generated. Lowenstam (1964) found that carbonate extracted from *Plexaura flexuosa* is

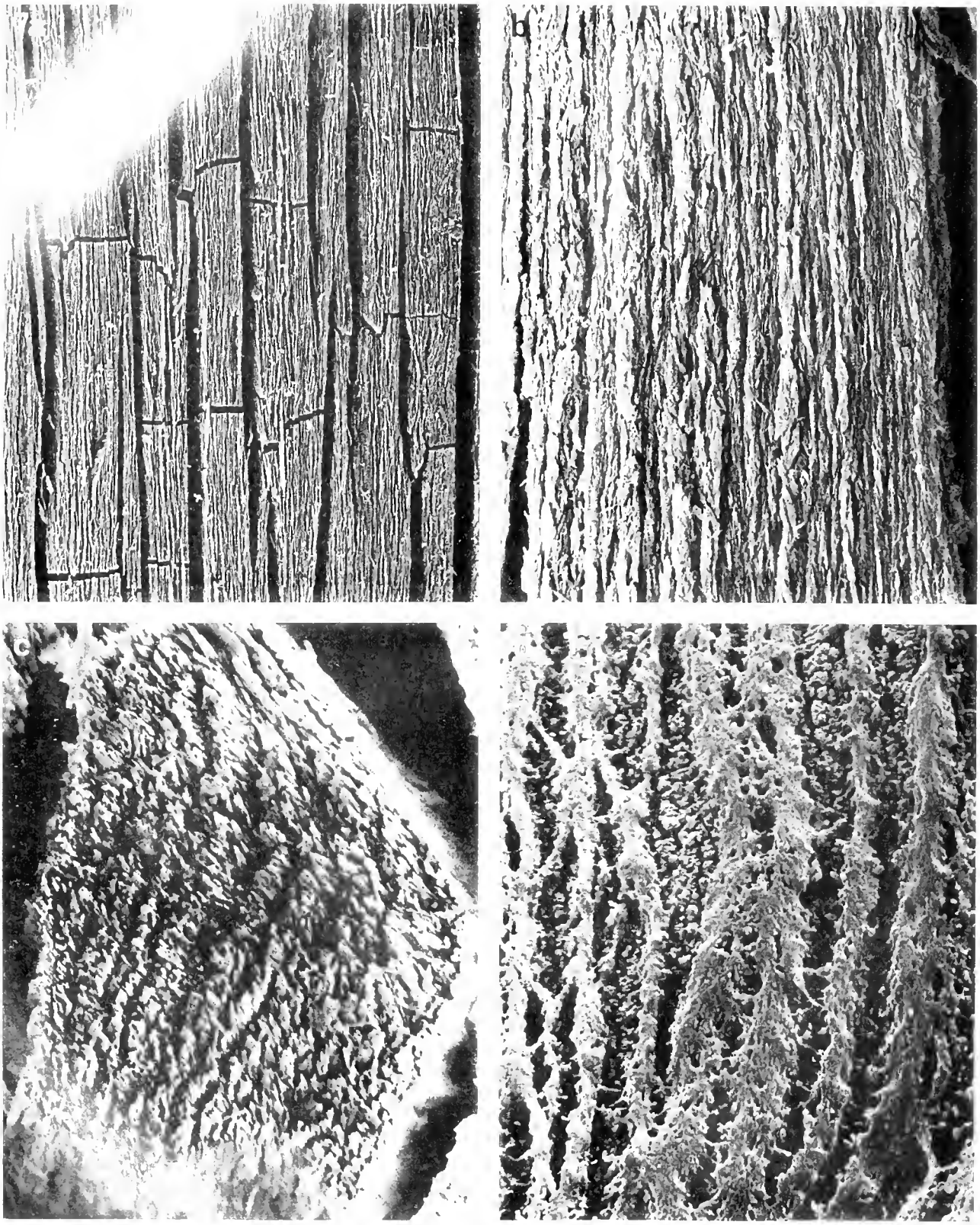

Figure [illegible]. (a) Bleach-etched edges of longitudinally cleaved plate loculi show the laminar organization of mineral [illegible] sclerosomin layers of *Lophogorgia cardinalis*. Note the lateral branching and fusion of calcified connections [illegible] adjacent plates. 470×. (b) Bleach-etched edge of a longitudinally cleaved plate loculus reveals rope-like rows of fine-grained, longitudinally oriented fine crystaline bodies. Grooves represent areas

Table II

A comparison of mechanical properties, associated structures, and habitat in Ellisella barbadensis, Lophogorgia cardinalis, Plexaurella, *and non-mineralized specimens*

Species	Tm	Ym	% Ca/Mg	Structure	Habitat
E. barbadensis	8.6	90	30	fiber-reinforced concentric rings	current
L. cardinalis	5.8	40	12	laminae of sheathed collagen fibers	current
Plexaurella	3.5	35	20	fusiform loculi separate from collagen	surge
Others	0.7	5–10	>1	no mineral	surge

Tm: torsion modulus, a measure of resistance to twist in Gdynes/cm^2.
Ym: approximated Young's modulus, a measure of stiffness.
% Ca/Mg: percentage of carbonate/dry weight of axis (Jeyasuria and Lewis, 1987; Esford and Lewis, 1990).

aragonitic, but obtained no definitive stain reaction. He also makes reference to an aragonitic axis in *Plexaurella dichotoma*, which is at odds with our determinations of high magnesium calcite in three other species from that genus.

A preliminary comparison of structure and some associated mechanical properties is instructive (Table II). The following tentative conclusions can be drawn from the table: (1) Unmineralized gorgonin has low stiffness and low torsion resistance. (The "other species" are exemplary.) (2) Mineral is used in different ways to stiffen gorgonin (compare the "Structure" with "Ym" columns). (3) Mineral content alone does not determine stiffness. (*Lophogorgia cardinalis* with half the mineral content of *Plexaurella* is somewhat stiffer.) (4) Mineral content alone does not determine torsional resistance. (*Lophogorgia cardinalis*, with half the mineral content of *Plexaurella*, is much more resistant to twist). (5) Incorporation of collagen into the mineral phase increases stiffness. (Individuals of both *Ellisella barbadensis* and *Lophogorgia cardinalis*, are stiffer than the *Plexaurella*, despite *Lophogorgia cardinalis* having far less mineral). (6) Separation of the mineral phase from the collagen fibers lowers both Young's and torsion moduli. Species of (*Plexaurella* have lower moduli than *Ellisella barbadensis* and *Lophogorgia cardinalis*). (7) Higher torsional, tensional, and compressional stiffness is used in current than in surge. (Consistently higher Ym and Tm are found in the two species that occur in the current zone). (8) The reinforced concrete style of mineralization found in *Ellisella barbadensis* produces very high stiffness and very high resistance to torsion. (9) The interconnected, lamellar, shield-like plates of sheathed collagen fibers produces moderately high stiffness and moderately high resistance to torsion with relatively little mineral in *Lophogorgia cardinalis*. (10) The lenticular crystalline loculi of species of *Plexaurella* are separate from the collagen fibers and produce moderately high stiffness, but moderately low resistance to torsional forces.

Acknowledgments

We thank L. Stobbs and J. Van Schagen of the Vineland Agriculture Canada Research Station for assistance with SEM, U. Brand, Department of Geological Sciences and M. Richardson, Department of Chemistry, Brock University, for assistance with X-ray diffraction and the Prime Minister's Office of the Government of Trinidad-Tobago for permission to collect gorgonians for this research.

Literature Cited

Addadi, L., J. Moradian, E. Shay, N. G. Maroudas, and S. Weiner. 1987. A chemical model for the cooperation of sulphates and carboxylates in calcite crystal nucleation: relevance to biomineralization. *Proc. Nat. Acad. Sci. USA* **84**: 2732–2736.

Barnes, R. D. 1980. *Invertebrate zoology, 4th Edition.* Pp. 164–169. Saunders College/Holt Rhinehart and Winston, Philadelphia.

Barnowski, T. F. 1991. SEM of the heavily calcified axial skeletons of three genera of Caribbean gorgonians. *Hons. B.Sc. Thesis.* Brock University, St. Catharines, Canada. 137 pp.

Bayer, F. M. 1961. *The Shallow Water Octocorallia of the West Indian Region.* Marinus Nijhoff. The Hague. 373 pp.

Carter, J. G., and G. R. Clark II. 1985. Classification and phylogenetic significance of molluscan shell microstructure; in *Mollusks: Notes for a short course*, D. J. Bottjer, C. S. Hickman, and P. D. Ward, eds. University of Tennessee, Dept. of Geological Sciences, Studies in Geology 13. 305 pp.

Chalker, B. E., and D. L. Taylor. 1978. Rhythmic variations in calcification and photosynthesis associated with the coral *Acropora cervicornis*. *Proc. R. Soc. Lond. B. Biol. Sci.* **201**: 179–189.

Esford, L. E., and J. C. Lewis. 1990. Stiffness of Caribbean gorgonians (Coelenterata, Octocorallia) and Ca/Mg content of their axes. *Mar. Ecol. Prog. Ser.* **67**: 189–200.

Gladfelter, E. H. 1984. A comparison of monthly rates of linear extension and calcium carbonate accretion measured over a year. *Coral Reefs* **3**: 51–57.

from which collagen has been removed. X-ray diffraction pattern is amorphous. 1400×. (c) Bleach-etched, transversely fractured plate loculus of *Lophogorgia cardinalis*. Note rows of carbonate, sleeve-like structures, many with hollow centres. Dark areas between rows remain from gorgonin removal. Carbonate is probably deposited around individual collagen fibers. (d) Acid-etched, transversely fractured plate loculus. Fused and melted ends of dense collagen-gorgonin layers form elevated ridges. Valleys contain ends of acid-eroded calcareous tubes. 2400×.

Goldberg, W. M. 1973. [illegible] of sclerotized collagen from the skeleton of a gorgon[illegible] *Comp. Biochem. Physiol.* **49:** 525–532.

Goldberg, W. M. [illegible]. Comparative Study of the chemistry and structure[illegible] and antipatharian coral skeletons. *Mar. Biol.* **35:** 253–[illegible]

Jeyasuria, [illegible] C. Lewis. 1987. Mechanical properties of the axial [illegible] in gorgonians. *Coral Reefs* **5:** 213–219.

Kingsley, R. J., and N. Watabe. 1984. Calcium uptake in the gorgonian *Leptogorgia virgulata*. The effects of ATPase inhibitors. *Comp Biochem. Physiol.* **79A:** 487–491.

Kingsley, R. J., and N. Watabe. 1987. Role of carbonic anhydrase in calcification in the gorgonian *Leptogorgia virgulata*. *J. Exp. Zool.* **241:** 171–180.

Koehl, M. A. R. 1982. Mechanical design in spicule reinforced connective tissues: Stiffness. *J. Exp. Biol.* **98:** 239–267.

Ledger, P. W., and S. Franc. 1978. Calcification of the collagenous axial skeleton of *Vertullum cynomorium* Pall (Cnidaria: Pennatulacea). *Cell Tissue Res.* **192:** 249–266.

Leversee, G. J. 1969. Composition and function of the axial skeleton in the gorgonian coral *Leptogorgia virgulata*. *Am. Zool.* **9:** 1115 (abstract).

Lowenstam, H. A. 1964. Coexisting calcites and aragonites from skeletal carbonates of marine organisms and their strontium and magnesium contents. Pp. 373–404 in *Recent Researches in the Fields of Hydrosphere, Atmosphere and Nuclear Geochemistry*, Y. Miyake, and T. Koyama, eds. Maruzeu Co., Ltd., Tokyo.

Lowenstam, H. A., and S. Weiner. 1989. *On Biomineralization*. Oxford University Press. New York. 324 pp.

Muss, M. L. 1964. The phylogeny of mineralized tissue. *Int. Rev. Gen. Exp. Zool.* **1:** 297–331.

Muzik, K., and S. A. Wainwright. 1977. Morphology and habitat of five fijian fans. *Bull. Mar. Sci.* **27:** 308–337.

Pearse, V. B., and L. Muscatine. 1971. Roles of symbiotic algae (zooxanthellae) in coral calcification. *Biol. Bull.* **141:** 350–363.

Ramsarnop, D. 1977. Common shallow-water gorgonians of Trinidad. *Living World* **2:** 21–32.

Roberts, H. H., S. N. Murray, and J. N. Suhayda. 1975. Physical processes in a fringing reef system. *J. Mar. Res.* **33:** 233–260.

Simkiss, K., and K. M. Wilbur. 1989. *Biomineralization: Cell biology and mineral deposition*. Academic Press, Inc. Toronto. 337 pp.

Telesnicki, G. J. 1990. A comparative study of the structure of gorgonian axial skeletons. *Hons. B.Sc. Thesis*. Brock University, St. Catharines, Canada. 140 pp.

Vincent, J. F. V. 1981. *Structural Biomaterials*. MacMillan Press Ltd., London. 206 pp.

Wainwright, S. A., W. D. Biggs, J. D. Currey, and J. M. Gosline. 1982. *Mechanical design in organisms*. Princeton University Press, New Jersey. 423 pp.

Wainwright, S. A. 1988. *Axis and Circumference: the Cylindrical Shape of Plants and Animals*. Harvard Univ. Press., Cambridge. 132 pp.

Weiner, S., W. Traub, and H. A. Lowenstam. 1983. *Biomineralization and Biological Metal Accumulation*. P. Westbroek and E. W. de Jong, eds. Dordrecht, Netherlands. Pp. 205–224.

Weise, L. 1988. *Cell and Tissue Biology: A Textbook of Histology, Sixth Edition*. Urban and Schwarzenberg, Inc., Baltimore, MD, U.S.A. 1158 pp.

Wilbur, M. K. 1984. Many minerals, several phyla, few considerations. *Am. Zool.* **24:** 839–845.

Reference: *Biol. Bull.* **183**: 297–303. (October, 1992)

Ion Transport in the Freshwater Zebra Mussel, *Dreissena polymorpha*

JANICE HOROHOV, HAROLD SILVERMAN, JOHN W. LYNN, AND THOMAS H. DIETZ*

Department of Zoology and Physiology, Louisiana State University, Baton Rouge, Louisiana, 70803

Abstract. The blood solute concentration (36 mosm) of pondwater acclimated zebra mussels is among the lowest found in freshwater bivalves. Blood ion concentrations were Na (11–14 m*M*) and Cl (12–15 m*M*), with lesser amounts of Ca (4–5 m*M*), HCO_3 (about 2–4 m*M*), and K (0.5 m*M*). Sodium, Ca and Cl transport rates were 20–30 μeq (g dry tissue · h)$^{-1}$ for pondwater acclimated mussels. The influx of both Na and Cl was stimulated by exogenous serotonin (0.1 m*M*). Sodium transport in zebra mussels was not inhibited by amiloride. Zebra mussels became isosmotic in 30 m*M* NaCl solutions and did not survive beyond a week in 45 m*M* NaCl. Zebra mussels are well adapted to their dilute freshwater habitat, but are more stenohaline than other freshwater bivalves as reflected by their intolerance of elevated ion concentrations in the bathing solution.

Introduction

The zebra mussel (*Dreissena polymorpha*) is the most recent freshwater bivalve introduced into the United States from Europe (Mackie *et al.*, 1989). Unlike other freshwater bivalves, adult zebra mussels attach to solid substrate with byssal threads and may reach densities exceeding $10^5/m^3$. In addition, reproduction involves gametes that are discharged into the water column and develop into free-swimming veliger larvae that may remain planktonic for weeks or months, allowing them to move considerable distances before settling (Mackie *et al.*, 1989; Morton, 1979).

Dreissena has been documented as a serious economic pest because of its propensity to foul raw-water systems, and there is extensive European literature on the ecology and gross morphology (Stanczykowska, 1977; Morton, 1979; Mackie *et al.*, 1989). However, there are few osmoregulatory studies and most physiological studies have focused on methods for control or extermination (Morton, 1979; Mackie *et al.*, 1989).

In a study by Fisher *et al.* (1991), a buffered artificial soft water was found to be lethal to *Dreissena*. Some artificial freshwater solutions are buffered with up to 30 m*M* KH_2PO_4 and 19 m*M* NaOH to maintain neutral pH (Porcella, 1981). This concentration of potassium and sodium and the ionic ratio are exceptional for an artificial freshwater but the primary solute responsible for the mortality in *Dreissena* is potassium (Fisher *et al.*, 1991). Others have noted that zebra mussel distribution is restricted by salinity (see Morton, 1979; Deaton and Greenberg, 1991). Studies demonstrating that zebra mussels are sensitive to ionic concentration have opened avenues for possible methods of controlling their populations. However, other studies have demonstrated that many fresh-water bivalves are killed by low concentrations of potassium (see Dietz and Byrne, 1990).

This report describes some of the characteristics of ionic and osmotic regulation in the zebra mussel and some conditions limiting their survival. Because of the potential similarities with indigenous bivalves, the basic biology of zebra mussels must be understood to be able to selectively control their numbers or distribution.

Materials and Methods

Animals

Zebra mussels (*Dreissena polymorpha*) were collected from Lake Erie near Cleveland, Ohio, and acclimated to artificial pondwater for a minimum of 5 days (Dietz,

Received 26 March 1992; accepted 20 July 1992.

* Address correspondence to: T. H. Dietz, Dept. Zoology and Physiology, Louisiana State University, Baton Rouge, LA 70803.

1979). Mussels were stored unfed in aerated pondwater at 22 ± 2°C before . Zebra mussels usually survived 6–8 weeks at 2 no mortality. For longer maintenance, mus held in pondwater at 16 ± 1°C and subseque sferred to room temperature for at least 24–48 h (usually 5 days) before use in experiments. We normally selected larger specimens for study (2–3.5 cm length) with a dry tissue mass of 15–40 mg.

To avoid contaminating local water systems with zebra mussels or veliger larvae, all acclimation water and animal containers were treated with 1% chlorine bleach for 24 h before being discarded. Mussels were dissected from the shell and dried at 95°C, and weighed before being discarded.

Blood analyses

Blood was collected by heart puncture (Fyhn and Costlow, 1975) and centrifuged 8000 g · min before use. We could routinely collect blood volume equal to 10% of the animal weight. However, the mantle cavity retains more pondwater than other freshwater bivalves and was more difficult to drain. Failure to drain the mantle cavity water in smaller zebra mussels will likely contaminate the blood sample if the syringe needle passes beyond the pericardial region. Total solute was determined by freezing-point depression. Sodium and potassium concentration were determined by flame emission, and calcium was assayed by atomic absorption spectroscopy. Chloride was determined by electrometric titration. The bicarbonate concentration in the blood was measured as CO_2 using a Hach Carle analytical gas chromatograph (Boutilier *et al.*, 1985). The bicarbonate concentrations were not routinely measured but were estimated from aliquots of blood that were equilibrated in air. From previous studies, 95–98% of the CO_2 would be in the form of bicarbonate over the pH range 7.5–8.1 (Byrne *et al.*, 1991).

Ion fluxes

Unidirectional ion influxes (J_i) were calculated by monitoring the disappearance of isotope from the bathing medium using previously described methods (Graves and Dietz, 1982). The animals were removed from their storage containers by cutting the byssal thread with scissors or scraping the thread from the container, not by pulling the thread from the animal. The mussels were rinsed in deionized water for about 30 min and transferred to a small container with the appropriate bathing solution. The animals ordinarily did not reattach with byssal threads during the brief period of study. Bath samples were collected at timed intervals and radioactivity determined by liquid scintillation counting. Net flux (J_n) was calculated from the change in ion concentration in the bathing medium. Unidirectional efflux (J_o) was calculated by difference ($J_o = J_i - J_n$).

The effects of exogenous biogenic amines on ion transport were determined by the addition of monoamines to bring the bathing medium concentration to 0.1 m*M*. Several biogenic amines (dopamine, epinephrine, norepinephrine, octopamine, and serotonin) were tested. All monoamine neurotransmitters were obtained from Sigma Chemical Company (St. Louis, MO).

Data are expressed as mean ± one standard error. The Student's *t*-test was used to compare means with equal variances, and differences were considered significant if $P < 0.05$. Time-course studies and the effects of ion concentrations on mussel blood, where variances were unequal, were analyzed by ANOVA and Scheffe's *F*-test on log transformed data.

Results

The blood composition of *D. polymorpha* acclimated to pondwater (PW) is shown in Table I. Zebra mussels were hyperionic to PW with sodium and chloride being the principal solutes. The measured solutes account for 88% of the total solute but there is an ion deficit ("other") of 5.1 m*M*. From another group of animals, we measured the total solute, all of the major ions and total blood CO_2. We noted that most of the missing solute (70%) was CO_2, probably in the form of HCO_3 at neutral to alkaline pH ("other" 3.7 ± 0.7 m*M*; CO_2 2.6 ± 0.4 m*M*; n = 6) (see Byrne *et al.*, 1991). Blood pH of 7.45 has been measured anaerobically from zebra mussels acclimated to pondwater at 23°C, thus 95% of the CO_2 would exist as HCO_3 (unpub. obs., R. Byrne, SUNY-Fredonia).

The blood solute in *D. polymorpha* is among the lowest recorded for freshwater mussels (see Dietz, 1979). To test their ability to osmoregulate, we challenged the mussels with NaCl added to pondwater and measured the blood ion concentrations after 96 h (Table II). There was a significant ($P < 0.01$) 11.8 m*M* rise in blood Na

Table I

Blood and pondwater ion composition in pondwater acclimated Dreissena polymorpha

Ion	Blood	Pondwater
Total Solute, mosm	36.0 ± 1.0	3.00
Na, m*M*	11.5 ± 1.1	0.70
Ca, m*M*	5.2 ± 0.4	0.40
K, m*M*	0.5 ± 0.0	0.05
Cl, m*M*	14.5 ± 0.5	1.35
Other (HCO_3), m*M*	5.1 ± 0.7	0.20

Mean ± SEM, n = 7. Total solute was rounded to 2 significant figures.

Table II

Blood ion concentration in Dreissena polymorpha *after 4 days acclimation to pondwater containing additional NaCl*

Added NaCl (m*M*)	n	mosm Total	Concentration (m*M*) Na	Ca	Cl	Other
0	15	35 ± 2[a]	10.9 ± 0.8[a]	5.1 ± 0.4	12.2 ± 0.9[a]	6.7 ± 0.9[a]
15	7	51 ± 1[b]	22.7 ± 1.7[b]	4.0 ± 0.5	15.6 ± 0.6[a]	8.6 ± 1.5[a,b]
30	9	76 ± 2[c]	32.3 ± 0.7[c]	5.2 ± 0.9	24.8 ± 1.3[b]	13.6 ± 1.6[b]
45	5	96 ± 3[d]	41.5 ± 1.7[d]	5.5 ± 1.0	29.6 ± 3.5[b]	19.4 ± 3.7[b]

Mean ± SEM. Total solute was rounded to 2 significant figures. [a,b,c,d] Values within a column with different letters are significantly different, $P < 0.05$ with Scheffe's F-test on log transformed data.

concentration at 15 m*M* NaCl accounting for 74% of the elevated total solute. The animals became isosmotic and isoionic for sodium in the 30 m*M* NaCl PW solution, but were hypoionic for Cl in 30 m*M* and 45 m*M* NaCl supplemented pondwater. Above 15 m*M* NaCl the rise in Na, Cl, and HCO_3 (but notably not Ca) contributed significantly to the rise in the total solute.

The addition of 15 m*M* NaCl to PW did not alter the survival of zebra mussels compared to PW acclimated controls. In contrast, some animals in 45 m*M* NaCl died 24 h after the acute transfer and some mortality occurred in animals placed in 30 m*M* NaCl by the second day. The majority of the zebra mussels were dead after 4 days in 45 m*M* NaCl, so we confined our acclimation studies to 4 days. The high standard error observed in the 45 m*M* NaCl group is an indication that the mussels were under physiological stress (Table II). We have not determined if step-wise acclimation favors survival above 45 m*M* NaCl, but acute transfer resulted in 100% mortality by 7 days (data not shown). The results shown in Table II were from animals that had been freshly collected. Repeating the experiment with animals that had been in the laboratory for over a month gave qualitatively similar results but survival time was reduced (data not shown).

The pronounced change in blood ion concentration when challenged with NaCl suggested these animals turn over salts at a rapid rate. This hypothesis was supported by the high ion fluxes measured in *D. polymorpha* (Table III). The PW acclimated animals were in a steady state for Na, Cl and Ca ($J_i = J_o$). The variability of ion fluxes was relatively high, in part, because of the small animal weight (less than 30–40 mg dry tissue) and the difficulty of sampling the bath without disturbing the mussels. Of the measured fluxes, only calcium efflux was significantly higher than Na efflux.

In a separate study, we demonstrated that Na uptake largely was independent of Cl by measuring the unidirectional fluxes from 0.5 m*M* Na_2SO_4 ($J_i = 14.0 \pm 2.7$, $J_o = 19.5 \pm 3.6$ μeq (g dry tissue · h)$^{-1}$, n = 5). In contrast, Cl uptake was significantly dependent on Na. When pondwater acclimated zebra mussels were transferred to 1 m*M* choline chloride, the unidirectional influx was significantly reduced ($J_i = 7.9 \pm 1.5$, $J_o = 49.6 \pm 5.9$ μeq (g dry tissue · h)$^{-1}$, n = 11). Although the Cl efflux was higher than reported in Table III, it was not higher than Cl efflux measured in animals collected at the same time and stored in PW for 2 months in the laboratory (PW controls $J_o = 32.7 \pm 7.5$ μeq (g dry tissue · h)$^{-1}$, n = 8).

The effect of the high transport rates on blood ion concentration in zebra mussels was evident from the time course of acclimation to 45 m*M* NaCl supplemented pond water (Table IV). Within 8 h, total blood solute was

Table III

Unidirectional ion fluxes in pondwater acclimated Dreissena polymorpha

Ion	n	Dry tissue mass, g	μeq (g dry tissue · h)$^{-1}$ Influx	Efflux	Net flux
Sodium	10	0.04 ± 0.00	22.34 ± 1.87	22.91 ± 1.99	−0.57 ± 1.16
Chloride	9	0.04 ± 0.00	24.82 ± 2.96	31.64 ± 5.31	−6.82 ± 4.96
Calcium	9	0.03 ± 0.00	29.04 ± 3.93	30.35 ± 2.37*	−1.31 ± 3.30

Mean ± SEM. * Significantly different than sodium efflux, $P < 0.05$.

Table IV

Change in blood ion [illegible] *in* Dreissena polymorpha *following acute transfer to pondwater containing 45 mM NaCl*

Hours		mosm Total	Concentration (m*M*) Na	Ca	Cl	K	Other
0	9	35 ± 1[a]	13.6 ± 0.2[a]	3.9 ± 0.3	15.0 ± 0.9[a]	0.6 ± 0.0	1.7 ± 0.6[a]
8	3	54 ± 6[b]	25.5 ± 5.0[b]	3.5 ± 0.8	23.3 ± 5.4[a,b]	0.5 ± 0.1	1.4 ± 3.8[a,b]
24	4	80 ± 6[c]	37.7 ± 3.6[c]	4.3 ± 1.1	28.9 ± 4.6[b]	0.4 ± 0.0	8.3 ± 1.8[b]
48	4	96 ± 3[c]	42.7 ± 2.3[c]	3.4 ± 0.7	36.6 ± 2.1[b]	0.3 ± 0.0	12.5 ± 4.2[b]
72	4	100 ± 2[c]	48.4 ± 2.2[d]	2.8 ± 0.3	41.7 ± 1.2[c]	0.3 ± 0.1	6.7 ± 0.7[b]

Mean ± SEM. Total solute was rounded to 2 significant figures. [a,b,c,d] Concentrations within a column having a different letter are significantly different, $P < 0.05$ by Scheffe's F-test on log transformed data.

elevated 54% due to the significant rise in Na that accounted for 62% of the solute gain and by 48 h the zebra mussels were isoionic for Na. The variability of blood ion concentration was high and the rest of the measured ions were not significantly different from controls until 24 h when Cl and HCO_3 became significantly elevated. Calcium and potassium did not change during the 3-day acclimation period. Although chloride was significantly less than Na ($P < 0.05$) on day 3, it was not significantly different from the 45 m*M* acclimation concentration. Elevation of blood bicarbonate concentration ("other") compensated for the Cl anion deficit. Because of the differential time course of changes in the measured blood ions, there was no evidence that the loss of body water due to the acute transfer to the hyperosmotic 45 m*M* NaCl was a predominant factor, although the potential for some water loss does exist.

In previous studies we have shown that the addition of serotonin to the bathing medium stimulated Na transport in other freshwater mussels (Dietz *et al.*, 1982). Serotonin (0.1 m*M*) also significantly elevated Na influx and net sodium flux in zebra mussels (Table V). Most animals displayed considerable motor activity, valve gaping, frequent valve closures, and extension of the foot. These behavioral responses to serotonin are similar in pattern to the response shown by unionids exposed to exogenous serotonin. The hyperextension of the foot and valve closures in *D. polymorpha* frequently caused an elevation of the bath ion concentration due to bleeding. In addition, some animals held in the laboratory for over a month failed to open during the flux study as indicated by fluxes near zero, and were excluded as outliers (fluxes exceeding 3 standard errors of the mean).

Because of the rapid ion turnover, and to prevent significant isotope backflux, unidirectional fluxes were measured over a short time of 1–2 h. We also extended the time of serotonin treatment to 3 h and measured the net Na and Cl fluxes in zebra mussels in PW (Table VI). Serotonin significantly reduced the spontaneous loss of Na experienced by this group of mussels but did not stimulate a net uptake, yet the same mussels experienced a net uptake of Cl. We also exposed zebra mussels to 0.1 m*M* concentrations of several other monoamine neurotransmitters (dopamine, epinephrine, norepinephrine, and octopamine) and measured the net flux of Na and Cl but we saw no significant change relative to control animals (data not shown).

Previous studies have indicated that freshwater mussels differ in the sensitivity of Na transport to amiloride inhibition (Dietz, 1978; McCorkle and Dietz, 1980). The

Table V

*Effects of serotonin (0.1 m*M*) added to pondwater on unidirectional sodium fluxes in pondwater acclimated* Dreissena polymorpha

Treatment	n	μeq (g dry tissue · h)$^{-1}$ Influx	Efflux	Net flux
Control	21	29.08 ± 2.15	35.48 ± 2.78	−6.41 ± 1.99
Serotonin	23	40.33 ± 3.83*	31.82 ± 4.82	8.44 ± 4.52*

Mean ± SEM. * Significantly different from controls, $P < 0.02$.

Table VI

*Effect of 0.1 m*M *serotonin in the bathing solution on net ion fluxes in pondwater acclimated* Dreissena polymorpha

Ion	Net flux μeq (g dry tissue · h)$^{-1}$ Control	Serotonin
Sodium	−7.12 ± 1.08 (19)	−1.93 ± 1.03 (20)**
Chloride	−1.88 ± 2.05 (19)	10.38 ± 4.93 (19)*

Mean ± SEM with number of animals in parenthesis. Significantly different from controls, *$P < 0.05$, **$P < 0.01$.

unionid bivalve sodium transport system is inhibited by amiloride. In contrast, corbiculid Na transport is not. Sodium transport in *D. polymorpha* was not inhibited by 0.5 m*M* amiloride (Table VII). Some mussels were slow to open their valves and initiate siphoning and this raised the variability of the measured fluxes. However, the amiloride-treated mussels that were observed to be open and siphoning had transport rates that equalled or exceeded the controls.

Table VII

Effects of amiloride (0.5 mM) addition to pondwater on unidirectional sodium fluxes in pondwater acclimated Dreissena polymorpha

	μeq (g dry tissue · h)$^{-1}$		
Treatment	Influx	Efflux	Net flux
Control	22.22 ± 4.24	25.04 ± 2.34	−2.92 ± 4.12
Amiloride	19.00 ± 5.96	30.34 ± 7.33	−11.34 ± 2.29

Mean ± SEM, n = 8.

Discussion

Dreissena polymorpha exhibited several characteristics that were significantly different from the other freshwater bivalves that have been studied. The Cl transport rate was higher than observed in other freshwater mussels and the rate of Na transport is equaled only by the fingernail clam *Musculium* (= *Sphaerium*) *transversum* (Dietz, 1979). Chloride transport was double the transport rate of fingernail clams and 10–20× that of unionids. This is the first report in a freshwater mussel of chloride transport being dependent on Na and Cl uptake being stimulated by exogenous serotonin. Preliminary data indicate that both Na and Cl transport also may be stimulated by serotonin in corbiculids (unpub. obs.). Serotonin has been reported to stimulate only sodium transport in unionid bivalves (Dietz *et al.*, 1982).

The blood of PW acclimated zebra mussels has significantly less total solute than other mussels and was composed primarily of NaCl with only about 2–4 m*M* HCO_3. Organic solutes contribute little to the total solute of freshwater mussels (Hanson and Dietz, 1976). The ionic composition in zebra mussel blood is similar to a Canadian unionid, *Anodonta grandis simpsoniana*, but differs from most other unionids in that they contain a combination of Na, Cl, and HCO_3 (Dietz, 1979; Byrne and McMahon, 1991). Corbiculid blood composition is largely NaCl at about twice the concentration found in *D. polymorpha*. *Corbicula fluminea* also has twice the calcium concentration as the zebra mussel (Dietz, 1979; Byrne *et al.*, 1989).

Acute transfer of zebra mussels to 45 m*M* NaCl resulted in an elevated blood NaCl concentration within 8 h, but 48 h was required for acclimation. *Corbicula fluminea* rapidly adjust blood total solutes within 12 h after being transferred from freshwater to 5‰ (172 mosm), but volume regulation is incomplete even after 120 h (Gainey, 1978). Zebra mussels became isosmotic and suffered considerable mortality when acutely transferred to NaCl solutions above 30 m*M*. In contrast, unionids become isosmotic above 50 m*M* NaCl and survive 75 m*M* NaCl and corbiculids can tolerate even higher solute concentrations (Dietz and Branton, 1975; Gainey, 1978).

Although *D. polymorpha* displayed high ion turnover rates, they were able to maintain a steady state in dilute pondwater. However, storage of zebra mussels in PW, without food, beyond 2 months led to an increase in mortality. Coincidentally, mussels maintained in the laboratory tended to lose solutes and ion fluxes became more variable, but this phenomenon has not been studied systematically.

Sodium transport in zebra mussels was the same in solutions of either NaCl or Na_2SO_4 indicating an independence from chloride transport. Unionid and corbiculid Na transport are also independent of Cl, using instead an apparent Na/H exchange component (Dietz, 1978; McCorkle and Dietz, 1980). We have not examined the exchange mechanism in zebra mussels. Recent studies have indicated that Na flux across amphibian skin is largely regulated by availability of intracellular protons rather than a directly coupled exchange mechanism (Harvey and Ehrenfeld, 1988; Kirschner, 1988).

This is the first evidence that Cl transport is dependent on Na in a freshwater mussel. These data indicate that there may be a NaCl co-transport system in *D. polymorpha*. This inference was further supported by the stimulation of both Na and Cl uptake by exogenous serotonin. Because we have not measured transepithelial electrical characteristics in zebra mussels, it is premature to speculate on primary or secondary transport mechanisms.

Both *Dreissena* and *Corbicula* have elevated Na transport rates compared to unionids. Zebra mussels share with *Corbicula* the unusual property that sodium transport is insensitive to amiloride (McCorkle and Dietz, 1980). Since *Corbicula* displays a substantial Na/Na exchange component not found in unionids, it is tempting to speculate that zebra mussels also may have a large Na/Na exchange mechanism contributing to the high isotope turnover, but this has not been measured. It is possible that these Na/Na exchange pathways present in some freshwater bivalves are insensitive to amiloride inhibition.

Alternatively, the large Na exchange diffusion component may be a characteristic of recent brackish-water ancestry of *Corbicula* and *Dreissena*. Although they have invaded freshwater independently, both genera contain species that inhabit brackish-water (for review see

McMahon, 1983; Mackie *et al.*, 1989; Deaton and Greenberg, 1991).

Freshwater animals are capable hyper-regulators and usually are able to tolerate hyperosmotic conditions that would more than double their normal total solute concentration (Deaton and Greenberg, 1991; Kirschner, 1991). *Dreissena* is uniquely stenohaline in showing elevated mortality at low solute concentrations (30 m*M* NaCl), and being incapable of surviving an acute transfer to 45 m*M* NaCl beyond a week. We have noted previously that *Corbicula* subjected to a loss of body water will shift Na and Cl out of the blood compartment presumably into the intracellular fluid (Byrne *et al.*, 1989). It is possible that the changes in intracellular ionic composition due to the gain in Na and Cl may be an attempt to preserve cell volume. Such a mechanism would have major limitations. Either the addition of NaCl to the cells or the resultant imbalance in the Na:K ratio could interfere with electrically excitable tissue (nerve, skeletal, cardiac muscle) and may be a critical factor limiting survival of *Dreissena polymorpha*.

Alternatively, Deaton and Greenberg (1991) have noted a correlation between the osmoregulatory capability of bivalves and their ability to mobilize calcium. They suggested that the mode of action of elevated calcium is to regulate membrane permeability. *Dreissena* blood calcium concentration was similar to other freshwater mussels but it remained constant during periods of hyperosmotic stress. Perhaps the critical feature leading to their stenohaline characteristic is their inability to add Ca as an osmolyte to the blood when under stress.

The variability in ion transport and the magnitude of ion losses in some *Dreissena polymorpha* acclimated to pondwater exceed the range found in other freshwater bivalves. Freshwater mussels are normally nocturnally active and tend to gain salts at night and lose ions during the day (Graves and Dietz, 1980; McCorkle-Shirley, 1982). Perhaps *Dreissena* has more pronounced diurnal rhythms of ion transport. Zebra mussels also form byssal threads and the secreted material may be in ionic form contributing to some of the apparent salt losses. Alternatively, *Dreissena* may be more sensitive to starvation conditions imposed by laboratory storage. Further studies are needed to resolve these issues.

The basis for zebra mussels' intolerance of salt loading is of fundamental interest. There have been few studies of salt tolerance in freshwater mussels and these studies provide little insight with regard to the physiological mechanism (Deaton and Greenberg, 1991). From an environmentally sound perspective, an ionic challenge is likely to be too nonspecific and detrimental to all freshwater bivalves to be a suitable method for general control of zebra mussel populations. However, KCl or NaCl may be useful in controlling zebra mussels in a specific case such as freshwater ballast in trans-oceanic vessels. The addition of 5–10% seawater, in this example, would be lethal to adult zebra mussels.

Acknowledgments

We thank Drs. Robert McMahon and Roger Byrne for providing the zebra mussels collected from Lake Erie and for the many suggestions and comments. Julie Cherry and Diondi Lessard provided technical assistance. This work was supported, in part, by the LSU Center for Energy Studies grant 91-01-11 and NSF grant DCB90-17461.

Literature Cited

Boutilier, R. G., G. K. Iwama, T. A. Heming, and D. J. Randall. 1985. The apparent pK of carbonic acid in rainbow trout blood plasma between 5 and 15°C. *Resp. Physiol.* **61:** 237–254.

Byrne, R. A., and B. R. McMahon. 1991. Acid-base and ionic regulation, during and following emersion, in the freshwater bivalve, *Anodonta grandis simpsoniana* (Bivalvia: Unionidae). *Biol. Bull.* **181:** 289–297.

Byrne, R. A., R. F. McMahon, and T. H. Dietz. 1989. The effects of aerial exposure and subsequent reimmersion on hemolymph osmolality, ion composition and ion flux in the freshwater bivalve, *Corbicula fluminea*. *Physiol. Zool.* **62:** 1187–1202.

Byrne, R. A., B. N. Shipman, N. J. Smatresk, T. H. Dietz, and R. F. McMahon. 1991. Acid-base balance during prolonged emergence in the freshwater bivalve, *Corbicula fluminea*. *Physiol. Zool.* **64:** 748–766.

Deaton, L. E., and M. J. Greenberg. 1991. The adaptation of bivalve molluscs to oligohaline and freshwaters: Phylogenetic and physiological aspects. *Malacol. Rev.* **24:** 1–18.

Dietz, T. H. 1978. Sodium transport in the freshwater mussel, *Carunculina texasensis* (Lea). *Am. J. Physiol.* **235:** R35–R40.

Dietz, T. H. 1979. Uptake of sodium and chloride by freshwater mussels. *Can. J. Zool.* **57:** 156–160.

Dietz, T. H., and W. D. Branton. 1975. Ionic regulation in the freshwater mussel, *Ligumia subrostrata* (Say). *J. Comp. Physiol.* **104:** 19–26.

Dietz, T. H., and R. A. Byrne. 1990. Potassium and rubidium uptake in freshwater mussels. *J. Exp. Biol.* **150:** 395–405.

Dietz, T. H., J. I. Scheide, and D. G. Saintsing. 1982. Monoamine transmitters and cAMP stimulation of Na transport in freshwater mussels. *Can. J. Zool.* **60:** 1408–1411.

Fisher, S. W., P. Stromberg, K. A. Bruner, and L. D. Boulet. 1991. Molluscicidal activity of potassium to the zebra mussel, *Dreissena polymorphia*: Toxicity and mode of action. *Aquatic Toxicol.* **20:** 219–234.

Fyhn, H. J., and J. D. Costlow. 1975. Anaerobic sampling of body fluids in bivalve molluscs. *Comp. Biochem. Physiol.* **52A:** 265–268.

Gainey, L. F. 1978. The response of the Corbiculidae (Mollusca: Bivalvia) to osmotic stress: The organismal response. *Physiol. Zool.* **51:** 68–78.

Graves, S. Y., and T. H. Dietz. 1980. Diurnal rhythms of sodium transport in the freshwater mussel. *Can. J. Zool.* **58:** 1626–1630.

Graves, S. Y., and T. H. Dietz. 1982. Cyclic AMP stimulation and prostaglandin inhibition of Na transport in freshwater mussels. *Comp. Biochem. Physiol.* **71A:** 65–70.

Hanson, J. A., and T. H. Dietz. 1976. The role of free amino acids in cellular osmoregulation in the freshwater bivalve, *Ligumia subrostrata* (Say). *Can. J. Zool.* **54:** 1927–1931.

Harvey, B. J., and J. Ehrenfeld. 1988. Role of Na^+/H^+ exchange in the control of intracellular pH and cell membrane conductances in frog skin epithelium. *J. Gen. Physiol.* **92:** 793–810.

Kirschner, L. B. 1988. Basis for apparent saturation kinetics of Na^+ influx in freshwater hyperregulators. *Am. J. Physiol.* **254:** R984–R988.

Kirschner, L. B. 1991. Water and ions. Pp. 13–107 in *Environmental and Metabolic Animal Physiology.* C. L. Prosser ed. Wiley-Liss, New York.

Mackie, G. L., W. N. Gibbons, B. W. Muncaster, and I. M. Gray. 1989. The zebra mussel, *Dreissena polymorpha.* A synthesis of European experiences and a preview for North America. Pp. 1–76 in *Water Resources Branch Great Lakes,* Ontario Ministry of the Environment, Ontario.

McCorkle, S., and T. H. Dietz. 1980. Sodium transport in the freshwater Asiatic clam, *Corbicula fluminea. Biol. Bull.* **159:** 325–336.

McCorkle-Shirley, S. 1982. Effects of photoperiod on sodium flux in *Corbicula fluminea* (Mollusca: Bivalvia). *Comp. Biochem. Physiol.* **71A:** 325–327.

McMahon, R. F. 1983. Ecology of an invasive pest bivalve, *Corbicula.* Pp. 505–561 in *The Mollusca, Vol. 6, Ecology,* W. D. Russell-Hunter, ed. Academic Press, San Diego.

Morton, B. 1979. Freshwater fouling bivalves. Pp. 1–14 in *Proceedings, First International Corbicula Symposium,* J. C. Britton, ed. Texas Christian University Research Foundation, Fort Worth.

Porcella, D. B. 1981. Bioassay methods for aquatic organisms. Pp. 615–649 in *Standard Methods for Examination of Water and Wastewater,* A. E. Greenberg, J. J. Conners, and D. Jenkins, eds. 15th edition. American Public Health Association, Washington, DC.

Stanczykowska, A. 1977. Ecology of *Dreissena polymorpha* (Pall). (Bivalvia) in lakes. *Pol. Arch. Hydrobiol.* **24:** 461–530.

Reference: *Biol. Bull.* **183**: 304–326. (October, 1992)

Morphology of the Brain of Crayfish, Crabs, and Spiny Lobsters: A Common Nomenclature for Homologous Structures

DAVID SANDEMAN[1], RENATE SANDEMAN[1], CHARLES DERBY[2], AND MANFRED SCHMIDT[3,*]

[1]*School of Biological Science, University of New South Wales, Sydney, NSW 2033, Australia,* [2]*Department of Biology, Georgia State University, Atlanta, Georgia, and* [3]*Whitney Laboratory, University of Florida, St. Augustine, Florida 32086*

Abstract. The morphologies of the cerebral ganglia (brains) of three infraorders of the decapod crustaceans (Astacura-crayfish; Brachyura-crabs; Palinura-spiny lobsters) are described. A common nomenclature is proposed for homologous nerve roots, brain regions, tracts, commissures, neuropils, and cell body clusters.

Introduction

Decapod crustaceans have been favored animals among neurobiologists for many years because they are comparatively large arthropods, have well-organized nervous systems and interesting behavior patterns ranging from reflexes to complex social interactions. Several fixed action patterns concerned with protection or escape are mediated by particularly well-defined sensory inputs and large neuromuscular systems, and, much research has been focused on these. The crayfish ventral nerve cord survives well in isolation and has also been exploited in the study of many aspects of the neurophysiology of the ventral ganglia (*e.g.*, Hoyle, 1977; Atwood and Sandeman, 1982; Wine and Krasne, 1982; Wiese *et al.*, 1990).

There is a growing interest, however, in the cerebral ganglia (brains) of the crustaceans. Initial studies on the brains of the spiny lobsters by Maynard in the 1960's (Maynard, 1962; Maynard, 1966; Maynard, 1969; Maynard and Sallee, 1970) came to an untimely end, but the description of the impulse traffic between the eye and the brain was continued by Wiersma and his colleagues (Wiersma *et al.*, 1982; Glantz and Pfeiffer-Linn, 1990) and the endocrine systems in the eyestalks have been particularly well investigated (Cooke and Sullivan, 1982; Arechiga *et al.*, 1990). The development of a semi-isolated preparation of the crab and then crayfish brain allowed the investigation of eye withdrawal, statocyst driven reflexes, chemoreceptive responses, and antenna II reflexes (Sandeman, 1969, 1971, 1989; Sandeman and Okajima, 1972; Silvey and Sandeman, 1976; Ache and Sandeman, 1980; Sandeman and Wilkens, 1982). Recently there has been a renewed interest in the crustacean cerebral ganglion, stimulated by more detailed anatomical studies and the description of a number of neuronal systems revealed by antibodies raised against various neurotransmitters and neuromodulators (see Wiese *et al.*, 1990).

The entry of researchers from many different fields into crustacean brain research has been accompanied by a certain confusion about the names of different parts of the brain. This confusion is probably the result of a large literature on the brains of the crustaceans, not all of which belonged to the decapods. Within the decapods, problems have been caused by various interpretations of the works of previous authors, and by the earlier authors themselves changing their minds about what to call a particular neuropil (*e.g.*, Hanström, 1924, 1925; 1947). Many recent descriptions of the brains of various decapods have perpetuated the errors or misconceptions of the earlier authors. Progress toward a standard nomenclature for the component neuropils, tracts, and cell bodies of the decapods was made by Tsvileneva and Titova (1985) who adopted the original nomenclature of Helm (1928) in their description of the brains of the crayfish and crab.

Received 14 February 1992; accepted 22 July 1992.

* Present address: Institut für Biologie, T. U. Berlin, 1000 Berlin 10, Germany.

The larger decapod crustaceans have life spans of many years and a brain that, in size and complexity, lies somewhere between the octopus and insects. Indications are that the brain and behavior of the crustaceans will attract considerable attention in the future (Wiese *et al.*, 1990). It is therefore timely that a nomenclature for brain morphology of the decapods be compiled for the commonly used species. In this report we suggest names for homologous components (*i.e.*, nerve roots, neuropils, tracts, and groups of cell bodies) that can be recognized in the brains of three infraorders of the decapod Crustacea: the Astacura (clawed lobsters and crayfish), Brachyura (crabs), and Palinura (spiny lobsters). We have chosen representatives from these infraorders because preparations already exist for the physiological investigation of the brains of these animals, and further studies will therefore most likely be done on them.

In selecting names for the various components we have sought, where possible, to keep terms that have been commonly used and to prefer names that do not imply function unless this has been clearly established. We have tried to remove ambiguities and show that the same components can be identified in the three different infraorders. We have included an Appendix which lists synonyms that have been used by other authors for the neuropil areas and cell body clusters we describe. Earlier authors have used the terms "lobe", "body", and "bridge" for several particularly clearly delineated neuropils. Although we prefer the term "neuropil," we have retained these terms as they are well entrenched in the literature on comparative studies of arthropod brains. We do not pretend that our system of nomenclature will apply to all members of the Phylum Crustacea, given their diversity and the very different morphology of the cerebral ganglia of some forms (Elofsson and Hessler, 1990).

Material and Methods

Brain morphologies of the three different types of decapod were compiled from serial sections of wax embedded and silver impregnated, or plastic embedded and osmium ethyl gallate stained material. *Cherax destructor* has been taken as the representative of the Astacura, *Scylla serrata* of the Brachyura, and *Jasus novaehollandiae* and *Panulirus argus* of the Palinura.

Results

Head Appendages

Several terms are used for the two pairs of antennae. We believe the most unambiguous to be antenna I and antenna II. Antenna I is equivalent to the antennule or first antenna, and antenna II to antenna or second antenna, terms that we also use.

Antenna I (ANT I): Basal segments contain the statocysts and muscles, and bear two sensory flagella both of which carry mechanoreceptive and chemoreceptive sensilla (Derby, 1982; Derby and Ache, 1984). The lateral flagellum bears special olfactory sensilla; the aesthetasc sensilla (Grünert and Ache, 1988).

Antenna II (ANT II): Basal segments contain muscles and bear a scale-like structure and a single long sensory flagellum carrying both mechanoreceptive and chemoreceptive sensilla (Tazaki and Shigenaga, 1974; Derby, 1982).

Nerve Roots

We define the nerve roots as those bundles of axons that extend from the brain or other central nervous ganglia and contain either sensory afferents, motor efferents, or both, but not interneurons. The tract of axons between the brain and the optic ganglia in the eyestalk is, therefore, not a nerve root because it forms a connection between central ganglia.

Anterior median nerve (AMNv): This short nerve bundle projects from the anterior surface of the brain and supplies the muscles of the median segment of the eyestalk. There is no information on afferents in this nerve bundle.

Oculomotor nerve (OMNv): The oculomotor nerve carries motor neurons to the muscles of the eyestalk. It also contains primary afferent axons from mechanoreceptors in this area. Motor neurons to some eye muscles have been found in the lateral protocerebral tract in crabs (Sandeman, 1964) and crayfish (Mellon, 1977).

Antenna I nerve (A_INv): Motor neurons to the muscles in the basal segments of antenna I are contained in this nerve together with the primary afferents from the receptors on the flagella and basal segments. To the best of our knowledge, all axons from the olfactory sensilla (aesthetascs) diverge from the main bundle and project exclusively to the olfactory lobe (see below) (Sandeman and Denburg, 1976; Mellon and Munger, 1990; Schmidt and Ache, 1990; Schmidt and Ache, 1992), non-aesthetasc chemosensory and mechanosensory afferents project to the lateral and median antenna I neuropil (Roye, 1986; Schmidt and Ache, 1990; Roye and Bashor, 1991; Schmidt *et al.*, 1992).

Antenna II nerve (A_{II}Nv): Motor neurons to the muscles in the basal segments of antenna II run in this nerve together with primary afferents from mechanoreceptors, proprioceptors, and chemoreceptors on the flagellum and the basal segments. All axons terminate in the same neuropil (see below). A number of subdivisions of the antenna II nerve for crayfish have been described (Habig and Taylor, 1982; Sandeman and Wilkens, 1982; Tautz and Müller-Tautz, 1983).

Tegumentary nerve (TNv): This is a purely sensory nerve carrying primary afferents from mechanoreceptors

and other sensilla [illegible] dorsal carapace (Kinnamon, 1979).

Posterior [illegible] *e* (PMNv): Projecting from the posterior o[illegible] [illegible]e median nerve carries interneurons be[illegible] [illegible]an and the oesophageal ganglion.

Brain Regions and Neuropils (Fig. 1)

There are three main divisions of the brain, protocerebrum, deutocerebrum, and tritocerebrum, reflecting the three ganglia that have fused to form it. The neuropils of the optic ganglia and lateral protocerebrum are located in the eyestalks of crayfish, crabs, and lobsters. The median protocerebrum and tritocerebrum are located medially.

Protocerebrum

The protocerebrum can be conveniently subdivided into three parts, the optic ganglia, the lateral protocerebrum and the median protocerebrum.

OPTIC GANGLIA. Contains three neuropils that are probably devoted to processing the information received by the photoreceptors of the retina.

Lamina (L): The first neuropil behind the retina, the lamina is geometrically structured.

External medulla (EM): Lying directly behind the lamina, the external medulla is similarly geometrically structured, but is also transversely layered.

Internal medulla (IM): The most proximal of the three neuropils in the optic ganglia, this too is geometrically organized and has clearly defined transverse bands.

LATERAL PROTOCEREBRUM. Contains two neuropils. In crayfish, crabs, and spiny lobsters the neuropils of the lateral protocerebrum lie in the distal segment of the eyestalk, directly proximal to the optic ganglia. In some anomurans the lateral protocerebrum is incorporated into the centrally located median protocerebrum.

Terminal medulla (TM): This complex neuropil is not geometrically organized but has a number of subdivisions (Blaustein *et al.*, 1988). It contains neurosecretory cells of the X-organ and its associated neurohaemal organ, the sinus gland, which together constitute one of the most important neuroendocrine systems in the crustaceans.

Hemiellipsoid body (HN): Positioned anterior to the terminal medulla, this neuropil sometimes has a glomerular structure, and is large and layered in some anomurans, a characteristic which led Hanström (1925) to postulate that it is homologous with the corpora pedunculata of the insects.

MEDIAN PROTOCEREBRUM. Forms the anterior part of the medially situated neuropils of the brain. It contains two paired medial and two unpaired median neuropils. (Throughout this paper we use the term *median* to describe a structure that straddles the midline, and *medial* to describe paired structures near or at the midline. Thus

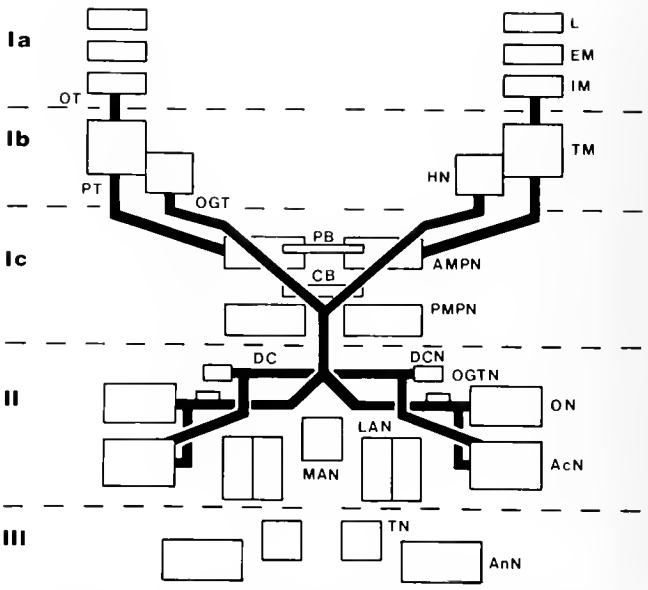

Figure 1. Brain regions and neuropils that can be identified in all three brain types and that are considered to be homologous. Heavy black bars represent the tracts and commissures linking the neuropil areas, shown as boxes. The roman numerals represent the divisions of the brain according to the way we have arranged them in the text of the paper: *i.e.*, I = protocerebrum (with three subsections); II = deutocerebrum; III = tritocerebrum. A key to the abbreviations is provided in Appendix 2.

the *median* protocerebrum is made up of two anterior *medial* protocerebral neuropils and two posterior *medial* protocerebral neuropils). While clearly discernible in some section planes, these four neuropils tend to fuse with one another dorsally and ventrally, making the distinction between them somewhat arbitrary. No primary afferent projections to the neuropils of the median protocerebrum have been reported.

Anterior medial protocerebral neuropil (AMPN): These two neuropils lie on each side of the midline at the anterior of the median protocerebrum.

Posterior medial protocerebral neuropil (PMPN): These two neuropils lie on each side of the midline, directly posterior to the anterior medial protocerebral neuropils.

Protocerebral bridge (PB): Embedded in the anterior edge of the anterior medial protocerebral neuropil, this V-shaped neuropil has a characteristic form containing many large through-running axons with fine side branches. In the crayfish *Cherax*, extra-retinal photoreceptors lying in the anterior of the brain terminate in the neuropil of the protocerebral bridge (Sandeman *et al.*, 1990).

Central body (CB): A cigar-shaped neuropil lying across the brain and dividing the anterior from the posterior medial protocerebral neuropils. The central body is a well-defined area of neuropil that immunocytochemical studies have shown to contain a wide variety of different neuroactive substances (Schürmann *et al.*, 1991).

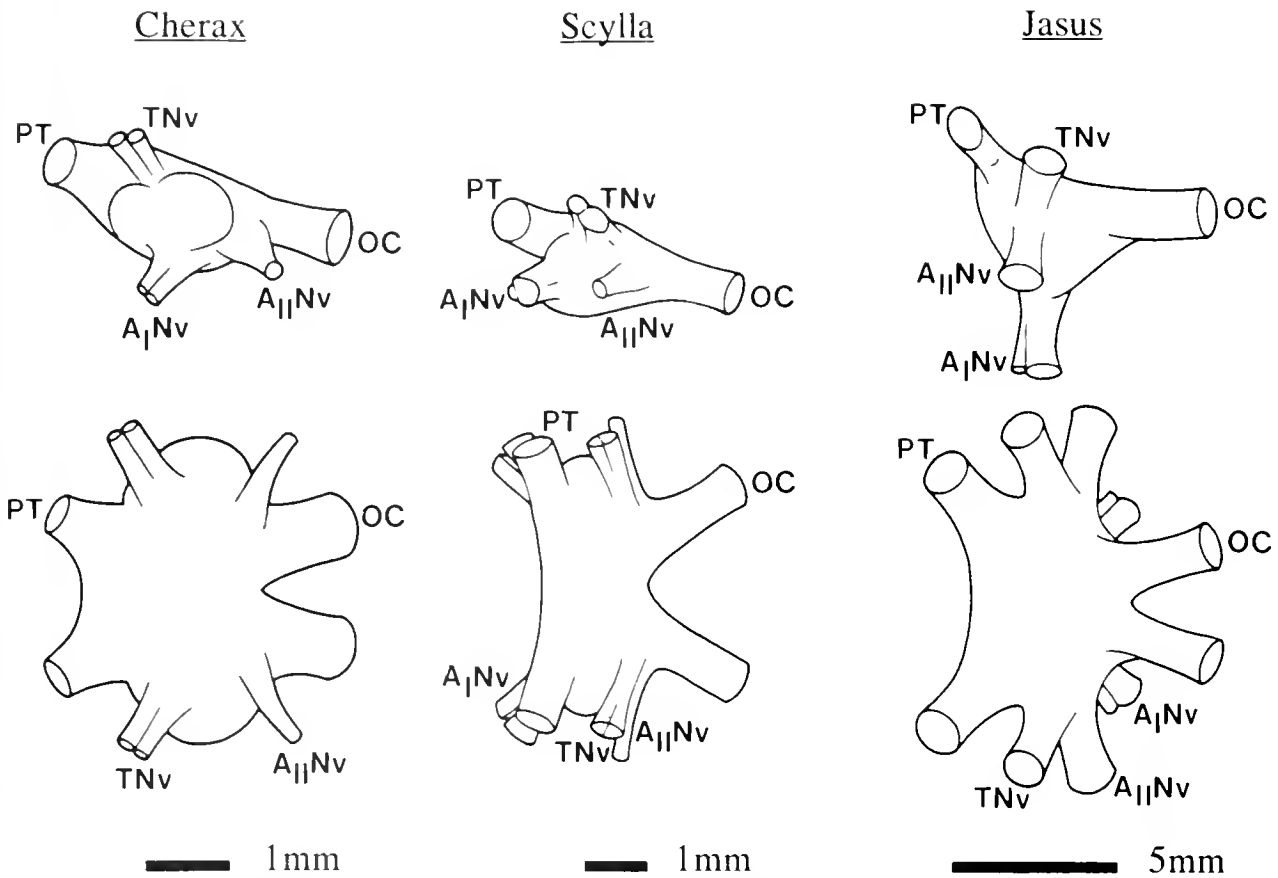

Figure 2. Camera lucida-traced outlines of the brains of *Cherax*, *Scylla* and *Jasus* seen from the side and from above. Anterior is to the left of the page. In the crayfish and crab, the oesophageal connectives and the protocerebral tract lie in nearly the same horizontal plane. In the spiny lobster the protocerebral tracts extend upwards, almost at right angles to the plane of the oesophageal connectives. Antenna 1 and antenna 2 nerve roots of the crayfish and the crab point anteriorly and ventrally, whereas those of the spiny lobster project almost directly ventrally. These differences are reflected in the organization of the neuropils within the brains of the three animals.

Deutocerebrum

Olfactory lobe (ON): The olfactory lobes are clearly delineated spheres lying on each side of the brain. They contain cone-shaped areas of densely packed synaptic fields—the olfactory glomeruli—arranged with their apices pointing to the center of the sphere. The olfactory lobes receive the primary afferent endings of the chemoreceptors on antenna I (Sandeman and Denburg, 1976; Mellon and Munger, 1990; Schmidt and Ache, 1990; Schmidt and Ache, 1992).

Lateral antenna I neuropil (LAN): Consisting of two clear subdivisions when viewed in frontal sections, the lateral antenna I neuropil on each side of the brain receives afferents from mechanoreceptors, statocysts, and non-aesthetasc chemoreceptors from the ipsilateral antenna I (Sandeman and Denburg, 1976; Yoshino *et al.*, 1983; Roye, 1986; Blaustein *et al.*, 1988; Schmidt and Ache, 1990). It also contains the synaptic fields of the motor neurons that control the movements of the ipsilateral antenna I (Roye and Bashor, 1991; Schmidt *et al.*, 1991). The lateral antenna I neuropils have sometimes been referred to as "parolfactory lobes" (see Appendix 1).

Median antenna I neuropil (MAN): A relatively diffuse block of neuropil that lies across the brain between or dorso-anterior to the lateral antenna I neuropils. The median antenna I neuropil fuses anteriorly with the posterior medial protocerebral neuropils, and posteriorly with the tegumentary and antenna II neuropils. Little is known about the projections to this area of the brain. Branches of descending interneurons related to statocyst inputs extend into the medial antenna I neuropil in both crabs (Fraser, 1974) and crayfish (Yoshino *et al.*, 1983). In the blue crab, mechanosensory afferents from sensilla at the base of antenna I project to the medial antenna I neuropil, where antenna I motorneurons also branch (Roye, 1986; Roye and Bashor, 1991). Primary afferents from the base

of the antennule have been observed that project to the medial antenna[1] neuropil in spiny lobsters (Schmidt, unpub. obs.)

Accessory lobe (AcN): The accessory lobes lie directly posterior to the olfactory lobes. They are larger than the accessory lobes in the crayfish, about the same size as the olfactory lobes in spiny lobsters, and very much smaller than the olfactory lobes in crabs. They contain large numbers of small round glomeruli. In the spiny lobster, the accessory lobes are subdivided into medial, central, and lateral layers containing glomeruli of different sizes (Maynard, 1966, 1971; Blaustein *et al.*, 1988). The accessory lobes do not appear to receive a direct input from primary afferent axons, nor have motor efferents been found that have their synaptic fields there.

Deutocerebral commissure neuropil (DCN): Small round ventrally situated neuropils characterized by receiving strong projections from the deutocerebral commissure and from the medial protocerebrum. Clearly defined in crayfish and spiny lobsters with large deutocerebral commissures, these neuropils have not yet been identified in the crab brain. No primary afferent inputs are known that project to the deutocerebral commissure neuropils, nor has the nature of the interneuronal input been defined. The subject of much confusion, these neuropils have been called "parolfactory lobes" in several recent publications (Tsvileneva and Titova, 1985; Sandeman *et al.*, 1988; Blaustein *et al.*, 1988) and are renamed here in accordance with our policy to avoid functional names where we can. See Appendix 1 for synonyms.

Olfactory globular tract neuropil (OGTN): First pictured in crayfish by Helm (1928) and labelled "z", attention was again drawn to this neuropil by Tsvileneva and Titova (1985). It appears to lie within, or very closely associated with, the olfactory globular tract at a point just before the tract reaches the olfactory and, when present, accessory lobes. Present also in crabs, this neuropil has assumed a greater significance since the branches of large serotonin immunoreactive neurons, associated with the accessory and olfactory lobes, have been found in this neuropil (Sandeman and Sandeman, 1987; Beltz *et al.*, 1990; Schmidt *et al.*, 1991). Connections between the olfactory globular tract neuropil and other parts of the nervous system have yet to be determined.

Tritocerebrum

Antenna II neuropil (AnN): These cylindrical neuropils are posterior to the accessory lobes in crayfish, posterior to the olfactory lobes in crabs, and postero-dorsal to the olfactory lobes in the spiny lobster. They are tapered laterally and often have a geometrically arranged pattern of axons running antero-posteriorly across them. The primary afferents from antenna II end in the antenna II neuropil which also contain the synaptic fields of the motor neurons that control the movements of antenna II (Sandeman and Wilkens, 1982; Habig and Taylor, 1982; Tautz and Müller-Tautz, 1983).

Tegumentary neuropil (TN): Each tegumentary nerve, carrying the afferent input from the dorsal carapace (Sandeman, 1969; Kinnamon, 1979), ends in a tight knot of neuropil dorsal and somewhat anterior to the medial margin of the antenna II neuropil.

Tracts and Commissures (Fig. 1)

Many tracts in the brains of the crustaceans link areas of neuropils, and a number of axon bundles cross the brain. We have restricted ourselves here to the largest and best known that can be unequivocally identified, when present, in the three infraorders.

Optic tract (OT): The optic tract links the last of the optic ganglia (internal medulla) to the lateral protocerebrum. Very short in the astacurans, brachyurans, and palinurans, it is often confused with the much longer protocerebral tract that links the terminal medulla to the median protocerebrum in these groups.

Protocerebral tract (PT): Axons in this tract link the terminal medulla and hemiellipsoid body with the anterior medial protocerebral neuropil and other areas of the brain. Sometimes inaccurately referred to as the "optic nerve" or "optic tract" (see Appendix 1).

Olfactory globular tract (OGT): The olfactory globular tract links the hemiellipsoid bodies and terminal medullae with the olfactory and accessory lobes on both sides of the brain by crossing the brain just dorsal to the central body neuropil. It typically contains very large numbers of small diameter axons (1 μm and less).

Deutocerebral commissure (DC): This commissure is large in crayfish and spiny lobsters, but cannot be identified with certainty in crabs. In crayfish it contains two populations of axon diameters that cross the brain between the two accessory lobes.

Oesophageal connectives (OC): These two large tracts link the brain with the suboesophageal ganglion and the ventral cord.

Cell Body Clusters

Homologous cell bodies are more difficult to identify than neuropils, tracts, and commissures. In some cases, such as the cells associated with the olfactory and accessory lobes, the cell bodies can be identified by their characteristic morphology, but in others there are no such criteria available. The projections of the primary neurites of a few cell bodies are known, but these are in the minority, and then information is often available for only one brain type.

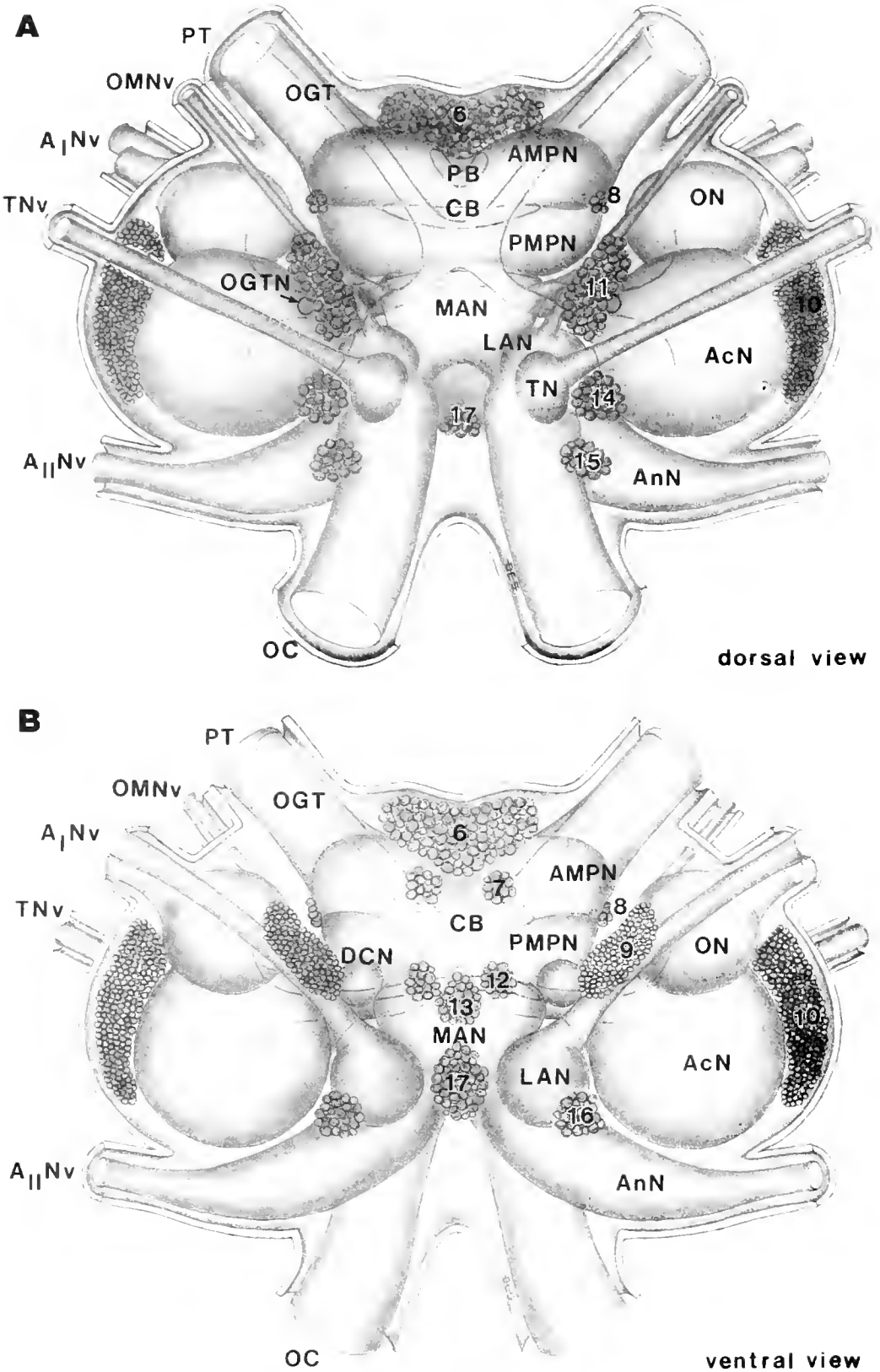

Figure 3A, B. Graphic reconstruction of the neuropils and cell clusters in dorsal and ventral views of the brain of the crayfish. This figure, and those for the crab and spiny lobster, were reconstructed from sectioned material, so that the proportions of the brain areas and positions of the cell clusters are reasonably accurately retained. The numbers and size of the cell bodies shown, however, do not represent the true situation, apart from indicating the difference between the characteristically small "globuli" cells associated with the accessory and olfactory lobes, and the larger cell bodies found elsewhere in the brain. A key to the abbreviations is provided in Appendix 2. See text for details.

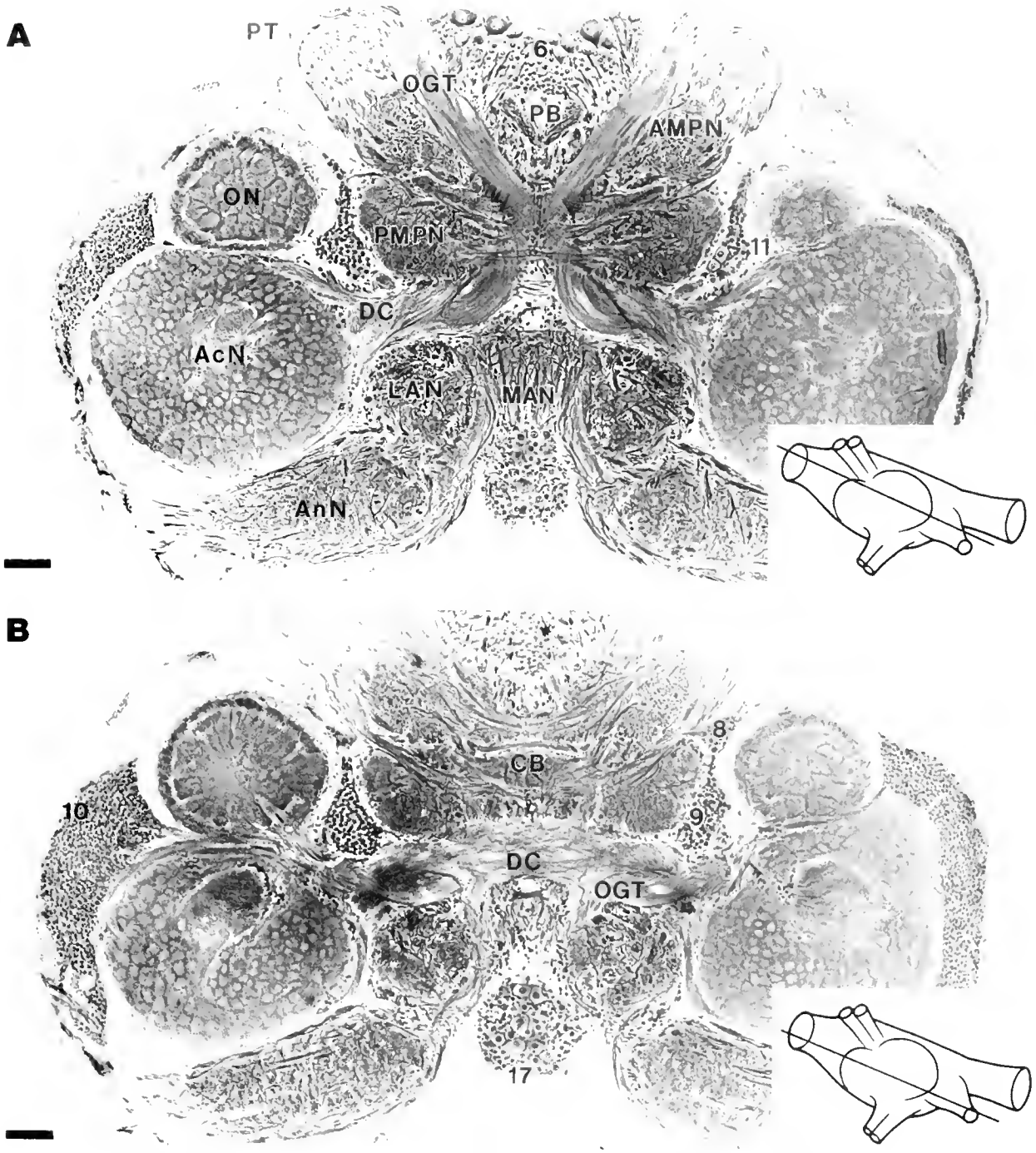

Figure 4. Horizontal sections of the brain of *Cherax*. In this and in the following figures, the planes of the sections are indicated on the inset diagram which shows the brain in side view with anterior on the left. Figure 4A includes the olfactory globular tract (OGT) which forms a chiasm at the center of the brain and then diverges to end in the olfactory (ON) and accessory (AcN) lobes. All the main neuropils can be seen in this plane. Figure 4B is a section through a more ventral plane and shows the deutocerebral commissure (DC) extending across the brain between the two accessory lobes. A and B show how the olfactory globular tract passes dorsally over the deutocerebral tract in the midline and then ventrally beneath it before entering the olfactory and accessory lobes. Scale bars = 100 μm.

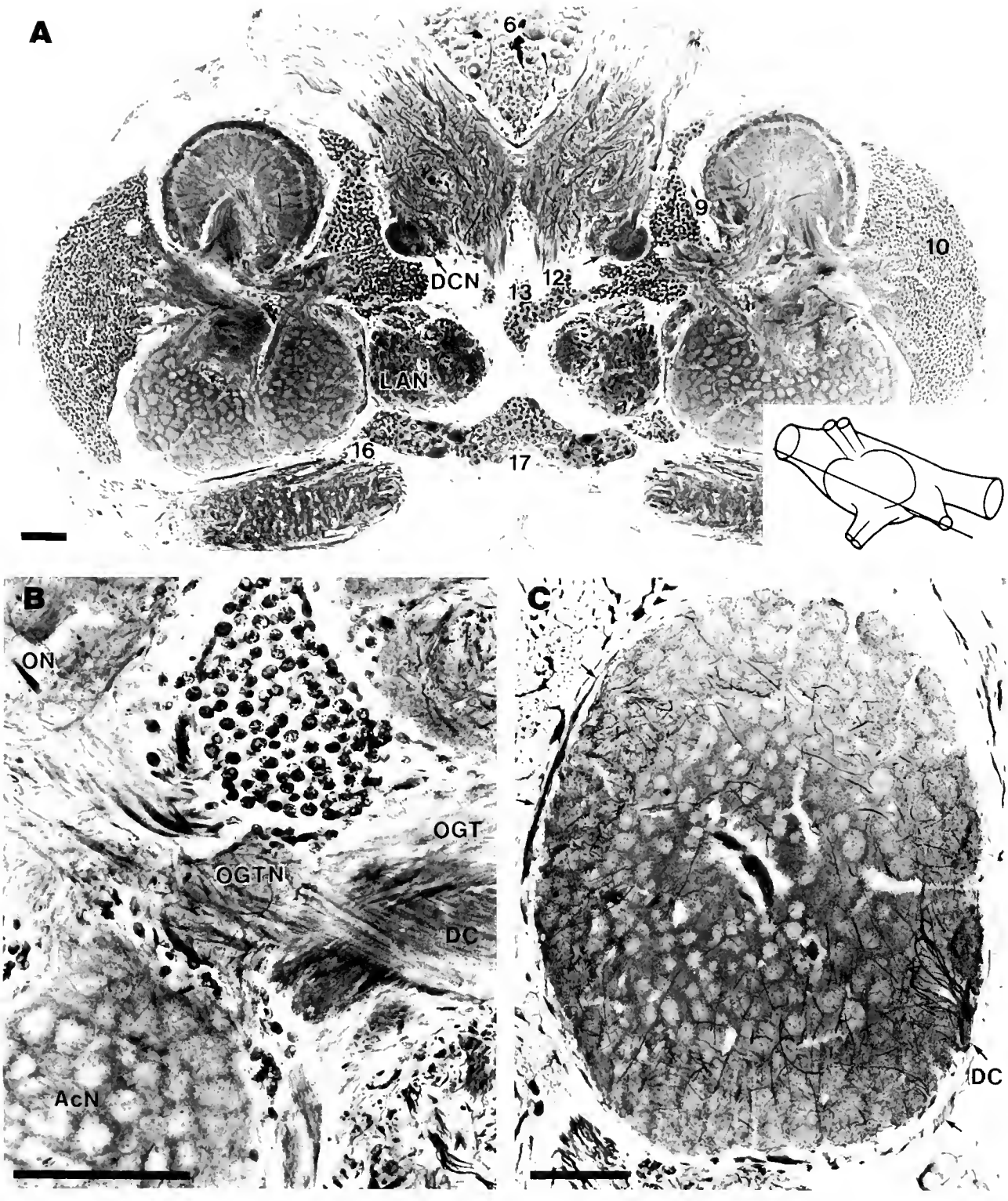

Figure 5. A. A horizontal section near the ventral surface of the *Cherax* brain. At this level the ventrally situated deutocerebral neuropils can be seen (DCN). The medial antenna I neuropil is no longer in the plane of the section, but the lateral antenna I neuropils (LAN) are still present as round areas, medial to the accessory lobes. Bundles of axons at their anterior margins are the beginning of the antenna I nerve root. The olfactory lobes are enclosed by the fine fibers of the axons from the chemoreceptors. These axons are also contained in the antenna I nerve root. B. The small olfactory globular neuropil (OGTN) contained within the fibers of the olfactory globular tract (OGT) at the point where the olfactory globular tract and the deutocerebral commissure (DCN) cross before projecting to the neuropils to the olfactory (ON) and accessory lobes (AcN). C. Darkly stained axons (arrows) from the deutocerebral tract (DC) penetrate the accessory lobe from the periphery to end in two layers of glomeruli in the lobe. Scale bars = 100 μm.

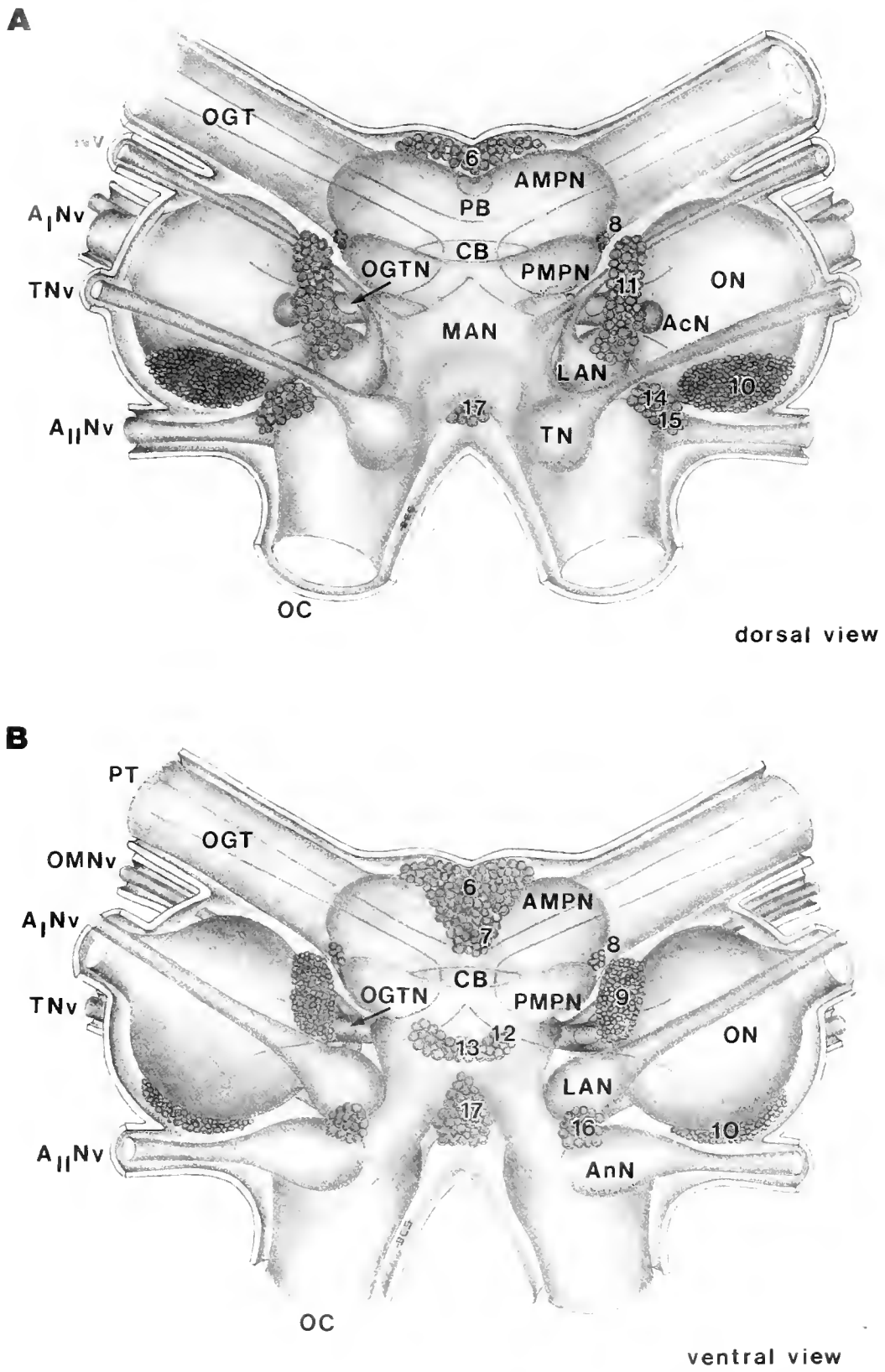

Figure 6A, B. Dorsal and ventral views of the brain of *Scylla serrata* as an example of a brachyuran. See text for details.

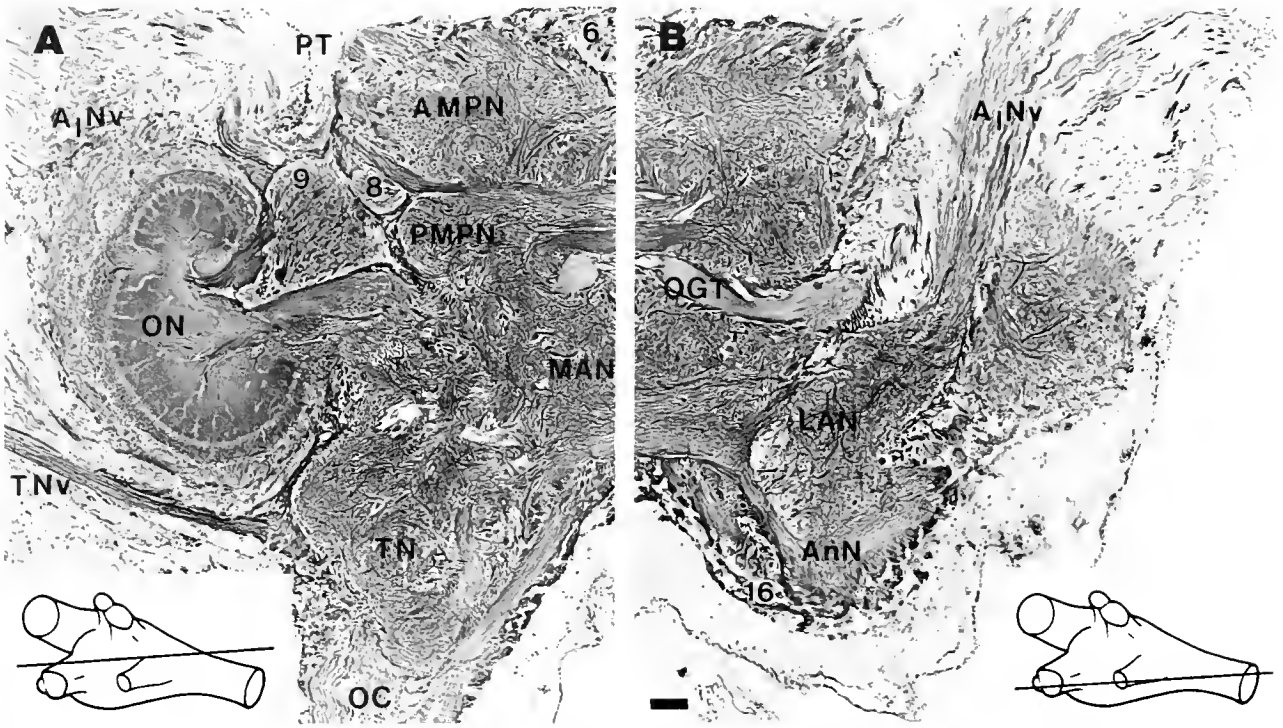

Figure 7. A horizontal section through the brain of *Scylla*. This section is slightly oblique, passing through more dorsal neuropils on the left (A) and more ventral neuropils on the right (B). The anterior medial protocerebral neuropils (AMPN) are larger than the posterior protocerebral neuropils. The olfactory lobes (ON) are also large and enclosed by many chemoreceptive fibers projecting from the antennules in the antenna I nerve root. The tegumentary nerve root and neuropil are prominent (A), whereas the lateral antenna I neuropil and the antenna II neuropil are relatively small (B). Scale bar = 100 μm.

The cell bodies are contained in clusters; some of these clusters are clearly recognizable in all brain types, some are not. In previous studies, cell body clusters have been given specific names, and these names differ from one brain type to another. Here, we describe the cell clusters according to the brain region in which they are found. In this way we avoid functional names for cell clusters that may be highly heterogeneous and that may contain the cell bodies of neurons with widely differing functions and projections.

We recognize 17 different clusters of cell bodies that appear to be common to all brain types; to simplify matters we have numbered the cell clusters, 1–17, from anterior to posterior. Tables in Appendix 1 provide cross references to the descriptions provided in this paper and by previous authors.

Protocerebrum[†]

OPTIC GANGLIA. In the optic ganglia we recognize (1) cell bodies that lie distal to the lamina, (2) cell bodies that lie distal or adjacent to the external medulla, and (3) cell bodies that lie adjacent to the internal medulla, or between the internal and terminal medulla.

Detailed information about the projections of many of the cell bodies in the optic ganglia is available for some crustaceans (Nässel, 1977; Sandeman, 1982).

LATERAL PROTOCEREBRUM. The lateral protocerebrum contains (4) cell bodies that lie adjacent to the terminal medulla, and (5) cell bodies that lie adjacent to the hemiellipsoid body.

Detailed information about the projections of some of the cell bodies in the lateral protocerebrum of spiny lobsters and crayfish is available (Blaustein *et al.*, 1988; Derby and Blaustein, 1988).

MEDIAN PROTOCEREBRUM. The median protocerebrum includes (6) a prominent medial cluster of cell bodies, some of which are very large; lying around the front of the brain and extending from the dorsal to ventral surfaces; (7) lateral cell bodies that may appear in some preparations as extensions of cell cluster 6 on the ventral surface of the brain and in others as separate groups; and (8) small lateral groups of cell bodies that lie on either side of the central body at the junction be-

[†] Numbers correspond to cell bodies labeled in Figures.

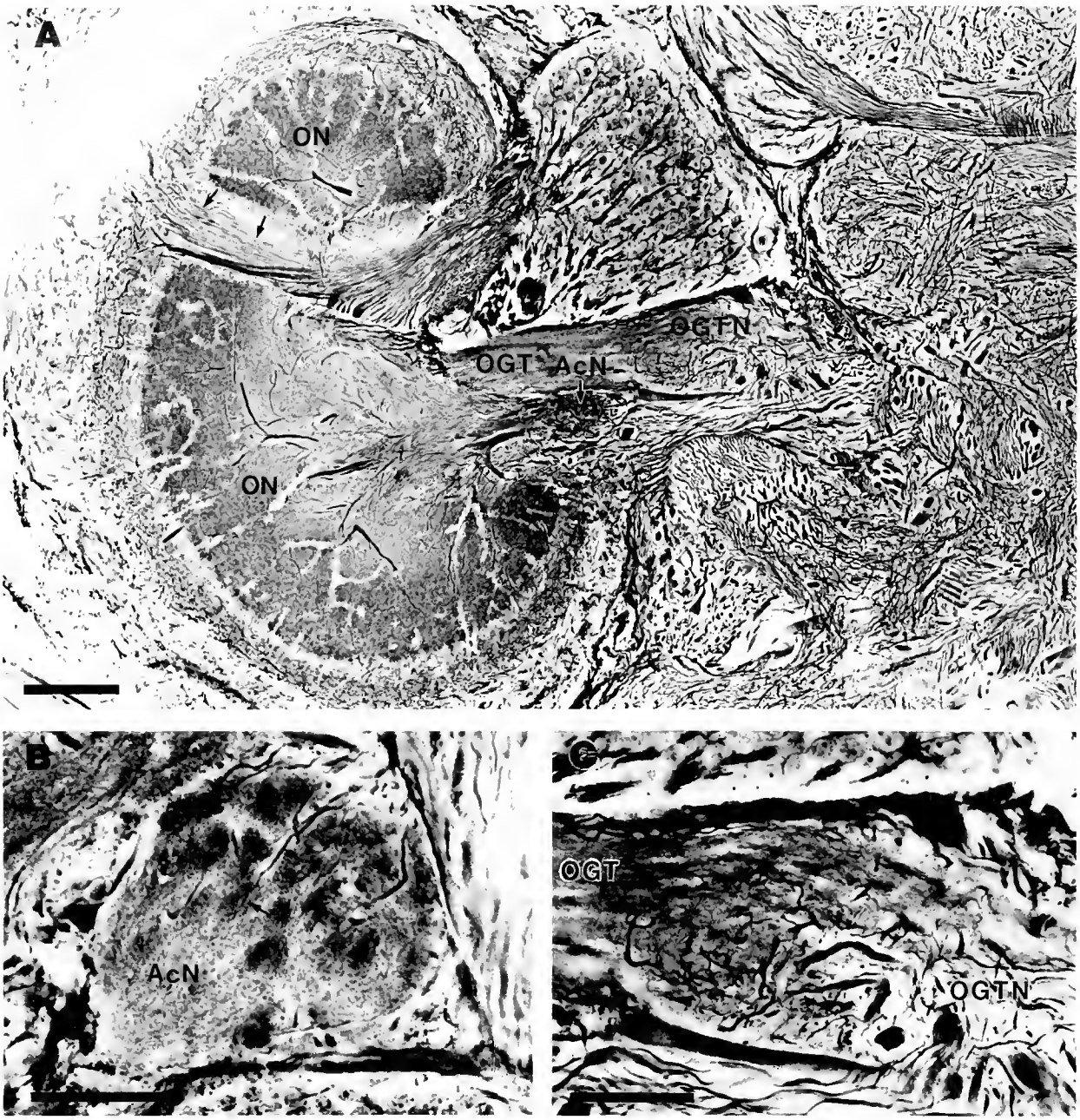

Figure 8. A. Horizontal section through the brain of *Scylla* (left side) showing the location of the olfactory globular tract neuropil (OGTN) and the small accessory lobe (AcN). Primary neurites (arrows) from the medial globuli cells in crabs pass through the neuropil of the olfactory lobe and spread out over its periphery. B. The reduced accessory lobe of crabs retains its glomerular structure and receives darkly staining axons (arrows) that end in the glomeruli. C. The olfactory globular tract neuropil is contained amongst the fibers of the olfactory globular tract. Scale bars = 8A, 100 μm; 8B = 25 μm; 8C = 50 μm.

tween the anterior and posterior medial protocerebral neuropils. These are subdivided in spiny lobsters.

Deutocerebrum

The cell bodies of the deuterocerebrum are recognized as follows: (9) Laterally situated, characteristically small cell bodies with nuclei that almost fill the cell lumen, lying ventrally between the anterior medial margin of the olfactory lobe and the posterior medial protocerebral neuropil, or ventral to the posterior part of the olfactory lobe. The primary neurites of these cells are directed towards the olfactory (and, when present, accessory) lobes.

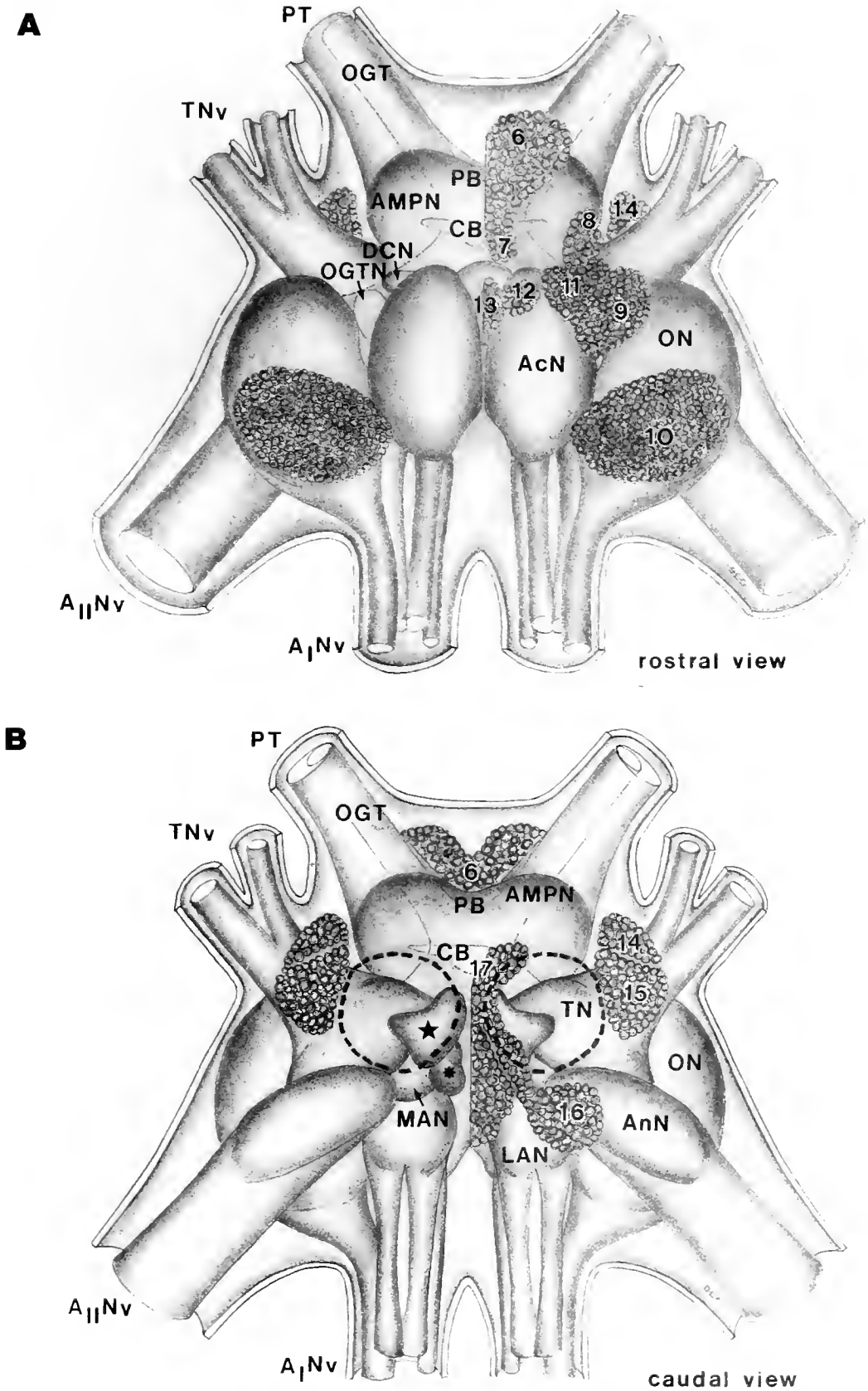

Figure 9 A, B. Rostral and caudal views of the brain of *Panulirus argus* as an example of a palinuran. Medially placed cell bodies in the drawings of *Panulirus* have been shown only on one side to avoid obscuring the underlying neuropil areas. See text for details.

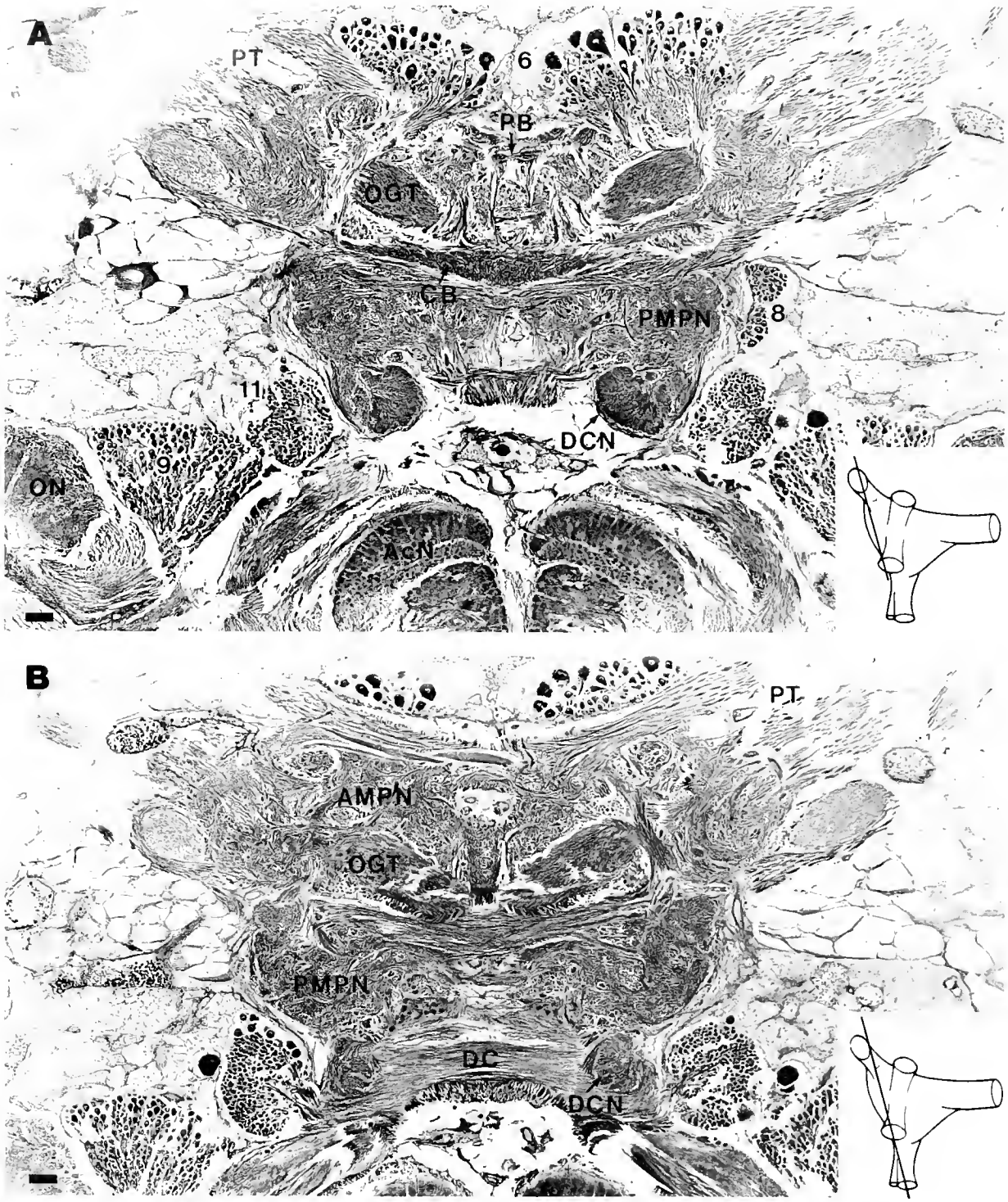

Figure 10. A. A frontal section passing through the medial protocerebral neuropils of *Jasus* and showing the location of the protocerebral bridge and central body (CB). The olfactory globular tracts (OGT) lie near the surface of the protocerebral tracts (PT) and in this section are converging on the center of the brain where they will form a chiasm. The deutocerebral neuropils (DCN) lie ventral to the posterior medial protocerebral neuropil (PMPN) as they do in *Cherax*. B. Further into the brain (equivalent to moving more dorsally in *Cherax*) the deutocerebral commissure (DC) can be seen with its connections to the deutocerebral commissure neuropils (DCN). Scale bars = 100 μm.

(10) Like the cell bodies of cell cluster 9, these are also small with nuclei that nearly fill the lumen. In the crayfish where the accessory lobe lies directly posterior to the olfactory lobe, these cell bodies constitute a large lateral group. In spiny lobsters, where the accessory lobes lie medial to the olfactory lobes, and in the crabs where the accessory lobes are very small, the above cell bodies lie posterior to the olfactory lobes. (11) A heterogeneous, laterally placed group, containing small and large cell bodies. They occupy the space between the olfactory lobes and the median antenna 1 neuropils on the dorsal side of the deutocerebrum. They are contiguous with cell cluster 10 in spiny lobsters. (12) Laterally situated cells, similar in makeup to cell cluster 11 and occupying about the same antero-posterior position, but lying on the ventral surface of the brain. (13) A medial group of cell bodies, lying on the ventral surface, and fused with cell cluster 12 in crabs and spiny lobsters.

Tritocerebrum

The following cell clusters are recognized in the tritocerebrum: (14) Small laterally situated groups of cell bodies lying over the anterior medial margin of the antenna II neuropil on the dorsal side of the brain. (15) A small laterally situated group of cells lying over the posterior medial margin of the antenna II neuropil on the dorsal side of the brain. Often fused with cluster 14. The primary neurites of cell bodies in 14 and 15 end in the antenna II neuropils in crayfish (Sandeman, unpub. obs.). (16) Laterally situated cell bodies on the ventral surface of the brain that lie directly below the anterior margins of the antenna II neuropil. Although they occupy a relatively caudal position in the brain, the primary neurites of virtually all these cell bodies extend to the deutocerebrum in the spiny lobster (Schmidt, unpub. obs.). (17) A medial cluster of cell bodies of different sizes, grouped between the oesophageal connectives, and spreading from the dorsal to the ventral surface of the brain and thence out over the ventral surface of the brain.

Brain Plans of the Different Infraorders

The shapes, and an indication of the relative sizes of the brains of the crayfish, crab, and spiny lobster, seen from the side and above, are shown in Figure 2. The folded nature of the spiny lobster brain, with the dorsally extending protocerebral tracts and ventrally projecting antenna I and antenna II nerve roots, is well demonstrated in side view.

Astacura (clawed lobsters and crayfish *e.g., Homarus, Procambarus, Astacus, Orconectes, Cherax, Euastacus, Pacifastacus*). The crayfish *Cherax destructor* has been used as an example of an astacuran brain. A dorsal view of the brain is shown in Figure 3A, and a ventral view in Figure 3B. Micrographs of horizontal sections taken through different planes are shown in Figures 4 and 5. The brain regions (proto-, deuto-, and tritocerebrum) lie almost in a single plane, so that most of the neuropils can be seen in both dorsal and ventral views.

The protocerebral tracts (PT) enter the anterior medial protocerebral neuropils (AMPN) antero-laterally. Enclosed within the neuropils of the median protocerebrum are the protocerebral bridge (PB) (Fig. 4A) and the central body (CB) (Fig. 4B). The olfactory globular tract (OGT) is also buried within the neuropils, but comes close to the dorsal surface where the protocerebral tracts enter the median protocerebrum (Fig. 4A).

The deutocerebrum is dominated by the laterally situated olfactory (ON) and accessory (AcN) lobes that are the origin of the olfactory globular tract. The small olfactory globular tract neuropils (OGTN) are embedded within the olfactory globular tract close to the point where it branches into the olfactory and accessory lobes (Fig. 5B). The deutocerebral commissure runs between the two accessory lobes and has strong projections to the deutocerebral commissure neuropil (DCN) on the ventral side of the brain (Figs. 4B, 5A). Axons from the deutocerebral commissure enclose the accessory lobe (AcN) and penetrate from the periphery of the lobe to end in glomeruli lying in two layers in the lobe (Fig. 5C). Fine axons from olfactory sensilla on the antenna I end in the olfactory lobe (Fig. 5A). No projections from peripheral sense organs or motor neurons have been described in the accessory lobes.

The lateral (LAN) and median (MAN) antenna I neuropils are located medial to the olfactory and accessory lobes (Figs. 4A, 5A). Axons in the antenna I nerve (A_1Nv) and in the oculomotor nerve (OMNv) both originate or end in these two neuropils. Axons in the oculomotor nerve also project to the posterior medial protocerebral neuropils (PMPN).

The tritocerebrum contains the tegumentary (TN) and antenna II (AnN) neuropils which receive inputs from the receptors on the carapace and antenna II, respectively. The motorneurons controlling the movements of antenna II are located in the antenna II neuropil.

Clusters of cell bodies are clearly delineated in the crayfish. The cell bodies associated with the olfactory and accessory lobes (9 and 10) are characteristically small with nuclei that almost fill the cell lumen. Cluster 10 is located laterally, a situation not shared with the crabs and spiny lobsters.

Brachyura (crabs; *e.g., Scylla, Carcinus, Callinectes, Hemigrapsus, Leptograpsus*). The crab *Scylla serrata* is taken as an example of a brachyuran. A dorsal view of the brain is shown in Figure 6A and a ventral view in

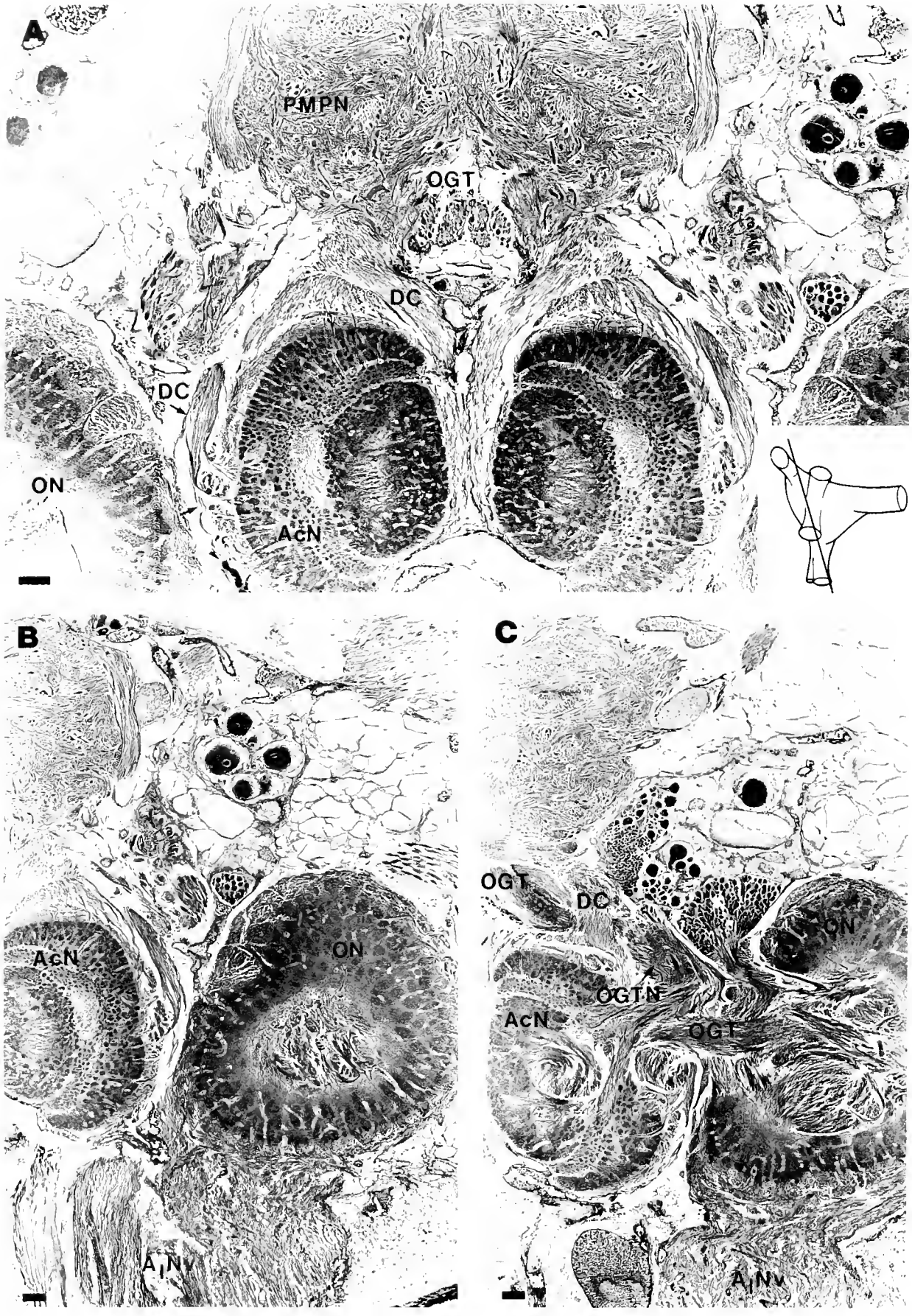
A
PMPN
OGT
DC
DC
ON
AcN
B
AcN
ON
AiNv
C
OGT
DC
ON
OGTN
AcN
OGT
AiNv

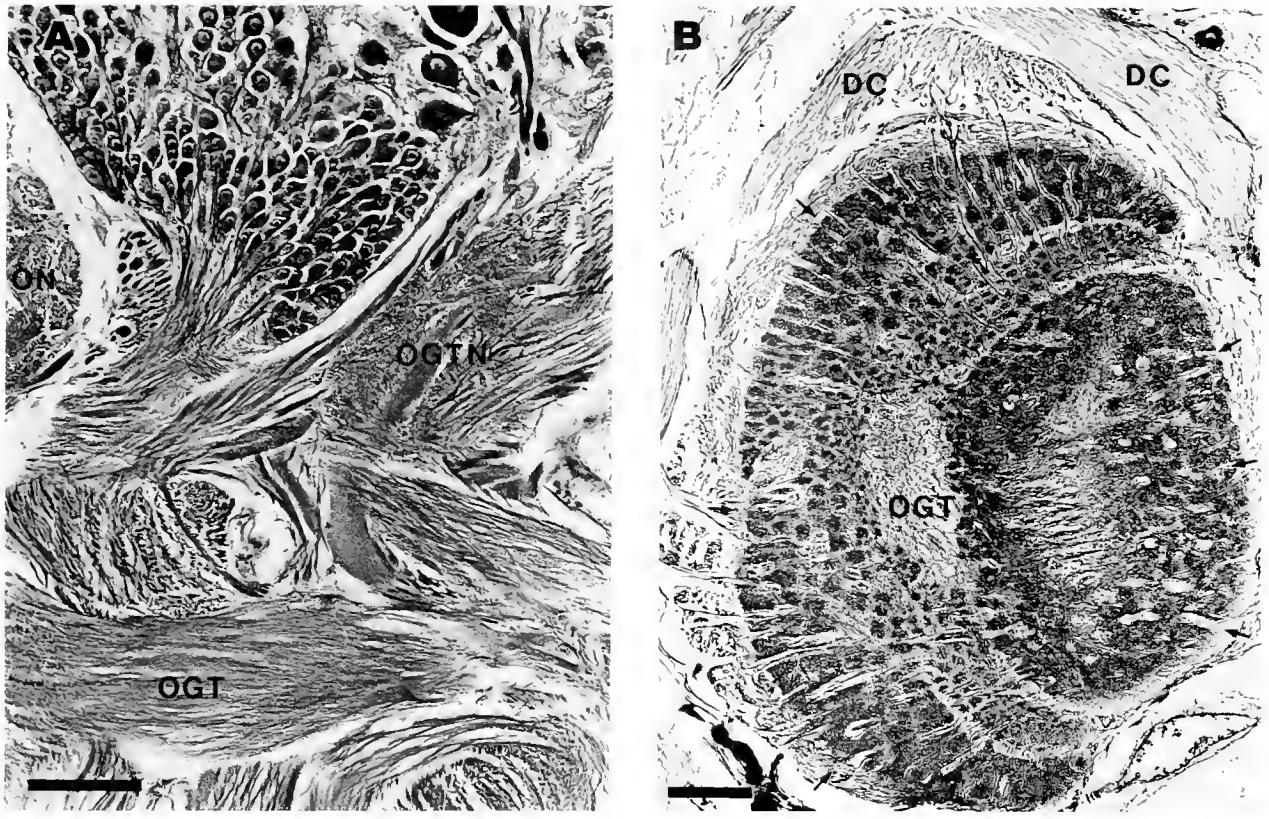

Figure 12. A. The olfactory globular tract neuropil on the left side of the brain of *Jasus*. As in the crayfish and crab, this neuropil is formed from arborizations among the fibers of the olfactory globular tract, just before it diverges into the olfactory and accessory lobes. B. The accessory lobe of *Jasus* has three layers of glomeruli, the outer two being cup shaped and the inner layer forming a spherical area of neuropil enclosed by the other two. Axons from the deutocerebral commissure (arrows) that enter from the lateral surfaces appear to reach all layers, whereas those that enter medially appear to stop within the central area of neuropil. Fine fibers from the olfactory globular tract (OGT) that enter the glomerular layers from within the lobe can be seen in the figure. Scales bars = 100 μm.

Figure 6B. Like the crayfish, the three brain regions of the crab brain lie in one plane so that most of the neuropils can be seen from both sides.

The protocerebral tracts are large in brachyurans and contain a number of axons of a large diameter. The anterior medial protocerebral neuropils (AMPN) are also proportionately larger than in crayfish. The protocerebral bridge (PB), central body (CB), and the olfactory globular tract (OGT) are not different from those of crayfish; they occupy the same sites and are similarly proportioned (Fig. 7).

Two features in the deutocerebrum distinguish the brachyuran brain from the crayfish (and spiny lobster). First, there is a marked reduction in the size of the accessory lobes (AcN). These are tucked in at the posteromedial edge of the olfactory lobes (ON). They are small but retain their glomerular structure (Fig. 8A, B). Second, a large deutocerebral commissure and the associated deu-

Figure 11. A. The large accessory lobes (AcN) are medial to the olfactory lobes (ON) in the palinurans. Axons in the deutocerebral commissure (DC) sweep around the olfactory globular tract and descend over the accessory lobes containing three layers of glomeruli. B. The right half of the brain of *Jasus* showing the axons from chemoreceptors on the antennule ascending and enclosing the laterally placed olfactory lobe (ON). Axons to the left of those projecting to the olfactory lobe end in the lateral antennal 1 neuropil. Both sets of axons are contained in the antenna I nerve root. C. A section through the center of the olfactory (ON) and accessory lobes (AcN) to show the branches of the olfactory globular tract (OGT) axons to both accessory and olfactory lobes. The olfactory globular tract neuropil (OGTN) lies close to where the olfactory globular tract enters the two lobes. Scale bars = 100 μm.

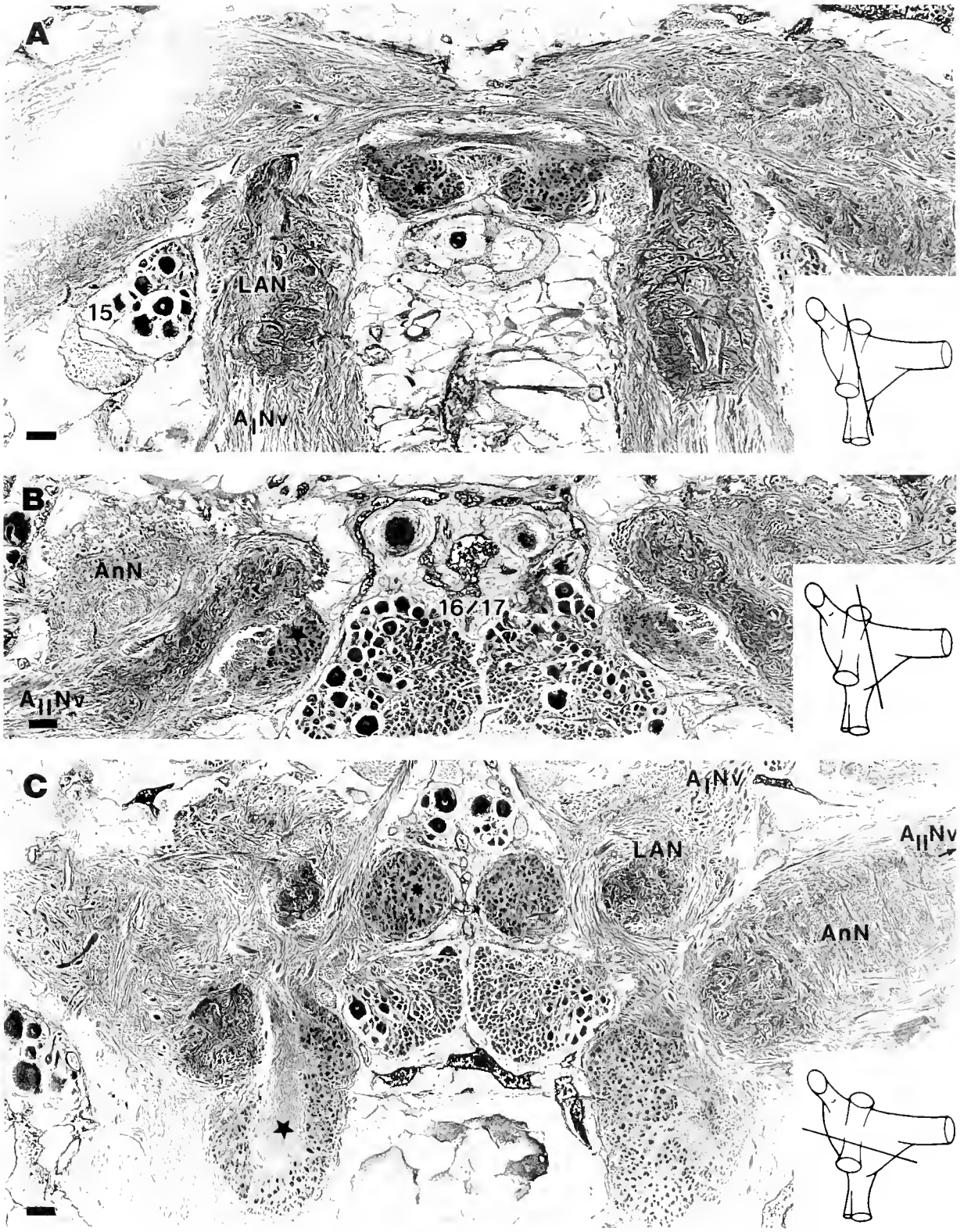

Figure 13. A. A frontal section of *Jasus* brain passing through the lateral antenna I neuropils (LAN) and the antenna II neuropils (AnN). Axons in the antenna I nerve root (A_INv) ascend from below to enter the lateral antenna I neuropil. The antenna II nerve roots (A_{II}Nv) enter the brain more laterally. The two areas of glomerular neuropil (asterisk) that lie between the lateral antenna I neuropils are the antennular glomeruli reported by Blaustein *et al.*, 1988, and are unique to spiny lobsters. B. A section taken further caudal to that shown in A passes through the caudal extremities of the antenna II neuropil

tocerebral neuropils have not yet been determined, although the axons that project to the accessory lobes do cross the brain and pass ventral to the olfactory globular tract at the midline. The olfactory globular tract neuropil (OGTN) (Fig. 8C) is present. The absence of a large accessory lobe results in the cell body cluster 10 occupying a position posterior to the olfactory lobe, instead of lateral to it as in the crayfish.

The lateral (LAN) and medial (MAN) antenna 1 neuropils are located medial to the olfactory lobes and are the origin or destination of motor and sensory neurons in the antenna 1 (A_1Nv) and oculomotor (OMNv) nerves (Fig. 7).

There is little difference between the tritocerebrum of the crayfish and the crab. The tegumentary nerve (TNv) in the crab ends in its neuropil (TN) which lies on the dorsal surface of the brain at the base of the oesophageal connectives. The antenna II neuropil (AnN) is proportionately smaller in the crab than in the crayfish, but occupies the same position. The second antennae of the crabs are also much smaller than those of the crayfish.

Clusters of cell bodies in the crab brain are very similar to those in the crayfish, with the exception of cluster 10 which has far fewer cell bodies than either the crayfish or spiny lobster and, as in the lobster, is located posterior to the olfactory lobe.

Palinura (spiny lobsters, slipper lobsters; *e.g., Jasus, Panulirus, Arctides, Ibacus*). Two lobsters, *Jasus novaehollandiae* and *Panulirus argus,* have been used here to represent the palinuran brain. Two characteristic features of the palinuran brain are present in all members of the group, namely a rotation of the medial protocerebral neuropils back over the deutocerebrum so that they come to lie dorsal to it, and the location of the large accessory lobes medial to the olfactory lobes. The upwardly folded median protocerebrum of the spiny lobster makes the "dorsal" and "ventral" views that are shown for the crayfish and crab less useful in depicting the spiny lobster brain morphology. For this reason the views that are shown are rostral (from in front) in Figure 9A and caudal (from behind) in Figure 9B. Dorsal is, therefore, at the top of the page, and ventral at the bottom in these figures.

The protocerebral tracts (PT) enter the anterior median protocerebrum (AMPN) dorso-laterally, and the protocerebral bridge (PB), central body (CB), and olfactory globular tract (OGT) can be found in the same places as in the other two brain types (Fig. 10A). The posterior medial protocerebral neuropils (PMPN) are hidden in the rostral view by the deutocerebral neuropils and by the tritocerebral neuropils in the caudal view.

The dominant deutocerebral neuropils are the olfactory (ON) and accessory (AcN) lobes and can be seen best in the rostral view. Quite unlike the organization in the crayfish, the four neuropils are lined up and thrust forward with the olfactory lobes flanking the medially located and slightly smaller, accessory lobes (Fig. 11A). The antenna I nerve (A_1Nv) projects ventrally (in the plane of the page in Fig. 4) and contains bundles of axons that end or originate in the lateral (LAN) and median (MAN) antenna 1 neuropils, or in the olfactory lobes (ON) (Fig. 11B, C). No projections from any nerve roots have been found that end in the accessory lobe. A large deutocerebral commissure connects the two accessory lobes, and axons from this project to the deutocerebral commissure neuropil (DCN) (Fig. 10A, B), also visible in the rostral view. As in crayfish, axons from the deutocerebral commissure penetrate the accessory lobe from the perimeter and end in spherical glomeruli. There are three layers of glomeruli in the spiny lobster accessory lobes, and the penetrating axons end in all (Fig. 12B). The olfactory globular tract, as in crayfish, branches into both the accessory and olfactory lobes (Figure 11C), and a small neuropil, the olfactory globular tract neuropil (OGTN) is associated with the tract just before the branch point (Figs. 11C, 12A).

The lateral (LAN) and median (MAN) antenna 1 neuropils are partly obscured by the tritocerebral neuropils, but can be seen in the caudal view. Two neuropils associated with the deutocerebrum in the spiny lobsters may be unique to those animals. These have been called the antennal and antennular glomeruli (Fig. 13) (Blaustein *et al.*, 1988). They are indicated in Figures 4B and 13A, B, C by a star and an asterisk respectively and have not been identified in the other two brain types.

The caudal view of the brain (Fig. 4B) shows how its folded nature brings the median protocerebrum to lie dorsal to the tritocerebral neuropils. The large tegumentary nerve (TNv) projects dorsally from the large tegumentary neuropils (TN) on the dorsal side of the tritocerebrum, close to the base of the oesophageal connectives. These project towards the observer in Figure 4B, and their positions are shown by two dashed circles. The antenna II neuropils (AnN) lie ventral to the oesophageal connectives as in the other two brain types, and the very large antenna II nerves (A_{II}Nv) project ventrolaterally.

Identification of the cell body clusters in the spiny lob-

---

and through a second pair of glomerular neuropil areas (star), the antennal glomeruli (Blaustein *et al.*, 1988), also unique to the spiny lobsters. (C) The antennular (asterisk) and antennal (star) glomeruli, and their relationship to the neuropils of the lateral antenna I and antenna II, can be clearly seen in a horizontal section through this area of the brain. Scale bars = 100 μm.

ster is less certain than in the other two brain types. The cells associated with the olfactory and accessory lobes are easily identified by their characteristically small size and large nuclei. Cluster 10, found lateral to the olfactory and accessory lobes in crayfish, are posterior to the olfactory lobes in the spiny lobster. Other cell clusters, such as 6, 7, 8, 11, and 17, are relatively certain to be homologues of the same clusters in the other two brain types. Less certain are the clusters 14, 15, and 16, and the large cluster adjacent to 17 which spreads out over the ventral surface of the brain between the lateral antenna 1 neuropils.

Discussion

In proposing a standard nomenclature for the components in the brains in three infraorders of the decapod crustaceans, we set out with the assumption that the same neural components (neuropils, tracts, cell clusters) would be represented in all three members of this phylogenetically close grouping. This has proved to be largely true, with the exception of the two deutocerebral neuropils in the spiny lobsters, the antennal and antennular glomeruli. These may either represent a special development of the spiny lobster, or the homologous areas in the crab and crayfish have not yet been recognized. The organization of the optic ganglia is remarkably constant within the three groups, perhaps because few degrees of freedom are allowed in a neuropil designed to compute the direction and velocity of images moving across the receptors of the retina.

If, as suggested by the similarity of the optic ganglia, common function leads to common neural structure, then the relative size of a neuropil area in the crustacean brain could be a reflection of the dominance of a particular sensory modality, as is the case with fish that live in clear or turbid water (Huber and Rylander, 1992). The brachyurans, for example, have large protocerebral tracts and large medial protocerebral neuropils, suggesting a reliance on the visual system. The second antennae are relatively small and the antenna II neuropil is also correspondingly reduced when compared with the crayfish and the spiny lobster. The spiny lobsters and crayfish brains are dominated by the antenna I and antenna II neuropils, olfactory lobes, and above all, accessory lobes. From what we know of the behavior of these animals they are night active and must rely heavily on tactile and olfactory senses.

To follow up these and other questions related to the brain and behavior in the crustaceans requires a much more precise knowledge of the brain neuroanatomy than what is presented here or known at the present stage. There is very little information, for example, about the connectivity between neuropils in the crustacean brains, and not even the function of the accessory lobe, central body, and protocerebral bridge have been understood. The demonstration of homologous neuronal components in the three brain types enhances the value of comparative studies and the establishment of a common nomenclature is a useful first step in this direction.

Acknowledgments

The concept of a common nomenclature for the larger decapods originated in a meeting organized by Drs. B. Ache and DeF. Mellon at the Symposium on Crustacean Pioneer Systems in Neurobiology, Sept. 7–9, 1989, in Hamburg, Germany. We thank Drs. Ache, Mellon, and others for their suggestions and encouragement and Rosa Ascencio for her technical assistance. The study was supported by an ARC research grant to DS and by grants from the DFG (Schm738/1-1 and 1-2) and NSF (#88-10261) to MS.

Literature Cited

Ache, B. W., and D. C. Sandeman. 1980. Olfactory-induced central neural activity in the Murray crayfish, *Euastacus armatus*. *J. Comp. Physiol.* **140:** 295–301.

Arbas, E. A., C. J. Humphreys, and B. W. Ache. 1988. Morphology and physiological properties of interneurons in the olfactory midbrain of the crayfish. *J. Comp. Physiol. A* **164:** 231–241.

Aréchiga, H., U. Garcia, and L. Martínez-Millán. 1990. Synaptic regulation of neurosecretory cell activity in the crayfish eyestalk. Pp. 373–380 in *Frontiers in Crustacean Neurobiology*, K. Wiese, W.-D. Krenz, J. Tautz, H. Reichert, and B. Mulloney, eds. Birkhäuser, Basel.

Atwood, H. L., and D. C. Sandeman. 1982. *The Biology of Crustacea*, Vol. 3, *Neurobiology: Structure and Function*. Academic Press, New York.

Beltz, B. S., M. S. Pontes, S. M. Helluy, and E. A. Kravitz. 1990. Patterns of appearance of serotonin and proctolin immunoreactivities in the developing nervous system of the American lobster. *J. Neurobiol.* **21:** 521–542.

Bethe, A. 1897. Das Nervensystem von *Carcinus maenas*. *Arch. Mikrosk. Anat. EntwMech.* **50:** 460–544.

Blaustein, D. N., C. D. Derby, R. B. Simmons, and A. C. Beall. 1988. Structure of the brain and medulla terminalis of the spiny lobster *Panulirus argus* and the crayfish *Procambarus clarkii*, with an emphasis on olfactory centers. *J. Crustacean Biol.* **8:** 493–519.

Bullock, T. H., and G. A. Horridge. 1965. *Structure and Function in the Nervous System of Invertebrates*. Vols. 1 and 2, W. H. Freeman, San Francisco.

Cooke, I. M., and R. E. Sullivan. 1982. Hormones and neurosecretion. Pp. 205–290 in *The Biology of Crustacea*, Vol. 3, *Neurobiology: Structure and Function*, H. L. Atwood and D. C. Sandeman, eds. Academic Press, New York.

Derby, C. D. 1982. Structure and function of articular sensilla of the lobster *Homarus americanus*. *J. Crustacean Biol.* **2:** 1–21.

Derby, C. D., and B. W. Ache. 1984. Quality coding of a complex odorant in an invertebrate. *J. Neurophysiol.* **51:** 906–924.

Derby, C. D., and D. N. Blaustein. 1988. Morphological and physiological characterization of individual olfactory interneurons connecting the brain and eyestalk ganglia of the crayfish. *J. Comp. Physiol.* **163:** 777–794.

Elofsson, R. 1983. 5-HT-like immunoreactivity in the central nervous system of the crayfish, *Pacifastacus leniusculus*. *Cell Tissue Res.* **232:** 221–236.

Elofsson, R., and R. R. Hessler. 1990. Central nervous system of *Hutchinsoniella macracantha* (Cephalocarida). *J. Crustacean Biol.* **10:** 423–439.

Fraser, P. J. 1974. Interneurons in crab connectives (*Carcinus maenas* L.): directional statocyst fibres. *J. Exp. Biol.* **61:** 615–628.

Glantz, R., and C. Pfeiffer-Linn. 1990. Synaptic mechanisms of a dual channel contrast detection system in the crayfish optic lobe. Pp. 157–164 in *Frontiers in Crustacean Neurobiology*, K. Wiese, W.-D. Krenz, J. Tautz, H. Reichert, and B. Mulloney, eds., Birkhäuser, Basel.

Grünert, U., and B. W. Ache. 1988. Ultrastructure of the aesthetasc (olfactory) sensilla of the spiny lobster, *Panulirus argus*. *Cell Tissue Res.* **251:** 95–103.

Habig, C., and R. C. Taylor. 1982. The crayfish second antennae. II. Motoneuron structure as revealed by cobalt chloride backfilling. *Comp. Biochem. Physiol. A* **72:** 349–358.

Hafner, G. S. 1973. The neural organization of the lamina ganglionaris in the crayfish: a Golgi and E. M. study. *J. Comp. Neurol.* **152:** 255–288.

Hamori, J., and G. A. Horridge. 1966. The lobster optic lamina. I. General organisation. *J. Cell Sci.* **1:** 249–256.

Hanström, B. 1924. Untersuchungen über das Gehirn insbesondere die Sehganglien der Crustaceen. *Ark. Zool.* **16:** 1–119.

Hanström, B. 1925. The olfactory centers in crustaceans. *J. Comp. Neurol.* **38:** 221–250.

Hanström, B. 1931. Neue Untersuchungen über Sinnesorgane und Nervensystem der Crustaceen. *Z. Morphol. Oekol. Tiere* **23:** 80–236.

Hanström, B. 1947. The brain, the sense organs, and the incretory organs of the head in the Crustacea Malacostraca. *Kungliga Fysiografiska Sällskapet, I Lund, Handlingar* **58:** 1–45.

Helm, F. 1928. Vergleichend-anatomische Untersuchungen über das Gehirn, insbesondere das "Antennalganglien" der Decapoden. *Z. Morphol. Oekol. Tiere* **12:** 70–134.

Hoyle, G. 1977. *Identified Neurons and Behavior of Arthropods*. G. Hoyle, ed., Plenum Press, New York. 594 pp.

Huber, R., and M. K. Rylander. 1992. Brain morphology and turbidity preference in *Notropis* and related general (Cyprinidae, Teleostei). *Environm. Biol. Fishes* **33:** 153–165.

Kinnamon, J. C. 1979. Tactile input to the crayfish tegumentary neuropile. *Comp. Biochem. Physiol. A* **63:** 41–50.

Kirk, M. D., B. Waldrop, and R. M. Glantz. 1983. A quantitative correlation of contour sensitivity with dendritic density in an identified visual neuron. *Brain Res.* **274:** 231–237.

Maynard, D. M. 1962. Organization of neuropil. *Am. Zool.* **2:** 79–96.

Maynard, D. M. 1966. Integration in crustacean ganglia. *Symp. Soc. Exp. Biol.* **20:** 111–149.

Maynard, D. M. 1969. Comments. Pp. 56–70 in *The Interneurons*, M. Brazier, ed., University of California Press, Los Angeles.

Maynard, D. M., and A. Sallee. 1970. Disturbance of feeding behavior in the spiny lobster, *Panulirus argus*, following bilateral ablation of the medulla terminalis. *Z. Vergl. Physiol.* **66:** 123–140.

Maynard, E. A. 1971. Microscopic localization of cholinesterases in the nervous system of the lobsters, *Panulirus argus* and *Homarus americanus*. *Tissue & Cell* **3:** 215–250.

Mellon, D. 1977. The anatomy and motor nerve distribution of the eye muscles in crayfish. *J. Comp. Physiol.* **121:** 349–366.

Mellon, D., and S. D. Munger. 1990. Nontopographic projection of olfactory sensory neurons in the crayfish brain. *J. Comp. Neurol.* **296:** 253–262.

Nässel, D. R. 1977. Types and arrangements of neurons in the crayfish optic lamina. *Cell Tissue Res.* **179:** 45–75.

Nässel, D. R., and R. Elofsson. 1987. Comparative anatomy of the crustacean brain. Pp. 111–133 in *Arthropod Brain. Its Evolution, Development, Structure, and Functions*, A. P. Gupta, ed., John Wiley and Sons, New York.

Roye, D. B. 1986. The central distribution of movement sensitive afferent fibers from the antennular short hair sensilla of *Callinectes sapidus*. *Mar. Behav. Physiol.* **12:** 181–196.

Roye, D. B., and D. P. Bashor. 1991. Investigation of single antennular motoneurons in the lateral antennular neuropil of *Callinectes sapidus*. *J. Crust. Biol.* **11:** 185–200.

Sandeman, D. C. 1964. Functional distinction between the optic and oculomotor nerves of *Carcinus*. *Nature* **201:** 302–303.

Sandeman, D. C. 1969. The synaptic link between the sensory and motor axons in the crab eye withdrawal reflex. *J. Exp. Biol.* **50:** 87–98.

Sandeman, D. C. 1971. The excitation and electrical coupling of four identified motoneurons in the brain of the Australian mud crab, *Scylla serrata*. *Z. Vergl. Physiol.* **72:** 111–130.

Sandeman, D. C. 1982. Organization of the central nervous system. Pp. 1–61 in *The Biology of Crustacea*, Vol. 3, *Neurobiology: Structure and Function*, H. L. Atwood and D. C. Sandeman, eds., Academic Press, New York.

Sandeman, D. C. 1989. Physical properties, sensory receptors and tactile reflexes of the antenna of the Australian freshwater crayfish *Cherax destructor*. *J. Exp. Biol.* **141:** 197–217.

Sandeman, D. C., and H. L. Atwood. 1982. *The Biology of Crustacea*, Vol. 4, *Neural Integration and Behavior*. Academic Press, New York. 327 pp.

Sandeman, D. C., and J. Denburg. 1976. The central projections of chemoreceptor axons in the crayfish revealed by axoplasmic transport. *Brain Res.* **115:** 492–496.

Sandeman, D. C., and S. E. Luff. 1973. The structural organization of glomerular neuropile in the olfactory and accessory lobes of the Australian freshwater crayfish, *Cherax destructor*. *Z. Zellforsch. Mikrosk. Anat.* **142:** 37–61.

Sandeman, D. C., and A. Okajima. 1972. Statocyst-induced eye movements in the crab *Scylla serrata*. I. The sensory input from the statocyst. *J. Exp. Biol.* **57:** 187–204.

Sandeman, D. C., and L. A. Wilkens. 1982. Motor control of movements of the antennal flagellum in the Australian crayfish, *Euastacus armatus*. *J. Exp. Biol.* **105:** 253–273.

Sandeman, D. C., R. E. Sandeman, and A. R. Aitken. 1988. Atlas of serotonin-containing neurons in the optic lobes and brain of the crayfish, *Cherax destructor*. *J. Comp. Neurol.* **269:** 465–478.

Sandeman, D. C., R. E. Sandeman, and H. G. de Couet. 1990. Extraretinal photoreceptors in the brain of the crayfish *Cherax destructor*. *J. Neurobiol.* **21:** 619–629.

Sandeman, R. E., and D. C. Sandeman. 1987. Serotonin-like immunoreactivity of giant olfactory interneurons in the crayfish brain. *Brain Res.* **403:** 371–374.

Schmidt, M., and B. W. Ache. 1990. Afferent projections to the midbrain of the spiny lobster revealed by biocytin. *Soc. Neurosci. Abstr.* **16:** 400.

Schmidt, M., and B. W. Ache. 1992. Antennular projections to the midbrain of the spiny lobster. II. Sensory innervation of the olfactory lobe. *J. Comp. Neurol.* **318:** 291–303.

Schmidt, M., E. Orona, and B. W. Ache. 1991. Parallel processing of chemosensory input in the brain of the spiny lobster. *Soc. Neurosci. Abstr.* **17:** 1018.

Schmidt, M., L. Van Ekeris, and B. W. Ache. 1992. Antennular projections to the midbrain of the spiny lobster. I. Sensory innervation of the lateral and medial antennular neuropils. *J. Comp. Neurol.* **318:** 277–290.

Schürmann, F-W., R. E. Sandeman, and D. C. Sandeman. 1991. Dense core vesicles and non-synaptic exocytosis in the central body of the crayfish brain. *Cell Tissue Res.* **265:** 493–500.

Silvey, G. E., and D. C. Sandeman. 1976. Integration between statocyst sensory neurons and oculomotor neurons in the crab *Scylla serrata* I. Horizontal compensatory eye movements. *J. Comp. Physiol.* **108:** 35–43.

Siwicki, K. K., and C. A. Bishop. 1986. Mapping of proctolin-like im-

munoreactivity in the nervous systems of lobsters and crayfish. *J. Comp. Neurol.* **243:** 435–453.

Strausfeld, N. J., and H. R. Nässel. 1980. Neuroarchitectures serving compound eyes of Crustacea and insects. Pp. 1–132 in *Handbook of Sensory Physiology,* Vol. VII/6, *Comparative Physiology and Evolution of Vision in Invertebrates,* H. Autrum, ed., Springer-Verlag, New York.

Tautz, J., and R. Muller-Tautz. 1983. Antennal neuropile in the brain of the crayfish: morphology of neurons. *J. Comp. Neurol.* **218:** 415–425.

Taylor, R. C. 1975. Integration in the crayfish antennal neuropile: topographic representation and multiple channel coding of mechanoreceptive submodalities. *J. Neurobiol.* **6:** 475–499.

Tazaki, K., and Y. Shigenaga. 1974. Chemoreception in the antenna of the lobster, *Panulirus japonicus. Comp. Biochem. Physiol. A* **47:** 195–199.

Titova, V. A. 1985. Neuropile topography in the cerebral ganglion of the crayfish. *J. Evol. Biochem. and Physiol.* **21:** 256–263.

Tsvileneva, V. A., and V. A. Titova. 1985. On the brain structures of decapods. *Zool. Jahrb. (Anat.)* **113:** 217–266.

Tsvileneva, V. A., V. A. Titova, and T. V. Kvashina. 1985. Brain topography of the shore crab *Hemigrapsus sanguineus. J. Evol. Biochem. and Physiol.* **21:** 394–400.

Wiersma, C. A. G., B. M. H. Bush, and T. H. Waterman. 1964. Efferent visual responses of contralateral origin in the optic nerve of the crab *Podophthalmus. J. Cell. Comp. Physiol.* **64:** 309–326.

Wiersma, C. A. G., J. L. M. Roach, and R. M. Glantz. 1982. Neural integration in the optic system. Pp. 1–32 in *The Biology of the Crustacea,* Vol. 4, *Neural Integration and Behavior,* D. C. Sandeman and H. L. Atwood, eds., Academic Press, New York.

Wiese, K., W.-D. Krenz, J. Tautz, H. Reichert, and B. Mulloney. 1990. *Frontiers in Crustacean Neurobiology.* Birkhäuser, Basel.

Wine, J. J., and F. B. Krasne. 1982. The cellular organization of crayfish escape behavior. Pp. 241–292 in *The Biology of Crustacea,* Vol. 4, *Neural Integration and Behavior,* D. C. Sandeman and H. L. Atwood, eds., Academic Press, New York.

Yoshino, M., Y. Kondoh, and M. Hisada. 1983. Projections of the statocyst sensory neurons associated with crescent hairs in the crayfish, *Procambarus clarkii* Girard. *Cell Tissue Res.* **230:** 37–48.

Appendix 1

The first listed and underlined name is the one we have preferred. Equivalents are listed below each preferred name. References indicate studies in which the names have been used but not necessarily the origin of the name.

Brain Divisions and Neuropils

Optic ganglia: (Kirk *et al.,* 1983; Titova, 1985; Tsvileneva and Titova, 1985; Blaustein *et al.,* 1988).
= optic lobes: (Sandeman and Luff, 1973; Nässel and Elofsson, 1987)
= optic masses: (Hanström, 1925)

Lamina: (Strausfeld and Nässel, 1980; Sandeman, 1982; Siwicki and Bishop, 1986)
= lamina ganglionaris: (Hanström, 1931, 1947; Bullock and Horridge, 1965; Maynard, 1966; Hafner, 1973; Elofsson, 1983; Kirk *et al.,* 1983; Siwicki and Bishop, 1986; Sandeman *et al.,* 1988; Blaustein *et al.,* 1988)
= optic lamina: (Hamori and Horridge, 1966)

External medulla: (Hanström, 1931, 1947; Bullock and Horridge, 1965; Sandeman, 1982; Elofsson, 1983; Siwicki and Bishop, 1986; Sandeman *et al.,* 1988; Blaustein *et al.,* 1988)
= medulla externa: (the above authors also use the latin version)
= medulla: (Strausfeld and Nässel, 1980; Kirk *et al.,* 1983; Nässel and Elofsson, 1987)

Internal medulla: (Hanström, 1931, 1947; Bullock and Horridge, 1965; Sandeman, 1982; Elofsson, 1983; Siwicki and Bishop, 1986; Sandeman *et al.,* 1988; Blaustein *et al.,* 1988)
= medulla interna: (the above authors also use the latin version)
= lobula: (Strausfeld and Nässel, 1980; Kirk *et al.,* 1983; Nässel and Elofsson, 1987)

Terminal medulla: (Hanström, 1931, 1947; Bullock and Horridge, 1965; Sandeman, 1982; Elofsson, 1983; Siwicki and Bishop, 1986; Sandeman *et al.,* 1988; Blaustein *et al.,* 1988)
= medulla terminalis: (the above authors also use the latin version)
= lobula plate: (Strausfeld and Nässel, 1980)

Hemiellipsoid body: (Hanström, 1931; Bullock and Horridge, 1965; Sandeman, 1982; Blaustein *et al.,* 1988)
= corpora pendunculata (Hanström, 1924, 1925)
= globuli (Hanström, 1925)

Anterior medial protocerebral neuropil:
= anterior optic neuropil: (Bullock and Horridge, 1965; Sandeman, 1982; Sandeman *et al.,* 1988; Blaustein *et al.,* 1988)
= anterior and lateral optic neuropil: (Titova, 1985; Tsvileneva and Titova, 1985)
= dorsal anterior and ventral optic neuropil: (Helm, 1928)

Posterior medial protocerebral neuropil:
= posterior optic neuropil: (Bullock and Horridge, 1965; Sandeman, 1982; Sandeman *et al.,* 1988; Blaustein *et al.,* 1988)
= posterior protocerebral neuropil: Tsvileneva and Titova, 1985)
= medial optic neuropil: (Helm, 1928)

Protocerebral bridge: (Helm, 1928; Bullock and Horridge, 1965; Sandeman, 1982; Tsvileneva and Titova, 1985; Sandeman *et al.,* 1988)

Central body: (Helm, 1928; Bullock and Horridge, 1965; Sandeman, 1982; Tsvileneva and Titova, 1985; Sandeman *et al.,* 1988)

Olfactory lobe: (Helm, 1928; Hanström, 1925, 1931, 1947; Bullock and Horridge, 1965; Sandeman, 1982; Tsvileneva and Titova, 1985; Sandeman *et al.,* 1988; Ache and Schmidt, 1988; Mellon and Munger, 1990)
= hemiglobulus anterior and posterior: (Bethe, 1897)

Lateral antenna I neuropil:
= lateral antennular neuropil: (Hanström, 1924; Helm, 1928; Sandeman, 1982; Titova, 1985; Tsvileneva and Titova, 1985; Sandeman and Sandeman, 1987; Sandeman *et al.*, 1988; Blaustein *et al.*, 1988)
= parolfactory lobe: (Hanström, 1947; Bullock and Horridge, 1965; Maynard, 1966; Sandeman and Luff, 1973; Sandeman, 1982; Tautz and Müller-Tautz, 1983; Yoshino *et al.*, 1983; Siwicki and Bishop, 1986; Nässel and Elofsson, 1987; Arbas *et al.*, 1988)

Median antenna I neuropil:
= medial antennal neuropil: (Bullock and Horridge, 1965; Sandeman, 1982; Tsvileneva and Titova, 1985; Sandeman and Sandeman, 1987; Blaustein *et al.*, 1988)

Accessory lobe: (Helm, 1928; Hanström, 1931, 1947; Bullock and Horridge, 1965; Sandeman, 1982; Tsvileneva and Titova, 1985; Sandeman and Sandeman, 1987; Sandeman *et al.*, 1988; Blaustein *et al.*, 1988)
= lobus accessorius (Hanström, 1925)
= neuropilum parvum: (Bethe, 1897)

Deutocerebral commissure neuropil:
= parolfactory lobe: (Titova, 1985; Tsvileneva and Titova, 1985; Sandeman and Sandeman, 1987; Sandeman *et al.*, 1988; Blaustein *et al.*, 1988)
= lateral glomeruli: (Mäynard, 1966; Sandeman, 1982)
= paracentral lobe: (Hanström, 1947;
= nebenlappen: (Hanström, 1924, 1925)
= uv neuropil: (Helm, 1928; Sandeman, 1982)

Olfactory globular tract neuropil:
= "z" neuropil figured by Hanström (1928). Also referred to by Tsvilineva and Titova (1985); Sandeman and Sandeman (1987); Sandeman *et al.*, (1988); Schmitt *et al.*, (1991)

Antenna II neuropil:
= antennal neuropil: (Bullock and Horridge, 1965; Taylor, 1975; Sandeman and Wilkens, 1982; Tsvileneva and Titova, 1985)
= antennary neuropil: (Helm, 1928; Sandeman, 1982)

Tegumentary neuropil: (Bethe, 1897; Helm, 1928; Sandeman, 1982; Tsvileneva and Titova, 1985)

Antennular glomeruli: (Blaustein *et al.*, 1988)

Antennal glomeruli: (Blaustein *et al.*, 1988)

Tracts and Commissures

Optic tract:

Protocerebral tract: (Tsvileneva and Titova, 1985; Sandeman *et al.*, 1988)
= optic tract: (Hanström, 1924; Bullock and Horridge, 1965; Sandeman *et al.*, 1975)
= optic nerve: (Wiersma *et al.*, 1964; Sandeman, 1964, 1982)

Olfactory globular tract: (Helm, 1928; Bullock and Horridge, 1965; Tsvileneva and Titova, 1985)
= tractus optico-globularis (Bethe, 1897)
= tractus optico-antennularis (Hanström, 1924)
= tractus olfactorio-globularis (Hanström, 1925)

Deutocerebral commissure: (Titova, 1985; Tsvileneva and Titova, 1985; Sandeman and Sandeman, 1987; Sandeman *et al.*, 1988; Blaustein *et al.*, 1988)
= antennular commissure: (Hanström, 1925; Sandeman, 1982)
= olfactory commissure: (Bullock and Horridge, 1965)

Oesophageal connectives: (Sandeman and Luff, 1973; Sandeman, 1982; Nässel and Elofsson, 1987; Sandeman *et al.*, 1988)
= circumoesophageal connectives: (Helm, 1928; Siwicki and Bishop, 1986; Blaustein *et al.*, 1988)
= pharyngeal connectives: (Hanström, 1924, 1947)

Cell Bodies

The cell body clusters have been given different names by different authors. As explained in the text, we identify 17 clusters of cell bodies. Our identifying number is given in the first column (Ref) in the following tables and can be used to determine, across the tables, which cell body clusters are homologous.

Blaustein and Derby (1988) (Procambarus *and* Panulirus) (The first column of abbreviations refers to *Procambarus*, the second to the analogous cell clusters in *Panulirus*)

Ref.	Cluster name	Abbreviation	
1.	—	—	
2.	—	—	
3.	—	—	
4.	Cell cluster C,D,E,F	C,D,E,F	C,D,E,F
5.	Cell cluster A,B,G	A,B,G	A,B,G
6.	Anterior cluster	AC	AC
7.	Anterior cluster	AC	AC
8.	Ventral paired anterior cluster	VPAC	VPALC
9.	Ventral paired lateral cluster	VPLC	VPMLC
10.	Lateral cluster	LC	VPPLC
11.	Dorsal anterior cluster	DAC	VPMLC
12.	Ventral paired medial cluster	VPMC	VPMC
13.	Ventral unpaired medial cluster	VUMC	VUMC
14.	Dorsal medial clusters	DMC	DPMC

15. Dorsal posterior [illegible]sters	DPC	DUMC
16. Ventral paired [illegible]rior clusters	VPPC	DUMC
17. Ventral [illegible]d posteri[illegible]ster	VUPC	DUMC

Tautz and Müller-Tautz (1984)

Ref.	Cluster name	Abbreviation
1.	—	
2.	—	
3.	—	
4.	—	
5.	—	
6.	Anterior cluster	ac
7.	Ventral paired anterior cluster	vpac
8.	—	
9.	Ventral paired lateral cluster	vplc
10.	Lateral cluster	lc
11.	Dorsal anterior cluster	dac
12.	Ventral paired medial cluster	vpmc
13.	Ventral unpaired medial cluster	vumc
14.	Dorsal medial cluster	dmc
15.	Dorsal posterior cluster	dpc
16.	Ventral paired posterior cluster	vppc
17.	Ventral unpaired posterior cluster	vupc

Sandeman (1982) (after Helm 1928) (Helm's nomenclature is included in parenthesis)

Ref.	Cluster name	Abbreviation
1.	—	
2.	—	
3.	—	
4.	—	
5.	—	
6.	Anterior medial cells (cellulae anteriores)	I
7.	Anterior medial cells (cellulae anteriores)	I
8.	Dorsal lateral cells (cellulae superiores laterales)	II
9.	Ventral lateral cells (included in the cellulae superiores laterales)	IV
10.	Olfactory lobe cells (cellulae lobi olfactorii)	III
11.	Dorsal lateral cells (cellulae superiores laterales)	II
12.	Anterior medial cells (cellulae anteriores)	I
13.	Anterior medial cells (cellulae anteriores)	I
14.	Posterior lateral cells (cellulae angulares)	V
15.	Posterior lateral cells (cellulae angulares)	V
16.	Posterior medial cells (cellulae posteriores)	VI
17.	Posterior medial cells (cellulae posteriores)	VI

Appendix 2

Abbreviations used in this paper:

APPENDAGES
ANT I: antenna I
ANT II: antenna II

NERVE ROOTS
AMNv: anterior median nerve
OMNv: oculomotor nerve
A_INv: antenna I nerve
A_{II}Nv: antenna II nerve
TNv: tegumentary nerve
PMNv: posterior median nerve

NEUROPILS
L: lamina
EM: external medulla
IM: internal medulla
TM: terminal medulla
HN: hemiellipsoid body
AMPN: anterior medial protocerebral neuropil
PMPN: posterior medial protocerebral neuropil
PB: protocerebral bridge
CB: central body
ON: olfactory lobe
LAN: lateral antenna I neuropil
MAN: median antenna I neuropil
AcN: accessory lobe
DCN: deutocerebral commissure neuropil
OGTN: olfactory globular tract neuropil
AnN: antenna II neuropil
TN: tegumentary neuropil

TRACTS AND COMMISSURES
OT: optic tract
PT: protocerebral tract
OGT: olfactory globular tract
DC: deutocerebral commissure
OC: oesophageal connectives

Reference: *Biol. Bull.* **183:** 327–338. (October, 1992)

Natural Sources and Properties of Chemical Inducers Mediating Settlement of Oyster Larvae: A Re-examination

MARIO N. TAMBURRI[1,2,*], RICHARD K. ZIMMER-FAUST[1,2], AND MARK L. TAMPLIN[3]

[1]*Department of Biological Sciences, University of Alabama, Tuscaloosa, Alabama, 35487,*
[2]*Department of Biological Sciences, Marine Science Program, and Belle W. Baruch Institute for Marine and Coastal Research, University of South Carolina, Columbia, South Carolina, 29208, and*
[3]*Institute of Food and Agricultural Sciences, University of Florida, Gainesville, Florida, 32611*

Abstract. Live adult oysters and biofilms were separated experimentally as potential sources of waterborne chemical inducers of settlement in oyster larvae (*Crassostrea virginica*). Bacteria films growing on external shell surfaces were removed by mechanical agitation and chemical oxidation. This technique removed >99% of the viable bacteria without disrupting the normal production of metabolites by the oysters, measured as the weight-specific production of ammonium and dissolved organic carbon (DOC). In comparison to the external biofilms, microfloral abundances in oyster tissues and on internal shell surfaces were numerically insignificant (≤0.1% of total). Biofilms growing on aged shell material without the living oyster served as a source of bacteria metabolites. Metabolites released in particle-free, artificial seawater (ASW) medium by biofilms and by adult oysters (lacking biofilms) were tested for effects on larval behavior, relative to ASW (control). The larvae were exposed to solutions in a Plexiglas® microcosm (30 ml capacity). Locomotory responses were video recorded under infrared illumination, then subjected to computer-video motion analysis. Oyster larvae responded similarly to waterborne substances released *both* from adult conspecifics and from biofilms. The responses included: larvae rapidly swimming vertically downward in the water column; their horizontal swimming speed then slowed while their rate of turning increased, which focused activity near the bottom; and finally, the larvae contacted the bottom and attached with their foot, indicating settlement. Further analysis demonstrates that the settlement-inducing compounds of each source have a molecular weight between 500 and 1000.

Received 30 December 1991; accepted 27 July 1992.

* To whom correspondence should be addressed at Department of Biological Sciences, University of South Carolina, Columbia, South Carolina, 29208.

Introduction

Adults of most marine invertebrates reproduce sexually, by shedding gametes into the surrounding seawater where external fertilization occurs (Simpson and Beck, 1965). The embryos then develop into larvae which may spend hours to months in the water column before metamorphosing into the juvenile form. Larvae are often suspended and carried by ocean currents that serve as the agents of dispersal for parental stocks (Quayle, 1969; Roff, 1974; Hamilton and May, 1977; Palmer and Strathmann, 1981; Levin, 1984). Larval dispersal is especially important for species with sessile or sedentary adults. A vast majority of sessile marine animals, such as barnacles, oysters, tube-dwelling worms, and bryozoans produce planktonic larvae.

Colonization of benthic environments requires that larvae both settle and metamorphose. Settlement is a reversible behavioral process which includes the contact and exploration of substrates by larvae before metamorphosis. Metamorphosis is an irreversible developmental process mediating the biochemical, physiological, and morphological transformation of an individual between distinct life forms. Settlement and metamorphosis can be distinct processes and, in some cases, appear to differ in their regulatory pathways (Bonar *et al.*, 1990; Coon *et al.*, 1990a),

although the compounds that induce settlement and metamorphosis are usually identical for larvae of a given species (*e.g.*, r. ... Morse, 1990). In any event, mechanisms of ... settlement and metamorphosis must be elucidated ... the processes controlling habitat colonization ... larvae can be fully understood.

Gregarious settlement by larvae can lead to aggregations of conspecific adults (Meadows and Campbell, 1972; Burke, 1986; Gotelli, 1990). Aggregation resulting from larval settlement may be critical when the adult form is sessile or sedentary and reproduces sexually by spawning gametes into surrounding waters. In these cases, the hydrodynamical properties of turbulent-flowing water tend to dilute and disperse gametes after release. This dilution decreases the likelihood of fusion between egg and sperm, a consequence similar to that of increasing distance between spawning individuals of opposite sexes (Pennington, 1985; Grosberg, 1987; Denny and Shibata, 1989; Levitan, 1991). In addition to improving reproductive success (Knight-Jones and Stevenson, 1950; Crisp, 1979), gregarious settlement that leads to aggregation among juvenile and adult conspecifics may increase protection from predation (Sebens, 1983; Keough, 1984), competitive ability (Buss, 1981), and filter-feeding efficiency (Hughes, 1978), while also reducing juvenile and adult mortality (Knight-Jones, 1951; Buss, 1979; Highsmith, 1982; Young, 1983). Since gregariousness is critical for many sessile and sedentary species, specific traits that promote the active selection of settlement sites by larvae should be expected.

Gregarious settlement is believed to occur in response to chemical cues emitted by adult conspecifics (see reviews by Crisp, 1974; Burke, 1986; Pawlik and Hadfield, 1990). Considerable progress in identifying chemical cues has been made in some cases (*e.g.*, Pawlik and Faulkner, 1986; Jensen and Morse, 1990), although substances mediating gregarious settlement have yet to be completely isolated and fully characterized. Since Cole and Knight-Jones (1939) first described gregarious larval settlement and metamorphosis in oysters, there has been debate about the sources of settlement-inducing compounds. Two schools of thought have emerged: one points to juvenile and adult oysters (Walne, 1966; Bayne, 1969; Hidu, 1969; Keck *et al.*, 1971; Veitch and Hidu, 1971; Hidu *et al.*, 1978); whereas the other finds that biofilms on oyster shell surfaces (Bonar *et al.*, 1986, Fitt *et al.*, 1989, 1990; Weiner *et al.*, 1989) are the source of inducer molecules. These contrasting viewpoints may result from differences in experimental approach. Significantly, the effects of substances released by live adult oysters and by biofilms have never been separately assayed in a single study.

We have now quantified larval responses to waterborne substances released by each source. Our results show that: (1) settlement inducers are produced both by oysters and biofilms, (2) larval settlement behavior in response to inducers from each source is essentially identical, and (3) the settlement inducers liberated by both sources have a molecular weight between 500 and 1000.

Materials and Methods

Larval cultures

Twelve day old larvae, raised from Chesapeake Bay oysters and spawned at the Virginia Institute of Marine Science, were shipped via overnight courier to our laboratory. They were maintained at 0.5 to 1.0 larvae/ml in a 1:1 mixture of oceanic and artificial seawater at 25 ppt salinity, pH 8.0, in a 25°C incubator with a 12:12 dark: light cycle (light on: 0700 h). Prior to use, the culture media was filtered to 0.22 μm and autoclaved for 15 min at 150°C and 15 psi. Cultures were aerated actively by air bubbled through Pasteur pipettes. The culture medium was changed daily to preclude the build-up of pathogenic bacteria (Loosanoff and Davis, 1963), and marine diatoms (*Isochrysis galbana* and *Pavlova lutheri*) were provided as food, at 2.5×10^4 cells/ml, once each day.

Oyster larvae are typically >250 μm in length and have pigmented eye spots when competent to settle and metamorphose (Galtsoff, 1964; Coon *et al.*, 1990a). Experiments were begun within 6 h after 100% of the larvae in a culture had developed eyes, and experiments were run for 24 h thereafter. The mean length of larvae tested was 310 μm ($\pm$11 μm SD).

Summary of experimental procedure

Due to the complexity of the protocol, the following brief overview is provided so that the various specific methods outlined later can be kept in perspective. Nine solutions (including controls) were prepared to isolate substances released by adult oysters, biofilms, and empty oyster shells (called 'cultch'). The ammonium and dissolved organic carbon (DOC) in each solution were measured as an indication of general metabolite levels.

Methods were developed for removing the bacterial films covering the outer surface of adult oysters and shell cultch. We focused on eliminating external biofilms because the microflora inside of oysters was numerically insignificant in comparison. The total number of bacteria in oyster tissues, on inner shell surfaces, and released into bath solutions during incubations of oysters were measured, and found to be $\leq$0.1% of the total on the external shell surfaces. The internal microflora are therefore not discussed further in this report; these data are available from M. N. Tamburri on request.

Oysters with their external biofilms removed served principally as a source of oyster metabolites. Biofilms growing either on live oysters that were clamped shut, or

Table I

Schematic representation of methods used to treat live oysters during the preparation of bath-water solutions for experiment I

Live oysters	Treatment: Clamps	Treatment: Scrub and chemical oxidation	Sources of dissolved compounds	Abbreviation
Test solutions				
(+)	(−)	(−)	Oyster + Biofilm + Shell	OBS
		(+)	Oyster + Shell	OS
	(+)	(−)	Biofilm + Shell	BS1
		(+)	Shell	S1
Control solutions				
(−)	(+)	(−)	Clamp	CC
	(−)	(−)	None	SWC1

(+) Indicates the presence of oysters or use of treatment; (−) indicates the absence of oysters or omission of treatment.

on aged shell cultch, served as a source of biofilm metabolites. The oysters were shut with C-clamps wrapped in sterile polyethylene. Epifluorescence microscopy, Most Probable Number (MPN) analysis, and direct plate counts were used to enumerate the bacterial densities found in biofilms, and to estimate the effectiveness of our biofilm removal technique.

The locomotory responses of larvae to test and control solutions were subjected to computer-video motion analysis. Settlement behavior was characterized as: downward movement, slowed swimming speed with increased horizontal turning near the bottom, and finally, contact with and attachment to the bottom. The solutions that induced oyster larvae to settle were serially diluted so that the relationship between inducer dose and larval behavior could be determined. In addition, solutions causing settlement of larvae were fractionated by molecular weight as a first step in the characterization and identification of the inducers. Specific methods used in our study are described in detail below.

Preparation of solutions

Live oysters and shell cultch were collected from reefs in Portersville Bay, Alabama, in May, 1990. These materials were transported to our laboratory at Dauphin Island, Alabama, in aerated seawater in polyethylene containers. The methods used in preparing solutions are shown schematically in Tables I and II. Test solutions were made by bathing either six oysters or six shells, for 4 h, in 4 l of sterile ASW held at the same temperature (27°C), salinity (17 ppt), pH (7.8), and dissolved oxygen (6.8 mg/l) as seawater at the collection site. Each group of oysters had a total wet tissue weight of 200 ± 18 gm, and a total shell surface area of 700–800 cm^2. After the 4 h bath, we removed the oysters or shells and adjusted the pH to 8.0 with 1 *M* NaOH, and the salinity to 25 ppt; these conditions are the same as those of the larval culture medium. The solutions were filtered to 0.22 μm, divided into 25 ml aliquots, and frozen at −87°C until used in experiments. All lab wares were sterilized before use, either by autoclaving (15 psi, 150°C, 15 min) or, when auto-

Table II

Schematic representation of methods used to treat oyster shell cultch during the preparation of bath-water solutions for experiment II

Shell cultch	Treatment: Scrub and chemical oxidation	Sources of dissolved compounds	Abbreviation
Test solutions			
(+)	(−)	Biofilm + Shell	BS2
	(+)	Shell	S2
Control solutions			
(−)	(−)	None	SWC1

(+) Indicates the presence of cultch or use of treatment; (−) indicates the absence of cultch or omission of treatment.

claving was impossible by rinsing with 70% isopropyl alcohol.

Our first experiment tested the capacity of solutions, prepared with adult oysters, to induce settlement of oyster larvae (Table I). Our second experiment tested the larval response to solutions containing compounds released only by biofilms and oyster shell material (Table II), and thus enlarged on the results of the first experiment.

Larval behavioral assays

Two to three hours before testing, the larvae were gently filtered from the culture media, rinsed, then placed at 0.5 larvae/ml in a separate container of ASW (25 ppt). This procedure removed the oyster larvae from their microalgal food, the exudates of which are known to influence the locomotory behavior (Zimmer-Faust and Tamburri, pers. obs.). Sixty larvae (±2) were then transferred, in 5 ml ASW, into a Plexiglas® microcosm (3 cm long × 3 cm wide × 4 cm high) containing 25 ml of a test or control solution. The solution containing the larvae was gently stirred for 5 s, then held briefly until the fluid came to rest. The microcosm was next placed into a darkened chamber at 25°C, where the larval movements were recorded on video tape. The chamber was illuminated with an infrared light source (>820 nm) oriented 90° to the axis of the video field. The use of infrared light was required because oyster larvae exhibit phototactic responses to visible wavelengths (Smith and Chanley, 1975). The larvae were taped with a Sony infrared-sensitive video camera (Model HVM-200) equipped with a Tamron 180 mm macrofocal lens. Video records made with a Panasonic (Model AG-6300) video cassette recorder, were stored on magnetic tape, and viewed with a Panasonic (Model TR-124MA) monitor.

During the experiments, we recorded the paths made by larvae as they: (1) swam vertically in the water column, and (2) swam horizontally near, then contacted the bottom. Eight replicate trials were run for each solution and recording position. Behavior was monitored during the initial 3 min of exposure, corresponding to the period of the maximum larval settlement response (Zimmer-Faust and Tamburri, pers. obs.). The order of test and control solutions was determined with a random numbers table, subject to the constraints that: each solution was presented in every block of nine trials; and no single solution was ever tested twice in succession. Individual larvae were tested only once, then discarded.

Vertical swimming in the water column. The video camera was mounted at the side of the microcosm to observe larvae swimming vertically, 1.5 cm (40–50 body lengths) above the bottom. The size of the viewing field was 6.9 mm × 6.8 mm, with a 1.5 mm depth. We programmed a computer-video motion analyzer to count the larvae moving vertically upward and downward across the viewing field. The number of larvae swimming downward was subtracted from the number swimming upward through the plane per unit time, giving a quantitative measure of net vertical flux. A negative value is net downward movement, while a positive value is net upward movement.

Horizontal swimming near, and settlement on bottom. The camera was mounted beneath the microcosm to view larvae as they swam in a horizontal plane (6.75 mm × 6.70 mm) at a distance, ≤1.2 mm (≈4 body lengths) above the bottom. Swimming paths were recorded and then subjected to computer-video motion analysis. We counted only those larvae that attached with the foot to the bottom during the observation period as a measure of settlement.

Computer-video motion analysis of larval responses to test and control solutions. We quantified swimming speed and turning behavior by replaying each video tape through a computer-video motion analysis system (Motion Analysis Corp., Model VP 110 and Expertvision software package) interfaced with an Amdek 386 microcomputer. The video sampling rate of the motion analysis hardware was set at 15 frames/s. Analysis of larval behavior consisted of determining swimming speed, net-to-gross displacement ratio (NGDR), rate of change in direction (RCDI), and path duration, for each swimming path. The RCDI is the angle turned per unit time, measured in degree/s. The NGDR is the ratio of the linear distance between the starting and ending points (net distance) and the total distance traversed by the path (gross distance). The NGDR measures the tendency of paths to be circular or twisted and reaches a minimum value of zero for looping or circular paths that have their origin and endpoint at the same spatial coordinates. An NGDR of 1.0 defines a completely straight path.

Data for all paths were pooled across trials for each test or control treatment. The effect of treatments was first assessed using ANOVA. Groups of treatment means were then compared using either *t*-tests or Student-Newman-Keuls multiple range comparisons (SNK). We used an experiment-wise error rate of $\alpha = 0.05$ to determine when comparisons were significantly different.

Initial characterization of settlement inducer

Dose-response curves. Experiments were performed to determine the magnitude of the larval responses to a dilution series of each solution causing settlement. The active solutions were diluted with ASW to 0.31×, 0.1×, 0.031×, and 0.01× their original concentrations. We also tested larval responses to a concentration series of ammonium chloride (pH 8.0), prepared with ASW at 10^{-4} to 3×10^{-7} *M*. Five trials were performed for each solution and concentration. The order of testing was randomized with the constraints described above.

Molecular weight fractionations. Each bath solution that caused settlement was tested both without being fractionated, and after fractionation according to molecular weight. Fractions were prepared by cascading ultrafiltration using a pressure vessel (Amicon Model 8400) and dialysis membranes with cutoffs of <10,000 (Amicon YM10), <1000 (Amicon YM1), and <500 (Amicon YC05) daltons. Ultrafiltrations were performed under a nitrogen atmosphere at 50 psi and 2°C. Five trials were conducted of each solution and ASW, and the order of testing was randomized.

Chemical determinations of metabolite levels

Ammonium and dissolved organic carbon (DOC) were measured to indicate the general metabolite levels of each solution (see Hammen *et al.*, 1966; Srna and Baggaley, 1976; Dame *et al.*, 1989). Ammonium determinations were made with an Alpkem (Model RFA/2) nutrient autoanalyzer, while DOC was measured with a Shimadzu (Model TOC-5000) total organic carbon analyzer.

Methods used in removing biofilms

Microflora were removed from the outer surfaces of cultch and live oyster shells by first vigorously scrubbing with a soft plastic bristle brush to manually dislodge most of the biofilm material. The oysters and cultch then were bathed in 2.5% sodium hypochlorite (NaOCl, Sigma Chemical Co., reagent-grade) for 5 min, which oxidized and further removed microorganisms from the shell surfaces. After the 5 min, each item was removed from the NaOCl and rinsed ten times with 200 ml of sterile ASW. The treated shells were bathed in 1 l of sterile ASW for 5 min, followed by a second set of ten rinses. Living oysters, with shells mechanically and chemically treated, resumed pumping within minutes of being returned to seawater medium.

As a precaution, we performed chemical assays to test that the final rinse waters were free of NaOCl. Rinse waters were analyzed colorimetrically for total chlorine according to the DPD method with N,N-diethyl-p-phenylenediamine reagent. A Hach spectrophotometer (Model DR 2000) was used to measure peak absorbence at 445 nm. Because final rinse waters and ASW both had identical chlorine levels (=2 μg/l), we conclude that the rinses removed all traces of NaOCl.

Microbiological determinations of external biofilms

A series of microbial techniques was used to determine the densities and taxonomic classifications of bacteria found on oyster shells, and to determine the effectiveness of the procedures used to remove biofilms. Three adult oysters and three cultch shells were treated to remove external biofilms through scrubbing and chemical oxidation (see above procedures). These items were then scrubbed for an additional 3 min, with a sterile brush, so that remaining biofilm materials were dislodged and collected in separate beakers each containing 400 ml phosphate buffered saline (PBS). The contents of each beaker were stirred, and four aliquots of 100 ml were then withdrawn. The bacteria in three of the aliquots were enumerated by epifluorescence microscopy, Most Probable Number (MPN) test, and direct plate counts. The numerically dominant bacteria in the fourth aliquot were classified taxonomically.

As a reference for comparison, we repeated the above procedures for an additional three adult oysters and three cultch shells, but with one exception. Shell surfaces were not mechanically and chemically treated initially to remove biofilms. This second group served as a standard by which to determine the effectiveness of scrubbing and chemical oxidation in removing biofilms from the surfaces of shells in the first group, and to identify the dominant bacteria in natural biofilms.

Epifluorescence microscopy. A 5-ml sample of each aliquot was diluted 100-fold with PBS, then 0.01% acridine orange (w/w) was added to stain bacteria cells (Hobbie *et al.*, 1974). We withdrew three 1 ml sub-samples from each of the diluted samples and filtered these separately onto Nucleopore membranes (0.22 μm pore size). The filters containing the stained bacteria were viewed through a fluorescence microscope (Zeiss, Model 47-30-28) and bacteria cells were enumerated according to the procedures of Hobbie *et al.* (1974).

Most Probable Number (MPN). A 10-ml sample of each aliquot was serially diluted ten-fold, 10^1 to 10^5, with PBS. Three, 1 ml sub-samples were then withdrawn from each of the dilutions and added separately to culture tubes, each containing 9 ml alkaline peptone broth. The tubes were incubated for 16 h at 35°C, after which turbidity and MPN estimates of bacteria were determined for each solution.

Direct plate counts. A 1-ml sample of each aliquot was diluted 100-fold with PBS. Three, 100 μl sub-samples were then withdrawn from each of the samples and spread separately on tryptic soy agar plates (TSA, +1% NaCl, Difco Corp.). The plates were incubated for 24 h at 35°C, after which individual colonies were counted.

Identification of dominant bacteria. A 1-ml sample of each aliquot was diluted 100-fold with PBS. Five 100 μl sub-samples of each aliquot were spread separately on replicate TSA plates. The plates were incubated for 24 h at 35°C, after which individual colonies were counted. Bacteria from each colony were then isolated by streaking on separate new TSA plates. These plates were next cultured for 24 h at 35°C. The isolated bacterial colonies were classified to at least the level of Family, by applying

Table III

Mean ammonium [illegible] determined from triplicate assays of bath-waters [illegible] presence of oysters (O), biofilms (B), and shell [illegible] -waters with only clamps (CC) or seawat[illegible] SWC) were controls

Experiment	Source*	NH_4 (μM)
I	OBS	31.0
	OS	17.5
	BS1	8.7
	S1	0.5
	CC	0.3
	SWC1	0.3
II	BS2	9.1
	S2	0.7
	SWC2	0.4

* The sources of dissolved compounds in these solutions are explained in Tables I and II.

the 23 biochemical analyses of the API 20E system (Analytab, Inc.).

Results

Chemical determinations of metabolites

Concentrations of ammonium in the prepared solutions were between 0.3 and 31.0 μM (Table III), while the dissolved organic carbon concentrations varied from 1.4 to 6.1 mg/l. These values are typical of levels reported for estuarine waters above oyster reefs (Stevens, 1983; Dame *et al.*, 1989; Zimmer-Faust and Tamburri, unpubl. data). Ammonium levels in the OBS, OS, BS1, and BS2 solutions were elevated above concentrations in the seawater control solutions (SWC1 and SWC2), indicating presence of dissolved metabolites, while ammonium levels measured in S1, S2, and CC solutions were nearly identical to the seawater controls, showing an absence of metabolite release. (Abbreviations are fully described in Tables I and II; briefly: O = oyster, B = biofilm, S = shell, and CC and SWC are clamp and seawater controls).

The concentrations of ammonium in the nine test and control solutions (Table III) demonstrate that the techniques used in preparing bath waters resulted in metabolite levels that differed in the expected manner. First, the biofilm removal technique was effective in reducing the amount of metabolites in the OS solution, and in eliminating metabolites in the S1 and S2 solutions. Though still elevated above SWC1, OS contained about half the ammonium as the OBS solution, while ammonium concentrations in S1, S2, SWC1, and SWC2 were essentially identical (all between 0.3 and 0.7 μM). Second, the clamp technique prevented the release of oyster metabolites. This conclusion is supported by our finding that ammonium concentration in BS1 (8.7 μM) was far less than that of the OBS solution (31.0 μM), and nearly identical to the concentration in the BS2 solution (9.1 μM). Third, the techniques of biofilm removal and clamping did not seem to affect metabolite production of the target source, oysters and biofilms, respectively. When ammonium concentrations of OS (17.5 μM) and BS1 (or BS2) solutions are added together, the total concentration of ammonium is similar to the level found in the OBS (31.0 μM) solution.

Microbial determinations

The density of bacteria (cells/cm^2) on external shell surfaces of live oysters and cultch were nearly identical (Table IV). In both cases, 70–75% of the bacteria were in the families Vibrionaceae and Pseudomonadaceae or in the genus *Flavobacteria*. When comparing external oyster shell surfaces, before and after treatment to remove biofilms, most probable numbers (MPN), and direct plate counts reveal a >99% reduction in the total number of viable bacteria (Table IV). The bacterial counts, under epifluorescence microscopy, of treated versus untreated oyster shells show a >90% reduction in bacteria cells. Be-

Table IV

Mean (±SEM) densities of bacteria (No./cm^2) occurring on shell surfaces of living oysters and cultch. Bacteria were counted on shell surfaces with, and without, treatment to remove bacteria biofilms

Experiment and source	Treatment	Most probable number (viable bacteria)	Direct plant count (viable bacteria)	Epifluorescence microscopy (total bacteria)*
I Oysters	Biofilms intact (untreated)	7.9×10^7	$3.1\ (\pm 0.1) \times 10^7$	$6.9\ (\pm 0.7) \times 10^6$
	Biofilms removed (treated)	1.4×10^3	$1.4\ (\pm 0.1) \times 10^3$	$5.9\ (\pm 0.7) \times 10^5$
	Mean % reduction	>99.9	>99.9	91.5
II Cultch	Biofilms intact (untreated)	1.1×10^7	$2.3\ (\pm 0.1) \times 10^7$	$9.1\ (\pm 0.8) \times 10^6$
	Biofilms removed (treated)	9.3×10^3	$1.9\ (\pm 0.1) \times 10^3$	$3.5\ (\pm 0.6) \times 10^5$
	Mean % reduction	>99.9	>99.9	96.2

* Total bacteria includes both living and dead cells.

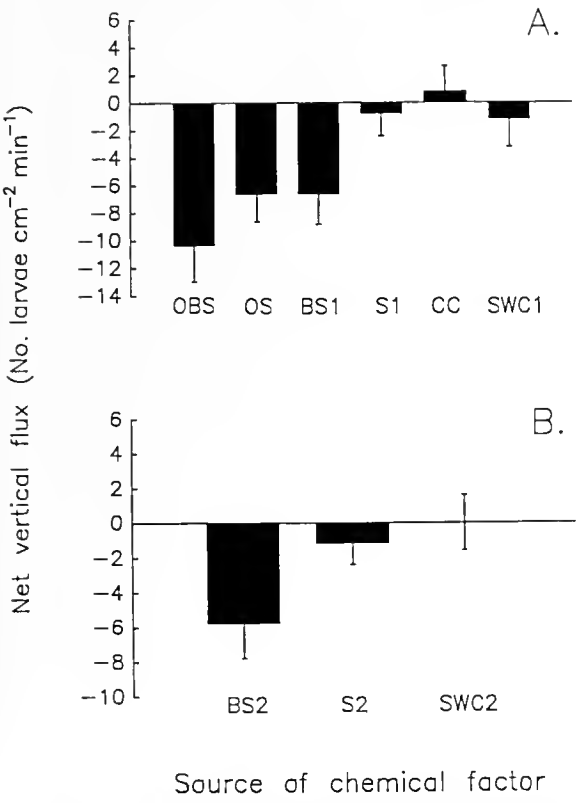

Figure 1A, B. Mean (±SEM) net vertical fluxes of oyster larvae swimming in the water column of the microcosm. Positive values indicate upward transport, while negative values indicate downward transport. The rank order of downward flux in response to solutions is: OBS > OS = BS1 = BS2 > S1 = S2 = CC = SWC1 = SWC2 (Student-Newman-Keuls multiple range comparison: $F = 9.53$; d.f. = 8, 63; $P < 0.0001$). The equal sign (=) designates vertical fluxes that are not significantly different. Abbreviations: oyster (O), biofilm (B), shell material (S), clamp control (CC), and seawater control (SWC).

cause epifluorescence microscopy estimates total bacteria, both living and dead, elevated levels in the treated groups are most likely due to the incorporation of dead cells in the counts.

Larval settlement behavior

The oyster larvae responded to waterborne compounds in the OBS, OS, BS1, and BS2 solutions in a manner indicative of settlement behavior. Larvae swimming in the water column rapidly (within the first 3 min) moved downward when exposed to the OBS, OS, and both BS solutions (Fig. 1). Response to the OBS solution was the largest, showing a significantly greater net downward flux of larvae than to either OS or BS solutions. There was no significant downward movement in response to any other solutions. When exposed to seawater controls (SWC1 and SWC2), larvae exhibited no net vertical movement (−1.00 ± 1.45 SEM and 0.00 ± 1.55 SEM). Larval responses to

Table V

Mean (±SEM) swimming speed of larvae in test and control solutions

Experiment	Solution*	Speed (mm/s)		# of paths analyzed
I	OBS	0.45 ± 0.03	A	71
	OS	0.55 ± 0.04	A	47
	BS1	0.51 ± 0.05	A	41
	S1	0.88 ± 0.05	B	16
	CC	0.93 ± 0.06	B	29
	SWC1	1.03 ± 0.09	B	24
II	BS2	0.51 ± 0.03	A	43
	S2	1.05 ± 0.06	B	25
	SWC2	1.02 ± 0.06	B	18

* Abbreviations: oyster (O), biofilm (B), shell material (S), clamp control (CC), and seawater control (SWC).

Capital letters designate speeds that are not significantly different (Student-Newman-Keuls multiple range comparison: $F = 23.47$; d.f. = 8,305; $P < 0.0001$).

substances released by shells alone (S1 and S2) and clamps (CC), were not significantly different than the responses seen in SWC's.

Larvae also altered their swimming behavior in response to the OBS, OS, and BS solutions, and tended to focus their activity near the bottom. Larvae decreased their swimming speeds (Table V), and they modified their path trajectories as expressed by decreasing NGDRs (Table VI), increasing RCDIs (Table VII), and increasing path durations (Table VIII).

Finally, significantly more larvae attached (with their foot) to the bottom of the microcosm in response to the

Table VI

Mean (±SEM) net-to-gross displacement ratio (NGDR) of larvae swimming in test and control solutions

Experiment	Solution*	NGDR		# of paths analyzed
I	OBS	0.61 ± 0.03	A	71
	OS	0.64 ± 0.03	A	47
	BS1	0.63 ± 0.04	A	41
	S1	0.87 ± 0.05	B	16
	CC	0.85 ± 0.03	B	29
	SWC1	0.82 ± 0.09	B	24
II	BS2	0.62 ± 0.03	A	43
	S2	0.84 ± 0.03	B	25
	SWC2	0.83 ± 0.04	B	18

* Abbreviations: oyster (O), biofilm (B), shell material (S), clamp control (CC), and seawater control (SWC).

Capital letters designate NGDRs that are not significantly different (Student-Newman-Keuls multiple range comparison: $F = 6.91$; d.f. = 8,305; $P < 0.0001$).

Table VII

Mean (±SEM) r… …irection (RCDI) of larvae swimming in test and co…

Experi…	…ution*	RCDI (°/s)		# of paths analyzed
I	OBS	99.77 ± 7.57	A	71
	OS	71.58 ± 6.58	B	47
	BS1	77.19 ± 8.65	B	41
	S1	43.36 ± 7.61	C	16
	CC	58.65 ± 5.85	C	29
	SWC1	51.42 ± 6.20	C	24
II	BS2	65.91 ± 5.15	B	43
	S2	53.83 ± 6.01	C	25
	SWC2	47.52 ± 4.61	C	18

* Abbreviations: oyster (O), biofilm (B), shell material (S), clamp control (CC), and seawater control (SWC).

Capital letters designate RCDIs that are not significantly different (Student-Newman-Keuls multiple range comparison: $F = 6.09$; d.f. = 8,305; $P < 0.0001$).

OBS, OS, and both BS solutions (Fig. 2). The greatest number of settlers were responding to OBS, significantly more than all other solutions. In contrast, when larvae were exposed to S1, S2, and CC solutions, the number of individuals attaching to the substrate was the same as the number settling in the SWC solutions.

In summary, oyster larvae responded to substances in the OBS, OS, and both BS solutions by moving rapidly downward in the water column, by focusing activity near the bottom (by slowing their swimming speed while turning more often), and finally, by increasing their contact and attachment to the substrate.

Initial characterization of settlement inducer

The above behavioral assays indicate that OBS, OS, BS1, and BS2 solutions all contained waterborne settlement factors. Further experiments were conducted with OBS, OS, and BS1 solutions to determine the dose-response relationships, and the molecular weights of settlement inducers. Data are reported only for the number of larvae that attached to the bottom during the observation period, thus simplifying our presentation of results.

Dose-response. Dose-response functions for each solution are expressed as the magnitude of settlement relative to ammonium concentration (Fig. 3). We chose ammonium as the standard, because: (1) it is the principal nitrogen metabolite produced by marine heterotrophic organisms, and (2) it is reported to induce settlement when in the un-ionized form (Coon *et al.*, 1990b). The OBS solution continued to induce significant settlement behavior when diluted 0.031-times its original concentration (0.9 μM ammonium) (Student's t-test: $t = 12.26$, d.f. = 8, $P < 0.001$). Both OS and BS1 solutions were similarly effective when diluted to 0.10-times their original concentrations (0.9 and 1.8 μM ammonium, respectively) (t-test: $t \geq 10.65$, d.f. = 8, $P < 0.001$, both comparisons). In contrast, larvae did not settle at rates significantly higher than seawater control (SWC1) in response to any test concentration of ammonium chloride.

Each dose-response curve was analyzed according to a non-linear regression model, assuming a hyperbolic relationship between concentration of the ammonium standard and the magnitude of settlement response (Statistical Analysis Systems, Carey, North Carolina, SAS version 6; also see theoretical arguments of Beidler, 1954; Maes, 1984). The curves generated for OBS, OS, and BS1 solutions all produced highly significant fits to the model (F-test: $F \geq 28.22$; d.f. = 2, 17; $P < 0.001$, all comparisons). Asymptotes and slopes of curves generated in response to OS and BS1 solutions were identical (t-tests: $P > 0.50$, both comparisons). However, there was a significant difference in the asymptotes between the dose-response curves describing settlement in response to OBS and either OS or BS1 solutions (t-tests: $P < 0.01$, both comparisons), but not in the slopes (t-test: $P > 0.05$, both comparisons).

Molecular weight fractionations. Compared with the seawater control (SWC1) larval settlement was significantly elevated in the <10,000 and <1000 molecular-weight fractions of OBS, OS, and BS1 solutions (SNK: critical range ≥ 1.201, $P < 0.01$) (Fig. 4). Levels of response were the same for these fractions and for solutions tested without fractionation (SNK: critical range ≥ 1.197, $P > 0.20$). The larvae did not settle at levels elevated from SWC1, when exposed to the <500 molecular-weight frac-

Table VIII

Mean (±SEM) path duration of larvae swimming in test and control solutions

Experiment	Solution*	Duration (s)		# of paths analyzed
I	OBS	8.45 ± 1.19	A	71
	OS	6.91 ± 0.65	B	47
	BS1	7.26 ± 0.80	B	41
	S1	4.19 ± 0.50	C	16
	CC	3.85 ± 0.31	C	29
	SWC1	4.05 ± 0.36	C	24
II	BS2	8.39 ± 0.89	A	43
	S2	4.20 ± 0.44	C	25
	SWC2	4.18 ± 0.48	C	18

* Abbreviations: oyster (O), biofilm (B), shell material (S), clamp control (CC), and seawater control (SWC).

Capital letters designate path durations that are not significantly different (Student-Newman-Keuls multiple range comparison: $F = 20.73$; d.f. = 8,305; $P < 0.0001$).

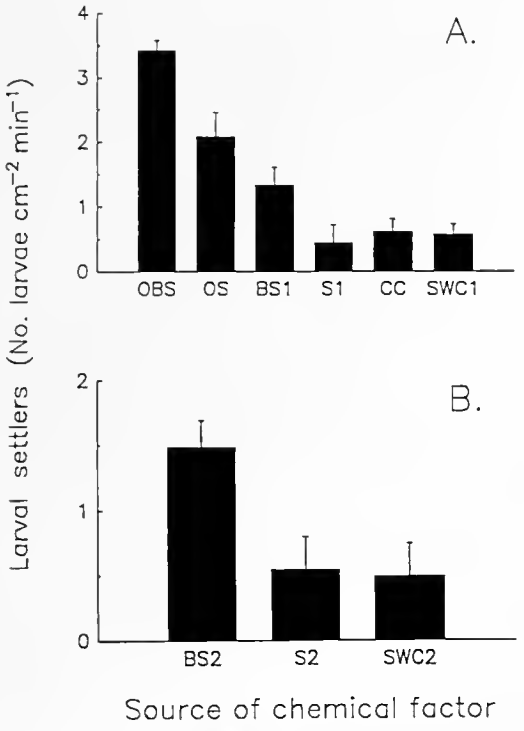

Figure 2A, B. Mean (±SEM) settlement rates of oyster larvae. The ranked order of settlement in response to solutions is: OBS > OS = BS1 = BS2 > S1 = S2 = SWC1 = SWC2 (Student-Newman-Keuls multiple range comparison: $F = 20.43$; d.f. = 8, 63; $P < 0.0001$). The equal sign (=) designates settlement rates which are not significantly different. Abbreviations: oyster (O), biofilm (B), shell material (S), clamp control (CC), and seawater control (SWC).

tions (SNK: critical range ≥ 0.981, $P > 0.20$). Consequently, the data indicate that the settlement inducers in each solution (OBS, OS, and BS1) have molecular weights between 500 and 1000 daltons.

Discussion

Ever since Cole and Knight-Jones (1939) first described the gregarious nature of larval settlement in oysters, there has been debate about the sources of chemical inducers. Two schools of thought have emerged: one reports juvenile and adult oysters to be the source of inducers, whereas the other finds the source in biofilms (references in Introduction). Our results suggest that these contrasting viewpoints have resulted largely from differences in experimental approach. In this study we have separated both proposed sources of settlement inducers by preparing and testing solutions that contain compounds released either by oyster or by their external biofilms. We report here that *both* sources produce waterborne substances rapidly provoking larval settlement.

The small size of oyster larvae (250–350 μm), and their sensitivity to handling, made them difficult subjects for

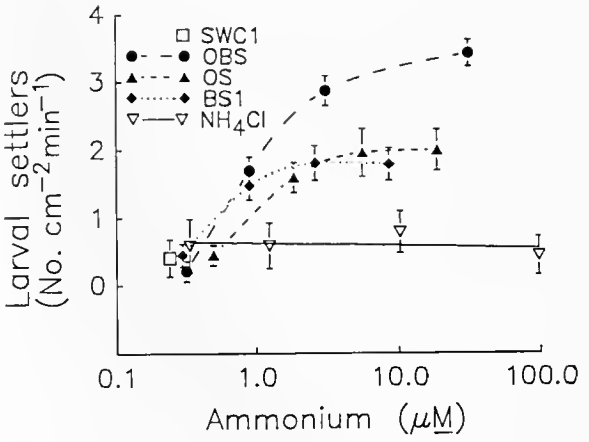

Figure 3. Dose-responses of oyster larvae to serial dilutions of OBS, OS, BS1, and ammonium chloride (NH_4Cl) solutions, relative to seawater control (SWC1). Responses are expressed as mean (±SEM) settlement rates; dosages are expressed in ammonium concentrations. Abbreviations: oyster (O), biofilm (B), and shell material (S).

experimental analysis. We overcame these difficulties by applying computer-video motion analysis to non-invasively track the paths made by individual larvae as they swam in the water column or crawled on the substrate. We found this technology to be indispensable to the study of larval behavior, because: (1) experimental chambers having large volumes (*e.g.*, 30–5000 ml; Zimmer-Faust, 1990; Weissburg and Zimmer-Faust, 1991; present study) can be used, which do not impede locomotory behavior, (2) locomotory paths can be tracked for many individual larvae simultaneously, and (3) data can be collected rapidly and in sufficient quantities from larvae held at low densities (1 or 2/ml), thereby avoiding interactions between larvas and density-dependent effects.

We isolated the oyster metabolites (from biofilm metabolites) during the preparation of the OS solution by

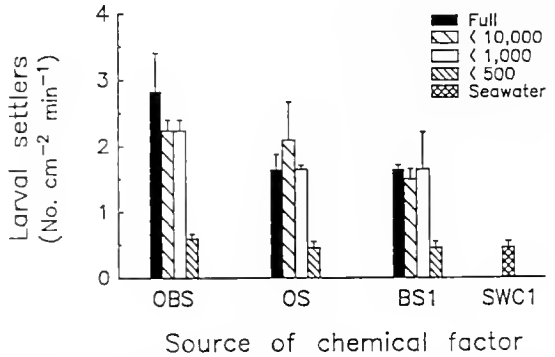

Figure 4. Mean (±SEM) settlement rates of larvae in response to seawater control (SWC1), and to OBS, OS, and BS1 solutions tested without fractionation (Full), and after fractionation by molecular weight to <10,000, <1000, and <500 daltons. Abbreviations: oyster (O), biofilm (B), and shell material (S).

minimizing the amount of biofilm organisms on the outer shell surfaces. Our efforts were focused on eliminating external biofilm bacteria in oyster tissues, on internal shell surfaces, and released during incubations of oysters were numerically insignificant (≤0.1%) compared with the total on external shell surfaces. Not only was there a >99% reduction in total viable bacteria after treatment to remove external biofilms, but there was also a large reduction in ammonium levels in the OS solution relative to the OBS solution. Significantly more larvae settled in response to the OS solution than in response to SWC1, but the reduction of metabolites in the OS solution coincided with a significant (≈2-fold) decrease in larval settlement response when compared to the OBS solution.

Biofilm metabolites were collected for assay by minimizing, or eliminating, the influence of live oysters in preparing the BS solutions. Both solutions (BS1 and BS2) induced significant settlement activity, although not to the same extent as the OBS solution. The reduction in settlement activity in BS1 and BS2 corresponded to a reduction in ammonium and DOC levels (relative to the OBS), yet the concentrations were almost identical in BS1 and BS2. These results indicate: (1) that the clamping technique is effective in preventing the oysters from releasing significant levels of metabolites in the BS1 solution, and (2) clamped oysters (BS1) and shell cultch with intact biofilms (BS2) both release substances evoking settlement. This second point clearly demonstrates that biofilms are producers of chemicals inducing oyster larval settlement.

The potential influence of the shell material itself was never completely isolated from oyster and biofilm (OBS, OS, BS1, and BS2). Nevertheless, both solutions prepared with shells alone (S1 and S2) had ammonium concentrations equal to seawater controls (SWC1 and SWC2). Because neither S1 nor S2 induced larvae to settle, the effect of shell material was negligible. We admit the technique used to remove biofilms was imperfect, because some cracks or crevices harboring pockets of viable bacteria probably went undetected. Still, the absence of settlement responses by larvae to S1 and S2 argues that sufficient amounts of bacterial biofilms were removed, so if inducers were produced, their levels were below the threshold for settlement.

Larvae responded similarly to oyster and biofilm metabolites by swimming actively downward to the bottom of the test chambers. Once near the bottom (within four larval body lengths), they decreased their swimming speed and net-to-gross displacement (NGDR), while they increasing their rate of turning (RCDI) in the horizontal plane. These changes in swimming near the bottom are consistent with site-restricted search (*e.g.*, see references on zooplankton by Buskey, 1984; Buskey and Stoecker, 1989; Weissburg and Zimmer-Faust, 1991). Clearly, increased turning may facilitate 'search' for specific microsites, because turning causes larvae to loop back focusing locomotory activity within a small area (*e.g.*, Koopman, 1980). The longer mean durations of paths recorded as larvae swam near the bottom in response to OBS, OS, BS1, and BS2 support this conclusion (Table VIII). The larvae tended to concentrate their swimming activities within an area the size of our viewing field (6.75 mm × 6.70 mm), or smaller. Larvae also attached with their foot and crawled on the bottom, clearly indicating a settlement response.

We have previously assayed behavior of larvae produced by Chesapeake Bay and Galveston Bay oysters. Oyster populations in these two regions are of different physiological strains (Groue and Lester, 1982; Buroker, 1983; King and Gray, 1989). Yet, the responses to oyster metabolites exhibited by larvae of both populations were the same (Zimmer-Faust and Tamburri, in prep.). Our current investigation shows that larvae behave in identical fashion to chemical factors released independently by adult oysters and by biofilms. Consequently, the sequence of behaviors in settlement is genetically conserved and appears stereotyped in response to chemical stimuli produced by both sources.

The molecular structures of compounds inducing settlement remain unresolved. Soluble bacterial metabolites ≤ 300 daltons, and ammonia, are proposed to elicit settlement responses (Fitt *et al.*, 1989, 1990; Coon *et al.*, 1990b). Our data seem to be in contrast with this hypothesis, because in each case fractions prepared at <500 daltons were ineffective as settlement stimuli. In fact, solutions of ammonium chloride did not induce settlement responses at concentrations tested in this study. The threshold for settlement induction by ammonium chloride (at pH 8.0) is 2.5 m*M* (Coon *et al.*, 1990b), a concentration 100-times higher than those in OBS, OS, and BS1 solutions maximally stimulatory to settlement in our dose-response experiments.

Additional investigation is needed to further identify the structures of settlement inducers. The narrow range of molecular weights of compounds stimulatory to settlement (500–1000 daltons), and the marked similarity between dose response curves for OS and BS1 solutions, argue for production of the same factors by both oysters and biofilms. Alternatively, we found the asymptote of the dose—response curve for the combined source (OBS) to be significantly higher than that for the dose—response to either single source, OS, and BS1. This difference between asymptotes suggests that each source might produce distinct inducers, differing in structure, yet acting together synergistically when combined in mixtures.

Acknowledgments

The authors express their sincere gratitude to Drs. M. J. Weissburg, J. R. Pennock, and J. M. Ward for

assistance on every aspect of this project. We are also grateful to Mr. K. Kurkowski for generously providing larvae and to Dr. D. R. Fielder for splendid editorial assistance. Comments by an anonymous reviewer were valuable in reminding us, "science is hard enough without placing constraints of absolute perfection on work with the unknown." We hope our final manuscript reflects the spirit of this reviewer's comments. Research was sponsored by awards from the National Science Foundation (R11-8996152, DIR-8954231 and DIR-9013187) and the Mississippi-Alabama Sea Grant Consortium (NA16RG0155-01 R/LR-27). The U.S. Government is authorized to produce and distribute reprints for governmental purposes notwithstanding any copyright notation that may appear hereon.

Literature Cited

Bayne, G. L. 1969. The gregarious behavior of the larvae of *Ostrea edulis* L. at settlement. *J. Mar. Biol. Assoc. U.K.* **49:** 327–356.

Beidler, L. M. 1954. A theory of taste stimulation. *J. Gen. Physiol.* **38:** 133–139.

Bonar, D. B., R. M. Weiner, and R. R. Colwell. 1986. Microbial-invertebrate interactions and potential for biotechnology. *Microb. Ecol.* **12:** 101–110.

Bonar, D. B., S. L. Coon, M. Walch, R. M. Weiner, and W. Fitt. 1990. Control of oyster settlement and metamorphosis by endogenous and exogenous chemical cues. *Bull. Mar. Sci.* **46:** 484–498.

Burke, R. D. 1986. Pheromones and gregarious settlement of marine invertebrate larvae. *Bull. Mar. Sci.* **39:** 323–331.

Buroker, N. E. 1983. Population genetics of the American oyster, *Crassostrea virginica*, along the Atlantic coast and the Gulf of Mexico. *Mar. Biol.* **75:** 99–112.

Buskey, E. J. 1984. Swimming patterns as an indicator of the roles of copepod sensory systems in the recognition of food. *Mar. Biol.* **79:** 165–175.

Buskey, E. J., and D. K. Stoecker. 1989. Behavioral responses of the marine tintinnid *Favella* sp. to phytoplankton: influence of chemical, mechanical and photic stimuli. *J. Exp. Mar. Biol. Ecol.* **32:** 1–16.

Buss, L. W. 1979. Habitat selection, directional growth and spatial refuges: why colonial animals have more hiding places. Pp. 319–327 in *Biology and Systematics of Colonial Organisms*, G. Larwood and B. R. Rosen, eds. Academic Press, New York.

Buss, L. W. 1981. Group living, competition, and the evolution of cooperation in a sessile invertebrate. *Science* **213:** 1012–1014.

Cole, J. A., and E. W. Knight-Jones. 1939. Some observations and experiments in the setting behavior of *Ostrea edulis*. *J. Cons. Int. Explor. Mer.* **14:** 86–105.

Coon, S. L., W. K. Fitt, and D. B. Bonar. 1990a. Competency and delay of metamorphosis in the Pacific oyster, *Crassostrea gigas* (Thunberg). *Mar. Biol.* **106:** 379–387.

Coon, S. L., M. Walch, W. K. Fitt, D. B. Bonar, and R. M. Weiner. 1990b. Ammonia induces settlement behavior in oyster larvae. *Biol. Bull.* **179:** 297–303.

Crisp, D. J. 1974. Factors influencing settlement of marine invertebrate larvae. Pp. 177–265 in *Chemoreception in Marine Organisms*, P. T. Grant and A. M. Mackie, eds. Academic Press, London.

Crisp, D. J. 1979. Dispersal and re-aggregation in sessile marine invertebrates, particularly barnacles. Pp. 319–327 in *Biology and Systematics of Colonial Organisms*, G. Larwood and B. R. Rosen, eds. Academic Press, New York.

Dame, R. F., J. D. Spurrier, and T. G. Wolaver. 1989. Carbon, nitrogen and phosphorus processing by an oyster reef. *Mar. Ecol. Pro. Ser.* **54:** 249–256.

Denny, M. W., and M. F. Shibata. 1989. Consequence of surf-zone turbulence for settlement and external fertilization. *Am. Nat.* **134:** 859–889.

Fitt, W. K., S. L. Coon, M. Walch, R. M. Weiner, R. R. Colwell, and D. B. Bonar. 1990. Settlement behavior and metamorphosis of oyster larvae (*Crassostrea gigas*) in response to bacterial supernatants. *Mar. Biol.* **106:** 389–394.

Fitt, W. K., M. P. Labare, W. C. Fuqua, M. Walch, S. T. Coon, D. B. Bonar, R. R. Colwell, and R. M. Weiner. 1989. Factors influencing bacterial production of inducers of settlement behavior of larvae of the oyster *Crassostrea gigas*. *Microb. Ecol.* **17:** 287–298.

Galtsoff, P. S. 1964. The American Oyster, *Crassostrea virginica* Gmelin. *Fish. Bull.* **64:** 1–480.

Gotelli, N. J. 1990. Stochastic models of gregarious larval settlement. *Ophelia* **32:** 95–108.

Grosberg, R. K. 1987. Limited dispersal and proximity-dependent mating success in the colonial ascidian *Botryllus schlosseri*. *Evolution* **41:** 372–384.

Groue, K. J., and L. T. Lester. 1982. A morphological and genetic analysis of geographical variation among oysters in the Gulf of Mexico. *Veliger* **24:** 331–335.

Hamilton, W. D., and R. M. May. 1977. Dispersal in stable habitats. *Nature* **269:** 578–581.

Hammen, C. S., H. F. Miller Jr., and W. H. Geer. 1966. Nitrogen excretion of *Crassostrea virginica*. *Comp. Biochem. Physiol.* **17A:** 1199–1200.

Hidu, H. 1969. Gregarious setting in the American oyster, *Crassostrea virginica* Gmelin. *Chesapeake Sci.* **10:** 85–92.

Hidu, H., W. G. Valleau, and F. P. Veitch. 1978. Gregarious setting in the European and American oysters-response to surface chemistry vs. waterborne pheromones. *Proc. Nat. Shellfish. Assoc.* **68:** 11–16.

Highsmith, R. C. 1982. Induced settlement and metamorphosis of sand dollar (*Dendraster excentricus*) larvae in predator-free sites: adult sand dollar beds. *Ecology* **63:** 329–337.

Hobbie, J. E., R. S. Daley, and S. Jasper. 1974. Use of Nucleopore filters for counting bacteria by epifluorescence microscopy. *Appl. Environ. Microbiol.* **33:** 1225–1228.

Hughes, R. N. 1978. Coloniality in Vermetidea (Gastropoda). Pp. 319–327 in *Biology and Systematics of Colonial Organisms*, G. Larwood and B. R. Rosen, eds. Academic Press, New York.

Jensen, R. A., and D. E. Morse. 1990. Chemically induced metamorphosis of polychaete larvae in both the laboratory and the ocean environment. *J. Chem. Ecol.* **16:** 911–930.

Keck, R., D. Maurer, J. C. Kauer, and W. A. Sheppard. 1971. Chemical stimulants affecting larval settlement in the American oyster. *Proc. Nat. Shellfish. Assoc.* **61:** 24–28.

Keough, M. J. 1984. Kin-recognition and the spatial distribution of larvae of the bryozoan *Bugula neritina* (L.). *Evolution* **38:** 142–147.

King, T. L., and J. D. Gray. 1989. Allozyme survey of the population structure of *Crassostrea virginica* inhabiting Laguna Madre, Texas, and adjacent bay systems. *J. Shellfish Res.* **8:** 448.

Knight-Jones, E. W. 1951. Gregariousness and some other aspects of the settling behavior of *Spirorbis*. *J. Mar. Biol. Assoc. U.K.* **30:** 201–222.

Knight-Jones, E. W., and J. P. Stevenson. 1950. Gregariousness during settlement in the barnacle *Elminius modestus*. *J. Mar. Biol. Assoc. U.K.* **32:** 281–287.

Koopman, B. O. 1980. *Search and Screening*. Pergamon Press, New York. 368 pp.

Levin, L. A. 1984. Life history and dispersal patterns in a dense infaunal polycheate assemblage: community structure and response to disturbances. *Ecology* **56:** 1185–1200.

Levitan, D. R. 1991. Influence of body size and population density on fertilization success and reproductive output in a free-spawning invertebrate. *Biol. Bull.* 181: 261–268.

Loosanoff, V. L., and [illegible] 1963. Rearing of bivalve mollusks. Pp. 1–136 in *Marine Biology*, F. S. Russell, ed. Academic Press.

Maes, F. W., [illegible] 1990. Problems with linear regression of pharmacological and biochemical data. *J. Theor. Biol.* **111:** 817–819.

Meadows, P. S., and J. I. Campbell. 1972. Habitat selection by aquatic invertebrates. *Adv. Mar. Biol.* **10:** 271–282.

Morse, D. E. 1990. Recent progress in larval settlement and metamorphosis: closing the gaps between molecular biology and ecology. *Bull. Mar. Sci.* **46:** 465–483.

Palmer, A. R., and R. R. Strathmann. 1981. Scale of dispersal in varying environments and its implications for life histories of marine invertebrates. *Oecologia* **48:** 308–318.

Pawlik, J. R., and D. J. Faulkner. 1986. Specific free fatty acids induce larval settlement and metamorphosis of reef-building tube worm *Phragmatopoma californica* (Fewkes). *J. Exp. Mar. Biol. Ecol.* **102:** 301–310.

Pawlik, J. R., and M. G. Hadfield. 1990. A symposium on chemical factors that influence the settlement and metamorphosis of marine invertebrate larvae: introduction and prospective. *Bull. Mar. Sci* **46:** 450–454.

Pennington, J. T. 1985. The ecology of fertilization of echinoid eggs: the consequence of sperm dilution, adult aggregation, and synchronous spawning. *Biol. Bull.* **169:** 417–430.

Quayle, D. B. 1969. Pacific oyster culture in British Columbia. *J. Fish. Res. Board Can.* **169:** 1–192.

Roff, D. A. 1974. Spatial heterogeneity and the persistence of populations. *Oecologia* **15:** 245–258.

Sebens, K. P. 1983. Larval and juvenile ecology of the temperate octocoral *Alcyonium siderium* Verrill II. Fecundity, survivorship, and juvenile growth. *J. Exp. Mar. Biol. Ecol.* **72:** 263–285.

Simpson, G. G., and W. S. Beck. 1965. Reproduction: larvae. Pp. 266–267 in *Life: An Introduction to Biology*, G. G. Simpson and W. S. Beck, eds. Harcourt, Brace and World, Inc., New York.

Smith, W. L., and M. H. Chanley. 1975. Provisions of light. Pp. 33–36 in *Culture of Marine Invertebrate Animals*. W. L. Smith and M. H. Chanley, eds. Plenum Press, New York.

Srna, R. F., and A. Baggaley. 1976. Rate of excretion of ammonia by the hard clam *Mercenaria mercenaria* and the American oyster *Crassostrea virginica*. *Mar. Biol.* **36:** 251–258.

Stevens, S. A. 1983. *Ecology of Intertidal Oyster Reefs: Food, Distribution and Carbon/nutrient Flow.* Ph.D. Dissertation, University of Georgia. 195 pp.

Veitch, F. P., and H. Hidu. 1971. Gregarious setting in the American oyster *Crassostrea virginica* Gmelin: I. Properties of a partially purified "setting factor." *Chesapeake Sci.* **12:** 173–178.

Walne, P. R. 1966. Experiments in large-scale culture of the oyster *Ostrea edulis*. *Fish. Invest. Lond. Ser. 2* **25:** 1–53.

Weiner, R. M., M. Walch, M. P. Labare, D. B. Bonar, and R. R. Colwell. 1989. Effect of biofilms of the marine bacterium *Alteromonas colwelliana* (LST) on the set of the oyster *Crassostrea gigas* (Thunberg, 1793) and *C. virginica* (Gmelin, 1791). *J. Shellfish Res.* **8:** 117–123.

Weissburg, M. J., and R. K. Zimmer-Faust. 1991. Ontogeny *versus* phylogeny in determining patterns of chemoreception: initial studies with fiddler crabs. *Biol. Bull.* **181:** 205–215.

Young, C. M. 1983. Functional significance of larval behavior in an intertidal population of the ascidian *Pyura haustor*. *Am. Nat.* **23:** 1021.

Zimmer-Faust, R. K. 1990. Settlement behavior of larvae is revealed using computer-video motion analysis. *Am. Zool.* **30:** 556A.

Reference: *Biol. Bull.* **183**: 339–380. (October, 1992)

Reports of Papers Presented at the General Scientific Meetings of the Marine Biological Laboratory

August 17–19, 1992

Short Reports appear in the following categories: Biophysics and Neurobiology (pp. 339–359); Cell and Developmental Biology (pp. 360–377); Comparative Physiology (pp. 377–379); and Marine Resources (pp. 379–380). This year's featured article is by K. K. Siwicki et al.

All Short Reports were reviewed by members of our Special Editorial Board. Board members include: Daniel Alkon (NIH/NINDS); George Augustine (Duke University Medical Center); Richard Chappell (Hunter College, CUNY); William Cohen (Hunter College, CUNY); Barbara Ehrlich (University of Connecticut Health Center); Sarah Garber (University of Alabama, Birmingham); Susan Hill (Michigan State University); Robert Josephson (University of California, Irvine); Alan Kuzirian (MBL); John Lisman (Brandeis University); James Olds (NIH); William Ross (New York Medical College); Robert Silver (Cornell University/New York College of Veterinary Medicine); Kathleen Siwicki (Swarthmore College); Darrell Stokes (Emory University); Ete Szuts (MBL); Bruce Telzer (Pomona College); Mark Terasaki (NIH/NINDS); Hiroshi Ueno (Osaka Medical College, Japan); Dieter Weiss (Technical University, Munich); and Steven Zottoli (Williams College).

In addition to the reports contained in this issue, the following papers were also presented, by title, at the meetings. The abstracts of these papers are available from the MBL Archives.

Biophysics and Neurobiology

Herr, Barbara, Melissa Watt, and Jelle Atema. "Information currents in Crustacea."

Herzog, E., N. Buelow, M. Kelly, U. Koch, K. Longnecker, H. Nelson, I. Harris, M. Powers, and R. Barlow, Jr. "Visual performance of *Limulus* day and night for different size targets."

Cell and Developmental Biology

Harrison, John, and Linda Deegan. "Stable isotope analysis of macroalgae as a primary producer in a salt pond food web."

Langford, G. M., S. A. Kuznetsov, F. F. Severin, N. R. Dudley, and D. G. Weiss. "Axoplasmic organelles move on exogenous actin filaments."

Lauzon, Robert J., and Meryl Y. Tucker. "Involvement of a clock mechanism in the regulation of zooid lifespan in the colonial ascidian *Botryllus schlosseri*."

Morrell, Candy M., and James A. Adams. "Toxicity of Verrucarin A to gametes and embryos of the purple sea urchin (*Arbacia punctulata*)."

Terasaki, Mark, and Thomas Reese. "Actin filaments in the interior of sea urchin eggs."

Weiss, D. G., S. A. Kuznetsov, and G. M. Langford. "Dual filament model of fast axonal transport."

Comparative Physiology

DuBois, A. B., G. M. Fox, and C. S. Ogilvy. "Hypoxia intensifies the blood pressure response to increased intracranial pressure in bluefish *Pomatomus saltatrix*."

Rome, L. C., D. Corda, and D. Swank. "Design of the scup muscular system."

Marine Resources

Bullis, Robert A., Roxanna M. Smolowitz, and Michael Syslo. "A histological technique for the detection of scrubbed lobsters by staining of the pleopod tegmental glands."

Bullis, Robert A., James R. Weinberg, and Alan Kuzirian. "A new parasite of *Nereis acuminata (Neanthes arenaceodentata)*: implications for a marine laboratory animal."

Rollenhagen, J., H. Chikarmane, and R. A. Bullis. "Rapid identification of marine bacterial pathogens using PCR fingerprinting."

The *Drosophila period* Gene and Dye Coupling in Larval Salivary Glands: A Re-evaluation

Kathleen K. Siwicki[1], Kimberly K. Flint[2], Jeffrey C. Hall[2], Michael Rosbash[2,3], and David C. Spray[4]
([1]Biology Department, Swarthmore College, Swarthmore, PA 19081-1397; [2]Department of Biology and [3]Howard Hughes Medical Institute, Brandeis University, Waltham, MA 02254-9110; and [4]Department of Neuroscience, Albert Einstein College of Medicine, Bronx, NY 10461-1602)

In 1987, Bargiello *et al.* (1) reported that mutations of the *period* (*per*) gene dramatically altered the extent of intercellular coupling in larval salivary glands, such that coupling was virtually absent in per^o glands and was quite extensive in per^s compared to wild type. These results, together with early immunochemical data and sequence analysis of the PER protein (1, 2, 3), were interpreted as indications that the PER protein was a proteoglycan, localized at the cell boundaries in larval salivary glands, and acting there to regulate intercellular communication (1). Recent evidence suggests that the PER protein is unlikely to be a proteoglycan (4), and raises questions about its presence in salivary glands (5, 6). Therefore, we have re-evaluated the influence of *per* genotype on intercellular coupling in larval salivary glands.

Working in two different laboratories, we performed two extensive series of Lucifer Yellow injections into salivary glands from larvae of various *per* genotypes. The same four *per* strains were used by both groups: the arrhythmic per^o mutant, the short-period per^s mutant, and two control strains—an isogenic per^+ stock and a transgenic strain (per^o; 13.2/13.2), wherein two copies of a fully functional 13.2 kb fragment of per^+ DNA are inserted into a per^o genetic background. The strains were coded so that experimenters were uninformed as to the genotype. As a historical note, after the first series of experiments (by K.F.F., J.C.H. and M.R.) had been completed, open discussions of their results stimulated a further series (by K.K.S. and D.C.S.).

Although the extent of dye coupling was evaluated by different criteria in the two laboratories, the results of both failed to show a correlation between *per* genotype and the extent of dye coupling in larval salivary glands (Tables IA, B). Although the median values of one data set (that in Table IB) reproduced the order $per^s > per^+ > per^o$ (with median values of 1.0, 0.8, and 0.5, respectively), the data displayed a wide range in the degree of coupling within each genotype, and mean values revealed no genotypic differences. Even within a single animal, the extent of dye spread could be highly variable; this was exemplified most prominently by two glands of a per^o; 13.2/13.2 animal: one gland showed extensive dye coupling, and the other showed no transfer at all.

The variability reported here contrasts markedly with the striking differences and small variability within genotypes reported previously (1). In attempting to understand this discrep-

Table I

A. Dye transfer in larval salivary glands

Genotype	Anterior injections	Posterior injections
per^o	4.8 (6)	3.5 (11)
per^+	1.0 (4)	4.2 (6)
per^s	3.0 (9)	2.0 (5)
per^o; 13.2/13.2	1.8 (14)	3.4 (6)

B. Dye transfer in larval salivary glands

Genotype	All glands	Small	Large	Early	Late
per^o	0.9 ± 0.2 (36)	0.2 ± 0.1 (13)	1.3 ± 0.2 (23)	0.9 ± 0.3 (9)	0.9 ± 0.2 (27)
per^+	0.8 ± 0.1 (31)	0.7 ± 0.1 (22)	0.9 ± 0.2 (9)	0.7 ± 0.2 (11)	0.8 ± 0.1 (20)
per^s	0.8 ± 0.1 (46)	0.07 ± 0.04 (16)	1.3 ± 0.1 (30)	0.9 ± 0.1 (12)	0.8 ± 0.1 (34)
per^o; 13.2/13.2	1.1 ± 0.2 (38)	0.5 ± 0.2 (11)	1.4 ± 0.2 (27)	1.1 ± 0.3 (11)	1.2 ± 0.2 (27)
Total	0.9 ± 0.07 (151)	0.4 ± 0.07 (62)	1.3 ± 0.08 (89)	0.9 ± 0.1 (43)	0.9 ± 0.08 (108)

A. In this series of experiments, dye transfer was scored as the number of cells filled 1–2 min after the beginning of each 30 s injection; the numbers of injections are in parentheses. These data are from cells whose resting potentials (pre-injection) were <-28 mV. Because anterior and posterior cells exhibit differences in electrical parameters (7), their scores were tabulated separately. In other cells whose resting potentials ranged from -27 mV to -12 mV ($n = 23, 9, 6$, and 9, respectively, for the 4 genotypes), similar results were obtained: there were no systemic genotypic variations from the average dye transfer score of 3.5 cells.

B. In this series of experiments, dye transfer was scored on a rating scale of 0–3 by two individuals who were blind as to the genotype, and the two scores for each injection were averaged. The numbers of injections are in parentheses. Larvae were maintained at 25°C in a 12 h light:12 h dark cycle. Data in the 'Early' column are from glands dissected between 1 and 3 h after 'lights-on'; data in the 'Late' column are from glands dissected within 2.5 h of 'lights-off.' Salivary glands were classified as small or large prior to injections.

ancy, we have compared subsets of our data with regard to location of injection (anterior *vs.* posterior gland regions in Table 1A), large *versus* small glands (Table 1B), and glands injected at different times of day (early *vs.* late in Table 1B). These restricted data sets revealed significantly weaker coupling in smaller glands than in larger glands, but no evidence for an effect of *per* genotype. Thus, while other variables affect coupling in this tissue, we conclude that the *per* gene itself does not detectably influence the extent of intercellular coupling in larval salivary glands.

We thank Daniel Goodenough, in whose laboratory some of these experiments were performed, for hospitality and guidance, and Marc Chanson and Matthew Clausen for help with scoring injections. This work was supported by NIH grants GM-33205 (to J.C.H. and M.R.), and NS-16524 (to D.C.S.), and NSF grant 9057703 (to K.K.S.).

Literature Cited

1. **Bargiello, T. A., L. Saez, M. K. Baylies, G. Gasic, M. W. Young, and D. C. Spray. 1987.** *Nature* **328:** 686–691.
2. **Jackson, F. R., T. A. Bargiello, S.-H. Yun, and M. W. Young. 1986.** *Nature* **320:** 185–188.
3. **Reddy, P., A. C. Jacquier, N. Abovich, G. Petersen, and M. Rosbash. 1986.** *Cell* **46:** 53–61.
4. **Rosbash, M., and J. C. Hall. 1989.** *Neuron* **3:** 387–398.
5. **Siwicki, K. K., C. Eastman, G. Petersen, M. Rosbash, and J. C. Hall. 1988.** *Neuron* **1:** 141–150.
6. **Liu, X., L. Lorenz, Q. Yu, J. C. Hall, and M. Rosbash. 1988.** *Genes Dev.* **2:** 228–238.
7. **van Venrooij, G. E. P. M., W. M. A. Hax, G. F. van Dantzig, V. Prijs, and J. J. Denier van der Gon. 1974.** *J. Membrane Biol.* **19:** 229–252.

Gating and Single Channel Properties of Gap Junction Channels in Hepatopancreatic Cells of *Procambarus clarkii*

Marc Chanson and David C. Spray (Department of Neuroscience, Albert Einstein College of Medicine, 1300 Morris Park Avenue, Bronx, NY 10461)

The crustacean hepatopancreas is responsible for major metabolic events in the organism, including enzyme secretion, absorption and storage of nutrients, molting, and vitellogenesis (1, 2). The multifunctional role of the hepatopancreas requires that its constituent cells be precisely coordinated so that the organ can produce appropriate responses. Hepatopancreocytes are connected by large gap junctions (3, 4), which are specialized transmembrane channels involved in direct cell-to-cell communication. In the crayfish, the morphological organization of gap junction plaques (as revealed by freeze-fracture methodology), as well as the extent of electrical coupling between neighboring cells (as revealed by coupling coefficient measurements with two microelectrodes) are modulated by the molting cycle and by the molting hormone crustecdysone (5, 6). These observations suggest that gap junctional communication may be involved in the function of crustacean hepatopancreatic cells.

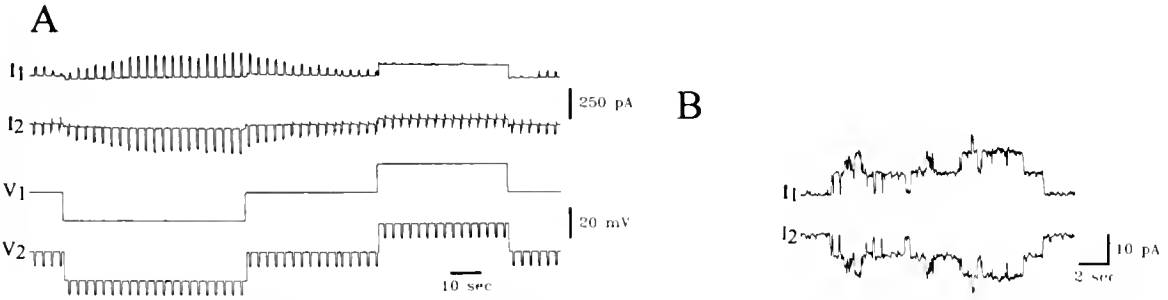

Figure 1. *(A) Inside-outside voltage dependence of junctional conductance between hepatopancreatic cell pairs. At the beginning of the experiment, both cells of the pair were held at a common holding potential of 0 mV (V_1 and V_2). Junctional conductance was determined by applying 10 mV pulses to cell 2. This protocol evoked a current, both in the pulsed cell (I_2), and in the non-pulsed cell (I_1). Although the latter current is only junctional, the current appearing in cell 2 is the sum of junctional (I_j) and non-junctional currents (I_{nj}). When both cells were hyperpolarized to −20 mV, I_j increased with time indicating the opening of gap junction channels. This effect is reversible when cells were held back to the initial holding potential. In contrast, when cells were depolarized to positive values (+20 mV), I_j was no longer detected indicating closure of gap junction channels. I_j could be resolved once again when the cells were clamped to 0 mV. (B) Single gap junction channel activity in hepatopancreatic cell pairs. To visualize single gap junction channels, a difference of potential was elicited across the junctional membrane by holding one cell of a pair at 0 mV and the second cell at −20 mV. Single gap junction channel openings and closures are recognized by simultaneous transitions of identical but opposite polarities in both cells of the pair. Upward transitions in I_1 indicate channel opening. Most current transitions correspond to a junctional conductance of about 250 pS. A similar junctional conductance value was observed when the pulsed cell was held at a positive voltage of 20 mV.*

To characterize the biophysical properties of the gap junction channels expressed between crustacean hepatopancreatic cells, we applied the dual patch clamp technique to freshly isolated cell pairs (Dissociated Cell Culture). For each experiment, the posterior lobes of one hepatopancreas were dissected and digested with collagenase. Cells released by this procedure were plated in Petri dishes. Then, one patch electrode was sealed on the membrane of each cell of a pair, and the whole cell configuration was achieved to allow individual voltage clamp of the cells. Electrodes were filled with a solution containing CsCl to reduce non-junctional currents. Junctional conductance was determined by measuring the current evoked in one cell of the pair by a voltage pulse applied to the second cell.

Under voltage clamp conditions, junctional conductance changes with membrane potential of the cells. As is shown in Figure 1A, when both cells were held at a membrane potential of 0 mV, only a small junctional current could be detected. This current increased dramatically when cells were hyperpolarized, whereas the channels closed during depolarizing voltage steps. These observations indicate that the gap junction channels underlying these changes exhibit inside-outside voltage dependence. To characterize these channels, each member of the pair was held at a different voltage, thus applying a driving force across the junctional membrane. As is shown in Figure 1B, single gap junction channel openings and closures can be identified by simultaneous transitions of identical amplitudes, but opposite polarities, in both cells of the pair. While a predominant elementary conductance of about 250 pS was detected, events of smaller sizes were also observed.

These results indicate that hepatopancreatic cells are connected by large gap junction channels, the gating of which is steeply dependent on membrane potential. While inside-out voltage dependence has previously been described (8, 9), this study reports the first recordings of single gap junction channel activity in an adult invertebrate tissue. The steep sensitivity of these channels to small membrane potential changes suggests that junctional communication between hepatopancreatic cells are of importance for tissue function.

M. C. was a Grass Foundation Fellow during the 1992 summer at the Marine Biological Laboratory, Woods Hole, MA.

Literature Cited

1. **McWhinnie, M. A., R. J. Kirchenberg, R. J. Urbansky, and J. E. Schwarz. 1972.** *Am. Zool.* **12:** 357–372.
2. **Adiyodi, R. G., and K. G. Adiyodi. 1972.** *Biol. Bull.* **142:** 359–369.
3. **Bunt, A. H. 1968.** *Crustaceana* **15:** 282–288.
4. **Gilula, N. B. 1972.** *J. Ultrastruct. Res.* **38:** 215–216.
5. **McVicar, L. K., and R. R. Shivers. 1984.** *Tissue and Cell* **16:** 917–928.
6. **McVicar, L. K., and R. R. Shivers. 1985.** *Cell Tissue Res.* **240:** 261–269.
7. **Neyton, A., and A. Trautmann. 1985.** *Nature* **317:** 331–335.
8. **Obaid, A. L., S. J. Socolar, and B. Rose. 1983.** *J. Membr. Biol.* **73:** 69–89.
9. **Verselis, V. K., M. V. L. Bennett, and T. A. Bargiello. 1991.** *Biophys J* **59:** 114–126.

Discontinuities in Action Potential Propagation Along Chains of Single Ventricular Myocytes in Culture: Multiple Site Optical Recording of Transmembrane Voltage (MSORTV) Suggests Propagation Delays at the Junctional Sites Between Cells.

S. Rohr[1,2] and B. M. Salzberg[1] ([1]Departments of Neuroscience and Physiology, University of Pennsylvania School of Medicine, Philadelphia, PA, and [2]Institute of Physiology, University of Bern, 3012 Bern, Switzerland)

Since one-dimensional cable theory was first applied to Purkinje fibers in the early 1950s, electrical conduction in heart muscle has generally been treated as continuous. Indirect evidence for discontinuous impulse propagation at the cellular level, due to gap junctions acting as intercellular resistive barriers, has only been presented during the last decade (1). For the case of longitudinal propagation under physiological conditions, this evidence was based exclusively on computer simulations (2, 3). To examine the possibility that action potential propagation in heart tissue is influenced, at the cellular level, by junctional delays, we measured transmembrane voltage changes with high temporal resolution at multiple sites along "one-dimensional" strands of single cardiac myocytes. The strands were constructed using photolithographically patterned growth in culture.

Multiple site optical recording of transmembrane voltage (MSORTV). The measurement apparatus was built around an inverted microscope (Zeiss, IM35), equipped for epifluorescence, and attached to a large micrometer driven X-Y positioner mounted on a vibration isolation table (Newport). An image of the preparation was projected onto a 12 × 12 array of silicon photodiodes (Centronics, MD-144-0) or onto the CCD sensor of a video camera (Sony XC-77). The photocurrents generated by the central 124 detectors were converted to voltages by first stage amplifiers and were further amplified by an A.C. coupled second stage. The variation in the response time constants among the amplifiers was <10 μs. The signals of all 124 diodes were multiplexed, digitized (maximum rate of 2000 frames per second), and stored in a computer (VME-bus Motorola 68030). Analog outputs from an arbitrarily selectable subset of up to 16 channels were routed in parallel to a fast PC-based data acquisition system (Northgate 486i equipped with a data acquisition card from Strawberry Tree, Inc.; 16 μs conversion time per

channel for 16 channels, with true 1 μs switching rate between channels). High resolution images of the myocyte cultures were recorded with a computer-based image acquisition system (Macintosh, equipped with a Data Translation framegrabber) connected to the video camera.

Cell cultures. Cultures were established according to conventional techniques (*c.f.* reference 4 for details). The cultures were kept in an incubator at 35°C in a water-saturated atmosphere of ambient air and 1.4% CO_2. Patterned growth was obtained by plating the cells onto coverslips precoated with patterns of a light-sensitive resin (photoresist) that rejected adhesion of cells (*c.f.* reference 4 for details). During the experiments, the cultures were mounted in a temperature-controlled experimental chamber and superfused at 5 to 10 ml/min with Hank's balanced salt solution (HBSS) at 35°C, pH 7.4. After the extracellular stimulating electrodes had been placed, the cells were stained with 60 to 80 μg/ml of the voltage sensitive dye DI-8-ANEPPS (5) for 5 min.

A typical experiment is illustrated in Figure 1. The recording was obtained from a 2-day-old culture. The cell strand was stimulated at 1.7 Hz with an extracellular electrode delivering 0.5-ms wide square pulses at twice threshold intensity. The electrode was placed at a sufficient distance from the recording site that only propagated action potentials could invade the region of interest. Recordings were made with a 100×, 1.25 N.A. objective providing a spatial resolution in the object plane of 15 × 15 μm for each detector element. Panel A shows the positions of the photodiode array pixels with respect to the outlines of the individual cells. In this example, two cells out of a strand could be imaged simultaneously. Panel B depicts the amplitude-normalized upstroke portion of the propagating action potential. Upstroke velocities in this example varied between 120 V/s and 195 V/s, and are comparable to values measured with intracellular electrodes in the same culture system (4). Although motion artifacts generated by contraction can distort the shape of most of the repolarization phase of the optically recorded action potential, the upstroke is entirely preserved because of the excitation-contraction coupling latency. Panel C illustrates propagation delays between contiguous photodetector fields. These are calculated as the average delay between 40% and 60% depolarization measured between adjacent photodetectors. This panel demonstrates that delays measured *along* individual cells ranged from 21 to 67 μs, and this contrasts with propagation delays in the overlap region between cells, which in this example were 131 and 101 μs, respectively. Comparable values for delays in the cell-to-cell contact region were found in three additional experiments (range: 85–135 μs; data not shown). The average conduction velocity in the experiment illustrated in Figure 1, as determined from the delay between the first and last detector element in the chain, was 0.32 m/s. This value is comparable to those found when imaging at lower spatial resolution, and to values obtained with extracellular recording electrodes spaced farther apart in the same culture system (4). This average conduction velocity is quite different from the much slower conduction in the overlap regions containing the cell-to-cell boundaries (0.13 m/s) and the more rapid conduction velocities measured along single cells (0.62 and 0.36 m/s). These results suggest that, although overall conduction velocity is normal, microscopic conduction is highly discontinuous in a single cell strand composed of coupled cardiac myocytes.

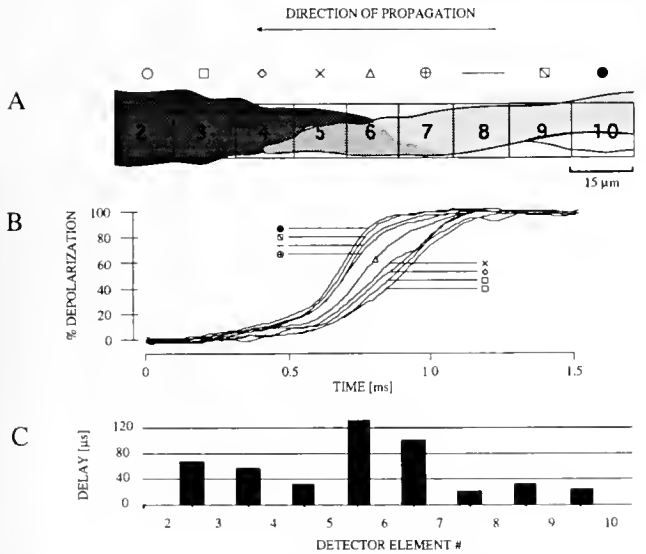

Figure 1. *Discontinuous action potential propagation along a chain of single ventricular myocytes in culture. (A) Outlines, based on a video image, of two ventricular myocytes superimposed on the 15 × 15 μm fields of 9 elements of the photodiode array. The overlap region between the two large cells (intermediate grey level) is mainly confined to pixels numbered 5–7, and propagation proceeds from the right to left. (B) Optical recordings (single sweeps) of the upstrokes of the action potential from individual pixels. The different symbols correspond to the detector labels in A. (C) Action potential propagation delays between successive segments of the strand (detector elements). Note the large delays as the impulse propagates through the overlap region (Elements 5–7).*

While these results were typical of experiments carried out on strands one myocyte wide, no obvious discontinuities in action potential propagation were found when we assessed impulse propagation in cell strands that were several cells across (data not shown). This is the expected result, if discontinuities in propagation were smoothed out by virtue of lateral electrical connections between the myocytes that averaged local differences in activation time.

We are grateful to Drs. Larry Cohen and Ana Lia Obaid for helpful discussions, to Leslie Loew, Rina Hildesheim, and Amiram Grinvald for gifts of molecular probes, and to Mel Decker of Optiquip for the loan of their low noise xenon arc system. Supported by Swiss NSF grant 823A-28424 (S.R.) and USPHS grant NS 16824 (B.M.S.).

Literature Cited

1. **Spach, M. S., W. T. Miller, III, D. B. Geselowitz, R. C. Barr, J. M. Kootsey, and E. A. Johnson. 1981.** *Circ. Res.* **48:** 39–54.
2. **Diaz, P. J., Y. Rudy, and R. Plonsey. 1983.** *Annals Biomed. Eng.* **11:** 177–189.
3. **Rudy, Y., and W. Quan. 1991.** *J. Cardiovasc. Electrophys.* **2:** 299–315.
4. **Rohr, S., D. G. Schölly, and A. G. Kléber. 1991.** *Circ. Res.* **68:** 114–130.
5. **Bedlack, R. S., M. D. Wei, and L. Loew. 1992.** *Neuron* (in press).

Optical Recording With Single Cell Resolution from a Simple Mammalian Nervous System: Electrical Activity in Ganglia from the Submucous Plexus of the Guinea-Pig Ileum

A. L. Obaid[1], D. J. Zoli[2], S. Rohr[3], and B. M. Salzberg[1] ([1]Departments of Neuroscience and Physiology, University of Pennsylvania School of Medicine, Philadelphia, PA; [2]Department of Pharmacology, Biocenter, Basel University, 4056 Basel, Switzerland; and [3]Institute of Physiology, University of Bern, 3012 Bern, Switzerland)

Nervous systems consisting of a limited number of elements would seem to offer the best hope for understanding, in detail, the dynamic electrical and chemical interactions that generate behavior. One approach to the study of simple nervous systems is literally to construct defined neuronal ensembles in culture, by allowing identified invertebrate neurons to interact synaptically (1), and to analyze their functional connectivity by using multiple site optical recording techniques (2, 3). These methods, combined with conventional electrophysiology, have been used to explore the collective behavior of defined neuronal ensembles or networks *in vitro*, and to discern dynamic patterns of functional connectivity (1). Because each ensemble of co-cultured *Aplysia* neurons was a unique anatomical entity, and because we wished to examine in a reproducible fashion a simple *mammalian* nervous system, we turned our attention to the submucous plexus of the guinea-pig ileum. The neurons of the enteric nervous system are arranged in plexuses confined to distinct planes in the gut wall, and each ganglion, like other neuronal systems involved in integrated behavior, contains sensory neurons, interneurons, and motor neurons.

The submucous plexus of the guinea-pig (4–6), in particular, has several properties that make it particularly amenable to Multiple Site Optical Recording of Transmembrane Voltage (MSORTV) (7, 8). First, the individual ganglia of the plexus each contain an average of only 8–10 neurons (12–29 μm in diameter), and these are arranged in a very thin ($\sim$15 μm thick) monolayer, presenting little or no barrier to diffusion of dyes or pharmacological agents. (A confocal image of a typical ganglion from the submucous plexus is shown in Fig. 1A). Second, the preparation can be dissected as a sheet of connective tissue containing the submucous neurons with their interconnecting nerve fibers and the submucosal vasculature (6); when stained with potentiometric dyes (9), the neuronal network yields extrinsic optical signals that are uncontaminated by mechanical artifact. Finally, the synaptic inputs to the ganglia are accessible to electrical stimulation, and a variety of excitatory and inhibitory synaptic inputs, both fast and slow, have already been described (4, 10–12).

The isolated submucous plexus was obtained from the small intestine of 150 g Hartley guinea-pigs that had been anesthetized by halothane inhalation and decapitated. The methods of dissection were essentially those of Hirst and McKirdy (4). With the goal of reducing background fluorescence from dye bound to residual smooth muscle and connective tissue, the isolated plexus was incubated for 2 h at room temperature in a Ringer's solution containing 100 U/ml Collagenase VII (Sigma C-0773) and 1 mg/ml Protease IX (Sigma P-6141). After this treatment, the preparation was kept in organ culture for 12 to 20 h, at room temperature, covered by Ringer's solution. All of the incubations took place in a chamber saturated with 95% O_2, 5% CO_2. The Ringer's solution contained (in m*M*): NaCl (120); $NaHCO_3$ (5); KCl (4.5); $CaCl_2$ (2.5); $MgCl_2$ (1.0); NaH_2PO_4 (0.5); HEPES (20); Glucose (11), pH adjusted to 7.4.

For the optical experiments, the preparation was mounted in a recording chamber attached to the fixed stage of an inverted microscope (Zeiss IM 35) equipped for epifluorescence. The tissue was then stained for 10 min with 100 μg/ml of the styryl dye, Di-8 ANEPPS (13), in Ringer's solution containing 0.95% DMSO and 0.34% Pluronic F-127. After staining, the plexus was continuously superfused with oxygenated Ringer's solution. All experiments were carried out at room temperature. The system for MSORTV was based on a 124 element photodiode array (Centronic) positioned in the image plane of the microscope which, in turn, was mounted on a large micrometer driven X-Y platform (1). Epi-illumination was provided by a 150 Watt Xenon arc lamp. Excitation was at 530 $\pm$ 25 nm, and the fluorescence emission was selected with a 560 nm dichroic mirror and an OG570 (Schott Glass Co.) barrier filter.

Optical recordings of electrical activity, with single cell resolution, were obtained from *in vitro* submucous plexus preparations using either a $\times$63 (Zeiss Planapochromat 1.4 na) or a $\times$100 (Nikon Achromat 1.25 na) objective. In an area 4 $\times$ 7 mm, 100–150 ganglia were examined for spontaneous activity.

The trace in Figure 1B is a 1-s segment of the output from a single pixel of the photodiode array. Rhythmic spiking in a single neuron is apparent. The five traces in Figure 1C are the digitized records from five selected photodiodes which were monitoring activity in five different neurons in another ganglion from the same plexus. Complex electrical activity is evident, with single detectors monitoring more than one cell, and single cells represented on several detectors (14). The spatiotemporal patterning of activity in this experiment is more clearly illustrated in Figure 1D, where the optical signals recorded by the central 48 elements of the photodiode array are superimposed on the corresponding regions of the projected image of the ganglion.

We observed "spontaneous" activity during 1-s recording periods in the majority of the ganglia monitored. But, under our illumination conditions, this activity lasted less than 10 s, and typically, the cells became quiescent after 4–5 s. We do not yet know what portion of the electrical behavior is induced by the incident light, or to what degree the ongoing activity of the plexus is suppressed by the excitation beam. However, photodynamic damage must perturb the system, because the same ganglion generally cannot be monitored twice. We are attempting to control phototoxicity in this system by using protective agents and by reducing the light intensity to the minimum compatible with an acceptable signal-to-noise ratio (1). Despite concerns about the present limitations of the experiments, the fluorescence

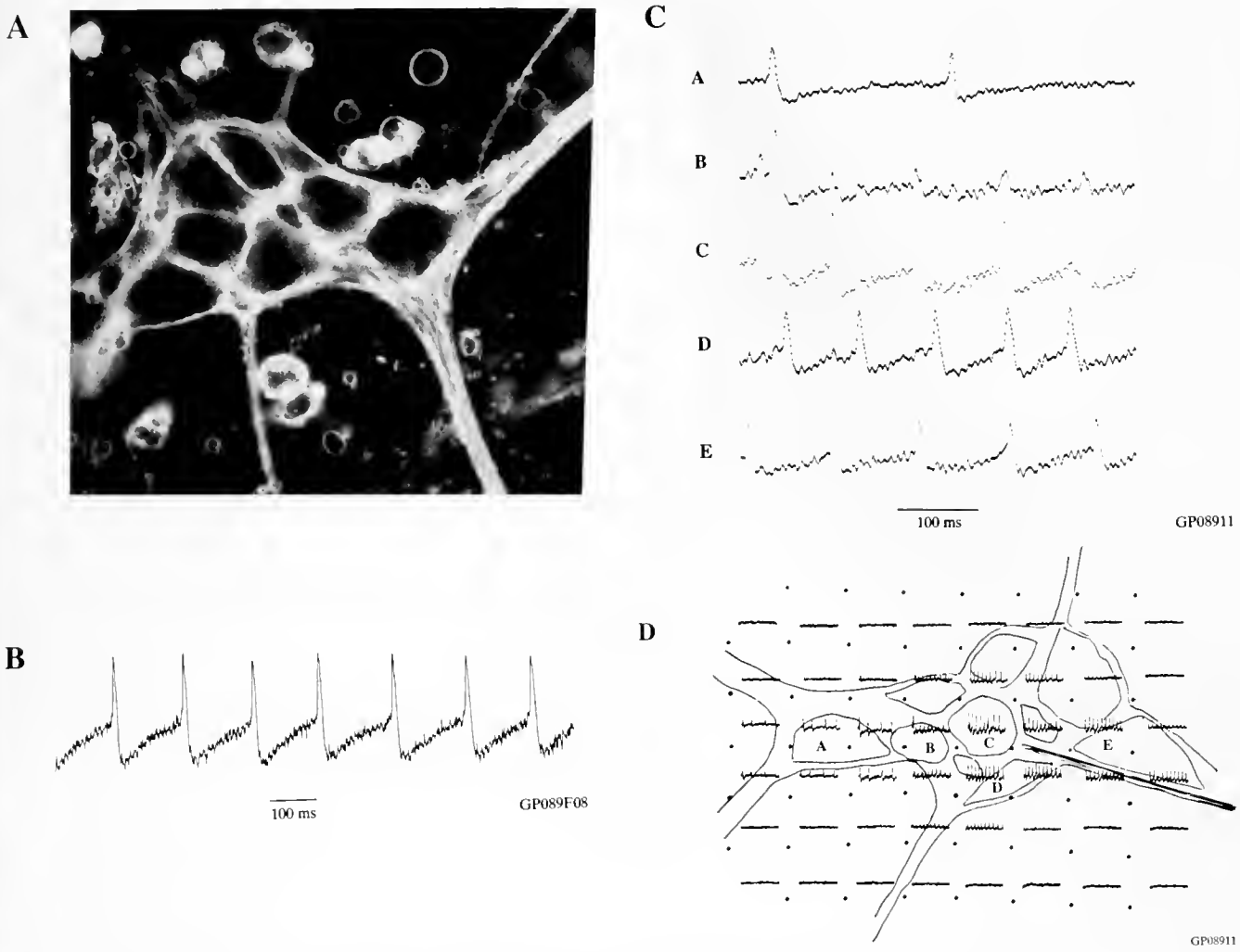

Figure 1. *Optical recordings from individual neurons of the submucous plexus of the guinea-pig ileum. (A) Confocal image of a typical ganglion from the submucous plexus. The ganglion was photographed through a ×100 (planapochromat, 1.4 n.a.) objective in a Zeiss Laser Scanning Microscope after staining with the potentiometric probe Di-8 ANEPPS. The section thickness was 0.5 μm. The width of the field was 128 μm. (B) Fluorescence signal from a single neuron in a different ganglion stained with Di-8 ANEPPS. An increase in fluorescence is shown as a downward deflection of the trace. Here, the fractional change in fluorescence (compared to background) was approximately 4%. Single sweep. The response time constant of the optical recording system was 300 μs. The AC coupling time constant of the second stage amplifier was 400 ms (GP089F08). (C) Fluorescence signals from five individual photodetectors positioned over different neurons in the same ganglion. The traces derive their dominant inputs from the cells labeled with the same letter in panel D (GP08911). (D) The outline of the ganglion projected onto the image of the central 48 pixels of the photodiode array. The individual optical traces are placed in their region of origin to illustrate the spatiotemporal patterning of the electrical activity in this ganglion.*

signals presented here represent the first optical recordings of electrical activity from mammalian ganglia with single cell resolution. Multiple site optical recording from the neurons of the submucous plexus of the enteric nervous system may facilitate a deeper understanding of neuronal interactions within and between ganglia in a relatively simple mammalian network.

We are most grateful to Annemarie Surprenant and Richard Evans for teaching us the submucous plexus preparation, and for their help and encouragement; to Larry Cohen's laboratory for data acquisition and analysis software; to Leslie Loew for Di-8 ANEPPS; to Steve Senft (Vital Images, Inc.) and Phil Presley (Carl Zeiss, Inc.) for use of the confocal imaging system; and to Mel Decker of Optiquip for the loan of their low noise Xenon arc system. Supported by USPHS grant NS 16824 and a Grass Fellowship to D.-J.Z. S.R. is a Fellow of the Swiss NSF (grant 823A-028424).

Literature Cited

1. **Parsons, T. D., B. M. Salzberg, A. L. Obaid, F. Raccuia-Behling, and D. Kleinfeld. 1991.** *J. Neurophysiol.* **66:** 316–333.

2. **Salzberg, B. M., A. Grinvald, L. B. Cohen, H. V. Davila, and W. N. Ross. 1977.** *J. Neurophysiol.* **40:** 1281–1291.
3. **Grinvald, A., L. B. Cohen, S. Lesher, and M. B. Boyle. 1981.** *J. Neurophysiol.* 45: 829–840.
4. **Hirst, G. D. S., and H. C. McKirdy. 1975.** *J. Physiol. Lond.* **249:** 369–385.
5. **Furness, J. B., and M. Costa. 1987.** *The Enteric Nervous System.* Churchill Livingstone, New York. 290 pp.
6. **Surprenant, A. 1989.** Pp. 253–263 in *Nerves and the Gastrointestinal Tract,* M. V. Singer and H. Giebell, eds. MTP Press Ltd., Boston.
7. **Salzberg, B. M. 1983.** Optical recording of electrical activity in neurons using molecular probes. Pp. 139–187 in *Current Methods in Cellular Neurobiology,* J. Barker and J. McKelvy, eds. John Wiley and Sons, Inc., New York.
8. **Grinvald, A., R. D. Frostig, E. Lieke, and R. Hildesheim. 1988.** *Physiol. Rev.* **68:** 1285–1366.
9. **Cohen, L. B., and B. M. Salzberg. 1978.** Optical measurement of membrane potential. Pp. 33–88 in *Reviews of Physiology, Biochemistry, and Pharmacology.* Springer-Verlag, Berlin-Heidelberg-New York.
10. **Surprenant, A. 1984.** *J. Physiol. Lond.* **351:** 343–361.
11. **North, R. A., and A. Surprenant. 1985.** *J. Physiol. Lond.* **358:** 17–33.
12. **Borstein, J. C., J. B. Furness, and M. Costa. 1987.** *J. Auton. Nerv. Syst.* **18:** 83–91.
13. **Bedlack, R. S., M. D. Wei, and L. Loew. 1992.** *Neuron* (In Press).
14. **Salzberg, B. M., A. Grinvald, L. B. Cohen, H. V. Davila, and W. N. Ross. 1977.** *J. Neurophysiol.* **40:** 1281–1291.

Potassium Current Composition and Kinetics in Toadfish Semicircular Canal Hair Cells

A. Steinacker, J. Monterrubio, R. Perez, and S. M. Highstein (Institute of Neurobiology, University of Puerto Rico, San Juan, PR, and *Washington University School of Medicine, St. Louis, MO)*

Sensory hair cells of acoustico-lateralis systems exhibit a variety of potassium currents in addition to a non-inactivating calcium current (1, 2, 3, 4). They also display resonating or spiking behavior under current clamp conditions (5, 6, 7, 8). These properties suggest configurations of ionic currents capable of coding complex attributes of a sensory stimulus. Because the response dynamics of primary afferents of the horizontal semicircular canals co-vary with their position of origin on the crista, a study of the ionic currents of the hair cells isolated from the crista may reveal links between ionic currents and functional coding capabilities of afferents.

Whole cell patch clamp methods were used to record the outward currents and membrane potential resonance of hair cells isolated from the horizontal semicircular canals of the toadfish, *Opsanus tau.* Toadfish were used for these experiments because of the similarity of semicircular canal systems between species, ease of removal of the canal structures and because of the large body of electrophysiological work published on the semicircular canal system in this species. Data were collected on line using Pclamp and a P/4 routine. Bath Ringer was a salt water teleost Ringer containing (in mM): NaCl 165, KCl 5, $MgCl_2$ 1, $CaCl_2$ 4, Hepes 10, adjusted to a pH of 7.2 with NaOH. Pipette Ringer was composed of (in m*M*): KCl 165, NaCl 5, $CaCl_2$ 0.5, $MgCl_2$ 1.5, K^+ EGTA 5.0, K^+ ATP 2.5 adjusted to pH 7.4 with KOH. Experiments were done at 15°C. Using a prepulse protocol that would detect both voltage- and time-dependent inactivation, as well as the kinetics of activation and inactivation, we found several classes of cells. In one class, most or all of the outward current showed no inactivation (Fig. 1A). This group included cells with either rapid or slow activation and deactivation kinetics. A second class of cells showed a rapid voltage-dependent inactivation of the outward current (Fig. 1B). At a −60 mV holding potential, this current was only partially inactivated (see Fig. 1B, upper data trace of current response to prepulse step to −10 mV from −60 mV holding potential). This current had fast activation and deactivation kinetics. The inactivating current

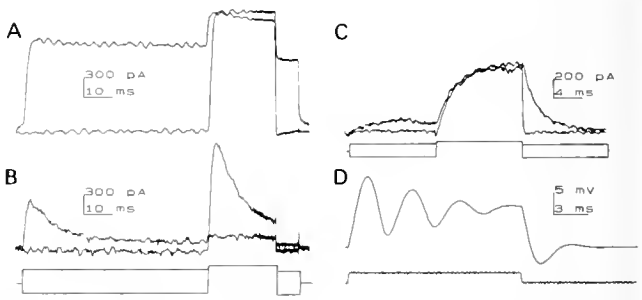

Figure 1. *Data from three different hair cells (A, B, C) illustrating differences in activation, inactivation and deactivation rates of the outward current. Voltage command protocol (A, B, lower left, C, below) consisted of a prepulse step from −60 mV holding potentials to either −110 or −10 mV followed by a test pulse to +10 mV and repolarization back to prepulse levels. (D) Current clamp record (from cell in C), produced high quality resonance of the membrane potential in response to 100 pA current command pulses (lower right frame). Note difference in time calibrations. This data was selected from a pool of 31 cells from which whole cell recordings have been made to date. The cells selected here are representative of the three classes, based on qualitative assessment of activation, deactivation and inactivation rates.*

has features resembling a current termed an A current in other hair cells (2, 9, 10). However, because its calcium dependence has not been tested, it cannot yet be differentiated from an inactivating calcium activated potassium conductance with similar kinetics that has been described (11, 12). A similar inactivating current was found in toadfish saccule that blocked rapidly with TEA, leaving behind a more rapidly inactivating current that was presumed to be an A current (8). The rapid activation seen in Figure 1B from a membrane holding potential close to physiological values (−60 mV) indicates that this current could play a significant role in sensory coding in these hair cells. Figure 1C, D shows another cell with no inactivation of outward current in the voltage clamp mode and resonance in the current clamp

mode, with a resonant frequency of 290 Hz at cell resting membrane potential. If resonance is coding characteristic frequency of a hair cell, this value is high for a system with low frequency response dynamics, such as the semicircular canals. The variety of ionic currents and high resonant frequency indicates the potential for complex coding by these hair cells.

This work was supported by NSF 9120497 and NIMH MH48190.

Literature Cited

1. **Art, J. J., and R. Fettiplace. 1987.** *J. Physiol. Lond.* **385:** 207–242.
2. **Hudspeth, A. J., and R. S. Lewis, 1988.** *J. Physiol. Lond.* **400:** 237–274.
3. **Fuchs, P. A., and M. G. Evans. 1990.** *J. Physiol.* **429:** 529–551.
4. **Steinacker, A., and A. Romero. 1991.** *Brain Res.* **556:** 22–32.
5. **Hudspeth, A. J., and D. P. Corey. 1977.** *Proc. Natl. Acad. Sci. USA* **74:** 2407–2411.
6. **Fuchs, P. A., Nagai, T., and Evans, M. G. 1988.** *J. Neurosci.* **8:** 2460–2467.
7. **Fuchs, P. A., and M. G. Evans. 1988.** *J Comp. Physiol. A.* **164:** 151–163.
8. **Steinacker, A., and A. Romero. 1991.** *Brain Res.* **574:** 229–236.
9. **Lang, D. L., and M. J. Correia. 1989.** *J. Neurophysiol.* **62:** 935–945.
10. **Housley, G. D., C. H. Norris, and P. S. Guth. 1989.** *Hearing Res.* **38:** 259–276.
11. **Pallotta, B. S. 1985.** *J. Physiol.* **363:** 501–516.
12. **Smith, P. A., K. Borvist, P. Arkhammar, P. Berggren, and P. Rorsman. 1990.** *J. Gen. Physiol.* **95:** 1041–1059.

Perforated Patch Recordings From Isolated Skate Bipolar Cells

Richard L. Chappell (Hunter College and Graduate Center of CUNY), Robert Paul Malchow, and Harris Ripps

The perforated patch method of voltage clamping was used to study the pharmacological properties of presumed bipolar cells (Fig. 1A) isolated enzymatically from the all-rod retina of the skate, *Raja erinacea* and *R. ocellata* (1). In accordance with the protocol of Rae *et al.* (2), amphotericin B was used to achieve the perforated patch. In addition to the amphotericin-DMSO solution (2), the pipette solution contained 204 m*M* KCl, 11 m*M* EGTA, 1 m*M* $CaCl_2$, 1 m*M* $MgCl_2$, and 5 m*M* HEPES, adjusted to pH 7.6 with KOH. The time required for amphotericin to insert itself into the cell membranes was quite variable; series resistances declined over the course of 2–3 min for some cells, while others required tens of minutes before a stable recording configuration was achieved. Series resistances varied from 50 to 250 Mohm, averaging 150 Mohm.

The majority of cells from which recordings were obtained responded to 100 μM GABA applied via bath superfusion. With the cells held at −45 mV, GABA elicited outward currents in 33 of 42 cells tested; the current could be markedly suppressed by 200 μM picrotoxin. Puffer pipettes with tip diameters of 2 μm were used in localizing the spatial sensitivity of bipolar cells to GABA. The five cells tested in this manner gave larger responses when the drug was applied to the dendrites and cell soma as compared to the axon or axon terminal (Fig. 1B). Further evidence that distal regions of the cell are sensitive to GABA was obtained in one experiment in which the cell retained its sensitivity to GABA even after the synaptic terminal was excised. Voltage ramps were used to estimate the reversal potential for the currents induced by GABA (Fig. 1C); the mean values were −67 mV (n = 6) when 10 μM GABA was used, and −65 mV (n = 7) when 100 μM was superfused. These values are considerably more negative than those obtained when using whole-cell recording methods with nearly equimolar concentrations of chloride inside and outside the cell (3). The present data suggest that the internal chloride concentration is approximately 19 m*M*.

The responses to other neurotransmitters were considerably more varied. Inward currents were elicited by 100 μM kainate in 32% of the cells tested (n = 31). Surprisingly, only two of fifteen cells tested gave detectable responses to 100 μM glutamate, and only one of eight cells tested responded to 100 μM APB (DL-2-amino-4-phosphonobutyric acid); none of the cells tested responded to 100 μM aspartate. These findings are consistent with those obtained by Lasater *et al.* (4) using intracellular recording methods; *i.e.*, isolated bipolar cells were almost always sensitive to GABA, but few responded to glutamate or its analogs. Perhaps some bipolar cells in the skate retina receive their input solely from the GABAergic horizontal cells, rather than directly from the glutamatergic photoreceptors. On the other hand, it is important to consider the possibility that glutamate receptors are lost in the course of cell isolation.

We also found that 19 of the 37 cells tested, when held at −45 mV, responded to superfusion with 100 μM glycine. Of these, 18 responded with an outward current, while one responded with an inward current. There was very little consistency in the responsivity of the cells to the various agents; *e.g.*, cells responsive to GABA might or might not also exhibit a sensitivity to glycine or kainate. The only pattern to emerge was that every cell that tested positively for kainate also responded to the application of glycine.

Based on their appearance in Golgi-stained sections, and the variability in their responses to drugs, it appears that there may be many different classes of bipolar cell in the all-rod retina of the skate. Two of these can be identified immunocytochemically: one shows immunoreactivity for protein kinase C; another stains positively for serotonin (5). Immunocytochemical methods are being employed in an attempt to distinguish between these two cell types in isolation. Twelve cells from which recordings were obtained were processed for serotonin immunoreactivity. Cells were bathed in serotonin in the presence of pargyline prior to

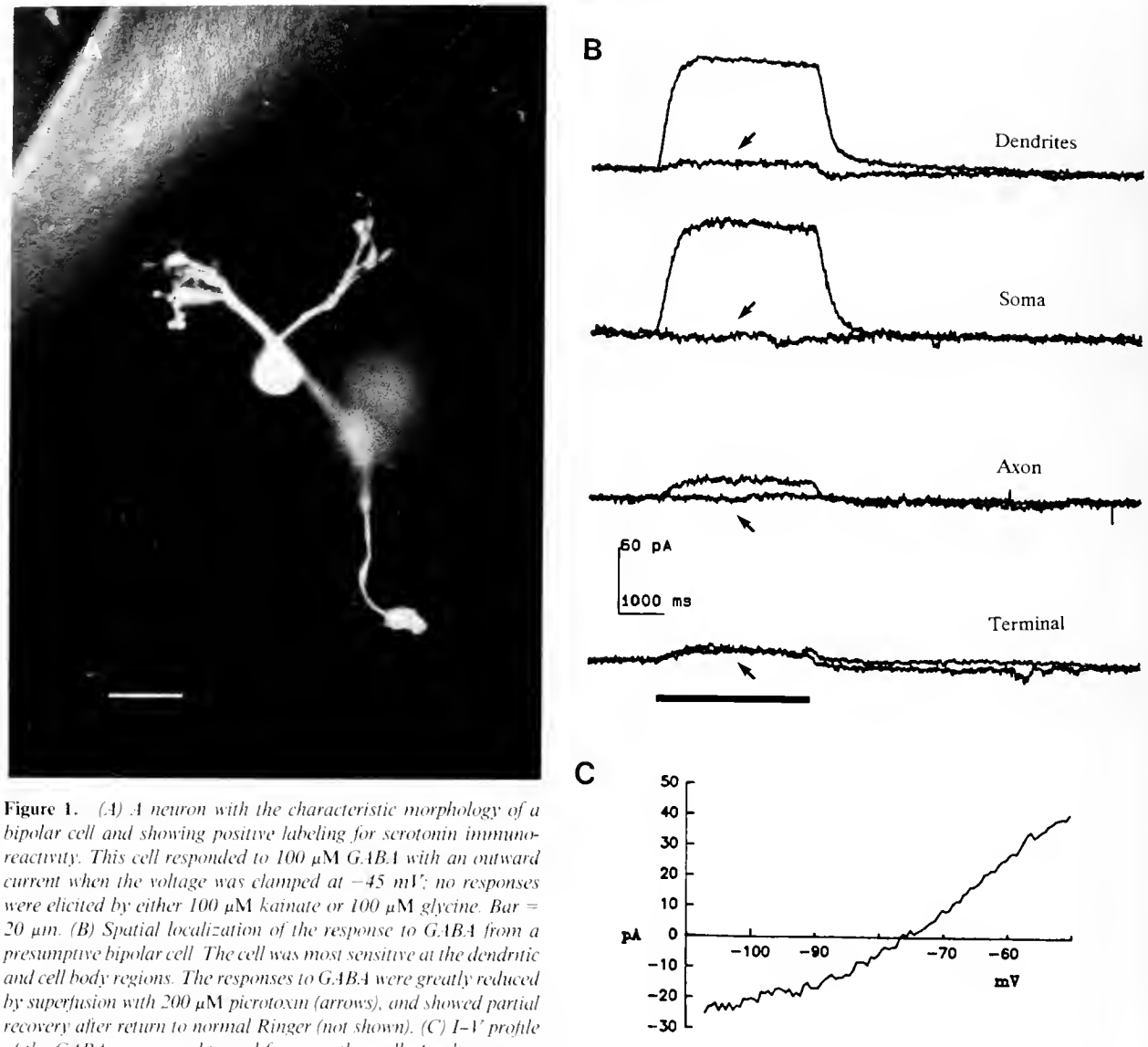

Figure 1. *(A) A neuron with the characteristic morphology of a bipolar cell and showing positive labeling for serotonin immunoreactivity. This cell responded to 100 μM GABA with an outward current when the voltage was clamped at −45 mV; no responses were elicited by either 100 μM kainate or 100 μM glycine. Bar = 20 μm. (B) Spatial localization of the response to GABA from a presumptive bipolar cell. The cell was most sensitive at the dendritic and cell body regions. The responses to GABA were greatly reduced by superfusion with 200 μM picrotoxin (arrows), and showed partial recovery after return to normal Ringer (not shown). (C) I–V profile of the GABA response obtained from another cell. A voltage ramp was applied, and currents obtained in elasmobranch Ringer were subtracted from the currents recorded after the addition of GABA. In this case, the resultant GABA-induced responses reversed from an inward to an outward current at about −76 mV.*

fixation, exposed to an antibody to serotonin, and reacted with an FITC-labelled secondary. Although positive labeling of the cells was often difficult to distinguish from background fluorescence, six of the cells appeared to show labeling above background; each of these cells had responded to superfusion of 100 μM GABA.

Supported by grants (EY-00777, EY-06516, and EY-09411) from the National Eye Institute. H. Ripps is a Research to Prevent Blindness Senior Scientific Investigator.

Literature Cited

1. **Malchow, R. P., *et al.* 1990.** *J. Gen. Physiol.* **95:** 177–198.
2. **Rae, J., *et al.* 1991.** *J. Neurosci. Methods* **37:** 15–26.
3. **Malchow, R. P., *et al.* 1991.** *Biol. Bull* **181:** 323–324.
4. **Lasater, E. M., *et al.* 1984.** *J. Neurosci.* **4:** 1966–1975.
5. **Schlemermeyer, E., and R. L. Chappell. 1991.** *Invest. Ophthal. Vis. Sci.* **32:** 1264.

Second-Order Electroreceptive Cells in Skates Have Response Properties Dependent on the Configuration of Their Inhibitory Receptive Fields

Aimee Salyapongse, Gregory Hjelmstad, and David Bodznick (Wesleyan University)

The elasmobranch electrosense is used to detect localized dipole-like electric fields of prey and to guide the fish's orientation in large scale uniform fields in its marine environment (1). Detection of these biologically relevant stimuli involve the second-order ascending efferent neurons (AEN), which receive convergent excitatory and inhibitory inputs from the primary afferents. This configuration allows the system to suppress ventilatory reafference without sacrificing sensitivity to external fields (2, 3). Unlike AENs, primary afferents are modulated by ventilation and have a simple receptive field (RF) comprising one electroreceptor pore. Afferents are excited by a cathode and inhibited by an anode at the pore. The response of primary afferents to a uniform field stimulus is predictable based on its dipole response and the length of its receptor canal, but this is not true for AENs. In this study, we examined the relationship between the response characteristics of AENs and their receptive fields.

AENs in the little skate *Raja erinacea* were identified by their antidromic response to a midbrain stimulus. Excitatory RFs (activated by cathode) and inhibitory RFs (activated by anode, inhibited by cathode) were mapped with a hand-held dipole. Intensity-response functions were then taken for both a dipole positioned 1 cm from the excitatory RF, and a uniform field oriented in the direction of the excitatory canal(s). Initial slopes of the intensity-response functions are a measure of the AEN's sensitivity to dipole and uniform fields.

All AENs respond well to dipole stimuli with a sensitivity greater than that of the primary afferents due to convergent inputs. The AENs' responses to uniform fields are quite variable, and only about ⅓ (9 of 28 studied) are predictable from their excitatory RFs alone. Instead, the characteristics of the inhibitory RF—its size, location, and relationship to the excitatory RF—determine an AEN's response to uniform fields.

The response of some AENs (2 of 28) to uniform fields is enhanced by having inhibitory and excitatory inputs from receptors whose canals are oppositely directed on the body surface (Fig. 1A). A uniform field of the correct orientation and polarity will not only activate the excitatory inputs but also reduce the tonic inhibitory inputs. The result is increased sensitivity to uniform fields beyond that expected by the excitatory canal length alone. Alternatively, by having excitatory and inhibitory inputs from receptors with canals oriented in the same direction, uniform field sensitivity of many AENs (12 of 28) is virtually eliminated, regardless of excitatory canal lengths (Fig. 1B).

In *Raja erinacea*, the configuration of the inhibitory RF with respect to the focal excitatory RF determines the response characteristics of AENs. While one might hypothesize that AENs could be categorized as either dipole or uniform field "specialists," such an absolute dichotomy does not appear to exist in the medulla.

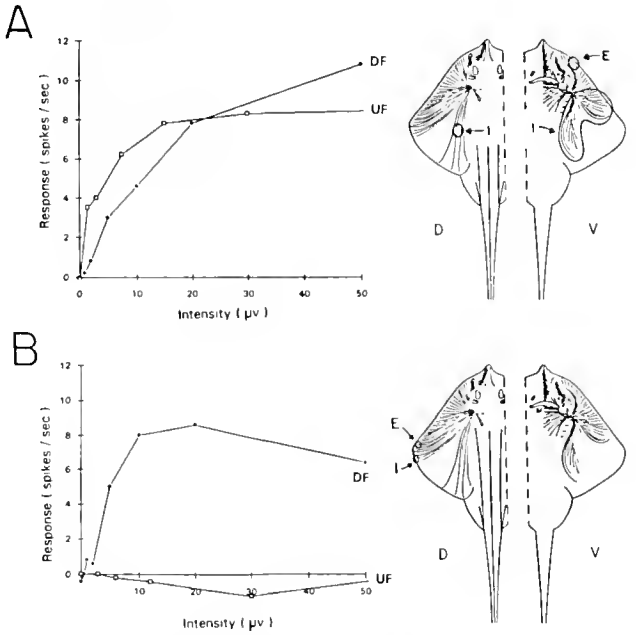

Figure 1. *Intensity-response functions for two AENs to 500 ms DC step dipole (DF) and uniform field (UF) stimuli. Responses to uniform fields were standardized by multiplying the stimulus intensity (μv/cm) by the effective canal length of receptors in the excitatory receptive field (vector canal length in the direction of the uniform field × 0.6, to compensate for effects of skin resistance). (A) Excitatory (E) and inhibitory (I) RFs on oppositely directed receptors enhance longitudinal uniform field sensitivity. (B) Excitatory and inhibitory fields in the same direction eliminate response to transverse uniform field.*

This work was supported by an NSF grant to DB, and a Hughes traineeship to AS.

Literature Cited

1. **Kalmijn, A. J. 1988.** Pp. 151–185 in *Sensory Biology of Aquatic Animals*, J. Atema *et al.*, eds. Springer-Verlag, New York.
2. **New, J. G., and D. Bodznick. 1990.** *J. Comp. Physiol.* **167A:** 295–307.
3. **Bodznick, D., and J. C. Montgomery. 1988.** *Biol. Bull.* **175:** 303.

Voltage-sensitive Dyes for Intracellular Application

Srdjan Antic, Leslie Loew, Joe Wuskell and Dejan Zecevic
(Institute for Biological Research, Belgrade, Yugoslavia)

The significance of regional properties of neurons for signal integration in functional neuronal networks is well established, but detailed analysis has been restricted because, in most cases, membrane potential changes in neuronal processes cannot be recorded with standard microelectrodes. Optical recording methods (1, 2) do allow simultaneous multi-site measurements from neuronal processes (3, 4). We inject voltage-sensitive dyes into individual neurons, and then record optically membrane potential changes from the cell soma and processes in situations where the source of the signal is known. The optical recording system is already optimized with respect to spatial and temporal resolution and signal-to-noise ratio. Better sensitivity, which is still required for the systematic analysis of subthreshold signal integration, can only come from better voltage-sensitive dyes.

The experiments were carried out on neurons from the suboesophageal ganglia of the terrestrial snail *Helix aspersa*. About 30 dyes have been tested for large optical signals after intracellular application. When signals from the cell body were compared, absorption measurements with some of the most sensitive oxonol (JPW1177, RH479, RH482, JPW1241, JPW1245) and merocyanine (WW375, JPW1124, NK2367) molecules were as effective as fluorescence measurements obtained with styryl dyes (RH461, RH437, JPW1114). Signal-to-noise ratio varied, in these measurements, from 1 to 4. However, fluorescence measurements are more effective in a situation where the image of the object (*e.g.*, thin axon or dendrite) is much smaller than the size of a detector. The other important aspect is that absorption dyes are significantly better in terms of photodynamic damage as compared to fluorescence molecules. All aspects of dye characteristics, including pharmacological effects, the rate of spread inside the neurons, and the rate of bleaching have to be considered in choosing the best dye for every particular preparation. We show here the results of using one of the best voltage-sensitive dyes, designated JPW1114, for intracellular application in *Helix* neurons.

The preparation was positioned on the stage of a microscope, and the light from a tungsten-halogen lamp was passed through an appropriate heat and interference filter and focused on the preparation for transmission or epifluorescence measurements. The image of the ganglion was formed by a 20×, .4 NA water immersion objective with an actual magnification, on our microscope, of 26×. The 464 element photodiode array was positioned in the objective image plane. The output of each photodiode was converted to voltage, amplified, and filtered before digitizing. Optical signals were sampled, digitized, and stored in a Motorola VMEbus computer. With a newly implemented provision for resetting the second stage amplifiers, the time that the preparation was exposed to high intensity light could be limited to the actual recording period (about 100 ms) plus an additional 30 ms. This procedure reduced the extent of photodynamic damage in fluorescence measurements.

Figure 1 illustrates the optical recording by epifluorescence. The neuron was stained intracellularly with the positively charged styryl dye, JPW1114, a close analog of widely used di-4-ANEPPS. The dye was pressure injected into the neuron from a microelectrode filled with a solution of 6 mg/ml dye in deionized H_2O. Optical recording is usually done several hours after the injection, allowing the dye to spread into the processes. Since the dye is fluorescent, the shape and size of the soma and processes could be observed by fluorescent microscopy with green excitation light (540/30 nm), a 570 nm dichroic mirror, and a RG610 barrier filter. Both absorption (not shown) and fluorescent signals corresponding to action potentials could be recorded from the cell soma with similar signal-to-noise ratios, but the signal-to-noise ratio in recordings from neuronal processes was markedly larger in fluorescence measurements. In measuring transmitted light from a process, most of the light falling on the photodiode does not carry signal, but adds to the noise.

Figure 1A illustrates the shape of the cell as obtained with a confocal microscope (BioRad facility, MBL, Woods Hole). Figure 1B shows a recording of the light intensity changes, from the 464 elements of the diode array, corresponding to action potentials evoked in the cell by brief transmembrane depolarizations. The size and shape of the neuron, as determined by the spatial distribution of optical signals on the photodiode array, corresponds to the photograph of the cell, with discrepancies due to light scattering and the effects of clearing the preparation in glycerol. Action potential signals from the cell soma and from two processes can clearly be distinguished, demonstrating sufficient spatial resolution that could, in principle, be improved with different objectives. The objectives we used are chosen so to provide adequate depth of field, but once areas of interest on the neuron are determined, higher magnification lenses with higher NA might be effectively used.

Since the shortest sampling interval with the full 464 array is 1.5 ms, a more appropriate time resolution was achieved with a subset of 150 photodiodes chosen to cover the image of the neuron, with a sampling interval of 0.5 ms; a recording is illustrated in Figure 1C. The time resolution is good enough that we can follow the spread of the signal along neuronal processes, as illustrated in Figure 1D. Optical signals lag behind the electrically recorded action potential (not shown) by about 1 ms, due to the low-pass filtering (cutoff frequency of 300 Hz) in optical measurements. This should, however, not influence the relative temporal relationship between optical signals from different parts of the neuron as long as they have similar rates of change. The signal from the soma (average of four different detectors from the soma) occurs about 0.5 ms after the spike in the axon (average of four different detectors from the axon), indicating that stimulation of the soma causes AP generation somewhere in the axon (spike initiating zone), and the signal spreads to the soma with a delay. This delay is probably real, since every point on

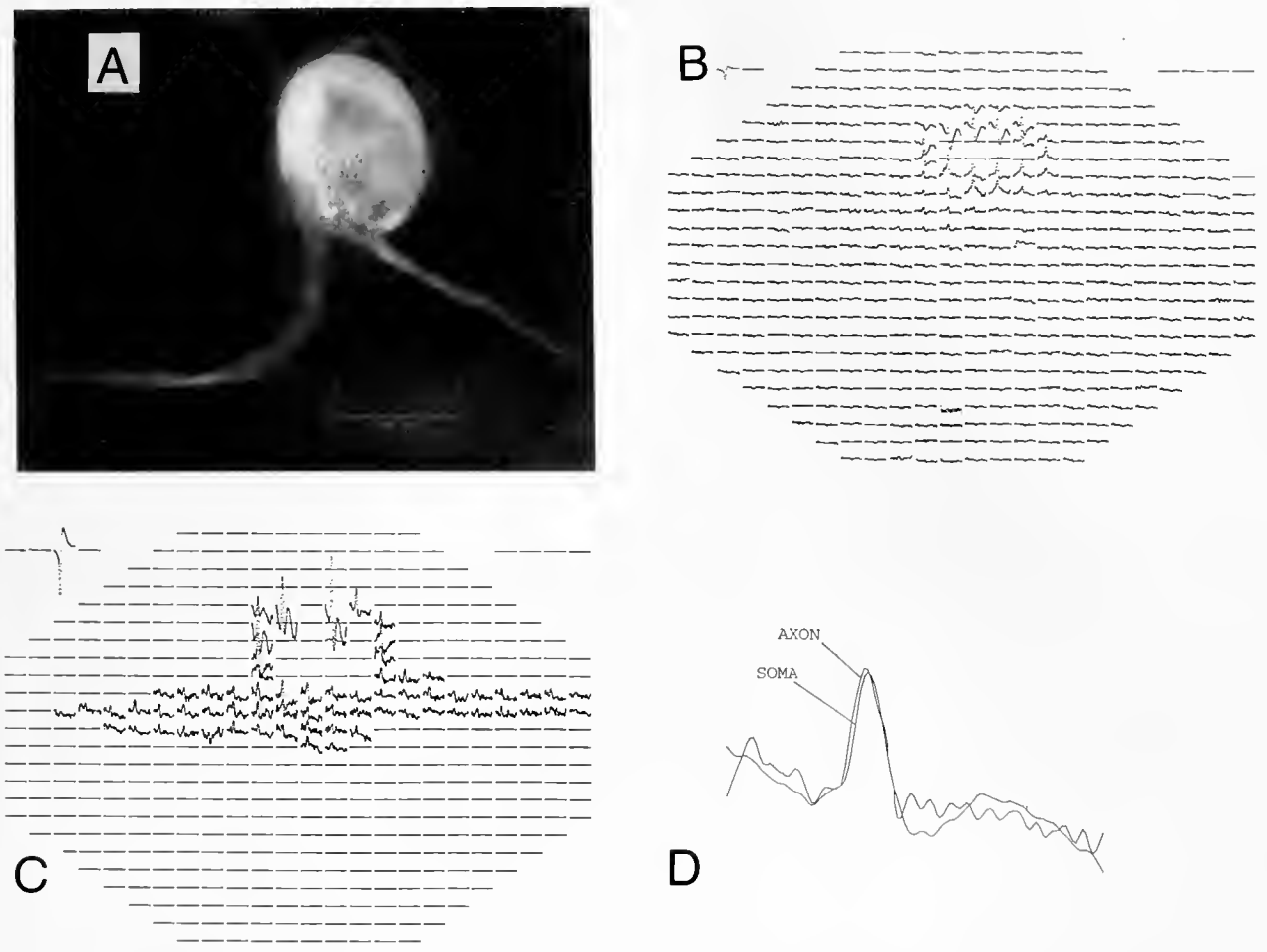

Figure 1. *(A) Fluorescence image of the cell obtained on a confocal microscope. (B) Optical recording from 464 elements of photodiode array. Average of 35 trials. Each photodiode receives light from the square area of 720 μm². The recorded changes in fluorescent light intensity, has been obtained with the green excitation light (interference filter 520/90 nm), a 570 nm dichroic mirror, and a RG610 barrier filter. Some signals (in B and C) from cell body area have been omitted from the figure being too large at the gain appropriate to show signals from processes. (C) Optical recording from a subset of 75 elements of the array with improved temporal resolution. Average of 76 trials. (D) Soma action potential appears with a delay of about 0.5 ms after axon signal; explanation in text.*

the rising phase of the axon signal occurs before the soma signal. The axon signal may also be wider than the soma spike, but the effect of noise could not be excluded.

With this type of recording, even with the sensitivity currently available, membrane potential changes along neural processes can be directly measured, and signal integration in a single cells can be analyzed.

We are grateful to Larry Cohen for help with the apparatus.

Literature Cited

1. **Cohen, L. B., and S. Lesher. 1986.** *Soc. Gen. Physiol. Ser.* **40:** 71–99.
2. **Zecevic, D., J-Y Wu, L. B. Cohen, J. A. London, H-P Hopp, X. C. Falk. 1989.** *J Neurosci.* **9:** 3681–3689.
3. **Ross, W. N., and V. Krauthamer. 1984.** *J Neurosci.* **4:** 659–672.
4. **Grinvald, A., B. Salzberg, V. Lev-Ram, and R. Hildesheim. 1987.** *Biophys. J* **42:** 195–198.

Squid Photoreceptors and Retinas: Content of Phosphatidylinositol-Bisphosphate and Inositol Trisphosphate

Ete Z. Szuts (Marine Biological Laboratory)

Phosphoinositidase C is the target enzyme of the G-protein cascade that mediates signal transduction in invertebrate photoreceptors (review in 1). Phosphoinositidase C, which catalyzes the formation of inositol 1,4,5-trisphosphate ($InsP_3$) and diacylglycerol from phosphatidylinositol-4,5-bisphosphate ($PtdInsP_2$), is critical for the generation of the photoreceptor potential. For example, electrical activity is absent in the eyes of *norp*A mutants of *Drosophila* that lack the active enzyme. The subcellular location of phototransduction is the rhabdomeric microvillus, which contains all the components of the enzyme cascade (rhodopsin, G-protein, and phosphoinositidase C). Although light-stimulated activation of the lipase has now been demonstrated in several invertebrates (horseshoe crab, squid and fruitfly), the levels of $PtdInsP_2$ and $InsP_3$ have been measured only indirectly with the use of radioactive tracers. The purpose of the experiments reported here was to measure the actual concentrations of $PtdInsP_2$ and $InsP_3$ within squid photoreceptors, for which the phosphoinositidase reaction has previously been characterized (2–4).

For analysis of $PtdInsP_2$ content, rhabdomeric membranes were purified under conditions that minimized changes in the endogenous content of phosphoinositides. Two dark-adapted eyecups from *Loligo pealei* were initially rinsed in oxygenated artificial seawater (480 m*M* NaCl; 10 m*M* KCl; 49 m*M* $MgCl_2$; 10 m*M* $CaCl_2$; 5 m*M* glucose; 10 m*M* Hepes; pH 7.8) maintained at 10°C, and were then frozen in isopentane cooled with liquid nitrogen. Freezing abolishes subsequent light-induced hydrolysis of $PtdInsP_2$ (4). The frozen eyecups were thawed in a solution containing 0.4 *M* NaCl, 20 m*M* EDTA, and 50 m*M* Hepes (pH 7.3), were homogenized and the rhabdomeric membranes purified within an hour by two successive centrifugations on sucrose step gradients (5). Each fraction, including the pellet of purified rhabdoms, was analyzed for its content of rhodopsin, protein, and polyphosphoinositide. To calculate the efficiency of recovery for $PtdInsP_2$, [^{3}H]$PtdInsP_2$ was added to the sample of purified rhabdoms prior to lipid extraction. Deacylated lipids were separated on anion-exchange columns, and the eluted fractions were assayed for radioactivity (to detect deacylated [^{3}H]$PtdInsP_2$) and for total phosphate (to detect deacylated $PtdInsP_2$). 0.27 ± 0.06 mol of $PtdInsP_2$ was recovered per mol rhodopsin (mean ± s.d., n = 6) in the purified rhabdoms of unstimulated photoreceptors. Losses during extraction, deacylation, and chromatography were found to be 92 ± 2%. If these losses are corrected for, the basal content of rhabdomeric membranes becomes 3.66 ± 0.85 mol $PtdInsP_2$ per mol rhodopsin. $PtdInsP_2$ represents 3.1 ± 0.7% of the total phospholipids in microvillar membranes, a value similar to that found in rat forebrain (6). Because rhodopsin concentration is ≈1.5 m*M* when averaged over the volume of a rhabdom (7), the results indicate that the concentration of $PtdInsP_2$ is ≈5 m*M* for a typical invertebrate rhabdom. No significant decrease was observed in $PtdInsP_2$ content, if, prior to freezing, retinas were stimulated with a flash that photoactivated 1% of the rhodopsin.

The $InsP_3$ content of squid retinas was measured with a radioreceptor assay (8). Pieces of dark-adapted eyecups were incubated for several minutes at 10°C in oxygenated artificial seawater. Individual pieces were stimulated with a ≈1-ms flash of varying intensity and were quenched with trichloroacetic acid 15 s after stimulation; at this time, the level of [^{3}H]$InsP_3$ is maximal following a similar stimulus (4). Water soluble inositol phosphates were extracted and assayed. The accuracy of the radioreceptor assay was verified by an independent technique using HPLC. The $InsP_3$ content of unstimulated retinas was 30 ± 9 nmol $InsP_3$ per g of tissue (mean ± S.D., n = 8), about twice as much as in rat brains (8). Retinal content also corresponded to 0.15 ± 0.05 mol $InsP_3$ per mol rhodopsin (mean ± S.D., n = 8).Because these measurements were performed with whole tissue, the subcellular distribution of the measured $InsP_3$ in dark-adapted retinas remains unknown. Photoactivating 1% of the visual pigment increased the $InsP_3$ content to 0.68 ± 0.22 $InsP_3$/rhodopsin (mean ± S.D., n = 9). A corresponding change in $PtdInsP_2$ could not have been detected in the previous measurements of that lipid, as the decrease was within experimental error. Because the distal segment contains the rhabdomeric microvilli, it is the most likely cellular source of the light-induced increase of 0.53 $InsP_3$/rho. Ultrastructural analysis of squid photoreceptors (9, 10) indicates that the distal segments contain about 0.4 μl cytoplasmic volume per nmol rhodopsin. As a result, the light-induced concentration of $InsP_3$ may be as high as ≈1 m*M* within the organelle. This value represents total concentration, as some of the molecules may be bound or sequestered. This is the highest $InsP_3$ concentration yet observed for any tissue or cell type.

The high levels measured for both $PtdInsP_2$ and $InsP_3$ in this study are indicative of the highly specialized function of invertebrate photoreceptors, for which the phosphoinositidase reaction is part of the central pathway of transduction.

This work was supported by research grant BNS-8912108 from NSF.

Literature Cited

1. **Shortridge, R. D., and W. L. Pak. 1991.** *Photochem. Photobiol.* **53:** 871–875.
2. **Szuts, E. Z., S. F. Wood, M. S. Reid and A. Fein. 1986.** *Biochem. J.* **240:** 929–932.
3. **Brown, J. E., D. C. Watkins, and C. C. Malbon. 1987.** *Biochem. J* **247:** 293–297.
4. **Wood, S. F., E. Z. Szuts, and A. Fein. 1989.** *J Biol. Chem.* **264:** 12970–12976.
5. **Kito, Y., T. Seki and F. M. Hagins. 1982.** *Meth. Enzymol.* **81:** 43–48.
6. **Nishihara, M. and R. W. Keenan. 1985.** *Biochim. Biophys. Acta* **835:** 415–418.
7. **Goldsmith, T. H. and R. Wehner. 1977.** *J. Gen. Physiol.* **70:** 453–490.
8. **Bredt, D. S., R. J. Mourey, and S. H. Snyder. 1989.** *Biochem. Biophys. Res. Comm.* **159:** 976–982.
9. **Tsukita, S., S. Tsukita and G. Matsumoto. 1988.** *J Cell Biol.* **106:** 1151–1160.
10. **Walrond, J. P., and E. Z. Szuts. 1992.** *J Neurosci.* **12:** 1490–1501.

High Resolution Measurement and Control of Chemical Stimuli in the Lateral Antennule of the Lobster *Homarus americanus*

George Gomez, Rainer Voigt, and Jelle Atema (Boston University Marine Program, Marine Biological Laboratory)

The lateral antennules of the American lobster, *Homarus americanus*, serve in distance orientation in turbulent odor plumes (1). Turbulent odor dispersal results in a chaotic series of odor pulses in different concentrations. Chemoreceptor cells may extract directional information from this temporal stimulus pattern. The study of temporal characteristics of aquatic chemoreceptors requires precise stimulus control, which is difficult to achieve due to boundary layer effects imposed by receptor organs. The antennular chemoreceptors are aesthetasc sensilla that form dense tufts on the ventral surface of the lateral antennule. Odor access is thus limited by a thick boundary layer surrounding the sensilla. To overcome boundary layer effects, the antennule periodically flicks (2). Flicking, together with the patchy nature of odor plumes (3), results in a pulsatile odor delivery to the aesthetasc chemoreceptors. The major goal of this study was to *measure and control* the stimulus delivery in an *in situ* preparation of a lobster lateral antennule and simultaneously record the neuronal responses of single chemoreceptor cells. We combined electrochemical measurements (IVEC-5, Medical Systems) of aquatic odor signals with a fast reproducible stimulus delivery system. The IVEC-5 voltammetry system measures tracer (dopamine) molecules at a spatial (30 μm) and temporal (5 ms) resolution similar to that of an aesthetasc sensillum (4) without affecting biological activity of neurons (5). The electrochemical probes used in this experiment were manufactured from 30 μm carbon fiber inserted and sealed into microelectrodes (4 mm O.D. sodalime glass). Prior to recording, the probes were calibrated and exhibited excellent linearity over a concentration range of 0–20 μM ($r^2 > 0.98$). The electrodes were charged to 0.55 V and current from dopamine oxidation at the electrode tip was sampled at 4 KHz; data points were summed and stored at 200 Hz and displayed on the computer screen for on-line verification.

A concentric pipette system was produced by the insertion of a 1 mm O.D. glass pipette (with its tip tapered and broken to about 0.15 mm I.D.) into a tapered 2 mm O.D./1.25 mm I.D. pipette (0.25 mm tip I.D.). The inner pipette delivered the stimulus solution with 20 μM dopamine tracer while the outer pipette delivered seawater (*i.e.*, wash); both solutions were pressurized to 5 psi. The ejection of fluids from both pipettes was controlled by solenoid valves (5 ms opening/14 ms closing time; Lee Co.) configured such that the stimulus and wash solutions were released alternately. Computer-controlled 5 V pulses triggered the valves and synchronized the stimulus recording with the electrophysiological recording. Stimulus and wash were driven forcibly into the boundary layer to contact the receptor surfaces; excess stimulus was carried away by a 30 ml/min flow superfusing the antennule.

Individual receptor cells were identified as follows. The stimulus pipette was positioned at the tip of an aesthetasc row of hairs and brief pulses were delivered, starting from the most distal segments and progressing toward the proximal end of the antennule. Once a response was observed, the stimulus pipette was positioned along the segment until the minimum response latency was observed. The IVEC probe was then positioned in the aesthetasc tuft at about 200 μm from the base of a sensillum. Our olfactometer allowed localization of the responding cell within one to one-half antennular segment. Because bulk transport processes dominate under these conditions, tracer and stimulus molecules behave similarly. The process used by the IVEC electrode to obtain concentration readings is dopamine molecules contacting and oxidizing at the carbon fiber. This process mimics the way chemoreceptors detect odors (*i.e.*, stimulus molecules must contact the receptor surfaces for a neuronal response to begin). This method cannot account for possible differences due to microscale turbulence that may exist around the sensilla and cause slight differences in the delivery of molecules to the IVEC probe and to the responsive aesthetasc sensillum.

The onset of the stimulus pulse occurs within 5 ms of the valve opening. Recorded pulses had a typical rise time (to 80% of maximum pulse amplitude) of 20 ± 15 ms and a clearance time of 80 ± 40 ms (from 80% of maximum pulse amplitude). A series of ten 100 ms square pulses could be reliably delivered with frequencies up to 4 Hz, varying in peak amplitude by 2.8 ± 1.2% (n = 5). Between different series of pulses in the same preparation, stimulus amplitude varied by 7.1 ± 3.6% (n = 5). In different preparations, variations in stimulus pipette characteristics and electrode configuration caused mean pulse amplitudes to vary within 19.8% (n = 6). Pulse shapes changed slightly due to varying onset times.

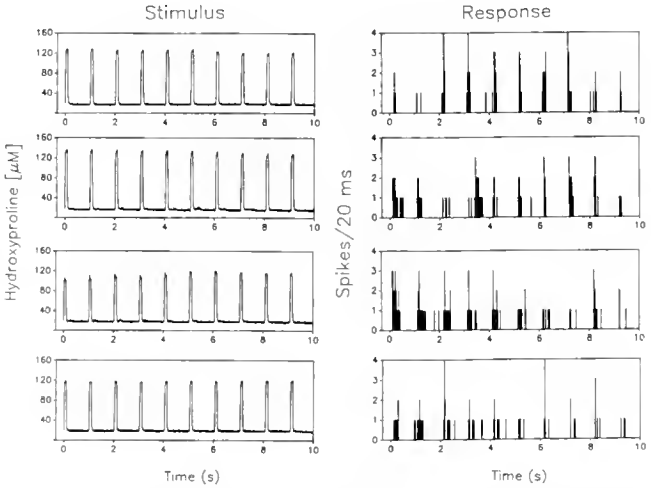

Figure 1. *Stimulus profiles* (i.e., *intensity-time plots) and corresponding responses (number of spikes in 20 ms) of a single chemoreceptor cell to four repetitions of 10 identical stimuli at 1 Hz. Stimulus pulses were highly reproducible; responses of the cell were variable.*

With accurate stimulus measurements in the vicinity of the receptor cells, we gained deeper insight into the response variability of single cells in the lobster antennules. A single hydroxyproline-sensitive cell responded to four identical series of ten 100 ms pulses, delivered at 1 Hz, with 11 ± 8 spikes per pulse (71% variation) and latencies of 114 ± 54 ms (48% variation; Fig. 1). Given an identical series of ten 100 ms pulses at 0.5 Hz, three different cells responded with 6.6 ± 1.9 spikes per pulse (30% variation) with latencies of 265 ± 43 ms (16% variation).

Future applications of this method include studies of temporal filter properties of aquatic chemoreceptor cells, *e.g.*, flicker-fusion and the effects of different pulse shapes. "Turbulent" odor patterns can also be programmed into the computer and played back to the receptor cells to mimic complex but replicated natural conditions.

Supported by NSF BNS 88-12952 to JA.

Literature Cited

1. **Devine, D., and J. Atema 1982.** *Biol. Bull.* **163:** 144–153.
2. **Schmitt, B. C., and B. W. Ache 1979.** *Science* **205:** 204–206.
3. **Atema, J. 1985.** Pp. 387–423 in *Physiological Adaptation of Marine Animals*, M. S. Laverack, ed. The Society for Experimental Biology, Cambridge U.K.
4. **Moore, P. A., G. A. Gerhardt and J. Atema 1989.** *Chem. Senses* **14(6):** 829–840.
5. **Hefti, F., and D. Felix 1983.** *J. Neurosci. Methods* **7:** 151–156.

Cranial Efferent Neurons Extend Processes Through the Floor Plate in the Developing Hindbrain

Eric Marsh, Ken Uchino, and Robert Baker (Department of Physiology and Biophysics, NYU Medical Center, New York, NY)

Cranial nerves III, IV, and VIII contain axons of contralateral efferent neurons in *all* adult vertebrates. Oculomotor neuroblasts appear to migrate across the midline (1), whereas trochlear motoneurons extend their axons through the roof of the aqueduct of Sylvius (2). The midline of the developing vertebrate hindbrain contains specialized neuroepithelial cells that have been postulated to act as a spatial organizer for both commissural and motor neurons (3, 4). Efferent neurons of the VIIIth nerve in all species, and dendrites in some, are distributed bilaterally in the hindbrain (5), but the establishment of a developmental pattern and relationship to the floorplate has never been well characterized for any embryo. The aim of this work was to describe the temporal/spatial organization of efferent neurons of the VIIIth nerve. Surprisingly, leading processes from some efferent neurons in every hindbrain cranial nerve, especially the Vth and VIIIth, exhibited a precocious association with the midline floor plate.

Cationic lipophilic dyes were applied onto the cut ends of dissected III–XII nerve roots in formaldehyde fixed embryos. Four different probes (DiI, DiQ, DiO, and DiA; Molecular Probes), each exhibiting a distinct lipid bilayer mobility, were used to enhance comparisons within the same specimen (Fig. 1A). Hindbrain whole-mounts cleared in glycerol were examined with epifluorescence, Nomarski, and confocal microscopy. Subsequently, the embryos were embedded in agarose and sectioned transversely with a Vibratome at 50 μm (Fig. 1C–D). The detailed descriptions and illustrations in Figure 1 derive from staged chick embryos (H-H 17–25), with key features corroborated in shark and mouse embryos.

By Stage 17, motoneurons are differentiated for all of the chick cranial nerves (6) with cell somata located adjacent to the floor plate on the side of dye application (ipsilateral) in rhombomeres (rh) 2–8 (Fig. 1A). Early as Stage 18, fine processes with apparent growth cones are observed in rh 2 extending toward and along the ipsilateral border of the floor plate (Fig. 1B). By Stage 19, many processes have crossed the midline and approach the contralateral edge of the floor plate (Fig. 1C). The diameters of these processes vary, from the barely observable, up to 2 μm. Although the processes are initially confined to the caudal half of rh 2, by Stage 22 many are observed in rh 3. At Stage 24 a few efferent neurons were observed near the midline of the floor plate, and a rare cell appeared on the contralateral side. The contralateral processes were still present in Stage 26 chick, E-12.5 day mouse and Stage 27 shark embryos.

A similar but more extensive pattern of migration and process formation was observed for efferent neurons with axons presumably entering the VIIIth cranial nerve. Processes extended slightly later in rh 4, but quickly appeared more numerous than those in rh 2 (Fig. 1E). By Stage 21, a large number of cell somata covered the entire rh 4 floor plate boundary and a few cells appeared contralaterally (Fig. 1F). At this time, very fine processes were also observed to reach the contralateral nerve root from ipsilaterally located cells. Extensive axonal crossing of VIIIth efferents was largely confined to rh 4 in the mouse, but the interchange included rh 5 by H-H 23 in the chick and rh 4–6 in the shark (7). By contrast, separate dye labeling of the VIIth and VIIIth nerves revealed only a few chick VIIth motoneurons with crossing processes, while none were seen in the mouse. Efferent neurons of the VI, IX, X, XI, and XIIth nerves also extended processes through the floor plate with more exuberance for branchiomotor than for somatomotor neurons. Notably, processes from neurons of the IIIrd nerve root did not appear in the midbrain midline until Stage 22 in the chick, and the first presumed migration of motoneurons was not observed until Stage 24.

These observations demonstrate that some efferent neurons of all the cranial nerves develop and extend growth cone-like processes into and across the embryonic floor plate, most strikingly for cells with axons in the Vth and VIIIth nerves. Efferent neurons of V through XII tender contralateral processes before

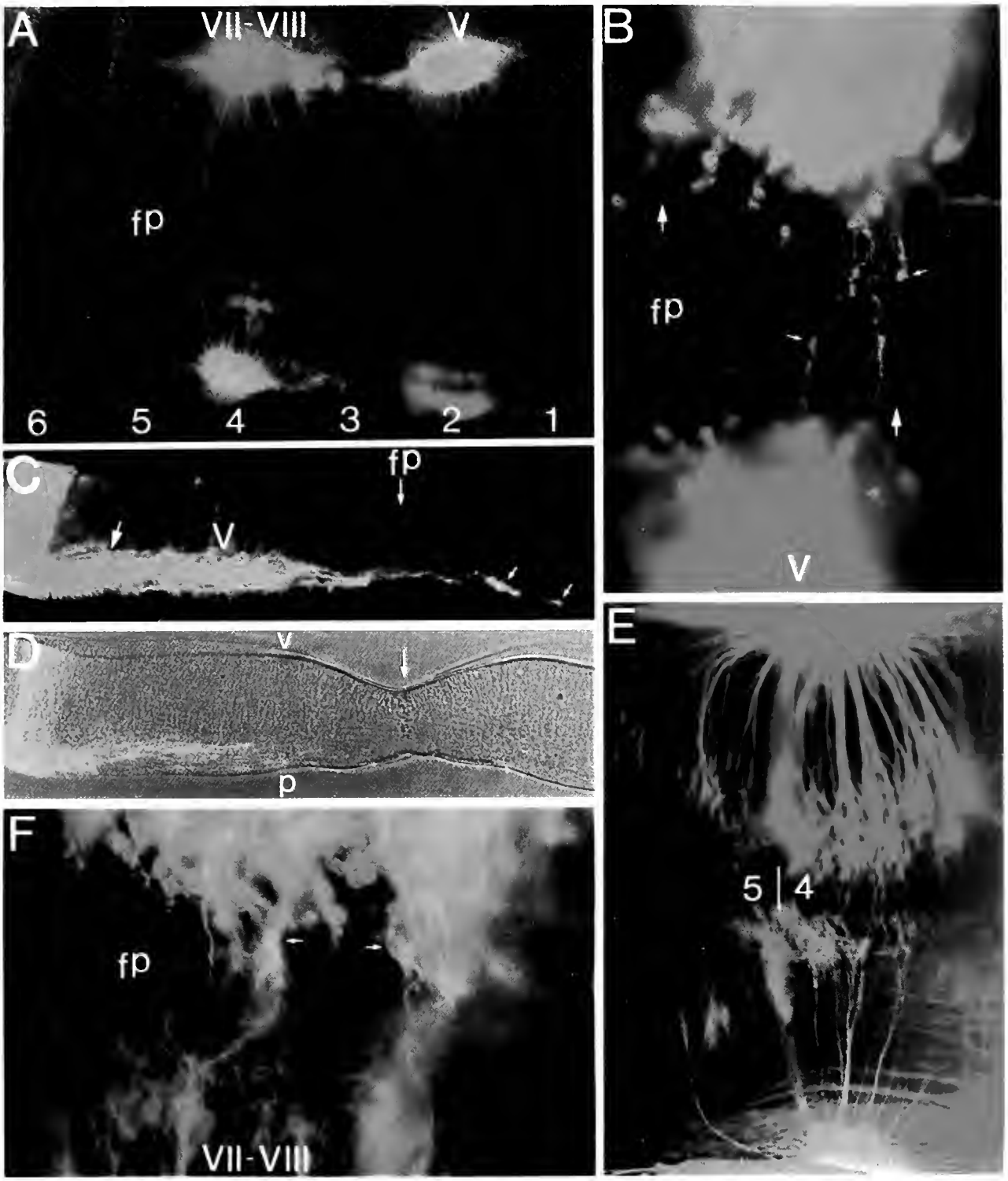

Figure 1. *A–A Stage 18 chick embryo hindbrain viewed ventrally with combined brightfield-epifluorescence illumination showing six rhombomeres and the exit points of cranial nerves V and VII–VIII at rh 2 and rh 4 respectively. DiO (red) and DiA (yellow) were applied to the right and left V th nerves respectively. DiO (green) and DiI (orange) to the right and left VII–VIIIth nerves. The micrograph shows motor cells and processes adjacent to the floorplate (fp) in the even numbered rhombomeres. B: Higher magnification of a Stage 19 chick hindbrain revealing V th nerve processes. DiO left, DiA right, in the midline with growth cones (small arrows) extending contralaterally across the floorplate (fp). Fibers are seen advancing on the ipsi- and contralateral side of the floorplate (large arrows). C: Transverse section through rh 2 showing the major*

either IIIrd or IVth motoneurons. Contralateral neurite outgrowth is initiated in rh 3 and rh 4. Leading processes remain robust and aligned with the rh 2/3 and rh 4/5 neuromeric boundary through the stages examined. Apparently, zones delimited by the processes of the floorplate act as guideposts that attract and direct the movement of neurons and their processes (8). Cells, neurites (presumed-dendrites), and axons advance towards and through the floor plate where they migrate axially adjacent to it, on either the ipsi- or contralateral side (Fig. 1B). Collectively, these observations suggest that the floor plate plays as significant a role in patterning the contralateral leading processes of hindbrain efferent neurons as it does for those of the intrinsic commissural neurons.

This work was supported by the National Eye Institute.

Literature Cited

1. **Puelles-Lopez, L., F. Malagon-Cobos, and J. M. Genis-Galvez. 1975.** *Exp. Neurol.* **47:** 459–469.
2. **Tello, F. 1922.** *Libro en honor de D. Santiago Ramon y Cajal.* Madrid, **1:** 205–258.
3. **Bovolenta, P., and J. Dodd. 1990.** *Development* **109:** 435–447.
4. **Jessel, T. M., P. Bovolenta, M. Placzek, M. Tessier-Lavigne, and J. Dodd. 1989.** *Ciba Found. Symp.* **144:** 255–280.
5. **Roberts, B. L., and G. E. Meredith. 1989.** Pp. 445–459 in *The Mechanosensory Lateral Line.* S. Coombs, P. Gorner, and G. Munz, eds. Springer-Verlag, Berlin.
6. **Lumsden, A., and R. Keynes. 1989.** *Nature* **337:** 424–428.
7. **Gilland, E., and R. Baker. 1992.** *Bio. Bull.* **183:** 000–000.
8. **Hirano, S., S. Fuse, and G. S. Sohal. 1991.** *Science* **251:** 310–313.

Longitudinal and Tangential Migration of Cranial Nerve Efferent Neurons in the Developing Hindbrain of *Squalus acanthias*

Edwin Gilland and Robert Baker (Department of Physiology and Biophysics, NYU Medical Center, New York, NY)

The organization of the embryonic hindbrain neuroepithelium provides three, roughly orthogonal, types of pathways for migrating neurons: radial (1), tangential (2) and longitudinal. Dye labeling of cranial nerves III–XII in embryos of the spiny dogfish shark, *Squalus acanthias,* demonstrates that migration of immature cranial nerve efferent neurons occurs predominantly along tangential and longitudinal pathways. Cationic lipophilic dyes (DiI, DiQ, DiO and DiA; Molecular Probes) were applied to either the peripheral trunks or severed roots of cranial nerves III–XII in formaldehyde-fixed dogfish embryos at Scammon Stages 24–28. After one to three days of dye diffusion, the hindbrains were cleared in glycerol and mounted flat for viewing with combined brightfield and epifluorescent illumination.

Retrogradely labeled efferent neurons were first visible as segmentally arrayed clusters of cells located in the primitive motor column adjacent to the floorplate (3). Because no other elongated processes were present on the cells, their first neuritic projections were the axonal processes that ran laterally along tangential paths to the root exit zones. The next phase of cranial efferent neuronal development involved either: (a) perikaryal translocation within the tangential axonal processes, resulting in "lateral migration" of the neuronal somata; or (b) projection of secondary, caudally directed processes along the edge of the floorplate, with concomitant caudal perikaryal translocation. Early lateral translocation predominated in a rostral population of trigeminal efferent neurons located in rhombomeres (rh) 2 and 3 (Fig. 1A, large arrow in B), a pattern similar to that seen during trigeminal development in amniotes (4). Early caudal translocation occurred in a subgroup of trigeminal neurons in rh 3 (Fig. 1B, small arrow) as well as the majority of efferent neurons of the branchial (VII, IX, X) and octavolateral (ALLN, VIII) nerves located in rh 4–8 (Fig. 1C).

The caudal translocation of efferent neuronal somata occurred over relatively long distances (Fig. 1A–C). Trigeminal efferent neurons migrated from rh 3 to a location adjacent to the abducens motoneurons in rh 6 (Fig. 1C, VI). Similarly, subgroups of octavolateral efferents were first seen at Stage 24 in rh 4 and rh 5, and by Stage 26 were located adjacent to efferent neurons of the IXth and Xth nerves in rh 7 and rh 8 (Fig. 1C). A significant number of the octavolateral efferents projected axons either contralaterally or bilaterally (Fig. 1E). All of the IXth nerve efferents that arose in rh 6 migrated caudally and became intermingled with the IXth nerve efferents of rh 7 (Fig. 1C).

In most of the branchial and octavolateral efferent neuronal populations, the caudal migration was followed by a second phase of tangential neurite extension (Fig. 1D–F). Laterally directed neurites were seen extending from the caudally migrated neuronal groups. At slightly later stages, the neuronal somata appeared to have translocated laterally within these putative dendritic domains, and the number of medially located somata was

fascicle (large arrow) to run laterally towards the Vth nerve exit zone, but some fibers with growth cones (arrows) reaching through the floorplate (fp). (D) Bright field illumination of C disclosing the distinctive midline floorplate area (arrow) as well as the pial (p) and ventricular (v) surfaces. (E) A Stage 21 chick embryo with labeled VIIIth nerves (DiI right, DiO left) demonstrating that most processes cross in rh4, and at the rh4/5 boundary. (F) High magnification of a Stage 23 VIIIth nerve label, (DiO and DiI) illustrating crossing processes and cells (arrows) within the floorplate (fp).

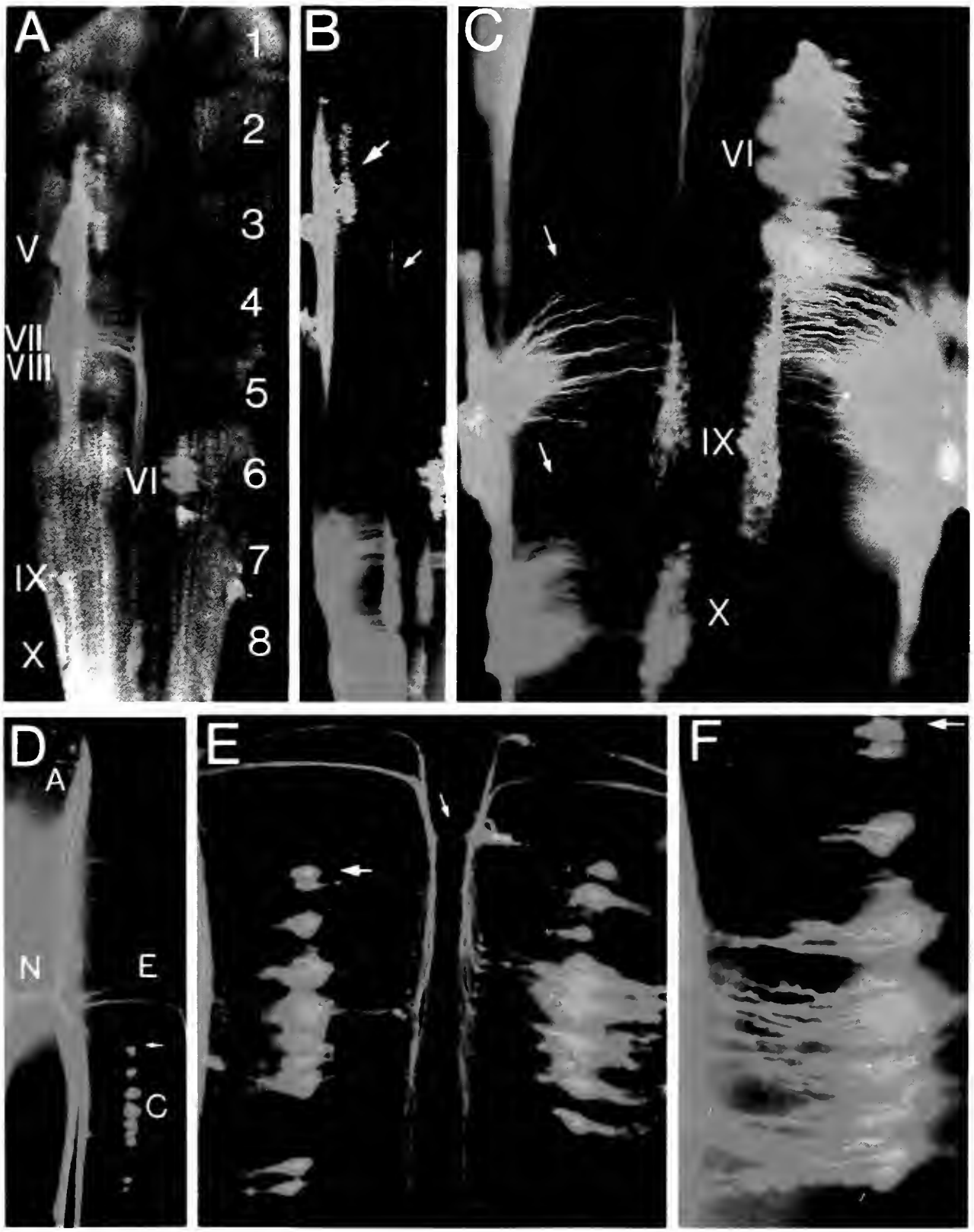

Figure 1. (A–C) *Stage 26 hindbrains viewed ventrally in either combined brightfield-epithonescence (A) or epithonescence alone (B and C). Rhombomeres 1–8 and nerve root exit zones I–X are indicated in A. The large and small arrows show the lateral and caudal subgroups of trigeminal motoneurons, respectively. In A and C, DiA (yellow) was applied to the right Vth and both IXth nerves. DiI (orange) to the right VII–VIII*

reduced. The complete sequence of (1) tangential (lateral) axonal projection from the medially located origin zone followed by (2) longitudinal [illegible] and then (3) tangential (lateral) perikaryal translocation resulted in a laterally open horseshoe configuration (Fig. 1). Transversely oriented somata were arranged in a ladder-like pattern within the basal plate. The putative dendritic processes extended laterally to the afferent fiber tracts while the axons of these cells ran medially and then ascended along the edge of the floor plate, from which they departed laterally in their original transversely oriented pathways to the root exits.

Many of the neuronal somata of cranial nerve efferent neurons come to lie far caudal to their root exit points. This pattern is brought about not by rostral extension of axons from caudal zones of origin, but rather from caudal perikaryal translocation of neurons born rostrally. The caudal translocation occurs over distances of one to three neuroepithelial segments. This characteristic pattern is repeated with few variations in all of the branchial and octavolateral efferent neuronal populations; by contrast, axial translocation does not occur in the "somatomotor" populations of nerves III, VI and XII.

This work was supported by the Grass Foundation and the National Eye Institute.

Literature Cited

1. **Edwards, M. A., M. Yamamoto, and V. S. Caviness. 1990.** *Neuroscience* **36:** 121–144.
2. **Bourrat, F. and C. Sotelo. 1990.** *J. Comp. Neurol.* **294:** 1–13.
3. **Gilland, E. and R. Baker. 1990.** *Biol. Bull.* **179:** 230.
4. **Heaton, M. B. and S. A. Moody. 1980.** *J. Comp. Neurol.* **189:** 61–99.

Localization of Myelin Proteins in the Developing Shark Spinal Cord

Robert M. Gould, Warren D. Spivack, Edwin Gilland, Harish C. Pant and Dan Tseng (Marine Biological Laboratory and NYS Institute for Basic Research in Developmental Disabilities, Staten Island, NY)

All but the most primitive vertebrates have heavily myelinated central (CNS) and peripheral (PNS) nervous systems; jawless fish have no myelin (1, 2). To understand how myelin sheaths evolved, we are studying the properties of myelination in cartilagenous fishes, descendants of the first animals with myelinated nervous systems (1, 2).

Both oligodendrocytes that myelinate the vertebrate CNS and Schwann cells that myelinate the PNS use the same two proteins to sculpture myelin. Protein zero, P_0, is the major protein component of fish myelin and of mammalian PNS myelin. It is an integral membrane protein (in fish it appears to be a family) with a single membrane spanning domain, and an extracellular domain like members of the immunoglobulin gene superfamily of cell adhesion proteins (3). Cells transfected with P_0 cDNA express this protein and aggregate (4, 5). This aggregation is speculated to be equivalent to joining external myelin membrane surfaces causing compaction. Myelin basic proteins, MBP, an alternatively spliced family of low molecular weight basic proteins that account for 15–30% of myelin protein, are believed to cause compaction of the cytoplasmic myelin leaflets (6). Together these proteins catalyze the "jelly-rolling" of myelin sheaths.

P_0 and MBP have been cloned from two sharks, *Heterodontus francesci* (7) and *Squalus acanthias* (Spivack, Zhong, Saavedra and Gould, in prep.). Amino acid sequences of both proteins show roughly 45% identity with mammalian P_0 and MBP. To study the developmental regulation of these proteins in Squalus acanthias spinal cord, polyclonal antibodies were prepared against gel-purified MBP and P_0. The P_0 antibody recognized several low molecular weight (24–28 kDa) and lower abundance high molecular weight (60–70 kDa) species in homogenates of adult shark medulla (Fig. 1A). The MBP antibody recognized two low molecular weight isoforms (14–16 kDa); slight cross-contamination was indicated by light staining of bands in the region corresponding to the P_0 doublet.

Bouin's fixed, paraffin embedded embryos 4, 5.5, and 13 cm long were used; at birth, neonates 24–28 cm long, contain heavily myelinated CNS and PNS. The present report focuses on motor tracts in the ventral funiculus, because they are among the first to be myelinated (Gould and Gilland, in prep.). With both rhodamine- and peroxidase-conjugated secondary antibodies, myelin tracts in the spinal cords of 13 cm embryos were heavily stained with both antibodies. With the 5.5 cm embryo, P_0 staining (Fig. 1B) was more widespread than was staining with the MBP

and DiQ (red) to the Xth nerves. DiA, DiI and DiO (green) labeled the rostral, middle and caudal rootlets of the left VIIth nerve in rh 6. C. Higher magnification view of the rh 6–8 region of Figure 1A. Abducens, glossopharyngeal and vagal efferent somata are indicated by VI, IX and X. The arrows indicate the transverse pathways of exiting IXth and Xth axons. D–F. Octavolateral efferent neurons labeled by application of DiI to the anterior lateral line nerve. The nerve root (N), afferent fibers (A), transverse efferent fibers (E) and efferent cell somata (C) are indicated in D. The arrows in D–F indicate the same cell in each panel. The extensive bilateral labeling shown in E results from a unilateral dye application. Although not in the plane of focus the meshwork of fibers crossing the floorplate is visible between the longitudinal axonal pathways (small arrow).

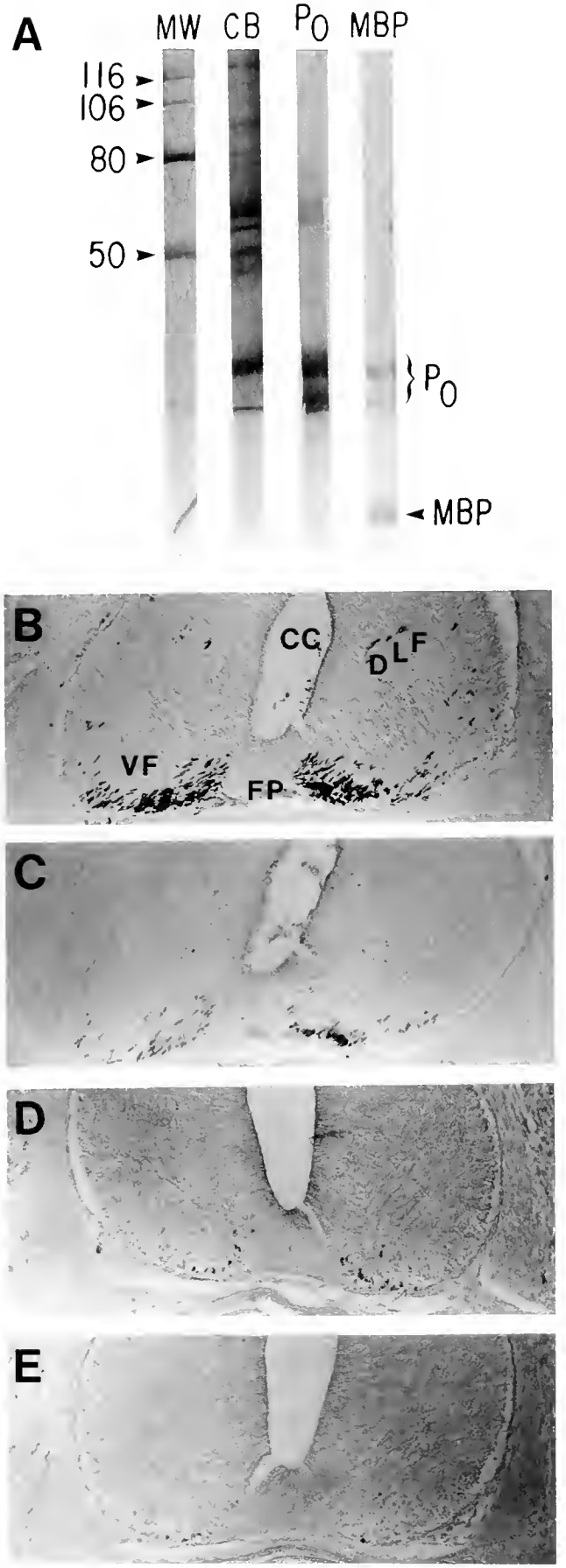

antibody (Fig. 1C). Likewise, in the corresponding region of the 4 cm embryo, P_0 staining (Fig. 1D) was stronger and more widespread than that of MBP. Uyemura *et al.* (8) used immunoblot to show that P_0 expression preceeded that of MBP in the chick sciatic nerve. Taken together, these results are in line with the possibility that the early expression of externally oriented P_0 may play a role in heterophilic interactions with molecules on the surfaces of the large caliber axons about to be myelinated. In this regard that the molecule designated for this role in mammals, myelin-associated glycoprotein (see 9, for review), is absent from shark (10).

These studies were supported by grants from the NIH (NS-13980) and National Multiple Sclerosis Society.

Literature Cited

1. **Young, J. Z. 1989.** *The Life of Vertebrates,* Third Ed., Clarendon Press.
2. **Waehneldt, T. V., J.-M., Matthieu, and G. Jeserich. 1986.** *Neurochem Int.* **9:** 463.
3. **Lemke, G., and R. Axel. 1985.** *Cell* **40:** 501.
4. **D'Urso, D., P. J. Brophy, S. M. Staugaitis, C. S. Gillispie, A. B. Frey, G. Spempak, and D. R. Colman. 1990.** *Neuron* **2:** 449.
5. **Filbin, M. T., F. K. Walsh, B. D. Trapp, J. A. Pizzey, and G. I. Tennekoon. 1990.** *Nature* **55:** 500.
6. **Omlin, F. X., H. deF. Webster, C. F. Palkovits, and S. R. Cohen. 1982.** *J Cell Biol* **95:** 242.
7. **Saavedra, R. A., L. Fors, Aebersold, B. Arden, S. Horvath, J. Sanders, and L. Hood. 1989.** *J Mol Evol* **29:** 149.
8. **Uyemura, K., K. Horie, M. Suzuki, and S. Uehara. 1979.** *J Neurochem* **32:** 779.
9. **Quarles, R. H., D. R. Colman, J. L. Salzer and B. D. Trapp. 1992.** In *Myelin Biology and Chemistry,* R. E. Martenson, ed. CRC Press, Boca Raton, FL.
10. **Zand, D., J. Hammer, R. Gould, and R. Quarles. 1991.** *J Neurochem.* **57:** 1076.

Figure 1. *(A) A homogenate of adult medulla was electrophoresed on 9% SDS-PAGE, transferred to a nitrocellulose membrane, and lanes were stained with coomassie blue (CB), anti-P_0 or anti-MBP. The position of molecular weight standards and P_0 and MBP are indicated. Paraffin sections of rostral spinal cord from 5.5 (B, C) and 4 (D, E) cm long embryos were stained with anti-P_0 (B, D) or anti-MBP (C, E) polyclonal antibodies and visualized with peroxidase. Positions of the central canal (CC), ventral funiculus (VF) and deep lateral funiculus (DLF) are indicated.*

Individual Actin Filaments Visualized by DIC (Nomarski) Microscopy

Andreas Stemmer (Marine Biological Laboratory)

I introduce a methodology for visualizing individual, non-fluorescent actin filaments by differential interference contrast (DIC or Nomarski) video microscopy.

To date, high-quality light microscopy imaging of individual actin filaments has been restricted to the use of fluorescent labels either directly attached to actin monomers or to phalloidin complexed with actin filaments (1). The high photon yield of these labels allows the detection of single filaments even with standard video or photo microscopical equipment. Unlabeled single actin filaments decorated with heavy meromyosin or S-1 have also been imaged in dark-field (2). To study the dynamics of actin assembly and disassembly and actin-based motility in living cells as well as cell-free extracts, an imaging mode is required that (i) provides high contrast, (ii) does not require fluorescent labels, which may shift equilibrium concentrations or otherwise interfere with the dynamics of the system, and (iii) is far less susceptible to the deleterious effects of other light scattering objects than is dark-field illumination.

DIC video microscopy combined with well corrected, high-numerical-aperture (NA) optics has proven capable of visualizing the dynamics of individual unlabeled microtubules (3), and bacterial flagella (4). But the mass per unit length of actin filaments is 10 times less than that of microtubules, so one might expect a contrast about 100 times lower. Over the time necessary to acquire an image, this low contrast would be even further reduced by the blurring effect of Brownian motion, thus creating a real challenge for light microscopy.

To explore the feasibility of visualizing single actin filaments in DIC, actin monomers isolated from rabbit skeletal muscle acetone powder were polymerized at room temperature in the presence of rhodamine-labeled phalloidin and subsequently diluted before being mounted on a slide or injected into a flow chamber. To minimize Brownian motion of filaments, coverslips were coated with poly-L-lysine or rabbit muscle myosin to provide a surface for adsorption and hence mechanical stabilization. This preparation also provided for the best possible resolution, allowing the maximum advantage of corrections designed into high-quality objectives. Light microscopy was performed on a Microphot-SA (Nikon, Inc.) equipped with a carefully selected 60×/1.4 NA DIC Plan Apochromat objective lens and corresponding 1.4 NA DIC condenser, a 100W Hg light source for epifluorescence, and a 100W Hg lamp with mirror, light scrambler (Technical Video, Inc.), broad-band green interference filter, and an external high-transmission polarizer mounted on the field lens for DIC illumination (all parts from Nikon, unless otherwise indicated). With the DIC illumination shuttered off, areas containing faint (single) as well as bright (bundled) actin filaments were identified by epifluorescence, oriented by rotating the microscope stage so that the long axis of faint filaments became predominantly perpendicular to the shear axis of the DIC set-up, and recorded with a SIT camera (Hamamatsu Photonics) and an Image-1 data acquisition and processing system (Universal Imaging Corp.). This procedure of first taking a fluorescent reference image assured unambiguous identification of actin filaments in the corresponding DIC image that was subsequently recorded with a Newvicon camera (Hamamatsu Photonics), because the strong DIC illumination completely and very rapidly bleached the rhodamine fluorescence. In addition, fluorescence intensities could be measured and analyzed for each acquired frame, establishing, as a control value, the actual number of individual actin filaments per apparent filament. Actin filament preparations were also checked in the electron microscope to assure that they consisted of single filaments.

As expected, actin bundles of two or more individual filaments were very easily visualized in DIC. Bundles identified, by discrete steps in fluorescence intensity, as being tapered were also recognized as such in DIC by contrast variations along the filaments similar to observations made on microtubules (5, 6). Visualizing single, immobilized actin filaments (Fig. 1) became possible once the microscope had been carefully tuned to allow for good transfer of high spatial frequencies. Although image quality improved when several frames (≤8) were averaged, detection of single filaments was just feasible at standard video rate.

Ultimately, it should be possible to visualize single actin filaments in their native cellular environment, thus allowing the direct study of transport, motility, and assembly or disassembly dynamics. This formidable task may require special specimen preparation techniques to improve the cellular optical properties,

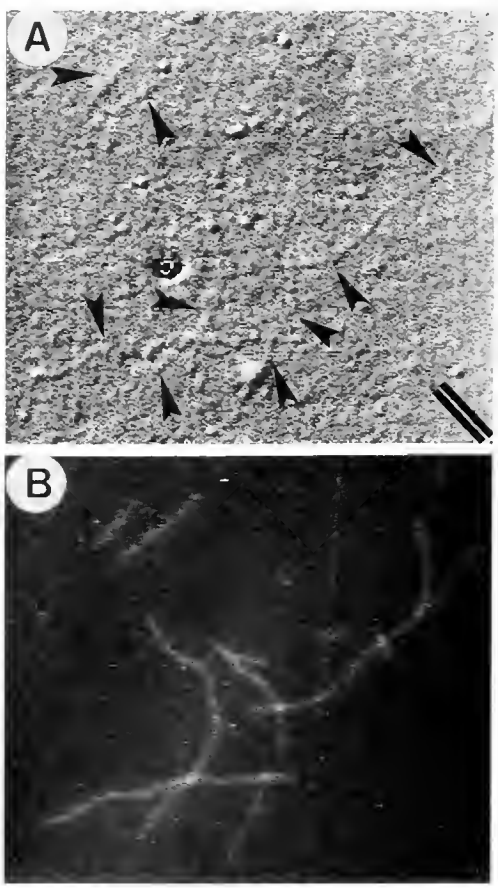

Figure 1. *(A) Unprocessed DIC image of single actin filaments (arrow heads). (B) Fluorescent reference image of identical filaments as shown in A. Note that in DIC contrast is maximal when filaments are oriented perpendicular to the shear axis of the Wollaston prism (double line in A) and minimal when parallel. Width of images is 21 μm.*

and faster than video rate imaging devices, such as shuttered cameras, that will maintain the contrast of filaments that are moving, growing or shortening, and also most likely undergoing rapid Brownian motion. For very short exposure times, brighter light sources, such as lasers, may be required as well.

I thank Nikon, Inc., for their 1992 Nikon Fellowship award. I am indebted to Dr. Shinya Inoué for his generous support and advice and Dr. Lewis Tilney for providing rabbit muscle acetone powder. Financial support through research grants R37GM31617-11 from NIH and MCB-8908169 from NSF (both to Dr. Shinya Inoué) and a Swiss National Science Foundation Fellowship is gratefully acknowledged.

Literature Cited

1. **Yanagida, T., M. Nakase, K. Nishiyama, and F. Oosawa. 1984.** *Nature* **307:** 58–60.
2. **Nagashima, H., and S. Asakura. 1980.** *J. Mol. Biol.* **136:** 169–182.
3. **Cassimeris, L., N. K. Pryer, and E. D. Salmon. 1988.** *J. Cell Biol.* **107:** 2223–2231.
4. **Block, S. M., K. A. Fahrner, and H. C. Berg. 1991.** *J. Bacteriol.* **173:** 933–936.
5. **Schnapp, B. J., J. Gelles, and M. P. Sheetz. 1988.** *Cell Motil. Cytoskel.* **10:** 47–53.
6. **Inoué, S. 1989.** *Methods Cell Biol.* **30:** 85–112.

Fluorescence Microscopy of Single Actin Filaments Labeled by Conjugation to Rhodamine

E. L. Bearer (Dept. of Pathology, Brown University, Providence, RI, and Marine Biological Laboratory)

Actin filaments have traditionally been visualized by electron microscopy or by fluorescence microscopy of filaments saturated with fluorescently labeled phalloidin (1, 2). The conjugation of a rhodamine fluorochrome directly onto actin monomers has made possible the observation of actin dynamics inside living cells (3). These filaments are easily observed when acting as a group or bundle, but are not bright enough to be detected as individual filaments (4). Individual actin filaments directly conjugated to fluorescein have been described, but this approach has not proved generally useful because of rapid photobleaching (4, 5). In this report, I describe a method to label actin monomers with rhodamine such that individual single filaments can be observed over long periods with computer-assisted video fluorescence microscopy.

Rabbit skeletal muscle actin was purified (5) and stored at a concentration of 7–10 mg/ml at 4°C in F-buffer [10 m*M* Tris,

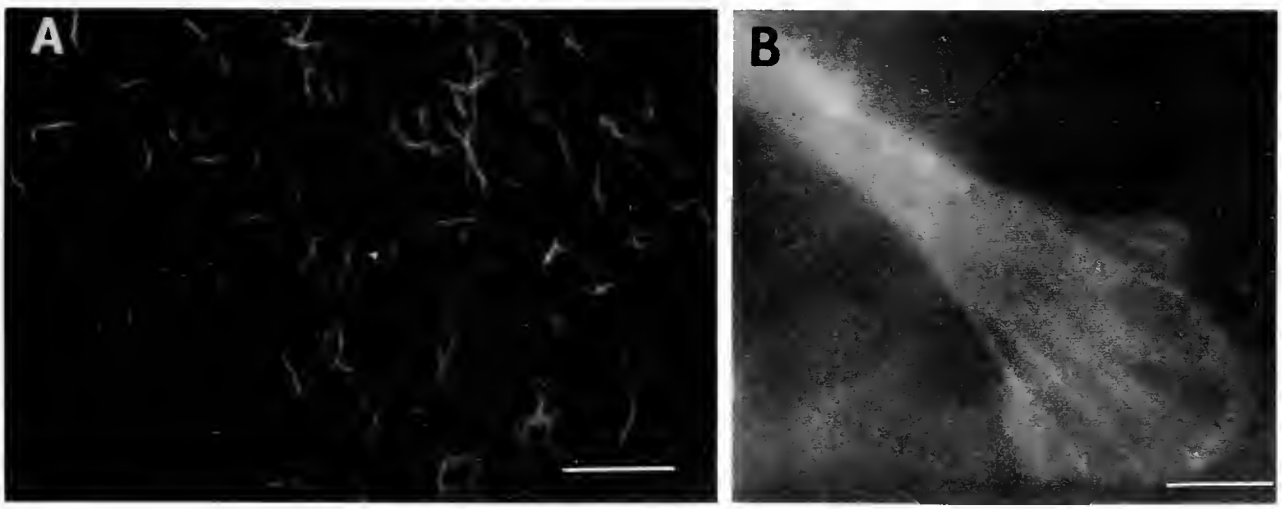

Figure 1. *(A) Filaments were formed by diluting 1 μl of thawed stock r-actin with 200 μl assay buffer (AB) (25 m*M *Imidazole, 25 m*M *KCl, 4 m*M *$MgCl_2$, and 5 m*M *DTT). The critical concentration was identified by observing the minimal concentration of protein required to form filaments* in vitro. *This was readily done by looking at different dilutions of the stock actin in AB by fluorescence microscopy. Filaments were visible without computer-enhanced video, and could be photographed directly onto 35 mm TMax ASA 3200 film with the Zeiss Axioscope available in the Zeiss facility at MBL. Parlodian-coated gold grids were coated with the same preparation of polymerized actin, either freeze-dried and rotary shadowed, or negatively stained with 1% uranyl acetate, and examined by electron microscopy. Only single filaments were found, and no bundles were observed. (B) The growth cone of a neurite produced by a neural crest cell from a* Xenopus laevis *embryo that had been injected with 1 ng of r-actin at the two-cell stage 3 days previously. Stress-fiber-like bundles and the ruffle at the leading edge contained fluorescent filaments. These filaments disappeared upon perfusion of the chamber with 10 μM cytochalasin B. The image was collected with the aid of Argus 10 image processing. Bars = 10 μ*

50 m*M* KCl, 2 m*M* $MgCl_2$, 1 m*M* ATP, and 0.2 m*M* dithiothreitol (DTT)]. Actin from this stock (5 mg) was dialyzed against 200 ml of reaction buffer (50 m*M* Pipes, pH 6.8, 50 m*M* KCl, 0.2 m*M* $CaCl_2$, 0.2 m*M* ATP) for 4 h at 4°C. This polymerized actin was diluted to 2–3 mg/ml with reaction buffer, and ATP was increased to 0.5 m*M*. 5(and6)carboxytetramethylsuccinimidyl ester (Molecular Probes, Eugene, OR) was added at a concentration of 3.2 mg/ml. The reaction is allowed to proceed on ice in the dark for 1.5 h. The actin was then pelleted at 50,000 × *g* for 1 h, the pellet resuspended in 0.5 ml of G-buffer (5 m*M* Tris, pH 8.1, 0.2 m*M* $CaCl_2$, 0.2 m*M* ATP, 0.2 m*M* DTT), and dialyzed against three changes of G-buffer for 36 h at 4°C. The depolymerized actin was passed over G-25 gel filtration column (Pharmacia). The first red peak was collected, pooled, polymerized for 1 h by addition of KCl to 50 m*M*, and centrifuged at 50,000 × *g* for 1 h at 4°C. The pellet was resuspended in 200 μl of G-buffer and dialyzed by floatation on a dialysis filter (Millipore) over three changes of 20 ml G-buffer for 18 h at 4°C. The dialysate was spun for 30 min in a Beckman TL 100 at 35,000 rpm. A typical procedure gave a final protein concentration of 1 mg/ml, and a ratio of fluorochrome to monomer of 3:1 (555 nm extinction coefficient).

Rhodamine-labeled actin (r-actin) formed filaments that were readily visible in the fluorescence microscope (Fig. 1A). Typically, the critical concentration ranged from 0.17 to 0.24 μ*M*. Electron microscopy was performed on the same preparation, and only single filaments were observed.

R-actin was injected into the animal cap of frog embryos at the two-cell stage. Neurons cultured 3 days later displayed cytochalasin-sensitive rhodamine-labeled filaments, demonstrating that the labelled actin behaved normally *in vivo* (Fig. 1B).

In conclusion, succinimidyl linkage of rhodamine to actin monomers produces actin filaments that are readily observed by fluorescence video microscopy, and thus will be an excellent tool for the study of actin filament dynamics, such as polymerization.

I wish to thank T. Reese and P. E. Gallant for help with electron microscopic analysis, and J. Zheng and M. M. Poo for *Xenopus* embryo injections. This work was supported by the Council for Tobacco Research.

Literature Cited

1. **Kron, S. J., Y. Y. Toyoshima, Q. P. Uyeda, and J. A. Spudich. 1991.** *Methods Enzymol.* **196:** 399–416.
2. **Bearer, E. L. 1991.** *J Cell Biol.* **115:** 1629–1638.
3. **Wang, Y.-L. 1991.** *Current Opin. Cell Biol.* **3:** 27–32.
4. **Simon, J. R., A. Gough, E. Urbanik, F. Wang, F. Lanni, B. R. Ware, and D. L. Taylor. 1988.** *Biophys. J.* **54:** 801–815.
5. **Honda, H., H. Nagashima, and S. Asakura. 1986.** *J Mol. Biol.* **191:** 131–133.
6. **Pardee, J. D., and J. A. Spudich. 1982.** *Methods Enzymol.* **85:** 164–181.

Bidirectional Gliding of Microtubules From Squid Axoplasm

S. A. Kuznetsov, G. M. Langford (Department of Biological Sciences, Dartmouth College, Hanover, NH 03755), and D. G. Weiss

ATP-dependent gliding of microtubules over a glass surface was first observed in preparations of axoplasm obtained from the giant axon of the squid (1, 2). Subsequently, gliding motility of microtubules has been used extensively to characterize the organelle motors responsible for anterograde and retrograde axonal transport; *i.e.*, kinesin and dynein (3, 4, 5). The early studies of microtubule-dependent organelle motility in axoplasm revealed that native microtubules (nMTs) exhibited principally kinesin-dependent gliding (6). Bidirectional gliding of nMTs in squid axoplasm preparations was expected to occur because both kinesin and dynein are present (3, 7, 8). However, bidirectional gliding has not been reported to date. The aim of this report is to provide evidence that MTs reverse direction while gliding, thereby exhibiting bidirectional gliding, and that the interaction of the MT-based motors kinesin and cytoplasmic dynein with the gliding nMTs can account for this phenomenon.

Axoplasm was obtained from the giant axons of the squid (*Loligo pealei*) by extrusion (9) and maintained in the axoplasmic dissociation buffer as previously described (10). The gliding movements of nMTs in axoplasm preparations were observed by AVEC-DIC video microscopy (2).

After extrusion, numerous nMTs dissociated from the bulk axoplasm and moved along the glass surface to which they were attached. Careful observation revealed that, in these preparations, bidirectional gliding was observed. Bidirectional gliding differs from typical continuous gliding; it includes movement for long distances (>15 μm) in one direction followed by a brief pause and then movement in the opposite direction at a faster velocity and for a shorter distance. The latter usually occurred for a distance equal to, or less than, the length of the nMT segment (2–10 μm). Bidirectional gliding nMTs showed several episodes of direction reversal with distinct differences in the velocity in the two directions.

Motion analysis of gliding motility was performed with a computer-assisted tracking program, and the data were quantitatively evaluated with the software packages PARTI-MOVI and SPSS (9). In the 27 preparations of extruded axoplasm examined in this study, 10 showed bidirectional gliding motion. In these 10 preparations, 14 nMTs were analyzed in detail, and 41 measurements of movement at the slower velocity were made. The slower velocity ranged between 0.22 and 0.61 μm/s with an average of 0.42 ± 0.10 μm/s. For the same 14 nMTs, 27 measurements were made of movement at the faster velocity. The faster velocity ranged between 0.46 and 1.79 μm/s with an average of 0.92 ± 0.33 μm/s. The slower velocity was similar to the average velocity reported for kinesin-dependent microtubule

Table I

Conditions for microtubule gliding

Treatment concentration		[ATP]	Continuous gliding	Discontinuous gliding	Bidirectional gliding
Control	—	2 m*M*	+	+	+
Control	—	—	+	+	+
Apyrase	5U/ml	—	−	−	−
Hexokinase	10U/ml				
+ glucose	5 m*M*	—	−	−	−
AMP-PNP	4 m*M*	—	−	−	−
Vanadate	10 μM	2 m*M*	+	−	−
	100 μM	2 m*M*	−	−	−
EDTA	5 m*M*	2 m*M*	−	−	−
EGTA	5 m*M*	2 m*M*	+	+	+
Cytochalasin B	10 μM	2 m*M*	+	+	+

(+) Gliding motility present in control and experimental; (−) gliding motility not observed in experimental, but present in control. In all experiments, half of axoplasm was used as control for axon quality and the presence of bidirectional gliding. In the case of EDTA treatment, Mg^{2+} and Ca^{2+} were omitted, and in the case of EGTA treatment, Ca^{2+} was omitted.

gliding (2, 3, 9), whereas the faster velocity was similar to the average reported for cytoplasmic dynein-dependent movement of microtubules (5).

Of all nMTs observed, about two thirds were in the process of gliding. Although, the majority (about 80%) of gliding nMTs exhibited movement at the kinesin-like velocity (continuous gliding), and a small fraction exhibited bidirectional gliding, a much smaller number of nMTs (less than 5%) showed discontinuous gliding exclusively at the dynein-like velocity. Microtubules in 8 of the 27 preparations exhibited movement at the dynein-like velocity while gliding in a discontinuous fashion. These nMTs exhibited Brownian motion when gliding and therefore appeared weakly attached to the glass surface. A given nMT moved for a short distance (less than the length of the nMT segment), paused while pivoting slightly due to Brownian forces, and then continued moving with the same relative velocity for a short distance. The average velocity was 0.96 ± 0.31 μm/s, a value not significantly different from the average for the faster velocity exhibited by nMTs undergoing bidirectional gliding.

To determine which motors were involved in bidirectional and discontinuous gliding, experiments with agents that influence these motilities were performed. Bidirectional and discontinuous gliding of nMTs required ATP (Table I). Depletion of endogenous ATP by the addition of hexokinase or apyrase inhibited movement. AMP-PNP, an inhibitor of dynein and especially of kinesin ATPase activity, blocked all forms of gliding, whereas 10 μM vanadate, an inhibitor of dynein ATPase activity, blocked bidirectional and discontinuous gliding. 100 μM vanadate inhibited all forms of gliding. EDTA, but not EGTA, also blocked bidirectional gliding. Therefore, agents that are known to block either kinesin- or dynein-dependent movement inhibited bidirectional gliding (Table I). Bidirectional and discontinuous gliding of nMTs were insensitive to 10 μm cytochalasin B; therefore actin filaments and actin-dependent motors were not involved.

In this report, we have shown that nMTs can undergo direction reversal while gliding. This is the first demonstration of directionality switching of gliding nMTs. The velocities of gliding in the two directions were distinctly different and corresponded to the velocities reported for kinesin-dependent (2, 3, 9) and cytoplasmic dynein-dependent (5) microtubule gliding. Furthermore, bidirectionality of gliding was abolished by either dynein or kinesin inhibitors, while disruption of the actomyosin system had no effect. These results lead us to conclude that two motors, kinesin and cytoplasmic dynein, are responsible for movement in the two directions rather than a single motor undergoing reversal of its direction of force generation.

We conclude that nMTs switch their polarity of gliding by alternately interacting with kinesin, a (+) end directed motor, and cytoplasmic dynein, a (−) end directed motor. Bidirectional gliding of nMTs may provide an assay for studying the regulation of directionality switching of organelle movement in axons and may serve as a model for motile systems, such as saltatory vesicle movement and possibly prometaphase chromosome oscillations during mitosis.

Supported by A. von Humboldt and MBL Fellowships (SAK), DFG grant We790/12-1 (DGW), and NSF grant BNS9004526 (GML).

Literature Cited

1. **Allen, R. D., and D. G. Weiss. 1985.** Pp 327–333 in *Cell Motility: Mechanism and Regulation,* H. Ishikawa, S. Hatano, and H. Sato, eds. University Press, Tokyo.
2. **Allen, R. D., D. G. Weiss, J. H. Hayden, D. T. Brown, H. Fujiwake, and H. Simpson. 1985.** *J Cell Biol* **100:** 1736–1752.
3. **Vale, R. D., B. J. Schnapp, T. S. Reese, and M. P. Sheetz. 1985.** *Cell* **40:** 559–569.
4. **Vale, R. D., T. S. Reese, and M. P. Sheetz. 1985.** *Cell* **42:** 39–50.
5. **Paschal, B. M., H. S. Shpetner, and R. B. Vallee. 1987.** *J Cell Biol* **105:** 1273–1283.
6. **Weiss, D. G., D. Seitz-Tutter, and G. M. Langford. 1991.** *J Cell Sci Suppl* **14:** 157–161.
7. **Gilbert, S. P., and R. D. Sloboda. 1989.** *J Cell Biol.* **109:** 2379–2394.
8. **Schnapp, B. J., and T. S. Reese. 1989.** *Proc. Natl. Acad. Sci. USA* **86:** 1548–1552.
9. **Weiss, D. G., G. M. Langford, D. Seitz-Tutter, and F. Keller. 1988.** *Cell Motil. Cytoskel* **10:** 285–295.
10. **Kuznetsov, S. A., G. M. Langford, and D. G. Weiss. 1992.** *Nature* **356:** 722–725.

Rapid Loading of Molecules into Animal Cells using a Radio-Frequency Electric Field

D. C. Chang (Hong Kong University of Science and Technology and Marine Biological Laboratory), D. S. Y. Leung, M. Ehrlich, and P. Q. Gao

The introduction of isolated genes or recombinant DNA into cultured cells is a key procedure in cell and molecular biological research. At present there are many methods for gene transfer. All of these methods have certain shortcomings. Most of them are strongly cell-type dependent (*i.e.*, they can work only on certain cells), and the transfer efficiency is frequently unsatisfactorily low. Furthermore, these methods often produce undesirable biological or chemical side-effects.

Recently, a new physical method has been developed (1). The cell membrane can be temporarily permeabilized by exposing the cell to a pulse of high intensity electric field (2). This process is attributed to the creation of resealable pores in the cell membrane and is thus called "electroporation." The electroporation method offers more advantages than most other methods. First, it is simple to use and is time efficient. It can also be used to inject a single cell or millions of cells. Second, because it is a physical method, electroporation is less dependent on cell type. Third, it has fewer harmful biological and chemical side effects. In the last several years, the electroporation method has been successfully used to introduce cloned genes into a wide variety of cells, including mammalian cell lines, isolated cells, plant cells, bacteria, and yeast (3, 4).

In addition to gene transfer, electroporation has the potential for use as a micro-injection method to introduce molecules other than DNA, such as second messengers, kinases, and kinase inhibitors, drugs, and antibodies into a large number of cells. We are currently working to improve this technology.

Our approach is to experiment with different wave forms and pulse protocols and to test their effects on cell survival rate and transfection efficiency. Our earlier results had suggested that, by using a radio-frequency (RF) electric field instead of the direct current (DC) field that is commonly used in conventional electroporation, one can significantly improve the transfer efficiency (5). This summer, we have used this RF electroporation method to introduce molecular probes into a variety of cell types, including mammalian cell lines, sea urchin eggs, and cultured neurons. The label molecules injected into the cells were rhodamine-conjugated Dextran (M.W. 10, 40, 70 KD), and CMV-β-galactosidase.

The design of the RF electroporation apparatus is described in reference 5. The cells were washed and suspended in a low ionic strength poration medium and transfered into cuvettes with two parallel electrodes 1 mm apart. A train of RF electric pulses was then applied (frequency 40 kHz, typical pulse width 2 ms, room temperature). The experimental variables include electric field strength, number of trains of pulses, number of pulses per train, and interval between pulses. Generally, the percentage of cells loaded with the injected molecules increases as electric field strength increases, while cell survival rates increase as electric field strength decreases (Fig. 1). Using an electric field strength close to the optimal range, 80% to 100% of the cells can be loaded with Dextran, and up to 50% of the cells can take up and express the β-gal gene. Under such conditions, approximately 50% of the total cells can survive. Loading of the molecules has no apparent effect on cell survival rate. Cell death is attributed mainly to the electrical treatment.

Table 1

Transfection efficiency using different pulse protocols

Cell type	Pulse protocol*	Optimal field (kV/cm)	Ratio of transfection efficiency**
K562	3 × 5 pulses (1.0 s interval)	1.3–1.4	1
	3 × 15 pulses (0.1 s interval)	0.8	3.05
3T6	1 × 15 pulses (0.1 s interval)	1.0	1
	1 × 5 pulses (0.1 s interval)	1.1	1.65
COS-M6	1 × 5 pulses (0.1 s interval)	1.3–1.4	1
	1 × 15 pulses (0.1 s interval)	1.1–1.2	1.64
	capacitor discharge (C = 500 μF, R = 100 Ω)	0.8–1.0	0.53

* "M × N pulses" indicates that M trains of electric pulses, each train containing N pulses were applied.

** Transfection efficiency is a measure of the amount of reporter gene expressed in the surviving cells multiplied by the survival rate. Results are the averages of three (K562, 3T6) and two (COS-M6) experiments.

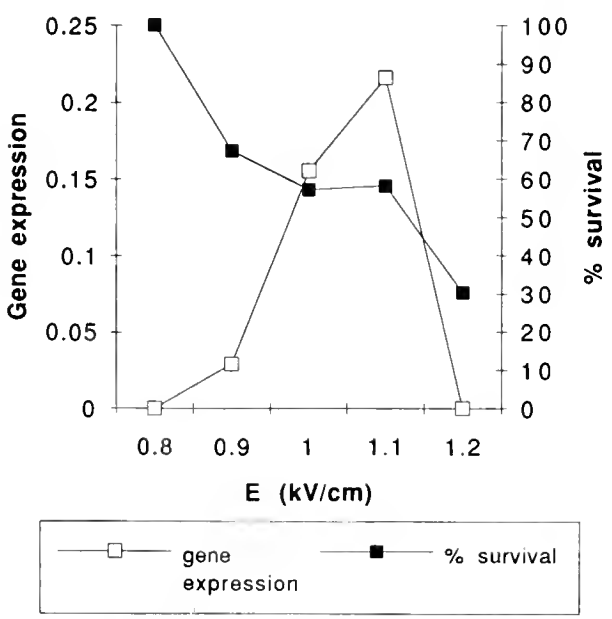

Figure 1. *Gene expression in the 3T6 cell line.*

Our results with three different cell lines (K562, 3T6, and COS-M6) are summarized in Table 1. The assay involved the transfection of the reporter gene, CMV-β-galactosidase (β-gal). We found that the optimal electrical parameters differ from one cell line to another. For example, K562, a suspended cell, favors long trains of many pulses, whereas the 3T6 cell, an attached cell, favors short trains of fewer pulses. The optimal electric field at which gene expression is maximized also clearly differs between cell types. Data in Table 1 also confirms that the RF field gives higher transfection efficiency than a DC field generated by capacitor discharge (CD).

Electroporation experiments with other cells (including eggs and neurons) were assayed using β-gal gene and fluorescent labeled Dextran. We showed that molecular probes can be introduced into these cells without lysing them. The experimental procedures, however, still require further refinement. A requirement critical to minimizing the disturbance of cell function when the cell is permeabilized, is to formulate special media to preserve the integrity of the cytoplasmic environment and to promote membrane resealing.

The authors wish to acknowledge the important contributions of Dr. David Epel in the sea urchin experiment, and Dr. Stephanie Kaech in the neuron experiment. Work was partially supported by grants from NSF, ATP and BRI to D.C.C.

Literature Cited

1. **Chang, D. C., B. M. Chassy, J. A. Saunders, and A. E. Sowers. 1992.** *Guide to Electroporation and Electrofusion,* Academic Press Inc., San Diego.
2. **Kinosita, K., and T. Y. Tsong. 1977.** *Nature* **268:** 438–441.
3. **Wong, T. K., and E. Neumann. 1982.** *Biochem. Biophys. Res. Commun.* **107:** 584–587.
4. **Potter, H. 1988.** *Anal. Biochem.* **174:** 361–373.
5. **Chang, D. C. 1989.** *Biophys. J.* **56:** 641–652.

Heterogenous Distribution of Fluorescent Phorbol Ester Signal in Living Sea Urchin Embryos

John H. Connor, James L. Olds, David S. Lester, Donna L. McPhie, Stephen L. Senft, Jennifer A. Johnston, Daniel L. Alkon (NINDS, National Institutes of Health)

The major protein receptor for the active phorbol esters is the Ca^{2+}/phospholipid-dependent protein kinase (PKC; 1, 2). Limited studies in which flouresecent phorbol esters were employed have suggested that such probes may be useful for studying PKC function in living cells (3, 4).

Initial experiments were performed with an established model membrane system specifically developed for analyzing biochemical and biophysical interactions between PKC and its lipid milieu (5, 6). BODIPY-labeled phorbol esters were chosen as they have a significantly higher quantum yield and are considerably more photo-stable than other phorbol ester compounds labelled with alternative fluorophores (7). Because similar concentrations of BODIPY phorbol ester (proprionoyl form) and the unlabeled phorbol ester inhibited the binding of ^{3}H-phorbol dibutyrate binding to purified PKC (IC_{50} = 20 nM), the fluorophore and the unlabelled analog compete probably for the same binding site. The emission spectra of the membrane-incorporated BODIPY probe (100 nM) were determined in different lipid mixtures and in the presence or absence of divalent cations and purified cytosolic PKC. When Ca^{2+} (100 μM), Mg^{2+} (5 mM), and PKC (10 μg/ml) were added to small unilamellar vesicles (SUVs) composed of the neutral phospholipid, phosphatidylcholine (PC; 50 μM), no significant change was seen in the fluorescent signal monitored on a spectroflourometer. Qualitatively different responses were monitored when the above components were added to SUVs composed of 50% PC and 50% of the PKC-activating acidic phospholipid, phosphatidylserine (PS). Mg^{2+} had little effect (9.5% decrease), whereas Ca^{2+} caused a significant increase on the emission spectrum (18.1%). Ca^{2+} is known to reorganize PS lipid structures, a process considered to be important in the mechanism of PKC activation (8). Addition of PKC to this Ca^{2+}:Mg^{2+}:lipid complex produced a 19% increase in the fluorescent signal, suggesting that specific protein-lipid and lipid-lipid interactions thereby altering the fluorescent properties of this probe.

The role of PKC in sea urchin egg activation has been well described (9). To gain further insight into PKC function during this process, we used established methods (10) to examine the behavior of BODIPY phorbol-ester under different conditions in eggs from *Lytichinus pictus.* Activation of eggs was induced by the dilution of dried sperm into artificial seawater. Unlabelled eggs examined with specific filters in epifluorescence microscopy showed an autofluorescence level that did not interfere with BODIPY labeling studies. Therefore, we determined both the optimal concentration of the fluorescent probe and the optimal time of incubation (Fig. 1A, B). Preincubation of eggs with BODIPY phorbol ester for 40 min at 25 nM was determined to be optimal and was used in successive experiments. Viewed with the Zeiss Universal Microscope, unfertilized eggs displayed a relatively homogenous degree of labelling. However, unfertilized eggs examined with a confocal microscope revealed a noticeable heterogeneity of intracellular fluorescence. Specifically, signal concentrated at the plasma membrane and was absent from the nucleus (Fig. 1C). Both zygotes and embryos had a noticably lower fluorescent signal than unfertilized eggs (42.3 $\pm$ 4.1 *vs.* 57.6 $\pm$ 1.4, respectively, arbitrary density units). In addition, the fluorescent signal due to BODIPY phorbol ester decreased with subsequent cell divisions in all embryos studied.

To confirm that the observed changes in BODIPY phorbol ester fluorescence are related to the PKC activation process, two factors known to modulate PKC activity, A23187 and arachidonic acid (2), were tested. The addition of both arachidonic acid (50 μM) and Ca^{2+} ionophore, A23187 (10 μM), produced no significant change in fluorescence. To determine the specificity of the BODIPY phorbol ester association with intracellular organelles, sperm and egg preparations were labelled with the mi-

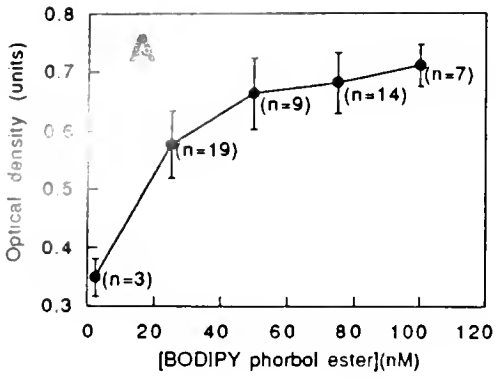

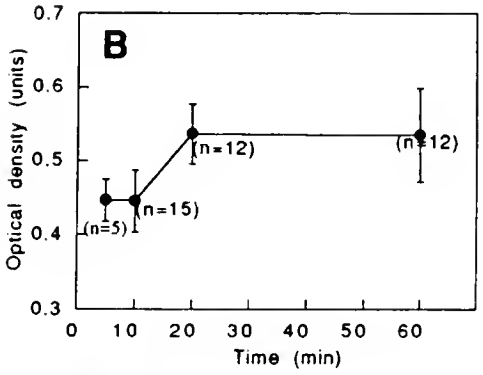

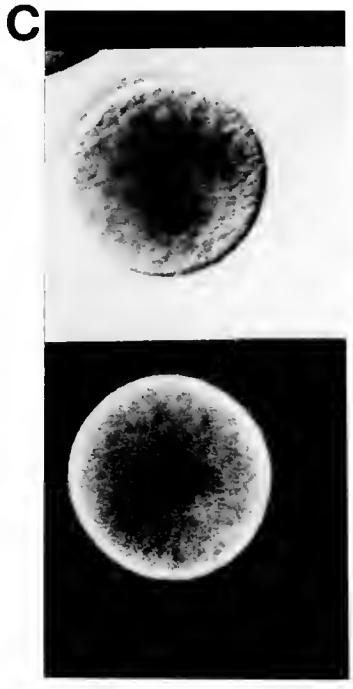

tochondrial fluorescent marker, rhodamine 123 (10 μM), and with BODIPY phorbol ester (Fig. 1C). In zygotes, the rhodamine signal was punctate and was interpreted as being associated with mitochondria. The BODIPY signal appeared coincident with the rhodamine signal and was also associated with other undefined intracellular structures.

These studies demonstrate that fluorescently labeled phorbol ester can be used as an analytical probe of the fertilization process in the sea urchin egg. Upon fertilization, fluorescent labeling decreases, and this can be interpreted in two ways: (1) the microenvironment of the probe changes resulting in a change in the fluoresence signal; or (2) the amount of phorbol ester receptor (*i.e.*, PKC) decreases upon fertilization. The lack of response in fertilized eggs to arachidonic acid and A23187 supports the notion that the PKC membrane association is altered in unfertilized eggs. Thus, the lack of effect of this agent suggests that the decrease in fluorescence observed here is not necessarily due to some change in the lipid environment of the phorbol ester. We are verifying this second possibility by studying the kinetics of BODIPY phorbol ester uptake into fertilized eggs.

Literature Cited

1. **Ashendel, C. L. 1985.** *Biochim. Biophys. Acta* **882:** 219–242.
2. **Nishizuka, Y. 1986.** *Science* **233:** 305–213.
3. **Liskamp, R. M. J., *et al.* 1985.** *Biochim Biophys. Res. Comm.* **131:** 920–927.
4. **Balazs, M., *et al.* 1991.** *J Cell Biochem* **46:** 266–276.
5. **Lester, D. S. 1990.** *Biochim. Biophys. Acta* **1054:** 297–303.
6. **Brumfeld, V., and Lester, D. S. 1990.** *Arch. Biochem. Biophys.* **245:** 140–146.
7. **Johnstone, I. D., *et al.* 1991.** *Anal. Biochem.* **198:** 228–237.
8. **Zidovetzki, R., and D. S. Lester. 1992.** *Biochim. Biophys. Acta* **1134:** 261–272.
9. **Shen, S. S., and L. A. Ricke. 1989.** *Comp. Biochem. Physiol.* **92b:** 251–254.
10. **Wolf, D. E., *et al.* 1981.** *Dev Biol.* **81:** 133–138.

Figure 1. *BODIPY phorbol ester flourescence in sea urchin eggs. (A) Optimization of dose response. Unfertilized eggs were incubated for 40 min at various concentrations of probe. The fluorescent signal was quantified on an MCID imaging system. All values are means ± standard deviation. The number of cells analyzed are shown below each point. (B) Optimization of incubation time. Unfertilized eggs were incubated in probe (25 nM) for various times in artifical seawater (pH 8.0, 18°C). Signal was quantified as in A. (C) Representative image of BODIPY probe incorporation in a living zygote under optimized conditions (see text). The accompanying image is under differential interference contrast microscopy.*

Inhibitory Effect of Tricyclic Antidepressant Drugs on Serotonin-induced Maturation of *Spisula* Oocyte

R. Juneja (Population Council), H. Ueno, S. S. Koide, and S. J. Segal

The neurotransmitter, serotonin (5-hydroxytryptamine, 5-HT), induces spawning (1) when injected into the gonads of the surf clam (*Spisula solidissima*). When added *in vitro* to isolated *Spisula* oocytes, 5-HT and various analogs induce germinal vesicle breakdown (GVBD) and stimulate $^{45}Ca^{2+}$ uptake (1–3). Verapamil, a phenylalkylamine Ca^{2+} channel blocker, effectively blocks 5-HT-induced maturation and $^{45}Ca^{2+}$ uptake by *Spisula* oocytes. Other Ca^{2+} channel blockers, such as dihydropyridine and Cd^{2+} are ineffective. In the present study, tricyclic antidepressants, which block 5-HT action by interfering with Ca^{2+} influx, were used to test the hypothesis that 5-HT induces GVBD by stimulating Ca^{2+} influx.

Induction of GVBD was assayed by adding 5-HT creatinine sulfate at a final concentration of 5 μM to a suspension of *Spisula* oocytes (2000/ml). Oocytes were examined for GVBD by light microscopy. The antidepressants, imipramine · HCl, desipramine · HCl and clomipramine · HCl, were tested at concentrations ranging from 1 to 100 μM. Imipramine, at a concentration of 2 μM, blocks 5-HT-induced GVBD. Desipramine and clomipramine are effective at 10 μM (Fig. 1a).

The effect of antidepressants on 5-HT-stimulated $^{45}Ca^{2+}$ uptake by *Spisula* oocytes was examined (Fig. 1b). 5-HT stimulates an accelerated uptake of $^{45}Ca^{2+}$ after a 2 min lag time. The stimulatory action of 5-HT was blocked by all antidepressants tested at a concentration of 20 μM and verapamil at a concentration of 50 μM. The most efficacious drug was imipramine.

In conclusion, 5-HT induces GVBD of *Spisula* oocytes by stimulating influx of extracellular Ca^{2+}, antidepressants block the Ca^{2+} uptake stimulated by 5-HT. Because the action of the antidepressants mimic that of the channel blocker, verapamil, they too may interfere with gating of Ca^{2+} channels. The bioassay system of 5-HT-induced GVBD of *Spisula* oocytes may prove to be a useful test to screen drugs for potential anti-serotoninergic activity.

This work is supported by a grant GAPS-9032 from the Rockefeller Foundation.

Literature Cited

1. **Hirai, S., T. Kishimoto, A. L. Kadam, H. Kanatani, and S. S. Koide. 1988.** *J. Exp. Zool.* **245:** 318–321.
2. **Kadam, A. L., and S. S. Koide. 1990.** *Invert. Reprod. Dev.* **18:** 165–168.
3. **Kadam, P. A., A. L. Kadam, S. J. Segal, and S. S. Koide. 1991.** *J. Shellfish Res.* **10:** 215–219.

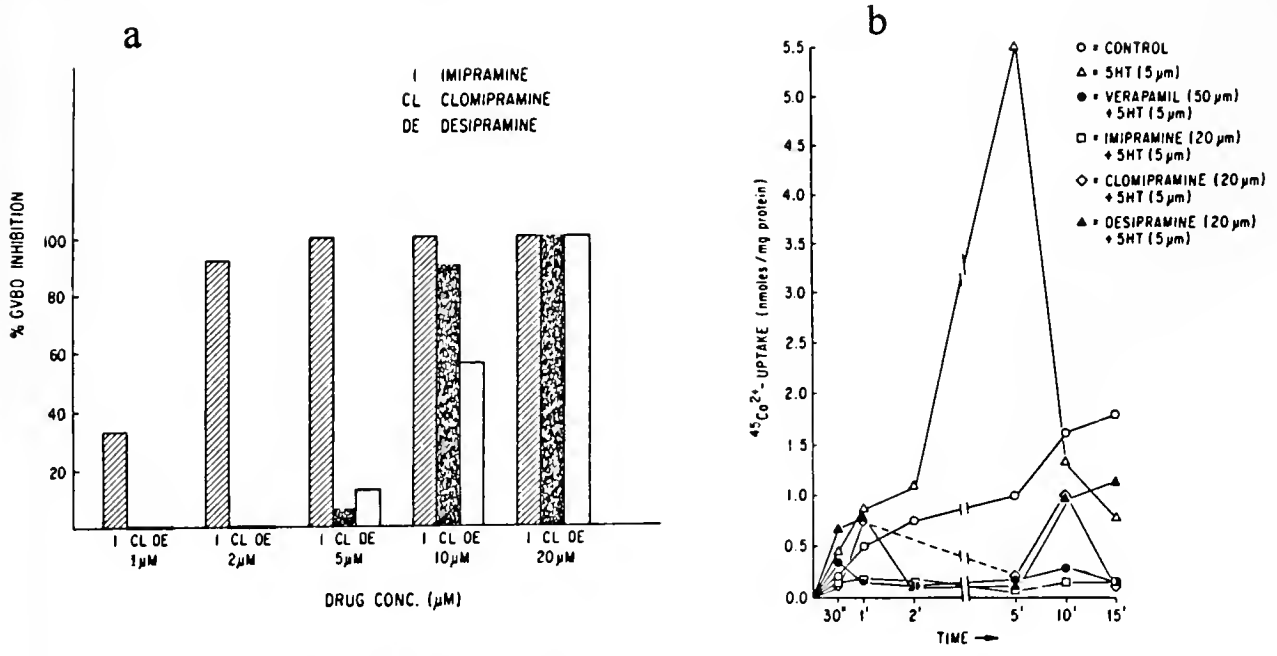

Figure 1. *Effects of tricyclic antidepressant drugs on* Spisula *oocytes. (a) Effect of varying concentrations of tricyclic antidepressant drugs on 5-HT-induced oocyte maturation. (b) Effect of tricyclic antidepressant drugs on time course of $^{45}Ca^{2+}$ uptake by* Spisula *oocytes. Final concentration of 5-HT was 5 μM. The tricyclic antidepressant drugs at 20 μM inhibited $^{45}Ca^{2+}$-uptake stimulated by 5-HT. The assay procedure is described in text. Values in figure are mean of three experiments repeated on three independent preparations.*

Cell Cycle Contraction Waves in *Xenopus* are Suppressed by Injecting Calcium Buffers

Andrew L. Miller (Marine Biological Laboratory), Richard A. Fluck and Lionel F. Jaffe

During the period of rapid metachronous cleavages that follow fertilization, the cortex of *Xenopus* eggs contracts before each cell division (1). These periodic events were termed "surface contraction waves." The wave that precedes the first cell division is most easily studied and has been described in detail. It is propagated in a circular manner from the animal pole, through the equator, and on to the vegetal pole. The surface contraction wave induces a change in the height of the egg. When the wave moves from the animal pole to the equator the egg rounds up, its maximum height occurring as the wave crosses the equator. In normally cleaving eggs, the maximum height of the egg in the rounding phase also corresponds to the appearance of the furrow at the animal pole. Eggs treated with antimitotic drugs (colchicine and vinblastine), although prevented from cleaving, undergo a series of periodic surface contraction waves timed closely to the cleavage cycle in untreated eggs. In addition, this cycle of contractions does not require the sperm nucleus, the egg nucleus, or the sperm centriole. Hara *et al.* proposed that a cytoplasmic biological clock present in vertebrate eggs operates independently of the nucleus and may be involved in regulating the cell cycle (1).

Our idea was to investigate the involvement of free cytosolic calcium elevation in the initiation and propagation of these surface contraction waves. To do this, we selected a relatively weak calcium buffer with a dissociation constant closely matched to localized calcium elevations already measured in large vertebrate eggs during early development and cytokinesis (2, 3). The buffer chosen was 5,5′-dibromo-BAPTA (K_D = 1.5 μM). Our experience in the use of such weak "shuttle" buffers led us to select a final buffer concentration of 2 mM for 5,5′-dibromo-BAPTA for these preliminary experiments. This assumes that 70% of the egg volume is inaccessible yolk, and that 70% of the remaining cytosol is water (4). As a control, we injected 5-mononitro-BAPTA (K_D = 40 μM) again to a final concentration of $\approx$2 mM. Facilitative diffusion theory predicts that for such a weak buffer, a final cytosolic concentration of 2 mM would be insufficient to suppress a local rise in free calcium in the 5 μM range (5). Sufficient calcium was added to the buffer injectates to set them at the resting pCa of the *Xenopus* cytosol. This was assumed to be 0.4 μM (6), which resulted in injectates having a 5:1 and a 100:1 ratio of buffer to calcium for 5,5′-dibromo-BAPTA and 5-mononitro-BAPTA, respectively.

Unfertilized *Xenopus* eggs were obtained by standard procedures and prick-activated. Fertilization membranes were then removed mechanically and the eggs mounted on agar platforms in optically clear cuvettes. These, in turn, were mounted in a modified low-power microscopy set-up that allowed simultaneous time-lapse video microscopy both from above the egg and from the side. Buffers were injected with a high pressure injection system (Medical Systems Corp. PLI-100) that accurately delivered precise, repeatable volumes. Eggs were allowed to relax and contract at least once before buffers were injected. We attempted to inject the buffers at the state of maximum contraction.

Figure 1A shows contractions that are similar, both in their periodicity and in their amplitude ($\approx$36 min and $\approx$18% of the maximum egg height, respectively), to those described by Hara *et al.* (1). In the 5-mononitro-BAPTA injection experiment illustrated in Figure 1B, the egg contracts to an average of 18.2% of its maximum height in the first two contractions before the buffer was injected. The mean figure for the eight contractions following the injection is 17.5%, indicating a minimal effect. When 5,5′-dibromo-BAPTA is injected at about the maximum state of contraction (Fig. 1C and D, respectively), it reduces the amplitude of the subsequent contractions by about two-fold, compared to that before the buffer was injected (*i.e.*, from 13.8% to a mean of 4.9% and from 15% to a mean of 9.2%, for Fig. 1C and D, respectively).

Although the degree of contraction was dramatically affected by the injection of 5,5′-dibromo-BAPTA, the periodicity of the cycle of contraction and relaxation clearly was not. The mean time between contraction peaks for Figure 1A, B, C and D are 36.0, 33.2, 33.0, and 34.5 min, respectively.

These preliminary buffer-injection experiments indicate that localized cytosolic calcium elevations do play a role in the propagation or modulation of surface contraction waves in parthenogenetically activated *Xenopus* eggs. The lack of any effect of the injected buffers on the periodicity of the contraction waves will require further investigation if we are to ascertain whether calcium plays a role in a basic cell cycle timing mechanism that resides in the cytoplasm, or more specifically, in the cortex of the egg.

This work was supported by NSF grants DCB-9103569 to LFJ, DIR-9211855 to LFJ & ALM, and DCB-9017210 to RAF.

Literature Cited

1. **Hara, K., *et al.* 1980.** *Proc. Natl. Acad. Sci. USA* **77:** 462–466.
2. **Fluck, R. A., *et al.* 1991.** *J. Cell Biol.* **115:** 1259–1256.
3. **Fluck, R. A., *et al.* 1992.** *Biol. Bull.* **183:** 70–77.
4. **McLaughlin, J. A., *et al.* 1991.** *Biol. Bull.* **181:** 345a.
5. **Speksnijder, J. E., *et al.* 1989.** *Proc. Natl. Acad. Sci. USA* **86:** 6606–6611.
6. **Busa, W., and R. Nuccitelli. 1985.** *J. Cell Biol.* **100:** 1325–1329.

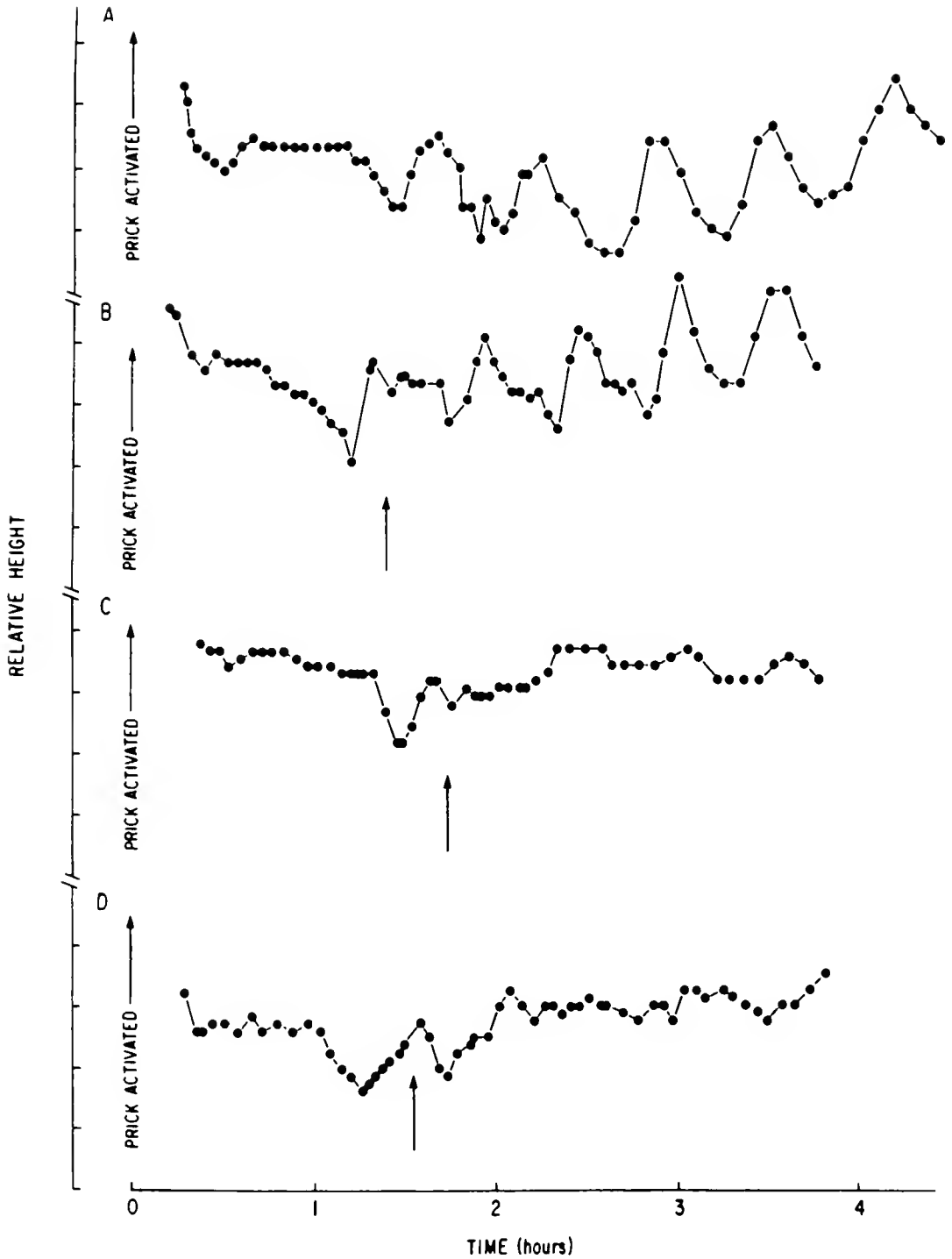

Figure 1. *Periodic changes in the height of parthogenetically activated* Xenopus *eggs. Arrows mark the time of buffer injection. Eggs were allowed to proceed through one relaxation and contraction cycle before injection. (A) Uninjected control; (B) egg injected with 5-monomtro-BAPTA to a final cytosolic concentration of 2 m*M. *(C, D) Eggs injected with 5,5'-dibromo-BAPTA to a final cytosolic concentration of 2 m*M

On the Calcium Pulse during Nuclear Envelope Breakdown (NEB) in Sea Urchin Eggs

Carole L. Browne (Marine Biological Laboratory), Andrew L. Miller, Robert E. Palazzo, and Lionel F. Jaffe

The relationship between a calcium pulse and NEB was critically reviewed by Hepler in 1989 (1) and more briefly reviewed by Tombes *et al.* in 1992 (2). With regard to eggs, Hepler concluded that "the evidence . . . supports the occurrence of a Ca pulse preceding NEB. . . However, there is much less agreement for the other phases of division . . ." We fully agree with Hepler but would add that the evidence has supported the need for (as well as the occurrence of) NEB pulses.

Particularly convincing is the report by Twigg *et al.* that injection of BAPTA calcium buffer into fertilized *Lytechinus* eggs at a final cytosolic concentration above about 2 m*M* regularly and permanently blocks NEB; while injection of CaEGTA at a final concentration of 25 m*M* so as to set free calcium at one micromolar regularly speeds NEB (3). This **indirect** evidence seems particularly cogent since this BAPTA effect is in quantitative agreement with shuttle buffer theory (4) as well as several other observations of inhibition by calcium buffer injections (4–7). Also consistent with a need for NEB pulses are reports that mitosis and NEB can be blocked by antibodies to intracellular calcium pumps (8–9), by antagonists to intracellular calcium channels (10) and by a specific peptide inhibitor to a Ca^{++}/calmodulin-dependent protein kinase (11).

On the other hand, **direct** evidence for NEB pulses has been less satisfactory. The first such report was primarily illustrated by a single recording showing six calcium peaks during the first cell cycle in *Lytechinus*, including one said to occur at NEB; however, as Hepler pointed out this particular egg was grossly abnormal and probably dispermic (12). The second group of such reports have only appeared in abstract form and seem impossible to critically assess (13). The third indicated that such pulses could only be seen regularly in *Lytechinus* eggs when they were activated by ammonia rather than fertilized (5). The latest reports that only 8 of 19 mouse eggs showed such pulses and is therefore cautious about their significance (2).

Here we briefly report observations of calcium pulses during first NEB in fertilized, monospermic *Lytechinus* eggs as observed via injection of the ultrasensitive h or f forms of the chemiluminescent protein, aequorin. [At cytosolic pCa's, but measured *in vitro*, these 'semi-synthetic' aequorins luminesce with about 30 to 60 times the intensity of natural aequorin (14).] In about 40 cases of aequorin-loaded, monospermic eggs that underwent normal first cleavage, all except one showed a striking calcium pulse that began within the minute that preceded NEB. The calcium level was observed to rise to a peak level of about 200 photons/s from a resting level of about 10 photons/s. These pulses usually rose to a peak within about 10 s and remained perceptible for about 30–60 s. Preliminary quantitation indicates that these pulses peak in the few micromolar range of free calcium while preliminary imaging of these pulses showed them to fill the whole egg.

However, to our considerable and continuing surprise, no detectible calcium pulses ever accompanied NEB during the second or later cell cycle in any of those two dozen eggs in which observations were continued beyond the first cell cycle. Subsequent tests for residual aequorin showed that an ample amount remained to have revealed later NEB pulses had they been present.

In four cases, we observed the course of free calcium in eggs that were visibly dispermic. In all of these cases, we again observed an extraordinarily large (about ten times usual) but otherwise typical pulse of aequorin light during NEBD. In three of these four dispermic eggs, the initial pulse was followed by a periodic series of pulses that continued until (delayed) cleavage occurred. The number of such additional pulses varied from 3 to 11, the pulse to pulse time was about 4 min and the amplitude tended to gradually decrease.

Finally, in two cases, we succeeded in observing the course of free calcium change in eggs that were immersed in calcium free seawater (containing 2 m*M* EGTA) right after fertilization. In both of these cases we observed an extraordinarily large (about ten times usual) but otherwise typical pulse of aequorin light during first NEB. Figure 1 illustrates one of these remarkable pulses. We suspect that giant pulses occur in calcium free seawater because much of the injected, ultrasensitive aequorin is normally destroyed by calcium entering the injection wound.

This is the first report of calcium pulses clearly and regularly

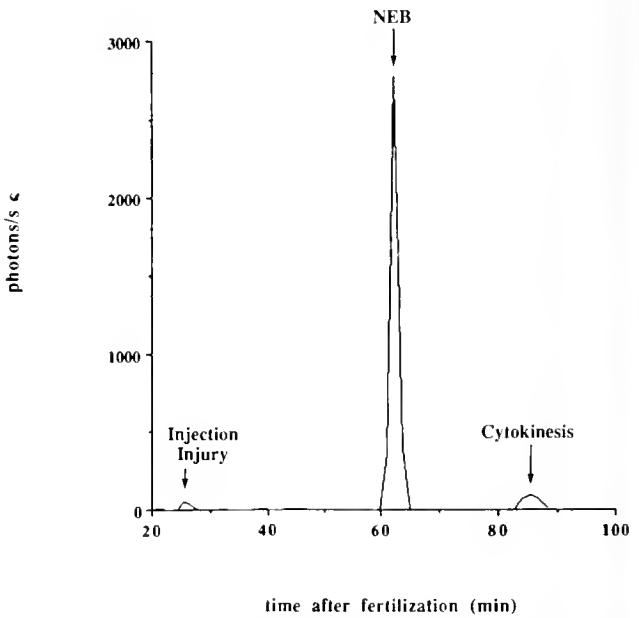

Figure 1. *NEB calcium signal from a* Lytechinus pictus *egg that was injected with f-aequorin about 20 min after fertilization and allowed to develop in calcium free artificial seawater. The resting level of about 10 photons/s was too small to appear on this linear graph. Similar NEB signals of about one tenth this height are regularly seen in* Lytechinus *eggs developing in natural seawater (see text). The smaller second signal accompanied cytokinesis. Such signals have only been seen occasionally.*

associated with NEB in fertilized cleaving eggs. It is also the first report that such pulses are absent during subsequent NEB's, do not require external calcium, and may be periodically repeated in dispermic eggs. The further use of ultrasensitive aequorins should make it possible to better characterize NEB calcium pulses and better study their function. In particular, it should now be possible to test the prediction that such pulses initially spread through the egg in the form of fast calcium waves (15).

We thank Osamu Shimomura for providing h- and f-aequorin and we were financially supported by NSF grants #DCB-9103569 to LFJ and DIR-9211855 to LFJ and ALM.

Literature Cited

1. **Hepler, P. K. 1989.** *J. Cell Biol.* **109:** 2567–2573.
2. **Tombes, R. M., C. Simerly, G. G. Borisy, and G. Schatten. 1992.** *J. Cell Biol.* **117:** 799–811.
3. **Twigg, J., R. Patel, and M. Whitaker. 1988.** *Nature* **332:** 366–369.
4. **Speksnijder, J. E., A. L. Miller, M. H. Weisenseel, T.-H. Chen, and L. F. Jaffe. 1989.** *Proc. Natl. Acad. Sci. USA* **86:** 6607–6611.
5. **Steinhardt, R., and J. Alderton. 1988.** *Nature* **332:** 364–366.
6. **Kao, J. P. Y., J. M. Alderton, R. Y. Tsien, and R. A. Steinhardt. 1990.** *J. Cell Biol.* **111:** 183–196.
7. **Miller, A. L., R. A. Fluck, and L. F. Jaffe. 1992.** *Biol. Bull.* (in press).
8. **Silver, R. B. 1986.** *Proc. Natl. Acad. Sci. USA* **83:** 4302–4306.
9. **Hafner, M., and C. Petzelt. 1987.** *Nature* **330:** 264–266.
10. **Silver, R. B. 1989.** *Dev. Biol.* **131:** 11–26.
11. **Baitinger, C., *et al.* 1990.** *J. Cell Biol.* **111:** 1763–1773.
12. **Poenie, M., J. Alderton, R. Y. Tsien, and R. A. Steinhardt. 1985.** *Nature* **315:** 147–149.
13. **Silver, R. B., and S. Inoué. 1987.** *Biol. Bull.* **173:** 420–421 (abstract); **Silver, R. B., O. Shimomura, and S. Inoué. 1989.** *J. Cell Biol.* **109:** 9a (two abstracts).
14. **Shimomura, O., B. Musicki, and Y. Kishi. 1989.** *Biochem. J.* **270:** 309–312.
15. **Jaffe, L. F. 1991.** *Proc. Natl. Acad. Sci. USA* **88:** 9883–9887.

Calcium Buffer Injections Block Ooplasmic Segregation in *Oryzias latipes* (Medaka) Eggs

Richard A. Fluck (Franklin and Marshall College), Vivek C. Abraham, Andrew L. Miller, and Lionel F. Jaffe

We used the calcium buffer, 5,5′-dibromo-BAPTA, to investigate the possible role of Ca^{2+} in ooplasmic segregation in the medaka fish egg. The unfertilized medaka egg consists of two compartments: a large (~1 mm in diameter) central yolk vacuole and a thin (~30 μm thick) peripheral layer of ooplasm; a unit membrane (the yolk membrane) separates the two compartments. Following activation of the egg, the bulk of the ooplasm and its inclusions move toward the animal pole and form a blastodisc there, while oil droplets and other, smaller inclusions move toward the vegetal pole (1). At 25°C, segregation is complete within about 70 min.

Throughout the period of segregation, zones of elevated cytosolic $[Ca^{2+}]$ are present at both the animal and vegetal poles of the medaka egg (2). To determine whether these zones are required for ooplasmic segregation, we injected dibromo-BAPTA (final concentration = 0.5–7.0 mM) into the ooplasm near the vegetal pole of the egg or near its equator (midpoint along the animal-vegetal axis) within 10 min after fertilization, using methods described previously (2). Our idea was to use this relatively weak calcium buffer (K_D = 1.5 μM) as a shuttle buffer to suppress or reverse the formation of needed high calcium zones in the micromolar range (3). Eggs were co-injected with sufficient Ca^{2+} to give free $[Ca^{2+}]$ in the injectate of 0.14 μM, 0.2 μM, or 0.3 μM and thus in the range of natural resting levels (4). Injections of such buffer/Ca^{2+} mixtures, set at the resting level of $[Ca^{2+}]$, cannot act by shifting $[Ca^{2+}]$ away from the resting level (3). To estimate the time required for the buffer to diffuse around the egg from the site of injection, we monitored the spread of fluorescein injected near the equator of the egg. We found that it reached the poles of the egg within 10 min of injection and the antipode of the injection site within 20 min.

Low concentrations of the buffer (≤2.0 mM) had little or no effect on the eggs, while higher concentrations of the buffer (≥2.6 mM) inhibited ooplasmic segregation and blocked cleavage at all three levels of $[Ca^{2+}]$ (Table I). The fact that the results were independent of pCa in this range confirms that the injectate was acting as a shuttle buffer. The slightly higher concentration of dibromo-BAPTA required to inhibit segregation and cleavage in the medaka egg *vs.* fucoid egg development may be due to a slightly higher calcium flux in the medaka egg.

The immediate reaction of the eggs to the injectate was an apparent expansion of the yolk membrane near the injection site, which caused the yolk vacuole to bulge into the ooplasm locally. At lower concentrations of buffer (<4 mM), this bulge usually subsided within 10 min. Sometimes, however, the yolk membrane over the bulge lysed; this was the predominant outcome at ≥4.0 mM buffer. This effect on the yolk membrane may have been caused by the initially high concentration of buffer near the injection site. Another consistent local response to the injection was the movement of nearby oil droplets away from the injection site and toward the top of the egg; this movement was over within 15 min.

Except for this early movement of oil droplets, segregation of ooplasm and oil droplets was strongly inhibited by ≥2.6 mM dibromo-BAPTA. The blastodisc formed slowly, and its final size was smaller than in control eggs; this effect was more pronounced in eggs in which we injected buffer near the equator. The effect of buffer injection on oil droplet movement also varied with the site of injection. When buffer was injected near the equator, oil droplet movement was strongly inhibited all along the animal-vegetal axis, but when it was injected near the vegetal pole, oil droplets moved away from both poles and formed a

Table 1

Inhibition of ooplasmic segregation in the medaka egg by the injection of 5,5'-dibromo BAPTA calcium buffer

[Free Ca^{2+}] μM	[Dibromo-BAPTA] mM*	N	Response of embryos: Lysed	Segregated normally	Cleaved	Formed embryonic axis
0.14	0.5–2.0	6	0	6	6	6
0.14	2.6–3.6	10	1	0	0	0
0.14	4.0–7.0	9	4	0	0	0
0.20	0.5–2.0	6	0	6	6	6
0.20	2.6–3.6	24	7	0	0	0
0.20	4.0–7.0	23	20	0	0	0
0.30	0.5–2.0	5	0	5	5	5
0.30	2.6–3.6	20	7	0	0	0
0.30	4.0–7.0	3	3	0	0	0

* Estimated final cytosolic concentration. See text.

ring just above the equator of the egg. Buffer concentrations ≥2.6 mM buffer also blocked cleavage. Control eggs and eggs in which we injected the buffer into the yolk vacuole developed normally.

In a previous study (2), 2.7 mM dibromo-BAPTA was shown to facilitate the diffusion of Ca^{2+} away from the poles of the medaka egg and thus substantially dissipate calcium gradients near them. The results of the present study suggest that these zones are necessary for the normal segregation of ooplasm and its inclusions in this egg.

Supported by NSF grants DCB-9017210 to RAF and DCB-9103569 to LFJ.

Literature Cited

1. **Abraham, V., and R. A. Fluck. 1991.** *J. Cell Biol.* **115:** 52a.
2. **Fluck, R. A., A. L. Miller, and L. F. Jaffe. 1992.** *Biol. Bull.* **183:** 70–77.
3. **Speksnijder, J. E., A. L. Miller, M. H. Weisenseel, T.-H. Chen, and L. F. Jaffe. 1989.** *Proc. Natl. Acad. Sci. USA* **86:** 6607–6611.
4. **Schantz, A. R. 1985.** *J. Cell Biol.* **100:** 947–954.

Natural Antioxidants Reduce Near-UV Induced Opacification and Filamentous Actin Damage in Dogfish (*Mustelus canis*) Lenses

Seymour Zigman (University of Rochester School of Medicine), Nancy S. Rafferty, and Steven Sooudi (Northwestern University School of Medicine)

We have shown that near-UV radiation, predominantly in the wavelength range of 320 to 400 nm (near UV_A), degrades F-actin, both in cells and in extracts of muscle (1, 2). In this study, the ability of several natural antioxidants to protect lens epithelial cell F-actin from UV degradation was studied.

Low levels of natural antioxidants were added to incubation media (elasmobranch Ringer's solutions) in which fresh dogfish (*Mustelus canis*) lenses were maintained in the presence and absence of near-UV_A radiation for 14 h. At an irradiance of 1.5 mW/cm^2 the lenses received 63 J/cm^2 of UV-A energy.

Slit-lamp photographs of unexposed control lenses (Fig. 1a), of UV-exposed lenses without (Fig. 1b) or with (Fig. 1c) A, C, E mixture are shown. Without UV exposure, the lenses remained clear, but with UV exposure they developed superficial cortical opacities (see Fig. 1). The presence of 10 μM α-tocopherol (E) or a mixture of 10 μM of E plus 10 μM β-carotene (A) plus 0.1 mM ascorbic acid (C) partially protected against opacification. Only the unprotected UV-exposed lenses developed an opacity.

F-actin normally appears in lens epithelial cells as stress fibers. Fluorescence microscopy of epithelial cells stained with rhodamine-phalloidin dye (a specific reactant for polymerized actin) revealed a large diminution of F-actin fluorescence after the cells had been exposed to near-UV_A (Fig. 1e) as compared to the unexposed control epithelia (Fig. 1d). Those lens epithelial cells exposed to UV with A, C, E added (Fig. 1g) retained their normal actin filaments. Surprisingly, the lens epithelial cells that were kept in the dark and also given A, C, E (Fig. 1f) exhibited greater F-actin fluorescence than the controls (Fig. 1d). This observation requires further investigation.

To quantitate the decrease of F-actin in these cells, a modified chemical assay for F-actin (3) was applied to extracts of lens-capsule epithelium from control or UV-exposed lenses, with or without A, C, E added to the medium. The results of the chemical assay used to determine polymerized actin was applied to 14,000 rpm supernates of lens capsule epithelia homogenized in polymerizing buffer [$MgCl_2$ (2 mM), KCl (50 mM), and ATP (2 mM)]. The 580 nm emissions due to 550 nm excitation were measured with an Aminco-Bowman fluorometer.

The values of F-actin fluorescence of dogfish lens capsule epithelia were determined in several experiments. UV-exposure diminished the F-actin by about 30 to 40% when no additives were present, but the control values were retained when A, C, E was added to the incubation medium. E alone also protected against a decrease of F-actin due to UV exposure. A and C were not protective. When supernatants of frozen lens capsule-epithelial homogenates were similarly UV-irradiated, a 43% loss of F-actin was observed.

The data support the following conclusions: Near-UV_A radiation at lower than solar levels leads to superficial dogfish lens opacities *in vitro*. These opacities are diminished when α-tocopherol (E), or a combination of E and β-carotene (A) and ascorbic acid (C), are present in the medium. A or C alone did not protect F-actin from degradation.

This radiation resulted in histologically observable damage to

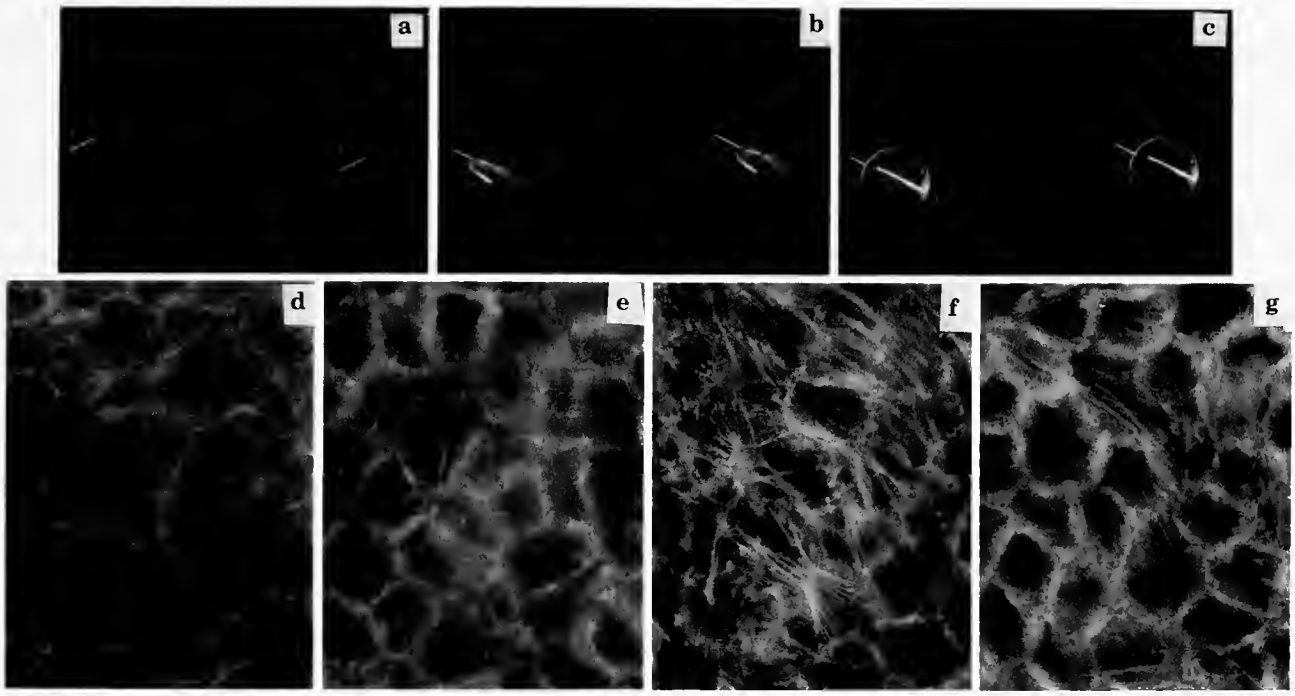

Figure 1. *Frames a, b, c are slit lamp photographs of dogfish lenses incubated in Ringer's solution as follows: time: 14 h; temperature: 20°C; photographed with Zeiss photographic slit lamp camera microscope using circular cool-white fluorescent light for illumination; (a) unirradiated control lens; (b) near-UV_A exposed lens; (c) near-UV_A-exposed lens plus A, C, E in the medium. Frames d, e, and f and g are fluorescence microscopic photographs of flat mounted lens epithelial cells stained with 0.66 μM rhodamine-phalloidin (d) unirradiated controls, (e) near-UV_A exposed lens; (f) controls plus A, C, E; (g) near-UV_A exposed lens plus A, C, E in the medium. Concentrations were: A at 10 μM, C at 0.1 mM, E at 10 μM.*

the lens epithelial cells and outer cortex (unpub. obs.). The radiation also resulted in the degradation of filamentous actin in the lens epithelial cells, as indicated by lower rhodamine-phalloidin fluorescence-binding to the stress fibers.

A fluorescence-binding assay, with rhodamine-phalloidin, of the amounts of polymerized actin left in dogfish lens epithelium after near-UV exposure also indicated an appreciable loss of polymerized actin. A, C, E added to the medium partially prevented the loss of polymerized actin. In fact, it markedly stimulated stress fiber fluorescence, even in unexposed cells.

As E alone did protect F-actin, the rationale for testing A, C, E was to observe possible synergistic effects. The data presently available seems to show a synergistic effect, but more data are needed to support this conclusion with confidence.

Near-UV_A radiation thus photooxidatively damages dogfish lens epithelial cells via F-actin degradation. Natural antioxidants protect against actin filament degradation and lens opacity formation significantly.

Research support was provided by NIH (EY 00698 and EY 00459) and RPB, Inc.

Literature Cited

1. **Zigman, S., N. S. Rafferty, and R. B. Wheeler, Jr. 1991.** *Biol. Bull.* **181:** 341–342.
2. **Zigman, S., N. S. Rafferty, B. S. Scholz, and K. Lowe. 1992.** *Exp. Eye Res.* **55:** (in press).
3. **Huang, Z., R. P. Haugland, W. You, and R. P. Haugland. 1992.** *Analyt. Biochem.* **200:** 199–204.

Nautilus Embryology: A New Theory of Molluscan Shell Formation

John M. Arnold (University of Hawaii, Manoa)

The classical theory of molluscan shell formation involves the secretion of ionic and molecular precursors by the mantle cells into a space between the mantle and periostracum where the definitive shell is formed (1).

Observations by scanning electron microscopy of the mantle and shell of the recently discovered embryos of *Nautilus belaunesis* (2) indicate that the large "proto-prisms" and "proto-platelets" are formed in intracellular vacoules and transported

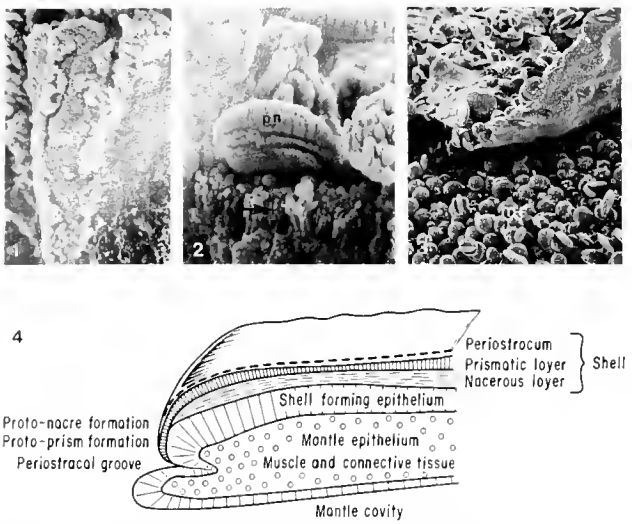

Figure 1. *Formation of an intracellular proto-prisms (pp). Subunits (su) with an outer coating attach to the intracellular organelle (here shown with the vacoule membrane removed) are condensed and incorporated into the structure of the proto-prism (si). To the right of the labeled proto-prism has the vacuole membrane intact. (ca 10,000×).* **Figure 2.** *Nacreous proto-platelet stack being transported through the cell surface into the space between the mantle layer and periostracum. The platelet is composed of several layers composed of condensing subunits which are larger at the margin that in the central region. The surface of the cell is covered with microvilli that contain subunits sized particles (arrow). It is proposed that the subunits are released from the microvilli to cement the proto-platelets and proto-prisms into sheets of either interior nacreous shell (illustrated here) or the outer layer of prismatic shell. (12,000×).* **Figure 3.** *Groups of proto-platelets emerging from the mantle surface (ms) into the space between the periostracum and mantle. The platelets are fused together to form a continous sheet which eventually fuses with the prismatic to form the embryonic shell (ca 2000×).* **Figure 4.** *Diagram of the mantle edge showing the proposed scheme of shell formation.*

through the mantle cell surface where they are assembled into the adult shell composed of prismatic and nacreous layers. The first figure shows the formation of a proto-prism from subunits. These subunits have two components: a core about 0.1 μm in diameter, and an outer coating that appears to be lost when the subunits form the shell. Figure 1 shows a proto-prism forming within a cell at the periostracal groove. On the surface the subunits are large and less dense than those that are incorporated into the proto-prismatic shell. Proto-prisms are transported out of the cell where they are assembled into a complete prismatic layer with the addition of extracellular subunits. Similar events occur in the cicatrix area of the early organogenic embryo. First the prismatic shell is laid down at the distal edge of the lip of the periostracal groove and later, the nacreous shell is laid down beneath it by cells back from the mantle edge.

Figure 2 shows a nacreous proto-platelet after it has been transported through the cell surface. The proto-platelet is composed of condensed subunits which form stacked discs. Each extracellular nacreous platelet is composed of several layers with large subunits being incorporated at the edges and surface. In the center of each platelet the subunits are smaller, presumably due to condensation and loss of an organic coat. The mantle cell surfaces are covered with a microvillar brush border that contains subunit sized granules.

Figure 3 shows the assemblage of proto-platelets into confluent sheets of definitive shell. At the mantle surface proto-platelets can be seen emerging through the cell surface. Against the inner surface of the periostracum (removed in this micrograph) the proto-platelets fuse into a continuous layer probably by interaction with subunits secreted into the extracellular space.

It is proposed that the actual aragonite shell is formed intracellularly and large components are assembled into proto-platelets or proto-prisms and are transported into the periostracal-mantle space where they are assembled into continuous layers of the definitive shell. This proposed mechanism is summarized and illustrated in Figure 4.

The author acknowledges the financial support of the Grass Foundation, the *Teuthis obscura* fund, and the help of the Waikiki Aquarium staff.

Literature Cited

1. **Wilbur, K. M., and A. S. M. Saleudin. 1985.** Pp 211–287 in *The Mollusca*, vol. 5. Academic Press.
2. **Arnold, J. M., and B. A. Carlson. 1986.** *Science.* **232:** 73–76.

The Effect of Deleting Opposite First Quartet Micromeres on the Development of the Polyclad *Hoploplana*

Barbara C. Boyer (Union College, Schenectady, NY 12308)

Embryos of the polyclad Turbellaria share many features with higher Spiralia (specifically annelids and mollusks); the most important of these are quartet spiral cleavage and developmental mechanisms involving autonomous specification followed by cell interactions (1, 2, 3).

The deletion of micomeres from eight-cell stage embryos of *Hoploplana inquilina*, including the ablation of two adjacent first quartet cells, resulted in larvae with abnormalities in morphology, eye number, and apical tuft (3). But this earlier series of experiments did not include the deletion of opposite pairs of first quartet micromeres: 1a and 1c, or 1b and 1d. This continuation study examined the localization of cytoplasmic determinants in the eight-cell embryo by deleting opposite micromeres.

When the gonads of *Hoploplana* are pierced with sharp needles, eggs and sperm pour out, producing zygotes lacking the egg shell membrane. About 15 min after formation of the first quartet, opposite micromeres 1a and 1c or 1b and 1d were deleted

with hand-pulled glass needles. The embryos were raised in Millipore-filtered seawater containing 100 units/ml penicillin and 200 mg/ml streptomycin for six days. The 46 larvae that resulted from deletion of 1a and 1c, and 35 from 1b and 1d ablation, were compared to the normal Muller's larva for abnormalities in morphology, eye number, and apical tuft. They were also compared to the 27 larvae produced after the removal of two adjacent micromeres.

In all experimental categories, about half of the embryos were morphologically normal, and abnormalities in the remainder involved primarily the absence or underdevelopment of larval lobes. Fewer than one quarter of the larvae were "swollen" (spherical and histologically very abnormal) and formed only when opposite blastomeres were deleted. The swollen syndrome is characteristic of both micromere and especially macromere-deleted embryos, occurring with increasing frequency as more cells are killed, and it is not a common phenomenon when only two micromeres are removed (3, 4). Therefore swollen embryos cannot be attributed to just the latter experimental series.

Only larvae with Muller's-like morphology were analyzed for eye development; the data are shown in Table I. Deletion of 1a and 1c produced a greater number of eyeless larvae than the deletion of 1b and 1d or two adjacent micromeres ($\chi^2 = 12.56$, 2 d.f., $P < 0.01$). Differences in the numbers of one-eyed larvae were not significant ($\chi^2 = 3.91$, d.f., $P > 0.05$), and no conclusions can be drawn from the small number of larvae with the normal two eyes. In single-eyed larvae, eye position was almost equally divided between right and left in all experiments, but ablation of two adjacent micromeres resulted in 63% of larvae with a centrally located eye as compared to 42% for 1b & 1d ablated embryos and 23% after removal of 1a & 1c; however, the sample size is too small for statistical analysis.

These results support the idea that although eye determinants are localized similarly to those in the higher Spiralia, they do not follow an invariant lineage. When 1a and 1c are deleted, for example, 39% of the larvae are eyeless, indicating that eye determinants are commonly localized in these blastomeres, as they are in mollusks such as *Ilyanassa* and *Crepidula* (5, 6). The 26% two-eyed larvae resulting from ablation of 1b and 1d and the 70% one-eyed larvae produced when two adjacent micromeres are deleted also are consistent with such localization. However, the relatively high percentage of larvae with a single eye following removal of opposite first quartet micromeres, as well as the 15% two-eyed and 7% eyeless larvae produced by absence of adjacent micromeres, indicate that eye determinants are not always segregated to opposite first quartet micromeres.

Table I

Effect of deleting two first quartet micromeres from embryos of Hoploplana

	Number of eyes				
Deletion	0	1	2	3 or more	Total
1a and 1c	12 (39%)	14 (45%)	4 (13%)	1 (3%)	31
1b and 1d	2 (7%)	14 (52%)	7 (26%)	4 (15%)	27
2 adjacent micromeres	2 (7%)	19 (70%)	4 (15%)	2 (7%)	27

Values in table represent the number of larvae from each experimental category.

The lack of strict correlation between specific deletions and loss of eyes, plus the common appearance of supernumerary eyes with macromere deletions in eight-cell stage embryos (4), suggest that eye development is complex, perhaps involving cytoplasmic localization, induction, and inhibition. The larger number of centrally located single eyes produced by deletion of two adjacent micromeres than by deletion of opposite micromeres may be caused by the asymmetry of the embryo that results from the former experiment.

The apical tuft was missing in 55% of larvae from 1a and 1c deletions, 71% of 1b and 1d deletions, and 85% when two adjacent micromeres were ablated; these proportions are significantly different ($\chi^2 = 7.71$, 2 d.f., $P < 0.05$). Thus apical tuft determinants are more likely to be localized in the 1b and 1d cell, but may go to 1a and 1c.

This study indicates that specific cytoplasmic determinants are localized in the first quartet micromeres at the eight-cell stage in *Hoploplana,* but these determinants are not consistently assigned to the same blastomeres in each embryo. When two micromeres are deleted, the larvae characteristically exhibit Muller's-like morphology but are abnormal in the development of anterior structures such as eyes and apical tuft. Eye determinants tend to be localized in the 1a and 1c blastomeres, and apical tuft determinants in 1b and 1d. Thus polyclads demonstrate some features of autonomous specification that is characteristic of many higher Spiralia, but do not exhibit an invariant cell lineage. This suggests that polyclads may have evolved from an ancestral form that was "experimenting" with the developmental mechanism of cytoplasmic localization.

This work was supported by NSF grant DCB-8817760.

Literature Cited

1. **Boyer, B. C. 1986.** *Int. J. Invert. Repro. Dev.* **9:** 243–251.
2. **Boyer, B. C. 1987.** *Roux's Arch. Dev. Biol.* **196:** 158–164.
3. **Boyer, B. C. 1989.** *Biol. Bull.* **177:** 338–343.
4. **Boyer, B. C. 1990.** *Biol. Bull.* **179:** 221.
5. **Clement, A. C. 1967.** *J. Exp. Zool.* **166:** 77–88.
6. **Conklin, E. G. 1897.** *J. Morphol.* **13:** 1–226.

Lindane (1, 2, 3, 4, 5, 6-Hexachlorocyclohexane) Affects Metamorphosis and Settlement of Larvae of *Capitella* species I (Annelida, Polychaeta)

Susan Douglas Hill (Department of Zoology, Michigan State University) and Leonard Nelson

Capitella sp. I, formerly part of the *Capitella capitata* complex (1), produces larvae that emerge from brood tubes as metatrochophores competent to settle and metamorphose into small worms in the presence of suitable substrate (2). Because the species is one of the early colonizers of disturbed and polluted areas (3) and maintains a high reproductive output under potential stress (4, 5), the response of larvae to toxic substances in the environment is of particular interest.

Lindane is a highly persistent chlorinated hydrocarbon insecticide. Compounds of this chemical class have very low water solubilities but are highly soluble in lipids and bioaccumulate (6). They adsorb to soil particles and occur in soil of high organic content (7). Toxic effects of lindane in mammals include convulsions, ataxia, prostration, and damage to fatty tissues (6) and, in sea urchins, inhibition of sperm motility (8, 9). Because capitellids occur in marine areas of high organic content and directly ingest the sediment, the response of larvae to lindane and related compounds may be of importance in recolonization.

We have addressed the following questions:

(1) Does lindane suspended in seawater affect the ability of *Capitella* sp. I larvae to settle and metamorphose?
(2) If there is an effect, is it reversible?
(3) Is embryonic development affected by amounts of lindane that interfere with normal settlement?

Competent larvae were exposed to graded amounts of lindane in seawater; their ability to settle in suitable substrate and to metamorphose into young worms was observed. Both the time to settlement and the numbers of metamorphosed worms and remaining larvae were determined for each treatment. Each dish received 10 competent larvae. All treatments and controls were run in duplicate.

In the first experiment, 6 lindane treatments ranging from 7.5 to 187.7 μmole/L were used. Within 2 h, 58 of 60 control larvae had settled, whereas only 35 of 120 lindane-treated larvae had moved into the substrate. The disappearance of larvae into the substrate was monitored daily. Worms and persisting larvae were counted after one week. Fifty-eight of the 60 control larvae had metamorphosed into healthy, feeding worms. No larvae were found. In all of the treatment groups combined, only five small, non-feeding worms were found. Twenty-two moribund larvae were retrieved. When the ratio of young worms to remaining larvae in the test group is compared with that of the controls, lindane is seen to have very significantly delayed and even prevented successful settlement and metamorphosis ($\chi^2 = 64$; $P < .001$).

In the presence of lesser amounts of lindane (0.087–17.5 μmole/L), some larvae in each category (*e.g.*, 95% in 0.087 μmole/L) settled and metamorphosed successfully (Table 1). Significantly fewer metamorphosed into young worms in combined treatment groups than in control groups ($\chi^2 = 15$; $P < .001$).

Table 1

Effects of increasing amounts of lindane on settlement and metamorphosis of larvae of Capitella *sp. I*

	Number at end of experiment		Percent of original animals metamorphosed
	Larvae	Worms	
Controls	0	20	100
Controls (acetone)	0	19	95
Lindane-treated (μmole/L)			
0.086	1	19	95
0.43	5	13	65
0.86	3	16	80
1.7	7	12	60
4.3	6	14	70
8.6	7	12	60
17.2	11	7	35

Each cohort originally consisted of 20 larvae in duplicate dishes of seawater-substrate (controls) or seawater-substrate-lindane (treatments). Acetone controls were included because lindane was dissolved in acetone.

To investigate the effects of duration of exposure, larvae were treated with 86 μmole/L of lindane (an amount that prevents settlement and metamorphosis) for 2, 4, 18, 24, 48, and 72 h, then removed to fresh seawater and provided with substrate. Treatments of up to 24 h did not interfere with settlement and metamorphosis. Longer exposures to lindane decreased survival. Some larvae from all groups metamorphosed into feeding worms. One week after treatment, 133 of the original 150 treated larvae were retrieved as young worms; however, only 4 out of 10 metamorphosed successfully following the 72-h exposure, and after either 48- or 72-h exposure, some worms were very small and non-feeding.

Capitella sp. I embryos developed normally when lindane was present in amounts found to inhibit settling. Eggs at late cleavage were removed from a single brood tube to assure uniformity of developmental stage and exposed to either 1.7 or 8.6 μmole/L lindane, or placed in Millipore-filtered seawater. Development proceeded at the same rate in all dishes, and swimming metatrochophores were present in 4 days. When maintained in lindane, treated metatrochophores largely failed to settle within 24 h. (Thirteen of 20 remained larvae.) Metatrochophores (19 of 20) from control dishes settled within 20 min.

In conclusion, exposure to lindane delays or prevents settlement and metamorphosis of *Capitella* sp. I larvae. Larvae appear able to recover from lindane exposures of short duration when

returned to fresh seawater. Under our experimental conditions, embryos undergo normal development into metatrochophores in the presence of lindane but the subsequent settlement and larval metamorphosis are inhibited.

Literature Cited

1. **Grassle, J. P., and J. F. Grassle. 1976.** *Science* **192:** 567–569.
2. **Butman, C. A., J. P. Grassle, and C. M. Webb. 1988.** *Nature* **333:** 771–773.
3. **Grassle, J. F., and J. P. Grassle. 1977.** Pp. 177–189 in *Ecology of Marine Benthos,* B. C. Coull, ed. Univ. S.C. Press.
4. **Hill, S. D., J. P. Grassle, and M. J. Ferkowicz. 1987.** *Biol. Bull.* **173:** 430.
5. **Hill, S. D., M. J. Ferkowicz, and J. P. Grassle. 1988.** *Biol. Bull.* **175:** 311.
6. **Murphy, S. D. 1986.** Pp. 519–581 in *Casarett and Doull's Toxicology,* 3rd ed, J. Doull, C. D. Klaassen, and M. O. Amdur, eds.
7. **Menzer, R. E., and J. O. Nelson.** Pp. 825–853 in *Casarett and Doull's Toxicology,* 3rd ed., J. Doull, C. D. Klaassen, and M. O. Amdur, eds.
8. **Nelson, L. 1987.** *Biol. Bull.* **173:** 327.
9. **Nelson, L. 1990.** *Bull. Eviron. Contam. Toxicol.* **45:** 876–882.

Flicking in the Lobster *Homarus americanus:* Recordings from Electrodes Implanted in Antennular Segments

Kathleen Berg[1], Rainer Voigt[2], and Jelle Atema[2] ([1]VA-MD Regional College of Veterinary Medicine, and [2]Boston University Marine Program, Marine Biological Laboratory)

The first antennae (antennules) of the American lobster have been defined behaviorally as olfactory organs (1). The base of an antennule consists of three segments (proximal, medial, and distal); the distal segment bears a lateral and a medial flagellum. As in the second antenna (8), each antennular segment has a pair of antagonistic muscles: a depressor and a levator. In addition, the medial and distal segments contain a third muscle. The muscles involved in antennular movements of *H. americanus* are similar to those described by Snow for *Pagurus alaskensis* (9).

Chemoreceptor cells of the lateral flagellum play an important role in complex adaptive behaviors such as food search (4), social recognition (5, 2), and orientation towards odor sources (3, 6). The distal half of each lateral flagellum bears on its ventral surface a dense tuft of aesthetasc sensilla; each sensillum is innervated by 200–300 bipolar chemoreceptor cells. Only the lateral antennule "flicks": the fast sudden downstroke of flicking creates a burst of high water velocity, which splays the hairs, reduces the boundary layer, and enhances stimulus access (7). This is followed by a slower upstroke. Both strokes appear variable in depth and velocity. The maximal flicking frequency is about 4 Hz. The downstroke is mediated by the depressor muscle in the distal segment; the levator muscle causes the slower upstroke. Conventionally, lobster muscle fibers have been classified by their sarcomere length into fast (<4 μm) and slow fibers (≥4–5 μm). Among all antennular muscles, only the depressor muscle in the distal segment contains a sizeable population of fast fibers as confirmed by histochemical staining for ATP-ase and NADH-diaphorase (C. K. Govind, pers. comm.).

The purpose of this study was to develop techniques that would allow us to correlate chemosensory orientation behavior in the lobster with antennular flicking behavior. Therefore, we measured the extracellular electrical activity in the distal segment associated with each flick in a freely moving lobster. Various wire types and implantation sites were tried. Best results were obtained with Teflon-coated platinum-iridium (Pt-Ir) wire (O.D.: 76 μm bare, 110 μm coated; A-M Systems). The best signal-to-noise ratio was obtained with differential recordings of the distal segment against either a second identical electrode in the medial segment or a larger indifferent electrode (Ag-AgCl wire) attached on to the animal's carapace. Less than 1 mm of insulation was removed and the tip was implanted through a small hole drilled through the exoskelton in a dorsal-medial position over the depressor muscle of the distal segment. The electrode was secured with cyanoacrylate cement and sealed with 5-minute epoxy. The extracellular activity was differentially amplified with standard electrophysiological equipment and recorded on a magnetic tape for later analysis.

Visual observation of the flicking motion indicated that attached electrodes caused only slight impairment of the depth of the flick. This and the signal-to-noise ratio of the recording im-

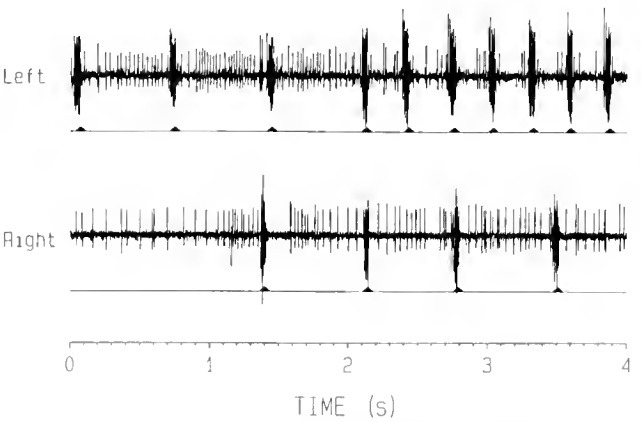

Figure 1. *Bilateral recordings of extracellular activity associated with antennular flicking. Upper Trace: each burst of 6–13 spikes of the larger unit is associated with a flick (arrowhead) of the left lateral antennule. Lower Trace: simultaneously recorded responses from the right lateral antennule.*

proved over a period of a few hours as the lobsters recovered from the implantation procedure. Clear responses were obtained for several days or until the lobster destroyed the Pt-Ir wires by grooming behavior. Bilateral implantation of electrodes into the distal segments showed reliable motor unit responses associated with antennular flicks on each side (Fig. 1). Simultaneous recording of motor unit activity and video taping of the flicking motion allowed synchronization of spike response and flicking behavior. We identified two spiking units in recordings from the distal segment on each side. The larger amplitude unit (Fig. 1) gave 50–100 ms bursts of 6–13 spikes preceding each flick. A second neuron gave more tonic responses (Fig. 1).

These results demonstrate that we can record quantitatively the bilateral flicking activity of freely moving animals. This will be important for future experiments on the decision making process involved in lobster orientation behavior in turbulent odor plumes.

This study has been supported in part by the Lucy and Jules Silver AQUAVET Research Fellowship and Madison Trust (KB) and NSF (IBN-9212650; JA) and NIH (2PO1NS25915-04A1; JA).

Literature Cited

1. **Atema, J. 1977.** Pp. 165–174 in *Olfaction and Taste VI,* J. Le Magnen and P. MacLeod, eds. Information Retrieval Ltd., London.
2. **Cowan, D. 1991.** *Biol. Bull.* **181:** 402–407.
3. **Devine, D. V., and J. Atema. 1982.** *Biol. Bull.* **163:** 144–153.
4. **Hazlett, B. A. 1971.** *J. Anim. Morphol. Physiol.* **18:** 1–10.
5. **Karavanich, C., and J. Atema. 1991.** *Biol. Bull.* **181:** 359–360.
6. **Moore, P. A., N. Scholz, and J. Atema. 1991.** *J. Chem. Ecol.* **17:** 1293–1307.
7. **Moore, P. A., J. Atema, and G. A. Gerhardt. 1991.** *Chem. Senses* **16:** 663–674.
8. **Sigvardt, K. A. 1977.** *J. Comp. Physiol* **118:** 195–214.
9. **Snow, P. 1973.** *J. Exp. Biol.* **58:** 745–765.

A Hemolytic Activity in the Blood of the American Horseshoe Crab, *Limulus polyphemus* that Resembles the Mammalian Complement System

Peter B. Armstrong (Laboratory for Cell Biology, Department of Zoology, University of California, Davis, CA 95616-8755), Margaret T. Armstrong, and James P. Quigley

A key to the survival of animals in a septic world is the operation of a variety of immune defense systems that kill or inactivate invading pathogens. In mammals, the complement system, which consists of about 20 proteins and about 40 receptor and regulatory proteins, is one of the principal immune systems present in the plasma (1). Lower vertebrates also have a complement system, though typically with a reduced number of components from the mammalian system (2). Among the various activators of the vertebrate complement system is C-reactive protein (3). The key protein of the complement system is C3, which binds to the surfaces of foreign cells by amide and ester linkages and marks the cells for cytolysis and phagocytosis. Covalent binding of C3 is mediated by an unusual internal thiol ester bond that is activated by proteolysis of C3 and that then reacts with nucleophiles in the environment (4). C3 belongs to the α_2-macroglobulin family of proteins.

In 1982, we identified α_2-macroglobulin in the plasma of the horseshoe crab, *Limulus polyphemus* (5). Our initial characterization of α_2-macroglobulin in *Limulus* was as a protease-binding protein (6, 7). We now present evidence that *Limulus* homologues to two components of the mammalian complement system, α_2-macroglobulin and C-reactive protein, function in a cytolytic system found in the plasma. This represents the first molecular characterization of a complement-like cytolytic system in an invertebrate.

The plasma of *Limulus* is of simple composition, with the three most abundant proteins being hemocyanin, α_2-macroglobulin (6, 7), and C-reactive protein (8). Both whole plasma and hemocyanin-depleted plasma cytolyze sheep erythrocytes

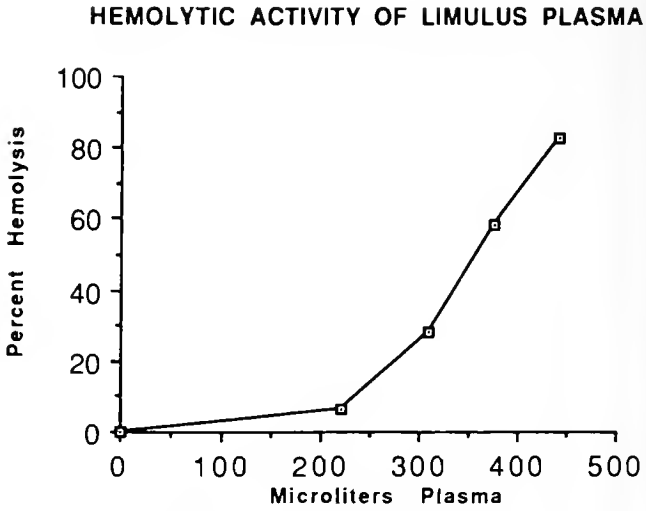

Figure 1. *Hemolysis of sheep erythrocytes by hemocyanin-depleted* Limulus *plasma.* Limulus *plasma was treated with 3% polyethylene glycol-8000 to remove most of the hemocyanin. Sheep erythrocytes were suspended in a barbital-buffered saline (71 mM NaCl, 0.15 mM $CaCl_2$, 0.5 mM $MgCl_2$, 2.5% glucose, 0.1% gelatin, 2.5 mM sodium barbital, pH 7.3) and exposed to different concentrations of hemocyanin-depleted plasma for 4 h on a table-top shaker at 25°C. At the completion of the incubation period, the erythrocytes were removed by centrifugation and extent of hemolysis was estimated by determining the concentration of hemoglobin released into the bathing medium by the optical absorbency at 412 nm. Complete hemolysis was produced by exposure of an aliquot of erythrocytes to distilled water.*

(the foreign cell model for these studies) (Fig. 1). The cytolytic activity is Ca^{+2}-dependent, since it was abolished both by EDTA and Mg^{+2}-EGTA. Activity was reduced by 70–80% if the plasma was treated with methylamine, which inactivates the internal thiol ester bond of *Limulus* α_2-macroglobulin. The cytolytic activity was restored by the addition of purified *Limulus* α_2-macroglobulin to methylamine-treated plasma. We propose that α_2-macroglobulin may play a role in the *Limulus* cytolytic system similar to that served by C3 in mammals, since C3 and α_2-macroglobulin are members of the same protein family and both require a functional thiol ester bond for activity. Thus, *Limulus* α_2-macroglobulin has both protease-binding and complement functions, whereas in vertebrates these functions have become segregated to different members of the α_2-macroglobulin family of proteins.

The involvement of C-reactive protein was demonstrated by complete inactivation of the cytolytic activity of plasma treated with phosphorylethanolamine or exposure to phosphorylethanolamine-sepharose and by the ability of purified C-reactive protein to produce hemolysis. Phosphorylethanolamine is a ligand for C-reactive protein. Activity of plasma that has been depleted of C-reactive protein by treatment with phosphorylethanolamine-sepharose was restored by addition of affinity purified *Limulus* C-reactive protein. The involvement of C-reactive protein in the cytolytic system of *Limulus* strengthens the notion that the cytolytic system of this invertebrate represents an evolutionary homolog of the vertebrate complement system, since C-reactive protein is a documented activator of the mammalian complement system.

In recombination trials, the sole necessary component for hemolysis was C-reactive protein. α_2-Macroglobulin was not required at high concentrations of C-reactive protein, but potentiated hemolysis at lower concentrations of C-reactive protein. At the concentrations found in the blood (α_2-macroglobulin = 1–2 mg/ml; C-reactive protein = 1–5 mg/ml), both components appear to be necessary, because the removal of C-reactive protein or the inactivation of α_2-macroglobulin eliminates or reduces the cytolytic activity of the plasma. Interestingly, C-reactive protein was inactive at the ionic strength of the hypotonic hemolysis buffer but became active at physiological ionic strength (0.15 molar NaCl).

Vertebrates depend upon the complement system to eliminate pathogens from vascular and tissue spaces. Our study is the first characterization of an immune defense system in the plasma of an invertebrate, the arthropod *Limulus*, that shows significant similarities to the mammalian complement system. Two components of the *Limulus* system are molecular homologs to important elements of the mammalian complement system. The evolution of the complement system is a topic of emerging interest in the discipline of comparative immunity.

This research was supported by Grant No. GM 35185 from the National Institutes of Health.

Literature Cited

1. **Law, S. K., and K. B. M. Reid. 1988.** *Complement.* IRL Press, Oxford. v. + 72 pp.
2. **Dodds, A. W., and A. J. Day. 1992.** In *The Molecular Biology and Biochemistry of Complement.* R. B. Sim, ed. MTP Press, Lancaster, UK. (in press).
3. **Jiang, H., J. N. Siegel, and H. Gewurz. 1991.** *J. Immunol.* **146:** 2324–2330.
4. **Law, S. K., and R. P. Levine. 1977.** *Proc. Nat. Acad. Sci. USA* **74:** 2701–2705.
5. **Quigley, J. P., P. B. Armstrong, P. Gallant, F. R. Rickles, and W. Troll. 1982.** *Biol. Bull.* **163:** 402.
6. **Quigley, J. P., and P. B. Armstrong. 1983.** *J. Biol. Chem.* **258:** 7903–7906.
7. **Quigley, J. P., and P. B. Armstrong. 1985.** *J. Biol. Chem.* **260:** 12715–12719.
8. **Robey, F. A., and T.-Y. Liu. 1981.** *J. Biol. Chem.* **256:** 969–975.

Monitoring Marine Resources: Ecological and Policy Implications Affecting the Scientific Collecting and Commercial Value of New England Conch (*Busycon*)

Ilene M. Kaplan and Barbara C. Boyer (Union College, Schenectady, NY 12308)

Socio-economic and ecological trends in the New England conch (*i.e.*, the commercial name for the whelk *Busycon*) fishery and concomitant changes in marine policy regarding the commerical fishing of conch are examined. These observations are part of an ongoing study of the New England conch fishery drawing from interviews of fishermen, seafood buyers and sellers, processors, market and restaurant owners, and government officials (1, 2, 3). Special attention was focussed on the availability of conch and recent policy changes limiting the commercial activity in this fishery, particularly as it pertains to small-scale fishermen (*i.e.*, pot fishermen). Conch is an interesting fishery to examine because it reflects changes that are occurring in the commercial fishing industry as a whole. Differences between traditional and non-traditional fishermen and their techniques are only some of the changes that the industry now confronts (4). There is also scientific interest in *Busycon;* it serves as a host organism for other marine life and as a subject for biological investigations in a number of different areas.

Fishermen in the coastal areas of Massachusetts typically receive 70 to 75 cents a pound for conch; fishermen in the Narragansett area of Rhode Island receive 35 to 45 cents a pound for smaller specimens. Lower prices are also paid for conch caught by draggers (*i.e.*, large-scale fishermen) because the product is often damaged. Market prices of conch in the shell range from 75 to 99 cents a pound. Smaller conch in Rhode Island may sell for 50 to 60 cents a pound. Conch salad ranges in price

from $3.49 to $7.99 a pound. Most sellers report that ethnic markets continue to be the mainstay of the domestic industry, with Chinatowns in the Boston, New York, and San Francisco areas being the largest markets. Foreign markets include Taiwan, Hong Kong, Singapore, and Japan.

Larger wholesalers of conch consistently state that the commercial value of the New England product is largely influenced by the depletion of the fishery in traditional waters of South America, the Caribbean, and Asia. This depletion has resulted in the steady climb of the commercial value of New England conch. Buyers, as well as fishermen, report turning to conch as other domestic fish stocks become depleted. Fishermen and wholesalers both voiced concerns over the possible depletion of the New England fishery, although buyers report indifference among some fishermen who have tried selling small, immature conch.

Overfishing of New England conch continues to be a potential problem as commercial interest increases and as the number of conch fishermen also increases. Variability in the processing and marketing conditions of conch also continues to be found, with rules governing quality control and seafood inspection largely done on an individual company basis. Interchangeable marketing terms are used, including calling conch "snail salad" in higher priced markets. Conch has become the popularized label for different species of gastropod in addition to the traditional *Strombus,* resulting in the sale of a product to consumers that is not accurately named.

In the last few years, regulations governing the conch fishery have been established in the state of Massachusetts. These include freezing the number of licenses issued, limiting the number of conch pots that a fisherman can have in the water at any one time to 200, and limiting conch fishing to daylight hours. Most recently, the Division of Marine Fisheries of Massachusetts created a closed season for conch, a minimum legal size (width) limit, and a ban on on-board processing of conch. Gear restrictions for conching in different coastal areas are also being specified.

Fishermen report being aware of these new policies, although most state that it is too early to tell how effective the policies will be or how they will impact their livelihood. We suggest further research in the area of compliance to policies and their enforcement and a need for improvements in government reports such as the use of consistent measures for weights and monetary values reported for conch. We also suggest improvements regarding policies for seafood inspection programs.

Fishermen also express a curiosity in the habits and biology of conch. Although the whelk *Busycon* has been the subject of some scientific investigations, there is much that is still not known about the species. A total of 245 specimens of *Busycon canaliculatum* were examined (185 females and 60 males) at the Marine Biological Laboratory in Woods Hole; all were over the minimum size limit of 2.75 inches in width. Consistent with earlier findings in our research, females appear to grow to larger sizes than males. The average size for females was 18.2 cm in length; the average size for males was 16.3 cm. Data collected since 1983 show consistently that males are smaller than females; in all years but one, a higher proportion of whelks below 15 cm in length were males. We suggest more research in the area of size and sex disparity.

The fate of unintentional catch in the fishing industry is also a concern with regard to the conservation of marine resources. For example, *Hoploplana inquilina,* a marine flatworm that lives comensally in the mantle cavity of *Busycon* and used in studies of developmental mechanisms (5), is unintentionally collected by conch fishermen. Overfishing of New England *Busycon* will have direct impact on this non-parasitic flatworm.

Continued investigations of the New England conch fishery are planned.

The authors gratefully acknowledge the support of the Woods Hole Oceanographic Institution and the Marine Biological Laboratory.

Literature Cited

1. **Kaplan, I., B. Boyer, and K. Santos. 1988.** *Biol. Bull.* **175:** 312.
2. **Kaplan, I., B. Boyer, and D. Hoffmann. 1989.** *Biol. Bull.* **177:** 327.
3. **Kaplan, I., B. Boyer, and D. Hoffmann. 1990.** *Biol. Bull.* **179:** 227.
4. **Kaplan, I. 1988.** *J. Cont. Eth.* **16:** 491–514.
5. **Boyer, B. 1986.** *Int. J. Invert. Repro. Dev.* **9:** 243–251.

CONTENTS

Volume 183 Number 3

THE BIOLOGICAL BULLETIN

DECEMBER, 1992

Published by the Marine Biological Laboratory

THE
BIOLOGICAL BULLETIN

PUBLISHED BY
THE MARINE BIOLOGICAL LABORATORY

DECEMBER, 1992

Printed and Issued by
LANCASTER PRESS, Inc.
3575 HEMPLAND ROAD
LANCASTER, PA

THE BIOLOGICAL BULLETIN

THE BIOLOGICAL BULLETIN is published six times a year by the Marine Biological Laboratory, MBL Street, Woods Hole, Massachusetts 02543.

Subscriptions and similar matter should be addressed to Subscription Manager, THE BIOLOGICAL BULLETIN, Marine Biological Laboratory, Woods Hole, Massachusetts 02543. Single numbers, $30.00. Subscription per volume (three issues), $77.50 ($155.00 per year for six issues).

Communications relative to manuscripts should be sent to Michael J. Greenberg, Editor-in-Chief, or Pamela L. Clapp, Managing Editor, at the Marine Biological Laboratory, Woods Hole, Massachusetts 02543. Telephone: (508) 548-3705, ext. 428. FAX: 508-540-6902. E-mail: pamcl@hoh.mbl.edu.

POSTMASTER: Send address changes to THE BIOLOGICAL BULLETIN, Marine Biological Laboratory, Woods Hole, MA 02543.

Second-class postage paid at Woods Hole, MA, and additional mailing offices.
ISSN 0006-3185

INSTRUCTIONS TO AUTHORS

The Biological Bulletin accepts outstanding original research reports of general interest to biologists throughout the world. Papers are usually of intermediate length (10–40 manuscript pages). A limited number of solicited review papers may be accepted after formal review. A paper will usually appear within four months after its acceptance.

Very short, especially topical papers (less than 9 manuscript pages including tables, figures, and bibliography) will be published in a separate section entitled "Research Notes." A Research Note in *The Biological Bulletin* follows the format of similar notes in *Nature*. It should open with a summary paragraph of 150 to 200 words comprising the introduction and the conclusions. The rest of the text should continue on without subheadings, and there should be no more than 30 references. References should be referred to in the text by number, and listed in the Literature Cited section in the order that they appear in the text. Unlike references in *Nature*, references in the Research Notes section should conform in punctuation and arrangement to the style of recent issues of *The Biological Bulletin*. Materials and Methods should be incorporated into appropriate figure legends. See the article by Lohmann *et al* (October 1990, Vol. **179**: 214–218) for sample style. A Research Note will usually appear within two months after its acceptance.

The Editorial Board requests that regular manuscripts conform to the requirements set below; those manuscripts that do not conform will be returned to authors for correction before review.

1. ***Manuscripts.*** Manuscripts, including figures, should be submitted in triplicate. (Xerox copies of photographs are not acceptable for review purposes.) The original manuscript must be typed in no smaller than 12 pitch, using double spacing (*including* figure legends, footnotes, bibliography, etc.) on one side of 16- or 20-lb. bond paper, 8½ by 11 inches. Please, no right justification. Manuscripts should be proofread carefully and errors corrected legibly in black ink. Pages should be numbered consecutively. Margins on all sides should be at least 1 inch (2.5 cm). Manuscripts should conform to the *Council of Biology Editors Style Manual*, 5th Edition (Council of Biology Editors, 1983) and to American spelling. Unusual abbreviations should be kept to a minimum and should be spelled out on first reference as well as defined in a footnote on the title page. Manuscripts should be divided into the following components: Title page, Abstract (of no more than 200 words), Introduction, Materials and Methods, Results, Discussion, Acknowledgments, Literature Cited, Tables, and Figure Legends. In addition, authors should supply a list of words and phrases under which the article should be indexed.

2. ***Title page.*** The title page consists of: a condensed title or running head of no more than 35 letters and spaces, the manuscript title, authors' names and appropriate addresses, and footnotes listing present addresses, acknowledgments or contribution numbers, and explanation of unusual abbreviations.

3. ***Figures.*** The dimensions of the printed page, 7 by 9 inches, should be kept in mind in preparing figures for publication. We recommend that figures be about 1½ times the linear dimensions of the final printing desired, and that the ratio of the largest to the smallest letter or number and of the thickest to the thinnest line not exceed 1:1.5. Explanatory matter generally should be included in legends, although axes should always be identified on the illustration itself. Figures should be prepared for reproduction as either line cuts or halftones. Figures to be reproduced as line cuts should be unmounted glossy photographic reproductions or drawn in black ink on white paper, good-quality tracing cloth or plastic, or blue-lined coordinate paper. Those to be reproduced as halftones should be mounted on board, with both designating numbers or letters and scale bars affixed directly to the figures. All figures should be numbered in consecutive order, with no distinction between text and plate figures. The author's name and an arrow indicating orientation should appear on the reverse side of all figures.

4. ***Tables, footnotes, figure legends, etc.*** Authors should follow the style in a recent issue of *The Biological Bulletin* in preparing table headings, figure legends, and the like. Because of the high cost of setting tabular material in type, authors are asked to limit such material as much as possible. Tables, with their headings and footnotes, should be typed on separate sheets, numbered with consecutive Roman numerals, and placed after

the Literature Cited. Figure legends should contain enough information to make the figure intelligible separate from the text. Legends should be typed double spaced, with consecutive Arabic numbers, on a separate sheet at the end of the paper. Footnotes should be limited to authors' current addresses, acknowledgments or contribution numbers, and explanation of unusual abbreviations. All such footnotes should appear on the title page. Footnotes are not normally permitted in the body of the text.

5. ***Literature cited.*** In the text, literature should be cited by the Harvard system, with papers by more than two authors cited as Jones *et al.*, 1980. Personal communications and material in preparation or in press should be cited in the text only, with author's initials and institutions, unless the material has been formally accepted and a volume number can be supplied. The list of references following the text should be headed Literature Cited, and must be typed double spaced on separate pages, conforming in punctuation and arrangement to the style of recent issues of *The Biological Bulletin*. Citations should include complete titles and inclusive pagination. Journal abbreviations should normally follow those of the U. S. A. Standards Institute (USASI), as adopted by BIOLOGICAL ABSTRACTS and CHEMICAL ABSTRACTS, with the minor differences set out below. The most generally useful list of biological journal titles is that published each year by BIOLOGICAL ABSTRACTS (BIOSIS List of Serials; the most recent issue). Foreign authors, and others who are accustomed to using THE WORLD LIST OF SCIENTIFIC PERIODICALS, may find a booklet published by the Biological Council of the U.K. (obtainable from the Institute of Biology, 41 Queen's Gate, London, S.W.7, England, U.K.) useful, since it sets out the WORLD LIST abbreviations for most biological journals with notes of the USASI abbreviations where these differ. CHEMICAL ABSTRACTS publishes quarterly supplements of additional abbreviations. The following points of reference style for THE BIOLOGICAL BULLETIN differ from USASI (or modified WORLD LIST) usage:

A. Journal abbreviations, and book titles, all underlined (for *italics*)

B. All components of abbreviations with initial capitals (not as European usage in WORLD LIST *e.g., J. Cell. Comp. Physiol.* NOT *J. cell. comp. Physiol.*)

C. *All* abbreviated components must be followed by a period, whole word components *must not* (*i.e., J. Cancer Res.*)

D. Space between all components (*e.g., J. Cell. Comp. Physiol.*, not *J.Cell.Comp.Physiol.*)

E. Unusual words in journal titles should be spelled out in full, rather than employing new abbreviations invented by the author. For example, use *Rit Vísindafjélags Islendinga* without abbreviation.

F. All single word journal titles in full (*e.g., Veliger, Ecology, Brain*).

G. The order of abbreviated components should be the same as the word order of the complete title (*i.e., Proc.* and *Trans.* placed where they appear, not transposed as in some BIOLOGICAL ABSTRACTS listings).

H. A few well-known international journals in their preferred forms rather than WORLD LIST or USASI usage (*e.g., Nature, Science, Evolution* NOT *Nature, Lond., Science, N.Y.; Evolution, Lancaster, Pa.*)

6. ***Reprints, page proofs, and charges.*** Authors receive their first 100 reprints (without covers) free of charge. Additional reprints may be ordered at time of publication and normally will be delivered about two to three months after the issue date. Authors (or delegates for foreign authors) will receive page proofs of articles shortly before publication. They will be charged the current cost of printers' time for corrections to these (other than corrections of printers' or editors' errors). Other than these charges for authors' alterations, *The Biological Bulletin* does not have page charges.

ERRATUM

The Biological Bulletin, Volume **183,** Number 2, page 343

The following correction should be noted in the research note by S. Rohr and B. M. Salzberg titled, "Discontinuities in action potential propagation along chains of single ventricular myocytes in culture: multiple site optical recordings of transmembrane voltage (MSORTV) suggests propagation delays at the junctional sites between cells" (*Biol. Bull.* **183:** 342–343).

The X-axis calibration in Figure 1B should be multiplied by 2, and the overall conduction velocity between the first and last elements in the chain (#2 and #10) should be 0.27 m/s and not, as stated in paragraph 4, 0.32 m/s.

CONTENTS

No. 1, August 1992

CONTENTS

No. 2, October 1992

No. 3, December 1992

ECOLOGY AND EVOLUTION

NEUROBIOLOGY AND BEHAVIOR

PHYSIOLOGY

RESEARCH NOTES

Reference: *Biol. Bull.* **183**: 381–386. (December, 1992)

Genetic Consequences of Blocking Polar Body I with Cytochalasin B in Fertilized Eggs of the Pacific Oyster, *Crassostrea gigas:* I. Ploidy of Resultant Embryos

XIMING GUO[1]*, KENNETH COOPER[2]**, WILLIAM K. HERSHBERGER[1], AND KENNETH K. CHEW[1]

[1]*School of Fisheries, WH-10, University of Washington, Seattle, Washington 98195, and*
[2]*Coast Oyster Company, Quilcene, Washington 98376*

Abstract. The effect of blocking polar body I (PB1) with cytochalasin B (CB) on the ploidy of embryos was studied in the Pacific oyster, *Crassostrea gigas*. To block the release of PB1, fertilized eggs were treated with CB (1.0 μg/ml) for 15 min beginning at 5 min post-fertilization at 25°C. The CB treatment and its control were repeated in three crosses. Ploidy of 8-h-old embryos was determined with karyological analysis.

In control groups, the majority of the cells (89.3%) had a diploid number of 20 chromosomes, although spontaneous haploids (0.7%), triploids (1.3%) and aneuploids (8.7%) were also encountered. In CB-treated groups, only 4.5% of the cells remained as diploid, and the majority were either triploid (15.6%), tetraploid (19.4%) or aneuploid (57.6%). Despite variation among the three crosses, contingency Chi-square analysis showed that the occurrence of triploids, tetraploids and aneuploids had a significant ($P = 0.0001$) dependence on the CB treatment. The majority of the aneuploids fell into two groups containing either 23–25 or 35–37 chromosomes. The production of triploids, tetraploids and aneuploids in specific distributions suggests that blocking PB1 complicates subsequent chromosome segregation.

Introduction

In most vertebrates, eggs usually mature after the completion of meiosis I. In the Pacific oyster, *Crassostrea gigas*, and many other marine mollusks, mature eggs are arrested at prophase of meiosis I (Ahmed, 1973; Lu, 1986; Strathmann, 1987). Only after fertilization or activation, do the eggs complete meiosis I and II, releasing two polar bodies. Delayed meiosis in eggs of the Pacific oyster provides a unique opportunity for manipulation of both polar body I (PB1) and polar body II (PB2). Although it has been well established that blocking the release of PB2 results in triploidy (reviewed by Beaumont and Fairbrother, 1991), it is still uncertain what ploidy will result from blocking PB1.

Stanley *et al.* (1981) first reported that cytochalasin B (CB) treatment applied during meiosis I resulted in triploid and tetraploid embryos in the American oyster, *Crassostrea virginica*, although only triploids survived to 8 months of age. Similarly, both triploid and tetraploid embryos were produced from blocking PB1 in the blue mussel *Mytilus edulis* (Yamamoto and Sugawara, 1988) and the Pacific abalone, *Haliotis discus hannai* (Arai *et al.*, 1986). In the Pacific oyster, however, only triploids were found when thermal shocks were applied during meiosis I (Quillet and Panelay, 1986). In a later study, blocking PB1 with CB in the Pacific oyster produced tetraploids, not triploids (Stephens and Downing, 1988; Stephens, 1989).

In the Pacific oyster, production of either meiosis I triploids or tetraploids is of interest. Triploid oysters have become an important part of the oyster culture industry because of their sterility (Allen, 1988; Allen *et al.*, 1989). Meiosis I triploids may grow better than meiosis II triploids (Stanley *et al.*, 1984) that are currently produced in commercial hatcheries. Tetraploids may be mated to diploids to produce all triploid progeny. However, available data are inconclusive, if not conflicting, on the ques-

Received 3 March 1992; accepted 31 July 1992.

* Corresponding author, present address: Haskin Shellfish Research Laboratory, Rutgers University, Box B-8, Port Norris, New Jersey 08349.

** Present address: 24888 Taree Drive NE, Kingston, Washington 98346.

tion of what ploidy is produced from blocking PB1. The lack of detailed ploidy analyses of early embryos may be partly responsible for the discrepancy. This study used extensive karyological analysis to determine the ploidy of 8-h-old Pacific oyster embryos following blocking PB1 with CB. It was anticipated that results of this study would clarify some of the confusion concerning the genetic consequences of blocking PB1.

Materials and Methods

Gamete preparation

Gametes were obtained by strip-spawning sexually mature Pacific oysters. To obtain eggs, female gonadal tissue was dissected into 2 l of seawater. The egg suspension was first passed through a 100 μm screen (Research Nets Inc.) to remove large tissue debris. Eggs about 50 μm in diameter were collected onto a 20 μm screen. Broken eggs and other smaller debris were washed off. The eggs were then re-suspended in 1 l of seawater, ready for fertilization.

To prepare sperm suspensions, 1 g of male gonadal tissue was completely suspended in 99 g of seawater. The large tissue debris were removed by passing the sperm suspension through a 20 μm screen. For fertilization, 5 ml of the sperm suspension was added to one million eggs suspended in 1 l of seawater. Fertilization, treatment, and embryo culture were all conducted at 25°C.

CB treatment

To block the release of PB1, 1.0 mg CB (Sigma) dissolved in 1.0 ml dimethyl sulfoxide (DMSO) was added to 1 l egg suspension at 5 min post-fertilization for 15 min. CB was removed by collecting and rinsing treated eggs on a 20 μm screen. Eggs were then returned to 0.1% DMSO in seawater for 30 min to remove residual CB. In the control groups, fertilized eggs were treated with only 0.1% DMSO. The embryos were stocked at a density of 20 embryos/ml. The experiment was repeated three times using three pairs of oysters as parents.

Determination of ploidy

Ploidy of the resultant embryos in both control and treated groups was determined by karyological analysis. Samples for karyological analysis were taken at 8 h post-fertilization. Embryos were first treated with 0.01% colchicine for 30 min. After the colchicine was removed, nine parts of a hypotonic solution (0.075 *M* KCl) was added to one part embryo suspension for 25–30 min. The hypotonic solution was then removed as completely as possible, and samples were fixed in a solution of one part glacial acetic acid and three parts of absolute methanol (v/v). About 15 min before staining, the fixative was replaced by 1:1 (v/v) glacial acetic acid and absolute methanol solution.

Embryo suspensions were dropped onto slides and air-dried. Slides were stained with Leishman's stain (Benn and Perle, 1986). The stock solution was made by dissolving 150 mg Leishman's stain (Sigma) in 100 ml methanol. The staining solution was prepared by mixing one part of the stock solution with three parts phosphate buffer (0.025 *M* KH_2PO_4, pH 6.8). The slides were stained for 10–15 min.

Only metaphase plates which showed no evidence of artificial chromosome loss were counted. Only one metaphase plate per embryo was scored and used to represent that embryo. Embryos with more than one countable metaphase were rare. A minimum of 50 metaphase plates from 50 embryos were counted for control and treatment groups of all replicates. Diploid Pacific oysters have 20 chromosomes (Ahmed and Sparks, 1967; Ahmed, 1973). In this study, ploidies were classified as the following: 10, haploid; 20, diploid; 29–30, triploid; 39–40, tetraploid; 49–50, pentaploid. All others were considered to be aneuploid.

Data analysis

For both control and treated groups, homogeneity among the three crosses was tested with Chi-square homogeneity analysis. Differences between the control and treated groups were then tested by contingency Chi-square analysis. The null hypothesis was that the occurrence of ploidies was independent of CB treatment.

Results

In the control groups, PB1 was released around 17 min post-fertilization, and PB2 was released around 35 min post-fertilization. In the CB-treated groups, PB1 was not observed at the time expected, but one polar body was released in most of the eggs between 35 and 45 min post-fertilization. The first mitosis in the treated groups appeared to be normal, except apparently less synchronized than that in the control groups.

At 8 h post-fertilization, all embryos developed to swimming trochophores, and the number of swimmers hatched was high in both treated and control groups (95–100%). However, abnormal trochophores were noticed in the CB-treated groups. The abnormal trochophores were either deformed or constantly swam in a circular motion.

In the control groups, the karyological analysis revealed that 89.3% of all cells examined had exactly 20 chromosomes (Table 1). Only 8.7% could be classified as aneuploids, of which, about half (4.7%) had 19 chromosomes, one quarter (2.0%) had 15–18 chromosomes, and one quarter (2.0%) had 21 chromosomes (trisomics). Spon-

taneous haploids and triploids were also observed in the control groups at a low frequency (0.7% and 1.3%, respectively). No tetraploids or pentaploids were found among the 150 cells counted from the control groups.

Compared with the control groups, all three CB-treated groups had dramatic increases in the proportion of polyploid and aneuploid cells; only about 4.5% of all cells remained as diploid (Table I). The majority of cells were either triploid (15.6%), tetraploid (19.4%) or aneuploid (57.6%) (Fig. 1). A low percentage of haploids and pentaploids were also recorded in the CB-treated groups. The mitotic index of CB-treated groups was noticeably lower than control groups.

For both the control and the treated groups, the homogeneity among crosses was accepted at a significance level of 95% for the frequencies of diploids, triploids, tetraploids and aneuploids. Homogeneity was not tested for haploids and pentaploids, where at least one cross had no occurrence of the ploidy tested (Table I). Because the number of haploids and pentaploids observed in all three crosses was low (0–4%), homogeneity among crosses was assumed. Consequently, data from all three crosses were used in a contingency Chi-square analysis to test the null hypothesis that the occurrence of ploidies is independent of the CB treatment. When all ploidies were analyzed in one Chi-square test (df = 5), the null hypothesis was rejected at a confidence level of 95%. When ploidies were tested separately (df = 1), however, the null hypothesis was accepted for haploids and pentaploids (Table I). On the other hand, the occurrence of diploids, triploids, tetraploids, and aneuploids showed a significant ($P = 0.0001$) dependence on whether or not the eggs were treated with CB for blocking PB1.

Although the homogeneity among crosses was statistically accepted, the CB-treated groups from different crosses had noticeable differences in the distribution of the different ploidies induced. For example, in the first cross, CB treatment induced 26% triploids, 24% tetraploids and 45% aneuploids, compared to 11%, 6%, and 72% of respective ploidies induced in cross 3 (Table I).

The distribution of pooled chromosome counts for the control and for the treated groups from the three crosses is shown in Figure 2. As expected, only one peak (at 2n = 20 chromosomes) was present in the control groups (Fig. 2A). In the treated groups, however, four peaks could be identified: triploids, tetraploids, and two aneuploid peaks, corresponding to chromosome counts of 23–25 and 35–37 (Fig. 2B).

Discussion

This study provides an estimate of the frequency of spontaneous aneuploidy in 8-h-old embryos of the Pacific oyster under our experimental conditions. It is unlikely that the aneuploidy in the control groups was caused by DMSO, although this study cannot rule out such a possibility. DMSO is widely used with cultured cells and embryos, and has no known effects on chromosome segregation. Comparable data have not been reported. Since karyological techniques tend to create chromosome losses and overestimate the occurrence of aneuploidy, the 8.7% aneuploids observed in this study may be considered as an upper limit of aneuploidy in the 8-h-old embryos. On the other hand, since the probability of creating trisomics by artifacts is low, the 2% trisomics observed here may provide a conservative low limit.

The formation of aneuploid gametes in mollusks may be common, particularly under environmental stress (Dixon, 1982). Gaffney *et al.* (1990) suggested that heterozygosity deficiency, a common phenomenon in mollusks, could be caused by the occurrence of aneuploids. In juvenile Pacific oysters, aneuploid cells were estimated to range from 4% to 36% (Thiriot-Quievreux *et al.*, 1988). Frequency of spontaneous aneuploids could be very different at different stages of the life cycle.

Table I

Percentage of different ploidies observed from normal fertilization (Control) and blocking PB1 (Treated) in the Pacific oyster

Cross	Group	Sample size	1n	2n	3n	4n	5n	An
1	Control	50	2.0	88.0	0.0	0.0	0.0	10.0
	Treated	54	0.0	5.5	25.9	24.1	0.0	44.5
2	Control	50	0.0	92.0	2.0	0.0	0.0	6.0
	Treated	50	0.0	2.0	10.0	28.0	4.0	56.0
3	Control	50	0.0	88.0	2.0	0.0	0.0	10.0
	Treated	65	1.5	6.2	10.8	6.2	3.1	72.3
Average	Control	(150)	0.7	89.3	1.3	0.0	0.0	8.7
	Treated	(169)	0.5	4.5	15.6	19.4	2.4	57.6
P-value (Chi-square)*			0.5313	0.0001	0.0001	0.0001	0.1639	0.0001

* The null hypothesis of the Chi-square test was that occurrence of each ploidy is independent of the CB treatment.

Ploidy was classified as: 10, haploid (1n); 20, diploid (2n); 29–30, triploid (3n); 39–40, tetraploid (4n); 49–50, pentaploid (5n); and others, aneuploid (An).

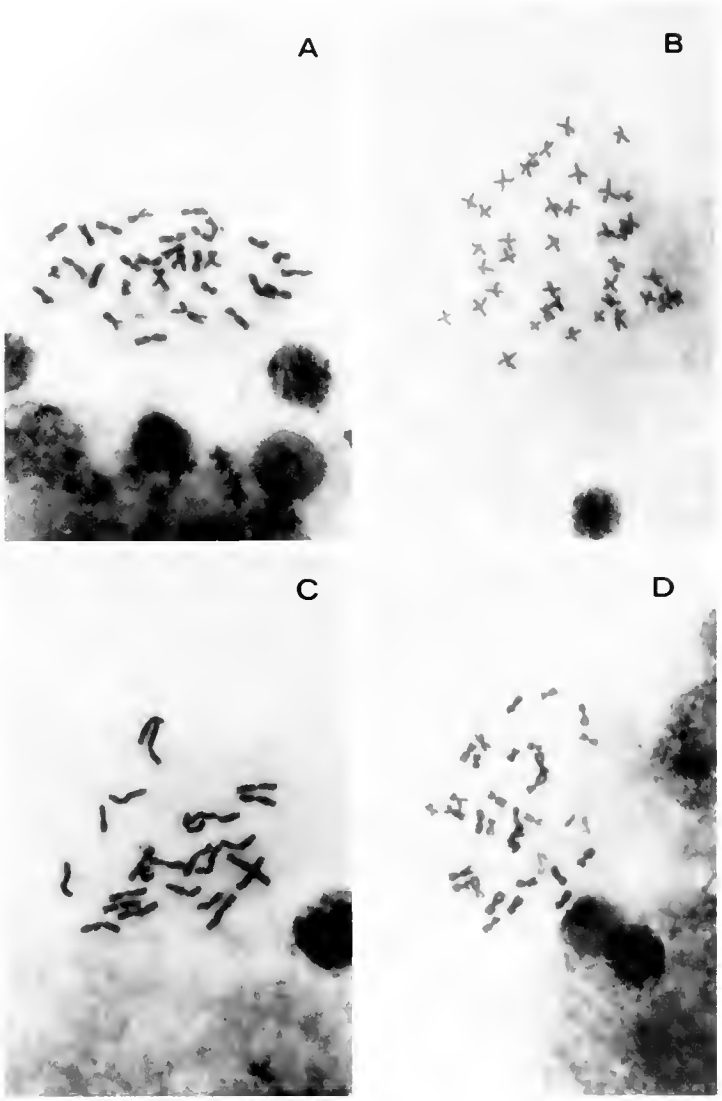

Figure 1. Metaphase plates of triploid (A), tetraploid (B) and aneuploid (C, D) cells produced from blocking polar body I with cytochalasin B in the fertilized eggs of the Pacific oyster.

Results from this study suggest that spontaneous haploids and triploids might occur in the Pacific oyster. Spontaneous triploids have been reported in amphibians and fish and are probably caused by fertilization of unreduced ova by diploid sperm (Fankhauser, 1945; Thorgaard and Gall [illegible] aploids could be caused by the failure of sperm [illegible] incorporation. Again, this study cannot comment about the possibility that the haploids and triploids [illegible] control groups were induced by the DMSO.

It is clear that the CB treatment applied during meiosis I was effective in preventing polar body release at 17 min post-fertilization, a time corresponding to the release of PB1. That the polar body released at 40 min post-fertilization (after CB treatment) is PB2 rather than the delayed PB1 has been previously suggested, based on the different fluorescence intensity of the two polar bodies (Stephens, 1989).

The detection of triploids and tetraploids from blocking PB1 in this study agrees with results from the American oyster (Stanley *et al.*, 1981), the blue mussel (Yamamoto and Sugawara, 1988), and the Pacific abalone (Arai *et al.*, 1986). Also, results of this study do not conflict with studies in which only triploid juveniles were observed from blocking PB1 (Stanley *et al.*, 1984; Downing and Allen, 1987). The lack of tetraploids at juvenile or adult stages was probably due to poor viability of tetraploids (Stanley *et al.*, 1981; Stephens, 1989; Guo, 1991). On the other hand, results of this study differ from other studies, in which only triploid embryos (Quillet and Panelay, 1986)

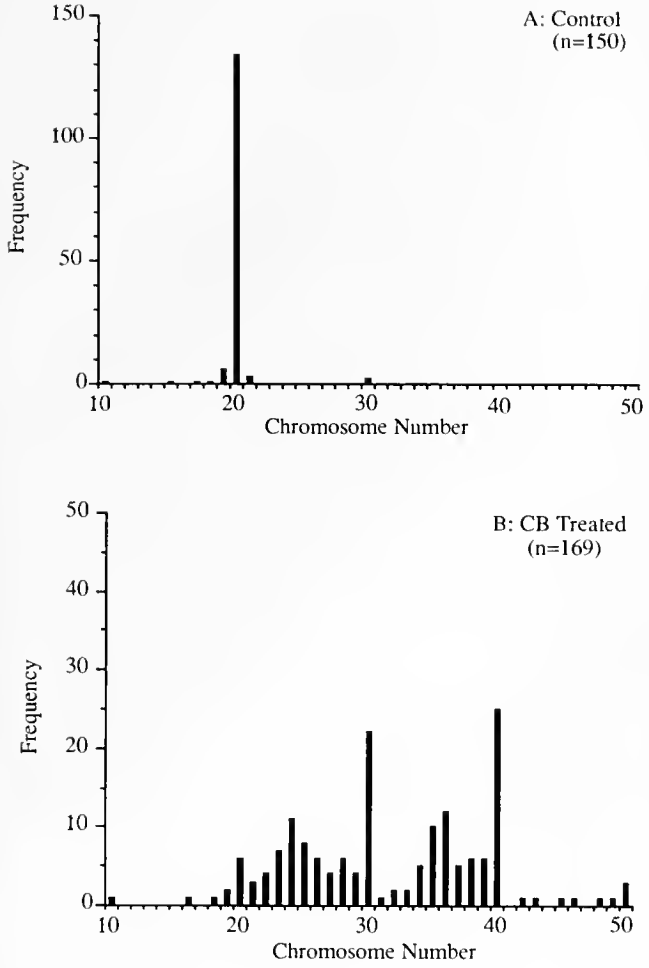

Figure 2. Chromosome counts in embryos resulting from normal fertilization (A:Control) and blocking polar body 1 with cytochalasin B (B:CB Treated) in the Pacific oyster; combined data from three crosses.

or only tetraploid larvae (Stephens, 1989) were observed from blocking PB1. This variation may be due to differences in experimental methods and conditions. For example, Quillet and Panelay (1986) used temperature shock instead of CB to block PB1, and Stephens (1989) treated zygotes at 18°C instead of at 25°C. Environmental factors, such as temperature, salinity, egg quality, timing and duration of CB treatment, all have effects on meiotic events and triploid induction (Lu, 1986; Downing and Allen, 1987). Variation in those environmental factors was probably also responsible for the different proportions of ploidies observed in the three crosses of this study.

The production of a large proportion of aneuploids from blocking PB1 was unexpected. Further, it was surprising that the aneuploids distributed around two peaks with 23–25 and 35–37 chromosomes. Aneuploids were commonly assumed to be artifacts caused by karyological treatment. In this study, comparison between the control and CB-treated groups clearly demonstrated that the aneuploids were a consequence of CB treatments, not artifacts. Also, the fact that the aneuploids formed two peaks minimized the possibility of artifacts being the explanation. The assumption of artifacts was probably the reason why aneuploids were not reported in previous studies. As a result, aneuploids were grouped into the closest euploid groups. For example, in the blue mussel with a diploid number of 28 chromosomes, Yamamoto and Sugawara (1988) classified cells with 35–48 chromosomes as triploids and those with 49–62 chromosomes as tetraploids. Also, Quillet and Panelay (1986) classified metaphase spreads with "about 20 chromosomes" as diploids, and those with "about 30 chromosomes" as triploids in the Pacific oyster. In studies where ploidy was determined at juvenile or adult stages (Stanley *et al.*, 1981; Downing and Allen, 1987), aneuploids were absent probably because they died in early embryonic development. Aneuploidy often leads to abnormality and death in higher animals. A preliminary study showed that the majority of aneuploids were not viable in the Pacific oyster (Guo *et al.*, 1989).

Survival of the resultant embryos from blocking PB1 was not recorded in this study. It was our experience with the Pacific oyster that blocking PB1 always resulted in higher mortalities than blocking PB2; the survival to D-stage was usually 20–40% for blocking PB1, and 60–80% for blocking PB2 (Guo and Cooper, unpub.). Downing and Allen (1987) also found that early CB treatments in the Pacific oyster produced higher mortalities at D-stage than late treatments. Differential mortality may also occur after D-stage. In the American oyster, the early CB treatment resulted in a higher mortality than the late treatment, as determined at 8 months post-fertilization, although the early treatment produced a larger number of D-stage larvae than the late treatments at 24 h post-fertilization (Stanley *et al.*, 1981). The high mortalities from blocking PB1 could be caused by the poor viability of aneuploids and tetraploids.

The production of triploids, tetraploids and a large proportion of aneuploids in specific distributions suggests that blocking PB1 complicates subsequent chromosome segregation. Mechanisms by which triploids, tetraploids and specific aneuploids are produced from blocking PB1 were investigated in a separate study; the results of that study are presented in the next paper (Guo *et al.*, 1992).

Acknowledgments

The authors would like to thank Dr. Standish K. Allen Jr. for his constructive comments on the manuscript, and the Coast Oyster Company for providing this study with broodstock and laboratory space. This project was partly funded by Washington State Sea Grant.

Literature Cited

Ahmed, M. 1973. Cytogenetics of oysters. *Cytologia* **38:** 337–347.

Ahmed, M., and A. K. Sparks. 1967. A preliminary study of chromosomes of two species of oyster (*Ostrea lurida* and *Crassostrea*). *J. Fish. Res. Bd. Canada* **24**(10): 2155–2159.

Allen, S. K., Jr. 1988. Triploid oysters ensure year-round supply. *Oceanus* **31**(3): 58–63.

Allen, S. K., Jr., S. L. Downing, and K. K. Chew. 1989. *Hatchery Manual for Producing Triploid Oysters.* University of Washington Press, Seattle.

Arai, K. F., F. Naito, and K. Fujino. 1986. Triploidization of the Pacific abalone with temperature and pressure treatments. *Bull. Japan Soc. Sci. Fish.* **52**(3): 417–422.

Beaumont, A. R., and J. E. Fairbrother. 1991. Ploidy manipulation in molluscan shellfish: a review. *J. Shellfish Res.* **10**(1): 1–18.

Benn, P. A., and M. A. Perle. 1986. Chromosome staining and banding techniques. Pp. 57–84 in *Human Cytogenetics: A Practical Approach.* D. E. Rooney, and B. H. Czepulkowski, eds. IRL Press Ltd, Oxford, England.

Dixon, D. R. 1982. Aneuploidy in mussel embryos (*Mytilus edulis* L.) originating from a polluted dock. *Mar. Biol. Lett.* **3:** 155–161.

Downing, S. L., and S. K. Allen Jr. 1987. Induced triploidy in the Pacific oyster *Crassostrea gigas:* optimal treatments with cytochalasin B depend on temperature. *Aquaculture* **61:** 1–15.

Fankhauser, G. 1945. The effects of chromosome number on amphibian development. *Q. Rev. Biol.* **20:** 20–78.

Gaffney, P. M., T. M. Scott, R. K. Koehn, and W. J. Diehl. 1990. Interrelationships of heterozygosity, growth rate and heterozygote deficiencies in the coot clam, *Mulinia lateralis. Genetics* **124:** 687–699.

Guo, X. 1991. Studies on tetraploid induction in the Pacific oyster, *Crassostrea gigas.* Ph.D. Dissertation, University of Washington, Seattle.

Guo, X., K. Cooper, and W. K. Hershberger. 1989. Aneuploid Pacific oyster larvae produced by treating with cytochalasin B during meiosis I. *J. Shellfish Res.* **8**(2): 448. (Abstract)

Guo, X., W. K. Hershberger, K. Cooper, and K. K. Chew. 1992. Genetic consequences of blocking polar body I with cytochalasin B in fertilized eggs of the Pacific oyster, *Crassostrea gigas:* II. Segregation of chromosomes. *Biol. Bull.* **183:** 387–393.

Lu, J. K. 1986. The combined effects of salinity and temperature on meiosis and early mitosis of the Pacific oyster (*Crassostrea gigas*) oocytes. M.S. Thesis, University of Washington, Seattle.

Quillet, E., and P. J. Panelay. 1986. Triploidy induction by thermal shocks in the Pacific oyster, *Crassostrea gigas. Aquaculture* **57:** 271–279.

Stanley, J. G., S. K. Allen Jr., and H. Hidu. 1981. Polyploidy induced in the American oyster, *Crassostrea virginica,* with cytochalasin B. *Aquaculture* **23:** 1–10.

Stanley, J. G., H. Hidu, and S. K. Allen Jr. 1984. Growth of American oysters increased by polyploidy induced by blocking meiosis I but not meiosis II. *Aquaculture* **37:** 147–155.

Stephens, L. B. 1989. Inhibition of the first polar body formation in *Crassostrea gigas* produces tetraploids, not meiotic I triploids. M.S. Thesis, University of Washington, Seattle.

Stephens, L. B., and S. L. Downing. 1988. Inhibition of the first polar body formation in *Crassostrea gigas* produces tetraploids, not meiotic I triploids. *J. Shellfish Res.* **7**(3): 550–551. (Abstract)

Strathmann, M. F. 1987. *Reproduction and Development of Marine Invertebrates of the Northern Pacific Coast.* University of Washington Press, Seattle.

Thiriot-Quievreux, C., T. Neol, S. Bougrier, and S. Dollot. 1988. Relationship between aneuploidy and growth rate in pair mating of the oyster, *Crassostrea gigas. Aquaculture* **75:** 89–96.

Thorgaard, G. H., and G. A. E. Gall. 1979. Adult triploids in a rainbow trout family. *Genetics* **93:** 961–973.

Yamamoto, S., and Y. Sugawara. 1988. Induced triploidy in the mussel, *Mytilus edulis,* by temperature shock. *Aquaculture* **72:** 21–29.

Reference: *Biol. Bull.* **183:** 387–393. (December, 1992)

Genetic Consequences of Blocking Polar Body I with Cytochalasin B in Fertilized Eggs of the Pacific Oyster, *Crassostrea gigas:* II. Segregation of Chromosomes

XIMING GUO[1]*, WILLIAM K. HERSHBERGER[1], KENNETH COOPER[2]**, AND KENNETH K. CHEW[1]

[1]*School of Fisheries, WH-10, University of Washington, Seattle, Washington 98195, and*
[2]*Coast Oyster Company, Quilcene, Washington 98376*

Abstract. The effect of blocking polar body I (PB1) with cytochalasin B (CB) on subsequent chromosome segregation was studied in fertilized eggs of the Pacific oyster, *Crassostrea gigas.* To block the release of PB1, fertilized eggs were treated with CB (1.0 μg/ml) for 15 min beginning at 5 min post-fertilization at 25°C. Chromosome segregation in both control and CB-treated eggs was analyzed with an acetic orcein stain.

In untreated eggs, ten maternal tetrad chromosomes went through meiosis I and II, and released two polar bodies, reaching a haploid number of 10 chromatids. In CB-treated eggs, meiosis I proceeded normally and produced two groups of dyads, ten in each group. However, blocking PB1 dramatically changed chromosome segregation in meiosis II. In the majority of the treated eggs (68%), the two groups of dyads from meiosis I entered meiosis II through a "tripolar segregation", although two other types of segregation, namely "united bipolar" (7%) and "separated bipolar" (12%) were also observed. After anaphase II, chromatids at the peripheral pole were released as polar body II (PB2). The release of two sets of chromatids as PB2 through either a united bipolar or a separated bipolar segregation resulted in the formation of meiosis I triploids (14%). The release of one set of chromatids as PB2 from an unmixed tripolar or a separated bipolar segregation formed meiosis I tetraploids (20%). Aneuploids (56%) were produced, primarily when the two groups of dyads from meiosis I united or overlapped before entering the tripolar segregation.

Received 3 March 1992; accepted 31 July 1992.

* Corresponding author, present address: Haskin Shellfish Research Laboratory, Rutgers University, Box B-8, Port Norris, New Jersey 08349.

** Present address: 24888 Taree Drive NE, Kingston, Washington 98346.

Introduction

It has been reported that blocking the release of polar body I (PB1) in the Pacific oyster, *Crassostrea gigas,* and other mollusks may result in triploidy (Quillet and Panelay, 1986; Arai *et al.,* 1986), tetraploidy (Stephens and Downing, 1988), or both (Stanley *et al.,* 1981; Yamamoto and Sugawara, 1988). In addition to the triploids and tetraploids reported, a previous study also revealed the production of high levels of aneuploids, which distributed unexpectedly around two peaks (Guo *et al.,* 1992). The production of triploids, tetraploids and aneuploids in specific distributions suggests that blocking PB1 may have complicated subsequent chromosome segregation.

The production of triploids and tetraploids from blocking PB1 may be explained by results from two studies. In the surf clam *Spisula solidissima,* Longo (1972) used electron microscopy to study the effects of CB on the formation of polar bodies. When CB blocked the formation of both polar bodies, he observed four groups of maternally derived chromatids, suggesting that two groups of dyad chromosomes from meiosis I might have entered meiosis II separately. If one or two of the four chromatid groups were released as PB2, tetraploids or triploids were produced. In the Japanese pearl oyster, *Pinctada fucata martensii,* blocking PB1 produced 3 or 4 maternally derived groups of chromatids; triploids or tetraploids were produced by releasing two or one set of chromatids (Komaru *et al.,* 1990).

Despite the findings that production of triploids from blocking PB1 is possible, the question still remains

whether triploids produced from blocking PB1 are genetically different from triploids produced from blocking PB2. It has been shown that meiosis I triploids have a higher level of heterozygosity and a higher growth rate than meiosis II triploids in the American oyster, *Crassostrea virginica* (Stanley *et al.*, 1984). Improved growth rate was also observed for meiosis I triploids in the Pacific oyster (Yamamoto *et al.*, 1988), in blue mussel, *Mytilus edulis* (Beaumont and Kelly, 1989), and in the pearl oyster, *Pinctada martensii* (Jiang *et al.*, 1991). Treatments applied at different times showed two windows for triploid induction, corresponding to the timing of meiosis I and II, respectively (Quillet and Panelay, 1986; Arai *et al.*, 1986; Yamamoto and Sugawara, 1988). However, cytological evidence of meiosis I triploid formation has never been reported. That tetraploids and aneuploids resulted from blocking PB1 adds further confusion to how meiosis I triploids are produced.

The mechanism by which aneuploids were produced from blocking PB1 is unknown. Overlapping of chromosome segregation during meiosis II observed by Longo (1972) may produce some aneuploids; however, specific distributions of aneuploids suggest that they were not created randomly (Guo *et al.*, 1992). Instead, the aneuploids may be created through specific patterns of chromosome segregation.

It was the objective of this study to investigate how chromosomes segregate and what is released as PB2, following inhibition of PB1 in fertilized eggs of the Pacific oyster.

Materials and Methods

Treatment and sampling

Gametes of the Pacific oyster were prepared according to methods described in Guo *et al.* (1992). Gamete handling and treatment were all conducted at 25°C. Two experimental groups were formed. In the first group, fertilized eggs were treated with 0.1% dimethyl sulfoxide (DMSO) only and allowed to develop as diploid controls. In the second group, fertilized eggs were treated with 1.0 μg/ml CB in 0.1% DMSO for 15 min beginning at 5 min post-fertilization. The experiment was repeated in a second cross using a different pair of oysters.

To study chromosome segregation, samples of developing zygotes from both groups were taken every 5 min until 80 min post-fertilization and fixed in 1:3 (v/v) glacial acetic acid and absolute ethanol. Ploidy level of 8-h-old embryos was determined with karyological analysis according to methods in Guo *et al.* (1992). Twenty-five metaphase plates were counted for each group.

Staining method

Initially, two acetic orcein stains were tested: 1% orcein stain in 45% acetic acid (in distilled water) and a lactic-acetic orcein stain (Darlington and La Cours, 1962; Lu, 1986). Both resulted in dark staining of the cytoplasm and, therefore, the contrast between chromosomes and cytoplasm was poor.

Subsequently, 0.5% orcein in 40%, 50%, 60%, 70% and 80% acetic acid was tested. Cytoplasmic staining became lighter with increasing concentrations of acetic acid. But with 80% acetic acid, the staining of chromosomes was slow, taking at least 24 h to obtain good contrast. Stain with 0.5% orcein in 60% acetic acid gave satisfactory contrast with 5–10 min of staining.

For staining, drops of fixed samples were spread on slides, and the excess fixative was allowed to run off the slides. Two drops of the modified acetic orcein stain were added, and the material was covered with a cover glass. After staining for 5 min, excess stain was removed by absorption onto filter paper. The cover glass was gently pressed and sealed with fingernail polish.

Slides were examined with a Zeiss compound microscope. Photographs were taken with Kodak TMX 400 black and white film.

Results

The mature oocyte of the Pacific oyster has a large germinal vesicle which is visible under the microscope without staining. Germinal vesicle breakdown (GVBD) usually occurs after the egg has been in the seawater for 20–40 min.

Pacific oysters have a diploid number of 20 chromosomes (Ahmed and Sparks, 1967; Ahmed, 1973). After GVBD, 10 tetrad (synapsed) chromosomes were scattered in the eggs. Shortly after fertilization (within 5 min), the 10 tetrads gathered closely and were apparently ready for meiosis I (Fig. 1A).

In both the control and the CB-treated groups, development of eggs was not completely synchronized. A small proportion (<5%) of the eggs developed very slowly. These slowly developing eggs reached metaphase I when the majority of the eggs had released the second polar body.

Chromosome segregation in the control groups

In the control groups, the 10 tetrads started to segregate at 5 min post-fertilization. Anaphase I was reached in the majority of the eggs at 10 min post-fertilization with 10 dyad chromosomes moving toward each division pole (Fig. 1B). At telophase I (around 15 min post-fertilization), the 10 dyads at the peripheral pole became more condensed and compacted (Fig. 1C). PB1 was released in the majority of the eggs by 20 min post-fertilization. The ten remaining dyads continued through meiosis II, and metaphase II was reached around 25 min post-fertilization.

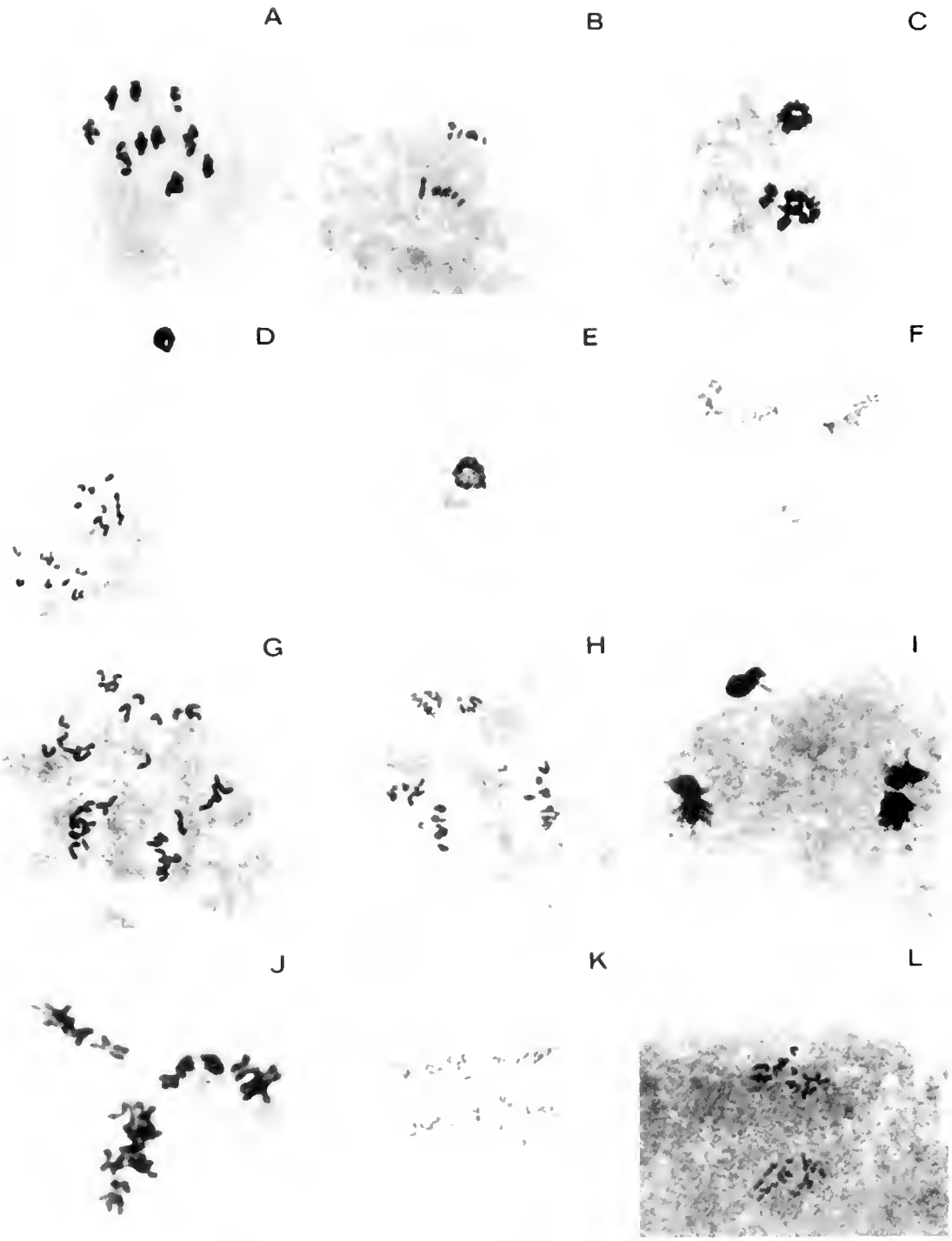

Figure 1. Segregation patterns observed in fertilized eggs of the Pacific oyster following normal fertilization (A–E) and blocking polar body I with cytochalasin B (F–L): A–E, meiosis in normal eggs; F–I, randomized tripolar segregation; J, unmixed tripolar segregation; K, united bipolar segregation; and L, separated bipolar segregation.

The remaining dyads segregated into anaphase II around 30 min post-fertilization (Fig. 1D). PB2 was released in the majority of the eggs by 35 min post-fertilization (Fig. 1E). The remaining 10 maternal chromatids became invisible. Fusion of pronuclei was not observed. Maternal chromosomes reappeared as 10 duplicated dyads before mitosis I. At the same time, 10 paternal dyads also became visible. The first mitotic division occurred between 55 and 65 min post-fertilization. The development of a normal diploid is schematically represented in Figure 2A.

Chromosome segregation in the treated groups

Tripolar segregation. Although CB may effectively block the release of PB1 (Guo *et al.*, 1992), the presence of CB had no apparent inhibitory effects on the segregation and movement of chromosomes during meiosis I. In the CB-treated groups, events during the first 15 min after fertilization were the same as in the untreated controls. Maternal chromosomes went through meiosis I and divided into two groups of dyads, and the peripheral group also condensed and compacted as in the control groups (Fig. 1C).

Differences in the pattern of chromosome segregation between the control and treated groups appeared between 15 and 20 min post-fertilization (10 min after CB treatment). In the treated eggs, the compacted group of dyads (ten) at the peripheral pole was not released as PB1 and started to dissociate, become individual dyads, and migrate back toward the remaining group of dyads. No polar body was released at 20 min post-fertilization when eggs in the control groups released PB1.

In the majority of treated eggs at 20 min post-fertilization, the two groups of dyads were united in a single cluster. At 25–30 min post-fertilization, the twenty dyads (ten from each group) randomly partitioned into three groups; each group (with 6–7 dyads on the average) was distributed on one of three division planes in a tripolar configuration (Fig. 1F). Between 30 and 35 min post-fertilization, the three groups of dyads at the three division planes entered anaphase II (Fig. 1G). During telophase II, each pole received chromatids from two adjacent groups of dyads and ended up with an average of 13–14 chromatids (Fig. 1H). After telophase II, all three groups of chromatids became condensed, and the group at the peripheral pole was released as PB2 [illegible] post-fertilization (Fig. 1I). This PB2 contained [illegible] average 13–14 chromatids; its release could leave the [illegible] aneuploid (Fig. 2C). Since the dyads from [illegible] appeared to group and segregate randomly, this tripolar segregation was referred to as "Randomized Tripolar" segregation (Fig. 2C). Although rare, eggs with two PB2s were also observed. The first mitosis in the CB-treated groups occurred between 60 and 75 min post-fertilization.

In some of the treated eggs, the two groups of dyads from meiosis I did not unite or overlap before entering a tripolar segregation. Instead, one group of dyads divided itself into the two division planes adjacent to the peripheral pole, and the other 10 dyads remained together at the inner division plane (Fig. 1J). Thus, a set of ten chromatids might be pulled to the peripheral pole and released as PB2 (Fig. 2D). The remaining 30 maternal chromosomes may unite with the paternal set of chromosomes and form a tetraploid. This type of tripolar segregation, in which the two groups of dyads appeared to be kept unmixed during metaphase II, was referred to as the "Unmixed Tripolar" segregation (Fig. 2D).

Intermediate to the randomized and unmixed tripolar segregations, the two groups of dyads would sometimes overlap by only 1–3 dyads. This tripolar segregation was referred to as "Overlapped Tripolar" segregation (picture not shown).

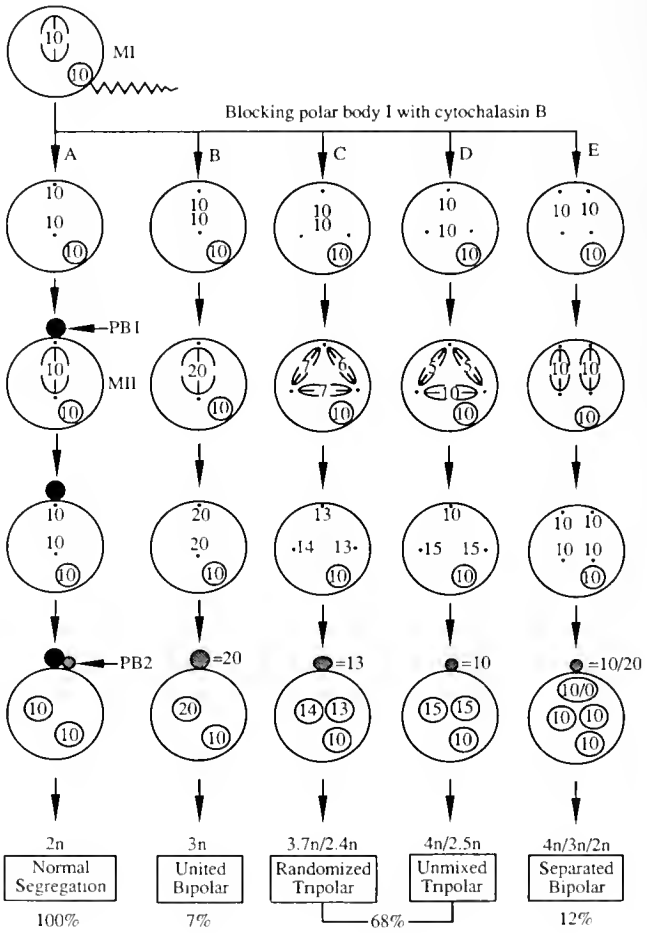

Figure 2. Schematic summary of segregation patterns observed in fertilized eggs of the Pacific oyster following normal fertilization (A) and blocking polar body I with cytochalasin B (B–E). Spindles and centrioles are hypothetical.

Table I

Percentage of different segregation patterns and ploidies observed from blocking polar body I with cytochalasin B in fertilized eggs of the Pacific oyster

	Segregation patterns (n = 50)				Ploidy levels (n = 25)			
Cross	Separated bipolar	United bipolar	Tripolar all	Unclassified patterns	3n	4n	An	Other
1	12	10	64	14	12	8	68	12
2	12	4	72	12	16	32	44	8
Average	12	7	68	13	14	20	56	10

All segregation patterns were determined at telophase II based on the number of maternal chromosome groups observed. Ploidy was abbreviated as 3n for triploids, 4n for tetraploids, An for aneuploids, and Other for haploids, diploids and pentaploids combined.

Other patterns of segregation. Tripolar segregations were common, but other segregation patterns were also found. In some cases, the two groups of dyads from meiosis I completely united and went through meiosis II in a single bipolar configuration (Fig. 1K). This type of segregation was referred to as "United Bipolar" segregation, which led to the formation of meiosis I triploids (Fig. 2B). In other cases, the two groups of dyads derived from meiosis I entered the second meiosis independently in two separate bipolar divisions (Fig. 1L; Fig. 2E). This segregation was referred as the "Separated Bipolar" segregation.

Segregation patterns and ploidy of resultant embryos. Due to the relatively short duration of metaphase and anaphase, it was difficult to estimate precisely frequencies of different tripolar segregations. Between anaphase II and the release of PB2, however, there was a relatively long period when the number of maternal chromatid groups could be reliably counted. The frequency of united bipolar segregation, tripolar segregation and separated bipolar segregation was determined by the presence of two, three and four maternal chromatid groups, respectively. As indicated by the presence of three maternal chromatid groups, the majority of the treated eggs in both crosses (68%) went through tripolar segregations following blocking PB1 (Table I). The two crosses had the same number of separated bipolar segregations, but differed in the percentage of the united bipolar segregations.

Overall, ploidies of the resultant embryos from the CB-treated groups consisted of 14% triploids, 20% tetraploids and 56% aneuploids (Table I). However, the two crosses differed considerably in the frequencies of tetraploids and aneuploids. CB treatment in the second cross produced more tetraploids (32%) but fewer aneuploids (44%) than that in the first cross (8% and 68%, respectively). About two-thirds of the aneuploids fell in the range of 23–26 and 34–38 chromosomes. In some aneuploid embryos where two cells were counted, chromosome numbers sometimes varied. In the control groups, over 90% of the cells counted could be classified as diploids.

Discussion

The acetic orcein stain provided a convenient and satisfactory tool for cytological analysis of Pacific oyster eggs. Meiotic events observed in normal diploid embryos agree with what has been described for the Pacific oyster (Lu, 1986). In treated groups, CB treatment effectively blocked the release of PB1 without inhibiting chromosome segregation and movement during meiosis I, which confirms observations by Longo (1972) and Komaru *et al.* (1990). However, blocking PB1 greatly changed chromosome segregation during the second meiotic division.

Segregation patterns following inhibition of PB1 observed in this study differ from that observed in the surf clam, *Spisula solidissima* by Longo (1972). When the formation of both polar bodies was blocked in fertilized eggs of the surf clam, four groups of maternally derived chromatids were most often produced, suggesting that the two groups of dyads from meiosis I might go through meiosis II through a separated bipolar segregation. In this study, the separated bipolar segregation was observed in only a small proportion of treated eggs (12%). The majority of the treated eggs (68%) went through a tripolar segregation to produce three groups of maternally derived chromatids (Table I). Although tripolar segregation was not described in his study, Longo (1972) did observe that sometimes three maternal pronuclei of unequal ploidy were present.

In the Japanese pearl oyster, *Pinctada fucata martensii*, Komaru *et al.* (1990) reported that three (20.6%) or four (17.6%) groups of maternally derived chromosomes were produced from blocking PB1. While the authors did not discuss how dyads segregated during meiosis II, it is likely that the four groups of maternal chromatids were formed through the separated bipolar segregation. However, there are two possible explanations why three groups of maternal chromosomes were observed by Komaru *et al.* (1990). One possibility is that the three groups of maternal chromosomes were produced through the tripolar segregations.

as described in this study. The other possibility is that one group of dyads from meiosis I did not divide during meiosis II, and the other group did. Evidence of the latter possibility was not found in this study, and in fact, dyads from meiosis I always entered meiosis II synchronously. It should be mentioned that in the Komaru *et al.* 1990 study, blocking PB1 produced 1.9% triploids and 98.1% diploids, suggesting that their CB treatment was not very effective.

Mechanisms for the formation of triploids, tetraploids and aneuploids are indicated by the segregation patterns we observed (Fig. 2). Triploids could be formed through either a united bipolar segregation (Fig. 2B), or a separated bipolar segregation (Fig. 2E). Triploids produced from a united bipolar segregation would undoubtedly be meiosis I triploids, which should be genetically different from meiosis II triploids. Triploids produced from a separated bipolar segregation were probably also meiosis I triploids, because the two chromatid sets released were most likely from two different divisions rather than from the same one. The formation of meiosis I triploids has been previously suggested by the fact that (1) treatments applied corresponding to meiosis I and II showed two windows of triploid induction (Arai *et al.*, 1986; Quillet and Panelay, 1986; Yamamoto and Sugawara, 1988) and (2) the triploids produced from treatment applied during meiosis I contained a higher level of genomic heterozygosity than triploids produced at meiosis II (Stanley *et al.*, 1984). However, this study does not rule out the possibility that blocking PB1 might overlap with blocking PB2 and produce meiosis II triploids as well (Downing and Allen, 1987).

Having shown that meiosis I triploids are genetically different from meiosis II triploids, this study does not necessarily imply that meiosis I triploids always have higher levels of heterozygosity than meiosis II triploids. Heterozygosity of meiosis I and II triploids is determined by the recombination rate (r). Considering only the maternal chromosome sets, the heterozygosity is predicted by "1 − r/2" in meiosis I triploids, and "r" in meiosis II triploids. Thus, meiosis I triploids would be more heterozygous than meiosis II triploids only if the recombination rate is lower than 2/3. In the Pacific oyster, a preliminary study estimated that the average recombination rate was close to [illegible] allozyme coding loci (Guo and Gaffney, in [illegible]).

Following [illegible] PB1, the release of one set of chromosomes [illegible] either a separated bipolar or an unmixed tripolar segregation will lead to the formation of a meiosis I tetraploid (Fig. 2D, E). Such tetraploids contain three maternal sets and one paternal set of chromosomes. Compared with tetraploids produced from blocking mitosis I, meiosis I tetraploids should have higher levels of heterozygosity. However, meiosis I tetraploids had very limited viability (Stephens and Downing, 1988; Stephens, 1989; Guo, 1991).

Aneuploids were apparently created as a consequence of the tripolar segregations. If the twenty dyads (ten from each group) derived from blocking PB1 enter the tripolar division randomly, the release of one of the three groups of chromatids in meiosis II left the egg, on average, with 26–27 maternally derived chromatids (Fig. 2C). The 26–27 maternally derived chromosomes plus the 10 paternally derived chromosomes would form an aneuploid with 36–37 chromosomes. In our previous paper (Guo *et al.*, 1992), karyological analysis has shown that induced aneuploids formed a peak around 35–37 chromosomes.

However, the question still remains as to how aneuploids with 23–25 chromosomes were formed. Besides creating aneuploids with 36–37 chromosomes, randomized tripolar segregation may suggest two other possibilities. First, two of the three groups of chromatids (13–14 per group) might be released as PB2s, leaving the egg with 13–14 maternal chromatids, which, combined with 10 paternal chromatids, form aneuploids with 23–24 chromosomes. The second possibility is that one group of chromatids was released as PB2, but another group failed to incorporate into the first mitosis or was incorporated into only one of the daughter cells, forming aneuploids with 23–24 chromosomes or mosaic aneuploids with 23–24/36–37 chromosomes (Fig. 2C). Evidence for both possibilities exists. In this study and in that of Komaru *et al.*, 1990, some eggs were observed to release two polar bodies after blocking PB1. Komaru *et al.* (1990) also found evidence that one group of maternal chromatids might be neither released as PB2 nor incorporated into the first mitosis. Similarly, aneuploids with, on the average, 25 chromosomes could also be produced from an unmixed tripolar segregation (Fig. 2D).

Difficulties in discriminating between the various types of tripolar segregations prevented direct correlation between segregation patterns and ploidies of resultant embryos. Increased incidence of aneuploids observed in the first cross was probably caused by a higher proportion of randomized tripolar segregations. It is possible that the two dyad groups from meiosis I united more frequently in eggs of the first cross than in eggs of the second cross, producing more randomized tripolar segregations in the first (increased aneuploidy) and more unmixed tripolar segregations in the second (increased tetraploidy).

The various tripolar segregations may also be responsible for the difference in ploidies reported from different studies on blocking PB1 (Stanley *et al.*, 1981; Quillet and Panelay, 1986; Stephens, 1989; Guo *et al.*, 1992). Results of this study indicate that formation of triploids, tetraploids or aneuploids depends on the configuration of the dyads when they enter the tripolar segregation. Since the movement of the two groups of dyads can be influenced

by many factors, such as temperature, salinity and egg quality (Lu, 1986; Downing and Allen, 1987), ploidies could vary greatly among species or in the same species with different experimental conditions. Stephens (1989) obtained a high percentage of tetraploids when she blocked PB1 at 18°C. Possibly at low temperature (18°C), the two groups of dyads from meiosis I moved too slowly to unite, primarily forming unmixed tripolar segregation and producing tetraploids.

In summary, CB-induced inhibition of PB1 in fertilized eggs of the Pacific oyster produced complicated patterns of chromosome segregation, yielding triploids, tetraploids and aneuploids in specific distributions. This study provided cytological evidence that blocking PB1 could produce meiosis I triploids that are genetically different from meiosis II triploids. Because meiosis I triploids exhibited faster growth rates than normal diploids and meiosis II triploids (Stanley *et al.*, 1984; Yamamoto *et al.*, 1988; Beaumont and Kelly, 1989; Jiang *et al.*, 1991), it may be necessary to re-evaluate blocking PB1 as an alternative method for triploid production. Although blocking PB1 usually produces lower survival and lower levels of triploids than blocking PB2, faster growth rate may compensate for the loss of eggs that are abundant in marine bivalves. It would be beneficial to test whether meiosis I triploids are indeed more heterozygous than meiosis II triploids (Stanley *et al.*, 1984), and whether treatments for blocking PB1 can be improved to produce more meiosis I triploids and fewer of other ploidies.

Acknowledgments

The authors would like to thank Dr. Standish K. Allen Jr. for his constructive comments on the manuscript, and the Coast Oyster Company for providing this study with broodstock and laboratory space. This project was partly funded by Washington State Sea Grant.

Literature Cited

Ahmed, M. 1973. Cytogenetics of oysters. *Cytologia* **38**: 337–347.

Ahmed, M., and A. K. Sparks. 1967. A preliminary study of chromosomes of two species of oyster (*Ostrea lurida* and *Crassostrea*). *J. Fish. Res. Bd. Canada* **24**(10): 2155–2159.

Arai, K. F., F. Naito, and K. Fujino. 1986. Triploidization of the Pacific abalone with temperature and pressure treatments. *Bull. Japan Soc. Sci. Fish.* **52**(3): 417–422.

Beaumont, A. R., and K. S. Kelly. 1989. Production and growth of triploid *Mytilus edulis* larvae. *J. Exp. Mar. Biol. Ecol.* **132**: 69–84.

Darlington, C. D., and L. F. La Cours. 1962. *The Handling of Chromosomes.* Hafner Publishing Co, New York.

Downing, S. L., and S. K. Allen Jr. 1987. Induced triploidy in the Pacific oyster *Crassostrea gigas:* optimal treatments with cytochalasin B depend on temperature. *Aquaculture* **61**: 1–15.

Guo, X. 1991. Studies on tetraploid induction in the Pacific oyster, *Crassostrea gigas.* Ph.D. Dissertation, University of Washington, Seattle.

Guo, X., K. Cooper, W. K. Hershberger, and K. K. Chew. 1992. Genetic consequences of blocking polar body I with cytochalasin B in fertilized eggs of the Pacific oyster, *Crassostrea gigas:* I. Ploidy of resultant embryos. *Biol. Bull.* **183**: 381–386.

Jiang, W., G. Xu, Y. Lin, and G. Li. 1991. Comparison of growth between triploid and diploid of *Pinctada martensii* (D.). *Tropic Oceanography,* **10**(3): 1–7. (In Chinese)

Komaru, A., H. Matsuda, T. Yamakawa, and K. T. Wada. 1990. Chromosome-behavior of meiosis-inhibited eggs with cytochalasin B in Japanese pearl oyster. *Nippon Suisan Gakkaishi* **569**: 1419–1422.

Longo, F. J. 1972. The effects of cytochalasin B on the events of fertilization in the surf clam, *Spisula solidissima* I polar body formation. *J. Exp. Zool.* **182**: 321–344.

Lu, J. K. 1986. The combined effects of salinity and temperature on meiosis and early mitosis of the Pacific oyster (*Crassostrea gigas*) oocytes. M.S. Thesis, University of Washington, Seattle.

Quillet, E., and P. J. Panelay. 1986. Triploidy induction by thermal shocks in the Pacific oyster, *Crassostrea gigas. Aquaculture* **57**: 271–279.

Stanley, J. G., S. K. Allen Jr., and H. Hidu. 1981. Polyploidy induced in the American oyster, *Crassostrea virginica,* with cytochalasin B. *Aquaculture* **23**: 1–10.

Stanley, J. G., H. Hidu, and S. K. Allen Jr. 1984. Growth of American oysters increased by polyploidy induced by blocking meiosis I but not meiosis II. *Aquaculture* **37**: 147–155.

Stephens, L. B. 1989. Inhibition of the first polar body formation in *Crassostrea gigas* produces tetraploids, not meiotic I triploids. M. S. Thesis, University of Washington, Seattle.

Stephens, L. B., and S. L. Downing. 1988. Inhibition of the first polar body formation in *Crassostrea gigas* produces tetraploids, not meiotic I triploids. *J. Shellfish Res.* 7(3): 550–551. (Abstract)

Yamamoto, S., and Y. Sugawara. 1988. Induced triploidy in the mussel, *Mytilus edulis,* by temperature shock. *Aquaculture* **72**: 21–29.

Yamamoto, S., Y. Sugawara, T. Nomaru, and A. Oshino. 1988. Induced triploidy in the Pacific oyster, *Crassostrea gigas,* and performance of triploid larvae. *Tohoku J. Agr. Res.* **39**(1): 47–59.

Reference: *Biol. Bull.* 183: 394–400. (December, 1992)

Protein, Vitellogenin, and Vitellin Levels in the Hemolymph and Ovaries during Ovarian Development in *Penaeus semisulcatus* (de Haan)

S. SHAFIR[1,2], M. TOM[1], M. OVADIA[2], AND E. LUBZENS[1]

[1]*National Institute of Oceanography, Israel Oceanographic & Limnological Research, P.O. Box 8030, Haifa 31080, Israel, and* [2]*Dept. of Zoology, Wise Faculty of Life Sciences, Tel Aviv University, Tel Aviv 69978, Israel*

Abstract. The concentration of vitellogenin (Vg) in the hemolymph of *Penaeus semisulcatus* was found to increase from an average of 50 μg ml^{-1} to 439 μg ml^{-1} in female shrimp during ovarian development. The most significant increase in Vg occurred concomitant with the increase in the vitellin (Vt) content of oocytes with an average diameter (AOD) ranging between 150 and 250 μm. The amount of Vt in the oocytes was found to increase linearly from a mean of 0.0126 mg to 4.55 mg per gm body weight. However, the percentage of Vt in the total protein was found to decrease, from 67% in ovaries with AOD of 150–250 μm, to 39.7% in ovaries with AOD of 350 μm or larger. The volume of the hemolymph was found to be 0.4 ml per gm body weight and did not change significantly during ovarian development. Assuming that Vg in the hemolymph represents either an extraovarian origin of Vt or an active secretion from the ovary, a turnover rate of two to three times per day was calculated over one full cycle of oocyte development. However, during the most significant increase in Vt in the ovary (in ovaries with AOD of 150–250 μm), the turnover rate in the hemolymph could reach seven to eight times per day. The results lead to the conclusion that the contribution of Vg to the formation of the ovary is quantitatively insignificant.

Introduction

Vitellogenesis is associated with several complex processes that lead to the formation of mature oocytes within the ovary. In crustaceans, substantial quantities of yolk accumulate within the developing oocytes, and serve to meet the basic requirements of embryonic and larval development, independent of the maternal organism (Adiyodi and Subramoniam, 1983). One of the major components of yolk is the lipoglycoprotein, vitellin (Vt). In several crustacean species, Vt was found to be synthesized by the ovary (Lui *et al.*, 1974; Lui and O'Connor, 1976, 1977; Dehn *et al.*, 1983; Eastman-Reks and Fingerman, 1985; Yano and Chinzei, 1987; Quackenbush, 1989a, b; Browdy *et al.*, 1990). Yano and Chinzei (1987) suggested that Vt was synthesized in the follicle cells of *Penaeus japonicus*. However, a protein that reacts immunologically to the antiserum prepared against purified Vt was detected in the hemolymph of vitellogenic females. This female-specific protein (FSP), known as vitellogenin (Vg), has been reported in all species studied so far (Kerr, 1969; Ceccaldi, 1970; Fyffe and O'Connor, 1973; Wolin *et al.*, 1973; Caubere *et al.*, 1976; Meusy, 1980; Dehn *et al.*, 1983; Ferrero *et al.*, 1983; Marzari *et al.*, 1986; Susuki, 1987; Tom *et al.*, 1987; Nelson *et al.*, 1988; Quackenbush and Keeley, 1988; Quackenbush, 1989a). Vg is one of the two lipoproteins known in crustacean hemolymph (Lee, 1990). A large increase in the concentration of Vg has been reported in the hemolymph during vitellogenesis. While some reports show that the appearance of Vg in the hemolymph is correlated with morphological changes in the ovaries antecedent to egg release, others show that Vg is at the highest concentrations prior to the maximum accumulation of yolk in the oocyte (Quackenbush, 1989b; Lee, 1990).

Several reports show evidence for extraovarian tissues engaged in Vg synthesis. Vg was reported to be produced

Received 20 December 1991; accepted 26 August 1992.

Abbreviations: AOD—Average oocyte diameter; SAT—Subepidermal adipose tissue; Vg—Vitellogenin; Vt—Vitellin; HEP—Hepatopancreas.

by the subepidermal adipose tissue (SAT) of anostracean (Van Beek *et al.*, 1987), isopod (Picaud, 1980; Souty and Picaud, 1981; Picaud *et al.*, 1989) and amphipod crustaceans (Croisille and Junera, 1980; Junera and Croisille, 1980). Vg was also found in the SAT of decapods (Meusy *et al.*, 1983; Vazquez-Boucard, 1985; Tom *et al.*, 1987). However, it was not identified as being synthesized by *in vitro* incubated SAT of *P. semisulcatus* (Fainzilber, 1988; Fainzilber *et al.*, 1992). Conflicting results were reported for Vg synthesis by the hepatopancreas (HEP) in decapods. Quackenbush and Keeley (1988) and Quackenbush (1989a, b) reported *in vitro* Vg synthesis in *Uca pugilator* and *P. vannamei*, respectively. However, Yano and Chinzei (1987) and Rankin *et al.* (1989) were unable to detect *de novo* Vg synthesis in HEP of *P. japonicus* and *P. vannamei*, respectively. Low levels of a Vt-immunoreactive protein were detected in *in vitro* incubated HEP in females of *P. semisulcatus* (Fainzilber, 1988; Fainzilber *et al.*, 1992). The possible contribution of Vg in the accumulation of Vt in the ovary is further suggested by work describing endocytosis in the ovary (Hinsch and Cone, 1969; Wolin *et al.*, 1973; Duronslet *et al.*, 1975; Zerbib, 1979; Beams and Kessel, 1980; Schade and Shivers, 1980; Zerbib and Mustel, 1984; Jugan and Soyez, 1985). Furthermore, Vg receptors were isolated from the ovarian cytoplasmic membranes of two decapod species (Jugan, 1985; Lavrdure and Soyez, 1988; Jugan and Van Herp, 1989). However, Lui and O'Connor (1976) suggested that Vg originated from resorbed oocytes.

The present investigation aims at elucidating the possible role of Vg and its contribution to oocyte development in *Penaeus semisulcatus*, which is a species of economic importance in Israel. We attempted to examine the hypothesis that Vg in the hemolymph is transported and taken up by the ovary, relying on the suggestion of Byard and Aiken (1984). They reported that the observed levels of FSP in the hemolymph were always higher prior to the maximum accumulation of yolk in the oocytes, and that they dropped off markedly prior to oviposition. The conclusion drawn by Byard and Aiken was that this pattern is consistent with the idea that the FSP represents an externally synthesized protein and is found at the highest level in hemolymph during the period when oocytes are accumulating the maximum amount of yolk. To examine this possibility, the concentration of Vg in the hemolymph, Vt in the ovary, and the volume of the hemolymph were determined during one cycle of ovarian maturation. The results enabled us to calculate the hypothetical turnover rate assuming that the entire Vt within the ovary originated from Vg circulating in the hemolymph.

An approach to vitellogenesis as a flow system, in which Vg is produced by an extraovarian tissue, released into the hemolymph, and subsequently taken up by the developing oocytes, was described in insects (Bakker-Grunwald and Applebaum, 1977). This approach was also attempted in the present paper, in order to reach conclusions on the possible dynamic flow of Vg in the hemolymph.

Materials and Methods

Chemicals

^{3}H Inulin (46/mCi/g) was purchased from New England Nuclear (U.S.A.). All other reagents were of analytical grade and were purchased from Sigma (U.S.A.), Merck (Germany) or Bio-Rad (U.S.A.).

Animals

Adult *P. semisulcatus* were collected in Haifa Bay, Israel. They were held in 3 m^3 running seawater tanks, at a density of 30 specimens per tank. Water was changed at a rate of 300% per day. Salinity was constant at 40‰, and temperature ranged from 18°C (winter) to 27°C (summer). The animals were fed once a day on a mixture of frozen fish, squid, shrimp and *Artemia*. Females were individually marked by clipping of the uropods, and ovarian development was monitored externally, according to the methods of Browdy and Samocha (1985). Moulting of marked females was also recorded by identifying the uropod coded cuts of the shedded exuviae.

Results of hemolymph volume, protein and Vg levels were related to the average oocyte diameter (AOD), measured according to Shlagman *et al.* (1986) in sacrificed animals.

Collection of hemolymph and the determination of its volume

Hemolymph was collected from animals bled after cutting off the anterior part of the cephalothorax near the base of the eyestalks. The hemolymph from each female was collected into a vial containing a known volume of 10% sodium citrate solution.

The hemolymph volume was determined by injecting 2 μCi of ^{3}H-inulin dissolved in 100 μl of sterilized seawater diluted to 30 ppt. Preliminary experimental results showed that the hemolymph radioactivity was stable for 24 h after the injection of the inulin. The hemolymph volume was calculated by measuring the dilution in the radioactivity of samples withdrawn 2 h after the injection of the labeled inulin.

Determination of proteins, Vg, and Vt concentrations

The total protein concentration in the hemolymph and ovaries was determined according to Bradford (1976), using bovine serum albumin as a standard.

The concentrations of Vg in the hemolymph samples and Vt in the ovarian homogenates were determined by

rocket [illegible] trophoresis (Jurd, 1981). The area form[illegible] rocket" precipitation lines was calcu[illegible] Graphplot series digitizer 7000 and com[illegible] concentrations of purified Vt subjected [illegible] rocket" preparation. The purified Vt and [illegible] polyclonal antibody used in these determinations were isolated and prepared as described in Browdy *et al.* (1990).

Experimental procedure

Two series of experiments were carried out. In Experiment 1, hemolymph samples were removed (as described previously) from 77 females that were at various stages of ovarian development, including females immediately after the moult. The hemolymph samples from each female were centrifuged (9000 × *g* at 4°C for 10 min in a Sorvall RC-5C U.S.A.) and the supernatant was stored at −70°C. In parallel, a small piece was removed from the ovaries of each female and fixed in formaldehyde (4% in seawater) for the measurements of AOD (see above). In these females, the protein and Vg concentration in the hemolymph were determined (see above) and related to the AOD.

In Experiment 2, 21 females were chosen individually, after monitoring for several days the moult and ovarian developmental stages. Females following moulting, those showing arrested ovarian development, and those with ovaries in progress of oosorption were rejected. Each female was injected with ^{3}H inulin (as described above). After 2 h, the females were weighed and bled and the hemolymph volume was determined as described above. Ovaries were dissected out and weighed. A small piece was fixed in formaldehyde and used for measurements of AOD. Two other samples (each weighing 0.1–0.2 g) were used for determinations of dry weight. They were placed in pre-weighed vials and dried at 60°C until reaching constant weight (about 48 h). The remaining part of the ovary was homogenized in 10 ml of phosphate buffer (0.1 *M*, pH 7.4) and centrifuged at 4°C and 9000 × *g* for 20 min (Sorvall RC-5C, U.S.A.). The supernatant of the ovarian homogenates and the hemolymph samples were stored at −70°C until they were used in the determinations of total protein, Vt and Vg concentrations.

Results

The co[illegible] of total protein and Vt specific protein (Vg) [illegible] mph was found to increase with the progres[illegible] development, shown by the increase in A[illegible]. The values obtained in Experiment 1 fo[illegible] and Vg of 77 females and 73 females, respe[illegible] pooled and divided into four size groups acco[illegible] their AOD. It can be clearly seen that females with [illegible] 150 μm or larger had similar

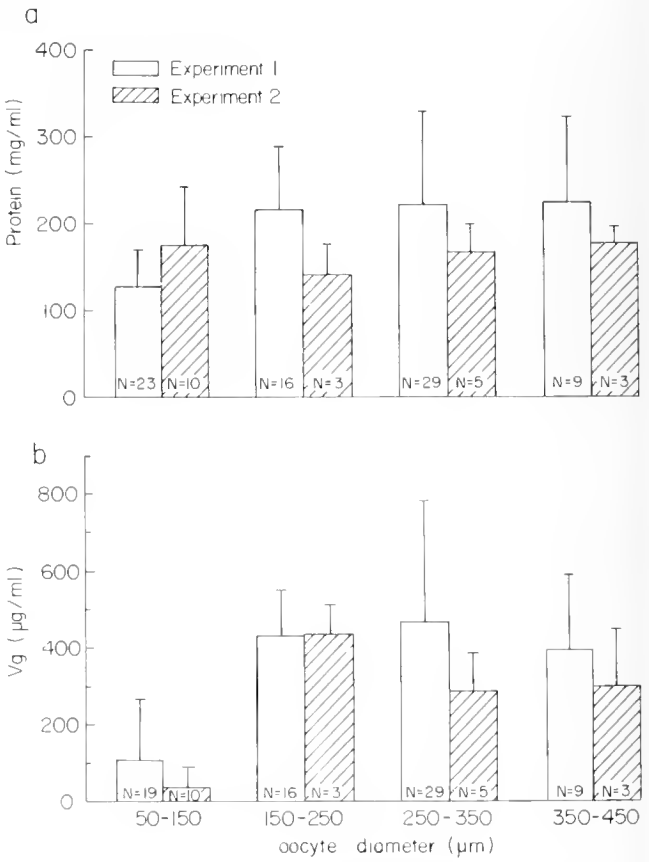

Figure 1. The concentration of (a) protein in mg ml^{-1} and (b) vitellogenin in μg ml^{-1} in the hemolymph (Experiments 1 and 2) related to the average oocyte diameter (AOD). The mean ± S.D. is shown for samples pooled into four size groups of AOD.

levels of total protein and Vg (one way ANOVA, $P > 0.05$). However, females at the initial stage of oocyte development (50–150 μm in AOD) show lower protein levels ($P < 0.001$) and Vg levels ($P < 0.0001$). Four of the examined females which were taken immediately after spawning showed an average of 430.0 ± 43.8 μg ml^{-1} of Vg in their hemolymph, and their results were not included in Fig. 1b. The highest average values of protein (247 ± 139 mg m^{-1}) and Vg (562 ± 410 μg ml^{-1}) were found in females with an AOD ranging between 250 and 300 μm. The lowest average values for protein (116 ± 32 mg ml^{-1}) and Vg (60 ± 95 μg ml^{-1}) were found in females with an AOD of less than 100 μm. The results from the 21 females (Experiment 2) were divided into 4 size groups according to the AOD of the ovaries (Fig. 1a, b). Some of the females included in the size class of 50–150 μm AOD were postmoult. This may have contributed to the large standard deviations in this group, relative to the others. Unlike the results shown earlier for Experiment 1, the total protein concentration in these females did not change with the AOD. However, Vg was virtually not

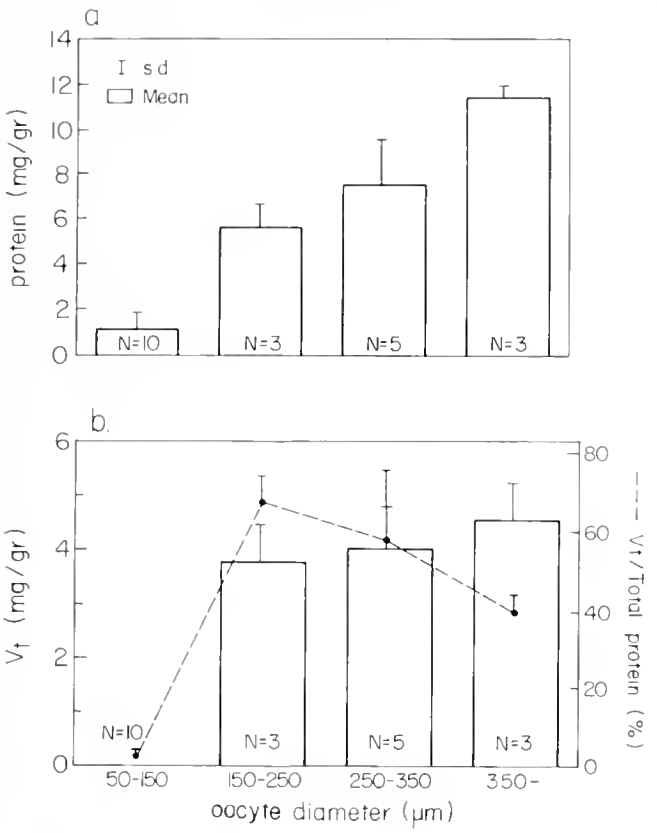

Figure 2. The total amount of protein (a) and vitellin (b) in mg/g fresh weight and the percent of vitellin out of the total amount of protein in ovaries of females at various stages of ovarian development. Results (mean ± S.D.) were pooled into four size groups according to the average oocyte diameter.

present in the hemolymph samples removed from females with an AOD of 50–150 μm.

The mean concentrations of Vg in the hemolymph in the four oocyte size groups of Experiment 1 were not statistically different from those of Experiment 2 (P ranging from 0.2 to 0.9). However, the mean concentration of protein in the hemolymph in females from Experiment 1 with oocytes ranging in size from 50–150 μm was significantly lower ($P < 0.02$) than that of females from the same size group in Experiment 2. These differences may be due to the fact that in Experiment 1 the 50–150 μm size group included post-moult females and post oviposition females, which were eliminated in Experiment 2.

The hemolymph volume did not change in relation to the AOD of the examined females (results not shown) and its average was 0.403 ± 0.114 ml per g body weight.

The total amount of protein in the ovary (in Experiment 2) increased linearly from an average of 1.14 ± 0.7 mg per g body weight to 11.4 ± 0.4 mg per g body weight (Fig. 2a). The amount of Vt in the ovaries increased significantly in ovaries with AOD of 150–250 μm and only slightly in ovaries with larger AOD (Fig. 2b). The Vt concentration in the ovaries was found to average 4.55 ± 0.66 mg per g body weight in ovaries with an AOD of 300 μm or larger. A significant increase in the relative amount of Vt in the total ovarian proteins was found when the AOD increased from 50–150 μm to 150–250 μm, similar to that found in the hemolymph. This ratio decreased significantly towards the end of ovarian development (Fig. 2b). The water content in the ovary was found to decrease linearly during oocyte maturation (Fig. 3), from 83% in immature females to 69.5% in mature ones. This could partially explain the increase in the total amount of protein in the ovaries mentioned earlier (Fig. 2a).

Discussion

The concentration of Vg in the hemolymph of *P. semisulcatus* was found to range from 50 μg ml^{-1} in females with undeveloped ovaries to a high average concentration of 439 μg ml^{-1} in females with oocytes larger than 150 μm AOD. These values constitute only 0.06 ± 0.09% to 0.27 ± 0.15% of the total proteins in the hemolymph of females with undeveloped or developed ovaries, respectively. The relatively large standard deviations probably stem from the attempt to correlate Vg level to the AOD in preset size classes. These values are much lower than those reported for *P. vannamei* (Quackenbush, 1989a), for *P. japonicus* (20 μg μl^{-1} at the maximum stage in vitellogenesis; Yano, 1987), for *Homarus americanus* (1 mg ml^{-1}; Nelson *et al.*, 1988), for *Cancer antennarius* (estimated as 175 mg dl^{-1}; Fig. 1 in Spaziani, 1988), for *Callinectes sapidus* (4.1 mg ml^{-1}; Lee and Puppione, 1988), or for *Macrobrachium rosenbergii* (12 mg ml^{-1}; Derelle *et al.*, 1986). Most of the protein in the hemolymph of several species of crustaceans was found to be associated with hemocyanin (Magnum, 1983; Depledge and Bjerregaard, 1989).

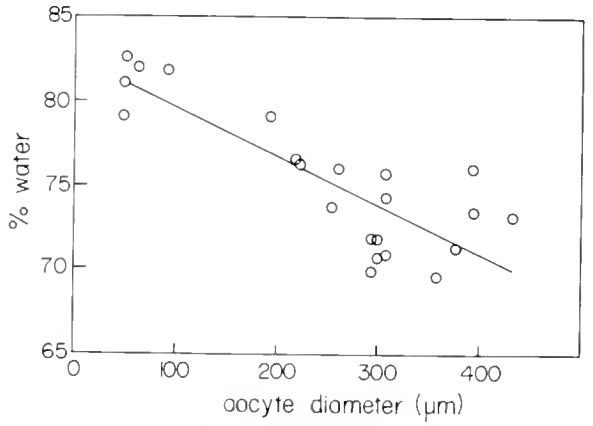

Figure 3. The percent of water in ovaries related to the average oocyte diameter (R2 = 0.814).

Table I

The calculated turnover rate of Vg in the hemolymph at four different stages of ovarian development, using the mean values of the hemolymph volume, Vg concentration, and the amount of Vt in the ovaries, at each stage

Average oocyte diameter (AOD; μm)	n	Hemolymph volume (ml per g body weight)	Vg in hemolymph (μg per g body weight)	Total amount of Vg in ovaries (mg per g body weight)	Increment in the amount of Vt in ovaries (mg per g body weight)	Turnover rate* (per day)	Turnover rate** (per day)
50–150	10	0.5317	1.145	0.0126	0.0126	0.16	0.16
150–250	3	0.4361	8.83	3.76	3.745	7.80	7.78
250–350	5	0.3573	5.63	4.03	0.2726	16.02	1.08
350–450	4	0.4720	7.40	5.11	1.0785	11.69	2.47

* Calculated from the total amount of Vt in ovaries.

** Calculated from the increment in the amount of Vt in ovaries.

The concentration of total protein was found to increase (in Experiment 1) in the hemolymph with the increase in oocyte size, staying at a stable level at later stages of oocyte development. However, no such trend was found in Experiment 2. It is possible that in Experiment 1, the lower concentrations could be attributed to females that were taken immediately after moulting, when their AOD was less than 100 μm. The hemolymph volume was reported to increase prior to moulting, and an inverse linear relationship between hemolymph volume and protein concentration was reported by Smith and Dall (1982).

As mentioned, the concentration of Vg in the hemolymph was found to increase dramatically during the initial stages of oocyte development, when the AOD was 150–250 μm. This increase occurred with a concomitant increase in the absolute and relative amount of Vt in the ovaries. A similar relationship between the increase of Vg in the hemolymph and oocyte development was reported by Lee and Puppione (1988) for *Callinectes sapidus*. However, in *Homarus americanus*, the increased Vg levels in the hemolymph preceded ovarian development (Byard and Aiken, 1984). In ovaries with AOD of 150–250 μm, the Vt constituted 67.7 ± 6.4% of the total proteins. This was reduced to an average of 39.7 ± 4.5%, suggesting that, in addition to Vt, other proteins (*e.g.*, the cortical crypts protein, see below) were synthesized in the ovary towards the end of ovarian maturation. In *P. vannamei*, Vt was found to constitute 5.3–20.9% of the total protein in spawns of fertile eggs (Quackenbush, 1989b).

The presence and synthesis of a cortical crypts protein was reported by Bradfield *et al.* (1989) to take place mainly at the period immediately before spawning in *P. vannamei*. Ovaries that were incubated *in vitro* were also found to synthesize 40–60% of the total proteins. Furthermore, the proportion of Vt was reduced in ovaries with AOD of 350 μm and larger (Browdy *et al.*, 1990). The increase in the total amount of protein deposited in the ovaries was inversely related to their water content, which was reduced from about 83% to 69.5% in the fully mature ovaries.

A flow system demonstrating the Vg flow in hemolymph towards the ovary in vitellogenic females was demonstrated in insects (Bakker-Grunwald and Applebaum, 1977). This model was based on the following data: (a) concentration of Vg and Vt in the hemolymph and ovary, respectively; (b) the rate of incorporation of injected labeled amino acid into Vg; and (c) the rate of incorporation of Vg by the ovary. In this paper, we present results in *P. semisulcatus* that are comparable to (a) above.

In crustaceans, the origin of Vg in the hemolymph is still problematic. In the case that Vg originates from extraovarian tissue, it could be assumed to be directed towards the ovary, where it is taken up and constitutes at least part of the Vt. This is the case in some crustacean species and in most insects which are also arthropods (Kanost *et al.*, 1990). However, several reports show that Vt is synthesized in the ovary (see references in the Introduction). In this case, Vg originates either by controlled secretion from the ovary (Yano and Chinzei, 1987), or by passive leakage from oocytes in the process of resorption. If Vg is actively secreted from the ovary, it could have a role in the transport of nutrients (*e.g.*, lipids) into the ovary from extraovarian tissues (*e.g.*, HEP). The data presented in the present paper allow us to consider the flow dynamics of such systems. From the total hemolymph volume, and the Vg and Vt concentrations in the hemolymph and ovaries, respectively, it is possible to calculate the hypothetical turnover rate of Vg in the hemolymph. This is presented in Table I. If it is assumed that the entire amount of Vt present in the ovaries is transported via the hemolymph as Vg, the calculated turnover rate is 2.5 times per day over one full cycle. In carrying out this calculation, it is assumed that one full cycle of oocyte development is linear and takes 10 days

(Browdy, 1988). However, if the full cycle is divided into four stages, the turnover rate must reach 7.78 per day, to account for the Vt accumulated in oocytes of 150–250 μm. The accumulation rate is reduced at later stages (Table I), to account for the increment in the amount of Vt accumulated in the ovaries.

The results presented here, on the increase in Vg concentration concomitant with the increase in the amount of Vt in the ovary, and those of Fainzilber *et al.* (1992) show that if there is an extraovarian source for Vt in *P. semisulcatus*, its contribution to Vt is quantitatively very low.

Acknowledgments

This research was supported by grants from the Israeli Ministry of Infrastructure and the Binational Agricultural Research and Development Fund (Project No. I-1435-88). Mr. S. Shafir was the recipient of a scholarship from the Baur Foundation.

Literature Cited

Adiyodi, K. G., and T. Subramoniam. 1983. Oogenesis, Oviposition and Oosorption, Arthropoda-Crustacea. Pp. 443–495 in *Reproductive Biology of Invertebrates. Vol. I*, K. G. Adiyodi, and R. G. Adiyodi, eds. Wiley, New York.

Bakker-Grunwald, T., and S. W. Applebaum. 1977. A quantitative description of vitellogenesis in *Locusta migratoria migratorioides*. *J. Insect Physiol.* **23**: 259–263.

Beams, H. W., and R. G. Kessel. 1980. Ultrastructure and vitellogenesis in the oocyte of the crustacean, *Oniscus asellus*. *J. Submicrosc. Cytol.* **12**(1): 17–28.

Bradfield, J. Y., R. L. Berlin, S. M. Rankin, and L. L. Keeley. 1989. Cloned cDNA and antibody for an ovarian cortical granule polypeptide of the shrimp *Penaeus vannamei*. *Biol. Bull.* **177**: 344–349.

Bradford, M. M. 1976. A rapid and sensitive method for the quantitation of microgram quantities of protein utilizing the principle of protein dye binding. *Anal. Biochem.* **72**: 248–254.

Browdy, C. L. 1988. Aspects of the reproductive biology of *Penaeus semisulcatus* de Haan (Crustacea; Decapoda; Penaeidae). Ph.D. Thesis, Tel-Aviv University.

Browdy, C. L., and T. M. Samocha. 1985. The effect of eyestalk ablation on spawning, molting and mating of *Penaeus semisulcatus* de Haan. *Aquaculture* **49**: 19–29.

Browdy, C. L., M. Fainzilber, M. Tom, Y. Loya, and E. Lubzens. 1990. Vitellin synthesis in relation to oogenesis in *in vitro* incubated ovaries of *Penaeus semisulcatus* (Crustacea, Decapoda, Penaeidae). *J. Exp. Zool.* **255**: 205–215.

Byard, E. H., and D. E. Aiken. 1984. The relationship between molting, reproduction and a hemolymph female specific protein in the lobster *Homarus americanus*. *Comp. Biochem. Physiol.* **77A**(4): 749–758.

Caubere, J. J., R. Lafon, F. Rene, and C. Sales. 1976. Maturation et ponte chez *Penaeus japonicus* en captivate esai de controle de cette reproduction a maguelone sur les cotes francaises. FAO Tech. Conf. on Aquacult., Kyoto, Japan. FIR:AQ/Conf./76/E.49.18 pp.

Ceccaldi, H. J. 1970. Evolution des proteines de l'hemolymphe de *Penaeus kerathurus* femelle durant la vitellogenese. *C. R. Sean. Soc. Biol.* **164**(12): 2572. (Abstract)

Croisille, Y., and H. Junera. 1980. Site of vitellogenin synthesis in *O. gammarella* (Crustacea, Amphipoda). Immunohistological demonstration of appreciable amounts of vitellogenin in the subepidermal adipose tissue of females in which secondary vitellogenesis is taking place. *C. R. Hebd. Seances Acad. Sci. Ser. D* **290**(23): 1489–1490.

Dehn, P. F., P. E. Aiken, and S. L. Waddy. 1983. Aspects of vitellogenesis in the lobster *Homarus americanus*. *Can. Tech. Rep. Fish. Aquat. Sci.* **1161**: iv + 24 pp.

Depledge, M. H., and P. Bjeregaard. 1989. Haemolymph protein composition and copper levels in decapod crustaceans. *Helgolander Meeresunters* **43**: 207–223.

Derelle, E., J. Grosclaude, J. J. Meusy, H. Junera, and M. Martin. 1986. ELISA titration of vitellogenin and vitellin in the freshwater prawn *Macrobrachium rosenbergii* with monoclonal antibody. *Comp. Biochem. Physiol.* **85B**(1): 1–4.

Duronslet, M. J., I. A. Yudin, R. S. Wheeler, and W. H. Clark Jr. 1975. Light and fine structural studies of natural and artificially induced egg growth of penaeid shrimp. *Proc. World Maricult. Soc.* **6**: 105–122.

Eastman-Reks, S. B., and M. Fingerman. 1985. *In vitro* synthesis of vitellin by the ovary of the fiddler crab *Uca pugilator*. *J. Exp. Zool.* **233**(1): 111–116.

Fainzilber, M. 1988. Vitellogenesis in the marine shrimp *Penaeus semisulcatus* de Haan. M.S. Thesis, Hebrew University, Jerusalem.

Fainzilber, M., M. Tom, S. Shafir, S. W. Applebaum, and E. Lubzens. 1992. Is there extraovarian synthesis of vitellogenin in penaeid shrimp? *Biol. Bull.* **183**: 233–241.

Ferrero, E. A., G. Graziosi, R. Marzari, and A. Mosco. 1983. Protein pattern variability of the hemolymph of mantis shrimp *Squilla mantis* L. (Crustacea, Stomatopoda). *J. Exp. Zool.* **225**: 341–345.

Fyffe, W. E., and J. D. O'Connor. 1973. Characterization and quantification of a crustacean lipovitellin. *Comp. Biochem. Physiol.* **47B**: 851–867.

Hinsch, G. W., and M. V. Cone. 1969. Ultrastructural observations of vitellogenesis in the spider crab *Libinia emarginata* L. *J. Cell Biol.* **40**: 336–342.

Jugan, P. 1985. Regulation de la croissance ovocytaire chez la crustace *Macrobrachium rosenbergii* (De Man). Demonstration d'une endocytose par recepteurs et approche du mode d'action de la neurohormone inhibitrice de la vitellogenese. Ph.D. Thesis. P. and M. Curie University, Paris.

Jugan, P., and D. Soyez. 1985. *In vitro* inhibitory effect of a sinus gland extract on oocyte endocytosis in the prawn *Macrobrachium rosenbergii*. *C. R. Acad. Sc. Paris 300 Ser. III* **(20)**: 705–709.

Jugan, P., and F. Van Herp. 1989. Introductory study of an oocyte membrane protein that specifically binds vitellogenin in the crayfish *Orconetes limosus*. *Invert. Reprod. Dev.* **16**(1–3): 149–154.

Junera, H., and Y. Croisille. 1980. Recherche du lieu de synthese de la vitellogenine chez le crustace amphipode *Orchestia gammarella* (Pallas). Mise en evidence d'une activation de la synthese proteique dans le tissu adipeus sous-epidermique en liaison avec la production de vitellogenine. *C. R. Acad. Sc. Paris* **290**: 703–706.

Jurd, D. R. 1981. Immunoelectrophoresis. Pp. 229–248 in *Gel Electrophoresis of Proteins—A Practical Approach*, B. D. Hames, and D. Rickwood, eds. IRL Press, Oxford.

Kanost, M. R., J. K. Kawooya, J. H. Law, R. O. Ryan, M. C. Van Heusden, and R. Ziegler. 1990. Insect hemolymph proteins. Pp. 299–396 in *Advances in Insect Physiology. Vol. 22*, P. D. Evans, and V. B. Wigglesworth, eds. Academic Press, London.

Kerr, M. S. 1969. The hemolymph proteins of the blue crab, *Callinectes sapidus* II. A lipoprotein serologically identical to oocyte lipovitellin. *Dev. Biol.* **20**: 1–17.

Laverdure, A. M., and D. Soyez. 1988. Vitellogenin receptors from lobster oocyte membrane, solubilization and characterization by a

solid phase binding assay. *J. Invert. Reprod. Dev.* **13**(3): 251–266.

Lee, R. F. 1990. Lipoproteins from the hemolymph and ovaries of marine invertebrates. *Comp. Environ. Physiol.* **7:** 187–207.

Lee, R. F., and D. L. Puppione. 1988. Lipoproteins I and II from the hemolymph of the blue crab *Callinectes sapidus*, lipoprotein II associated with vitellogenesis. *J. Exp. Zool.* **248**(3): 278–289.

Lui, C. W., and J. D. O'Connor. 1976. Biosynthesis of lipovitellin by the crustacean ovary. II. Characterization and *in vitro* incorporation of amino acids into the purified subunits. *J. Exp. Zool.* **195:** 41–52.

Lui, C. W., and J. D. O'Connor. 1977. Biosynthesis of crustacean lipovitellin. III. The incorporation of labeled amino acids into the purified lipovitellin of the crab *Pachygrapsus crassipes*. *J. Exp. Zool.* **199:** 105–108.

Lui, C. W., B. A. Sage, and J. D. O'Connor. 1974. Biosynthesis of lipovitellin by the crustacean ovary. *J. Exp. Zool.* **188**(3): 289–296.

Magnum, C. P. 1983. Oxygen transport in the blood. Pp. 382–428 in *Biology of Crustacea. Vol. 5*, D. E. Bliss, ed. Academic Press, New York.

Marzari, R., E. Ferrero, A. Mosco, and A. Savoini. 1986. Immunological characterization of the vitellogenic proteins in *Squilla mantis* hemolymph (Crustacea Stomatopoda) *Exp. Biol. (Berl.)* **45**(2): 75–80.

Meusy, J. J. 1980. Vitellogenin, the extraovarian precursor of the protein yolk in Crustacea: a review. *Reprod. Nutr. Dev.* **20**(1A): 1–21.

Meusy, J. J., H. Junera, P. Cledon, and M. Martin. 1983. Vitellogenin in a decapod crustacean *Palaemon serratus*, identification, immunological similarity to vitellin synthesis and role of the eyestalks. *Reprod. Nutr. Dev.* **23**(3): 625–640.

Nelson, K., B. Heyer, E. Johnson, D. Hedgecock, and E. S. Chang. 1988. Photoperiod-induced changes in hemolymph vitellogenins in female lobsters (*Homarus americanus*). *Comp. Biochem. Physiol.* **90B**: 809–821.

Picaud, J. L. 1980. Vitellogenin synthesis by the fat body of *Porcellio dilatatus* Brandt (Crustacea, Isopoda). *Int. J. Invert. Reprod* **2:** 341–349.

Picaud, J. L., Souty-Grosset, C., and G. Martin. 1989. Vitellogenesis in terrestrial isopods: Female specific proteins and their control. *Monitore Zool. Ital. (N.S.) Monogr.* **4:** 305–331.

Quackenbush, S. L. 1989a. Vitellogenesis in the shrimp *Penaeus vannamei*: *in vitro* studies of the isolated hepatopancreas and ovary. *Comp. Biochem. Physiol.* **94B**(2): 253–261.

Quackenbush, S. L. 1989b. Yolk protein production in the marine shrimp *Penaeus vannamei*. *J. Crust. Biol.* **9**(4): 509–516.

Quackenbush, S. L., and L. L. Keeley. 1988. Regulation of vitellogenesis in the fiddler crab *Uca pugilator*. *Biol. Bull.* **175:** 321–331.

Rankin, S. M., J. Y. Bradfield, and L. L. Keeley. 1989. Ovarian protein synthesis in the South American white shrimp *Penaeus vannamei*, during the reproductive cycle. *Invert. Reprod. Dev.* **15:** 27–33.

Schade, M. L., and R. R. Shivers. 1980. Structural modulation of the surface and cytoplasm of oocytes during vitellogenesis in the lobster *Homarus americanus*. An electron microscope protein tracer study. *J. Morph.* **163:** 13–26.

Shlagman, A., C. Lewinsohn, and M. Tom. 1986. Aspects of the reproductive activity of *Penaeus semisulcatus* de Haan along the southeastern coast of the Mediterranean. *P.S.Z.N.I. Mar. Ecol.* **7:** 15–22.

Smith, D. M., and W. Dall. 1982. Blood protein, blood volume and extracellular space relationships in two *Penaeus* spp. (Decapoda, Crustacea). *J. Exp. Mar. Biol. Ecol* **63:** 1–15.

Souty, C., and J. L. Picaud. 1981. Vitellogenin synthesis in the fat body of the marine crustacean Isopoda *Idotea balthica basteri* during vitellogenesis. *Reprod. Nutr. Dev.* **21**(1): 95–102.

Spaziani, E. 1988. Serum high-density lipoprotein in the crab, *Cancer antennarius* Stimpson. II. Annual cycles. *J. Exp. Zool.* **246:** 315–318.

Susuki, S. 1987. Vitellin and vitellogenin of the isopod *Armadillidium vulgare*. *Zool. Sci.* 3(6): 1013.

Tom, M., M. Goren, and M. Ovadia. 1987. Localization of the vitellin and its possible precursors in various organs of *Parapenaeus longirostris* (Crustacea, Decapoda, Penaeidae). *Int. J. Invert. Reprod. Dev.* **12:** 1–12.

Van Beek, E., M. Van Brussel, G. Crel, and A. De Loof. 1987. A possible extraovarian site for synthesis of lipovitellin during vitellogenesis in *Artemia sp.* (Crustacea: Anostraca). *Int. J. Invert. Reprod. Dev.* **12:** 227–240.

Vazquez-Boucard, C. 1985. Identification preliminaire du tissu adipeux chez le crustace decapode *Penaeus japonicus* Bate a l'aide d'antilipovitelline. *C. R. Acad. Sc. Paris* **300**(3): 95–97.

Wolin, E. M., H. Laufer, and D. F. Albertini. 1973. Uptake of the yolk protein, lipovitellin, by developing crustacean oocytes. *Dev. Biol.* **35:** 160–170.

Yano, I. 1987. Effect of 17α-hydroxy-progesterone on vitellogenin secretion in Kuruma prawn, *Penaeus japonicus*. *Aquaculture* **61:** 49–57.

Yano, I., and Y. Chinzei. 1987. Ovary is the site of vitellogenin synthesis in kuruma prawn, *Penaeus japonicus*. *Comp. Biochem. Physiol.* **86B**(2): 213–218.

Zerbib, C. 1979. Ultrastructural study of the oocyte during vitellogenesis in the crabs *Astacus astacus* and *A. leptodactylus*. *Int. J. Invert. Reprod* **1**(5): 289–296.

Zerbib, C., and J. J. Mustel. 1984. Incorporation of tritiated vitellogenin into the oocytes of the crustacean amphipod *Orchestia gammarellus*. *Int. J. Invert. Reprod. Dev.* **7**(1): 63–68.

Reference: *Biol. Bull.* **183:** 401–408. (December, 1992)

Control of Hatching in an Estuarine Terrestrial Crab I. Hatching of Embryos Detached From the Female and Emergence of Mature Larvae

MASAYUKI SAIGUSA

College of Liberal Arts & Sciences, Okayama University, Tsushima 2-1-1, Okayama 700, Japan

Abstract. Embryos of the terrestrial crab *Sesarma haematocheir* hatch simultaneously just prior to their release into water. Larval hatching occurs synchronously when the embryos are attached to a female, and the role of the female in this synchrony has been investigated. Clusters of embryos (200–2000 berries in each cluster) were detached from ovigerous females, and their hatching was compared with that of embryos attached to the females. Of the detached embryos in a cluster, either all hatched, or none hatched. A remarkable feature was that the success of hatching of these detached eggs depended upon the time of hatching of the eggs still attached to the female. Clusters of embryos that were detached from the female within 48–49.5 h of the projected time of larval release all hatched successfully, and swimming zoeas appeared. But embryos that had been detached from the female for longer periods did not hatch at all, though they were obviously alive. These results suggest a hatching process different from the embryonic development process. The female may trigger this process. In addition, detached eggs hatched later than eggs attached to the female, and their hatching was less synchronized. These observations suggest that the female not only initiates hatching, but also enhances the synchrony of hatching.

Introduction

Studies over the past 50 years have demonstrated that many biological rhythms are driven by an endogenous pacemaker which, when coupled to an environmental cycle, adjusts the phase of the rhythm to local time. In contrast to the abundance of information about the timing systems in terrestrial animals, our knowledge of the mechanisms and ecological significance of such systems in marine organisms is severely limited. The reasons are evident: relatively inaccessible habitats, technical difficulties in monitoring the activity, and the noise that is often observed in locomotor activity patterns. Notwithstanding these restrictions, clearly-demarcated biological rhythms associated with reproductive activity have been demonstrated in a variety of marine animals; *e.g.*, a polychaete (Franke, 1985), intertidal midges (Koskinen, 1968; Hashimoto, 1976), and estuarine crabs (DeCoursey, 1979, 1983; De Vries and Forward, 1989). This paper also concerns a rhythmical reproductive activity, focussing on the control of larval hatching in a marine crustacean.

Fertilized eggs of most marine crustaceans are attached by a funiculus to the abdominal appendages of the female, and are ventilated by the female during embryonic development. When the development is complete, the outer egg membrane breaks, and the larvae hatch. These larvae are released into water with a special fanning behavior of the female's abdomen. Larval release is generally a short-lived event, and the timing is often correlated with such environmental periodicities as day-night, tidal, or lunar cycles. In lobsters (Ennis, 1973; Branford, 1978; Moller and Branford, 1979), for example, larvae hatch at the same time each night. The fiddler crab *Uca* also releases larvae for several minutes, in synchrony with nocturnal high water (DeCoursey, 1979, 1983). Such a short and precisely timed event implies that the timing of larval emergence from the egg capsule must be synchronized within each batch of embryos. Accordingly, we must ask whether the timing of hatching is controlled by the embryo itself, or by the female.

Previous studies of this problem have produced conflicting results. For the lobster *Homarus gammarus*, some investigators indicated that an endogenous factor in the

Received 2 May 1991; accepted 26 August 1992.

embryo itself sets the hatching time (Pandian, 1970; Ennis, 1973). Forward and Lee Chiasson (1983) showed that embryos control the timing of hatching, and suggested that the role of the female is to synchronize the development of the embryos. On the other hand, Branford (1978) showed that the female lobster controls the timing of hatching. This study is also aimed at this general problem, and the focus is on the distinction between the control of the hatching process and the control of embryonic development.

Females of the crab *Sesarma haematocheir* were used in these experiments. Each female incubates 20,000–60,000 eggs on her abdomen. While incubating, the females remain hidden under litter on the slopes of steep, wooded hills overlooking small estuaries. After the embryos have developed for a month, the female emerges, descends to the riverside, and releases her zoea larvae into the water. Larval release occurs at night. Release is synchronized with the time of high water (Saigusa, 1982, 1985), and the timing is endogenously controlled (Saigusa, 1986). Field observations (Saigusa, 1992) demonstrated that larval hatching occurs on the bank, just before the larval release, and not in the water.

Thus, release behavior is caused by the stimulus of hatching; *i.e.*, what is actually controlled is the timing of larval hatching from each egg, not the release behavior itself. Hence, the main questions to be answered are: (1) how do the larvae hatch simultaneously; (2) how is the timing synchronized to the time of high tide at night; and (3) does the female, or do the embryos, control the timing of hatching? To answer all of these questions, many experiments will be necessary. But as a first step, the hatching time and hatching synchrony of detached embryos were compared with those of embryos attached to the female.

Materials and Methods

Female *Sesarma haematocheir* bearing eggs that appeared likely to hatch within 1–10 days (see Saigusa, 1988 for signs) were collected from the field at Kasaoka, Okayama Prefecture (Saigusa, 1982), and brought into the laboratory. The dates of collection were: 23 and 27 September 1988; 18 and 29 July 1989, 6, 14, and 28 August 1989; 3 [illegible]00; and 5 September 1990. The females were maintained in experimental rooms where light and temperature were controlled. A 15 h light:9 h dark photoperiod, similar to that in the field, was employed (light-on at 5:00; light-off at 20:00). Temperature was maintained constant at 25°C. Groups of 1–5 females were selected and placed in four experimental rooms under the same conditions of light and temperature. Embryos were then detached from these females. Hatching of the larvae from these eggs, the swimming ability of the larvae, and the timing of these events were compared with embryos still attached to the female. (The terms 'egg' and 'embryo' are used synonymously in this paper. The embryo is considered as such until it hatches; it is then called a zoea larva.)

Detached eggs were prepared as follows. A cluster of embryos (200–2000 berries) was removed from the female together with a portion of the ovigerous hairs. This cluster was then suspended—by cotton thread tied to a horizontal nylon thread—in the center of a small plastic container (usually with a diameter of 8 cm and a depth of 6 cm). This container was then placed into a 1 l glass beaker containing about 600 ml of diluted, clean seawater. (The seawater was sterilized by boiling, and diluted with distilled water to a salinity of 10‰). The water was strongly aerated with an air stone placed in the bottom of the container (for a figure, see Saigusa, 1992).

The embryo cluster was detached from the female at various times of day for experimental purposes (*e.g.*, Fig. 2). In the 1988 experiments, detachment from, and binding to the nylon thread were carried out with a small hand-held flashlight during the dark period. The intensity of the light was very much reduced. The procedure was difficult with a hand-held light, so a head-attached light covered with a few sheet of red cellophane was used in the experiments of 1989 and 1990. To reduce the influence of light as much as possible, the manipulation of each sample was completed rapidly, *i.e.*, within 5 min. Thus, each female experienced the light at different times, and only briefly (Fig. 2c). Almost all of the crabs released their zoeas within 4-5 days after having been placed in the experimental rooms. Therefore, such a weak and brief light is not likely to have affected the timing of hatching, either of the isolated embryos, or of the embryos attached to the females.

Detached eggs that did not hatch were placed in a beaker for 7–10 days, and if vigorous aeration and turbulence were provided, these isolated embryos remained alive. Detached eggs hatched on the same night as those still attached to the female, and all of the larvae emerged from their egg cases on a single night, or by noon of the following day, at the latest. After the larvae escaped into the water, the empty egg cases still remained attached to the ovigerous hairs. Therefore, I easily determined whether hatching had occurred and what proportion of the swimming larvae had emerged. This examination was mostly carried out during the light period, and a stereo-microscope was used as required.

In some of the experiments, the hatch time of detached eggs was monitored. At intervals of 30 min or 1 h, the plastic container in which an egg cluster was being maintained was transferred to another beaker with a similar quantity of diluted (10‰) seawater. The original beaker was then removed from the experimental room, and the number of swimming zoeas was counted with the help of

a pipette. This exchange of beakers was made during the dark phase under the illumination of a hand-held flashlight covered with red cellophane.

Each female from which some embryos had been detached was also monitored, and the time of larval release recorded. The recording system consisted of a sensor unit (infrared source-receiver) and a controller unit with a photoelectric switch. The sensor unit was placed in the experimental room, and the controller unit was set outside the room. The larval release could thus be monitored without a change in ambient light. The female was confined in a perforated plastic cage suspended from the rim of a 1 or 2 l glass beaker containing diluted, clean seawater (500 or 750 ml; salinity at about 10‰). Only the bottom of the beaker was immersed in the water. When the larvae were released, they fell through the perforations and into the beaker, where they triggered the photoelectric switch. The output of this system was monitored by an event recorder (Saigusa, 1986). Females release their larvae as soon as hatching is completed, so the time of release clearly marks the completion of hatching.

The time of day that each female released her attached larvae was compared with the time of hatching from the eggs that had been detached from her. However, the day during which a female released her larvae could not be precisely estimated. The signs of hatching only appear on the day of larval release (*i.e.*, a few zoeas begin to swim in the glass beaker only a few hours before larval release). Many of the data were like those set out in the upper two sections of Table 1. Hence, many comparisons of detached and attached embryos were necessary; *i.e.*, 250 samples from 110 females were examined.

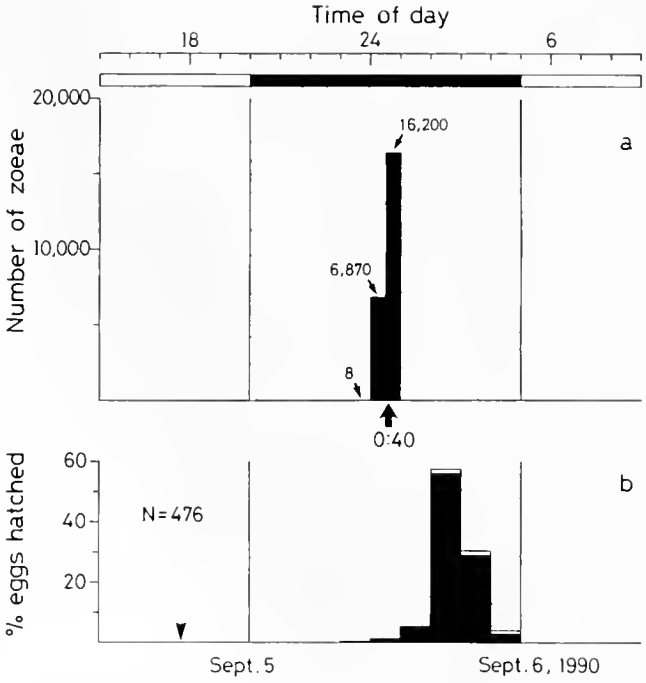

Figure 1. Comparison of the hatching of embryos attached to a female with the hatching of embryos separated from that female. (a): hatching profile of the female-attached eggs. The container holding the ovigerous female was placed in a new beaker every 30 min, and the number of zoeas that had escaped from the female was counted (number and time indicated by small arrows). The female exhibited release behavior at 0:40 on 6 September 1990, when all of the hatched larvae were liberated into the water (upward arrow). Some of eggs that hatched remained at prezoeal stage, and sank to the bottom of the beaker. Only the swimming zoeas were counted. (b): distribution of hatching in the separated eggs. Detachment occurred at 17:45 on 5 September. Hatching was monitored every hour. (Open square indicates the number of prezoeas submerged at the bottom of the beaker). N: total number of emerged larvae. Dotted area shows the dark period. Only these experiments were carried out at 25 ± 1°C.

Results

Figure 1a indicates the hatching profile of the eggs attached to a female. The female moved about in the perforated cage, and her body was frequently soaked in water in the glass beaker. On 5 September, as the time of larval release approached, several hatched larvae escaped from the female's abdomen, and were observed swimming in the beaker (23:30–24:00; Fig. 1a). Shortly after a rapid increase in the number of swimming zoeas in the beaker, the female vigorously vibrated her body to release all of the remaining larvae into the water; this triggered the photoelectric switch (0:40 on 6 September). These observations indicate that almost all of the eggs attached to the female hatch within an extremely brief period. The exact time required for the completion of hatching could not be determined because the eggs are attached in a mass, but it was not more than 1 h in this female.

Embryos separated from females before larval release all hatched on the same night as those attached to the female (Fig. 1b). A feature of such instances was that the hatching of detached embryos was not as simultaneous as that of attached embryos; *i.e.*, detached embryos started hatching shortly before the time of larval release by the female and continued for over 7 h. In the experiment shown in Figure 2, eggs were detached from the female at different times on the day of larval release, and the times of hatching were compared. These embryos all hatched, but as in the study illustrated in Figure 1b, hatching extended for 5–6 h. Figure 2c gave no evidence that the red light, on for 5 min, affected the time of hatching of the detached eggs. The time of hatching of eggs detached on the day of larval release (Fig. 3a) were compared with the time of hatching of eggs separated one day before that release (Fig. 3b). The eggs all hatched on the same night as the larval release in this case, too. And as in Figures 1b and 2, the simultaneity of hatching deteriorated. Thus, the eggs detached from the female on the

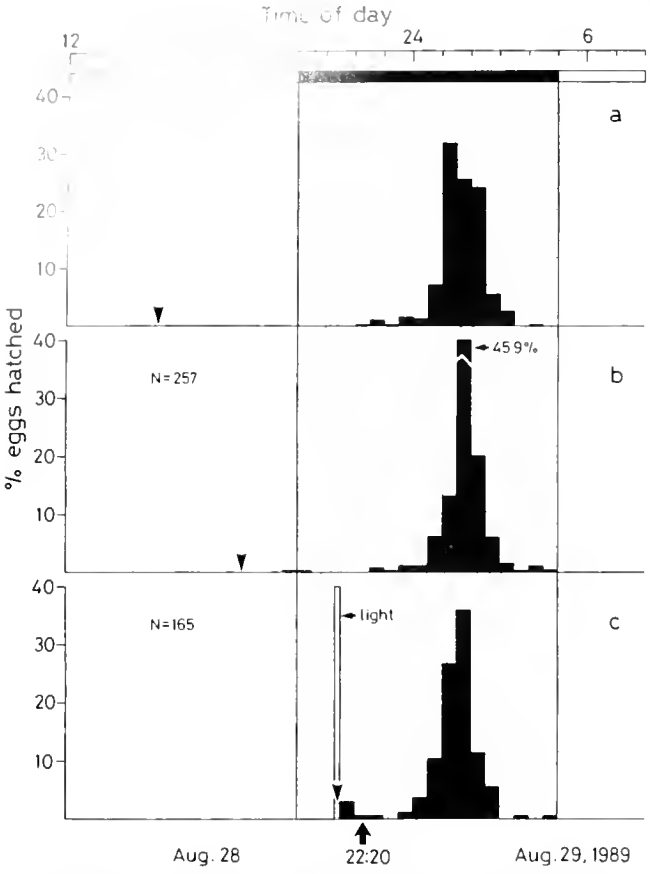

Figure 2. Comparison of the hatching from the eggs detached from a single female at different times on the day of larval release. Times of removal (downward arrows): (a) 15:12; (b) 18:06; (c) 21:25 on 28 August 1989. In figure 2c a red light was used for 5 min to remove the egg cluster. Larval release of the female: 22:20 on 28 August 1989 (upward arrow). N: total number of larvae emerged.

day of larval release and one day earlier all hatch regardless of light conditions.

In contrast to these results, most embryos detached more than 2 days before larval release did not hatch. When such detached embryos were placed in a beaker for a week or longer, hatching occurred sporadically. Those larvae that did [illegible] had poorly developed telsons, dorsal spines, and [illegible]inal appendages. Thus, they were premature la[illegible]rezoeas), and they almost never developed int[illegible]e prezoeas sank to the bottom of the beaker.

Embryos enc[illegible] membrane remained alive, if they were aerate[illegible] beat was clearly recognizable under the mic[illegible] and movements of the embryos were often observed through the transparent egg capsule. These movements are a common feature of embryos attached to the female. Fungi and protozoans were never observed to overgrow the surface of eggs. Nevertheless, the local environment of a detached egg cluster may differ from that of an attached cluster and may be less suitable for development. In that case, the induction of hatching and the appearance of swimming larvae should be dependent on the interval between detachment and natural (female-attached) hatching. If this possibility is accepted, then the hatching rate of the isolated eggs should gradually decrease as the time of separation from the female increases.

As a test of this hypothesis, embryos were detached at various times of day before the larval release by the female, and the hatching success rate was recorded. For this purpose, many ovigerous females that were expected to release larvae within a few days were collected from the field and brought to the laboratory. They were set individually in the apparatus used to record larval release. Eggs were detached from these females several times per day, and the success of their hatching was monitored. Table I summarizes the results from three specimens that released their larvae on 16, 20, and 18 August, respectively. Eggs separated from female B–5 all hatched on the same night as the larval release by the female, but the embryos detached from another female, A–15, all failed to hatch. Finally, of the embryos from female C–14, most failed, but the embryos contained in the last cluster of eggs to be detached did hatch. The time of each trial, from detachment of the eggs to the larval release by the mother female, is listed in Table I.

Experiments similar to those presented in Table I were carried out with 250 samples from a total of 110 females. These experiments demonstrate that induction of hatching

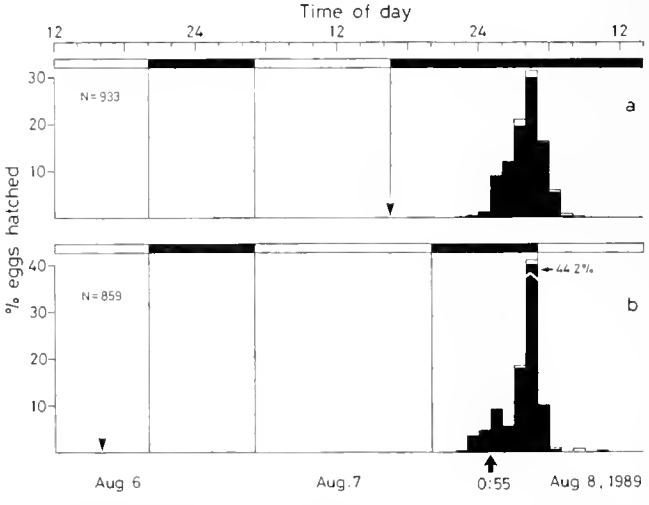

Figure 3. Comparison of the hatching from eggs detached from a single female on the day of larval release (a) with the hatching from eggs detached one day before the larval release (b). Times of removal (downward arrows): (a) 16:20 on 7 August 1989 (hatching was monitored in dark conditions after detachment); (b) around 16:00 on 6 August 1989. N: total number of larvae emerged. Larval release of this female: 0:55 on 8 August 1989 (upward arrow).

Table I

Hatching profiles of detached embryos and larval release by the female

Female identification number	Time of day of detachment	Larval release by the female
B–5	14 Aug. 21:07 (○), 23:06 (○) [27:13] [25:14] 15 Aug. 21:27 (○) [02:53]	16 Aug. 00:20
A–15	15 Aug. 22:17 (×) [99:23] 16 Aug. 02:01 (×), 23:00 (×) [95:39] [74:40] 17 Aug. 01:38 (×), 03:09 (×) [72:02] [70:31]	20 Aug. 01:40
C–14	14 Aug. 20:17 (×), 22:56 (×) [76:43] [74:04] 15 Aug. 21:10 (×) [51:50] 16 Aug. 00:17 (×), 02:35 (○) [48:43] [46:25]	18 Aug. 01:00

○: A cluster of eggs from which all larvae hatched.

×: A cluster of embryos which did not hatch. Hatching time of the embryos attached to the female is expressed as the time of larval release by that female. The female identification number is that of the appartus in which larval release was monitored.

depends upon the time of larval release by the female, not on the time of egg detachment (Fig. 4 top panel). Those embryos that had been separated from the female for more than about 48 h prior to the larval release exhibited neither hatching nor swimming zoeas. Closer examination of the data presented in Figure 4 (top panel) shows that the drastic change in hatching success occurred within a critical interval: 48–49.5 h (the shadowed interval in Fig. 4 bottom panel).

A question that still remains is whether clusters of embryos detached successively from a single female would hatch or not depending on the time of larval release. To answer this question, I examined the hatchability of embryos obtained from at least two egg clusters that were taken from a single female within several hours before or after the 48 h interval leading up to larval release. The resulting data (similar to those for female C–14 in Table I) were selected from among the values in Figure 3b. All 14 instances showed the same tendency (Table II). A comparison of the time at which each embryo cluster was detached from a female, with the time of larval release by that female, led to the hypothesis that there is a critical interval at 48–49.5 h before the time of larval release.

Discussion

A major question raised by these observations is whether the timing of hatching in crustaceans is controlled by the embryo itself, the female, or both. Previous studies have led to different conclusions. Pandian (1970) suggested that a clock that sets the hatching time is within the egg. Ennis (1973) also proposed an endogenous factor controlling the timing of hatching, but was inconclusive about whether it is in the embryo or in the mother.

More direct evidence derives from the experiments in which a portion of embryos were separated from a female, and the time of hatching of those detached embryos was compared with that of the embryos still attached to the female. In some crustaceans, the embryos can complete their development and hatch as viable larvae even when they are separated from the mother. Branford (1978) reported that *Homarus* eggs removed more than 10 days prior to larval release still hatched. Similarly, in the estuarine crab *Rhithropanopeus*, hatching occurred when the embryos were separated 1–5 days before larval release by the female (Forward and Lohmann, 1983). Detached embryos of *Homarus* hatched rhythmically in a 24 h LD cycle, but arrhythmically under constant light (LL) or constant dark (DD) conditions (Branford, 1978). This might suggest an exogenously cued hatching rhythm. On the other hand, when the ovigerous female was kept in DD conditions, larval hatching showed a marked 24 h rhythmicity, so Branford (1978) concluded that any endogenous component of the rhythm is located in the female. The results of Forward and Lohmann (1983) were somewhat different from those of Branford (1978): embryos removed from the female within two days of larval release hatched at a similar time to the larvae released by the female; hatching synchrony deteriorated with longer removal times. From these results, Forward and Lohmann (1983) concluded that the timing of hatching is controlled by the embryo, and that the role of the female is to synchronize embryo development.

In *Sesarma haematocheir*, when some eggs were detached from the female, and their hatching was compared with the eggs left attached to the female, the hatching synchrony of the detached eggs decreased (Fig. 1). These features have also been observed in other crabs inhabiting estuaries: *Neopanope sayi*, *Uca pugilator*, and *Sesarma cinereum* (De Vries and Forward, 1991). Desynchronization and delay of hatch time increased when the eggs were aerated at 15°C (unpub. data). So temperature is clearly one of the factors affecting the timing of hatching in detached eggs. But the data of Figure 1 cannot be explained in terms of temperature alone; the desynchronization and delay of hatch time could be due to the absence of some cue from the female.

Furthermore, if the embryos of *Sesarma haematocheir* were detached from the female sooner than 48–49.5 h before larval release, then only sporadic hatching (delayed by a week) occurred, and the larvae produced did not swim (Fig. 4 and Table II). To explain the failure of

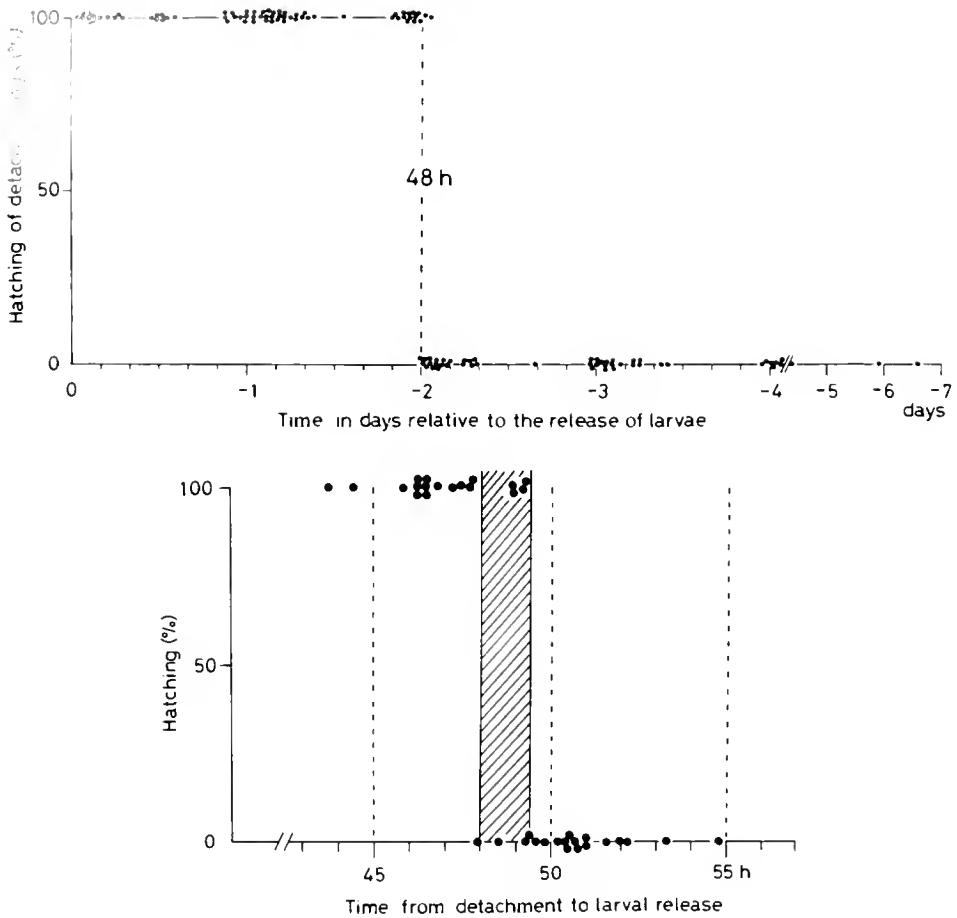

Figure 4. Relation between the success of hatching in detached egg clusters and the time of separation of those eggs from the females. Top panel: Hatching profile of eggs separated from the female 0–7 days before the larval release. The data were obtained from 110 females collected during July and August, 1989. Black dots represent the percentage of larvae hatched from an isolated egg cluster. Due to the large number of trials (250 samples), especially in the region of 24 h, 48 h, and 36 h, some data obtained around those times are indicated by one dot when the results were identical. Bottom panel: A closer examination of hatching from eggs detached 10 h before, and 10 h after, a critical interval—*i.e.*, 48–49.5 h before larval release by their females. The critical interval (shading) is indicated by hatching; other symbols are the same as in the top panel.

hatching and swimming in prematurely detached embryos. I postulated a process of hatching that, once initiated, requires 48–49.5 h until the motor activity of the embryo becomes high enough for swimming. Indeed, this process and ... tual timing of hatching are controlled by the embry... under detached conditions (Fig. 4, top). Howev... ation of the hatching process is not likely to b... within each embryo, as well. If this were th... moved more than two days before the actual ..., ng would all hatch. Hatching of detached egg... llowed an "all-or-nothing" pattern, with a drastic ... at about 48 h before larval release (Fig. 4, bottom). These results suggest that the timing that triggers the start of the hatching process is determined by the female.

Larval release by *S. haematocheir* coincides with the time of high water at night. The phase of this rhythm is endogenously controlled, and the internal period is about 24.5 h (Saigusa, 1986, 1988). Since larval release occurs as a result of synchronous hatching, the timing of hatching would actually be under 24.5 h circa-tidal control. As mentioned above, the hatching process might start between 48 and 49 h before the larval release. In the field, this would occur roughly two nights before the time of high tide, although the physiological mechanisms underlying the commencement of hatching are not yet known.

The embryos of most crustaceans are surrounded by two principle membranes: an outer egg-capsule, and a very delicate inner membrane investing the embryo. The common properties of hatching in the Crustacea are that

Table II

Hatching profiles of the embryos detached from individual females

Time of day the eggs were detached from a female [Time to larval release]			Larval release by the female
1. Jul. 18, 21:03 (×) [53:42]	Jul. 19, 01:25 (○) [49:20]	Jul. 20, 01:20 (○) [25:25]	21 Jul. 02:45
2. Jul. 18, 21:10 (×) [50:55]	Jul. 19, 01:34 (○) [46:31]	Jul. 20, 01:26 (○) [22:39]	21 Jul. 00:05
3. Jul. 18, 22:30 (×) [48:30]	Jul. 19, 02:45 (○) [44:15]	Jul. 19, 22:30 (○) [24:30]	20 Jul. 23:00
4. Jul. 18, 22:43 (×) [49:42]	Jul. 19, 02:45 (○) [45:40]	Jul. 19, 22:20 (○) [26:05]	21 Jul. 00:25
5. Jul. 18, 22:49 (×) [50:21]	Jul. 19, 02:50 (○) [46:20]	Jul. 19, 22:30 (○) [26:40]	21 Jul. 01:10
6. Jul. 18, 22:55 (×) [50:25]	Jul. 19, 02:58 (○) [46:22]	Jul. 19, 22:35 (○) [26:45]	21 Jul. 01:20
7. Jul. 18, 22:58 (×) [50:57]	Jul. 19, 03:00 (○) [46:45]	Jul. 19, 22:38 (○) [26:57]	21 Jul. 01:45
8. Jul. 31, 00:05 (×) [96:05]	Jul. 31, 22:00 (×) [50:10]	Aug. 1, 01:02 (○) [47:08]	3 Aug. 00:10
9. Aug. 14, 20:10 (×) [51:30]	Aug. 14, 22:47 (○) [48:53]	Aug. 15, 21:00 (○) [26:40]	16 Aug. 23:40
10. Aug. 14, 20:22 (×) [49:48]	Aug. 14, 23:00 (○) [47:10]	Aug. 15, 21:12 (○) [24:58]	16 Aug. 22:10
11. Aug. 15, 21:32 (×) [50:58]	Aug. 16, 00:55 (○) [47:35]	Aug. 16, 02:53 (○) [45:37]	18 Aug. 00:30
12. Aug. 15, 21:36 (×) [49:14]	Aug. 16, 01:00 (○) [45:50]	Aug. 16, 02:56 (○) [43:54]	17 Aug. 22:50
13. Aug. 16, 22:53 (×) [50:22]	Aug. 17, 01:34 (×) [47:41]	Aug. 17, 03:06 (○) [46:09]	19 Aug. 01:15

○: A cluster of eggs, all of which hatched.

×: A cluster of eggs, in which hatching was never observed. Time of day of hatching in the eggs attached to the female is shown by the time of larval release by the female. See female C-14 in Table I for another example. Braces on the right side indicate results that were obtained in the same experimental room.

the rigid outer membrane bursts first, and the inner membrane then emerges from the outer membrane. Emergence of this thin membrane occurs gradually in some species and very quickly in others (Marshall and Orr, 1954). Different hatching mechanisms have been proposed. Osmotic hatching has been suggested in a number of Crustacea (Yonge, 1937; Marshall and Orr, 1954; Davis, 1959, 1965). On the other hand, in the lobster *Homarus*, Davis (1964) proposed that breaking of the egg capsule is caused by the swelling of the embryo itself, due to an uptake of ambient water. Furthermore, in the amphipods *Corophium* (Fish and Mills, 1979), spines on the embryonic cuticle of the telson are used to break the membranes in hatching.

The outer membrane of *S. haematocheir* embryos, like that of other Crustacea, is also ruptured by pressure from within. The pressure responsible for bursting could be brought about by the larva, which swells, possibly due to the absorption of ambient water (Saigusa, 1992). This type of hatching makes the synchronization of the large number of embryos attached to the female even more difficult to understand. The temporal correlation between the hatching of the embryos attached to the female, and that of the detached embryos, suggests that a physical or chemical stimulus, transmitted from the female to each embryo, must be responsible for establishing hatching synchrony. De Vries and Forward (1991) postulated a hatching enzyme released by the embryo, and suggested that the timing of its release is controlled either by the embryo itself, or by the mother. In *S. haematocheir*, the stimuli that induce the hatching process and enhance hatching synchrony are unknown. Nor is it even clear that a hatching enzyme is released by the embryo.

Acknowledgments

I thank Mr. A. Betchaku (Faculty of Education, Okayama University) who kindly helped with the collection of crabs at Kasaoka.

Literature Cited

Branford, J. R. 1978. The influence of daylength, temperature and season on the hatching rhythm of *Homarus gammarus*. *J. Mar. Biol. Assoc. U.K.* **58:** 639–658.

Davis, C. . . . hatching in the eggs of some fresh-water . . . 5–29.

Davis . . . the hatching process in aquatic inver- . . . closion in the American lobster, *Homarus* . . . wards (Astacura, Homaridae). *Am. Midl. Nat.* . . .

. . . 1985. A study of the hatching process in aquatic inver- . . . brates. XX. The blue crab, *Callinectes sapidus*, Rathbun. *Chesapeake Science* **6**: 201–208.

DeCoursey, P. J. 1979. Egg-hatching rhythms in three species of fiddler crabs. Pp. 399–406 in *Cyclic Phenomena in Marine Plants and Animals*, E. Naylor, and R. G. Hartnoll, eds. Pergamon Press. Oxford.

DeCoursey, P. J. 1983. Biological timing. Pp. 107–162 in *The Biology of Crustacea VII. Behavior and Ecology*, F. J. Vernberg, and W. B. Vernberg, eds. Academic Press. Washington.

De Vries, M. C., and R. B. Forward, Jr. 1989. Rhythms in larval release of the sublittoral crab *Neopanope sayi* and the supralittoral crab *Sesarma cinereum* (Decapoda: Brachyura). *Mar. Biol.* **100:** 241–248.

De Vries, M. C., and R. B. Forward, Jr. 1991. Control of egg-hatching time in crabs from different tidal heights. *J. Crustacean Biol* **11:** 29–39.

Ennis, G. P. 1973. Endogenous rhythmicity associated with larval hatching in the lobster *Homarus gammarus*. *J. Mar. Biol. Assoc. U.K.* **53:** 531–538.

Fish, J. D., and A. Mills. 1979. The reproductive biology of *Corophium volutator* and *C. arenarium* (Crustacea: Amphipoda). *J. Mar. Biol. Assoc. U.K.* **59:** 355–368.

Forward, R. B. Jr., and K. J. Lohmann. 1983. Control of egg hatching in the crab *Rhithropanopeus harrisii* (Gould). *Biol. Bull.* **165:** 154–166.

Franke, H. D. 1985. On a clocklike mechanism timing lunar-rhythmic reproduction in *Typosyllis prolifera* (Polychaeta). *J. Comp. Physiol. A* **156:** 553–561.

Hashimoto, H. 1976. Non-biting midges of marine habitats (Diptera: Chironomidae). Pp. 377–414 in *Marine Insects*, L. Cheng, ed. North-Holland Publishing Company. Amsterdam.

Koskinen, R. 1968. Seasonal emergence of *Clunio marinus* Haliday (Dipt., Chironomidae) in western Norway. *Annales Zoologici Fennici* **5:** 71–75.

Marshall, S. M., and A. P. Orr. 1954. Hatching in *Calanus finmarchicus* and some other copepods. *J. Mar. Biol. Assoc. U.K.* **33:** 393–401.

Moller, T. H., and J. R. Branford. 1979. A circadian hatching rhythm in *Nephrops norvegicus* (Crustacea: Decapoda). Pp. 391–397 in *Cyclic Phenomena in Marine Plants and Animals*, E. Naylor and R. G. Hartnoll, eds. Pergamon Press. Oxford.

Pandian, T. J. 1970. Ecophysiological studies on the developing eggs and embryos of the European lobster *Homarus gammarus*. *Mar. Biol* **5:** 154–167.

Saigusa, M. 1982. Larval release rhythm coinciding with solar day and tidal cycles in the terrestrial crab *Sesarma*. *Biol. Bull.* **162:** 371–386.

Saigusa, M. 1985. Tidal timing of larval release activity in non-tidal environment. *Jpn. J. Ecol.* **35:** 243–251.

Saigusa, M. 1986. The circa-tidal rhythm of larval release in the incubating crab *Sesarma*. *J. Comp. Physiol. A* **159:** 21–31.

Saigusa, M. 1988. Entrainment of tidal and semilunar rhythms by artificial moonlight cycles. *Biol. Bull.* **174:** 126–138.

Saigusa, M. 1992. Observations on egg hatching in the terrestrial crab *Sesarma haematocheir*. *Pac. Sci.* **46:** 484–494.

Yonge, C. M. 1937. The nature and significance of the membranes surrounding the developing eggs of *Homarus vulgaris* and other Decapoda. *Proc. Zool. Soc. Lond. A* **107:** 499–517.

Reference: *Biol. Bull.* **183:** 409–417. (December, 1992)

Aspects of the Fertilization Ecology of Broadcast Spawning Corals: Sperm Dilution Effects and *in situ* Measurements of Fertilization

JAMIE OLIVER[1], AND RUSS BABCOCK[2,3]

Australian Institute of Marine Science, PMB 3 Townsville MC, Townsville, 4810, Australia

Abstract. A series of laboratory and field experiments was carried out to determine the effects of gamete dilution on fertilization rates in three species of reef coral. Gametes remained viable for 2 h after spawning, but one species exhibited signs of reduced fertility 3–4 h after spawning. Sperm dilution trials carried out in the laboratory indicated that fertilization reaches a maximum at sperm concentrations of 10^5–10^6 per ml, with reduced fertilization occurring at both higher and lower concentrations.

Estimates of "fertilization potential" in the field were obtained by exposing eggs to water samples taken from the field at various times and locations following episodes of coral spawning. This sampling program indicated that on nights when only small numbers of coral spawned (minor spawning), the fertilization potential was much lower than on major spawning nights. On major spawning nights, fertilization potential was consistently high just after spawning, but became spatially variable thereafter. The percentage of fertilization in field-collected samples of eggs and embryos just after spawning was also higher during major spawning nights than during minor spawning nights.

These measurements indicate that gamete dilution can play an important role in limiting the fertilization of coral eggs in the field during natural spawnings. It follows, therefore that corals are under considerable selective pressure to spawn synchronously in order to generate high gamete concentrations in the water column and thus to maximize the probability of successful fertilization. In addition to spawning in synchrony, corals also minimize the effects of gamete dilution by spawning buoyant gamete bundles that accumulate at the sea surface, and by spawning during periods of low water motion.

Received 10 May 1991; accepted 30 September 1992.

[1] Present Address: Great Barrier Reef Marine Park Authority, P.O. Box 1379, Townsville, 4810, Australia.

[2] Contribution Number 688 of the Australian Institute of Marine Science.

[3] Authorship in order of decreasing fertility.

Introduction

Fertilization is a critical and possibly limiting event in the life history of organisms that shed their gametes into the environment. Although behavioral phenomena such as spawning aggregations and synchronous gamete release are often presumed to have evolved as mechanisms to enhance fertilization (Giese and Pearse, 1974; Johannes, 1978; Babcock *et al.*, 1986; Pearse *et al.*, 1988), it is only recently that work on theoretical (Denny and Shibata, 1989) and actual (Pennington, 1985; Yund, 1990; Levitan, 1991; Levitan *et al.*, 1992) rates of *in situ* fertilization in broadcast spawning marine invertebrates have been studied. These studies suggest that gamete dilution in the field can result in very low fertilization rates, and that aggregation and spawning synchrony function to maximize fertilization. Working with echinoids in conditions of moderate current intensity, Pennington (1985) demonstrated that sperm concentrations and levels of fertilization rapidly decreased to low levels (<15%) at distances greater than 1 m from spawning males, and that sperm were short-lived. He concluded that gamete wastage due to the lack of successful fertilization could be significant in natural populations and that, though there was little consensus on whether aggregation is a characteristic feature of spawning echinoids, such aggregations could play a vital role in promoting fertilization. Similarly, Yund (1990) found that *in situ* fertilization of hydroid eggs during periods of calm water decreased substantially beyond 3 m from a source of sperm. In the brooding ascidian *Botryllus schlosseri*, Grosberg (1991) demonstrated that fertilization

from a known sperm [illegible] was reduced to negligible levels at distances of [illegible]0 cm. Recent work by Levitan (1991) and [illegible] (1992) has demonstrated that increases [illegible]ction size and aggregation can substantially [illegible]tilization success in sea urchins.

The [illegible]ates by Denny and Shibata (1989) of gamete diffusion agree well with the experimental results mentioned above and suggest that, except in a very restricted set of circumstances, fertilization rates are likely to be extremely low. Nevertheless, the effectiveness of synchrony and aggregation behavior in ensuring high concentrations of sperm around eggs can be inferred from the presence of mechanisms that prevent polyspermy in the eggs of several echinoid species (Schuel, 1984).

Although the studies cited above have described fertilization rates achievable under specific experimental arrangements of male and female individuals (or discrete gamete samples acting as simulated individuals), few, if any measurements of fertilization rates have been made during natural spawning in an unmanipulated population. Such studies are essential in order to verify the existence of postulated strategies for increasing fertilization rates in environments where dilution effects are overwhelming.

The problems of gamete dilution are particularly acute in sessile organisms because their lack of motility precludes aggregation during spawning events. Thus sessile, broadcast-spawning organisms must rely on other mechanisms, such as synchronous spawning or aggregation during the settlement stage, to ensure fertilization. Probably the most spectacular example of synchronous spawning in sessile marine invertebrates is the annual mass-spawning of reef building corals on the Great Barrier Reef (Harrison *et al.*, 1984; Willis *et al.*, 1985; Babcock *et al.*, 1986; Oliver *et al.*, 1988) and in other parts of the Pacific (Heyward, 1988; Heyward *et al.*, 1987). On the Great Barrier Reef, over 130 species of coral are known to participate in this annual reproductive event, with over 30 species spawning on the same night (Willis *et al.*, 1985). These spawning episodes are highly predictable and, for many of the species involved, last for less than an hour every year. That corals synchronize their reproductive activities to this degree, even when such a strategy can lead to the loss of an entire year's [illegible]oductive effort through chance events such as heavy [illegible] (Harrison *et al.*, 1984), may reflect an overriding [illegible]hieve adequate concentrations of sperm and eg[illegible]ter column. Indeed, many of the hypothese[illegible]pt to explain the timing of coral spawnin[illegible]h as spawning predominantly on low neap [illegible]nchrony have been concerned with the wa[illegible]ming may optimize successful fertilization ([illegible], 1986).

In this stud[illegible]vestigate several aspects of the fertilization biolog[illegible] mass spawning corals, with particular emphasis on factors that may influence successful fertilization in the field. We focus on three basic questions. (1) What is the optimal sperm concentration for fertilization of coral eggs? (2) How long after spawning do gametes remain capable of successful fertilization? (3) What is the spatial and temporal variability of fertilization in the field during nocturnal spawning events?

Materials and Methods

Study sites

Corals for these experiments were obtained from fringing reefs at two near-shore locations on the central Great Barrier Reef near Townsville, Australia (Fig. 1). The first of these sites was at Geoffrey Bay, Magnetic Island (19°10′S 146°51′E), where gametes were obtained from corals that spawned between October 27 and November 1, 1988, and October 16 through 18, 1989. The second site was at Pioneer Bay, Orpheus Island (18°35′S 146°29′E), where corals spawned one month later, between November 25 and 31 during both years.

Gamete collection

The species studied were *Montipora digitata*, *Favites pentagona*, and *Platygyra sinensis*. All three species are simultaneous hermaphrodites, releasing well-formed bundles containing both eggs and sperm (egg-sperm bundles). The eggs are highly buoyant and the bundles float rapidly to the surface where they break apart, usually within half an hour of release. If conditions are calm, the eggs, sperm, and associated mucus accumulate at the surface to form large, conspicuous "coral spawn slicks" (Oliver and Willis, 1987). Fertilization is not likely to occur until at least half an hour after spawning, since polar body extrusion does not occur before this time in faviids (*e.g.*, *Platygyra* and *Favia*) and may take even longer in acroporids (Babcock and Heyward, 1986).

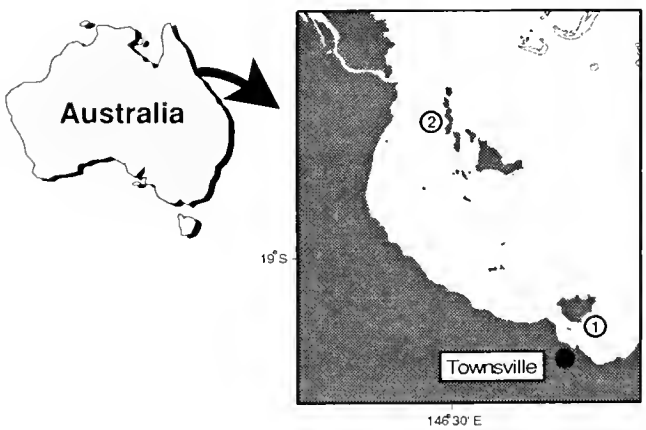

Figure 1. Map showing study locations at Geoffrey Bay, Magnetic Island (1) and Pioneer Bay, Orpheus Island (2).

The selected species all spawn on separate nights. In most species, spawning takes place on just one night, but in *M. digitata* spawning takes place over three nights, with the majority of spawning occurring on the second night (Heyward and Collins, 1985; Babcock *et al.*, 1986). Late in the afternoon on the day of spawning, ripe colonies were collected and placed, either in separate buckets, or in individual aquaria, with running water and aeration. The aquaria were left static after sunset to facilitate the collection of gametes.

The egg-sperm bundles used in these experiments were collected as soon as they reached the surface and were held in a small quantity of sperm-free seawater that had been collected in the afternoon, prior to spawning, about 1 km offshore from the island. The egg-sperm bundles were gently agitated at frequent intervals, until all the bundles broke apart, physically separating the eggs and sperm. This process took between 10 and 20 min. The eggs were then harvested with a wide-mouthed plastic pipette and rinsed to remove adherent sperm as follows.

The eggs were placed in 30 ml plastic vials, the bottoms of which had been replaced with 100 μ or 200 μ plankton mesh, depending on egg size. The vials then were partially immersed in sperm-free water, and the eggs were rinsed by agitation of the vial. After the rinse, the vials were rapidly transferred to a fresh volume of sperm-free water. This process was repeated nine times and the eggs were retained in the sperm-free water for later use. Each fertilization experiment included a set of washed eggs to which no sperm were added. This served as a control for either inadequate washing, or contamination by extraneous sperm. The original volumes of water in which the egg-sperm bundles were allowed to separate (approximately 300 ml), were used to provide concentrated sperm suspensions. Sperm concentrations in these undiluted suspensions were determined with a haemocytometer.

The first set of experiments carried out in 1988 resulted in a significant number of fertilized embryos which then developed abnormally. Subsequent trials with glass, polystyrene, and polycarbonate vials for egg-sperm incubations showed that, compared with glass, both types of plastic vial increased the proportion of abnormal embryos. Similar adverse effects caused by plastic have been reported by Dinnel *et al.*, 1987. All subsequent experiments in 1989 were carried out with glass vials. The vials were opened and soaked in seawater for 6 h before use.

Sperm dilution effects

The concentration of undiluted sperm was adjusted to about 10^7–10^8 ml $^{-1}$. These suspensions were then serially diluted 10 times (50% or 30% per dilution) in sperm-free water to provide a standard range of sperm concentrations (10^3–10^8 ml^{-1}). The sperm concentration was verified with a haemocytometer for one or two of the dilutions in each trial and was found to be within 10% of that predicted from the dilution factor. For each concentration, 25 ml of sperm suspension were added to three replicate 30 ml plastic (1988) or glass (1989) vials. These contained about 100 eggs in a small volume (<1 ml) of sperm-free water. Controls received the same volume of sperm-free water. The vials were sealed and placed in the sea where they received natural, irregular agitation. All egg-sperm combinations were carried out no more than 45 minutes after the serial dilutions were prepared. After three hours, the vials were retrieved from the sea, and the eggs scored to record the proportion which had been fertilized. All eggs that were at or beyond the two-cell stage were considered to have been fertilized.

Gamete age effects

Eggs of *Montipora digitata* and *Platygyra sinensis* were mixed with sperm at known concentrations at 30-min intervals to assess the potential longevity of gametes. The sperm concentration used was one that yielded the highest fertilization rates in initial trials. The sperm was stored at the dilution at which it was to be used, until the time the gametes were mixed. The protocol for sample preparation, incubation, and counting was the same as that described above for sperm dilutions. In these experiments, both eggs and sperm were allowed to age simultaneously. The effects of egg or sperm age could not be investigated separately.

Sperm concentrations in the field

Fertilization in the field was measured either by determining the percentage of fertilized eggs in the water column following spawning events, or by estimating the "fertilization potential" of discrete water samples taken at different times and locations around the reef. This second index was determined by incubating the water samples with washed eggs obtained from corals that had spawned in the laboratory. This assay allowed us to determine the likely percentage of eggs that would be fertilized by sperm in a particular water mass during times when very few eggs were present in the water. "Fertilization potential" thus provides a way of estimating the probability of successful fertilization for corals that spawn at a slightly different time or place than the majority of the population.

On the afternoon before spawning, two buoys were placed over the zone of greatest abundance of the coral species under investigation. The buoys were positioned about 250 m apart, parallel to the reef front. Divers monitored populations of *P. sinensis* and *M. digitata* for signs of spawning behavior (egg-sperm bundles can be observed within the colony before their release). As the first bundles

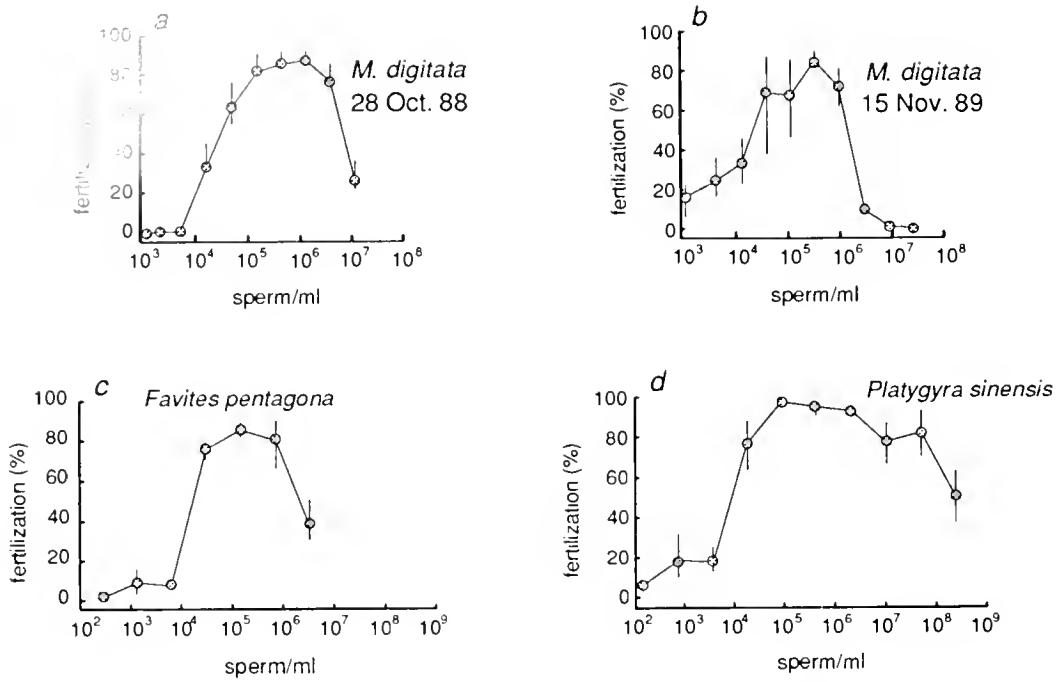

Figure 2. Sperm dilution series for *Montipora digitata* on two different nights (a, b), and for *Favites pentagona* (c) and *Platygyra sinensis* (d). Each series was run independently on separate nights. Values represent mean and ranges from three replicate vials.

were released, samples of seawater were taken from the surface adjacent to the buoys, and from the surface midway between them. The water samples were collected in 1 liter plastic bottles and transferred within 30 min to the laboratory where they were mixed with laboratory-spawned eggs in the manner described for the sperm dilutions. Although the field water samples occasionally contained some eggs, these were removed prior to mixing.

In an attempt to track patches of sperm near the surface during the hours after spawning, drogues ("X" vanes floating in the top 15 cm of the water column) were deployed above areas of actively spawning corals. Although these drogues track the near surface layer under calm conditions, they are not reliable indicators of water movement in the first few millimeters once wind speeds exceed 2–5 knots. As weather conditions during most spawning periods were calm, with occasional slight breezes, the drogues were used to increase the chances of finding patches of high sperm concentration. The drogues were tracked for hours, and samples were taken both adjacent to (within) and between the drogues at 30–60 minute intervals.

During spawning of *Montipora digitata* at Magnetic Island in 1989, natural (*in situ*) fertilization rates were examined by means of a series of single neuston net tows made between drogues. In addition, dip samples were taken from any visible slicks of coral spawn that were encountered. Sampling with tows or dips was concurrent with the water sampling described above. The resulting eggs and embryos were subsequently preserved and counted.

Results

Sperm dilutions

Sperm dilution experiments were successfully carried out on three occasions with *Montipora digitata* and on one occasion each with *Favites pentagona*, and *Platygyra sinensis*. In all cases there was a broad optimum for fertilization at densities between 10^5 and 10^6 sperm/ml (Fig. 2). At concentrations below 1000 sperm/ml, fertilization rates were low. At very high sperm concentrations ($>10^6$ per ml), there is evidence of inhibition of fertilization, although this was less obvious in *Platygyra sinensis* (Fig. 2d).

Gamete age

The gametes of both *Platygyra sinensis* and *Montipora digitata* lost little viability for at least 2 hours after spawning (Fig. 3). Those of *Platygyra sinensis*, which were kept for a longer period (4.5 h) before being mixed, showed depressed levels of fertilization commencing at about 3 hours (Fig. 3). After about 3 hours, the eggs began to disintegrate, so no further viability studies were possible.

In situ gamete concentrations and fertilization rates

Fertilization potential of water samples. In 1988, water samples were taken on one night only, during a mass

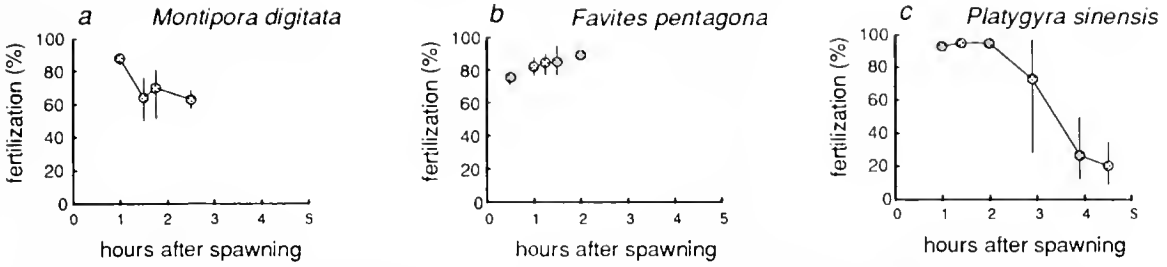

Figure 3. Gamete age effects. Fertilization rates (mean and ranges) for gametes of *Montipora digitata* and *Platygyra sinensis*, combined at varying times after spawning. Eggs and sperm were separated at the time of spawning and later re-combined with gametes from other colonies. Male and female gametes were of the same age at the time of mixing.

spawning event that included many faviid species. Weather conditions at the time of spawning were calm and the sea was glassy. During the first 1.5 to 2 h after spawning, large numbers of eggs from *P. sinensis* and other corals were visible at the sea surface around and near the drogues. The drogues moved slowly over the reef flat and were situated some 10–20 m off the edge of the reef by the time the last sample was taken 3.5 hours after spawning. The data in Figure 4 represent the pooled results from samples taken adjacent to, and midway between two drogues, since there was virtually no difference between the samples. Figure 4 clearly shows the fertilization potential for *Platygyra sinensis* rising to nearly 100% just after the initiation of spawning. During the next hour, rates were variable but slightly lower. By 3 hours after spawning, fertilization had dropped quite rapidly to near zero. This decrease is not due solely to an age effect, since it occurred earlier and was more pronounced than the reduction of fertilization observed in a concurrent longevity trial in the lab (Fig. 4). Samples were also taken from 1 m below the surface beginning 1.5 hours after spawning. These exhibited levels of fertilization very similar to the surface samples (Fig. 4), indicating that by this time the gametes were well mixed within at least the top meter of the water column. Statistical analysis of the results (Table I) indicate that by 1.5 hours after spawning, fertilization rates were significantly lower than those observed in the laboratory, and that fertilization decreased significantly in all treatments after 3 hours.

In 1989, seawater samples were taken over three consecutive nights during the spawning of *Montipora digitata* (Fig. 5). Fertilization rates were consistently low at all times and in all locations during the first and last nights of spawning. During the second night, which was the major night of spawning, fertilization rates were highly variable in space and time. For samples taken next to and between the two buoys anchored on the reef flat (Fig. 5c), fertilization rates were high at two of the three locations

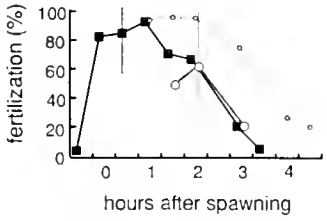

Figure 4. Fertilization rates for *Platygyra sinensis* resulting from water samples taken on the night of spawning. Each data point represents the mean and representative ranges of replicate vials (three sites each with three replicate vials). Time of spawning was determined by field observations. Solid squares: pooled results from single samples taken beside each drogue and midway between. Open circles: similarly pooled results from samples taken 1 m below the surface. Small circles and dashed line: results of gamete longevity trial using eggs spawned in the lab at the same time as the field, and a sperm concentration of approximately 500 sperm/ml.

Table I

(a) Two-way ANOVA for fertilization rates for Platygyra sinensis *samples at different times (1.5, 2, 3 h) after spawning and under different conditions (= Treatments: surface, 1 m,* in vitro*). The analysis was restricted to those times when all three treatments were sampled*

Source	df	SS	MS	F	*P*
Time	2	3296.2	6648.1	16.04	0.00
Treatment	2	7029.5	3514.7	8.48	0.002
Time × treatment	4	2548.9	637.2	1.54	0.233

(b) Tukey's Studentized Range test (HSD) α = .05, df = 18

Time/treatment level	Group	Mean	n
1.5 h	A	89.1	9
2 h	A	69	9
3 h	B	35.9	9
in vitro	A	87.2	9
surface	B	57.8	9
1 m	B	49.7	9

during the first hour but remained very low at all fixed locations thereafter. This suggests that eggs and sperm drifted off the reef flat during the first hour after spawning. Samples taken adjacent to, and between the two drogues (Fig. 5b) showed a similar pattern of initially high fertilization in two out of three locations followed by a rapid decrease. Two hours after spawning, only one drogue, located in a slick of eggs, was associated with high concentrations of sperm. By 3 h after spawning, fertilization was virtually zero for both drogues. But samples taken at this time from two ends of a surface slick of eggs, showed high rates of fertilization that were comparable to rates obtained in the lab with sperm at optimal concentration. Thus, after the first hour, high concentrations of sperm were found only in association with slicks (that occupy the first few millimeters of the water column), but were not consistently found next to drogues (which track the top 15 cm of water).

The difference in overall fertilization rates between the second night, when high rates of fertilization were obtained in some samples, and the first and third nights, when fertilization was consistently low, can be related to the intensity of coral spawning during this period. Table II shows

Table II

Percentage of Montipora digitata *colonies spawning on 14, 15 and 16 November 1989, compared to the percentage of fertilization from field water samples taken on the same night within an hour of spawning*

Date	% Spawning	% Fertilization (SD)
14th	16	1.01 (2.1)
15th	71	49.0 (37.3)
16th	3	0.2 (0.5)

Spawnings took place at Pioneer Bay, Orpheus Island. The same corals were observed each night, with some removal and replacement of stressed colonies. Numbers of colonies observed were: 14th, n = 15; 15th, n = 17; 16th, n = 12.

the proportion of colonies, collected for spawning studies, that spawned on each of the three nights. It can be seen that high fertilization rates occurred only on the night when a larger proportion of the colonies spawned.

Fertilization of eggs collected in situ. Fertilization rates of eggs in plankton samples taken from the sea surface in 1989 during the spawning of *M. digitata* at Magnetic Island reflected the same pattern as that seen over the three

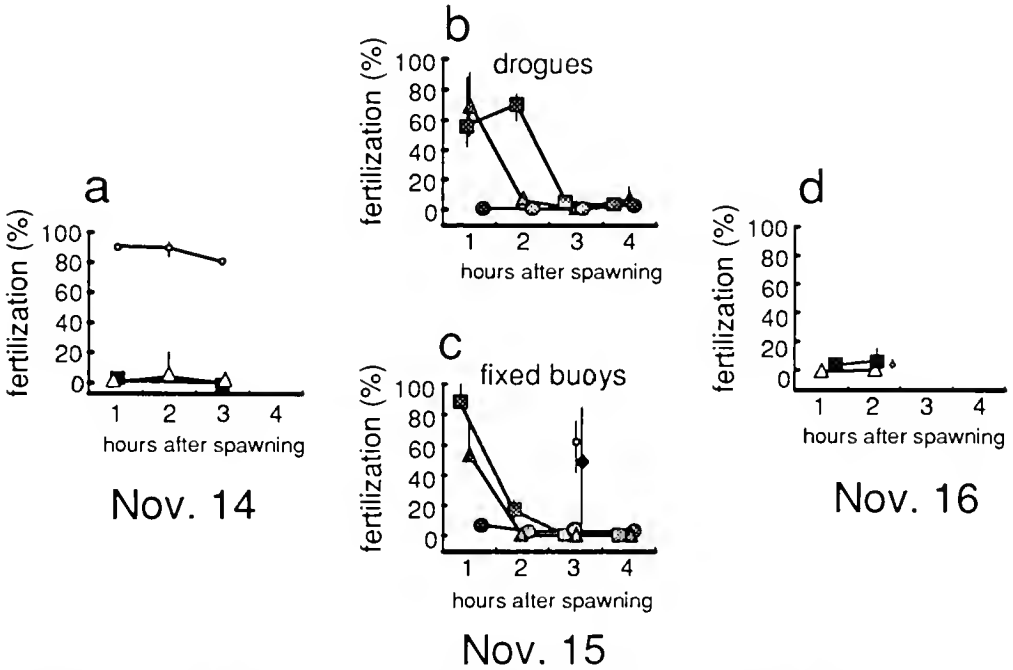

ure 5. Fertilization rates resulting from water samples taken on the three major spawning nights for *ora digitata*, Orpheus Island in 1989. All error bars represent sample ranges. (a): Data for November sed squares: pooled data from samples beside and between drogues. Open Triangles: pooled data les at and between fixed buoys on the reef flat. Small circles and dashed line: fertilization rates he lab with sperm at optimal concentrations. (b), (c): Data for November 15th (the major ight) showing results from each of three samples taken at (squares and circles) and between two drogues (b) and two fixed buoys (c). Diamonds show data from two samples (20 m apart) of slick of eggs. Small circle shows results of a laboratory fertilization trial using optimum sperm co tation. (d): Data for November 16. Symbols as for (a).

nights of spawning at Pioneer Bay. We assume that the vast majority of these eggs came from *M. digitata* since this was the only species observed to spawn on the first two nights in question, and only one other species of *Montipora*, (restricted to the reef slope) was observed to spawn on the third night. With the exception of the genus *Porites* (which spawns 4–6 nights after the full moon), the eggs of *Montipora* can be distinguished from those of other corals by the presence of zooxanthellae.

Again, the highest rates of fertilization were recorded on the second night of spawning (Fig. 6), when large numbers of spawning colonies were observed by divers, and eggs were conspicuous at the water's surface throughout the sampling period. On the previous night, no spawning corals were observed by divers, and only a few eggs could be seen at the water's surface immediately after spawning. Fertilization rates were correspondingly low on this night, and on the last night, when winds were stronger. Although numerous colonies of *M. digitata* were seen spawning on the last night, only moderate numbers of eggs were seen on the water's surface after spawning, and no obvious concentrations were visible after that time. In Figure 6, the proportion of fertilized eggs appears to increase with time because cleavage is not initiated until 1–2 hours after spawning.

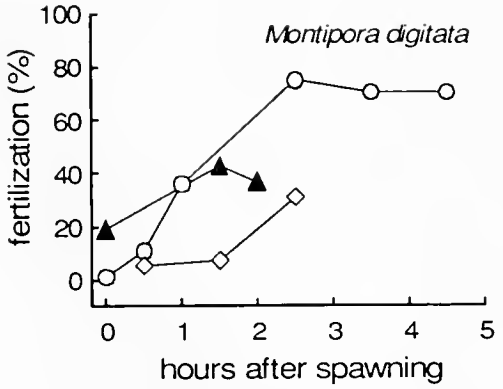

Figure 6. Fertilization rates for eggs of *Montipora digitata* obtained from plankton tows, Geoffrey Bay. Samples were obtained from single four-minute plankton tows during the nights of the 16th, 17th, and 18th of October 1989 at Geoffrey Bay, Magnetic Island (1st–3rd nights after full moon). Triangles: 16 October. Weather: winds 5–10 knots, some eggs seen in water immediately after time of spawning, but no spawning colonies observed in the field. Spawning itself observed only in aquaria. Circles: 17 October. Weather: winds 10 knots, many corals seen spawning and many eggs visible at the water's surface throughout sampling. Diamonds: 18 October. Weather: winds 10–15 knots. Many corals seen spawning. Moderate numbers of eggs visible after spawning but no obvious concentrations of eggs after this time.

Discussion

Fertilization rates of *Montipora digitata*, *Platygyra sinensis*, and *Favites pentagona* were all strongly influenced by sperm concentration, with optimal concentrations at about 10^5–10^6 sperm/ml. The pronounced decrease in fertilization rate at low sperm concentrations is presumably due to the decreased probability of successful egg-sperm encounters. Fertilization rates also declined at high sperm concentrations and were usually negligible above 10^7 sperm/ml. This reduction in fertilization rate may be due to the combined influences of decreased oxygen, increased CO_2, and lower pH. The inactivity of echinoid and ascidian sperm under these conditions is well documented (Chia and Bickell, 1983), and the existence, if not the cause, of this phenomenon has been known for some time (Lillie, 1915). Similar effects of high sperm concentrations on fertilization rates have been also reported for the bivalve *Mytilus edulis* (Ginzburg, 1975, cited in Sprung and Bayne, 1984). Our results therefore suggest that coral sperm are inactive when they are highly concentrated within egg-sperm bundles at the time of spawning, and that they are unlikely to be capable of full activity during the early stages of fragmentation of these bundles. This delay in the activation of sperm may be advantageous to corals for two different reasons. First, the delay may provide time for gametes from different colonies to mix, thus enhancing the chances of successful cross-fertilization. This would be especially important in those corals that are incapable of self-fertilization (Heyward and Babcock, 1986). Second, because Babcock and Heyward (1986) have shown that final egg maturation does not occur in many corals until 30 min after spawning, a delay in sperm activation would prevent energy reserves of the sperm from being expended prematurely.

Our experiments on gamete longevity indicate that the capacity for fertilization remains high for up to 2 h after spawning. In *P. sinensis*, where gamete viability was examined for a longer period, fertilization declined after 2 h, but remained substantially above zero (20–30%) for up to 4.5 h. Although the age of both eggs and sperm varied in these experiments, it is likely that the drop in fertilization rates with time probably reflects a progressive drop in sperm motility as the limited energy reserves in each sperm cell are depleted. Sperm respiration (and hence energy expenditure) is known to increase at low densities (Chia and Bickell, 1983), so the results presented here may not necessarily reflect the average longevity for gametes in the field, where more pronounced dilution effects could reduce the period of viability for most sperm.

Fertilization potential in the field exhibited several clear patterns. First, in both years of this study, there was a marked trend for high initial fertilization rates followed by a steady decline after 2–3 hours (Fig. 4). The decline was probably due to a combination of both dilution and ageing of gametes. Second, during 1989, when samples were taken over several nights, there was clear evidence

that the fertilization potential in the water column was drastically reduced on nights other than the principal spawning night, probably due to rapid dilution of the small volume of gametes released on these nights (Fig. 5, Table II). During major spawning nights, the concentration of sperm was patchy, and enhanced levels of fertilization were found for a much longer period in certain drifting patches than in areas over the reef flat where spawning occurred (Fig. 5b, c). These patches of high fertilization potential (*i.e.*, high sperm concentration) were invariably associated with concentrations of eggs and embryos (coral spawn slicks) at the sea surface.

The principal conclusions to be drawn from these results are that high sperm concentrations are important for successful fertilization, and that this is most effectively achieved by synchronization of the spawning event. Individuals that spawn either on a different night, or at a different time from the main spawning event, are clearly disadvantaged by a substantial reduction in the probability of successful fertilization of their gametes. The results of the *in situ* sampling of eggs during 1989 also support this conclusion since the percentage of fertilized eggs obtained from surface tows was twice as high during the main spawning night as on other nights.

The critical role that gamete concentration plays in the successful fertilization of marine organisms has been highlighted by the theoretical models of Denny and Shibata (1989), and by empirical studies on sea urchins, hydroids and ascidians (Pennington, 1985; Levitan, 1991; Levitan *et al.*, 1992; Yund, 1990; Grosberg, 1991). All of these studies showed that gametes are rapidly diluted and that fertilization is very low unless some means of creating high gamete concentrations is used.

High concentrations of gametes can be created and maintained in a number of ways during spawning events. These include: aggregation of spawning individuals; gregarious settlement of sessile organisms, resulting in high concentrations of spawners once sexual maturity is reached; spawning during periods of low water volume or low water exchange; and production of gametes that tend to resist dispersal in one way or another. For sessile invertebrates, such as corals, the options are somewhat restricted because adults cannot aggregate at the time of spawning. In contrast to many intertidal species, they are usually confined to a restricted or densely populated substratum. Sessile invertebrates such as crinoids (Kubota, 1980) and polychaetes (Caspers, 1984) commonly achieve high levels of gamete concentration through the timing of their spawning behavior, and this is clearly a mechanism exploited by corals (Willis *et al.*, 1985; Babcock, 1986; Richmond and Hunter 1990; this paper). In addition, many corals overcome their lack of mobility by spawning buoyant egg-sperm bundles that may themselves aggregate at the surface of the sea. In these aggregates, gametes are much more concentrated than they would be if they were spread throughout the water column. A similar effect is achieved in polychaetes through the swarming of epitokes at the sea surface (Caspers, 1984). Furthermore, in corals, mucus associated with the testes acts to bind the spawned material together in a surface slick that resists dispersion by wind and waves (Oliver and Willis, 1987; pers. obs.). Finally, corals on the Great Barrier Reef tend to spawn during the falling tide of a neap cycle, when the dispersive effects of tidal currents are at a minimum, and when the volume of water over the reef flat is reduced for a prolonged period. Thus corals appear to have evolved a number of behavioral and physical adaptations to overcome the problem of gamete dilution in the ocean.

Although the need to achieve high concentrations of gametes after spawning may underlie the high level of synchrony that exists within each coral species, it does not explain why so many different species should spawn on the same night of the year (Harrison *et al.*, 1984; Babcock *et al.*, 1986). Indeed, there would appear to be some disadvantage in spawning at the same time as other congenerics due to an increased probability of producing inviable hybrids (Hodgson, 1988).

Although our results suggest that quite high levels of fertilization occurred in the field during the main spawning nights, these field observations should be repeated when weather conditions are less calm. If most spawning occurs on a night when the winds are high, then the resulting wave action would cause a much higher degree of vertical mixing of the buoyant gametes. This would probably reduce both post-spawning gamete concentrations, and fertilization rates below those observed in the present study. In species that rely on the concentrating effects of buoyant gametes, weather may play a critical role in determining fertilization rates and the success of spawning for any one year.

Acknowledgments

We wish to thank Geoff Cheah, Caroline Christie, Phil Davies, Udo Engelhardt, Peter Harrison, Terri Seaman, and Angus Thompson for assistance with the fieldwork. John Benzie, John Chisholm, Dick Miller, Craig Young, and Michael Greenberg provided many helpful comments on the manuscript.

Literature Cited

Babcock, R. C., and A. J. Heyward. 1986. Larval development of certain gamete spawning scleractinian corals. *Coral Reefs* **5:** 111–116.

Babcock, R. C., G. D. Bull, P. L. Harrison, A. J. Heyward, J. K. Oliver, C. C. Wallace, and B. L. Willis. 1986. Synchronous spawnings of 105 scleractinian coral species on the Great Barrier Reef. *Mar. Biol.* **90:** 379–394.

Caspers, H. 1984. Spawning periodicity and habitat of the palolo worm *Eunice viridis* (Polychaeta: Eunicidae) in the Samoan Islands. *Mar. Biol.* **79:** 229–236.

Chia, F. S., and L. R. Bickell. 1983. Echinodermata. Pp. 545–620 in *Reproductive Biology of Invertebrates*, Vol. 2: Spermiogenesis and Sperm Function, K. G. and R. G. Adiyodi, eds. John Wiley and Sons, New York.

Denny, M. W., and M. F. Shibata. 1989. Consequences of surf-zone turbulence for settlement and external fertilization. *Am. Nat.* **134:** 859–889.

Dinnel, P. A., J. M. Link, and Q. J. Stober. 1987. Improved methodology for a sea urchin sperm cell bioassay for marine waters. *Arch. Environ. Toxicol.* **16:** 23–32.

Giese, A. C., and J. S. Pearse. 1974. Introduction: general principles. Pp. 1–49 in *Reproduction of Marine Invertebrates*, Vol. 1: Acoelomate and Pseudocoelomate Metazoans, A. C. Giese, and J. S. Pearse, eds. Academic Press, New York.

Grosberg, R. K. 1991. Sperm-mediated gene flow and the genetic structure of a population of the colonial ascidian *Botryllus schlosseri*. *Evolution* **45:** 130–142.

Harrison, P. L., R. C. Babcock, G. D. Bull, J. K. Oliver, C. C. Wallace, and B. L. Willis. 1984. Mass spawning in tropical reef corals. *Science* **223:** 1186–1189.

Heyward, A. J., and R. C. Babcock. 1986. Self- and cross-fertilization in scleractinian corals. *Mar. Biol.* **90:** 191–195.

Heyward, A. J., and J. D. Collins. 1985. Growth and sexual reproduction in the scleractinian coral *Montipora digitata* (Dana). *Aust. J. Mar. Freshw. Res.* **36:** 441–446.

Heyward, A. J. 1988. Reproductive status of some Guam corals. *Micronesica* **21:** 272–274.

Heyward, A. J., K. Yamazato, T. Yeemin, and M. Minei. 1987. Sexual reproduction of coral in Okinawa. *Galaxea* **6:** 331–343.

Hodgson, G. 1988. Potential gamete wastage in synchronously spawning corals due to hybrid inviability. *Proc. 6th Int. Coral Reef Symp., Townsville* **2:** 707–714.

Johannes, R. E. 1978. Reproductive strategies of coastal marine fishes in the tropics. *Environ. Biol. Fishes* **3:** 65–84.

Kubota, H. 1981. Synchronisation of spawning in the crinoid *Comanthus japonica*. Pp. 69–74, in *Advances in Invertebrate Reproduction*, W. H. Clark, Jr., and T. S. Adams, eds. Elsevier-North Holland, New York.

Levitan, D. R. 1991. Influence of body size and population density on fertilization success and reproductive output in a free-spawning invertebrate. *Biol. Bull.* **181:** 261–268.

Levitan, D. R., M. A. Sewell, and Fu-Shiang Chia. 1992. How distribution and abundance influence fertilization success in the sea urchin *Strongylocentrotus franciscanus*. *Ecology* **73:** 248–254.

Lillie, F. 1915. Studies of fertilization. VII. Analysis of the fertilizing power of sperm suspensions of *Arabacia*. *Biol. Bull.* **28:** 229–251.

Oliver, J. K., and B. L. Willis. 1987. Coral-spawn slicks in the Great Barrier Reef: preliminary observations. *Mar. Biol.* **94:** 521–529.

Oliver, J. K., R. C. Babcock, P. L. Harrison, and B. L. Willis. 1988. Geographic extent of mass coral spawning: clues to ultimate factors. *Proc. 6th Int. Coral Reef Symp., Townsville* **2:** 803–810.

Pearse, J. S., D. J. McClary, M. A. Sewell, W. C. Austin, A. Perez-Ruzafa, and M. Byrne. 1988. Simultaneous spawning of six species of echinoderms in Barkley Sound, British Columbia. *Int. J. Invert. Reprod. Dev.* **14:** 279–288.

Pennington, J. T. 1985. The ecology of fertilization of echinoid eggs—the consequences of sperm dilution, adult aggregation and synchronous spawning. *Biol. Bull.* **169:** 417–430.

Richmond, R. H., and C. L. Hunter. 1990. Reproduction and recruitment of corals: comparisons among the Caribbean, the tropical Pacific and the Red Sea. *Mar. Ecol. Prog. Ser.* **60:** 185–203.

Schuel, H. 1984. The prevention of polyspermic fertilization in sea urchins. *Biol. Bull.* **167:** 271–309.

Sprung, M., and B. L. Bayne. 1984. Some practical aspects of fertilizing the eggs of the mussel *Mytilus edulis*. *J. Cons. Int. Explor. Mer.* **41:** 125–128.

Willis, B. L., R. C. Babcock, P. L. Harrison, J. K. Oliver, and C. C. Wallace. 1985. Patterns in the mass spawning of corals on the Great Barrier Reef from 1981 to 1984. *Proc. 5th Int. Coral Reef Congr., Tahiti* **4:** 343–348.

Yund, P. O. 1990. An *in situ* measurement of sperm dispersal in a colonial marine hydroid. *J. Exp. Zool.* **253:** 102–106.

Reference: *Biol. Bull.* 183: 418–432. (December, 1992)

Reproductive Integration in Reef Corals

KERYEA SOONG[1] AND JUDITH C. LANG[2]

[1]*Division of Biological Sciences, University of Texas, Austin, Texas 78712, and*
[2]*Texas Memorial Museum, University of Texas, Austin, Texas 78705*

Abstract. The extent of colonial integration in structurally simple animals like scleractinian corals is poorly understood. We have used sexual reproductive characters (location of fertile polyps and colony size at maturation) to assess colony-level individuality, *i.e.*, the development, in coral colonies, of characters above the polyp level. Ten morphologically-diverse species of reef corals were used: *Acropora cervicornis, A. palmata, Diploria clivosa, D. strigosa, Favia fragum, Montastrea cavernosa, Porites astreoides, P. furcata, Siderastrea radians,* and *S. siderea.*

In no species were equally fertile polyps homogeneously distributed throughout a colony. Most inhomogeneities of fertile polyps could be attributed to intra-colony position or ontogenetic effects. The results of simple manipulations simulating natural wounds in three massive species strengthen the evidence that the position of polyps within a colony determines fertility.

Small colonies are not reproductive. Puberty size (colony size at maturation) could be explained by the infertility pattern along the colony margin, which does not require colony-level integration. Shape-related growth constraints could also produce the puberty size patterns found in massive corals. Infertility in the short radial polyps of *A. palmata* and in the axial polyps of *A. cervicornis* provided the only clear evidence of reproductive integration in this study: both are related to a morphological characteristic (polyp dimorphism) commonly associated with integration in colonial invertebrates.

Introduction

Colonial corals are composed of iterated units that usually originate from a single zygote. The degree of integration of colonial animals has long been the focus of scientific interest (Beklemishev, 1969; Hubbard, 1973; Sandberg, 1973; Rosen, 1979; Ryland, 1979; Shelton, 1979; Chapman, 1981; Mackie, 1986; Harvell, 1991). The objective of this study is to understand the extent to which the modules (*e.g.*, zooids, polyps, *sensu* Chapman, 1981) of a colony are interdependent and act as one unit; *i.e.*, how much individuality a colony has attained. Increasing individuality at the colony or genet level sets a higher stage at which selection could operate directly (Schopf, 1973; Buss, 1987).

Colonies of hydrozoans, bryozoans, and some other marine invertebrates are polymorphic, with two or more kinds of modules, each of which is capable of some vital functions (Hyman, 1940). A certain degree of integration is necessary in polymorphic colonies since differentiated modules cannot exist on their own. Indeed, an evolutionary tendency towards higher integration exists in colonial organization, at least in some lineages (Beklemishev, 1969; Boardman and Cheetham, 1973; Coates and Oliver, 1973; Coates and Jackson, 1985).

When modules are isomorphic and presumably have the same ability to perform all necessary living functions (Hyman, 1940), the level of individuality achieved by a colony is less obvious. For example, most colonial species of the highly successful scleractinian reef corals are composed of morphologically similar polyps. Differentiation of polyps does occur in some species (Veron, 1981; Foster, 1985), such as acroporids, which show a considerable degree of morphological variation between the axial polyps at their branch tips and the radial polyps that develop on their walls (Veron and Wallace, 1984).

Morphologically identical polyps that are produced by extratentacular budding in some colonies have been termed individuals (Duerden, 1902; Wells, 1973). Most colonial corals are classified as aggregates of independent polyps, since polypal (or rather its skeletal counterpart, the corallite) attributes constitute most of the taxonomic

Received 21 February 1992; accepted 31 July 1992.

Present address of Keryea Soong: Institute of Marine Biology, National Sun Yat-sen University, Kaohsiung, Taiwan (80424), Republic of China.

characters of scleractinian species (Vaughan and Wells, 1943; Wells, 1956). This line of thinking—*i.e.*, that coral colonies are merely aggregates of polyps—would appear to be justified by the plasticity of gross colony shape (Barnes, 1973; Foster, 1979; Veron and Pichon, 1982) and the indeterminate growth (Sebens, 1987) of most reef coral colonies.

However, a certain degree of functional integration may occur even within the structurally simple reef corals. For example, polyp retraction is coordinated within colonies of some species (Shelton, 1982); soluble organic compounds and Ca^{++} are translocated among polyps (Pearse and Muscatine, 1971; Taylor, 1977), and skeletal regeneration tends to restore symmetry of colony shape (Stephenson and Stephenson, 1933; Connell, 1973; Loya, 1976). One might conclude that colonies act as individuals. Moreover, ecologists tend to treat whole colonies as individuals (Connell, 1973; Hughes, 1984; Chornesky, 1989).

The above contrasting views about whether a coral colony is an aggregation of polyps or an integrated unit have yet to be reconciled. In comparing species, inferences of integration have been based on morphological characters, because function and structure are often correlated. In reef corals, branching colony shapes, dimorphic polyps, intratentacular budding (especially when it is incomplete, as in the meandroid condition), common (cerioid) walls, perforations in walls, and a well-developed coenosarc (soft tissues not belonging to individual polyps) are all thought to provide evidence of integration (Table I). Few data are available to test these assumptions. However, Hubbard (1973) found sediment-shedding ability, an expression of behavioral integration, to be greater in meandroid corals than in other corals which are considered less integrated morphologically.

In this study sexual reproductive characters were used to assess the nature of coloniality in reef corals. From an evolutionary point of view, the integration of sexual reproductive (hereafter called reproductive) activities within a coral colony should present no conflict among polyps, since all the constituent polyps are presumably of the same genotype [but see Buss (1982) for a discussion of the likely effects of somatic mutations]. Reproduction has been studied for many years in scleractinian corals (Duerden, 1902; Vaughan, 1909), but most research has concentrated on population level characteristics, *e.g.*, sexuality, reproductive mode, and spawning time (see reviews by Fadlallah, 1983; Harrison and Wallace, 1990; Richmond and Hunter, 1990). In some species, fertile polyps are distributed unevenly within the colony (Harrigan, 1972; Wallace, 1985; Kojis, 1986; Chornesky and Peters, 1987). Moreover, colony size, rather than age, is the primary factor determining reproductive status in two species (Kojis and Quinn, 1985; Szmant-Froelich, 1985). These two phenomena (fertile polyp location and fertile colony size) might be used as evidence for reproductive integration since, in each case, a reproductive character appears to be expressed beyond the level of single polyps.

In each of the ten morphologically diverse species of reef corals studied, we found uneven distribution of fertile polyps in the colony, and colony size-related maturation. Nonetheless, we argue that, except for the dimorphic polyps of *Acropora*, each of these patterns could have a simpler explanation. Indeed, at present there is little unamunambiguous evidence for reproductive integration in the isomorphic genera of reef corals.

Materials and Methods

Within colony infertility—observations

Ten species of shallow water corals (Table I) were monitored for reproductive activities along the Caribbean coast

Table I

Characteristics postulated to reflect potentially higher levels of morphological integration

Species	Branching	Dimorphic	Extratentacular budding	Meandroid	Common wall	Perforate walls	Coenosarc
Acropora cervicornis (Lamarck)	Y	Y	Y	N	N	Y	Y
Acropora palmata (Lamarck)	Y	Y	Y	N	N	Y	Y
Porites furcata Lamarck	Y	N	Y	N	Y	Y	N
Porites astreoides Lamarck	N	N	Y	N	Y	Y	N
Diploria clivosa (Ellis and Solander)	N	N	N	Y	Y	N	N
Diploria strigosa (Dana)	N	N	N	Y	Y	N	N
Siderastrea radians (Pallas)	N	N	Y	N	Y	N	N
Siderastrea siderea (Ellis and Solander)	N	N	Y	N	Y	N	N
Montastrea cavernosa (Linnaeus)	N	N	Y	N	N	N	N
Favia fragum (Esper)	N	N	N	N	N	N	N

"Y" implies higher integration than "N" (Wells, 1973; Jackson, 1979; Oliver and Coates, 1987). Species are ranked according to the number of "Y"s.

of Panama between July, 1987, and August, 1988. During their respective reproductive seasons, whole colonies (in the case of species of small size), or samples from various parts of large colonies were collected at random, preserved, and decalcified by means of standard techniques (Soong, 1991).

Except for *Favia fragum*, fecundity was estimated after dissection by directly counting eggs, or measuring the size of gonads with a dissecting microscope or, for species with small gonads, by histological preparations. In *F. fragum*, planulae are easier to observe than eggs, so the number of planulae per polyp were counted under the dissecting microscope as an estimate of brood size or fecundity. For all species, the identity of ovaries, spermaries, and planulae (if present) were confirmed by histology (Soong, 1991).

Owing to numerous instances of partial colony mortality, edge zones in *Siderastrea siderea* can occur virtually everywhere over the surface. Therefore, data for this species were collected separately for colony margins on both vertical and horizontal surfaces. Variations in tissue thickness within colonies were noticed in five species; those in *Siderastrea* spp. and *Porites furcata* were measured under a dissecting microscope.

Within colony infertility—manipulations

A series of field experiments was initiated to determine the possible causes of the infertile colony margins found in three species of massive corals. The scheme basic to all the manipulations was to create artificial margins across the centers of healthy, undamaged colonies (*Siderastrea siderea*—20–70 cm in diameter; *Porites astreoides*—15–25 cm; and *S. radians*—3.5–8 cm). A cut about 1 cm deep and 2 mm wide was made across the entire midregion of each colony with a hacksaw, effectively severing all soft tissue connections between the two sides of the cut. In one group consisting of 10 specimens per species, ("tissue cut"), the two halves remained connected by dead skeletal material. In a second group of 10 colonies ("cut and fill"), underwater epoxy (Birkeland, 1976) was used to fill and cover the open wounds and to fill the gaps created by sawing. A third group of 10 colonies ("total cut;" 20 colonies were used in *S. radians*) were separated into halves when the skeletal connection was completely severed. After manipulation, all colonies remained larger than the estimated puberty size (see below) for the species. This experiment was initiated in February–March 1988, before the start of gametogenesis in *S. siderea*. The other two species reproduce year round in Panama (Soong, 1991). Patterns of fertile polyp distribution were determined by dissection or histology four to five months later, at the end of July, and were compared with undisturbed colonies collected in the same habitat. The reverse experiment—tying two marginal pieces together to create an artificial "central condition"—was not employed, because preliminary trials showed that the trimming necessary to fit the pieces together removed the original marginal polyps.

Relationship between colony size and maturation

When a species was in reproductive condition (Soong, 1991), one sample of tissue (about 5×5 cm) was collected from the center of healthy-looking colonies of various known sizes. All specimens were examined after fixation, decalcification, and dissection. In species with small, inconspicuous gonads (*P. furcata, P. astreoides* and *Diploria clivosa*), histological slides were prepared from each specimen; in the remainder, histological confirmation of reproductive condition was limited to some randomly chosen specimens. For brooding species, reproductive data were collected during various months throughout the year. Fertility in the broadcasting species was assessed within one to two months of their annual spawning periods. Each sample was rated qualitatively as either infertile (no gonads), or fertile (gonads or planulae present in the sample). If colony size data were available, samples collected for study of colony infertility were also used to assess maturation.

Colonies of each species were ranked, from smallest to largest, and the size at which most colonies become mature was then assessed. Colony size was calculated as the surface area: the product of the maximal length and width of the living tissue (both dimensions measured in the field). In *A. palmata*, colony size was estimated by summation of the surface area of all the branches and the base. In the ramose *Acropora cervicornis* and *P. furcata*, the lengths of the living branches were taken as a measure of size. Puberty size was defined operationally as equal to the surface area or live-branch length of the smallest colony (or branch) in the first group of 20 consecutively ranked colonies (or branches) of which 90% or more were fertile.

Sample sizes in these studies ranged from 41 in *D. strigosa* (relatively rare) to 501 in *S. radians*.

Results

Within colony infertility—observations

Marginal areas. In no species were equally fertile polyps homogeneously distributed, and infertile polyps were generally associated with colony margins (summary in Table II). *Favia fragum* was the only massive species studied in which marginal polyps were fertile. These marginal polyps also carried planulae (average 73% of marginal polyps, n = 77 colonies, each colony large enough to have five central polyps), although their mean brood size was significantly lower than that of the central polyps (Wilcoxon's signed-ranks test, $T_s = 55$, $P < 0.01$, n = 77

Table II

Location of infertile polyps in fecund colonies of ten species of reef corals

Species	Colony shape	Location of infertile polyps	No. of colonies
Favia fragum	Massive	none, but 27% of marginal polyps lack planulae (*vs.* 7% of central polyps lacking planulae)	77
Siderastrea radians	Massive	0 to 0.25–0.5 cm from margin (one to two rows of polyps)	65
Porites astreoides	Massive	0 to 0.5–1.5 cm from margin (three to 10 rows of polyps)	10
Montastrea cavernosa	Massive	0 to 0.5–1 cm from margin (one row of polyps)	16
Siderastrea siderea	Massive	0 to 0.7–2 cm from margin on horizontal surface (at least two rows of polyps); 0 to 1–4 cm from margin on vertical surface (more than three rows of polyps)	17
Diploria strigosa	Massive	0 to 1–3.5 cm from margin (meandroid and lacks distinct polyps)	12
Diploria clivosa	Encrusting	0 to 1–4 cm from margin (meandroid and lacks distinct polyps)	9
Acropora cervicornis	Branching	0 to 2–6 cm from tip, 0 to 1–4.5 cm from base; and any shaded areas along branches	26; 11
Acropora palmata	Branching	0 to 3–10 cm from tip at spawning; 0 to 2–3.5 cm from basal margin at spawning, shorter infertile zone earlier in the year	23; 8
Porites furcata	Branching	0 to 0.5 cm from tip, 0 to 1–3 cm from base (>50% of whole branch length)	178

colonies, Fig. 1). Regardless of how fertility was measured, all other massive corals had an infertile marginal area equivalent to the width of at least one polyp (Table II), as exemplified in *S. radians* (Fig. 2).

In *Siderastrea radians*, the frequency of fertile polyps showed no significant correlation with colony size, either in the marginal row (Spearman's r = 0.08, $P > 0.05$, n = 20), or in the penultimate row (Spearman's r = 0.40, $P > 0.05$, n = 20) of polyps. The infertile area of large colonies of *S. siderea* was significantly wider on vertical surfaces than on the corresponding horizontal surfaces of the same specimens (Sign test, n = 13, t = 0, $P < 0.01$). The width of these infertile areas, however, showed no significant correlation with colony size (vertical margin, Spearman's r = −0.15, $P > 0.05$, n = 21 colonies; horizontal margin, Spearman's r = −0.15, $P > 0.05$, n = 18 colonies). A gradient of increased fecundity was observed in the first few centimeters of the fertile region for horizontal surfaces (Fig. 3).

In branching species, the distribution of fertile polyps was clearly related to the growth axis of the branches. For example, in *Porites furcata*, fertile polyps were concentrated in the distal half of the branches, but their abundance decreased again near the growing tip (Fig. 4). Usually the basal margin of the branches was lighter in color,

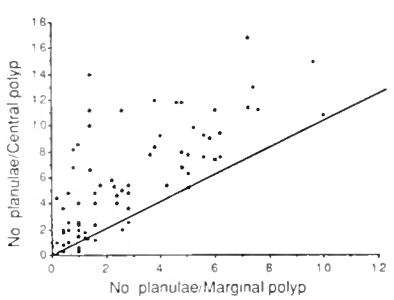

Figure 1. Brood sizes of central *versus* marginal polyps in *Favia fragum*. Mean number of planulae per polyp based on five marginal polyps per colony and (depending upon colony size) up to five central polyps per colony; each point represents one colony. The diagonal line indicates equal brood size in marginal and central polyps.

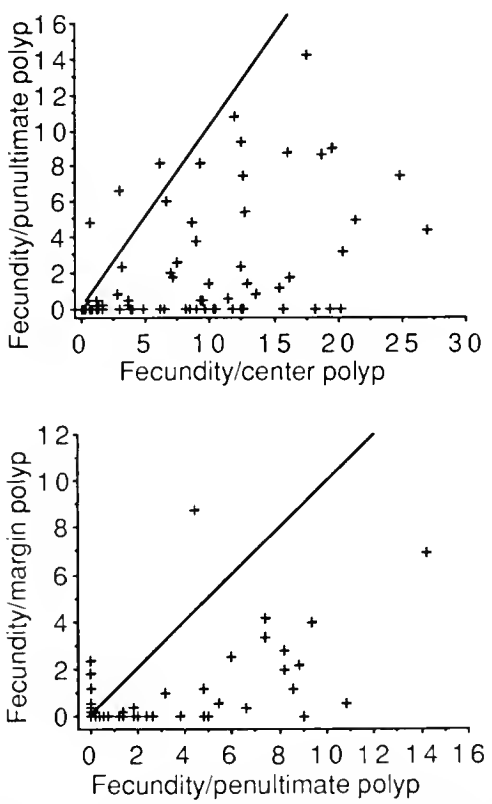

Figure 2. Fecundity of polyps within colonies of *Siderastrea radians*. Fecundity: mean number of eggs per polyp, based on five polyps per location in each colony. Penultimate polyp: row of polyps immediately adjacent to margin polyps. Difference significant among the three groups (Friedman test, T = 102.8, $P < 0.01$; pair-wise tests between any two groups also significant using Wilcoxon's signed-ranks test).

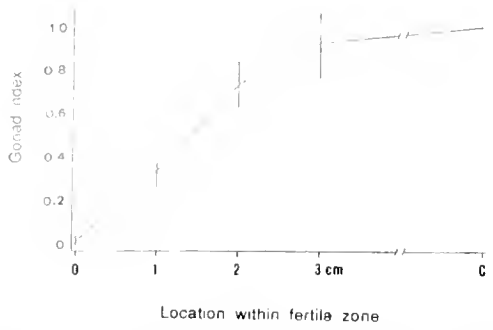

Figure 3. Fecundity gradient on horizontal surface of *Siderastrea siderea* Gonad index: mean gonad length × frequency of gonads (ovaries or spermaries), based on two randomly chosen mesenteries per polyp in each of ten randomly chosen polyps) at any given location relative to that in the center of the horizontal surface of the colony. Vertical bars represent the standard errors of the mean. 0: beginning of fertile zone, C: center of the horizontal surface. n = 8 male and 8 female colonies.

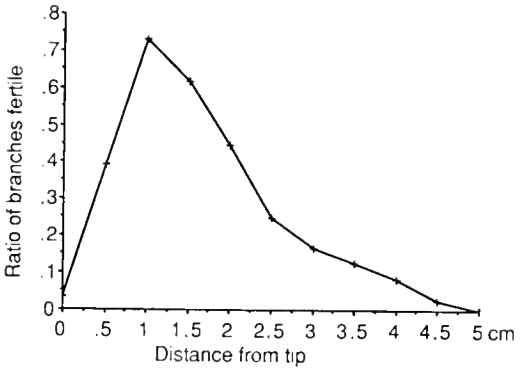

Figure 4. Probability of gonad occurrence along the branches of fertile, female *Porites furcata* At any position (at one cm intervals) along the branch, probability of gonad occurrence, *i.e.*, number of female branches having ovaries at that position relative to the total number of fertile, female branches checked; n = 178 branches.

presumably due to fewer endosymbiotic zooxanthellae. Soft tissue thickness also tapered toward the base, and the internal mesenterial filaments were degenerate.

In *Acropora cervicornis,* the large axial polyps and the basal tissues (1–4.5 cm from the base) of the branches were infertile, whereas gonads located within 2 to 6 cm of the branch tips always had smaller eggs than those in the mid-region of the branches (n = 21 branches).

In *A. palmata,* the pattern apparently changed with the annual reproductive cycle. When oogenesis was first noticed in February, small eggs were found in the whole colony. No gonads were present in the polyps that we presumed to have been produced after the onset of oogenesis. Infertile areas were observed in the encrusting bases (n = 5 colonies, end of July) and along the growing edges of branches (n = 3 colonies, shortly before the presumed spawning event in September).

Non-marginal areas. Relatively fine-scale variations were found within the fertile regions of some species. The few polyps of *F. fragum* undergoing intratentacular division (each with two discrete mouths enclosed by a common body wall) contained significantly more planulae than did five adjacent non-dividing polyps (Wilcoxon's signed-ranks test, $T_s = 2$, $P < 0.01$, n = 17 comparisons from 11 colonies). What are presumed to be young polyps within the non-marginal areas of *S. radians, S. siderea* and *P. furcata* could be identified in the colony, both from their fewer cycles of septa and their conical vertical profiles ("old" polyps have full cycles of septa and cylindrical vertical profiles). These young polyps were usually infertile, whereas intermediate-sized polyps carried some gonads, but were less fecund than adjacent, fully developed, cylindrical polyps (for *S. radians,* Table III; for *S. siderea,* Table IV; in both species, Wilcoxon's signed-ranks test, $T_s = 0$, $P < 0.01$). Small polyps carried eggs after reaching a tissue thickness of about 3.2 mm, and were estimated to be about eight months old, since the average skeletal increment of *S. siderea* in Panama is about 5 mm per year (H. Guzman, pers. comm.). The age of the infertile margins was more than 2 years old in *S. siderea,* judging from skeletal thicknesses (about 2 cm) at their vertical edges.

As described for Indo-Pacific acroporids (Wallace, 1978; Veron and Wallace, 1984), radial polyps on the upper surfaces of *A. palmata* could be classified into two types—ones with long polyp walls (thus exert), and others which have almost no walls. The frequency of fertile polyps was significantly higher in long polyps than in adjacent short polyps (5 large and 5 small polyps from each of 15 colonies, pooled, G = 66.2, $P < 0.01$). When only fertile

Table III

Fecundity of young and old polyps within the fertile area of Siderastrea radians

Colony	Number of eggs per polyp (sample size)	
	Old polyp	Young polyp
1	6.2 (5)	1.6 (5)
2	15.8 (5)	5.0 (5)
3	13.6 (5)	3.8 (5)
4	19.6 (5)	0 (5)
5	20.4 (5)	6.8 (5)
6	27.0 (5)	0 (5)
7	17.6 (5)	5.0 (5)
8	24.8 (5)	1.6 (5)
9	15.4 (5)	1.7 (5)
10	18.2 (5)	3.4 (5)
11	21.4 (5)	4.6 (5)

Table IV

Relative fecundity of polyps within fertile colonies of Siderastrea siderea

Colony	Relative fecundity		
	Large polyp	Medium polyp	Small polyp
1	100% (10)	1% (5)	0% (2)
2	100% (10)	56% (2)	1% (7)
3	100% (10)	15% (4)	9% (5)
4	100% (10)	10% (4)	1% (4)
5	100% (10)	0% (7)	—
6	100% (10)	0% (1)	0% (4)
7	100% (10)	40% (6)	1% (9)
8	100% (10)	0% (3)	0% (11)
9	100% (10)	—	3% (3)
10	100% (10)	0% (3)	—

Number in parenthesis indicates sample size.

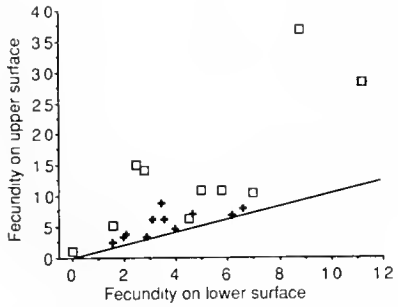

Figure 5. Comparison of fecundity between the upper and the lower surfaces of *Acropora palmata*. Mean area fertility (square): mean number of fertile polyps per cm^2, based on 2-32 cm^2/colony. Mean fertile polyp fecundity (cross): mean number of eggs per fertile polyp, based on 10 to 166 polyps per colony. The diagonal line indicates equal numbers on both surfaces.

polyps were compared, the number of eggs per fertile polyp was also significantly higher in the long polyps (Wilcoxon's signed-ranks test, $T_s = 0$, $P < 0.05$, n = 6 colonies, 6–14 polyps/colony). Short polyps, however, were more than 50% of the polyps on the upper surfaces (n = 5 colonies). Along the mid-branch regions, gonads were absent in areas where polyp density was low and the soft tissues were relatively thin, possibly as a result of shading (n = 11 colonies). Regenerated portions, where live tissues lack polypal mouths, were also infertile.

The upper surfaces of branches of *A. palmata* had a much higher fecundity than lower surfaces, as there were more fertile polyps per unit surface area (Wilcoxon's signed-ranks test, $T_s = 0$, $P < 0.01$, n = 10 colonies, Fig. 5), and larger numbers of eggs within fertile polyps (Wilcoxon's signed-ranks test, $T_s = 0$, $P < 0.01$, n = 11 colonies, Fig. 5). In addition, the soft tissues on the upper surfaces of *A. palmata* were at least twice as thick as those of the lower surfaces (measured from decalcified soft tissues), and their corresponding rate of vertical skeletal increment was about twice as great, as evidenced by growth bands revealed by X-ray of skeletal slabs from seven colonies. Central polyps on the horizontal surfaces of *S. siderea* also had thicker tissues (unpub. data) and longer gonads, and a proportionately larger number of mesenteries were carrying gonads than those on vertical surfaces. Thus the fecundity of horizontal polyps was significantly higher than that of the vertical polyps (Wilcoxon's signed-ranks test, $P < 0.01$, n = 16 colonies, Fig. 6).

Within colony infertility—manipulations

One month after the initiation of each experiment, colonies were checked for possible adverse responses to manipulations. Except for one colony of *S. siderea* which showed some discoloration and had become pink along its new artificial margin, all others looked normal, with no visible wound-related necroses. (This marginal discoloration also occurs naturally in some colonies of *S. siderea*). Seven specimens of *S. radians* were collected, and dissection revealed that the severed polyps still contained gonads.

Success retrieving the experimental colonies varied among species and treatments 5–6 months after manipulation. In *S. siderea*, only some (n = 8) of the "tissue cut" and "total cut" specimens were recovered, so the data for all the manipulated colonies were pooled. In *P. astreoides*, the only species with notable new growth, the wounds of simple "tissue cut" specimens were covered by a thin layer of regenerating tissues, and the "total cut" specimens showed some new growth along the margin.

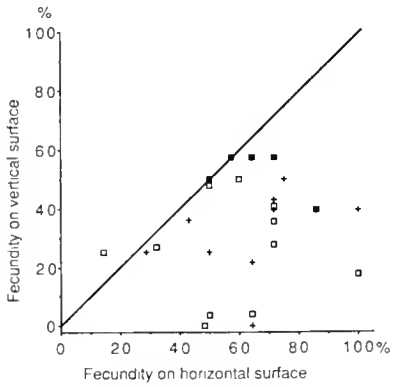

Figure 6. Comparison of fecundity between vertical and horizontal surfaces of *Siderastrea siderea*. For each surface on each colony, relative gonad lengths (cross): mean gonad length based on two randomly chosen mesenteries per polyp in 10 randomly-chosen polyps per sample, relative to the largest estimate of mean gonad length from any location in any colony. Relative fecundity (square): fecundity (see gonad index in Fig. 3 legend) relative to largest estimate of fecundity in any colony.

As an artificial margin was not successfully maintained in the above treatments, only the "cut and fill" specimens were checked for gonads. Seven "cut and fill," eight "tissue cut" and 15 "total cut" specimens were retrieved for *S. radians* and lumped together, since all three treatments showed the same trend, *i.e.*, the fecundity of the artificial margins was intermediate between that of the centers and the natural margins (significant differences with Wilcoxon's signed-ranks test: center > artificial margin, $T_s = 0$, $P < 0.01$, n = 29 colonies; artificial margin > natural margin, $T_s = 3.5$, $P < 0.01$, n = 11 colonies).

Except in *S. radians*, an infertile zone was found along every artificial margin. In *S. siderea*, the width of this newly generated infertile zone was comparable to the horizontal margins in natural colonies (difference insignificant, Wilcoxon's two-sample test, $U_s = 195$, $P > 0.05$, $n_1 = 18$, $n_2 = 16$, two-tail), and most (16/18) of the artificial margins had more than one row of infertile polyps. In the "cut and fill" specimens of *P. astreoides*, no significant difference was found between the infertile widths of the natural and manipulated margins (Wilcoxon's two-sample test, $U_s = 69.5$, $P > 0.05$, $n_1 = 10$, $n_2 = 10$, $P > 0.05$, two-tail). In *S. radians*, the polyps along the artificial margins remained fertile, although their fecundity was significantly lower than that of centrally located polyps in the same colonies (Wilcoxon's signed-ranks test, $T_s = 0$, $P < 0.01$, Table V).

Table V

Fecundity of polyps after manipulation in Siderastrea radians

	Number of eggs per 20 mesenteries						
Colony #	Center	Natural margin	Artificial margin	Colony #	Center	Natural margin	Artificial margin
1	20	13	—	16	12	6	—
2	20	7	0	17	12	3	—
3	20	2	2	18	11	5	7
4	18	2	—	19	10	1	0
5	17	17	—	20	9	—	0
6	17	8	—	21	9	3	—
7	17	3	—	22	8	8	0
8	16	15	—	23	8	3	—
9	16	6	0	24	8	3	—
10	15	14	—	25	8	0	—
11	15	2	—	26	7	3	—
12	15	2	0	27	6	2	0
13	14	7	0	28	3	3	—
14	13	6	—	29	3	2	0
15	13	5	—	30	3	0	—

Relationship between colony size and maturation

All ten species of western Atlantic reef corals studied showed size-correlated reproductive activities, with larger colonies having much higher fertility rates (Table VI).

Estimates of puberty size ranged from 2.3 cm^2 to 195 cm^2 in the seven species of massive reef corals (Table VII). The puberty size estimate of the massively branching *A. palmata* was very large (1600 cm^2). Puberty size estimated as branch length was 17 cm in *A. cervicornis*, and 1.4 cm in *P. furcata*.

Discussion

An integrated colony with polyps specialized for various roles would seem to be adaptive in reef environments, even in the absence of obvious morphological differentiation. Caution should be exercised in inferring integration, however, as exemplified by the clonal sea anemone, *Anthopleura elegantissima*, where an individual clonemate may have a different size, division rate, defensive tissues, and fertility according to its position in a patch (Francis, 1976). Since clonemates of *A. elegantissima* are separated, these differences develop in the absence of any connections after the polyps have divided. In a coral colony with morphologically connected polyps, heterogeneous patterns may similarly represent developmental stages or the independent responses of polyps to their own surroundings. Colony-level integration should be invoked only if inhomogeneities in form or function cannot be explained by microenvironmental or ontogenetic effects.

In the following sections, patterns of reproductive unevenness found in different species of colonial corals are discussed in relation to presumptive environmental or ontogenetic factors or, in the two acroporids, used as evidence for integration (Table VIII).

Within colony infertility patterns—marginal areas

Regardless of colony size and shape, the results for these ten species clearly indicate that the marginal polyps differ reproductively from the central polyps of the same colonies. What is the reason for this marginal pattern? Chornesky's (1989) observations may offer a good environmental explanation. Her study of natural encounters between colonies of *Porites* and *Agaricia*, showed that the margins of certain corals are in a dynamic state of temporary advances and retreats. Not only is the energy requirement for these confrontations potentially high (Rinkevich and Loya, 1985), but the continuing physical presence of the tissues themselves is less certain. In addition to competition, encroaching predators, such as snails, sea stars, and fire worms are more likely to attack at colony margins (J. Hayes, pers. comm.). An investment in somatic tissues, which can expand or fight along the margin, is presumably more important than one in reproductive tissues, which only increases the stake upon losing (Hughes and Jackson, 1985).

In the manipulated specimens of *S. siderea*, *S. radians*, and *P. astreoides*, some form of reduced fertility appeared in all artificially generated margins (see Results). Polyps

Table VI

Frequency of fertile colonies in each collected size class

Species		Size class (surface area of live colony; cm^2)						
		0–4	4–15	15–60	60–250	250–1000	1000–4000	>4000
Favia fragum	% fertile	63	93	94	—	—	—	—
	n	38	74	17	—	—	—	—
Siderastrea radians	% fertile	50	86	97	100	—	—	—
	n	64	206	208	23	—	—	—
Porites astreoides	% fertile	0	9	19	79	94	100	—
	n	4	12	26	47	55	11	—
Diploria clivosa	% fertile	0	0	40	57	93	100	100
	n	1	5	5	14	29	23	3
Diploria strigosa	% fertile	—	—	20	42	100	100	100
	n	—	—	5	12	9	6	9
Montastrea cavernosa	% fertile	—	0	100	92	100	94	100
	n	—	1	6	13	20	18	5
Siderastrea siderea	% fertile	0	0	0	47	96	100	96
	n	3	4	7	19	27	13	23
Acropora palmata	% fertile	—	0	0	7	31	43	88
	n	—	4	9	14	16	7	33
		Size class, branch length (cm)						
		<1	1–2	2–7	5–9	9–13	13–17	>17
Porites furcata	% fertile	0	77	94	—	—	—	—
	n	5	39	252	—	—	—	—
Acropora[1] *cervicornis*	% fertile	—	—	—	0	38	59	89
	n	—	—	—	4	13	17	18

"n" is the number of colonies examined.
[1]: Only thick branches (>1 cm diameter).

along the artificial margins originally had been in the center of colonies, and would be expected to be fully fertile had there been no manipulations. Alternatively, these results could be attributed to wounding caused by the operation itself, rather than the changed location of the polyps. Polyps not operated upon but close to the artificial margins, however, also became infertile in *P. astreoides* and *S. siderea*. Thus, regardless of its causes, the experimentally-induced infertile marginal response was not simply due to the age of the polyps.

The infertile bases of the branching *A. cervicornis* and *P. furcata* are subject to adverse environments, due to reduced access to water flow and sunlight. Encroachment by fouling organisms is a constant threat here, particularly to *P. furcata* which has compact colonies. The nearly infertile bases in branches of *P. furcata* make up more than 50% of the live tissue cover (Fig. 5), and all are older polyps, raising the alternative possibility of polyp senescence (Palumbi and Jackson, 1983). In *P. furcata* the fate of individual polyps may be predetermined. Live branches of *P. furcata* average 3.5 cm in length (pers. obs.), and their annual extension in the study area is about 2.0–3.7 cm (Meyer and Birkeland, 1975); hence the life expectancy of an individual polyp is about one to two years. Since oogenesis and embryogenesis are lengthy processes, basally located polyps should not be able to complete their investment in reproduction before dying. But the microenvironment near the branch bases may also deteriorate to the point that developing gonads can no longer be supported in the polyps.

The infertile tips of three branching species (*P. furcata*, *A. cervicornis* and *A. palmata*) could be the result of a time constraint, since all the polyps (except the terminal axial polyps in *Acropora*) are young, and oogenesis takes at least six months in the two acroporids (Soong, 1991).

The prominent, non-reproductive axial polyps of *A. cervicornis* indicate colony-level integration. Axial polyps are not young since they give rise to the radial polyps in the branch. They have less chlorophyll and lower photosynthetic rates, yet higher rates of skeletal deposition, than the radial polyps (Goreau, 1963). The nutrients that axial polyps receive from radial polyps (Pearse and Muscatine, 1971; Taylor, 1977; Gladfelter, 1983) presumably contribute to the fast rates of branch extension in

Table VII

Reproductive [illegible] species of reef corals in Panama

Species	No. of colonies	Size range of samples (cm^2)	Puberty size:area (length)	Smallest reproductive colony l × w (cm)	Width of infertile margin: median; range (cm)
Non-branching					
Favia fragum	129	0.25–19.6	2.3 (1.5)	0.6 × 0.6	none
Siderastrea radians	501	0.2–128	4.0 (2)	1.3 × 1.1	0.25; 0.25–0.5
Porites astreoides	155	4–2,530	70 (8.4)	3 × 2	1; 0.5–1.5
Montastrea cavernosa	63	12–10,000	20 (4.5)	5 × 4	1; 0.5–1
Diploria clivosa	79	4–5,400	12 (11)	7 × 5	2; 1–4
Siderastrea siderea	117	2–20,164	156 (12.5)	9 × 7	1; 0.7–2 (horizontal surface) 2; 1–4 (vertical surface)
Diploria strigosa	41	36–62,500	195 (14)	7 × 6	2; 1–3.5
Branching					
Acropora palmata	84	9–40,000	1600	16 × 8	tip: 5; 3–10 base: 3; 2–3.5
Acropora cervicornis	52	5–29	17*	9 (length)	tip: 4; 2–6 base: 3; 1–4.5
Porites furcata	296	0.6–6	1.4*	1 (length)	~50% branch length

* Size measured in cm^2 of surface area of live colonies, except for *A. cervicornis* and *P. furcata*, for which branch length in cm is given.

acroporids (Shinn, 1976; Oliver *et al.*, 1983; Tunnicliffe, 1983). Apparently, the differentiation of axial polyps is not terminal, since non-growing axials do reproduce (Oliver, 1984).

Within colony infertility patterns—non-marginal areas

New polyp generation, whether by intra- or extra-tentacular budding, may take a long time to complete in scleractinian corals (Stephenson and Stephenson, 1933), since skeletal development underlying the soft tissues is involved (Goreau, 1963; Barnes, 1973). But in *F. fragum*, which buds intratentacularly, reproductive ability is not compromised during polyp multiplication and colony growth. Extratentacular budding, occurring in most of the other corals of this study, produces a mosaic of polyps of various sizes and developmental stages. Young polyps are infertile, and we suspect that their other functions, *e.g.*, feeding, may also be rudimentary.

The s[illegible] polyps on the upper surface of *A. palmata* have a di[illegible]hed morphology and a lower fertility than the long p[illegible]ue, perhaps, to crowding. On the under surfaces, wi[illegible]lyp density is less than 50% of that on the upper sur[illegible] polyp size is much more homogeneous (pers. obs.). S[illegible] polyps on the upper surfaces do not appear to be you[illegible] they are scattered throughout the upper surface of the branch, and parallel corallite growth revealed by X-radiographs indicates that they are unlikely to have been generated later than the long polyps (pers. obs.). Although their function has not been determined, the infertility of the short radial polyps in *A. palmata*

Table VIII

Explanations for uneven distribution of fertile polyps within colonies

Explanations	Based on	Phenomenon
Environmental effects	Observations and Manipulations	1. infertile colony margins: most species 2. low-fertility on vertical surface of colonies: *S. siderea* 3. low-fertility on shaded surfaces of colonies: *A. palmata*
Ontogenetic effects	Observations	1. juvenile polyps budded extratentacularly 2. juvenile polyps along colony margins 3. juvenile polyps at tips of branching corals
Integration	Observations	1. short radial polyps: *A. palmata* 2. axial polyps: *A. cervicornis*

presumably represents a second example of reproductive integration in acroporid corals.

Relationship between colony size and maturation

Colony size acts as another colony-level reproductive character. As a simple example, young polyps estimated at one to two years old (see Table III, IV) in a large colony of *S. siderea* carry eggs, but much older polyps in a small colony below puberty size for its species are infertile. But how do individual polyps "know" the size of their colony?

After reaching a certain minimum colony size, corals may start reproducing due to microenvironmental changes imposed upon each polyp. The polyps in a large colony simply experience a different environment from those in a small colony, and the combined effect on many polyps produces what appears to be a colony-level character. For example, as colonies of the marine hydroid *Podocoryne carnea* become larger and their zooids become denser, elevated levels of CO_2 in the center of the colony may induce the development of generative zooids which are responsible for sexual reproduction (Braverman, 1962; Braverman, 1963).

The distribution of fertile polyps provides a model for explaining puberty size. Small colonies may fail to reproduce, not because of their small sizes *per se*, but because virtually all of their polyps are marginally located. Hence no colony-level integration would exist. The above hypothesis would be falsified if: (1) no marginal infertility existed in large reproductive colonies; (2) the critical size at which a colony becomes reproductive is much larger than that predicted from the extent of the marginal infertility pattern; or (3) only specialized polyps are reproductive.

Of the seven massive corals studied here, six species have infertile margins, whereas marginal polyps in the small *F. fragum* are fertile but have a lower fecundity than the corresponding central polyps (Table VII). For each species, the smallest fertile colonies were recorded and its dimension compared to the width of its infertile margin (Table VII). If marginal infertility is directly additive, we would expect a colony with a radius greater than that of the width of the infertile margin to be reproductive, since (as in two *Siderastrea* spp.) there is no relationship between the width of the infertile margin and colony size. In most species, however, the smallest reproductive colonies are a little larger than is expected from this simple extrapolation of infertile margins. The additional infertility may be explained as follows.

In a small colony, any polyp is likely to be subject to marginal influences from all directions, whereas in a large colony marginal polyps at any location are less likely to be affected by environmental perturbations on the opposite margins of the colony. Moreover, as indicated by the gradient of increasing fecundity found in the first few centimeters of the fertile region, marginal effects on polyp fertility extend beyond the infertile marginal area. To be reproductive, therefore, a colony should be larger than the size obtained by simple extrapolation from its infertile margins.

In addition to the proposal about environmental and ontogenetic effects, at least one other hypothesis can explain the reproductive size effect without invoking colony integration. Using an idealized hemispherical, massive colony as a model, the number of polyps is directly proportional to the square of the radius of the colony, since all the polyps are on the surface of the colony; *i.e.*,

$$N = c \cdot r^2 \tag{1}$$

where N is the number of polyps, r is radius of the colony, and c is a constant. The number of polyps in the following year is approximately

$$N_{(t+1)} = c \cdot (r + a)^2 \tag{2}$$

where "a" is annual vertical skeletal increment, *i.e.*, the increase in radius of the hemispherical colony. The annual increase per polyp would be

$$\frac{c \cdot (r + a)^2 - c \cdot r^2}{c \cdot r^2} = \frac{2 \cdot r \cdot a + a^2}{r^2} \tag{3}$$

According to Equation (3), if the annual skeletal increment, "a" remains constant and is small relative to r, the per polyp growth rate will be decreasing as colony size (or r) increases (Fig. 7). In other words, if a colony increases in diameter at the same linear rate, and its shape remains the same, the investment of each polyp in somatic growth (polyp proliferation) would decrease with increasing colony size. Assuming energy intake per polyp is independent of colony size, the excess energy available to polyps in large colonies could be used in reproduction. The critical point, *i.e.*, whether skeletal increment "a" is constant, or at least does not increase throughout a coral's life span, is supported by numerous studies (Connell,

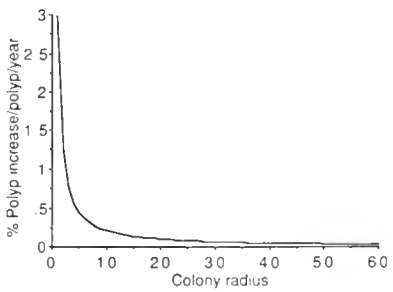

Figure 7. Model of the increase in polyp number as a function of the colony radius in a hemispherical colony. Unit of colony radius in terms of average annual skeletal increment.

1973; Nazaki *et al.*, 1978; Droffel, 1982; Hudson, 1985; Hughes and Jackson, 1985).

A closer look at the above hypothesis indicates that the curvature of the skeletal surface (Barnes, 1973), rather than colony size *per se*, is important in determining reproductive status. Given the same absolute vertical increment (or radial increase), a polyp in a colony of high curvature (usually a small colony) can invest more energy in growth since relatively more space will be available to add new polyps, whereas a polyp in a colony of low curvature (and usually large) would have little room for the addition of new polyps. (For the same reason, the lumpy surfaces present in large colonies of some species (Barnes, 1973; Isdale, 1977; Hughes and Hughes, 1986) effectively change the curvature of their surface and increase their surface area, presumably thereby maintaining the high growth rate of individual polyps.) Therefore, all of the observed patterns of uneven fertile polyp distribution in massive species are explicable without invoking integration.

In branching species, two factors are obviously important in the distribution of fertile polyps. The infertile tips in the three species studied are all young polyps (except for the axial polyps of acroporids). The infertile basal part of *A. cervicornis* and *P. furcata* are both associated with some degree of environmental degradation. The infertility of short branches in these two species could be explained by considering both an ontogenetic effect at the tips and an environmental effect at the bases. A branch would have to be long enough to have mid-regional polyps devoid of both effects to be reproductive.

Environmental and ontogenetic effects, however, cannot satisfactorily explain the size effect in *A. palmata*. Colonies with encrusting bases only (no standing branches) generally are small and non-reproductive, but none of the 13 medium sized (100–625 cm^2) encrusting colonies were fertile, and only one of nine colonies with small branches (100–644 cm^2) carried gonads. In large colonies with several fully developed branches (>3000 cm^2), however, marginal polyps along encrusting bases and growing edges of branches have been observed to carry eggs at the beginning of oogenesis. Obviously, the difference in fertility between a small and large colony of *A. palmata* is more than a simple combination of environmental and ontogenetic effects acting on individual polyps. Reproductive integration in colonies of *A. palmata* is likely

Morphological integration

As mentioned in the Introduction, many morphological characters have been proposed as being correlated with integration (see Table 1). Summarizing these characters, the species studied here seem to constitute a gradient, with the two acroporids having the highest potential for being morphologically integrated, and *F. fragum* having the lowest potential. We will assess the extent to which these characters appear to relate to reproductive integration.

Colony shapes. Although relationships between colony shape and extent of integration have often been proposed (Jackson, 1979; Silen, 1981; Oliver and Coates, 1987; McKinney and Jackson, 1989), shape itself does not necessarily imply any given level of organization, as exemplified below.

Graus and Macintyre (1976, 1982) found that realistic growth forms of *Montastrea annularis* can be simulated simply by programming polypal growth rates to vary as a function of the intensity and distribution of light, which itself varies with location on a colony and depth. In these simulations different colony shapes are generated as a result of individual polyps responding independently to environmental gradients across a colony. A simple "rule change" at the module level, or some environmental variation, can easily produce various complex colony shapes without invoking higher levels of integration (see also Harper and Bell, 1979; Bell, 1986; Gottlieb, 1986, for modular plants).

In branching species, new polyps are concentrated at the growing tips, and polypal age increases down the branch from the tip. The segregation of young and old polyps in these colonies could easily initiate the development of colony integration through temporally differentiated life history traits of individual modules (Bonner, 1965). For example, the translocation of materials to the growing tips in *Acropora* (Pearse and Muscatine, 1971), a clear case of colony integration, could have evolved as a character of individual polyps, in which polypal age or developmental stage is the factor determining whether to export or import nutrients. Similarly, polyps could be genetically programmed to grow when young, to reproduce later, and to engage in defense when old. At any rate, the persistent developmental gradient along the branch, corresponding to predictable environmental (selective) gradients, could facilitate the development of temporal differentiation in polypal functions. The same effect in a massive species, where young and old polyps are more evenly distributed within the colony, would be more difficult to develop, since environmental gradients are imposed upon heterogeneously-aged polyps. The view that branching corals have a higher potential to develop integration concurs with Jackson's (1979) general argument, that branching colonial animals should be more integrated because their basal attachment is critical to the survival of the whole colony.

Polyp dimorphism. In this study, dimorphism of polyps (Table 1) is associated with reproductive integration. Both acroporids have polyps of divergent morphology and both

species appear to be reproductively integrated. Direct inference of integration from morphology is supported here.

Budding types. Conflicting inferences about integration can be drawn from an examination of the modes of budding in corals. Duerden (1902) and Wells (1973) noted that polyps produced intratentacularly lack directive mesenterial couples (but see Matthai, 1926); daughter polyps, therefore, differ morphologically from the original polyp. Based on this morphological difference, they suggested that the entire colony formed by intratentacular budding should be regarded as an individual, whereas extratentacular budding produces many identical individuals (polyps) aggregated as a colony. The observations in this study, however, suggest just the opposite from a reproductive perspective. A colony produced by complete intratentacular budding (*F. fragum*) is homogeneous with respect to the fertility of its polyps (and by inference, other functions as well); an extratentacularly budded colony, in contrast, is a mosaic of large, old, fertile polyps intermixed with small, young, infertile or less fertile polyps. Integration should be higher in the latter, since at any moment, the young developing polyps are presumably more dependent on other polyps.

Other morphological characters. None of the reproductive data gathered during this study provided support for any of the other morphological characters (Table I) that are commonly used to imply integration. For example, reproductive fertility patterns in the two meandroid *Diploria* spp. resembled those of the extratentacularly budded *Montastrea cavernosa* and *Siderastrea siderea.*

Adaptiveness of integration

The ability to conduct signals, either through a primitive colonial nervous system, or through excitable epithelia is an important attribute of a true colony. In addition, the ability to share resources should set colonies clearly apart from mere aggregates of individually-acting polyps (Mackie, 1986). Judging by these non-reproductive criteria, reef corals do possess a certain extent of integration (see Introduction).

Many other marine invertebrates are also colonial, and some (including cnidarians) have developed much higher levels of integration. Why are colonial reef corals different? There are several possible reasons:

(1) Reef corals are sessile. Highly coordinated behavior among polyps may not be as important as it is in pelagic colonial organisms (*e.g.*, siphonophorans), for which locomotory activity is necessary (Mackie, 1986).

(2) Unlike many soft-bodied polymorphic species, most reef corals settle on hard substrata, and each polyp deposits calcium carbonate as it grows, hence no other differentiated supporting mechanism is necessary.

(3) One possible advantage of most polyps potentially being able to reproduce is that a "mutant polyp" would be less likely to reap all the reproductive success of the colony (Buss, 1982). Considering that a large, massive coral colony may live for centuries or even millennia, the occurrence of somatic mutations would appear to be inevitable, and the low level of integration might be adaptive after all.

(4) Ecologically, coral colonies are often separated into ramets (Hughes and Jackson, 1980). A less integrated colony with totipotent polyps may be better able to adjust to new conditions after environmental changes or damage (Chornesky, 1989).

(5) Most reef corals harbor zooxanthellae and are therefore less dependent upon external feeding for their carbon (Edmunds and Davis, 1989). The more homogeneous distribution of sunlight relative to the more patchily distributed zooplankton may allow less colony integration than in sedentary colonial animals lacking photosymbionts.

(6) Developmental constraints may be a non-selectionist's explanation for low integration in these corals.

In conclusion, a coral colony is an individual, in the sense that it is genetically homogeneous, and the constituting polyps are coordinated physiologically by their physical connections. Evolutionarily, a coral colony cannot be considered an individual, in the sense that the genet is a better unit of selection (Janzen, 1977), whereas the polyp characters are what is directly controlled by genetics.

Acknowledgments

Among the many people who contributed to this research, we would like especially to thank Dr. Jeremy B. C. Jackson for offering opportunities for the field study and sharing many ideas, Dr. Esther Peters for diagnosing histological problems, Ms. Jennifer H. H. Lin Soong for helping with the field and laboratory work, and Drs. Joseph C. Simon, Terry P. Hughes and one anonymous reviewer for providing valuable comments on an early version of the manuscript. This research was partly supported by Smithsonian Tropical Research Institute.

Literature Cited

Barnes, D. J. 1973. Growth in colonial scleractinians. *Bull. Mar. Sci* **23:** 280–298.

Beklemishev, W. N. 1969. *Principles of Comparative Anatomy of Invertebrates* University Chicago Press, Chicago, IL.

Bell, A. D. 1986. Evolutionary and non-evolutionary theories of senescence. *Phil. Trans. R. Soc. Lond* **B313:** 143–159.

Birkeland, C. 1976. An experimental method of studying corals during early stages of growth. *Micronesica* **12:** 319–322.

Boardman, R. S., and A. H. Cheetham. 1973. Degrees of colony dominance in stenolaemate and gymnolaemate bryozoa. Pp. 121–220 in *Animal Colonies: Development and Function Through Time.*

R. S. Boardman, A. H. Cheetham and W. A. Oliver, eds. Dowden, Hutchinson and Ross, Inc., PA.

Bonner, J. T. 1965. *Size and Cycle: An Essay on the Structure of Biology.* Princeton University Press, Princeton, NJ.

Braverman, M. H. 1962. Studies on hydroid differentiation. I. *Podocoryne carnea* culture methods and carbon dioxide induced sexuality. *Exp. Cell Res.* **26:** 301–306.

Braverman, M. H. 1963. Studies on hydroid differentiation. II. Colony growth and the initiation of sexuality. *J. Embryo. Exp. Morph.* **11:** 239–253.

Buss, L. W. 1982. Somatic cell parasitism and the evolution of somatic tissue compatibility. *Proc. Natl. Acad. Sci. USA* **79:** 5337–5341.

Buss, L. W. 1987. *The Evolution of Individuality.* Princeton University Press, Princeton, NJ.

Chapman, G. 1981. Individuality and modular organisms. *Biol. J. Linn. Soc.* **15:** 177–183.

Chornesky, E. A. 1989. Repeated attack and retaliation during spatial competition between corals. *Ecology* **70:** 843–855.

Chornesky, E. A., and E. C. Peters. 1987. Sexual reproduction and colony growth in the scleractinian coral *Porites astreoides*. *Biol. Bull.* **172:** 161–177.

Coates, A. G., and J. B. C. Jackson. 1985. Morphological themes in the evolution of clonal and aclonal marine invertebrates. Pp. 67–106 in *Population Biology and Evolution of Clonal Organisms.* J. B. C. Jackson, L. W. Buss, and R. E. Cook, eds. Yale University Press, New Haven, CT.

Coates, A. G., and W. A. J. Oliver. 1973. Coloniality in zoantharian corals. Pp. 3–27 in *Animal Colonies: Development and Function Through Time,* R. S. Boardman, A. H. Cheetham and W. A. J. Oliver, eds. Dowden, Hutchinson and Ross, Inc., PA.

Connell, J. E. 1973. Population ecology of reef building corals. Pp. 205–245 in *Biology and Geology of Coral Reefs,* O. A. Jones and R. Endean, eds. Academic Press, London.

Druffel, E. M. 1982. Banded corals: changes in oceanic carbon-14 during the little ice age. *Science* **218:** 13–19.

Duerden, J. E. 1902. The significance of budding and fission. *Ann. Mag. Nat. Hist. ser. 7* **10:** 382.

Edmunds, P. J., and P. S. Davis. 1989. An energy budget for *Porites porites* (scleractinia), growing in a stressed environment. *Coral Reefs* **8:** 37–43.

Fadlallah, Y. H. 1983. Sexual reproduction, development and larval biology in scleractinian corals, a review. *Coral Reefs* **2:** 129–150.

Foster, A. B. 1979. Phenotypic plasticity in the reef corals *Montastraea annularis* (Ellis and Solander) and *Siderastrea siderea* (Ellis and Solander). *J. Exp. Mar. Biol. Ecol.* **39:** 25–54.

Foster, A. B. 1985. Variation within coral colonies and its importance for interpreting fossil species. *J. Paleontol.* **39:** 1359–1381.

Francis, L. 1976. Social organization within clones of the sea anemone *Anthopleura elegantissima*. *Biol. Bull.* **150:** 361–376.

Gladfelter, E. H. 1983. Circulation of fluids in the gastrovascular system of the reef coral *Acropora cervicornis*. *Biol. Bull.* **165:** 619–636.

Goreau, T. F. 1963. Calcium carbonate deposition by coralline algae and corals in relation to their roles as reef builders. *Ann. N.Y. Acad. Sci.* **109:** 127–167.

Gottlieb, L. D. 1986. The genetic basis of plant form. *Phil. Trans. R. Soc.* [illegible]**3:** 197–208.

Graus, R. R., and J. G. Macintyre. 1976. Light control of growth form in colonial reef corals: computer simulation. *Science* **193:** 895–897.

Graus, R. R., and J. G. Macintyre. 1982. Variation in growth forms of the reef coral *Montastrea annularis* (Ellis and Solander): A quantitative evaluation of growth response to light distribution using computer simulation. Pp. 441–464 in *The Atlantic Barrier Reef Ecosystem at Carrie Bow Cay, Belize I. Structure and Communities,* K. Rutzler and G. Macintyre, eds. Smithsonian Institute Press, Washington, DC.

Harper, J. L., and A. D. Bell. 1979. The population dynamics of growth form in organisms with modular construction. Pp. 29–52 in *Population Dynamics,* R. M. Anderson, B. D. Turner, and L. R. Taylor, eds. Blackwell Sci. Pub., London.

Harrigan, J. F. 1972. The planula larva of *Pocillopora damicornis:* Lunar periodicity of swarming and substratum selection behavior. Ph.D. Dissertation, University of Hawaii.

Harrison, P. L., and C. C. Wallace. 1990. Reproduction, dispersal and recruitment of scleractinian corals. Pp. 133–207 in *Coral Reefs, Ecosystems of the World 25,* Z. Dubinsky, ed. Elsevier, New York.

Harvell, C. D. 1991. Coloniality and inducible polymorphism. *Am. Nat.* **138:** 1–14.

Hubbard, J. A. E. B. 1973. Sediment-shifting experiments: A guide to functional behavior in colonial corals. Pp. 31–42 in *Animal Colonies: Development and Function Through Time,* R. S. Boardman, A. H. Cheetham, and W. A. J. Oliver, eds. Dowden, Hutchinson and Ross, Inc., PA.

Hudson, J. H. 1985. Long-term growth rates of *Porites lutea* before and after nuclear testing: Enewetak Atoll (Marshall Islands). *Proc. 5th Int. Coral Reef Symp.* **6:** 179–185.

Hughes, D. J., and R. N. Hughes. 1986. Metabolic implications of modularity: studies on the respiration and growth on *Pilosa electra*. *Phil. Trans. R. Soc. Lond.* **B313:** 28–37.

Hughes, T. P. 1984. Population dynamics based on individual size rather than age: a general model with a reef coral example. *Am. Nat.* **123:** 778–795.

Hughes, T. P., and J. B. C. Jackson. 1980. Do corals lie about their age? Some demographic consequences of partial mortality, fission and fusion. *Science* **209:** 713–715.

Hughes, T. P., and J. B. C. Jackson. 1985. Population dynamic and the life histories of foliaceous corals. *Ecol. Mono.* **55:** 141–166.

Hyman, L. H. 1940. *The Invertebrates: Protozoa Through Ctenophora.* McGraw-Hill, New York.

Isdale, P. 1977. Variation in growth rate of hermatypic corals in a uniform environment. *Proc. 3rd Int. Coral Reef Symp.* **2:** 403–408.

Jackson, J. B. C. 1979. Morphological strategies of sessile animals. Pp. 499–555 in *Biology and Systematics of Colonial Animals.* G. Larwood and B. R. Rosen, eds. Academic Press, London.

Janzen, D. H. 1977. What are dandelions and aphids? *Am. Nat.* **111:** 586–589.

Kojis, B. L. 1986. Sexual reproduction in *Acropora (Isopora)* species (Coelenterata: Scleractinia). I. *A. cuneata* and *A. palifera* on Heron Island reef, Great Barrier Reef. *Mar. Biol.* **91:** 291–309.

Kojis, B. L., and N. J. Quinn. 1985. Puberty in *Goniastrea favulus*, age or size limited? *Proc. 5th Int. Coral Reef Symp.* **4:** 289–294.

Loya, Y. 1976. Skeletal regeneration in a Red Sea scleractinian coral population. *Nature* **261:** 490–491.

Mackie, G. O. 1986. From aggregates to integrates: physiological aspects of modularity in colonial animals. *Phil. Trans. R. Soc. Lond.* **B313:** 175–196.

Matthai, G. 1926. Colony-formation in astraeid corals. *Phil. Trans. R. Soc. Lond.* **B214:** 313–356.

McKinney, F. K., and J. B. C. Jackson. 1989. *Bryozoan Evolution.* Allen and Unwin, London.

Meyer, D. L., and C. Birkeland. 1975. Biological monitoring data. Pp. 358–370 in *Environmental Monitoring and Baseline Data,* D. M. Windsor, eds. Smithsonian Institute, Washington, DC.

Nazaki, Y., D. M. Rye, K. K. Turekian, and R. E. Dodge. 1978. A 200 year record of carbon-13 and carbon-14 variations in a Bermuda coral. *Geop. Res. Let.* **5:** 825–828.

Oliver, J. K. 1984. Intra-colony variation in the growth of *Acropora formosa*: extension rates and skeletal structure of white (zooxanthellae free) and brown-tipped branches. *Coral Reefs* **3:** 139–147.

Oliver, J. K., B. E. Chalker, and W. C. Dunlap. 1983. Bathymetric adaptations of reef building corals at Davis Reef, Great Barrier Reefs, Australia. I. Long-term growth responses of *Acropora formosa*. *J Exp. Mar. Biol. Ecol.* **73:** 11–35.

Oliver, W. A. J., and A. G. Coates. 1987. Phylum Cnidaria. Pp. 140–193 in *Fossil Invertebrates*, R. S. Boardman, A. H. Cheetham, and A. J. Rowell, eds. Blackwell Scientific Publication, London.

Palumbi, S. R., and J. B. C. Jackson. 1983. Aging in modular organisms: ecology of zooid senescence in *Steginoporella* sp. (Bryozoa, Cheilostomata). *Biol. Bull.* **164:** 267–278.

Pearse, J. S., and L. Muscatine. 1971. Role of symbiotic algae (zooxanthellae) in coral calcification. *Biol. Bull.* **141:** 350–363.

Richmond, R. H., and C. L. Hunter. 1990. Reproduction and recruitment of corals: comparisons among the Caribbean, the tropical Pacific, and the Red Sea. *Mar. Ecol. Prog. Ser.* **60:** 185–203.

Rinkevich, B., and Y. Loya. 1985. Intraspecific competition in a reef coral: effects on growth and reproduction. *Oecologia* **66:** 100–105.

Rosen, B. R. 1979. Modules members and communes. A postscript introduction to social organisms. Pp. XIII–XXXV in *Biology and Systematics of Colonial Animals*, G. Larwood and B. R. Rosen, eds. Academic Press, London.

Ryland, J. S. 1979. Structural and physiological aspects of coloniality in bryozoa. Pp. 211–242 in *Biology and Systematics of Colonial Animals*, G. Larwood and B. R. Rosen, eds. Academic Press, London.

Sandberg, P. A. 1973. Degree of individuality in cheilostome bryozoa: skeletal criteria. Pp. 305–316 in *Animal Colonies: Development and Function Through Time*, R. S. Boardman, A. H. Cheetham, and W. A. J. Oliver, eds. Dowden, Hutchinson and Ross, Inc., PA.

Schopf, T. J. M. 1973. Ergonomics of polymorphism: its relation to the colony as the unit of natural selection in species of the phylum ectoprocta. Pp. 247–294 in *Animal Colonies: Development and Function Through Time*, R. S. Boardman, A. H. Cheetham, and W. A. Oliver, eds. Dowden, Hutchinson and Ross, Inc., PA.

Sebens, K. P. 1987. The ecology of indeterminate growth in animals. *Ann. Rev. Ecol. Syst.* **18:** 371–407.

Shelton, G. A. B. 1979. Co-ordination of behavior in cnidarian colonies. Pp. 141–154 in *Biology and Systematics of Colonial Animals*, G. Larwood and B. R. Rosen, eds. Academic Press, London.

Shelton, G. A. B. 1982. Anthozoa. Pp. 141–154 in *Electrical Conduction and Behavior in 'Simple' Invertebrates*, G. A. B. Shelton, ed. Glarendon Press, Oxford.

Shinn, E. A. 1976. Coral reef recovery in Florida and the Persian Gulf. *Environ. Geol.* **1:** 241–254.

Silen, L. 1981. Colony structure in *Flustra foliacea* (Linnaeus). *Acta Zoologica* **62:** 219–232.

Soong, K. 1991. Sexual reproductive patterns of shallow-water reef corals in Panama. *Bull. Mar. Sci.* **49**(3): 832–846.

Stephenson, T. A., and A. Stephenson. 1933. Growth and asexual reproduction in corals. *Great Barrier Reef Exp. 1928–1929* **3:** 168–217.

Szmant-Froelich, A. 1985. The effect of colony size on the reproductive ability of the Caribbean coral *Montastrea annularis* (Ellis and Solander). *Proc. 5th Int. Coral Reef Symp.* **4:** 295–300.

Taylor, D. L. 1977. Intra-colonial transport of organic compounds and calcium in some Atlantic reef corals. *Proc. 3rd Int. Coral Reef Symp.* **1:** 432–436.

Tunnicliffe, V. 1983. Caribbean staghorn coral population—Pre-hurricane Allen conditions in Discovery Bay, Jamaica. *Bull. Mar. Sci.* **33:** 131–151.

Vaughan, T. W. 1909. Geology of the keys, the marine bottom deposits, and recent corals of southern Florida. *Carnegie Inst. Wash. Yearbook* **8:** 140–144.

Vaughan, T. W., and J. W. Wells. 1943. Revision of the suborders, families, and genera of the Scleractinia. *Geol. Soc. Amer. Spec. Paper* **44:** 1–363.

Veron, J. E. N. 1981. The species concept in scleractinia of eastern Australia. *Proc. 4th Int. Coral Reef Symp.* **2:** 183–186.

Veron, J. E. N., and M. Pichon. 1982. Scleractinia of Eastern Australia. Part IV Poritidae. *Aust. Inst. Mar. Sci. Mono. Ser.* **5:** 1–159.

Veron, J. E. N., and C. C. Wallace. 1984. Scleractinian of Eastern Australia. Part V. Family Acroporidae. *Aust. Inst. Mar. Sci. Mono. Ser.* **6:** 1–485.

Wallace, C. C. 1978. The coral genus *Acropora* (Scleractinia: Astrocoeniina: Acroporidae) in the central and southern Great Barrier Reef Province. *Mem. Qd. Mus.* **18:** 273–319.

Wallace, C. C. 1985. Reproduction, recruitment and fragmentation in nine sympatric species of the coral genus *Acropora*. *Mar. Biol.* **88:** 217–233.

Wells, J. W. 1956. Scleractinia. Pp. 328–444 in *Treatise on Invertebrate Paleontology, pt. F. Coelenterata*, R. C. Moore, ed. Geol. Soc. Amer., and University Kansas Press, Lawrence, KS.

Wells, J. W. 1973. What is a colony in anthozoan corals? P. 29 in *Animal Colonies: Development and Function Through Time*, R. S. Boardman, A. H. Cheetham, and W. A. J. Oliver, eds. Dowden, Hutchinson and Ross, Inc., PA.

Reference: *Bi* 183: 432–439. (December, 1992)

Morphogenetic Movements and Assembly of Strobilae into Zooidal Systems in Early Colony Development of the Compound Ascidian *Polyclinum planum*

A. R. HOLYOAK[1]

Department of Biology, University of California, Santa Cruz, California 95064

Abstract. Large-scale developmental processes, such as the morphogenetic movement of constructional sub-units within colonies of modular organisms, require self-assembling mechanisms. The compound ascidian *Polyclinum planum* is a modular organism. In the present study, colonies of *P. planum* were subjected to light-shock, and the development of the released tadpole larvae was followed in the laboratory from settlement, through the formation of oozooids and, finally, small colonies. Oozooids strobilated in 40 to 78 days. The number of post-abdominal strobilae produced per oozooid depended on post-abdomen length, but the timing of strobilation did not. Thoracic and abdominal remnants of *P. planum* parent zooids regressed completely; only the post-abdominal strobilae regenerated to form new zooids. Regenerating strobilae moved through the tunic into the region once occupied by the parent zooid, and formed a zooidal system around a pocket-like common cloacal cavity. Expansion of the thoraxes of regenerating zooids within the young colony produced the cylindrical to capitate shape of small, single-system colonies. The observed non-regeneration of the thoracic and abdominal remnants of *P. planum* differs markedly from their reported fates in other polyclinid ascidians. These observations shed light on the "rules of asso[illegible]" that govern formation of young *P. planum* colonies.

Introduction

Self-a[illegible]echanisms proceed without the direct control [illegible]ular cell's DNA, usually occurring outside the cell and often at levels higher than that of the cell (Bonner, 1974; Adair, 1988; Edelman, 1988; Vreeland and Laetsch, 1988). Thus, development on an even broader scale must rely heavily upon supra-cellular activity.

Modular organisms demonstrate such large-scale organizational activities in their development and growth (Harper *et al.*, 1986). They grow through the iteration of functional units (modules), and in colony-forming species, the arrangement of modules in relation to each other determines colony shape and organization.

Compound ascidian tunicates are modular organisms. The diverse ways in which ascidian blastozooids (their modules) arise has been reviewed by Berrill (1935, 1951); Brien (1948, 1958); Nakauchi and Kawamura (1966); Nakauchi (1982); and Monniot *et al.* (1991).

Oozooid development, strobilation, and colony organization in ascidians of the family Polyclinidae have received considerable attention (Brien, 1924, 1925, 1936; Scott, 1952; Trason, 1957; Nakauchi, 1966, 1970, 1974, 1977, 1979, 1980a, b, 1981, 1982, 1986, 1987; Freeman, 1971; Nakauchi and Kawamura, 1974, 1978). These studies show that zooid production in polyclinid ascidians is by strobilation of either the abdomen or post-abdomen, or of both the abdomen and the post-abdomen. Descriptions of bud fates and system formation in this family have consistently shown that all buds—thoracic, abdominal, and post-abdominal—regenerate, with the thoracic remnant of the parent zooid usually regenerating to become the center of a new system of zooids (Brien 1936; Nakauchi 1966, 1970, 1977, 1979, 1981, 1986, 1987; Freeman 1971; Nakauchi and Kawamura 1974, 1978).

In the present paper, I use direct observation and time-lapse videomicroscopy to describe the strobilation of oo-

Received 1 M[illegible] 30 September 1992.

[1] Current address: [illegible] Biology, Manchester College, North Manchester, Indiana

zooids and blastozooids and the self-assembling movement and organization of consequent zooids into systems in the compound ascidian *Polyclinum planum*.

Materials and Methods

Early stages of colony morphogenesis in *Polyclinum planum*, from settled larvae through the formation of systems of zooids, were studied in culture at the Long Marine Laboratory, Santa Cruz, California. Larvae were obtained from colonies collected intertidally at Hopkins Marine Station, Pacific Grove, California. Larval release was induced by holding colonies in running seawater in the dark for at least 48 h, and then subjecting them to bright incandescent illumination (3.5×10^{20} to 5.5×10^{20} photons $cm^{-2}\ s^{-1}$). Zooids released their larvae 1–30 min after the initiation of the light shock. The tadpole larvae emerged from the common cloacal openings and swam directly toward the brightest light source, where they were easily collected and transferred to drops of water on 75 × 50 mm glass slides. They settled within 30 min. Cohorts of larvae were collected in this way in February and November 1990, and in April 1991.

Developing oozooids, and the colonies they subsequently produced, were maintained in 0.2 μm-filtered, aerated seawater, in closed, plastic 5-l containers. The containers were held at ambient laboratory seawater temperature (about 14°C; Fig. 1) by partial immersion in a running-seawater table. At least twice a week, when the water in the containers was changed, cultures were fed Liquifry marine food (concentration: 2 drops per liter) and unicellular algae: *Dunaliella* and *Isochrysis* (100 ml of each alga; approximate cell densities of 10,000 to 15,000 cells ml^{-1}). Liquifry is a commercial food for filter-feeding invertebrates in marine aquaria; its main ingredients are dextrin, pea flour, whole egg, yeast, spinach: 3.5% protein, 1.6% fat, 1% fiber. Liquifry was used successfully by Boyd *et al.* (1986) to rear laboratory-cultured Monterey *Botryllus schosseri*.

The post-settlement growth and development of each *Polyclinum planum* oozooid or colony was monitored weekly. The maximum lengths of every zooid's thorax, abdomen, and post-abdomen, the longest visible blood vessel in the tunic, and the total length of each oozooid or colony, including its tunic, was measured. These body parts were observed with an inverted microscope through the glass slide on which the cultures were growing.

Time-lapse videomicroscopy was used to augment the observations described above, and to record the pattern of zooid strobilation, the regeneration of strobilae, and the organization of multiple-zooid systems. A Panasonic PV-604 video camera was fitted to a dissection microscope, and the camera's pre-programmed time-lapse feature taped these events for one second of every minute. Strobilation of three zooids, the regeneration of about 15 strobilae, and the organization of two multiple-zooid systems were recorded in this manner.

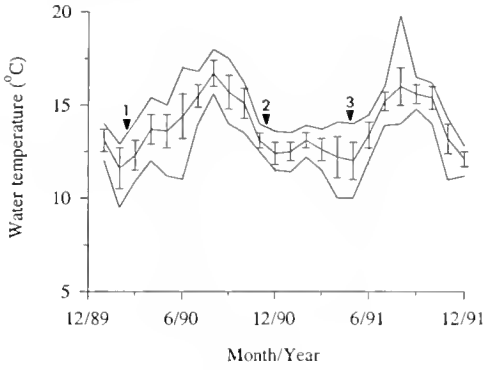

Figure 1. High, low, and mean monthly seawater temperatures (±SD) in seawater tables of the Long Marine Laboratory, Santa Cruz, California, from January 1990 through December 1991 (data provided courtesy of J. S. Pearse). Settlement dates of cohorts of *Polyclinum planum* followed during this study are indicated by arrows: 1 = 14 Feb 1990; 2 = 7 Nov 1990; 3 = 26 Apr 1991.

Results

Laboratory cultures of *Polyclinum planum* larvae, released after light shock, settled on glass slides on 14 February 1990 (n = 20 larvae), 7 November 1990 (n = 70), and 26 April 1991 (n = 32). These cohorts were maintained in culture until 27 November 1990, 3 June 1991, and 19 August 1991, respectively. The zooids showed evidence of feeding as soon as their oral and atrial apertures opened; *i.e.*, food was clearly visible in the gut, and fecal pellets were constantly produced.

Polyclinum planum oozooids strobilated on average 55.1 days after larval settlement (SD = 7.4 days; n = 92 oozooids). The earliest strobilation occurred in 40 days, and the latest at 78 days. Oozooids produced the body regions typical of all polyclinid ascidians: thorax, abdomen, and post-abdomen, as well as at least one test vessel that extended into the tunic from near the heart (Fig. 2).

The initiation of zooidal strobilation was signalled by the atrophy of the test vessels and by the regression of the thorax and abdomen. The oozooid's thorax soon separated from its abdomen at the esophagus. Next, the abdomen separated from the post-abdomen, and the former zooid was now divided into isolated thoracic, abdominal, and post-abdominal remnants. The isolated post-abdomen then produced one or more strobilae, the number depending on total post-abdominal length (Fig. 3). The lack of significance between the lengths of post-abdomens

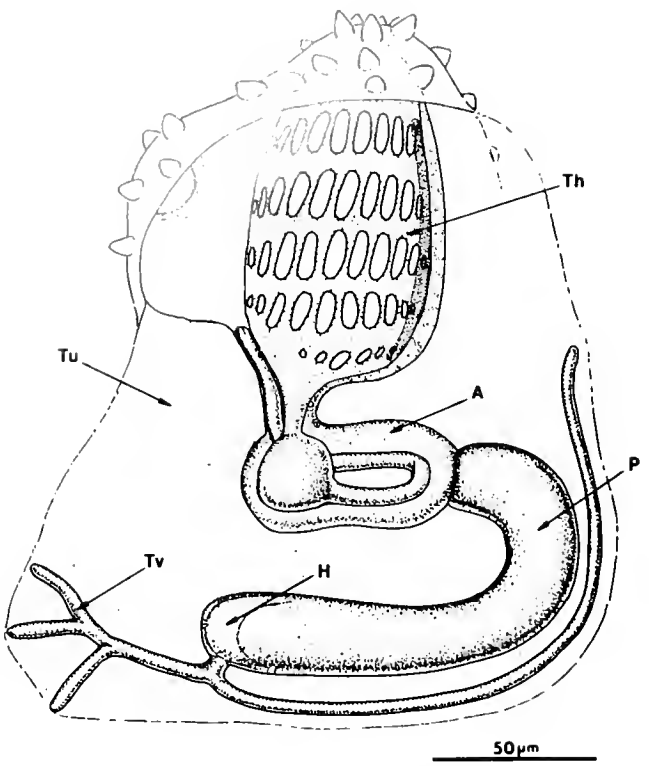

Figure 2. Fully developed oozooid of *Polyclinum planum* as viewed through the slide to which it is attached (A—abdomen; P—post-abdomen; H—heart; Th—thorax; Tv—test vessel; Tu—tunic). Tuberculate region at the top is the surface of the tunic around the oozooid's oral and cloacal apertures.

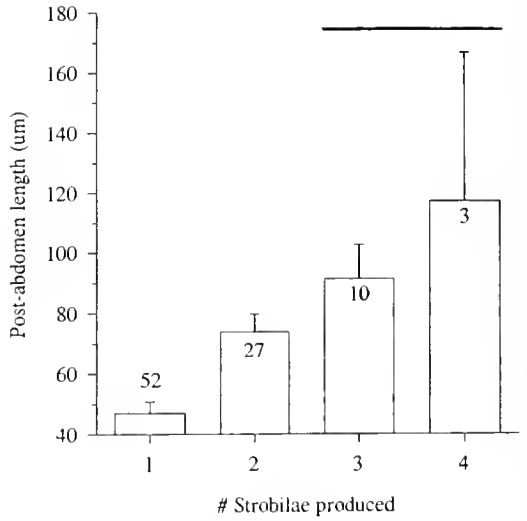

Figure 3. Mean post-abdomen lengths for groups of zooids producing 1 (n = 52 zooids), 2 (n = 27), 3 (n = 10), or 4 (n = 3) post-abdominal strobilae. Error bars are standard deviations. A Tukey multiple comparisons test revealed significant differences between post-abdomen lengths of zooids producing 1, 2, and 3 strobilae, but not between those producing 3 or 4 strobilae, as indicated by the Tukey-bar on the figure.

giving rise to three strobilae and those giving rise to four may be attributed to the small number of zooids (n = 3) that produced four post-abdominal strobilae. Although the number of strobilae produced was a function of post-abdomen length, the timing of strobilation was not (Fig. 4). Post-abdominal strobilae were pinched off sequentially, beginning "proximally," at the end formerly next to the abdomen, and proceeding "distally" toward the end farthest from the abdomen (Fig. 5).

Post-abdominal strobilae regenerated into whole blastozooids, while the thoracic and abdominal remnants regressed completely (Fig. 6). These regressing elements became [illegible]nular, possibly supplying nutrients to the regenerating [illegible]bilae. (The regressed thorax precluded feeding at this [illegible]. All of the post-abdominal strobilae showed polarized [illegible]opment. That is, in each new strobila, a new thorax [illegible]domen formed at the end closest to the former abdomen.

Time-lapse [illegible]ordings revealed the pattern of development in the [illegible]rating strobilae. First, the strobilae produced a clear [illegible]ge at the end of the strobila formerly proximal to the abdomen (Fig. 5E–G; Fig. 6A). This clear bulge was the new developing thorax. At the same time, a smaller clear area—the heart—appeared at the end of the strobila opposite that of the new thorax. At this point, a strobila consisted of a post-abdomen and a thorax. Fi-

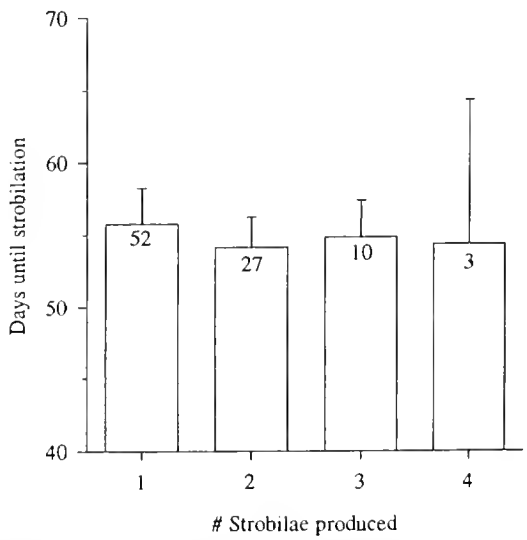

Figure 4. Time from larval settlement to strobilation of the oozooid, comparing oozooids producing 1 (n = 52 zooids), 2 (n = 27), 3 (n = 10), or 4 (n = 3) post-abdominal strobilae. Error bars are standard deviations. One-way ANOVA of the four groups of zooids indicated no significant differences between the four groups ($F = 0.30 < 2.76 = F_{0.05(3,60)}$; $P > 0.5$).

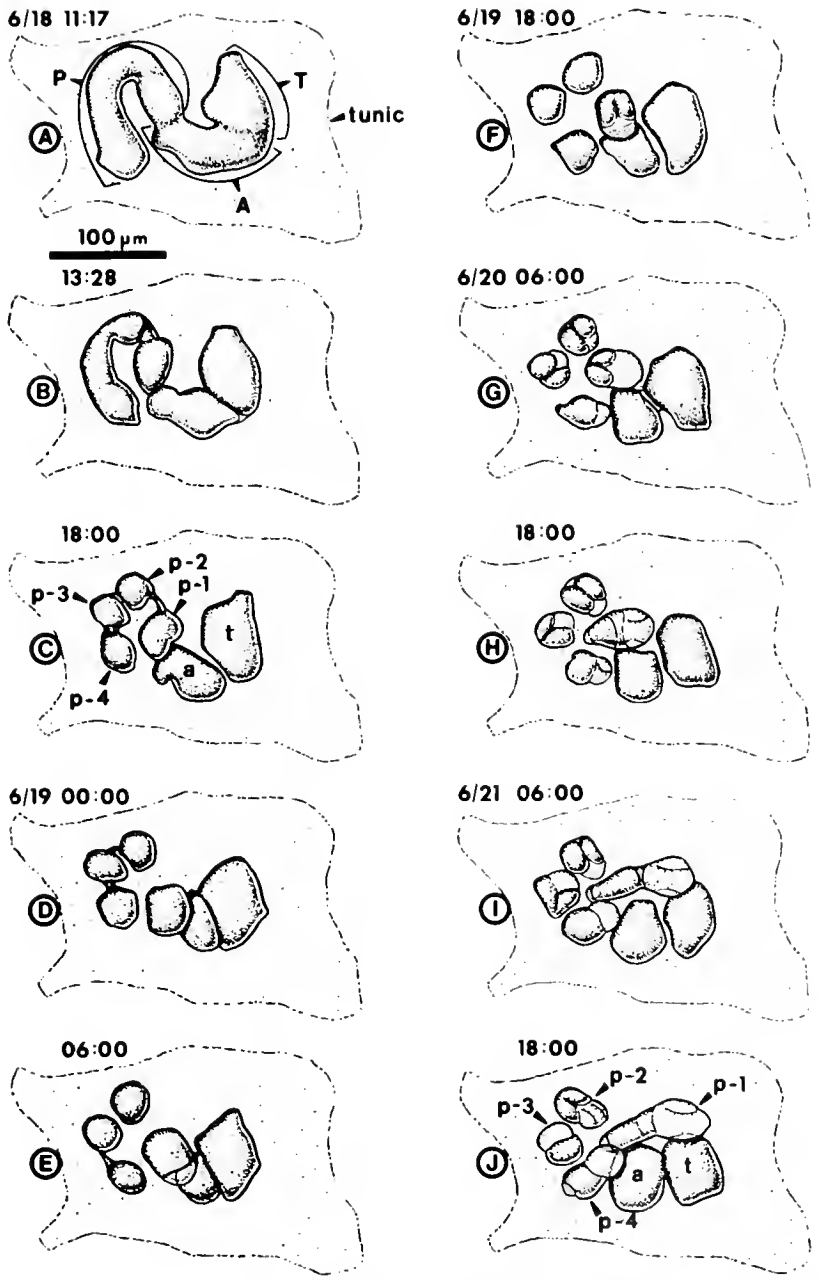

Figure 5. Pattern of strobilation of a *Polyclinum planum* oozooid, drawn from time-lapse video record (T—thorax; A—abdomen; P—post-abdomen; t—thoracic remnant; a—abdominal remnant; p-1 to p-4—post-abdominal strobilae). Read down columns, Figures A to J.

nally, an abdomen developed between the post-abdomen and the thorax. Each of the three body regions then increased in size, and were continuing to grow as the taping sessions ended.

Growth of the three body regions of the new blastozooid was accompanied by the movement of the entire bud through the colony's tunic, with the new thorax always in the lead. Rhythmic contractions of the post-abdomen, and then of the abdomen, occurred during these movements. Thoraxes, however, did not exhibit similar contractions as they expanded. Time-lapse video recordings showed that the mean contraction rate of post-abdomens was 42 min (pooled mean; SD = 15 min), and for the abdomens, 35.5 min (SD = 14 min). These "developmental contractions" occurred over a much longer period than either the mean heart rate of these zooids ($\bar{x}$ = 54

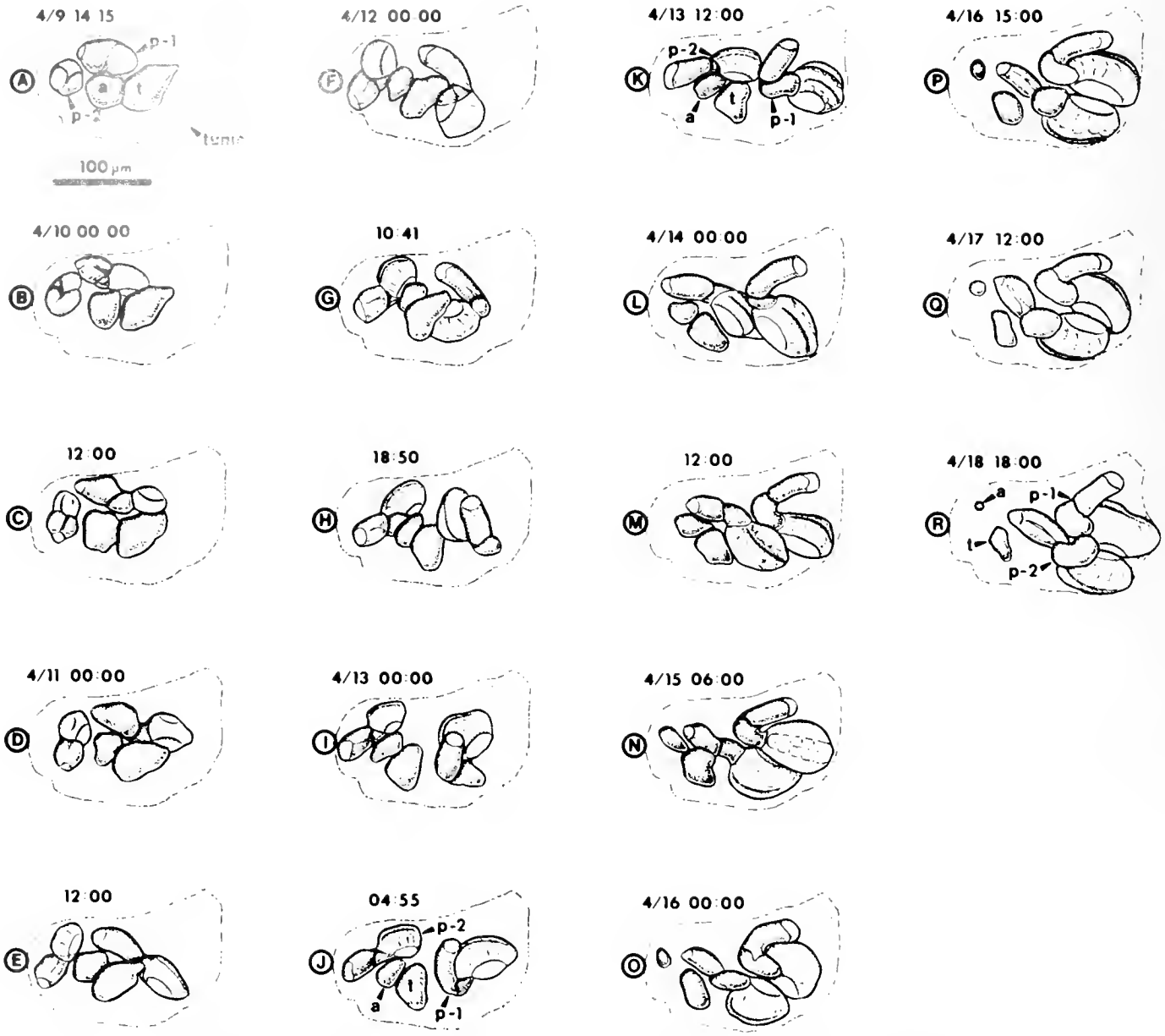

Figure 6. Two regenerating post-abdominal strobilae in the laboratory, drawn from time-lapse video record (t—thoracic remnant; a—abdominal remnant; p-1, p-2—regenerating post-abdominal strobilae). Note the decrease in size of thoracic and abdominal remnants as the post-abdominal strobilae regenerate. Read down columns, Figures A to R.

beats/min, SD = 2 beats/min), or the interval between the reversal of blood flow through the zooid's body, which occurred about every 2 min.

Regenerative buds always moved toward the region previously occupied by the thorax of the parent zooid, displacing the degenerating parent zooid's thoracic and abdominal remnants (Fig. 6). Once in place, the new blastozooids arranged themselves into a zooidal system. The thoraxes of new zooids rotated until their endostyles lay farthest from each other, and their atrial (cloacal) languets lay closest. Once their rotation was completed, the zooids' cloacal (atrial) apertures emptied into the new system's pocket-like common cloacal cavity.

The aggregation of thoraxes, and their subsequent growth and expansion, swelled the thoracic region of the new colony's single system of blastozooids. This swelling gave the colony a somewhat cylindrical to capitate shape, with its one common cloacal cavity and aperture at the

top (Fig. 7). The base of the colony now formed the beginning of the peduncle that characterizes larger, multisystem colonies in this species.

Discussion

From these results, we can formulate at least tentative "rules of assembly" by which modules are formed and by which systems of zooids are organized during early colony development in *Polyclinum planum*. These rules are listed and discussed below.

First, post-abdomen length determines the number of strobilae produced per bout of strobilation (see Fig. 3). It may well be that post-abdomen growth is regulated by nutrition, as previously discussed by Freeman (1971), and that better nutrition will result in the production of more strobilae and, therefore, faster growth of the colony.

The initiation of strobilation appears to be internally regulated. The timing of strobilation of zooids did not differ significantly between zooids producing 1, 2, 3, or 4 post-abdominal strobilae (see Fig. 4). These results cast doubt on Brien's (1968) suggestion that lengthening of the post-abdomen leads to impaired blood circulation in it, and that this circulatory congestion triggers strobilation. Freeman (1971), on the other hand, reported that increased *thorax* length is related to strobilation. Freeman's siamese twin experiments (1971), in which a single zooid had both an older and a younger thorax, showed that the younger thorax determines the initiation of strobilation. A similar thorax or entire-zooid age-size effect may also determine the onset of strobilation in *Polyclinum planum*.

Polyclinum planum's pattern of strobilation resembles that of other polyclinids (Nakauchi, 1982). And the timing of strobilation in *P. planum* is close to that of the only congener studied so far: *P. aurantium* (40–70 days; Nakauchi, 1981).

Second, only post-abdominal strobilae regenerate; the thoracic and abdominal remnants completely regress. The fates of the isolated thoracic and abdominal elements of iterating *Polyclinum planum* zooids do not conform to those of other polyclinids. In other polyclinids, the thoracic and abdominal elements can also regenerate into new zooids. My results with *P. planum* show that the production of solely post-abdominal zooids occurred consistently in all cohorts, at different times of the year, and independently of post-abdomen length. But whether this strobilation pattern also occurs in the field, or is only an artifact is still unclear.

Reviewing other species, Nakauchi (1981) suggests that, under normal conditions, the polyclinid thoracic remnant persists and regenerates an abdomen and post-abdomen, but that the thorax and even the abdomen regress during "survival budding" (his term) under adverse conditions.

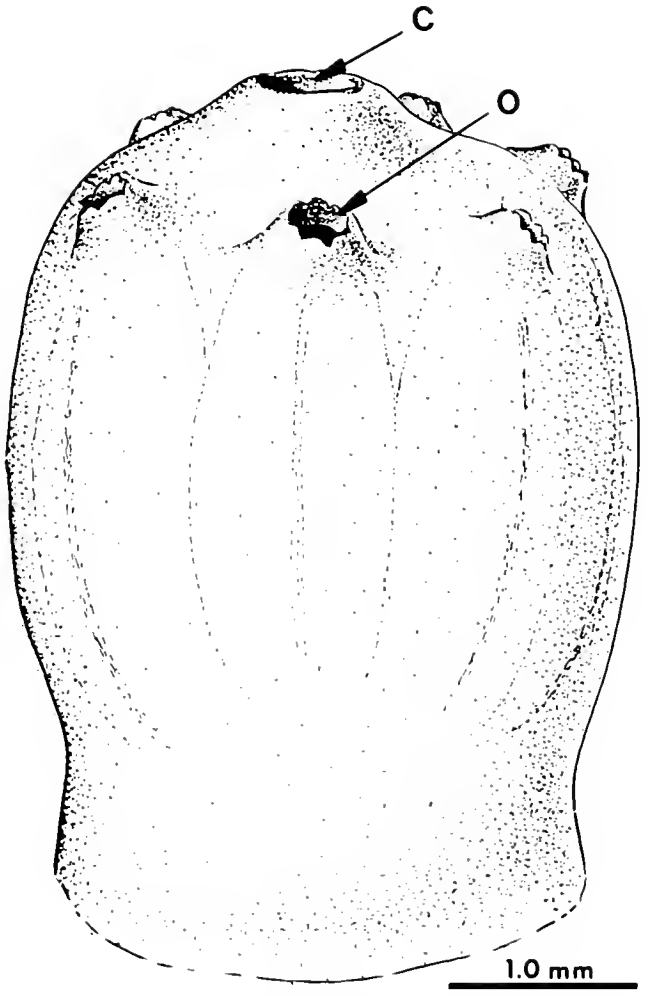

Figure 7. A young single-system colony of *Polyclinum planum* comprised of six zooids (C—common cloacal opening; O—oral aperture). Thoraxes of blastozooids are visible through the tunic. Blastozooids are much larger than oozooids (see Fig. 2) in this species.

Could my cultures have been under stress? Possibly, but zooids that can produce multiple post-abdominal buds certainly have enough energy stores to support the regeneration of their thoracic and abdominal fragments, if those fragments have the ability to regenerate at all. In *Polyclinum planum*, evidently, only post-abdominal fragments have this ability. On the other hand, laboratory culture and an artificial diet can produce stress resulting in abnormal growth.

If the strobila fates of *Polyclinum planum* can be further substantiated by rearing specimens in the field (which has not been attempted), then the pattern of strobilation reported here may warrant the addition of a new strobilation type to Nakauchi's (1982) inventory.

Third, all regenerating post-abdominal strobilae exhibit identical polarity in regeneration. The thorax, and then

the abdomen, each develop at the proximal end, and a new post-abdomen and heart develop at the distal end. This phenomenon facilitates the organization of an entire zooidal system from the regenerating strobilae, since strobilae tend to be oriented in the same direction as they are produced.

Fourth, regenerating strobilae move through the tunic as they develop, so that their thoraxes eventually lie in the space left by the regressed thorax of the parent zooid (see Fig. 6). This orderly arrangement is consistent with that reported by Nakauchi and Kawamura (1974, 1978) for regenerating strobilae of the polyclinid *Aplidium multiplicatum*. They found that regenerating strobilae move within the tunic, typically to a site either currently or previously occupied by a grown zooid or by a regenerating thoracic fragment. They proposed that grown zooids produce some attractant substance that organizes the movements of regenerating strobilae. Identifying any such attractant and its source would help us understand the control of self-assembly at levels higher than that of the individual module. But, of course, several other mechanisms, even pressure-differentials within the tunic or varying polymerization of polysaccharides in newer tunic, might also be hypothesized as controlling movement at this level.

Time-lapse video recordings of regenerating strobilae showed that their post-abdomens and abdomens had cyclic contractions as they moved through the tunic. These developmental contractions occurred over fairly long periods ($\bar{x}$ = 35 min for abdomens; $\bar{x}$ = 42 min for post-abdomens). The contractions are probably not driven by blood-flow reversals, or by the heart rate itself, because those phenomena operate within much shorter time frames. The causes and effects of these developmental contractions and the ultrastructural changes they generate within strobilae are, as yet, unstudied.

Fifth, system formation in *Polyclinum planum* commences as the thoraxes of regenerating strobilae aggregate in the region once occupied by the parent zooid's thorax. Thoraxes of newly regenerated blastozooids rotate until their endostyles lie on the rim of the circular system, and their future cloacal apertures point toward the center of the new system.

Sixth, as zooids reorient themselves this way, each zooid opens via oral (incurrent) and cloacal (excurrent) apertures. Each zooid maintains its own small oral siphon and aperture, which opens directly to the surface of the colony, while its cloacal aperture opens into a pocket-like common cloacal cavity that receives water from all zooids in the system. The system's common cloacal cavity opens to the surface of the colony as a rather large common cloacal aperture, slightly raised on a siphon.

Seventh, since several regenerating strobilae may result from the post-abdominal fragmentation of a single parent zooid, regenerating blastozooids must necessarily crowd into a limited space as they move toward the colony's surface. In the smallest colonies, this crowding, followed by the expansion of thoraxes and the production of tunic material by new zooids, enlarges the whole colony and generates the usual capitate shape. It is not yet clear that all regenerating *Polyclinum planum* zooids successfully reach the surface of the colony and join a system, especially in larger, multi-system colonies; some may well be crowded out and die.

In very young colonies, with few zooids or with only one or two post-abdominal strobilae, crowding does not tend to be a factor, nor do such colonies (*e.g.*, Fig. 6) assume the upright posture typical of the species, until more zooids are produced.

The events of module development and zooid regeneration are certainly under genetic control, but the forces governing system formation and whole colony morphogenesis remain problematic. How might genetic coding within the cells of a zooid extend its influence to the spatial arrangement of systems in which a zooid is only a modular component? Perhaps Nakauchi and Kawamura's (1978) "attractants"—substances produced by the parent zooid that affect movement of regenerating strobilae—hold a clue. System formation, including the molding of a common cloacal cavity and aperture and the differentiation of the whole colony into a basal peduncle and a lofted, zooid-bearing region, are important morphogenetic events. Genetic explanations provide for the production of the materials involved in these processes, but other contributing factors—physical ones like the effects simply of crowding zooids, and environmental ones like seasonal fluctuations in availability of food or nearness of other colonies—just as surely play their roles in guiding or molding these larger events in the self-assembly of the colony.

Although these tentative "rules of assembly" describe the production of strobilae and the formation of zooidal systems, still higher-order rules most certainly govern processes such as differentiation of an older *Polyclinum planum* colony into a peduncle and a zooid-bearing lobe, and influence morphogenetic changes in the zooid-bearing lobe as it increases in size and changes from a semispherical to a discoid shape—the shape by which *P. planum* is most often recognized in the field.

Acknowledgments

I thank A. T. Newberry, J. S. Pearse, C. M. Young, and two anonymous reviewers for helpful comments on the manuscript. Support for this study was provided by

the Department of Biology, University of California at Santa Cruz, the Friends of the Long Marine Laboratory, the American Museum of Natural History (Lerner Gray Fund for Marine Research), and the Earl and Ethel Myers Oceanographic and Marine Biology Trust.

Literature Cited

Adair, W. S. 1988. Organization and *in vitro* assembly of the *Chlamydomonas reinhardtii* cell wall. Pp. 25–41 in *Self-Assembling Architecture, the 46th Symposium of the Society for Developmental Biology*, J. E. Varner, ed. Alan R. Liss, Inc., New York.

Berrill, N. J. 1935. Studies in tunicate development. IV. Asexual reproduction. *Phil. Trans. R. Soc. Lond. Ser B* **225:** 327–379.

Berrill, N. J. 1951. Regeneration and budding in tunicates. *Biol. Rev.* **26:** 456–475.

Bonner, J. T. 1974. *On Development.* Harvard University Press. Cambridge, MA.

Boyd, H. C., S. K. Brown, J. A. Harp, and I. L. Weismann. 1986. Growth and culture of laboratory-cultured Monterey *Botrylus schossen*. *Biol. Bull.* **170:** 91–109.

Brien, P. 1924. Le bourgeonnement chez *Aplidium zostericola*. *Extrait Bull. de la Classe des Sci. Acad. Royal. Bel.* **(1924):** 603–610.

Brien, P. 1925. Contribution a l'etude de la blastogenese des tuniciers bourgeonnement chez *Aplidium zostericola* (Giard,). *Arch. Biol.* **35:** 155–203.

Brien, P. 1936. Formation des coenobies chez les Polyclinidae. *Annales Soc. Royal Zool. Belg.* **67:** 63–73.

Brien, P. 1948. Morphologie et reproduction des tuniciers. Pp. 553–1040 in *Traite de Zoologie, Vol. 11*, P. P. Grasse, ed. Masson, Paris.

Brien, P. 1958. La reproduction asexuee. *Ann Biol* **34**(5/6): 241–262.

Brien, P. 1968. Blastogenesis and morphogenesis. *Adv Morphog* **7:** 151–203.

Edelman, G. M. 1988. *Topobiology.* Basic Books, Inc., New York.

Freeman, G. 1971. A study on the intrinsic factors which control the initiation of asexual reproduction in the tunicate *Amaroucium constellatum*. *J Exp. Zool.* **178:** 433–456.

Harper, J. L., B. R. Rosen, and J. White. 1986. Preface. The growth and form of modular organisms. *Phil. Trans. R Soc. Lond. B* **313:** 3–5.

Monniot, C., F. Monniot, and P. Laboute. 1991. *Coral Reef Ascidians of New Caledonia.* Orstom, Paris.

Nakauchi, M., and K. Kawamura. 1966. Asexual reproduction of ascidians. Pp. 471–478 in *Advances in Invertebrate Reproduction 4*, M. Porchet, J-C. Andries, and A. Dhainaut, eds. Elsevier Sci. Publ. New York.

Nakauchi, M., and K. Kawamura. 1974. Behavior of buds during common cloacal system formation in the ascidian, *Aplidium multiplicatum*. *Rep. Usa Mar. Biol. Sta* **21:** 19–27.

Nakauchi, M., and K. Kawamura. 1978. Additional experiments on the behavior of buds in the ascidian, *Aplidium multiplicatum*. *Biol. Bull.* **154:** 453–462.

Nakauchi, M. 1966. Budding and colony formation in the ascidian *Amaroucium multiplicatum*. *Jpn. J. Zool.* **15:** 151–172.

Nakauchi, M. 1970. Asexual reproduction in *Amaroucium yamazii* (a colonial ascidian). *Publ. Seto Mar. Biol. Lab.* **17:** 309–328.

Nakauchi, M. 1974. Development and budding in the oozooids of polyclinid ascidians. 1. *Sidneioides snamoti*. *Rep. Usa Mar. Biol. Stn.* **21:** 1–18.

Nakauchi, M. 1977. Development and budding in the oozooids of polyclinid ascidians. 2. *Rutterella pulchra*. *Annot. Zool. Jpn.* **50:** 151–159.

Nakauchi, M. 1979. Development and budding in the oozooids of polyclinid ascidians. 3. *Aplidium solidum*. *Annot. Zool. Jpn.* **52:** 40–49.

Nakauchi, M. 1980a. Development, strobilation, and regeneration in the oozooids of *Aplidium nordmanni* (a colonial ascidian). *Mem. Fac. Sci. Kochi Univ. Ser. D Biol.* **1:** 11–22.

Nakauchi, M. 1980b. Oozooids of *Parascidia areolata* (a polyclinid ascidian). *Rep. Usa Mar. Biol. Inst.* **2:** 19–23.

Nakauchi, M. 1981. Development and budding in the oozooids of *Polyclinum aurantium* (a colonial ascidian) (Protochordata). *J. Zool. Lond.* **194:** 1–9.

Nakauchi, M. 1982. Asexual development of ascidians: its biological significance, diversity and morphogenesis. *Am. Zool.* **22:** 753–763.

Nakauchi, M. 1986. Oozooid development and budding in the polyclinid ascidian, *Parascidia flemingii* (Urochordata). *J. Zool. Lond. (A)* **208:** 255–267.

Nakauchi, M. 1987. Strobilation and colony formation in the ascidian, *Aplidium californicum*. *Mem. Fac. Sci. Kochi Univ. Ser. D Biol.* **8:** 9–14.

Scott, S. F. M. 1952. The developmental history of *Amaroecium constellatum*. III. Metamorphosis. *Biol. Bull.* **103:** 226–241.

Trason, W. B. 1957. Larval structure and development of the oozooid in the ascidian *Euherdmania claviformis*. *J. Morphol.* **100:** 509–546.

Vreeland, V., and W. M. Laetsch. 1988. Role of alginate self-associating subunits in the assembly of *Fucus* embryo cell walls. Pp. 77–96 in *Self-Assembling Architecture, the 46th Symposium of the Society for Developmental Biology*, J. E. Varner, ed. Alan R. Liss, Inc, New York.

Reference: Biol. Bull. 183: 440–447. (December, 1992)

The Effect of Palp Loss on Feeding Behavior of Two Spionid Polychaetes: Changes in Exposure

SARA M. LINDSAY AND SARAH A. WOODIN

Department of Biological Sciences, University of South Carolina, Columbia, South Carolina, 29208

Abstract. The effects of sublethal predation on foraging behavior are potentially important. Such predation changes both the condition of the individual and the cost or risk associated with further predation. Tissue loss to predators is a very common phenomenon in marine sedimentary environments; often the tissue lost is the organism's feeding structure. We asked how the loss of feeding structures would affect the foraging behavior of two species of spionid polychaetes, and whether the responses to palp loss are predictable. *Rhyncospio glutaeus* and *Pseudopolydora kempi japonica* represent the ends of a spectrum of risk associated with tissue exposure during feeding. In both species, the loss of one or both palps significantly increased the amount of tissue exposed, and the frequency of exposure, but not the duration of each exposure. All changes were consistent with the normal foraging behaviors of these species. Estimates of relative energy gain suggest that these responses may partially mitigate the effect of palp loss, although potentially increasing the risk of predation.

Introduction

Predation can have profound effects on the foraging behavior of prey organisms, influencing when, where, on what, and how they feed (Lima and Dill, 1990). Trade-offs between food acquisition and risk of predation are common, such as reductions in time spent feeding when predation risk is high (Stein and Magnuson, 1976), use of energetically inferior but secure patches or habitats in the presence of predators (Werner *et al.*, 1983; Gilliam and Fraser, 1987; Holbrook and Schmitt, 1988), reduced handling time in areas with less cover (Valone and Lima, 1987), and reduced general activity levels in the presence of predators (Holomuzki and Short, 1988; Main, 1987). Whether animals make such trade-offs can depend on predator abundance, food abundance, the condition of the animal, or a combination of these features (Milinski and Heller, 1978; Mangel and Clark, 1986).

Tissue loss from sublethal predation affects the condition of individuals by changing their physiological state. In addition, such tissue loss may also change the cost or risk associated with further predation [*e.g.*, tailless lizards are more likely to be captured by predators than lizards with intact tails (Dial and Fitzpatrick, 1984; Vitt and Cooper, 1986)]. Sublethal predation is common in marine environments. For example, sediment dwellers (infauna) frequently lose body parts that are exposed above the sediment surface (brittlestar arms: Bowmer and Keegan, 1983; tentacles and tails of worms: De Vlas, 1979a, b; Woodin, 1982; Clavier, 1984; Zajac, 1985; siphons of clams: Edwards and Steele, 1968; Peterson and Quammen, 1982; De Vlas, 1985). Colonial forms living on hard surfaces are often only partially eaten by their predators (Harvell, 1984; Harvell and Suchanek, 1987). Such tissue losses affect growth, reproduction, and activity (growth: De Vlas, 1979b; Peterson and Quammen, 1982; Coen and Heck, 1991; Harvell, 1984; Harvell and Suchanek, 1987; reproduction: Zajac, 1986; Wahle, 1985; activity: Woodin, 1984; Clements, 1985). Moreover, the loss of sensory structures on exposed body parts may impair such organisms' ability to detect predators.

Infaunal animals respond immediately to partial predation by changes in activity and behavior, and thus can be readily used to investigate short term responses to tissue loss. This is particularly true because: (1) the infauna live within a partial predator refuge, the sediment (Virnstein, 1979; Blundon and Kennedy, 1982); (2) their response to predation risk is easily quantifiable as relative exposure outside the sediment; and (3) the tissues lost are often

Received 7 April 1992; accepted 22 September 1992.

feeding structures the loss of which directly affects foraging.

Organisms losing feeding structures would appear to have three options representing trade-offs between energetic requirements and risk of further predation: (1) no change in foraging behavior, (2) reduced exposure during foraging, or (3) increased exposure during foraging. Increased exposure might compensate for changes in food intake due to loss of feeding structures but may also increase the risk of further predation. For example, after losing their siphon tips, some bivalves move closer to the sediment surface to maintain their access to the overlying water (Zwarts, 1986). For infauna such as bivalves, predation risk increases as depth in sediment decreases (Blundon and Kennedy, 1982; Zwarts, 1986). Decreased exposure of remaining tissues reduces risk but carries the potential cost of reduced feeding rates and, for bivalves, less access to oxygenated water for respiration. Similarly, infauna that feed on the sediment surface with tentacles or palps may expose more of their body segments following loss of all or part of these feeding structures.

Sih (1987) predicted that animals under increased predation risk should decrease their exposure. In the application of this prediction, predation risk is typically defined by predator abundance, activity levels, and proximity to prey. Use of refuges by prey modifies such predation risk. Similarly, these elements of risk contribute to interactions between sublethal predators and prey (*e.g.,* Levinton, 1971). However, tissue loss may cause physiological and behavioral changes that affect a prey organism's use of refuges. In this study we addressed this modification of refuge use, asking whether, following tissue loss and in the absence of predators, the prey's stereotypical foraging behavior is modified in a way that would change the probability or cost of a second attack. Our goal was to determine how the loss of feeding appendages, a common phenomenon among infauna, would affect tissue exposure in the absence of predators.

For surface-feeding polychaetes such as spionids, feeding incurs risk of tissue loss because it involves exposure of body segments, palps, or both. By removing different amounts of the feeding apparatus (*e.g.,* one *versus* two palps), we could explicitly test whether such tissue losses would result in increased or decreased exposure of body segments. Since infauna escape into the sediment, increased exposure of the body on the sediment surface or shallower burrowing depth are equivalent to increased risk (Blundon and Kennedy, 1982; Zwarts, 1986; Woodin and Merz, 1987). We chose two species that represent extremes of spionid feeding behavior and, given the different feeding behaviors, asked whether the responses to sublethal predation are predictable from a knowledge of normal foraging modes.

Materials and Methods

Study organisms

Rhyncospio glutaeus (Ehlers) and *Pseudopolydora kempi japonica* Imajima and Hartman, are spionid polychaetes common in the intertidal zone of False Bay, San Juan Island, Washington, U. S. A. (48° 29′N: 123° 04′W). *Pseudopolydora* occurs in the high intertidal zone, and *Rhyncospio* in the lower intertidal zone. Both species commonly lose their palps in nature. In 1989 and 1990, 17% of *Rhyncospio* and 8% of *Pseudopolydora* collected from False Bay were regenerating one palp; 10% of *Rhyncospio* and 10% of *Pseudopolydora* collected were regenerating two palps (total collected, n = 466 and 355, respectively). In the absence of high particle flux, both spionid species are surface deposit feeders (Woodin, 1982; Miller and Jumars, 1986). When intact, *Rhyncospio* feeds on the surface by extending both its palps and its body segments (Woodin, 1982), sometimes even feeding directly upon the sediment with its mouth. *Pseudopolydora* rarely extends its body segments, feeding only with its palps on the surface (Woodin, 1982). Both *Rhyncospio* and *Pseudopolydora* have translucent palps, but *Rhyncospio* has about three times as many translucent anterior segments as *Pseudopolydora* (Woodin, 1982). *Rhyncospio* may be up to 15 mm long; *Pseudopolydora* can reach lengths of 30 mm (Wilson, 1984). Worms used in this study were 10 to 15 mm long (*Rhyncospio*), and 15 to 20 mm long (*Pseudopolydora*). The length of the translucent portion of the worms in these size ranges is on average 3.2 mm (15 setigers plus head: *Rhyncospio*) *vs* 1.2 mm (4 setigers plus head: *Pseudopolydora*) (Woodin, 1982; Lindsay, unpubl. data).

Palp removal and behavioral observations

Worms collected from False Bay and transported to the Friday Harbor Laboratories (University of Washington) were stored in sediment cores in a running seawater table. Worms were selected for palp removal within 10 days of collection. Only those with intact, long palps and with no other obvious damage were used. All of the worms selected for observation were relaxed in 1:1 isotonic $MgCl_2$: seawater for 2–3 minutes. There were three treatment groups, worms with 0, 1, or 2 palps removed. The palps were removed at the base where they join the peristomium. *Rhyncospio* palps require a small pull to remove, but *Pseudopolydora* palps drop off easily. After a recovery period (3–5 min) in fresh seawater, the worms were added singly to containers of sieved (0.5 mm mesh) defaunated sediment from False Bay. The mud had been frozen, thawed, rinsed with fresh seawater, placed into containers, and aged in an outdoor seawater tank for 24 h where it developed a surface algal layer. The containers

were 3 cm in diameter, and 9.5 cm deep. After palp removal, worms were allowed a minimum of 24 h to recover from handling before their feeding behavior was recorded on videotape.

Because suspension feeding should be impossible after complete palp loss, this study was restricted to observations of surface deposit feeding behavior, and all observations were made in still seawater. The containers with the worms were submerged in a 1 l beaker of seawater set inside a larger tub of flowing seawater for temperature control. The worms were filmed at night under cool, dark red-filtered fiber optic lights. A video camera attached to a dissecting microscope (at 6×) was suspended above the container. Due to the high resolution of S-VHS videotaping, the palps and segments were both clearly visible against the sediment surface in the low light conditions used for filming.

To limit the range of regenerative states, the worms were placed into their individual containers in groups of nine: three worms per treatment. All nine worms were filmed, and then another group of nine was prepared. All of the worms within a group were typically filmed within 3–4 days of palp removal (in most cases, one worm per treatment per night; *i.e.*, a total of three worms per night). The order in which the worms from each treatment were filmed each night was random. Worms were filmed only if the core surface showed evidence of feeding activity (feces). A total of 36 *Rhyncospio* were filmed: control, n = 11; one palp removed, n = 12; two palps removed, n = 13. A total of 35 *Pseudopolydora* were filmed: control, n = 11; one palp removed, n = 12; two palps removed, n = 12.

Quantifying behavior and statistics

Each worm was videotaped continuously for 2 h, enabling the measurement of true frequencies and durations of behaviors, as well as the times at which feeding behavior patterns stopped and started (Martin and Bateson, 1986). Within the 2 h for a given worm, there were multiple periods during which segments or palps were exposed outside the tube (range: 1 to 68 emergence periods). Each time a worm emerged, we counted the number of segments and palps exposed separately, and the duration of their exposure (seconds). The exposures were considered to have ended when segments or palps withdrew below the tube edge. For clarity of presentation and data analysis, the prostomium and peristomium together were counted as one segment. The prostomium and peristomium are, of course, segmental in the spionids, and are, together, about equivalent to one anterior setiger in both species (Lindsay, pers. obs.). These data were summarized along two time scales: the full 2 h period, and a per emergence scale; thus the frequency, duration and quantity of segment and palp exposure could be described (see Table I).

Table I

Behavioral variables analysed in this study

2-hour time scale
Frequency:
Frequency of segment exposure
Frequency of palp exposures
Duration:
Proportion of 2 h during which any segments were exposed
Proportion of 2 h during which any palps were exposed
Longest duration the maximum number of segments were exposed in 2 h (s)
Quantity:
Mean number of segments exposed in 2 h
Maximum number of segments exposed in 2 h
Per-emergence time scale
Duration:
Duration of segment exposures
Duration of palp exposures
Duration the maximum number of segments were exposed per emergence
Quantity:
Mean number of segments exposed per emergence
Maximum number of segments exposed per emergence

For the 2 h time scale, all variables resulted in one value per worm. For the per emergence time scale, means of the per emergence values for individuals were the data analysed. Potential detectability of a worm by visual predators will increase with increasing frequency or duration of exposure and with increasing amount of tissue (*i.e.*, body segments) exposed.

Variables summarized on a per emergence time scale had distributions within an individual worm, but comparison among all individuals required a single value for each worm. We used the mean of a variable as the value per individual. Although the mode may be a good descriptor of an individual distribution when assessing behavior, it was often not available, did not necessarily occur frequently (a mode could be due to 2 observations out of 25), and was typically equal to or within one standard deviation of the mean of the distribution.

ANOVA was used to determine the effect of palp removal on the behavior variables, with *a posteriori* Bonferroni multiple comparisons among treatment means. When necessary, variables were transformed to meet the assumptions of ANOVA and to correct heteroscedasticity, as noted in Table II (homoscedasticity tested by Scheffé-Box test, Sokal and Rohlf, 1981). All data analysis was done using PC-SAS, version 6.04 (SAS Institute Inc., Cary, North Carolina).

Results

Palp removal had a significant effect on the frequency of segment and palp exposure in *Pseudopolydora;* both increased with palp loss (Table IIA, Figure 1A). The frequency of segment and palp exposure did not change significantly with palp loss in *Rhyncospio* (Table IIA).

Table II

Effect of palp removal on spionid feeding behavior variables

Behavior variable	*Rhyncospio* Treatment mean 0	1	2	F	sig	*Pseudopolydora* Treatment mean 0	1	2	F	sig
A. *2-hour time scale*										
a,b Frequency of segment exposure	16.69	21.71	15.17	0.89	ns	2.28	4.60	7.72	2.95	*
Mean number of segments exposed in 2 h	3.70	4.45	5.32	3.24	*	1.14	1.13	1.56	1.91	ns
Maximum number segments exposed in 2 h	10.09	11.83	12.23	0.62	ns	1.73	1.83	3.25	4.54	**
a,c Longest duration maximum number segments out in 2 h (s)	11.32	9.08	12.77	0.28	ns	32.67	51.14	44.99	0.67	ns
a,b Proportion of 2 h that segments were exposed	0.05	0.09	0.07	0.59	ns	0.002	0.004	0.01	2.46	ns
Frequency of palp exposure	24.64	20.67	NA	1.44	ns	14.27	19.17	NA	7.08	**
Proportion of 2 h that palps were exposed	0.27	0.35	NA	1.07	ns	0.83	0.90	NA	0.84	ns
B. *Per-emergence time scale*										
a,d Mean number segments out per emergence	3.12	3.56	4.84	7.02	****	1.09	1.07	1.44	1.59	ns
a,d Maximum number segments out per emergence	3.72	4.41	6.52	8.01	****	1.21	1.12	1.73	2.77	*
a,b,d Duration maximum number segments out per emergence (s)	12.73	10.98	13.64	0.67	ns	2.98	4.73	4.38	0.47	ns
b,d Mean duration segment exposures (s)	24.26	26.46	32.30	0.93	ns	4.39	5.57	7.24	0.50	ns
a,d Mean duration palp exposures (s)	77.16	110.9	NA	1.96	ns	435.3	370.8	NA	0.35	ns

[a] *Rhyncospio:* Variable was square-root transformed in analysis; back-transformed means given.

[b] *Pseudopolydora:* Variable was square-root transformed in analysis; back-transformed means given.

[c] *Pseudopolydora:* Variable was log (x + 1) transformed in analysis; back-transformed means given.

[d] Variable has a distribution across an individual. Means of per emergence values were used in the analysis; both species.

Results of one-way ANOVA with palp removal as the main effect. Palp removal treatments are 0, 1, or 2 palps removed. When variables were transformed to meet assumptions of ANOVA, back-transformed treatment means are given. Results of Bonferroni multiple comparisons are given in the figure or text for variables with F values significant at $P \leq 0.05$. Probability of significance is indicated as follows: *: $P < 0.10$, **: $P \leq 0.05$, ***: $P \leq 0.01$, ****: $P \leq 0.005$, n.s.: not significant, NA: not applicable.

The total proportion of time that any segments were exposed over the 2 h observation period was low for both species and did not change significantly with palp loss (Table IIA). Similarly, palp loss did not significantly affect the total time palps were exposed in either species (Table IIA). Neither the mean duration of segment exposures nor the mean duration of palp exposures changed significantly with palp loss in either *Rhyncospio* or *Pseudopolydora* (Table IIB). Another duration variable of interest, in terms of exposure outside the sediment refuge, is the amount of time the maximum amount of tissue is exposed by a worm. The longest duration that the greatest number of segments were exposed in 2 h showed no significant difference with palp loss for either *Rhyncospio* or *Pseudopolydora* (Table IIA). Similarly, palp loss had no effect on the length of time that the maximum number of segments were exposed per emergence in either species (Table IIB).

Measures of the quantity of segment exposure increased significantly with palp removal in both *Rhyncospio* and *Pseudopolydora* (Table II). The mean number of segments that were exposed in a 2 h period increased from 3.7 (control average) to 5.3 segments for *Rhyncospio* with no palps (two palps removed) (Table IIA, Fig. 1B). Intact *Pseudopolydora* on average extended only one segment, and this did not change significantly with palp removal. The maximum number of segments exposed in the 2 h period represents the furthest degree to which a worm exposed its body during the period. *Pseudopolydora* with two palps removed extended significantly more segments at maximum in the 2 h than intact worms, although the increase was small, from 1.7 to 3.2 segments (Table IIA, Bonferroni multiple comparison test, $\alpha = 0.05$). Over a 2 h period, *Rhyncospio* exposed at maximum 10 to 12 segments, showing no significant response to palp removal (Table IIA).

Rhyncospio with no palps (two palps removed) extended significantly more segments at maximum per emergence than those with one or two palps (Fig. 1C, Table IIB). In fact, the difference between an average of 3.7 (control) and 6.5 segments (two palps removed) exposed represents an 80% increase in the average maximum amount of tissue exposed by the worms per emergence. While the maximum number of segments exposed per emergence was statistically greater than controls for *Pseudopolydora* with no palps (Table IIB), the difference be-

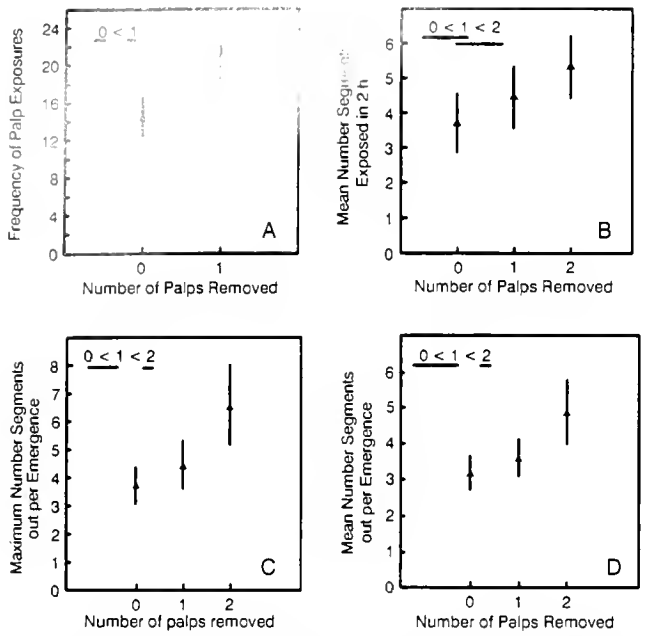

Figure 1. The effect of palp removal on tissue exposure by *Rhyncospio* and *Pseudopolydora* (means and 95% C.I.). Inequalities indicate the results of Bonferroni multiple comparisons among means. Treatments underlined by the same line are not significantly different at an $\alpha = 0.05$ experimentwise error rate. (A) Frequency of palp exposure, *Pseudopolydora;* (B) Mean number of segments exposed in 2 h, *Rhyncospio;* (C) Maximum number of segments out per emergence, *Rhyncospio;* (D) Mean number of segments out per emergence, *Rhyncospio.* In (C) and (D) back-transformed means and 95% C.I.s are plotted: Bonferroni results are for comparisons made among transformed means used in the ANOVA.

tween 1.2 (control) and 1.7 segments (two palps removed) is quite small.

The mean number of segments worms exposed per emergence is consistent with the mean number of segments exposed in the 2 h period. *Pseudopolydora* with no palps (two palps removed) tended to expose more segments per emergence than those with one or two palps, but the change is very small and not significant (Table IIB). *Rhyncospio* with no palps exposed significantly more segments per emergence than those with one or two palps (Fig. 1D and Table IIB).

Because both spionid species have anterior body segments are relatively translucent and presumably cryptic (e.g., 1982), increases in the quantity of segment exposure were also considered with respect to the coloration of tissue exposed. Both *Rhyncospio* and *Pseudopolydora* increased the quantity of segment exposure in response to palp loss (Table II). But the maximum number of segments exposed per emergence by *Rhyncospio* (6.5 ± , X ± S.D., n = 13) (Fig. 1C) is well within the range of translucent anterior segments reported by Woodin (1982): 15.1 ± 3.2 (X ± S.D., n = 42). In fact, the maximum number of segments exposed in the 2 h by *Rhyncospio* with no palps, 12.2 ± 4.4 (X ± S.D., n = 13), is also within the range of translucent segments. The same is true for *Pseudopolydora.* The maximum number of segments exposed in 2 h by individuals with no palps, 3.2 ± 1.5 (X ± S.D., n = 12) (Table IIA), is within the range of translucent anterior segments reported by Woodin (1982): 4.3 ± 3.7 (X ± S.D., n = 51).

The normal feeding behavior of *Rhyncospio* would appear to involve more risk than that of *Pseudopolydora:* exposure of more segments (and more metric length: 0.74 mm *vs.* 0.27 mm) with greater frequency and duration (controls, Table II), as well as longer periods of exposure to aquatic predators, because *Rhyncospio* lives in the lower intertidal zone. The occurrence of worms in the field regenerating one palp seems to support this; twice as many *Rhyncospio* as *Pseudopolydora* were found regenerating one palp (17%: n = 466 and 8%: n = 355, respectively; these proportions are significantly different, z-test, z = 3.83, $P \leq 0.05$). However, the percentage of worms regenerating two palps was the same for both species: 10%. The translucence of the anterior tissues (*i.e.,* crypsis) probably decreases detectability of spionids by visual predators, but does not render them invisible. Following palp loss, all increases in body segment exposure were within the translucent portions of the worms.

Discussion

For prey, risk is a measure of exposure determined by predator access, abundance, and activity, as well as by the behavior of prey. In these experiments, we measured changes in refuge use by infaunal prey (spionid polychaetes) following tissue loss. Because the sediment acts as a partial refuge from predation for infauna (Virnstein, 1979; Blundon and Kennedy, 1982), any increase in exposure on the sediment surface represents increased risk in the same sense that emergences from other refuges, such as crevices and complex structures, represent increased risk (fish: Sale, 1971; brittlestars: Sides, 1981; harpacticoid copepods: Coull and Wells, 1983). Thus, in our experiments we equated risk with increases in emergence of spionids onto the sediment surface following tissue loss. These experiments were conducted in the absence of predators or competitors. Clearly, the presence of either of these may affect the behavior of the spionids. In the presence of predators or competitors we would expect a reduction in the differences in exposure between worms with palps and worms with no palps due mainly to decreased activity of all worms. This expectation is based upon numerous observations that infauna (particularly spionids) withdraw into the sediment with changes in light intensity, shadowing, vibration, water pressure, physical contact with tubes or body parts etc., all of which are

presumably associated with predators (*e.g.*, fish and shrimp), competitors (*e.g.*, other spionids), or even with physical events which could cause damage to the animal. Our results, then, represent a baseline description of the effect of tissue loss on behavior and refuge use.

Increased exposure with tissue loss

Juvenile flatfish, such as plaice and dab, are well-known partial predators, with bivalve siphons and polychaete tentacles constituting the majority of their diets (Edwards and Steele, 1968; De Vlas, 1979a). These predators scan the sediment surface for prey and pounce upon it; dab in particular rely on visual cues, whereas plaice also employ chemical detection of prey (De Groot, 1971). Given such predators, the frequency, duration, and quantity of tissue exposure directly contribute to prey detectability. By simple chance, more frequent exposure increases the chance of detection. Similarly, a predator will have more time to identify prey as the duration of prey exposure increases. The quantity of its tissue exposed will also contribute to prey detectability.

For both *Rhyncospio* and *Pseudopolydora*, feeding behaviors following palp loss were expansions of their normal feeding behaviors, with no radical alterations; thus intact feeding behaviors may be useful for predicting the behavioral response of spionid polychaetes to palp loss. *Rhyncospio* often exposes segments during feeding, while *Pseudopolydora* does not (controls, Table II). Loss of feeding structures in *Rhyncospio* resulted in much greater exposure of segments than in *Pseudopolydora* (Table IIB). *Pseudopolydora* feeds primarily with its palps, and following loss of one palp, frequency of exposure of the remaining palp increased. Tissue loss caused increased exposure of anterior tissues in both species (Table II), and this increased exposure should be associated with increased risk.

Trade-offs of risk and energy?

The behavioral options for foraging animals lie on a continuum between energy maximization (at the expense of predator avoidance) and risk minimization (at the expense of feeding). Loss of feeding structures might constrain infauna to feed at, or closer to, either of these extremes. For instance, spionids with no palps may either expose body segments to feed upon the surface with their mouths (at the expense of increased chance of detection by predators), or these worms may not feed at all, remaining within the sediment refuge.

We observed increased tissue exposure following palp loss in both species of spionids examined. Assuming that all exposure is associated with feeding, the advantage of continued feeding might contribute to the observed increase in exposure. The worms probably did not face starvation, as evidenced by the presence of feces on cores within 2 to 5 days after removal of two palps from worms of both species. Nevertheless, continued and increased exposure for feeding may speed palp regeneration, thereby minimizing the impact of palp loss. Do the observed increases in exposure result in increased energy gain? Although we did not measure growth in these experiments, by relating the time spent feeding to intake rate and hence energy gain, we can make some estimates of the energy gain associated with the responses of these polychaetes.

Assuming no changes in the efficiency of digestion and assimilation following palp loss, energy gain will be directly related to intake rate. If we assume that a worm with one palp feeds with 50% of the collection efficiency of an intact worm and that time spent feeding is proportional to energy intake, then we can use our data on palp and segment exposure times to estimate relative energy gain per treatment by the following calculations: for the control, (time that the two palps are exposed $\times$ 1); for worms with one palp, (time that the palp is exposed $\times$ 0.5); with no palps, (time that the segments are exposed). Exposure times are calculated by multiplying the frequency of exposure by the duration of exposure, using appropriate treatment means from Table II. Note that, in over 99% of the cases, when the segments are exposed, the palps are exposed; thus only in the no palp treatment must we use segment exposure times in the calculations. For these calculations, we have assumed that all exposure is associated with feeding. For *Rhyncospio*, at least, this is probably not true and further study may reveal shifts in the time spent feeding following palp loss.

By the above calculation, loss of one palp by *Rhyncospio* would reduce the worm's relative energy intake by 40%, and loss of both palps would result in a 74% reduction relative to controls. For *Pseudopolydora*, the reductions are even more dramatic: 43% and 99%. Note that, for both species, the relative reduction in energy gain following the loss of one palp is less than the 50% that would be expected if there were no changes in exposure.

Woodin's (1984) data on weights of feces of another spionid, *Spiophanes bombyx*, following palp loss suggest no change in efficiency following the loss of one palp, but reduced efficiency following the loss of two palps. Changing our calculations to time exposed, with no adjustment for one or two palps present, we find no significant change between controls and one palp treatments for *Rhyncospio* (*i.e.*, no difference in palp exposure times, Table II) but still a 74% reduction for the no palp treatment. *Rhyncospio* is similar to *Spiophanes* in its feeding mode, and this pattern of reduction is similar as well. Woodin (1984) saw no reduction in fecal weights of *Spiophanes* with one palp, but observed a 35% reduction in fecal weights of those with no palps. For *Pseudopolydora*, assuming no change in efficiency following the loss of one palp, relative energy

intake would increase [illegible] for the one palp treatment relative to controls (due to the significant increase in palp exposure in the one palp treatment) and would be reduced by 99% for the no palps treatment.

From both calculations, loss of both palps, a common phenomenon for numerous species including *Rhyncospio* and *Pseudopolydora*, has striking effects on relative energy gain. These calculations also show that increased palp exposure by *Pseudopolydora* with one palp ablated resulted in an apparent increase in relative energy gain. But, because *Pseudopolydora* did not change its segment exposure after losing both palps, as predicted by normal foraging behavior, it incurred a 99% reduction in relative energy intake. Normal feeding behavior in *Rhyncospio* involves segment exposure and, after the loss of two palps, the amount of segment exposure increased (Table II). But, to compensate for the loss of both palps, the frequency and duration of segment exposure would have to increase, and they did not (Table II), resulting in a 74% reduction in relative energy intake. Whether the changes in frequency, duration, and quantity of tissue exposure are a reflection of the relative risk of these three behaviors awaits further study.

Another factor that might contribute to energy gain is the area of sediment surface to which a worm may have access. This feeding area is directly determined by the amount of tissue exposed, which as we have shown, increased with palp loss. We describe the feeding area available to a worm as circular, with the tube opening at the center. The radius of this circle is determined by the average length of tissue exposed, which is the sum of segment and palp lengths. Segment length is equivalent to the product of the length per anterior segment (*Rhyncospio:* 0.2 mm; *Pseudopolydora:* 0.24 mm) and the average number of segments exposed in 2 h (Table IIA, treatment means). Palp length is the average palp length of worms in the appropriate treatment (*Rhyncospio* controls: 2.7 mm; *Pseudopolydora* controls: 10.2 mm).

By this calculation, the feeding area of intact *Rhyncospio* is 37.0 mm^2. Following palp loss, the feeding radius is determined by the length of body segments exposed. For *Rhyncospio* with no palps, the feeding area is 3.5 mm^2. For *Rhyncospio* in this study, loss of two palps resulted in a 90% reduction of the average area accessible for feeding.

Intact *Pseudopolydora* have longer palps than intact *Rhyncospio*, therefore, a longer feeding radius as well. For intact *Pseudopolydora* in this study, the feeding area is 344.0 mm^2, because *Pseudopolydora* with no palps extended very few segments, their potential feeding area was drastically reduced. The feeding area of *Pseudopolydora* with no palps is 0.4 mm^2!

Like the relative energy gain calculations, these suggest that palp loss will dramatically reduce the accessible feeding area for these worms. Although *Rhyncospio* with no palps significantly increased its exposure of segments (Table II), this increase was not enough to compensate for the loss of palps. The feeding area of *Pseudopolydora* with no palps was even more drastically reduced. In terms of energy gain, the relative importance of these changes in feeding area following palp loss will be modified by the hydrodynamic regime of the worms' habitat and by particle re-supply rates. High particle re-supply rates may mitigate the effect of a reduced feeding area (Miller *et al.*, 1984).

These results emphasize the need to consider the foraging behavior of infauna with respect to the effects of partial predation, particularly because infauna often lose feeding structures. Like lethal predation risk, partial predation can influence when (Levinton, 1971) and where (this paper) infauna feed. For spionids losing palps, the potential advantage to continued feeding and therefore faster palp regeneration may cause increases in the exposure of the remaining tissues (Table II, Fig. 1). These increases in exposure may mitigate the effect of palp loss on relative energy intake but may also increase risk. Given the demonstrated changes in feeding behavior following palp loss in spionid polychaetes and the potential increase in risk associated with increased tissue exposure, consideration of the regenerative state of the animal and consequent changes in behavior is especially important in foraging models of infauna.

Acknowledgments

Comments by J. Eckman, D. Lincoln, P. Rawson, S. Stancyk, M. Greenberg, and two anonymous reviewers improved the manuscript. Dr. A. O. D. Willows, Director of the Friday Harbor Marine Laboratories, University of Washington, kindly made the facilities of the laboratories and the protected habitats available. S. M. L. thanks M. Strathmann, B. Stell, and G. Mackie who provided welcome musical respite from filming and scoring. This material is based upon work supported under a National Science Foundation Graduate Fellowship to S. M. L. Additional support was provided by NSF grant OCE-8900212 to S. A. W.

Literature Cited

Bowmer, T., and B. F. Keegan. 1983. Field survey of the occurrence and significance of regeneration in *Amphiura filiformis* (Echinodermata: Ophiuroidea) from Galway Bay, west coast of Ireland. *Mar. Biol.* **74:** 65–71.

Blundon, J. A., and V. S. Kennedy. 1982. Refuges for infaunal bivalves from blue crab, *Callinectes sapidus* (Rathbun), predation in Chesapeake Bay. *J. Exp. Mar. Biol. Ecol.* **65:** 67–81.

Clavier, J. 1984. Production due to regeneration by *Euclymene oerstedi* (Claparede) (Polychaeta: Maldanidae) in the maritme basin of the Rance (Northern Brittany). *J. Exp. Mar. Biol. Ecol* **75:** 97–106.

Clements, L. A. J. 1985. Post-autotomy feeding behavior of *Micropholis gracillima* (Stimpson): Implications for regeneration. Pp. 609–615 in *Proceedings of the 5th International Echinoderm Conference,* B. F. Keegon, and B. D. S. O'Connor, eds. Galway, Ireland.

Coen, L. D., and K. L. Heck, Jr. 1991. The interacting effects of siphon nipping and habitat on bivalve (*Mercenaria mercenaria* (L.)) growth in a subtropical seagrass (*Halodule wrightii* Aschers) meadow. *J. Exp. Mar. Biol. Ecol.* **145:** 1–13.

Coull, B. C., and J. B. J. Wells. 1983. Refuges from fish predation: experiments with phytal meiofauna from the New Zealand rocky intertidal. *Ecology* **64:** 1599–1609.

De Groot, S. J. 1971. On the interrelationships between morphology of the alimentary tract, food and feeding behaviour in flatfishes (Pisces: Pleuronectiformes). *Neth. J. Sea Res.* **5:** 121–196.

De Vlas, J. 1979a. Annual food intake by plaice and flounder in a tidal flat area in the Dutch Wadden Sea, with special reference to consumption of regenerating parts of macrobenthic prey. *Neth. J. Sea Res.* **13:** 117–153.

De Vlas, J. 1979b. Secondary production by tail regeneration in a tidal flat population of lugworms (*Arenicola marina*) cropped by flatfish. *Neth. J. Sea Res.* **13:** 362–393.

De Vlas, J. 1985. Secondary production by siphon regeneration in a tidal flat population of *Macoma Balthica*. *Neth. J. Sea Res.* **19:** 147–164.

Dial, B. E., and L. C. Fitzpatrick. 1984. Predator escape success in tailed versus tailless *Scincella lateralis* (Sauria: Scincidae). *Anim. Behav.* **32:** 301–302.

Edwards, R., and J. H. Steele. 1968. The ecology of 0-group plaice and common dabs at Loch Ewe. 1. Population and food. *J. Exp. Mar. Biol. Ecol.* **2:** 215–238.

Gilliam, J. F., and D. F. Fraser. 1987. Habitat selection under predation hazard: test of a model with foraging minnows. *Ecology* **68:** 1856–1862.

Harvell, C. D. 1984. Why nudibranchs are partial predators: intracolonial variation in bryozoan palatability. *Ecology* **65:** 716–724.

Harvell, C. D., and T. H. Suchanek. 1987. Partial predation on tropical gorgonians by *Cyphoma gibbosum* (Gastropoda). *Mar. Ecol. Prog. Ser.* **38:** 37–44.

Holbrook, S. J., and R. J. Schmitt. 1988. Effects of predation on foraging behavior: mechanisms altering patch choice. *J. Exp. Mar. Biol. Ecol.* **121:** 170–180.

Holomuzki, J. R., and T. M. Short. 1988. Habitat use and fish avoidance behaviors by the stream-dwelling isopod *Lirceus fontinalis*. *Oikos* **52:** 79–86.

Levinton, J. S. 1971. Control of Tellinacean (Mollusca: Bivalvia) feeding behavior by predation. *Limnol. Oceanogr.* **16:** 660–662.

Lima, S. L., and L. M. Dill. 1990. Behavioral decisions made under risk of predation: a review and prospectus. *Can. J. Zool.* **68:** 619–640.

Main, K. L. 1987. Predator avoidance in seagrass meadows: prey behavior, microhabitat selection, and cryptic coloration. *Ecology* **68:** 170–180.

Mangel, M., and C. W. Clark. 1986. Towards a unified foraging theory. *Ecology* **67:** 1127–1138.

Martin, P., and P. Bateson. 1986. *Measuring Behaviour.* Cambridge University Press, Great Britain. 200 pp.

Milinski, M., and R. Heller. 1978. Influence of a predator on the optimal foraging behaviour of sticklebacks (*Gasterosteus aculeatus* L.). *Nature* **275:** 642–644.

Miller, D. C., and P. A. Jumars. 1986. Pellet accumulation, sediment supply, and crowding as determinants of surface deposit-feeding rate in *Pseudopolydora kempi japonica* Imajima & Hartman (Polychaeta: Spionidae). *J. Exp. Mar. Biol. Ecol.* **99:** 1–17.

Miller, D. C., P. A. Jumars, and A. R. M. Nowell. 1984. Effects of sediment transport on deposit feeding: scaling arguments. *Limnol. Oceanogr.* **29:** 1202–1217.

Peterson, C. H., and M. L. Quammen. 1982. Siphon nipping: its importance to small fishes and its impact on growth on the bivalve *Protothaca staminea* (Conrad). *J. Exp. Mar. Biol. Ecol.* **63:** 249–268.

Sale, P. F. 1971. Extremely limited home range in a coral reef fish: *Dascyllus aruanus* (Pisces; Pomocentridae). *Copeia* **1971:** 324–327.

Sides, E. M. 1981. Aspects of space utilization in shallow-water brittle-stars (Echinodermata, Ophiuroidea) of Discovery Bay, Jamaica. Ph.D. Dissertation, University of the West Indies, Mona, Jamaica.

Sih, A. 1987. Predators and prey lifestyles: an evolutionary and ecological overview. Pp. 203–224 in *Predation: Direct and Indirect Impacts on Aquatic Communities,* W. C. Kerfoot and A. Sih, eds. University Press of New England, Hanover, NH.

Sokal, R. R., and F. J. Rohlf. 1981. *Biometry,* 2nd edition. W. H. Freeman & Co., San Francisco, CA. 776 pp.

Stein, R. A., and J. J. Magnuson. 1976. Behavioral response of crayfish to a fish predator. *Ecology* **57:** 751–761.

Valone, T. J., and S. L. Lima. 1987. Carrying food items to cover for consumption: the behavior of ten bird species feeding under the risk of predation. *Oecologia* **71:** 286–294.

Virnstein, R. W. 1979. Predation on estuarine infauna: Response patterns of component species. *Estuaries* **2:** 69–86.

Vitt, L. J., and W. E. Cooper, Jr. 1986. Tail loss, tail color, and predator escape in *Eumeces* (Lacertilia: Scincidae): age-specific differences in costs and benefits. *Can. J. Zool.* **64:** 583–592.

Wahle, C. M. 1985. Habitat-related patterns of injury and mortality among Jamaican gorgonians. *Bull. Mar. Sci.* **37:** 905–927.

Werner, E. E., J. F. Gilliam, D. J. Hall, and G. G. Mittelbach. 1983. An experimental test of the effects of predation risk on habitat use in fish. *Ecology* **64:** 1540–1548.

Wilson, W. H., Jr. 1984. Non-overlapping distributions of spionid polychaetes: the relative importance of habitat and competition. *J. Exp. Mar. Biol. Ecol.* **75:** 119–127.

Woodin, S. A. 1982. Browsing: important in marine sedimentary environments? Spionid polychaete examples. *J. Exp. Mar. Biol. Ecol.* **60:** 35–45.

Woodin, S. A. 1984. Effects of browsing predators: activity changes in infauna following tissue loss. *Biol. Bull.* **116:** 558–573.

Woodin, S. A., and R. Merz. 1987. Holding on by their hooks: anchors for worms. *Evolution* **41:** 427–432.

Zajac, R. N. 1985. The effects of sublethal predation on reproduction in the spionid polychaete *Polydora ligni* Webster. *J. Exp. Mar. Biol. Ecol.* **88:** 1–19.

Zwarts, L. 1986. Burying depth of the benthic bivalve *Scrobicularia plana* (da Costa) in relation to siphon-cropping. *J. Exp. Mar. Biol. Ecol.* **101:** 25–39.

Reference: *Biol. Bull* 183: 448–455. (December, 1992)

Phylogenetic Relationships between Solitary and Colonial Ascidians, as Inferred from the Sequence of the Central Region of their Respective 18S rDNAs

HIROSHI WADA[1], KAZUHIRO W. MAKABE[1,*], MITSUAKI NAKAUCHI[2] AND NORIYUKI SATOH[1]

[1]*Department of Zoology, Faculty of Science, Kyoto University, Kyoto 606–01, and* [2]*The President, Kochi University, Kochi 780, Japan*

Abstract. Ascidians (tunicates) are primitive chordates. In spite of their elevated phylogenetic position in the animal kingdom, ascidians have evolved a varied reproductive repertoire; some of them live as individuals (solitary ascidians), while others form colonies (colonial ascidians). Colonial ascidians propagate asexually by budding and strobilation, and they have an extensive capacity for regeneration. However, the orthodox taxonomic classification of ascidians categorizes them into two major groups (the orders Enterogona and Pleurogona), irrespective of their solitary or colonial life style. To examine whether the orthodox classification of ascidians is substantiated by molecular phylogeny, the complete nucleotide sequence of a region of about 1000 base pairs in the central part of their respective 18S rDNAs was determined, and the sequences were compared among five solitary and three colonial ascidians. The phylogenetic tree deduced from these results suggests that the three species of Enterogona and the five species of Pleurogona examined form discrete and separate groups irrespective of their potential to form colonies. Therefore, a solitary or colonial life style is likely to have developed independently after the divergence of the two major groups of ascidians.

Introduction

Ascidians (subphylum Urochordata, class Ascidiacea), or sea squirts, are ubiquitous, sessile marine animals that can be classified as members of about 2,300 species. Since a tadpole-type larva with a well-organized notochord is formed, ascidians are regarded as one of the most primitive types of chordate (Kowalevsky, 1986; Berrill, 1955). Recent studies of the molecular phylogeny of the animal kingdom by comparison of sequences of 5S rRNA (Hori and Osawa, 1987) and 18S rRNA (Field *et al.*, 1988) support this view; namely, ascidians are more closely related to vertebrates than to invertebrates. This view is also supported by recent studies of the structure of genes for muscle actin (Kusakabe *et al.*, 1992). In spite of such an elevated phylogenetic position in the animal kingdom, ascidians have evolved a wide variety of patterns and modes of development. Some of them live as individuals (solitary ascidians), while others form colonies (colonial ascidians). Solitary ascidians propagate exclusively by sexual reproduction, whereas colonial ascidians reproduce both sexually, and asexually by budding and strobilation (Berrill, 1935; Nakauchi, 1982). In addition, colonial ascidians have an extensive capacity for regeneration. On the basis of these differences, ascidians were initially classified as solitary (or simple) or as members of colonial (or compound) groups (Savigny, 1816). This classification is rather convenient for explanations of various phenomena in the fields of developmental and cell biology.

The modern and more orthodox taxonomic classification of ascidians is based mainly on the morphology of the branchial sac and the gonad, and at present, ascidians are subdivided into two orders, the Enterogona and Pleurogona (Lahille, 1886; Huus, 1940; Berrill, 1936, 1950; Millar, 1966; Kott, 1969; Monniot and Monniot, 1973). The Enterogona, in which each individual has a single gonad, contains two subgroups, namely, Aplousobran-

Received 6 [illegible] cepted 30 September 1992.

* Present address: [illegible] tment of Biology, California Institute of Technology, Pasadena, California 91125.

Table I

Distribution of PCR, cloning, and sequencing errors

Position in sequence	Individual 1		Individual 2	
	Clone 1	Clone 2	Clone 1	Clone 2
297	C	C	G	C
328	A	A	C	A
352	G	C	G	G
511	G	A	G	G
525	T	T	T	C
595	C	T	T	T
773	T	T	T	C
802	G	A	A	A
857	G	G	A	G

chiata and Phlebobranchiata; members of the former subgroup have a simple branchial sac, and members of the latter have a branchial sac with longitudinal vessels. The Pleurogona, in which each adult has a pair of gonads, contains two subgroups, namely, the Stolidobranchiata and Aspiraculata: members of the former subgroup have a folded branchial sac with longitudinal vessels, and members of the latter live in the deep sea and are macrophagous. Some aspects of the taxonomical interpretation of Aspiculata remain controversial (Kott, 1969; Monniot and Monniot, 1973).

Nucleotide sequence data provide new insight into metazoan phylogenetic relationships and complement the extensive data obtained by paleontological, morphological and developmental analyses. In particular, the sequences of 16–18S and 23–28S ribosomal RNA or DNA provide molecular markers that are useful in attempts to evaluate both long- and short-range phylogenetic relationships within the animal kingdom (Field *et al.*, 1988; Lake, 1990; Christen *et al.*, 1991). In the present investigation, we determined the sequence of a region of about 1000 base pairs (bp) in the central part of the 18S rDNA from eight ascidians, including three colonial species. By comparing these sequences, we analysed the phylogenetic relationship among these ascidians. Our main interest was in determining whether the modern, orthodox taxonomic classification is supported by the sequence data from 18S rDNA, and whether the life style of solitary and colonial ascidians developed independently of the divergence of the two major groups of ascidians.

Materials and Methods

Ascidians

Eight species of ascidians, three from the order Enterogona and five from the order Pleurogona, were examined in this study. The former included *Ciona savignyi, Perophora japonica, Ascidia sydneiensis samea,* and the latter included *Halocynthia roretzi, Pyura mirabilis, Styela clava, Polyandrocarpa misakiensis,* and *Symplegma reptans. Per. japonica, Poly. misakiensis* and *Sym. reptans* are colonial ascidians; the five others are solitary ascidians.

```
          143
18S rRNA:GTTTACTTTGAAAAAATTAGAGTGTTCAAA-CAGGCTGTTCGCCTGCATAGTGTTGCATGGAATAATGGAAT
18S rDNA:.............................G.....................................

AGGACCTCGGTTCTATTTTGTTGGTTTTCGGAGCACGAGGTAATGATTAAGAGGGAC?GACGG?GCCGTCCG
.....................................................A.....G.G......

T?CTCTGCCGTTAGAGGTGAAATTCTTGGATCGGCGGAAGACGAACTACTGCGAAAGCATTCGCC?AGAATG
.A.....................................................................A......

TTTTCTTT?ATC?AGA-CGAAAGTCAGAGGTTCGAAGACGATCAGATACCGTCCTAGTTCTGACTATAAACG
........A...A...G.....................................................

                                                                      504
ATGCCAACTAGCGATCGGGAGGCGTTACCATGACGACCTTTCCG?CAGCTTCCGGGAAACCAAAGTCTTTG
.....................................G.....................
```

Figure 1. Comparison between the nucleotide sequence of a region of the 18S rDNA of *Styela clava*, determined in the present study, and that of 18S rRNA, as reported by Field *et al.* (1988). The data for 18S rRNA were kindly provided by Dr. Rudolf A. Raff of Indiana University.

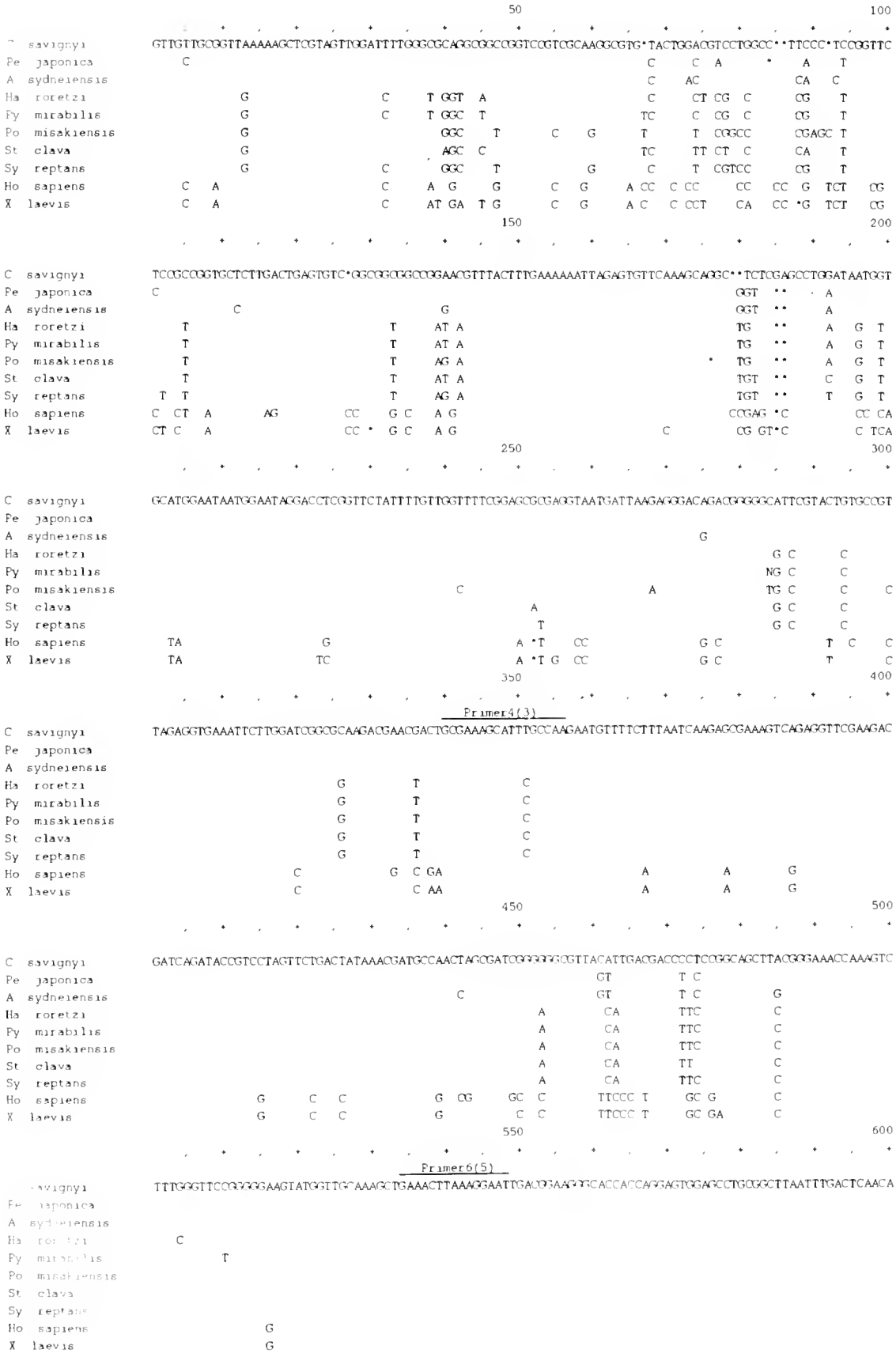
50
100
C savignyi GTTGTTGCGGTTAAAAAGCTCGTAGTTGGATTTTGGGCGCAGGCGGCCGGTCCGTCGCAAGGCGTG*TACTGGACGTCCTGGCC**TTCCC*TCCGGTTC
Pe japonica
A sydneiensis
Ha roretzi
Py mirabilis
Po misakiensis
St clava
Sy reptans
Ho sapiens
X laevis
150
200
C savignyi TCCGCCGGTGCTCTTGACTGAGTGTC*GGCGGCGGCCCGAACGTTTACTTTGAAAAAATTAGAGTGTTCAAAGCAGGC**TCTCGAGCCTGGATAATGGT
Pe japonica
A sydneiensis
Ha roretzi
Py mirabilis
Po misakiensis
St clava
Sy reptans
Ho sapiens
X laevis
250
300
C savignyi GCATGGAATAATGGAATAGGACCTCGGTTCTATTTTGTTGGTTTTCGGAGCGCGAGGTAATGATTAAGAGGGACAGACGGGGGCATTCGTACTGTGCCGT
Pe japonica
A sydneiensis
Ha roretzi
Py mirabilis
Po misakiensis
St clava
Sy reptans
Ho sapiens
X laevis
350
400
Primer4(3)
C savignyi TAGAGGTGAAATTCTTGGATCGGCGCAAGACGAACGACTGCGAAAGCATTTGCCAAGAATGTTTTCTTTAATCAAGAGCGAAAGTCAGAGGTTCGAAGAC
Pe japonica
A sydneiensis
Ha roretzi
Py mirabilis
Po misakiensis
St clava
Sy reptans
Ho sapiens
X laevis
450
500
C savignyi GATCAGATACCGTCCTAGTTCTGACTATAAACGATGCCAACTAGCGATCGGGGGGCGTTACATTGACGACCCCTCCGGCAGCTTACGGGAAACCAAAGTC
Pe japonica
A sydneiensis
Ha roretzi
Py mirabilis
Po misakiensis
St clava
Sy reptans
Ho sapiens
X laevis
550
600
Primer6(5)
savignyi TTTGGGTTCCGGGGGAAGTATGGTTGC*AAAGCTGAAACTTAAAGGAATTGACGGAAGGGCACCACCAGGAGTGGAGCCTGCGGCTTAATTTGACTCAACA
Pe japonica
A sydneiensis
Ha roretzi
Py mirabilis
Po misakiensis
St clava
Sy reptans
Ho sapiens
X laevis

Figure 2.

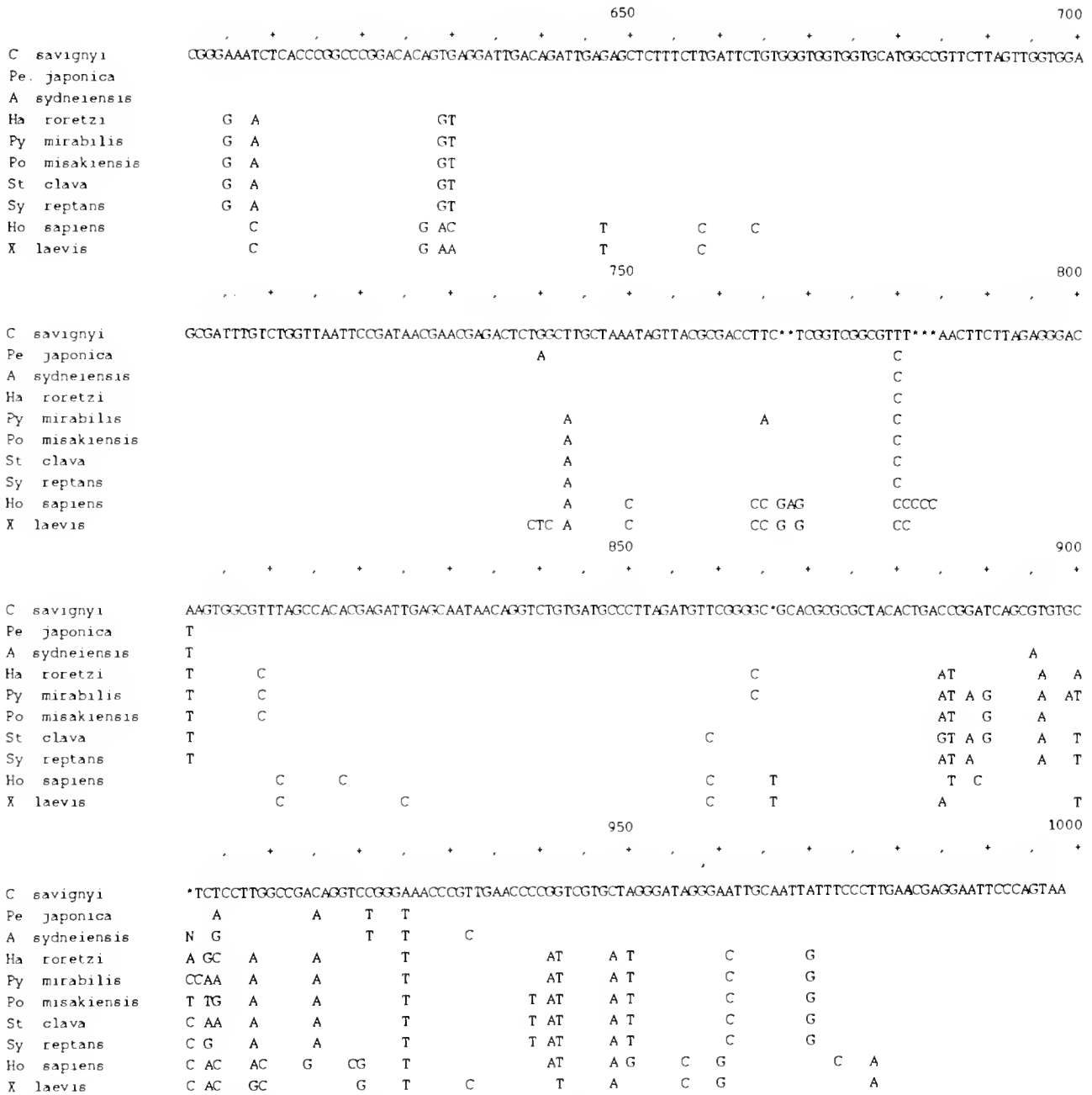

Figure 2. Alignment of the central regions of the 18S rDNAs from eight ascidians analysed by the present study, *Homo sapiens* and *Xenopus laevis* (Neefs *et al.*, 1990). All the bases are shown for *Ciona savignyi* and only bases different from these are shown for other species. Asterisks indicate deletions. The four primers used for sequencing are shown by underlining.

Per. japonica, *Poly. misakiensis*, and *Sym. reptans* were generously provided by Dr. K. Kawamura, Kochi University, Japan.

Isolation of DNA

The gonad or the whole animal was frozen in liquid nitrogen and kept at −80°C until used. Frozen and powdered samples were lysed in TE buffer (10 m*M* Tris-HCl, 0.1 *M* EDTA, pH 8.0) that contained 0.5% sodium dodecyl sulfate. After digestion of samples with proteinase K (100 μg/ml) at 50°C for 3 h, DNA was extracted with phenol and precipitated in ethanol and an equal volume of 5.0 *M* ammonium acetate. Samples resuspended in TE buffer were further purified by treatment with RNase A

Table II

Structural similarity and evolutionary distance data for ascidian 18S rDNA sequences

Species	*C.s.*	*P.j*	*A.s.s.*	*H.r.*	*Py m.*	*Po m.*	*St.c.*	*Sy.r.*	*H.s.*	*X.l.*
Ciona savignyi		0.0218	0.0250	0.0641	0.0697	0.0697	0.0641	0.0675	0.1258	0.1233
Perophora japonica	21		0.0166	0.586	0.0630	0.0675	0.0586	0.0630	0.1221	0.1221
Ascidia sydneiensis samea	24	16		0.0653	0.0709	0.0720	0.0664	0.0686	0.1233	0.1245
Halocynthia roretzi	60	55	61		0.0145	0.0271	0.0239	0.0229	0.1331	0.1355
Pyura mirabilis	65	59	66	14		0.0271	0.0208	0.0229	0.1355	0.1380
Polyandrocarpa misakiensis	65	63	67	26	26		0.0282	0.0197	0.1367	0.1417
Styela clava	60	55	62	23	20	27		0.0208	0.1355	0.1392
Symplegma reptans	63	59	64	22	22	19	20		0.1318	0.1355
Homo sapiens	113	110	111	119	121	122	121	118		0.0454
Xenopus laevis	111	110	112	121	123	126	124	121	43	

The lower-left half of the table gives the number of substitutions in which gaps are not included. The upper-right half of the table gives the evolutionary distance values (average number of nucleotide substitutions per sequence position) determined by the Jukes and Cantor (1969) formula.

(20 μg/ml) at 37°C for 1 h and then precipitated in ethanol.

Amplification of the central region of 18S rDNA

A region of about 1000 bp from the central part of 18S rDNA was amplified by the polymerase chain reaction (PCR; Saiki *et al.*, 1988) in a Perkin Elmer Cetus thermal cycler. Amplifications were performed in 100 μl of 50 m*M* KCl, Tris-HCl (10 m*M*, pH 9.0), 0.1% Triton X-100, with 0.2 m*M* each dNTP, 100 p*M* primer, template DNA (10–100 μg) and 2 U *Taq* DNA polymerase (Promega). Primer-1 (5′-CAG(CA)CCCGCGGT-AAT(TA)C-3′) and Primer-2 (5′-ACGGGCGGTGTGT(AG)C-3′), the latter being identical to Primer C of Field *et al.* (1988), were used for amplification. The temperature regimen for

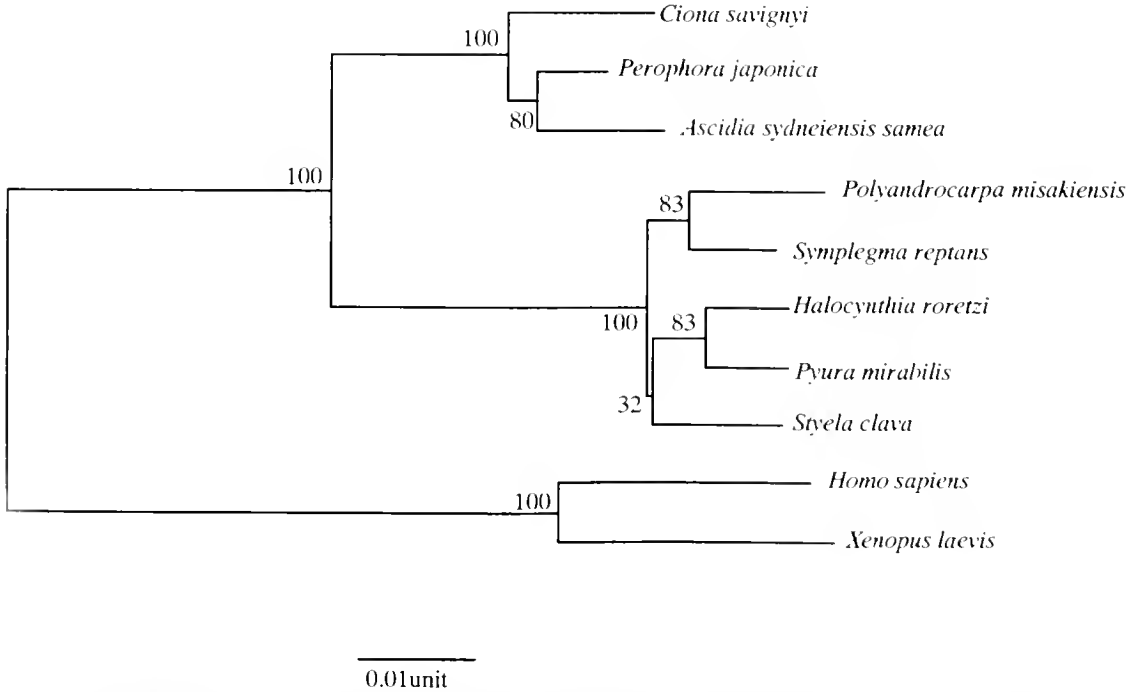

Figure 3. Phylogenetic tree of eight ascidians, as deduced by the neighbor-joining method. The scale bar indicates an evolutionary distance of 0.01 nucleotide substitution per sequence position. Numbers at each branch indicate the percentage of times a node was supported in 200 bootstrap pseudoreplications by neighbor-joining method.

30 cycles was 1 min at 92°C, 2 min at 55°C, and 3 min at 72°C.

Cloning and sequencing of the amplified DNA

Amplified DNA was purified by electrophoresis in 0.8% agarose, inserted into the *Bam*HI site of the vector pBluescriptII SK(+) (Stratagene), and cloned. Sequencing was performed by the dideoxy chain-termination method (Sanger *et al.*, 1977) using Sequenase ver 2.0 (USB) and [^{35}S]-dATP (Amersham). In addition to Primers 1 and 2, Primer-3 (5′-GCGAAAGCATTTGCCAA-3′), Primer-4 (antisense analog of Primer-3), Primer-5 (5′-GAAAC-T(TC)AAAGGAAT-3′), and Primer-6 (antisense analog of Primer-5) were used for sequencing.

Comparison of sequences and inferences about phylogeny

Sequences were aligned on the basis of maximum nucleotide similarity. Using the aligned sequences, evolutionary distance values were calculated pair-wise as described by Jukes and Cantor (1969). The phylogenetic tree was inferred from an analysis of results by the neighbor-joining method of Saitou and Nei (1987). The degree of support for internal branches of the tree was further assessed by bootstrapping (Felsenstein, 1985).

Results and Discussion

Validity of the methodology

Genomic DNA was extracted from each of eight ascidians. The central region of 18S rDNA was amplified by PCR using synthetic oligonucleotide primers (Primers 1 and 2). Amplification yielded a single band of DNA of about 1000 bases in length. The product of PCR was subsequently inserted into the *Bam*HI site of pBluescriptII SK(+) and cloned. The complete nucleotide sequence of the fragment was determined by the dideoxy termination-chain method using six primers. The sequences we determined in the present study correspond to positions 656–1643 in the sequence of human 18S rRNA (Neefs *et al.*, 1990).

Amplification of certain DNA fragments by PCR with the aid of Taq DNA polymerase may result in a few mismatched bases per 1 kilobase of DNA. Such misamplification causes confusion in the interpretation of results. To examine this possibility, we first selected two individuals of *H. roretzi,* and determined the nucleotide sequences of the 1000-bp-long portion of 18S rDNA twice for each specimen by separate amplification and cloning. As shown in Table I, there were four mismatches in the nucleotide sequences when two independent analyses of individual 1 were compared, and five mismatches in the case of individual 2. However, no mismatches occurred at identical positions in the two individuals. Therefore, one can distinguish changes in nucleotide sequence caused by misamplification during the PCR from those that are specific to individuals in the natural population. In this study we examined at least two clones of each of eight species. When the nucleotide sequences of the two clones were identical, we took this sequence as that of this species. When the sequences were not identical, we performed a third cloning.

The partial nucleotide sequence of 18S rRNA of the ascidian *Styela clava* has already been reported (Field *et al.*, 1988), and the relevant data were kindly provided by Dr. Rudolf A. Raff of Indiana University. To examine still further the validity of the present method, we determined the nucleotide sequence of the 18S rDNA of this species and compared it with that of the 18S rRNA. The nucleotide sequences of two regions of 18S rDNA, each of about 300 bases, were compared with the corresponding sequences in 18S rRNA. The nucleotide sequence of one region of the 18S rDNA was identical to that of a region of the 18S rRNA (data not shown). The result for the other region is shown in Figure 1. Seven bases in the 18S rRNA in this region were not determined in the previous study (Field *et al.*, 1988). We were able to identify all of the bases. We also identified two bases that may have been missed in the previous study. We found that there was a single-base mismatch between the results of the two studies, which may be a difference caused by individuality. Therefore, the present method is apparently valid for an analysis of the molecular phylogeny of ascidians.

Complete nucleotide sequences of rRNA genes including 18S rDNA of the ascidian *Herdmania momus* have been reported by Degnan *et al.* (1990), but we did not include the *H. momus* 18S rDNA sequence in the present study.

Partial nucleotide sequences of the 18S rDNAs from eight ascidians

The complete nucleotide sequences of a region of about 1000 bp in the central part of the 18S rDNA of eight species of ascidians are summarized in Figure 2. As mentioned previously, these sequences correspond to positions 656–1643 in the sequence of human 18S rRNA (cf. Neefs *et al.*, 1990). Alignment of the nucleotide sequences from the eight ascidian species revealed some interesting features. In some regions, the nucleotide sequences are highly conserved; very few changes are evident among the eight species. In particular, the sequences from position 511 to position 742 are completely identical among the five species of the order Pleurogona. In contrast, nucleotide sequences of other regions, such as positions 32–92 and

positions 885–950, are highly variable. Sequences of yet another region vary only moderately. These differences may reflect differences in the functional importance of the regions in the 18S rRNA. In addition, the five species of the order Pleurogona clearly share common nucleotide sequences, as do the three species of the order Enterogona. However, the nucleotide sequences from the two groups are very different, suggesting the early divergence of the two groups of ascidians during evolution.

Phylogenetic relationships

Structural similarity and evolutionary distance values were calculated pair-wise (as described by Jukes and Cantor, 1969) between the sequences aligned in Figure 2 and those of *Homo sapiens* and *Xenopus laevis;* the results are summarized in Table II. A phylogenetic tree was constructed by the neighbor-joining method (Saitou and Nei, 1987), by reference to the distance values of Table II. The phylogenetic tree (Fig. 3) indicates that the eight ascidians examined here can be subdivided into two groups, corresponding to the orders Enterogona and Pleurogona. That is, the relationships between the partial nucleotide sequences of 18S rDNAs support the modern and orthodox classification, but not the classification of ascidians into solitary and colonial groups.

Among species of the order Pleurogona, two pyuride ascidians, namely, *Pyu. mirabilis* and *H. roretzi*, and two styelide ascidians, namely, *Poly. misakiensis* and *Sym. reptans*, form discrete groups, because a high percentage of bootstrap analysis was given. However, the exact position of another styelide, *Styela clava*, was not determined in this study. The Styelidae form one of three families that include both solitary and colonial species (the others are Cionidae and Octacnemidae), and the Styelidae are divided into two subfamilies, namely, the Polyzoinae (colonial) and the Styelinae (solitary). Although the present results suggest the divergence between the two subfamilies, it is uncertain at present whether *Styela clava* is more closely related to the Styelidae or the Pyuridae.

Ascidians were initially classified as solitary and colonial species (Savigny, 1816). Around the turn of the century, however, ascidians were classified, mainly by reference to the morphology of the branchial sac and the gonad, into three major groups: the suborder Aplousobranchiata (colonial ascidians with a simple branchial sac, spicardia present, and gonads located within the gut loop), the suborder Phlebobranchiata (solitary and colonial ascidians with longitudinal vessels within the branchial sac, and gonads located within the gut loop), and the Stolidobranchiata (solitary and colonial ascidians with a folded branchial sac that contains longitudinal vessels, and gonads located to one side of the pharyngeal baskets) (Lahille, 1886; Huus, 1940). Recent investigations into the morphology of internal organs and lifestyles tend to support such a classification (Berrill, 1950; Millar, 1966; Kott, 1969; Monniot and Monniot, 1973). As shown by the present study, the comparison of nucleotide sequences of 18S rDNA also supports this orthodox classification.

In the present study, we included only three of nine families of the order Enterogona and two of five families of the order Pleurogona. The molecular phylogeny, as deduced by comparisons of nucleotide sequences from 18S rDNAs of species within all known families of ascidians is the focus of further investigations.

Acknowledgments

We thank Dr. Kazuo Kawamura of Kochi University for his kind help in collecting the samples. We also thank Dr. T. Miyata and Mr. N. Iwabe for their kind help in construction of the phylogenetic tree, and Ms. Kazuko Hirayama for assistance. This work was supported by a Grant-in-Aid (01304007) from the Ministry of Education, Science and Culture, Japan, and by a grant from the Aquatic Invertebrate Laboratory, Tokyo, Japan.

Literature Cited

Berrill, N. J. 1935. Studies in tunicate development. IV. Asexual reproduction. *Phil. Trans. Roy. Soc. London Ser. B* **225:** 327–379.

Berrill, N. J. 1936. Studies in tunicate development. V. The evolution and classification of ascidians. *Phil. Trans. Roy. Soc. London Ser. B* **226:** 43–70.

Berrill, N. J. 1950. *The Tunicata with an Account of the British Species.* Roy Soc. London.

Berrill, N. J. 1955. *The Origin of Vertebrates.* Oxford University Press, London.

Christen, R., A. Ratto, A. Baroin, R. Perasso, K. G. Grell, and A. Adoutte. 1991. An analysis of the origin of metazoans, using comparisons of partial sequences of the 28S RNA, reveals an early emergence of triploblasts. *EMBO J.* **10:** 499–503.

Degnan, B. M., J. Y. Clifford, J. Hawkins, and M. F. Lavin. 1990. rRNA genes from the lower chordates *Herdmania momus:* structural similarity with higher eukaryotes. *Nuc. Acid Res.* **18:** 7063–7070.

Felsenstein, J. 1985. Confidence limits on phylogenies: an approach using the bootstrap. *Evolution* **39:** 783–791.

Field, K. G., G. J. Olsen, D. J. Lane, S. J. Giovannoni, M. T. Ghiselin, E. C. Raff, N. R. Pace, and R. A. Raff. 1988. Molecular phylogeny of the animal kingdom. *Science* **239:** 748–753.

Hori, H., and S. Osawa. 1987. Origin and evolution of organisms as deduced from 5S ribosomal RNA sequences. *Mol. Biol. Evol.* **4:** 445–472.

Huus, J. 1940. Ascidiacea. Pp. 545–692 in *Handbuch der Zoologie,* Vol 5, Pt 2, Kukenthal and Krumbach, eds. Walter de Gruyter, Berlin & Leipzig.

Jukes, T. H., and R. C. Cantor. 1969. Evolution of protein molecules. Pp. 21–132 in *Mammalian Protein Metabolism,* H. N. Munro, ed. Academic Press, New York.

Kott, P. 1969. Antarctic Ascidiacea. *Antarct. Res. Ser. Washington* **13:** 1–239.

Kowalevsky, A. O. 1866. Entwicklungsgeschichte der einfachen Ascidien. *Mem. Acad. Sci. St. Petersb.* 7e ser. **10**(15): 1–19.

Kusakabe, T., K. W. Makabe, and N. Satoh. 1992. Tunicate muscle actin genes: Structure and organization as a gene cluster. *J. Mol. Biol.* **227:** 955–960.

Lahille, F. 1886. Sur la classification des Tuniciers. *C. R. Acad. Sci. Paris* **102:** 1573–1575.

Lake, J. A. 1990. Origin of the Metazoa. *Proc. Natl. Acad. Sci. U. S. A.* **87:** 763–766.

Millar, R. H. 1966. Evolution in ascidians. Pp. 519–534 in *Some Contemporary Studies in Marine Science*, H. Barnes, ed. George Allen & Unwin Ltd., London.

Monniot, C., and F. Monniot. 1973. Clefmondiale des genres d'ascidies. *Arch. Zool. Exp. Gen.* **113:** 311–367.

Nakanchi, M. 1982. Asexual development of ascidians: Its biological significance, diversity, and morphogenesis. *Am. Zool.* **22:** 753–763.

Neefs, J.-M., Y. Van de Peer, L. Hendriks, and R. De Wachter. 1990. Compilation of small ribosomal subunit RNA sequences. *Nucleic Acids Res.* **18:** 2237–2317.

Saiki, R. K., D. H. Gelfand, S. Stoffel, S. J. Scharf, R. Higuchi, G. T. Horn, K. B. Mullis, and H. A. Erlich. 1988. Primer-directed enzymatic amplification of DNA with a thermostable DNA polymerase. *Science* **239:** 487–491.

Saiton, N., and M. Nei. 1987. The neighbor-joining method: a new method for reconstructing phylogenetic trees. *Mol. Biol. Evol.* **4:** 406–425.

Sanger, F., S. Nicklen, and A. R. Coulson. 1977. DNA sequencing with chain-terminating inhibitors. *Proc. Natl. Acad. Sci. U. S. A.* **74:** 5463–5467.

de Savigny, M. J. C. L. 1816. Memoires sur les Animaux sans Vertebres. Part 2, Fasc 1. *De Crapelet, Paris.* 260 pp.

Reference: *Biol. Bull.* 183: 456–462. (December, 1992)

Spectral Tuning of Chemoreceptor Cells of the Third Maxilliped of the Lobster, *Homarus americanus*

FRANK COROTTO, RAINER VOIGT, AND JELLE ATEMA

Boston University Marine Program, Marine Biological Laboratory, Woods Hole, Massachusetts 02543

Abstract. This is the first investigation of the spectral tuning properties of single chemoreceptor cells of the third maxillipeds (mouthparts) of the lobster *Homarus americanus*. These organs are used, among other functions, for chemical recognition of food. Based upon extracellular recordings of action potentials, we report on 53 cells identified with a 15-compound equimolar mixture of mostly amino acids in an artificial seawater background (applied mixture concentration 150 μM). Subsequently, all cells were tested with each compound separately. Cells were generally narrowly tuned to a single compound. Twenty-five percent of the cells sampled responded best to L-glutamate, 17% to betaine, 11% to taurine, and 9% to ammonium chloride. There was no consistent second best stimulus for these four cell populations. Two other populations were more broadly tuned: one responded best to hydroxy-L-proline and the other to L-arginine. Some cells responded to both compounds. Arginine-sensitive cells (not necessarily "arginine-best" cells) tended to respond also to a lesser degree to leucine. Hydroxy-L-proline-sensitive cells tended to respond to a lesser degree to glycine. Among the lobster's chemoreceptive organs, the tuning of the maxillipeds is the broadest of all and resembles the tuning of the walking legs more than that of the antennules or antennae.

Introduction

The lobster *Homarus americanus* uses several chemoreceptive appendages to locate, manipulate and ingest food (see for review Atema, 1985). Lobsters orient toward a distant food odor source using the lateral rami of the biramous antennules (here simply "lateral antennules"), and to a lesser extent the walking legs (Devine and Atema, 1982). Similar behavioral functions of the antennules have been reported in spiny lobsters (Reeder and Ache, 1980). Near an odor source, lobsters locate food by probing the substrate with the legs until the source is contacted (Derby and Atema, 1982), as do crabs (Schmidt and Gnatzy, 1987). The legs pass the food to the endopodites of the third maxillipeds immediately prior to and during ingestion. Although food quality is probably assessed throughout by all these appendages, they serve different specific functions in the feeding sequence (Derby and Atema, 1982).

Behavioral evidence supports a gustatory, food-evaluating function of the maxilliped. Lobsters require sensory input from maxillipeds to eat; animals with deafferented maxillipeds dropped their food (Derby and Atema, 1982). Maxillipeds are also involved in assessing food palatability. *H. americanus* readily eats filter discs soaked in mussel (*Mytilus edulis*) extract, but is less eager to accept them if the extract is laced with tannic acid (Derby *et al.*, 1984). Although tannic acid receptors are present in the antennules and legs (and presumably in the mouthparts as well), lobsters began to reject the discs only after holding them in their mouthparts. Similarly, the shrimp *Macrobrachium rosenbergii* rejects quinine-laced food only after holding it in its mouthparts (Steiner and Harpaz, 1987), and the banana prawn *Penaeus merguiensis* passes both edible and inedible material to its mouthparts where inedible material is rejected (Hindley, 1975). Although crustaceans appear to use their legs as initial gustatory appendages, they may pay special attention to food being held in their mouthparts which provide a final quality check. A functionally similar arrangement is found in catfish; they use an extraoral sense of taste to locate food odor sources, but the intraoral sense of taste determines palatability (Atema, 1977).

Received 9 June 1989; accepted 1 September 1992.

Single chemoreceptor cells of the lateral antennules (Johnson and Atema, 1983; Weinstein *et al.*, 1990), medial antennular rami ("medial antennules"; Tierney *et al.*, 1988), antennae (Voigt and Atema, 1992), and legs (Johnson *et al.*, 1984) were evaluated with a similar series of compounds selected to probe their spectral tuning. It was found that (1) most receptor cells were surprisingly narrowly tuned, and (2) different appendages contained different blends of cell populations as defined by the single compound to which they were most responsive. The lateral antennules contained prominent populations of cells narrowly tuned to either taurine or hydroxy-L-proline (*i.e.*, "Tau-best" and "Hyp-best" cells); the medial antennules had prominent populations of Hyp-best, Tau-best, and L-arginine-best cells. The antennae were dominated by a Hyp-best cell population. In contrast, leg cell populations were narrowly tuned to either L-glutamate (Glu), betaine (Bet), ammonium chloride (NH_4^+) or Hyp. The occurrence of different blends of cell populations in different appendages may be related to different behavioral functions. Physiologically, the chemoreceptive properties of the maxillipeds have not been studied in any detail.

In this study, we evaluated the tuning properties of chemoreceptor cells in the maxilliped to a series of fifteen compounds, including thirteen used in previous studies of other lobster appendages.

Materials and Methods

Lobsters were obtained from local fishermen and were maintained in unfiltered seawater at the Marine Biological Laboratory in Woods Hole. They were fed squid or fish twice weekly. Experimental methods were adapted from Johnson *et al.* (1984). The endopodite of the third maxilliped was severed along the merus and placed in a two-compartment preparation chamber where the dactyl and propus were superfused with a stimulus carrier flow of artificial sea water (ASW; flow rate 20 ml/min). The dissected sensory nerve was bathed in *Homarus* Ringer's (Govind and Lang, 1981). The tip of the dactyl was cut off to allow the introduction of a cannula for perfusion with oxygenated Ringer's, which maintained viability for 2–3 h. Action potentials were monitored extracellularly from afferent axons with a suction electrode. Responses were recorded on magnetic tape for later analysis.

Chemoreceptor cells were initially identified by their response to 50 μl of an equimolar search mixture (Mix) of 15 single compounds (Table I, note abbreviations) each at a final peak concentration of 10 μ*M* (*i.e.*, total Mix concentration of 150 μ*M*) injected into the ASW carrier flow. An equimolar mixture is equally effective as a search stimulus as is a naturally proportioned mixture (Weinstein *et al.*, 1990) and—despite the common effects of "mixture suppression" (see Discussion)—the most efficient method of finding cells responsive to the individual components of the mixture.

Table I

Test stimuli

Compounds	Abbreviations
L-Aspartate	Asp
L-Glutamate	Glu
Ammonium chloride	NH_4^+
L-Proline	Pro
Sucrose	Suc
L-Lysine	Lys
L-Glutamine	Gln
Betaine	Bet
L-Arginine	Arg
Hydroxy-L-Proline	Hyp
Ethanol	EtOH
L-Alanine	Ala
Glycine	Gly
Taurine	Tau
L-Leucine	Leu
Search mixture—an equimolar mixture of the above compounds	Mix

Once identified, responsive cells were tested with each of the fifteen single compounds (injected as 50 μl volumes), again with a final peak concentration of 10 μ*M*. For Glu-sensitive cells, 10 μ*M* is at the middle of the mean concentration-response function (see Fig. 3) and well above the thresholds of most of these cells. By measuring conductivity within the stimulation chamber after injecting a 50 μl pulse of 1 *M* NaCl into a flow of deionized water, we found that stimuli passed over the maxilliped as a pulse of one second duration at half peak height. ASW contained very low concentrations of some of the compounds tested, but rather high NH_4^+ levels (*e.g.*, $[NH_4^+]$ = 1–2 μ*M*, [Asp] = 5 n*M*, [Gly] = 26 n*M*; HPLC measurements courtesy of Dr. Donal Manahan, University of Southern California).

Stimuli were injected at one minute intervals, during which the stimulation chamber and stimulus introduction port were vigorously flushed with ASW. Stimuli were injected in the order shown in Table I, with every sixth stimulus being Mix as a test for viability. This order was chosen to represent a haphazard (random) sequence of strong and weak stimuli, as determined from previous experiments of chemoreceptor cells in the lateral antennules and walking legs. Responses to the four Mix stimuli showed no systematic decline in magnitude. Thus we infer that preparation viability was maintained throughout the experiments, and that order-bias was not significant. One cell was rejected because its sensitivity to Mix decreased by 60% over the course of the experiment. A few other cells showed response variability to Mix of greater than 60% throughout the experiment, however, because there

was no trend to lower or higher responses, but rather a variability around some fairly constant mean response, these cells were included.

To assess our choice of test concentration, concentration-response functions were determined for 10 Glu-sensitive cells; the spectral properties of these cells were not investigated. The cells were identified by their response to a 10 μM pulse of Glu. Five minutes were allowed to disadapt the cell from the repeated exposures to Glu inherent in searching for a single unit. Then, cells were probed with ascending concentrations of Glu in log steps, from 10^{-11} M to 10^{-3} M.

Single cell responses were identified visually from an oscilloscope trace on the basis of amplitude [with the assistance of a window-discriminator (Frederick Haer & Co., New Brunswick, ME)], waveform, and latency. Because different cells responded with different temporal patterns, response magnitude was assessed as the total number of spikes. Response durations were less than 5 s. Only six cells were spontaneously active at a low frequency (about 0.1 Hz), while others fired occasional bursts of spikes. The responses of the six cells that fired spontaneously at a constant frequency were corrected by subtracting, from the response frequency, the mean spontaneous spike frequency prior to stimulation, as in Johnson *et al.* (1984). Cells that fired in spontaneous bursts were not recorded because the resulting data could not be interpreted. We present only cells for which complete tuning spectra were determined.

The tuning breadth of cells was described by the H-metric (Smith and Travers, 1979), a measure of diversity:

$$H = -K \sum P_i \log_{10} P_i,$$

where H is a measure of response diversity, K is a scaling constant (a function of the number of compounds tested), and P_i is the proportional response of each of the 15 test compounds. The metric is scaled from 0 to 1, where $H = 0$ designates a cell responding to only one stimulus, and $H = 1$, a cell responding equally to all stimuli. The tuning breadth of cells was computed without responses to Mix or ASW.

Cells were classified by their best response to a single compound. Cells that responded best to Mix are occasionally termed "Mix-best" cells, although they are classified by their best single compound stimulus. A best-compound classification for receptor cells does not by itself imply a well-defined cell population.

Results

The results are based on the responses from 53 cells. Overall, the greatest response—in terms of the total number of spikes generated in all cells—was elicited by Mix, followed by Glu, Tau, Bet, Arg, Hyp, Leu, NH_4^+ and Gly; the remaining seven compounds and ASW were poor stimuli (Table I).

Nineteen cells (36%) responded best to Mix (Fig. 1) including two cells (#46; #49) that responded best to both Mix and to one single compound. The remaining 34 cells responded best to one or another single compound. The 19 Mix-best cells were widely distributed among the cell populations as defined by their best *single* compound. They included 1 of the 13 Glu cells (#1–#13), 1 of 6 Tau (#14–#19), 2 of 8 Bet (#20–#27), 3 of 5 NH_4^+ (#28–#32), 4 of 6 Arg (#33–#38), 3 of 9 Hyp (#40–#48), and 2 of 3 Gly cells (#49–#51). Of the three remaining Mix-best cells, one (#53) responded to none of the single compounds (Figs. 1, 2); the other two responded best to Leu (#39) and Lys (#52) respectively. Two of the cells classified here as Arg-best responded equally well to Hyp (#34) or Leu (#38), one of the Hyp-best cells responded equally to Gly (#44), and one Gly-best cell responded equally to Hyp and Bet (#51; Fig. 2). The latter were all low responses of only a few spikes. Thus, the classification of these latter cells is obviously arbitrary.

The most stimulatory single compound was Glu, which elicited a total of 341 spikes from 17 cells; 13 of these responded better to Glu than to the other single compounds. Eight compounds (Glu, Tau, Bet, Arg, Hyp, Leu, NH_4^+ and Gly) accounted for 89% of all the spikes generated by single compound stimuli in all cells of this study.

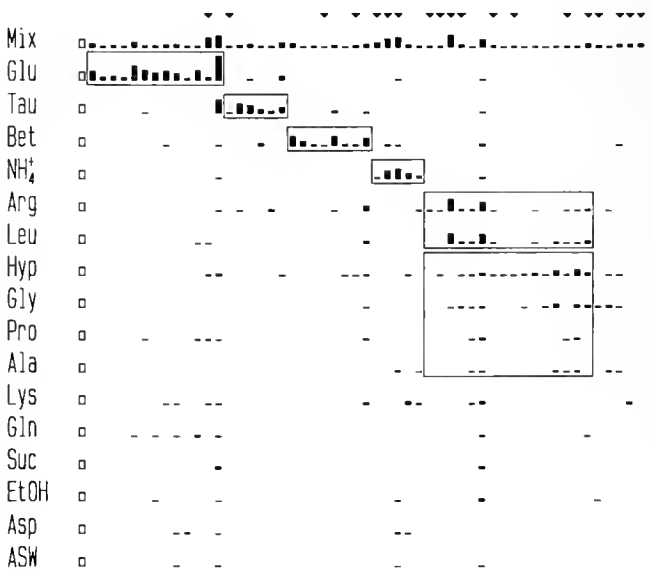

Figure 1. Responses of 53 chemoreceptor cells of the lobster maxilliped. Each column represents the responses (total number of spikes) of a cell to the stimuli on the left. Cells are grouped in best-compound populations, starting with the single compound (Glu) that caused the largest total number of spikes. Open scale bars on far left represent 25 spikes. Arrowheads indicate cells in which the mixture caused an equal or stronger response than their best compound. Boxes reflect response correlations; see text.

Lys, Pro, Ala, Gln, Suc, EtOH and Asp were relatively ineffective stimuli, each compound eliciting less than 40 spikes in all cells; few cells responded best to these stimuli. These 7 compounds and ASW accounted for the remaining 11% of all spikes. ASW stimuli caused 7 spikes in 4 cells.

Fourteen of the 53 cells (28%) responded to only one of the 15 single compounds (Fig. 2). Thirteen cells responded to only two, eight cells to three, and seven cells to four compounds. The remaining ten cells were more broadly tuned. Four of these 10 cells also responded to ASW, including two cells, #13; #38, (Fig. 2) that responded to almost all compounds. This response was probably not caused by a contamination of ASW because carrier flow and ASW stimulus were identical. Perhaps these ASW-responsive cells are both chemo- and mechanoreceptive (Hatt, 1986). Tuning breadth varied across the major cell populations (Table II). As a population, Glu, Tau and Bet cells were most narrowly tuned.

Cells grouped by their best single compound (Figs. 1, 2) formed populations within which the responses to all single compounds tended to be correlated with one another ($P < 0.01$, Pearson's Product moment correlation coefficient). These results were similar to the correlation values for responses of lobster walking leg receptor cells (Johnson *et al.*, 1984; data not shown). Within the Glu, Tau, Bet and NH_4^+ cell populations, no single compound was a consistent second best stimulus for the population.

Responses to six compounds—Arg, Leu, Hyp, Gly, Pro, and Ala—appeared correlated, particularly Arg with Leu and Hyp with Gly (Figs. 1, 2). Eleven of the 18 cells that responded to Arg also responded to Leu, usually to a lesser degree. Four of the six Arg-best cells (Fig. 2) had strong Leu responses. Similarly, eleven of the 23 cells that responded to Hyp (but were not necessarily Hyp-best cells) responded also, and usually to a lesser degree, to Gly. Five of the nine Hyp-best cells had strong Gly responses. Interstimulus Pearson product-moment correlations showed that responses to Arg were correlated with responses to Leu (r = 0.99), and Hyp with Gly (r = 0.77). Pro and Ala responses were correlated, and both were correlated with Hyp and Gly responses.

Individual concentration-response functions for nine Glu-sensitive cells possessed unique characteristics (Fig. 3). At the highest three stimulus concentrations, one outlier cell (not shown) fired at rates 3–5 times the mean. Thresholds ranged from 10^{-8} *M* to 10^{-5} *M*. Some cells saturated at 10^{-5} *M*, others did not saturate at the highest

Table II

Response breadth of major chemoreceptor cell populations based on responses to 15 single compounds

Population	Median H	Mean H	Range	N
Glu	0.11	0.16	0–0.50	13
Tau	0.19	0.17	0–0.32	6
Bet	0.14	0.19	0–0.59	8
NH_4^+	0.38	0.27	0–0.57	5
Hyp	0.25	0.31	0–0.55	5
Arg	0.37	0.42	0–0.82	6
Gly	0.44	0.37	0.17–0.50	3

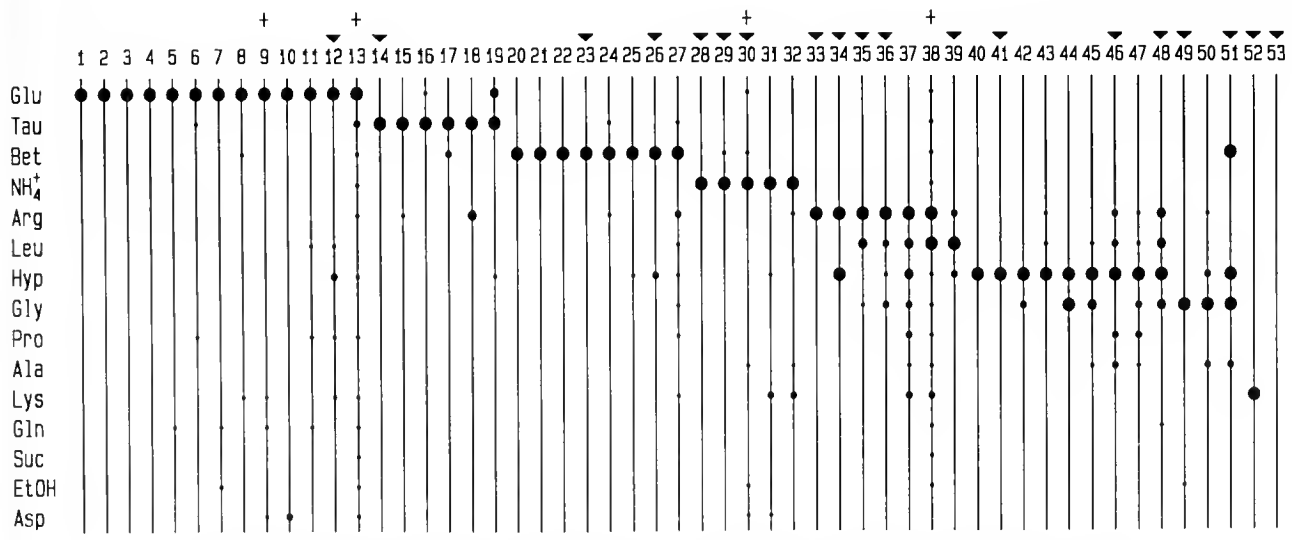

Figure 2. Spectral tuning shown as responses of all cells to all single compounds normalized to the best response (largest dot) of each cell. Decreasing dot sizes represent responses of 70–99%, 30–69%, and less than 30% of that cell's maximum response. Arrowheads indicate cells in which the mixture caused an equal or stronger response than their best compound. Crosses indicate cells responding to ASW.

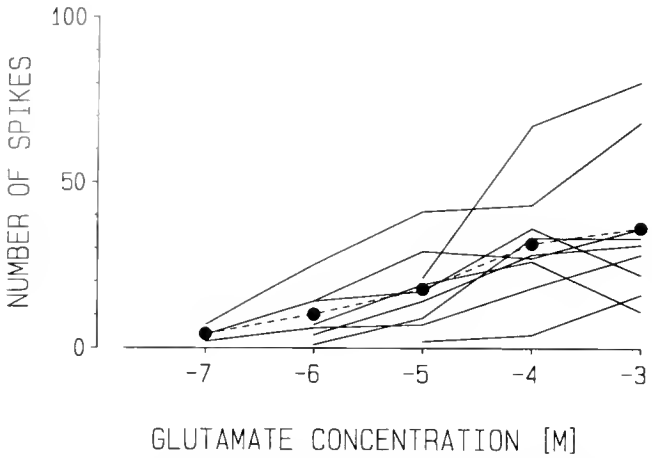

Figure 3. Glu-response functions of nine glutamate-sensitive cells. Five cells responded with one single spike to 10^{-8} *M* Glu (data not shown). There were no responses to Glu concentrations less than 10^{-8} *M*. Mean response function is broken line.

test concentration (10^{-3} *M*). Three cells showed greatly reduced responses at the highest test concentration. The mean response function (not including the outlier cell) increased rather linearly from 10^{-7} to 10^{-4} *M*, and then saturated.

In 19 cells, the mixture elicited an equal or stronger response than any single compound tested (Fig. 1). Sixteen of these cells had low firing rates, responding with less than 15 spikes to their best compound. Thus, they were rare among generally strongly responding Glu- and Tau-cells and common among generally weakly responding Arg, Hyp, NH_4^+ and Gly-cells (Fig. 1). Taking as a criterion a response difference of two spikes (representing about 15%, determined as response variability; Merrill, 1992), nine cells responded more strongly to the mixture than to their best single compound. In six of these cells, the response to the mixture was more than 15% stronger than the *sum* of the responses to all single compounds. In four of these cells, the response to the mixture was twice as strong as the *sum* of the responses to single compounds (Fig. 4).

In 37 cells (Fig. 4), the response to the mixture was 15% smaller than the *sum* of the responses to the single compounds. In 32 of these cells, the sum was twice as strong as the response to the mixture.

Discussion

This study shows that the tuning spectra of chemoreceptor cell populations (defined by best compound) of the third maxillipeds of the lobster *H. americanus* are similar to the tuning spectra of prominent cell populations found in other lobster chemoreceptor appendages. The most remarkable difference with respect to its other appendages is that no single best cell population dominated the maxillipeds (Fig. 2). The maxillipeds are characterized by mostly narrowly tuned Glu- (24.5%), Tau- (11.3%), Bet- (17.0%), NH_4^+- (9.4%), Arg- (11.3%), and Hyp-best cell populations (17.0%), with one or two cells responding best to Leu, Lys, or Gly. Overall, the response spectrum of the maxilliped resembles that of the walking legs, but the latter is more strongly dominated by Glu-best cells (37.9%), in addition to NH_4^+ (15.2%), Hyp- (16.7%), and Bet-best cell populations (10.6%), and some Lys-, Tau-, Leu-, and Asp-best cells (Johnson *et al.*, 1984). In contrast to these thoracic appendages, the cephalic appendages are Hyp-cell dominated. The lateral antennules contain many cells narrowly tuned to Hyp (47.3%), Tau (15.3%), and Glu (10.2%) (Johnson and Atema, 1983; Weinstein *et al.*, 1990). The medial antennules contain large populations of Hyp- (26.4%), Tau- (24.5%), and Arg-best cells (20.8%) and a few Bet- and NH_4^+-best cells (Tierney *et al.*, 1988). The second antenna was dominated by a Hyp-best cell population (85.1%) with small Tau- (10.6%) and Bet-cell populations (4.3%) (Voigt and Atema, 1992). For a further discussion of organ tuning see Voigt and Atema (1992).

Tuning breadth is generally dependent on stimulus intensity; chemoreceptor cells become more broadly tuned at higher stimulus intensities (Ogawa *et al.*, 1974; Voigt and Atema, 1992). Our test concentration of 10 μM was well above threshold for most of the Glu-sensitive cells tested (Fig. 3). Even at this stimulus intensity, four of the cell populations (Glu, Tau, Bet, NH_4^+) were narrowly tuned (Table II). Yet, more broadly tuned cells were not uncommon, *i.e.*, Arg and Hyp cell populations.

The Arg-best cells often responded second best to Leu. In fact, Arg and Leu were so highly correlated (r = 0.97) that one might suspect that they bind to the same receptor site, despite the different net charges they carry at the pH

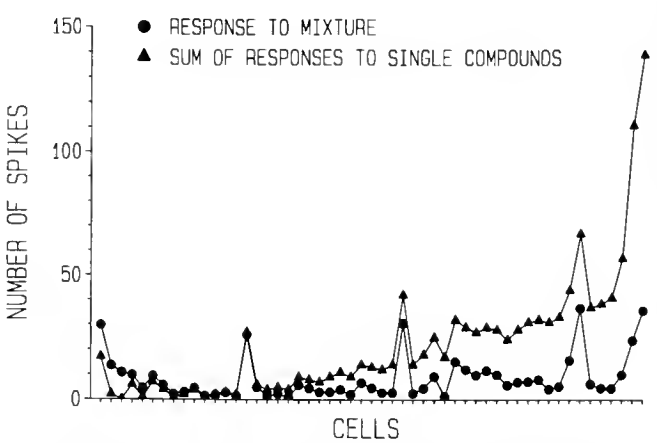

Figure 4. Responses of all 53 cells to the mixture (circle) and to the sum of their responses to 15 single compounds (triangle), ordered by the magnitude of the response difference.

of ASW. However, Arg and Leu are not as tightly coupled in receptor cells identified in other chemoreceptor organs and Leu is not always second best; Leu-best cells, including cell #39 in this study (Fig. 2), are not uncommon in the lobster. This would argue for the general independence of separate Arg and Leu receptor sites. The close Arg-Leu response correlation in certain cells would then be based on a specific ratio of simultaneously expressed Arg and Leu binding receptors. In other cells and organs this ratio would be different and variable. This idea appears to have general appeal (Atema *et al.*, 1989; Buck and Axel, 1991; Dionne, 1992). Similar arguments can be made for Hyp and Gly coupling which appears significant ($r = 0.77$) in this study but is not a general rule for lobster receptor cells. The determinant of the particular blends of receptor expression in chemoreceptor cells is now one of the most intriguing unsolved issues in chemosensory research.

Some maxilliped receptor cells showed enhanced responses, and other cells reduced responses to mixture stimuli, whether compared to the response to their best compound or to the *sum* of responses to all individual mixture components (Fig. 4). This has also been seen in other chemoreceptor organs studied (*e.g.*, Atema *et al.*, 1989; Voigt and Atema, 1992). A common way of expressing mixture suppression (or mixture enhancement) is to compare the observed response to the mixture with an expected response calculated as the sum of responses to individual mixture components, with or without adjustments for the slope of the individual concentration-response functions (Caprio *et al.*, 1989; Daniel and Derby, 1987). Since we did not determine concentration-response functions, we have assumed, conservatively, that mixture responses more than 50% greater or smaller than the sum of the responses to the mixture components reflect enhancement and suppression, respectively. By this criterion we have identified four cells showing mixture enhancement, and 32 cells showing mixture suppression. It is likely that such robust phenomena would be seen under any number of different model assumptions for mixture enhancement and suppression.

We also found 19 cells (38%) that responded equally or more strongly to the mixture (Figs. 1, 4). Similar Mix-best cells were found in *H. americanus* legs (Gerardo *et al.*, 1989). In comparison with data from cephalic appendages, this is a surprisingly large percentage of cells. In the medial antennule, 96% of the cells surveyed gave smaller responses to the mixture than to the sum of responses to individual compounds, whereas only 4% showed enhanced responses (Tierney *et al.*, 1988). Enhanced responses to the mixture were seen before to be characteristic of weakly responding cells (Atema *et al.*, 1989). This was confirmed here: while most other cells were tested well above their thresholds, as shown by the response magnitude for their best compound, most of the Mix-best cells responded with less than ten spikes to their best single compound (Fig. 4). This suggests that the Mix-best cells were tested close to their threshold. Moderately stimulatory compounds might have been subthreshold stimuli when presented alone, thus appearing to be ineffective (Figs. 1, 2). However, when presented as part of Mix, responses to several individual compounds may have been summed, leading to a stronger response to the mixture than to the best single compound or the sum of all responses to the individual components. Therefore, the high percentage of Mix-best cells found in this study may be the result of relatively low stimulus concentrations used here.

The stimulus-response function of Glu cells (Fig. 3) is similar to results obtained from leg chemoreceptors (Derby and Atema, 1982; Johnson *et al.*, 1984, 1985). A 10^{-7} *M* threshold may reflect the ambient concentration of Glu in coastal seawater (2×10^{-8} *M;* Mopper and Lindroth, 1982). The one very highly responsive cell (216 spikes to a brief stimulus pulse of 10^{-4} *M* Glu) is an anomaly thus far.

As interesting as the physiological and genetic basis for tuning diversity among receptor cells, is the behavioral function of this diversity. Why are so many cells narrowly tuned? Why are cephalic receptor organs tuned to Hyp and Tau whereas thoracic appendages are tuned to Glu, Bet or NH_4^+? We may understand the extreme narrow tuning of many insect pheromone receptor cells as an evolutionary response to sexual selection and communication that may have sharpened the tuning specificity of signal and receptor. But narrow tuning in chemoreceptor cells involved in feeding is unusual, and its function not immediately obvious (Johnson *et al.*, 1984; Derby and Atema, 1988). Narrow tuning might improve the detection of key compounds in a (food) mixture odor against ambient chemical (noise) backgrounds. Thus it could enhance chemical orientation in odor plumes via such compounds as Hyp or Tau, which occur in very low background concentrations in natural seawater (Mopper and Lindroth, 1982) and are good indicators of released body fluids (see discussion in Johnson and Atema, 1986). This may suggest an explanation for the presence of many Tau and Hyp cells in the antennules and antennae. The case for narrow tuning of Glu, Bet, and NH_4^+-best cells of the walking legs and maxillipeds is more difficult to make.

It may be easier to explain the blend of differently tuned cell populations in different organs than it is to suggest a strong argument for narrow tuning of individual receptor cells. If Hyp and Tau have good qualities as distance signals, then both narrow cell tuning and the dominance of their cell populations in antennules may be understood. In contrast, legs are used to both locate (Devine and Atema, 1982; Moore *et al.*, 1991) and to evaluate food (Derby and Atema, 1982), and they require rather precise

and complex blends of amino acids before full behavioral responses can be elicited (Borroni *et al.*, 1986). Their discrimination function may require a more equally distributed blend of cell populations. Maxillipeds do not serve any function in orientation or localization, but play a critical role in evaluating food (Derby and Atema, 1982; Derby *et al.*, 1984). This pure evaluation function may be reflected in the nearly equal distribution of tuning populations reported in this study.

Acknowledgments

This paper is part of F. C.'s Masters Degree Thesis at the Boston University Marine Program. The research was supported in part by grants from the Whitehall Foundation and the National Science Foundation (BNS 85-12585) to J. A. and a Boston University Graduate Fellowship to F.C.

Literature Cited

Atema, J. 1977. Functional separation of taste and smell in fish and crustacea. Pp. 165–174 in *Olfaction and Taste VI*, J. Le Magnen and P. MacLeod, eds. Information Retrieval Ltd., London.

Atema, J. 1985. Chemoreception in the sea: adaptations of chemoreceptors and behavior to aquatic stimulus conditions. *Soc. Exp. Biol. Symp.* **39:** 387–423.

Atema, J., P. F. Borroni, B. R. Johnson, R. Voigt, and L. S. Handrich. 1989. Adaptation and mixture interactions in chemoreceptor cells: mechanisms for diversity and contrast enhancement. Pp. 83–100 in *Perceptions of Complex Smells and Tastes*, D. L. Laing, W. Cain, R. McBride, and B. W. Ache, eds. Academic Press, Sydney.

Borroni, P. F., L. S. Handrich, and J. Atema. 1986. The role of narrowly tuned taste cell populations in lobster (*Homarus americanus*) feeding behavior. *Behav. Neurosci.* **100:** 206–212.

Buck, L., and R. Axel. 1991. A novel multigene family may encode odorant receptors: A molecular basis for odor recognition. *Cell* **65:** 175–188.

Caprio, J., J. Dudek, and J. J. Robinson II. 1989. Electro-olfactogram and multiunit olfactory receptor responses to binary and trinary mixtures of amino acids in the channel catfish, *Ictalurus punctatus*. *J. Gen. Physiol.* **84:** 403–422.

Daniel, P. C., and C. D. Derby. 1987. Mixture interaction analysis: a polymodal model for multiple-receptor systems which incorporates the Beidler equation. *Chem. Senses* **12:** 417–423.

Derby, C. D., and J. Atema. 1982. The function of chemo- and mechanoreceptors in lobster (*Homarus americanus*) feeding behavior. *J. Exp. Biol.* **98:** 317–327.

Derby, C. D., P. M. Reilley, and J. Atema. 1984. Chemosensitivity of the lobster *Homarus americanus* to secondary plant compounds: unused receptor capabilities. *J. Chem. Ecol.* **10:** 879–892.

Derby, C. D., and J. Atema. 1988. Chemoreceptor cells in aquatic invertebrates: peripheral mechanisms of chemical signal processing in decapod crustaceans. Pp. 365–385 in *Sensory Biology of Aquatic Animals*, J. Atema, R. R. Fay, A. N. Popper, and W. N. Tavolga, eds. Springer-Verlag, New York.

Devine, D., and J. Atema. 1982. Function of chemoreceptor organs in spatial orientation of the lobster, *Homarus americanus:* differences and overlap. *Biol. Bull.* **163:** 144–153.

Dionne, V. E. 1992. Chemosensory responses in isolated olfactory receptor neurons from Necturus maculosus. *J. Gen. Physiol.* **99:** 415–433.

Gerardo, H. F., R. Voigt, and J. Atema. 1989. Self- and cross-adaptation in chemoreceptor cells. *Chem. Senses* **14:** 702. (Abstract)

Govind, C. K., and F. Lang. 1981. Physiological identification and asymmetry of lobster claw closer motoneurons. *J. Exp. Biol.* **94:** 329–339.

Hatt, H. 1986. Responses of bimodal neurons (chemo- and vibration-sensitive) on the walking legs of the crayfish. *J. Comp. Physiol. A* **159:** 611–617.

Hindley, J. P. R. 1975. The detection, location, and recognition of food by juvenile banana prawns, *Penaeus merguiensis* de Man. *Mar. Behav. Physiol.* **3:** 193–210.

Johnson, B. R., and J. Atema. 1983. Narrow-spectrum chemoreceptor cells in the antennules of the American lobster, *Homarus americanus*. *Neurosci. Lett.* **41:** 145–150.

Johnson, B. R., R. Voigt, P. F. Borroni, and J. Atema. 1984. Response properties of lobster chemoreceptors: tuning of primary taste neurons in walking legs. *J. Comp. Physiol.* **155:** 593–604.

Johnson, B. R., P. F. Borroni, and J. Atema. 1985. Mixture effects in primary olfactory and gustatory receptor cells from the lobster. *Chem. Senses* **10:** 367–373.

Johnson, B. R., and J. Atema. 1986. Chemical stimulants for a component of feeding behavior in the common Gulf Weed Shrimp, *Leander tenuicornis* (Say). *Biol. Bull.* **170:** 1–10.

Merrill, C. L. 1992. Reliability and specificity of hydoxy-L-proline sensitive chemoreceptor cells. Ph.D. Thesis, Boston University, Boston, Massachusetts.

Moore, P. A., N. Scholz, and J. Atema. 1991. Chemical orientation of lobsters, *Homarus americanus*, in turbulent odor plumes. *J. Chem. Ecol.* **17:** 1293–1307.

Mopper, K., and P. Lindroth. 1982. Diel and depth variations in dissolved free amino acids and ammonium in the Baltic Sea determined by shipboard HPLC analysis. *Limnol. Oceanogr.* **27:** 336–347.

Ogawa, H., S. Yamashita, and M. Sato. 1974. Variation in gustatory nerve fiber discharge pattern with change in stimulus concentration and quality. *J. Neurophysiol.* **37:** 443–457.

Reeder, P. B., and B. W. Ache. 1980. Chemotaxis in the Florida spiny lobster, *Panulirus argus*. *Animal Behav.* **28:** 831–839.

Schmidt, M., and W. Gnatzy. 1987. Contact chemoreceptors on the walking legs of the shore crab, *Carcinus maenas*. In Taste and Olfaction IX, S. D. Roper and J. Atema, eds. *Ann. N. Y. Acad. Sci.* **510:** 589–590.

Smith, D. V., and J. B. Travers. 1979. A metric for the breadth of tuning of gustatory neurons. *Chem. Senses Flav.* **4:** 215–229.

Steiner, J., and S. Harpaz. 1987. Behavior stereotypes or food acceptance and the rejection of 'bitter' food in the fresh water prawn, *Macrobrachium rosenbergii*. *Chem. Senses* **12:** 89–97.

Tierney, A. J., R. Voigt, and J. Atema. 1988. Response properties of chemoreceptors from the medial antennular filament of the lobster *Homarus americanus*. *Biol. Bull.* **174:** 364–372.

Voigt, R., and J. Atema. 1992. Tuning of chemoreceptor cells of the second antenna of the American lobster (*Homarus americanus*) with a comparison of four of its other chemoreceptor organs. *J. Comp. Physiol. A* **171:** (in press).

Weinstein, A., R. Voigt, and J. Atema. 1990. Spectral tuning of lobster olfactory cells and their response to defined mixtures and natural food extracts. *Chem. Senses* **15:** 651–652. (Abstract)

Reference: *Biol. Bull.* **183**: 463–475. (December, 1992)

Nervous System of the Tornaria Larva (Hemichordata: Enteropneusta). A Histochemical and Ultrastructural Study

S. SH. DAUTOV[1] AND L. P. NEZLIN[2]

[1]*Institute of Marine Biology FEBS Academy of Sciences of Russia 17, Palchevsky str., 690041 Vladivostok, Russia, and* [2]*Institute of Developmental Biology Academy of Sciences of Russia 26, Vavilov str., 117808 Moscow, Russia*

Abstract. Transmission electron microscopy (TEM) and histochemical approaches were used to investigate the topology and ultrastructure of the nervous system of the tornaria larva of an enteropneust, *Balanoglossus proterogonius*. Cholinesterase activity was detected in the epithelium of the pre- and postoral ciliary bands. Groups of catecholamine-containing cells (CA) were detected at the anterior tip of larva, in the ventral epidermis behind the mouth, and in the stomach wall near its junction with the intestine. Single CA neurons were detected in the telotroch epithelium. Axon tracts are described in ciliary band epithelia. At the base of the aboral plate, epithelial nerve cells form a ganglion-like cluster. Single neuron-like cells and single axons and axonal tracts were found in the epithelium of digestive tract. The data were compared with ones from the literature and with those obtained from other marine invertebrate larvae. The properties of the neural elements and their possible functions are discussed.

Introduction

The tornaria is the principle free-swimming larva of enteropneusts (Phylum Hemichordata, Class Enteropneusta). Despite some differences, all tornaria have much in common. They have three ciliary bands serving as locomotory or feeding organs: the preoral and postoral bands are used for both swimming and collecting of food particles; but the adoral band (telotroch) is used for locomotion only (Strathmann and Bonar, 1971, 1976; Strathmann *et al.*, 1972). The ventrally-located mouth leads to the digestive tract, which is divided into three parts. An apical plate with a tuft of sensory cilia and paired eyespots are located at the anterior tip of the body.

Tornaria look very much like the hypothetical ancestral echinoderm larva, the dipleurula, and they were originally described as asteroid larvae (Müller, 1850; Krohn, 1854). Later Metschnikoff (1870) showed tornariae to be the free-swimming larvae of enteropneusts. At present, tornariae and echinoderm larvae are classified together as the "dipleurula type" of larvae (Ivanova-Kazas, 1978). The neuromorphology of several echinoderm larvae has been studied with light and electron microscopy and biogenic amines have been visualized histochemically (Burke, 1978, 1983a, b; Nezlin *et al.*, 1984; Bisgrove and Burke, 1986, 1987; Burke *et al.*, 1986; Chia *et al.*, 1986; Nakajima, 1987).

The nervous system of the tornaria remains essentially unknown. Ivanova-Kazas (1978) referred to a nerve plexus under the base of the apical plate, but only the structure of the eyespots has been described in detail (Branderburger *et al.*, 1973). We present ultrastructural and histochemical evidence for the larval nervous system of tornaria and compare it to that known for larval echinoderms.

Materials and Methods

Tornaria identified as *Tornaria ancoratae* (Damas and Stiastny, 1961) were collected from plankton of Vostok Bay, Sea of Japan in September-October from a depth of 5–20 m (the majority of tornariae were collected near the bottom).

For transmission electron microscopy (TEM), larvae were fixed in a solution of 2.5% glutaraldehyde (Sigma) in 0.05 *M* cacodylate buffer (pH 7.0) with 0.142 *M* NaCl and 0.283 *M* sucrose for 1 h at 5°C, rinsed in 0.1 *M* cacodylate buffer, and postfixed in 2% osmium tetroxide

Received 9 August 1991; accepted 26 August 1992.

in 0.05 *M* cacodylate buffer with 0.205 *M* NaCl and 0.389 *M* sucrose. After dehydration in a graded series of ethanol and acetone solutions, samples were embedded in Epon-Araldite. Sections were cut with an LKB-3 Ultracut, stained with uranyl acetate followed by lead citrate, and observed with a JEOL-100B electron microscope.

Cholinesterase activity was localized by the direct thiocholine method (Koelle and Friedenwald, 1949), with acetylthiocholine iodide (Sigma) as a substrate. Catecholamine-containing cells were visualized by the glyoxilic acid-induced fluorescence technique (de la Torre and Surgeon, 1976; Sharp and Atkinson, 1980). Larvae were incubated in a solution containing 2% glyoxilic acid (Fluka) and 4% sucrose in 0.1 *M* phosphate buffer (pH 7.4, 18°C) for 10–20 min. The specimens were then placed on a glass slide, dried with a stream of hot air (80°C, 5 min), and mounted in liquid paraffin under a glass coverslip. The larvae were examined with a UV epifluorescence microscope (ML-2). To be confident about the specificity of the reaction, ascorbic acid was substituted for the glyoxilic acid in some samples.

Results

This tornaria larva has a barrel shaped body with a sharply pointed anterior end bearing paired eyespots (Fig. 1). Its triangular oral field is surrounded by the preoral ciliary band. The dorsal field is greater in area than the oral field. Tentacles are absent.

The tornariae are present in plankton from late August until late October. All of the specimens are morphologically identical, so these larvae probably belong to the same species. *Balanoglossus proterogonius* Belichov (Van-der Horst, 1933) which was described from this region of Sea of Japan. Adults of this enteropneust species have not been collected recently from Vostok Bay.

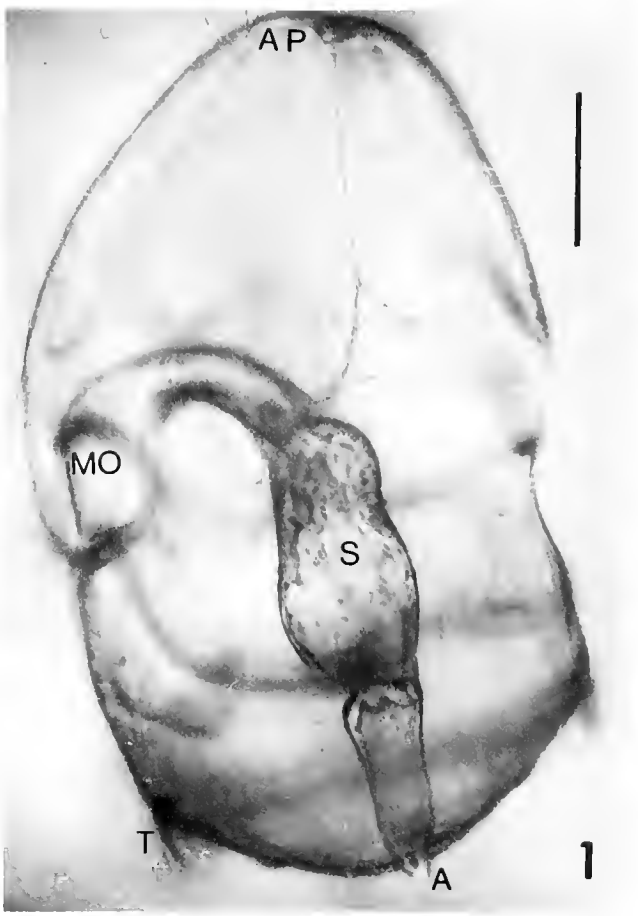

Figure 1. Left lateral view of a fully developed tornaria *Tornaria ancoratae* from plankton of Vostok Bay of Sea of Japan. A, anus; AP, apical plate; MO, mouth; S, stomach; T, telotroch. Scale bar = 100 μm.

Transmission electron microscopy

A cross section of the ciliary band is shown in Figure 2. It consists of fusiform cells organized as a pseudostratified epithelium. Each cell bears on its apical surface a single cilium surrounded by a collar of microvilli. The cilium has a typical axonemal complex (9 + 2). The ciliated band is 6-12 cells wide. A nerve tract containing 15-20 axons lies between the epithelial cells and their subjacent basal lamina. Additionally, some axons occur at the base of the band outside the tract but still superjacent to the basal lamina. The axons are 0.2–1.5 μm in diameter; the cytoplasm contains microtubules, mitochondria, rough endoplasmic reticulum, and vesicles of different types. Both clear vesicles, 50 nm in diameter, and vesicles with electron-dense cores, 200 nm in diameter, are found within these axons (Figs. 3, 4). Some ciliated cells of the band have a process that enters the axonal tract. Adjacent to the tract several subepithelial neuron-like cells have been found. These cells have no detectable cilia. They too have processes that may enter the nerve tract (Fig. 3). The apical ends of the epithelial cells are connected by tight junctions.

Except at the ciliary bands, the body wall is composed of a squamous epithelium. Adjacent to its base, axons are present singly or in small bundles (Figs. 5, 6). Axons can also pass within grooves, either between adjacent epithelial cells, or embedded in one of them (Figs. 7, 8).

At the anterior end of the body, a thick cuboidal epithelium constitutes the aboral plate with its tuft of cilia. Here at the base of the epithelium, a cluster of nerve cells forms what appears to be a ganglionic mass (Fig. 9). The cluster is surrounded by the neurites of the nerve plexus (Fig. 10); these neurites contain mitochondria, microtubules and diverse vesicles.

Lateral to the ganglion the epithelium becomes thinner. Here a group of special cells occurs in the epithelium (with 5–10 cilia each); they are thus quite different from the other epithelial cells (Fig. 11). They have a lobate nucleus and a rough outer surface covered with

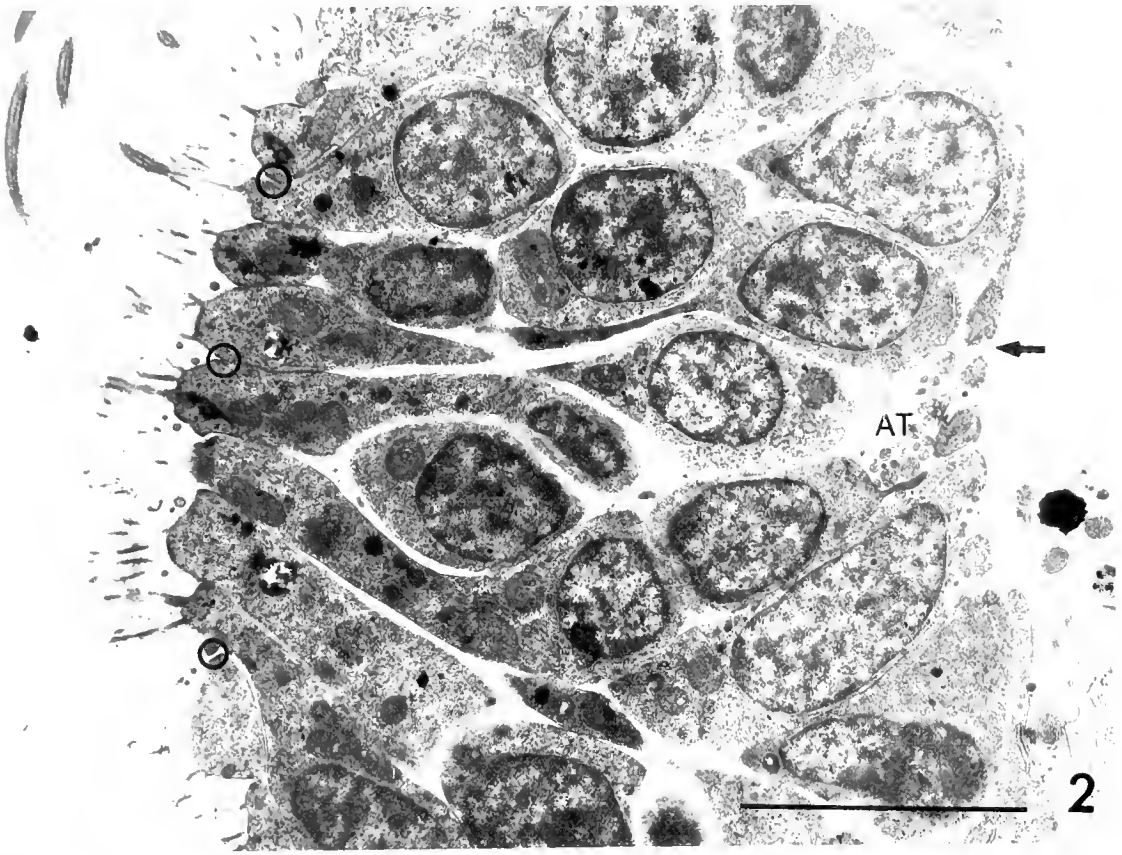
AT
2


AT
3


A
4

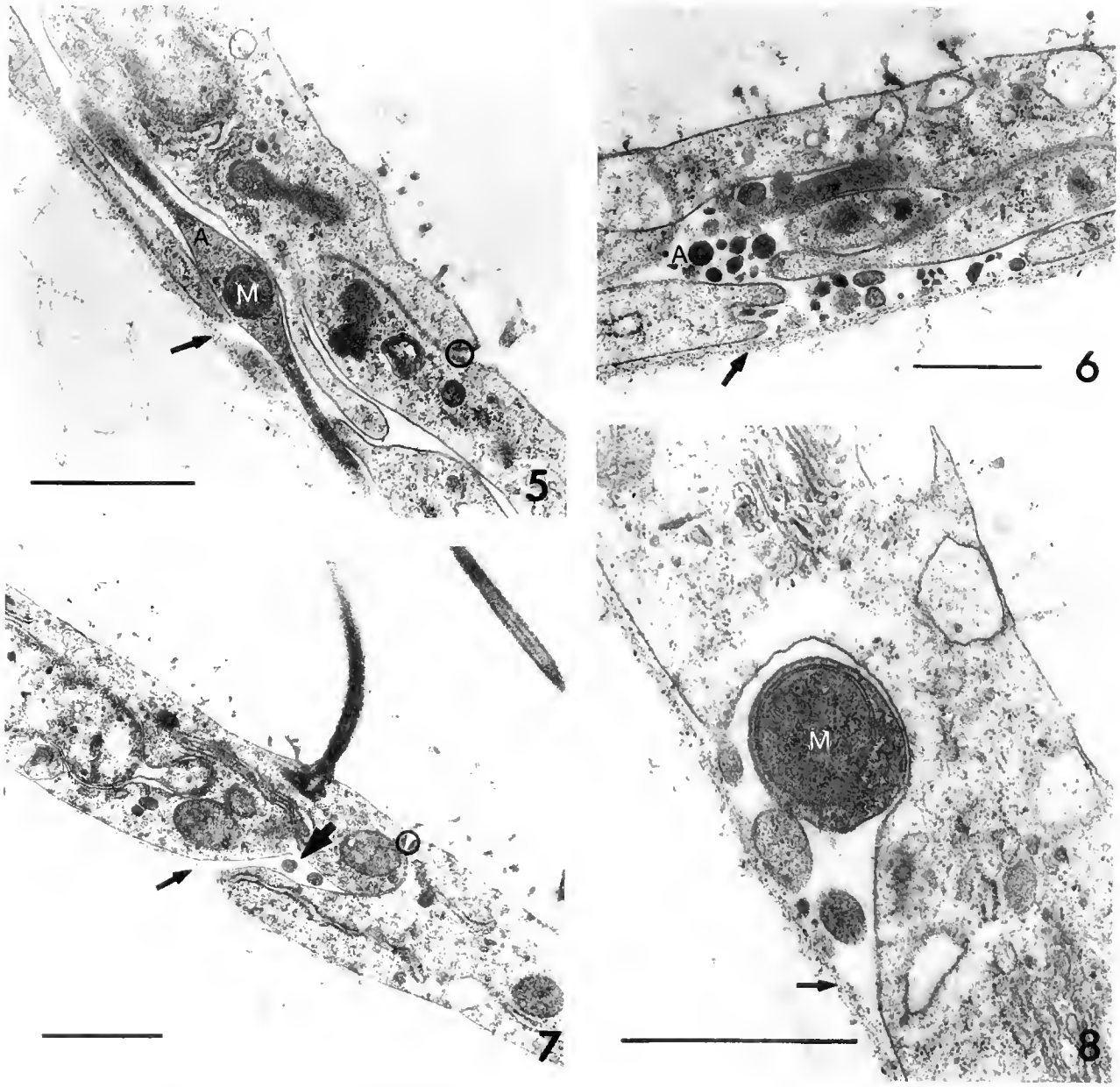

Figure 5. TEM. Longitudinal section of single axon (A) containing mitochondria (M) in the body wall outside ciliary band near basal lamina (arrow). Circle indicates tight junction. Scale bar = 1 μm.

Figure 6. TEM. Cross section of the axonal tract (A) inside the body wall epithelium. Arrow indicates a basal lamina. Scale bar = 2 μm.

Figure 7. TEM. Two axons (large arrow) between adjacent cells of the body wall. Small arrow indicates a basal lamina. Circle indicates tight junction. Scale bar = 2 μm.

Figure 8. TEM. Several axons inside groove in inner side of the body wall cell. Larger axon contains mitochondrion (M). Arrow indicates basal lamina. Scale bar = 2 μm.

Figure 2. Transmission electron microscopy (TEM). Cross section of ciliary band with axonal tract (AT) in its base near a basal lamina (arrow). Circles indicate tight junctions. Scale bar = 5 μm.

Figure 3. TEM. Cross section of nerve (AT) in the base of ciliary band near a basal lamina (arrow). Some axons contain transparent vesicles. Basal part of epithelial cell gives process to the tract. Scale bar = 1 μm.

Figure 4. TEM. Solitary axons at the base of the ciliary band near the basal lamina (arrow). One axon (A) contains electron dense-core vesicles. Scale bar = 1 μm.

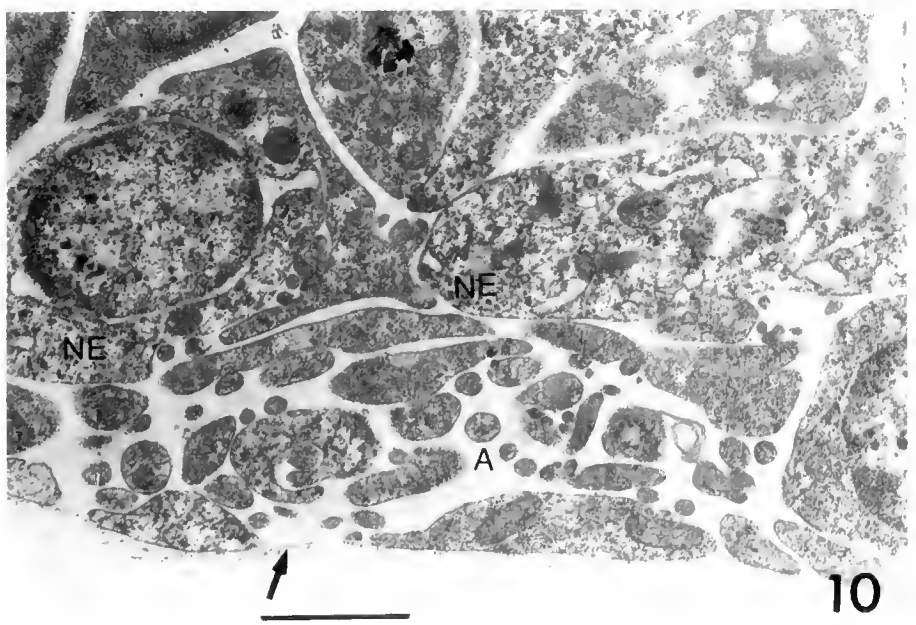

Figure 9. TEM. A part of the apical plate with a cluster of neuron-like cells (NE) and axons (A) at the base of the epithelium near a basal lamina (arrow). Circles indicate tight junctions. Scale bar = 2 μm.

Figure 10. TEM. Axons and neurons (NE) in the apical plate. Nerve plexus (A) is at the base of epithelium adjacent to basal lamina (arrow). Scale bar = 1 μm.

microvilli. In the apical region, the cytoplasm includes the Golgi complex, mitochondria and cisternae of rough endoplasmic reticulum (RER). Some cells have many large clear vacuoles. Tracts consisting of 3–5 axons each run between basal parts of these cells and the basal lamina. Around the ganglion, several axonal tracts each containing about fifty fibers, pass under the body wall (Fig. 12).

The epithelium of the esophagus is built from cuboidal multiciliated cells. Close to their bases numerous axonal tracts, of 10–20 fibers each, pass in different directions between the epithelial cells and the basal lamina (Fig. 13).

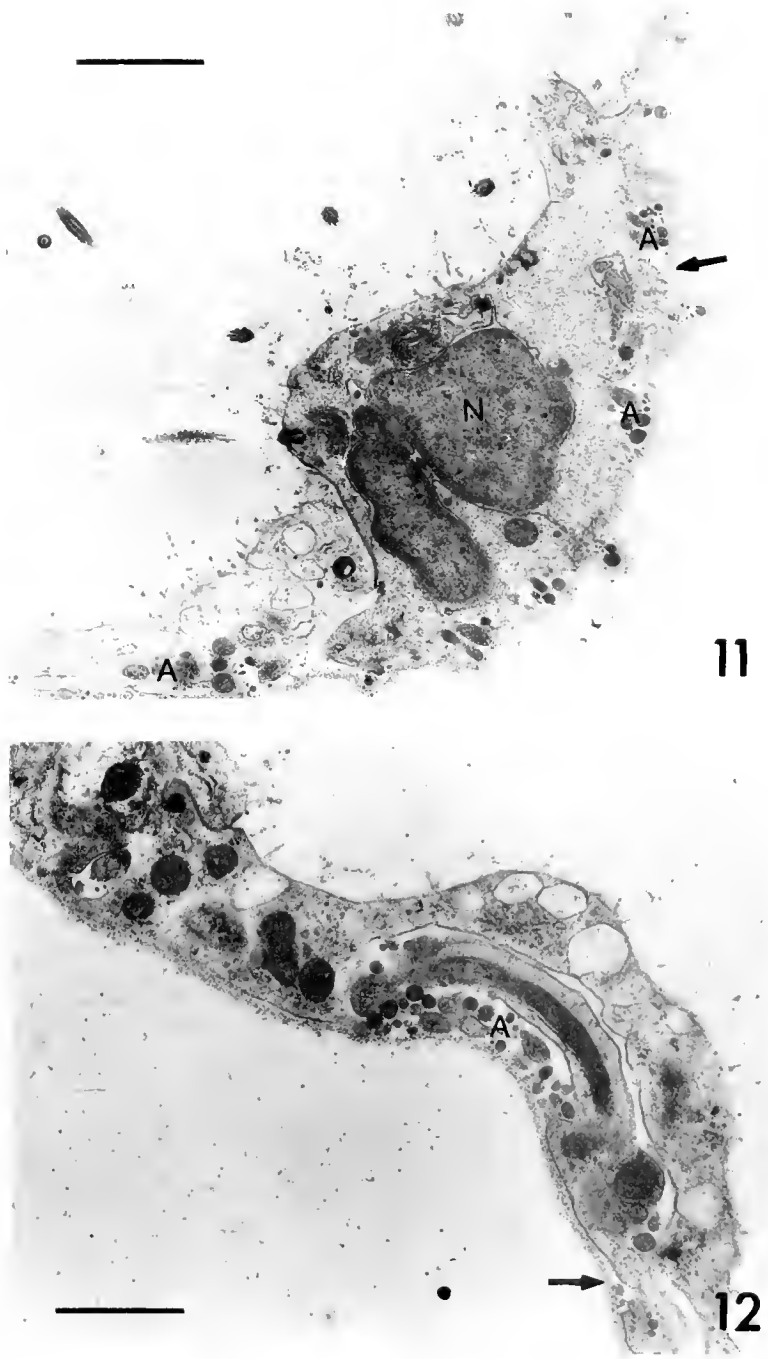

Figure 11. TEM. Epithelial cell lying laterally to the apical plate (frontal section) with lobate nucleus (N) and axonal tracts (A) at the base. Arrow indicates a basal lamina. Scale bar = 2 μm.

Figure 12. TEM. Axons (A) passing at the base of the body wall from the apical ganglion. Arrow indicates a basal lamina. Scale bar = 1 μm.

Several cells of the epithelium send processes to these tracts. Behind the mouth opening a group of subepithelial cells and numerous nerve fibers are present (Fig. 14). Muscle cells, which presumably assist in swallowing of food, lie at the base of esophageal epithelium coated by the layers of a basal laminae (Figs. 13, 14).

The epithelium of the stomach consists of cells of different types. At their bases only a few solitary axons were detected (Fig. 15).

Near the junction of the stomach with the intestine are 3–4 nerve tracts (Fig. 16). Each tract contains not more than ten axons. We detected some cells where processes

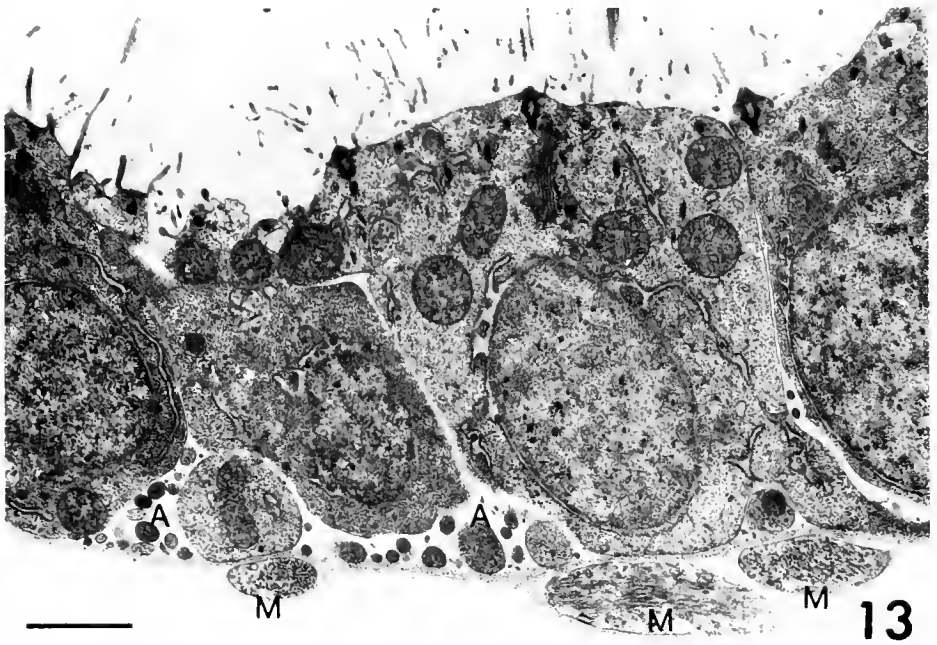

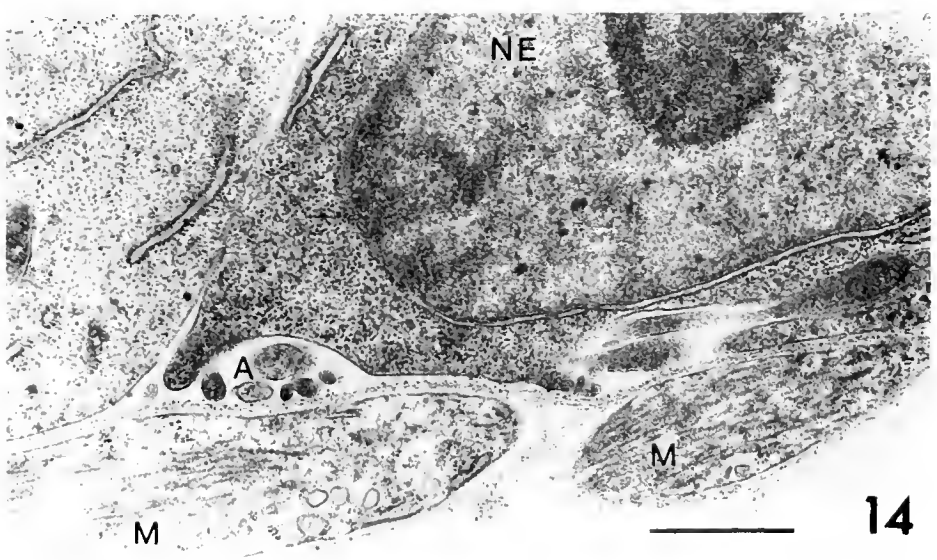

Figure 13. TEM. Longitudinal section of the esophagus showing ciliated epithelial cells, nerves (A) near the basal lamina and muscle cells (M) coated by layers of a basal lamina. Scale bar = 1 μm.

Figure 14. TEM. Neuron-like cell (NE) in the esophagus epithelium with axons (A) at its base. M, muscle cells surrounded by layers of the basal lamina. Scale bar = 2 μm.

that entered to the tract arose from the basal surface. The cytoplasm of the cells has high electron density and includes numerous mitochondria, RER, and vesicles.

The telotroch consists of multiciliated epithelial cells (Fig. 17). In addition to cilia, these cells have microvilli on their external surfaces. At the base of the telotroch, several tracts consisting of a few axons each run the length. Some cells with a very electron-dense cytoplasm lie in the epithelium. Processes extend from the base of these cells to the nerve tract. Another ciliary ring is situated between the telotroch and the anal opening. It consists of flat multiciliated cells with very few microvilli on their outer surfaces. Few axons run along this ring in grooves between adjacent cells (Fig. 18).

Histochemistry

Cholinesterase activity occurs in the epithelium along the length of the pre- and postoral ciliary bands, but not in the telotroch (Fig. 19).

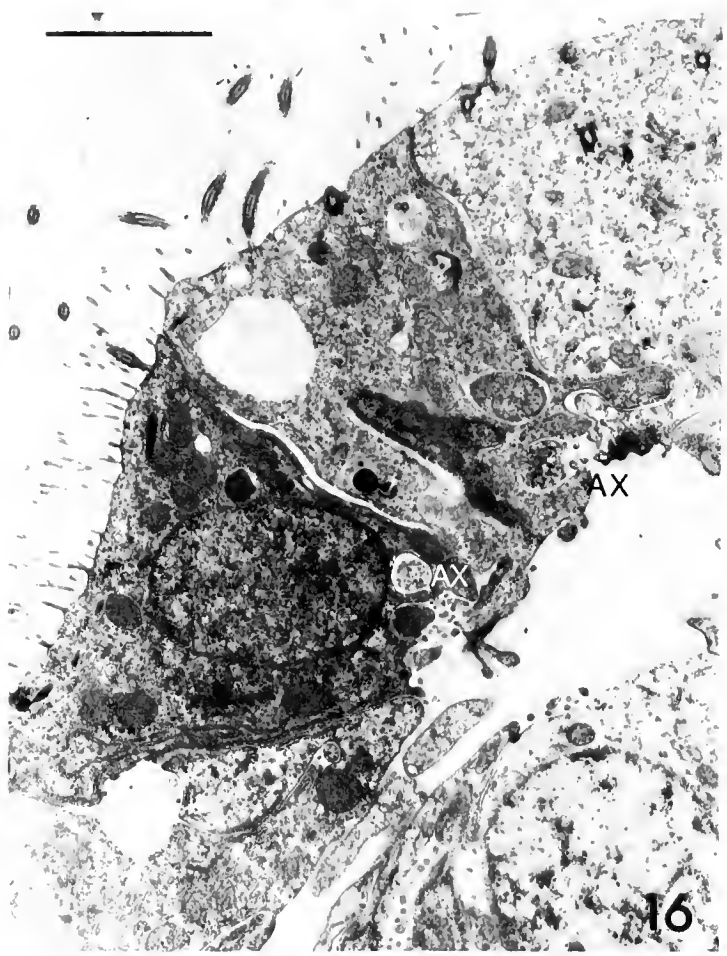

Figure 15. TEM. Epithelium of the stomach. Several axons (A) lie at its base adjacent to basal lamina. Scale bar = 2 μm.

Figure 16. TEM. Longitudinal section of part of the pyloric sphincter with axonal tracts (AX) at the base of the epithelium. Scale bar = 2 μm.

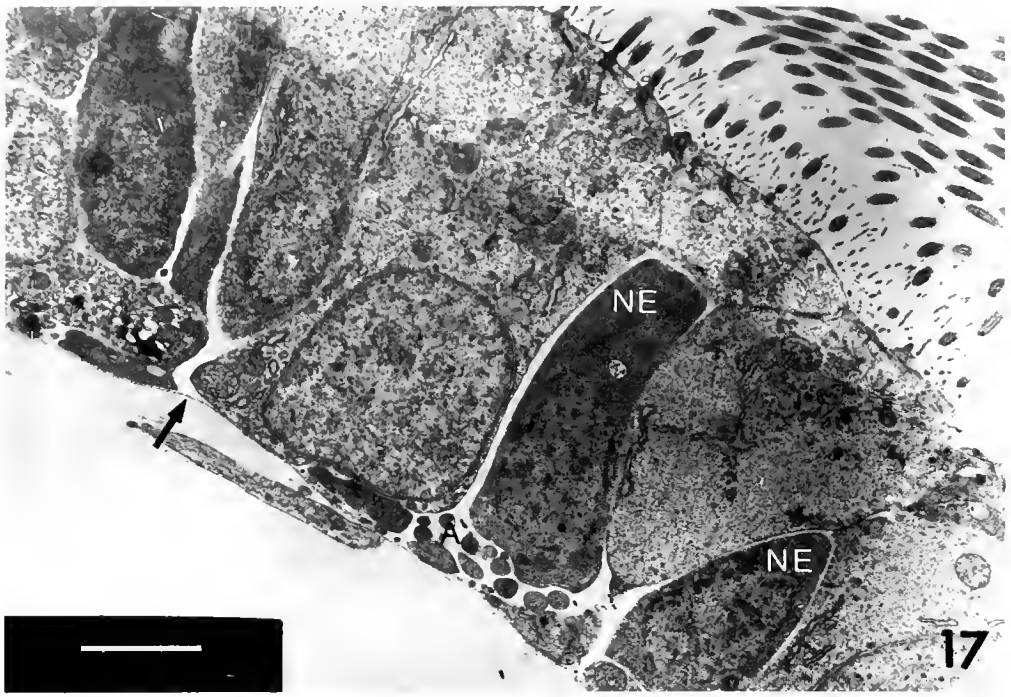

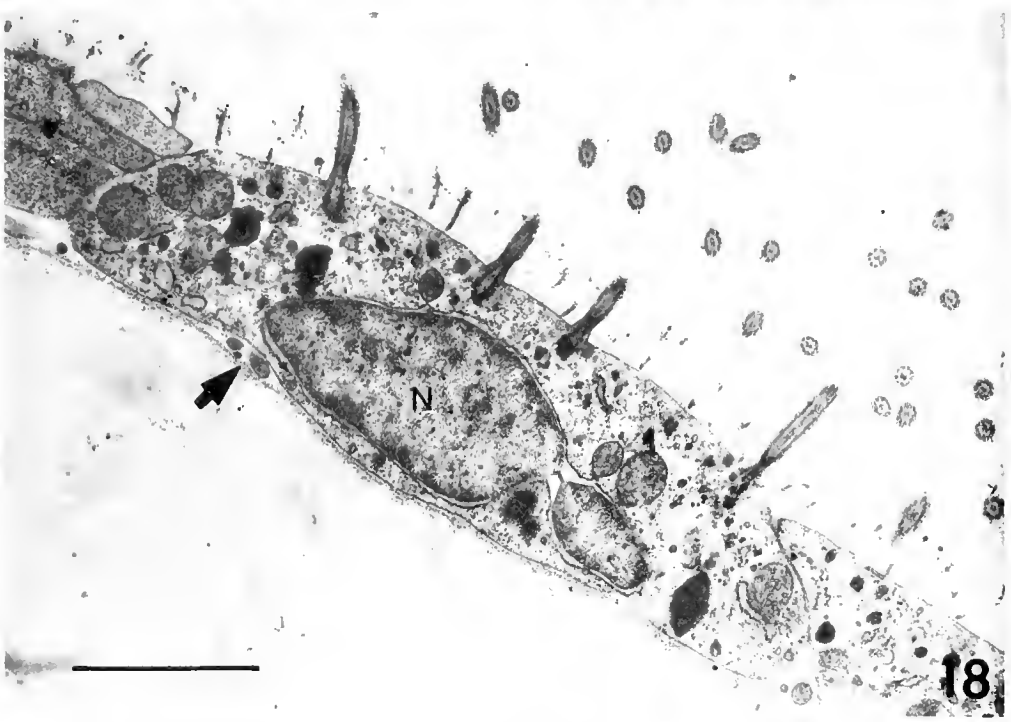

Figure 17. TEM. Cross section of the posterior ciliary band (telotroch) with the axonal tract (A) and two neuron-like cells (NE). Arrow indicates a basal lamina. Scale bar = 2 μm.

Figure 18. TEM. Cross section of the ciliary ring between telotroch and anal opening. Multiciliated cell with lobated nucleus (N) is shown. Axons (arrow) pass between it and its basal lamina. Scale bar = 1 μm.

Bright green fluorescence in glyoxilic acid preparation reveals what appear to be accumulations of the nerves (Fig. 20). The aboral plate appears as a cluster of fluorescent cells at the anterior tip of the larva (Fig. 21). A group of about 30–40 cells lies just between the eyespots. These cells extend their axons subepithelially along ciliary bands. A second group of nerve cells is located in the ventral part of the larva just behind the mouth opening (Fig. 22).

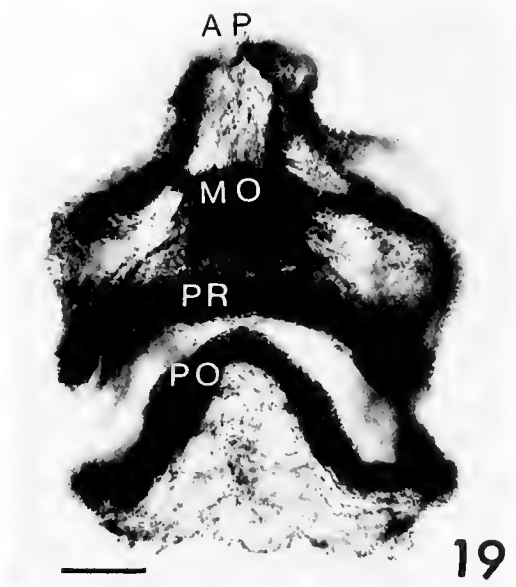

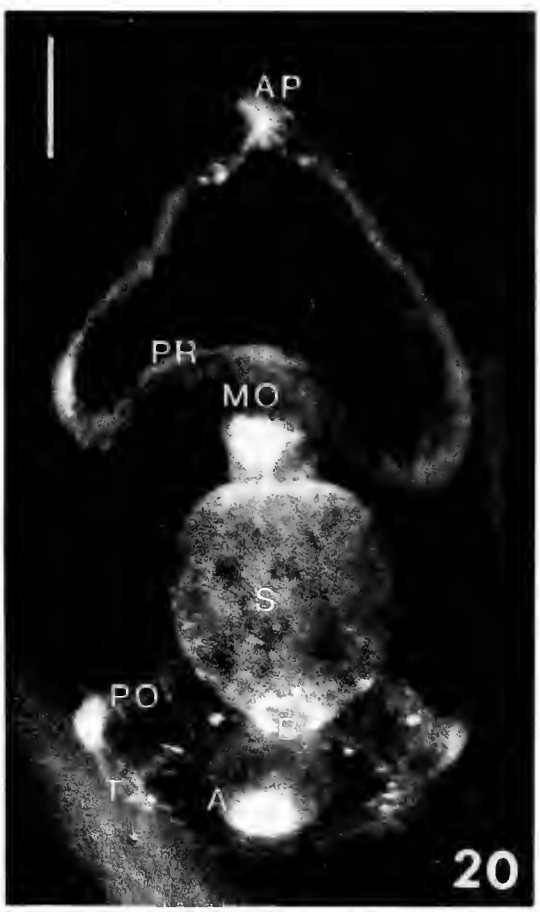

Axons from these cells pass anteriorly and enter the preoral ciliary band forming the circumoral nerve ring. In addition, a tract of axons passes backward in the ventral midline. These axons enter the postoral ciliary band.

In the stomach wall near the entrance to the intestine, the axons of a group of about ten fluorescent cells form a ring (Fig. 23). Several axons connect this ring with the axonal tract in the postoral band. Fluorescent cells in the epithelium of the telotroch all send axons into the postoral tract too (Fig. 23). In the telotroch itself, no fluorescent axonal tracts were detected. Axonal tracts which pass along the ciliary bands include no more than several fluorescent axons (Fig. 24). Green fluorescing cells in the telotroch send processes to the postoral nerve tract (Fig. 25). Bright nonspecific fluorescence was observed around the anus opening (Figs. 20, 23). No green fluorescing cells or fibers were found there.

Discussion

The tornaria exhibit a coordinated behavior which consists of swimming while permanently rotating about a long body axis and feeding on planktonic unicellular algae or organic particles (Strathmann and Bonar, 1976). Both locomotion and feeding are affected by the activity of the ciliary bands. But unlike echinoderm larvae, the tornaria has a specialized locomotory ciliary band, the telotroch, in addition to the pre- and postoral ciliary bands, which also capture and transfer food particles to the mouth. As in planktotrophic echinoderm larvae, this process is accomplished in tornaria by a local reversal of ciliary beat when food particles are contacted (Strathmann and Bonar, 1971, 1976). Cilia of the telotroch beat synchronously, bringing about a metachronal ciliary wave, but some parts of the telotroch may stop beating while other parts continue. This mechanism is involved in larval orientation and control of locomotion. Coordination of locomotion and feeding allow us to suppose that the behavior of tornaria is controlled by the nervous system. A standard method for identifying certain nerve cells is the histochemical localization of biogenic monoamines—*e.g.*, dopamine, noradrenaline, L-tyrosine, serotonin—by treatment with a solution of glyoxilic acid (Keenan and Koopowitz, 1981). Nerve elements thus found in the tornaria are localized along the ciliary bands. Groups of neuron bodies—*i.e.*, ganglia—lie in the apical plate and behind the mouth opening, and nerve tracts run subepithelially, reflecting the configuration of the ciliary bands. In addition, single catecholamine-containing (CA) cells are

Figure 19. Cholinesterase activity zones (dark parts of the specimen). Ventral view of the entire larva. AP, apical plate; MO, position of the mouth opening; PR, preoral ciliary band; PO, postoral ciliary band. Scale bar = 100 μm.

Figure 20. Glyoxilic acid-induced fluorescence (GAF). Total ventral view of entire larva. AP, apical plate; MO, mouth opening; B, border between the stomach and the intestine; S, stomach; T, telotroch; A, anus; PR, preoral ciliary band; PO, postoral ciliary band. Scale bar = 100 μm.

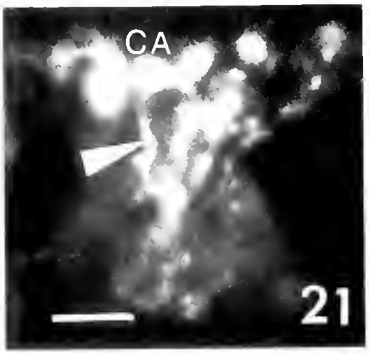
CA
21


CA
22


24

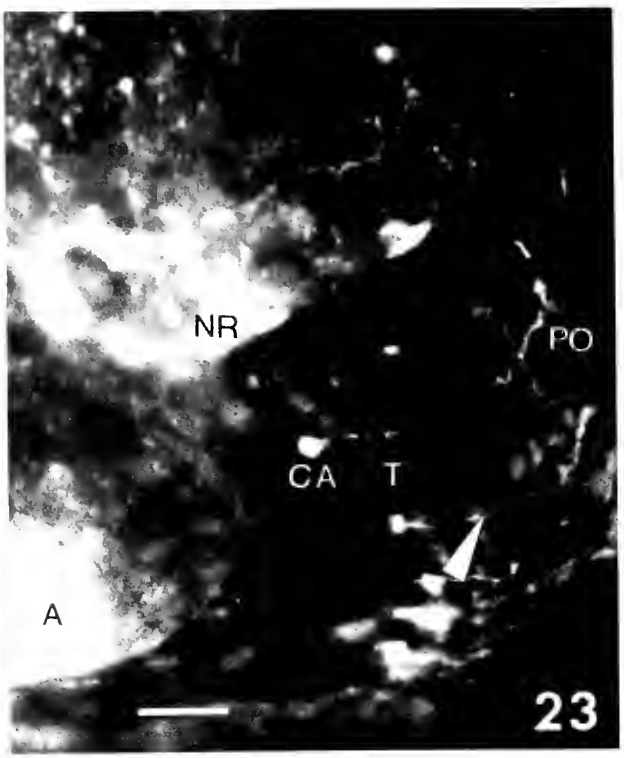
NR
PO
CA
T
A
23

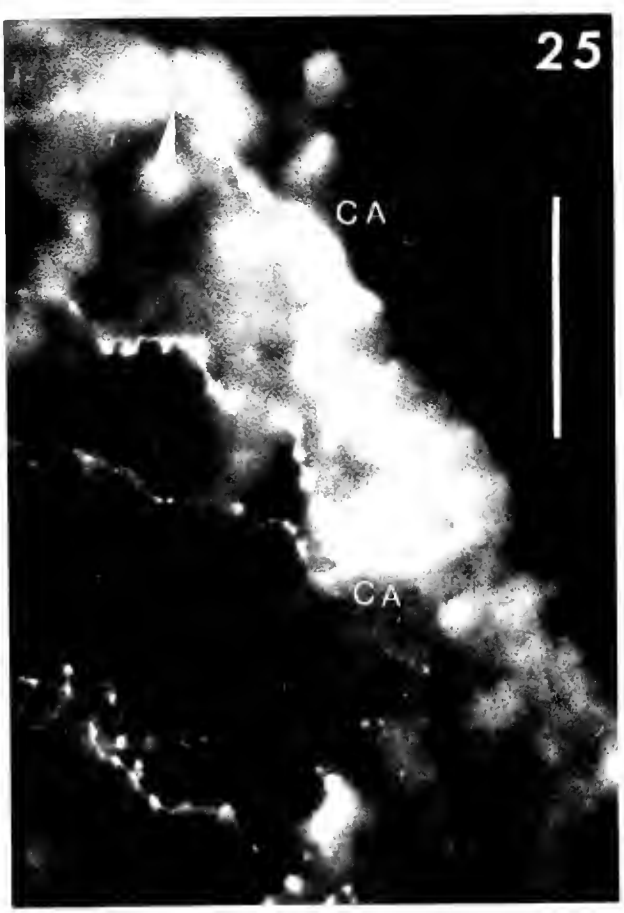
25
CA
CA

localized in epithelia of the postoral ciliary band and the telotroch. Cholinesterase is detected in ciliary bands, excluding the telotroch.

The electron microscopic data agree with the histochemical ones. Subepithelial strands of cell processes were found in the ciliary bands. The ultrastructure of these processes (*i.e.*, the presence of vesicles, microtubules, and mitochondria) clearly suggests that they are axons. Two cell types that send processes to the nervous tracts can be distinguished. The first are ciliated cells found in the epithelia and telotroch, which send axons from their bases. Subepithelial processes originates from the second type of nonciliated cells especially in the region of aboral and esophageal ganglia. The first type of neuron may perform a sensory function, whereas the second type may be an inter- or motoneuron. Similar cells and nerve plexes adjacent to basal lamina were described earlier in the ocelli of the tornaria of *Ptychodera flava* (Branderburger *et al.*, 1973). Unfortunately, no morphologically distinct synapses, either between nerve cells, or between neural and muscle cells, were found in the tornaria. Our assumption that these cells are neural is mainly based on their ultrastructural localization being coincident with the distribution of cells containing biogenic amines (specific neurotransmitters). The apparent absence of synapses is a common feature of marine invertebrate planktotrophic larvae, since no ultrastructural investigations have revealed these structures in pilidia larvae of nemertines (Lacalli and West, 1984), echinoderm larvae (Burke, 1983a, b), or in the actinotrocha larvae of phoronids (Hay-Schmidt, 1989). The detection of catecholamines and of cholinesterase activity suggests that monoamine and cholinergic regulatory mechanisms occur in the tornaria. Evidently there are additional neurotransmitters in the nervous system of tornaria. This is confirmed by the presence of various vesicles in neurons and their axons, and in neuron-like cells and axons, detected in regions of the larva, that exhibit no cholinergic activity and no specific monoamine fluorescence.

In starfish and holothurian larvae, which are morphologically similar to tornaria, the nervous system includes nerve cords lying in the subepithelial layer under ciliary bands and near the esophagus, and many nerve cells containing monoamines lying near the cords (Burke, 1983a; Nezlin *et al.*, 1984; Burke *et al.*, 1986). A similar distribution of neural elements was described in sea urchin larvae (Burke, 1983a; Bisgrove and Burke, 1987). In actinotroehs, intraepithelial nerves pass from the apical ganglion along the midline and around the edge of the epistome (preoral hood). Other nerves are located around the tentacular ring and the posterior ciliary band or telotroch (Hay-Schmidt, 1989). These last neurons, containing catecholamines, are situated in the epithelium along the ciliary bands (Nezlin, 1988). In actinotrochs and tornaria, an apical and a subesophageal mass of nervous cells were detected. In the anterior end of auricularia and bipinnaria, accumulations of catecholamine-containing neurons are absent. Nevertheless, in the "apical ganglion" of auricularia and bipinnaria of several species, massed serotoninergic neurons were shown immunohistochemically (Nakajima, 1988), in one case with antibodies directed against serotonin (Burke *et al.*, 1986).

Despite a strong similarity to echinoderm larvae in ultrastructural localization of neural elements, tornaria differ from them in having catecholamine-containing neurons concentrated in the aboral and esophageal ganglia, and in axons running along the ciliary bands. Posteriorly, solitary catecholamine ciliated cells, connected by axons with nerve tracts, lie in the ciliary band epithelium.

Earlier, Burke (1978, 1983a) suggested that the function of catecholamine-containing neurons in planktotrophic larvae is the coordination of swimming and feeding. Bisgrove and Burke (1987) also pointed out the same possible function for dopaminergic neurons in larval arm epithelia of echinopluteus. The finding of two types of catecholamine cells in tornaria, one concentrated in two subepithelial ganglia sending axons along ciliary bands, and the second scattered in the ciliary band epithelia, allows us to suggest that these cells perform similar functions.

The lack of cholinesterase activity in the telotroch of tornaria probably means that locomotion in tornaria is not acetylcholine dependent. In bipinnaria, cholinesterase is detected throughout the entire ciliary band system. Moreover, in bipinnaria of the asteroid *Lethasterias fusca*, locomotion is controlled by a cholinergic system (Dautov and Semenova, 1988). Thus, the tornaria probably differs

Figure 21. GAF. Catecholamine-containing cells (CA) and their processes (arrow head shows one) in the region of apical plate. Scale bar = 15 μm.

Figure 22. GAF. The cluster of catecholamine containing cells (CA) behind the mouth opening and axonal tract passing from it posteriorly (arrow head). Scale bar = 15 μm.

Figure 23. GAF. Posterior view at the region of postoral ciliary band (PO), telotroch (T), and anus (A). Nerve ring at the junction of stomach and intestine (NR) is shown. Solitary catecholamine containing cells (CA) of telotroch give processes (arrow head shows one) to postoral ciliary band. Scale bar = 15 μm.

Figure 24. GAF. Processes of catecholamine-containing cells (arrow head) in the ciliary band epithelium. Scale bar = 15 μm.

Figure 25. GAF. Catecholamine-containing cells (CA) in the epithelium of telotroch, each having a single process (arrow head). Scale bar = 15 μm.

from the bipinnaria not only in the topology of CA elements but also in the distribution of acetylcholine-containing cells.

In this regard, it is interesting to note that actinotrocha larvae have in their telotroch (a specialized locomotor ciliary band) neither cholinergic- nor catecholamine-containing cells (Nezlin, 1988). Presumably, in the course of adaptive evolution, larvae of certain marine invertebrates—echinoderms, phoronids, and enteropneusts—acquired a set of common morphological and behavioral features. This commonality is especially marked in the bipinnaria and tornaria. Notwithstanding these similarities, however, there are presumed different physiological mechanisms of behavioral regulation.

Literature Cited

Bisgrove, B. W., and R. D. Burke. 1987. Development of the nervous system of the pluteus larva of *Strongylocentrotus droebachiensis*. *Cell Tissue Res.* **248:** 335–343.

Branderburger, I. L., R. M. Woollacott, and R. M. Eakin. 1973. Fine structure of eyespots in tornarian larvae (Phylum: Hemichordata). *Z. Zellforsch.* **142:** 89–102.

Burke, R. D. 1978. The structure of the nervous system of the pluteus larvae of *Strongylocentrotus purpuratus*. *Cell Tissue Res.* **191:** 233–247.

Burke, R. D. 1983a. Development of the larval nervous system of the sand dollar, *Dendraster excentricus*. *Cell Tissue Res.* **229:** 145–154.

Burke, R. D. 1983b. The structure of the larval nervous system of *Pisaster ochraceus* (Echinodermata: Asteroidea). *J. Morphol.* **178:** 23–35.

Burke, R. D., D. G. Brand, and B. W. Bisgrove. 1986. Structure of the nervous system of the auricularia larva of *Parastichopus californicus*. *Biol. Bull.* **170:** 450–460.

Chia, F. S., R. D. Burke, R. Koss, P. V. Mladenov, and S. S. Rumrill. 1986. Fine structure of the doliolaria larva of the feather star *Florometra serratissima* (Echinodermata: Crinoidea), with special emphasis on the nervous system. *J. Morphol.* **189:** 99–120.

Damas, D., and G. Stiastny. 1961. Les larves planctoniques d'Enteropneusts (Tornaria et Planctosphaera). *Mem. Acad. roy. Belgique* C 1, Sci. 2, ser. **15** (2): 1–70.

Dautov, S. Sh., and M. M. Semenova. 1988. Participation of cholinergic system in the regulation of locomotion of star fishes larvae. Pp. 81–83, in *Prostye Nervnye Sistemy*. Leningrad, Nauka. (in Russian)

Hay-Schmidt. 1989. The nervous system of the actinotrocha larva of *Phoronis muelleri* (Phoronida). *Zoomorphology* **108**(6): 333–352.

Ivanova-Kazas, O. M. 1978. *Comparative Embryology of Invertebrates Echinoderms and Hemichordates*. Moscow, Nauka. (in Russian)

Keenan, C. L., and H. Koopowitz. 1981. Limitations in identifying neurotransmitters within neurons by fluorescent histochemistry techniques. *Science* **214:** 1151–1152.

Koelle, G. B., and J. S. Friedenwald. 1949. A histochemical method for localizing cholinesterase activity. *Proc. Soc. Exp. Biol. Med.* **70:** 617–622.

Krohn, A. 1854. Beobachtungen uber Echinodermenlarven. *Arch. Anat. Physiol. Wissensch.* 208–213.

Lacalli, T. C., and J. E. West. 1985. The nervous system of a pilidium larva: evidence from electron microscope reconstructions. *Can. J. Zool.* **63:** 1909–1916.

Metschnikoff, E. 1870. Untersuchungen uber die Metamorphose einiger Seethiere. Ueber Tornaria. *Z. Wiss. Zool.*, Bd XXII.

Müller, J. 1850. Über die Larven und die Metamorphose der Echinodermen. *Abhandl. Acad. Wiss.* Berlin, for **1848:** 75–110.

Nakajima, Y. 1987. Localization of catecholaminergic nerves in larval echinoderms. *Zool. Sci.* **4**: 293–299.

Nakajima, Y. 1988. Serotoninergic nerve cells of starfish larvae. Pp 235–239 in *Echinoderms Biology*. Burke *et al.*, eds. Balkema, Rotterdam.

Nezlin, L. P. 1988. The development of monoaminergic elements of the nervous system in the actinotroch—planctonic larvae of *Phoronopsis harmeri*. *Journal evolutsyonnoy biochimii i fisiologii* **24**: 76–80. (in Russian)

Nezlin, L. P., S. Sh. Dautov, and V. V. Malakhov. 1984. Topography of catecholamine containing neurons in larval development of starfishes. *Doklady Akademii Nauk SSSR.* **278:** 983–985. (in Russian)

Sharp, M. J., and H. J. Atkinson. 1980. Improved visualization of dopaminergic neurons in nematodes using the glyoxilic acid fluorescence method. *J. Zool. Lond.* **190:** 273–284.

Strathmann, R. R., and D. Bonar. 1971. Tornaria's water-working revisited. *Am. Zool.* **11:** 517.

Strathmann, R. R., and D. Bonar. 1976. Ciliary feeding of tornaria larvae of *Ptychodera flava* (Hemichordata: Enteropneusta). *Mar. Biol.* **34:** 317–324.

Strathmann, R. R., T. Jahn, and J. R. C. Fonseca. 1972. Suspension feeding by marine invertebrate larvae: clearance of particles by ciliated bands of a rotifer, pluteus, and trochophore. *Biol. Bull.* **142:** 505–519.

de la Torre, J., and J. Surgeon. 1976. A methodological approach to rapid and sensitive monoamine fluorescence using a modified glyoxilic acid technique: the SPG-method. *Histochem.* **49:** 81–93.

Van der Horst, K. 1933. Enteropneusts of the seas of the USSR. *Issl. morei SSSR* **19:** 73–78.

Reference: *Biol. Bull.* 183: 476–481. (December, 1992)

Increased Reactive Oxygen Intermediate Production by Hemocytes Withdrawn from *Crassostrea virginica* Infected with *Perkinsus marinus*

ROBERT S. ANDERSON[1], KENNEDY T. PAYNTER[2], AND EUGENE M. BURRESON[3]

[1]*Chesapeake Biological Laboratory, University of Maryland System, P. O. Box 38, Solomons, Maryland 20688,* [2]*Department of Zoology, University of Maryland, College Park, Maryland 20742, and* [3]*Virginia Institute of Marine Science, School of Marine Science, The College of William and Mary, Gloucester Point, Virginia 23062*

Abstract. *Perkinsus marinus* is a protozoan parasite responsible for a major infectious disease of the Eastern oyster, *Crassostrea virginica*. Nonspecific immunity was assayed in oysters with known intensities of infection so that the physiological responses of the host elicited by the parasite could be better understood. This report describes the capacity of hemocytes to generate reactive oxygen intermediates during the progression of the disease. The hemocytes constitute the major internal defense effector system of oysters, and cytotoxic oxygen species are thought to play central roles in antimicrobial activities of hemocytes and other phagocytic cells. Production of oxyradicals by both resting and phagocytically stimulated hemocytes was quantified by luminol-augmented chemiluminescence. Hemocytes from oysters with heavy *Perkinsus* infections produced significantly higher levels of chemiluminescence than their counterparts withdrawn from lightly or moderately infected individuals. Furthermore, in addition to a higher chemiluminescent activity per cell, the total circulating hemocyte count was elevated in the heavily infected animals. Therefore, advanced cases of this disease seem to be characterized by hemocyte activation and recruitment, with concomitant exuberant production of hemocyte-derived reactive oxygen intermediates. The resultant oxidant load may participate in the pathogenesis of the disease.

Received 1 June 1992; accepted 14 September 1992.

Abbreviations: CL = chemiluminescence; CSM = cell supported medium; MB = Mobjack Bay; ROI = reactive oxygen intermediates.

Introduction

Upon appropriate stimulation, phagocytic cells typically undergo a burst of respiratory activity and manufacture large quantities of cytotoxic oxidants. This activity was first reported in mammalian neutrophils and macrophages, but has subsequently been observed in phagocytes from most vertebrates and invertebrates. The details of the production of reactive oxygen intermediates (ROIs) by these cells may be found in reviews by Badwey and Karnovsky (1980), DeChatelet *et al.* (1982), Klebanoff (1982), Babior (1984), and Babior *et al.* (1988). Cell-derived ROIs can participate in protective antimicrobial mechanisms and mediate various kinds of host tissue injury. The ultimate source of these oxidants is the superoxide anion ($O_2^{\cdot}-$) produced by the one-electron reduction of oxygen at the expense of NADPH; the reaction is catalyzed by a membrane-bound flavoprotein oxidase. Superoxide undergoes enzymatic dismutation to produce hydrogen peroxide (H_2O_2), which may give rise to other highly toxic species, such as the hydroxyl radical ($^{\cdot}OH$), via the Fenton reaction, or hydrochlorous acid (HOCl) via myeloperoxidase. The roles of phagocyte-generated ROIs in the pathogenesis of certain mammalian diseases has gained considerable recent attention (*e.g.*, see Halliwell, 1988; Cerutti *et al.*, 1988) particularly with regard to inflammatory cell damage of the vascular endothelium in atherosclerosis, tissue injury during myocardial ischemia and reperfusion, immune complex-induced acute lung injury, and glomerulonephritis. The health of aquatic organisms may also be effected by oxidative stress (DiGiulio

et al., 1989). The mechanisms underlying oxidant damage of cells are numerous but are thought to include: decreased ATP levels via inhibition of mitochondrial oxidative phosphorylation, increased DNA strand breaks and other structural and functional alterations of nucleic acids, interference with intracellular enzymes, peroxidation of membrane lipids with concomitant reduction in structural integrity, and various other deleterious interactions with cell membrane proteins and lipids (Fantone and Ward, 1982; Kako, 1987; Cochrane *et al.*, 1988).

As previously noted, the respiratory burst and accompanying production of ROIs are not restricted to mammalian phagocytes. The literature on these activities by molluscan hemocytes has been expanding since the initial report of H_2O_2 release from scallop amebocytes by Nakamura *et al.* (1985). Recently, the hemocytes of many molluscan species have been shown to produce O_2^- and H_2O_2 (Dikkeboom *et al.*, 1987 and 1988; Adema *et al.*, 1991a; Bachère *et al.*, 1991a; Pipe, 1992), and this activity may be modulated by exposure to certain environmental contaminants (Larson *et al.*, 1989; Fisher *et al.*, 1990; Anderson *et al.*, 1992a, 1992b) or by microbial infection (LeGall *et al.*, 1989, 1991; Hervio *et al.*, 1989). Myeloperoxidase activity has also been measured in bivalve hemocytes (Schlenk *et al.*, 1991). The subject of ROI expression by molluscan phagocytes has been reviewed recently by Adema *et al.* (1991b).

As is the case for of oxyradicals in other species, molluscan ROIs probably participate in antimicrobial defense, but they also have a destructive potential. The balance between ROI production and activities of protective mechanisms (superoxide dismutase (EC 1.15.1.1), catalase (EC 1.11.1.6), glutathione peroxidase (EC 1.11.1.9), glutathione, vitamins A, C and E, β carotene, etc.) is critical in determining the extent of oxidative damage. The contribution of ROIs from activated hemocytes to oxidant loads already present due to normal or pollution-enhanced oxyradical production (reviewed by Livingstone *et al.*, 1989, 1990; Winston *et al.*, 1990; Winston, 1991) could theoretically overwhelm the antioxidant defense mechanisms of mollusks.

In this paper we report that hemocytes from oysters heavily infected with the protozoan parasite *Perkinsus marinus* produce significantly elevated levels of ROIs; the possibility that this contributes to the pathogenesis of the disease is raised.

Materials and Methods

Animals

The oysters (*Crassostrea virginica*) used in this study were spawned in July 1989 and introduced as spat into an area with low *Perkinsus* (the Wye River, MD, salinity ~eight ppt) in September 1989. Two groups from this population were transferred to a high *Perkinsus* site in Mobjack Bay, VA (~20 ppt salinity): the first group on 14 April 1991, and the second group on 28 July 1991. Both the *Perkinsus* prevalence and the higher salinity of Mobjack Bay favored infection and progression of the disease in the transplanted oysters (Paynter and Burreson, 1991). The above transfer protocol was designed to make available oysters with a wide spectrum of disease stages.

Both groups of Mobjack Bay oysters were sampled twice (on 10 and 17 September 1991), held on ice, and transported to the laboratory within 24 h of collection. They were numbered and housed at ambient temperatures and salinity (23°C, 20 ppt) in aerated aquaria. Hemolymph samples were withdrawn from the adductor muscle sinus for chemiluminescence (CL) studies and for hemocyte enumeration; all of the hemolymph samples were collected within three days of receipt of the oysters. The animals were replaced in the aquaria; all specimens living at the end of the hemolymph collection period (three days) were individually diagnosed and staged for *Perkinsus* by the thioglycollate method (Ray, 1952, 1966).

Oysters that became moribund before they could be diagnosed by the thioglycollate method were fixed in Davidson's AFA and examined by histology. Histological diagnoses have been found to provide slightly lower estimates of infection levels than the thioglycollate method. Based on this experience, the histological diagnoses were adjusted slightly to enable them to be expressed by the thioglycollate scoring method. In this study, 55 diagnoses were carried out via thioglycollate, and 25 were initially performed by histology and converted to thioglycollate scores. To quantify the level of infection in individual oysters, the subjective criteria of light, moderate, and heavy, based on Ray (1952), were given the numeric values of 1, 3, and 5, respectively.

Reactive oxygen intermediate determination

The production of ROIs by oyster hemocytes was quantified by measuring luminol-augmented chemiluminescence (CL) before and after phagocytic stimulation. To obtain the hemocytes, several ml of hemolymph were withdrawn from the adductor muscle sinus via a small notch cut in the edge of the valves. An aliquot was placed on a hemacytometer and the total cell count determined; the remaining hemolymph was further processed for CL evaluation. The hemolymph was incubated for 15 min at room temperature in a plastic petri dish, during which time the majority of the cells became firmly attached. Filter-sterilized ambient water from the oyster tanks (FA) was then used to gently wash off the fluid phase of the hemolymph and any unadhered cells. The cell monolayer was then overlaid with FA and incubated for 2.5 h at room temperature. During this period the cells became

progressively more loosely attached and could be finally washed free and resuspended in FA. These cells retained phagocytic activity, but showed little of the clumping typically encountered during the centrifugation and resuspension of freshly collected cells. The hemocytes were removed from suspension by centrifugation (200 *g*, 15 min), resuspended in cell support medium (CSM), and counted. The composition of CSM was 0.5% antibiotic solution (10,000 U penicillin, 10 mg streptomycin, and 25 μg amphotericin B/ml), 5% fetal calf serum, and 1 mg/ml glucose in FA. One ml aliquots of the hemocyte suspension (10^6 cells in CSM) were placed in small scintillation vials. From this point on, all steps were carried out in a dark room under dim red illumination. To each vial was added 0.3 ml FA and 1 ml luminol (250 μM in FA), and the vials were placed in a scintillation counter programmed for single photon monitoring. The vials were counted at 0.3 min intervals for about 10 min to establish the level of unstimulated, background CL for each sample. Then 0.2 ml of a suspension of heat-killed, washed yeast cells (final particle:hemocyte ratio = ~20:1) were added to the vials to provide phagocytic stimulation. The vials were counted at 0.3 min intervals for about 2 h after the addition of yeast.

Chemiluminescence (counts per min) was recorded directly on computer disks and as printed output from the scintillation counter. The background (basal) CL level was defined as the cpm recorded immediately before the addition of the phagocytic stimulus. The peak CL was the maximal CL response elicited by the phagocytic event (corrected for background). The total CL response was expressed as the area under the phagocytically induced portion of the curve (estimated by a polygon summation method).

The raw CL data were not normally distributed and were transformed (ln [1 + X]) to permit statistical analysis of variance; multifactor ANOVA was performed as appropriate. Differences between data groups were considered significant if $P < 0.05$ (F-test). Post hoc tests (Fisher PLSD and Scheffe F-test) were also run and significance at the 95% level determined.

Results

Batch differences

Two batches of oysters, taken a week apart, were sampled from each of the two transplanted groups in Mobjack Bay. The possibility that the two batches were significantly different from each other with regard to mean levels of CL activity was investigated. The level of infection showed no significant difference between batches within the groups. The various raw CL parameters showed a trend (batch 1 < batch 2); after log transformation, the only parameter to show this effect was total CL ($P = 0.0298$).

Table I

Intensities of Perkinsus marinus *infection in oyster groups with different residency times in Mobjack Bay (MB)*

Infection level*		
Group 1 (7 wks in MB; n = 39)	Group 2 (22 wks in MB; n = 41)	*P* value (ln [1 + X] transformed data; F-test, one factor ANOVA)
1.6 ± 0.2	3.8 ± 0.3	0.0001

* Each oyster scored for level of infection: 1 = light, 3 = moderate, 5 = heavy.

Because of the highly significant differences reported below between the two transplanted groups, with regard to all CL parameters and infection levels, the batch effects were considered minimal, and the data were analyzed by two factor ANOVA using group data and levels of infection.

Group differences

As outlined in Materials and Methods, the two groups were derived from the same spawning, but differed with regard to the period spent in Mobjack Bay (MB), during which time they were exposed to increased salinity, increased *Perkinsus* exposure, and other environmental factors present in that location. As expected, the mean level of infection recorded for group 2 (~22 weeks in MB) was higher than that of group 1 (~7 weeks in MB), as seen in Table I. Table IIa indicates that the background,

Table II

Luminol-augmented chemiluminescence by 10^6 hemocytes from oysters infected with Perkinsus marinus

a: Hemocytic chemiluminescence (mean cpm ± SEM) from oyster groups with different intensities of *Perkinsus marinus* infection.

CL parameter	Group 1 Lightly infected (n = 39)	Group 2 Heavily infected (n = 41)	*P* value (F-test, two factor ANOVA, ln [1 + X] transformed data)
Background	121 ± 22	347 ± 49	0.0294
Peak	276 ± 107	1,050 ± 174	0.0031
Total	23,632 ± 9,266	80,720 ± 13,513	0.0098

b: Hemocytic chemiluminescence (mean cpm ± SEM) from individual oysters with various levels of *P. marinus* infection.

CL parameter	Level of infections: Light (n = 38)	Moderate (n = 13)	Heavy (n = 28)	*P* value (calculated as above)
Background	128 ± 20	105 ± 22	452 ± 62	0.0115
Peak	305 ± 105	253 ± 85	1,388 ± 229	0.0036
Total	24,834 ± 8,336	18,506 ± 6,499	108,771 ± 18,265	0.0057

peak, and total CL parameters of the more heavily infected group were significantly greater than the comparable values of the lightly infected group. The Fisher PLSD and Scheffe F-tests were also significant at the 95% level when the CL parameters were compared between groups.

Correlation of CL parameters with levels of infection in individuals

Since groups differed with regard to average levels of infection, and the CL responses seemed to be related to the levels of infection, we asked whether infection intensities were directly correlated with magnitude of CL responses in individual oysters. Diagnostic data and CL values were available for each oyster, and these data were analyzed for individuals without consideration of the particular groups from which they were collected. Table IIb shows that there were significant differences between mean CL parameters in oysters with light, moderate, or heavy *Perkinsus* infections. However, further examination showed that these differences were significant (95% level, Fisher PLSD and Scheffe F-test) when comparing light *versus* heavy or moderate *versus* heavy infections, but not when comparing light *versus* moderate. Significant CL response differences can apparently only be seen between oysters with heavy *Perkinsus* infections and those with less intense infections. Since none of the oysters in this study were totally *Perkinsus*-free, we do not yet know whether uninfected oysters can be differentiated from lightly or moderately infected individuals based on their CL responsiveness.

When their relative contributions to the observed variation (induction) of CL parameters were analyzed (data in Tables IIa and b compared), the effects were clearly more associated with the levels of infection than with the group. Moreover, there were no significant interactions between individual and group infection level effects ($P > 0.2$ for background, peak, and total CL).

Total hemocyte counts in Perkinsus-infected oysters

During the preparation of cells from batch 1 for CL assays, we noticed that the hemolymph from the heavily infected group sometimes seemed more turbid than that from the lightly infected group. This was tentatively ascribed to the presence of elevated numbers of circulating hemocytes; therefore, hemocyte counts were carried out on the second batch (n = 36). The total hemocyte counts in the second group of oysters (the more heavily infected group of Mobjack Bay transplants) were not significantly higher than those recorded for the lightly infected group (Table IIIa). But if the hemocyte data were grouped according to diagnostic scores of individual oysters (Table IIIb), the correlation between heavy intensity of infection and hemocyte numbers was noticeable, and the differences between these groups were significant. Post hoc tests were also run to determine the significance of the differences observed between cell counts from oysters with different *Perkinsus* diagnostic scores. These results showed that significant differences (at the 95% level, Fisher PLSD test) were encountered when comparing light *versus* heavy and moderate *versus* heavy, but not light and moderate. This was reminiscent of the findings when chemiluminescence data were compared according to these classifications.

Table III

Effects of Perkinsus marinus *infection on total hemocyte count (THC) in* Crassostrea virginica

a: Hemocyte numbers in lightly and heavily infected groups, as defined in Table I.

Total hemocyte count × 10^6/ml, mean ± SEM		
Group 1 Lightly infected (n = 18)	Group 2 Heavily infected (n = 18)	*P* value (ln [1 + X] transformed data, F-test, two factor ANOVA)
2.78 ± 0.66	4.15 ± 0.65	0.267

b: Hemocyte numbers in individual oysters with known intensities of infection.

	Levels of infection			*P* value
	Light (n = 20)	Moderate (n = 6)	Heavy (n = 10)	(calculated as above)
THC × 10^6 (mean ± SEM)	2.52 ± 0.47	2.95 ± 0.54	5.68 ± 1.15	0.002

Discussion

The method of transferring groups of oysters into Mobjack Bay at different times successfully produced populations with significantly different average levels of *Perkinsus* infection. However, at the times of sampling, no oysters were obtained that were entirely free of the sporozoan parasite. In an attempt to understand the status of the oysters' internal defense mechanisms during the course of the infection, the chemiluminescence (CL) response of hemocytes withdrawn from these oysters was determined. We knew that reactive oxygen intermediates (ROIs) produced by hemocytes were probably important to antimicrobial defense and that luminol-augmented CL is a sensitive method of ROI quantitation. Therefore, we predicted that decreased CL might be associated with *Perkinsus* infection, either as a result of the disease, or as a component of decreased resistance to the disease. Indeed, there is evidence that such is the case for certain other infections in bivalves. For example, the parasite *Bonamia*

ostreae failed to stimulate CL production after ingestion by *Ostrea edulis* hemocytes (Hervio *et al.*, 1989; Bachère *et al.*, 1991b) and similar inhibition of CL followed phagocytosis of Rickettsiales-like organisms by the cells of *Pecten maximus* (LeGall *et al.*, 1991). But the data reported here show that established *Perkinsus* infections apparently have the opposite effect: the hemocytes produce large amounts of ROIs, both at rest and after phagocytic stimulation.

The experimental groups varied with regard to residence time in Mobjack Bay (length of exposure to elevated salinity and to any environmental contaminants that might be present), as well as with regard to average level of infection. Although the water chemistry at the Mobjack Bay site was not analyzed, the area is considered to be relatively clean. Furthermore, exposure of bivalves to environmental pollutants can result in hemocyte CL suppression (Larson *et al.*, 1989; Fisher *et al.*, 1990; Anderson *et al.*, 1992a, b), but rarely causes enhancement. Preliminary studies in this laboratory have failed to produce ROI modulation in hemocytes after salinity changes greater than that (8–20 ppt) experienced by the oysters in this study. Furthermore, since this salinity shock occurred a minimum of seven weeks before the oysters were collected; the animals probably had ample time to recover from this physiological stress. Therefore, the differences in CL responses observed between the groups are probably due to differences in *Perkinsus* infection intensities.

The relationship between infection and CL activity was further clarified when considered for individually diagnosed animals without regard to experimental group designations. Statistical analysis of the data showed that both resting and induced CL parameters in oysters with heavy infections were elevated compared to oysters with light or moderate infections. Clearly, as the disease progressed, the circulating hemocytes produced greater amounts of ROIs and developed an increased capacity for ROI release upon phagocytic stimulation. In short, these cells appear to be activated, perhaps as a result of endocytosis of the *Perkinsus* organism itself; the sporozoan may be resistant to intracellular destruction and appears to be disseminated within the host via transport in hemocytes.

Although the mechanism of increased CL responsiveness of hemocytes from *Perkinsus*-infected oysters is not known, the phenomenon seems to be established. Preliminary results reported here also indicate that the total hemocyte count per ml hemolymph is higher in oysters with heavy infections. These two factors could work together to generate oxidant loads that could produce various forms of inflammatory cell damage in oysters during the later stages of infection, and play a role in the pathogenesis of the disease.

Acknowledgments

Expert technical assistance was provided by Laurie M. Mora, Lisa L. Brubacher, and Juanita Walker. This study was funded in part by NOAA Grant NA16FL0400–01.

Literature Cited

Adema, C. M., E. C. van Deutekom-Mulder, W. P. W. van der Knaap, E. A. Meuleman, and T. Sminia. 1991a. Generation of oxygen radicals in hemocytes of the snail *Lymnaea stagnalis* in relation to the rate of phagocytosis. *Dev. Comp. Immunol.* **15:** 17–26.

Adema, C. M., W. P. W. van der Knaap, and T. Sminia. 1991b. Molluscan hemocyte-mediated cytotoxicity: the role of reactive oxygen intermediates. *Rev. Aquatic Sci.* **4:** 201–223.

Anderson, R. S., L. M. Mora, and S. A. Thomson. 1992a. Exposure of oyster macrophages to particulate brass suppresses luminol-augmented chemiluminescence. *Toxicologist* **12:** 391.

Anderson, R. S., L. M. Oliver, and D. Jacobs. 1992b. Immunotoxicity of cadmium for the eastern oyster (*Crassostrea virginica* [Gmelin, 1791]): effects on hemocyte chemiluminescence. *J. Shellfish Res.* **11:** 29–33.

Babiur, B. M. 1984. Oxidants from phagocytes: agents of defense and destruction. *Blood* **64:** 959–966.

Babior, B. M., J. T. Curnutte, and N. Okamura. 1988. The respiratory burst oxidase of the human neutrophil. Pp. 43–48 in *Oxygen Radicals and Tissue Injury*, B. Halliwell, ed. Fed. Amer. Soc. Exp. Biol. (for the Upjohn Company), Bethesda, MD.

Bachère, E., D. Hervio, and E. Mialhe. 1991a. Luminol-dependent chemiluminescence by hemocytes of two marine bivalves, *Ostrea edulis* and *Crassostrea gigas*. *Dis. Aquat. Org.* **11:** 173–180.

Bachère, E., V. Boulo, P. Godin, L. Goggin, D. Hervio, G. LeGall, A. Morvan, and E. Mialhe. 1991b. *In vitro* chemiluminescence studies of marine bivalve defence mechanisms and responses against specific pathogens. *Dev. Comp. Immunol.* **15:** S102.

Badwey, J. A., and M. L. Karnovsky. 1980. Active oxygen species and the functions of phagocytic leukocytes. *Ann. Rev. Biochem.* **49:** 695–726.

Cochrane, C. G., I. U. Schraufstätter, P. Hyslop, and J. Jackson. 1988. Cellular and biochemical events in oxygen injury. Pp. 125–136 in *Oxy-Radicals in Molecular Biology and Pathology*, P. A. Cerutti, J. Fridovich and J. M. McCord, eds. Alan R. Liss, Inc., NY.

Cerutti, P. A., I. Fridovich, and J. M. McCurd, eds. 1988. *Oxy-Radicals in Molecular Biology and Pathology.* Alan R. Liss, Inc., N. Y.

DeChatelet, L. R., G. D. Long, P. S. Shirley, D. A. Bass, M. J. Thomas, F. W. Henderson, and M. S. Cohen. 1982. Mechanisms of the luminol-dependent chemiluminescence of human neutrophils. *J. Immunol.* **129:** 1589–1593.

DiGiulio, R. T., P. C. Washburn, R. J. Wenning, G. W. Winston, and C. S. Jewell. 1989. Biochemical responses in aquatic animals: a review of determinants of oxidative stress. *Environ. Toxicol. Chem.* **8:** 1103–1123.

Dikkeboom, R., J. M. G. H. Tijnagel, E. C. Mulder, and W. P. W. van der Knaap. 1987. Haemocytes of the pond snail *Lymnaea stagnalis* generate reactive forms of oxygen. *J. Invertebr. Pathol.* **49:** 321–331.

Dikkeboom, R., W. P. W. van der Knaap, W. van den Bovenkamp, J. M. G. H. Tijnagel, and C. J. Bayne. 1988. The production of toxic oxygen metabolites by haemocytes of different snail species. *Dev. Comp. Immunol.* **12:** 509–520.

Fantone, J. C. and P. A. Ward. 1982. Role of oxygen derived free radicals and metabolites in leukocyte-dependent inflammatory reactions. *Am. J. Pathol.* **107:** 297–418.

Fisher, W. S., A. Wishkovsky, and F.-L. E. Chu. 1990. Effects of tributyltin on defense-related activities of oyster hemocytes. *Arch. Environ. Contam. Toxicol.* **19:** 354–360.

Halliwell, B., ed. 1988. *Oxygen Radicals and Tissue Injury* Federation of American Societies for Experimental Biology, Bethesda, MD.

Hervio, D., E. Bachère, E. Mialhe, and H. Grizel. 1989. Chemiluminescent responses of *Ostrea edulis* and *Crassostrea gigas* to *Bonamia ostrea* (Ascetospora). *Dev. Comp. Immunol.* **13:** 449.

Kako, K. J. 1987. Free radical effects on membrane protein in myocardial ischemia/reperfusion injury. *J. Mol. Cell. Cardiol.* **19:** 209–212.

Klebanoff, S. J. 1982. Oxygen-dependent cytotoxic mechanisms of phagocytes. Pp. 111–162 in *Advances in Host Defense Mechanisms, Vol 1*, J. I. Gallin and A. S. Fauci, eds. Raven Press, NY.

Larson, K. G., B. S. Roberson, and F. M. Hetrick. 1989. Effect of environmental pollutants on the chemiluminescence of hemocytes from the American oyster *Crassostrea virginica*. *Dis. Aquat. Org.* **6:** 131–136.

LeGall, G., E. Bachère, E. Mialhe, and H. Grizel. 1989. Zymosan and specific rickettsia activation of oxygen free-radicals in *Pecten maximus* hemocytes. *Dev. Comp. Immunol.* **13:** 448.

LeGall, G., E. Bachère, and E. Miale. 1991. Chemiluminescence analysis of the activity of *Pecten maximus* hemocytes stimulated with zymosan and host-specific Rickettsiales-like organisms. *Dis. Aquat. Org.* **11:** 181–186.

Livingstone, D. R., M. A. Kirchin, and A. Wiseman. 1989. Cytochrome P-450 and oxidative metabolism in molluscs. *Xenobiotica* **19:** 1041–1062.

Livingstone, D. R., P. Garcia Martinez, X. Michel, J. F. Narbonne, S. O'Hara, D. Ribera, and G. W. Winston. 1990. Oxyradical production as a pollution-mediated mechanism of toxicity in the common mussel, *Mytilus edulis* L., and other molluscs. *Funct. Ecol.* **4:** 415–424.

Nakamura, M., K. Mori, S. Inooka, and T. Nomara. 1985. *In vitro* production of hydrogen peroxide by the amoebocytes of the scallop, *Patinopecten yessoensis* (Jay). *Dev. Comp. Immunol.* **9:** 407–417.

Paynter, K. T., and E. M. Burreson. 1991. Effects of *Perkinsus marinus* infection in the Eastern oyster, *Crassostrea virginica*. II. Disease development and impact on growth rate at different salinities. *J. Shellfish Res.* **10:** 425–431.

Pipe, R. K. 1992. Generation of reactive oxygen metabolites by the haemocytes of the mussel *Mytilus edulis*. *Dev. Comp. Immunol.* **16:** 111–122.

Ray, S. M. 1952. A culture technique for the diagnosis of infections with *Dermocystidium marinum*, Mackin, Owen and Collier, in oysters. *Science* **116:** 360–361.

Ray, S. M. 1966. A review of the culture method for detecting *Dermocystidium marinum*, with suggested modifications and precautions. *Proc. Natl. Shellfish. Assoc.* **54:** 55–69.

Schlenk, D., P. Garcia Martinez, and D. R. Livingston. 1991. Studies on myeloperoxidase activity in the common mussel, *Mytilus edulis L. Comp. Biochem. Physiol.* **99C:** 63–68.

Winston, G. W. 1991. Oxidants and antioxidants in aquatic animals. *Comp. Biochem. Physiol.* **100C:** 173–176.

Winston, G. W., D. R. Livingstone, and F. Lips. 1990. Oxygen reduction metabolism by the digestive gland of the common marine mussel, *Mytilus edulis* L. *J. Exp. Zool.* **225:** 296–308.

Reference: *Biol. Bull.* 183: 482–489. (December, 1992)

The Function of the Madreporite in Body Fluid Volume Maintenance by an Intertidal Starfish, *Pisaster ochraceus*

JOHN C. FERGUSON

Department of Biology, Eckerd College, St. Petersburg, Florida 33733, and Friday Harbor Laboratories, University of Washington, Friday Harbor, Washington 98250

Abstract. The madreporite has been viewed as superfluous and unnecessary because starfish can keep their tube feet inflated by osmotic mechanisms alone. Recent evidence has suggested, however, that the madreporite may be significant in the replenishment of general body fluid. This hypothesis has been tested. The madreporite openings of an intertidal starfish, *Pisaster ochraceus*, were obstructed with cement, and the animals were used in controlled experiments to compare weight (volume) changes under stable conditions, in response to air drying and recovery, and during adaptations to hyper- and hypoosmotic environments. Over a period of days, normal animals showed positive and negative volume fluctuations of up to about 20% (in part related to posture). Animals with obstructed madreporites generally did not gain weight and were significantly less able to maintain body volume or recover from fluid losses resulting from the stresses applied. The madreporite seemed to contribute little to the initial osmotic responses, but it did participate in subsequent volume readjustments in a hyperosmotic medium that had induced fluid losses. Obstruction of the madreporite did not impede tube foot activity, but may have caused some diversion of general body fluid to the ambulacral system. Rates of seawater uptake through the madreporite of 2.2–2.6 $\mu l\ g^{-1}\ h^{-1}$ were calculated from observed maximum mean differences in weight changes.

Introduction

A sieve-like structure known as the madreporite is conspicuously located on the aboral disk of most starfish. The madreporite contains pores that mostly open into a reinforced ciliated duct, the stone canal, which in turn leads to the oral side of the body and a system of canals extending to the tube feet (Ferguson and Walker, 1991). Although many scientists have assumed that the function of the madreporite is to admit seawater to the tube feet, thus supporting their operation as hydraulic devices, Hyman (1955) pointed out that there was little reliable evidence for that assumption, and that any fluid loss and replacement from this "water vascular system" must be slight. Further, Robertson (1949) showed that the fluid found within the tube feet of *Marthasterias glacialis* was different from seawater, being especially elevated in potassium ion concentration. These observations led Binyon (1961, 1962, 1964, 1966, 1976a, b, 1979, 1980, 1984) to examine the dependence of tube feet on madreporitic water inflow much more closely. He found that in *Asterias rubens*, these appendages continued to function quite well, even if all the water passages were plugged, the madreporite removed, or the arms separated entirely from the disk. After measuring pressure levels and permeability factors, he concluded that tube foot activity must be sustained by the osmotic influx of water directly through their walls. Additional evidence of the importance of osmotic factors came from Prusch and Whoriskey (1976) and Prusch (1977), who not only directly measured the osmotic elevations of tube foot fluid in *Asterias forbesi*, but also demonstrated in these tube feet an active transport system for potassium ions that is capable of sustaining the osmotic differences. More recently, Ferguson (1990a) has provided data on 14 species of starfish, all showing osmotic elevation of ambulacral fluids.

These studies have convinced many modern workers that the madreporite cannot be important to the normal operation of tube feet. Disconcertingly, there are few data

Received 1 August 1990; accepted 26 August 1992.

to show that the structure does anything else either. A number of functions have been suggested, *e.g.*, that it is some kind of sense organ, a secretory or excretory device, an emergency relief valve, or a supplementary pump that functions only in periods of stress, but evidence for these kinds of functions is trivial (Binyon, 1964; Nichols, 1966; Prusch, 1977).

Noting this confusion, Ferguson (1987) initiated a series of experiments on *Echinaster graminicola* to explore the function of the madreporite. Although he confirmed many of the findings of earlier workers, he observed that the body weight of this species diminished when its madreporite was obstructed. Further, a fluorescently labeled high-molecular weight dextran tracer put into seawater could be found in the body fluids of the animals after a period—a pattern that was largely inhibited when the madreporite was obstructed. Additional study with this tracer method (Ferguson, 1989) established quantitatively that modest amounts of seawater do reach the ambulacral fluid (presumably through the madreporite), but that an even greater volume (nearly 60% of total influx) somehow moves directly into the perivisceral coelomic cavity. Fluorescent microbeads have been used to verify madreporitic inflow in *Leptasterias hexactis,* and point to passage through the Tiedemann's bodies (enigmatic structures on the oral water ring canal) as the probable major route of seawater movement from the madreporite and stone canal to the perivisceral coelomic cavity (Ferguson, 1990b).

From these studies, then, is emerging a new view of the role of the madreporite. It does serve to admit seawater into the starfish body, but this admission is less significant with respect to the inflation of the tube feet, in which osmotic factors predominate, than to fluid replenishment throughout the whole organism and the size control of other fluid compartments. If this is the case, obstruction of the madreporite should have a much more profound effect on volume control (and weight) than on tube foot activity. Such effects might be especially evident in an intertidal species, such as *Pisaster ochraceus,* which appears to experience frequent changes in its fluid volume as a result of tidal stranding, complex postural adjustments, and estuarine salinity variations. These possibilities have been examined in the present study.

Materials and Methods

Work was carried out on specimens of *Pisaster ochraceus,* mostly weighing between 200 and 800 g, collected from rocks at low tide within a few kilometers of the Friday Harbor Laboratories in the San Juan Islands of Washington. The animals were kept in seawater tables for several days before use to ensure their health and stability under laboratory conditions. The seawater temperature remained nearly constant in the short term, between 7 and 9°C, and its osmotic concentration was measured at about 885 mosmol kg^{-1}. During the experiments, the starfish were confined to vessels lined with paper toweling so that they could be removed easily and without damage to their tube feet. The animals were not fed, but they normally eat little during the winter months, when the work was done.

Weight changes of animals were recorded as an indirect measurement of fluid volume variation. The specimens were first blotted dry in a consistent manner with paper toweling for several minutes and then weighed on an electronic balance. As a species adapted to an intertidal existence, *P. ochraceus* took this handling very well, and the wet weights obtained from individual animals were repeatable within 0.20%.

Osmotic measurements were made on some specimens. Small samples of perivisceral coelomic fluid (about 0.5 ml) were withdrawn from these specimens with a syringe and allowed to settle in a capped vial for several minutes. At least three replicates of the samples were analyzed in a Wescor 5500 vapor pressure osmometer, along with ambient seawater for comparison. Studies showed that these measurements were accurate to within 2 mosmol kg^{-1} osmotic difference with 95% confidence.

Because preliminary work had suggested that the effects of madreporite obstruction might take some time to appear, a number of different procedures were explored for sealing this structure without otherwise harming the animals. The approach finally used was quite effective. Commercial hydraulic cement (a mixture of Portland cement and lime) was further triturated to a fine powder with a mortar and pestle. The surface of the madreporite was scraped away with a dissecting needle and the debris blotted up. A small quantity of cement, freshly mixed with a minimum amount of distilled water, was then placed on the wound and worked around with the needle. After the cement had set for several minutes, the animal was returned to seawater, where the plug became fixed firmly in position and quite hard over the next several hours. *Pisaster* tolerated this operation very well, and specimens usually could be kept for up to ten days with the opening still tightly sealed.

Most experiments involved measuring daily changes in the wet weight of six madreporite-obstructed specimens (tests), as well as those of a similar group of unaltered animals (controls). The null hypothesis is that obstructing the madreporite should have no effect on the frequencies of measured daily weight gains and losses; the alternative is that the treatment should prevent weight gains from madreporite fluid uptake and lead to a decrease in weight through gradual fluid losses.

Since the wide range of initial body weights of the specimens available for use could potentially bias many statistical approaches, conclusions were drawn exclusively

from the gain or loss of weight from one measurement to the next. The data were assessed with SPSS-X using a non-parametric two-sample median test. This test evaluated a 2 × 2 contingency matrix of control group and test group daily weight changes above and below a prescribed median of zero. With more than 30 cases, this computes a chi-square statistic and a corresponding probability that the two samples are drawn from populations with the same median. An assumption underlying this approach is that, on any day, a normal undisturbed specimen has an equal chance of showing either a positive or negative weight fluctuation, not materially affected by previous responses. Because a runs test failed to show that observed daily variations of normal animals were statistically predictable, and because these variations were always small relative to the wide ranges of total fluctuations tolerated, this assumption seemed justified.

Four main sets of experiments were undertaken. The first examined the variation of animals kept under stable laboratory conditions for up to 10 days. The second examined responses of animals under similar stable conditions following 12 h of resting on wet paper toweling in air, simulating a prolonged tidal stranding that might leave them dehydrated. The third and fourth sets of experiments examined the fluid volume responses of animals which had been subjected to modest (about 6%) salinity changes that would not be excessively stressful, but comparable to those that might be commonly encountered in their estuarine environment. In these latter experiments, specimens were placed in either hyperosmotic or hypoosmotic media prepared by adding "Instant Ocean" sea salts or distilled water to aquaria of seawater. To monitor changes in the osmotic concentration of the coelomic fluids, we used several additional specimens.

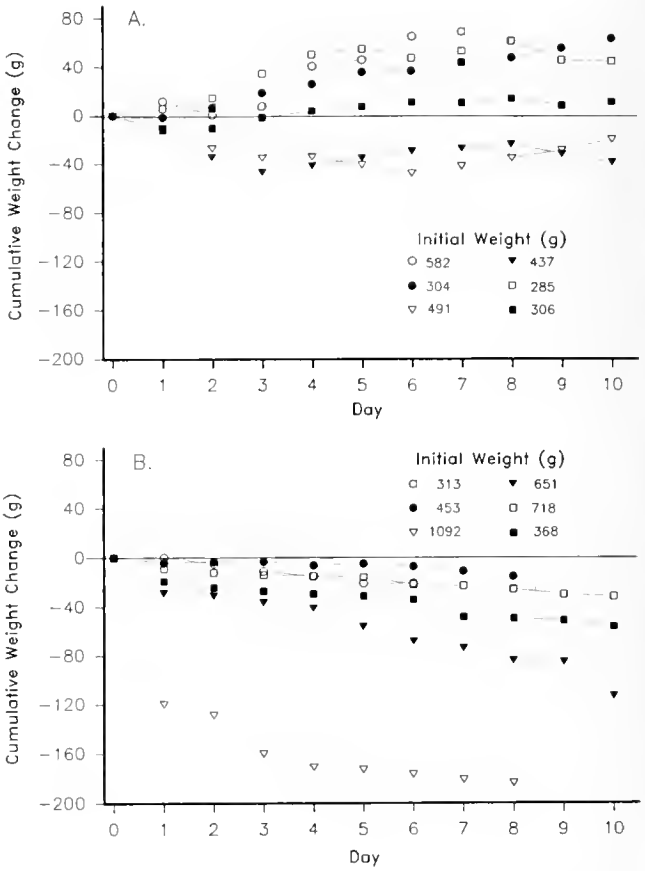

Figure 1. Cumulative change in weight (fluid volume) of specimens of *Pisaster ochraceus* while maintained under stable laboratory conditions for 7 to 10 days. (A) Intact animals (n = 6) have 39 daily periods of increase, 18 of loss. (B) Madreporite-obstructed animals (n = 6) have 2 minor periods of increase, 47 of loss, and 3 no change.

Results

Stable conditions

Groups of control and test animals were monitored daily for weight (fluid volume) changes exhibited in a stable laboratory environment, where neither temperature nor salinity varied beyond detectable limits. The patterns of their cumulative responses may be seen in Figure 1. The weights of individual animals were found to fluctuate spontaneously, over a range of about 20%. These variations appeared to be correlated, at least in part, with postural changes. *Pisaster* is a very "stiff" species, and individuals were observed to hold the same contorted position for many days. When they relaxed and spread out, as they were prone to do after being handled for weighing, their volumes often gradually increased. Within the experimental period of up to 7 to 10 days, every control specimen demonstrated numerous daily intervals of weight gain, as well as instances of daily weight loss. The test animals, on the other hand, showed only 2 minor daily periods of weight increase out of the 52 measurements taken, both within the limits of experimental precision; they had 47 instances of weight loss and three instances of no change. The median test confirmed that the daily responses of the two groups were significantly different ($P < 0.001$). By the final weighing, all 6 test animals had lost weight from the beginning, while 4 of the control animals had gained and 2 had lost weight. In all cases, obstruction of the madreporite had no perceptible effect on the functioning of the tube feet.

Air dehydration

During a 12 h period of exposure to air while resting on moist toweling, both control and test animals lost around 6 to 8% of their body weights (Fig. 2). A good deal of this change appeared to be due to evaporative water loss rather than draining of fluid, as shown by an analysis of the osmotic concentration of the coelomic fluids of

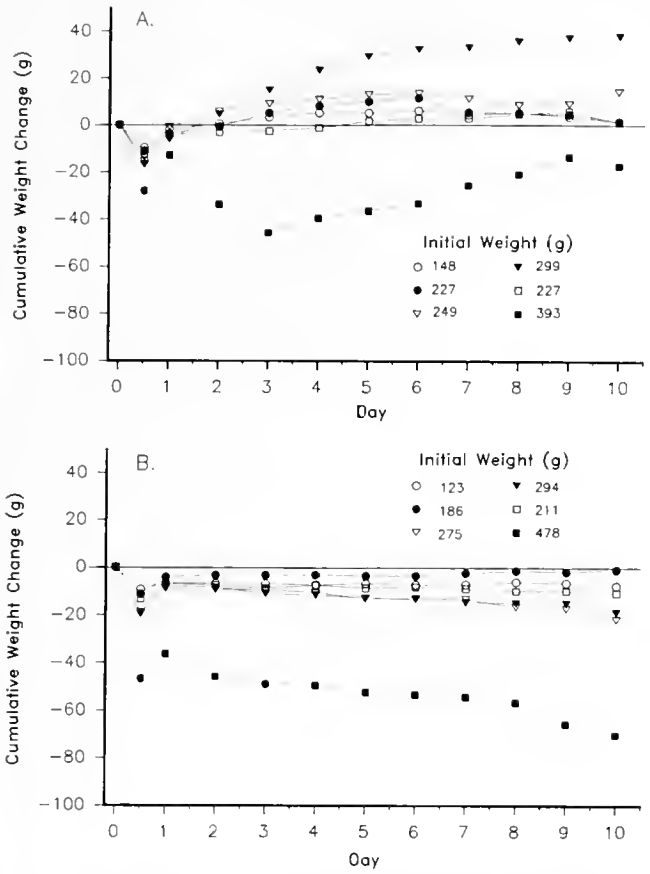

Figure 2. Cumulative change in weight of specimens exposed to the dehydration of a simulated tidal stranding of 12 h and then returned to stable seawater. All regained weight with their re-establishment of osmotic equilibrium after return to seawater. (A) Intact animals (n = 6). (B) Madreporite-obstructed animals (n = 6). After the first day, intact animals (A) show 41 daily periods of gain and 13 loss; test animals (B) 10 minor gains, 39 loss, and 5 no change. The minor gains in the latter group might be due to seal leakage, fluid taken into the stomach, or residual osmotic factors.

four similarly treated normal animals. After 12 h of dehydration, their coelomic fluid osmolality (mean ± S.E.) was elevated 52.1 ± 3.0 mosmol kg^{-1} (5.9%) above ambient seawater, while their weight (mean ± S.E.) had dropped 11.9 ± 2.7 g (6.8%). After 12 h of reimmersion in seawater, their coelomic fluid osmotic level had equilibrated to within 1.1 ± 0.1 mosmol kg^{-1} (0.2%) of ambient seawater, but their weight was still 9.0 ± 2.7 g (5.1%) below the initial mean. Thus, they had gained some water in recovery, but had mainly lost osmolytes. All the control animals quickly assumed normal behavior once they were back in seawater. They then showed 41 daily intervals of weight gain and 13 of loss. The test group (Fig. 2b), like the control animals, also rapidly recovered some weight in seawater, in correspondence with the period of osmotic readjustment. Thereafter, while the control animals gained and fluctuated in weight daily, the test group mostly lost weight: 39 instances to 10 minor gains and 5 instances of no change. The episodes of minor weight gain were observed in 2 of the 6 test animals and could have been caused by leakage around the madreporite seals, fluid taken into the stomach, or residual osmotic factors. Again, a median test confirmed a highly significant difference ($P < 0.001$) between the daily weight change patterns of the two groups. At the end of the experiment, 5 of the 6 control animals showed an overall weight gain, while all 6 tests specimens had lost weight.

Hyperosmotic conditions

Both control (n = 5) and test (n = 6) animals rapidly lost weight for the first 3 to 6 h after being subjected to an osmotic increase in their media from 878 to 935 mosmol kg^{-1}, a change of 6.5% (Fig. 3). By 6 h, both groups appeared to have reached substantial osmotic equilibrium, as monitored by coelomic fluid samples taken from sim-

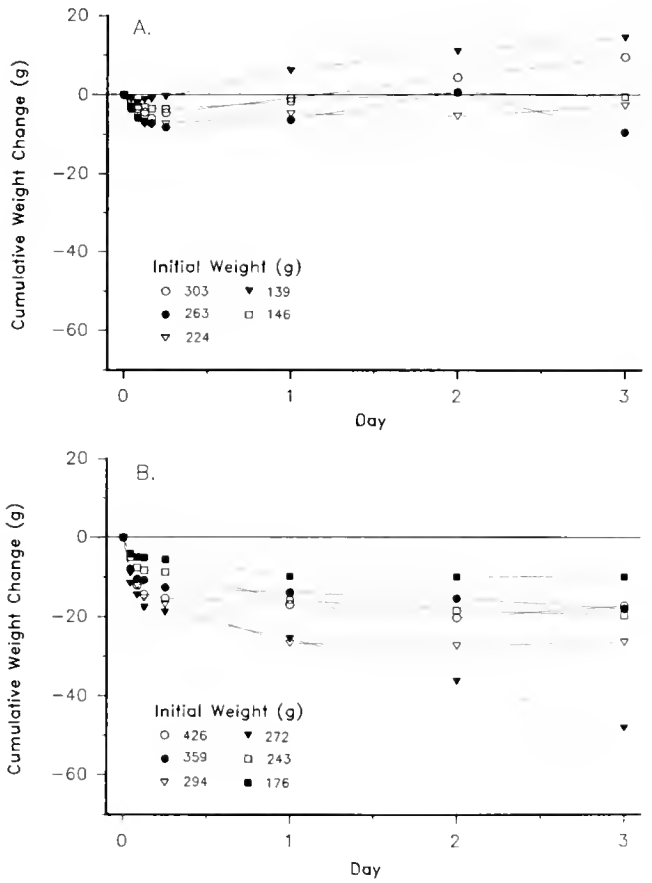

Figure 3. Cumulative weight responses of animals to an osmotic increase in their medium from 878 to 935 mosmol kg^{-1} (6.5%). (A) Intact specimens (n = 5). (B) Madreporite-obstructed specimens (n = 6). Both groups lose fluid over the first few hours while osmotically adjusting. Following the 6 h mark, intact animals (A) show 12 intervals of gain and 3 loss; test animals (B) show 2 gain, 14 loss, and 2 no change.

ilarly treated animals (Fig. 4). Following this period of osmotic adjustment, all of the control animals regained weight for the next 18 h (Fig. 3a). Over the next two days they showed seven instances of weight gain and three of loss. In contrast, all the test animals (Fig. 3b) continued to lose weight for the 18 h following the initial period of adjustment. Thereafter, they had 8 instances of loss, 2 of gain and 2 of no change. The differences in these patterns (after the 6 h adjustment period) were highly significant ($P < 0.001$) by median test analysis.

Hypoosmotic conditions

When exposed to a 6.2% osmotic decrease in the medium, from 885 to 830 mosmol kg^{-1}, 4 of the 6 animals in both the control and test groups temporarily gained weight in the first 4 h, apparently as a manifestation of the osmotic fluxes taking place (Fig. 5). As with the previous experiment, measurements of the coelomic fluids

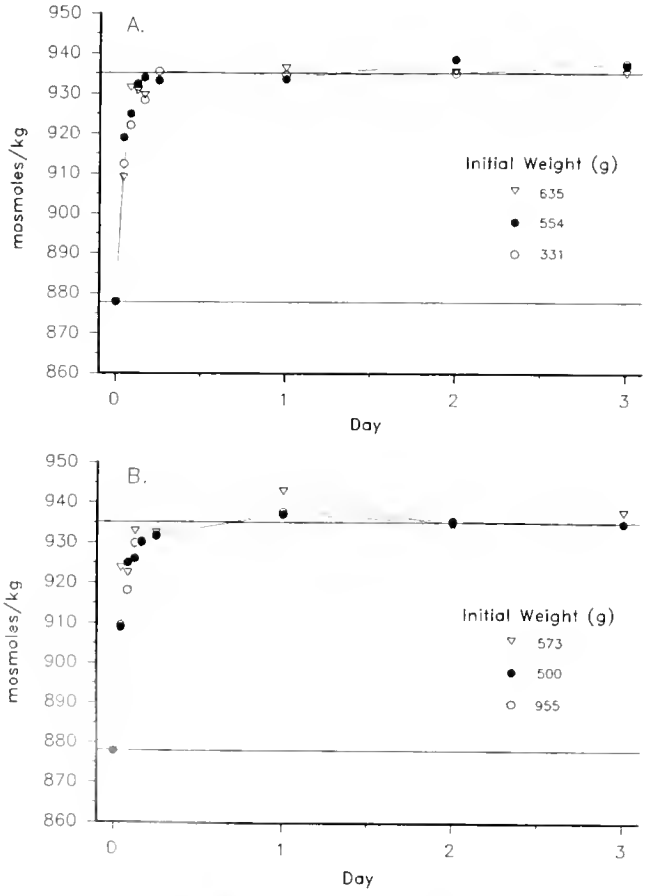

Figure 4. Osmotic changes in the perivisceral coelomic fluid of animals exposed to an increase in their medium from 878 to 935 mosmol kg^{-1}. (A) Intact animals (n = 3). (B) Madreporite-obstructed animals (n = 3). There is little obvious difference in the responses of the two groups, both of which have substantially completed osmotic adjustments by 6 h.

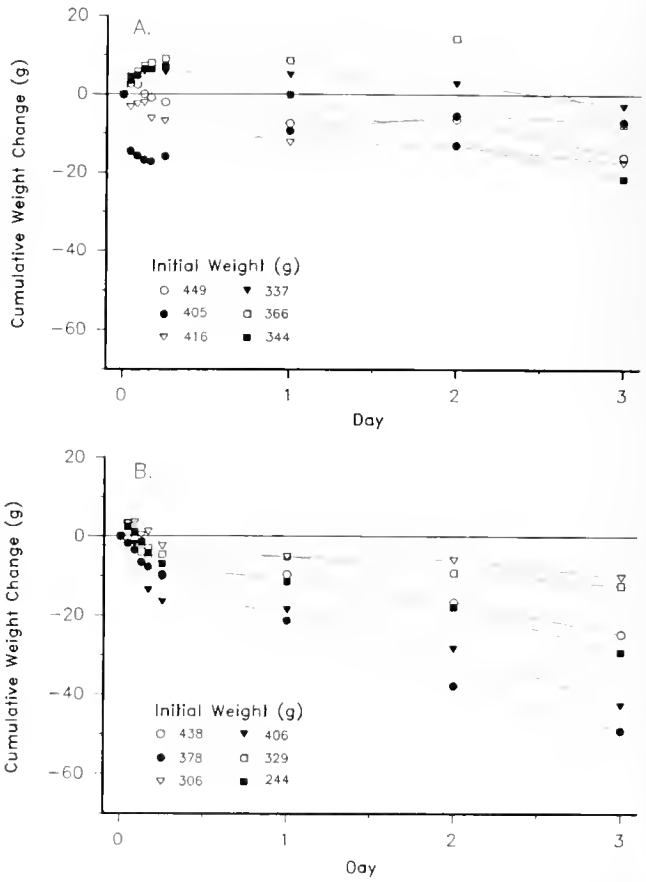

Figure 5. Cumulative weight responses of animals to an osmotic decrease in their medium from 885 to 830 mosmol kg^{-1} (6.2%). (A) Intact specimens (n = 6). (B) Madreporite-obstructed specimens (n = 6). Individuals in both groups show some initial swelling. Following the 6 h mark, intact animals (A) have 4 intervals of gain and 10 loss; test animals (B) show loss in all instances except 1 no change.

of comparable animals showed that osmotic adjustments of both groups were nearly complete within 4 to 6 h (Fig. 6). For the 18 h after this period, 5 of the 6 control animals lost weight (Fig. 5a). The next day there were three losses and three gains, and the following day, all losses. The test group, on the other hand, showed only losses, except for one instance of no change (Fig. 5b). The transfer to a hypoosmotic medium may have been more stressful to the animals than a transfer in the other direction. In any case, the control animals recorded too few episodes of weight gain, and thus do not show that they responded in a significantly different way from the test animals (median test: $P = 0.112$).

Discussion

All four sets of experiments demonstrated markedly reduced capacity of madreporite-obstructed specimens of *Pisaster ochraceus* to retain their fluid volume, even

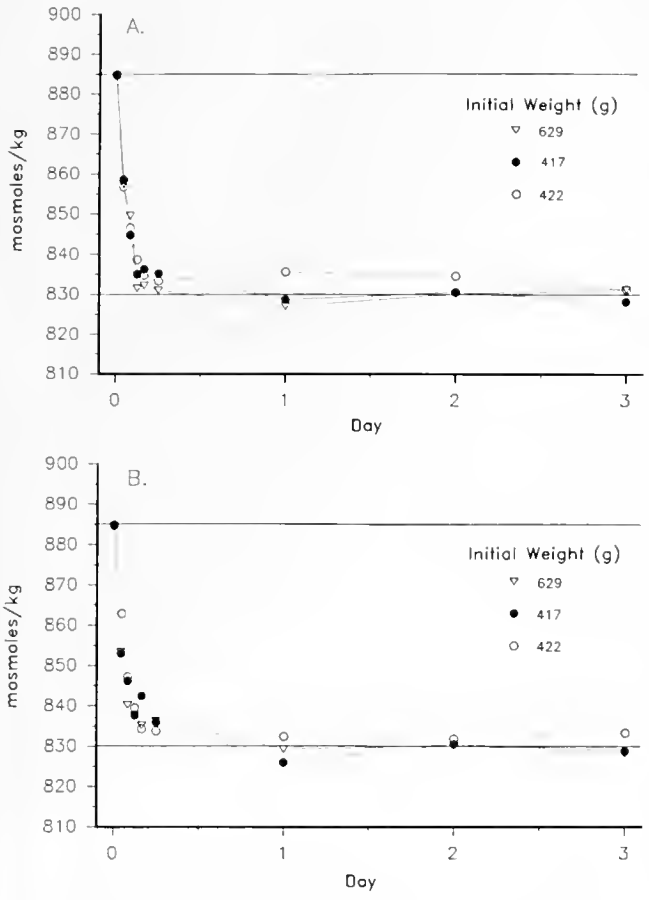

Figure 6. Osmotic changes in the perivisceral coelomic fluid of animals exposed to an osmotic decrease in their medium from 885 to 830 mosmol kg^{-1}. (A) Intact specimens (n = 3). (B) Madreporite-obstructed specimens (n = 3). There is little obvious difference in the responses of the two groups, both of which have substantially completed osmotic adjustments by 6 h.

though the activity of their tube feet appeared undiminished. In fact, every single test specimen weighed less at the end of the study than it did at the beginning. On the other hand, control groups were able to exhibit normal weight fluctuations throughout, except following hypoosmotic stress. Every control specimen showed a period of weight gain, and at the end of the study, 11 weighed more than they did at the start and 12 less (including the hypoosmotic group). Not surprisingly, statistical comparisons by the median test confirmed a highly significant difference between the control and test groups (except following hypoosmotic stress). Thus, these observations strongly support the alternative initial hypothesis: that obstruction of the madreporite should substantially prevent animals from gaining weight and from retaining their body fluid. Although some differences may exist among other asteroid species, and certainly between echinoderm classes, with their different anatomical arrangements, slow but steady inflow of seawater through the madreporite is undoubtedly a basic adaptation for fluid volume maintenance in *P. ochraceus* and probably other starfish. This seawater influx appears to provide a general replenishment of the body fluids, probably the flushing of excretory products, and homeostatic response to changing needs, especially those brought on by alteration in posture, stranding, or fluid losses occurring with osmotic adjustment. The madreporite probably also contributes some water to the tube feet (Ferguson, 1987, 1989, 1990b), although those structures can be kept inflated by the osmotic mechanism previously described and perhaps by fluid diversion through the axial sinus pore (Ferguson, 1991).

The responses shown here by normal animals to salinity changes (as well as osmotic elevation resulting from dehydration) were as might be expected from previous work, reviewed by Binyon (1966, 1972), Diehl (1986), and Stickle and Diehl (1986). After transfer to either hyper- or hypoosmotic medium, rapid exchange of ions and water takes place across the integument, leading to near osmotic equilibrium within a few hours. Binyon (1961, 1964, 1976a,b, 1980, 1984), in his work with *Asterias rubens*, found that the integument was quite permeable to both ions and water, although not necessarily equally. Ellington and Lawrence (1974) and Diehl and Lawrence (1984) similarly demonstrated rapid, but uneven, flux of ions and water in *Luidia clathrata* during hypoosmotic adjustment, leading to some volume increase, which took several days to abate. Shumway (1977) apparently saw such a response in *A. rubens, Solaster papposus, Henricia sanguinolenta,* and *Astropecten irregularis*, as did Ferguson (1987) in *E. graminicola*. In the major previous work on *P. ochraceus*, however, Stickle and Ahokas (1974) indicate that osmotic adjustment of body fluid during a simulated tidal cycle over a 20‰ salinity range lagged behind ambient seawater and never reached completion. They further stated that there was "little change" in percentage of body water during the cycle. Their graphical data, however, do seem to show some such change, so perhaps their different judgment was only a matter of perspective and the different intentions of the experiments. In any case, the animals in the present study, when transferred directly to the equivalent of about a 1.9‰ salinity change, rapidly reached near osmotic equilibrium with their altered environments, but not such rapid volume stability. The presence or absence of a functional madreporite made relatively little difference in osmotic adjustment, but the madreporite played a significant role in subsequent readjustments of body volume after transfer to a hyperosmotic medium that produced a rapid fluid loss.

By comparing the rates of weight loss by madreporite-obstructed animals to the rates of weight gain by normal specimens, the present data can be used to make specific

estimates of the rate of flow of seawater into the madreporite of *P. ochraceus*. The maximum difference between the control and test groups might be expected to occur in circumstances where the controls are in apparent need of augmenting their body fluids, while the test animals are unable to do so and are suffering physiological losses. Such a situation existed in the hyperosmotically stressed animals between the time that they had largely completed their osmotic adjustment, at 6 h, and before the control specimens had replenished much of their body fluid, at 24 h. Figure 3 shows that within this period, there is indeed a conspicuous difference between the two groups. The six test animals had a weight loss (mean ± S.E.) of 1.16 ± 0.76 $\mu g\ g^{-1}\ h^{-1}$, whereas the five control specimens had a corresponding weight gain of 1.05 ± 0.90 $\mu g\ g^{-1}\ h^{-1}$. The sum of these, 2.21 $\mu l\ g^{-1}\ h^{-1}$, is an estimate of fluid uptake. That value is in agreement with a madreporite flow rate of 2.27 $\mu l\ g^{-1}\ h^{-1}$ measured in *E. graminicola* by fluorescent tracer methodology (Ferguson, 1989). By similar arithmetic, the most rapid rate of weight increase noted in any of the normal control animals in the present study (Fig. 1) corresponds to a net gain of 2.60 $\mu l\ g^{-1}\ h^{-1}$, a value that seems to be well within the reasonable capability of their system.

How seawater taken up reaches the perivisceral coelomic cavity may in part be revealed by other recent work, including some in which fluorescent microbeads were used as a tracer (Ferguson, 1990b). The model developing is that seawater is drawn in through the madreporite by strong currents generated in the ciliated stone canal. This seawater mixes with recirculated fluid from the axial sinus, which also opens into the upper end of the stone canal. The result is a high pressure composite fluid that is pumped into the ring canal. From there, the composite fluid appears to be filtered through the Tiedemann's bodies and tube feet ampullae, counteracting fluid loss from the perivisceral coelom to the higher osmotic concentration in the tube feet.

Other factors also may be involved in body fluid maintenance. A persistent slight osmotic elevation exists in the perivisceral coelomic fluid of most species, although in *P. ochraceus* it is almost negligible [0.47 ± 0.59 mosmol kg^{-1} (± S.E.)] (Ferguson, 1990a). In forms with a more flaccid integument, such as *Pycnopodia helianthoides*, osmotically elevated coelomic fluid [2.18 ± 0.53 mosmol kg^{-1} (± S.E.)] may be of more substantial importance (Ferguson, 1990a). Further studies of the volume responses of *P. helianthoides* would be particularly interesting, but unfortunately, preliminary work has shown that it does not tolerate the present experimental approach. Bulk fluid movement through the digestive systems of starfish might also influence fluid volume relationships (Ferguson, 1987).

How much regulatory control starfish actually have over their fluid volume is also open to question. The present study has demonstrated a net tendency for animals to take up seawater through their madreporites and to contribute that seawater to fluid volume maintenance under a variety of conditions. However, the body weights of the starfish fluctuated widely and could not be considered fixed at any point. So there is as yet little evidence of a sensitive central volume regulatory mechanism other than that achieved from the general balance of water uptake and loss from the several largely independent processes of bulk fluid movement, osmotic uptake and adjustment, pressure filtration, degree of exposure of permeable surfaces (especially on the tube feet), and adjustment of compartment size with posture and feeding. Nevertheless, these animals consistently maintain a low hydrostatic pressure in their body cavities. This is probably only 1 or 2 mm of water in magnitude, but it supports the respiratory papulae and allows extrusion of the cardiac stomach during feeding. This pressure seems to be maintained primarily by the contractile force of the body wall musculature and connective tissue. These animals may be using muscle tone to regulate a low fluid pressure, while allowing their volume to range rather widely. The fluid pressures in these forms are low and so difficult to measure accurately that they have not yet been successfully studied.

Literature Cited

Binyon, J. 1961. Salinity tolerance and permeability to water of the starfish *Asterias rubens* L. *J. Mar. Biol. Assoc. U. K.* **41:** 161–174.

Binyon, J. 1962. Ionic regulation and mode of adjustment to reduced salinity of the starfish *Asterias rubens* L. *J. Mar. Biol. Assoc. U. K.* **41:** 49–64.

Binyon, J. 1964. On the mode of functioning of the water vascular system of *Asterias rubens* L. *J. Mar. Biol. Assoc. U. K.* **44:** 577–588.

Binyon, J. 1966. Salinity tolerance and ionic regulation. Pp. 359–378 in *Physiology of Echinodermata*, R. A. Boolootian, ed. Wiley-Interscience, New York.

Binyon, J. 1976a. The permeability of the podial wall to water and potassium ions. *J. Mar. Biol. Assoc. U. K.* **56:** 639–647.

Binyon, J. 1976b. The effects of reduced salinity upon the starfish *Asterias rubens* L., together with a special consideration of the integument and its permeability to water. *Thalassia Jugoslav.* **12:** 15–20.

Binyon, J. 1979. Ion movements and oxygen requirements of asteroids—a theoretical consideration. *Comp. Biochem. Physiol.* **62A:** 639–640.

Binyon, J. 1980. Osmotic and hydrostatic permeability of the integument of the starfish *Asterias rubens*. *J. Mar. Biol. Assoc. U. K.* **60:** 627–630.

Binyon, J. 1984. A re-appraisal of the fluid loss resulting from the operation of the water vascular system of the starfish, *Asterias rubens*. *J. Mar. Biol. Assoc. U. K.* **64:** 726.

Diehl, W. J. 1986. Osmoregulation in echinoderms. *Comp. Biochem. Physiol.* **84A:** 199–205.

Diehl, W. J., and J. M. Lawrence. 1984. The effect of salinity on coelomic fluid osmolyte concentration and intracellular water content in *Luidia clathrata* (Say) (Echinodermata: Asteroidea). *Comp. Physiol. Biochem.* **79A:** 119–126.

Ellington, W. R., and J. M. Lawrence. 1974. Coelomic fluid volume regulation and isosmotic intracellular regulation by *Luidia clathrata* (Echinodermata: Asteroidea) in response to hypoosmotic stress. *Biol. Bull.* **146:** 20–31.

Ferguson, J. C. 1987. Madreporite and anus function in fluid volume regulation of a starfish (*Echinaster gramunicola*). Pp. 603–609 in *Echinoderm Biology: Proceedings of the Sixth International Echinoderm Conference, Victoria/23–28 August 1987*, R. D. Burke, P. Mladenov, P. Lambert, and R. L. Parsley, eds. Balkema, Rotterdam.

Ferguson, J. C. 1989. Rate of water admission through the madreporite of a starfish. *J. Exp. Biol.* **145:** 147–156.

Ferguson, J. C. 1990a. Hyperosmotic properties of the fluids of the perivisceral coelom and watervascular system of starfish kept under stable conditions. *Comp. Physiol. Biochem.* **95A:** 245–248.

Ferguson, J. C. 1990b. Sea water inflow through the madreporite and internal body regions of a starfish (*Leptasterias hexactis*) as demonstrated with fluorescent microbeads. *J. Exp. Zool.* **255:** 262–271.

Ferguson, J. C., and C. W. Walker. 1991. Cytology and function of the madreporite systems of the starfish *Henricia sanguinolenta* and *Asterias vulgaris*. *J. Morphol.* **210:** 1–11.

Hyman, L. 1955. *The Invertebrates IV. Echinodermata.* McGraw-Hill, New York.

Nichols, D. 1966. Functional morphology of the water-vascular system. Pp. 219–244 in *Physiology of Echinodermata*, R. A. Boolootian, ed. Wiley-Interscience, New York.

Prusch, R. D. 1977. Solute secretion by the tube foot epithelium in the starfish *Asterias forbesi*. *J. Exp. Biol.* **68:** 35–43.

Prusch, R. D., and F. Whoriskey. 1976. Maintenance of fluid volume in the starfish water vascular system. *Nature* **262:** 577–578.

Robertson, J. D. 1949. Ionic regulation in some marine invertebrates. *J. Exp. Biol.* **26:** 182–200.

Shumway, S. E. 1977. The effects of fluctuating salinities on four species of asteroid echinoderms. *Comp. Physiol. Biochem.* **58A:** 177–179.

Stickle, W. B., and R. Ahokas. 1974. The effects of tidal fluctuation of salinity on the perivisceral fluid composition of several echinoderms. *Comp. Physiol. Biochem.* **47A:** 469–476.

Stickle, W. B., and W. J. Diehl. 1986. The effects of salinity on echinoderms. Pp. 235–285 in *Echinoderm studies II*, M. Jangoux and J. M. Lawrence eds. Balkema, Rotterdam.

Reference: *Biol. Bull.* **183**: 490–499. (December, 1992)

Respiratory, Blood, and Heart Enzymatic Adaptations of *Sebastolobus alascanus* (Scorpaenidae; Teleostei) to the Oxygen Minimum Zone: A Comparative Study

T.-H. YANG, N. C. LAI, J. B. GRAHAM, AND G. N. SOMERO[1]

Marine Biology Research Division, Scripps Institution of Oceanography, University of California, San Diego, La Jolla, California 92093-0202

Abstract. The scorpaenid fishes *Sebastolobus alascanus* and *Scorpaena guttata* have similar life styles but differ in their depth distributions: *S. guttata* lives in shallow water (< 180 m); adult *S. alascanus* occur predominantly on the upper continental slope (400–1200 m) where the oxygen minimum zone (OMZ) prevails and ambient temperature is much colder. Respiratory properties and the activities of heart-tissue enzymes of these species were compared to determine the effect of different thermal and ambient O_2 regimens on metabolism. Measured over the appropriate habitat temperature ranges, the oxygen consumption (VO_2) of *S. alascanus* is two to four times less than that of *S. guttata*. Correction for differences in habitat temperature accounted for over 50% of this reduction. The depth-related decrease in VO_2 for these two benthic fishes is less than that observed for pelagic fishes. The VO_2 of *S. guttata* decreases at O_2 concentrations below 1 ml/l, whereas the VO_2 of *S. alascanus* is regulated down to 0.3 ml/l. The ventilation frequency (Vf) of both species increases in progressive hypoxia; but at < 0.5 ml/l, the Vf of *S. guttata* declines, while that of *S. alascanus* does not. When measured at the same temperature, pH and CO_2, the blood-O_2 affinity of *S. guttata* is significantly lower than that of *S. alascanus*. The anaerobic/aerobic enzyme activity ratio of pyruvate kinase to citrate synthase, which correlates with the ability of heart tissue to tolerate hypoxia, is significantly higher for *S. alascanus* than *S. guttata*. Lactate dehydrogenase (LDH) activity in freshly collected *S. alascanus* is also significantly above that of specimens acclimated to normoxic water in the laboratory. Only the skeletal muscle isozyme of LDH (LDH-A) is present in the heart of *S. alascanus*, whereas *S. guttata* has both LDH-A and heart (LDH-B) isozymes. Data for metabolic rate, critical O_2 tension, blood oxygen affinity, and heart metabolic enzyme profiles all show essential adaptations of *S. alascanus* for life in the OMZ.

Received 15 June 1992; accepted 18 September 1992.

[1] To whom correspondence should be addressed. Present address: Department of Zoology, 3029 Cordley Hall, Oregon State University, Corvallis, OR 97311–2914.

Introduction

A large body of evidence documents that organisms living at greater ocean depths generally have lower metabolic rates than related shallower-living species (for review, see Childress and Thuesen, 1992). Explanations for the depth-related reduction in metabolism have invoked a number of factors including the direct influences of the physical environment (*e.g.*, temperature, pressure, light, oxygen) and biotic forces such as food availability and predator-prey interactions. One approach to unraveling the complex interrelationships between depth and both the physical and biological influences on metabolic rate has been to compare the same or ecologically similar species in regions of the ocean where the suite of depth-related factors is different (cf. Childress and Mickel, 1985; Childress *et al.*, 1990; Cowles *et al.*, 1991; Torres *et al.*, 1979; Torres and Somero, 1988). For example, experiments by Childress and colleagues, comparing the metabolism of midwater crustaceans occurring in the eutrophic California current and in the relatively oligotrophic waters off Hawaii, have shown that visual predator-prey interactions, but not food availability, is the major selective force for the depth-related reduction in metabolic rate (Cowles *et al.*, 1991).

The depth-related reduction in metabolism observed in many benthic species is due primarily to temperature

(Childress and Mickel, 1985; Childress *et al.*, 1990). Relative to pelagic species, benthic organisms are generally less active, are restricted to a narrower habitat range, and cannot make short term vertical migrations. These restrictions may force many benthic inhabitants of the oxygen minimum zone (OMZ) to endure hypoxia permanently. In such cases, both temperature and hypoxia could potentially contribute to the depth-related reduction in metabolism.

In this paper, we have adopted the "comparative environmental approach" in order to differentiate between the potential effects of temperature and oxygen availability on the metabolism and respiratory adaptations of two closely related benthic fishes with different depth distributions. We have compared the metabolic properties of two scorpaenid fishes: the shortspine thornyhead (*Sebastolobus alascanus*) and the spotted scorpionfish (*Scorpaena guttata*). These two genera are considered to be closely related members of the family Scorpaenidae. Both are common off the coast of California and have similar life histories, producing floating eggs and pelagic larvae, and living on the bottom as adults. These species differ, however, in their depth distributions (Fig. 1): *S. guttata* is commonly found between the intertidal and 180 m, whereas *S. alascanus* occurs much deeper. Juveniles of *S. alascanus* occur on the continental shelf, and larger individuals extend into deeper waters (400–1200 m) and into the oxygen minimum zone (Wakefield and Smith, 1990) which prevails in the depth range of 600–1000 m. The concentration of O_2 in the OMZ can be lower than 0.3 ml/l (Hunter *et al.*, 1990). Thus, during much of its adult life, *S. alascanus* encounters extremely low O_2 concentrations.

Childress (1968, 1971, 1975) showed that crustaceans living in the OMZ are able to do so aerobically. Special adaptations for hypoxia in the lophogastrid mysid, *Gnathophausia ingens*, include: an increased ventilation capacity, large gill surface area, a very low critical O_2 tension, high cardiac output, and a high oxygen affinity hemocyanin (Childress, 1971; Belman and Childress, 1976; Sanders and Childress, 1990). To determine whether a similar suite of adaptations occurs in *S. alascanus*, we compared this species and *S. guttata* for their ventilatory frequencies (Vf) and VO_2 in response to decreasing O_2 concentration, and also measured their blood Hb-O_2 affinities. To study ambient hypoxia effects on tissue function, we compared the activities of heart metabolic enzymes, lactate dehydrogenase (LDH), pyruvate kinase (PK), malate dehydrogenase (MDH), and citrate synthase (CS). Heart enzymes are of interest because the tolerance of this organ to hypoxia has been previously correlated with the ratios of activities of aerobically- and anaerobically-poised enzymes (Gesser and Poupa, 1974). Additionally, the expression of LDH isozymes changes with

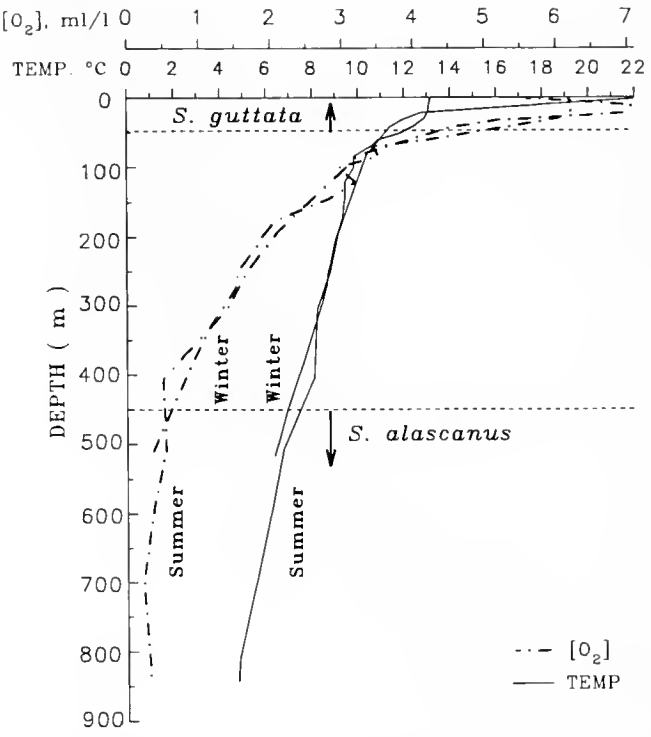

Figure 1. Winter and summer oxygen concentration and temperature profiles for waters off the San Diego coast in relation to the depth distribution of *Scorpaena guttata* and *Sebastolobus alascanus*. Arrowheads and dashed lines indicate the depths where the specimens were caught. Temperature and O_2 data are from CalCOFI cruise 8901 and 8908, station 93.30 (Anonymous, 1989, 1990; SIO Ref. 89–26, and 90–19).

environmental O_2 content (Lindy and Rajasalmi, 1966; Acker, 1988). We determined whether the expression of heart-type (LDH-B) and muscle-type (LDH-A) isozymes of LDH in heart reflect the ambient O_2 levels of these two fishes.

Materials and Methods

Collection and maintenance of animals

Specimens of *S. alascanus* were caught by long-line fishing at depths of 500 to 700 m off the Southern California coast and held in chilled seawater (5–8°C) without light. Fish were held for two to four days prior to the VO_2 measurements and were then used for blood and tissue studies. Some fish were acclimated to 9 ± 0.5°C in aerated running seawater for at least three months, during which they were fed either live or frozen shrimp every two days. Fish tissue used for enzyme analyses was stored at −80°C.

Specimens of *S. guttata* were caught either with SCUBA or by hook and line in shallow coastal waters (<15 m) during summer; they were maintained in flowing ambient seawater (~18°C) on a 12 h light/dark regime. Some of these fish were used for VO_2 measurements at 18°C, which

began three days after capture. Others were used for blood sampling. Another group was acclimated to 9 ± 0.5°C in aerated, running seawater. These fish were fed on chopped squid or fish every two days. After three months of acclimation, the VO_2 measurements were made and tissue samples removed for enzyme analyses.

Oxygen consumption

Routine oxygen consumption rates were measured in a thermostatted closed system. Depending on the size of the fish, respiratory chambers of different volumes (about 1, 5, 7, and 10 liter) made of clear PVC pipe were used. A peristaltic pump was used to circulate the water in the chamber. Clark-type polarographic oxygen electrodes were used to measure O_2 concentration via a Radiometer PHM72 or YSI54A monitor and O_2 concentration was recorded on chart paper. The electrode was calibrated with air-saturated and nitrogen-bubbled seawater at experimental temperature. The resultant O_2 data, obtained in either units of torr (Radiometer) or mg/l (YSI), were converted to standard units of concentration (ml/l) by means of the appropriate equations and O_2 solubility values (Weiss, 1970).

Measurements on *S. alascanus* were made at 4 and 9°C. Those for *S. guttata* were made at 18°C (freshly caught) and 9°C (acclimated). All fish were fasted for at least 48 h prior to the experiments and were placed in the respirometer containing air-saturated seawater 10 h before the measurements began. To avoid circadian effects, the VO_2 measurements were done between 0800 and 1300 h. Except for periodic checks of the system made under dim light, metabolic determinations were made in the dark. Most data were obtained between O_2 tensions of 90% to 40% saturation. In experiments designed to test the abilities of the two species to regulate their oxygen consumption rates at decreasing O_2 tensions, a Wöstoff pump was used to regulate O_2 concentration by mixing different proportions of nitrogen and air. About 15 min were needed to change the O_2 concentration, and fish were exposed to each concentration for an additional 45 min. After VO_2 measurements, the fish was removed and its volume was replaced by fresh seawater for a 3-h measurement of background microbial respiration. The background rate, when significant, was subtracted from the rate determined with a fish in the respirometer.

Ventilation frequency

Ventilation frequencies were counted while the VO_2 was being measured on size-matched specimens of *S. guttata* and *S. alascanus* maintained under different O_2 tensions at 9°C. The time required for 5 or 10 opercular beats was recorded and Vf was calculated; the mean of three measurements was used.

Determination of whole blood oxygen dissociation curves

Blood samples were drawn from caudal vein punctures into heparinized syringes and placed on ice. The sampling time for blood was kept short, usually less than 10 min for *S. guttata*, and 20 min for *S. alascanus*. Several drops of solution containing 10 mmol/l Tris/NaOH in 0.9% NaCl (pH 10) were added to buffer roughly 5 ml of blood. Hematocrit was determined by spinning 10 μl of blood in a microhematocrit centrifuge for 10 min.

To determine half saturation of oxygen (P_{50}), 180 μl samples were incubated at a series of O_2 pressures at constant CO_2 (2 torr) in an Astrup Micro Tonometer AMTl at 5, 9, and 20°C for at least 10 min. Total O_2 content was measured by the method of Tucker (1967). The blood O_2 and CO_2 partial pressure and pH were determined at the incubation temperature with a Radiometer blood gas microsystem (BMS-MK2). Oxygen-carrying capacity was determined by incubating the blood sample with 220 torr PO_2 for 20 min. The percentage of O_2 saturation of hemoglobin was calculated, and the P_{50} and Hill coefficient (n) were determined using the Hill equation.

Measurements of heart metabolic enzyme activities

Hearts were removed and homogenized on ice in conical glass homogenizers (Kontes Duall-21,23) with 30 volumes of 10 mmol/l Tris-HCl, pH 7.2 at 20°C. All enzymatic activities were assayed on freshly prepared homogenates without centrifugation. Measurements were done at 20 ± 0.1°C in a Perkin-Elmer Lambda 3B UV/VIS spectrophotometer. Activities of lactate dehydrogenase (LDH), pyruvate kinase (PK), malate dehydrogenase (MDH), and citrate synthase (CS) were assayed according to Somero and Childress (1980), except that Tris buffer was replaced by imidazole buffer.

Comparison of heart, white muscle, and brain LDH isozymes and determination of the pyruvate apparent K_m

To compare the LDH isozymes of heart and white muscle of *S. alascanus* and *S. guttata*, the tissue homogenates were electrophoresed in 7.5% polyacrylamide gels and detected by activity stain (Brewer, 1970).

In kinetic experiments, the enzyme activities were assayed in 80 mmol/l imidazole/Cl buffer, pH 7.2 at 20°C containing 150 μ*M* NADH, and a range of pyruvate concentrations from 0.1 to 1.0 mmol/l (Coppes and Somero, 1990). Enzymes were obtained from the supernatants of tissue homogenates prepared in 10 mmol/l Tris/Cl buffer and centrifuged at maximal speed in an Eppendorf microcentrifuge for 5 min. Apparent K_m values were determined from Lineweaver-Burke plots using a weighted lin-

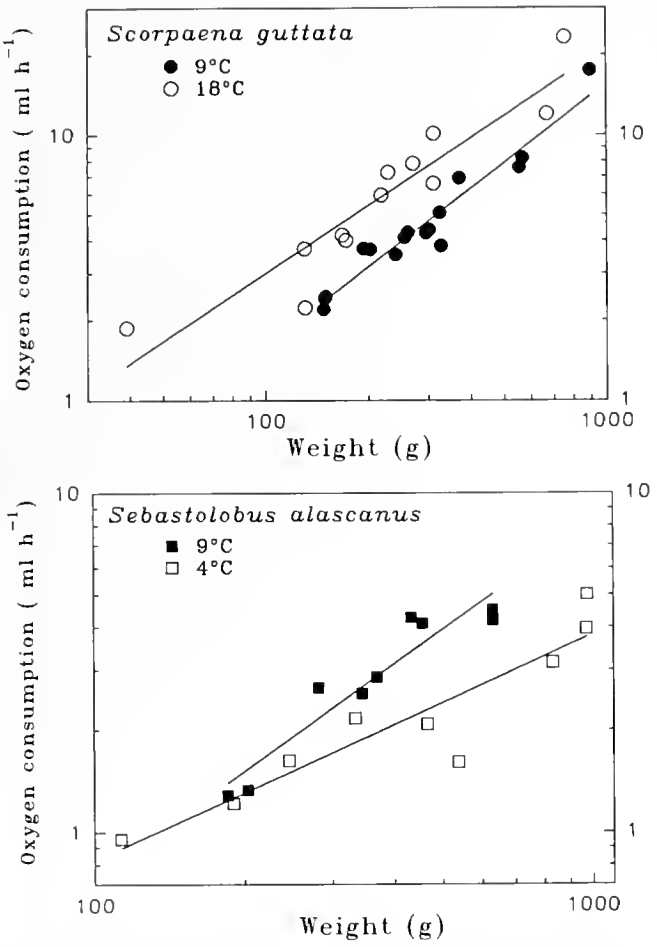

Figure 2. Regressions of VO_2 on body mass (M) for *Scorpaena guttata* and *Sebastolobus alascanus*. Equations for *S. guttata*: 18°C, Log VO_2 = −1.22 + 0.848 Log M, r^2 = 0.869; 9°C, Log VO_2 = −1.78 + 0.989 Log M, r^2 = 0.931. For *S. alascanus*: 9°C, Log VO_2 = −2.22 + 1.04 Log M, r^2 = 0.899; 4°C, Log VO_2 = −1.41 + 0.663 Log M, r^2 = 0.856.

ear regression technique (Wilman software: Brooks and Suelter, 1986).

Statistical analysis

Linear regression analysis of log-transformed data was used to calculate the relationship between VO_2 and body mass. The regression lines were tested by analysis of covariance (ANCOVA). An unpaired Student t-test was used to compare the results of P_{50} values and enzyme activities. The Tukey HSD pairwise analysis of variance (Wilkinson, 1990) was used to compare anaerobic/aerobic enzyme activity ratios between species. $P < 0.05$ was taken as the criterion for significant differences.

Results

VO_2 and temperature

Relationships between VO_2 and body mass at each temperature are shown for both species in Figure 2. Scaling equations describing the regression of VO_2 on mass at each test temperature are shown in Table I. Although there were no significant differences in the slopes of the four lines, their intercepts did differ ($P < 0.001$). Interspecific VO_2 comparisons (Table I) feature the regression-calculated VO_2 of a 250 g fish (median body mass) at each temperature, along with the 95% confidence intervals of the value. The VO_2 of *S. guttata* at 18°C, the temperature at which specimens were caught [and which was near the high end of its habitat range (about 10–20°C)], is 3.4 and 4.3 times that of *S. alascanus* at 9 and 4°C (habitat temperature range), respectively. At 9°C, however, the VO_2 of *S. guttata* is only about twice that of *S. alascanus*. The Q_{10} of the VO_2 for *S. alascanus* between 4 and 9°C is 1.58; that for *S. guttata* between 9 and 18°C is 1.75.

The effect of oxygen concentration on Vf and VO_2

Figure 3 shows the effects of O_2 concentration on the Vf and VO_2 of two individuals of *S. guttata* and *S. alascanus*. The VO_2 of *S. alascanus* at 9°C is virtually unaffected by O_2 concentration down to 0.3 ml/l, where it is reduced to about 85% of the rate seen at higher O_2 concentrations. In contrast, the VO_2 of *S. guttata* begins to decline at about 1 ml/l, and the decrease in rate is abrupt: at 0.3 ml/l, the rate is reduced to only 30% of that at higher O_2 concentrations.

The ventilation frequencies of both species showed a similar response to reduced O_2 content down to O_2 concentrations near 0.5 ml/l: Vf dramatically increased as O_2 content decreased below 2 ml/l (Fig. 3). As O_2 concentration decreased below 0.5 ml/l, differences between these two species appeared. The Vf of *S. alascanus* showed no decline at the lowest concentration, while that of *S. guttata* decreased. Although not quantified, the opercular stroke volume, as indicated by the extent of opercular expansion, increased for both species as O_2 content decreased.

Table I

Oxygen consumption rates of Sebastolobus alascanus *and* Scorpaena guttata *at different temperatures*

Species/ temperature	n	$VO_2 = a * M^b$	VO_2 (250 gr), (95% CI)
S. alascanus			
4°C	9	$VO_2 = 0.0391 * M^{0.663}$	1.52, (±0.32)
9°C	9	$VO_2 = 0.0061 * M^{1.04}$	1.91, (±0.16)
S. guttata			
18°C	12	$VO_2 = 0.0604 * M^{0.848}$	6.52, (±1.14)
9°C	16	$VO_2 = 0.0167 * M^{0.989}$	3.94, (±0.30)

Regression equation describes VO_2 (ml/l) in relation to gram body mass (M). VO_2 values for 250-g fish are regression estimates. Parenthetic values are the 95% confidence intervals (CI).

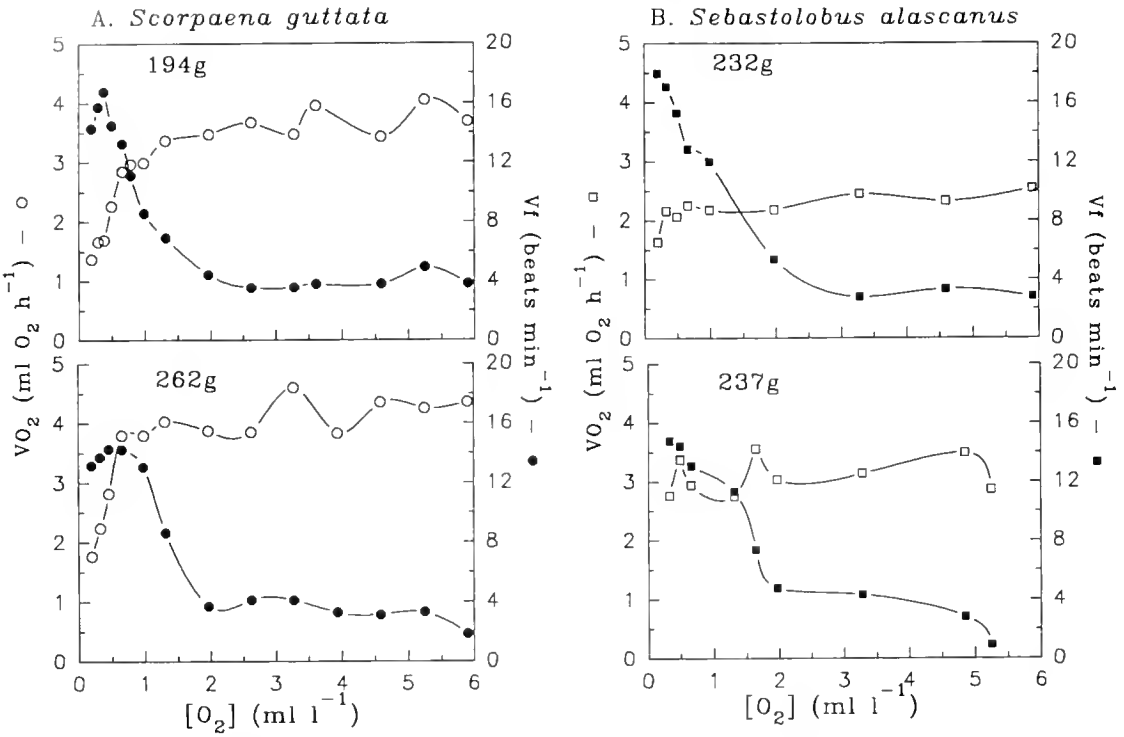

Figure 3. Effects of O_2 concentration on the ventilation frequency and oxygen consumption of two *S guttata* (A) and *S. alascanus* (B).

Whole blood hematocrit and oxygen affinity

The hematocrits of *S. alascanus*, 15.5 ± 3.6 (Mean ± S.D.; n = 9), and *S. guttata* (16.8 ± 2.8; n = 10) are not significantly different. Neither did the two species differ in total blood O_2 capacity [*S. alascanus*, 2.38 ± 0.78 mmol O_2/l (Mean ± S.D.; n = 9); *S. guttata* 2.72 ± 0.51 mmol O_2/l (n = 15)]. Comparison of the O_2 dissociation curves for the two species at 5°C reveals the higher O_2 affinity of *S. alascanus* (Fig. 4). The insert in Figure 4 expresses the Hb-O_2 affinities of the two species in the form of Hill plots. The slopes of these lines, Hill coefficients (n), provide an index of Hb-subunit cooperativity. Statistical analysis shows these n values were not different. Comparisons of blood P_{50} values for *S. guttata* and *S. alascanus* (Table II) show that at all temperatures and under similar conditions of pH and CO_2 partial pressure, *S. alascanus* has a significantly ($P < 0.05$) lower P_{50} than *S. guttata*.

Metabolic enzymes

The activities of four heart-tissue metabolic enzymes (LDH, PK, MDH, and CS) were compared to determine whether acclimation of *S. alascanus* to higher O_2 concentrations would lead to a shift in the aerobic *vs.* anaerobic poise of metabolism. Activities of the glycolytic enzymes LDH and PK were significantly higher ($P < 0.05$) in the freshly caught (hypoxia-dwelling) *S. alascanus*, compared to fish acclimated in normoxia (Table III). A significant difference is also seen for MDH activity ($P < 0.05$). On the other hand, the activity of CS, a key aerobic metabolic

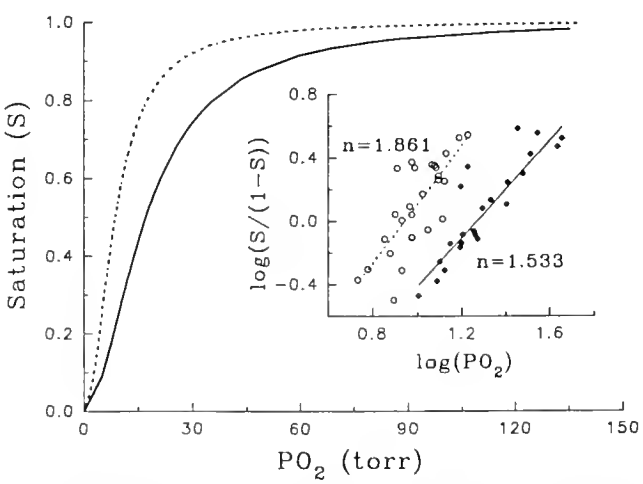

Figure 4. Oxygen equilibrium curves for the whole blood of *Sebastolobus alascanus* (dashed line and open symbols) and *Scorpaena guttata* (solid line and closed symbols) at 5°C, pH 7.9. Inset shows the Hill plots for both data sets within 20% and 80% saturation (S), and the Hill coefficient (n).

Table II

Blood oxygen affinity of Scorpaena guttata *and* Sebastolobus alascanus *measured at different temperatures*

Species	n	Temp. °C	PCO_2, torr	pH	P_{50} (O_2, torr)
S. guttata	5	20	1.9 ± 0.6	7.87 ± 0.41	24.2 ± 5.9
	5	9	1.8 ± 0.3	7.86 ± 0.18	21.8 ± 2.4
	4	5	1.7 ± 0.2	7.93 ± 0.12	18.8 ± 2.0
S. alascanus	4	20	2.1 ± 0.3	7.72 ± 0.11	13.9 ± 2.5
	1	9	1.8	7.87	9.9
	4	5	1.8 ± 0.7	7.92 ± 0.08	7.2 ± 1.5

Values are mean ± SD.

enzyme, was always the same, whether measured in freshly caught or laboratory-acclimated fish. Except for PK, the activities of enzymes measured in *S. guttata* are higher than in both acclimated and freshly caught *S. alascanus* (Table III).

The PK/CS ratio of freshly caught *S. alascanus* is significantly ($P < 0.05$) higher than those of the acclimated group and *S. guttata*. Although the PK/CS ratio tended to be higher in the acclimated *S. alascanus* than in *S. guttata*, the difference is not significant.

Figure 5 shows the K_m values for pyruvate of white muscle and heart LDH for both *S. alascanus* and *S. guttata*. In *S. alascanus* the K_m of white muscle is identical to that of heart, suggesting that the LDH isozyme composition is identical in both tissues. In *S. guttata* the LDHs of white muscle and heart have different K_m values, with that of heart LDH being significantly lower. Gel electrophoresis (Fig. 5) confirms that only one isozyme of LDH occurs in heart, red muscle, and white muscle of *S. alascanus*. In *S. guttata* both white and red muscle have the same single isozyme, but there are at least two isozymes expressed in the heart. In both species multiple isozymes of LDH occur in brain.

Discussion

Metabolic rate

This study of *S. alascanus* and *S. guttata* is one of the first to compare the effects of habitat depth, temperature, and ambient O_2 on the metabolic rates of confamilial benthic species with similar life styles, but different depth distributions. Because both fishes are benthic and accommodate well to respirometer confinement, the routine VO_2 estimates made for them very likely approach the minimal rates needed for maintenance metabolism.

Very few VO_2 measurements for benthic OMZ-dwelling fishes are presently available. The VO_2 reported for a single (48 g) specimen of *S. alascanus* by Siebenaller (1984) agrees closely with our results. Smith and Brown (1983) measured the VO_2 of *Sebastolobus altivelis*, which is closely related to *S. alascanus* and has an overlapping depth distribution range (although *S. altivelis* occurs slightly deeper). Their estimates were made *in situ* at 1300 m and at O_2 concentrations from about 0.6 to 0.3 ml/l. When corrections are made for temperature and body mass, our VO_2 estimate for *S. alascanus* is about three times higher than the Smith and Brown (1983) value for *S. altivelis*. The differences may be partly explained by methodology. The *S. alascanus* in our work were collected at 500–700 m and held at one atm pressure prior to respirometry, which was done at relatively high O_2 concentrations. In contrast, the *S. altivelis* used for the *in situ* VO_2 measurement by Smith and Brown were collected and remained at a greater depth and did not experience normoxia. Although we cannot predict how the pressure difference of 130 atm in the two studies would affect the respiration of *Sebastolobus*, the differences in O_2 tension between the two experiments seem unlikely to account for a significant fraction of the observed VO_2 difference. This is because the O_2 tensions in the range of those used in the study of *S. altivelis* did not cause a significant reduction in the respiration rate of *S. alascanus* (Fig. 3). Also, the findings of Siebenaller and Somero (1982)—that the average activities of ATP-generating enzymes in white muscle of *S. alascanus* were two-fold higher than in *S. altivelis*—support our conclusion that these two *Sebastolobus* species differ in their metabolic rate. Species differences in the activities of ATP-generating enzymes like LDH and CS in white muscle have been shown to correlate strongly with differences in VO_2 (Childress and Somero, 1979; Torres and Somero, 1988; Yang and Somero, in prep.).

Table III

Metabolic enzyme activities for hearts of Sebastolobus alascanus *and* Scorpaena guttata

	S. alascanus		*S. guttata*
	Field n = 9	Acclimated n = 8	Acclimated n = 17
LDH	183 ± 73[1]	89 ± 28	318 ± 133
PK	87 ± 27[1]	57 ± 15	84 ± 24
MDH	236 ± 63[1]	161 ± 37	513 ± 133
CS	13.7 ± 3.5[ns]	11.7 ± 2.2	20.1 ± 5.0
LDH/CS	13.9 ± 5.8[1]	7.4 ± 1.3[2]	15.3 ± 4.1[ns]
PK/CS	6.62 ± 2.66[1]	4.81 ± 0.66[ns]	4.03 ± 0.65[3]

The values are mean ± SD. The unit for enzyme activity is U/g tissue. LDH: lactate dehydrogenase; PK: pyruvate kinase; MDH: malate dehydrogenase; CS: citrate synthase. Statistical comparisons show significant differences ($P < 0.05$): 1—field and acclimated *S. alascanus*; 2—acclimated *S. alascanus* and *S. guttata*; 3—field *S. alascanus* and *S. guttata*; ns—not significant.

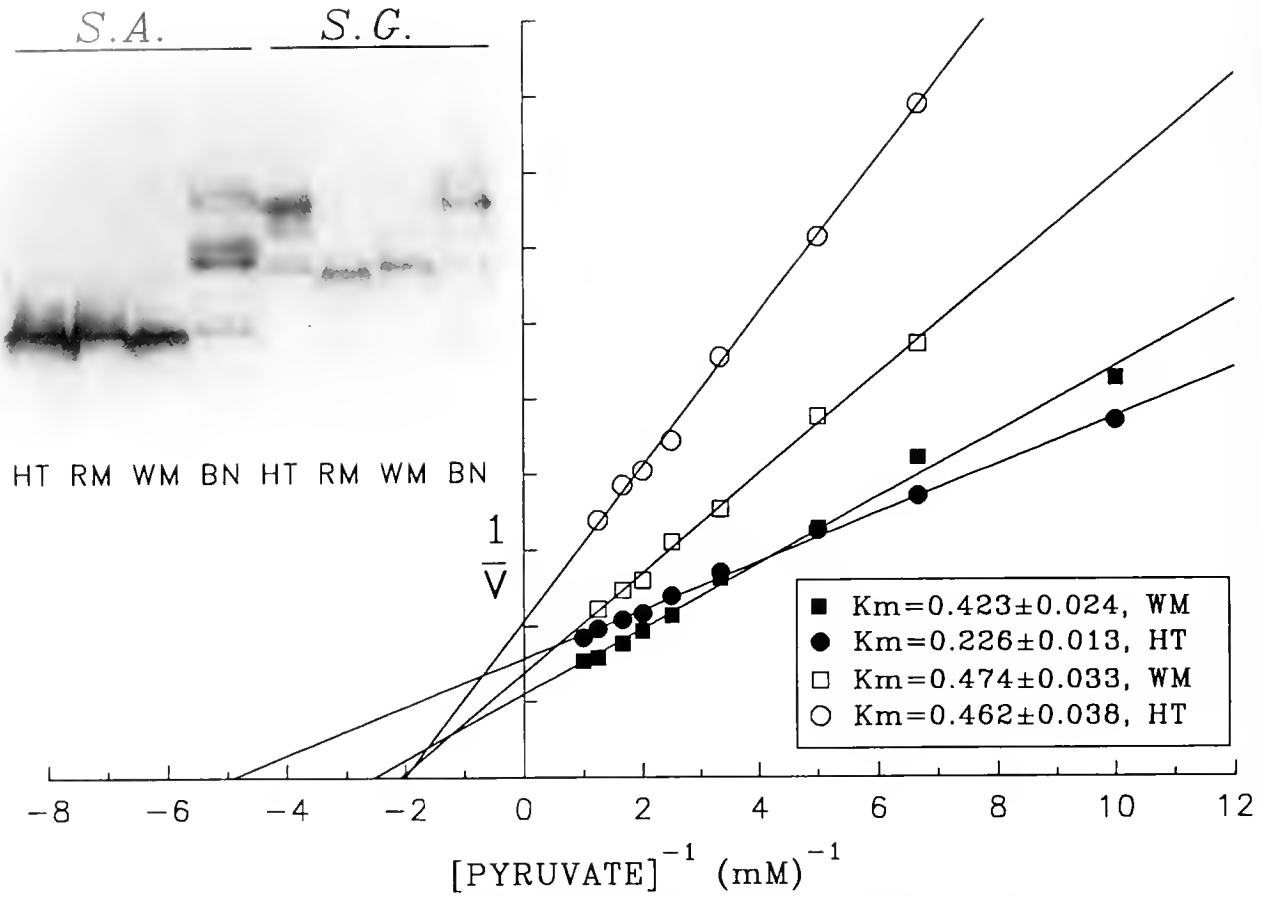

Figure 5. Kinetic and electrophoretic differences between LDH values of *Sebastolobus alascanus* and *Scorpaena guttata*. Lineweaver-Burke plots show the dependence of velocity on pyruvate concentration. K_m values (±S.E.) for pyruvate of white muscle and heart LDH values of *S. guttata* (SG; closed symbols) and *S. alascanus* (SA; open symbols) at 20°C are given in the inset. The polyacrylamide gel shows the activity stain of LDH isozymes in brain (BN), heart (HT), red muscle (RM), and white muscle (WM), of both species.

When compared to the oxygen consumptions of epi- and mesopelagic fishes from coastal California waters (Torres *et al.*, 1979) and Antarctic waters (Torres and Somero, 1988) at comparable depths and temperatures, the VO_2 values of both *S. guttata* and *S. alascanus* were lower than those of pelagic fishes. Moreover, in these two benthic scorpaenids, VO_2 values do not show the order of magnitude decrease with depth found for pelagic fishes (Torres and Childress, 1979; Torres and Somero, 1988). At habitat temperatures, the VO_2 of *S. guttata* was three to four times higher than that of *S. alascanus*. When acclimated and measured at the same temperature (9°C), the VO_2 of *S. guttata* was only twice that of *S. alascanus*. This means that temperature accounts for more than 50% of the depth-related decline in metabolic rate seen for these two benthic fishes. A similar conclusion was reached in studies of benthic crustaceans (Childress *et al.*, 1990; Childress and Mickel, 1985). Thus, for both benthic fishes and crustaceans, the depth-related decrease in metabolism is more attributable to changes in temperature than to changes in factors such as light and locomotory requirements (cf. Childress and Somero, 1979; Childress *et al.*, 1990).

Respiratory adaptations to the OMZ

Oxygen concentration in the OMZ can be as low as 0.2 ml/l and can form a barrier to the distribution of marine organisms (White, 1987). Animals with less oxygen demand would therefore be favored in this environment. Thus, the low metabolic rate of *S. alascanus*, compared to that of the shallow-living confamilial *S. guttata*, may be the result of adaptations to the OMZ as well as to temperature and other depth-related effects. To live in this low O_2 habitat, *S. alascanus* has important respiratory adaptations in addition to a low VO_2. It is a stronger O_2

regulator than *S. guttata,* and its critical O_2 concentration (P_c) is less than 0.4 ml/l, compared to 1 ml/l for *S. guttata.* Although the physiological significance of P_c is controversial, the P_c is regarded as the tension below which tissue oxygen delivery is not sufficient to support aerobic metabolism (Grieshaber *et al.,* 1988).

To maintain a constant VO_2 while environmental O_2 concentration varies, a fish must adjust its ventilatory water flow (Forgue *et al.,* 1989). Although only the ventilation frequency was measured (Figs. 3a and 3b), a notable increase in stroke volume was observed when O_2 concentration decreased. The decline in Vf of *S. guttata* at very low O_2 concentrations (<0.5 ml/l) indicated a loss in its ability to extract O_2. At these same low O_2 concentrations, *S. alascanus* was still able to regulate its VO_2.

Differences in oxygen extraction are attributable to blood O_2-binding properties (Malte and Weber, 1987). Over the ranges of temperature, pH, and PCO_2 at which these experiments were done, the whole blood of *S. alascanus* has a significantly higher O_2 affinity than that of *S. guttata* (Table II). At 9°C, the P_{50}s of both species approximate their P_cs (Fig. 3 and Table II). (Note for this comparison that at 9°C, 1 ml O_2/l = 24 torr.) In view of their close functional link, our finding of a coherence between the independently estimated parameters, P_c and P_{50}, is not surprising. In the case of *S. alascanus,* a low P_c and P_{50} are clearly adaptive in facilitating O_2 uptake in the OMZ, as are the respiratory adaptations of *Gnathophausia ingens.* Nevertheless, the high O_2 affinity of *S. alascanus* seems only marginally sufficient for aerobic respiration at the ambient tensions typical in the OMZ. At the usual OMZ tension of 5 to 12 torr, the blood of *S. alascanus* would be less than 80% saturated (Fig. 4). Exposure to the lowest O_2 tensions could lead to a further left shift of the dissociation curve through mechanisms of allosteric modulation (Weber and Jensen, 1988). Alternatively, *S. alascanus* may be able to sustain a partially anaerobic metabolism, a suggestion supported by the enzymatic profiles (discussed below).

While our dissociation curve data suggest that *S. alascanus* may be partially hypoxic in the OMZ, this conclusion cannot be made strongly at present due to three uncertainties. First, our P_{50} data are based on fish that had been in normoxia for about 24 h and subjected to stresses related to capture and handling. A slight right shift due to a decreased intracellular pH during blood sampling might be expected in our study; on the other hand, physical disturbance could result in an adrenergic response which has been shown to offset the Bohr effect (for review, see Weber and Jensen, 1988). Furthermore, we have no knowledge of how hydrostatic pressure may affect the O_2 binding of hemoglobin. A low P_{50} like that found for the blood of *S. alascanus* could, of course, pose difficulties for unloading oxygen in the respiring tissues. Further analysis of the regulation of oxygen affinity, *e.g.,* through Bohr effects and organophosphate modulation, is needed to address the question of oxygen unloading. Finally, the prediction of a partial hypoxia for *S. alascanus* would be opposite to what has been shown in bathypelagic crustaceans (Childress, 1968, 1971, 1975; Sanders and Childress, 1990).

Our studies with adult fishes provide no indication of how the blood O_2 affinity of *S. alascanus* changes in the course of its ontogenetic vertical migration into deeper water and the OMZ.

Metabolic enzymes of the heart

A notable finding of this research is that the laboratory-acclimated *S. alascanus* differed from the freshly caught population in their levels of heart metabolic enzymes. Our observations enable us to rule out the possibility that these differences were the result of body size, exercise, or nutrition. First, fish in the field and laboratory-acclimated populations were of the same size range, and no scaling effect of enzyme activity was found in our study. Second, although our acclimated *S. alascanus* were confined in the laboratory for more than three months, the finding that heart CS activities (an index of aerobic metabolic capacity) were essentially the same in both groups argues against the idea that reduced exercise resulted in the difference. Finally, the effect of nutritional level on the differences between freshly caught and acclimated fishes is ruled out because there is no long term starvation effect on heart enzyme activities (although activities in muscle are reduced; Yang and Somero, in prep.).

Although commonly viewed as an aerobic organ, the hearts of some vertebrates can tolerate hypoxia (Wegener, 1988). Our enzyme data suggest that, as an adaptation to the OMZ, the heart of *S. alascanus* maintains a relatively high potential for ATP generation by glycolysis, and that this capacity may become important during periods when activity levels exceed aerobic capacity. In Table III, we show that the glycolytic enzymes PK and LDH were significantly higher in low oxygen-acclimatized field fish than in those experiencing laboratory normoxia. MDH also differed in these two groups, which may reflect its dual role in both aerobic and anaerobic energy production (Hochachka and Somero, 1984).

In addition to activity levels, the anaerobic/aerobic enzyme ratio may very likely indicate the heart's anaerobic tolerance. A survey of five teleosts by Gesser and Poupa (1974) revealed no correlation between the acute anoxia tolerance of isolated hearts and the activities of PK, LDH, and cytochrome oxidase (also an oxidative indicator). These workers did, however, find a positive correlation between the ratio of PK and cytochrome oxidase activities and anoxia tolerance. Because cytochrome oxidase activity

is significantly reduced by freezing, we were unable to measure the same ratio as Gesser and Poupa (1974). However, CS is also a good indicator of aerobic ATP generation, and we were able to compare *S. alascanus* and *S. guttata* for their ratios of PK/CS. As shown in Table III, this ratio in field *S. alascanus* is significantly higher than that in either acclimated *S. alascanus* or *S. guttata.*

The LDH/CS ratios (Table III) do not completely follow the trend seen for the PK/CS ratios. The LDH/CS ratio of field *S. alascanus* was nearly twice that of laboratory-acclimated *S. alascanus,* and thus was consistent with a greater anaerobic poising of heart metabolism in field fish. However, neither ratio was higher than that of *S. guttata.* The high LDH/CS ratio found in *S. guttata* may be a consequence of the occurrence of two LDH isoforms in its heart, but only one in the heart of *S. alascanus* (Fig. 5). In white muscle and heart of *S. alascanus,* only LDH-A is expressed, as judged by the agreement of the K_m of pyruvate with published values for the LDH-A of other vertebrates (Yancey and Somero, 1978; Coppes and Somero, 1990). The lower K_m of pyruvate for the heart LDH of *S. guttata* indicates the presence of LDH-B, and the electrophoretic pattern shows that both isozymes are expressed in this tissue. Therefore, the high LDH activities in *S. guttata* heart may represent capacities for substantial oxidation of lactate by LDH-B, as well as the ability to produce lactate by LDH-A. Although the activity staining of gels is not a quantitative measure of enzyme activity, Figure 5 does indicate the presence of relatively higher LDH-B than LDH-A in the heart of *S. guttata.* By contrast, the absence of LDH-B in the heart of *S. alascanus* would lower the efficiency for lactate oxidation. Therefore, the high LDH/CS ratio and high LDH activity in the heart of *S. guttata* may reflect a high aerobic capacity (*i.e.,* lactate oxidation by LDH-B to form pyruvate), rather than a high anaerobic capacity (by LDH-A).

The occurrence of only LDH-A in the heart of *S. alascanus* and the higher LDH activity in freshly caught fish are interesting findings in the context of factors regulating LDH gene expression. LDH-A can be induced by hypoxia in the hearts of chicken embryos and in rat tumor cells (Lindy and Rajasalmi, 1966; Acker, 1988), and it has been proposed that the expression of LDH isozymes reflects tissue PO_2 (Acker, 1988). We used native gel electrophoresis to look for differential expression of LDH isozymes in the heart of field and laboratory-acclimated *S. alascanus,* but found no evidence for oxygen-related shifts in gene expression.

Our data suggest that the exclusive presence of LDH-A in the heart of *S. alascanus* may be related to limited availability of O_2 in its environment. Although a number of fishes are known to have only LDH-A in their hearts, factors relating to this have not always been clear. Data for the Antarctic fishes *Notothenia neglecta* (Fitch, 1989) and *Channichthys rhinoceratus* (Feller and Gerday, 1987; Feller *et al.,* 1991) strongly support the idea that the sole presence in heart of LDH-A may relate to O_2 availability. *Notothenia* has a reduced blood hemoglobin, and in *Channichthys,* the ice fish, hemoglobin and myoglobin are absent. During exercise the hearts of these two fishes could become hypoxic due to shortfalls in O_2 delivery. Thus, the presence of LDH-A and high glycolytic enzyme activities might be an adaptation for ATP production by anaerobic metabolism (Gesser and Poupa, 1973, 1974; Hansen and Sidell, 1983).

Oxygen availability to the heart may form the basis for similar biochemical characteristics in the cardiac tissues of *S. alascanus* and the two Antarctic species. In the case of *S. alascanus* heart, O_2 availability is limited by environmental O_2 concentration, whereas in the Antarctic fishes, it is limited by blood O_2 carrying capacity. In *S. alascanus,* the gene for LDH-B is not lost, but expressed in the brain (Fig. 5). The exclusive use of LDH-A in the hearts of these diverse species may thus be a convergence to limited oxygen supply that allows continuous glycolytic flux by reducing pyruvate to lactate during anaerobic metabolism.

Acknowledgments

We gratefully acknowledge the assistance of Mr. Ronald McConnaughey in collecting specimens. During part of the studies, T.-H. Yang was supported by a graduate student fellowship from the Department of Education, Taiwan, R. O. C. These studies were supported by National Science Foundation grants DCB-8812180 and DCB-9206660 to G. N. Somero.

Literature Cited

Acker, H. 1988. Possible mechanisms of O_2 sensing in different cell types. Pp. 65–75 in *Oxygen Sensing in Tissues,* H. Acker, ed. Springer-Verlag, Berlin.

Anonymous. 1989. Data report: physical, chemical and biological data. *SIO Ref.* 89–26.

Anonymous. 1990. Data report: physical, chemical and biological data. *SIO Ref.* 90–19.

Belman, B. W., and J. J. Childress. 1976. Circulatory adaptations to the oxygen minimum layer in the bathypelagic mysid *Gnathophausia ingens. Biol. Bull.* **150:** 15–37.

Brewer, G. J. 1970. P. 85 in *An Introduction to Isozyme Techniques.* Academic Press, New York.

Brooks, S. P. J., and C. H. Suelter. 1986. Estimating enzyme kinetic parameters: a computer program for linear regression and non-parametric analysis. *Int. J. Bio-Med. Comput.* **19:** 89–99.

Childress, J. J. 1968. Oxygen minimum layer: vertical distribution and respiration of the mysid *Gnathophausia ingens. Science* **160:** 1242–1243.

Childress, J. J. 1971. Respiratory adaptations to the oxygen minimum layer in the bathypelagic mysid *Gnathophausia ingens. Biol. Bull.* **141:** 109–121.

Childress, J. J. 1975. The respiratory rates of midwater crustaceans as a function of depth of occurrence and relation to the oxygen min-

imum layer off Southern California. *Comp. Biochem. Physiol.* **50**A: 787–799.

Childress, J. J., D. L. Cowles, J. A. Favuzzi, and T. J. Mickel. 1990. Metabolic rates of benthic deep-sea decapod crustaceans decline with increasing depth primarily due to the decline in temperature. *Deep-Sea Res.* **37:** 929–949.

Childress, J. J., and T. J. Mickel. 1985. Metabolic rates of animals from the hydrothermal vents and other deep-sea habitats. *Biol. Soc. Wash. Bull.* **6:** 249–260.

Childress, J. J., and G. N. Somero. 1979. Depth-related enzymic activities in muscle, brain and heart of deep-living pelagic marine teleosts. *Mar. Biol.* **52:** 273–283.

Childress, J. J., and E. V. Thuesen. 1992. Metabolic potential of deep-sea animals: regional and global scales. Pp. 217–236 in *Deep-Sea Food Chains and the Global Carbon Cycle,* G. T. Rowe, and V. Pariente, eds. Kluwer Academic Publishers, Dordrecht.

Coppes, Z. L., and G. N. Somero. 1990. Temperature-adaptive differences between the M_4 lactate dehydrogenases of stenothermal and eurythermal sciaenid fishes. *J. Exp. Zool.* **254:** 127–131.

Cowles, D. L., J. J. Childress, and M. W. Wells. 1991. Metabolic rates of midwater crustaceans as a function of depth of occurrence off the Hawaiian Islands: food availability as a selective factor? *Mar. Biol* **110:** 78–83.

Feller, G., and C. Gerday. 1987. Metabolic pattern of the heart of hemoglobin- and myoglobin-free Antarctic fish *Channichthys rhinoceratus. Polar Biol.* 7: 225–229.

Feller, G., J.-P. Pauly, A. Smal, P. O'Carra, and C. Gerday. 1991. The lactate dehydrogenase of the icefish heart: biochemical adaptations to hypoxia tolerance. *Biochim. Biophys. Acta.* **1079:** 343–347.

Fitch, N. A. 1989. Lactate dehydrogenase isozymes in the trunk and cardiac muscles of an Antarctic teleost fish, *Notothenia neglecta,* Nybelin. *Fish Physiol. Biochem.* **6:** 187–195.

Forgue, J., B. Burtin, and J. C. Massabuau. 1989. Maintenance of oxygen consumption in resting *Silurus glanis* at different levels of ambient oxygenation. *J. Exp. Biol.* **143:** 305–319.

Gesser, H., and O. Poupa. 1973. The lactate dehydrogenase system in the heart and skeletal muscle of fish: a comparative study. *Comp. Biochem. Physiol.* **46**B: 683–690.

Gesser, H., and O. Poupa. 1974. Relations between heart muscle enzyme pattern and directly measured tolerance to acute anoxia. *Comp. Biochem. Physiol.* **48**A: 97–103.

Grieshaber, M. K., U. Kreutzer, and H. O. Pörtner. 1988. Critical PO_2 of euryoxic animals. Pp. 37–48 in *Oxygen Sensing in Tissues,* H. Acker, ed. Springer-Verlag, Berlin.

Hansen, C. A., and B. D. Sidell. 1983. Atlantic hagfish cardiac muscle: metabolic basis of tolerance to anoxia. *Am. J. Physiol.* **244:** R356–R362.

Hochachka, P. W., and G. N. Somero. 1984. *Biochemical Adaptation* 537 pp. Princeton University Press, Princeton.

Hunter, J. R., J. L. Butler, C. Kimbrell, and E. A. Lynn. 1990. Bathymetric patterns in size, age, sexual maturity, water content, and caloric density of dover sole, *Microstomus pacificus. CalCOFI Rep.* **31:** 132–144.

Lindy, S., and M. Rajasalmi. 1966. Lactate dehydrogenase isozymes of chick embryo: response to variations of ambient oxygen tension. *Science* **153:** 1401–1403.

Malte, H., and R. E. Weber. 1987. The effect of shape and position of the oxygen equilibrium curve on extraction and ventilation requirement in fishes. *Respir. Physiol.* **70:** 221–228.

Sanders, N. K., and J. J. Childress. 1990. Adaptations to the deep-sea oxygen minimum layer: Oxygen binding by the hemocyanin of the bathypelagic mysid, *Gnathophausia ingens* Dohrn. *Biol. Bull.* **178:** 286–294.

Siebenaller, J. F. 1984. Analysis of the biochemical consequences of ontogenetic vertical migration in a deep-living teleost fish. *Physiol. Zool.* **57:** 598–608.

Siebenaller, J. F., and G. N. Somero. 1982. The maintenance of different enzyme activity levels in congeneric fishes living at different depths. *Physiol. Zool.* **55:** 171–179.

Smith, K. L., Jr., and N. O. Brown. 1983. Oxygen consumption of pelagic juveniles and demersal adults of the deep-sea fish *S. altivelis,* measured at depth. *Mar. Biol.* **76:** 325–332.

Somero, G. N., and J. J. Childress. 1980. A violation of the metabolism-size scaling paradigm: activities of glycolytic enzymes in muscle increase in larger-size fish. *Physiol. Zool.* **53:** 322–337.

Torres, J. J., B. W. Belman, and J. J. Childress. 1979. Oxygen consumption rates of midwater fishes as a function of depth of occurrence. *Deep-Sea Res.* **26**A: 185–197.

Torres, J. J., and G. N. Somero. 1988. Vertical distribution and metabolism in Antarctic mesopelagic fishes. *Comp. Biochem. Physiol.* **90**B: 521–528.

Tucker, V. A. 1967. Method for oxygen content and dissociation curves on microliter blood samples. *J. Appl. Physiol.* **23:** 410–413.

Wakefield, W. W., and K. L. Smith, Jr. 1990. Ontogenetic vertical migration in *S. altivelis* as a mechanism for transport of particulate organic matter at continental slope depths. *Limnol. Oceanogr.* **35:** 1314–1328.

Weber, R. E., and F. B. Jensen. 1988. Functional adaptations in hemoglobins from ectothermic vertebrates. *Ann. Rev. Physiol.* **50:** 161–179.

Wegener, G. 1988. Oxygen availability, energy metabolism, and metabolic rate in invertebrates and vertebrates. Pp. 13–35 in *Oxygen Sensing in Tissues,* H. Acker, ed. Springer-Verlag, Berlin.

Weiss, R. F. 1970. The solubility of nitrogen, oxygen and argon in water and seawater. *Deep-Sea Res.* **17:** 721–735.

White, B. N. 1987. Oceanic anoxic events and allopatric speciation in the deep sea. *Biol. Oceanogr.* **5:** 243–259.

Wilkinson, L. 1990. *SYSTAT: The System for Statistics.* SYSTAT, Evanston.

Yancey, P. H., and G. N. Somero. 1978. Temperature dependence of intracellular pH: its role in the conservation of pyruvate apparent Km values of vertebrate lactate dehydrogenases. *J. Comp. Physiol.* **125:** 129–134.

Reference: *Biol. Bull.* **183**: 500–502. (December, 1992)

Glutathione (GSH)-Induced Bud Initiation in *Hydra oligactis*

JAMES A. ADAMS* AND MICHAEL A. WARD**

**Department of Natural Sciences, University of Maryland Eastern Shore, Princess Anne, Maryland 21853, and **Department of Biological Sciences, Tennessee State University, Nashville, Tennessee 37208*

Budding in the genus Hydra *was first described in the scientific literature, and sketched, by Leeuwenhoek (1). Since that time, budding has continued to be a popular problem for developmental biologists who study* Hydra *(2, 3, 4). The relationship between feeding and budding was established in mass culture experiments performed by a number of investigators (5, 6, 7, 8, 9). The discovery by Schaller (10) of a low-molecular-weight peptide released by the nerve cells of* Hydra *in response to feeding or injury, and her determination that this polypeptide acts as a mitogen (11), taken together with studies showing a correlation between the mitotic index and the budding rate in* Hydra *(7, 12, 13) left little doubt that feeding and budding are causally related. Recent studies continue to reinforce the observation that reduced glutathione (GSH), or glutathione derivatives, can elicit the feeding response in* Hydra *(14, 15). But the literature is mute about the possibility that GSH, which causes a mechanical feeding response in* Hydra *(16), might also stimulate budding. This study was designed to test that possibility. The specific objectives were (a) to determine whether exposure to GSH leads to a significant increase in the rate of bud initiation in starved* Hydra oligactis; *(b) to determine by employing decapitated* H. oligactis, *whether any observable GSH effect can occur without mediation by the head of the hydra; and (c) to determine whether any GSH induction of budding is additive to that elicited by feeding. All of these objectives were met, and we propose that GSH plays a (significant) role in the cascade of events heading to budding in* Hydra.

H. oligactis individuals were purchased from Carolina Biologieal Supply Co. (Burlington, North Carolina) and subcultured in an artificial pondwater (APW) medium (17) at 19°C. The animals were fed *Artemia salina* (Wards) nauplii daily, and the medium was changed approximately 3 h after feeding. Mass culture were kept in 8″ Pyrex dishes. All hydras used in this study possessed one stage-one bud (9). All animals were starved for 24 h before use.

A 10^{-5} molar solution of GSH was prepared with APW. Where GSH treatment is indicated, the culture medium contained 10^{-5} *M* GSH. The medium was discarded each day and replaced with fresh medium containing GSH. For the groups exposed to APW alone, the medium was also changed daily. Seventy-five animals were used for each treatment. Each animal was kept in an individual, 16 × 50 mm, numbered Petri dish to allow for individual data collection.

Following initial 24-h pre-experimentation starvation periods, hydras were treated in the following ways.

(a) Unfed controls were starved throughout the 96-h period of the study.
(b) Animals fed on alternate days were fed on days one and three of the study.
(c) Alternate day-fed animals with GSH exposure were treated as those in (b) above but with the addition of 10^{-5} *M* GSH to the medium.
(d) Hyposomally transected animals (*i.e.*, "decapitated") were prepared at the initiation of the GSH observation period and were continuously starved for the entire 96-h period.
(e) Finally, decapitated and GSH-exposed animals were treated as in (d) above, except that 10^{-5} *M* GSH was added to the culture medium.

Recorded observations of bud initiation reflect new buds only. The original stage-one of each animal was not

Received 4 February 1992; accepted 1 October 1992.

Table I

The effect of glutathione (GSH) on bud initiation in Hydra *under various treatments*

Treatment	Incubation time			
	24 h	48 h	72 h	96 h
Unfed control	2	9	14	22
Unfed with GSH	22*	41*	58*	66*
Alternate day fed control	3	19	29*	43*
Alternate day fed with GSH	15*	56*	65*	83*
Decapitated control	3	29	35	38
Decapitated with GSH	22*	56*	63*	82*

Brackets indicate pairwise comparisons.
* $P < 0.05$, *t*-test.
n = 75 for each treatment group.

included. Point-to-point comparisons of bud initiation were performed with a two-tailed *t*-test. Bud numbers were assessed at 24-h intervals.

All of the data are presented in Table I. When starved *H. oligactis* bearing a single stage one bud are exposed to reduced glutathione, the rate of bud initiation is significantly higher than that of unexposed controls during all three observation intervals. By the end of the 96-h incubation period, the GSH-treated animals displayed a 3-fold increase in the rate of bud initiation. Moreover, decapitation had no influence on this GSH-induced budding (Table I): at all three observation intervals, decapitated animals treated with GSH displayed significantly elevated rates of bud initiation when compared with headless but untreated controls.

When hydras were fed on alternate days, an increased rate of bud initiation was expected. Table I also shows that animals fed on alternate days have a higher rate of bud initiation than starved controls. Although alternate day feeding significantly increased the rate of bud initiation, the addition of GSH led to a further significant increase over the already accelerated rate caused by feeding alone (Table I). We selected alternate day feeding as an experimental condition because we had already determined that daily feeding produces a maximum budding rate, thus obscuring any additional effect of GSH (unpub.).

In summary, our results clearly show that at all recorded intervals and under all experimental conditions, hydras treated with GSH have significantly higher rates of bud initiation than untreated control animals. Further, because GSH was fully effective when tested on decapitated animals, the mechanical feeding response cannot be responsible for the increased bud initiation. We have also shown that the effect of GSH is additive to that elicited by feeding and decapitation; *i.e.*, the combined effects of alternate day feeding and GSH exposure on intact hydras are similar to the effects of GSH and decapitation. Finally, GSH receptors have been demonstrated and characterized in *H. vulgaris* (18).

We propose, therefore, that the tripeptide glutathione plays a central role in the sequence of molecular and cellular events leading to the production of buds in *Hydra*. The sites of action of GSH are, however, not yet evident.

When hydras feed, GSH is presumed to be released from their prey, although this hypothesis has never been validated. Feeding has also been presumed to release a polypeptide with mitogenic and morphogenic activities from endogenous stores in *Hydra* (11). This polypeptide (*i.e.*, 'head activator') is also released by transection of the head or other injury (10) and stimulates both budding and head regeneration. But the rise in the mitotic index subsequent to feeding is more likely to be due to a release from inhibition caused by feeding (19).

Thus, although alternate day feeding and decapitation are equally efficient at stimulating bud initiation, we cannot be sure that their mechanisms of action are identical. As for GSH, it may be a part of the cascade of events initiated by head activator; it may be one of the signals initiating the cascade; or it may act through another pathway altogether.

Acknowledgments

We thank Robert A. Nesby, Abiodun Adibi, and Amuel Kennedy for technical assistance, and Jasmine D. Adams for inspiration. This work was supported in part by NIH Grant RR08092.

Literature Cited

1. **Leeuwenhoek, A. 1702–1703 (1704).** Part of a letter from Mr. Leeuwenhoek concerning green weeds growing in water and some Animalicula found about them. *Philos. Trans. Lond.* **23:** 1304–1311.
2. **Tannreuther, G. W. 1909.** Observations on the germ cells of *Hydra*. *Biol. Bull.* **16:** 205–209.
3. **Goetsch, W. 1929.** Das Regenerations-material und sein experimentele Beeinflussung. Versuch zur einheitlichen Beurteilung der Regenerative. *Wilhelm Roux' Arch. Entwicklungsmech. Organismen.* **117:** 211–311.
4. **Kanauew, J. 1930.** Zur Frage Bedeutung der Interstitiellen Zellen Bei *Hydra*. *Wilhelm Roux' Arch. Entwicklungsmech. Organismen.* **122:** 736–759.
5. **Loomis, W. F. 1953.** The cultivation of *Hydra* under controlled conditions. *Science* **117:** 565–566.
6. **Stiven, A. E. 1962.** The effect of temperature and feeding on the intrinsic rate of increase of three species of *Hydra*. *Ecology* **43:** 325–328.
7. **Campbell, R. D. 1967.** Tissue dynamics of steady state growth in *Hydra littoralis*. I. Patterns of cell division. *Dev. Biol.* **15:** 487–502.
8. **Shostak, S. 1968.** Growth in *Hydra viridis*. *J. Exp. Zool.* **69:** 431–446.
9. **Shostak, S., J. W. Bisbee, C. Askin, and R. V. Tammariello. 1968.** Budding in *Hydra viridis*. *J. Exp. Zool.* **192:** 43–56.

10. **Schaller, H. C. 1973.** Isolation and characterization of a low-molecular-weight substance activating head and foot formation in *Hydra*. *J. Embryol. Exp. Morphol.* **29:** 27–38.
11. **Schaller, H. C. 1976.** Action of the head activator as a growth hormone in *Hydra*. *Cell Differ.* **5:** 1–11.
12. **Campbell, R. D. 1965.** Cell proliferation in *Hydra*. An autoradiographic approach. *Science* **148:** 1231–1232.
13. **Clarkson, S. G., and L. Wolpert. 1967.** Bud morphogenesis in *Hydra*. *Nature* **214:** 780–783.
14. **Spencer, A. N. 1989.** Neuropeptides in the Cnidria. *Am. Zool.* **29:** 1213–1225.
15. **Hanai, K., M. Sakaguchi, S. Matsuhashi, K. Hori, H. Morita, S. D. Roper, and Atema-Jeds. 1987.** Monoclonal antibodies to multiple glutathione receptors mediating the feeding response of *Hydra*. Taste and Olfaction. *Ann. New York. Acad. Sci.* **510:** 335–337.
16. **Loomis, W. F. 1955.** Glutathione control of the specific feeding reactions of *Hydra*. *Ann. New York Acad. Sci.* **62:** 208–209.
17. **Loomis, W. F., and H. M. Lenhoff. 1956.** Growth and sexual differentiation of *Hydra*. *Ann. New York Acad. Sci.* **62:** 208–209.
18. **Bellis, S. L., W. Grosvenor, G. Kass-Simon, and D. E. Rhoads. 1991.** Chemoreception in *Hydra vulgaris* (*attenuata*): initial characterization of two distinct binding sites for L-glutamic acid. *Biochem. Biophys. Acta* **1061:** 89–94.
19. **Herman, K., and S. Berking. 1987.** The length of S-phase and G sub (2)-phase of epithelial cells is regulated during growth and morphogenesis on *Hydra attenuata*. *Development* **99:** 33–39.

Reference: *Biol. Bull.* **183**: 503–506. (December, 1992)

The Zooxanthellal Tubular System in the Giant Clam

JOHN H. NORTON[1], MALCOLM A. SHEPHERD[1],
HELEN M. LONG[1], AND WILLIAM K. FITT[2]

[1]*Queensland Department of Primary Industries, Oonoonba Veterinary Laboratory, P. O. Box 1085, Townsville 4810, Queensland, Australia, and* [2]*University of Georgia, Department of Zoology, 724 Biological Sciences Building, Athens, Georgia 30602*

Giant clams (family Tridacnidae) are special in that they contain large numbers of symbiotic dinoflagellates, Symbiodinium sp., *commonly called zooxanthellae which live in the clam's siphonal mantle (hypertrophied siphonal tissues) (1) and are important in its nutrition (2, 3). In 1946, Mansour (4) partially described a tubular system arising from the clam stomach, extending into the mantle and containing zooxanthellae. However, the eminent scientist Sir Maurice Yonge (5, 6) disputed its existence. Subsequently, Yonge's views appear to have suppressed further investigations of Mansour's observations. The zooxanthellae have been universally regarded as living in the hemal spaces of the mantle (2, 5, 7, 8, 9). This study, however, has confirmed the presence of the tubular system indicated by Mansour and has shown that the zooxanthellae live within a branched, tubular structure that has no direct connection with the hemolymph. The existence of this tubular system has important implications for our understanding of the symbiosis between tridacnids and their symbiotic algae.*

During a study of the anatomy and histology of giant clams, numerous *Tridacna gigas*, from a few millimeters to 35 cm in shell length, were dissected. Tissues were fixed in 10% seawater formalin, processed by routine histological methods, including serial sectioning, and stained with hematoxylin and eosin (H & E). Additional stains included Masson's trichome for muscle tissue, periodic Acid-Schiff (PAS) and PAS/diastase for glycogen, starch, neutral mucopolysaccharides and glycoproteins, and an Alcian Blue stain to delineate the tertiary zooxanthellal tubes.

The zooxanthellal tubular system was found to commence as a single primary tube, originating from one of the digestive diverticular ducts of the stomach (Figs. 1a, b). It passes dorsally and posteriorly between the digestive diverticula, and then between the crystalline style sac and the muscular wall that encloses the digestive and reproductive organs. Above the digestive organs, it divides into right and left tubes. These tubes pass close to the dorsal aspect of the muscular wall, then through this muscular wall and into the kidney parenchyma. Both tubes travel through the kidney in a more ventral direction, until they leave the kidney and enter the root of the middle ctenidial suspensory ligament. The tubes continue to travel posteriorly, where they become embedded in the connective tissue sheath of the adductor muscle. While traversing the posterior portion of the adductor muscle, each tube gives off a branch which is embedded in the floor of the excurrent water chamber. Each primary tube associated with the zooxanthellae passes toward the end of the adductor muscle, and dorsally into the root of the siphonal mantle, before branching both anteriorly and posteriorly. One or more main branches run along inside the root of the siphonal mantle close to the circumpallial artery, the circumpallial vein, and the pallial nerves. Secondary zooxanthellal tubes branch into the upper levels of the inner fold of the siphonal mantle, where they terminate in convolutions of thin tertiary tubes with blind ends. These tertiary tubes contain the zooxanthellae. Other secondary branches form tertiary tubes in other organs, such as in the connective tissue surrounding the adductor muscle and in the connective tissues of the bulbus arteriosus of the heart, the pericardium, the ctenidia, and the lateral mantle.

The primary zooxanthellal tubes (Fig. 2) have an epithelial lining of cuboidal to low columnar cells with long cilia and are surrounded by a thin zone of muscle fibers. The secondary tubes (Fig. 3) are thin-walled and

Received 14 May 1992; accepted 22 September 1992.

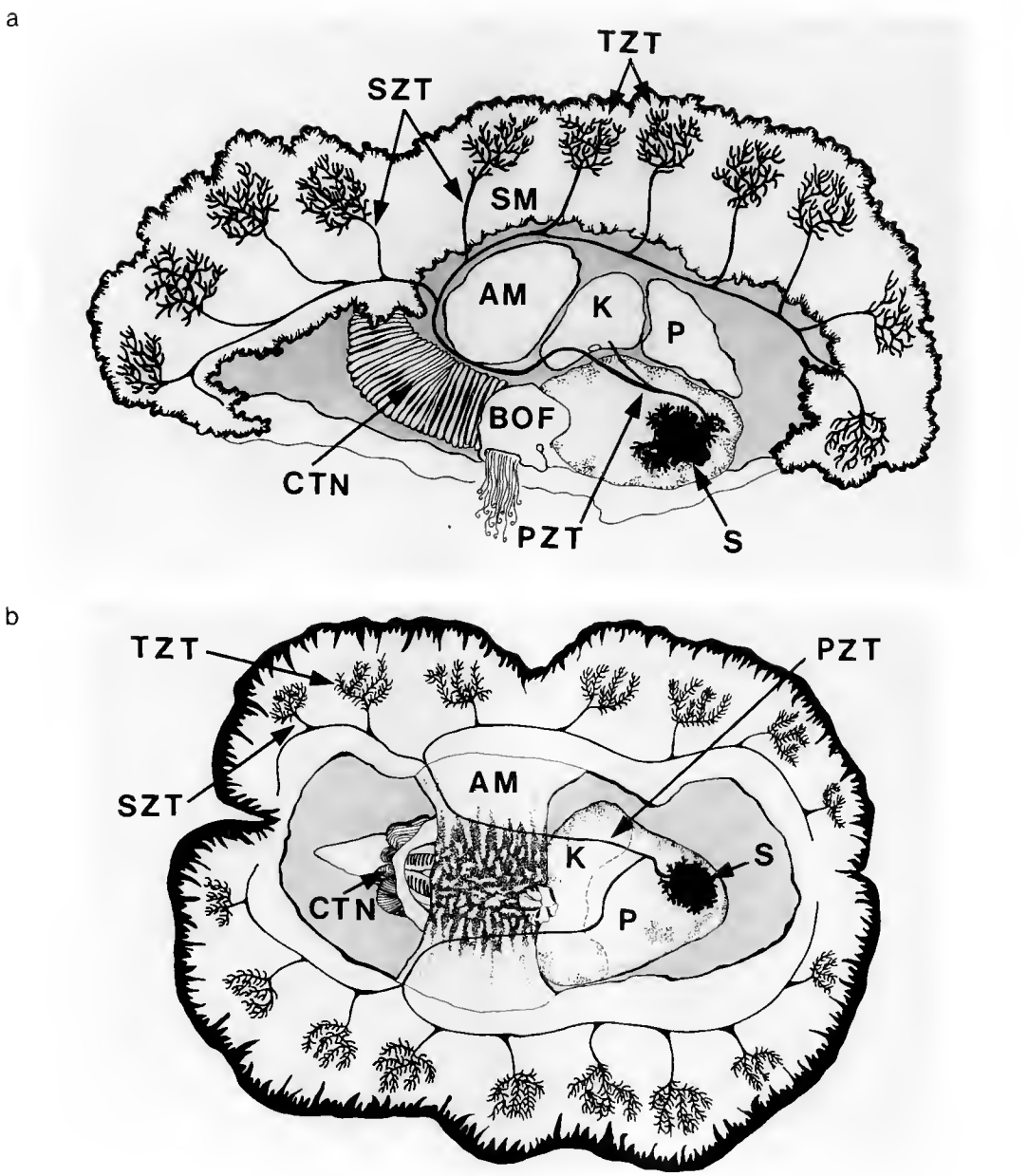

Figure 1. *Diagrammatic view of the path followed by the zooxanthellal tube through a giant clam. The black, highly branched structure on the surface of the stomach (S) in both a and b is the mass of digestive diverticular. Note that the primary zooxanthellal tube (PZT) originates from one of the diverticular ducts. a: Medial view of a bissected clam. b: Dorsal view of a bissected clam.*

Abbreviations: AM = adductor muscle, BOF = byssal organ/foot, CTN = ctenidia, K = kidney, P = pericardium, PZT = primary zooxanthellal tube, S = stomach, SM = siphonal muscle, SZT = secondary zooxanthellal tube, TZT = tertiary zooxanthellal tube.

are lined by ciliated epithelial cells with thin cytoplasm and small, prominent dark nuclei. Similar cells line the tertiary tubes (Fig. 3), but these cells appear to lack cilia. In naturally occurring bleached mantles, *i.e.*, in mantles lacking zooxanthellae, the tertiary zooxanthellal tubes atrophy.

No zooxanthellae were observed living free in the hemal sinuses, explaining previous reports that zooxanthellae are not found in hemolymph samples from giant clams (10, 11). Although some elements of the tubular system associated with the zooxanthellae were partially described by Mansour (4), he did not recognize that the tertiary zooxanthellal tubes have blind ends and do not communicate with the hemolymph system. Parts of the tubular system have been described previously by others (2, 12), but interpreted as communicating with the hemolymphatic system.

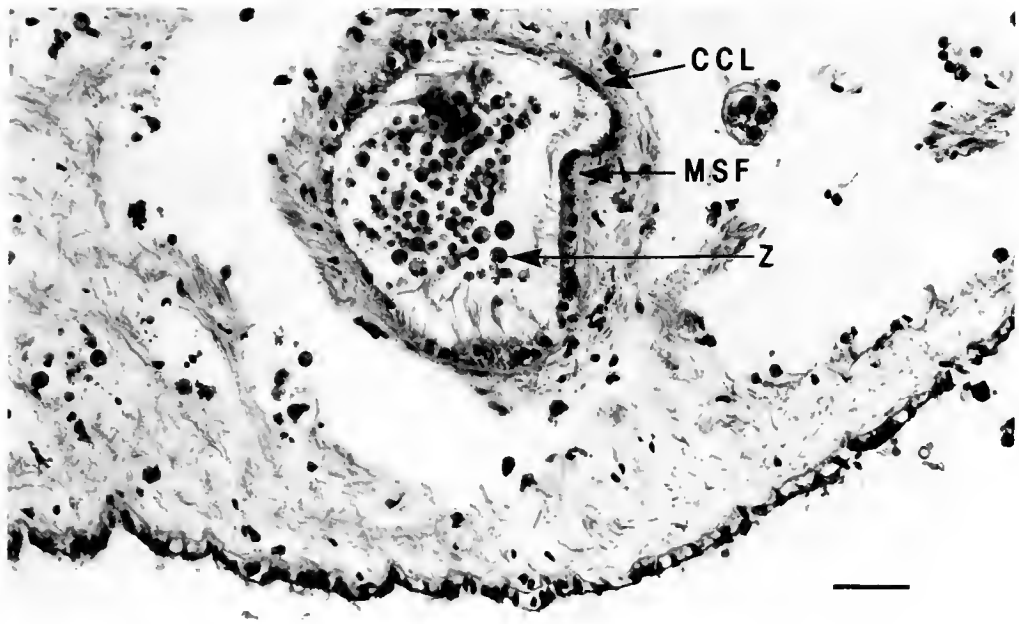

Figure 2. *A primary zooxanthellal tube (transverse section, H & E stain, Bar = 19 μm)*
Abbreviations: CCL = ciliated columnar epithelium, MSF = muscle fibers; Z = zooxanthellae

Our observations resolve much of the controversy that has existed over the past 50 years concerning the location and fate of zooxanthellae in the giant clams (2, 4, 5, 6, 7, 9, 10, 11, 13, 14, 15, 16, 17). The existence of this system simplifies the interpretation of previous data on the way the symbiosis functions. For example, Yonge (16) drew attention to the need to regulate the numbers of zooxanthellae that reproduce in the siphonal mantle. Yonge hypothesized that the algae are culled from the siphonal mantle by amoebocytes, wherein they are digested, and

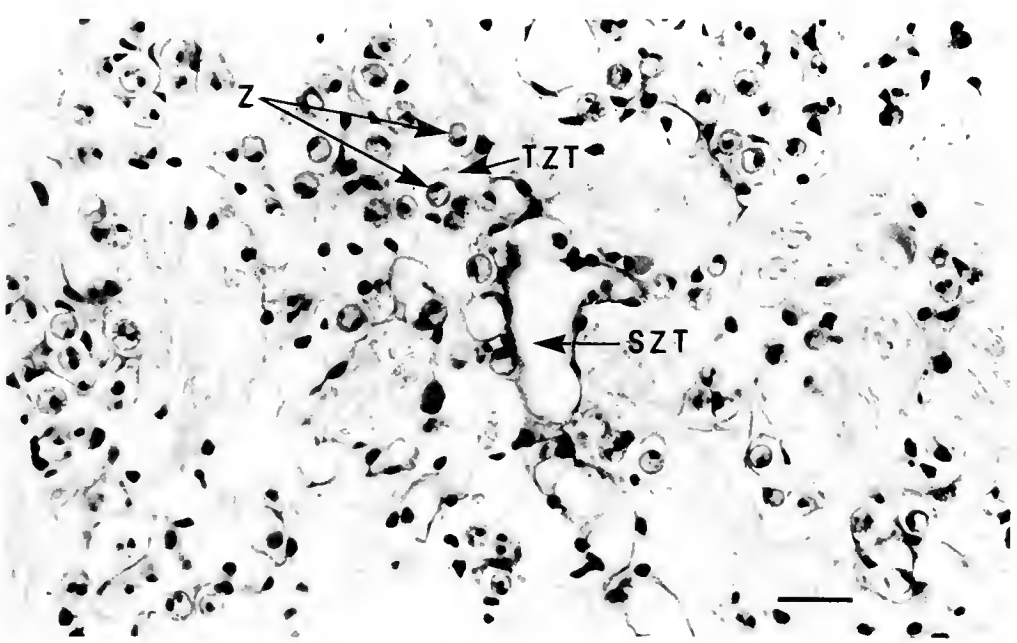

Figure 3. *Secondary and tertiary zooxanthellal tubes in the siphonal mantle (transverse section, Alcian Blue stain, Bar = 23 μm).*
Abbreviations: SZT = secondary zooxanthellal tube, TZT = tertiary zooxanthellal tube, Z = zooxanthellae

that the indigestible remains accumulate in the kidneys (18). As has been stated before, there is no evidence of this, and the algae move from the siphonal mantle to the stomach. Healthy zooxanthellae observed in the stomach (19), pass through the intestine and the rectum (2, 20) and are released in the feces; thus these algae, by an unknown mechanism, are able to resist host digestion. This route is also available for the mass expulsion of zooxanthellae from clams exposed to elevated environmental temperatures (21). Furthermore, there is no direct connection between the hemolymph and the stomach, via the tubes associated with the zooxanthellae, that would allow digestive enzymes into the hemolymphatic system (7). The entire branched tubular system associated with the zooxanthellae communicates with the stomach via a single opening, which is visible in clams that are only a few weeks old (22), and which would appear to explain the initial entry of zooxanthellae into the mantle (12).

The definition of this tubular system has implications for our understanding of the nutritional relationship between the giant clams and their zooxanthellae. It also reveals that the giant clam-zooxanthellae symbiosis is actually like other known invertebrate-algal symbioses, being intimately associated with the digestive system of the host (23).

Acknowledgments

We thank J. Lucas, D. Yellowlees, and A. Rees for comments on this paper. We also thank the Australian Centre for International Agricultural Research, Canberra, for financial assistance, and M. Dashorst for artwork.

Literature Cited

1. **Yonge, C. M. 1975.** Giant clams. *Sci. Am.* **232:** 96–105.
2. **Trench, R. K., D. S. Wethey, and J. W. Porter. 1981.** Observations on the symbiosis with zooxanthellae among the Tridacnidae (mollusca, bivalvia). *Biol. Bull.* **161:** 180–198.
3. **Fisher, C. R., W. K. Fitt, and R. K. Trench. 1985.** Photosynthesis and respiration in *Tridacna gigas* as a function of irradiance and size. *Biol. Bull.* **169:** 230–245.
4. **Mansour, K. 1946.** Communication between the dorsal edge of the mantle and the stomach of *Tridacna*. *Nature (Lond.)* **157:** 844.
5. **Yonge, C. M. 1953.** Mantle chambers and water circulation in the Tridacnidae (Mollusca). *Proc. Zool. Soc. (Lond.)* **123:** 551–561.
6. **Yonge, C. M. 1953.** The monomyarian condition in the Lamellibranchia. *Trans. R. Soc. Edinb.* **62:** 443–478.
7. **Fankboner, P. V., and R. G. B. Reid. 1991.** Nutrition in giant clams (Tridacnidae). Pp. 195–209 in *The Bivalvia—Proceedings of a Memorial Symposium in Honour of Sir Charles Maurice Yonge, Edinburgh, 1986*, B. Morton, ed. Hong Kong University Press, Hong Kong.
8. **Kawaguti, S. 1966.** Electron microscopy on the mantle of the giant clam with special references to zooxanthellae and iridophores. *Biol. J. Okayama Univ.* **12:** 81–92.
9. **Fankboner, P. V. 1971.** Intracellular digestion of symbiotic zooxanthellae by host amoebocytes in giant clams (Bivalvia: Tridacnidae), with a note on the nutritional role of the hypertrophied siphonal epidermis. *Biol. Bull.* **141:** 222–234.
10. **Yonge, C. M. 1936.** Mode of life, feeding, digestion and symbiosis with zooxanthellae in the tridacnidae. *Sci. Rep. Great Barrier Reef Exped. 1928–1929* **1:** 283–331.
11. **Mansour, K. 1946.** Source and fate of the zooxanthellae of the visceral mass of *Tridacna elongata*. *Nature (Lond.)* **158:** 130.
12. **Fitt, W. K., and R. K. Trench. 1981.** Spawning, development, and aquisition of zooxanthellae by *Tridacna squamosa* (Mollusca: Bivalvia). *Biol. Bull.* **161:** 213–235.
13. **Goreau, T. F., N. I. Goreau, and C. M. Yonge. 1973.** On the utilization of photosynthetic products from zooxanthellae and of a dissolved amino acid in *Tridacna maxima* f. *elongata* (Mollusca: Bivalvia). *J. Zool. (Lond.)* **169:** 417–454.
14. **Reid, R. G. B., P. V. Fankboner, and D. G. Brand. 1984.** Studies on the physiology of the giant clam *Tridacna gigas* Linne—I. Feeding and digestion. *Comp. Biochem. Physiol.* **78A:** 95–101.
15. **Morton, B. 1978.** The diurnal rhythm and the processes of feeding and digestion in *Tridacna crocea* (Bivalvia: Tridacnidae). *J. Zool. (Lond.)* **185:** 371–387.
16. **Yonge, C. M. 1980.** Functional morphology and evolution in the tridacnidae (Mollusca: Bivalvia: Cardiacea). *Rec. Aust. Mus.* **33:** 735–777.
17. **Reid, R. G. B., P. V. Fankboner, and D. G. Brand. 1984.** Studies of the physiology of the giant clam *Tridacna gigas* Linne—II. Kidney function. *Comp. Biochem. Physiol.* **78A:** 103–108.
18. **Fitt, W. K., G. A. Heslinga, and T. C. Watson. 1992.** Utilization of dissolved inorganic nutrients in growth and mariculture of the tridacnid clam *Tridacna derasa*. *Aquaculture*, in press.
19. **Fitt, W. K., C. R. Fisher, and R. K. Trench. 1986.** Contribution of the symbiotic dinoflagellate *Symbiodinium microadriaticum* to the nutrition, growth and survival of larval and juvenile tridacnid clams. *Aquaculture* **55:** 5–22.
20. **Ricard, M., and B. Salvat. 1977.** Faeces of *Tridacna maxima* (Mollusca: Bivalvia), composition and coral reef importance. *Proc. 3rd Coral Reef Symp., Miam.* **1:** 496–501.
21. **Estacion, J. S., and R. D. Braley. 1988.** Growth and survival of *Tridacna gigas* juveniles in an intertidal pond. Pp. 191–192 in *Giant Clams in Asia and the Pacific*, J. W. Copland, and J. S. Lucas, eds. Monograph No. 9, Australian Centre for International Agricultural Research, Canberra.
22. **Lee, P. S. 1990.** *Aspects of the Biology of Metamorphosis in Tridacnid Clams, with Special Reference to* Hippopus hippopus. M.S. Thesis, James Cook University, Townsville, Queensland.
23. **Trench, R. K. 1979.** The cell biology of plant-animal symbiosis. *Ann. Rev. Plant Physiol.* **30:** 485–531.

INDEX

D

E

F

G

H

I

J

K

L

M

N

O

P

Q

R

S

T

U

V

W

Y

Z

CONTENTS